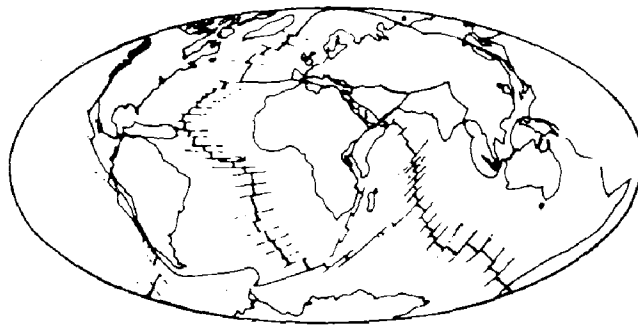


Extension Division

Proceedings
of the

International Symposium on Earthquake Structural Engineering

August 19-21, 1976



In Two Volumes

Vol. I

Second Edition
Edited by
FRANKLIN Y. CHENG



University of Missouri - Rolla



Proceedings of the
**International Symposium on
Earthquake Structural Engineering**

In two volumes
Volume I

August 19-21, 1976
St. Louis, Missouri, U.S.A.

Edited by
Franklin Y. Cheng
Professor of Civil Engineering

Department of Civil Engineering
University of Missouri - Rolla

Presented by
Department of Civil Engineering
Extension Division
University of Missouri - Rolla

PLANNING COMMITTEE

F.Y. Cheng, Symposium Director, University of Missouri - Rolla
J.H. Senne, Symposium Co-director, University of Missouri - Rolla
G.E. Lorey, University of Missouri - Rolla
J.B. Heagler, University of Missouri - Rolla
W. Kratzer, University of Missouri - Rolla
E.C. Murphy, University of Missouri - Rolla

TECHNICAL COMMITTEE

A.H-S. Ang, University of Illinois at Urbana-Champaign
F.Y. Cheng, Coordinating Chairman, University of Missouri - Rolla
C.G. Culver, National Bureau of Standards, Washington, D.C.
T.V. Galambos, Washington University
J.E. Goldberg, Purdue University and University of Illinois - Chicago Circle
W.A. Nash, University of Massachusetts-Amherst
O.W. Nuttli, St. Louis University

Preceding page blank



PREFACE

The 89 papers contained in these two volumes constitute the proceedings of the International Symposium on Earthquake Structural Engineering, which was held in St. Louis, Missouri, and presented by the University of Missouri - Rolla. The symposium was endorsed by the American Society for Engineering Education; the St. Louis and Mid-Missouri sections of the American Society of Civil Engineers; and the Joint Committee on Tall Buildings established by the International Association for Bridge and Structural Engineering, the American Society of Civil Engineers, the American Institute of Architects, the American Institute of Planners, the International Federation for Housing and Planning, and the International Union of Architects.

A large quantity of effective research has been put forth in the various areas of destructive earthquakes, seismicity, ground motions, earthquake instrumentation, earthquake zoning, and disaster prevention. In each, a tremendous amount of world-wide information has been accumulated that should be discussed and disseminated in specialized conferences, such as the one held in St. Louis, to provide for interaction and cooperation among researchers, educators, practitioners, and civil authorities in the field of earthquake structural engineering and to focus attention on structural design so as to minimize the destructive and killing effects of earthquakes. It is hoped that the presentations and discussions contained herein will contribute significantly toward this end.

It is not possible here to thank each and every person who contributed toward the organization of the conference, but sincere appreciation is extended to the authors for their cooperation and contributions and to all the Technical Committee members and Session Chairmen for their untiring efforts.

Special appreciation is expressed to the NSF for its partial financial support in publishing these proceedings. We are grateful for the assistance of Drs. S.C. Liu and J.B. Scalzi, Program Managers of Earthquake Engineering, Division of Advanced Environmental Research and Technology of the National Science Foundation, and for the encouragement and support of Drs. D. Thompson, Vice Chancellor, G.E. Lorey, Dean of Extension, and J.S. Johnson, Dean of School of Engineering, Prof. J.K. Roberts, Assist. Dean of School of Engineering, of the University of Missouri - Rolla. Last, but not least, the cooperation of the Planning Committee and University staff is acknowledged with thanks, and the skilled assistance of Mrs. Ann Mitchell and Margot Lewis in typing portions of the proceedings deserves special mention.

Rolla, Missouri, August 1976

Franklin Y. Cheng
Joseph H. Senne

Preceding page blank

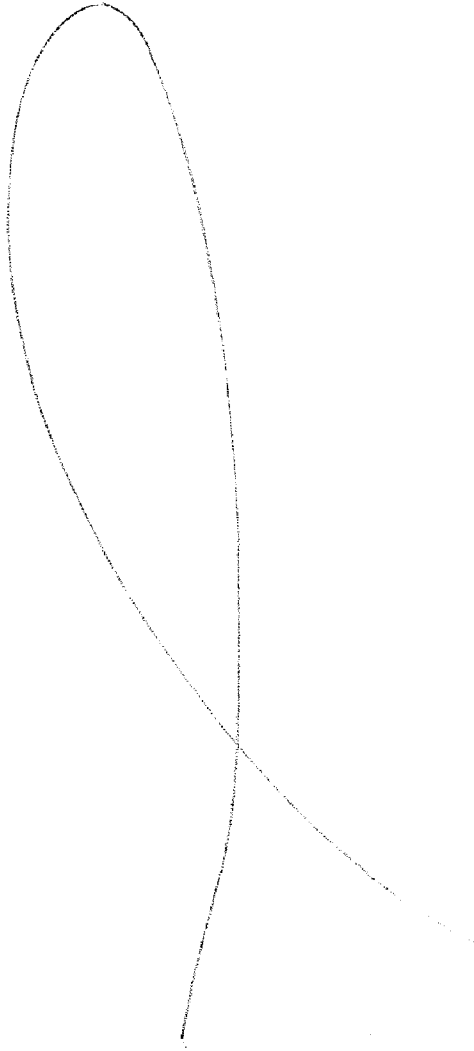


TABLE OF CONTENTS

Volume I

Page

PROGRAM.....	XI
INVITED LECTURE	
On the Specification of a Design Earthquake	
O.W. Nuttli.....	1
TECHNICAL SESSION NO. 1A--BUILDINGS AND BRIDGES	
A Study of the Effect of the Frequency Characteristics of	
Ground Motions on Nonlinear Structural Response	
A.T. Derecho, G.N. Freskakis and M. Fintel.....	21
Seismic Retrofitting for Highway Bridges	
A. Longinow, R.R. Robinson, K.H. Chu and J.D. Cooper.....	37
The Non-Linear Deformations in the Ground Base of Large-Panel	
Buildings Under Oscillations	
G.A. Shapiro and G.N. Ashkinadze.....	51
Dynamic Behavior of Cable Stayed Bridges	
E.A. Egeseli and J.F. Fleming.....	59
Modal Analysis and Seismic Design of Tall Building Frames	
P. Paramasivam, S. Nasim and S.L. Lee.....	73
Development in Structural Solutions of Multi-Storey Seismic-	
Proof Frameless Buildings of In-Situ Reinforced Concrete in	
USSR	
M.E. Sokolov and Y.V. Glina.....	83
The Inelastic Seismic Response of Bridge Structures	
R.D. Sharpe and A.J. Carr.....	91
Effect of Coupling Earthquake Motions on Inelastic Structural	
Models	
F.Y. Cheng and K.B. Oster.....	107
TECHNICAL SESSION NO. 1B--FOUNDATION AND	
STRUCTURE INTERACTION	
The Effect of Foundation Compliance on the Fundamental	
Periods of Multi-Story Buildings	
E. Mendelson and I. Alpan.....	127
Inverted-Pendulum Effect on Seismic Response of Tall Buildings	
Considering Soil-Structure Interaction	
T.H. Lee.....	147
On the Use of Precast Pile-Foundations in Construction of Earth-	
quake-Proof Large-Panel Buildings	
L.D. Martynova, Y.A. Simon, V.F. Zakharov and N.V.	
Kondratyev.....	161
Some Seismic Response Solutions for Soil-Foundation-Building	
Systems	
J.K. Minami and J. Sakurai.....	169
Response of Structures Embedded in the Ground to Travelling	
Seismic Waves	
E.G. Prater and M. Wieland.....	183
Some Comparisons of Dynamic Soil-Structure Analyses	
G.R. Johnson, H.I. Epstein and P. Christiano.....	199

Gypsum Layer in Soil-Structure Systems Y.C. Hung and M.D. Snyder	215
The Soil Foundation-Structure Interaction Under the Action of Earthquake Loads I. Ciongradi and N. Ungureanu	233
INVITED LECTURE	
Protection of Communications Facilities in Earthquake Areas N.J. Decapua and S.C. Liu	253
TECHNICAL SESSION NO 2A--ANALYSIS AND DESIGN	
Critical Excitation and Response of Free Standing Chimneys P.C. Wang, W. Wang, R. Drenick and J. Vellozzi	269
Dynamic Analysis of Elastic-Plastic Space Frames N.F. Morris	285
On the Limit Analysis of Box-Unit Buildings Under Static and Dynamic Effects T.I. Nassonova and M.J. Fraint	299
Dynamic Response of Cantilever Beam-Columns with Attached Masses Supported on a Flexible Foundation A.N. Kounadis	305
Vibrations and Interactions of Layered Beam Foundations V.N. Shah and T.C. Huang	315
Generating Response Spectra from Displacement and Velocity Time History Input A. Chuang, T.H. Lee, D.A. Wesley and S. Lu	331
A Simplified Nonlinear Seismic Response Analysis of Structures Including Vertical Ground Motion D.R. Bervig	345
Response of an Elasto-Plastic Spherical Structure in a Fluid to Earthquake Motions D. Srimahachota, T. Hongladaromp and S.L. Lee	375
Dynamic Response of Retaining Walls During Earthquake C.S. Yeh	387
Dynamic Response of Bridge Grid Under Moving Force N. Munirudrappa	393
A New Method for Numerical Integration of Equations of Motion J.E. Goldberg	413
Sheraton Hotel in Santo Domingo, Dom. Rep.: Analysis, Design, and Construction Techniques A.A. Ricart Nouel	423
TECHNICAL SESSION NO.2B--DYNAMIC TESTS ON STRUCTURES	
Reversing Load Tests of Five Isolated Structural Walls A.E. Fiorato, R.G. Oesterle, Jr. and J.E. Carpenter	437
Dynamic Behavior of a Reinforced Concrete Spray Tower T.J. Fowler, and D.M. Williams	455
Experimental Studies on Hysteretic Characteristics of Steel Reinforced Concrete Columns and Frames M. Wakabayashi and K. Minami	467

Static and Dynamic Tests of a Large-Size Model of a Frameless In-Situ Reinforced Concrete Residential Building	
Y.V. Barkov and Y.V. Glina	481
Experimental Study on Reinforced Concrete Truss Frames as Earthquake-Resistance Elements	
T. Shimazu and Y. Fukuhara	489
Ductile Behavior of Coupled Shear Walls Subjected to Reversed Cyclic Loading	
A.R. Santhakumar	501
Earthquake Response of Guyed Towers	
A.V. du Bouchet	513
Experimental Study on Reinforced Concrete Columns with Special Web-Reinforcements	
H. Umemura, T. Shimazu, S. Tadehara, T. Konishi and Y. Abe	527
Torsional Response at Large Eccentricities	
K.J. Meyer and I.J. Oppenheim	541
INVITED LECTURE	
Establishment of Design Earthquakes--Evaluation of Present Methods	
V.V. Bertero in collaboration with R.A. Herrera and S.A. Mahin	551
TECHNICAL SESSION NO. 3A--ANALYSIS AND DESIGN	
A Unified Approach to Designing Structures for Three Components of Earthquake	
A.K. Gupta and S.L. Chu	581
Resizing of Frames Subjected to Ground Motion	
V.B. Venkayya and F.Y. Cheng	597
Problems in Establishing and Predicting Ductility in Aseismic Design	
S.A. Mahin and V.V. Bertero	613
Shear Coefficient and Shear Force Distribution in Nuclear Power Plant Structures due to Seismic Loading	
N.C. Chokshi and J.P. Lee	629
Evaluation of the Reservoir Effect on the Dynamics of Dams	
H.U. Akay and P. Gulkan	643



PROGRAM

Registration **Wednesday, August 18, 1976**

6:00 p.m. - 9:00 p.m., Mississippi Room

Thursday, August 19, 1976

7:30 a.m. - 5:00 p.m., Registration, Mississippi Room

8:15 a.m. **OPENING SESSION**, Mississippi Room

Presiding: J.H. SENNE, University of Missouri - Rolla

Welcome Remarks

J.H. POELKER, Mayor of St. Louis

Representative of Honorable J.W. SYMINGTON, U.S. Congressman

D. THOMPSON, Vice Chancellor, University of Missouri - Rolla

9:05 a.m. **INVITED LECTURE**, Mississippi Room

Presiding: T.V. GALAMBOS, Washington University

On the Specification of a Design Earthquake, by O.W. NUTTLI, St. Louis University

9:40 a.m. Coffee Break

10:00 **SESSION IA**, Mississippi Room

BUILDINGS AND BRIDGES

Chairman:

T.V. GALAMBOS, Washington, University

Co-Chairman:

W.A. ANDREWS, University of Missouri - Rolla

A Study of the Effect of the Frequency Characteristics of Ground Motions on Nonlinear Structural Response, by A.T. DERECHO, G.N. FRESKAKIS, and M. FINTEL, U.S.A.

Seismic Retrofitting for Highway Bridges, by A. LONGINOW, R.R. ROBINSON, K.H. CHU, and J.D. COOPER, U.S.A.

The Non-Linear Deformations in the Ground Base of Large-Panel Buildings Under Oscillation, by G.A. SHAPIRO and G.N. ASHKINADZE, U.S.S.R.

Dynamic Behavior of Cable Stayed Bridges, by E.A. EGESELI, and J.F. FLEMING, U.S.A.

Modal Analysis and Seismic Design of Tall Building Frames, by P. PARAMASIVAM, S. NASIM, and S.L. LEE, Singapore

Development in Structural Solutions of Multi-Storey Seismic-Proof Frameless Buildings of In-Situ Reinforced Concrete in USSR, by M.E. SOKOLOV and Y.V. GLINA, U.S.S.R.

The Inelastic Seismic Response of Bridge Structures, by R.D. SHARPE, and A.J. CARR, New Zealand

Effect of Coupling Earthquake Motions on Inelastic Structural Models, by F.Y. CHENG and K.B. OSTER, U.S.A.

10:00 **SESSION IB**, Illinois Room
FOUNDATION AND STRUCTURE INTERACTION

Chairman:

M. ALIZADEH, Shannon & Wilson, Inc.

Co-Chairman:

W.A. NASH, University of Massachusetts - Amherst

The Effect of Foundation Compliance on the Fundamental Periods of Multi-Storey Buildings, by E. MENDELSON, and I. ALPAN, Israel
Inverted-Pendulum Effect on Seismic Response of Tall Buildings Considering Soil-Structure Interaction, by T.H. LEE, U.S.A.

On the Use of Precast Pile-Foundations in Construction of Earthquake-Proof Large-Panel Buildings, by L.D. MARTYNOVA, Y.A. SIMON, V.F. ZAKHAROV, and N.V. KONDRATYEV, U.S.S.R.

Some Seismic Response Solutions for Soil-Foundation-Building Systems, by J.K. MINAMI and J. SAKURAI, Japan

Response of Structures Embedded in the Ground to Traveling Seismic Waves, by E.G. PRATER and M. WIELAND, Switzerland

Some Comparisons of Dynamic Soil-Structure Analyses, by G.R. JOHNSON, H.I. EPSTEIN, and P. CHRISTIANO, U.S.A.

Gypsum Layer in Soil-Structure Systems, by Y.C. HUNG and M.D. SNYDER, U.S.A.

The Soil Foundation-Structure Interaction Under the Action of Earthquake Loads, by I. CIONGRADI and N. UNGUREANU, Romania

12:00 Lunch

1:30 - 2:10 **INVITED LECTURE**, Mississippi Room

Presiding: V.V. BERTERO, University of California-Berkeley

Protection of Communications Facilities in Earthquake Areas, by S.C. LIU, National Science Foundation

2:15 **SESSION 2A**, Mississippi Room
ANALYSIS AND DESIGN

Chairman:

T.C. HUANG, University of Wisconsin-Madison

Co-Chairman:

V.B. VENKAYYA, U.S. Air Force Flight Dynamics Laboratory, Wright Patterson, Ohio

Critical Excitation and Response of Free Standing Chimneys, by P.C. WANG, W.WANG, R. DRENICK, and J. VELLOZZI, U.S.A.

Dynamic Analysis of Elastic-Plastic Space Frames, by N.F. MORRIS, U.S.A.

On the Limit Analysis of Box-Unit Buildings Under Static and Dynamic Effects, by T.I. NASSONOVA and M.J. FRAINT, U.S.S.R.

2:15 **SESSION 2B**, Illinois Room
DYNAMIC TESTS ON STRUCTURES

Chairman:

M. FINTEL, Portland Cement Association

Co-Chairman:

V.V. BERTERO, University of California-Berkeley

Reversing Load Tests of Five Isolated Structural Walls, by A.E. FIORATO, R.G. OESTERLE, JR. and J.E. CARPENTER, U.S.A.

Dynamic Behavior of a Reinforced Concrete Spray Tower, by T.J. FOWLER and D.M. WILLIAMS, U.S.A.

Experimental Studies on Hysteretic Characteristics of Steel Reinforced Concrete Columns and Frames, by M. WAKABAYASHI, and K. MINAMI, Japan

3:00 Coffee Break

3:30

Dynamic Response of Cantilever Beam-Columns with Attached Masses Supported on a Flexible Foundation, by A.N. KOUNADIS, Greece

Vibrations and Interactions of Layered Beam Foundations, by V.N. SHAH and T.C. HUANG, U.S.A.

Generating Response Spectra from Displacement and Velocity Time History Input, by A. CHUANG, T.H. LEE, D.A. WESLEY and S. LU, U.S.A.

A Simplified Nonlinear Seismic Response Analysis of Structures Including Vertical Ground Motion, by D.R. BERVIG, U.S.A.

Response of an Elasto-Plastic Spherical Structure in a Fluid to Earthquake Motions, by D. SRIMAHACHOTA, T. HONGLADAROMP, Thailand and S.L. LEE, Singapore

Dynamic Response of Retaining Walls During Earthquake, by C.S. YEH, Republic of China

Dynamic Response of Bridge Grid Under Moving Force, by N. MUNIRUDRAPPA, India

Static and Dynamic Tests of a Large-Size Model of a Frameless In-Situ Reinforced Concrete Residential Building, by Y.V. BARKOV and Y.V. GLINA, U.S.S.R.

Experimental Study on Reinforced Concrete Truss Frames as Earthquake Resistance Elements, by T. SHIMAZU and Y. FUKUHARA, Japan

Ductile Behavior of Coupled Shear Walls Subjected to Reversed Cyclic Loading, by A.R. SANTHAKUMAR, India

Earthquake Response of Guyed Towers, by A.V. du BOUCHET, U.S.A.

Experimental Study on Reinforced Concrete Columns with Special Web-Reinforcements, by H. UMEMURA, T. SHIMAZU, S. TADEHARA, T. KONISHI and Y. ABE, Japan

Torsional Response at Large Eccentricities, by K. J. MEYER and I.J. OPPENHEIM, U.S.A.

A New Method for Numerical Integration of Equations of Motion
by J.E. GOLDBERG, U.S.A.
Sheraton Hotel in Santo Domingo, Dem. Rep.: Analysis, Design, and Construction Techniques, by A.A. RICART NOVEL, Dom. Rep.

Friday, August 20, 1976

8:00 - 12:00 Registration, Mississippi Room

8:30 - 9:10 **INVITED LECTURE**, Mississippi Room

Presiding: J.B. SCALZI, National Science Foundation

Establishment of Design Earthquakes--Evaluation of Present Methods, by V.V. BERTERO, University of California-Berkeley

9:15 **SESSION 3A**, Mississippi Room
ANALYSIS AND DESIGN

Chairman:

J.B. SCALZI, National Science Foundation

Co-Chairman:

R.E. DAVIS, McDonnell Douglas Automation Co.

A Unified Approach to Designing Structures for Three Components of Earthquake, by A.K. GUPTA and S.L. CHU, U.S.A.

Resizing of Frames Subjected to Ground Motion, by V.B. VENKAYYA and F.Y. CHENG, U.S.A.

Problems in Establishing and Predicting Ductility in Aseismic Design, by S.A. MAHIN and V. V. BERTERO, U.S.A.

10:00 Coffee Break

10:30

Shear Coefficient and Shear Force Distribution in Nuclear Power Plant Structures due to Seismic Loading, by N.C. CHOKSHI and J.P. LEE, U.S.A.

Evaluation of the Reservoir Effect on the Dynamics of Dams, by H.U. AKAY and P. GULKAN, Turkey

Dynamic Response Characteristics of an Elasto-Plastic Structure on a Random Soil Ground, by T. KOBORI, Y. INOUE and M. KAWANO, Japan

Some Design Considerations of Earthquake Resistant Reinforced Concrete Shear Walls, by T. PAULAY, New Zealand

Earthquake Resistance of Structures with Suspended Masses, by N.A. NIKOLAENKO and I.N. BURGMAN, U.S.S.R.

9:15 **SESSION 3B**, Illinois Room
CODES AND REGULATIONS

Chairman:

J.E. GOLDBERG, Purdue University and University of Illinois-Chicago

Co-Chairman:

V.R. BUSH, International Conference of Building Officials

On Specifications for Earthquake-Resistant Design of the Honshu-Shikoku Bridges [JSCE-1974], by I. KAWASAKI and E. KURIBAYASHI, Japan

Comparison of Aseismic Steel Building Design Practice in Japan and USA, by P.H. CHENG, U.S.A.

Comparative Study of the New Turkish Earthquake Resistant Design Code, by M. CELEBI, Turkey

Application of Structural, Mechanical and Electrical Codes and Standards in the Design of Safety Related Structures, Components, and Systems for Nuclear Power Plants, by D.S. MEHTA and B.L. MEYERS, U.S.A.

On Specifications for Earthquake-Resistant Design of Highway Bridges [Jan. 1971], by K. KAWAKAMI, E. KURIBAYASHI, T. IWASAKI and Y. IIDA, Japan

The New Turkish Aseismic Code: A Critical Evaluation with Emphasis on Soil Amplification Considerations, by A. GURPINAR, Turkey

Earthquake Dynamic Environment within Buildings, by K.L. MERZ, U.S.A.

Earthquake Response of a Tall Multi-Flue Stack, by P. KARASUDHI, Y.C. TSAI and K.P. CHAU, Thailand

On Earthquake Resistant Design of a Submerged Tunnel, by C. TAMURA and S. OKAMOTO, Japan
Seismic Design of the Veteran's Administration Hospital at Loma Linda, California, by W.T. HOLMES, U.S.A.

12:00 Lunch

1:30 - 2:10 **INVITED LECTURE**, Mississippi Room
Presiding: S.C. LIU, National Science Foundation

Risk and Safety Analysis in Earthquake-Resistant Design, by A. H-S. ANG, University of Illinois at Urbana-Champaign

2:15 **SESSION 4A**, Mississippi Room
SAFETY, RELIABILITY, AND POWER PLANT STRUCTURES

Chairman:

S.C. LIU, National Science Foundation

Co-Chairman:

J.T.P. YAO, Purdue University

Structural Damage and Risk in Earthquake Engineering, by D.S. HSU, J.T. GAUNT and J.T.P. YAO, U.S.A.

On Non-Stationary Spectrum and Mean Square Response of a Simple Structural System to Earthquake Excitation, by T. KOBORI and Y. TAKEUCHI, Japan

Dynamic Earthquake Analysis of a Bottom Supported Industrial Boiler, by N. J. MONROE and N. DASA, U.S.A.

2:15 **SESSION 4B**, Illinois Room
GROUND MOTIONS, CONSTRUCTION AND REPAIR OF STRUCTURES

Chairman:

O.W. NUTTLI, St. Louis University

Co-Chairman:

J.L. BEST, University of Missouri - Rolla

Methodology for Incorporating Parameter Uncertainties Into Seismic Hazard Analysis for Low Risk Design Intensities, by R.K. mcguire, U.S.A.

Epoxy Repair of Structures, by J.M. PLECNIK, J.E. AMRHEIM, W.H. JAY, and J. WARNER, U.S.A.

A California Structural Engineer Shares Three Years of On-Site Experiences in the Design of Repairs for Buildings in Managua, by P.J. CREGAN, Nicaragua

3:00 Coffee Break

3:30

Effects of Earthquake Input in Seismic Responses of Nuclear Power Plant Sites, by B.T.D. LU, J.A. FISCHER and J. Peir, U.S.A.

Discrete Modeling of Containment Structures, by Y.J. LIN and A.H. HADJIAN, U.S.A.

Seismic Risk Analysis of Nuclear Power Plant Sites Including Power Spectrum Simulation of Future Earthquake Motion, by A. GURPINAR, Turkey

Safety of Seismic Protective Systems with Reserve Elements, by I.M. EISENBERG, U.S.S.R.

Seismic Dynamic Parametric Study on Finite Element Model of Nuclear Power Plant Facility, by J.S. TERASZKIEWICZ, U.S.A.

Troika for Earthquake-Resistant Building Design, by J.R. TISSELL, U.S.A.

Safety of Cities During Severe Earthquakes, by O.C. MANN, U.S.A.

Evaluation of Greek Strong Motion Records, by P.G. CARYDIS and J.G. SBOKOS, Greece

Behavior of Reinforced Concrete Structures During the Managua Earthquake, by G. ESTRADA-URIBE, Columbia

Site Response Analysis for Earthquake Loading, by Y.S. LOU, S.J. DIXON and C.R. MacFADYEN, U.S.A.

Approximate Random Vibration Analysis of Elastoplastic Multi-Degree-of-Freedom Structures, by G. GAZETAS and E.H. VANMARCKE, U.S.A.

Probabilistic Approach to Ultimate Aseismic Safety of Structures, by M. YAMADA and H. KAWAMURA, Japan

Seismic Analysis of Hyperbolic Cooling Towers by the Response Spectrum Method, by P.L. GOULD, S.K. SEN and H. SURYOUTOMO, U.S.A.

6:20 p.m. Social Hour, Illinois Room

7:20 p.m. Banquet

Presiding: J.K. ROBERTS, University of Missouri - Rolla

SUBJECT: Structural Damage Caused by Guatemala Earthquakes of 4 and 6 February 1976, by J. ROESSET, Massachusetts Institute of Technology

Saturday, August 21, 1976

8:30 a.m. **INVITED LECTURE**, Mississippi Room

Presiding: P.L. GOULD, Washington University

Observational Studies on Earthquake Response of Buildings in Japan, Y. OSAWA, M. MURAKAMI, and T. MINAMI, University of Tokyo, Japan

9:15 a.m. **SESSION 5**, Mississippi Room **STRUCTURAL ELEMENTS AND SPECIAL STRUCTURES**

Chairman:

P.L. GOULD, Washington University

Co-Chairman:

A.H. HADJIAN, Bechtel Power Corporation

Discrete Modeling of Symmetric Box-Type Structures, by A.H. HADJIAN, and T.S. ATALIK, U.S.A.

Inelastic Seismic Response of Isolated Structural Walls, by G.N. FRESKAKIS, A.T. DERECHO and M. FINTEL, U.S.A.

Effects of Sectional Shape on the Strength and Ductility of Slender Structural Walls in Earthquake-Resistant Multistory Buildings, by S.K. GHOSH and M. FINTEL, U.S.A.

10:00 Coffee Break

10:20

On the Shear Pinched Hysteresis Loops, by M. CELEBI, Turkey

Confined Concrete in Compression Zones of Structural Walls Designed to Resist Lateral Loads Due to Earthquakes, by P.H. KAAR, A.E. FIORATO, J.E. CARPENTER, and W.G. CORLEY, U.S.A.

Response of an Empty Cylindrical Ground Supported Liquid Storage Tank to Base Excitation, by S.H. SHAABAN and W.A. NASH, U.S.A.

Seismic Design of Liquid Storage Tanks to Earthquakes, by P.C. CHEN and R.B. BARBER, U.S.A.

Analysis of Non-Uniform Coupled Shear Walls With Two Rows of Openings, by A.R. SANTHAKUMAR, India

Aseismic Design Examples of Prestressed Concrete Water Tank, by A. SAKURAI, C. KURIHARA and T. IWATATE, Japan

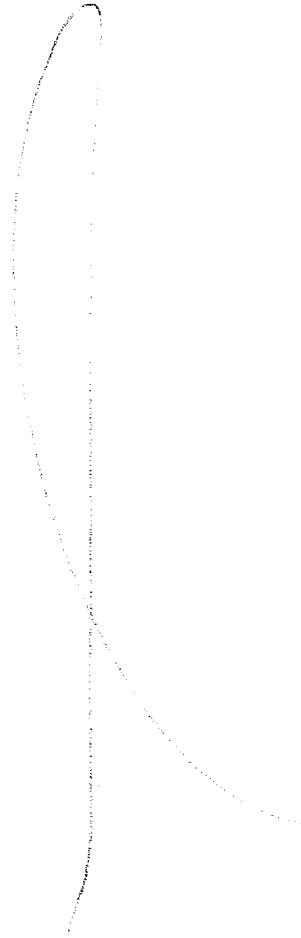
A New Structural Model for Shear Walls Analysis, by N. UNGUREANU, Romania

Response of Reinforced Concrete Chimneys to Earthquake Forces, by C.K. RAMESH and P.V. FADNIS, India

12:20 Closing Remarks

F.Y. CHENG, University of Missouri - Rolla

12:30 Adjourn



INTERNATIONAL SYMPOSIUM ON
EARTHQUAKE STRUCTURAL ENGINEERING

St. Louis, Missouri, USA, August, 1976

1

ON THE SPECIFICATION OF A DESIGN EARTHQUAKE

OTTO W. NUTTLI

Professor of Geophysics

Saint Louis University

St. Louis, Missouri, U. S. A.

SUMMARY

This paper discusses some of the more common means of specifying the design earthquake motion at a site. They include: estimation of the peak acceleration or the modified Mercalli intensity at the site, selection of an existing strong motion accelerogram which is scaled up or down to give the proper peak acceleration at the site, calculation of response spectra and/or Fourier spectra from the selected strong motion records, construction of typical response spectra which are scaled up or down so that their zero-period level corresponds to the expected peak acceleration, estimation of the sustained levels and the durations of ground acceleration, velocity and displacement at discrete frequencies, selection of an existing strong motion accelerogram which is scaled up or down to fit the sustained acceleration levels, and construction of synthetic time histories of the ground motion by making use of mathematical-physical models of the earth structure and of the earthquake source mechanism.

INTRODUCTION

The purpose of a design earthquake is to provide the structural engineer with a specification of the maximum ground motion to be encountered at a site during the lifetime of a structure, so that the engineer can design the structure to withstand the effects of the earthquake. Depending upon the use and importance of the building, the phrase "withstand the effects of an earthquake" can mean anything from not collapsing and no loss of life (e.g. school and office buildings) to no structural and little architectural damage, with the structure remaining operational (e.g. hospitals, nuclear power plants, communication facilities).

There are various ways in which the seismologist or earthquake engineer can present the design earthquake motion to the structural engineer. In general they vary from the elementary to the highly sophisticated, some of which exceed the present state-of-the-art. Some are purely empirical, whereas others employ models of the earthquake process and of earth structure for calculating the ground motion. All the methods involve assumptions which simplify or idealize actual conditions.

The purpose of this paper is to acquaint the structural engineer with the ways in which design motion can be presented, with the type of information about the earthquakes and the Earth itself which is needed to estimate the design motion, and with the present state-of-the-art concerning the specification of design earthquake motion.

MEANS OF PRESENTING DESIGN EARTHQUAKE MOTION

In terms of information contained, the most complete design motion would consist of time histories of the ground acceleration, velocity and displacement. These would be calculated, assuming a knowledge of the time history in the immediate neighborhood of the earthquake, of the geological structure between the source region and the site, and of the topography and soil conditions at the site. Figure 1 is an example of what such time histories would look like, although the accelerogram in that figure is an observed rather than a computed one. The velocity and displacement time histories were obtained by numerical integration of the accelerogram.

The accelerogram shows one horizontal component of motion at Pacoima Dam, about 8 km away from the epicenter of the San Fernando, California earthquake of February 9, 1971. Note that the frequency of the waves varies between about 20 and 1 Hz, and that in the mid-portion of the accelerogram there are high frequency waves which override lower frequency ones. The maximum acceleration, which occurs shortly after 7.5 sec, appears to result from the constructive interference

of approximately 3 Hz and higher frequency waves. Also note the dispersive character of the low frequency waves, beginning at about 2.5 sec and continuing until the end, with in general the lowest frequency waves arriving first. These probably are surface waves originating from the initial fault breakage. The higher frequency waves that override them, on the other hand, more likely are body waves originating at various points on the fault as the rupture advanced in jerky steps. This latter type of motion is particularly difficult to model mathematically, because there is no way of knowing in advance of the earthquake the exact time history of the fault rupture.

The ground velocity and ground displacement time histories of Figure 1 show principally the effect of the large amplitude, low frequency surface waves. In the velocity record one can see what appears to be both fundamental and higher mode waves, the fundamental mode in general having the lower frequency. As the base of the pier to which the strong motion instrument at Pacoima Dam was attached suffered a 0.5° permanent tilt because of the earthquake, part of the displacement on the ground displacement record may be showing the response of the instrument to tilt, rather than to actual ground displacement (Trifunac and Hudson, 1971).

Rather than specify the actual time history of the ground motion, one can give the displacement, velocity or absolute acceleration response spectra. The response spectrum is a measure of the maximum motion of a simple linear oscillator with a specified amount of damping when the oscillator is subjected to the ground acceleration time history. If ω is the natural angular frequency of the oscillator, n is the fraction of critical damping of the oscillator, and

$$\omega_n = \omega \sqrt{1 - n^2} \quad (1)$$

the displacement response spectrum is given by (Housner, 1970)

$$S_d = |y(t, \omega, n)|_{\max} = \left| \frac{1}{\omega_n} \int_{\tau=c}^{\tau=t_m} \ddot{z}(\tau) \exp[-n\omega_n(t-\tau)] \sin \omega_n(t-\tau) d\tau \right| \quad (2)$$

where y is the displacement of the oscillator, \ddot{z} is the ground acceleration and t_m is the time t for which the absolute value of the integral (or the displacement of the oscillator) is a maximum. The integral must be evaluated at each angular frequency ω for which a value of the response spectrum is desired. In general t_m will be a function of ω .

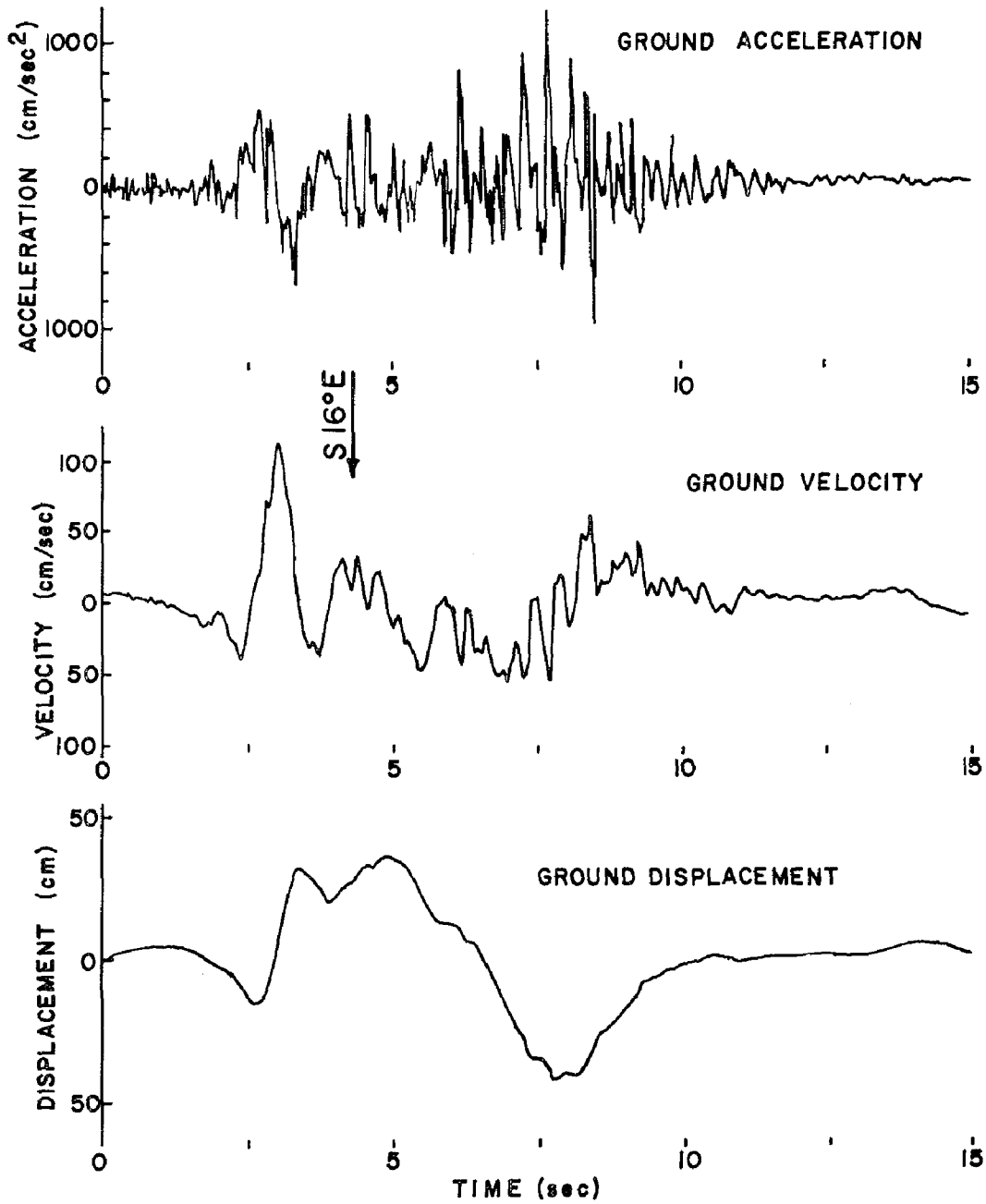


Figure 1. Strong ground motion (horizontal S16^oE component) at Pacoima Dam, 8 km from the epicenter of the 1971 San Fernando, California earthquake (adapted from Trifunac and Hudson, 1971)

The pseudovelocity response spectrum, S_{pv} , is given by (Housner, 1970)

$$S_{pv} = \omega S_d \quad (3)$$

and the acceleration response spectrum, S_a , by

$$S_a = \omega^2 S_d. \quad (4)$$

Figure 2 shows the response spectra for the Pacoima Dam horizontal component accelerogram of the San Fernando, California earthquake of February 9, 1971. (The accelerogram was shown as Figure 1.) Note that the effect of increased damping is to reduce the value of S_{pv} . It also can be observed that the largest values of S_{pv} and S_a occur at periods of less than 2 sec. In general, the larger the earthquake, the longer the periods at which the peak in the velocity response spectrum occurs if the distance from the epicenter remains constant (Housner, 1970). If the size of the earthquake is kept constant but the epicentral distance allowed to increase, there also will be a shift of the peak in the velocity response spectrum to the longer periods because the higher frequency waves undergo greater attenuation in traveling through the Earth.

One shortcoming of the response spectra curves is that, by themselves alone, they cannot give a complete picture of the effects of the time history of the acceleration duration (Trifunac and Hudson, 1971). Trifunac and Hudson noted that the San Fernando earthquake, with strong ground motion lasting about 7 sec, would have caused many buildings and bridges that were only partially damaged to have collapsed if the shaking had continued for another few seconds. They observed that it is mainly this effect of the duration of shaking on structural damage that calls for detailed investigations of the pattern of the time release of earthquake energy.

In addition to or in place of the response spectra one can also calculate the Fourier amplitude spectra of the ground acceleration, velocity and displacement. These spectra will indicate the periods, or period range, of ground motion that contain large accelerations, velocities and displacements. Fourier methods also suffer from the fact that they give no information about the duration of the motion. Housner (1970) showed that the undamped velocity spectrum is almost identical to the Fourier amplitude spectrum of the ground acceleration.

There are many seismic areas of the world for which there are either none or at most a few strong motion records of earthquakes. Most of the United States with the

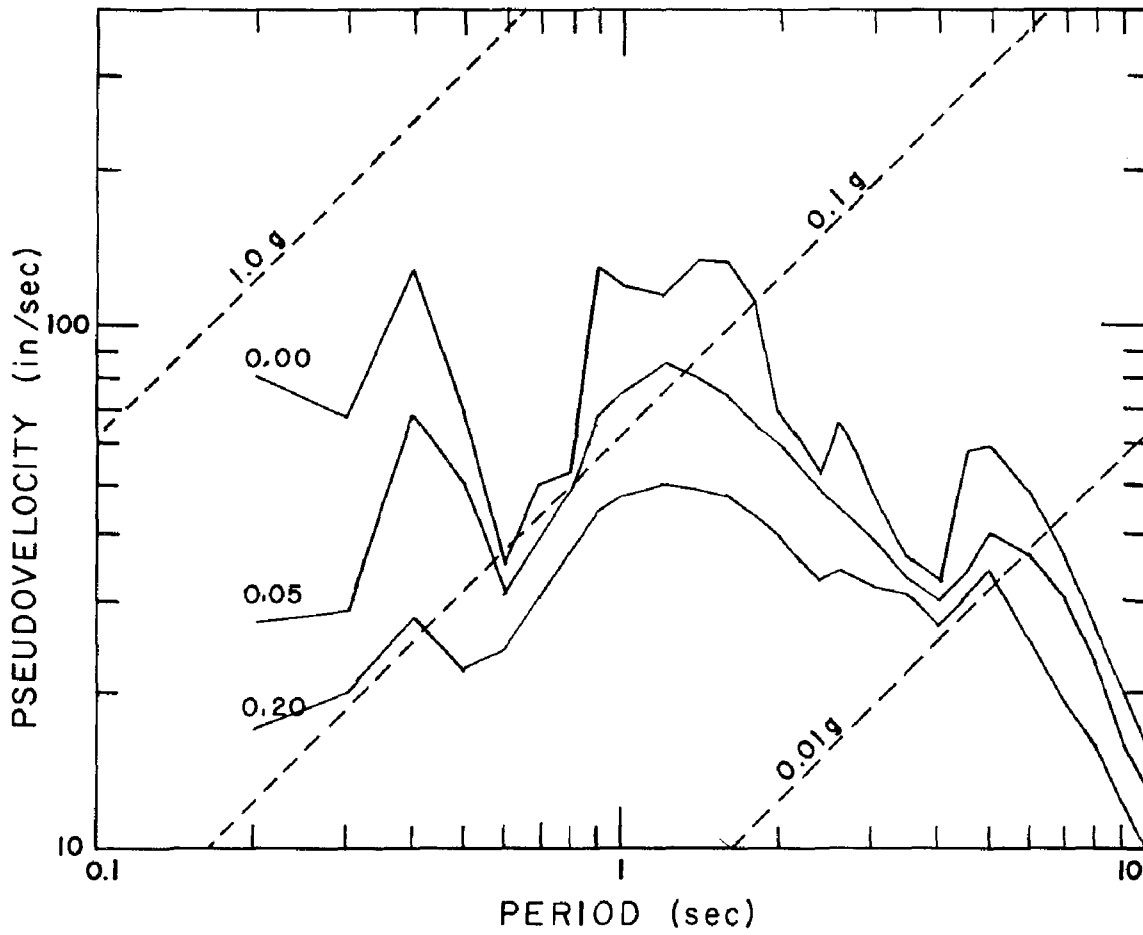


Figure 2. Response spectra derived from Pacoima Dam accelerometerogram of Figure 1 (data from Trifunac and Hudson, 1971). The numbers on the curves indicate the fraction of critical damping.

exception of California falls in this category. If one is unwilling to use strong motion records from one geographic region for specifying design motion in another, he must look at other methods of specifying design motion than those discussed to this point.

One such method (Nuttli, 1973a) estimates the level of the ground acceleration, velocity and displacement for certain discrete wave frequencies. These ground motion values, together with their durations, are given as a function of distance from the epicenter. The values specified are not spectral values, but rather the amplitudes that would be obtained by direct measurement in the time domain from strong motion records, if such records were available. By estimating ground motions at, say, 5, 1 and 0.2 Hz, one can provide some idea of the ground motion in the short, intermediate and long period ranges.

Another widely used method merely estimates the peak value of the ground acceleration (sometimes also velocity and displacement). It is the least satisfactory of all the methods because it provides no information about either the wave frequency of the peak ground motion or of the duration of the motion. Although there have been numerous attempts to correlate peak acceleration (or peak velocity) with damage (ordinarily expressed in terms of a modified Mercalli or some other intensity value), the correlation usually is low, with individual values differing by as much as plus or minus one order of magnitude from the mean value.

INFORMATION NEEDED TO SPECIFY DESIGN EARTHQUAKE MOTION

The first kind of information that is needed to specify the design earthquake motion at a site is the location of all potential earthquakes near the site. This implies that one can accurately identify and locate the seismically-active regions of the world. Unfortunately, this is not the case. In most parts of the world our historical record of earthquakes goes back no farther than a few hundred years, which is far too little a time to give a representative picture of the seismicity of an area. To supplement these data we can look for fault structures, and for evidence of movement on them in recent times by displacements in very young geological strata. Such data, when available, can give additional information about the return or recurrence time of the large magnitude earthquakes that are responsible for most of the fault displacement. Not all faults, however, show evidence of recent geological movement. In such cases microearthquake studies can be made in the vicinity of the fault, to determine if there is evidence of present-day activity. Sometimes the spatial coordinates of the micro-

earthquake hypocenters will help to delineate the horizontal and vertical dimensions of the active portion of the fault surface. These microearthquake studies, along with focal mechanism studies which determine the orientation of the surface across which faulting occurs and the direction of dislocation on that surface, can serve to identify a fault as active even though there have been no observable surface displacements on it. Examples of such areas are the New Madrid fault zone of southeast Missouri and adjacent states, the Ouachita Mountain front of Arkansas and eastern Oklahoma, and the Wabash Valley fault zone on the Illinois-Indiana border.

Along with the location of the active faults one also needs information about the maximum size of an earthquake to be expected in a given region. Normally this information is given in the form of a maximum magnitude earthquake. Richter and Gutenberg (Richter, 1935; Gutenberg and Richter, 1936, 1956) defined three types of magnitude scales. The first, which Richter called local magnitude (M_L), is a measure of the maximum ground motion in the frequency range of about 1 to 10 Hz for California earthquakes. This scale can only be properly used in areas where the surficial geology is similar to that of California and thus gives the same attenuation of high frequency waves. The second and third scales, which ordinarily make use of the amplitudes of waves recorded at great distances from the epicenter, are nearly independent of regional variations in geology. The one, called body-wave magnitude (m_b), is a measure of the size of the wave motion at a frequency of about 1 Hz. The other, called surface-wave magnitude (M_S), is a measure of the size of the wave motion at a frequency of 0.05 Hz. Unfortunately both M_L and M_S are commonly called the Richter magnitude, although for individual earthquakes they can differ by more than one order of magnitude from each other, the one being a measure of the excitation of short-period seismic wave energy and the other a measure of the excitation of very long-period wave energy.

If the shape of the spectrum of the ground motion were the same for all earthquakes, then all we would need to know in addition to that shape would be the level of the spectrum, which could be specified by one of the magnitudes. However, this is not the case. Factors such as the depth of the earthquake, the orientation of the fault surface and of the dislocation across the fault surface, the stress drop, the area of fault rupture and the time history of the rupture process all influence the shape and level of the spectrum in the source region of the ground motion. For large earthquakes in some source regions the first three of these factors remain nearly constant, and thus can be determined from a study of previous earthquakes in those regions.

The motion in the source region is transmitted through the Earth to the site in the form of wave motion. As it propagates it is attenuated, both because of geometrical spreading of the wave fronts and because of scattering and absorptive losses. The former, which is independent of wave frequency, depends on the vertical and horizontal variations in the elastic moduli and density of the rock layers. This so-called velocity structure can be determined from independent studies of the travel times and amplitudes of body waves and of the dispersion of surface waves. The latter is frequency dependent, and shows wide variation in different geologic regions for waves with periods less than 5 seconds (Nuttli, 1973b; Mitchell, 1975). The higher frequency waves in general are the most strongly absorbed. Thus as the epicentral distance increases the peak in the spectrum of the ground motion is shifted towards the lower frequencies, so that the seismic risk at large distances applies principally to tall or long structures having natural periods of vibration of one or more seconds.

Finally, soil conditions at the site can affect the ground motion there. The effect of a thick soil layer in general is to lower the acceleration values at the upper soil surface (compared to the values at its base), and to increase the velocities and displacements at the upper surface (Trifunac and Brady, 1975). Inasmuch as damage or seismic intensity values correlate better with ground velocity than with ground acceleration (Hudson, 1970; Nuttli, 1973c), the effect of a thick soil layer is to increase the damaging ground motions. In addition, certain soils liquefy when subjected to vibratory motion, i.e. they take on some properties of a fluid. Seed (1970) cites examples of earthquake-induced ground vibrations producing compaction and associated settlement of cohesionless soil deposits. If these cohesionless materials are water saturated, then their compaction is accompanied by an increase in pore water pressure in the soil and a consequent movement of water from the voids, resulting in the eruption of sand, mud and water in the form of sandblows and mudboils. Sandblows, over an area about 150 km in length, were a common phenomenon of the New Madrid earthquakes of 1811 and 1812 (Fuller, 1912). Soil liquefaction on sloping grounds, which results in flow slides, was extensive in the 1811-1812 New Madrid earthquakes, the 1920 Kansu Province, China earthquake, the 1960 Chile earthquake, the 1964 Alaska earthquake and the 1970 Peru earthquake.

STATE-OF-THE-ART FOR SPECIFYING DESIGN EARTHQUAKE MOTION

The simplest method of presenting design earthquake motion is by means of a hazard map, such as that of Alger-

missen (1969). Figure 3 shows his map for the United States. Zone 0 corresponds to no damage, zone 1 to minor damage with modified Mercalli intensities of V and VI to be expected, zone 2 to moderate damage with intensity of VII and zone 3 to major damage with intensities of VIII and greater. Alternately, using empirical relations, one can assign a maximum acceleration (or ground velocity) for each of the zones. Although the methodology is simple, there are some practical problems that arise. First of all, the maximum intensity or acceleration values jump discontinuously from one zone to another, whereas more realistically they should change smoothly. Secondly, the map gives no weight to the frequency of occurrence of earthquakes, so that regions such as Charleston, South Carolina which have experienced just one damaging earthquake in historic times are placed in the same zone 3 as coastal California, which has experienced a number of damaging earthquakes. Thirdly, because the map is developed mainly on the basis of historic activity, it does not show the places where future large earthquakes might occur but which have not yet experienced damaging earthquakes. Finally, as was pointed out previously, a single maximum intensity or maximum acceleration value is inadequate for many design purposes.

At the present time much work is being done to revise Algermissen's map in order to overcome some of its limitations, particularly the first two that were mentioned above. To overcome the third, separate maps of active fault systems in the United States are being prepared. Unfortunately, however, most of our knowledge of active fault systems is restricted to the western United States.

There are several approaches that have been used to overcome the problem of how to design with just a peak magnitude value. One is to select an existing strong motion accelerogram made at a place with similar site conditions to those of the place under investigation and at about the same epicentral distance, and to scale it up or down by the ratio of the accelerations. This is a fairly good procedure if the regional geology and attenuative properties of the Earth are the same in the region under investigation as the place where the accelerograms are obtained. As with all methods which employ peak acceleration values, it suffers from the fact that large peak accelerations can arise from fortuitous constructive interference of several wave arrivals, so that the peak acceleration may be physically unrelated to the overall amplitude level of the accelerogram and to the destructive potential of the ground motion. Once an accelerogram is adopted, one can readily construct response spectra for various fractions of critical damping.

A second approach is to construct an average set of

response spectra curves, based on accelerograms from a number of large earthquakes. The acceleration response spectral curves will approach a limiting value at small periods, independent of the amount of damping. In practice these curves can then be scaled up or down by the ratio of the design peak acceleration to the zero-period acceleration limit for the standard curves, the assumption being that most peak accelerations occur at short periods.

Instead of mapping the seismic hazard of a region, such as was done by Algermissen (1969), one can map the regions in which earthquakes of a given magnitude can be expected to occur. Figure 4 shows an example of such a map. Region A is the place where earthquakes as large as $m_b = 7.5$ can be expected to occur, region B where earthquakes as large as $m_b = 6.5$ can be expected to occur, and region C where earthquakes as large as $m_b = 6.0$ can be expected to occur. Accompanying this map is a table or set of curves, showing how the ground acceleration, velocity and displacement for several selected frequencies fall off with epicentral distance. Figure 5 shows such a set of ground acceleration curves for an earthquake in region A. For the curves of Figure 5 Nuttli (1973a) preferred to use the sustained maximum values of the ground motion rather than individual peak values, where the sustained maximum is the level attained for at least three cycles of the motion of a selected period. For a particular site one may have to make two sets of calculations of the sustained maximum motion, one for a nearby earthquake of smaller magnitude and one for a more distant earthquake of large magnitude.

An alternate to using directly for design purposes the values taken from the curves of Figure 5 is to use the values from the curves to select and scale an existing strong motion accelerogram. After this is done one can compute response spectra, as described previously.

Because the body-wave amplitudes decrease more rapidly with distance than the surface-wave amplitudes, one does not have to go too far from the epicenter before the surface-wave motion is dominant. No definite numerical value can be assigned to this critical distance, as it depends upon the size and depth of the earthquake and the length of faulting, as well as upon the frequency-dependent absorptive properties of the transmitting medium. For the distances at which the surface-wave motion is dominant, one can construct a fairly adequate synthetic time history of the ground motion (acceleration, velocity or displacement) by calculating the motion produced by the surface waves alone. To do this one must assume a knowledge of the depth of the earthquake, of the orientation of the fault plane and the dislocation on it, of the velocity structure of the source and transmission

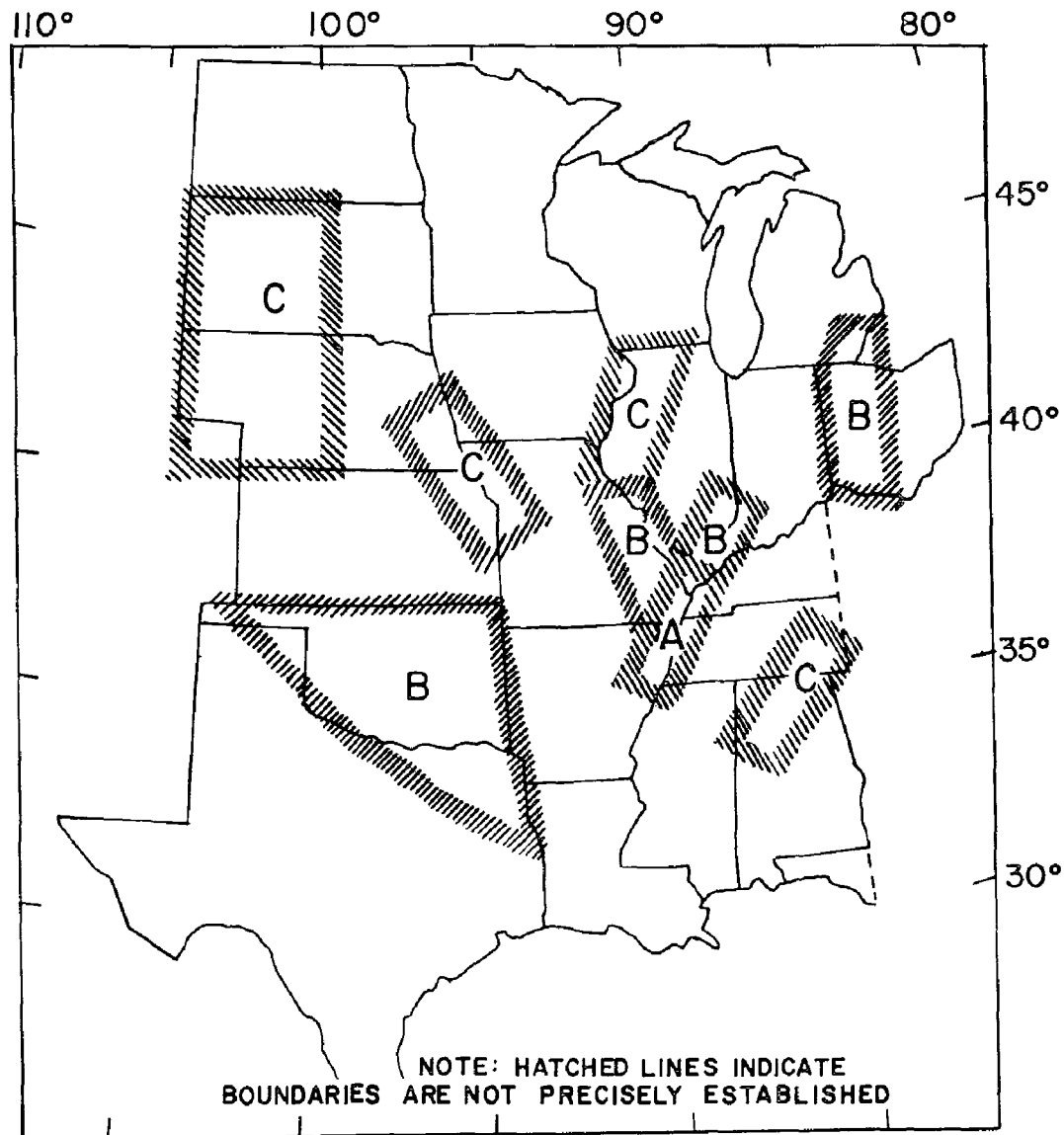


Figure 4. Design earthquake zoning map of central United States, showing regions where earthquakes of a specified magnitude can be expected to occur (adapted from Nuttli, 1973a)

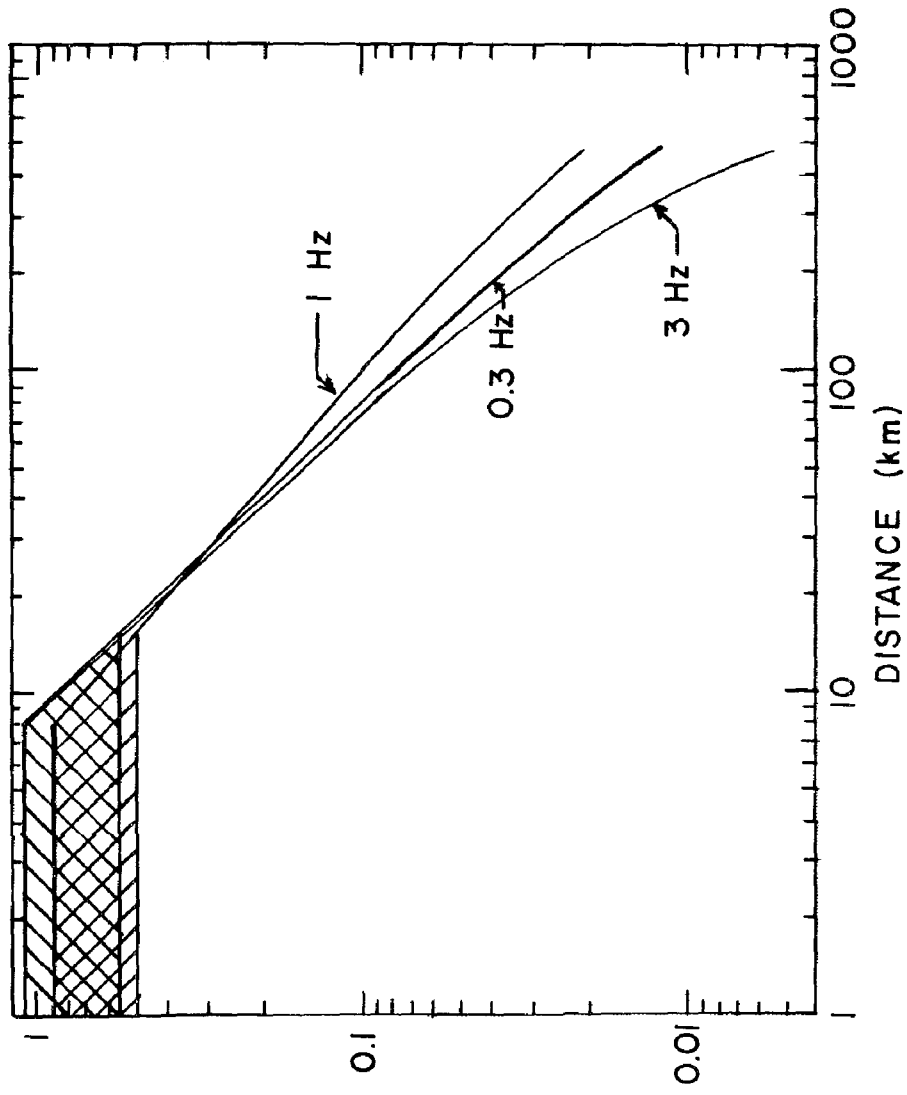


Figure 5. Ground acceleration as a function of wave frequency and horizontal distance for an $m_b = 7.5$ earthquake occurring in the central Mississippi Valley (region A of Figure 4). The accelerations are sustained maximum values, rather than peak values (adapted from Nuttli, 1973a)

region, of the time history of the dislocation and of the size of the earthquake, expressed in terms of its seismic moment. Figure 6 is an example of the Love wave ground velocity and displacement, computed for earthquakes at focal depths of 2.5, 9.5 and 19.5 km, for a central United States type geology and a seismic moment of 10^{24} dyne-cm (about $m_0 = 5.7$). This motion represents the contribution of the fundamental and the first eight higher modes of Love waves, for wave periods of 1.5 to 400 sec. In order to include the contribution of shorter period waves one would have to include many additional higher modes in the calculations, which would result in a formidable computing problem.

Figure 7 shows the effect of change of focal depth on the spectra of the Love wave motion at a distance of 1000 km. As the depth is decreased the short period level increases greatly, due to a stronger excitation of the fundamental-mode wave. At these short periods the fundamental-mode waves damp out faster than the higher-mode waves, so in the near-field region the surface wave amplitudes vary even more greatly with focal depth. Thus, in the near-field region of a very shallow earthquake the fundamental-mode surface waves will be destructive, even for earthquakes with m_0 as small as 4.

Although the surface-wave motion can be adequately modeled by a point (in space and time) source for the purposes discussed above, this is not the case for the body-wave motion in the near-field region. Each jerk-like motion of the fault surface will correspond to a new source of body waves, acting according to no definite physical law. That is, there is no way in advance we can know what the time separation between jerky breaks will be. Thus it is a much more difficult task to produce realistic synthetic time histories of body-wave motion in the near-field region (where the body waves are potentially damaging) than it is for the surface-wave motion. In fact, the present state-of-the-art is such that adequate synthetic time histories of neither the body-wave nor the surface-wave near-field motion are available for predictive purposes. Thus we shall have to continue to rely principally on strong-motion records of actual earthquakes, and hope to build a sufficiently large collection that we can eventually describe a set of "typical" near-field records.

CONCLUSION

The purpose of this paper has been to explain to structural engineers the kinds of design motion information that the seismologist can provide him, and to point out the limitations of such data and the assumptions made in arriving at them. Depending upon the cost, location and intended use

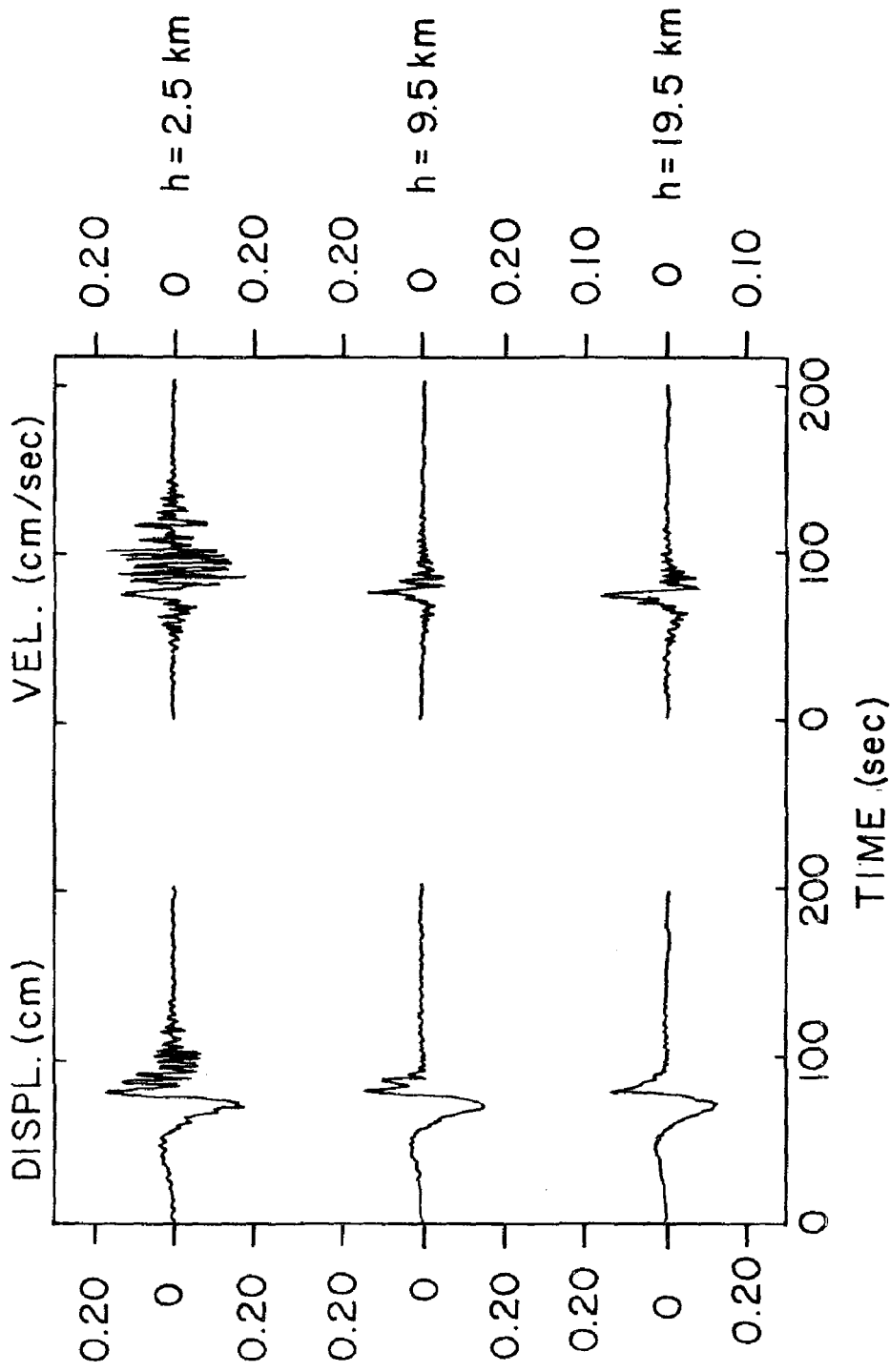


Figure 6. Synthetic velocity and displacement time histories of Love wave motion at 250 km distance for an $m_b = 5.7$ earthquake, assuming a central United States earth structure (adapted from Herrmann and Nuttli, 1975).

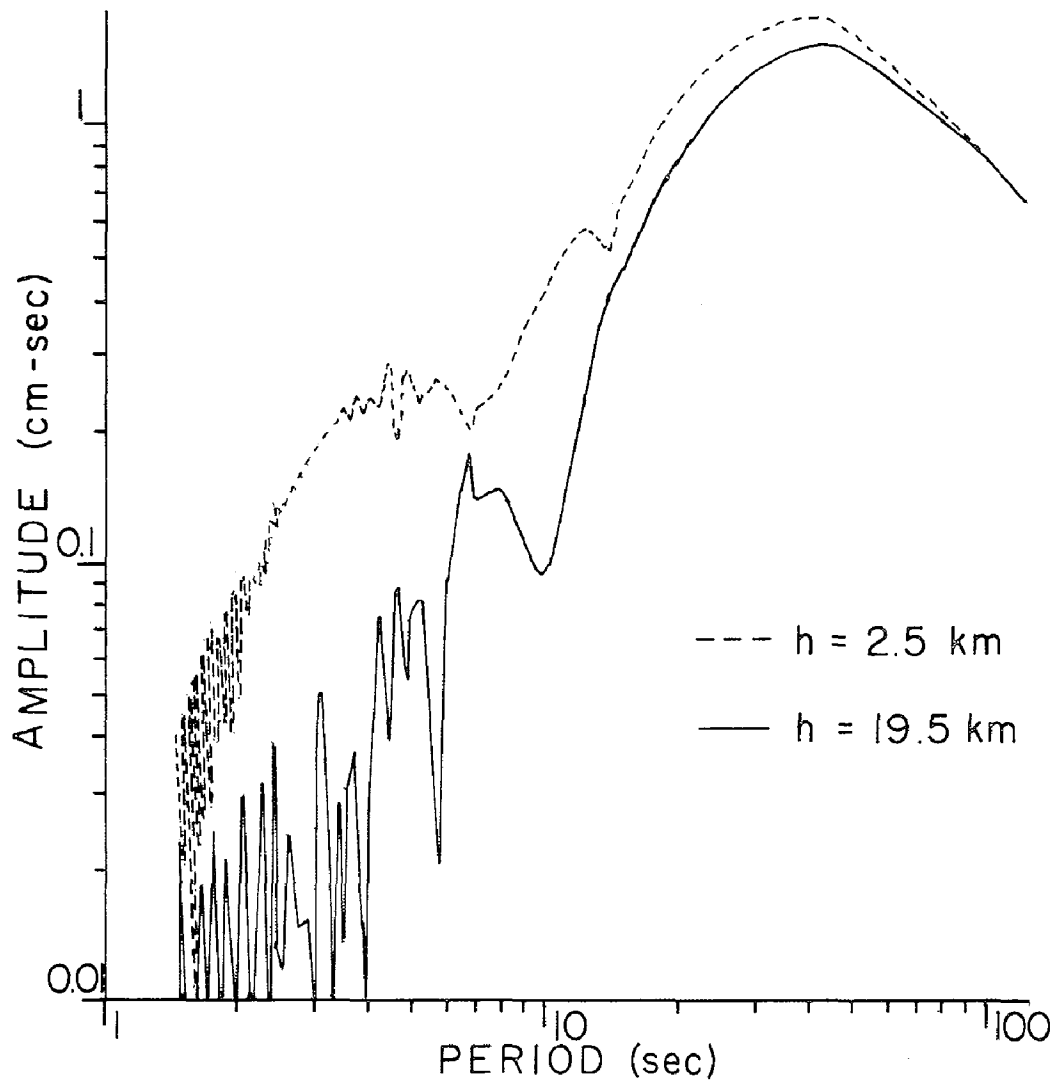


Figure 7. Love wave spectra at 1000 km distance as a function of focal depth, assuming a central United States earth structure (adapted from Herrmann and Nuttli, 1975)

of the structure, the design parameters may be as simple as a single peak acceleration value to as complex as a synthetic time history of the ground acceleration, velocity and displacement. As the latter is beyond the present state-of-the-art for ground motions in the near-field region, seismologists and earthquake engineers will have to extend their efforts to record the ground motion in such regions, to be able empirically to build up sets of typical time histories of the ground motion.

ACKNOWLEDGMENT

This research was supported by a grant from the National Science Foundation (Grant DES74-22852-A01).

REFERENCES

- Algermissen, S. T. "Seismic Risk Studies in the United States" Proceedings of the Fourth World Conference on Earthquake Engineering, Santiago, Chile, vol. 1, 1969, pp. 14-27.
- Fuller, M. B. "The New Madrid Earthquake" U. S. Geological Survey Bulletin 494, 1912, 118 pp.
- Gutenberg, B. and C. F. Richter "On Seismic Waves, 3" Gerland's Beiträge zur Geophysik, vol. 47, 1936, pp. 73-131.
- Gutenberg, B. and C. F. Richter "Magnitude and Energy of Earthquakes" Annali di Geofisica, vol. 9, 1956, pp. 1-15.
- Herrmann, R. B. and O. W. Nuttli "Ground-Motion Modelling at Regional Distances for Earthquakes in a Continental Interior, II. Effect of Focal Depth, Azimuth, and Attenuation" Earthquake Engineering and Structural Dynamics, vol. 4, 1975, pp. 59-72.
- Housner, G.W. "Strong Ground Motion" in Earthquake Engineering, edited by R. L. Weigel, Prentice-Hall, 1970, pp. 75-91.
- Hudson, D.E. "Ground Motion Measurements" in Earthquake Engineering, edited by R. L. Weigel, Prentice-Hall, 1970, pp. 107-125.
- Mitchell, B. J. "Regional Rayleigh Wave Attenuation in North America" Journal of Geophysical Research, vol. 80, 1975, pp. 4904-4916.
- Nuttli, O. W. State-of-the-Art for Assessing Earthquake Hazard in the United States, Report 1: Design Earthquakes for the Central United States, U. S. Army Engineer Waterways Experiment Station, Mississippi, Misc. Paper 5-73-1, 1973a, 55pp.
- Nuttli, O. W. "Seismic Wave Attenuation and Magnitude Relations for Eastern North America" Journal of Geophysical Research, vol. 78, 1973b, pp. 876-885.

- Nuttli, O. W. "The Mississippi Valley Earthquakes of 1811 and 1812: Intensities, Ground Motion and Magnitudes" Bulletin of the Seismological Society of America, vol. 63, 1973c, pp. 227-248.
- Richter, C. F. "An Instrumental Earthquake Scale" Bulletin of the Seismological Society of America, vol. 25, 1935, pp. 1-32.
- Seed, H. B. "Soil Problems and Soil Behavior" in Earthquake Engineering, edited by R. L. Wiegel, Prentice-Hall, 1970, pp. 227-251.
- Trifunac, M. D. and A. G. Brady "On the Correlation of Seismic Intensity Scales with the Peaks of Recorded Strong Ground Motion" Bulletin of the Seismological Society of America, vol. 65, 1975, pp. 139-162.
- Trifunac, M. D. and D. E. Hudson "Analysis of the Pacoima Dam Accelerogram" in Strong-Motion Instrumental Data on the San Fernando Earthquake of Feb. 9, 1971, edited by D. E. Hudson, Earthquake Engineering Research Laboratory of California Institute of Technology and Seismological Field Survey of National Oceanic and Atmospheric Administration, 1971, pp. 205-208.

INTERNATIONAL SYMPOSIUM ON
EARTHQUAKE STRUCTURAL ENGINEERING

21

St. Louis, Missouri, USA, August, 1976

A STUDY OF THE EFFECT OF THE FREQUENCY CHARACTERISTICS
OF GROUND MOTIONS ON NONLINEAR STRUCTURAL RESPONSE

A. T. DERECHO
Principal Structural Engineer

G. N. FRESKAKIS
Senior Structural Engineer

MARK FINTEL
Director

Engineering Services Department
Portland Cement Association
Skokie, Illinois, 60076, U.S.A.

SUMMARY

In conducting deterministic nonlinear dynamic response studies of a specific structure, it is essential to know what general type of accelerogram to use as input in order to obtain a good estimate of the expected maximum response with a limited number of analyses. Insofar as dynamic structural response is concerned, the major parameters characterizing the ground motion are intensity, duration and frequency content. The effects of intensity and duration on dynamic response have been studied by a number of investigators. However, little has been done to study the effect of the frequency characteristics of the input motion. This report presents the results of nonlinear dynamic analyses of isolated structural walls with hysteresis loops characterized by a stiffness that decreases with increasing amplitudes of inelastic deformation. A rough basis for classifying accelerograms in terms of their damped velocity spectra as "broad band" and "peaking" is proposed. The results of the study indicate that when extensive yielding occurs in a structure, so that a significant change in the effective period of vibration results, a broad band accelerogram is likely to produce a more severe response compared to a peaking accelerogram of the same intensity and duration. On the other hand, when only minor yielding occurs so that no significant increase in the effective period results, a peaking record will more likely produce the more severe response.

INTRODUCTION

The economic provision of adequate stiffness, strength and deformation capacity in earthquake-resistant structures depends on a realistic assessment of the maximum forces and deformations which are likely to occur during the expected life of the structure. For a particular site, wide variations in the character of the free field motion can occur as a result of variations in the source location, mechanism, and the transmission path properties. This variation would be greater if the potential earthquake foci were widely separated.

The variation in the character of the ground motion at a site indicates the desirability of considering a number of representative input motions when undertaking an analysis to determine the likely maximum response of a particular structure. However, where inelastic analyses (considered essential in a determination of

Preceding page blank

deformation requirements) are concerned, only a very limited number of such runs are possible in most cases. In recognition of this limitation, it was felt desirable to develop a means of classifying accelerograms into fairly broad categories according to certain basic properties, so that reasonably good estimates of the maximum response of structures to potential earthquakes could be obtained on the basis of a limited number of analyses.

GROUND MOTION PARAMETERS

Insofar as dynamic structural response is concerned, the principal ground motion parameters are intensity, duration, and frequency content. Intensity is used as a characteristic measure of the amplitude of the acceleration pulses in a record. Duration refers to the length of the record during which relatively large amplitude pulses occur, with due allowance for a reasonable build-up time. The frequency characteristics of a given ground motion have to do with the energy content of the different component waves making up the motion.

Although the effects of intensity and duration on dynamic structural response have been studied by a number of investigators, ⁽²⁾ very little has been done to study the effect of the frequency characteristics of the input motion, particularly with respect to the objective mentioned above.

This study presents the results of the dynamic nonlinear analyses of isolated structural walls with hysteresis loops characterized by a stiffness which decreases with increasing amplitudes of inelastic deformation. The study of the effect of the frequency characteristics of the input motion was undertaken primarily in an effort to narrow down the number of accelerograms which could be used in a parametric study while still providing a reasonable estimate of the maximum response under a likely combination of unfavorable conditions.

Frequency Characteristics

A typical strong-motion accelerogram shows an extremely complex series of oscillations. Any such record may be thought of as a superposition of simple, constant-amplitude waves each with a different frequency, amplitude and phase. The importance of knowing the frequency characteristics of a given input motion lies in the phenomenon of resonance or quasi-resonance, which occurs when the frequency of the exciting force or motion approaches the frequency of the structure. Near-maximum response to earthquake excitation can be expected if the dominant frequency components occur in the same frequency (or period) range as the dominant effective frequencies (or periods) of a structure.

A convenient way of studying the frequency characteristics of an accelerogram is provided by the Fourier amplitude spectrum. This spectrum provides a frequency decomposition of the accelerogram, indicating the amplitude (in units of velocity - a measure of the energy content) of the component at a particular frequency. Another commonly used measure of the frequency content of an accelerogram is the velocity response spectrum. This is a plot showing the variation of the maximum absolute value of the relative velocity of a linear single-degree-of-freedom

system with the undamped natural period (or frequency) when subjected to a particular input motion. Figure 1 (from Ref. 1) shows the relative velocity response spectra for the N-S component of the 1940 El Centro record, for different values of the damping factor. The dashed curve in Fig. 1 is the corresponding Fourier amplitude spectrum. Hudson⁽⁵⁾ has shown that when the maximum response of a system occurs at the end of a record, the undamped relative velocity response spectrum has a form identical to that of the Fourier amplitude spectrum of the ground acceleration. Otherwise, these two plots are only roughly similar. As in the Fourier spectrum, the peaks in the velocity response spectrum reflect concentrations of the input energy at or near the corresponding frequencies. For damped systems, these peaks are reduced, the reduction being greater for the shorter period systems. It is pointed out that the velocity response spectrum reflects the effects of the intensity and frequency content, but not necessarily the duration, of the input.

Although both Fourier amplitude and undamped velocity response spectra exhibit a jagged character, with peaks and troughs occurring at close intervals, it is usually possible to recognize a general trend in the overall shape of the curve. By noting the general shape of the spectrum in the frequency range of interest, a characterization of the input motion in terms of frequency content can be made. While this procedure represents a rather crude method for classifying accelerograms in terms of frequency content, it nevertheless provides a sufficient basis for determining the potential severity of a given input motion in relation to a specific structure.

In this study, where a viscous damping coefficient of .05 of critical for the first mode was used as the basic value for the dynamic analysis model, the 5% damped velocity response spectra corresponding to 10 seconds of a number of representative records were examined. Figure 2 shows the velocity response spectra for the N-S and E-W components of the 1940 El Centro record (Imperial

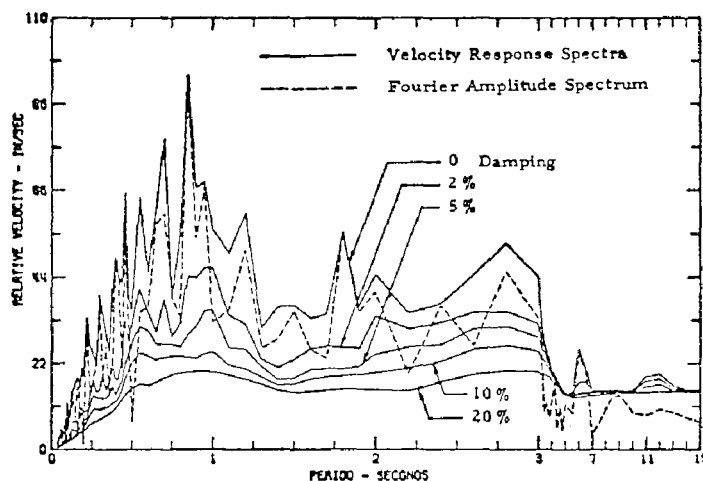


Fig. 1 - Velocity response spectra - 1940 El Centro, N-S component (from Ref. 1)

Valley Earthquake, May 18, 1940). On the basis of this examination, two general categories were recognized, namely:

- (1) a "peaking" accelerogram with a spectrum exhibiting dominant frequencies over a well-defined period range. The N-S component of the 1940 El Centro record is an example of this class.
- (2) a "broad-band" accelerogram with a spectrum that remains more or less flat over the period range of interest. The vertical component of the 1940 El Centro record may be classified under this category.

A sub-class of the broad-band category is a record with a spectrum which increases with increasing period within the period range of interest. This may be referred to as a "broad-band ascending" accelerogram. The E-W component of the 1940 El Centro record is typical of this type of record.

The above two cases are illustrated schematically in Fig. 3.

For a linear structure, where the dynamic behavior is dominated by its fundamental mode (as in most reinforced concrete multistory buildings with structural walls), a strong response can be expected when the fundamental period falls within the peaking range of the input motion, i.e., within the period range where the dominant components of the input motion occur. Lesser response can be expected if the dominant period of the structure falls outside the peaking range.

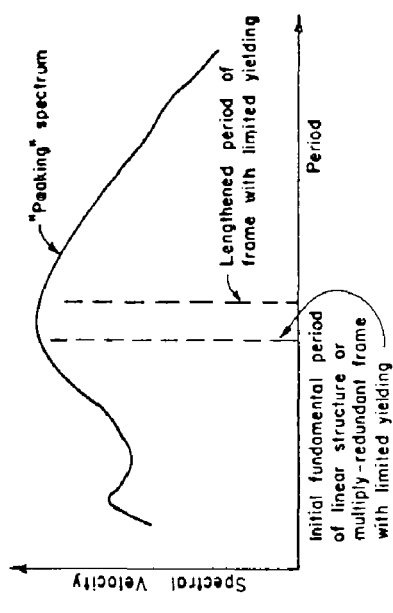
Duration

Because of the significant computer cost involved in dynamic inelastic analysis, particularly for the coupled wall and frame-wall systems planned for the subsequent phases of this investigation, it was decided at the outset to use a duration of 10 seconds of the base excitation for most analyses. Only when studying the effect of duration on the response were 20-second records used.

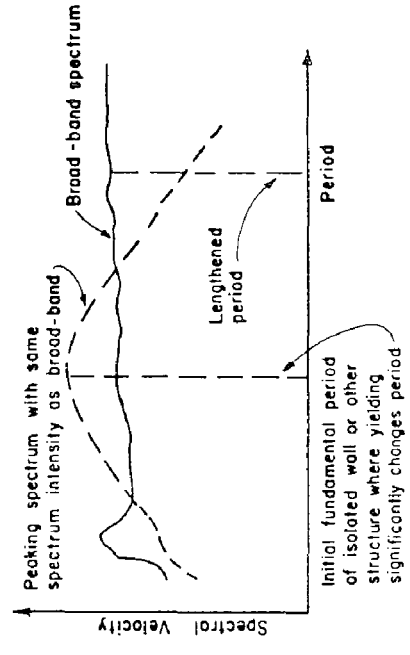
Intensity

The best parameter to use as a characteristic measure of the amplitude of the acceleration pulses within the period range of interest has not been clearly established. Some investigators have chosen to normalize accelerograms on the basis of the peak acceleration. Others have chosen to normalize their input accelerograms in terms of the "spectrum intensity", i.e., the area under the relative velocity spectrum curve between bounding values of the period representing the limits of the period range of interest. Still others have used the root-mean-square (rms) acceleration.

If the intensity measure is to reflect the variation of acceleration amplitude over the period range of interest, the measure must have the character of an average. By this criterion, the peak acceleration is a poor measure. The spectrum intensity taken over the period range of interest, and using a reasonable damping value, should yield a more representative measure of intensity.



(a) Peaking Spectrum



(b) Broad-band Spectrum

Fig. 3 - Typical shapes of damped response spectra

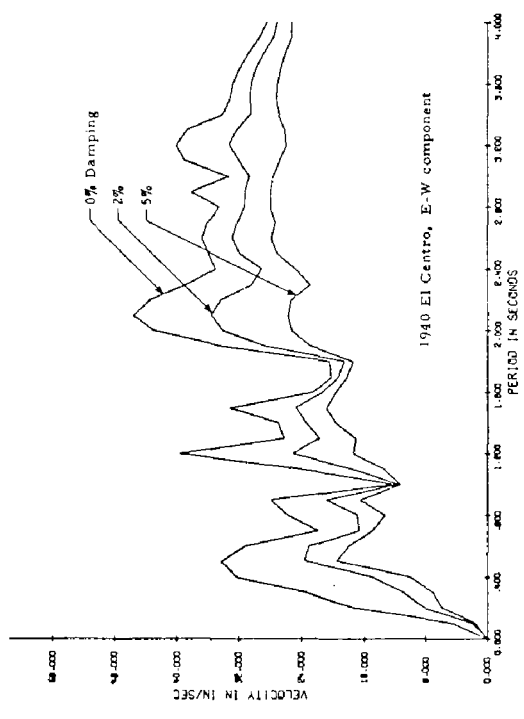
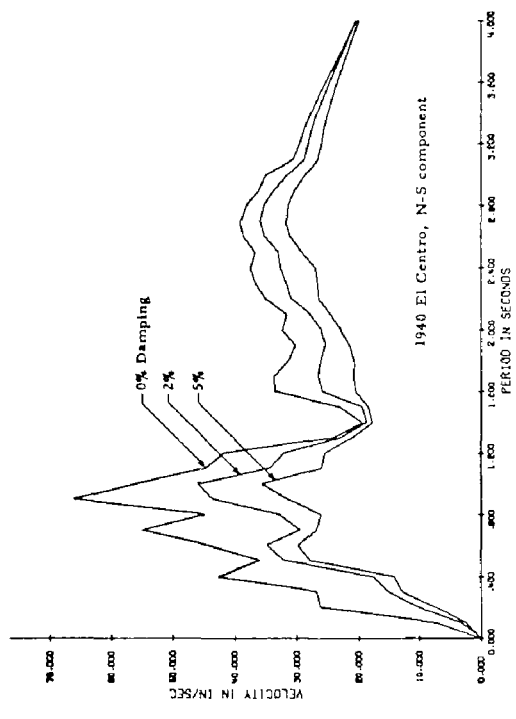


Fig. 2 - Velocity response spectra corresponding to first 10 seconds of 1940 El Centro record

Table 1 - Summary of Input Motions Considered in Study of Frequency Characteristics

Set	Structure Period T_1 (sec.)	Input Motion	Frequency Characteristics	Intensity Normalization Factor ^a
a	1.4	1971 Pacoima Dam S16E component	Peaking (0)	0.59
		1971 Holiday Inn, Orion, E-W comp.	Peaking (+)	3.22
		Artificial Accelerogram S1	Broad band	1.65
		1940 El Centro, E-W component	Broad band, ascending	1.88
		1940 El Centro, N-S component	Peaking (0)	1.50
b	0.8	1940 El Centro, E-W component	Broad band, ascending	1.88
		1971 Holiday Inn, Orion, E-W comp.	Peaking (-)	3.22
c	2.0	1940 El Centro, E-W component	Broad band, ascending	1.88

^a Calculated to yield a 5% damped spectrum intensity (for the range 0.1 to 3.0 sec.) equal to 1.5 times the 5% damped spectrum intensity of the N-S component of the 1940 El Centro record, i.e., 1.5 (SI) base. In all cases, only the first 10 seconds of each accelerogram was considered.

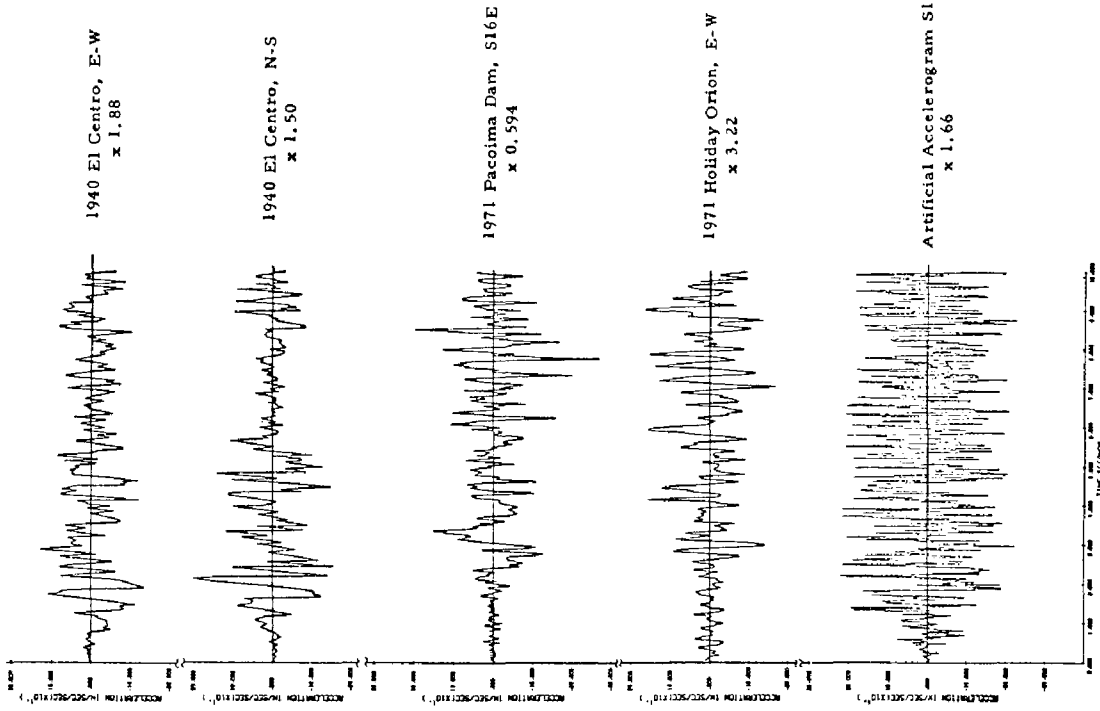


Fig. 4 - Ten-second duration normalized accelerograms

DYNAMIC ANALYSIS OF ISOLATED STRUCTURAL WALLS

In order to study the effect of the frequency characteristics of the input motion on the dynamic inelastic response of isolated reinforced concrete structural walls, and to confirm the qualitative observations made above, three separate sets of analyses were made. The analyses were carried out using the program DRAIN-2D⁽⁷⁾ developed at the University of California, Berkeley, as modified to include the Takeda decreasing stiffness model.⁽⁸⁾

The three sets considered are listed in Table 1. These sets correspond to structures with fundamental periods of 1.4, 0.8 and 2.0 sec., respectively. All five of the accelerograms used were normalized to 1.5 times the 5%-damped spectrum intensity (SI) of the N-S component of the 1940 El Centro record,* the normalization factors being listed in Table 1. The normalized accelerograms are shown in Fig. 4, and the corresponding 5%-damped velocity spectra are shown in Fig. 5. The entries in the fourth column of Table 1 indicate the classification of the accelerogram in terms of the general features of the velocity spectra relative to the initial fundamental period of the structure. Thus, a "peaking(+)" classification indicates that the peak in the velocity spectrum occurs at a period value greater than that of the fundamental period of the structure considered. A "broad band" classification refers to an accelerogram with a 5% damped velocity spectrum which remains more or less flat over a region extending from the fundamental period of the structure considered to at least 2 seconds greater.

Brief Description of Structure

The isolated structural wall considered in the analyses forms part of a hypothetical 20-story building consisting of a series of parallel walls, as shown in Fig. 6. The moment-rotation relationship for the wall is characterized by a decrease in the reloading stiffness with increasing deformations beyond yield.⁽⁷⁾ The structure is described in more detail in Ref. 4.

In an effort to cut down on the computer time required for each analysis without sacrificing accuracy in the results (the frequency content of the input motion being only one of the parameters considered in the overall investigation), preliminary analyses were run to determine the possibility of using a model with a reduced number of lumped masses. Alternative "equivalent" models with 5, 8 and 12 lumped masses were tried and the results compared with those for the 20-mass model. On the basis of these studies, the 12-mass model shown in Fig. 7 was chosen for the parametric investigation. In order to obtain a reliable estimate of the deformation requirements in the hinging region near the base of the wall, the concentrated masses were spaced closer together (resulting in shorter elements) in the lower portion of the model.

*In the following discussion, the 5%-damped spectrum intensity (SI) of the first 10 seconds of the N-S component of the 1940 El Centro record, for the period range 0.1 sec. to 3.0 sec., will be denoted by "(SI)_{base}" (which has a value of 70.15 in).

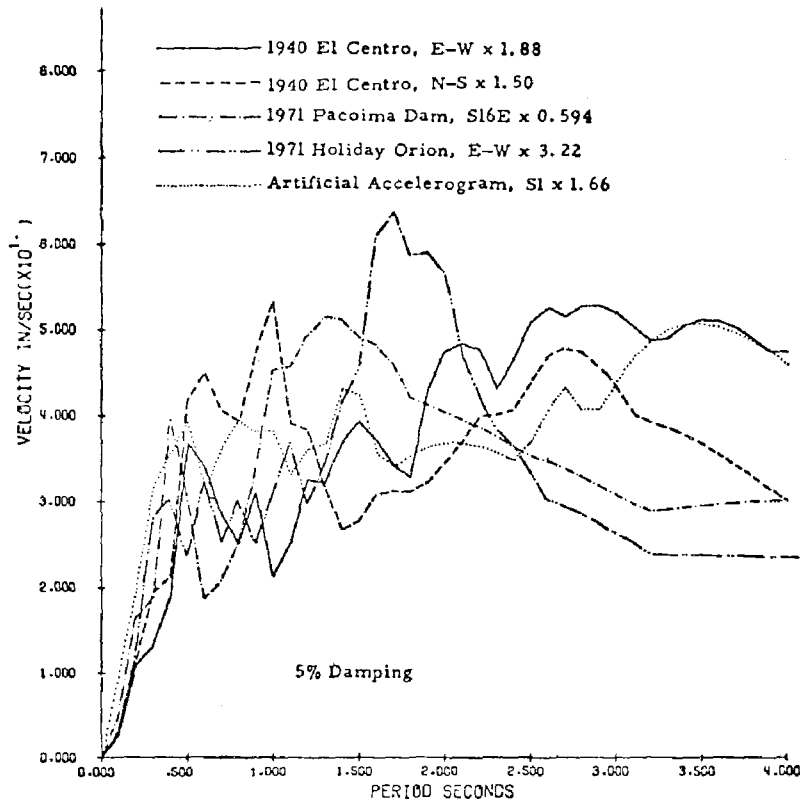


Fig. 5 - Relative velocity response spectra corresponding to first 10 seconds of normalized input motions

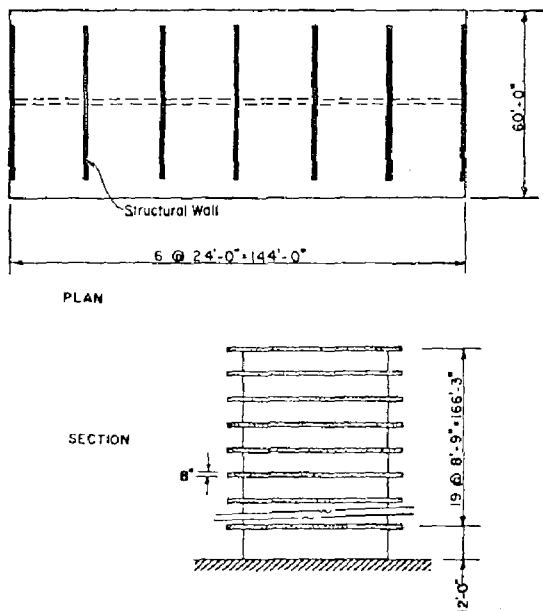


Fig. 6 - Twenty-story building with 'isolated' structural walls

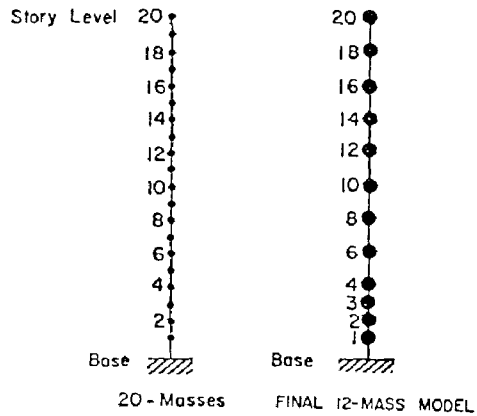


Fig. 7 - Dynamic analysis models

DISCUSSION OF RESULTS

(a) Fundamental Period of Structure, $T_1 = 1.4$ sec., $M_y = 500,000$ in-kips
 Envelopes of response values for the structure with period of 1.4 sec. and yield level, $M_y = 500,000$ in-kips, are shown in Fig. 8. Figures 8a, b, and d indicate that the E-W component of the 1940 El Centro record, classified as "broad band ascending" with respect to frequency characteristics, produces relatively greater maximum displacements, interstory displacements and ductility requirements than the other three input motions considered. However, the same record produces the least value of the maximum horizontal shear, with the artificial accelerogram S1* producing the largest shear, as shown in Fig. 8c. Because all the structures yielded and the slope of the second, post-yield branch of the assumed moment-rotation curve is relatively flat, the moment envelopes for this case do not show any significant differences among the four input motions used.

An idea of the variation with time of the flexural deformation at the base of the wall under each of the four input motions of set (a) in Table 1 is given by Fig. 9. This figure shows the normalized rotations of the node at story level "1", which represents the total rotation occurring in the first story. To plot the curves in Fig. 9, the rotations have in each case been divided by the absolute values of the corresponding rotation when first yielding occurred. The two dashed lines on each side of the zero axis (at ordinates +1.0 and -1.0) thus represent the yield level for all cases.

It is interesting to note in Fig. 9 that although the intense motion starts relatively early under the artificial accelerogram S1, yielding first occurs under the 1940 El Centro E-W motion. The magnitude of the rotation at the first yielding cycle, however, is greater under both S1 and the Pacoima Dam S16E record, a "peaking (0)" accelerogram. The Holiday Inn, Orion Blvd. record, a "peaking (+)" accelerogram, as expected produced a much lower response during the first few seconds, since the velocity spectrum for this motion (see Fig. 5) peaks at a period greater than the initial fundamental period ($T_1 = 1.4$ sec.) of the structure. As the structure yields and the effective period increases, however, the response under this excitation increases gradually.

It is significant to note in Fig. 9 that as yielding progresses and the effective period increases, it is the "broad band ascending" type of accelerogram (in this case, the El Centro E-W component) which excites the structure most severely, while response to the other types of accelerogram--and particularly the peaking accelerograms--tend to diminish. An indication of the change in fundamental period of a structure as the hinging (yielded, "softened") region progresses from the first story upward is given by Fig. 10, for different values of the yield stiffness ratio. The figure is based on the properties of a structure with initial fundamental period, $T_1 = 1.4$ sec.

* Generated using Program SIMQKE (Ref. 5).

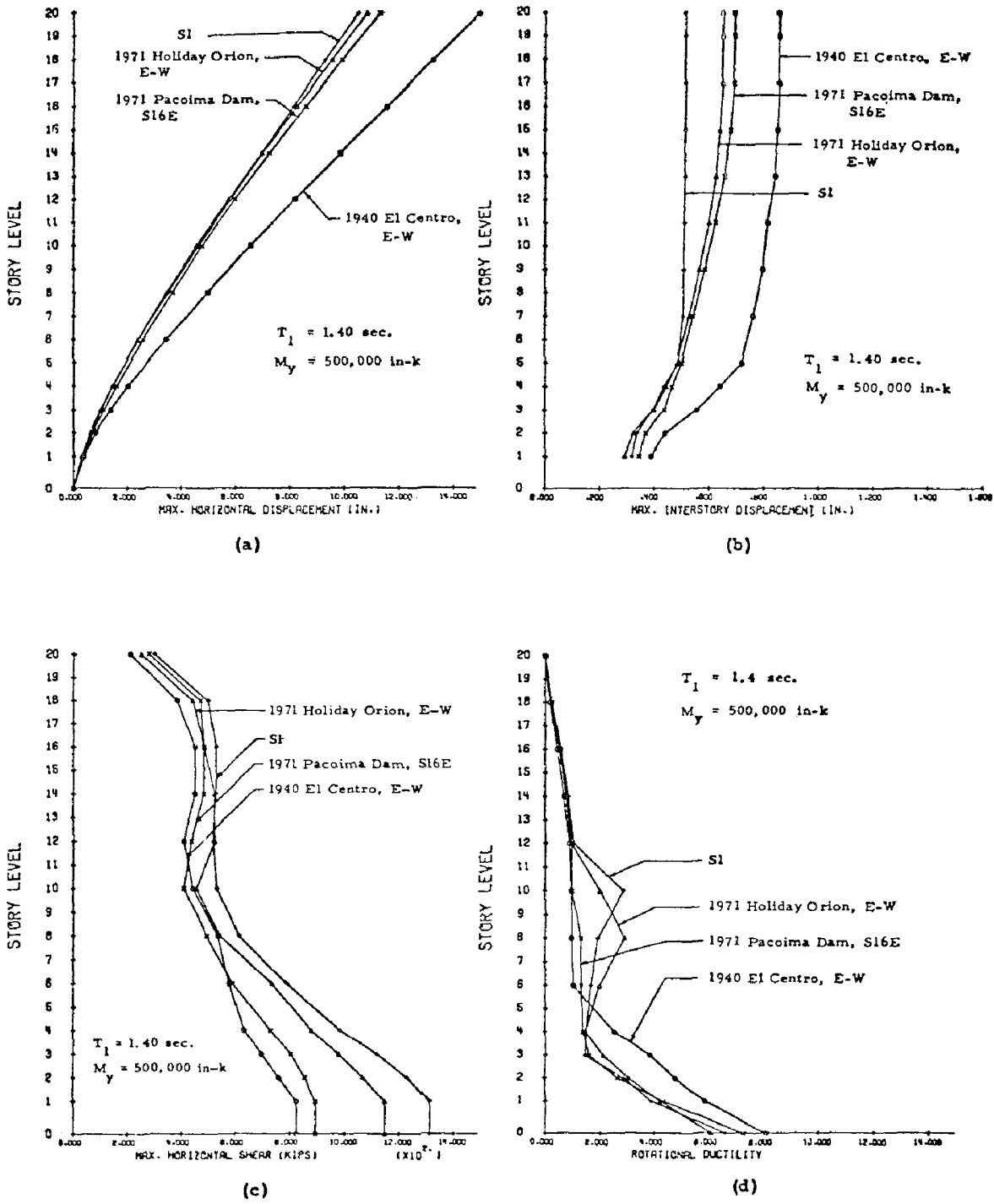


Fig. 8 - Response envelopes for wall with $T_1 = 1.4$ sec. and $M_y = 500,000$ in-k

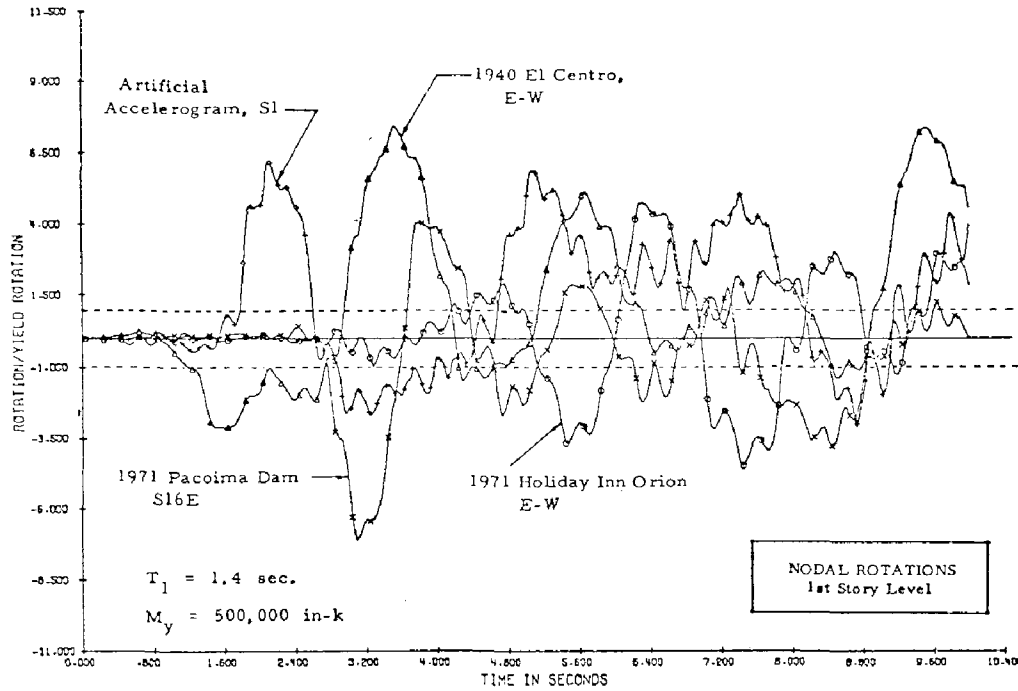


Fig. 9 - Rotation in first story vs. time for ground motions with different frequency characteristics

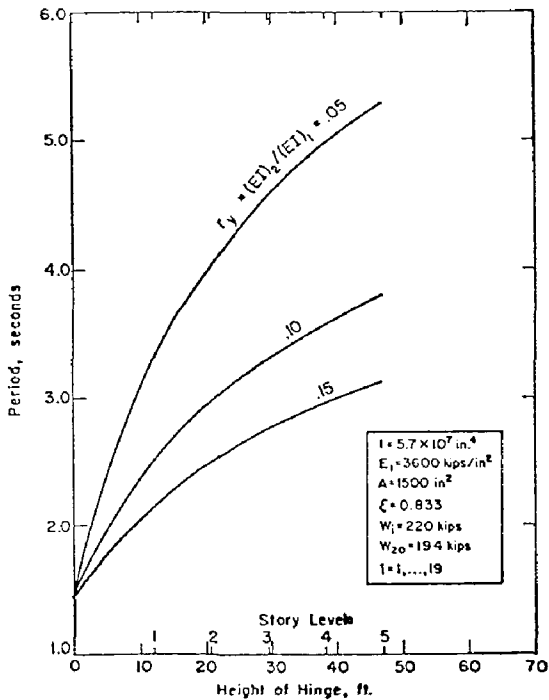


Fig. 10 - Fundamental period vs. height of yield hinge, 20-mass cantilever

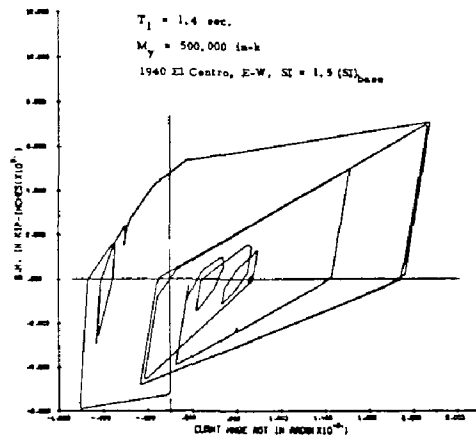


Fig. 11 - Moment at base vs. plastic hinge rotation in first story

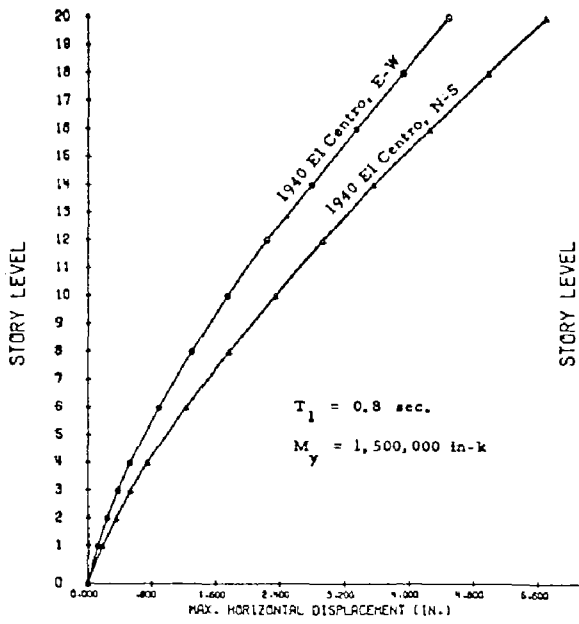
It is pointed out that since the structure goes through unloading and re-loading stages as it oscillates in response to the ground motion (see Fig. 11), the general behavior reflects the effects of both the "elastic" or unloading stiffness, as well as its yield or reloading stiffness. The effect of each stiffness value will depend on the duration of the response under each stiffness value, and this in turn will depend on the character of the input motion. When yielding occurs early, and for the type of structure considered here in which the condition at the critical section (i.e., the base of the wall) determines to a large degree the response of the structure, it may be reasonable to assume that both elastic and yield stiffness play about equal roles in influencing the "effective period" of the structure. In the Takeda model⁽⁸⁾ of the hysteretic loop, the initial portions of the reloading branches of the moment-rotation loops (see Fig. 11) will have stiffness values intermediate between the initial elastic and the yield stiffness of the primary curve.

(b) Fundamental Period of Structure, $T_1 = 0.8$ sec., $M_y = 1,500,000$ in-kips

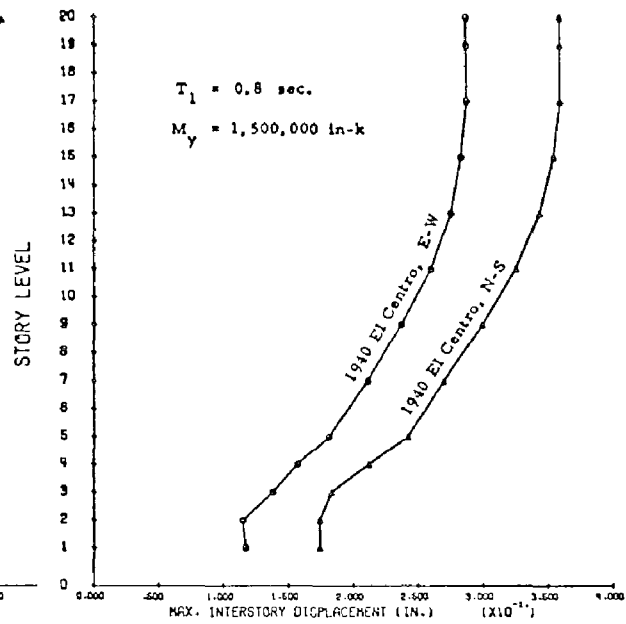
To study the effects of frequency characteristics for the case of short-period structures with relatively high yield levels, a "peaking (0)" accelerogram (N-S component of the 1940 El Centro) and a "broad band ascending" type (E-W component of the 1940 El Centro) were considered.

Figure 12, which shows response envelopes for this case, indicates that the peaking accelerogram consistently produces a greater response in the structure than a broad band record. It will be noted from a comparison of Fig. 12d and Fig. 8d that the ductility requirements are not only significantly less for this structure with a high yield level, but that yielding has not progressed as high up the structure as in the case of the structure considered under (a), with period $T_1 = 1.4$ sec. and a low yield level. For the type of structure considered here, where the displacements of the lower stories are generally in phase (fundamental mode predominating), the magnitude of the ductility requirements at the base of the wall is a direct function of the extent to which yielding has progressed up the height of the wall.

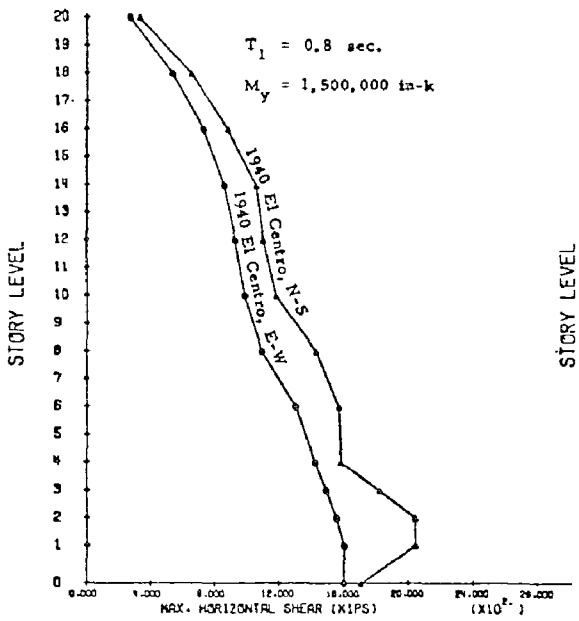
The greater response of the structure under the N-S component of the 1940 El Centro (peaking) follows from the fact that the dominant frequency components for this motion occur in the vicinity of the period of the structure (and also around 2.75 sec., see Fig. 5). In this region the E-W component has relatively low-power components. Also, because of the high yield level of the structure, yielding was not extensive, particularly under the E-W component and apparently did not cause the period of the yielded structure to shift into the range where the higher powered components of the E-W motion occur. On the other hand, under the N-S component of 1940 El Centro, Fig. 12d indicates yielding to have progressed up to the 4th story level, as against the 2nd story level under the E-W component. The greater extent of this yielding, and the accompanying increase in the effective period of the structure, could easily have put the structure within the next peaking range of the input motion.



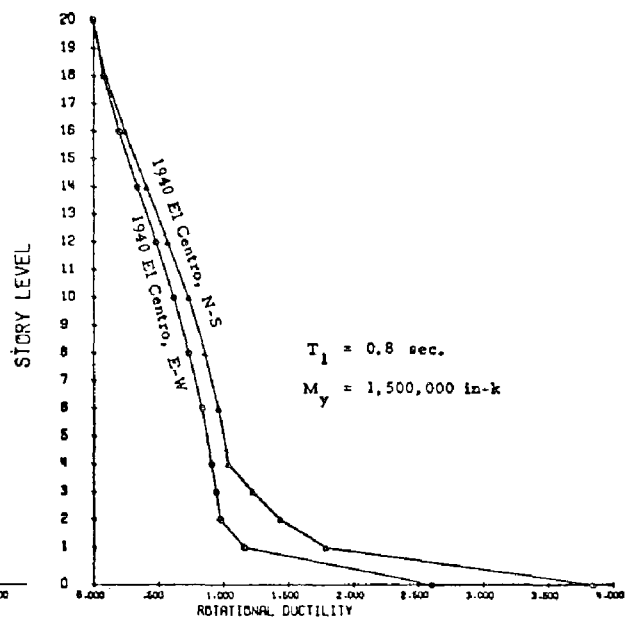
(a)



(b)



(c)



(d)

Fig. 12 - Response envelopes for wall with $T_1 = 0.8 \text{ sec.}$ and $M_y = 1,500,000 \text{ in-k}$

(c) Fundamental Period of Structure, $T_1 = 2.0$ sec., $M_y = 500,000$ in-kips

For this structure, the peaking accelerogram used was the E-W component of the record taken at the first floor of the Holiday Inn on Orion Boulevard, Los Angeles, during the 1971 San Fernando earthquake. The record has a 5%-damped velocity spectrum that actually peaks at about 1.75 sec. and may thus be classified as a "peaking (-)" accelerogram relative to the structure considered. The other input motion considered is the E-W component of the 1940 El Centro record ("broad band ascending").

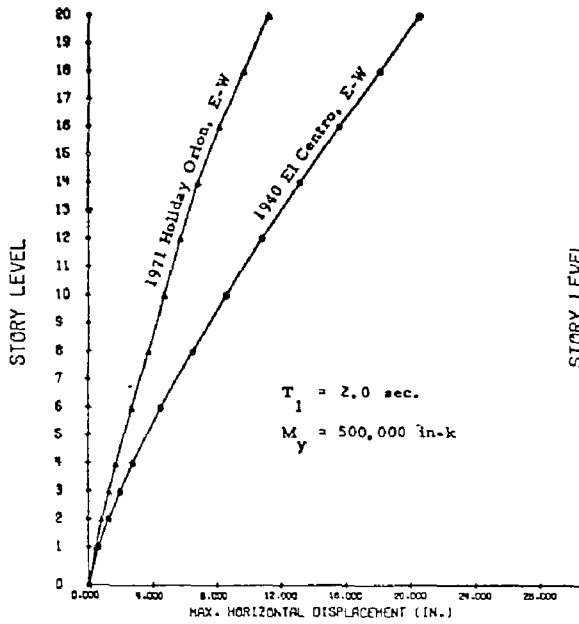
The response envelopes of Fig. 13 indicate, as in case (a), that where yielding is significant, the horizontal and interstory displacements, as well as the ductility requirements near the base are greater for the broad band accelerogram than for the peaking motion. Also, as in case (a), the extensive yielding which occurs near the base results in a reduction of the lateral inertial forces or shears. Thus, Fig. 13c, like Fig. 8d, shows the maximum shears corresponding to the E-W component of the 1940 El Centro to be less than those for the other input motions.

SUMMARY AND CONCLUSIONS

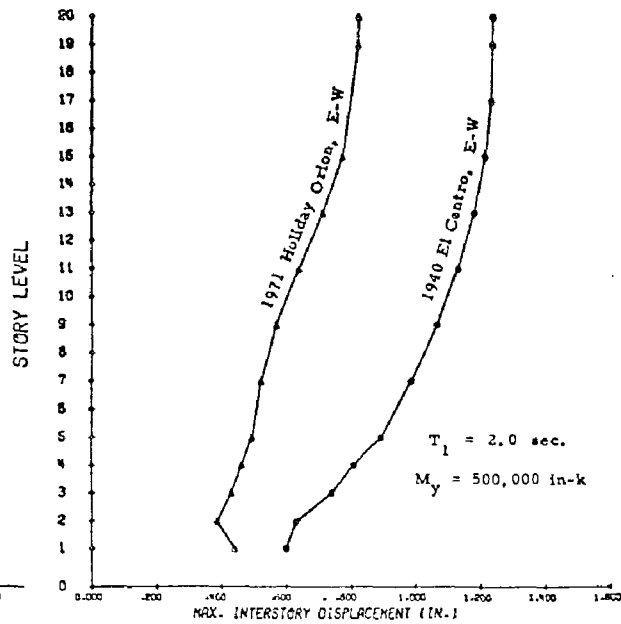
The results presented above indicate that the frequency content of the input motion can significantly affect the dynamic response of isolated walls. By classifying accelerograms in terms of their 5%-damped velocity response spectra as "peaking" or "broad band", a clear relationship was noted between the frequency characteristics of the input motion and the dynamic response of yielding structures.

Specifically, it was noted that where significant yielding can be expected in a structure, i.e., yielding which would appreciably lengthen the effective period of vibration, an input motion with a velocity spectrum of the "broad-band ascending" type is likely to produce more severe deformations than other types of motion of the same intensity and duration. For cases where only nominal yielding is expected so that the effective period of vibration is not significantly changed, "peaking" type accelerograms tend to produce more severe deformations. Since the extent of yielding is a function of both the earthquake intensity and the yield level of the structure, as well as the frequency characteristics of the input motion, these factors must be considered in selecting an input motion for a given structure for the purpose of producing near-maximum response. The above observations are important when it is desired to undertake a limited number of analyses for the purpose of determining near-maximum response for use in design.

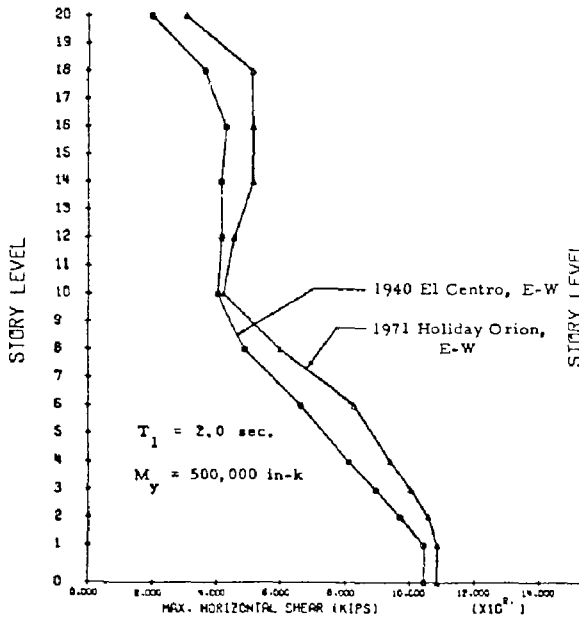
It is recognized that considerations of the probable epicentral distance and geology which affect the frequency content of the ground motion at a site may logically rule out the possibility of dominant frequency components occurring in certain frequency ranges. Thus, because the high frequency components in seismic waves tend to be attenuated more rapidly with distance than the low frequency components, it might be reasonable to expect that beyond certain distances, depending on the geology, most of the high frequency components from a given source would be damped out so that only the low frequency (long-period) components need be reckoned with.



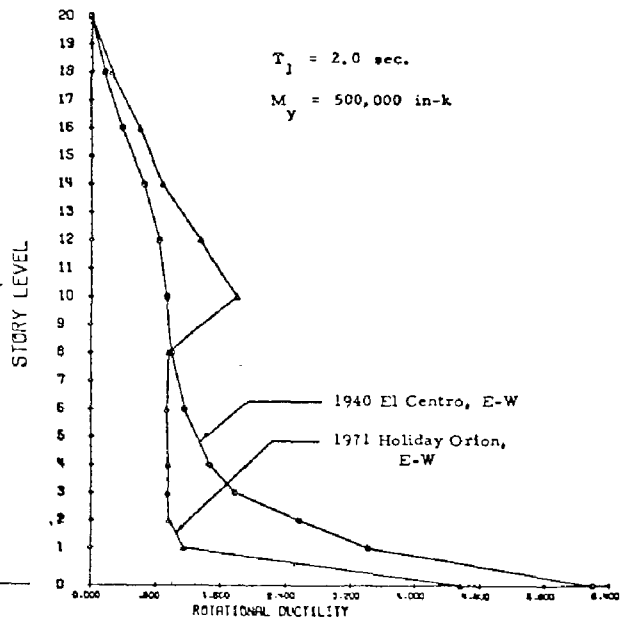
(a)



(b)



(c)



(d)

Fig. 13 - Response envelopes for wall with $T_1 = 2.0 \text{ sec.}$ and $M_y = 500,000 \text{ in-k}$

ACKNOWLEDGEMENT

The study reported here is part of a broader investigation directed towards the development of design procedures for earthquake-resistant structural walls sponsored by the National Science Foundation (RANN) under Grant No. GI-43880. This report is based on material presented in Ref. 3.

The help extended by S.K. Ghosh in incorporating the necessary plotting routines into Program DRAIN2D and by L. Eric Fugelso in the study of earthquake intensity is much appreciated.

REFERENCES

1. Analysis of Strong Motion Earthquake Accelerograms, Vol. III-Response Spectra, Part A-Accelerograms IIA001 through IIA030, Report EERL 72-80, California Institute of Technology, Earthquake Engineering Research Laboratory, August 1972.
2. Clough, R.W., and Benuska, K.L., "FHA Study of Seismic Design Criteria for High-Rise Buildings", Report HUD TS-3, Federal Housing Administration, Washington, D.C., August 1964.
3. Fintel, M., Derecho, A. T., Freskakis, G.N., Fugelso, L.E., and Ghosh, S.K., "Structural Walls in Earthquake-Resistant Structures--Analytical Investigation, Progress Report", Report to National Science Foundation (RANN), Portland Cement Association, August 1975.
4. Freskakis, G.N., Derecho, A.T., and Fintel, M., "Inelastic Seismic Response of Isolated Structural Walls", Proceedings International Symposium on Earthquake Structural Engineering, St. Louis, Missouri, August 1976.
5. Gasparini, D., "SIMQKE: A Program for Artificial Motion Generation", Internal Study report No. 3, Dept. of Civil Engineering, Massachusetts Institute of Technology, January 1975.
6. Hudson, D.E., "Some Problems in the Application of Response Spectrum Techniques to Strong-Motion Earthquake Analysis", Bulletin of the Seismological Society of America, Vol. 52, No. 2, April 1962.
7. Kanaan, A.E., and Powell, G.H., "General Purpose Computer Program for Inelastic Dynamic Response of Plane Structures", (DRAIN-2D), Report No. EERC 73-6. Earthquake Engineering Research Center, University of California, Berkeley, April 1973. Modified by Litton, R., and Powell, G.H., to include Takeda decreasing stiffness model and by S.K. Ghosh to include plotting capabilities.
8. Takeda, T., Sozen, M.A., and Nielsen, N.N., "Reinforced Concrete Response to Simulated Earthquakes", Journal of the Structural Division, ASCE, Proc. Vol. 96, ST12, December 1970.

INTERNATIONAL SYMPOSIUM ON
EARTHQUAKE STRUCTURAL ENGINEERING

37

St. Louis, Missouri, USA, August, 1976

SEISMIC RETROFITTING FOR HIGHWAY BRIDGES

A. LONGINOW AND R. R. ROBINSON
IIT Research Institute
Chicago, Illinois

K. H. CHU
Illinois Institute of Technology
Chicago, Illinois

J. D. COOPER
Federal Highway Administration
Washington, D.C.

SUMMARY

The San Fernando earthquake of February 9, 1971 has demonstrated that bridges located in high risk seismic zones and which were designed in accordance to the then prevailing AASHTO design criteria may not possess adequate seismic resistance. This narrative describes an effort which was undertaken to develop a set of practical retrofit measures that can be employed on existing bridges so as to reduce damage and minimize the threat to life should an earthquake occur. The process leading to the identification of potential bridge weaknesses, selection of retrofit measure and verification of its adequacy is illustrated using two analysis procedures i.e., a detailed analysis method and a simplified one.

INTRODUCTION

The San Fernando earthquake of February 9, 1971 caused considerable damage to highway bridges. A report (Ref. 1) on the postearthquake damage sustained, recommended that existing bridges in earthquake prone areas be re-examined to determine their seismic resistance, and if not adequate, be modified to at least prevent collapse in the event of a strong seismic loading.

The study described in this narrative (Ref. 3) was motivated as a result of the extensive damage sustained by bridges during the 1971 San Fernando earthquake. Its purpose was to develop a set of practical retrofit measures that can be employed on existing bridges so as to reduce damage and minimize the threat to life should an earthquake occur.

The study emphasized conventional steel and reinforced concrete highway bridges. Seven bridges were selected from potentially active seismic zones of this country, and formed the basis of the study. Each bridge was first analyzed in its "as built" condition to determine if a problem existed. Those which responded in a failure mode were appropriately "modified" to

reflect a retrofit and were then reanalyzed to determine the adequacy of the particular retrofit.

Observed failure modes for conventional bridge structures subjected to seismic loading can be grouped into two categories; i.e., substructure failures (pier or abutment) and hence loss of support capacity, and superstructure collapse due to excessive relative motion at support bearings. Both types of failure occurred during the San Fernando earthquake and both were considered in Ref. 3. Structural failure and damage to bridges may also be caused by inadequate foundation strength or load-bearing degradation during the course of seismic loading. Soil liquefaction is an example of this failure mode. It was not specifically considered in Ref. 3 since the problem is one of bridge foundation material rather than of the bridge structure itself.

The following five bridge retrofit concept categories were identified and several concepts were developed for each.

- Superstructure horizontal motion restrainers for hinges, expansion joints, bearings, etc.
- Bearing support restrainers - vertical
- Bearing area widening techniques
- Column (pier) strengthening
- Footing strengthening

Specific retrofit concepts produced were selected based on feasibility and practicality.

Before taking any steps to retrofit an existing bridge, it is necessary to decide (a) whether the bridge actually needs retrofitting, and (b) if it does, what type or types of retrofit measures to employ. For a retrofit measure to be cost-effective it must be both practical and economically feasible to employ. In the context of this study the purpose of a given retrofit measure is to minimize damage so that the bridge can remain in at least emergency use, rather than to eliminate it entirely.

To satisfactorily answer question (a), a structural, seismic analysis of the subject bridge needs to be performed. First there should be a simplified structural analysis which adequately considers the principal modes of bridge response when subjected to the probable, site dependent seismic loading. Should the results prove marginal as far as probable failure is concerned, then a more detailed structural analysis may be necessary to reach a decision. If the analysis (simplified or detailed) indicates that some type of failure (extensive enough so that the bridge could not remain in even emergency use) will occur, the retrofit measure(s) to be employed should be based on the mode and extent of failure. It is important to consider that strengthening a component which is susceptible to a particular mode of seismic damage may actually lead to a different mode of failure, or possibly to failure of another component.

Once the retrofit measure has been chosen, its effectiveness in minimizing damage should be investigated using an appropriate structural analysis

procedure. The process leading to the selection of adequate retrofit concepts is an iterative one.

It is important to emphasize that seismic and structural considerations are not the only ones that need to be considered in the overall bridge retrofit decision process. A partial list of other decision factors entering the process is given.

- The importance of the bridge to the given locality based on the type of highway, traffic volume and accessibility of other crossings.
- Replacement or repair costs based on estimated damage including lost time.

BRIDGE RETROFIT MEASURES

A retrofit measure is any means of increasing the seismic resistance of an existing bridge. It is likely that there are many possibilities; the problem is to find those which are cost-effective. A brief summary of some retrofit measures that should be considered for bridges in high risk seismic zones:

- (a) Restricting longitudinal, vertical, and lateral relative displacements of the superstructure at expansion joints, bearing seats, etc., by means of cables, tie bars, shear keys, extra anchor bolts, metal stoppers, etc.
- (b) Restricting rigid body motion of the superstructure by connecting (e.g., with high strength steel cables) to a supporting or an adjacent foundation or pier cap, enlargement of bearing areas, stoppers at edges of bearing areas, etc.
- (c) Reducing induced vibrations by installation of energy absorbing devices such as elastomeric bearing pads at bearing seats, or adaptation of the new Japanese "shock absorber" type of damper which allows slow movement, such as displacement due to creep, shrinkage, and temperature change with negligible resistance, but develops a large resistance in the case of a rapid displacement; i.e., high velocity, such as can be caused by an earthquake (Ref. 4).
- (d) Strengthening of supporting structures: As a specific example, increasing the strength of an existing column by adding longitudinal and spiral reinforcement to the exterior of the column and then bonding the added reinforcement with a new layer of high strength concrete using pressure grouting procedures and/or gunite. The additional longitudinal reinforcement could also be extended into the cap and the footing thus increasing the flexural strength of the column-to-cap and column-to-footing connections (Fig. 1).

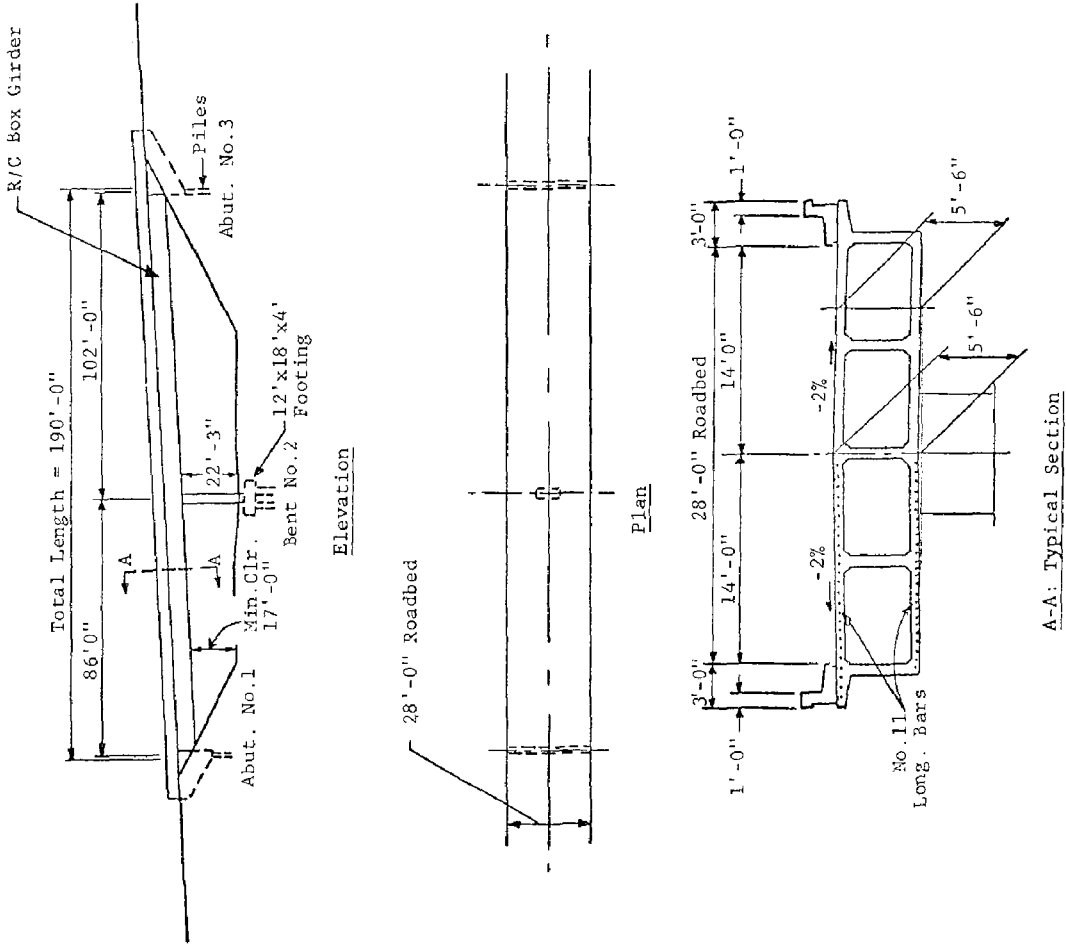


Fig. 2 Bahia Overcrossing, 5 miles N.W. of Benecia, California

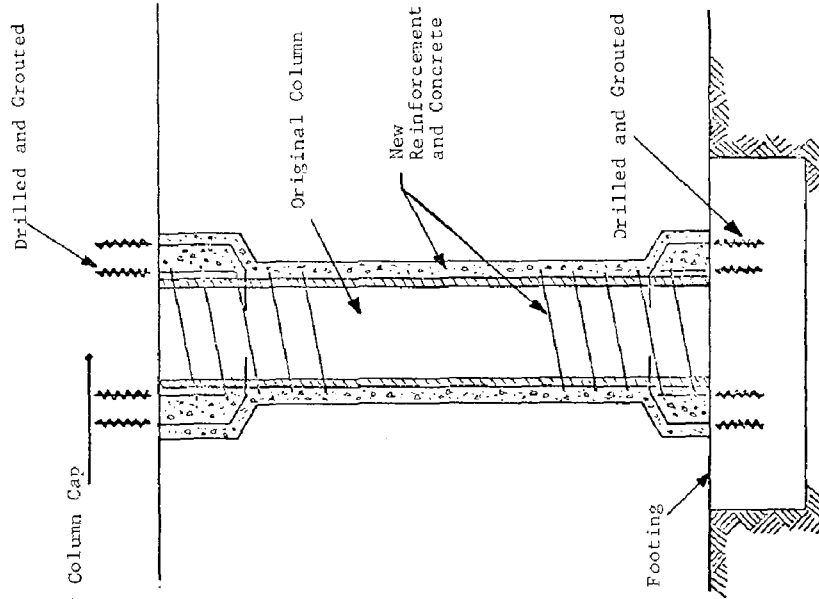


Fig. 1 Strengthening of R/C Column

BRIDGE ANALYSIS, RESULTS AND RETROFIT MEASURES EMPLOYED

The bridge chosen for illustration is the Bahia Overcrossing, Bridge Number 23-161, near Benecia, California (Fig. 2). It is a two-span continuous reinforced concrete box girder, built-in at the abutments, with a single column reinforced concrete bent, (3 ft by 8 ft) cross section, as the intermediate support. The abutments are founded on a single row of piles with sufficient flexibility to minimize stresses from thermal movement. The intermediate support is founded on a spread footing with piles. The soil of the bridge site consists, primarily, of loose to dense dark brown silt with some fine to coarse sand and gravel. This bridge was first analyzed using a nonlinear dynamic analysis method and was subsequently analyzed using a simplified procedure. Details of the two analysis techniques are given in Ref. 3.

For the detailed method, the bridge is modeled as a space frame (Fig. 3), and subjected to a hypothetical earthquake in the form of ground surface displacement time histories (Fig. 4) based on a statistical evaluation of the seismicity of the site. The bridge is first analyzed as built to determine: whether retrofitting is necessary, and if so, to define the failed component(s). The candidate retrofit measure(s) is then incorporated into the bridge model and the analysis performed again.

Nonlinear Dynamic Analysis

Figure 5 is a moment-time history resulting from the application of the vertical and horizontal (in the longitudinal direction) seismic ground motions. By comparing the dynamic response with the ultimate moment it is observed that the bending moment at the top of the column, approaches and exceeds the ultimate value for a duration of approximately 16 seconds correlating with the period of strongest vertical and horizontal motion.

The nonlinear analysis demonstrates that at least one area of the bridge should be considered for retrofitting. The area most vulnerable to damage is the top portion of the column. An obvious retrofit possibility is to strengthen the column using the method illustrated in Fig. 1. Figure 6 shows the bending moment variation at the top of the retrofitted column. The largest magnitude attained is 88 percent of the computed ultimate bending moment for the retrofitted column. The addition of the longitudinal reinforcing bars and concrete to the exterior of the column causes an increase in the maximum bending moment experienced by the column during the seismic loading. The ratio of the moment for the retrofitted case to the unretrofitted is 1.19. At the same time, the retrofit leads to a 61 percent increase in the ultimate moment.

Simplified Analysis

For the simplified analysis method, the predominant mode for a given bridge is assumed to be horizontal and can be resolved into two orthogonal directions, longitudinal and lateral. If the lateral restoring force or resistance of the structure is considerably larger than that in the longitudinal direction, then the lateral response does not govern and can be ignored. Vertical vibrations are also important for some bridges and for piers rigidly connected to the girders. An approximate consideration of such vibration is shown in this example.

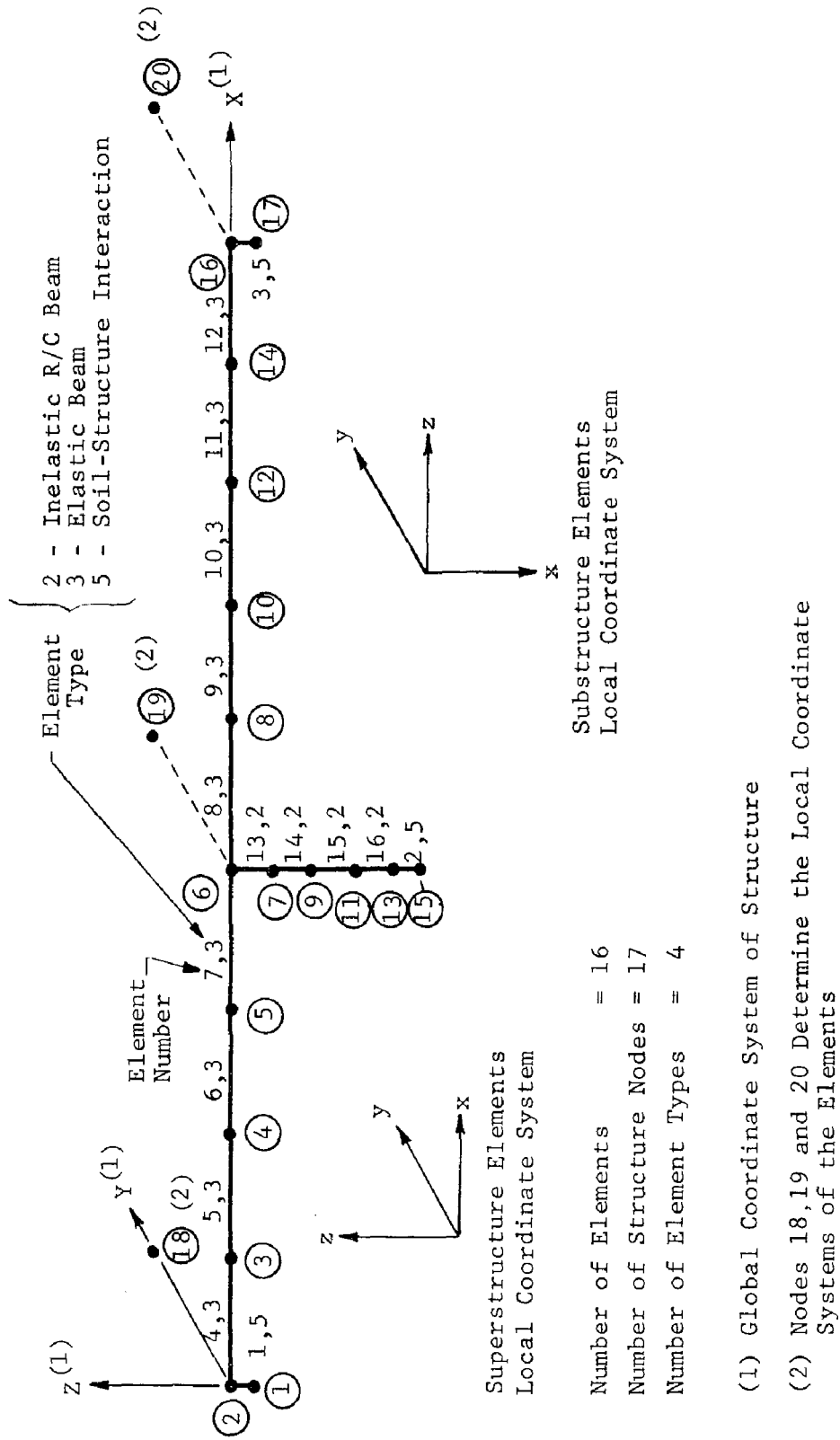
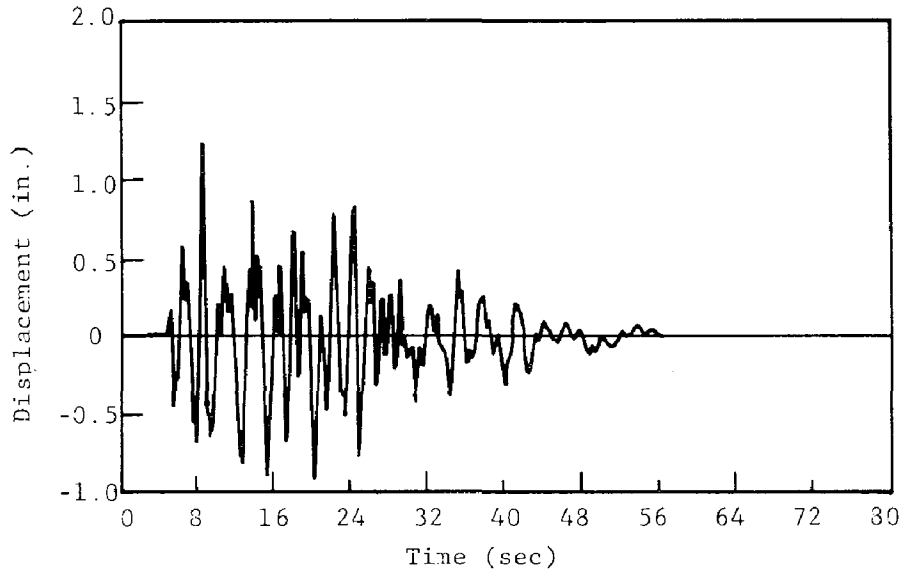
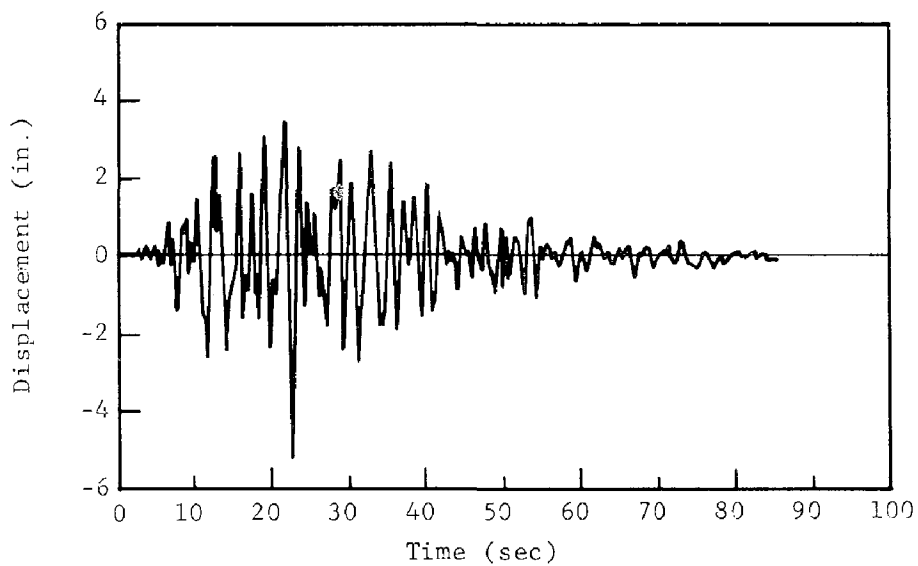


Fig. 3 Finite Element Model for Nonlinear Analysis of the Bahia Crossing Bridge, Benecia, California



(a) Simulated Ground Motion - Vertical



(b) Simulated Ground Motion - Horizontal

Engineering Seismicity: 5.295
 Richter Magnitude: 8.10
 Maximum Horizontal Ground Displacement (in.): 5.25
 Maximum Vertical Ground Displacement (in.): 1.25
 Maximum Horizontal Ground Acceleration (g): 0.32
 Maximum Vertical Ground Acceleration (g): 0.26
 Portion of Record Used in Bridge Analysis = 3.4 - 44.8 sec

Fig. 4 Benecia, California Bridge Site Seismic Characteristics

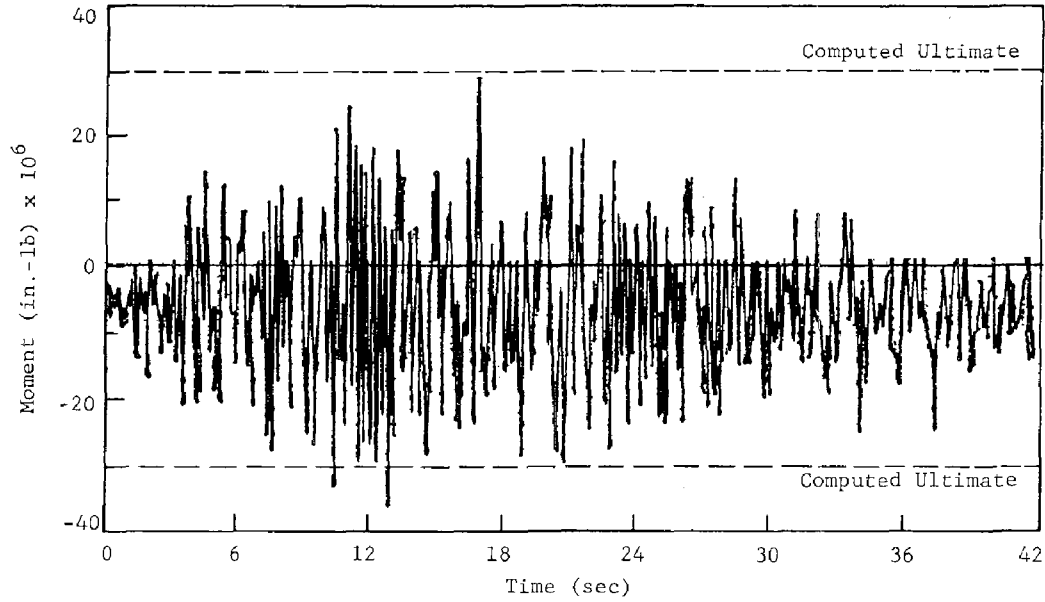


Fig. 5 Bending Moment - Time Variation at Top of Pier (Middle of Element 13)

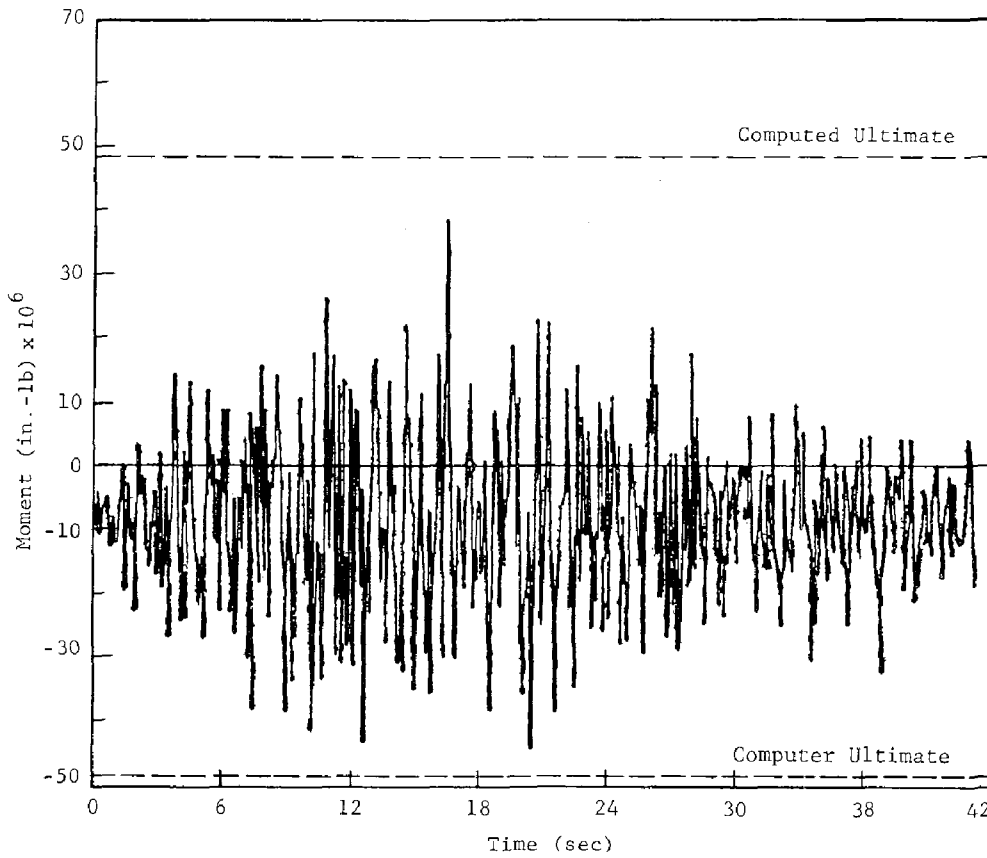


Fig. 6 Bending Moment - Time Variation at Top of Retrofitted Pier (Middle of Element 13)

The following assumptions are made for the simplified analysis concerning structural idealization.

- (1) Rollers and expansion joints are considered to be frictionless,
- (2) Expansion joints are assumed capable of transmitting longitudinal forces only if longitudinal ties are provided through the joint.
- (3) Skewed bridges are analyzed as if they were unskewed. (i.e., the longitudinal stiffness is assumed to be perpendicular to the skewed piers).
- (4) Horizontally curved bridges are analyzed by converting the structural properties into the chord line direction (which is nominally referred to as the longitudinal direction) and perpendicular to the chord (lateral) direction.

For the analysis of a particular element of a curved bridge, the longitudinal and lateral earthquake loading (accelerations) are individually resolved into the principal directions (parallel and perpendicular) of the element. Since the seismic motion can act in both the positive and negative directions, the absolute values of these results are added vectorially to obtain the appropriate element loads.

Each bridge is idealized separately in the longitudinal and lateral directions as single degree of freedom systems. This is done by determining an equivalent mass and spring stiffness for the bridge in each of the two directions by combining the individual stiffness from the various contributing bridge components.

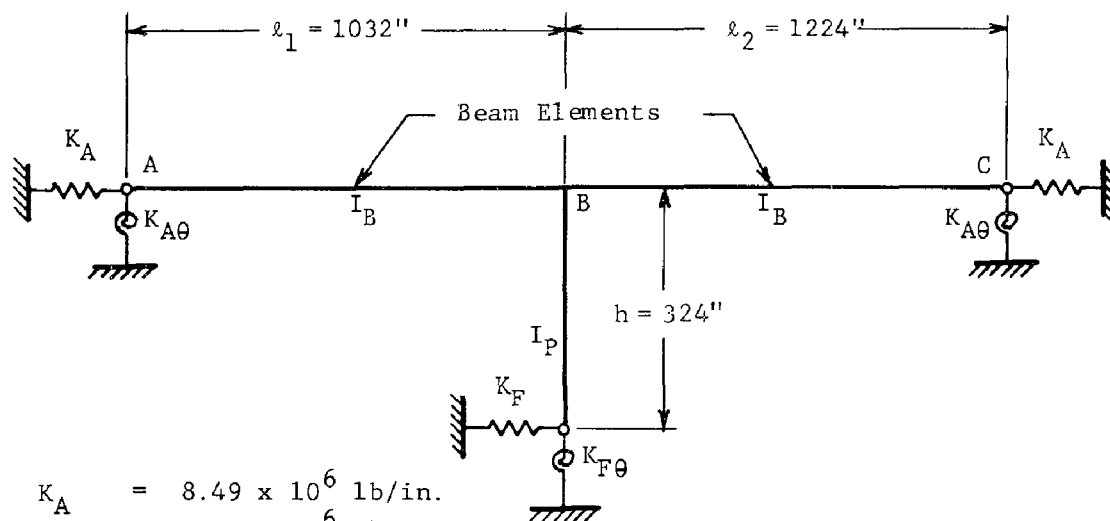
It is assumed that failure will not occur if the analysis indicates that the following overloading and/or yielding conditions will occur.

- (1) A plastic hinge occurring at the bottom of a pier that is fixed at the top as long as the pier is not an isolated one between expansion joints.
- (2) The bending moment for a reinforced concrete pier (based on the elastic response spectrum seismic loading) does not exceed three times the ultimate moment of the section. This is based on the fact that the seismic acceleration will be reduced by a factor of $1/\sqrt{2\mu-1}$ where μ is the ductility factor. For reinforced concrete, a value of $\mu = 5$ is commonly used.
- (3) If, due to vertical vibrations, a plastic hinge forms at the top of a pier which is monolithic with the superstructure and the pier is framed into a transverse superstructure diaphragm. Failure will not occur as long as no plastic hinge develops at the bottom of the pier.

It is assumed that the bridge will fail if the analysis indicates that any of the following conditions will occur.

- (1) The anchor bolts of fixed bearings fail by shear.
- (2) A plastic hinge is formed at the bottom of a pier that is hinged at the top if no additional lateral stability is provided by the adjacent piers or abutment.
- (3) Piles are subjected to excessive lateral forces which create large horizontal displacements of the structure. Vertical piles in good soil subjected to more than 15 kips (each) lateral force are considered to be excessive. Clay is considered as a poor soil for providing lateral resistance for piles.
- (4) Slip-out of pins in hinge connections or bearings due to excessive horizontal or vertical relative motion.

The simplified analysis technique is demonstrated by application to the as built Benecia bridge (see Fig. 7). Some selected results are compared with the nonlinear analysis discussed previously.



$$\begin{aligned}
 K_A &= 8.49 \times 10^6 \text{ lb/in.} \\
 K_F &= 11.60 \times 10^6 \text{ lb/in.} \\
 K_{A\theta} &= 1.55 \times 10^9 \text{ lb-in./radian} \\
 K_{F\theta} &= 63.80 \times 10^9 \text{ lb-in./radian} \\
 (EI)_B &= (3 \times 10^6)(5.48 \times 10^6) \text{ lb-in}^2 \\
 (EI)_P &= (4.73 \times 10^6)(3.73 \times 10^5) \text{ lb-in}^2 \\
 A_B &= 7708 \text{ in}^2, A_P = 3456 \text{ in}^2 \\
 M_B &= 1.80 \text{ lb-sec}^2/\text{in}^2
 \end{aligned}$$

Fig. 7 Simplified Analysis Model of Benecia Bridge

Vertical Response Analysis: The stiffness of span 2 for rotation about the lateral axis of the bridge (Y) is $4EI_B/l_2 = 5.35 \times 10^{10}$ lb/inch/radian. This is nearly 30 times the stiffness of the abutment ($K_{A\theta}$) thus the structure can be assumed to be hinged at the abutments. For the bent, the comparable rotational stiffness is $K_{P\theta} = 4KI_P/h = 2.18 \times 10^{10}$ lb-inch/radian. Since the pier foundation rotational stiffness ($K_{F\theta}$) is nearly three times as stiff, the base of the pier will be assumed as fixed.

The length of the spans is approximately the same, and it can be assumed that the spans will vibrate approximately as simple beams for the determination of their natural frequency for vertical response. For span 2, the frequency of vertical vibration is

$$F = (\pi/2\ell_2^2) \sqrt{(EI)_B/m_B}$$

$$= 3.17 \text{ cps}$$

From Fig. 8 for a maximum vertical ground acceleration of 1.0 g a peak acceleration of 4.2 g is obtained for a structure with this frequency. For the 0.26 g maximum vertical ground acceleration predicted for the bridge site, the vertical seismic forces are derived from an equivalent acceleration of $\alpha_z = (0.26) \times (4.2) = 1.09 \text{ g}$. From this acceleration, the midspan moment from the vertical seismic load is estimated as $M_2 = (1 - 0.2)\alpha_z m_B \ell_2^2 / 8 = 0.114 \times 10^9 \text{ inch-lbs}$. The continuity factor $(1 - 0.2)$ indicates that the bending moment at the pier (M_{BC}) is 0.4 times the simple beam moment for purposes of estimating the midspan moment for vertical seismic loading. Adding the static bending moment of $0.077 \times 10^9 \text{ lb-inch}$ results in a total moment of $0.191 \times 10^9 \text{ lb-inch}$. This is less than 9 percent higher than the peak value obtained from the nonlinear dynamic analysis.

The rotation (θ_B) at the top of the pier can be computed based on the above variation in the bending moment for the vertical seismic load. That is, the moment variation resulting from a uniform vertical seismic load of 1.09 times the superstructure dead load with zero moment at the right abutment and a value of M_{BC} at the pier. The result is $\theta = 0.75M_2\ell_2/(3EI_B) = 0.00212 \text{ radian}$. With this rotation at the top of the pier and zero rotation at the bottom (fixed) the bending moment at the top is $M_{BD} = K_P\theta$ (θ) = $46.0 \times 10^6 \text{ lb-inch}$. The moment at the bottom of the pier is of opposite sign and one-half this magnitude. The shear resulting from this distribution of moments is $H_P = 1.5M_{BD}/h = 21.3 \times 10^4 \text{ lbs}$. Assuming a linear variation in the moment at the center of the top and bottom elements of the pier are $M_{top}^P = 37.4 \times 10^6$ and $M_{bot}^P = 14.4 \times 10^6 \text{ lb-inch}$. These will be modified by the moments from the longitudinal loading before comparing the results with the nonlinear dynamic analysis.

Longitudinal Response Analysis: The important stiffness parameters for longitudinal seismic load calculations are:

$$\begin{aligned} \text{Abutments (each): } K_A &= 8.49 \times 10^6 \text{ lb/inch} \\ \text{Span 1: } K_1 &= EA_B/\ell_1 = 22.4 \times 10^6 \text{ lb/inch} \\ \text{Span 2: } K_2 &= EA_B/\ell_2 = 18.9 \times 10^6 \text{ lb/inch} \\ \text{Pier: } K_P &= 3EI_P/h^3 = 0.163 \times 10^6 \text{ lb/inch} \end{aligned}$$

The combined stiffness (K_X) is obtained from

$$K_X = (1/K_A + 1/K_1)^{-1} + (1/K_P + 1/K_F)^{-1} + (1/K_A + 1/K_2)^{-1}$$

$$= 12.14 \times 10^6 \text{ lb/inch}$$

The weight of the superstructure $W_B = 1.57 \times 10^6$ lb and the equivalent weight of the pier (which is approximately one-fourth the weight of the pier) is $W_{Pe} = 24,000$ lbs. The combined mass of the structure for longitudinal seismic response is $M = (W_B + W_{Pe})/g = 4,130$ lb-sec²/inch. With these parameters (K_X and M) the effective frequency is determined from $f = \sqrt{K_X/M}/(2\pi) = 8.65$ cps.

From Fig. 8 for a maximum longitudinal ground acceleration of 1.0 g a peak acceleration of 3.7 g is obtained. For the 0.32 g maximum horizontal ground acceleration predicted for the bridge site, the seismic longitudinal forces are derived from an equivalent acceleration of $a_x = 0.32 (3.7) = 1.18$ g. The total longitudinal force (H) for the structure is a_x times the combined mass (M) above, there results $H = 1.89 \times 10^6$ lbs. Assuming that this force is distributed in proportion to the longitudinal stiffnesses of the component elements of the bridge, the shear force in the pier is $H_p = H (K_p/K_X) = 24,200$ lbs. This shear force causes moments at the center of the top and bottom elements of the pier of $M_{Top}^p = 1.0 \times 10^6$ lb-inch and $M_{bot}^p = 6.9 \times 10^6$ lb-inch.

Combined Vertical and Longitudinal Seismic Results: Adding the pier shears from the vertical and horizontal analyses yields $H = (21.3 + 2.42) \times 10^4 = 23.72 \times 10^4$ lbs. This compares almost exactly with the dynamic response analysis value of 23.4×10^4 lbs. In a similar manner, the combined bending moment at the center of the top and bottom elements of the pier are $M_{Top}^p = 38.4 \times 10^6$ and $M_{bot}^p = 21.3 \times 10^6$ lb-inch. These also compare quite favorably with the dynamic analysis peak values of 36.4×10^6 and 27.5×10^6 , respectively.

CONCLUSIONS

From the observations made during this research program, the following conclusions can be made.

- (1) Bridges that are located in high risk seismic zones that were designed for earthquake loading according to the AASHTO Design Criteria may suffer substantial structural damage, and in some cases collapse can be anticipated. This conclusion is based on analyses performed on several bridges in Ref. 3. Each bridge was subjected to a predicted seismic load of the highest severity that would occur during the life of the bridge.
- (2) A similar conclusion to the above is made for structures located in highly active seismic regions that were designed for more stringent earthquake loads than the AASHTO code.
- (3) The current seismic design criteria for bridges and the methods of analysis for this loading are in a state of flux. This conclusion is based on two observations:
 - seismic design criteria have changed drastically in the last decade for both buildings and bridge structures built in regions where the earthquake risk is high; and

- comprehensive methods of dynamic structural analysis have not been used, to the extent required, to develop a rational system of simplified seismic design loading conditions for various bridge structures.

For example, the influence of the soil material at the bridge site and the vertical earthquake motions are not included in design codes; but, they are potentially important factors in the specification of seismic bridge loads.

- (4) The simplified method of analysis used in this project for the seismic analysis of bridges is a potentially adequate tool for deciding what type of retrofit is required, if any. At some time in the future when additional comprehensive numerical studies are available, the simplified analysis should be reviewed and compared with these new results for possible modifications to the method.

REFERENCES

1. Jennings, P. C. and Wood, J. H.; "Earthquake Damage to Freeway Structures," Engineering Features of the San Fernando Earthquake of February 9, 1971, Report EERL 71-02, June 1971.
2. Newmark, N. M.; Blume, J. A.; and Kapur, K. K.; "Seismic Design Spectra for Nuclear Power Plants," J. Power Division, ASCE, Nov. 1973.
3. Robinson, R. R., et al; "Structural Analysis and Retrofitting of Existing Highway Bridges Subjected to Strong Motion Seismic Loading," for Federal Highway Administration, IIT Research Institute, May 1975.
4. Shunji Inomata; "Japanese Practice in Seismic Design of Prestressed Bridges," PCI Journal, July-Aug. 1972.

INTERNATIONAL SYMPOSIUM ON
EARTHQUAKE STRUCTURAL ENGINEERING

51

St. Louis, Missouri, USA, August, 1976

THE NON-LINEAR DEFORMATIONS IN THE GROUND BASE
OF LARGE-PANEL BUILDINGS UNDER OSCILLATIONS

G.A.SHAPIRO, Techn.D.,
G.N.ASHKINADZE, Dipl. Engineer

TSNIIEP zhylysha
Moscow, USSR

SUMMARY

It is assumed that compressive deformation of the ground are elastic-plastic and the ground cannot act under tension. Basing on these assumptions, there was developed a non-linear calculation model of the large-panel building base under rocking oscillations. Good corroboration of the calculation model was obtained in the vibration tests of 1/4 life size model of the 10-storey building erected on the ground base. Principal dynamic properties and seismic response of buildings on the non-linear ground base are dealt with in this paper.

INTRODUCTION

It is known that the base deformability bears an important effect up on the performance of the large-panel building under vibrations. For example, displacement caused by rocking oscillations of the 8-9-storey large-panel building amounts to so per cent complete upper floor displacement by small vibrations [2].

It is natural to assume that the non-linear response of the building has to an even greater degree to depend on the non-linear response of bases. According to the data of high-capacity vibration tests the stiffness of bases can be considerably reduced as the intensity of vibrations increases. The authors often elicited this dependence by the vibration tests of buildings and models [2].

In contrast to non-linear structural stiffness that of the base comes back almost completely after vibrating has been stopped.

However, the non-linear processes taking place in the ground base of the building under heavy vibrations and their influence on the dynamic behaviour of system "building-ground" has not been studied as yet.

THEORETICAL RESEARCH

It is very important to take into account the fact that the non-linear deformations of the ground take place even under small strains and the residual deformations are considerable.

The common stress-strain relation for the ground under compression is shown in Fig 1 [1].

However, this diagram is normally used for calculating centrally loaded foundations which are not taken off base.

The displacement caused by rocking of the building like rigid massif on the ground accounts for a large part of complete vibration displacement. The breaking of contact between the foundation part and the ground can take place in the large-panel multistorey building under rocking of this type.

It will be convenient in the following analysis to accept the calculation scheme of vacillating building as an absolutely rigid massif and to add the diagram of the ground deformation column to horizontal section 3-4-3. This part of the diagram shows an arbitrary motion of the foundation part when breaking contact (Fig.1).

The above assumption that the building is an absolutely rigid massif allows for simplifying the problem of the pure deformation of ground base. The vibrations of designed model can be written in the form of an equation:

$$\ddot{\varphi} + \gamma \omega \dot{\varphi} + \frac{M(\varphi)}{m \cdot H^2} = \frac{P(t)}{mH} \quad (1)$$

in which

φ - angle of foundation rotation,

γ, ω - coefficient of resistance, and natural frequency of linear vibrations,

$M(\varphi)$ - non-linear force characteristics of the base,

m, H - building mass reduced to the point of applying the external load, and building height,

$P(t)$ - external load: vibrational $P\alpha^2 \sin \omega t$ or seismic

The complete diagram of elementary ground column in mathematic terms is the following relation:

$$P_i = C_i y_i + d_i$$

Coefficients C_i, d_i depend on the sequence of loadings. Force characteristics $M(\varphi)$ can be found from the equilibrium equation

$$\begin{cases} M - N \frac{\Delta l (n-1)}{2} + \Delta l^2 \sum_{i=1}^n [(C_i y_i + d_i)(i-1)] = 0; \\ N - \Delta l \sum_{i=1}^n (C_i y_i + d_i) = 0. \end{cases} \quad (2)$$

From (2)

$$M(\varphi) = \varphi \left(S_1 - \frac{S_2^2}{S_3} \right) \Delta l^3 + N \Delta l \left(\frac{n-1}{2} - \frac{S_2}{S_3} \right) + \Delta l^2 \left(\frac{S_2 S_4}{S_3} - S_5 \right), \quad (3)$$

$$y_{\text{left}} = \frac{N + \varphi \Delta l^2 S_2 - \Delta l S_4}{\Delta l S_3},$$

$$y_i = y_{\text{left}} - \varphi \Delta l (i-1),$$

where

$$S_1 = \sum_{i=1}^n c_i (i-1)^2, \quad S_2 = \sum_{i=1}^n c_i (i-1),$$

$$S_3 = \sum_{i=1}^n c_i, \quad S_4 = \sum_{i=1}^n d_i, \quad S_5 = \sum_{i=1}^n d_i (i-1)$$

Taking into account (3), the motion equation (1) can be integrated by numerical method, for example, by modified Runge-Cutt's method. The procedure of numerical method corresponds to successive loading of the system.

To calculate the above system under vibrational or seismic effects, the program for the computer has been elaborated. This program can be too used for calculating system under static alternating load. In this case, the procedure of step by step method is the same as the above, but the integration of equation (1) is substituted with the following calculation:

$$\varphi = \frac{M - N \Delta l \left(\frac{n-1}{2} - \frac{S_2}{S_3} \right) - \Delta l^2 \left(\frac{S_2 S_4}{S_3} - S_5 \right)}{\Delta l^3 \left(S_1 - \frac{S_2^2}{S_3} \right)} \quad (4)$$

THE PECULIARITIES OF NON-LINEAR BASE DEFORMATIONS UNDER VIBRATIONS

Results of calculations show that partial breaking of contact between the foundation and the base exerts the greatest influence on the base response (Fig.2).

If the ground deformations are elastic, the base stiffnesses can be decreased in 2.5 times, when $e_{bz} = 0,5L$ (Fig.3). The plastic deformations enlarge the angle of foundation rotation and reduce the stiffness in addition (Fig. 2,3). The plastic condensation of the ground enlarges the breaking area of the foundation under rocking vibrations as shown in Fig.3.

At the same time, the forms of hysteresis loops, angle rotations, resonance curve and small value of absorption coefficient testifies to the insignificant display of plastic

properties of ground. For the system with single-side ties that insignificant display is caused by a sharp decrease in the area of hysteresis loop (to compare Fig. 4a and 4b). The non-linear-elastic nature of building vibrations under vibration tests is too explained by this fact.

EXPERIMENTAL STUDY OF NON-LINEAR BASE DEFORMATIONS

To verify the calculation scheme there weve made the vibration tests of 10-storey building model. The scale of the model was 1/4. The model was erected on the ground. The tests were carried out by means of vibration generators which were placed on the upper floor. In these tests displacement of the foundation as related to the ground was specially measured. The 4,5 mm crack after breaking the contact was reached (Δ_{cz}) as well as the 1,5 mm chink by ground condensation (Δ_{ch}) - (Fig.3,6). The relations hip $M(\psi)$ (Fig 2) values of crack form of resonance curves and the line well confirm the theoretical values.

Therefore the above calculation scheme may be used for calculating actual buildings.

THE ANALYSIS THE BASE NON-LINEAR DEFORMATION EFFEKT UPON VIBRATIONS AND SEISMIC RESPONSE OF A 8-STOREYS LARGE-PANEL BUILDING IN ALMA-ATA

The building bases upon boulder bed. Dimensions of foundation slab are 34,6 x 16,1 x 0,5 m.

For this building the non-linear processes noted above lead to the 2-3 times decrease in the bases stiffness. If the well confirm the theoretical values. Therefore the above calculation scheme may be used for calculating actual buildings.

THE ANALYSIS THE BASE NON-LINEAR DEFORMATION EFFECT UPON VIBRATIONS AND SEISMIC RESPONSE OF A 8-STOREYS LARGE-PANEL BUILDING IN ALMA-ATA

The building bases upon boulder bed. Dimensions of foundation slab are 34,6x16,1x0,5 m.

For this building the non-linear processes noted above lead to the 2-3 times decrease in the bases stiffness. If the deformations of the structure is not taken into account, the natural frequency is decreased 1.4-1.75 times, and it is decreased 1,25-1.5 times if the elastic deformations of the structure are considered. (Fig.7). Hence the impulsive load is approximately twice decreased deformations of the structure is not taken into account, the natural frequency is decreased 1,4-1,75 times, and it is decreased 1,25-1,5 times if the elastic deformations of the structure are considered (Fig.7).

Hence, the impulsive load is approximately twice decreased.

But it is necessary to take into account that the about 2 times reduction of the contact area corresponds to the above decrease of the load (Fig.2). This makes the conditions of ground strength worse.

There was made the calculation of the building base under accelerogram of Hollister, 1949 [5]. In this accelerogram the accelerations were 2 times increased. If the non-linear base deformation is taken into account, the moment, applied to the base is 2,5-3 times less, but the length breaking area can exceed 0,5 L (Fig.8). Therefore in line with the USSR Building Codes [3] the stability of the ground may be unprovided for.

CONCLUSIONS

On the basis of theoretical and experimental studies there was developed a design model of the base of large-panel and stone buildings with regard to the breaking of the foundation off the ground, and to the plastic deformations of the latter. Such a design scheme makes it possible to calculate the base for the static, vibro and earthquake effects.

The most important result of the base non-linear deformations is the decrease in the forces under vacillations as well as in the foundation resting area on the base.

The partial breaking of the foundation off the ground, as well as the formation of the crack caused by ground compression may lead to the appearance of a certain suspension of building structures, which calls for additional forces and ought to be taken in to account in design, for instance, when applying methods [4].

Under earthquake loads notwithstanding the double or even triple reduction of forces, there may arise in the non-linearly deformable bases the short-term combinations of the moments exceeding rated values, as well as of the breaking area lengths exceeding the allowable values (0,5 foundation length), which threatens the stability conditions of the base.

REFERENCES

1. Баркан Д.Д. Динамика оснований и фундаментов. М., Стройиздат, 1948.
2. Вибрационные испытания зданий. М., Стройиздат, 1972.
3. Рекомендации по проектированию оснований и фундаментов зданий и сооружений, возводимых в сейсмических районах. М., НИИОСП им. Герсеванова, 1975.

4. Сергеев Д.Д. Проектирование крупнопанельных зданий для сложных геологических условий. М., Стройиздат, 1973.
5. Хачиян Э.Е. Определение сейсмических сил для четырехэтажной рамы по акселерограммам землетрясений. В сборнике "Исследования по сейсмостойкости здания", Ереван, АИСМ Госстроя Арм.ССР, 1966.

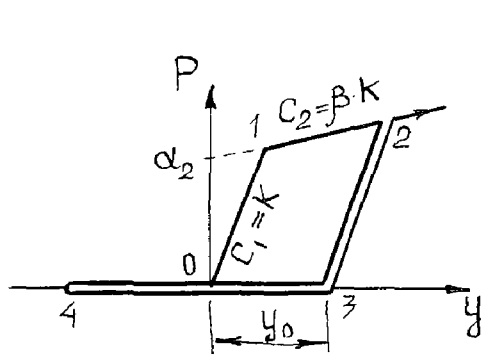


Fig. 1

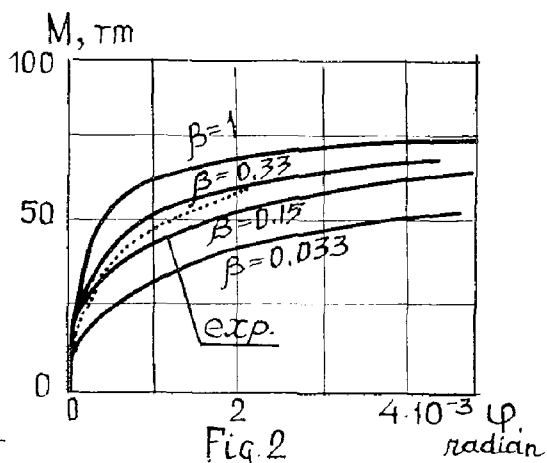


Fig. 2

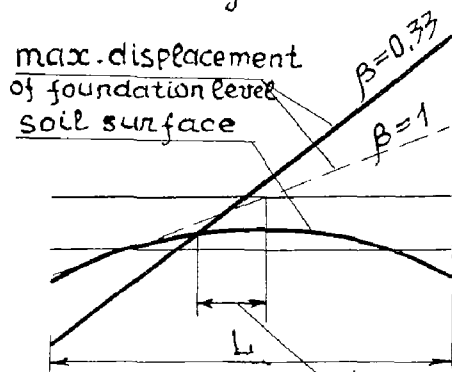


Fig. 3

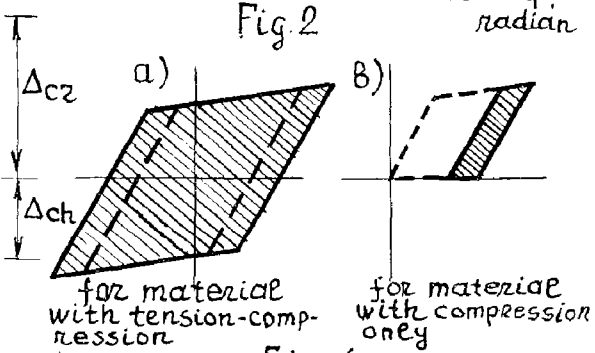


Fig. 4

Increase of area
breaking of contact
by plastic deformation

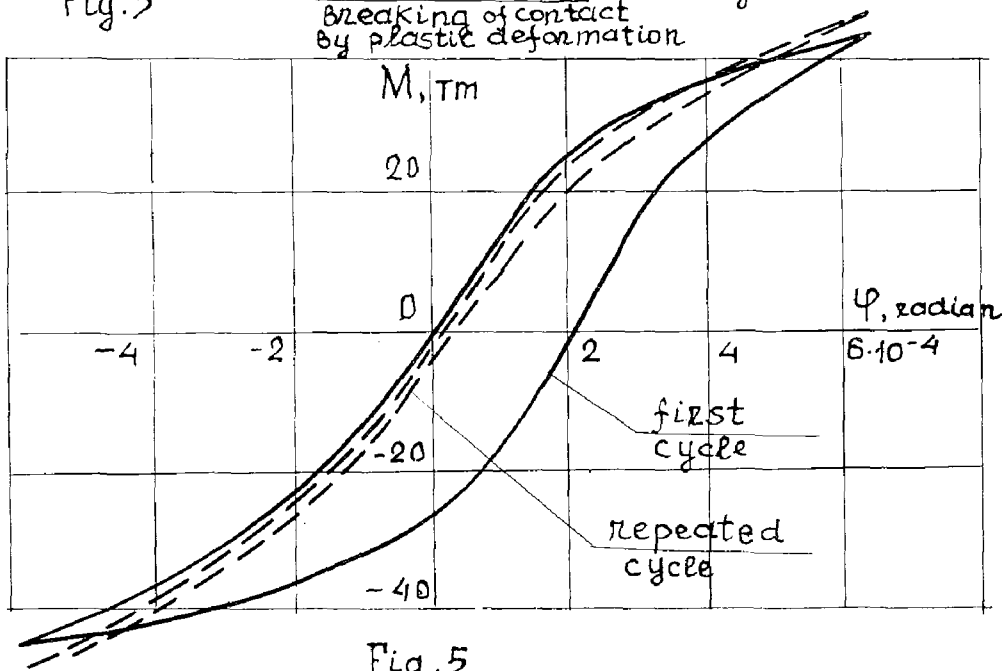


Fig. 5

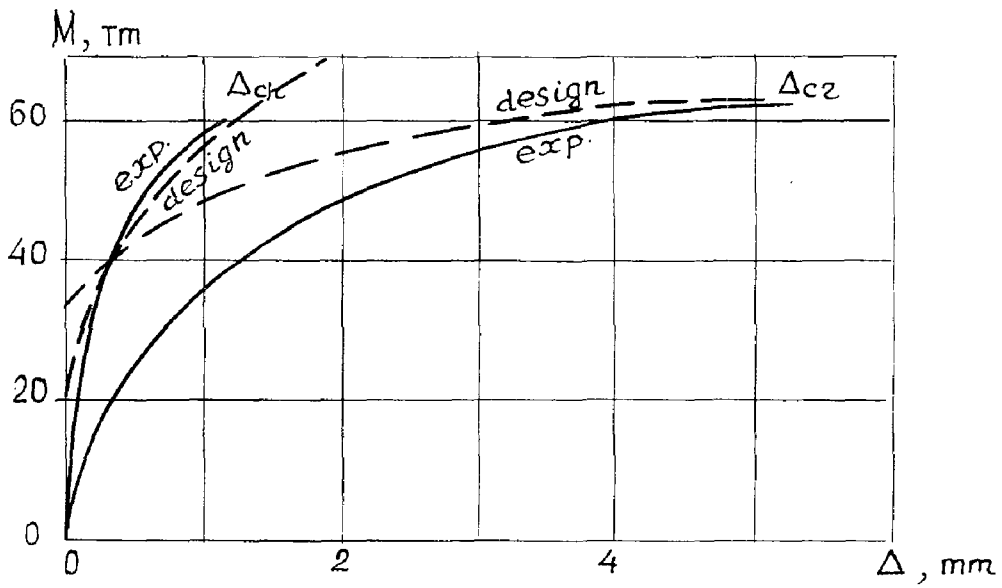


Fig. 6

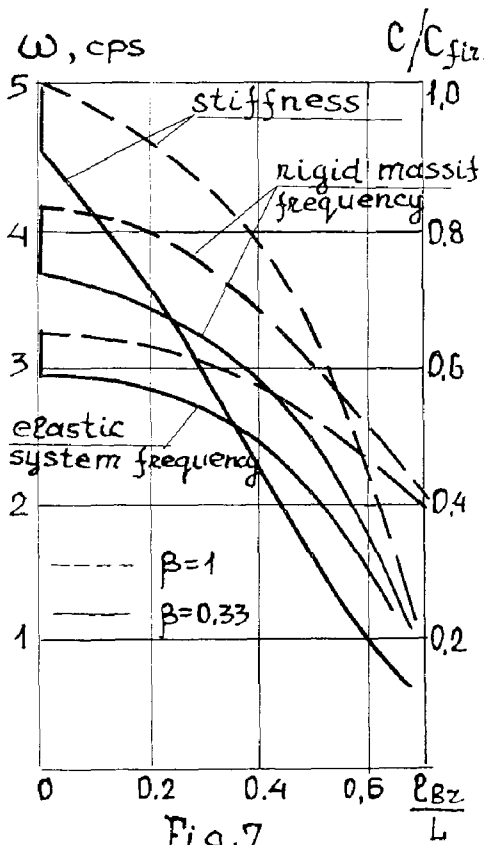


Fig. 7

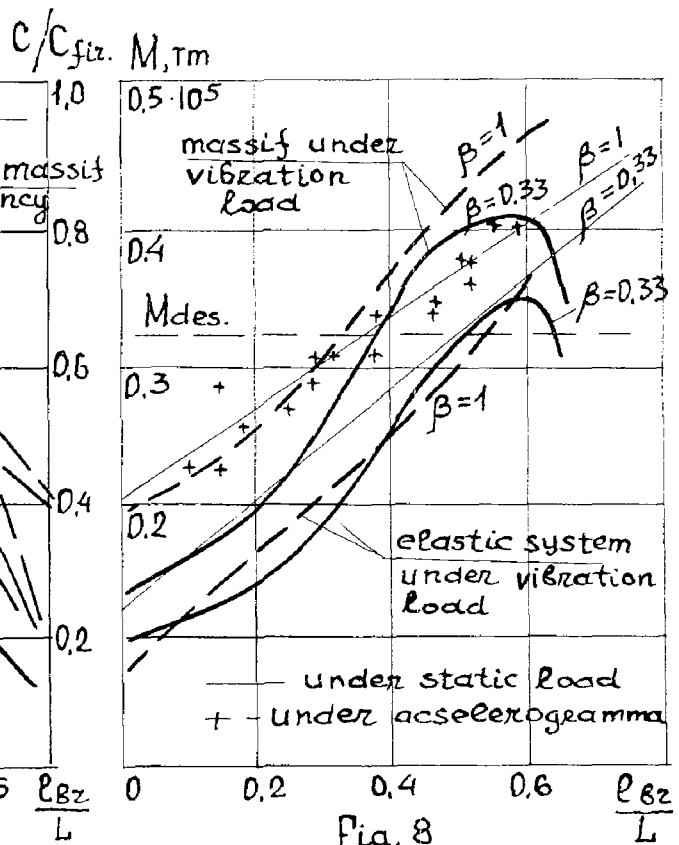


Fig. 8

INTERNATIONAL SYMPOSIUM ON
EARTHQUAKE STRUCTURAL ENGINEERING

St. Louis, Missouri, USA, August, 1976

59

DYNAMIC BEHAVIOR OF CABLE STAYED BRIDGES

Engin A. Egeseli
Design Engineer
Avondale Shipyards, Inc.
New Orleans, Louisiana

John F. Fleming
Associate Professor of Civil Engineering
University of Pittsburgh
Pittsburgh, Pennsylvania

SUMMARY

A procedure is described for analyzing a cable stayed bridge subjected to dynamic loads. The procedure considers nonlinear behavior of both the cables, due to changing sag, and the towers and girders, due to the interaction of axial and bending deformations. It is concluded that the nonlinearity of the structure must be considered in determining the stiffness of the structure in the dead load state, however, a linear dynamic analysis from the dead load state will give results well within normally required design accuracy. Damping in the structure should be considered.

INTRODUCTION

A cable stayed bridge is a nonlinear statically indeterminate structure in which the girder is supported elastically at points along its length by inclined cable stays. A wide variety of geometric configurations have been utilized in cable stayed bridge construction, as shown in Figure 1a. This type of bridge construction differs from the conventional suspension bridge since the girder is supported by individual inclined cable members, attached directly to the tower, rather than by hangers which are supported by one main cable suspended between the towers, as shown in Figure 1b.

Since World War II, approximately 60 cable stayed bridges have been built throughout the world, or are presently under consideration. The popularity of this type of structure is increasing, therefore it is important that the design engineer have available convenient techniques for their analysis and design. It is particularly important that knowledge be available concerning their behavior under various types of loads. The static behavior of cable stayed bridges has been studied by

a number of previous investigators, however, very little significant information has been presented concerning their dynamic behavior.* Because of their increased flexibility, low weight and low damping it is difficult to extrapolate their dynamic behavior from the known dynamic characteristics of girder and truss bridges.

The study presented here is concerned with a comparison of linear and nonlinear dynamic analysis procedures for a single plane cable stayed bridge under earthquake loading. For comparison purposes, the response of the structure is considered under both the longitudinal and vertical components of the May 18, 1940 El Centro California Earthquake (4).

NONLINEAR BEHAVIOR OF CABLE STAYED BRIDGES

Even though the material in the members in a cable stayed bridge behaves in a linear elastic manner, the overall force-deformation relationships for the structure are nonlinear. This nonlinear behavior is a result of both the axial force-deformation relationships for the inclined cable stays and the combined axial and bending force-deformation relationships for the towers and girders being nonlinear. Both of these nonlinear effects are due to geometric changes which occur in the members due to the applied loads on the structure, however, the individual behavior of the two types of members is completely different.

A cable, supported at its ends, and subjected to its own weight and an externally applied axial tensile force will sag into the shape of a catenary. The axial stiffness of the cable will change with changing sag, which in turn changes with displacement of the cable ends. For conventional truss members the sag due to self weight can be safely ignored, however, for cable members it must be considered if an accurate analysis is to be performed.

The displacement of the cable ends, which result from deformations in the structure due to the applied loads, have three distinct effects upon the cable. The first is a change in strain in the cable material. This change in strain can be considered to be linear and is governed by the material modulus. Second, there is a rearrangement of the individual wires in the cable cross section under changing load. This deformation, which is known as constructional stretch, is permanent, however, it is usually eliminated by the cable manufacturer by prestretching the cable to a load greater than the working load during the manufacturing process. Third, there is the change in sag of

*For a complete review of previous work and also a good bibliography see references 1,2,3.

the cable, exclusive of material deformation. This change in sag is governed by the length of the cable, the weight of the cable and the tensile force in the cable. It is this change in sag which causes the nonlinear force-deformation relationship for the cable since the change in sag does not vary linearly with cable tension.

The second non-linear consideration in cable stayed bridges is the behavior of the towers and girders when they are subjected to combined bending and axial loads. Structural members which carry both axial forces and bending moments are subjected to an interaction between these two effects. The lateral deflection of a member causes additional bending moment when subjected to a simultaneously applied axial force, thus altering the flexural stiffness. In a like manner the presence of bending moments will affect the axial stiffness of the member. For most structures the interaction between the flexural and axial stiffnesses can be ignored; however, due to the large displacements which can occur in cable stayed bridges this interaction should be considered.

Since the force-deformation relationships for cable stayed bridges are nonlinear, their analysis under the action of applied loads is more complicated than for conventional structures. Statically applied loads on a structure will always be in equilibrium with the internal member forces resulting from the deformation in the members. For a linear structure the stiffness can be formulated in terms of the deformations with nonchanging proportionality constants. For nonlinear structures these proportionality constants change with changing load and in most cases cannot be represented by a simple algebraic expression, thus increasing the difficulty in obtaining a solution for the resulting equations. One popular way of solving nonlinear structural equations for static loads is by making use of successive linear analyses, either by assuming the load to be applied incrementally with a corresponding linear structural behavior for each increment, or by assuming linear behavior for the total load application and iterating until the correct equilibrium position is obtained. Either approach should give essentially the same result. In the analyses presented here, an iterative approach is used to determine the displacements and member stresses under the structure dead load.

COMPUTATION OF STRUCTURAL STIFFNESS

A convenient method for considering the nonlinearity in the inclined cable stays is to consider an equivalent straight chord member with an equivalent modulus of elasticity. The equivalent modulus of elasticity combines both the effects of material and geometric deformations. Hence, the axial stiffness of the equivalent member for any particular combination of cable sag and cable tension is the same as

the axial stiffness of the actual cable. This approach has been used successfully by several previous investigators (2,3).

If the change in tension of a cable during a load increment is not large the axial stiffness of the cable will not significantly change during the load increment. For this situation, the equivalent modulus of elasticity can be considered to be constant and is given by:

$$E_{eq} = E / \left\{ 1 + \left[(wL)^2 \frac{AE}{12T^3} \right] \right\} \quad (1)$$

where E is the material modulus, L is the horizontal projected length of the cable, w is the weight per unit length of the cable, A is the cross section area and T is the cable tension before the load increment is applied. In many situations, due to the flexibility of cable stayed bridges, the displacements and resulting changes in member forces during the application of a load increment are not small. As the cable ends move during the load application the equivalent modulus will change as a result of the changing cable tension. For this situation, the equivalent modulus of elasticity over the load increment is:

$$E_{eq} = E / \left\{ 1 + \left[(wL)^2 \frac{(T_i + T_f) AE}{24T_i^2 T_f^2} \right] \right\} \quad (2)$$

where the subscripts i and f represent the initial and final values of cable tension during the load increment. By using the concept of an equivalent modulus of elasticity the individual member stiffness matrix for any inclined cable stay for any value of cable tension can be written in the form:

$$\left[K_m \right]_i = \begin{bmatrix} AE_{eq}/L & -AE_{eq}/L \\ -AE_{eq}/L & AE_{eq}/L \end{bmatrix}_i \quad (3)$$

The nonlinear behavior of the towers and girders, due to large deformations in the members, can be considered by introducing the concept of stability functions. The modified member stiffness matrix will be of the form:

$$\left[K_m \right]_i = \begin{bmatrix} k_{11} S_5 & 0 & 0 & k_{14} S_5 & 0 & 0 \\ 0 & k_{22} S_1 & k_{23} S_2 & 0 & k_{25} S_1 & k_{26} S_2 \\ 0 & k_{32} S_2 & k_{33} S_3 & 0 & k_{35} S_2 & k_{36} S_4 \\ k_{41} S_5 & 0 & 0 & k_{44} S_5 & 0 & 0 \\ 0 & k_{52} S_1 & k_{53} S_2 & 0 & k_{55} S_1 & k_{56} S_2 \\ 0 & k_{62} S_2 & k_{63} S_4 & 0 & k_{65} S_2 & k_{66} S_3 \end{bmatrix}_i \quad (4)$$

where S_i is a stability function which accounts for interaction of the axial and bending flexibilities. The derivation of these stability functions can be found in a number of standard texts in the area of structural analysis(5).

In order to perform a dynamic analysis of a structural system the total structural stiffness matrix must be determined. By using the previously described individual member stiffness matrices the structural stiffness matrix for any loading state can be determined by the standard assembly procedure.

DYNAMIC ANALYSIS

The results presented in this discussion are for a mathematical model, as shown in Figure 2, which represents with some modification a single load bearing plane of the Nordbrücke Bridge at Dusseldorf, Germany. For convenience, the dimensions were rounded off in converting from metric units to feet. Cable areas were similarly rounded off to correspond to dimensions of cables manufactured in the United States. Whereas the actual structure has a tapered tower, the mathematical model has a constant area and moment of inertia which was taken to be equal to that at the base of the tower in the actual structure. The actual girder has a varying cross-section, while in the mathematical model the average area and moment of inertia is used.

The girder is supported vertically at the towers, but is assumed to be independent of the towers so that there is no moment transfer between the girder and the towers. The towers are assumed to be fixed at their bases. It is assumed that the cable has an initial prestress so that it is capable of supporting a negative force increment during the application of any load increment.

The mathematical model has 22 nodes and 31 individual members. For the dynamic analysis, the mass of the structure was assumed to be lumped at the nodes. Both translational and rotational inertias were initially considered, however, at a later point in the analysis the rotational inertias were neglected since their effect was negligible. The modal damping coefficients were computed by using an approximate approach described by Biggs (6).

The method employed in the dynamic analysis is a step by step integration algorithm, developed by Argyris (7), which works in terms of the inertia force vector and its time derivatives at the beginning and end of a time step. This is an iterative approach which approximates the displacements by a fifth degree polynomial with time. An integration step of 0.3 times the smallest natural period of the system is used.

One of the advantages of this procedure is that it does not involve matrix inversion when a lumped mass matrix is employed. Another is that in most other procedures, when the number of degrees of freedom is large, the capacity of the core memory is insufficient and external storage units must be used thus greatly increasing the computation time. In the procedure employed here, the nodal forces are calculated directly from the total displacements so that there is no need to store the global structural stiffness matrix.

The mathematical model was analyzed, considering both linear and nonlinear dynamic response, for the vertical and horizontal components of the El Centro Earthquake. The conditions considered were:

- a) Linear dynamic response, using the stiffness at the dead load deformed state, assuming the structure behaved linearly during the application of the dead load (L-L).
- b) Linear dynamic response, using the stiffness at the dead load deformed state, considering the nonlinear behavior of the structure during the application of the dead load (NL-L).
- c) Nonlinear dynamic response, using the stiffness at the dead load deformed state, considering the nonlinear behavior of the structure during the application of the dead load (NL-NL). In order to account for the nonlinear behavior during the dynamic response the structure stiffness matrix was recomputed at the end of each time step.

RESULTS AND CONCLUSIONS

The first step in the dynamic analysis was to compute the natural frequencies and mode shapes for the bridge in the dead load deformed state in order to determine the length of time step required in the stepwise integration procedure. The lowest frequency of the structure is 0.4 cps due to its lightness and high flexibility.

The dynamic response of the structure to the vertical component of the El Centro Earthquake is shown in Figures 3 through 8. Figures 3, 5, and 7 show the variation of vertical displacement of the girder at node 7, moment in the girder at the tower, and tension in Cable 1, assuming no damping in the structure, for the L-L, NL-L, and NL-NL cases. Similar curves are shown in Figures 4, 6, and 8 for the NL-NL case assuming damping of six, five and three percent of critical damping in the first, second and third modes respectively. The variation of the displacement of the top of the tower at node 8, along the

longitudinal axis of the bridge, is shown in Figures 9 and 10, for the damped and undamped cases, for the horizontal component of the El Centro Earthquake.

It can be seen that for the undamped responses which are presented the computed results for the NL-L and NL-NL cases are almost identical for each quantity considered and are significantly different than the L-L case. The L-L case underestimates the displacements and the moments while giving mixed results for the cable tension.

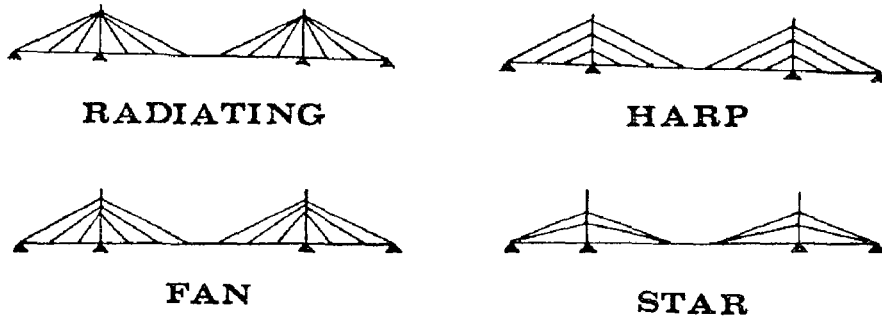
The effect of the small amount of damping considered in the analyses is considerable. The amount of reduction in the response ranges from 25 to 35 percent.

Two general conclusions can be made, based upon the results presented here and similar results obtained during the total investigation. The first conclusion is that the NL-L and NL-NL cases demonstrate almost the same dynamic behavior throughout the time of loading. This is an important observation since a linear dynamic analysis of the structure is far less complicated and requires far less computer time than a nonlinear dynamic analysis. For accurate results, however, nonlinear behavior of the structure must be considered when determining the structure stiffness matrix in the dead load state for use in the dynamic analysis. The second conclusion is that damping has a significant effect upon the response of the structure and should be considered during the analysis. Further investigation is necessary to determine accurate values for the damping coefficients to be used.

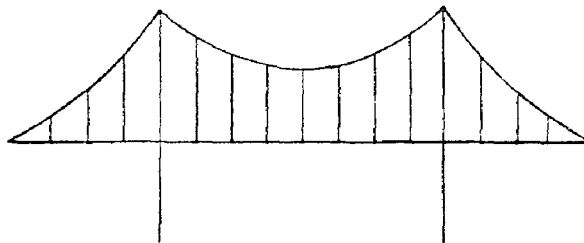
REFERENCES

1. Podolny, W. and Fleming, J. F. "Historical Development of Cable-Stayed Bridges," Proceedings, American Society of Civil Engineers, Vol. 98, No. ST9, September 1972
2. Podolny, W. "Static Analysis of Cable-Stayed Bridges," Ph.D. Dissertation, School of Engineering, University of Pittsburgh, 1971
3. Egeseli, E. A., "The Nonlinear Dynamic Response of a Cable-Stayed Girder Bridge to Various Loadings," Ph.D. Dissertation, School of Engineering, University of Pittsburgh 1975
4. "Strong Motion Earthquake Accelerograms, Digitized and Plotted Data, Vol. II," Report EERL 71-50, California Institute of Technology, Earthquake Engineering Research Laboratory
5. Harrison, H. B. "Computer Methods in Structural Analysis," Prentice-Hall, Inc. 1973

6. Biggs, J. M. "Introduction to Structural Dynamics," McGraw-Hill Book Co., 1964
7. Argyris, J. H., Dunne, P. E. and Angelopoulos, T. "Nonlinear Oscillations Using the Finite Element Technique," Computer Methods in Applied Mechanics and Engineering, Vol. 2, March 1973



(a)



(b)

Figure 1

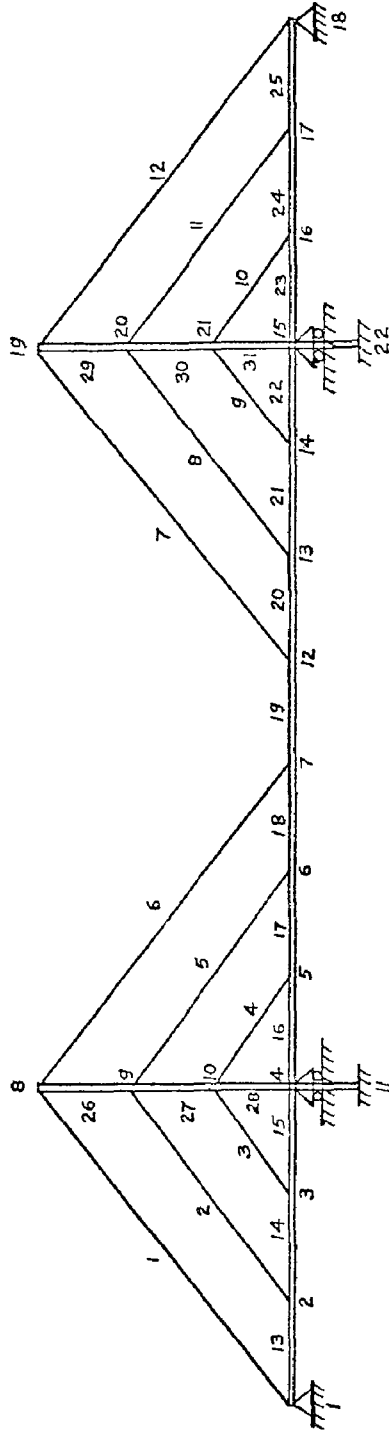


Figure 2

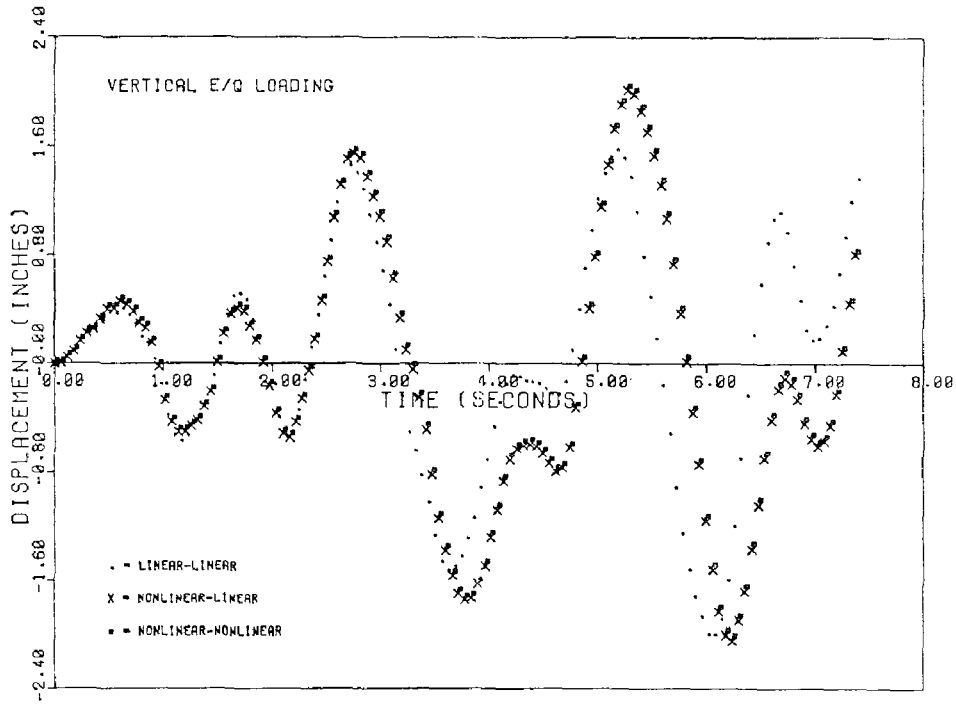


Figure 3

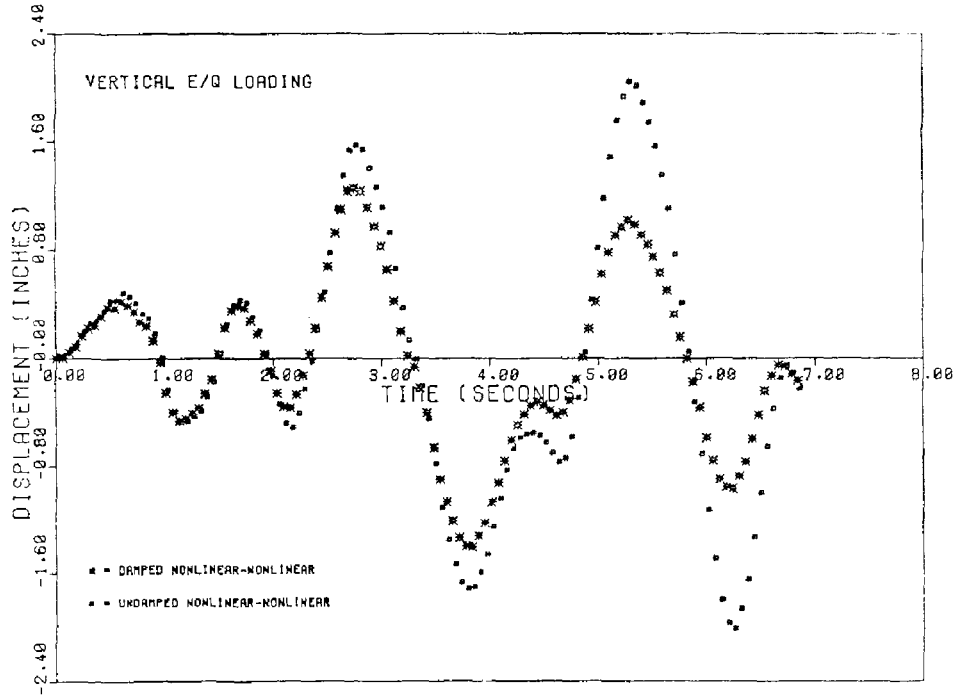


Figure 4

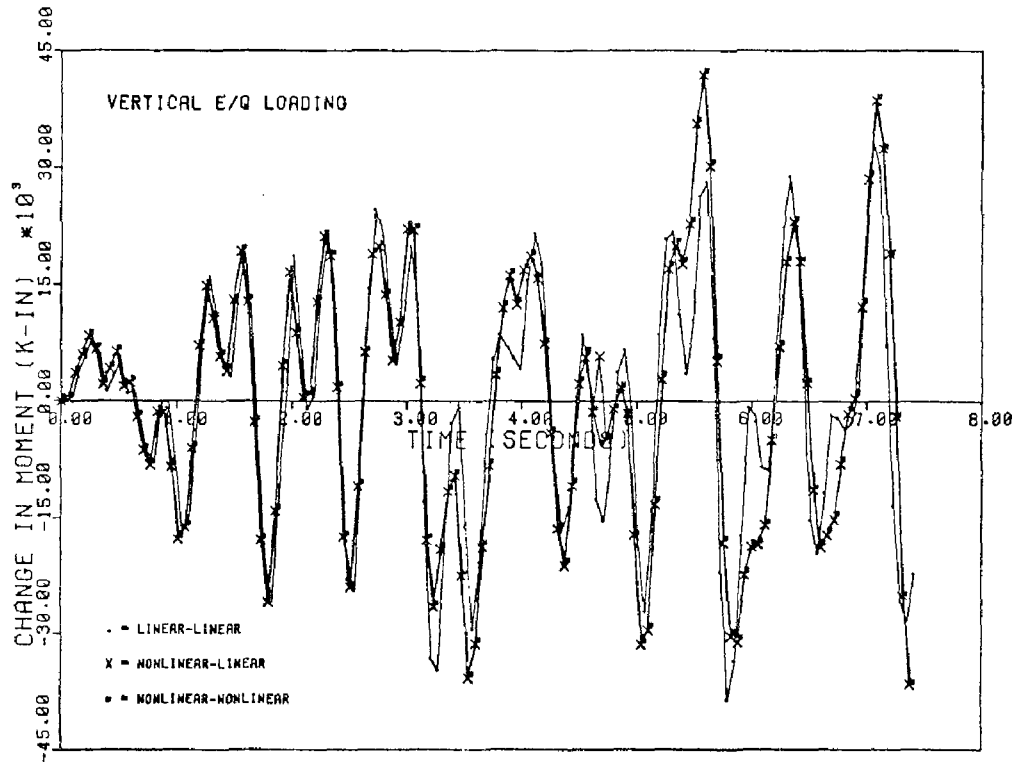


Figure 5

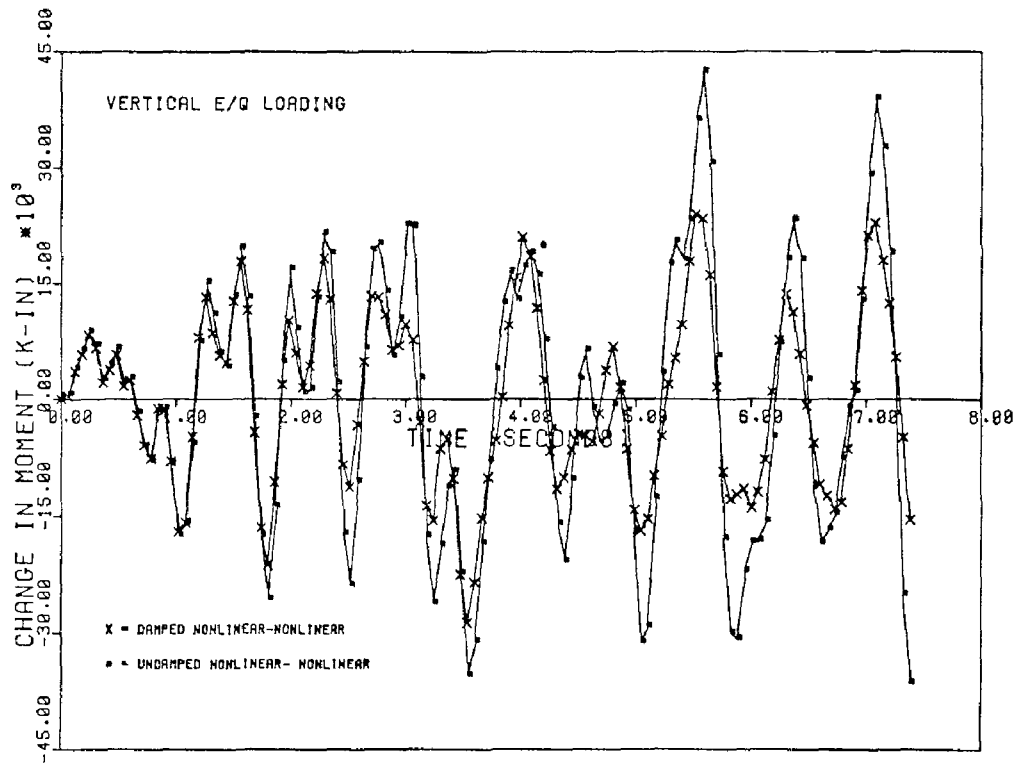


Figure 6

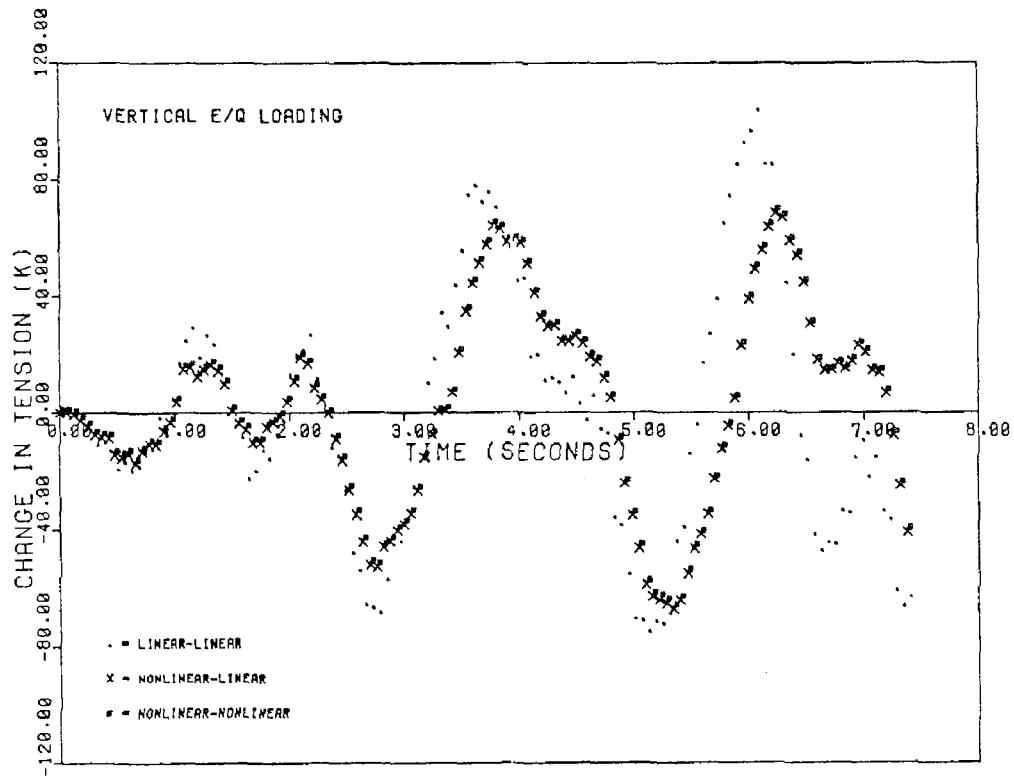


Figure 7

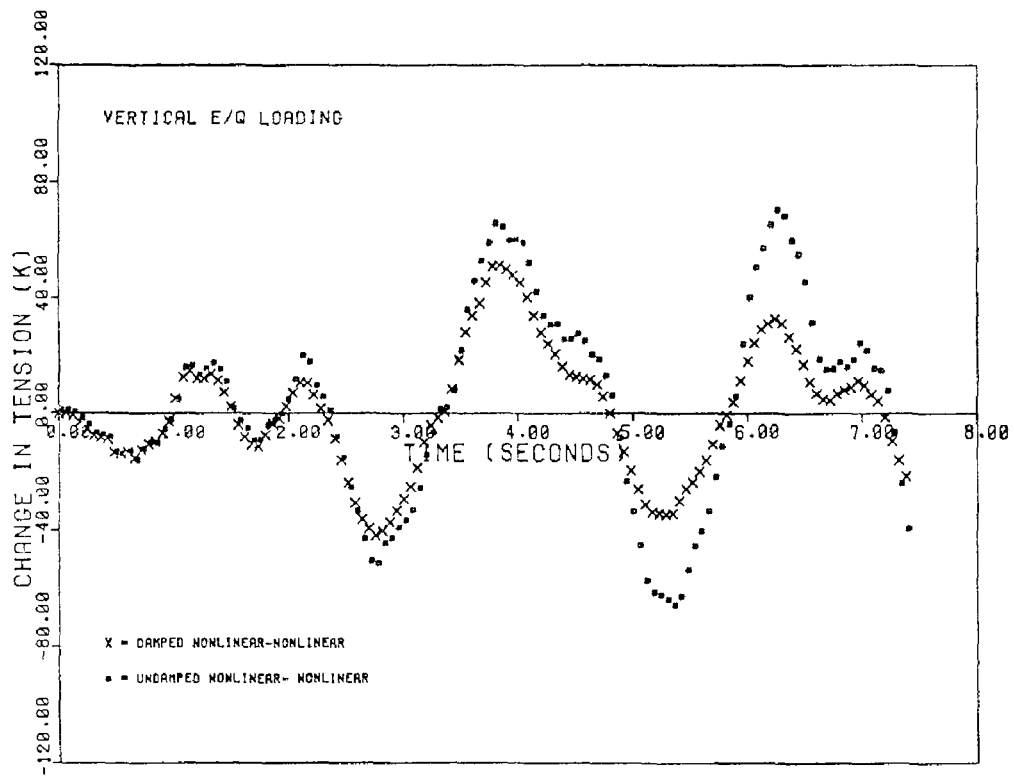


Figure 8

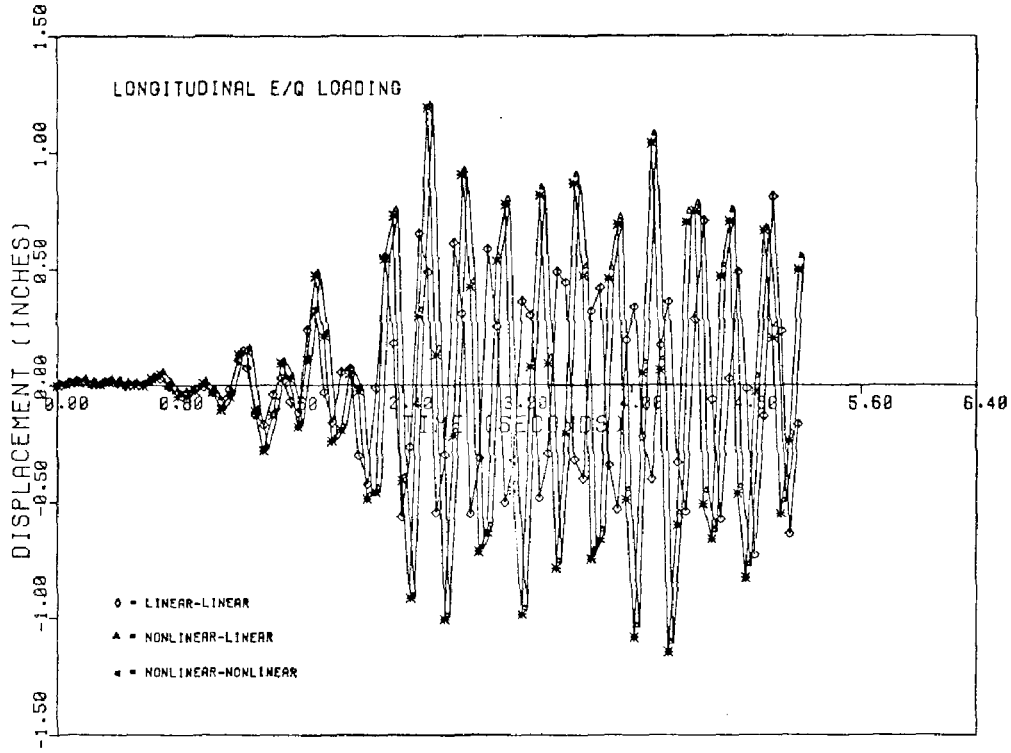


Figure 9

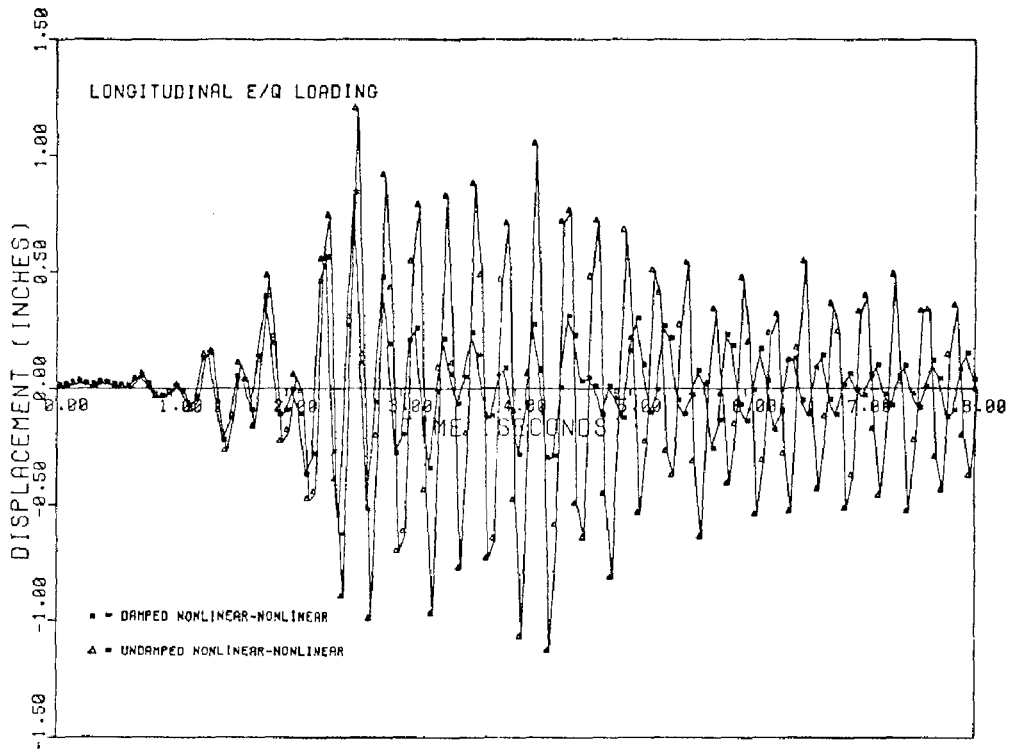


Figure 10

INTERNATIONAL SYMPOSIUM ON
EARTHQUAKE STRUCTURAL ENGINEERING

73

St. Louis, Missouri, USA, August, 1976

MODAL ANALYSIS AND SEISMIC DESIGN
OF TALL BUILDING FRAMES

P. PARAMASIVAM
Senior Lecturer
Department of Civil Engineering
University of Singapore
Singapore

S. NASIM
Structural Engineer
Ang Thian Soo and Partners
Consulting Engineers
Singapore

S.L. LEE
Professor and Head
Department of Civil Engineering
University of Singapore
Singapore

SUMMARY

An iterative method for the modal analysis of tall building frames based on lumped mass idealisation is presented. The method takes into consideration the flexibility of the horizontal members and allows distinct rotations of the joints in each storey. The iteration converges rapidly and the required computation can be carried out in a small computer. The application of the proposed method to the seismic design of tall buildings is illustrated with the aid of earthquake response spectrum. The effect of damping and the contributions of the lower modes to the seismic response of the structures are investigated. The storey shear coefficients obtained verified the whipping action observed on the top few storeys. The design procedure is simple and suitable for practical design.

INTRODUCTION

The importance of dynamic analysis of tall buildings has been enhanced by the recent trend towards more highrise buildings in some metropolitan centres. In designing the structures to withstand the effects of seismic and wind forces, the study of their dynamic behaviour is useful in general and necessary in some special cases.

The present study deals with a frequency analysis of tall building frames and its application in the determination of the probable maximum response of the structure when subjected to base excitation due to earthquake. Discrete methods of iterative nature which are relatively simple are commonly used in practical design for frequency analysis (1, 2, 3)*. These methods are more suitable to the analysis of building frames as the mass is mainly concentrated at each floor level. The proposed iterative method, while similar to the procedure presented by Goldberg, Bogdanoff

* Numbers in parenthesis refer to the listing of references.

and Moh (2) in that it takes into account the flexibility of the horizontal members, differs with it by allowing distinct rotations of the joints in each storey.

The procedure for the seismic design of building frames with the aid of the proposed modal analysis and an earthquake response spectrum is suggested with an illustrative example. The effect of damping on the earthquake response, the contribution of the lower modes to the seismic response of the structure, and the whipping action of the top few storeys are discussed.

MODAL ANALYSIS

The frequency analysis is based on lumped mass idealisation using slope deflection equations. The detailed derivation of the governing equations was presented by Paramasivam, Yeh and Nasim (4) and the salient features are outlined in the following. The equations of motion are obtained by equating the inertia forces acting on all the floors above a particular storey to the shearing forces acting on the columns of that storey. Thus the total shear S_i acting on the columns of the i -th storey can be written as

$$S_i = \sum_{k=i}^n M_k w^2 y_k \quad (1)$$

where M_k and y_k denote the mass and displacement of the k -th storey respectively, w the circular frequency and n the total number of floors. In Eq. 1, y_k is positive toward the right and S_i is positive if acting toward the left at the column base. The storey shear can be expressed in terms of the column moments in the form

$$M_i^C = S_i h_i \quad (2)$$

where M_i^C represents the sum of the moments acting on both ends of all the columns of the i -th storey, positive counter clockwise, and h_i is the height of the i -th storey.

The sum of the column moments acting at both ends of all the columns of i -th storey can be expressed in terms of the joint rotations and relative storey displacement by means of the slope deflection equations in the form

$$M_i^C = \sum_{j=1}^m K_{i,j}^C (12R_i - 6\theta_{i,j} - 6\theta_{i-1,j}) \quad (3)$$

where

$$R_i = (y_i - y_{i-1})/h_i \quad (4)$$

In these equations, $\theta_{i,j}$ denotes the rotation of joint j on the i -th floor, m the number of columns on the floor $K_{i,j}^C$ denotes the stiffness of the j -th column of the i -th storey, the stiffness being the flexural rigidity of

the member divided by the length. Similarly, the sum of the moments acting at the top of the i -th storey columns can be written as

$$M_{i,i-1}^C = \sum_{j=1}^m K_{i,j}^C (6R_i - 4\theta_{i,j} - 2\theta_{i-1,j}) \quad (5)$$

Eliminating R_i between (3) and (5) leads to

$$M_{i,i-1}^C = \frac{M_i^C}{2} - \sum_{j=1}^m K_{i,j}^C (\theta_{i,j} - \theta_{i-1,j}) \quad (6)$$

Similarly the sum of the moments acting at the bottom of the $(i+1)$ -th storey columns can be derived as

$$M_{i,i+1}^C = \frac{M_{i+1}^C}{2} - \sum_{j=1}^m K_{i+1,j}^C (\theta_{i,j} - \theta_{i+1,j}) \quad (7)$$

In a similar manner, the sum of the moments acting on both ends of all the beams on a floor level can be expressed in terms of the joint rotations. Since the sum of the beam and column moments acting on all the joints at a floor level must vanish, the sum of the column moments of two consecutive storeys, $M_i^C + M_{i+1}^C$, in view of Eqs. 6 and 7, can be expressed in terms of the joint rotations in the form

$$\begin{aligned} M_i^C + M_{i+1}^C &= 2 \sum_{j=1}^m K_{i,j}^C \theta_{i,j} + 2 \sum_{j=1}^m K_{i+1,j}^C \theta_{i,j} + 12 \sum_{j=2}^{m-1} K_{i,j}^b \theta_{i,j} \\ &+ 12 \sum_{j=2}^{m-1} K_{i,j+1}^b \theta_{i,j} - 2 \sum_{j=1}^m K_{i,j}^C \theta_{i-1,j} - 2 \sum_{j=1}^m K_{i+1,j}^C \theta_{i+1,j} \\ &+ 12 (K_{i,1}^b \theta_{i,1} + K_{i,m}^b \theta_{i,m}) \end{aligned} \quad (8)$$

where $K_{i,j}^b$ denotes the stiffness of the j -th beam on the i -th floor.

The iterative process starts with the simplifying assumption that all the joint rotations on a floor level are equal to the average value $\bar{\theta}_i$. Introducing the ratios $C_{i,j} = \theta_{i,j} / \bar{\theta}_i$ into Eqs. 3 and 8, in view of Eqs. 1, 2 and 4, leads to, respectively,

$$\frac{y_i - y_{i-1}}{h_i} = \frac{(\sum_{k=i}^n M_k w_k^2 y_k) h_i}{12 \sum_{j=1}^m K_{i,j}^C} + \frac{\sum_{j=1}^m (k_{i,j}^C C_{i,j}) + \sum_{j=1}^m (k_{i,j}^C C_{i-1,j}) \bar{\theta}_{i-1}}{2 \sum_{j=1}^m K_{i,j}^C} \quad (9)$$

$$\begin{aligned}
& \left(\sum_{k=i}^n M_k w^2 y_k \right) h_i + \left(\sum_{k=i+1}^n M_k w^2 y_k \right) h_{i+1} = -2 \sum_{j=1}^m (K_{i,j}^c C_{i-1,j}) \bar{\theta}_{i-1} \\
& + 2 \left[6 \left\{ K_{i,1}^b C_{i,1} + \left(\sum_{j=2}^{m-1} K_{i,j}^b + \sum_{j=2}^{m-1} K_{i,j+1}^b \right) C_{i,j} + K_{i,m}^b C_{i,m} \right\} \right. \\
& \left. + \sum_{j=1}^m K_{i,j}^c C_{i,j} + \sum_{j=1}^m K_{i+1,j}^c C_{i,j} \right] \bar{\theta}_i - 2 \left(\sum_{j=1}^m K_{i+1,j}^c C_{i+1,j} \right) \bar{\theta}_{i+1} \quad (10)
\end{aligned}$$

The equilibrium equation of joint i, j can be written in the form

$$\begin{aligned}
& K_{i,j}^b \theta_{i,j-1} + K_{i+1,j}^c (2\theta_{i,j} + \theta_{i+1,j}) + K_{i,j}^c (2\theta_{i,j} + \theta_{i-1,j}) \\
& + 2K_{i,j}^b \theta_{i,j} + 2K_{i,j+1}^b \theta_{i,j} + K_{i,j+1}^b \theta_{i,j+1} = 3K_{i+1,j}^c R_{i+1} \\
& + 3K_{i,j}^c R_i \quad (11)
\end{aligned}$$

Introducing the assumption that the ratio between the end rotations of all the columns on a storey is identical and the notations

$$\phi_{i+1,i} = \theta_{i+1,j} / \theta_{i,j} \quad (12)$$

$$\phi_{i-1,i} = \theta_{i-1,j} / \theta_{i,j} \quad (13)$$

Eq. 11 simplifies into the form

$$\begin{aligned}
& K_{i,j}^b \theta_{i,j-1} + \left[K_{i+1,j}^c (2 + \phi_{i+1,i}) + K_{i,j}^c (2 + \phi_{i-1,i}) + 2K_{i,j}^b \right. \\
& \left. + 2K_{i,j+1}^b \right] \theta_{i,j} + K_{i,j+1}^b \theta_{i,j+1} = 3K_{i+1,j}^c R_{i+1} + 3K_{i,j}^c R_i \quad (14)
\end{aligned}$$

For the first iteration, the coefficient $C_{i,j}$ is assumed to be unity. The iteration starts from the top floor where the floor displacement y_n , taken as the amplitude factor, is set equal to unity. Assuming a reasonable first approximation of the frequency w , the values of y_{n-1} and $\bar{\theta}_{n-1}$ are found in terms of $\bar{\theta}_n$ using Eqs. 9 and 10. This calculation is repeated downward until the displacement and rotation of the ground floor, y_0 and θ_0 are found in terms of $\bar{\theta}_n$. The boundary conditions at $i = 0$ are $\bar{\theta}_0 = 0$ and $y_0 = 0$. The first boundary condition yields the value of $\bar{\theta}_n$, which in turn leads to the first approximation of y_0 which, in general, will be different from zero. The above procedure is repeated with another trial value of w until the second boundary condition at the base is satisfied. When this is done, the values of the joint rotations $\theta_{i,j}$ on each floor are determined by applying Eq. 14 to each floor.

For the second iteration, the average values of the floor rotations $\bar{\Theta}_i$ and the second approximation of $C_{i,j}$ are computed from the values of $\Theta_{i,j}$ obtained in the first approximation. The iterative process is repeated as discussed above until the values of $C_{i,j}$ between consecutive cycles attain the desired accuracy.

With the final values of $\Theta_{i,j}$, the corresponding values of y_i are calculated by applying Eq. 9 to each floor, starting at the top floor, and the stress resultants are readily determined by means of the slope-deflection equations.

DESIGN PROCEDURE USING EARTHQUAKE RESPONSE SPECTRUM

The above analysis can be used to determine the natural frequencies and corresponding mode shapes of building frames, and to estimate the total maximum response of the structures when subjected to earthquake excitation with the aid of earthquake response spectrum (5). The maximum earthquake displacement y_{\max} corresponding to each mode is computed from the relationship

$$y_{\max} = S_d y_n L^* / M^* \quad (15)$$

where S_d is the spectral displacement, y_n the top displacement, L^* and M^* are the earthquake participation factor and generalised mass, respectively, as defined by

$$L^* = \sum_{i=1}^n M_i y_i \quad (16)$$

$$M^* = \sum_{i=1}^n M_i y_i^2 \quad (17)$$

and M_i is the lumped mass of the i -th floor.

The displacements and stress resultants corresponding to the maximum earthquake displacement are computed for the different modes. The maximum response is then determined by superimposing the response of the desired number of the lower modes, using the root-mean-square procedure (5).

ILLUSTRATIVE EXAMPLE

The 10-storey building frame shown in Fig. 1 is considered to illustrate the design procedure. The first three natural frequencies are found to be 3.2929, 9.1429 and 15.2950 rad/sec and the corresponding periods are 1.9088, 0.6875 and 0.4109 seconds respectively. Response spectra (5) based on the spectral velocity resulting from the N-S acceleration component recorded at EI Centro, California earthquake in May, 1940 for different damping ratios and 20% g are used to illustrate the design procedure.

The maximum earthquake displacements and the corresponding mode shapes for the first three modes, for damping ratios of 1%, 2% and 5%, are shown in Fig. 2. The effective earthquake loading, i.e. the storey shears, are calculated for each mode. The maximum storey shears are obtained by taking the root of the sum of the squares (RMS) of the shear values of the first three modes. The results for various damping ratios are presented graphically in Fig. 3. The resultant base shears for damping ratios of 1%, 2% and 5% are found to be 12.4%, 11.4% and 8.5% of the building weight respectively. The lateral force coefficients, i.e., the ratio between the difference of consecutive storey shears and the corresponding storey weight, are shown in Fig. 4.

CONCLUSION

The proposed iterative method is a generalised version of the procedure proposed by Goldberg et. al. (2) allowing distinct joint rotations. The consideration of distinct rotations of the joints yields a more flexible structure and reduces the natural frequency.

The contributions of the higher modes to the earthquake response of the structure considered are small in comparison with that of the first mode, and satisfactory preliminary designs can be based on the first mode response alone as can be seen from Fig. 3. From the lateral force coefficients shown in Fig. 4, it is observed that there is a significant increase in shear towards the top few storeys, substantiating the whipping action commonly observed in this type of structures.

The proposed method is suitable for practical design purposes, the computation work being relatively simple. In fact the entire calculations can be carried out with the aid of a desk top calculator or a mini computer.

REFERENCES

- (1) Biggs, J.M., "Introduction to Structural Dynamics", McGraw Hill Inc., New York, 1964.
- (2) Goldberg, J.E., Bogdanoff, J.L. and Moh, Z.L., "Forced Vibrations and Natural Frequencies of Tall Building Frames", Bulletin of the Seismological Society of America, June 1969, pp. 33-47.
- (3) Newmark, N.M. and Rosenblueth, F., "Fundamentals of Earthquake Engineering", Prentice Hall Inc., Englewood Cliffs, New Jersey, 1964.
- (4) Paramasivam, P., Yeh, C.S. and Nasim, S., "Dynamic Analysis of Building Frames", Journal of Sound and Vibrations, June, 1975, pp. 103-112.
- (5) Wiegel, L.R., "Earthquake Engineering", Prentice Hall Inc., Englewood Cliffs, New Jersey, 1970.

$K^B = 0.399 \times 10^7$ kgf m (for all beams)
 Mass = 7395.36 kgf sec²/m (for all floors)

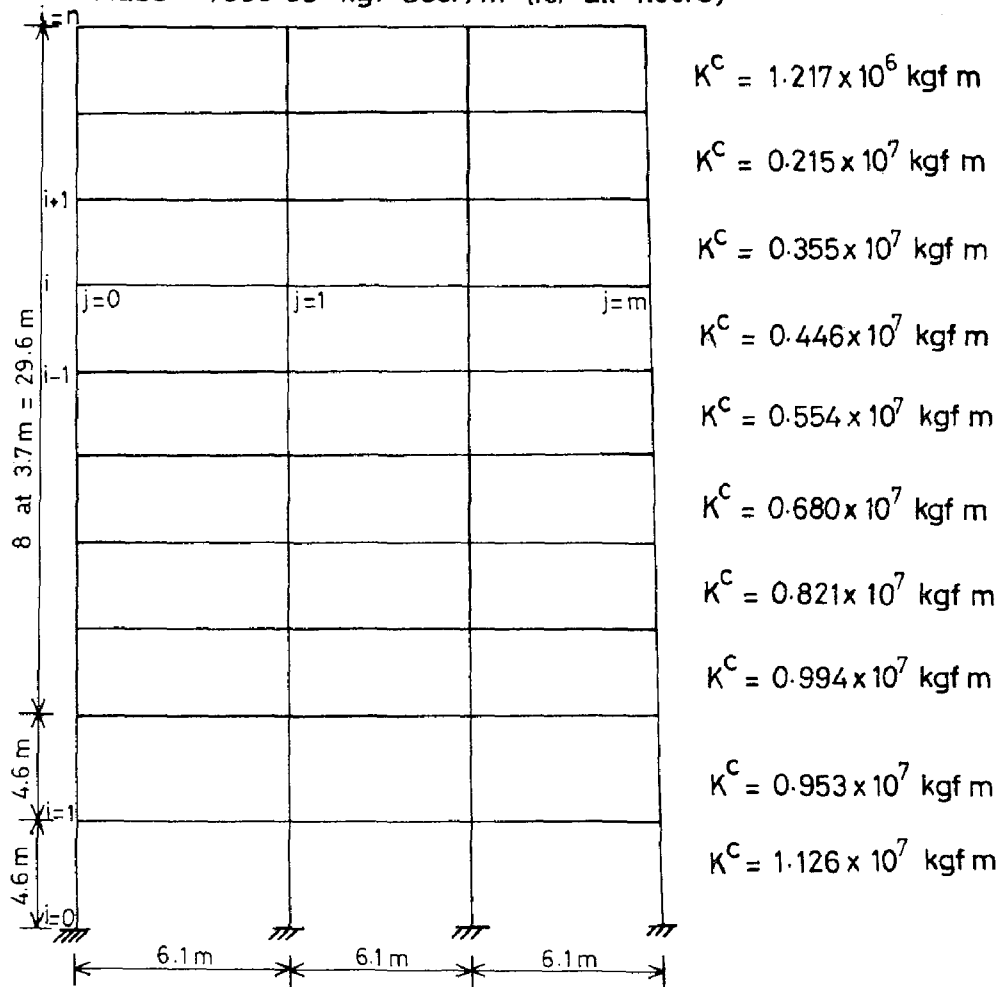


FIG. 1 BUILDING FRAME

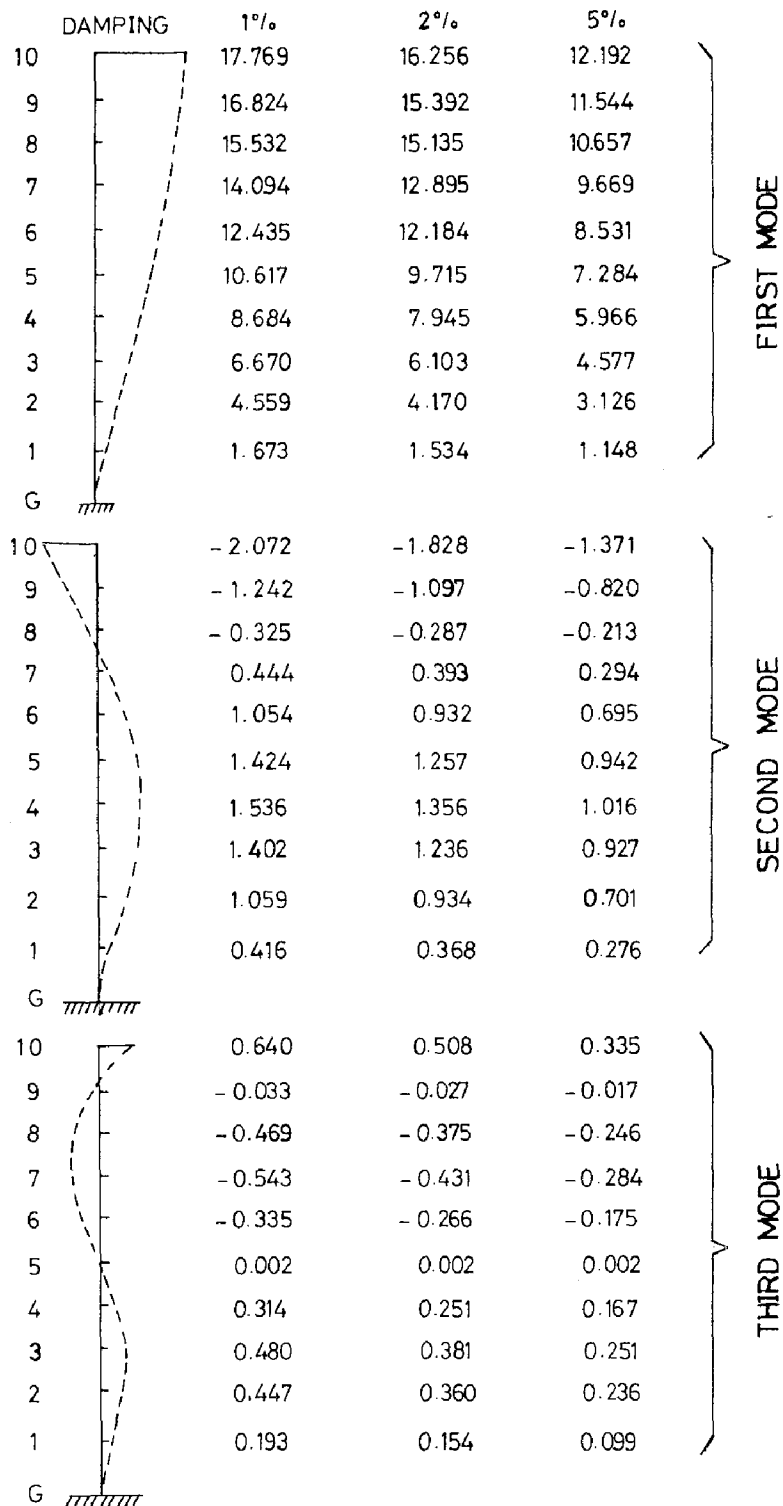


FIG.2 FLOOR DISPLACEMENTS (cm.) FOR VARIOUS DAMPING RATIOS

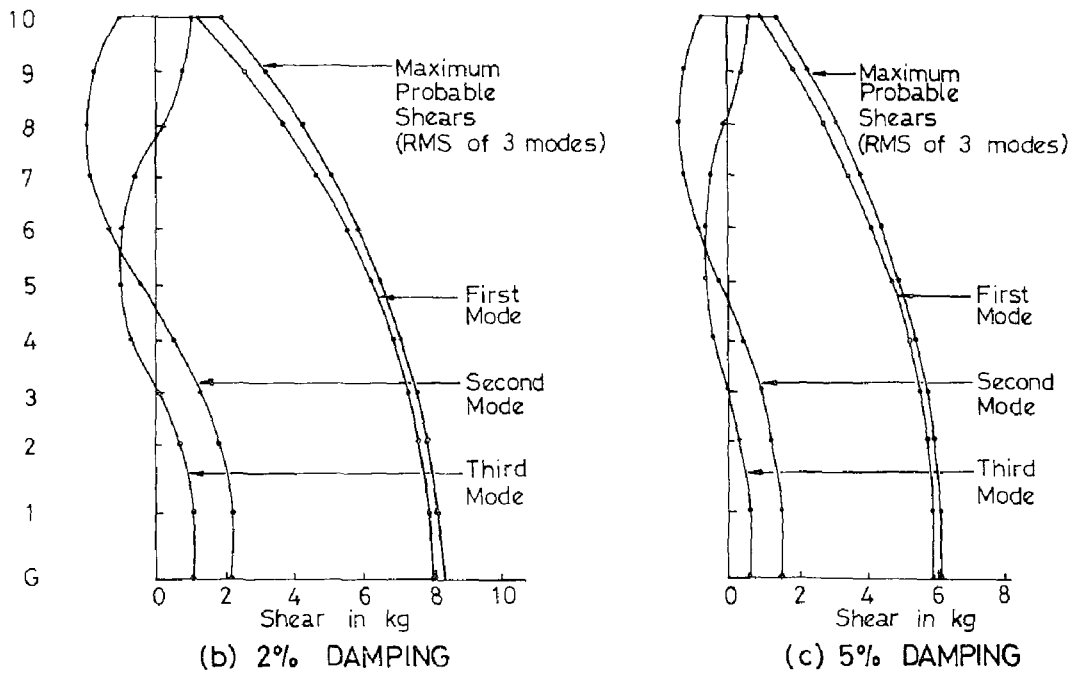
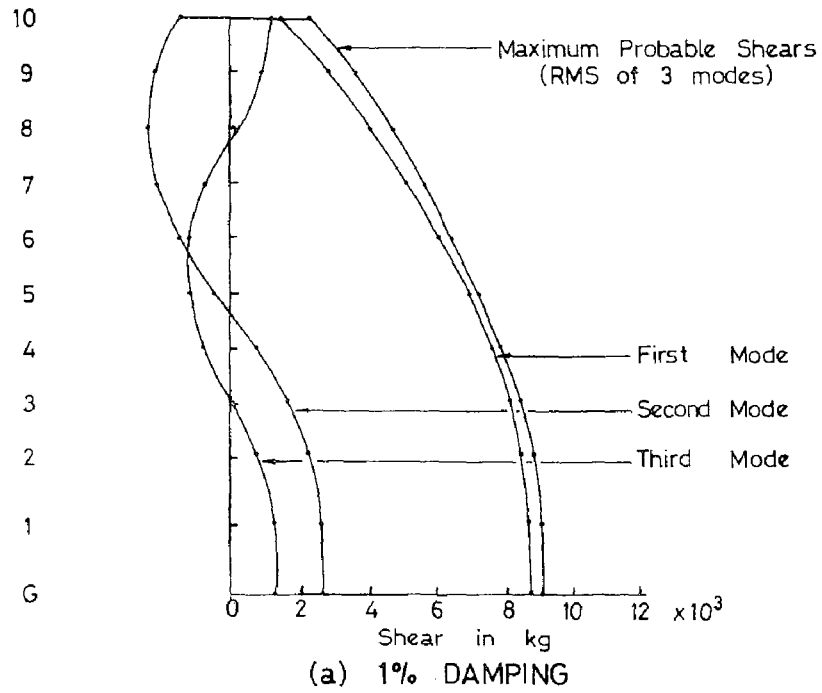


FIG. 3 STOREY SHEARS FOR VARIOUS DAMPING RATIOS

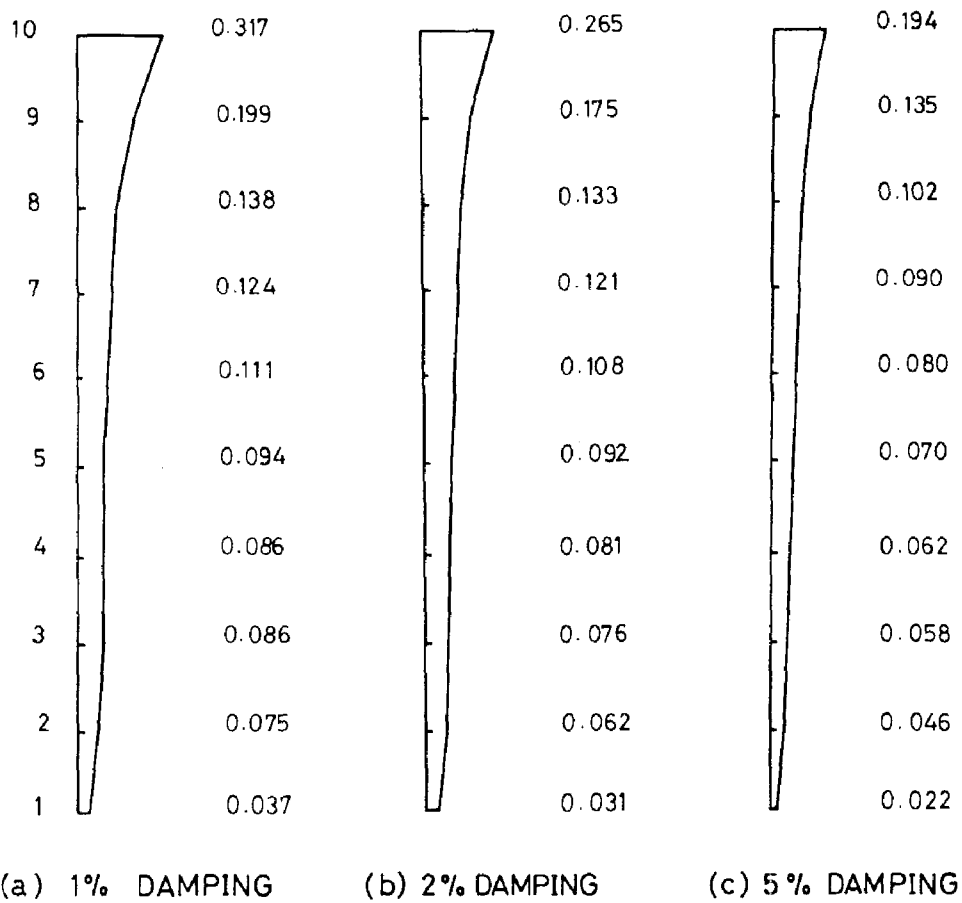


FIG. 4 LATERAL FORCE COEFFICIENTS FOR VARIOUS DAMPING RATIOS

INTERNATIONAL SYMPOSIUM ON
EARTHQUAKE STRUCTURAL ENGINEERING

83

St. Louis, Missouri, USA, August, 1976

DEVELOPMENT IN STRUCTURAL SOLUTIONS OF MULTI-STOREY
SEISMICPROOF FRAMELESS BUILDINGS OF IN-SITU REINFORCED
CONCRETE IN USSR

M.E.SOKOLOV, Techn.M,

Yu.V.GLINA, Dipl.Eng.

TSNIIEP zsilischa
Moscow, USSR

SUMMARY

The report deals with the main preconditions of in-situ housing development in seismic regions of the USSR as well as with a short survey of the subject. The paper includes the principal structural solutions of in-situ seismicproof buildings of frameless type: structural schemes, walls, floor slabs, methods of reinforcement.

The experience in the field of designing of such buildings is described too, particularly, static and dynamic calculations.

INTRODUCTION

In the USSR the construction of public and residential frameless buildings with the application of in-situ reinforced concrete using modern industrial methods has been carried out since the mid-sixties. The construction is preconditioned by a number of social-economic, architectural-town planning and technical requirements.

Population growth in big towns and new settlements demanded a comprehensive and efficient land use. It has entailed higher buildings in towns and variety in town-planning and architectural solutions for civil construction.

In seismic regions, besides the above-mentioned factors, the problems of seismic stability and durability of buildings in combination with economical consumption of building materials and capital investments are of primary importance.

In view of the fact that frameless in-situ buildings possess high bearing capacity, spatial rigidity and stability they meet the above requirements to a greater degree than other buildings.

At present in-situ construction is carried out on a wider scale in towns located in seismic regions.

In the European part of the USSR the following town-

resorts can be presented as an example: Sochi, Yalta; Kishinev and Baku, the capitals of the Union Republics; in the Asian part of the USSR - Alma-Ata, Dyushambe, Ashkhabad, Frunze - the capitals of Union Republics too. Reinforced concrete in-situ construction is under way in such towns as Erevan, Tashkent and other towns of the USSR.

Owing to a wide range of plastic and structural properties of in-situ concrete, some completed buildings are designed with expressive architectural and spatial forms, thus, performing the role of town-planning focal points.

15-storey sanatorium "Actor" and 14-storey residential buildings in Sochi, 16-storey residential buildings in Baku and Kishinev as well as 25-storey hotel in Alma-Ata are the most interesting designs from architectural and structural point of view.

STRUCTURAL SOLUTIONS

In-situ and precast - in-situ frameless buildings are designed according to the following structural schemes:

- with in-situ bearing internal and external walls in longitudinal and transverse direction;

- with in-situ bearing internal walls in longitudinal and transverse direction and with external curtain walls out of panels or large-size blocks.

The buildings of the first structural scheme are characterized with high seismic stability and, thus, being more universal, they can be erected in regions with seismic force from 7 up to 9 points, in future it is expected they are to be constructed in areas with seismic force - 10; the buildings of the second structural scheme are aimed for regions with seismic force - 7 and 8.

Industrial methods with the application of repeatative forms and shuttering are employed for in-situ construction.

As a rule, for buildings of the first scheme slip-forms or large-size shuttering (boards) are used; for the second scheme progressive shuttering (tunnel) is practiced.

One of the most important factors of seismic structural designing is the choice of material for bearing walls. At the beginning a heavy concrete was used for in-situ walls, as a rule, and external in-situ walls were three-layered: internal bearing layer, insulating layer (pads) external protective layer. This solution leaves much to be desired from technological point of view: considerable labour expenditure;

difficulty in ensuring the stability of insulation and the designed thickness of the bearing layer.

The application of structural thermal insulating concretes based on porous artificial aggregates (keramzite, agloporite) has come into common practice in current in-situ housing. From one side it allows to reduce the weight of a building and, accordingly, the value of inertia loads under seismic effects, and from the other side it permits to simplify the structure of external in-situ walls and the technology of their erection. The keramzite concrete buildings were constructed in Alma-Ata and Baku and agloporite concrete buildings - in Dyushambe. The specific weight of concrete based on light aggregates, in completed buildings makes up from 1400 up to 1800 kg/m³ with prism concrete strength being 205 kg/cm².

Experimental investigations are under way aimed at reducing specific weight of porous aggregate concretes owing to optimum composition of concrete mortar and proper granular size of aggregates. At the same time the improvement of strength properties is in the scope of research.

External bearing walls are assembled out of large-size blocks or panels. Blocks and curtain panels are made, as a rule, out of thermal insulating concretes based on artificial or local porous aggregates. The specific weight of such concretes amounts from 800 kg/m³ up to 1200 kg/m³ depending upon the weight of aggregates particularly upon the weight of small-size granulars.

Considerable reduction in weight of buildings can be obtained when asbestos cement curtain panels with effective thermal insulating layer are used for external walls.

In some regions with certain local raw materials being available or where the manufacturing of such panels are efficient from economical point of view the application of such panels in in-situ construction is being investigated and preparatory work is in a full swing.

The following types of floor slabs are employed: precast, precast - in-situ or in-situ. Precast floor slabs are room-size panels with wall spacing being up to 3.6m or they are cavity slabs with prestressed reinforcement with wall spacing being up to 6.3m.

Precast - in-situ floors consist of two parts: precast slab and in-situ reinforced concrete. In-situ floor slabs are structurally interconnected with walls with the help of projections in certain areas (slip-form method) or continuous ties are provided along the contour ("tunnel" method).

The experience has shown that in-situ floor slabs are more preferable from structural point of view as it allows to ensure the designed rigidity of floor slabs in their plane with less material expenditure and without additional measures connected with concreting the dowels and with welding the inserts required in precast floor slabs.

The reinforcement of in-situ walls and floor slabs consists of flat welded frames, nets and spatial frames. Reinforcement elements are made at special plants. As a rule for working reinforcement of walls, hot-rolled steel of high rigidity with rated resistance - 3400 kgf/cm^2 is used, for floor slabs cold-drawn reinforcement wire with rated resistance - from 2500 up to 3150 kgf/cm^2 is employed. Hot-rolled reinforcement steel with rated resistance 2100 kgf/cm^2 is practiced for manufacturing reinforcement.

While designing vertical in-situ diaphragms, special attention is being paid to the reinforcement of the most important elements - lintels and the joints between the lintels and the walls as well as to the reinforcement along door and window openings. Strength tests have proved, particularly, the efficiency of evenly distributed reinforcement of lintels.

All seismic calculations of in-situ buildings are performed on the basis of dynamic theory of seismic stability developed and adopted in the USSR. Automatic programmes calculated with the help of computers "Minsk-22" "M-222" and other have come into common use. The programmes are developed by the following Institutes: TSNIISK, TSNIIEP zsilischa and KievZNIIEP.

At present certain methods allowing exact determination of spatial behaviour of in-situ frameless structures are considered to be very perspective, particularly, the method based on the theory of "thin-walled rods". At the same time the methods of "approximate calculations" are investigated as well, they are intended for evaluation of seismic loads and bearing capacity of buildings at the early stage of designing.

While calculating and designing in-situ seismicproof buildings, laboratory and field results are taken into consideration. Field tests of 13 and 16-storey precast - in-situ buildings in Kishinev carried out by TSNIIEP zsilischa are of special interest.

B I B L I O G R A P H Y

1. Altshuller E.M., Bondard Ja.P., Glina Y.V., Rudoy V.M., Tsirik Ja.I. Industrial in-situ housing in large cities in the USSR. Moscow, GOSINTI, 1975
2. Lishak V.I. Modern methods of horizontal loads calculation for frameless buildings. Moscow, TSNTI, Gosgrazhdanstroy, 1972.
3. Sokolov M.E., Agronovskiy V.D. Strength and crackresistance of r.c. lintels of panel walls under transverse forces. "Concrete and reinforced concrete", 1971, N 11.

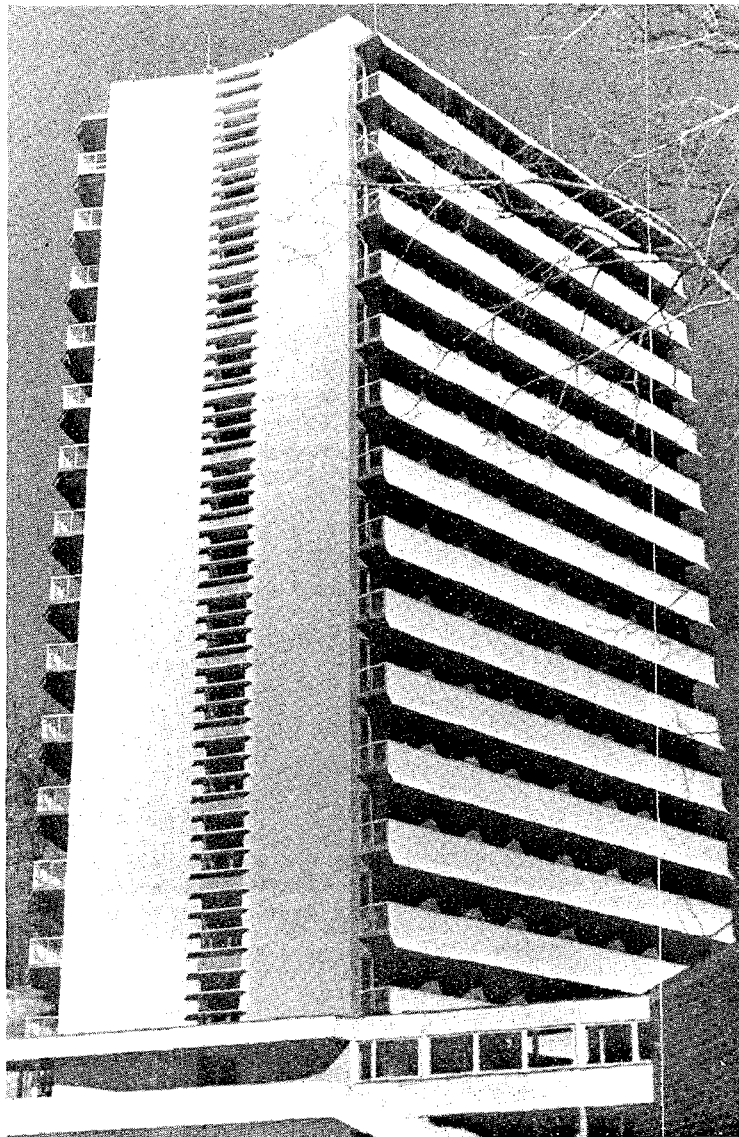


Fig. 1. 15-storey sanatorium in Sochi

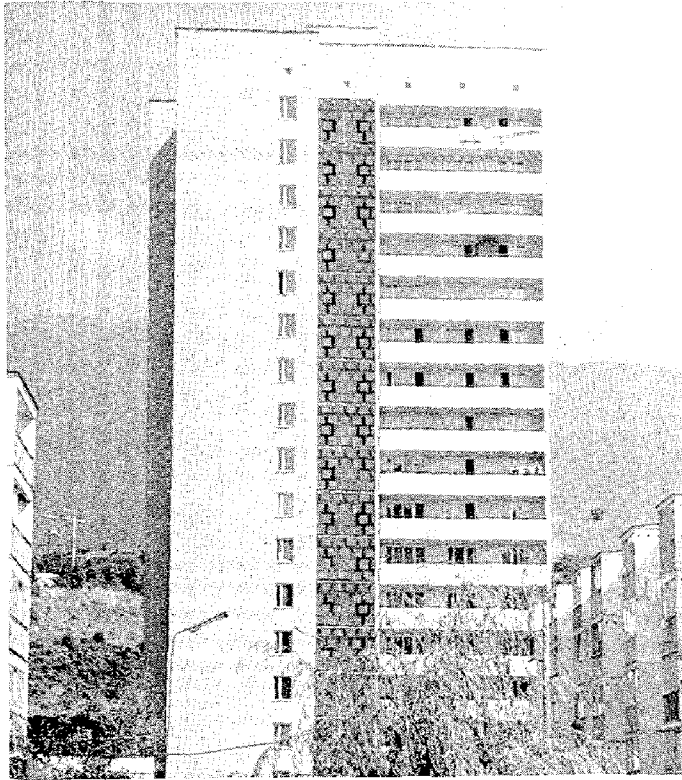


Fig.2. 16-storey resi-
dential building
in Yalta

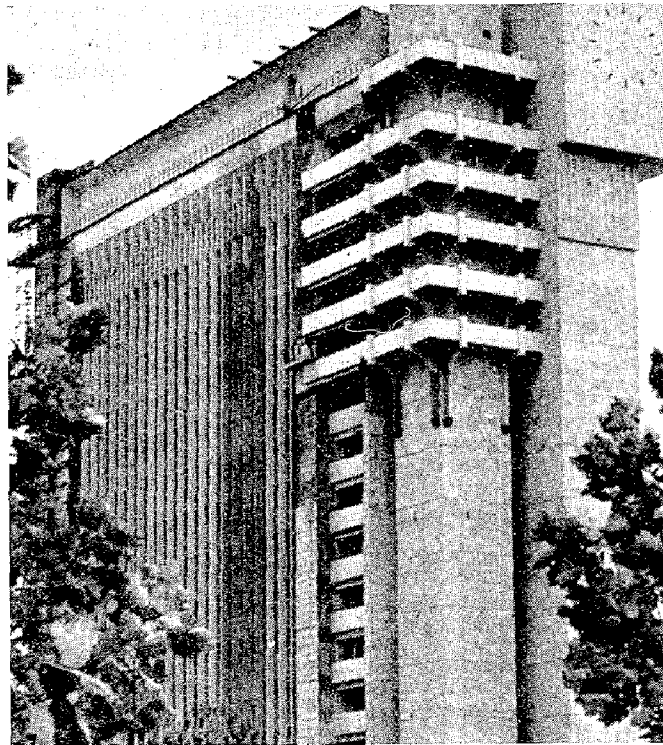


Fig.3. 18-storey ad-
ministrative
building in
Tashkent

INTERNATIONAL SYMPOSIUM ON
EARTHQUAKE STRUCTURAL ENGINEERING

91

St. Louis, Missouri, USA, August, 1976

THE INELASTIC SEISMIC RESPONSE OF BRIDGE STRUCTURES

RICHARD D. SHARPE^I and ATHOL J. CARR^{II}

^I Engineer, Beca Carter, Hollings & Ferner, Consulting Engineers,
Auckland, New Zealand.

^{II} Senior Lecturer, Department of Civil Engineering, University
of Canterbury, Christchurch, New Zealand.

SYSNOPSIS

This paper describes the application of an inelastic dynamic analysis of two very different bridge structures subjected to an earthquake excitation. The paper discusses the effects on the response of the structures of variations in the moment-curvature relationships of the piers and also the effects of the interaction of the axial forces in the members with the yield moments.

INTRODUCTION

Bridge structures differ from the usual building structures in that structures are usually very simple and that when they enter the inelastic range there is very little opportunity for a redistribution of member forces. Further, it is possible that the bridge structures may readily form dynamic collapse mechanisms upon the formation of only a small number of inelastic regions within their structural systems.

An inelastic dynamic analysis program is used to analyse bridge structures for arbitrary seismic excitations. The analysis allows for the interactive effects of the member axial forces on their yield moments and also permits the choice of three possible moment-curvature relationships.

The first example is a continuous multi span bridge which is provided with seismic gaps at the central pier and at the abutments and the initial aim of the analysis was to determine the necessary widths of these gaps to prevent hammering between the sections of the bridge and its abutments. The second structure is a tall reinforced concrete bridge pier, together with its supporting pile cap and piles, the pier being one of several supporting a multispan, box girder bridge. The effects of the axial-force moment interaction are important in the inelastic response of the pile system and the consequences of the different

Preceding page blank

movement-curvature relationships are studied.

THE METHOD OF ANALYSIS

The method of analysis and the computer program used for these analyses is due to Sharpe (5) which was developed for the dynamic analysis of two dimensional framed structures of arbitrary geometry and for an arbitrary time-history of seismic loading in both horizontal and vertical directions.

THE FRAME MEMBERS

For the purposes of this program it was essential that the beam-model should be such that its critical sections had the ability to track any generalized moment-curvature function. In particular, the Ramberg-Osgood (4) curvilinear hysteretic function and the standard bi-linear function - a special case of the latter being the elastic-perfectly plastic hysteresis.

As the emphasis was being placed on inertia loading of the structure, it was not considered necessary to make provision for the loading of the framed members with loads distributed along their length, such loadings, should they arise, are easily accommodated by the provision of joints along the member. The critical sections of all members occur at their interfaces with other members. To achieve this modelling rigid end-blocks are located between these interfaces and the modelled joints at the intersection of the member centrelines.

A suitable model, which has to simulate the correct moment-rotation and axial stiffness characteristics at these interfaces, is that due to Gibbertson (3). It is, simply, a one-dimensional prismatic beam with sprung hinges incorporated at the critical sections. By varying the rotational spring stiffnesses, it is possible to model the full range of situations, from that of a pinned end to one in which the beam is linearly elastic along its entire length.

The theoretical discontinuity of slope, which occurs at the critical sections of the beam-model, extends over an infinitely small length, whereas the plastic hinge length in the real beam has a length which varies with both the amount of curvature and the type of material. To relate the rotation of the theoretical hinge to the real plastic curvature, a constant hinge length for the beam member is supplied together with the other data on the members section properties.

The interaction between the axial force and the bending moments affects the yield moment behaviour of such members at columns in buildings and piers and piles in bridge systems and this is allowed for which the yield interaction diagram shown in figure 6.

THE STRUCTURES STIFFNESS, MASS AND DAMPING MATRICES

Once the stiffnesses of the individual member stiffnesses have been determined the stiffness matrix of the entire structure is assembled by the Direct Stiffness method. At the same time the mass matrix, of either the "Lumped" or "Consistent" [1] form, and the damping matrix are formed.

The damping matrix is obtained by the method proposed by Caughey [5] and is a combination of proportions of both the mass and stiffness matrices of the structure, the proportions being determined so as to provide a specified percentage of critical damping at each of two specified frequencies. These frequencies may be supplied as input data or taken as the first two natural frequencies of free-vibration of the linear elastic structure.

TIMEWISE INTEGRATION OF THE EQUATIONS OF MOTION.

The equations of motion for the structure are integrated, for equalised time steps, by a step by step integration method [7] where the accelerations are assumed to be constant during the time step, the method having been shown to be stable and accurate [6].

At the end of each time step the equilibrium of the critical sections of each member is checked and the stiffnesses adjusted accordingly. If, due to a change in stiffness, member equilibrium is no longer satisfied, the out of balance of these member forces is corrected during the next time step.

To improve interpretation of the results from the analysis, every time step in which the location of plastic hinges changes within the structure, a picture, showing all plastic hinges is printed together with any tabulated output.

THE DURHAM STREET RAILWAY OVERBRIDGE

The Structure

The bridge deck, simply-supported on piers formed on piles driven into alluvial material, will carry traffic over a series of main-trunk railway tracks. Built of reinforced and prestressed concrete in two sections with artificially-constructed approach embankments. In order that the two deck sections, when excited by an earthquake, should neither hammer each other nor be interfered with by the abutments, an attempt was made to predict a width for the three seismic- and expansion-gaps incorporated in the structure.

The idealization

The bridge was reduced to the centre-line frame depicted in figure 1. An initial assumption was made that the deck would not lift off any of its supports. The model sliding bearings, are idealized to the extent that they allow infinite movement in a horizontal direction. The seismic gap necessary in the real structure, is then at least the peak-to-peak amplitude of the relative motion. The deck, being simply-supported at the top of the piers, did not require the possibility that it might develop plastic hinges to be considered.

Equivalent viscous damping was set at five per cent of critical for the first two modes and Initial-condition moments due to shrinkage, temperature and creep were supplied by the designers as were yield moments for the bases of the piers

The analyses

The left and right halves of the bridge were found to have undamped natural frequencies of 2.789 and 2.879 Hz, respectively.

A purely elastic dynamic analysis was performed using the first ten seconds of the North-South and vertical components of the El Centro, May 18, 1940 earthquake which was scaled, at the request of the designers to give a maximum horizontal ground acceleration of 0.23 g. The displacement responses of the two halves, measured horizontally at the top of the central pier and with respect to the ground, are shown plotted in figure 2a. The initial displacements, due to the initial moments introduced to represent the effects of shrinkage in the prestressed deck, have been eliminated from the plot (figure 3a) of the relative displacements of the two decks. Hence, the gap required between the deck sections is the 'dynamic' gap alone.

The second analysis attempted was of a non-linear type, with only the columns being permitted to develop perfectly plastic hinges at their bases when the predicted yield moments were reached. For a collapse mechanism, it is only necessary for all the piers of either half of the bridge to yield at ground level. However, this is not a sufficient condition for a dynamically excited structure to become unstable and collapse. Recovery is possible if an incremental ground acceleration in the prevailing direction of collapse causes the supports to catch up with the collapsing deck.

With the same earthquake as used in the elastic analysis, the left half of the bridge formed a collapse mechanism after 1.72 seconds, followed by that of the right at 1.99 seconds. Both halves recovered briefly from this state before finally entering their respective collapse mechanisms at 2.20 and 2.15 seconds of

earthquake. The corresponding horizontal deflections of the decks at these latter times were -14.6 and 11.2 mm.

To confirm that the previous analysis had, by chance, shown the bridge just reaching the sensitive critical stage, a further analysis, using the same yield moments and earthquake, was implemented. The moment-curvature relationship at the pier bases was changed to that of a bi-linear hysteretic function in which the initial section remained the same as before. The second branch of the function was allocated a slope of ten per cent of the initial stiffness, in an attempt to simulate approximately the residual stiffness at a section. As a result, both bridge-sections again reached the stage where all the pier-bases had plastic hinges present concurrently, but catastrophic collapse was prevented from occurring by the presence of the small residual stiffness. Figures 2b and 3b show this response, both as a plot of the concurrent deck displacement and of the relative deck movement. A summary is given in table 1. The maximum section ductility recorded at any of the pier-bases was approximately 6 - which indicates that only moderate yielding took place.

Both sides of the bridge experienced some permanent drift which tended to widen permanently any seismic gap incorporated at the time of construction. If the earthquake's direction was reversed it might have been of the opposite effect. The real structure is not in as much danger of total collapse under the design earthquake as these initial analyses tend to indicate. The need for continuity in the road surface would ensure that further restraints on the horizontal movement of the deck would be imposed if a sufficiently severe earthquake was encountered. The inclusion of restraining devices, such as rubber buffering and sacrificial shear pins, would, if the abutments did not collapse, significantly decrease the response.

The permanent plastic horizontal drift, which is becoming apparent in the last five seconds of the non-linear response, is significant if the possibility of an eventual failure, due to repeated stress-relief and incremental collapse, is to be considered. A purely elastic analysis, on the other hand, will give no indication of the permanent drift likely.

THE AUCKLAND UPPER HARBOUR CROSSING

The structure

This provides a good example of a bridge structure in which there are very few members or places at which energy-absorption, through plastic work, can take place. The analysis is that of pier 'five' - in a direction perpendicular to that of the bridge axis, and is probably the most critical of those supporting the bridge deck. The structure, figure 4, consists of a hollow, thin-walled, reinforced concrete pier which supports the box-girder deck. The pier is mounted on an almost square and relatively inflexible pile-cap which is, in turn, supported by four identical

circular piles driven vertically for some distance into the harbour floor. The first ten seconds of the North-South and vertical components of the El Centro, May 18, 1940 earthquake accelerogram were used for all the analyses on this structure.

The idealization

The symmetrical nature of the plane-frame model of the pier enabled the four piles to be analytically replaced by two with twice the individual strength. The program could have coped with two co-linear pairs of members, but this would have unnecessarily introduced extra kinematic degrees of freedom and members. The assumption that the pile-cap was infinitely stiff meant that the horizontal degrees of freedom associated with the tops of the piles and the bottom of the pier could all be coupled together. To further stiffen the pile-cap, the associated rotations were also coupled. This latter coupling implies that the rotations will be identical at the relevant nodes and the rotational masses summed and made to act on one common degree of freedom. The ability of the program to handle rigid end-blocks meant that the considerable differences between the interfaces and the centre-line intersections could be accounted for in both the stiffness calculations and the positioning of the possible plastic hinge sections. Both horizontal, vertical and rotational mass was lumped at the intersections of all members. The basic moment-curvature relationship employed was elasto-plastic in form. Damping was ten per cent of critical for the first two modes, whose natural frequencies of free vibration were 0.65 and 3.4 Hz respectively.

The analyses

Three different analyses were carried out. They were...

- a) an elastic analysis,
- b) an elasto-plastic analysis in which the critical sections had only one constant value for the yield moment,
- c) an elasto-plastic analysis in which the moment - axial load interaction criteria was permitted to control the ultimate strength of the vertical members.

The horizontal displacement responses of the deck (figure 5) in the three analyses illustrate how the formation of the plastic hinges has allowed sufficient energy to be absorbed to reduce noticeably the deck displacement. This is particularly evident in the last four seconds of the responses. The maximum non-linear response was decreased by approximately seven per cent. Examination of the printed time-history showed that significant plasticity was not encountered until after 5.4 seconds of the earthquake. The effect of the energy-absorption did not show up in the plotted response (figure 5) until its next peak at about one second later - even though the former peak was also that at which the maximum response occurred.

The sensitivity of the structure to a changed criteria for the development of plastic hinges can be seen by an inspection of the differences in response between that using the obviously more correct moment - axial load interaction criteria and that in which the members' yield moments were fixed at a constant value. The response for the latter of these two cases (figure 5c) shows a very marked curtailment in the response after about seven seconds of excitation, resulting in the appearance of a significant permanent drift of the same magnitude as the curtailment.

An examination of the moment - axial load histories for the critical section at the top of the left-hand pile (figure 6) shows how the need for the interacting yield criteria. The overall geometry of the structure results in the bending moment in the piles being an almost linear function of the axial load. The heavily banded nature of the graphed relationship confirms this, the vertical width of the band reflecting the response of the bridge-deck and pile-cap to the vertical component of the earthquake. The imposition of either type of yield criteria on the pile moments is seen to be not very severe in the case of this excitation. In the absence of the ability for the yield criteria to be stipulated in terms of such interaction curves, provided that a linear prediction could be made (as in the case of these piles), a simple calculation would seem to be sufficient for an estimation of single positive and negative yield moments.

The moment - axial load interaction for the pier member's base section is similarly very strongly banded, but differs from that of the piles in that the imposed yield criteria is much more severe. It can be seen that the choosing of more accurate single yield moments for the non-interaction analysis should, because of the narrow banding of the actual path of the moment - axial load response, give results which are similar to those of the analysis which had an interactive capability.

In order to confirm this a fourth analysis, incorporating these modified yield moment values, was carried out. Yield moments of 6.51×10^6 N m for the double pile and 25.1×10^6 N m for the pier were specified. These were, approximately, ten per cent smaller than those for the previous similar analysis (i.e. analysis b.). When compared to the analysis, the ductility required doubled for an increase in maximum horizontal deck displacement, from 95.7 mm to 108 mm. The permanent drift, estimated from the apparent offset of the response after ten seconds of excitation, more than doubled. A comparative summary is given in table II.

The sensitivity of the structure to small changes in the member yield criteria is understandable when it is realized that the dynamic system is working in the region of a boundary condition plateau - namely, the yield criteria. The small number of members means that the loss of incremental stiffness at one or two critical member sections proportionately alters the total incremental stiffness of the structure much more significantly

much more significantly than the same number of changes in, for example, a ten-storey, four-bay frame with ninety members.

The only time that a collapse mechanism formed in the piles was after 5.54 seconds in that analysis in which the re-calculated yield moments were used instead of an interaction criteria. It was present for only 0.04 seconds. However, the formation of a plastic hinge at the base of the pier member also constitutes a collapse mechanism - this being observed in all the inelastic analyses. Again, this hinge was never present for any significant length of time.

CONCLUSIONS

Both bridge structures are seen to be sensitive to the characteristics of their plastic hinges. The nature of the differences between the linear and non-linear responses is not predictable because of this sensitivity. It is interesting to note that the formation of a potential collapse mechanism in a structure is a necessary (but not sufficient) condition for a failure under dynamic loading. In both cases, the analyses benefitted the designers by showing them the range in which they could expect their structures to respond if modelled with non-linear elements.

REFERENCES

1. Archer J.S., "Consistent Mass Matrix for Distributed Mass Systems" Journal of the Structural Division, ASCE, Vol. 89, No. ST4, Proc. Paper 3591, August 1963, pp, 161-178.
2. Caughey T.K., "Classical Normal Modes in Damped Linear Dynamic Systems" Journal of Applied Mechanics, ASME, Vol. 27, No. 2, Paper 59-A-62, June 1960, pp 269-271.
3. Giberson M.F., "Two Nonlinear Beams with Definitions of Ductility", Journal of the Structural Division, ASCE, Vol. 95, No. ST2, Proc. Paper 6377, February, 1969, pp 137-157.
4. Kaldjidu M.J., "Moment Curvature of Beams as Ramberg-Osgood Functions" Journal of the Structural Division, ASCE, Vol. 93. No. ST5, Proc. Paper 5488, October 1967, pp 53-65.
5. Sharpe. Richard D., "The Seismic Response of Inelastic Structures" Ph.D. Thesis, Department of Civil Engineering, University of Canterbury, November, 1974.
6. Sharpe R.D., and Carr A.J., "A Stable Integration for Nonlinear Dynamic Analyses" Computational Methods in Nonlinear Mechanics, Texas Institute for Computational Mechanics, University of Texas at Austin, Texas. September, 1974, pp 777-786.
7. Wilson E.L., and Clough R.W., "Dynamic Response by Step by Step Matrix Analysis" Symposium on use of Computers in Civil Engineering", Laboratoria Nacionalde Engenharia Civil, Lisbon, Portugal, October, 1962.

	Elastic analysis		Bi-linear analysis	
	Left deck	Right deck	Left deck	Right deck
Natural frequency of undamped fundamental mode (Hz)	2.789	2.879	2.789	2.879
Maximum deck displacement (horizontally) (mm)	20.2	18.3	23.1	25.4
Maximum amplitude of deck displacement (mm)	38.4	36.1	58.0	38.9
Maximum relative displacement of deck ends (mm)	11.5		25.0	
Maximum seismic gap required to prevent butting (mm)	5.9		9.4	

TABLE 1: SUMMARY OF RESULTS FOR DURHAM STREET RAILWAY OVERBRIDGE

	Maximum horizontal deck displacement (mm)	Maximum horizontal pile-cap displacement (mm)	Maximum plastic rotation of hinge of pier base (rads)	Maximum plastic rotation of hinge at top of left pile (rads)	Estimated permanent horizontal drift of deck (mm)
a) Elastic analysis	102	49.7	-	-	1
b) Elasto-plastic with no interaction	95.7	-46.3	-1.53×10^{-3}	3.66×10^{-4}	30
c) Elasto-plastic with interaction	-94.8	-46.6	-0.73×10^{-3}	4.39×10^{-4}	8
Elasto-plastic (no interaction) revised yield values	108	-49.7	-3.6×10^{-3}	8.30×10^{-4}	64

TABLE II: SUMMARY OF RESULTS OF ANALYSES OF PIER 5, TRANSVERSE DIRECTION, AUCKLAND UPPER HARBOUR CROSSING.

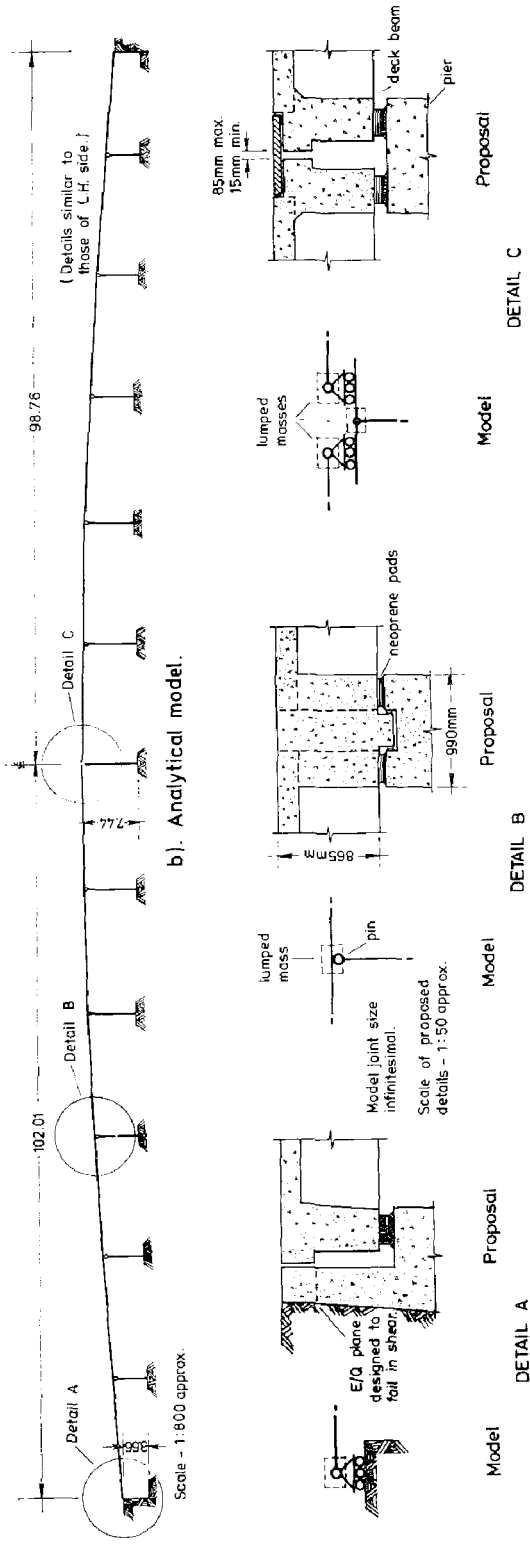
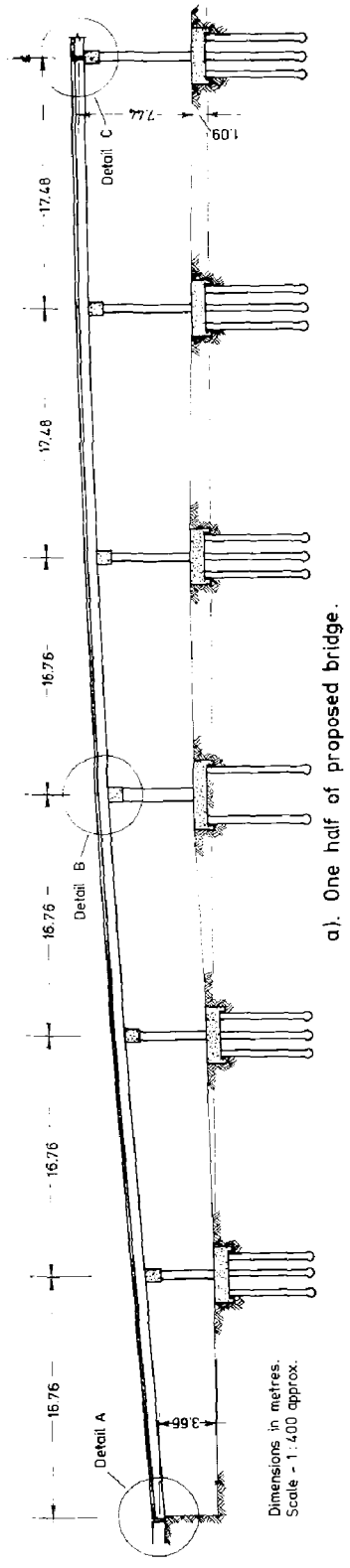


FIGURE 1 : DURHAM STREET RAILWAY OVERBRIDGE, CHRISTCHURCH.

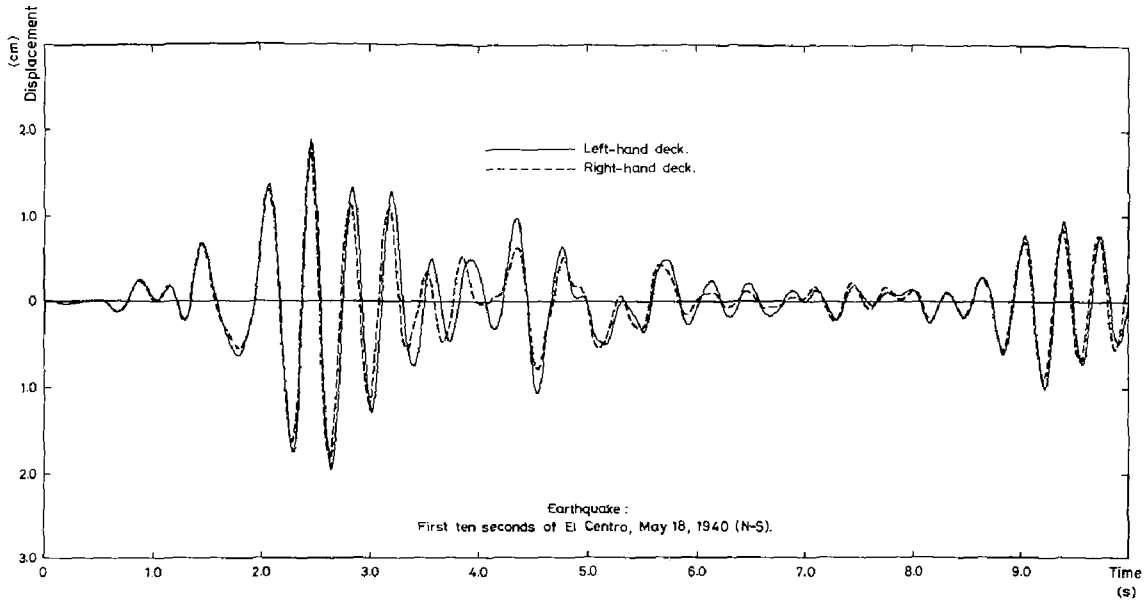


FIGURE 2a : HORIZONTAL DISPLACEMENT RESPONSES OF RAILWAY OVERBRIDGE DECKS - ELASTIC.

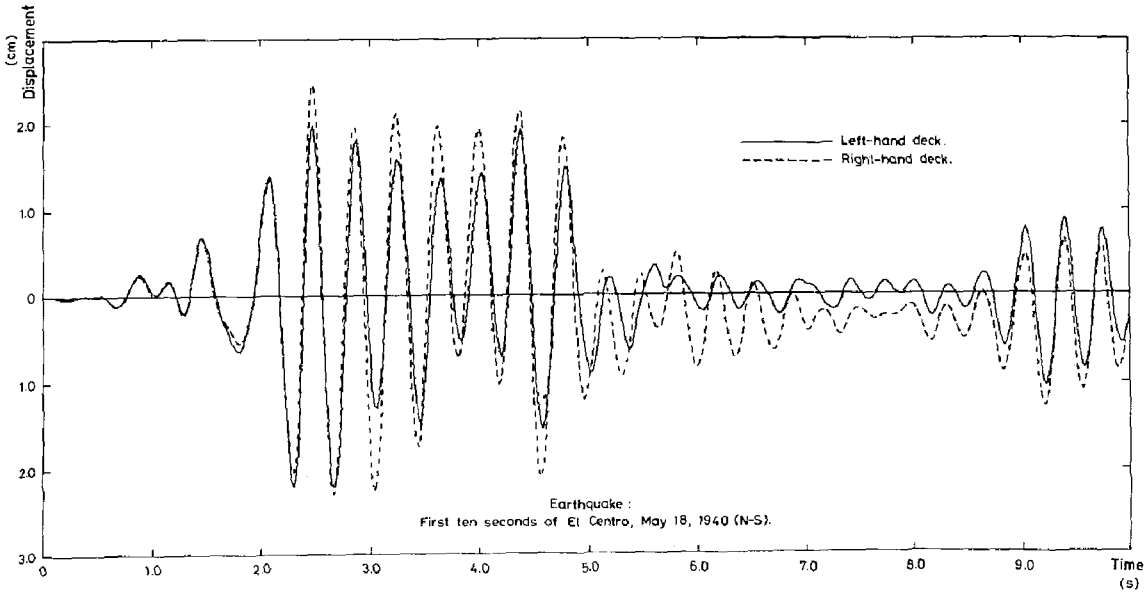


FIGURE 2b : HORIZONTAL DISPLACEMENT RESPONSES OF RAILWAY OVERBRIDGE DECKS - BI-LINEAR.

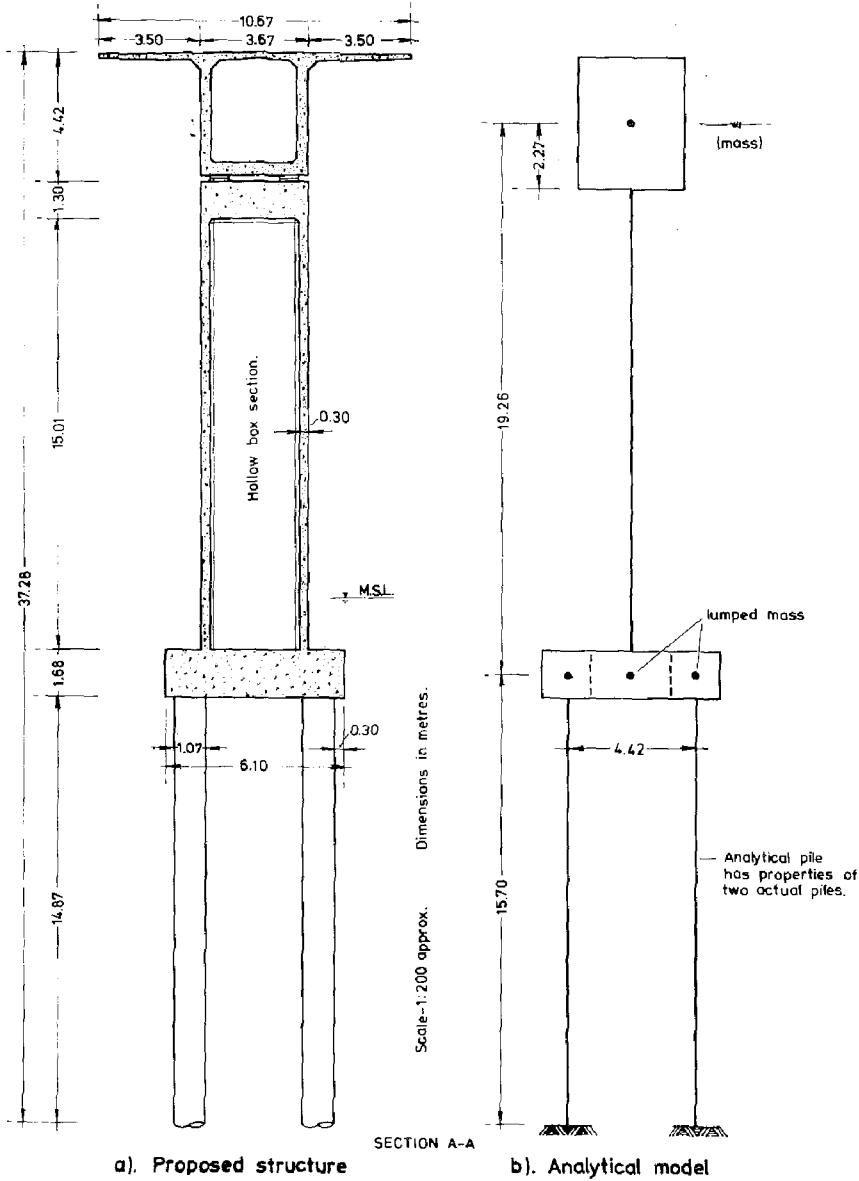
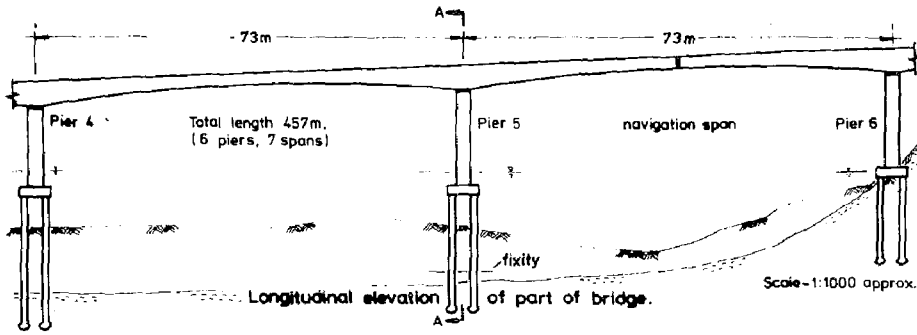


FIGURE 4 : AUCKLAND UPPER HARBOUR CROSSING - PIER 5.

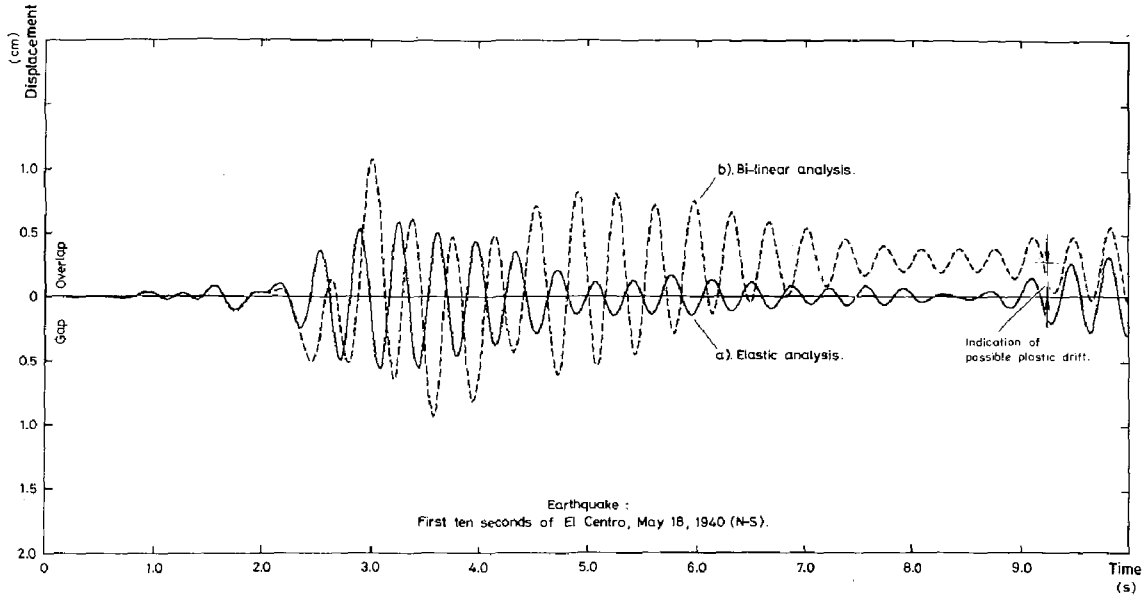


FIGURE 3 : RELATIVE HORIZONTAL DISPLACEMENT RESPONSES OF RAILWAY OVERBRIDGE DECKS.

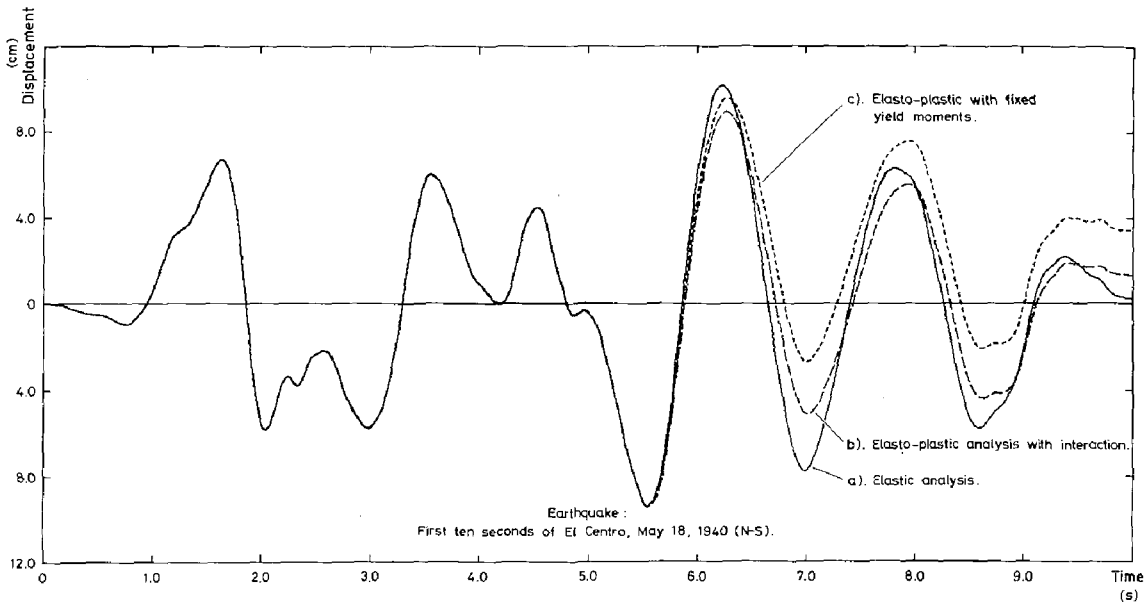


FIGURE 5 : HORIZONTAL DISPLACEMENT RESPONSES OF HARBOUR-CROSSING DECK.

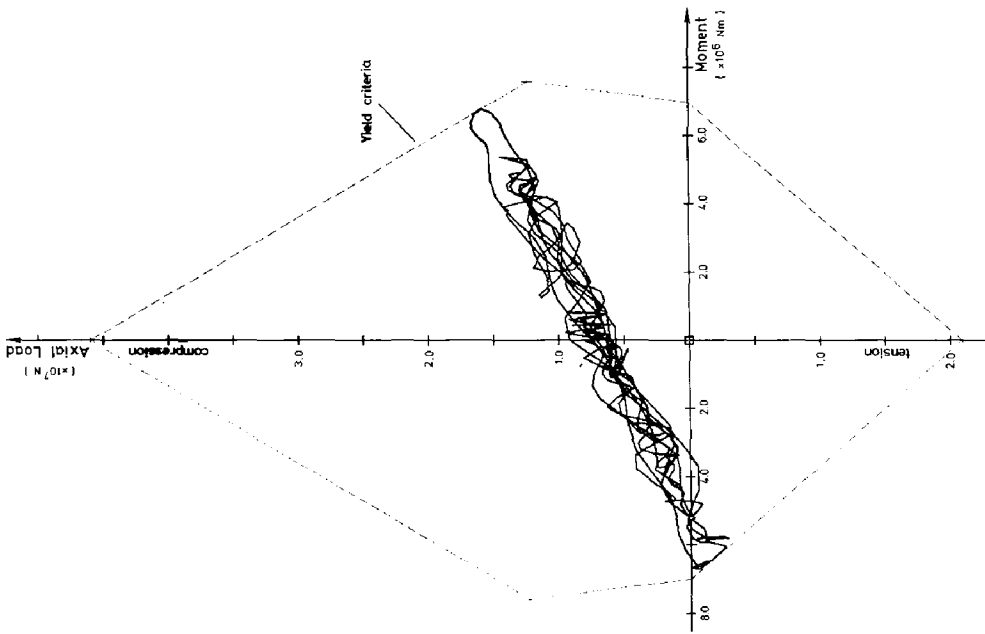


FIGURE 6 : MOMENT - AXIAL LOAD HISTORIES AT TOP OF LEFT-HAND PILE.
ELASIO-PLASTIC WITH INTERACTION.

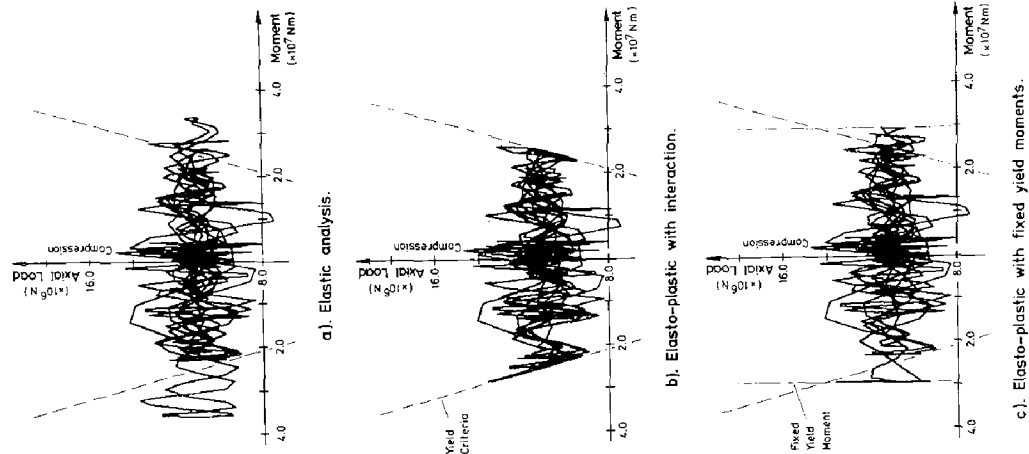


FIGURE 7 : MOMENT - AXIAL LOAD HISTORIES AT BASE OF PIER.

INTERNATIONAL SYMPOSIUM ON
EARTHQUAKE STRUCTURAL ENGINEERING

107

St. Louis, Missouri, USA, August, 1976

EFFECT OF COUPLING EARTHQUAKE MOTIONS ON
INELASTIC STRUCTURAL MODELS

FRANKLIN Y. CHENG¹ and KENNETH B. OSTER²

1. Professor 2. Research Assistant

Department of Civil Engineering, University of Missouri-Rolla
Rolla, Missouri U. S. A.

SUMMARY

Response parameters have been studied for two structural models subject to the coupling earthquake motions of the vertical and horizontal components of the 1940 El Centro. Bilinear material behavior, P-delta effect, damping, and the reduction of plastic moment capacity have been considered in the investigation. The structural models are lumped mass in nature. One model has masses lumped at structural joints, and the other has additional nodes at the centers of individual girders. Structures analyzed consist of a 4-story-3-bay and a 10-story-single-bay rigid frame. The results show that the model containing nodes at girder centers can realistically reveal the effect of coupling earthquake motions on structural systems and that the significance of a vertical earthquake component depends on the structural parameters. The observation is based on a comparison of displacement response, energy absorption, and the ductility and excursion ratios of the systems analyzed.

INTRODUCTION

The effect of parametric excitation on structural response and stability was described by Cheng [1] in 1974. Cheng and Oster recently published a report on the effect that vertical earthquake motion has on the dynamic response of elastic structures with various natural frequencies [2]. It is obvious that the inclusion of the vertical earthquake component is essential in exemplifying the real behavior of a structural system. However, the structural model used in such an analysis should provide a sufficient means for adapting the effects of this inclusion. The purpose of this report is to show the effect of vertical earthquake motion on two lumped mass models. The response parameters used for comparison are the maximum horizontal floor displacements, maximum relative horizontal floor displacements, maximum vertical floor displacements, energy absorptions, and ductility and excursion ratios.

Model 1 is the traditional spring-mass system in which the mass of each floor is lumped at the joints connected by columns and girders. The floor mass consists of girder weight, superimposed mass, and the half weight of the columns located above and below the floor. Model 2 is similar to Model 1 except one additional node is assumed at the center of each girder. The mass lumped at the

Preceding page blank

girder node is half of the floor mass distributed on the member.

FORMULATION OF MOTION EQUATION

The motion equation for a multidegree system includes viscous damping, P-delta effect, and both horizontal and vertical earthquake components. It can be expressed as

$$[M] \{\ddot{x}\} + [C] \{\dot{x}\} + ([K] - [K_s]) \{x\} = -[M] \{\ddot{x}_g\} \quad (1)$$

in which $[M]$ = mass matrix; $[C]$ = damping matrix; $[K]$ = structural stiffness matrix; $[K_s]$ = geometric matrix; $\{\ddot{x}_g\}$ = ground acceleration vector; and $\{\ddot{x}\}$, $\{\dot{x}\}$, and $\{x\}$ = acceleration, velocity, and displacement of the structural nodal coordinates respectively.

For the study of nonlinear structural systems, the numerical integration should be performed on the basis of a stepwise technique for which the motion equation of Eq. (1) can be written in the following incremental form:

$$[M] \{\Delta\ddot{x}\} + [C] \{\Delta\dot{x}\} + ([K] - [K_s]_{t+\Delta t}) \{\Delta x\} = -[M] \{\ddot{x}_g\} + [\Delta K_s] \{x\}_t \quad (2)$$

in which $\{\Delta\ddot{x}\} = \{\ddot{x}\}_{t+\Delta t} - \{\ddot{x}\}_t$, $\{\Delta\dot{x}\} = \{\dot{x}\}_{t+\Delta t} - \{\dot{x}\}_t$, $\{\Delta x\} = \{x\}_{t+\Delta t} - \{x\}_t$,

$\{\Delta\ddot{x}_g\} = \{\ddot{x}_g\}_{t+\Delta t} - \{\ddot{x}_g\}_t$, and $[\Delta K_s] = [K_s]_{t+\Delta t} - [K_s]_t$. Because earthquake

motions primarily cause linear inertial forces, the rotatory inertial forces associated with lumped masses are relatively small and can be neglected. Thus, the number of linear equations in Eq. (2) can be reduced by solving for the nodal rotations, $\{\Delta x_\theta\}$, in terms of nodal translations as

$$\{\Delta x_\theta\} = -[K_{11}]^{-1} [K_{12}] \begin{Bmatrix} \Delta x_v \\ \Delta x_s \end{Bmatrix} \quad (3)$$

in which $[K_{11}]$ and $[K_{12}]$ are submatrices of $[K]$, and $\{\Delta x_v\}$ and $\{\Delta x_s\}$ are incremental vertical and horizontal displacements respectively. The insertion of Eq. (3) into Eq. (2) results in the final incremental form of the motion equation as shown below:

$$[M] \begin{Bmatrix} \Delta\ddot{x}_v \\ \Delta\ddot{x}_s \end{Bmatrix} + [C] \begin{Bmatrix} \Delta\dot{x}_v \\ \Delta\dot{x}_s \end{Bmatrix} + [K^{11}] \begin{Bmatrix} \Delta x_v \\ \Delta x_s \end{Bmatrix} = -[M] \begin{Bmatrix} \Delta\ddot{x}_g \\ \Delta\ddot{x}_g \end{Bmatrix} + [\Delta K_s] \begin{Bmatrix} x_v \\ x_s \end{Bmatrix}_t \quad (4)$$

in which $[K^{11}] = [K_{22}] - [K_{12}]^T [K_{11}]^{-1} [K_{12}] - [K_s]_{t+\Delta t}$, and $\{\Delta\ddot{x}_g\}$ and $\{\Delta\dot{x}_g\}$ represent incremental vertical and horizontal earthquake components respectively. Newmark's integration technique was formulated for previous work (2, 5) and has been used successfully for this study.

STIFFNESS MATRIX FOR INELASTIC MATERIAL

Material behavior is assumed to be bilinear as shown in Fig. 1 for which the stiffness of a member may be assumed to consist of an elastoplastic component and an elastic component as discussed by Giberson [3]. The structural stiffness matrix, $[K]$, must be modified when one end or both ends of a constituent member become plastic or change from plastic to elastic. The member stiffness corresponding to the four possible deformation stages are given in the recent work of

Cheng and Oster [2]. The plastic moment capacity is reduced according to the interaction equations in the AISC manual [4] for columns and ideal plastic moment is used for girders.

GEOMETRIC MATRIX

The P-delta effect, which results from a vertical earthquake component and the structural weight, can be simply illustrated by studying the single mass system shown in Fig. 2. As sketched in the accompanying figure, the shear, $K_g x_g$, is due to the overturning moment produced by the vertical forces. The magnitude of shear per unit displacement is $K_g = W - m \ddot{y}_g / L$ in which W is the structural weight, M the structural mass, \ddot{y}_g the vertical earthquake component, and L the member length. The geometric matrix of multistory structures can be established in a similar manner.

DAMPING MATRIX

The general expression of the damping matrix can be expressed in a linear combination of mass and stiffness as

$$[C] = \alpha [M] + \beta [K] \quad (5)$$

in which α and β are constants based on the fundamental natural period of a structure system. For an inelastic structural system, the stiffness matrix, $[K]$, varies during a response period; consequently, the combined form of mass and stiffness cannot constantly represent the assumed damping coefficients, $[C]$. Therefore, the mass proportional damping is used in this study for which $\alpha = 2\lambda p_n$ and $\beta = 0$. The term λ is the fraction of critical damping, and p_n is the fundamental frequency of the structural system.

ENERGY FORMULATION

Consideration of the energy absorption of a structure may serve two purposes. First, the overall behavior of the structure can be determined by using the energy measurements. If a structure is able to store the total input energy in the form of elastic strain energy, the integrity of the structure will be greater than that of the same structure for which a part of the input energy must be dissipated by strain energy through permanent sets. Also the integrity of one structure will be greater than another if the one is necessary to dissipate less strain energy when both are subject to the same earthquake motion. Second, a means of checking the accuracy of the response solution is provided. Based on the law for the conservation of energy, the total input energy absorbed by a structure must be equal to the stored energy (TSE) in the form of both elastic energy (ESE) and kinetic energy (EKE) that is added to the dissipated energy resulting from permanent set (DSE) and damping (EDD). The general expression for energy conservation at time t may be written as

$$TIE_t = ESE_t + EKE_t + DSE_t + EDD_t \quad (6)$$

The individual terms in Eq. (6) are:

$$TIE_t = \sum_{t=0}^t (v_{ave} \Delta x_g + R_{yave} \Delta y_g + \{F_p\}^T \{\Delta x_s\}_{ab}) \quad (7)$$

$$ESE_t = \sum_{i=1}^{NM} \frac{L_i}{6EI_i} (M_{2i-1}^2 - M_{2i-1} M_{2i} + M_{2i}^2) \quad (8)$$

$$EKE_t = \frac{1}{2} \sum_{j=1}^{N_f} M_j (\dot{x}_j + \dot{x}_g)^2 + \frac{1}{2} \sum_{k=1}^{N_m} M_k (\dot{y}_k + \dot{y}_g)^2 \quad (9)$$

$$DSE_t = \sum_{j=1}^{N_j} \sum_{i=1}^{N_i} \Delta t M_{pc} \Delta \theta_i (1 - p) \quad (10)$$

$$EDD_t = ([C]^T \{\dot{x}\}_{ave})^T \{\dot{u}_s\}_{ave} \Delta t \quad (11)$$

The respective notations in Eqs. (7) to (11) are:

V_{ave} = average shears during incremental time at structural supports not including shears resulting from P-delta effect,

Δx_g = incremental horizontal ground displacements,

R_{yave} = average vertical reactions during incremental time at structural supports,

Δy_g = incremental vertical ground displacements,

$\{F_p\} = [K_s] \{x_s\}$, horizontal forces at floor levels due to P-delta,

$\{\Delta x_s\}_{ab} = \{\Delta x_s + \Delta x_g\}$, absolute horizontal displacement vector,

NM = number of members,

L_i = length of member i,

E = modulus of elasticity of the structural member,

I_i = cross-sectional moment of inertia of member i,

M_{2i-1} = moment at end 2i-1 of member i at time t,

M_{2i} = moment at end 2i of member i at time t,

N_f = number of floors,

N_m = number of lumped masses,

M_j = mass of jth floor,

M_k = lumped mass k,

\dot{x}_j = horizontal velocity of floor j,

\dot{x}_g = horizontal ground velocity at time t,

\dot{y}_k = vertical velocity of mass k relative to the base at time t,

\dot{y}_g = vertical ground velocity at time t,

$N_{\Delta t}$ = number of time increments at which the joint j (member end j) is in plastic range,

N_j = number of joints,

M_{pc} = reduced plastic moment for columns, ideal plastic moment for girders,

$\Delta\theta_i$ = incremental end rotation during time increment i,

p = strain hardening ratio,

$\{\dot{x}\}_{ave}$ = average relative transverse velocity vector over Δt , and

$\{\dot{u}_s\}_{ave}$ = average absolute transverse velocity over Δt .

The amount of error in the incremental integration technique is determined as a percent of the total input energy. The following equation is used to calculate the percentage of error after every time increment, Δt .

$$\% \text{ Error} = \frac{[TIE - (TSE + TDE)]}{TIE} \quad (100) \quad (12)$$

DUCTILITY AND EXCURSION RATIOS

The ductility ratio μ , used in this investigation is defined as the ratio of the total rotation, θ_t , of a joint (member end) divided by the yielding rotation, θ_y , of the joint as

$$\mu = \frac{\theta_t}{\theta_y} = \frac{\theta_y + \alpha}{\theta_y} = 1 + \frac{\alpha}{\theta_y} \quad (13)$$

in which α is equal to the plastic rotation of the joint as sketched in Fig. 1.

The excursion ratio, ϵ , of a joint (member end) is defined as the sum of total plastic rotation, of the joint during an earthquake record divided by its yielding rotation and may be expressed as

$$\epsilon = \frac{N}{\sum_{i=1}^N \mu} \frac{\alpha_i}{\theta_y} = \sum_{i=1}^N \frac{\mu_i}{\mu} (\mu_i - 1) \quad (14)$$

in which N_{μ} is equal to the total number of times in which the joint has suffered plastic deformation during the response.

EXAMPLES AND COMPARISONS

A 4-story-3-bay frame has been analyzed for Models 1 and 2 as shown in Fig. 3. A comparison of the displacement response resulting from both horizontal and vertical earthquakes is given in Fig. 4. The effect of the vertical component on energy absorption of the elastic models of 1 and 2 is shown in Figs. 5 and 6. Similarly, the comparisons of energy absorption of elastoplastic models resulting from a horizontal earthquake only and horizontal plus vertical components are given in Figs. 7 and 8 respectively. The ductility and excursion ratios of the columns and girders of Models 1 and 2 are given in Fig. 9. Note that the comparison of four cases for each floor refers to maximum values of any of the nodes on that floor. Fig. 10 shows the maximum vertical displacements at the girder centers of Model 2.

The ten-story-one-bay rigid frame shown in Fig. 11 has also been studied for comparison of response parameters for which the yielding stress is 36 kip/sq in. and the plastic moment capacity is increased by 2.5. The displacement response at the girder center of each floor is shown in Fig. 12. The comparisons of input and dissipated energy with and without damping are given in Figs. 13 and 14. These two figures reveal the significant effects of damping and material behavior on energy absorption, which, however, does not deviate noticeably for Models 1 and 2 of this structural system. The maximum relative floor displacements associated with elastic and elastoplastic Models 1 and 2 are shown in Fig. 15 in which the comparisons are based on a horizontal earthquake only, a horizontal earthquake and the P-delta effect, and horizontal and vertical earthquakes plus the P-delta effect. The ductility and excursion ratios of the girders for Models 1 and 2 are shown in Fig. 16. This structure has strong columns that have only plastic hinges developed at the supporting base during the entire response period. It is apparent that the P-delta effect has a significant influence on the displacement response, whereas the vertical earthquake does not influence this strong columnal structure noticeably. However, there is a remarkable difference in the ductility and excursion ratios between Models 1 and 2.

CONCLUSIONS

Two lumped mass models, 1 and 2, are used to study response parameters of damped and undamped inelastic systems subject to coupling horizontal and vertical earthquake motions. The response parameters are expressed in terms of the displacement response of the columns and girders, energy absorption, maximum relative floor displacements and ductility and excursion ratios. From two examples of four-story-three-bay and ten-story-one-bay rigid frames, it has been observed that Model 2, which has the masses lumped on girder centers and structural joints, can best describe the behavior of structural systems subject to both horizontal and vertical earthquakes. The significant effect of a vertical earthquake on displacement response depends on structural parameters. The examples show that the vertical earthquake affects more on model 2 than model 1, particularly on structures with weaker columns and that the vertical earthquake demands a great deal of ductility in girders of all structures.

For the work reported on here, the percentage of error ranged from less than 0.5 to 2.0%. The larger values occurred in the 10-story structure. This error level is felt to be sufficient for the investigation reported on in this paper.

ACKNOWLEDGEMENTS

This report is a partial work from the research project sponsored by the National Science Foundation, RANN Program Grant No. GI 34966. This support is gratefully acknowledged.

REFERENCES

1. Cheng, F. Y., "Finite Element Analysis of Structural Instability by Association of Pulsating Excitations," presented at the 1974 International Conference on Finite Element Methods in Engineering, August 1974, Australia, Proceedings pp. 597-610.
2. Cheng, F. Y., and Oster, K. B., "Ultimate Instability of Earthquake Structures," *Journal of the Structural Division, ASCE*, Vol. 102, May 1976, pp. 961-972.
3. Giberson, M. F., "Two Nonlinear Beams with Definitions of Ductility," *Journal of the Structural Division, ASCE*, Vol. 95, No. ST8, Proc. Paper 6377, Feb., 1969, pp. 137-157.
4. Manual of Steel Construction, 7th ed., American Institute of Steel Construction, New York, N. Y., 1970.
5. Newmark, N. M., "A Method of Computation for Structural Dynamics," *Journal of the Engineering Mechanics Division, ASCE*, Vol. 85, No. EM3, Proc. Paper 2094, July 1959, pp. 67-94.

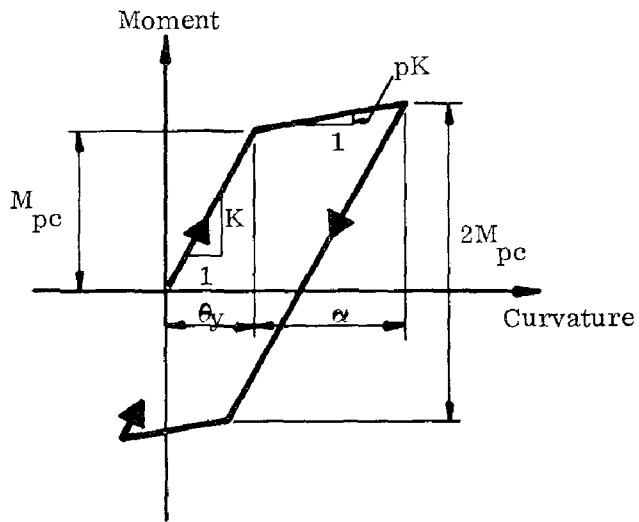


Fig. 1. Nonlinear Hysteresis Loop
 M_{pc} = Reduced Plastic Moment

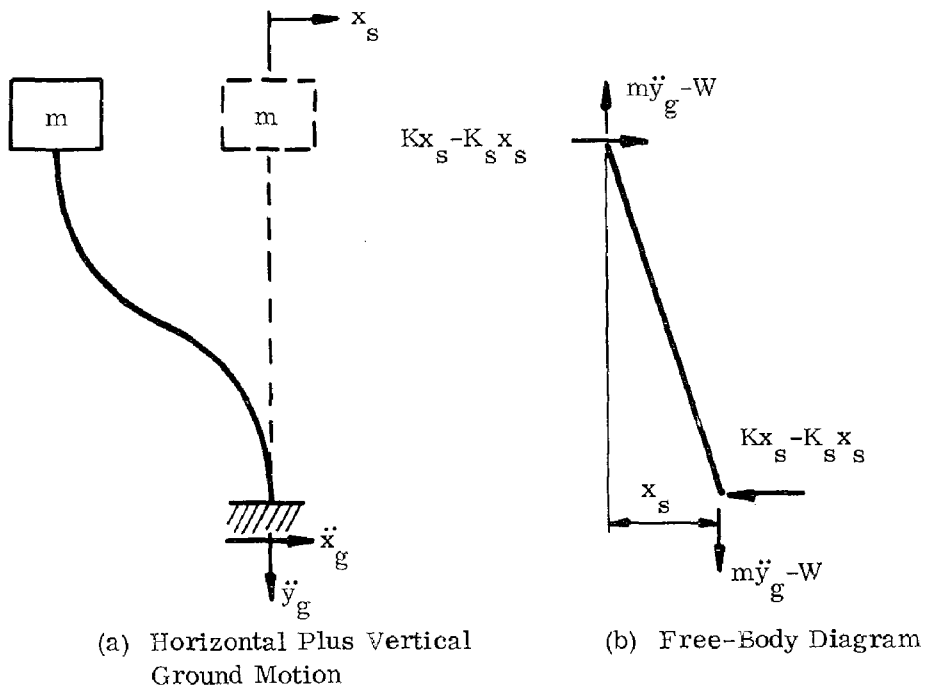


Fig. 2. Single-Mass-System

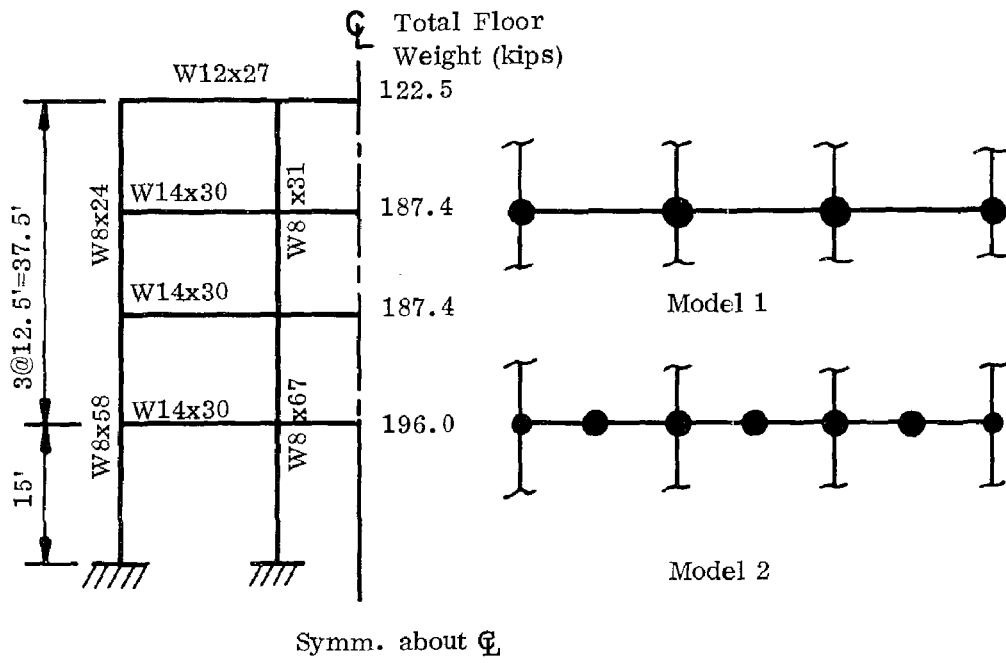


Fig. 3 4-Story-3Bay Frame

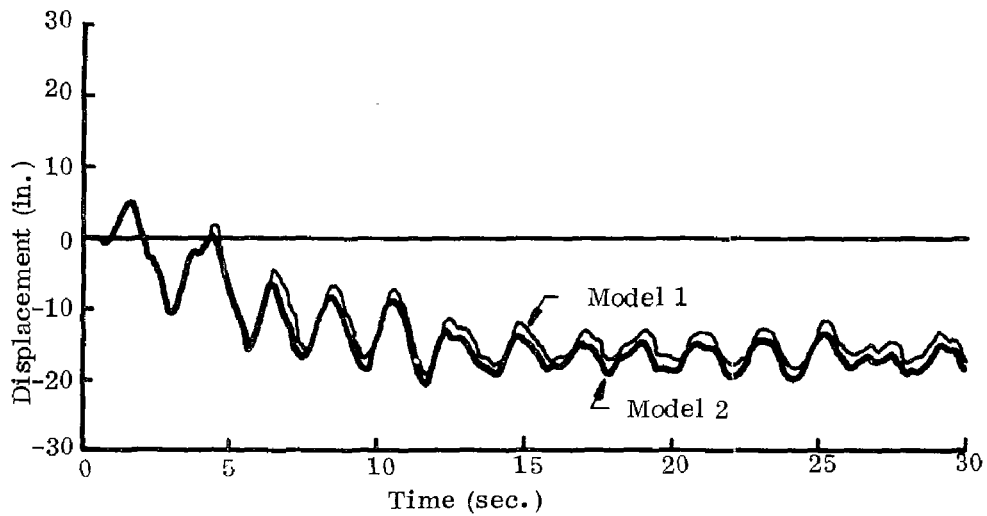


Fig. 4. Top Floor Displacement of Fig. 3
Elasto-Plastic System, 3% Damping
1940 El Centro Earthquake

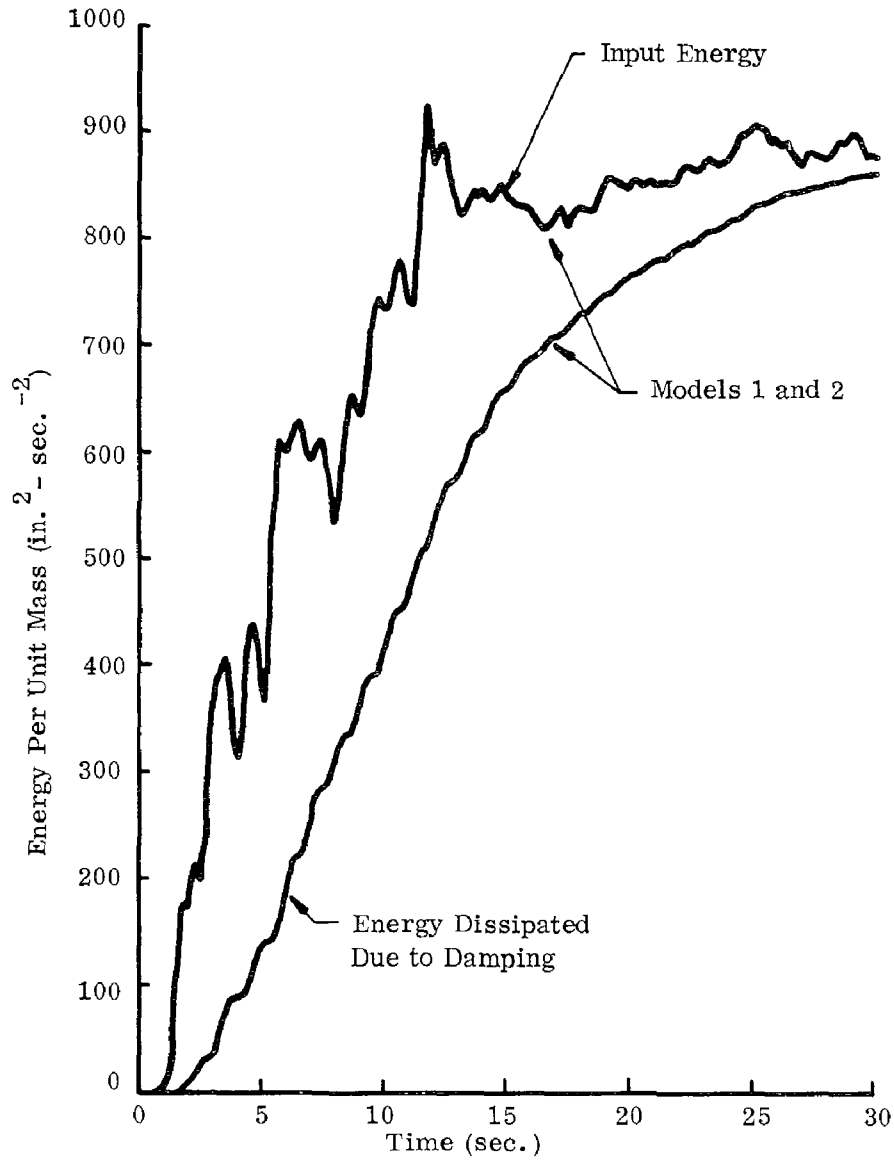


Fig. 5. Energy Plot of Fig. 3
Elastic System, 3% Damping
1940 El Centro Earthquake
N-S Component Only

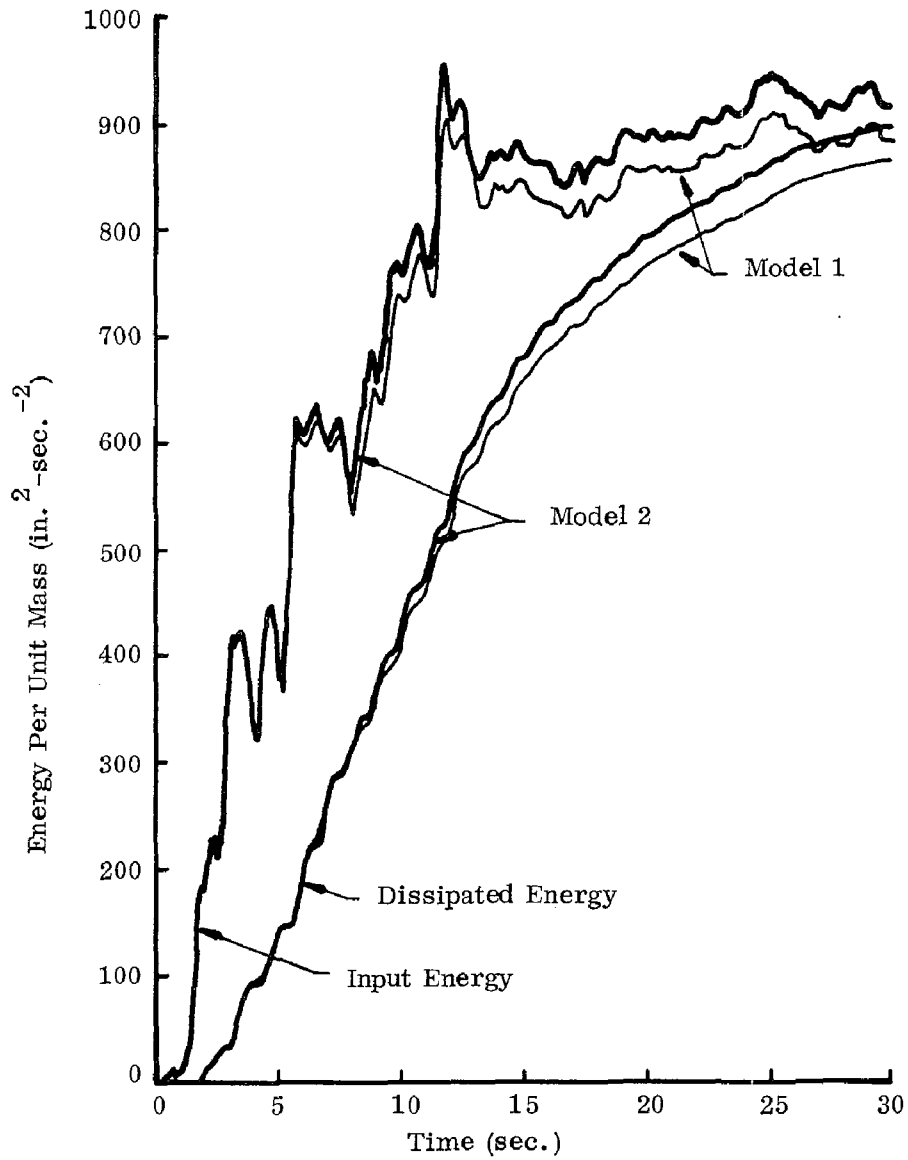


Fig. 6. Energy Plot of Fig. 3
 Elastic System, 3% Damping
 1940 El Centro Earthquake
 N-S Plus Vertical Component

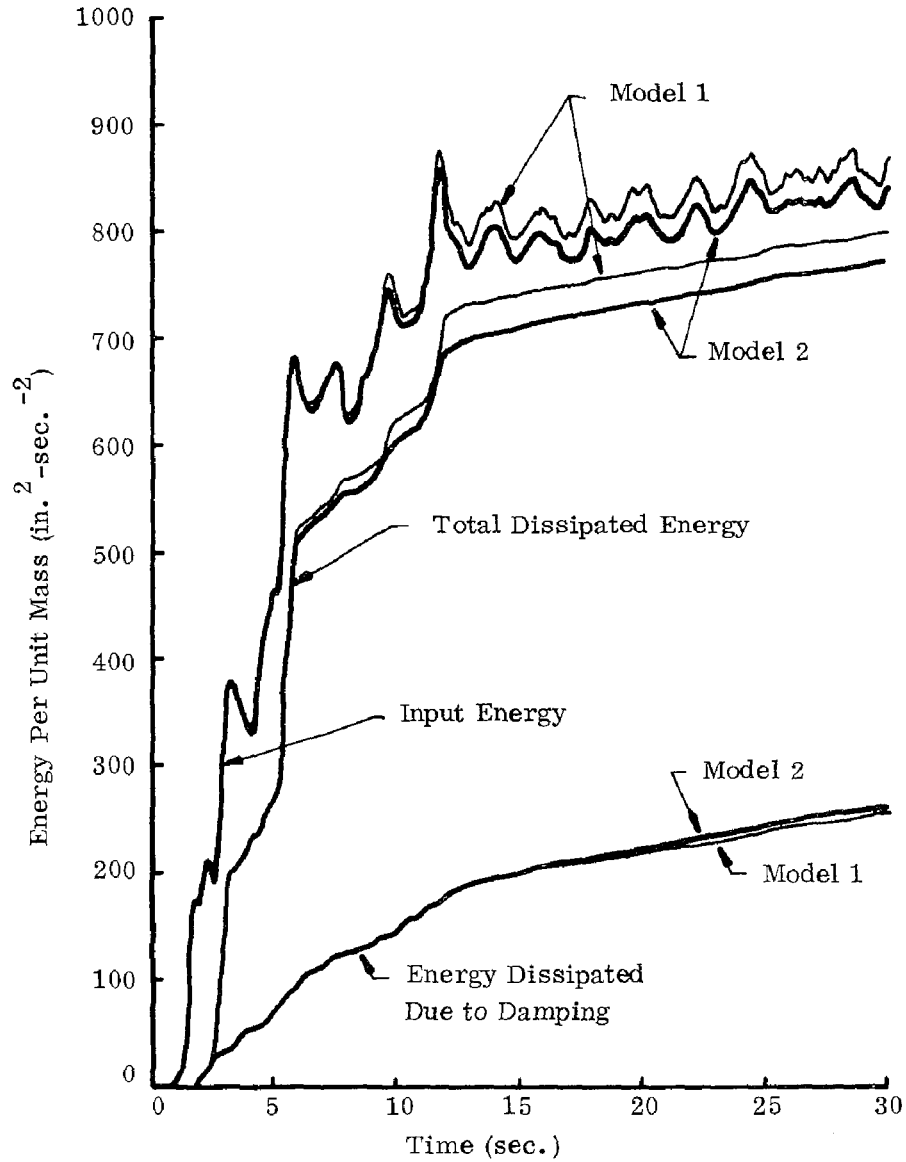


Fig. 7. Energy Plot of Fig. 3
 Elasto-Plastic System, 3% Damping
 1940 El Centro Earthquake
 N-S Component Only

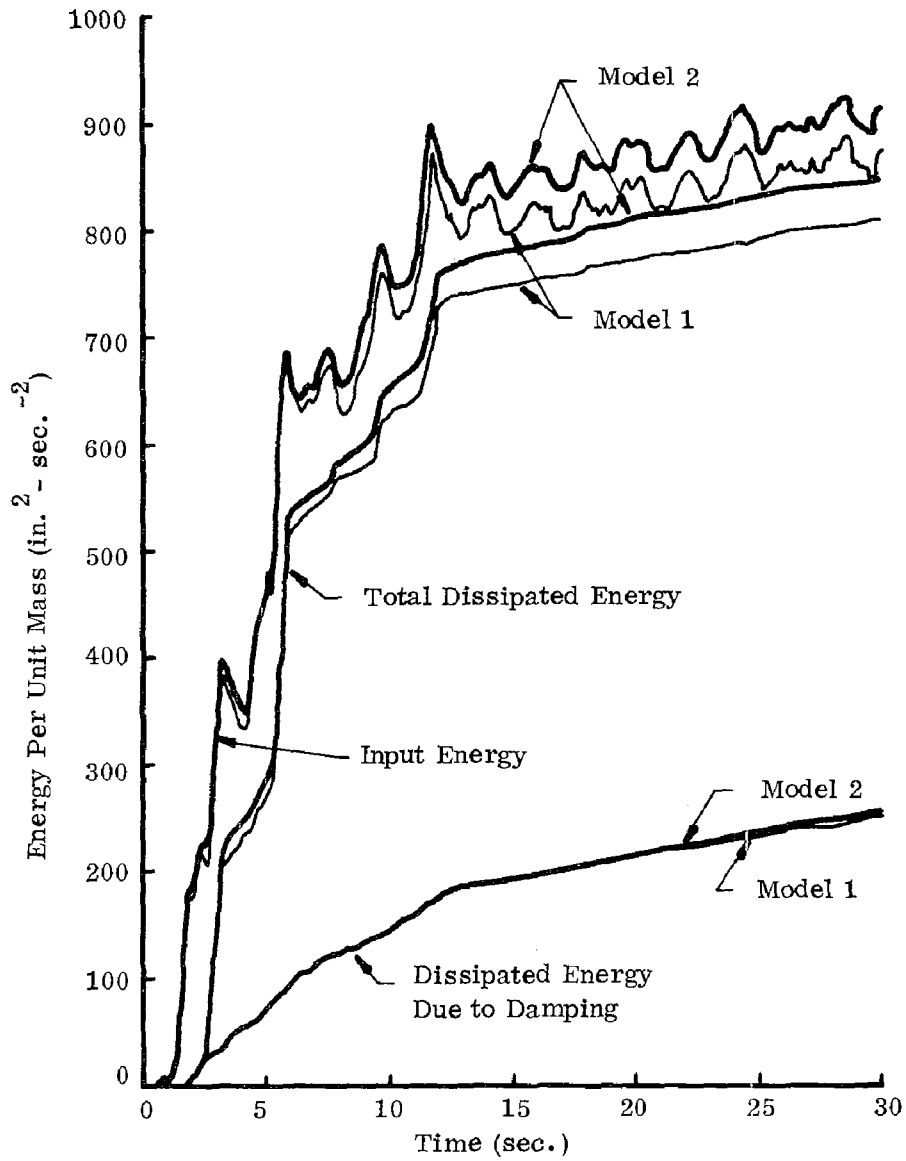


Fig. 8. Energy Plot of Fig. 3
 Elasto-Plastic System, 3% Damping
 1940 El Centro Earthquake
 N-S Plus Vertical Component

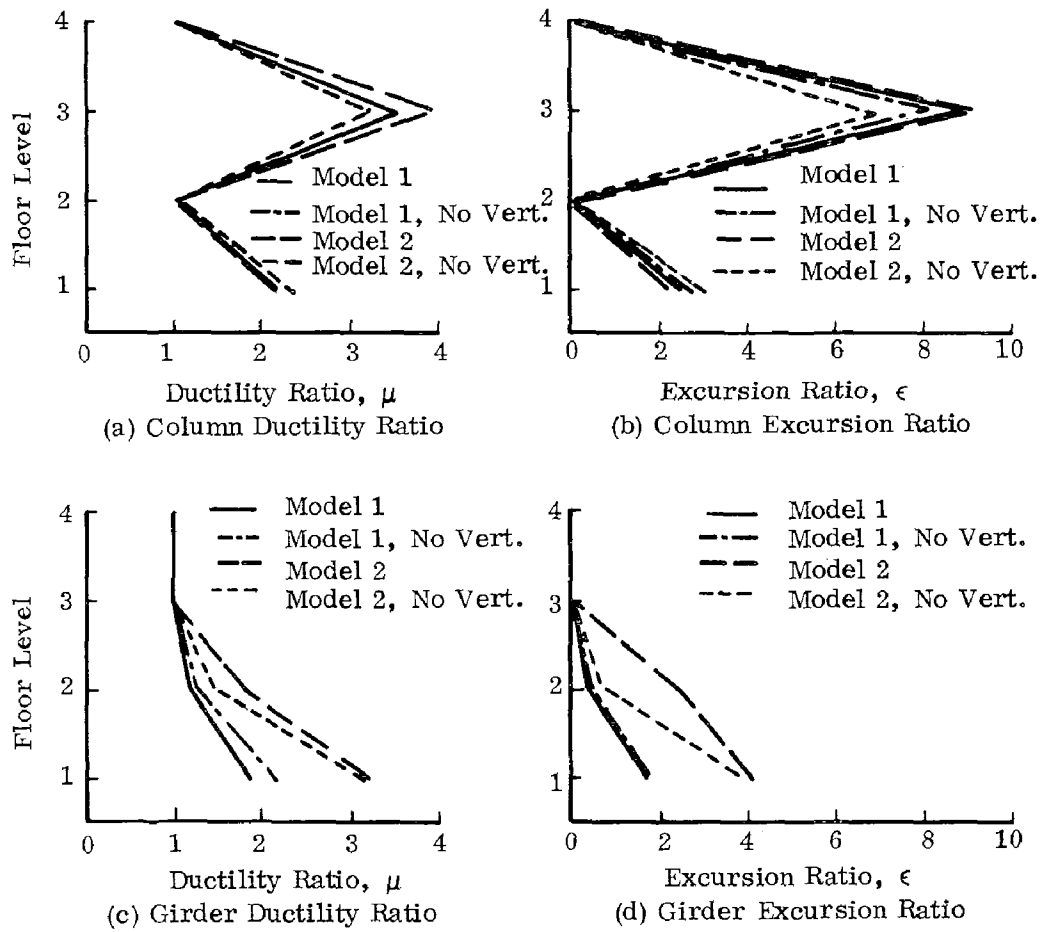


Fig. 9. Elasto-Plastic System of Fig. 3
1940 El Centro, N-S Plus Vertical Component

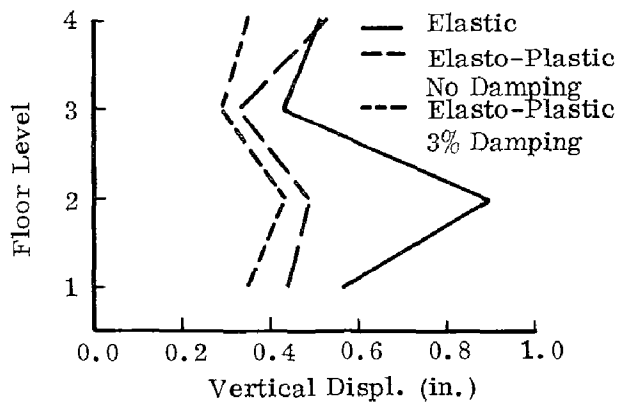


Fig. 10. Maximum Vertical Displacement at the
Center of Girders, Model 2 of Fig. 3

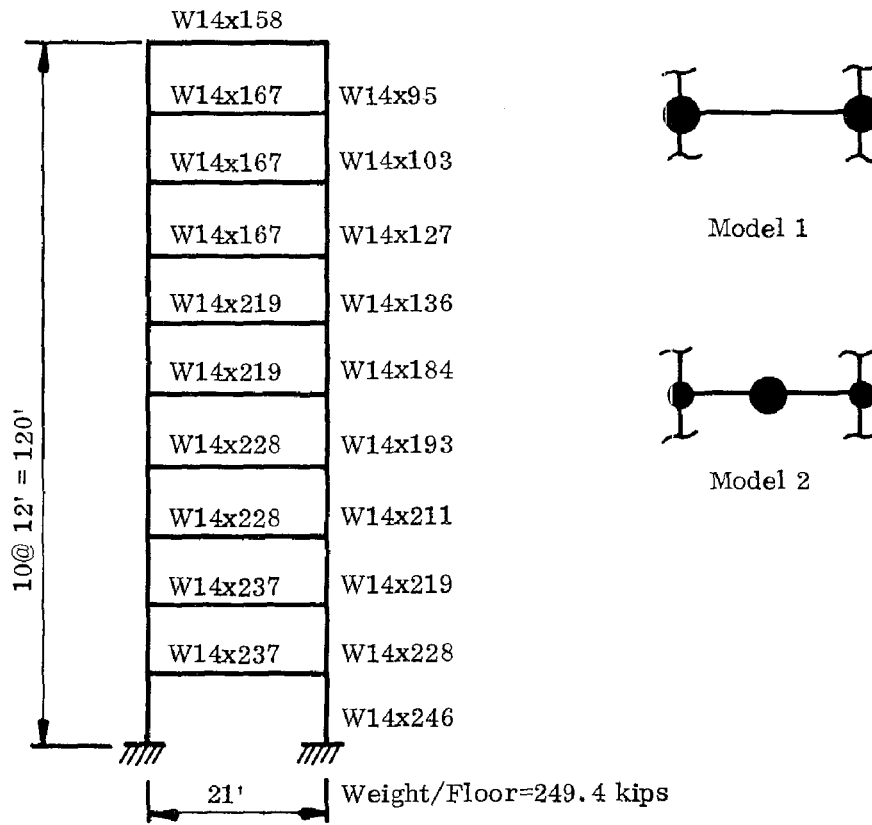


Fig. 11. 10 Story Frame

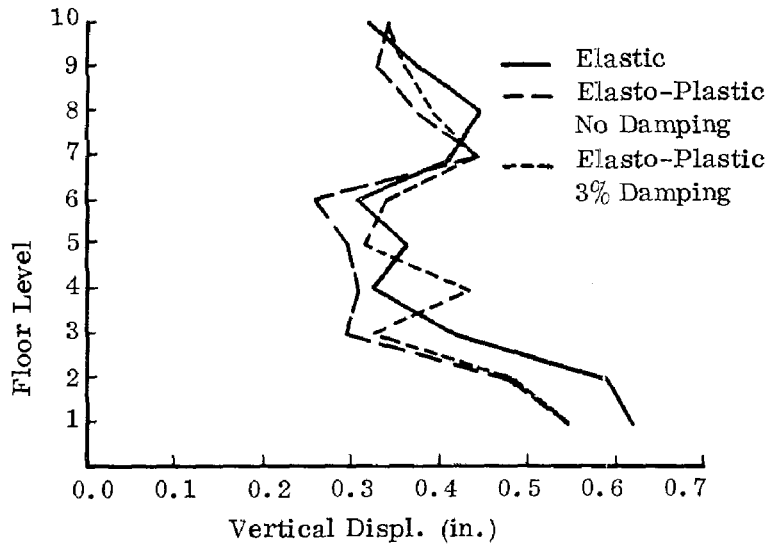


Fig. 12. Maximum Vertical Displacement at the Center of girders, Model 2 of Fig. 11.

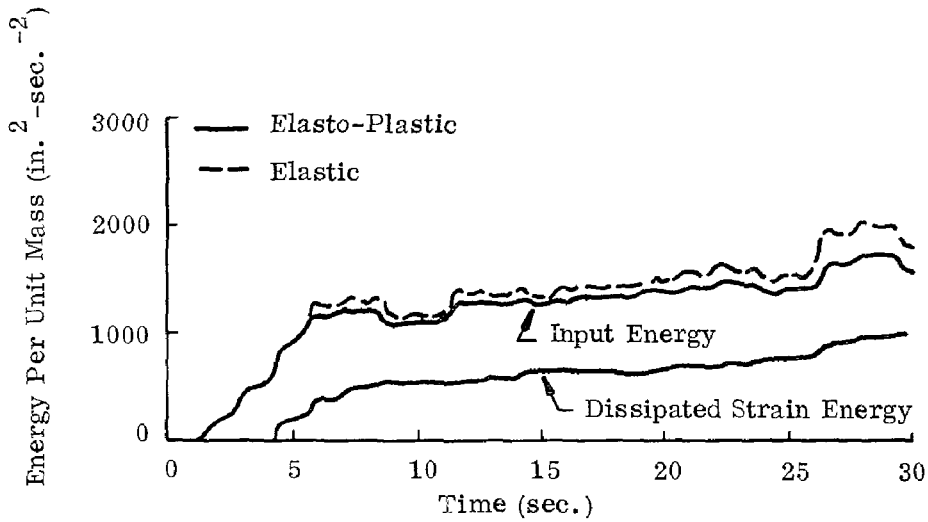


Fig. 13. Energy Plot of Fig. 11, No Damping

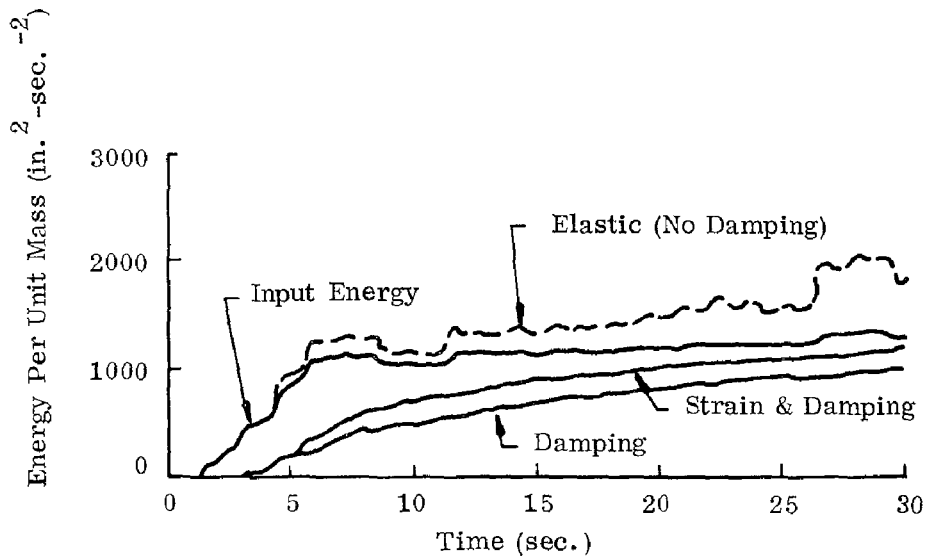


Fig. 14. Energy Plot of Fig. 11
Elasto-Plastic System, 3% Damping

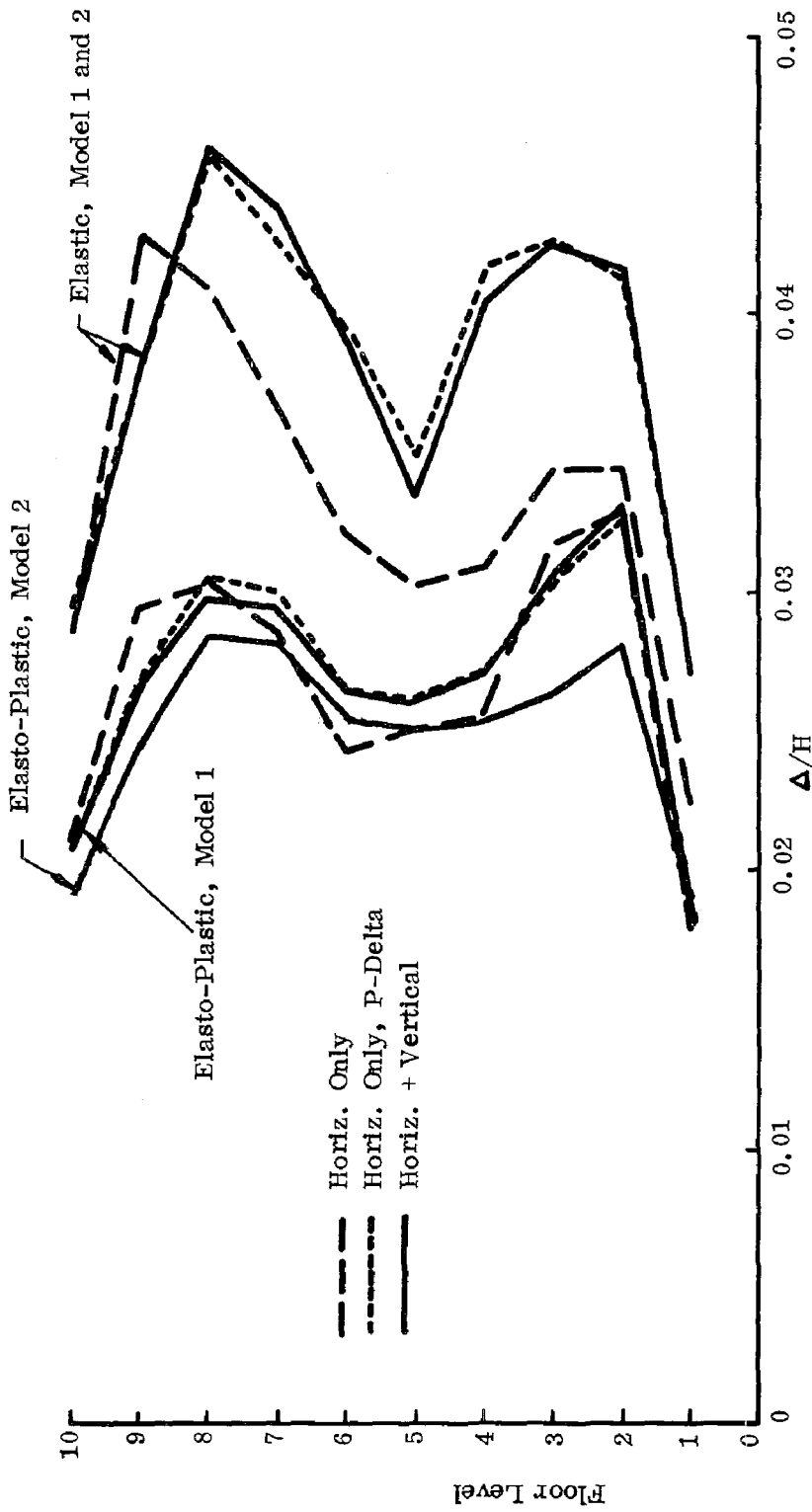


Fig. 15. Maximum Relative Floor Displacement of Fig. 11
1940 El Centro Earthquake, No Damping

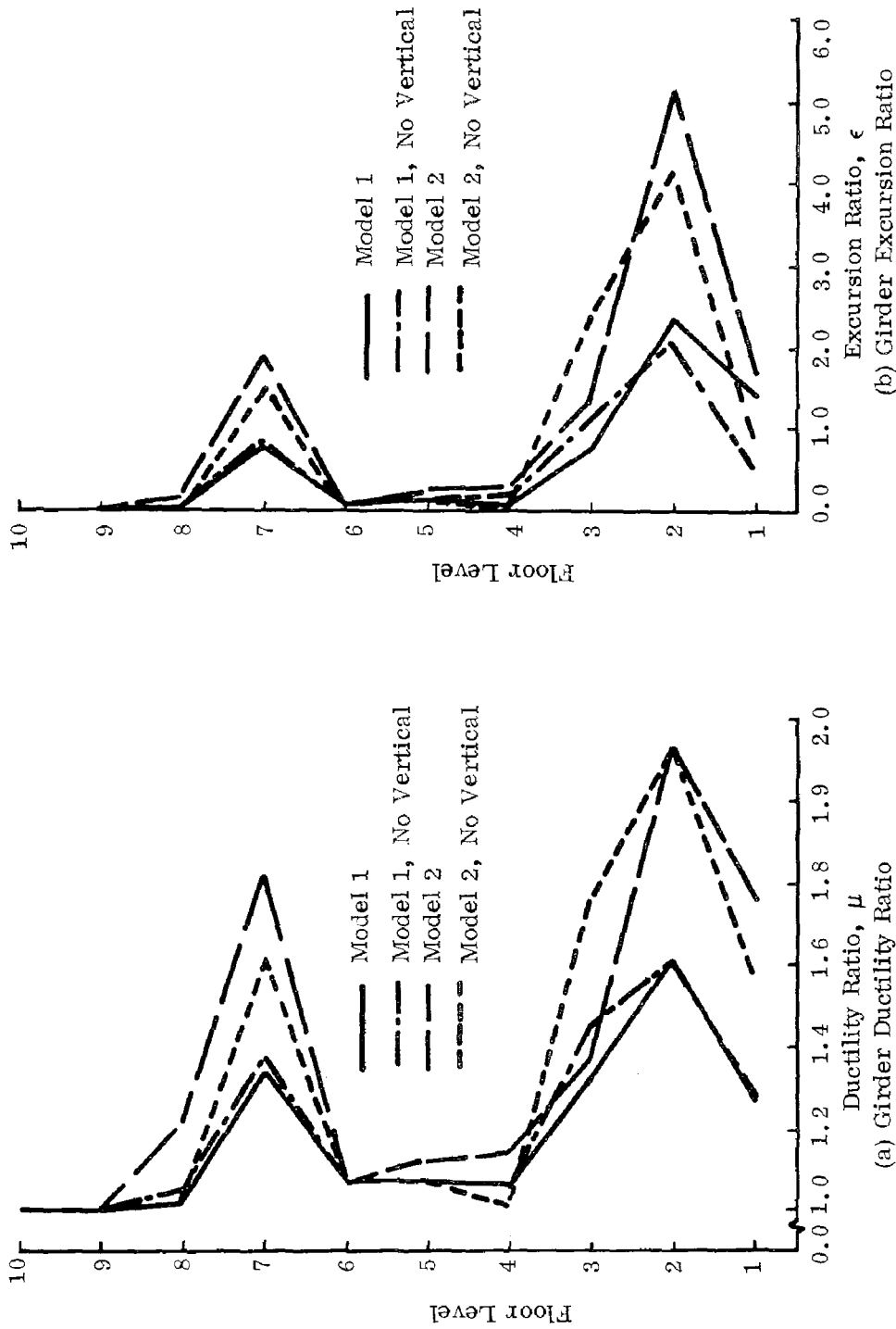


Fig. 16. Elasto-Plastic System of Fig. 11
1940 El Centro Earthquake, No Damping

INTERNATIONAL SYMPOSIUM ON
EARTHQUAKE STRUCTURAL ENGINEERING

127

St. Louis, Missouri, USA, August, 1976

THE EFFECT OF FOUNDATION COMPLIANCE ON THE FUNDAMENTAL
PERIODS OF MULTI-STOREY BUILDINGS

E. MENDELSON* and I. ALPAN**

Lecturer* and Professor**

Faculty of Civil Engineering, Technion - Israel

Institute of Technology

Haifa , Israel

Summary

The study deals with the effect of soil structure interaction on the fundamental periods of framed reinforced concrete multi-storey structures. Typical structures of various heights and several foundation systems are examined, as the relevant soil parameters are varied for each foundation system.

An approximate formula for the fundamental period, with the consideration of the elastic compliance of the foundation, is presented. This formula shows the effect of soil structure interaction to increase the fundamental period of the structure.

The influence of the elastic compliance is shown as particularly pronounced in the cases of isolated footings on sand and of raft foundation on soft clay. This influence increases with the height of the structure.

The influence of the compliance is small in the case of pile foundations and it decreases with increase in the height of the structure.

Preceding page blank

1. Introduction

In many investigations it has been shown that the interaction between a structure and the foundation soil increases the fundamental period of the structure and thus affects its response to earthquake stimuli.

Studying this problem, various mechanical models have been proposed to represent the properties of the foundation medium. Thus, for example, Lycan and Newmark(4)* Fleming et al(3) and Merritt and Housner(6) investigated two dimensional shear buildings with the foundation soil represented by a spring or a spring-mass combination, and Mendelson and Baruch(5) analysed the response of a non symmetric multi-storey structure, with a raft foundation, with the sub-soil being represented by a massless spring.

In these investigations only the vertical and rocking motions of the foundations were considered, whereas horizontal translations were not allowed for.

On the other hand, Parmelee et al(8) examined a one-storey structure in rocking and sliding motion and Muto(7) obtained the response of a framed structure, with the foundation soil represented by springs allowing for both rocking and sliding, while the participating soil mass is being added to that of the foundation.

The lateral dynamic response of pile foundations was examined by Alpan(1), who used the theory of beams on elastic supports(Winkler Model), and by Penzien(9), who used a similar model with non linear springs and with participating soil masses added to those of the piles.

In the present work the influence of the elastic foundation compliance on the fundamental period of typical framed reinforced concrete structures of 5,10 and 15 stories is examined. The following, commonly occurring, foundation systems are considered:

- (a) Isolated footings on sand.
- (b) A raft on a clay layer, overlying solid rock.
- (c) Piles penetrating a clay layer and supported by underlying solid rock.

Similarly, the influence of varying the soil parameters for each of the foundation system is also examined.

In view of the considerable uncertainty in assuming the soil mass participating in the motion of a foundation system,

* Numbers in parantheses refer to the list of references at the end of the paper.

the sub-soil is represented here by massless springs, enabling, as appropriate, rocking and sliding motions of the foundations. The relevant spring constants are determined from simple and practical relations based on elastic theory combined with empirical evidence.

The effect of the dynamic soil structure interaction in a general case may be expressed by an approximate formula, proposed by Mendelson and Baruch(5), for the fundamental period of a structure on an elastic subgrade. The validity of this formula is checked again in view of the results of the present work.

The computations connected with the present work were carried out by using the STRUDL II computer program(14).

2. An Approximate Formula for the Fundamental Period.

Mendelson and Baruch(5) have proposed, following Dunkerley's approximation(12), the following formula to estimate the fundamental period of a structure based on an elastic subgrade:

$$T_{ap} = \sqrt{T_o^2 + T_s^2} \quad (1)$$

where:

- T_{ap} = approximate fundamental period,
- T_o = fundamental period of the structure as supported by rigid subgrade,
- T_s = period of the structure, considered as being a rigid body elastically supported.

A similar formula has been presented by Merritt and Housner(6) for a one-storey structure:

$$T = \left(1 + \frac{h^2 k}{k_\theta}\right)^{1/2} \cdot 2\pi \sqrt{\frac{m}{k}} \quad (2)$$

where:

- T = period,
- h = height of structure,
- k = stiffness of structure,
- k_θ = stiffness of subgrade in rocking ,
- m = mass of structure
- $\frac{h^2 k}{k_\theta}$ = ratio between the elastic soil compliance and the flexibility of the structure.

The generalization of equation 2 to allow for an approximate determination of the fundamental period of multi-storey structures leads to considerable discrepancies if compared to actual values. The difference is due to the fact that in the model

represented by this equation the entire mass of the structure is concentrated at its top. In equation 1, on the other hand, the values of T_0 and T_1 are obtained in accordance with the actual mass distribution in the structure, and therefore there is a good agreement between the approximation and reality, as shown in reference 5.

3. Mechanical Models of Foundation-Soil Systems

3.1 Isolated footings on sand

The elastic compliance of the footings is assumed, in this case, as due to the compression of springs representing the foundation soil (Fig 1). A preliminary analysis of this system has shown sliding to have but a negligible effect on the period. Thus the proposed model does not include the possibility of sliding.

The computation of the relevant spring constant for an isolated footing follows the approach of Alpan(2) based on the following quite simple but adequate assumptions:

- (a) Uniform vertical pressure at any given depth.
- (b) Vertical pressure at a given depth to follow the relation (Fig 2):

$$\sigma_z = \frac{\sigma_0}{\left(1 + \frac{z}{2r_0}\right)^2} \quad (3)$$

where:

- σ_z = vertical pressure at a given depth,
- σ_0 = pressure under the footing,
- z = depth below footing,
- r_0 = equivalent radius of footing.

- (c) The elastic modulus of the sand - E_z varies linearly with depth as follows:

$$E_z = E_0 \left(1 + \alpha \frac{z}{r_0}\right) \quad (4)$$

where:

- E_0 = elastic modulus of sand at footing depth,
- $\alpha \frac{E_0}{r_0} = \frac{\partial E}{\partial z}$ = rate of increase of the elastic modulus with depth; a function of the relative density of the sand.

Appropriate integration of the infinitesimal strains within the simplified stress cone yields the spring constant of an individual footing:

$$k = \frac{E_o \cdot r_o}{(1-\gamma^2) \cdot I(\alpha)} \quad (5)$$

where:

k = spring constant,
 γ = Poisson's ratio, approximately 0.3 for sands,
 $I(\alpha)$ = a function, decreasing with increasing α , with maximum value of 0.5 for $\alpha=0$.

For the use with the approximate formula (equation 1) the general spring constant in rocking of the foundation system is obtained as:

$$k_{\theta} = \sum X_i^2 \cdot k_i \quad (6)$$

where:

k_{θ} = general spring constant in rocking,
 X_i = co-ordinate of footing i relative to the axis of rotation.

3.2 Raft foundation on a clay layer.

The raft, of dimensions B by L rests on a clay layer of thickness d (Fig 3a) and constant elastic modulus E . The clay layer, as previously mentioned, overlies a solid rock mass. The elastic behaviour of the clay is represented by one spring for the rocking mode and by a second one for the sliding mode (Fig.3b).

The spring constant for rocking - k_{θ} may be expressed according to Shieneis (11) as follows:

$$k_{\theta} = \frac{E \cdot L \cdot B^2}{i_{\gamma\tau} \cdot k_{\lambda}} \quad (7)$$

where:

E
 $i_{\gamma\tau}$ and k_{λ} = coefficients, depending on B, L and d

The spring constant for sliding - k_x is obtained by using a semi-empirical relationship given by Savinov (10):

$$k_x = k_{x0} \left(1 + \frac{2(B+L)}{\Delta \cdot B \cdot L}\right) \sqrt{\frac{\sigma}{\sigma_o}} \quad (8)$$

with

$$k_{x0} = \frac{(1.7 \times 10^{-3}) E \cdot B \cdot L}{(1+\gamma)(1-0.5\gamma)} \quad (\text{kgf/cm}) \quad (9)$$

where:

E = elastic modulus of the clay in kgf/cm^2 ,

B, L = raft dimensions in cm,

$\Delta = 10^{-2} \text{ cm}^{-1}$ = empirical coefficient,

γ = Poisson's ratio, approximately 0.5 for clays,

σ = pressure under the raft (kgf/cm^2),

$\sigma_0 = 0.1-0.2 \text{ kgf/cm}^2$ = empirical reference pressure.

3.3 Pile foundations

The structure is supported by piles penetrating a clay layer of thickness d and constant elastic modulus E , and having their tips supported by massive rock underlying the clay (Fig 4a).

The individual pile may be considered as a column with lateral elastic support, hinged at the bottom and with partial rotational restraint at the top (Fig 4b). The pile head rotation depends, on the bending stiffness of the pile itself, and on the stiffness of the structural elements (beams and columns) jointed at the pile head.

The spring constant of the lateral elastic support may be obtained from analogy with the model of a line load acting on an elastic half space (13) as shown in Fig 5:

$$k = \frac{P}{u} = \frac{\pi E}{2.1 \ln\left(\frac{R}{r}\right)} = \frac{E}{\beta} \quad (10)$$

where:

k = spring constant per unit length,

p = load per unit length,

u = displacement under the load,

$\frac{R}{r}$ = "influence radius" ratio.

Following empirical evidence published by Alpan (1) the value of $\beta = 2.18$ was adopted.

The actual analysis of the dynamic system under consideration was based on a lumped parameter model, i.e. the piles were divided into sections supported by discrete springs.

For use with the approximate formula (equation 1) the general spring constant for horizontal motion of the foundation system, $-k_x$, is defined as the force at ground level per unit displacement x , with restrained rotation at the pile heads.

4. The Buildings

A typical floor plan of the buildings selected for illustration is shown in Fig 6. The length of the buildings is 30.0 m, their width 12.0 m, the height of a storey is 3.0 m, and the number of stories is 5, 10 and 15 as stated before.

The structures consist of reinforced concrete slabs of 14 cm thickness, seven identical frames which provide structural stiffness in the short ("B") direction and four similar frames in the long ("L") direction as evident from Fig 6. All the beams are of the same cross section whereas the columns vary in accordance with their axial load, as shown in Fig 7.

In the cases of isolated footings and pile foundations the columns are fixed in foundation beams of the regular cross section, and in the case of raft foundation the columns are fixed in the raft which is considered as infinitely rigid. The external walls as well as the partitions are not considered to contribute to the structural stiffness.

The analysis was based on a lumped mass model with the masses lumped at the floor levels. Each lumped mass, including the mass of the floor, the walls, the partitions, the columns and 20% of the live load, was taken as $330 \text{ kgf}\cdot\text{sec}^2/\text{cm}$.

In the analysis, only the lateral oscillations in the "B" direction were considered.

5. The Foundation Systems

5.1 Isolated Footings on Sand

The footings were dimensioned in accordance with their static load, assuming two types of sands of the following properties:

(a) Relative density of $D_r = 50\%$, permissible bearing pressure of $3.0 \text{ kgf}/\text{cm}^2$ and elastic modulus at the surface of $E_o = 150 \text{ kgf}/\text{cm}^2$.

(b) Relative density of $D_r = 90\%$, permissible bearing pressure of $6.0 \text{ kgf}/\text{cm}^2$ and elastic modulus of $E_o = 250 \text{ kgf}/\text{cm}^2$.

The ratios α/r_o were found in accordance with the relative densities as 0.9 for the first case and 0.85 for the second one and for the appropriate equivalent radii, $I(\alpha)$ and the spring constants k were determined (see equations 4 and 5).

The dimensions of the footings, the associate spring constants and the general spring constants in rocking are given in Table 1.

As may be seen from Table 1, the difference between the spring constants for the two sands is not too significant. Thus only the stiffer sand ($D_r = 90\%$) was considered in the computations of the fundamental periods.

5.2 Raft on a Clay Layer

The raft dimensions were taken as 13.0 by 31.0 m, the thickness of the clay layer was taken as 10.0 m and the elastic moduli of the clay was assumed as 150 and 250 kgf/cm².

The geometry of the system yielded, for the computation of the spring constant in rocking (equation 7), the following values of the sequent coefficients:

$$i_{\gamma\tau}^E = 2.67 \quad \text{and} \quad k_{\lambda} = 0.85$$

As may be seen from equations 8 and 9, the spring constant in sliding depends, in addition to the elastic modulus of the clay, on the contact pressure on the clay, and thus on the height of the structure.

The values of the spring constants for the various structures are given in Table 2.

5.3 Pile Foundations

The thickness of the clay layer was again taken as 10.0m and the elastic moduli, as before, were 150 and 250 kgf/cm². The pile diameters, uniform for each building, were determined from the maximum static load with a permissible stress of 50 kgf/cm². The pile diameters, their mass per unit length, and the general spring constants for all the cases are given in Table 3.

6. The Approximate Fundamental Period

For use with the approximate formula (equation 1), T_0 were determined for the structures being hinge supported on rigid subgrade (Fig 8).

Values of T_s were obtained from:

$$T_s = 2\pi \sqrt{\frac{m}{k_{\theta}} \left(\frac{h^2}{3} + \frac{B^2}{12} \right)} \quad (11)$$

for the cases of isolated footings and raft foundations, and from:

$$T_s = 2\pi \sqrt{\frac{m+0.5 m_p}{k_x}} \quad (12)$$

for the case of pile foundations,

where:

- m = total mass of the building, assumed uniformly distributed throughout the height,
- m_p = total mass of the piles,
- h = height of building,
- B = width of building,
- k_{θ} = general spring constant in rocking,
- k_x = general spring constant for horizontal motion,

The values of T_0 and T_s are given, together with the other results in Table 4.

7. The Results

The fundamental periods for all the cases examined as well as the approximate values are presented in Table 4, and shown as a comparative illustration in Figure 9. In this figure the ratio T/T_0 is shown versus the squared ratio $(T_0/T_s)^2$ which in fact expresses the ratio between the flexibility of the structure and that of the foundation soil (cf. Fig.2 of reference 6).

The variation of the period ratio with the number of stories is illustrated in Fig. 10.

The practical significance of a change in period due to the soil structure interaction lies in the influence of this change on the seismic force acting on the structure. This force, according to various seismic codes of practice, is inversely proportional to $(T)^{1/3}$. Thus the ratio of the seismic forces $V/V_0 = (T_0/T)^{1/3}$, also presented in Table 4, essentially indicates the influence of the foundation compliance in comparison with non-yielding supports.

As an additional effect of the computations, the periods of some of the higher modes were also obtained, only to confirm, as has been known before (5), that the influence of the foundation compliance on the periods of the higher modes is negligible.

8. Conclusions

The influence of the foundation compliance on the fundamental period is particularly pronounced in the case of isolated footings on sand and that of a raft on a clay layer. This influence increases with the height of the structure. The main contributing factor in these cases appears to be the flexibility of the foundation system in the rocking mode. Introducing a constraint against sliding (i.e. $k_x = \infty$) does not influence the period significantly.

The influence of the foundation compliance appears to be small in the case of pile foundations. This influence decreases further with an increase in the height of the building (or rather its slenderness, i.e. its height to width ratio) since the pile diameters, and hence their stiffness are increased to allow for the higher loads transmitted.

The difference in the compliance effects of the various foundation systems becomes evident in the taller buildings, while in the lowest buildings (5 stories) it is practically negligible.

The approximate relationship, given by equation 1, appears to furnish reasonably accurate values for the periods. The deviation between the approximate and the more exact values obtained for the fundamental period are essentially due to the difference in the computation models used for obtaining T_0 and T . In the computations for T_0 , the columns are fixed at their bases in foundation beams of the regular cross section with the result of certain rotational flexibilities of the joints. In determining T , the rotational stiffnesses at the bases of the columns are increased significantly when the columns are also fixed in the pile heads or in the rigid raft.

For the cases examined in this paper, the influence of foundation flexibility on the probable seismic forces is not too pronounced. The maximum influence was obtained in case C 2.1 (15 stories building with raft foundation on soft clay) and amounted to a reduction of 15% of the seismic force. Nevertheless, a greater influence may be expected for stiffer structures (for example, shear wall structures) founded on soft soil, as seems to be indicated by the findings presented in reference 5.

References

1. Alpan, I., "The Dynamic Response of Pile Foundation to Lateral Forces", Proc. 5th World Conference on Earthquake Engineering, Vol. 2, Paper No. 229, Rome 1974, p. 1840 - 1850.
 2. Alpan, I., "The Settlement of a Rigid Disc on an Inhomogeneous Elastic Half-Space", Annales des Travaux Publics de Belgique, Vol. 127, No. 4, August 1974.
 3. Fleming J.F., Screwvala F.N. and Konder R.L., "Foundation Superstructure Interaction Under Earthquake Motion", Proc. 3rd World Conference on Earthquake Engineering, New Zealand 1965, Vol.1, p. 22-30.
 4. Lycan D.L. and Newmark N.M., "Effect of Structure and Foundation Interaction", Journal of the Engineering Mechanics Division, ASCE, Vol 87, No. EM 5, October 1961, p.1-31.
 5. Mendelson E and Baruch M. "Earthquake Response of Non-Symmetric Multi-Storey Structures", The Structural Engineer, Vol 57, No. 2, February 1973, p 61-70.
- Merritt R.G. and Housner G.W., "Effect of Foundation Compliance on Earthquake Stresses in Multi-Storey Buildings", Bulletin of the Seismological Society of America, Vol, 44, October 1954, p. 551-569.
- Ats, K. "Dynamic Response of the K-II Building to the San Fernando Earthquake", International Journal of Earthquake Engineering and Structural Dynamics. Vol.1,1973,p. 33-43.

8. Parmelee R.A., Perelman D.S., Lee S.L. & Keer L.M., "Seismic Response of Structure-Foundation Systems", Journal of the Engineering Mechanics Division, ASCE, Vol 94, No. EM 6, December, 1968, p 1295-1315.
9. Penzien, J., "Soil-Pile Foundation Interaction", in Earthquake Engineering (Ed. R.L. Wiegel), Prentice-Hall, Englewood Cliffs, N.J., 1970, p. 349-381.
10. Savinov, D.A., "The Modern Construction of Machine Foundations and their Calculation", (In Russian), Stroizdat, Moscow, 1964.
11. Schineis, M. "Verkantung des Starren Rechtecksfundaments bei Momentenbeanspruchung und elastisch-isotropem Baugrund" Die Bautechnik, No. 2, 1965, p. 58-64.
12. Thomson, W.T., "Vibration Theory and Applications", Prentice-Hall, Englewood Cliffs, New Jersey 1965.
13. Timoshenko, S. and Goodier J.N., "Theory of Elasticity", McGraw-Hill Book Company, New York, 1957.
14. ICES STRUDL II, The Structural Design Language, Engineering User's Manual, MIT, Department of Civil Engineering, 1968.

Relative density of sand	Number of stories	External Column		Internal Column		General spring constant (10^{10} kgfcm/Rad)
		Footings Dimensions (cm)	Spring Constant (10^3 kgf/cm)	Footings Dimensions (cm)	Spring Constant (10^3 kgf/cm)	
50%	5	135/135	62.7	180/180	83.7	36.4
	10	185/185	86.1	250/250	116.0	50.0
	15	230/230	107.0	305/305	142.0	62.0
90%	5	95/95	70.0	125/125	92.0	40.5
	10	135/135	99.5	180/180	132.5	57.5
	15	160/160	118.0	215/215	159.0	68.5

TABLE 1 ISOLATED FOOTINGS ON SAND

Elastic modulus of clay(kgf/cm ²)	Number of Stories	Spring constant for		Spring constant for sliding(10^5 kgf/cm)
		focking(10^{10} kgf cm/Rad)	focking(10^{10} kgf cm/Rad)	
150	5	33.0	33.0	23.7
	10	33.0	33.0	33.5
	15	33.0	33.0	41.1
250	5	55.0	55.0	39.5
	10	55.0	55.0	55.7
	15	55.0	55.0	68.5

TABLE 2 SPRING CONSTANTS, REPRESENTING CLAY LAYER UNDER RAFT FOUNDATION

Elastic Modulus of clay kgf/cm ²	Number of Stories	Pile diameter (cm)	Mass of an Individual pile per lm (kgf sec ² /cm/m)	General spring constant (10 ⁴ kgf/cm)
150	5	50	0.480	50.2
	10	70	0.945	70.0
	15	85	1.395	85.0
250	5	50	0.480	75.5
	10	70	0.945	94.0
	15	85	1.395	125.0

TABLE 3 PILE FOUNDATIONS

TABLE 4. EFFECT OF FOUNDATION COMPLIANCE ON THE FUNDAMENTAL PERIODS AND ON SEISMIC LOADS

Case	Number of Stories	Foundation System	Elastic modulus of soil kgf/cm ²	T ₀ sec	T _s sec	Tap sec	T sec	$\frac{T}{T_0}$	$\frac{V}{V_0}$
A1		Isolated footings	250		0.408	0.808	0.808	1.16	0.95
A21			150		0.453	0.830	0.832	1.20	0.94
A22	5	Raft	250	0.695	0.350	0.780	0.784	1.13	0.96
A31			150		0.400	0.803	0.820	1.18	0.95
A32		Piles	250		0.327	0.770	0.790	1.14	0.96
B1		Isolated footings	250		0.882	1.42	1.42	1.28	0.92
B21			150		1.16	1.61	1.58	1.43	0.89
B22	10	Raft	250	1.11	0.900	1.43	1.40	1.26	0.93
B31			150		0.462	1.20	1.25	1.13	0.96
B32		Piles	250		0.397	1.18	1.22	1.10	0.97
C1		Isolated footings	250		1.44	2.12	2.14	1.37	0.90
C21			150		2.08	2.60	2.55	1.63	0.85
C22	15	Raft	250	1.56	1.61	2.24	2.23	1.43	0.89
C31			150		0.550	1.64	1.73	1.11	0.96
C32		Piles	250		0.416	1.61	1.69	1.08	0.98

Fig. 1 :
Mechanical model of isolated footings as a foundation system.

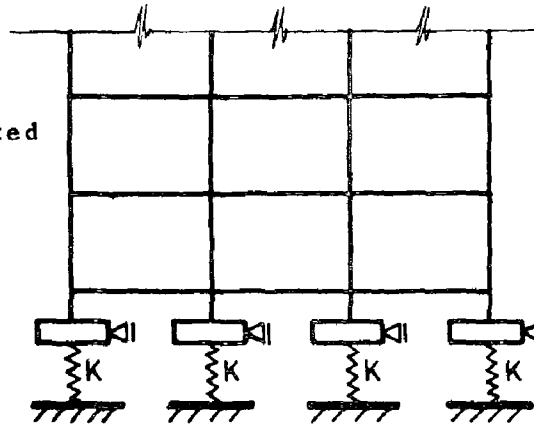


Fig. 2 :
Stress distribution under circular footing.

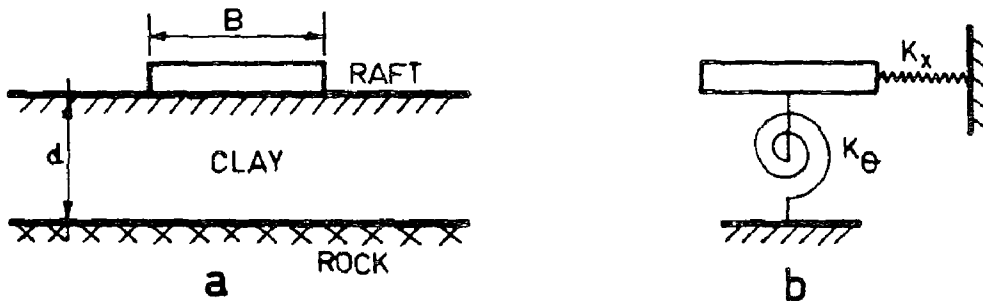
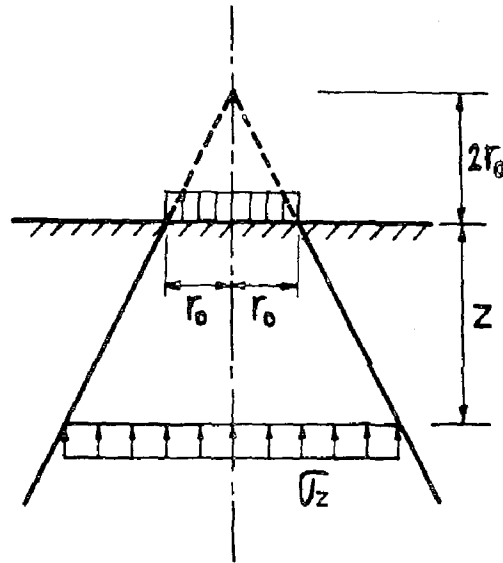


Fig. 3 : Mechanical model of a raft foundation.

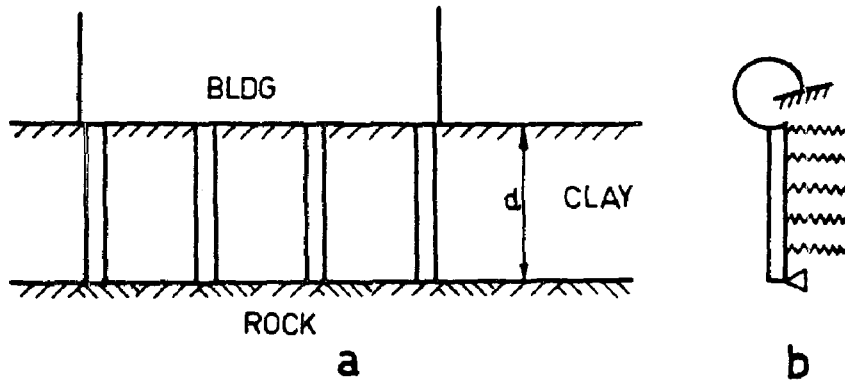


Fig. 4 : Mechanical model of a system of pile foundation.

Fig. 5 :
Elastic half space
under a line load.

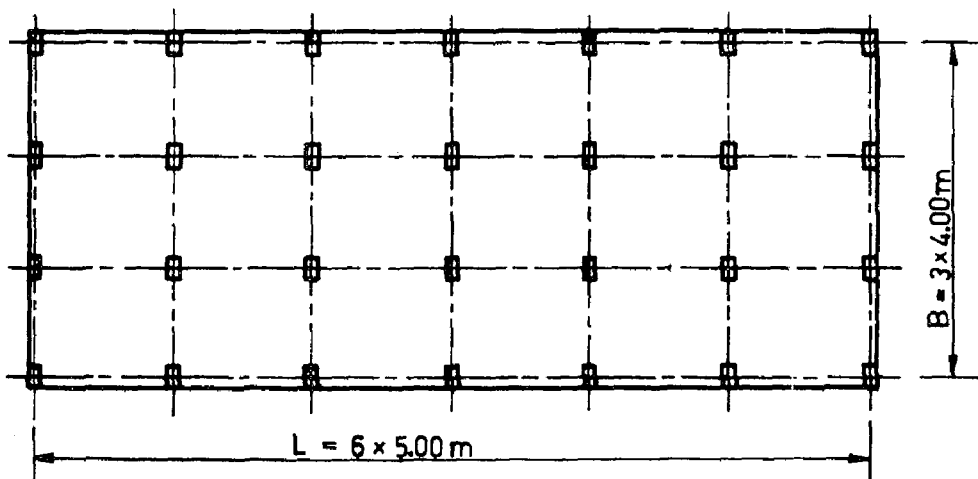
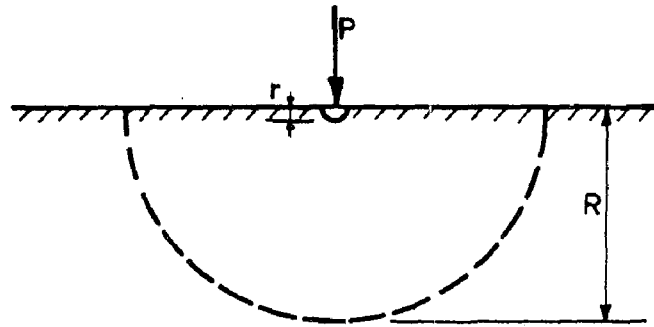


Fig. 6 : Typical floor plan of structures.

All cross sections of beams are 20/50 cm.

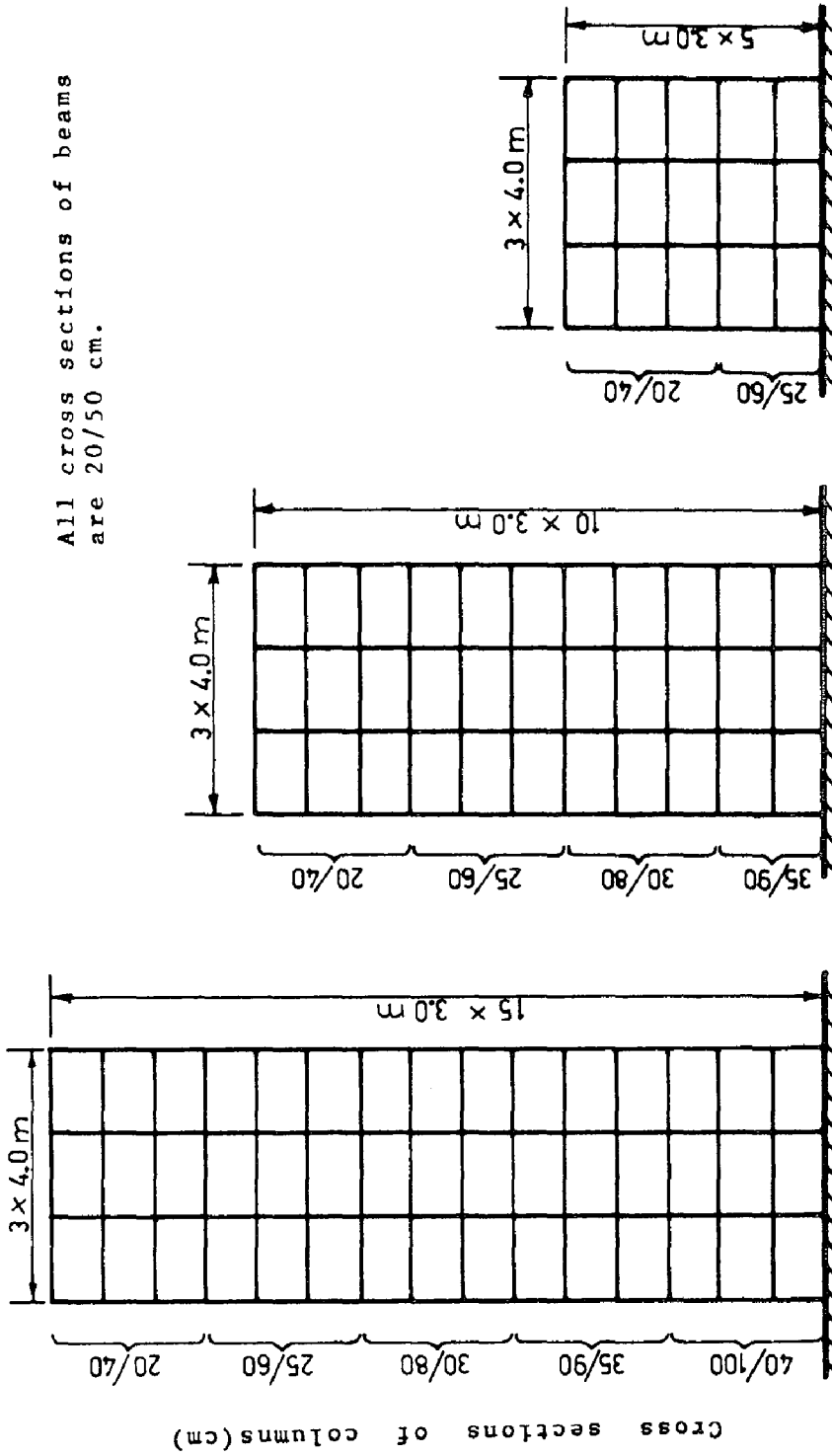


Fig. 7 : Elevation and detail of frames.

Fig. 8 : Idealized supports for computation of T_0

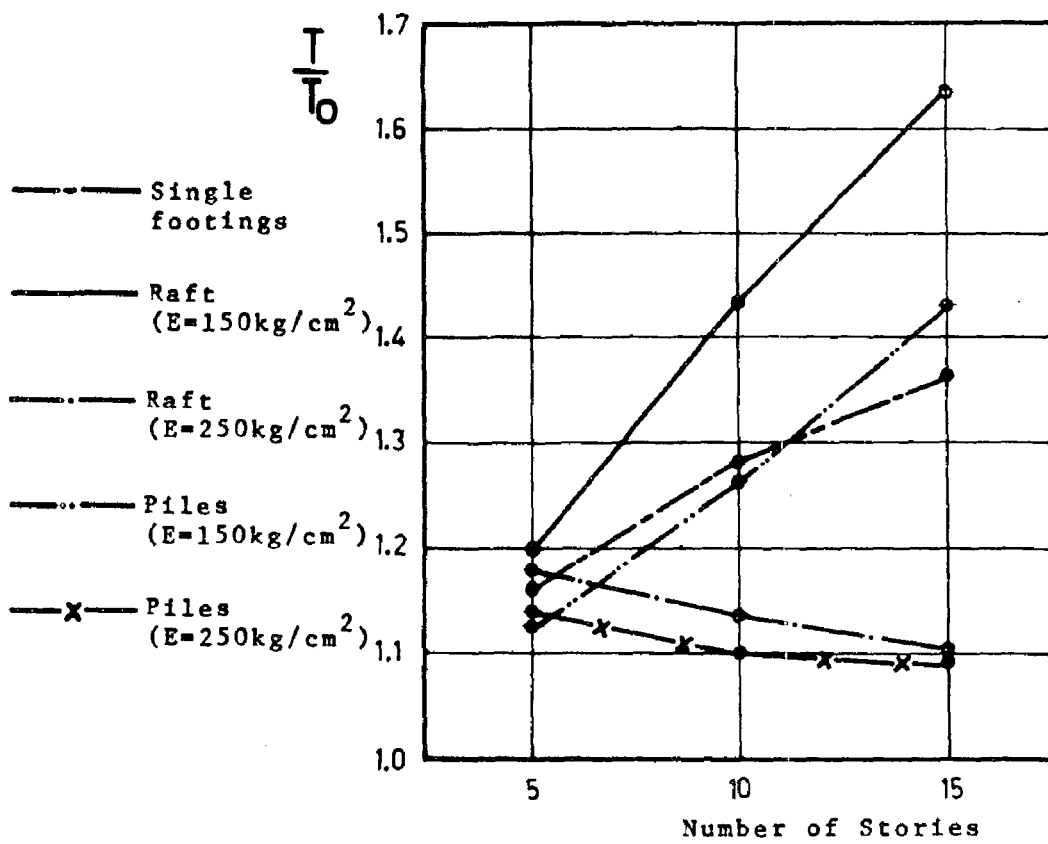
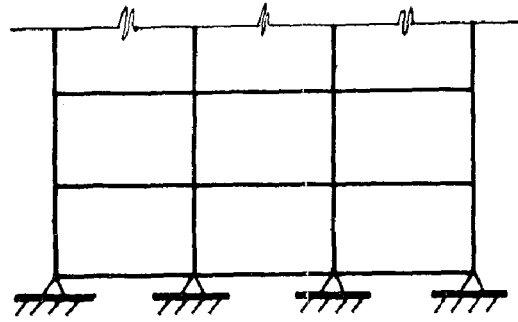


Fig. 10 : The fundamental period as influenced by building height and foundation system.

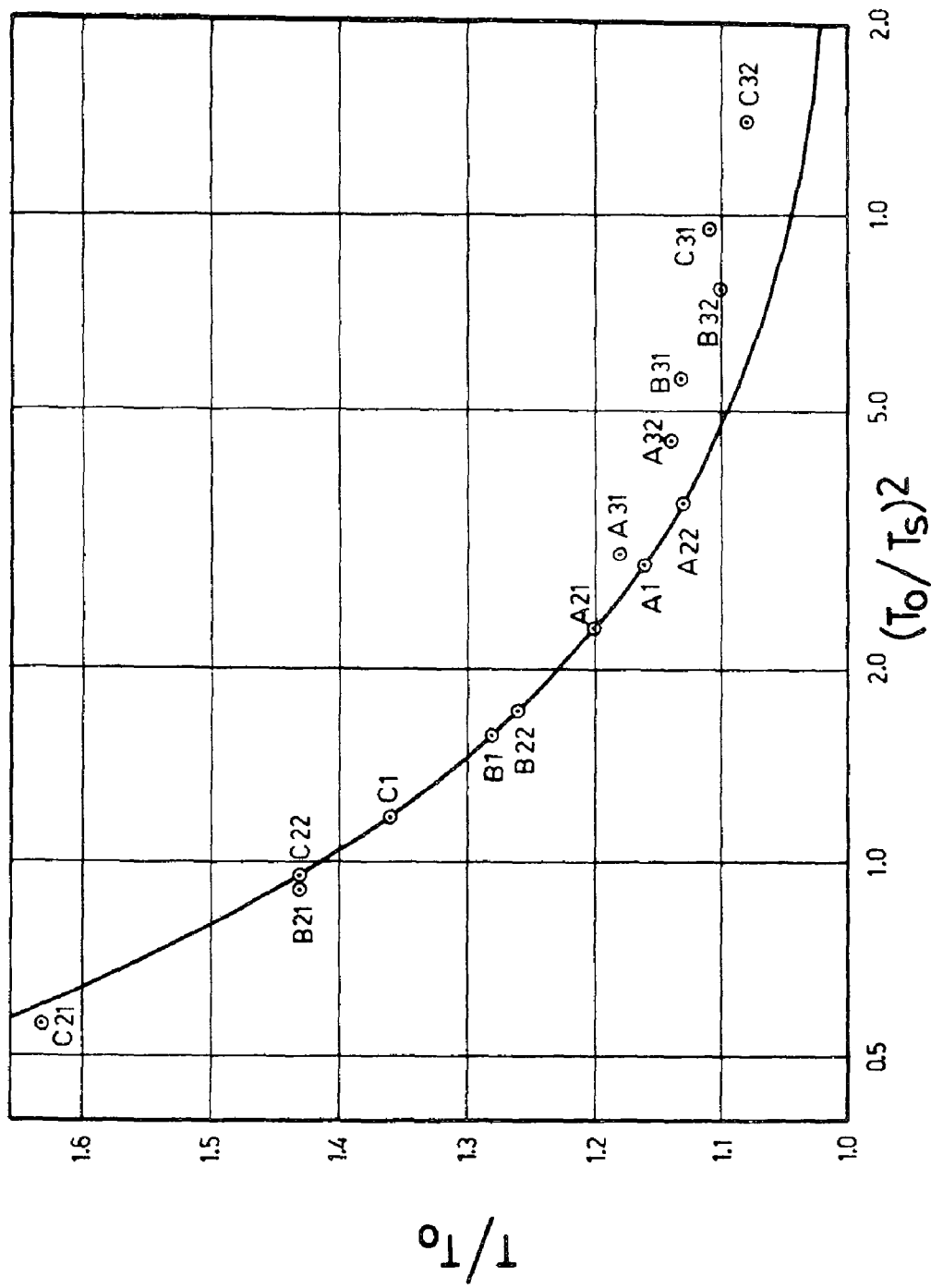


Fig. 9 : The influence of foundation compliance on the period.

INTERNATIONAL SYMPOSIUM ON
EARTHQUAKE STRUCTURAL ENGINEERING

147

St. Louis, Missouri, USA, August, 1976

INVERTED-PENDULUM EFFECT ON SEISMIC RESPONSE OF TALL
BUILDINGS CONSIDERING SOIL-STRUCTURE INTERACTION

TEH H. LEE

Senior Staff Engineer

General Atomic Company

San Diego, California, United States

ABSTRACT

The analyses of seismic response of high rise buildings have been customarily performed without taking into account the dynamic effects resulting from the dead weight of the structures. In the event of an earthquake disturbance, the rotation of the building due to soil-structure interaction will shift the center of gravity of the building laterally. This means that, while responding to the excitations due to ground motion, the system will behave as an inverted pendulum influenced by its own weight. Furthermore the phenomena can be shown to be coupled with the structural deformation which causes the centers of gravity of the structural members to move laterally. Although it is known to seismic analysts that this gravitational effect depends primarily upon the aspect ratio of the system and the foundation stiffness, its significance has not been accurately quantified for tall buildings on soft ground where the soil-structure interaction effect is playing an important role.

This paper demonstrates how the phenomena can be studied by using a soil-structure interaction model. Modified governing equations were derived and incorporated in an interaction analysis utilizing fixed-base modes of the superstructures. In this manner, the problem was investigated by modelling the soil medium as an elastic half-space. The inverted pendulum effects, with and without the consideration of structural deformation, are discussed on the basis of the numerical results obtained.

Preceding page blank

1. INTRODUCTION

The dynamic effects of gravity loads on structural response during earthquake has long been recognized by engineers. In the early studies of this problem, highly simplified models were used to obtain a qualitative assessment of the phenomenon. The change observed in these investigations when considering gravity influence was a reduction in the natural frequencies of the system (see, for example, Newmark [1]). The effects are more pronounced for tall structures, such as high-rise buildings, on soft ground and are insignificant for squat structures founded on rock. Technically speaking, the phenomenon depends to a large extent on the aspect ratio of the structure and the foundation stiffness which governs the rotation of the system during earthquake. Very little has been done so far for an accurate determination of the effect upon the dynamic response of the structural masses or members. Due to difficulty in deriving the modified governing equations for complex structures with gravity loads, the inclusion of gravitational influence in soil-structure interaction models has not yet been made feasible.

In the present paper, it will be demonstrated how the gravity effects may be incorporated in a model as complicated as a three-dimensional system in which the soil-structure interaction effects are accounted for by coupling the structure with an elastic half-space. This was accomplished by modifying the potential energy expression associated with gravity load and then deriving the modified governing equations using the Lagrange's equations of motion. In essence, the new equations govern the motions of a seismic model in which the structure-base system will behave as a flexible inverted pendulum while responding to the disturbances from the ground motions.

2. MATHEMATICAL FORMULATION

Consider, for the moment, the two-dimensional structure on an elastic half-space as shown in Figure 1. Rigorous derivation of its equations of motion including gravity effects associated with both the rigid-body rotation and the structural deformation may be achieved by considering the potential energy change resulting from gravity load. The mathematical formulation is, in general, rather involved. However, for a preliminary investigation, an insight to the problem can be obtained by taking an idealized model (Figure 2a) in which the structural deformation is characterized by lateral deflections of masses only. In this case, the necessary terms in the equations of motion reflecting gravity influence can be derived by only considering the change in potential energy due to rigid-body rotation of the system plus the lateral deflections of the masses. For instance, the potential energy change, V_g , at the i th mass, m_i , will be (Figure 2b)

$$V_g = - m_i g \left(h_i \frac{\theta^2}{2} + u_i \theta \right) \quad (1)$$

where g is the gravitational constant, h_i is the elevation of mass as indicated in Figure 2, θ is the base rotation and u_i is the lateral deflection of mass along x_1 -direction. Adding the potential energy change from all masses and extending the analysis to three-dimensional problem, the expression for the total change in potential energy resulting from gravity load due to building rotation and lateral deflections of N superstructure masses (ignoring contribution from the base mass) may be written, for small rotations, as follows:

$$V_g = - \sum_i^N \left[m_i g \left(h_i \frac{\theta_3^2}{2} + u_i \theta_3 \right) + m_i g \left(h_i \frac{\theta_1^2}{2} - w_i \theta_1 \right) \right] \quad (2)$$

where θ_1, θ_3, u_i and w_i are coordinate variables.

In writing the above equations, the notation for three-dimensional analysis has been used. The three components of rotation ($\theta_1, \theta_2, \theta_3$) and mass displacement relative to base (u, v, w) are defined corresponding to the three axes (x_1, x_2, x_3) in their respective coordinate frames.

Substituting Eq. (2) into the Lagrange's equations of motion yields the following additional terms representing gravity influence

$$\frac{\partial V_g}{\partial u_i} = - m_i g \theta_3, \quad (i = 1, 2, \dots, N) \quad (3)$$

$$\frac{\partial V_g}{\partial w_i} = m_i g \theta_1, \quad (i = 1, 2, \dots, N) \quad (4)$$

$$\frac{\partial V_g}{\partial \theta_1} = - g m_t \bar{h} \theta_1 + g \sum_j^N m_j w_j \quad (5)$$

$$\frac{\partial V_g}{\partial \theta_3} = - g m_t \bar{h} \theta_3 - g \sum_j^N m_j u_j \quad (6)$$

where m_t is the superstructure total mass and \bar{h} is the elevation distance of the superstructure center of mass as defined by the equation

$$\bar{h} = \frac{\sum_i^N m_i h_i}{m_t} \quad (7)$$

Note that for the problem considered here, contribution to V_g does not involve torsional rotation θ_2 .

The governing equations for a three-dimensional soil-structure interaction model using elastic half-space for ground simulation have been previously presented by Lee and Wesley ([2], [3]). Using the notation adopted in those papers and adding the gravity influence as given by Eqs. (3)-(6), the modified governing equations may be written

$$[\mathcal{M}] \{\ddot{q}\} + [C] \{\dot{q}\} + [K] \{q\} = - [P] \{\ddot{U}_B\} + g [\Psi]^t [T^m] \{U_B\}, \quad (8)$$

$$\begin{aligned}
 & (\left[M^B \right] + \left[A \right]^t \left[m \right] \left[A \right]) \left\{ \ddot{U}_B \right\} + \left[P \right]^t \left\{ \ddot{q} \right\} \\
 & - g m_t \bar{h} \left[T^1 \right] \left\{ U_B \right\} - g \left[T^m \right]^t \left[\Psi \right] \left\{ q \right\} = \left\{ \bar{f} \right\}. \quad (9)
 \end{aligned}$$

where the symbols used were already defined in [3] except that new matrices $[T^m]$ and $[T^1]$ have been introduced. The matrix $[T^m]$ contains zeros and masses. The elements in $[T^1]$ are zeros and unity. The symbol $[]^t$ denotes the transpose.

For harmonic response, Eq. (8) may be solved for $\{q\}$ to give the following expressions:

$$\left\{ \bar{q} \right\} = - \left[\tilde{D} \right] \left[P \right] \left\{ \bar{U}_B \right\} + g \left[\tilde{D} \right] \left[\Psi \right]^t \left[T^m \right] \left\{ \bar{U}_B \right\} \quad (10)$$

$$\left\{ \bar{q} \right\} = \left[D \right] \left[P \right] \left\{ \bar{U}_B \right\} - g \left[D \right] \left[\Psi \right]^t \left[T^m \right] \left\{ \bar{U}_B \right\} \quad (11)$$

where a bar over the column matrix designates the complex amplitude and $\left[\tilde{D} \right] = \frac{1}{\omega^2} \left[D \right]$. The matrix $[D]$ is a modal amplification matrix which has been defined in [3]. Substituting Eqs. (10)-(11) in Eq. (9) yields

$$\begin{aligned}
 & (\left[M^I \right] + g \left[T^m \right]^t \left[\Psi \right] \left[\tilde{D} \right] \left[P \right]) \left\{ \bar{U}_B \right\} \\
 & - \left(g m_t \bar{h} \left[T^1 \right] + g \left[P \right]^t \left[D \right] \left[\Psi \right]^t \left[T^m \right] \right. \\
 & \quad \left. + g^2 \left[T^m \right]^t \left[\Psi \right] \left[\tilde{D} \right] \left[\Psi \right]^t \left[T^m \right] \right) \left\{ \bar{U}_B \right\} = \left\{ \bar{f} \right\} \quad (12)
 \end{aligned}$$

where $\left[M^I \right] \equiv \left[M^B \right] + \left[A \right]^t \left[m \right] \left[A \right] + \left[P \right]^t \left[D \right] \left[P \right]$

The base displacement column matrix \bar{U}_B can be decomposed into two terms

$$\left\{ \bar{U}_B \right\} = \left\{ \bar{U}_G \right\} + \left\{ \bar{U}_I \right\} \quad (13)$$

in which $\{\bar{U}_G\}$ is the column matrix of ground motion and $\{\bar{U}_I\}$ is known as the column matrix of interaction displacement. Replacing $\{\bar{f}\}$ by the elastic half-space impedance functions in the following manner ([2] , [3])

$$\{\bar{f}\} = [K(i\omega)] \{\bar{U}_I\} \quad (14)$$

where $[K(i\omega)]$ is a 6 x 6 matrix containing impedance functions, the final equations can be put in the following form

$$\begin{aligned} & (\omega^2 [M^*] + g m_t \bar{h} [T^1] + g [K^D] + [K(i\omega)]) \{\bar{U}_I\} \\ & = - (\omega^2 [M^*] + g m_t \bar{h} [T^1] + g [K^D]) \{\bar{U}_G\} \end{aligned} \quad (15)$$

where $[M^*]$ corresponds to the dynamic feedback from the structure due to its inertia. It is defined as

$$[M^*] \equiv [M^I] + g [T^m]^t [\Psi] [\tilde{D}] [P] \quad (16)$$

and the term involving $[K^D]$ representing the influence due to structural deformation is defined by

$$[K^D] \equiv [P]^t [D] [\Psi]^t [T^m] + g [T^m]^t [\Psi] [\tilde{D}] [\Psi]^t [T^m] \quad (17)$$

Eq. (15) can be solved for $\{\bar{U}_I\}$ when the ground motion $\{\bar{U}_G\}$ is prescribed.

When structural deformation is neglected, the gravity influence comes from only one term

$$g m_t \bar{h} \left[T^1 \right] \quad (18)$$

which corresponds to the gravity load effects when the entire structure-base system behaves as a rigid inverted-pendulum. In this case, the total weight of the building gm_t and the \bar{h} parameter (or the aspect ratio parameter \bar{h}/r_0 where r_0 is the base radius) will play an important role.

3. NUMERICAL RESULTS

The modified governing equations derived in the preceding chapter retain the gravitational effects which are coupled with the soil-structure interaction. Numerical results were obtained for a tall building simulated by an idealized two-mass superstructure on rigid circular base with $h_1 = 250\text{ft}$ and $h_2 = 125\text{ft}$. The center of mass of the superstructure is at $\bar{h} = 168.6\text{ft}$ and the aspect ratio parameter is $\bar{h}/r_0 = 2.8$. The ground motion was taken to be harmonic and the data generated were in terms of frequency response for a two-dimensional problem. For the preliminary investigation conducted here with simplifying assumption introduced for the structural deformation, the major effect comes from the dynamic behavior of a rigid inverted pendulum. The gravitational influence was found to diminish to an insignificant level for buildings having low aspect ratios built on relatively stiffer ground. Quantitatively, when the shear wave velocity V_s in the elastic half-space is greater than 500 FPS, gravity influence is negligible for $\bar{h}/r_0 < 3$.

Figure 3 shows the frequency response of the top mass in the vicinity of the first peak obtained with consideration of gravity influence as compared to that determined by conventional analysis ignoring gravity. As the shear wave velocity V_s of the elastic half-space reduces, the rotation (rocking) of the building becomes greater, and the top mass amplification rises. The phenomena observed here agree with those previously found by Parmelee [4]. Apparently, the influence of gravity load tends to reduce the resonant frequencies of the system and the frequency shift becomes larger as V_s drops. Another important finding is that the dynamic amplification of top mass was found to be higher when gravitational effects were included in the analysis.

The gravitational influence resulting from structural deformation characterized by lateral deflection only is not significant judging from the numerical results generated for this problem. This was expected because the lateral displacement of the structural masses is primarily due to the rigid-body rotation of the system and the lateral deflection is secondary in this case. The numerical values of the top mass frequency response obtained with and without considering lateral deflection of masses are displayed in Table I.

Table I. INFLUENCE OF STRUCTURAL DEFORMATION

Excitation Frequency, Hz	Top Mass Amplification ($V_s = 150$ FPS)	
	Lateral Deflection Neglected	Lateral Deflection Considered
.0720	41.938	43.456
.0725	70.353	74.168
.0730	123.245	124.203
.0735	78.936	74.700
.0740	45.339	43.626
.0745	30.946	30.098

4. CONCLUSIONS

The influence of gravity load characterizing the dynamic behavior of a flexible inverted pendulum has been incorporated into a seismic model which accounts for the soil-structure interaction effects. The formulation is applicable to more involved three-dimensional models. Although the initial study discussed here was conducted for a simple system with idealized structural deformation, it has revealed important quantitative information regarding the nature of the gravitational influence on the building response during earthquake.

The gravity effect does not become a significant factor unless building is tall. It needs not be considered in seismic analyses of short and squat structures such as nuclear reactors. The effect, however, becomes relatively more important for tall buildings when foundation softening is developing during seismic disturbances.

The potential energy change associated with structural deformation was highly idealized. This results in the very small changes as shown in Table I. The gravity influence contributed from structural deformation is expected to be greater when more rigorous expressions are used for the work done by gravity forces. These include the consideration of the shortening of distance in the axial direction as the structure deforms. Such problems will be treated in future papers.

5. DISCLAIMER

The work presented in the paper is a personal product of the author who is responsible for the accuracy of the results and the opinions herein expressed. It does not necessarily reflect the official views of his employer.

6. REFERENCES

1. Newmark, N. M., and Emilio Rosenblueth, Fundamentals of Earthquake Engineering, 1971, Prentice-Hall Inc.,
PP. 53 - 56.
2. Lee, T. H. and D. A. Wesley, "Soil-Foundation Interaction of Reactor Structures Subjected to Seismic Excitation", Proc. 1st Int. Conf. Struct. Mech. in Reactor Technology, Berlin, Germany, September 1971, Paper K3/5.
3. Lee, T.H. and D. A. Wesley, "Soil-Structure Interaction of Nuclear Reactor Structures Considering Through-Soil Coupling Between Adjacent Structures", Nuclear Engineering and Design, 24, 374-387 (1973).
4. Parmelee, R. A., "Building-Foundation Interaction Effects", Journal of the Engineering Mechanics Division, ASCE, EM2, pp. 131-151.

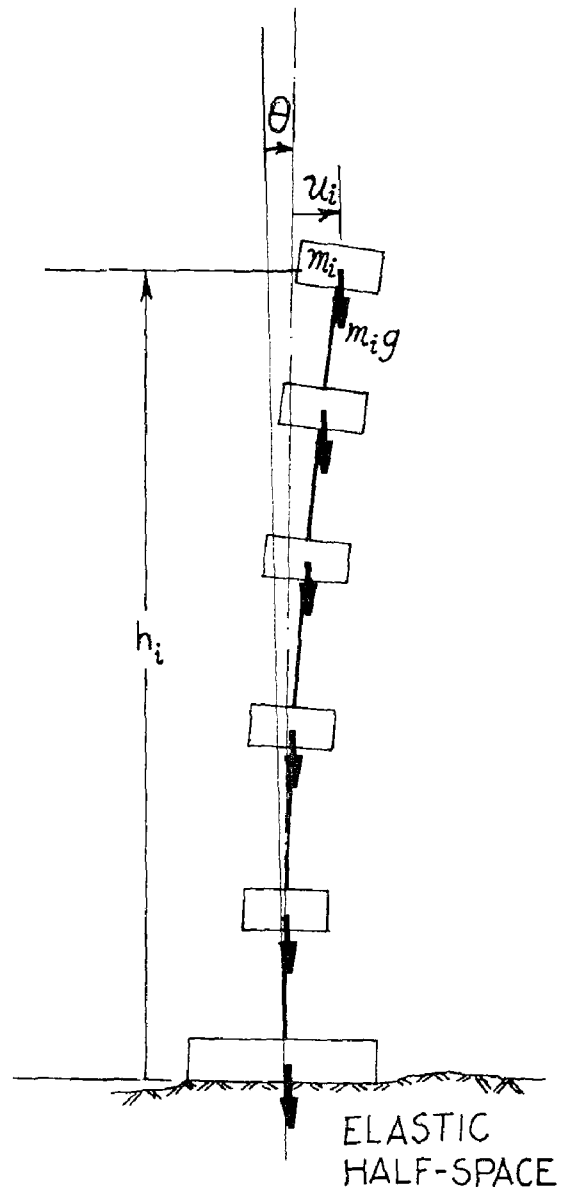


FIGURE 1. THE INVERTED-PENDULUM EFFECT ASSOCIATED WITH DYNAMIC RESPONSE

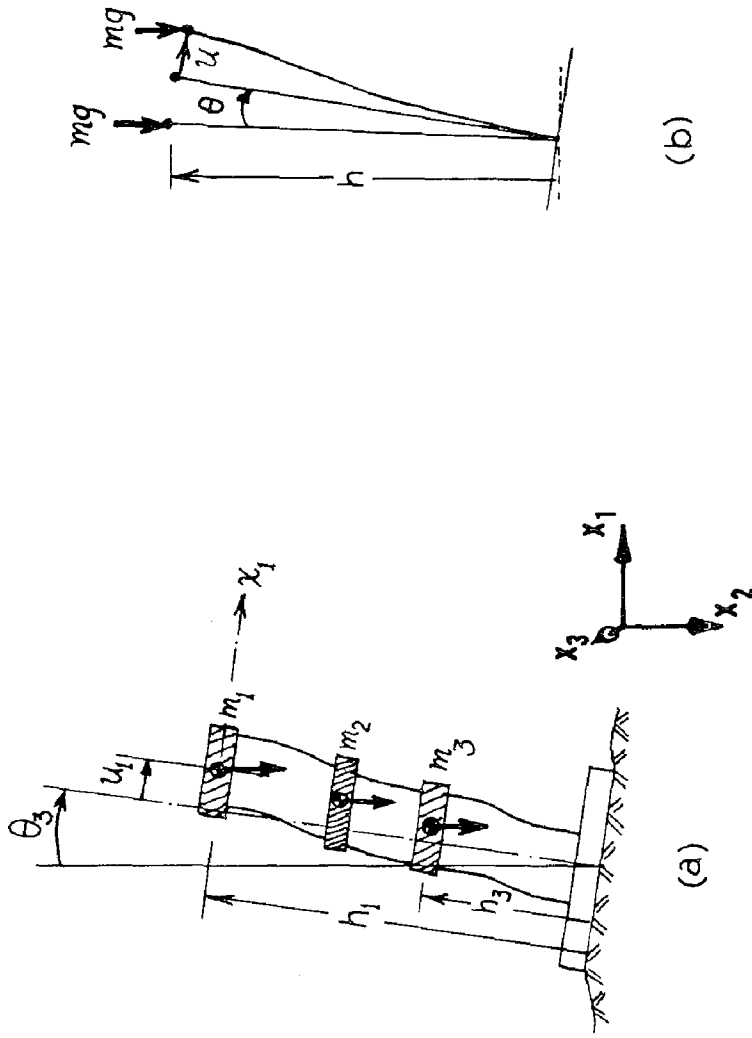


FIGURE 2. IDEALIZED STRUCTURAL DEFORMATION AND POTENTIAL ENERGY CHANGE

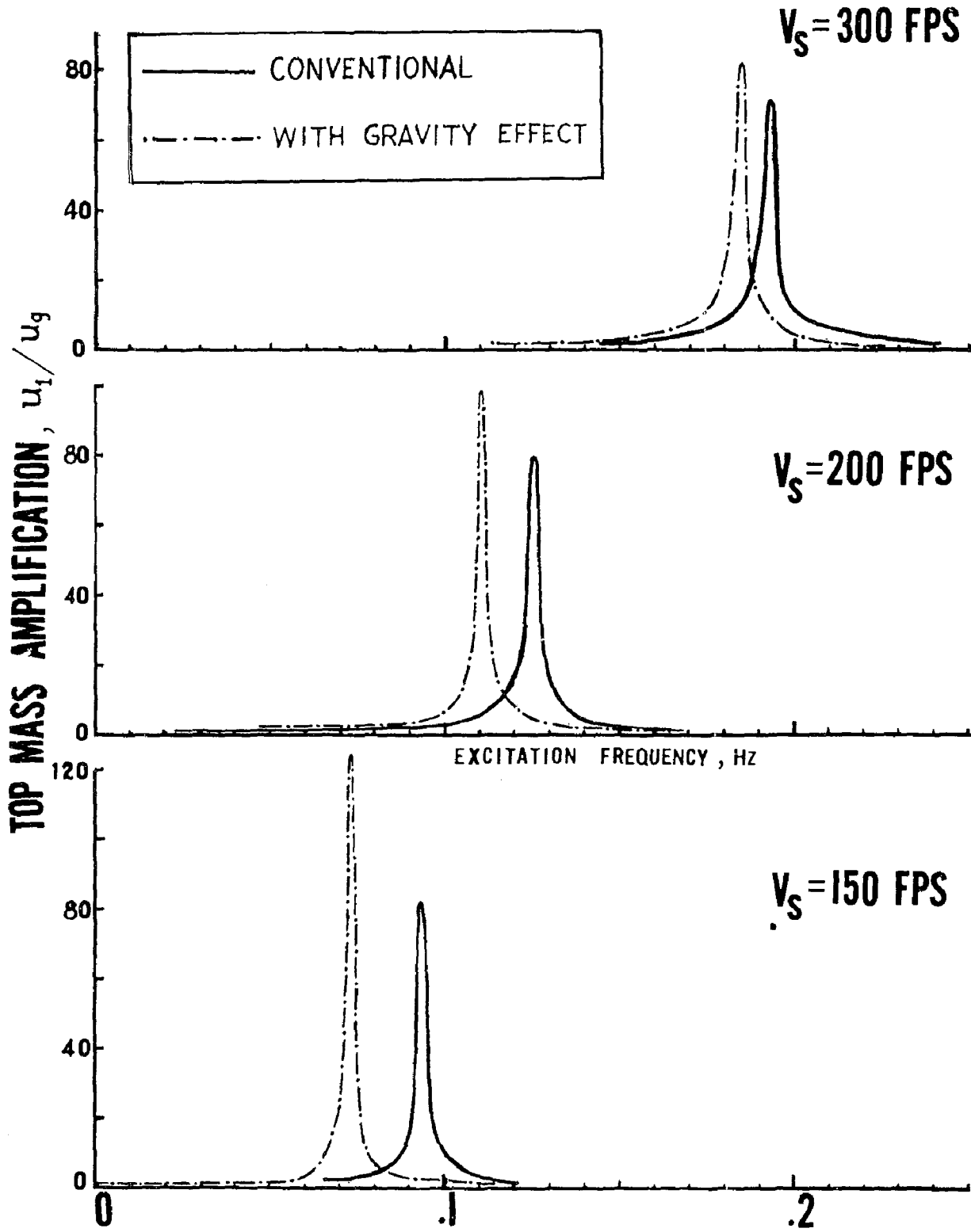


FIGURE 3. COMPARISON OF FREQUENCY RESPONSE CONSIDERING SOIL-STRUCTURE INTERACTION

INTERNATIONAL SYMPOSIUM ON
EARTHQUAKE STRUCTURAL ENGINEERING

161

St. Louis, Missouri, USA, August, 1976

ON THE USE OF PRECAST PILE-FOUNDATIONS IN CONSTRUCTION
OF EARTHQUAKE-PROOF LARGE-PANEL BUILDINGS

L.D. Martynova, Techn.M., TSNIEP zhylisha,
Y.A. Simon, Dipl.Eng., TSNIEP grajdanselstroy,
V.F. Zakharov, Dipl.Eng., Alma-Ata housing construction
N.V. Kondratyev, Dipl.Eng. integreted enterprise, Moscow,
Alma-Ata, USSR.

SUMMARY

This paper presents the results of the research of earthquake large-panel dwelling houses on precast pile-foundations under conditions of bed on building site of the unstable soil.

The calculation dynamic scheme of building, the results of natural tests of fragment of precast pile-foundation and large-panel 5-storey house by means of high capacity inertial vibrator are being discussed.

Rigidity of pile-foundation plays a significant role in the total deformation of a large-panel house, but practically it doesn't influence the frequency of its oscillation as was established in the results of the tests.

Rigidity of pile-foundation is determined both by the rigidity of grating and by piles.

The calculation dynamic scheme of large-panel building on the pile-foundation may be represented as a cantilever elastically-jammed in level grating and pile-foundation in the form of one storey frame.

Besides the investigations show that all constructions above precast pile-foundation of building and also their joints possess sufficient strength in order to resist earthquake of various intensity.

INTRODUCTION

The most part of earthquake territory of Soviet Union have the unstable and yielding ground.

Large-scale erection in this conditions of large-panel dwelling houses required the implementation of earthquake building of progressive shapes of foundation and pile-foundations, in particular.

The results of investigations.

The pile foundation represents a through construction and consists of separate slender pivot-piles, dispersed in ground and connected in level upper part beam framework in distinction from foundation plate and wall. The perception and average of seismic influence of ground on building takes place not on the level of solid foundation plate as in the case of foundation wall and plate, but only on the level of grating by based on of large-panel building on pile foundation

The total oscillations of the building on the whole remains qualitative identical to the oscillations of the building on solid foundation however the pillars experience bending deformations and piles absorb part of energy, transfer oscillation to the ground.

Calculation scheme of large-panel building in pile-foundation one can take as cantilever system in the form of pivot with a number of points compacts on its height, which is based on rigid disk (grating) that is supported by a number of slender pivot-piles.

For the sake simplification the calculation of a building in this case comes to the calculation of its above foundation part and separately the pile-foundation.

The cantilever pivot elastically-jammed in level grating is taken as a calculation scheme of above foundation part. The pile-foundation in its turn can be in the form of one storey frame, which is acted by of vertical load and seismic forces which in level grating.

The calculation above foundation part of building is done according to general used rules of calculation of large-panel buildings on rigid foundation, but taking into account the yielding pile-foundation.

The calculation of frame is being done in accordance with the ordinary rules of construction mechanics in assumption of static action of external forces. The distribution of seismic forces among separate bearing vertical constructions of frame (piles) is being done in dependence of construction solution of horizontal disk (grating).

The most favourable solution of pile foundation can be achieved by safe secure of horizontal ties of all piles in system. This condition demanded the organization of monolithic grating.

However monolithic reinforcement grating requires the organization of planking, application in big volume of manual labour, quality control of placing of concrete in mounting

and in winter conditions is heating of concrete or application of special admixtures. All this results in reduction of degree of industrialization of pile-foundations and prolonging the time of building.

One can avoid all these lacks by means of organization of precast grating, transferring a considerable part of work into factory conditions.

The problem of possible use of precast grating was examined on the basis of special investigations devoted to the study of earthquake-proof of large-panel buildings on precast pile-foundations in conditions of bedding unstable soil of small power on construction site (5-6 m).

The construction schemes of experimental house are given in figure 1.

The principal bearing elements of pile foundation are rammed reinforcement grating-poles, which cut through slack soil and with their lower ends rest on dense incompressible stratum of gravel-pebbles deposits and a beam of grating. Conjugate of beam of grating with piles is performed by means of reinforcement heads of piles (fig.1a). The heads of piles having through holes are put on the heads of two or three piles monolithing of cavity of holes with small-grained concrete is the next.

Joining of precast beams of grating with each other and with heads is performed by means of welding of laying details.

The strength of separate structures of foundation, its joinings and hardness and stability of pile-foundation on the whole by influence in it of horizontal vibrating loadings of seismic type was the first step in the investigation.

The fragment of precast pile foundation which composited 1/5 part of experimental house was erected at one of from building sites and was subjected to natural tests.

The fragment was loaded with calculated vertical statical loading which was imitated by the weight of panels stacking against each other.

The panels were displaced aside from the central axle of fragment in order to place a powerful vibration machine inertial action with the help which and are conduct tests.

The total volume of tests included a number of consecutive cycles of vibration loading with the increasing indignant force.

This was achieved by modification of mass debalances in vibrators.

The fragment was introduced into resonance at every stage of tests by easy change of rate rotation of debalances this was done twice - in increasing and in falling of rate rotation (frequency of oscillations).

Registration of horizontal transferences of grating in the process of forced oscillation of pile-foundation was performed by means of apparatuses in all intersection of grating beams.

The resonance curves were got as a result of treatment of oscillogram which represents the record of horizontal transferences of fragment under all cycles its vibration loading (fig.2).

Moreover the test fragment is in two resonance states on two first stages of loading and in two following - in one.

In the diapason close to the first resonance peak the whole mass of grating and bailast of loading moved progressively in the direction of the action of insurrected force and at the approach of second resonance peak simultaneously with horizontal transference of beam torsion oscillations of mass bailast of weight moved around their own central axes of perpendicular to the action of vibration machine.

As the law of inertial excitement of constructions by vibration load can be considered of harmonious, the inertial forces at the moment of passing resonance with sufficient degree of precision can be determined by ordinary formula:

$$S_i = m \cdot a, \quad (1)$$

where S_i - inertial force t;

m - total mass of oscillating system in t·sec²/m

a - acceleration with oscillate system in m/sec² and accordingly being determined by formula

$$a = 4 \pi^2 \varphi^2 A_i, \quad (2)$$

where φ - frequency of oscillation of system in cps.

A_i - amplitude of oscillations of points system in the level to be defined in m.

The inertial forces were determined for every stage of loading in accordance with the fixed φ and A_i on adducing above formulas, taking the whole mass of loading grating applied in level of head of pile.

In spite of some defects while testing in constructions

of grating (weak sides of heads, insufficient anchoring of laying details in beams of grating) the fact of taking the most part of horizontal inertial force by fragment (which equals approximately 80% from calculation in earthquake force 9) showed that pile-foundation of such construction can possess sufficient strength, rigidity, stability from the earthquakes of different intensity.

Natural test of two-section 5 storied dwelling was conducted to study the behaviour of large-panel building on precast pile-foundation under seismic forces. The roof of the house lacked at the time of the test as some vibromachines had to be located on the floor of the 5 story.

The test of dwelling was conducted in the same way as in the case of a fragment (the same method).

The total volume of test consisted of a number of cycles of vibro-loading of dwelling both in transverse and in longitudinal directions.

Records of horizontal and vertical oscillations of dwelling were conducted synchronously with the help of set of vibro-apparatus.

Horizontal oscillations of dwelling were registered in 7 levels of its height and vertical oscillations were registered in the level of grating.

The analysis of resonance curves (fig.3) has shown that dwelling under test in all cycles of vibration loading is only in one resonance state, but in most dangerous one.

The criterion of the behaviour of large-panel dwelling on precast pile-foundation in earthquake can be taken the form of its oscillation (fig.4) which is nearing to the form typical to the system shear with bending (this corresponds to the modern calculation of large-panel building on rigid foundation), but with additional components of oscillation and displacement their values prove the significant role of pliability of pile-foundation in the total deformability of a dwelling.

The pliability of pile-foundation is determined by its rigidity which is the combination of rigidity of grating and piles, the most part of rigidity of pile-foundation being provided by the rigidity of grating.

So for example, coefficient of rigidity of pile-foundation of the experimental house was $0,504 \cdot 10^6$ t/m, and coefficient of rigidity of grating was $0,329 \cdot 10^6$ t/m. The rigidity of piles has to be taken into account otherwise it will lead to the decrease of calculation of seismic load.

The rigidity of piles can be neglected when the rigidity of grating is much more than that of piles.

The substitution of solid foundation by pile-foundation influences greatly the elastic deformation of a building and the frequency changes insignificantly.

This doesn't allow - to decrease the value of dynamic coefficient in the well-known formula on determining seismic calculation force.

The intensity of oscillations of building was increased in comparison with original loading by 7 times for transverse and by 13,5 times for longitudinal in the process of testing and under successive increase of mass debalances.

The forces in building were achieved which equalled 86-90% of calculation for force 9. Visible fractures and cracks were not discovered in construction of building and pile-foundation. The lack of fractures accounts for more favorable conditions of foundation work in the system of a building than separate foundation from one side and the change of reinforcement of head piles on the other side.

In spite of the visible lack of fracture the decrease of resonance frequency of oscillation of the system "building-foundation" was registered in every cycle of loading this accounts for the decrease of original rigidity of the system due to the development of plastic deformations in joints and due to the irreversible pressing down of ground in contact with construction of pile-foundation.

CONCLUSIONS

1. The conducted investigations allowed to determine the influence of pile-foundation on the dynamic work of large-panel building, to check the strength of separate constructions of building and precast grating and also the joints under dynamic loadings nearing the calculated loadings under force 9.

2. It is established that the structure of pile-foundation doesn't result in significant change of dynamic calculated scheme of large-panel building and this scheme is being considered in the calculation of the building with a rigid foundation (wall, and plate). In this very case the elastic jam of cantilever pivot in level of grating is being introduced into calculation scheme of building thus reaching the registration of pliability of pile-foundation.

3. The rigidity of piles should be taken into account as well as the rigidity of grating in the determining of the rigidity of pile-foundation. The rigidity of piles can be neglected only in the case when it is much less than that of grating.

4. In the course of test the forces were excited comprising 90% of calculation for seismic force 9. However no visible fractures and cracks in above foundation construction of building and in grating were discovered although the amplitude of oscillation of upper floor reached its maximum value in 7,8 mm and in grating - 3,4 mm.

5. The data received as a result of these investigations permit to make a conclusion that large-panel buildings on precast pile-foundations can be earthquake-proof as well as the buildings on solid foundations.

REFERENCES

1. Дотлибов А.М., Мартынова Л.д. Строительство крупнопанельных домов на свайных фундаментах в сейсмических районах на просадочных грунтах малой мощности. М., ЦНТИ, 1973.
2. Шапиро Г.А., Мартынова Л.д., Симон Ю.А., Захаров В.Ф., Кондратьев Н.В. О сейсмостойкости крупнопанельных зданий на сборных свайных фундаментах. Ж. "Жилищное строительство", №2, 1976.
3. Вибрационные испытания зданий. Под редакцией проф. Г.А. Шапиро, М., Стройиздат, 1972 г.

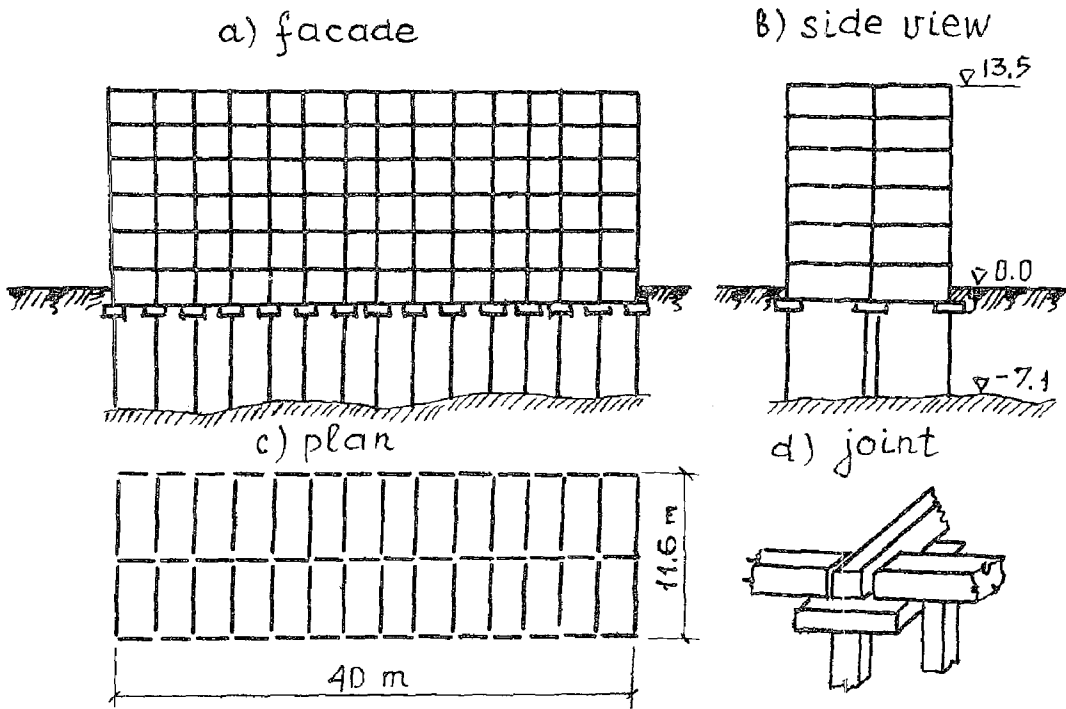


Fig. 1

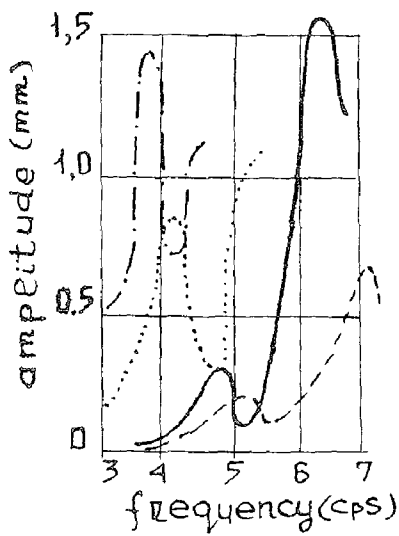


Fig. 2

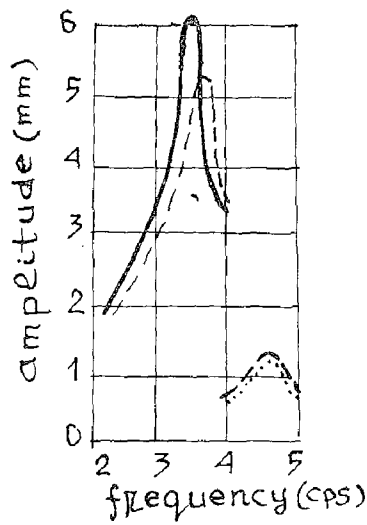


Fig. 3

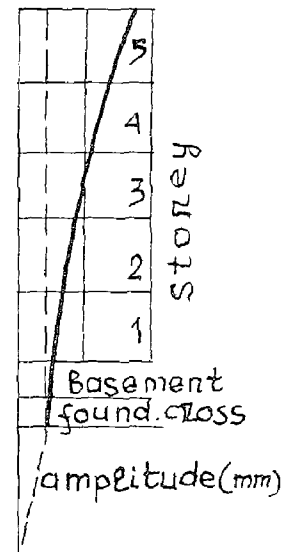


Fig. 4

INTERNATIONAL SYMPOSIUM ON
EARTHQUAKE STRUCTURAL ENGINEERING

St. Louis, Missouri, USA, August, 1976

169

SOME SEISMIC RESPONSE SOLUTIONS FOR
SOIL-FOUNDATION-BUILDING SYSTEMS

By J. KAZUO MINAMI* and JOJI SAKURAI**

* Professor and ** Assoc. Professor, Waseda University

Tokyo Japan

SUMMARY

Behavior of buildings in earthquakes, taking into consideration the interaction effects of the supporting ground and the foundation consisting of basement, piles and piers, the energy dissipative capacities (damping) of soils, and the influence of the vertical component of earthquake motion, has been investigated by means of a cyclic truss type model that represents a soil-foundation-building (SFB) vibratory system. The well-known 1940 El Centro and 1952 Taft earthquake wave forms have been used, normalized to 100 gal horizontal and 60 gal vertical components which are fed into the SFB system at the base of the surface soil layers. The buildings considered range from low to medium height, 1 to 15 storeys above the ground level. The damping of the building is assumed to be 3% of critical and 10% and 20% damping ratios have been assigned to the hard, soft and filled soil types. The case of uniform damping ratio of 5% for the soil and the building has also been studied for the purpose of comparison.

Seismic response in terms of base shear coefficient, base axial force coefficient and base overturning moment coefficient has been determined by performing hundreds of simulation experiments. Some of the findings do not conform to long established concepts but they provide satisfactory explanations for building damage observed in the past.

1. INTRODUCTION

The paper prepared by the ASCE-SEAOC Joint Committee on Lateral Forces of Earthquake and Wind (1), published in April 1951 as ASCE Proceedings, Separate 66 presented a rational dynamic approach method of estimating the earthquake forces acting on buildings and laid the foundation for current earthquake resistant design practice. The recommended lateral force provisions were based on the seismic response spectra for the one-mass vibrating system fixed at the base to a rigid supporting medium for some U.S. earthquakes by M.A. Biot and E.C. Robison. The Joint Committee also included recommendations for future study and invited investigators to substantiate, modify or refine the recommended provisions.

The authors of this paper have obtained some deterministic seismic response solutions for the soil-foundation-building (SFB) systems which are presented herein. 2-span buildings ranging from low, medium to moderate heights (15 storeys) supported on hard, soft, and filled ground are considered. The foundation of the system consists of basement, piles and piers to provide adequate support and stability to the buildings. Much attention has been directed to the study of the superstructure behavior under earthquake conditions but more attention should be directed to the study of the soil and foundation aspects if rational progress is to be achieved in earthquake resistant design. Recent research in soil dynamics has indicated that energy dissipative capacity of soils is significant and the vertical component of earthquakes, usually ignored in earthquake resistant analysis, may also be important in certain cases. These two aspects have been studied by performing simulation experiments using the SFB interacting models with the famous El Centro, 1940 earthquake and the Taft, 1952 earthquake as input wave forms at the base of the surface soil layers.

Certain other aspects of the seismic response problem have been investigated and published as progress reports since 1969. Evidence to substantiate, modify or refine the findings would be welcomed.

2. SOIL-FOUNDATION-BUILDING MODEL

Fig. 1 shows the model used in the investigation reported in this paper. The surface soil formation consists of three layers, each of 5 meter thickness and divided into 5 meter mesh in the horizontal direction. Masses are concentrated at the intersections of the members. The vertical, horizontal and diagonal members are proportioned to have the necessary areas and stiffnesses to represent the soil types. The special feature of the model is that the soil layers are continuous in the horizontal direction so that in this model, the buildings are located at 50m on centers. Our studies on the influence of adjacent buildings on the seismic response have revealed that when the separation distance is of the order of 40m,

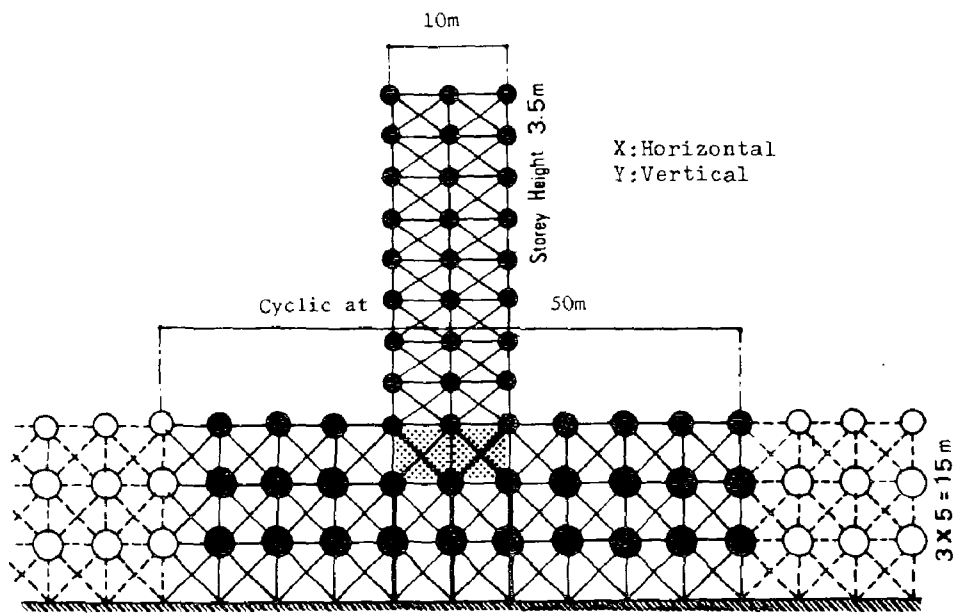


Fig.1 Typical Cyclic Truss Type Model

**Table 1 Periods of Vibration of Model Buildings
Fixed at GL, (sec)**

Storeys above GL	1st Mode	2nd Mode	3rd Mode
1	0.085	0.025	0.022
2	0.172	0.069	0.039
3	0.247	0.098	0.062
5	0.420	0.165	0.103
8	0.702	0.269	0.166
10	0.857	0.303	0.182
15	1.470	0.522	0.315

Table 2 Shear Moduli of Soil Types (kg/cm^2)

Soil Layer	Hard	Soft	Filled
Top	443	102	27
Middle	1034	236	64
Bottom	1330	305	82
Computed from shear wave velocities	1058	265	66

there is practically no interaction between the buildings. (2) The vibrational characteristics of the soil types are expressed by the predominant periods of vibration, namely approximately 0.25 sec for the hard soil, 0.50 sec for the soft soil and 1.0 sec for the filled ground to represent soil conditions in uptown, downtown, and filled areas of Tokyo. The upper two layers represent the actual vibrational characteristics of the surface soil formation and the third layer elements represent the characteristics of the deeper portion.

The building has been modeled as two 5m span width of 10m with a storey height of 3.5m above ground and 5m storey height for the basement portion. The masses are concentrated at the intersections of columns and girders and the elements proportioned to have the necessary areas and stiffnesses with the diagonal elements providing the required rigidities. Buildings of 1, 2, 3, 5, 8, 10 and 15 storeys have been analyzed. The foundation of the buildings consists of one or no basement supported by piles or piers reaching the firm bed formation 15m below the ground surface.

The natural periods of the modeled buildings considered fixed at the base are given in Table 1. The shear moduli of the different soil types for each soil layer and the values obtained from shear wave velocities are shown in Table 2. The latter values correspond fairly well with those for the middle layer. Poisson's ratio of 0.49 has been chosen based on the investigations of Akio Hara (in Japanese). The natural periods of the modeled soil types are 0.248 sec, 0.518 sec and 0.999 sec in the fundamental mode for the hard, soft and filled soil types respectively which are close to the values initially assumed for the three soil types.

Internal viscous damping of 3% for the building and 10% and 20% for each soil type has been assumed in the analysis based on the research of Seed and Idriss (3) and Kenji Ishihara (in Japanese) which indicate that damping values are strain dependent and the assumed values are to be expected in the strain range of 0.001. For the purpose of comparison, the seismic response for the case of uniform damping ratio of 5% assigned to both the soil and the building has also been obtained.

3. METHOD OF ANALYSIS

3.1 Stiffness Matrix

The soil and the buildings have been transformed to a cyclic truss type model as explained and shown in Fig. 1. Prestressed concrete piles are provided for buildings of 3 or more storeys and piers for 10 and 15 storey buildings. The piles are considered as flexural members fixed at the pile tip in the firm bed formation and to the building foundation at the pile butt and the stiffnesses determined for these conditions. Piers are considered to undergo shear and flexural deformations under the same assumed boundary conditions and the stiffnesses determined for formulating the stiffness matrix.

x, \dot{x}, \ddot{x} : displacement, velocity and acceleration vectors in the horizontal direction

y, \dot{y}, \ddot{y} : same vectors as above in the vertical direction

Eq. 4 may be rewritten as follows:

$$\begin{bmatrix} [C] & [M] \\ [M] & [0] \end{bmatrix} \begin{Bmatrix} \dot{x} \\ \dot{y} \\ \ddot{x} \\ \ddot{y} \end{Bmatrix} + \begin{bmatrix} [K] & [0] \\ [0] & -[M] \end{bmatrix} \begin{Bmatrix} x \\ y \\ \dot{x} \\ \dot{y} \end{Bmatrix} = \begin{Bmatrix} 0 \\ 0 \\ 0 \\ 0 \end{Bmatrix} \quad (5)$$

wherein $[0]$: zero matrix

Pre-multiplying Eq. 5 by Eq. 6, Eq. 7 is obtained

$$\begin{bmatrix} [K] & [0] \\ [0] & [M] \end{bmatrix}^{-1} \quad (6)$$

$$\begin{bmatrix} -[K]^{-1} \cdot [C] & -[K]^{-1} \cdot [M] \\ [I] & [0] \end{bmatrix} \begin{Bmatrix} \dot{x} \\ \dot{y} \\ \ddot{x} \\ \ddot{y} \end{Bmatrix} = \begin{Bmatrix} x \\ y \\ \dot{x} \\ \dot{y} \end{Bmatrix} \quad (7)$$

wherein $[I]$: unit matrix

Assuming $\begin{Bmatrix} x \\ y \end{Bmatrix} = \begin{Bmatrix} u \\ v \end{Bmatrix} \lambda^t$ in Eq. 7, the

following equation is obtained.

$$\frac{1}{\lambda} \begin{Bmatrix} u \\ v \end{Bmatrix} = \begin{bmatrix} -[K] \cdot [C] & -[K] \cdot [M] \\ [I] & [0] \end{bmatrix} \begin{Bmatrix} u \\ v \end{Bmatrix} \quad (8)$$

wherein

$$\begin{Bmatrix} u \\ v \end{Bmatrix} = \begin{Bmatrix} \psi u \\ \lambda \psi u \end{Bmatrix}$$

Using the values of $1/\lambda_j$ obtained from Eq. 8,

h_j and T_j values may be computed from Eqs. 10 and 11.

$$\lambda_j = \psi_j + i \phi_j = -h_j \omega_j + i \sqrt{1 - h_j^2} \omega_j \quad (9)$$

$$h_j = -\psi_j / \sqrt{\psi_j^2 + \phi_j^2} \quad (10)$$

$$T_j = 2\pi / (\omega_j \sqrt{1 - h_j^2}) = 2\pi / \phi_j \quad (11)$$

wherein h_j : damping ratio for the j -mode

T_j : natural period in the j -mode

ω_j : circular frequency for undamped j -mode

The complex eigenvectors corresponding to the above may be obtained from Eq. 12. The amplitude jA_k for the point in the j -mode and the phase difference angle $j\theta_k$ may be determined from Eq. 13.

$$\{U\} = \{v\} + i \{w\} \quad (12)$$

$$jA_k = \sqrt{v_k^2 + w_k^2}, \quad j\theta_k = \tan^{-1}(jw_k/jv_k) \quad (13)$$

3.3 Response Calculations

The earthquake response has been calculated by using the characteristic values obtained by the method explained in 3.2 and the damping ratios obtained for the varied damping factors by superposing the first 15 mode values. The buildings under study being low to moderate in height, the effect of wave propagation is considered to be minor and the phase angle difference between the masses has been neglected to simplify computations.

Input earthquake data for the 1940 El Centro and 1952 Taft tremors are those contained in volume II Part A, Earthquake Engineering Research Laboratory, EERL 75-50, California Institute of Technology, Sept. 1971. Appreciation is expressed to the EERL staff for making available such valuable information. Maximum horizontal acceleration has been reduced to 100 gal and the maximum vertical acceleration to 60 gal for both earthquakes and they are fed-in at -15m from the ground surface where a firm base formation is assumed to exist.

The 100 gal horizontal input produces acceleration response at the free field ground surface of approximately 410 gal, 290 gal and 190 gal for the hard soil for 5%, 10% and 20% damping ratios respectively for the El Centro earthquake; 270 gal, 225 gal and 145 gal for the hard soil for the same conditions from the Taft earthquake. The 60 gal vertical input produces random vertical acceleration response at the free surface ranging from 40 gal to 240 gal in all soil types from the two earthquakes.

Modified linear acceleration method has been used to compute the seismic response.

4. RESULTS OF STUDY

4.1 Natural Periods and Damping Ratios

Fig. 2 shows the relation between the circular frequencies and damping ratios for the 5 storey (N5) building without a basement (BO) supported on hard soil. The three light lines indicate 3% damping for the building, 10% and 20% damping for the soil, all in the fundamental mode respectively. The heavy solid line is for 3% building damping and 10% soil damping; the broken line is for 3% building damping and 20% soil damping. The circles on or near the three light lines indicate the damping ratio values for the

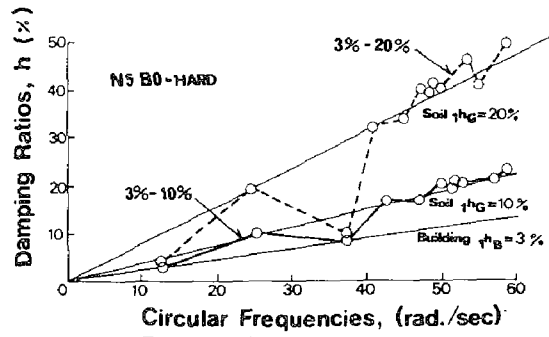


Fig.2 Relation Between Circular Frequencies and Damping Ratios

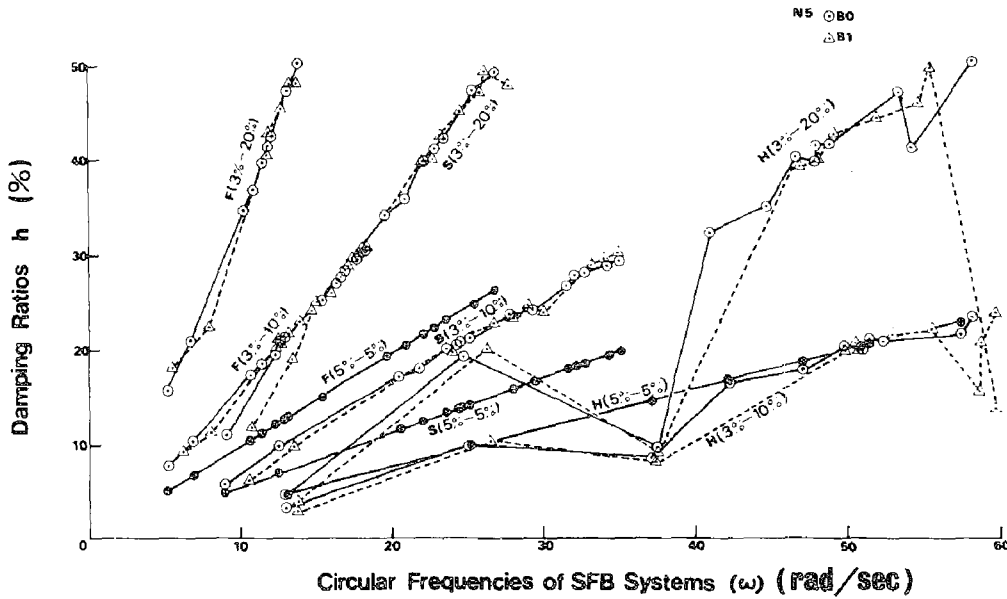


Fig.3 Relation Between Circular Frequencies and Damping Ratios for Different Soil Types

first, second, third, ... modes from the left and increasing toward the right. It is clear from this figure that assigning varied damping values to the building and the soil do not affect the circular frequencies in any particular mode. This is also true for the case when damping is neglected altogether. This is also evident in Fig. 3 and it may be concluded that values of the natural period of the SFB systems without damping may be used for engineering purposes.

It is common in practice to assume that damping ratios are proportional to the circular frequencies but the relationships shown in Figs. 2 and 3 indicate otherwise.

Fig. 3 is similar to Fig. 2 but three soil types with varied damping values are shown for the five storey building (N5) with (B1) and without a basement (BO). F (3%-20%) denotes filled ground with 3% building damping and 20% soil damping; S (3%-10%) denotes soft soil with 3% damping ratio for the building and 10% damping ratio for the soil; and H (5%-5%) denotes hard soil with uniform 5% damping for both the building and the soil.

The damping ratios are in general proportional to the circular frequencies for the filled and soft soil types but not so for the hard soil type. Within the scope of this investigation, the damping ratios are proportional to the circular frequencies for low buildings supported on soft soils but this relationship does not hold for taller buildings supported on any type of ground.

4.2 Displacement and Acceleration Response

The values of the maximum horizontal displacements and accelerations for the SFB systems due to simultaneously acting horizontal and vertical earthquake components varied only slightly, compared to the case of horizontal component acting alone. In general, the horizontal and the vertical components of earthquake motion may be considered separately and the results combined.

The acceleration response in the vertical direction at the base and top of buildings does not vary much but the response is greater for the hard soil than for the softer soils.

4.3 Stresses at the Base of Buildings

The maximum stresses acting at the ground level of buildings are important parameters in earthquake resistant design. One of the parameters is the base shear coefficient C_B , (the ratio of the first storey shear divided by the building weight above that level). Similarly important are the base overturning moment coefficient, C_M (overturning moment at the ground level divided by the product of the building weight and the height to the center of gravity) and the base axial force coefficient,

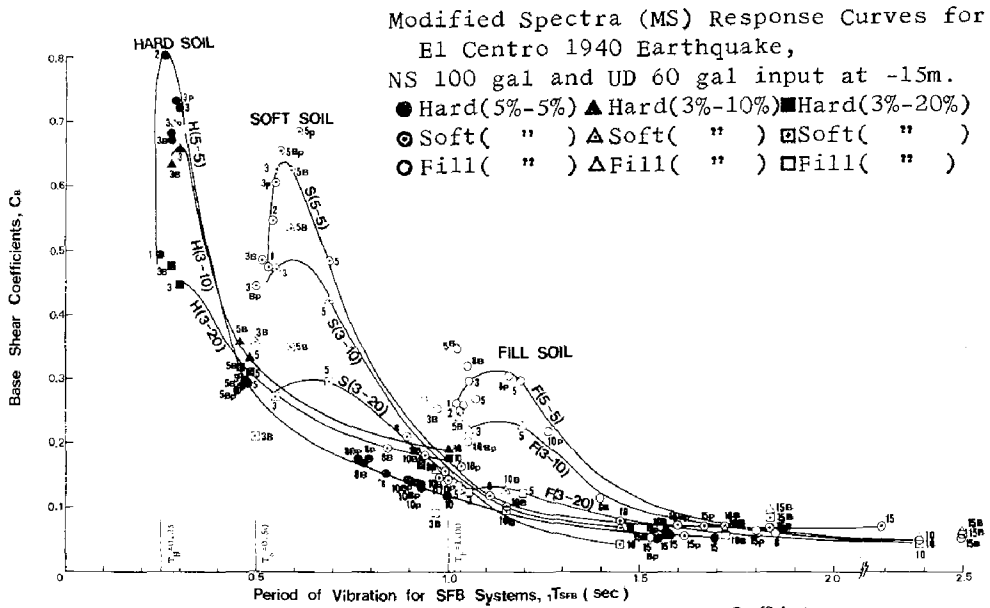


Fig.4 Relation Between Period of Vibration for SFB Systems and Base Shear Coefficients

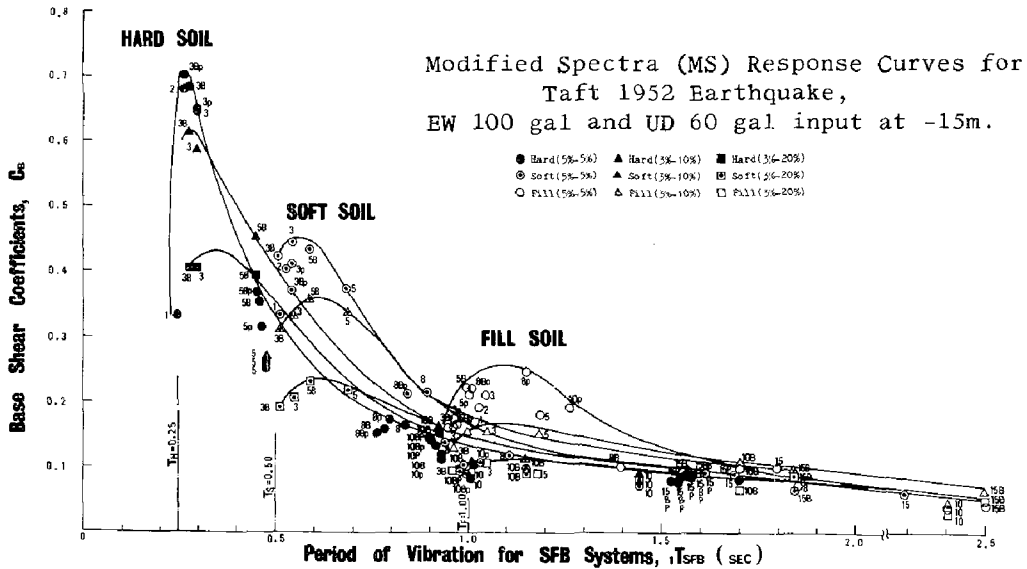


Fig.5 Relation Between Natural Periods for SFB Systems and Base Shear Coefficients

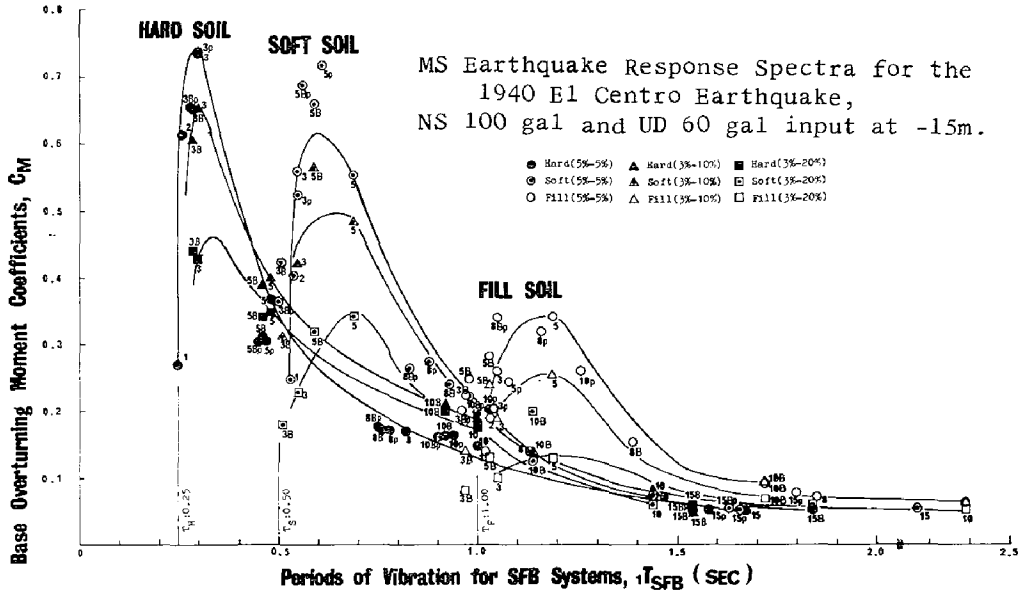


Fig. 6 Relation Between Natural Periods for SFB Systems and Base Overturning Moment Coefficients

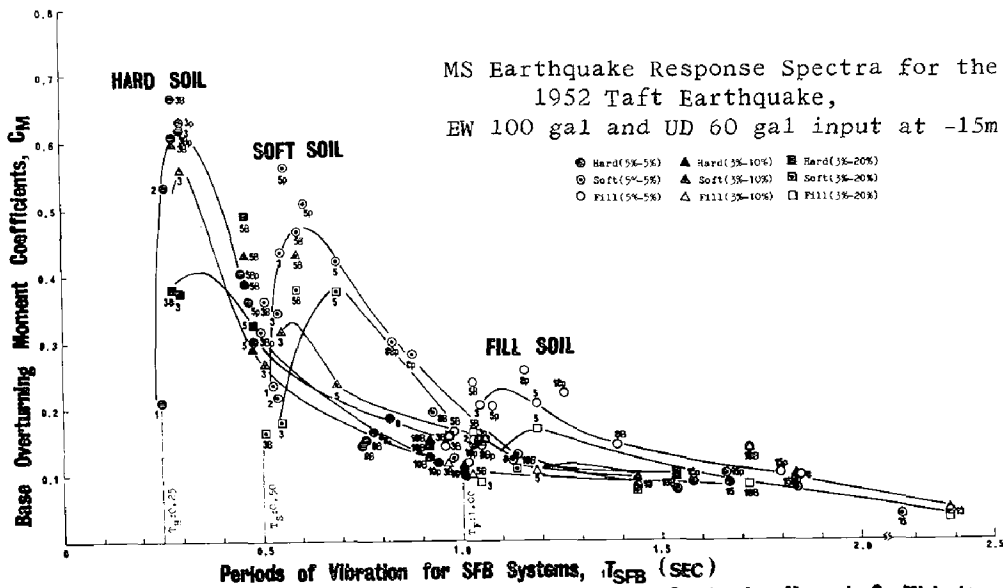


Fig. 7 Relation Between Natural Periods for SFB Systems and Base Overturning Moment Coefficients

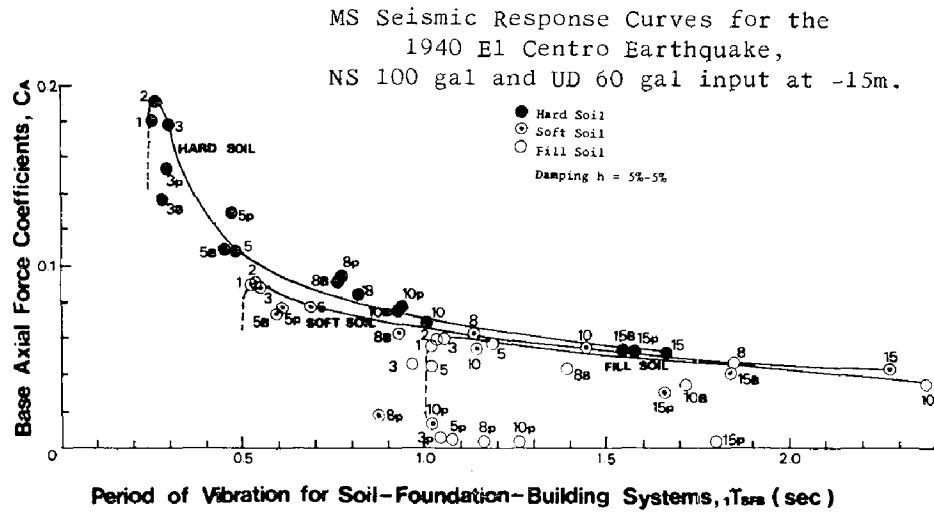


Fig. 8 Relation Between SFB System Period of Vibration and Base Axial Force Coefficients

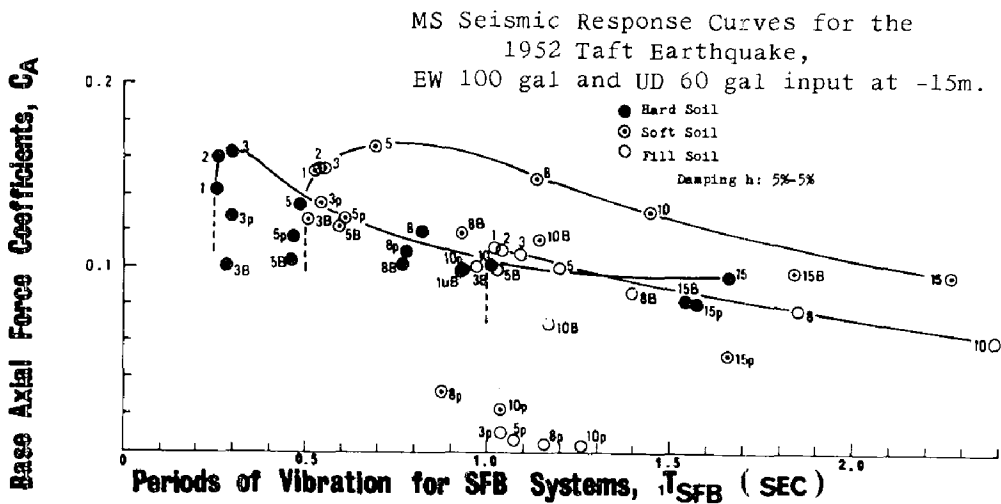


Fig. 9 Relation Between Natural Periods and Base Axial Force Coefficients

C_A , (axial forces in the columns at the base divided by the building weight).

Base Shear Coefficient, C_B

The MS (Minami-Sakurai's Modified Spectra) Response Curves for the hard, soft and filled soil types and varied damping ratios, with and without basements, piles and piers are plotted in Fig. 4 for the 1940 El Centro earthquake and in Fig. 5 for the 1952 Taft earthquake. These MS response curves are for 100 gal horizontal and 60 gal vertical inputs at -15m below the ground level as previously explained. The values of C_B are plotted against the fundamental periods of the soil-foundation-building systems which differ from the usually plotted response curves that are drawn against the fundamental periods of the buildings assumed fixed at the ground level without consideration of the foundation construction and the nature of the supporting soil. The numbers near plotted points indicate the number of storeys above grade, B denotes basement, p-piles and P-piers.

Several salient features are to be noted, as follows: 1. Low buildings move or ride with the motion of the ground and the natural periods of low buildings that are less than the predominant period of the ground are suppressed; 2. Base shear coefficients are largest for the hard type soil, least for the filled ground and intermediate for the soft soil; 3. Response values are largest for the uniform 5% building and 5% soil damping ratios, least for 3% building and 20% soil damping and intermediate for 3% building and 10% soil damping ratios; 4. Soil-foundation-building interaction effects are pronounced for the hard and soft soil types for the range of natural period of approximately 1.2 secs and less. For the filled ground type, 1.8 sec to 1.0 sec range; 5. For tall buildings with natural periods exceeding the above maximum SFB system periods, the soil type need not be considered. However, adequate foundation construction (piles or piers) must be used to transmit the permanent and temporary loads to the satisfactory bearing medium.

Base Overturning Moment Coefficient, C_M

The relationship between C_M and the SFB natural periods is shown in Fig. 6 for the El Centro earthquake and in Fig. 7 for the Taft earthquake. The general shapes of the Modified Spectra curves are similar to those for the C_B curves. Comparison of C_M with C_B indicates that for low buildings $C_M < C_B$; for medium height buildings $C_M \approx C_B$; and $C_M > C_B$ for taller buildings.

The maximum C_M values occur for the hard soil, least for the soft type soil. These values are reduced as the soil damping ratios are increased from 5% to 10% to 20%. For the same ranges in the natural period of the SFB systems, the same observations apply in this instance also as mentioned in connection with the C_B response curves. It should

be noted that large C_M response occurs for relatively small buildings; N3 in the case of hard soil and N5 for the soft soil.

Base Axial Force Coefficients, C_A

The relationship between C_A and the natural period of SFB systems is shown in Fig. 8 for the El Centro earthquake and in Fig. 9 for the Taft earthquake. This parameter may be considered to indicate either an increase or decrease in the building weight. The C_A values of 0.15-0.2 are due to 60 gal vertical component input at -15m from the ground surface. For near focus earthquakes, greater changes in the column stress conditions may occur and, in combination with the horizontal earthquake component effects, may not be dismissed as being insignificant as it usually is in current earthquake resistant design practice. This is particularly so for long span buildings and cantilevered portions of buildings.

Acknowledgment

Some forty undergraduate and graduate students in the Dept. of Architecture of Waseda University have participated and contributed efforts in attaining the aim of gaining new knowledge, understanding, and insight on this important problem in earthquake engineering from 1967 to date. The authors express deep appreciation for their cooperation.

References

1. Anderson, Blume, Degenkolb, Hammil, Knapik, Marchand, Powers, J.E. Rinne (Chairman), Sedgwich and Sjorberg: Lateral Forces of Earthquake and Wind, Trans. ASCE, Vol. 117, 1952.
2. Sakurai, J. and Minami, J.K.: Some Effects of Nearby Structures on the Seismic Response of Buildings, Proc. 5WCEE, Rome, 1973.
3. Seed, H.B. and Idriss, I.M.: Soil Moduli and Damping Factors for Dynamic Response Analyses, Univ. of California, EERC 70-10, 1970.
4. Foss, K.A.: Coordinates which Uncouple the Equations of Motion of Damped Linear Dynamic Systems, ASME, Journal of Applied Mechanics, Vol. 57 -A-86, 1957.

INTERNATIONAL SYMPOSIUM ON
EARTHQUAKE STRUCTURAL ENGINEERING

183

St. Louis, Missouri, USA, August, 1976

RESPONSE OF STRUCTURES EMBEDDED IN THE GROUND TO TRAVELLING

SEISMIC WAVES

E.G. PRATER, Institute of Foundation Engineering and
Soil Mechanics

M. WIELAND, Laboratory of Hydraulics, Hydrology
and Glaciology

Federal Institute of Technology, Zurich

Switzerland

ABSTRACT

The interaction of a long structure with the ground is investigated using the theory of wave propagation. The special feature of the investigation is the consideration of the spacial variations of the input motions applied at points on the boundary of the system. In the illustrative problem the underground is assumed to consist of horizontal layers terminated by vertical transmitting boundaries, and a horizontal soil-rock interface. Nonlinear soil behaviour is accounted for using a Ramberg-Osgood model for the deviatoric stress-strain behaviour. The equations of motion are discretized using central finite differences in space and time. The use of a dual grid gives more efficient discretization and greatly simplifies the relations at interfaces and boundaries. The analysis of travelling wave motions does not give rise to much extra computational effort as compared with the case in which the spacial variations of input motions are ignored. This is not the case with the finite element method, which becomes much less efficient for travelling wave analysis.

INTRODUCTION

In current earthquake structural engineering design it is usual to assume that the input motion is uniform along the base of the structure, or, as the case may be, of the soil-structure system. In other words, the underground is assumed to be perfectly rigid and to move as a whole. This assumption is not too restrictive if the horizontal dimensions of the structure are small in comparison with the wavelengths of significant components of the earthquake motion. For certain structures, however, this will not be the case, and it will be necessary to take into account the propagating nature of earthquake motions, i. e. the boundary conditions must be formulated for travelling wave input.

In many structural analyses a part of the underground is included in the structural model in order to investigate the interaction of the structure with the ground. This, of course, adds greatly to the cost of the numerical investigation, especially as a realistic inclusion of an underground consisting of soil layers requires an as-

segment of nonlinear stress-strain properties to the soil [1, 2].

If a structure is important enough to consider the problem of soil-structure interaction it is only realistic to incorporate travelling earthquake motion into the analysis. Since there is but scanty information available about differential earthquake motions at points in the ground [3], and in any case at points underlying the structure in question, it is necessary as a first approximation to assume a single travelling seismic wave which remains unchanged as it passes through the part of the underground not included in the structural model [4]. Thus the boundary motions are considered to be a phase-dependent phenomenon only.

The further away from the structure the artificial boundary line is drawn the more realistic the structural model becomes. It is often convenient, however, to let the artificial boundary coincide with a soil-rock interface, the underlying rock being, to all practical purposes, rigid in comparison with the soil. The speed of the input travelling wave is then determined by the physical characteristics of the rock. Due to the presence, in general, of underlying rock at a practical depth the bottom boundary condition is more easily taken care of. What presents the greatest problem from a practical point of view are the artificial side boundaries terminating the structural model. The problem arises from the reflections that take place at these boundaries. These spurious reflections contaminate the solution and limit the length of time for which it is valid [5].

The treatment of artificial boundaries is a rather knotty problem. The usual practice is to place them as far as possible from the structure as is economically feasible. If the structure is discretized with much refinement (using finite elements or finite difference approximations) it is usually not economically possible to place the artificial boundaries far away from the structure: some investigators have placed them at a distance of about two times the diameter of foundation away from the structure [6, 2]. If, on the other hand, only coarse discretization is used for the structure the position of the boundaries may be extended further into the underground [7]. For an underground composed of horizontal layers some improvement in the analysis may be effected by finding first the free field solution using a one-dimensional model analysis and then applying the free field accelerations (or displacements) at the artificial boundaries.

In this paper simple transmitting boundaries devised by Lysmer and Kuhlemeyer [8] have been used. Energy is absorbed at the boundaries using viscous elements. They were originally used in finite elements analysis, but have also found application in finite difference codes for nuclear shock loading [9]. This special type of boundary only functions if the incident wave impinges on the boundary at an angle greater than about 40° , i. e. not at grazing incidence. For the purposes of this investigation it has been assumed that the direction of the wave front makes a small angle with the horizontal so that the above condition is satisfied on the side boundaries. It is also considered unnecessary to apply the free field solution to these boundaries in the case of an underlying rock medium.

Relatively few papers dealing with travelling seismic waves have appeared in the literature. Dibaj and Penzien [10] have considered an earth dam resting on a rigid base, and Dezfulian and Seed [4] have considered the response of soil formations with sloping rock boundaries. The authors [11] have investigated the hydrodynamic forces on gravity dams due to travelling waves with both vertical and horizontal components. More recently Wolf [7] has considered a nuclear installation (idealized as a plate on an elastic foundation in which slip and uplift of the plate is possible) for travelling shear wave motions. Other references to buildings, bridges and underground pipelines are given in [3]. In most investigations to date the finite element method of analysis has been used. This method may be rather inefficient for travelling wave input depending upon the number of base nodal points. Thus Kaldjian [12] has utilized higher order finite elements (using very few elements) to investigate dam-foundation interaction for spacial variation in the ground motion. The finite difference method, however, does not present this problem as the spacial variation of the seismic wave may be incorporated directly through the boundary conditions into the equations for wave propagation.

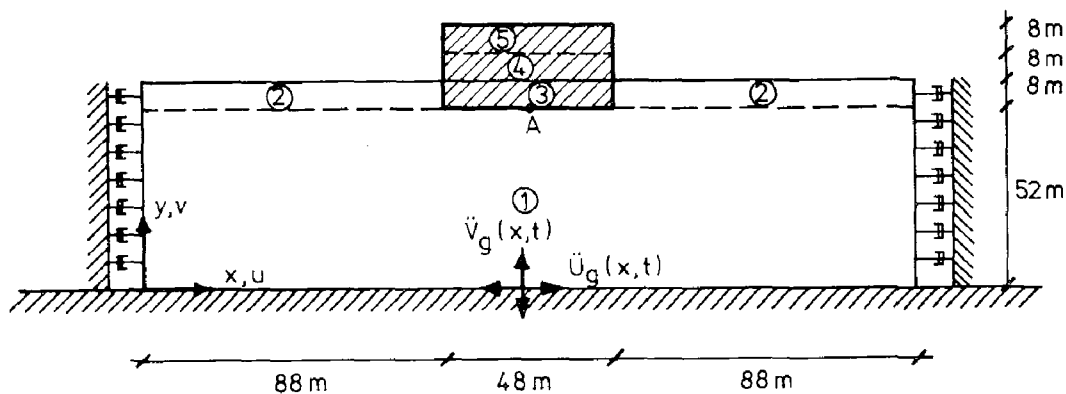


Fig. 1 Geometry of an idealized nuclear power plant embedded in the ground.

Material properties in the 5 zones :

① Ramberg-Osgood material

$$G_o = 1480 \text{ kp/cm}^2, \tau_y = 15 \text{ kp/cm}^2, R = 3, \gamma = 2.1 \text{ t/m}^3, \zeta = 7 \%$$

Elastic properties in zones ② - ⑤

②	$E = 2000 \text{ kp/cm}^2$	$\nu = 0.35$	$\gamma = 2.0 \text{ t/m}^3$	$\zeta = 15 \%$
③	$E = 25000 \text{ kp/cm}^2$	$\nu = 0.2$	$\gamma = 1.1 \text{ t/m}^3$	$\zeta = 2 \%$
④	$E = 70000 \text{ kp/cm}^2$	$\nu = 0.2$	$\gamma = 1.0 \text{ t/m}^3$	$\zeta = 2 \%$
⑤	$E = 40000 \text{ kp/cm}^2$	$\nu = 0.2$	$\gamma = 1.5 \text{ t/m}^3$	$\zeta = 2 \%$

THE PROPOSED MODEL

In recent years much effort has gone into designing nuclear power plants for seismic loading. An important aspect of the seismic design is the structural interaction of the nuclear reactor containment vessel with the surrounding ground. The nuclear reactor building is a massive structure which is embedded usually several metres in the ground. The shape of the structure lends itself to axisymmetric analysis and finite element codes have been written which incorporate the arbitrary nature of the seismic loading by approximating it by a Fourier series with a finite number of terms [13]. Recent designs have used such codes in preference to simplified one or two-dimensional spring-mass models [6]. In some cases, however, where particular aspects of the analysis require special investigation it may be justified to carry out a two-dimensional plane strain analysis. For example, Seed and Idriss [2] investigated the soil-structure interaction problem with nonlinear stress-strain models suited to soil behaviour using a finite element code written for plane strain conditions. The chief point of the present investigation is to evaluate the influence of travelling seismic waves and energy absorbent transmitting boundaries. Since nonlinear finite element codes incorporating these features are not available the authors have written a program based upon the finite difference method for this purpose. For convenience a plane strain model was chosen to represent the structural behaviour of the power plant system. The idealization of the system is shown in Fig. 1. The rigidity of the structure is based upon the data supplied in reference [2].

THE FIELD EQUATIONS

The differential equations of motion are the well known damped wave equations *

$$\rho \ddot{u}_i + K \dot{u}_i = T_i \quad \dots \dots \dots (1)$$

where $T_i = \sigma_{ij,j} + b_i$

where the dot notation implies differentiation with respect to time. Equation (1) is valid for any type of material behaviour.

The strain displacement relations are given by

$$e_{ij} = \frac{1}{2}(u_{i,j} + u_{j,i}) \quad \dots \dots \dots (2)$$

For elastic behaviour the stress-strain relations are

$$\sigma_{ij} = C_{ijkl} e_{kl} \quad \dots \dots \dots (3)$$

For plane strain conditions with cartesian coordinates x and y equations (2) and (3) reduce, for isotropic behaviour, to

$$\begin{aligned} \sigma_{xx} &= (\lambda + 2\mu) \frac{\partial u_x}{\partial x} + \lambda \frac{\partial u_y}{\partial y} \\ \sigma_{yy} &= \lambda \frac{\partial u_x}{\partial x} + (\lambda + 2\mu) \frac{\partial u_y}{\partial y} \quad \dots \dots \dots (4) \\ \sigma_{xy} &= \mu \left(\frac{\partial u_x}{\partial y} + \frac{\partial u_y}{\partial x} \right) \end{aligned}$$

Substitution of the relations expressed in equation (4) into equation (1) leads to a formulation of the problem in terms of the field variable u_i . Alternatively, the

* The symbols used are defined in the notation

algorithmus may be so written that equations (1) and (4) are used in conjunction with one another. In this way one works with lower order equations, and both the stress and displacement fields are obtained directly. Together with the boundary conditions these equations define the problem completely.

THE NUMERICAL METHOD

The finite difference method using central finite differences has been found to be quite suitable for solving the equations of wave propagation. In using the stress-strain relations together with the wave equations (in an alternative manner) it is convenient to specify the unknown discrete displacements and stresses at staggered grid points, thus allowing the use of central finite differences in all equations. In effect, four grids are superimposed over one another, one for normal stresses σ_{xx} , σ_{yy} , one for shear stresses σ_{xy} , one for horizontal displacement u_x and one for vertical displacement u_y . The system of interlacing nets as it is so called, is described in detail elsewhere [11]. Apart from the advantage of using lower order difference equations, a better approximation for the shear stresses is obtained and the formulation of boundary conditions is greatly simplified.

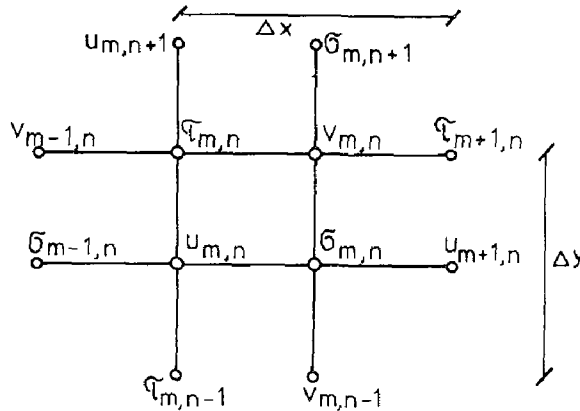


Fig. 2 System of interlacing nets

The discretisation of equation (1) in the time domain takes the form

$$\frac{\rho}{\Delta t} (\dot{u}_i^{t+1} - \dot{u}_i^t)_{m,n} + \frac{K}{2} (\dot{u}_i^{t+1} + \dot{u}_i^t)_{m,n} = (T_i^{t+\frac{1}{2}})_{m,n} \dots (5)$$

where m and n define the position of the field variable u_i

It follows that the velocity at time $t+1$ is given by

$$\dot{u}_i^{t+1} = [T_i^{t+\frac{1}{2}} + (\frac{\rho}{\Delta t} - \frac{K}{2})\dot{u}_i^t] \frac{1}{\frac{\rho}{\Delta t} + \frac{K}{2}} \dots (6)$$

The displacements are obtained by simple integration, viz:

$$u_i^{t+\frac{1}{2}} = u_i^{t+\frac{1}{2}} + \Delta t \dot{u}_i^{t+1}$$

The numerical scheme, which is explicit, belongs to a class which is only conditionally stable. To ensure stability the iterative speed must be less than the velocity of wave propagation in the material. For a region subdivided into rectangular mesh elements of sides Δx , Δy the following condition (after Courant et al.) must be fulfilled if the errors at some time step do not become magnified

with time :

$$\Delta t \leq \left\{ \frac{8}{\lambda + 2\mu} \frac{1}{\left[\left(\frac{1}{\Delta x} \right)^2 + \left(\frac{1}{\Delta y} \right)^2 \right]} \right\}^{\frac{1}{2}} \dots \dots \dots (7)$$

This formula is valid for the interior of a homogeneous medium. In practice, it is adequate to fix the time step, according to equation (7), for the stiffest sub-region of the physical system. Alternatively, it may be preferable to employ an implicit numerical scheme, e.g. that proposed by Newmark [see, for example, reference 14]. Spatial discretisation for T_i in equation (1), i.e. for terms $\frac{\partial \sigma_{xx}}{\partial x}$ etc., and in the stress-strain relations for $\frac{\partial u_x}{\partial x}$ etc., presents no difficulties [11]. See Fig. 2.

CONDITONS AT AN INTERFACE BETWEEN TWO MEDIA

In general, when an elastic wave reaches an interface between two media reflection and refraction take place. For the condition of no slip at the interface the following conditions hold. Denoting the quantities in the two media by suffices a and b

(i) equality of displacements

$$(u_i)_a = (u_i)_b \dots \dots \dots (8)$$

(ii) equality of normal and shear stresses

$$\begin{aligned} (\sigma_{nn})_a &= (\sigma_{nn})_b \\ (\sigma_{ns})_a &= (\sigma_{ns})_b \end{aligned} \dots \dots \dots (9)$$

The stress or displacement free boundary presents a special case of these conditions, in that the right hand sides of equations (8) and (9) become zero. Using interlacing nets and simple interpolations it is a trivial matter to express the interface conditions in discretised form. The stresses are assumed to be continuous across the interface.

SEISMIC LOADING

In accordance with the nature of wave propagation the seismic loading is introduced via the boundary conditions. In this case the right hand side of equation (8) is replaced by a known time dependent function.

$$\begin{aligned} (u_x)_a &= u_g(x, t) \\ (u_y)_a &= v_g(x, t) \end{aligned} \dots \dots \dots (10)$$

If the ground disturbance acts simultaneously at all points in contact with the rigid underground

$$\begin{aligned} u_g(x, t) &= u_0(t) \\ v_g(x, t) &= v_0(t) \end{aligned} \dots \dots \dots (11)$$

For travelling wave input the wave arrives at each point of the bottom boundary with a time dependant phase shift. In this case

$$u_g(x, t) = u_0(t - x/V_t) \dots \dots \dots (12)$$

etc.

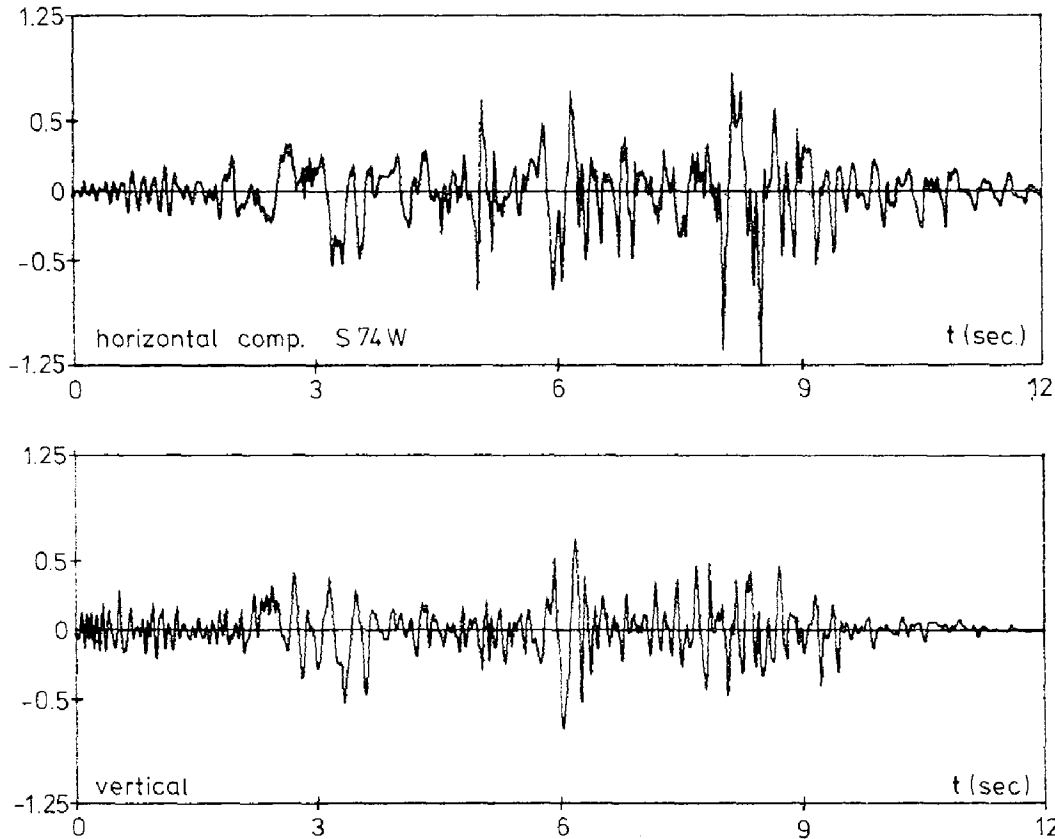


Fig. 3 Strong motion phase of the San Fernando Earthquake 1971, Station: Paicomo Dam. (Max. horizontal acceleration: 1.25 g, max. vertical acceleration: 0.72 g)

TRANSMITTING BOUNDARIES

Using two specialised equations of motion at the side boundaries, namely

$$\sigma_{xx} = - a \rho C_p \dot{u}_x \quad \dots \dots \dots (13)$$

and

$$\sigma_{xy} = - b \rho C_s \dot{u}_y \quad \dots \dots \dots (14)$$

where a, b are constants and C_p , C_s are the velocities of compression and shear waves respectively of the material beyond the boundary, very small reflections are produced and energy propagates to the region outside of the boundary. This is true if the waves impinge at angles which are not near grazing incidence. Optimum dissipation is dependent on the choice of a and b and the angle of incidence. For adequate results it is sufficient to set $a = b = 1$, [8]. It should be pointed out that equations (13) and (14) were derived, strictly speaking, for linear elastic materials. In the absence of published work for nonlinear materials it has been assumed by the authors that transmitting boundaries may be used, equations (13) and (14) being continually adjusted for the changes in the instantaneous values of the tangent shear modulus μ . When the transmitting bound-

aries are deleted from the system the usual roller boundary condition is applied. Fig. 2 shows the details of the computational grid scheme. On the transmitting boundaries shear stress (σ_{xy}) and horizontal displacements (velocity \dot{u}_x) are located. Thus, for the purposes of coding, the normal stress (σ_{xx}) and the vertical velocity (\dot{u}_y) at half a grid length ($\frac{\Delta x}{2}$) away from the boundary are used in the discretized form of equations (13) and (14).

MATERIAL PROPERTIES

Damping Characteristics :

Linear viscous damping may be introduced into the system through the term $K\dot{u}_1$ in equation (1). If ω_0 is the fundamental frequency of the discretized system the critical value of viscous damping for the fundamental mode is given by

$$K_{crit} = 2 \rho \omega_0 \dots \dots \dots (15)$$

Variable damping throughout the system is achieved by assigning different percentages of critical damping at the various discrete displacement points, i.e.

$$K = \xi K_{crit} \dots \dots \dots (16)$$

In the actual program used both ρ and K were assumed constant for each material zone.

Seed and Idriss [1] have shown that damping is strongly strain dependent, being rather low at small strains but increasing to over 20% at strains less than 1%. A bilinear hysteretic model idealizing real stress strain behaviour was used in some investigations, and later the concept of an equivalent linear parameter for approximating nonlinear hysteretic characteristics was introduced [1]. In the present study nonlinear hysteretic damping is obtained using the Ramberg-Osgood model. This model is used for the bottom soil layer, and in all zones of the system viscous damping of varying amounts is assumed. An experimental check on the critical damping (obtained using a finite element code to determine ω_0) was carried out, and K_{crit} adjusted to suit the nonlinear soil-structure system.

Stiffness Characteristics :

The Ramberg - Osgood model is now very well-known in both structural engineering [15,16] and the seismic analysis of soil layer systems [17, 18]. The equations have been used either to describe load-displacement characteristics in structural members or the shear stress-strain characteristics of soils. As a first approximation towards the 2-dimensional study of seismic loading of soil deposits it has been assumed that the volumetric behaviour is linear elastic without tension cut-off. The deviatoric behaviour is described by the following Ramberg-Osgood constitutive law

$$(\gamma_{oct} - \gamma_0) / c \gamma_y = (\tau_{oct} - \tau_0) / c \tau_y + \alpha \left| (\tau_{oct} - \tau_0) / c \tau_y \right|^R \dots \dots (17)$$

where $\tau_{oct} = \frac{1}{3} \left[(\sigma_{xx} - \sigma_{yy})^2 + (\sigma_{yy} - \sigma_{zz})^2 + (\sigma_{xx} - \sigma_{zz})^2 + 6(\sigma_{xy}^2 + \sigma_{xz}^2 + \sigma_{yz}^2) \right]^{\frac{1}{2}}$
 i.e. shear behaviour is characterised by the behaviour in the octahedral plane (τ_{oct} , γ_{oct}). The model has four parameters α , R , γ_y , τ_y where the γ_y and τ_y define a reference point for the stress-strain curve, which is usually asso-

Three cases were investigated:

- a) rigid underground ($V_t = \infty$); transmitting side boundaries.
- b) travelling wave input ($V_t = 1500$ m/sec); rigid side boundaries.
- c) as b) but with transmitting side boundaries.

The assumed material properties are shown in Fig. 1.

For numerical stability the time step was chosen as $\Delta t = 0.002$ sec, as determined by the wave velocity in zone 4. This value of Δt corresponds to a frequency of about 200 Hertz, and permits a good approximation of the acceleration seismograms, which have a maximum frequency of less than 20 Hertz.

The critical damping of the system is $K_{crit} = 3.8t \cdot \text{sec} \cdot \text{m}^{-4}$, where $\omega_0 = 9.1 \text{ sec}^{-1}$.

The time response for displacement and principal stress components for the three cases a), b), c) given above are shown in Figs. 5, 6 and 7 for a point (A) on the axis of symmetry at the base of the reactor foundation. The displacements given are relative to the ground displacement immediately below point A. A comparison of cases a) and c) shows that the particular travelling wave investigated does not have a substantial influence on the displacement response either qualitatively or quantitatively. Some differences are evident, however, in the stress response. The greatest differences occur between cases b) and c), namely between rigid and transmitting side boundaries. In Table 1 the extreme values of stresses and displacements at point A (Fig. 1) for the three above mentioned cases are given.

	u_{max} [cm]	v_{min} [cm]	$\sigma_{\gamma max}$ [kp/cm ²]	$\sigma_{\gamma min}$ [kp/cm ²]
case a	9.6	- 11.4	4.0	- 7.7
case b	12.2	- 14.1	5.5	- 8.8
case c	8.4	- 11.5	3.7	- 6.4

Table 1: Extreme values of stress and displacement at point A (cf. Fig. 1)

The dominant frequency of the displacements is in the region of the fundamental frequency of the system. The frequencies of the stresses, however, are much higher and are in the same order of magnitude as the earthquake frequencies. It should be added that in the reactor structure still higher stress frequencies occur because of the greater speeds of wave propagation and the presence of wave reflections. In one case the Ramberg - Osgood material was replaced by elastic material. The influence on the results was not significant. This may be explained by the fact that the shear stresses produced by the seismic loading were well below the stress parameter τ_y in the Ramberg - Osgood model, and the behaviour was quasi-elastic. Another consequence of this was the low value of nonlinear hysteretic damping.

In Fig. 8 the extreme values (i. e. limiting envelope to the curves) of stress and displacement along the base of the reactor foundation are shown.

ciated with the yield point. The initial shear modulus, G_0 , is defined by

$$G_0 = \frac{\tau_y}{\gamma_y}$$

Streeter et al. [17] assume τ_y about 80% of the shear stress at yield for a soil material. γ_o and τ_o define the point of most recent stress reversal. The parameter c equals 1 for the 'skeleton' curve and 2 for the 'branch' curve (i. e. unloading or reloading). For $c = 1$, $\gamma_o = \tau_o = 0$.

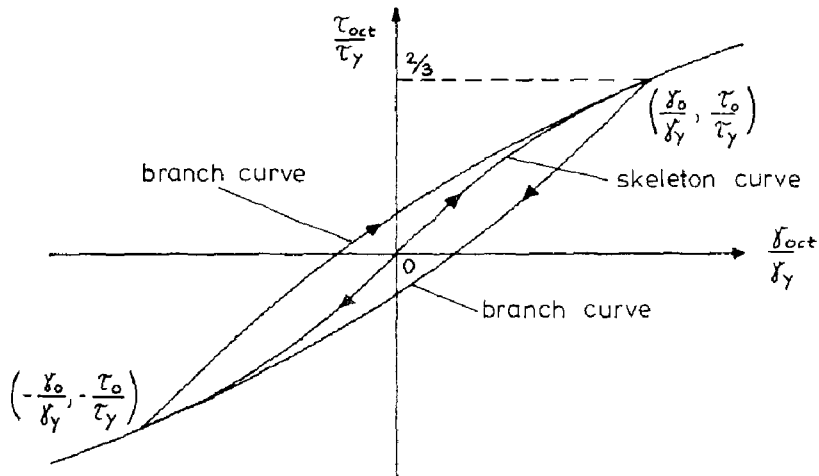


Fig. 4 Stress-strain behaviour of Ramberg-Osgood hysteretic model for material zone 1 .

The curves were constructed with the following material characteristics:

$$G_0 = 1480 \text{ kp/cm}^2, \quad R = 3, \quad \tau_y = 15 \text{ kp/cm}^2$$

For sand good correlation with experimental data has been found for $\alpha = 1.0$ and $R = 3$, [17]. These values have been adopted in this paper. In fact, the parameter R is the decisive parameter in the model. It enables behaviour between elastic ($R = 1$) and elastic-ideal plastic ($R = \infty$) to be modelled. Thus for simple cantilever structures Solnes et al. [16] assume $R = 10$.

The hysteresis behaviour of this simple nonlinear four parameter model is illustrated in Fig. 4.

SOME NUMERICAL RESULTS

The system shown in Fig. 1 was subjected to the seismic loading using vertical and horizontal components of a registered earthquake (San Fernando - 1971 - Paicomo Dam). These seismograms are shown in Fig.3 for strong motion phase of duration of 12 seconds. The seismograms were not scaled down so that relatively large ground accelerations of peak magnitude of the order 1.25g, were fed into the system.

A stiffness of the underlying rock, giving a travelling wave velocity of 1500 metres/sec, was assumed, but otherwise ignored in the analysis.

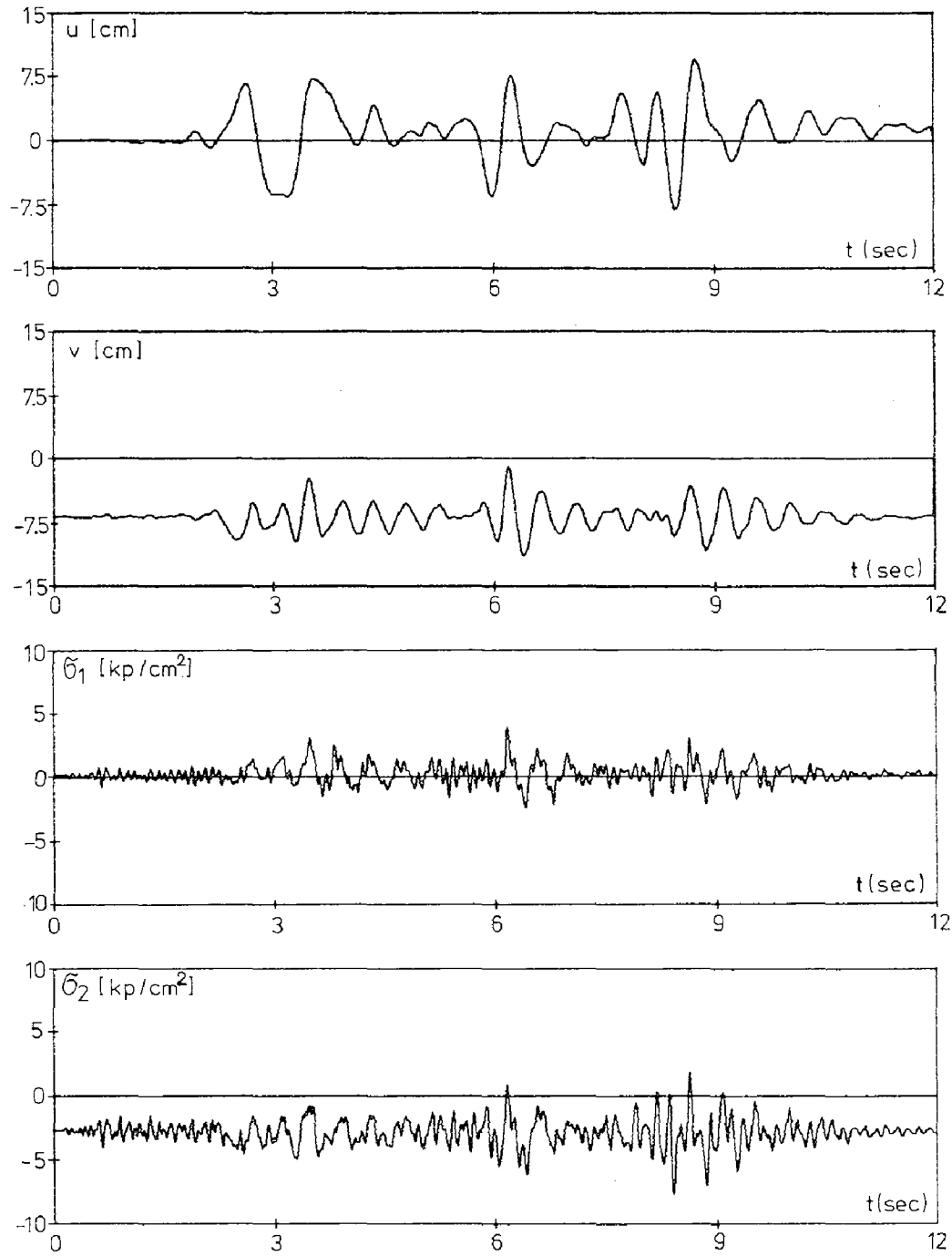


Fig. 5 Response of point A: relative displacements ($u(t)$ horizontal and $v(t)$ vertical) and principal stresses ($\sigma_1(t)$ and $\sigma_2(t)$), cf. case a.

System: transmitting boundaries, cf. Fig. 1

Loading: infinite travelling wave velocity $V_t = \infty$

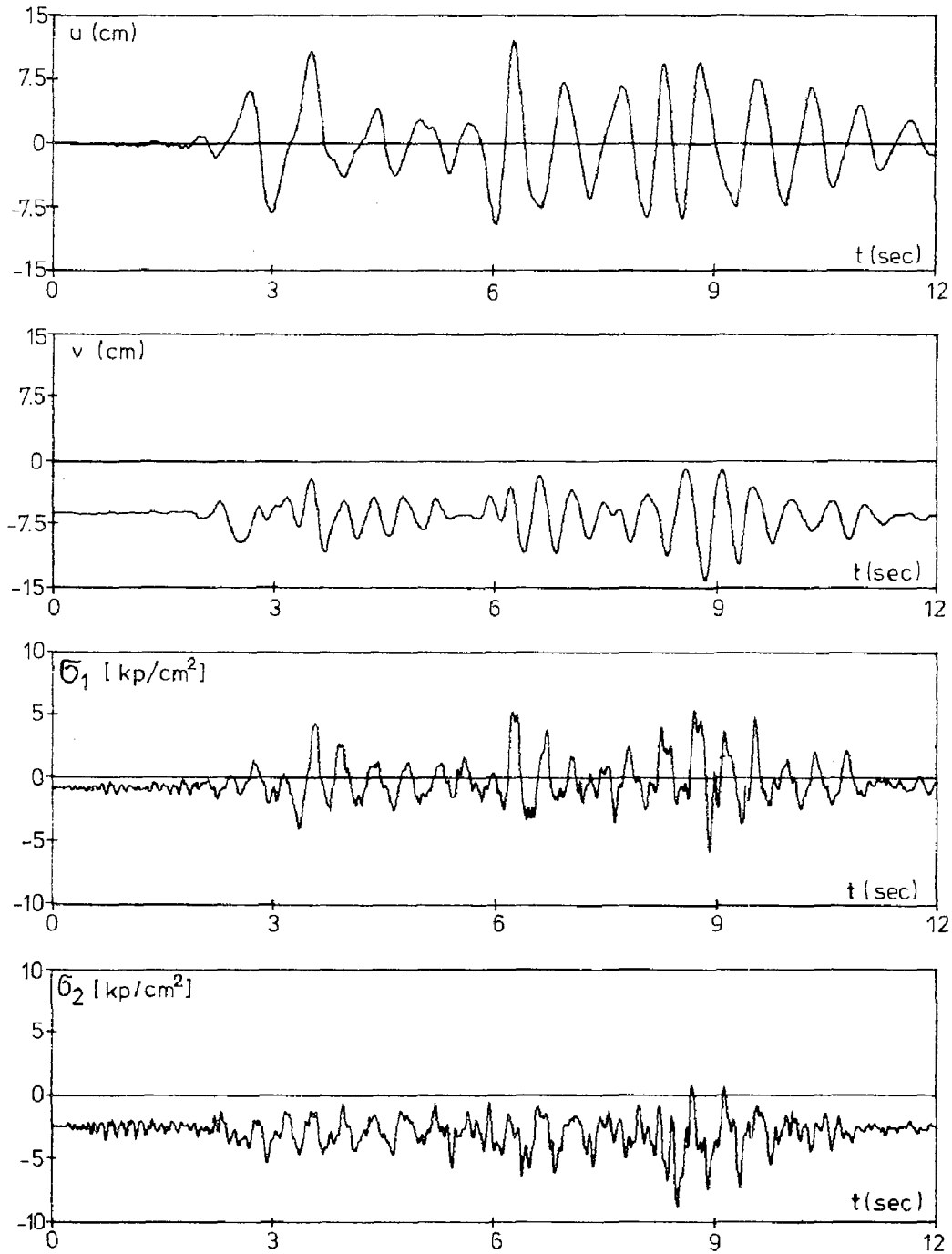


Fig. 6 Response of point A: relative displacements ($u(t)$ horizontal and $v(t)$ vertical) and principal stresses ($\sigma_1(t)$ and $\sigma_2(t)$), cf. case b. System: rigid side boundaries. Loading: travelling wave, velocity $V_t = 1500$ m/sec

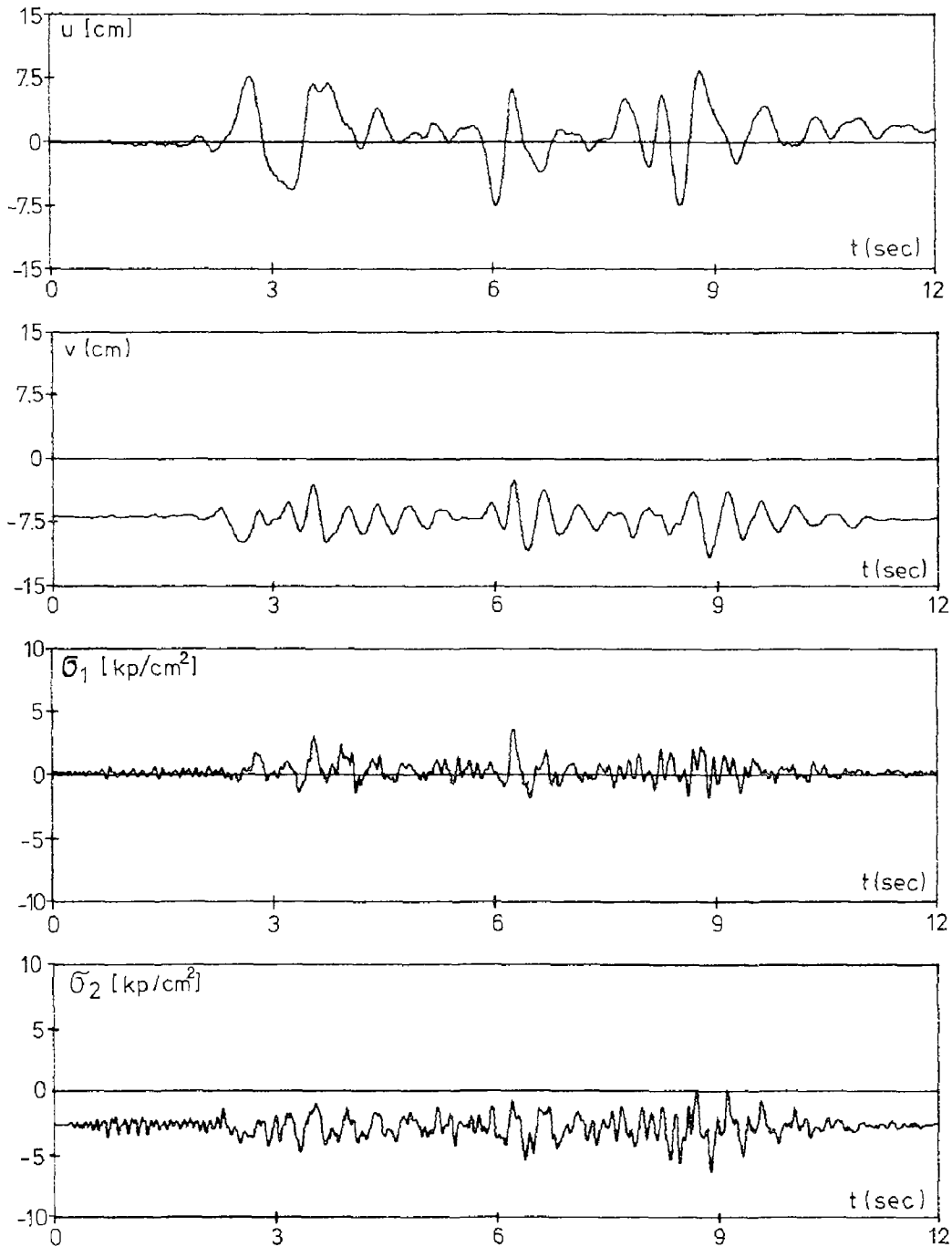
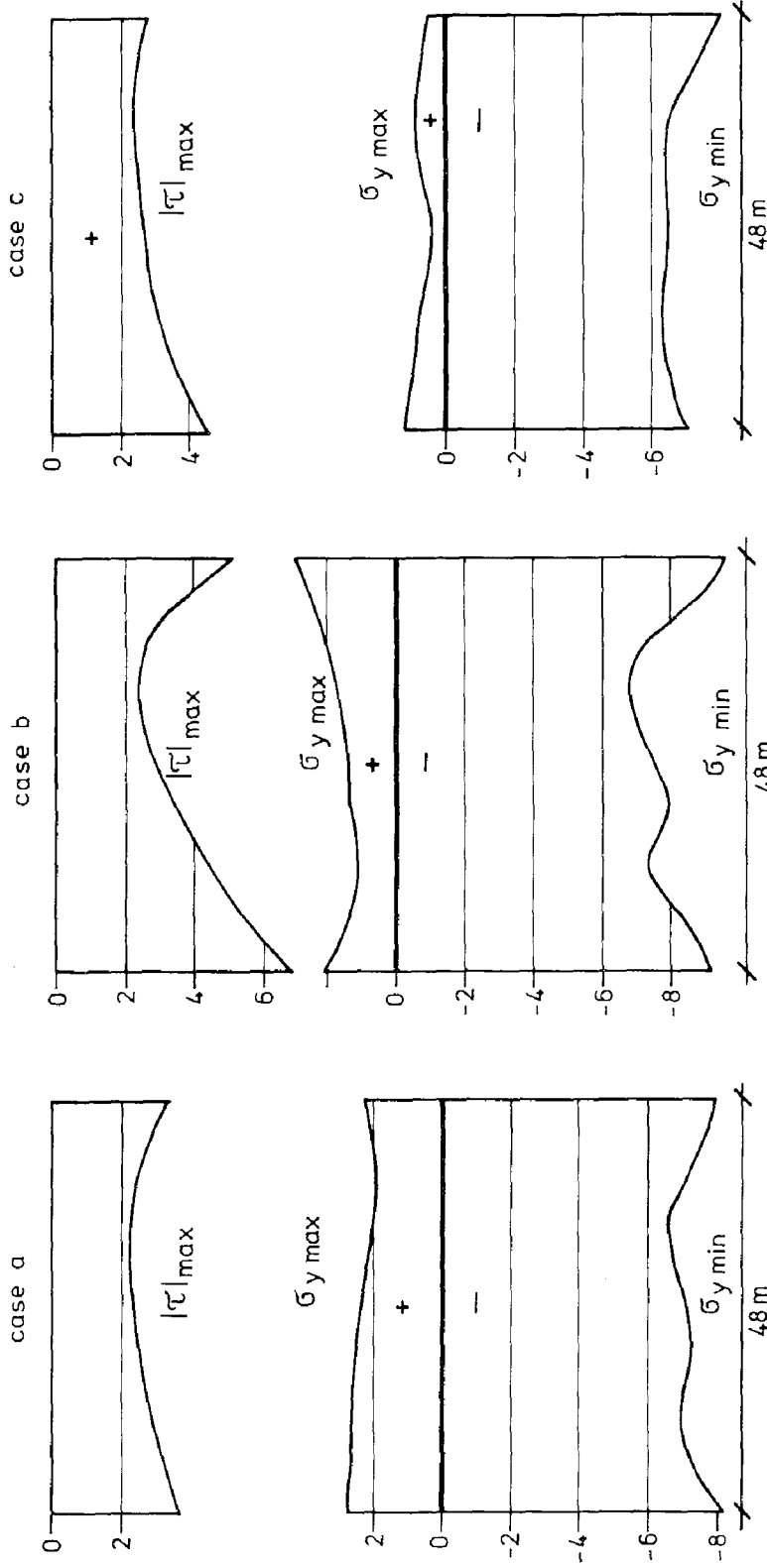


Fig. 7 Response of point A: relative displacements ($u(t)$ horizontal and $v(t)$ vertical) and principal stresses ($\sigma_1(t)$ and $\sigma_2(t)$), cf. case c.
 System: transmitting boundaries
 Loading: travelling wave, velocity $V_t = 1500$ m/sec.



Scale for stresses: $1 \text{ cm} = 2 \text{ kp/cm}^2$

Fig. 8 Maximum shear $|\tau|_{max}$ and extreme values of vertical stress $\sigma_{y max}$, $\sigma_{y min}$ acting on the base of the foundation of the reactor. Self-weight has been taken into account.

Case a. rigid underground, $V_t = \infty$, transmitting side boundaries

Case b. travelling wave, $V_t = 1500 \text{ m/sec}$, rigid side boundaries.

Case c. travelling wave, $V_t = 1500 \text{ m/sec}$, transmitting side boundaries

CONCLUSIONS

The analysis of the response of a nuclear reactor soil-structure system for seismic loading, taking into account the self-weight of the structure to properly simulate the nonlinear stress-strain behaviour of the ground, shows

1. A travelling wave of velocity 1500/sec through the underlying rock reduces the maximum response by about 10-15% as compared with the upper bound case, a rigid underground. The lower the velocity of the travelling wave the greater is this effect, and both quantitative and qualitative differences are to be expected.
2. The choice of the side boundary conditions substantially influences the results. Transmitting boundaries reduce the stress and deformation responses by up to 30% as compared with fixed boundaries.
3. The influence of the nonlinear hysteretic model is not significant in the range of small shear stresses $\tau_{oct} / \tau_y < 0.2$. The increased computational effort (about 2.5 times as much computer time) is hardly justified in the lower stress range.
4. Should travelling waves be of importance in the analysis it is economical to introduce them into existing finite difference codes.

NOTATION

u_i	:	displacement vector*
σ_{ij}	:	stress tensor
b_i	:	body force vector
e_{ij}	:	strain tensor
C_{ijkl}	:	components of the elasticity tensor
ρ	:	material density
K, K_{crit}	:	viscous damping coefficients
λ, μ	:	Lame's elasticity constants
T_i	:	static equilibrium term in the wave equation
Δt	:	time step
u_g, v_g	:	horizontal and vertical ground displacement
u_o, v_o	:	seismic disturbance
x, y	:	cartesian coordinates
V_t	:	speed of travelling wave
C_s, C_p	:	S-wave and P-wave velocities respectively
ω_o	:	fundamental frequency
ξ	:	percentage critical viscous damping
$\tau_{oct}, \epsilon_{oct}$:	octahedral stresses and strains
$c, R, \alpha, \tau_y, \beta, G_o$:	constants for Ramberg-Osgood model
g	:	acceleration due to gravity

* In the tensor notation $u_{i,j}$ denotes differentiation with respect to the coordinate x_j .

BIBLIOGRAPHY

1. Seed H. B. and Idriss I. M., 'Influence of Soil Conditions on Ground Motions during Earthquakes', Jnl. ASCE, SM 1, Jan. 1969, pp. 99 - 137.
2. Seed H. B. and Idriss I. M., 'Soil - Structure Interaction of Massive Embedded Structures during Earthquakes', 5th World Conf. Earth. Eng., Rome, 1973, pp. 1881 - 1890.
3. Despeyroux J., 'Design of Special Structures' Reporters Summary Session B-4, 4th World Conf. Earth. Eng., Chile, 1969, pp. 106 - 108.
4. Dezfulian H. and Seed H. B., 'Seismic Response of Soil Deposits underlain by Sloping Rock Boundaries', Report No. EERC 69-9, University of Calif., Berkeley.
5. Boore D. M., 'Finite Difference Methods for Seismic Wave Propagation in heterogeneous Materials', Methods in Computational Physics, 11, 1972, Ed. Adler B. et al., Academic Press, pp. 1 - 37.
6. Isenberg J. and Adham A. M., 'Interaction of Soil and Power Plants in Earthquakes', Jnl. ASCE, PO 2, Oct. 1972, pp. 273 - 291.
7. Wolf J. P., 'Seismic Response due to Travelling Shear Wave...', Specialist Meeting, Anti-Seismic Design of Nuclear Installations, Paris, 1975.
8. Lysmer J. and Kuhlemeyer R. L., 'Finite Dynamic Model for Infinite Media', Jnl. ASCE, EM 4, Aug. 1969, pp. 859 - 77.
9. Baladi G. Y., 'Ground Shock Calculation Parameter Study', Technical Report S-71-4, No. 2, 1972, U.S. Army Engineer Waterways Experiment Station, Vicksburg, Miss.
10. Dibaj M. and Penzien J., 'Response of Earth Dams to Travelling Seismic Waves', Jnl. ASCE, SM 2, March, 1969, pp. 541 - 59.
11. Prater E. G. and Wieland M., 'Hydrodynamic Pressures on Dams', Symposium, Numerical Analysis of Dams, Swansea, U. K., Sept. 1975, pp. 685 - 707.
12. Kaldjian M. J., 'Foundation-Dam Interaction and Spatial Variation in Ground Motion', 5th World Conf. Earth Eng., Rome, 1973, pp. 1004 - 7.
13. Ghosh S. and Wilson E. L., 'Dynamic Stress Analysis of Axisymmetric Structures under Arbitrary Loading', Report No. EERC-69-10, Univ. of Calif., Berkeley, 1969.
14. Ang A. H. -S., 'Numerical Approach for Wave Motions in Nonlinear Solid Media', Proc. Conf. Matrix Methods in Struct. Mechs., Dayton, Ohio, 1966, pp. 759-778.
15. Kaldjian M. S. and Fan W. R. S., 'Earthquake Response of a Ramberg-Osgood Structure', Jnl. ASCE, ST 10, Oct., 1968, pp. 2451 - 65.
16. Solnes J. et al., 'Earthquake Response of Ramberg-Osgood Systems with Gravity Effects', 5th World Conf. Earth. Eng., Rome, 1973, pp. 1830 - 37.
17. Streeter V. L. et al., 'Soil Motion Computations by Characteristics Method', Jnl. ASCE, GT 3, March, 1974, pp. 247 - 263.
18. Faccioli E. and Ramirez J., 'Earthquake Response of Nonlinear Hysteretic Soil Systems', Int. Jnl. Earth. Eng. and Struct. Dynamics, 4, 1976, pp. 261-76.

INTERNATIONAL SYMPOSIUM ON
EARTHQUAKE STRUCTURAL ENGINEERING

199

St. Louis, Missouri, USA, August, 1976

SOME COMPARISONS OF DYNAMIC SOIL-STRUCTURE ANALYSES

By

GORDON R. JOHNSON

Principal Development Engr.
Government and Aeronautical Products Div., Honeywell Inc.
Minneapolis, U.S.A.

HOWARD I. EPSTEIN

Assistant Prof. of Civil and Mineral Engrg.
University of Minnesota
Minneapolis, U.S.A.

PAUL CHRISTIANO

Associate Prof. of Civil Engrg.
Carnegie-Melon University
Pittsburgh, U.S.A.

SUMMARY

For the lumped parameter and finite element methods applied to dynamic soil-structure interaction problems, the effect of various parameters and possible sources of error are investigated through a limited parametric study. Single and multi-degree-of-freedom systems with various mass ratios, with and without internal and radiation damping, are subjected to severe loadings. The single-degree-of-freedom system consists of a rigid disk resting on the surface of an elastic stratum. Five-mass models are used for the multi-degree-of-freedom systems. For the lumped parameter model, a rational procedure is presented to find appropriate springs, dashpots, effective masses and equivalent modal damping. This study considers the vertical motion of surface-mounted axi-symmetric structures on a homogeneous elastic stratum underlain by bedrock. For these problems, it is demonstrated that the lumped parameter method can produce results that give good general agreement with finite element results which include the soil. The results indicate that it is possible to apply the lumped parameter method to problems beyond those of a harmonic forcing function and an elastic half-space.

INTRODUCTION

The lumped parameter method, based on elastic half-space theory, and the finite element method are the two most common treatments currently being used for dynamic soil-structure interaction problems. Each method has unique advantages and disadvantages which are somewhat dependent on the characteristics of the specific problem. Both methods are used extensively, but an evaluation of the accuracy of each is not possible for most cases due to the lack of exact solutions or test data.

The lumped parameter method evolved from analytical solutions obtained for a harmonic forcing function acting on a rigid disk mounted on the surface of an elastic half-space. In 1966, Lysmer and Richart [13] developed an analog solution for the vertical case by setting the soil spring equal to the static stiffness coefficient; then, a constant damping coefficient was selected which gave the closest agreement to the elastic half-space solution. Hall [6] developed similar analog solutions for the sliding and rocking cases; in the latter case, an effective mass was used to match the resonant frequencies. The effect of soil-structure interaction for earthquake problems was investigated by Parmelee et al. [e.g. 15] by expanding the elastic half-space results of Bycroft [3] to a two-mass model. Sarrazin, Roesset and Whitman [18] examined the interaction effects of the various parameters used in a similar lumped parameter model. In order to utilize the modal method for multi-degree-of-freedom systems, several techniques have been developed to represent the soil dashpots by equivalent modal damping [2, 4, 10, 17, 20].

An important advantage of the lumped parameter method over the finite element method is that the soil resistance is represented by a limited number of springs and dashpots, and the resulting model is relatively simple. In addition to the economic savings which result, it is also feasible to obtain mode shapes and natural frequencies. If the dynamic loads are well defined, the modal method of analysis can then be used to determine a time history response, and a response spectrum analysis can also be performed. The most important advantage associated with this method, however, is that it easily takes into account the three-dimensional nature of the problem.

Because of the derivation of the lumped parameters, good accuracy is obtained for problems involving harmonic forces acting on surface-mounted structures situated on a homogeneous, elastic half-space. Although some work has included one or more of the following: nonharmonic loading, partial embedment of the foundation, the presence of bedrock, and inhomogeneous soil [8, 12, 14, 15, 18], the accuracy of the lumped parameter method under these conditions has not been clearly established.

With the finite element method, such aspects as embedment and stratification can be accurately represented [21]. Problems that can be considered as two-dimensional, such as the long earth dam subjected to an earthquake, as studied by Wilson [23], are ideally suited to the finite element method. Spatially varying material damping may also be accommodated [7] using stepwise numerical integration procedures. A problem which occurs in the finite element model, however, is the necessity to absorb the energy which reaches the boundary in order to simulate the unbounded soil. Viscous boundary dashpots were derived by Lysmer and Kuhlemeyer [12] to absorb this energy. The results are good for harmonic forcing functions, but these dashpots have yet to be proven adequate for general loading and geometry.

A distinct disadvantage of the finite element method is that, due to computational limitations, it is not generally feasible to analyze the three-dimensional case. Isenberg and Adham [8] performed an earthquake analysis for a circular three-dimensional structure by considering only a

two-dimensional plane strain section through the center of the structure. Although the embedment, bedrock and layered soil can be represented, the simplification to two dimensions can introduce significant errors into the analysis [e.g. 11, 19].

The present work includes a limited parametric analysis which compares solutions obtained by the lumped parameter and finite element methods. Included is a rational procedure to determine the appropriate springs, dashpots, effective masses and equivalent modal damping for the lumped parameter model. The effects of various parameters and possible sources of errors are identified for both methods. While no claim of proof is made as regards accuracy of the two treatments, the results indicate that it is possible to apply the lumped parameter method to problems beyond those that involve a harmonic forcing function and an elastic half-space.

PROBLEM SELECTION

Due to limitations in the two methods, there are few problems available for comparative purposes. Even for problems that can be solved by both methods, an absolute evaluation of each method cannot be made due to the lack of exact solutions or test data. Therefore, any evaluation of accuracy must come from a comparison of these two approximate methods. Any meaningful comparison of the two methods must minimize the number of variables considered.

A problem for the lumped parameter method must be one for which springs, dashpots and effective masses can be obtained; for the finite element method, the problem usually needs to be two dimensional. Since an infinite half-space problem could introduce significant errors into the finite element analysis at the lower horizontal boundary of the model, the comparison problem is chosen to be bounded by bedrock beneath the soil.

This study considers the vertical motion of axi-symmetric structures mounted on the surface of a homogeneous elastic stratum underlain by a rigid base. This case was selected because the lumped parameter variables (spring, dashpot and effective mass) can be determined from existing solutions [3, 22]. This allows an independent comparison to be made with the finite element results. The dashpots are determined from Warburton's amplification data [22] which includes depths to bedrock up to 4.0 radii. The maximum depth of 4.0 radii is selected herein because this will result in higher effective radiation damping, and this damping has a significant effect on the response of the system.

The two structural configurations shown in Figure 1 are considered for comparison of the two methods. The first comprises a rigid disk resting on the surface of the elastic stratum, and will be referred to as the single-degree-of-freedom (SDF) system. The other configuration, similarly founded on the stratum, consists of five equal masses connected by springs having equal stiffnesses, and will be referred to as the multi-degree-of-freedom (MDF) system. The springs that connect the MDF masses are dependent on the mass and are selected to produce a fundamental natural frequency of 5.0 cps for the system when the soil is considered to be rigid. This is accomplished by setting $k/M = 1637 \text{ sec}^{-2}$; this corresponds to a frequency in the

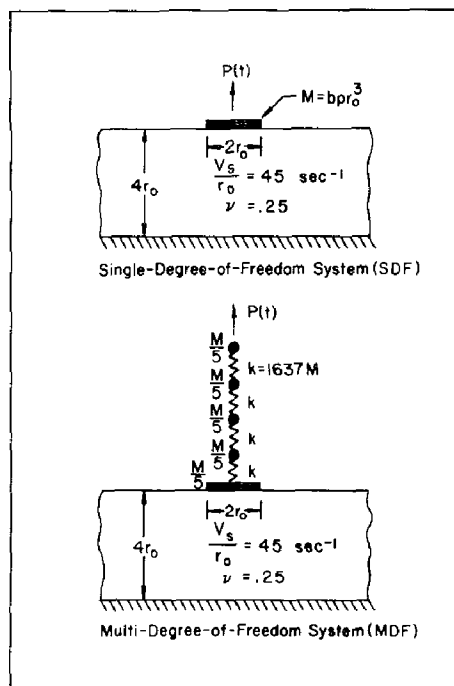


Figure 1 - Structural Configurations for the Example Problems

same range as the resonant frequencies for the SDF system, and should allow for significant soil-structure interaction.

The mass of the structure, M , is expressed in terms of a dimensionless mass ratio, b , given as

$$b = \frac{M}{\rho r_0^3} \quad (1)$$

where ρ is the density of the soil and r_0 is the radius of the foundation. Mass ratios of 5, 10, 20 and 30 are considered herein, and Poisson's ratio is $\nu = 0.25$, as these values correspond to those used by Warburton. The resonant frequency data are presented in the form of dimensionless frequencies, a_0 . For this parametric study, it is desirable to introduce time into the analysis. The resonant frequencies, f , are related to the dimensionless frequencies by

$$f = \frac{a_0}{2\pi r_0} \sqrt{\frac{G}{\rho}} = \frac{a_0}{2\pi} \frac{V_s}{r_0} \quad (2)$$

where G is the shear modulus and $V_s = \sqrt{G/\rho}$ is the shear wave velocity of the soil. For constant a_0 only the ratio of V_s/r_0 affects the resonant frequency. For this study, the range of 3-5 cps was selected for the

SDF systems resonant frequencies. This range is obtained by setting $V_s/r_0 = 45 \text{ sec}^{-1}$.

Two loading conditions are considered herein. The first is a suddenly applied constant force, P_0 , for which the maximum undamped amplification of a SDF system is 2.0. The second loading, shown in Figure 2, is

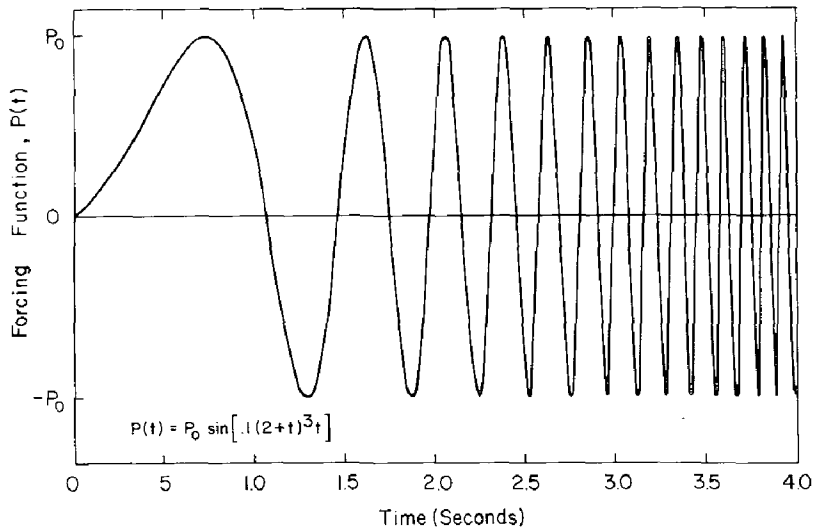


Figure 2 - Sine Sweep Forcing Function

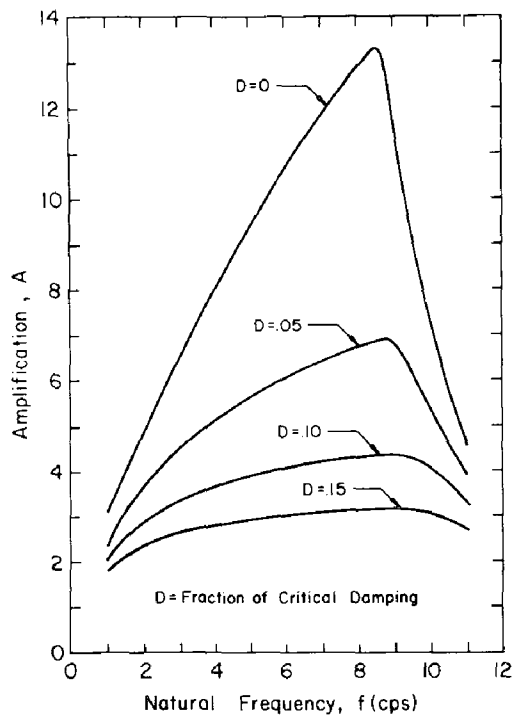


Figure 3 - Response Spectrum for the Sine Sweep Forcing Function

designated as the sine sweep forcing function. It consists of 13 cycles, with an initial frequency of less than 1.0 cps to a final frequency of about 10 cps. It is a more severe loading condition than the first, because it can cause significantly higher amplifications, and the response is dependent on the natural frequency of the system. This forcing function is not intended to represent an actual loading condition, but is selected instead to provide a critical basis for comparison of the lumped parameter and finite element methods. The response spectrum for the sine sweep forcing function is shown in Figure 3 as a function of the undamped natural frequency, f , of a SDF system for various fractions of critical damping, D . The resonant frequencies of the example SDF systems fall within the range of the sine sweep forcing function.

LUMPED PARAMETER MODELS

The lumped parameter models, shown on the left side of Figure 4, are intended to represent the actual systems shown in Figure 1. The soil is represented by a spring and dashpot for both the SDF and MDF configurations. Also, an effective mass, \bar{M} , is introduced to match Warburton's resonant frequencies [22]. The soil spring, K_z , for a stratum thickness = $4 r_0$ and $\nu = 0.25$, is taken equal to $7.35 Gr_0$ [9]. The dashpot represents both radiation damping and material damping in the soil. For the present, only radiation damping is considered, and the dashpot coefficients can be determined from Warburton's data. From the resonant amplifications, A , given in column 2 of Table 1, it is possible to obtain the effective fractions of critical damping, D , for a SDF system from

$$A = \frac{1}{2D \sqrt{1-D^2}} \tag{3}$$

The effective radiation damping fractions for vertical motion, D_z , obtained from Warburton's vertical amplifications, are shown in column 3 of Table 1. The values are significantly lower than for the infinite half-space [16].

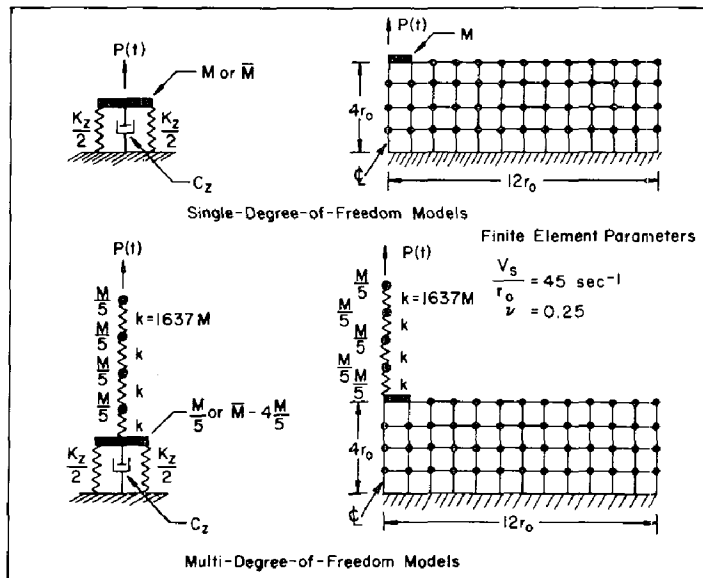


Figure 4 - Models for the Lumped Parameter and Finite Element Methods

Table 1 - Parameters for the SDF System

Mass Ratio b (1)	Amplification A (2)	Effective Damping D_z (3)	Resonant Frequency f (cps) (4)	Effective Mass Ratio m (5)	Damping Coefficient C_o (6)
5	4.2	.120	4.52	3.10	1.455
10	7.2	.0696	4.09	1.93	1.193
20	19	.0263	3.42	1.39	.638
30	34	.0147	3.00	1.21	.437

The effective mass, \bar{M} , can be obtained from the resonant frequency data of Warburton. Frequencies which result from $V_s/r_o = 45 \text{ sec}^{-1}$ are shown as a function of the mass ratio in column 4 of Table 1. The effective mass can now be found by using these frequencies, the damping fractions in column 3 of the table, and the appropriate spring constant. To be consistent with Warburton's data, Bycroft's spring stiffness [3] is used to obtain the effective mass ratio, m, shown in column 5 of Table 1, where

$$m = \frac{\bar{M}}{M} \quad (4)$$

It is now possible to determine the dashpot coefficients for a SDF system since the damping constant is given by

$$C_z = 2 D_z \sqrt{K_z \bar{M}} = C_o r_o^2 \sqrt{G \rho m} \quad (5)$$

where C_o is a dimensionless dashpot coefficient given in column 6 of Table 1. C_o includes the effect of Poisson's ratio, the damping fraction, the stiffness coefficient, and the mass ratio, b. Since this coefficient and therefore the damping constant, C_z , are dependent upon the mass (actual or effective) they must be consistent with the mass selected for the analysis.

The dashpot coefficients come from the amplification data that occur at the resonant frequencies. For most practical applications this is probably adequate because it is at the resonant frequency that the maximum response occurs. If the forcing frequency is far removed from the resonant frequency, the damping is less important. Although the dashpot coefficients have been derived from data for a SDF system, it is reasonable to use the same values for the MDF system. For a MDF system on a flexible soil, the fundamental resonant frequency will always be less than that of a SDF system with the same total mass. If the resonant frequency of the MDF system is only slightly less than that of the SDF system, the MDF system is essentially acting as a rigid body, and a similar condition exists for both systems. If the resonant frequency of the MDF system is much lower, the soil-structure interaction effects will be minimized and the dashpot coefficients become less important.

FINITE ELEMENT MODELS

The models used for the finite element analyses contain 467 elements and 263 nodes, and are similar to that given previously [9]. The concentrated masses are located at a grid spacing equal to the radius of the disk, r_0 , as shown on the right side of Figure 4, thereby resulting in a condensed model having 102 degrees of freedom for the MDF example case. For the resonant frequencies given in Table 1, the spacing of the concentrated masses varies from 1/10 to 1/15 the length of a shear wave, and is well within the limits suggested by Lysmer and Kuhlemeyer [12]. For some of the following cases investigated, no damping is considered; for others, dashpots are placed along the vertical outer boundary of the model. The boundary dashpots are taken as those derived by Lysmer and Kuhlemeyer. The representation of internal damping is discussed subsequently.

RESULTS FOR THE SDF SYSTEMS

For the lumped parameter model, the response to the two loading conditions can be obtained by any routine numerical integration technique. As computer run time is insignificant, accurate time-history responses can be obtained by using an integration time increment that is much smaller than the period of vibration. Moreover, the maximum amplification can be obtained directly from response spectra if the undamped natural frequency and fraction of critical damping are known. For the finite element model, solutions were obtained by a matrix integration procedure developed by Wilson [23]. As described subsequently, the Wilson technique utilizes a diagonal mass matrix and a damping matrix which is expressed as a function of the mass and stiffness matrices. For the present study, it was necessary to modify the procedure to include a diagonal damping matrix so as to incorporate the boundary dashpots. The time increment used for the sine sweep analyses is .01 sec. Since the fundamental natural frequencies are less than 5.0 cps, the selection of this time increment ensured at least 20 increments for each cycle at resonance.

A comparison of the results for the suddenly applied constant force is presented in Figure 5 as the amplification, A , versus mass ratio, b . The upper limit shown is the amplification which occurs for the lumped parameter model when the radiation damping is ignored; the lower limit shown is taken to be the amplification corresponding to half-space radiation damping. When radiation damping is properly included, the amplifications for the lumped parameter model are only 1 to 7 percent higher (depending on b) than for the finite element model. In the former case, the amplification for a suddenly applied force is independent of the natural frequency of the system. The amplifications for both the actual mass and the effective mass are therefore identical, and depend only on the fraction of critical damping.

For the purpose of comparing the behavior of the lumped parameter and finite element models, the sine sweep forcing function provides a more severe test. The amplifications which result from this loading condition are shown in Figure 6. The upper limit amplifications are between 7.2 and 13.3 when the actual mass is used, and between 6.7 and 9.3 using the effective mass. The undamped upper limits increase as the mass ratio decreases, because, as can be seen from the response spectrum (Figure 3), amplifications increase with increasing frequency in the range of frequencies considered. For a specified mass ratio, the actual mass will have higher

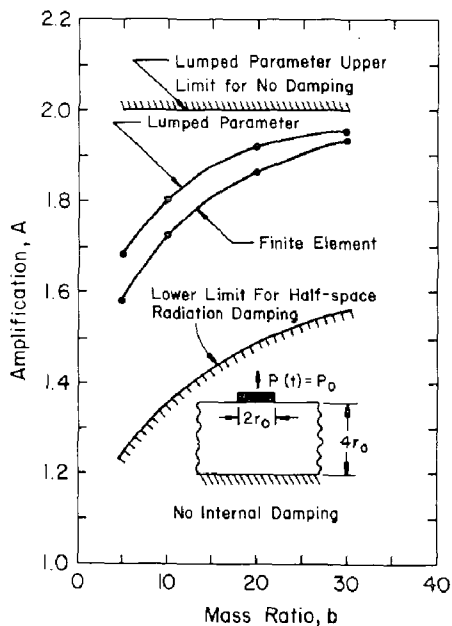


Figure 5 - Amplification for the SDF Systems Subjected to a Suddenly Applied Constant Force

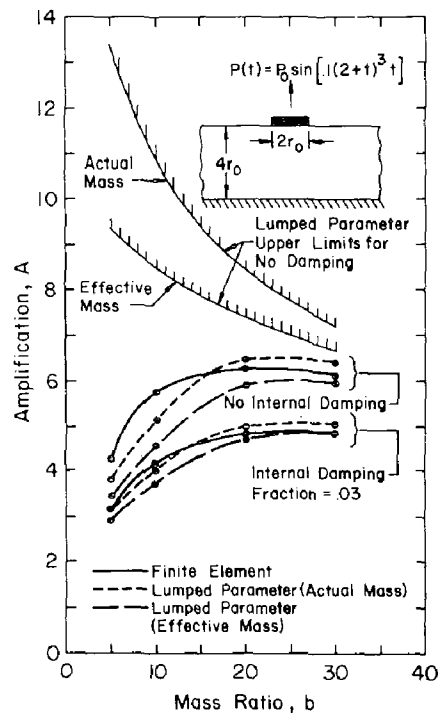


Figure 6 - Amplification for the SDF Systems Subjected to the Sine Sweep Forcing Function

amplifications than the effective mass because the natural frequency is higher in the former case. When radiation damping is included, amplifications decrease as the mass ratio decreases. This is because the radiation damping is higher for the lower mass ratios and more than offsets the higher undamped amplifications.

For the case of no internal material damping, shown in Figure 6, there is fairly good general agreement between the results of the two methods. Amplifications for the lumped parameter method are as much as 11 percent lower than the finite element amplifications for the actual mass, and are as much as 21 percent lower for the effective mass. Utilization of damping fractions for the half-space would again significantly lower the lumped parameter results.

Part of the differences shown in Figure 6 may be due to the presence of the vertical boundary of the finite element model. The boundary dashpots represent the "standard viscous boundary" as presented by Lysmer and Kuhlemeyer [12] and have not been shown to provide accurate solutions for this type of dynamic loading condition. For the case of the suddenly applied constant force, the amplifications for the finite element method are consistently lower than for the lumped parameter method, whereas for the

sine sweep, the amplifications for the finite element method are generally higher than for the lumped parameter method. The boundary does not affect the results for the suddenly applied constant force because of the short time interval required to attain the maximum amplification. For the case of the sine sweep, however, the maximum amplification takes place after several wave reflections have possibly occurred at the outer vertical boundary. The results were essentially the same when the boundary dashpots were removed. Also, for the case of $b = 5$, the amplification obtained from the finite element results is slightly higher than the resonant amplification predicted by Warburton [22]. It therefore appears reasonable to assume that the finite element results are high and are probably due to the presence of the boundary.

Inclusion of internal material damping is accomplished with the lumped parameter method simply by adding it to the radiation damping. With the finite element method, however, the internal damping is represented by the damping matrix, $[C]$, and is expressed as a function of the mass and stiffness matrices, $[M]$ and $[K]$, i.e.

$$[C] = \alpha [M] + \beta [K] \quad (6)$$

the fraction of critical internal damping is frequency dependent and is commonly expressed as follows:

$$D_i = \frac{\alpha}{4\pi f_i} + \beta \pi f_i \quad (7)$$

in which D_i is the fraction of critical damping in the i th mode and f_i is the natural frequency of the i th mode. For the present analysis, α and β were chosen to be 0.75 sec^{-1} and 0.0012 sec , respectively, so that the internal damping fraction is approximately equal to .03 in the range of resonant frequencies considered for this problem. When internal damping in the soil is included, the influence of the boundary diminishes because the elastic waves are partially damped as they approach and return from the vertical boundary. For an internal damping fraction equal to .03 the results are in better agreement than for the case of no internal damping; the maximum difference is reduced to about 10 percent.

In addition to the amplifications shown in Figure 6, time history responses are shown for the case of $b = 5$. The responses obtained from the finite element method, and from the lumped parameter method using the actual mass, are shown for the case of no internal damping in Figure 7. The normalized displacement, $\bar{\delta}$, is the dynamic displacement due to $P(t)$ divided by the static displacement due to P_0 . The maximum absolute value is equal to the amplification, A . The finite element response increases uniformly for about 3 sec and then oscillates somewhat erratically, with the maximum response occurring at about 3.7 sec. Again, it seems probable that the later oscillations are high due to the vertical boundary of the finite element model. The response of the lumped parameter model increases at a slower rate. As the natural frequency of the system with the actual mass is higher than with the effective mass, the model is responding more to the higher frequency portion of the sine sweep which occurs at the later times.

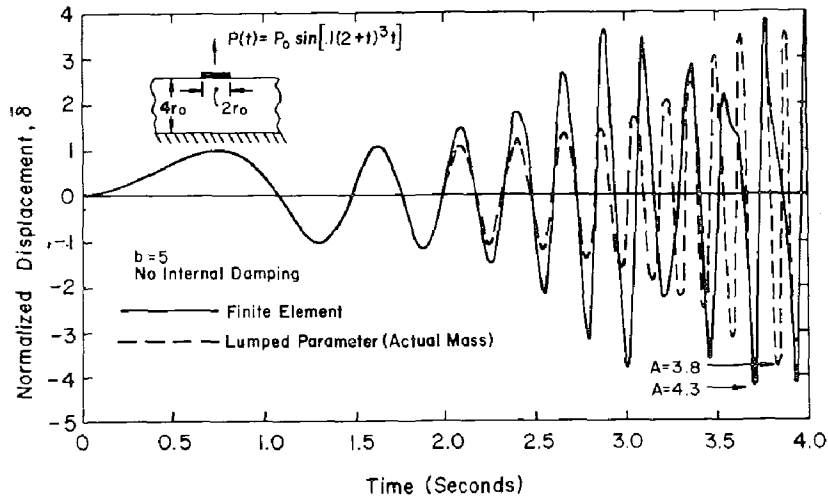


Figure 7 - Time History Responses to the Sine Sweep Forcing Function for a SDF System without Internal Damping

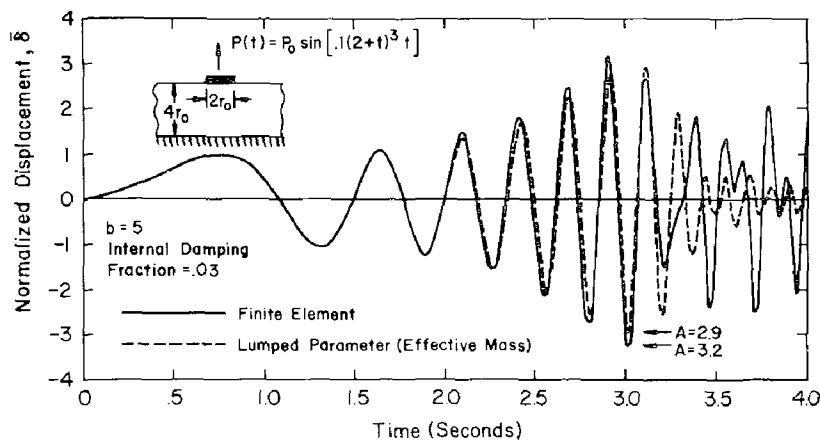


Figure 8 - Time History Responses to the Sine Sweep Forcing Function for a SDF System with Internal Damping

In Figure 8, the response of the finite element model is compared to that of the lumped parameter model with the effective mass. The internal damping fraction is taken equal to .03. A higher value was not selected because it could diminish the effect of the radiation damping. The results are in good agreement; both displacements increase at a similar rate until the maximum displacement is achieved at 3.0 sec. Inclusion of the additional mass lowers the natural frequency of the lumped parameter model to approximately that of the finite element model. As a result, both achieve the maximum displacement during the portion of the forcing function which corresponds to the resonant frequency. The finite element response decays less rapidly and this may again be due to the presence of the vertical boundary.

RESULTS FOR THE MDF SYSTEMS

With the finite element method, there are no additional problems associated with considering a MDF structure rather than a SDF system. Use of a lumped parameter model requires that when an effective mass is used, the additional mass be included with the base mass of the structure. The fundamental frequencies for the lumped parameter models are shown in columns 2 and 3 of Table 2. They are lower than the corresponding SDF frequencies because of the flexibility of the structure.

Table 2 - Parameters for the MDF System

Mass Ratio b	Fundamental Frequency		Energy Fraction		Damping Fraction	
	f_1 (cps)		γ_1		D_1	
	Actual Mass	Effective Mass	Actual Mass	Effective Mass	Actual Mass	Effective Mass
(1)	(2)	(3)	(4)	(5)	(6)	(7)
5	4.45	4.07	.220	.521	.0264	.0625
10	4.02	3.67	.386	.604	.0269	.0420
20	3.40	3.15	.587	.703	.0154	.0185
30	2.98	2.83	.695	.758	.0102	.0111

When internal structural damping is neglected, the lumped parameter solutions may be obtained directly because the dashpots which represent the soil can be expressed as a diagonal damping matrix. The governing equations can be solved using numerical integration techniques such as that of Fu [5] or of Wilson [23]. The method of Fu is directly applicable because it utilizes a diagonal damping matrix whereas the Wilson technique must be modified to accommodate a diagonal damping matrix.

When internal damping is included, it is usually necessary to utilize the modal method of analysis because the resulting damping matrix is not diagonal, and it is difficult to construct the damping matrix to properly account for damping in both the soil and the structure. When the modal method of analysis is used, it is necessary to represent the soil and structural damping by equivalent modal damping which can be approximated by the commonly used procedure presented by Biggs and Whitman [2], or by other techniques. In the case of only vertical motion, the Biggs-Whitman formulation reduces to

$$D_i = \frac{D_z E_{zi} + D_s E_{si}}{E_{zi} + E_{si}} \quad (8)$$

where D_i is the equivalent modal damping for the i th mode, D_z is the damping fraction for vertical motion, D_s is the damping fraction for the structure and E_{zi} and E_{si} represent the energy stored in the soil and in the structure, respectively, for the i th mode.

No Structural Damping - The case of no structural damping is of interest because the lumped parameter solutions can be obtained with both dashpot damping and equivalent modal damping. Amplifications of the top mass in the lumped parameter and finite element models subjected to the sine sweep forcing function are shown in Figure 9. Only radiation damping is included. Since no internal damping is included, the finite element amplifications are probably high due to the vertical boundary. The lumped parameter results with dashpot damping are obtained with the modified technique of Wilson [23]. When the modal method is employed, the lumped impulse method of Biggs [1] is used. The equivalent modal damping is determined from Eq. (8) with $D_s = 0$, hence

$$D_i = \frac{E_{zi}}{E_{zi} + E_{si}} D_z = \gamma_i D_z \quad (9)$$

in which γ_i represents the fraction of the total energy stored in the soil spring in the i th mode. D_z is given in column 3 of Table 1.

As shown in Figure 9, the amplification is lower when the effect of soil-structure interaction is included than when the stratum is rigid, as the decrease in frequency from 5.0 cps, and the radiation damping both cause a decrease in amplification (Figure 3). It can be seen that amplifications for the lumped parameter model utilizing the actual mass and its associated dashpot are as much as 30 percent higher than the finite element amplifications; however, amplifications for the lumped parameter model utilizing the effective mass are as much as 26 percent lower than the finite element amplifications. The significant decrease caused by the inclusion of the effective mass can be explained by looking at the first mode of vibration. The energy fraction stored in the soil spring for mode 1, γ_1 , is given for the actual mass and the effective mass in columns 4 and 5 of Table 2. The soil spring contains more of the total energy for the case of the effective mass, and the energy ratio increases as the mass ratio increases. To obtain the equivalent modal damping fractions for the first mode, the effective radiation damping fractions in column 3 of Table 1 are multiplied by γ_1 , in columns 4 and 5 of Table 2, leading to columns 6 and 7 of Table 2. Amplifications of the lumped parameter model with equivalent modal damping are consistently lower than those of the model with a dashpot. This generally occurs for viscous damping and the technique has recently been expanded to include a frequency factor which tends to reduce the damping [4, 17, 20].

Adjusted Modal Damping Fractions - Since modal damping is an approximation to dashpot damping, and since the amplifications for the dashpot damping are available for the case of no internal structural damping, it is possible to adjust the equivalent modal damping fractions to give better correlation with the dashpot damping results. This procedure is demonstrated by considering the effective mass case for $b = 5$. As shown in Figure 9, the amplification of the top mass is 14 percent lower for the Biggs-Whitman modal damping solution than for the dashpot damping solution. If the modal damping fractions, for each mode, are reduced by 30 percent, the amplification of the top mass for the modal damping solution is equal to that of the dashpot damping solution. Note that the base amplifications or the amplifications of any other point on the structure could be equated instead of the top amplifications. Also, the amplifications of various points on the structure could be averaged

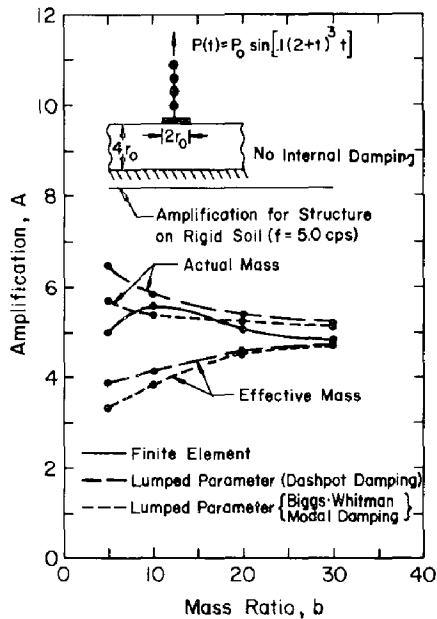


Figure 9 - Top Amplification for the MDF Systems (Without Internal Damping) for the Sine Sweep Forcing Function

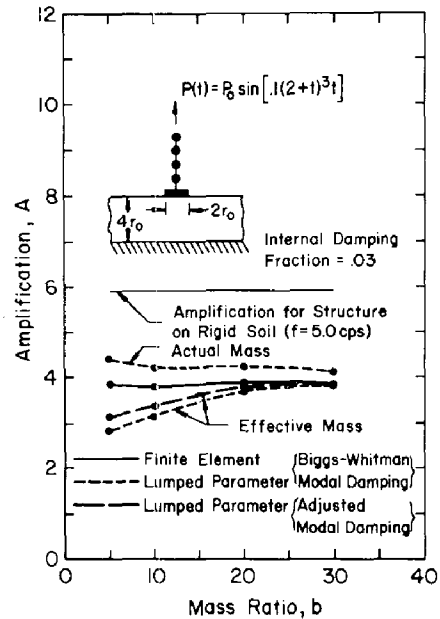


Figure 10 - Top Amplification for the MDF Systems (With Internal Damping) for the Sine Sweep Forcing Function

in some manner, and average amplifications could then be equated. The difference in amplifications for various points on the structure can then be determined to obtain an indication of the overall accuracy. The result of the adjusted damping fractions is that the relative damping between the various modes, as determined by the Biggs-Whitman procedure, is maintained because all modes are adjusted by the same percentage.

Results With Structural Damping Included - The same problem is now altered to incorporate internal damping. The internal damping fractions for the soil and the structure are both set equal to .03. The internal damping in the soil can be added directly to the radiation damping. For the lumped parameter method with modal damping (not adjusted) the modal damping fractions, obtained from Eq. (8), are .03 higher than those used for the earlier analyses.

The amplifications of the top mass are shown in Figure 10. It can be seen that the amplification for rigid soil is equal to 5.9. For the case of no internal damping, the amplification is 8.2. This reduction is due entirely to the effect of the structural damping. For the lumped parameter method with modal damping and actual mass, the amplifications are as much as 15 percent higher than the corresponding finite element amplifications. These differences would be increased if the modal damping fractions would be adjusted. For the case of the effective mass, the lumped parameter amplifications are as much as 27 percent lower than the finite element amplification if the Biggs-Whitman modal damping fractions are used. The maximum difference is reduced to about 19 percent when the adjusted damping fractions are used. The results for the two methods show good general agreement, but not as good as for the SDF system. Again, it appears that the effective mass should be used for the lumped para-

meter method; also, the adjusted modal damping fractions should be used, particularly if the amplification is very sensitive to damping.

CONCLUSIONS

In this paper, dynamic analyses have been performed using the lumped parameter and finite element methods. Included is a rational procedure to obtain springs, dashpots, effective soil masses and equivalent modal damping fractions for the lumped parameter method. The effects of various parameters have been examined. A limited parametric analysis has been performed to compare the results of the two methods. Single and multi-degree-of-freedom systems with various mass ratios, with and without internal soil and structural damping, have been subjected to two loading conditions. For these problems, it has been demonstrated that the lumped parameter method can produce results which give good general agreement with finite element results which include the soil.

BIBLIOGRAPHY

1. Biggs, J.M., Introduction to Structural Dynamics, McGraw-Hill, New York, 1964.
2. Biggs, J.M., and Whitman, R.V., "Soil-Structure Interaction in Nuclear Power Plants," Proceedings of Third Japanese Symposium on Earthquake Engineering, Tokyo, Japan, 1970.
3. Bycroft, G.N., "Forced Vibration of a Rigid Circular Plate on a Semi-infinite Elastic Space and on an Elastic Stratum," Philosophical Transactions of the Royal Society of London, Vol. 248, January, 1956.
4. Epstein, H. I., Johnson, G.R., and Christiano, P., Discussion of "Modal Damping for Soil-Structure Interaction," Journal of the Engineering Mechanics Division, ASCE, Vol. 100, No. EM6, December, 1974.
5. Fu, C. C., "A Method for the Numerical Integration of the Equations of Motion Arising from a Finite-Element Analysis," Journal of Applied Mechanics, ASME, Vol. 37, Series E, No. 3, September, 1970.
6. Hall, J.R., "Coupled Rocking and Sliding Oscillations of Rigid Circular Footings," Proceedings of International Symposium on Wave Propagation and Dynamic Properties of Earth Materials, Albuquerque, N.M., August, 1967.
7. Idriss, I. M., Seed, H.B., and Serff, N., "Seismic Response by Variable Damping Finite Elements," Journal of the Geotechnical Engineering Division, ASCE, Vol. 100, No. GT1, January, 1974.
8. Isenberg, J., and Adham, S. A., "Interaction of Soil and Power Plants in Earthquakes," Journal of the Power Division, ASCE, Vol. 98, No. P02, October, 1972.
9. Johnson, G.R., Christiano, P., and Epstein, H.I., "Stiffness Coefficients for Embedded Footings," Journal of the Geotechnical Engineering Division, ASCE, Vol. 101, No. GT8, August, 1975.
10. Johnson, T., and McCaffery, R., "Current Techniques for Analyzing Structures and Equipment for Seismic Effects," Proceedings ASCE Structures Conference, New Orleans, 1969.
11. Lefebvre, G., Duncan, J.M., and Wilson, E.L., "Three-Dimensional Finite Element Analysis of Dams," Journal of the Soil Mechanics and Foundations Division, ASCE, Vol. 99, SM7, July, 1973.
12. Lysmer, J., and Kuhlemeyer, R.L., "Finite Dynamic Model for Infinite Media," Journal of the Engineering Mechanics Division, ASCE, Vol. 95, No. EM4, August, 1969.

13. Lysmer, J., and Richart, F.E., "Dynamic Response of Footings to Vertical Loading," Journal of the Soil Mechanics and Foundations Division, ASCE, Vol. 92, No. SM1, January, 1966.
14. Novak, M., and Beredugo, Y., "Vertical Vibration of Embedded Footings," Journal of the Soil Mechanics and Foundations Division, ASCE, Vol. 98, No. SM12, December, 1972.
15. Parmelee, R.A., and Wronkiewicz, J.H., "Seismic Design of Soil-Structure Interaction Systems," Journal of the Structural Division, ASCE, Vol. 97, No. ST10, October, 1971.
16. Richart, F.E., Hall, J.R., and Woods, R.D., Vibrations of Soils and Foundations, Prentice-Hall, 1970.
17. Roesset, J.M., Whitman, R.V., and Dobry, R., "Modal Analysis for Structures With Foundation Interaction," Journal of the Structural Division, ASCE, Vol. 99, No. ST3, March, 1973.
18. Sarrazin, M., Roesset, J.M., and Whitman, R.V., "Dynamic Soil-Structure Interaction," Journal of the Structural Division, ASCE, Vol. 98, No. ST7, July, 1972.
19. Tsai, N.C., Discussion of "Interaction of Soil and Power Plants in Earthquakes," Journal of the Power Division, ASCE, Vol. 99, No. PO2, November, 1973.
20. Tsai, N.C., "Modal Damping for Soil-Structure Interaction," Journal of the Engineering Mechanics Division, ASCE, Vol. 100, No. EM2, April, 1974.
21. Waas, G., and Lysmer, J., "Vibrations of Footings Embedded in Layered Media," Proceedings of Symposium on Applications of the Finite Element Method in Geotechnical Engineering, Vicksburg, Miss., May, 1972.
22. Warburton, G.B., "Forced Vibration of a Body on an Elastic Stratum," Journal of Applied Mechanics, ASME, Vol. 24, March, 1957.
23. Wilson, E.L., "A Method of Analysis for the Evaluation of Foundation-Structure Interaction," Proceedings of Fourth World Conference on Earthquake Engineering, Santiago, Chile, January, 1969.

NOTATION

A	= displacement amplification;
a_0	= dimensionless frequency;
b	= dimensionless mass ratio (See Eq. 1);
C_0, C_z	= dashpot coefficients (See Eq. 5);
D	= fraction of critical damping;
E	= stored energy;
f	= resonant frequency;
G	= soil shear modulus;
K_z	= soil spring stiffness;
M	= total mass of structure;
\bar{M}	= effective mass of soil and total mass of structure;
m	= dimensionless mass ratio (See Eq. 4);
P_0	= maximum magnitude of applied force;
$P(t)$	= applied force (function of time);
r_0	= radius of the foundation;
t	= time;
V_s	= soil shear-wave velocity;
α, β	= constants in Eqs. 6 and 7;
γ	= energy fraction (See Eq. 9);
$\bar{\delta}$	= normalized displacement; and
ρ	= soil density.

INTERNATIONAL SYMPOSIUM ON
EARTHQUAKE STRUCTURAL ENGINEERING

215

St. Louis, Missouri, USA, August, 1976

GYPSUM LAYER IN SOIL-STRUCTURE SYSTEMS

Y.C. Hung and M.D. Snyder

Assistant Project Engineers

E. D'Appolonia Consulting Engineers, Inc.

Pittsburgh, Pennsylvania, U.S.A.

SUMMARY

The motion of an embedded foundation will differ during an earthquake from the free field as a result of the soil-structure interaction. For most of the sites, the soil profile is horizontally layered. This paper is to investigate the extent of the interaction of structure, foundation and soil when the soil layer is interrupted by the presence of a relatively stiff gypsum layer of irregular profile. The site studied for a reactor building consists mainly of layers of sand, clay, sandstone and gypsum.

Two finite element models were constructed to investigate the effect of the gypsum geometry in the proximity of the reactor building. One finite element model assumes the horizontal layering of the soil profile with a uniform thickness of gypsum layer interbedded, while the other considers the actual profile with a varying thickness of gypsum layer interbedded. Plane strain elements were used for the soil layers, reactor foundation and reactor building structural systems.

Static and dynamic aspects of the layering effect were studied. The static analysis was undertaken by applying vertical, horizontal and moment loadings to the foundation mat to assess the influence of the gypsum layer on the static soil spring constants. The dynamic analyses were performed to study the influence of the gypsum layer on the soil-structure interaction. Complex transfer functions were determined between bedrock and the structure-foundation to evaluate the dynamic characteristics of each soil profile from the two finite element models.

INTRODUCTION

Although in most cases the soil layers underneath a structure are horizontally extended, the existence of a tilted, and rather rigid layer of an undulatory nature could have influence on the soil-structure interaction. In the case of a nuclear power plant in the proximity of a thick and tilted gypsum layer, a detailed evaluation of influence upon seismic response is mandatory.

To study the effect of a gypsum layer, the model of an actual soil profile was accompanied by a model with assumed horizontal layering. These two finite element models were developed using plane strain elements for the soil layers, reactor foundation and reactor building structural systems. Thus, the dynamic coupling between the soil and structure was included.

The dynamic responses of the soil-structure systems were evaluated in terms of complex transfer functions which were determined between the bedrock, the foundation mat and the structural elements. The effect of the geometry of the gypsum layer on natural frequency and amplification factors was assessed. In this manner, the dynamic characteristics of each profile were evaluated relative to the differences in soil-structure interaction effects and the design ground response spectra.

The static analyses were performed by applying vertical, horizontal and moment loadings to the foundation mat. This evaluates the effect of the geometry of the gypsum layer on the static soil spring constants.

STRAIN COMPATIBLE SOIL PROPERTIES

Suppose that a sand-clay formation of layered soil is interbedded with gypsum which possesses a high shear wave velocity. The soil properties determined from in-situ geophysical testing are then incorporated with the soil profile in the model. Consider a reactor building which is underlain by seven formations as shown in Fig 1. The upper formations are sands and clay. These are underlain by a thin layer of sandstone, a relatively thick layer of overconsolidated clay and a 15 meter thick layer of gypsum interbedded with clay. The clay-gypsum layer is, in turn, underlain by stiff and more pure gypsum. A horizontally layered model with this soil profile is so constructed for the SHAKE⁽⁴⁾ computer program. Briefly, the computer program SHAKE analyzes one-dimensional shear wave propagations in layered media. Each layer is assumed to be homogeneous and isotropic and to be infinite in horizontal extent. A linear visco-elastic system is assumed, however, non-linear behavior is considered in an approximate, piece-wise linear manner.⁽³⁾ The computer program SHAKE was used to deconvolute the surficial time history to determine subsurface seismic strains and compatible soil modulus and damping values for the site stratigraphy and soil properties. An artificial time history with a response spectra enveloping a USAEC Regulatory Guide 1.60⁽⁶⁾ smooth design ground response spectra for 7 percent damping normalized to a peak ground acceleration of 0.18 g was used in the SHAKE runs. Figure 2 shows a comparison of the smooth design ground response spectrum and the response spectrum corresponding to the artificial time history.

Table 1 shows the results of the SHAKE runs in the form of strain dependent shear modulus and damping values for the various soil strata. These properties, which are compatible with the seismic strain levels

resulting from the Safe Shutdown Earthquake, were used for the soil properties in the two finite element models.

REACTOR BUILDING MODEL

For purposes of this investigation, a lumped mass model of a typical reactor building was adopted for this study. The lumped mass model is shown in Fig 3 and was taken from Ref 1. The massless beams in the lumped mass model represent the containment building and reactor internal structures. This lumped parameter model of the reactor building was analyzed for its dynamic characteristics in the form of mode shapes, natural frequencies and participation factors assuming fixed-base condition.

To be consistent with the plane strain geotechnical finite element models used for the static and dynamic analyses, a plane strain model for the reactor building was derived from the lumped mass model to preserve its natural frequencies. This was achieved by judicious selection of material properties for the plane strain elements, mass distribution and the physical width of the model. The height of the plane strain models was restrained to equal the actual height of the reactor building components in the lumped parameter model. The properties of the lumped mass model such as magnitudes of the various masses and the stiffness characteristics of the beams were distributed over the plane strain elements so as to preserve the natural frequencies. The plane strain representations of the reactor building components were then incorporated into the finite element models of the soil profiles and reactor foundation mat.

HORIZONTALLY LAYERED FINITE ELEMENT MODEL

The effect of the geometry of the interbedded gypsum layer was evaluated by comparing the static and dynamic responses of the actual profile with an assumed horizontally layered profile. A finite element model using two-dimensional plane strain elements having two translational degrees of freedom at each node was developed for the horizontally layered soil system. The symmetry of the soil profile about the centerline of the reactor building enabled the size of the model to be reduced through the use of symmetric and anti-symmetric boundary conditions. A symmetric half of the finite element model used for the horizontally layered soil profile as well as the representation of the reactor building are shown in Fig 5. The depth of the finite element model was taken to be 110 meters, or approximately 45 meters into the stiff gypsum layer underlying the site. This boundary, which was taken as rigid for both static and dynamic analyses, was the location of the prescribed harmonic motion for the dynamic analyses.

The dimensions of the finite element model can influence the results of dynamic finite element analyses significantly. Valid results require a reasonable prediction of free-field effects sufficiently far from the reactor building. Therefore, a parametric study was undertaken whereby the width of the horizontally layered finite element model was varied. Harmonic analyses with specified horizontal motion of the rigid base were then performed. In addition, exactly the same horizontal layering was used to obtain amplification functions using the SHAKE program which yields an exact solution for the horizontally layered profiles. Figure 4 shows the harmonic response, using

computer program LUSH,⁽²⁾ of Node A of the finite element model in Fig 5 compared to the exact solution from the SHAKE analysis. Node A of the finite element model represents the surface point farthest removed from the reactor building. Comparison of the two finite element solutions shown in Fig 4 to the SHAKE solution indicate that the 240 meter wide finite element model yields a favorable prediction of the free-field harmonic response.

The symmetry of the horizontally layered soil profile about the centerline of the reactor building was utilized to minimize the size of the finite element model. However, the use of symmetry in the finite element modeling necessitated the use of symmetric and anti-symmetric boundary conditions in static and dynamic analyses of the horizontally layered site. For a vertical harmonic excitation of the rigid base or the vertical static loading of the reactor building foundation mat, the displacement field is symmetric about the centerline of the reactor building. Consequently, a boundary condition of zero horizontal displacement was applied to all nodes along the centerline of the reactor building. This represented the symmetric conditions for both the static and dynamic analyses. For a horizontal harmonic excitation of the rigid base or the horizontal static loading of the reactor building foundation mat, the displacement field is anti-symmetric about the centerline of the reactor building. Consequently, a boundary condition of zero vertical displacement was applied to all nodes along the centerline of the reactor building. This represented the anti-symmetric conditions for both the static and dynamic analyses. The same boundary conditions as used for the horizontal excitation were used for the static analysis of moment loading of the foundation mat. The boundary conditions at the outer boundaries of the finite element model are discussed in later Sections.

The strain compatible soil properties determined from the SHAKE analysis of the horizontally layered site were used for the finite element models for both the ANSYS⁽⁵⁾ static analyses and LUSH dynamic analyses. ANSYS is a structural analysis computer program while LUSH is a dynamic analysis computer program for soil-structure system. Consequently, no iterations on the strain dependent soil properties were required for the LUSH dynamic analyses. For the static analyses, damping was not a consideration. Only the shear modulus values and Poisson's ratio were required for the ANSYS finite element model. For the dynamic analyses, the strain compatible hysteretic damping values as determined from the SHAKE analysis were used for the LUSH finite element model. Consequently, the damping was frequency independent representing the true hysteretic nature of the material damping in soil deposits. Table 1 shows the soil properties for various layers used for both the static and dynamic finite element models.

The dynamic finite element analysis requires a finite element mesh size which is small in comparison to the wave length. The size of the finite elements, therefore, depends upon the shear and compression wave velocities of the soil strata and the frequency range of excitation over which results are desired. A finite element mesh size of less than or equal to one-fifth (1/5) of the wave length of interest was used. The wave length is dependent upon the frequency of excitation f , shear wave velocity v_s and compression wave velocity v_c , according to:

$$\lambda_c = \frac{v_c}{f} \quad (1)$$

$$\lambda_s = \frac{v_s}{f} \quad (2)$$

where λ_c and λ_s are the compression and shear wave lengths respectively. Since the shear wave velocity is less than the compressional wave velocity, the shear wave velocity of the individual soil strata will govern the finite element mesh size required for each layer as a function of the maximum frequency of interest. Thus, the LUSH criterion results in an element mesh size, d , such that

$$d < \frac{1}{5} \lambda_s = \frac{v_s}{5f} \quad (3)$$

The program capabilities of LUSH require all matrix solutions to be performed in-core. This results in limitations on the dynamic matrix band width which in turn limits the mesh size of the finite element model by providing an upper bound on the frequency which may be considered. For the horizontally layered model, the wave propagation, either compressional or shear, is assumed to be vertical. Consequently, the element mesh size criteria is only restrictive in terms of the vertical element height except in the region directly beneath the reactor building where wave reflections are possible in non-vertical directions resulting from soil-structure interaction. However, the wave reflections and refractions for the actual gypsum layer profile are multi-directional. Thus, the mesh size requirement for the actual profile finite element model was found to restrict the maximum frequency considered to 10 Hz for shear wave propagation with a slightly higher frequency for compressional wave propagation. To preserve compatibility between the two finite element models, the horizontally layered model was developed for a maximum frequency of 10 Hz for shear wave propagation.

ACTUAL PROFILE FINITE ELEMENT MODEL

A finite element model of the actual soil profile including the inter-bedded gypsum layer was developed for both static and dynamic analyses. As shown in Fig 6, the finite element model of the actual profile utilizes two-dimensional plane strain finite elements having two translational degrees of freedom per node. Unlike the horizontally layered finite element model, the layer contours prohibit the use of symmetry conditions. Analogous to the horizontally layered finite element model, the plane strain representation of the reactor building was incorporated into the finite element model of the actual site profile.

For compatible results with the horizontally layered finite element model, the depth of the actual profile model was taken below the lowest point of the dipping gypsum layer. The width-to-depth ratio of the model affects the results of a dynamic finite element analysis. To be consistent with the horizontally layered model, the half-width of the actual profile model was taken to be 240 meters. Since the entire region on each side of the reactor building foundation mat was included, no recourse was made to symmetric and anti-symmetric boundary conditions.

Analogous to the horizontally layered model, only the shear modulus values and Poisson's ratios were required for the ANSYS model used for the static analyses. The material damping values used for LUSH model dynamic

analyses are the hysteretic damping values shown in Table 1. For the model of the actual profile, the interbedded gypsum layer gives rise to wave reflections and refractions at any angle beneath the reactor building because of its geometry. Consequently, it was necessary to utilize square shaped elements having diagonals of the order of one-fifth (1/5) of the shear wave lengths of the various materials throughout the region except near the boundaries. This restriction, coupled with the core limitations of the LUSH program, dictated a maximum frequency of 10 Hz for consideration in the dynamic analysis based on shear wave propagation. Analogous to the horizontally layered model, slightly higher frequency compressional waves can be represented by the actual profile model.

STATIC ANALYSIS

To evaluate the effect of the geometry of the interbedded gypsum layer on the static soil spring constants for the reactor building foundation mat, static loads were applied to each of the finite element models corresponding to the horizontally layered site and the actual profile. Three static loading conditions (vertical, horizontal and moment) were considered.

Vertical loading of 100 kips (45,359 kg) was applied to the finite element representation of the foundation mat. For the horizontally layered finite element model, recourse was made to the symmetry conditions. The boundary conditions at the outer periphery of both finite element models were taken as rigid along the base of the model with zero prescribed horizontal displacements along the nodes of the vertical boundaries of both the horizontally layered model and the actual profile model. For all static loading cases, the results were observed to be relatively insensitive to the boundary conditions along the vertical peripheral boundaries, indicating an adequate modeling of half space characteristics.

Horizontal loading of 100 kips (45,359 kg) was applied to the finite element model of the foundation mat. For the horizontally layered finite element model, recourse was also made to the anti-symmetric boundary conditions. Rigid boundary conditions were specified along the base of both finite element models while zero prescribed vertical displacements were specified at all nodes along the vertical boundaries of the model for the actual profile. Analogous to vertical loading, the results were also found to be relatively insensitive to the boundary conditions along the vertical boundaries.

Moment loading was applied to the foundation mat in both finite element models through the use of concentrated vertical forces at the nodes of the finite element representation of the mat. The vertical concentrated forces were linearly distributed so as to produce zero net vertical loading on the mat while yielding a moment of 100 kip-feet (13825 kg-M). Anti-symmetric boundary conditions along the centerline of the reactor building was also used for the horizontally layered model. The boundary conditions at the outer peripheral boundaries were taken to be the same as for the horizontal loading case.

It was assumed that the vertical mat loading would be sufficient to retain compressive soil pressures along all soil/foundation interfaces such that the possibility of lift-off of the mat under moment loading was not considered in the analysis.

For vertical loading of the horizontally layered model, the results indicate no coupling of vertical and rocking deformation. However, coupling exists for vertical loading of the actual profile model. Thus, comparison of these two cases illustrates that one effect of the geometry of the gypsum layer is to couple vertical and rocking motion of the reactor building.

The horizontal loading of the mat for the horizontally layered finite element model reveals a coupling of horizontal and rocking motion of the mat. This is expected since the line of action of the horizontal loading does not pass through the center of rotation; the horizontal mat loading, therefore, also produces a moment loading of the foundation mat. This same effect is observed for the actual profile where the coupled horizontal rocking motion is more pronounced for the same loading. Thus, another effect of the tilted gypsum layer is to increase the degree of coupled rocking/horizontal motion compared to the horizontally layered site.

Using the nodal displacements obtained from the computer runs along with the applied loads for each load case, lumped parameter stiffness matrices were calculated for both the horizontally layered model and the actual profile model by equating the work done to the strain energy of each model. The resulting stiffness matrices for the horizontally layered site and actual profile are shown in Table 2. The presence of off-diagonal terms in the stiffness matrices signifies the presence of coupled motion. Thus, the coupling stiffness between vertical and rocking motion present in Table 2 for the actual profile is absent from the stiffness matrix in Table 2 for the horizontally layered site. This confirms the coupling effects deriving from the geometry of the interbedded gypsum layer.

In general, a comparison of the two stiffness matrices in Table 2 indicates that in addition to introducing coupled vertical and rocking motion, the overall effect of the geometry of the interbedded gypsum layer is to increase the site stiffness 10 to 20 percent over the horizontally layered stiffness values, based on the approximation used to represent the average depth of the stiff gypsum layer.

DYNAMIC ANALYSIS

To evaluate the effect of the geometry of the interbedded gypsum layer on the seismic response of the reactor building, the transfer function between the underlying stiff and more pure gypsum and the structure was determined for both finite element models by applying a harmonic excitation to the base of the finite element models of varying frequency from 0.4 Hz to 10 Hz. The LUSH finite element program was used to formulate the stiffness matrix $[K]$ and mass matrix $[M]$ for each of the two finite element models. Damping is simulated through the use of complex moduli in defining the stiffness matrix.⁽²⁾ While the LUSH program utilizes harmonic analysis to formulate a complex transfer function to perform time history response analyses based on Fourier Transform methods, it is not written to directly perform only harmonic analyses. Consequently, a separate program was developed utilizing the appropriate subroutines of the LUSH program which solve the dynamic matrix equation:

$$([K] - \omega^2[M]) \{X\} = -[M] \{a\} \quad (4)$$

where $\{X\}$ is the vector of nodal displacements relative to the fixed base, $\{a\}$ is the vector of applied accelerations (unity for degrees of freedom in the excitation direction and zero for the remaining degrees of freedom), ω is the circular frequency of excitation ($2\pi f$) with f varied from 0.4 Hz to 10 Hz.

For the vertical harmonic excitation, the stiffness, mass and damping matrices were formulated for both finite element models. The harmonic excitation was applied at all the nodes on the base of the finite element models while the boundary condition at all nodes along the outer vertical boundaries was taken to be zero horizontal displacement. For the horizontal harmonic excitation, the boundary condition at the peripheral vertical boundary was taken to be zero vertical displacement at all nodes along the vertical boundary. The horizontal excitation was applied at all the nodes on the base of both models.

For comparison of the dynamic effects resulting from the geometry of the interbedded gypsum, the transfer functions were obtained for the locations at top of reactor building, base of foundation mat and free field away from reactor structure for both the horizontally layered model and the actual profile model. For purposes of this analysis, the transfer function for absolute acceleration, $A(\omega)$, is defined as the complex frequency response or magnification factor resulting from an absolute base acceleration given by:

$$a(t) = 1.0e^{i\omega t} \quad (5)$$

This implies that the absolute response to the base acceleration is complex and may be written as:

$$\ddot{u}(t) = A(\omega)e^{i\omega t} \quad (6)$$

where, in general, $A(\omega)$ is a complex valued function containing both amplitude and phase information. While the transfer function is thus complex, only the amplitude values were plotted against frequency. Figures 7 through 9 show the response to horizontal excitation and Figs 10 through 12 to the vertical excitation for the above locations.

The transfer functions between the base of the finite element models at a depth of 110 meters and the structural components of the reactor structure illustrate the differing dynamic characteristics between an assumed horizontally layered site and the actual profile. The differences are, therefore, a direct result of the geometry of the interbedded gypsum layer since the dynamic characteristics of the structure remained constant.

CONCLUSION

The results of the static analyses indicate that the effect of the geometry of the interbedded gypsum layer is to increase the overall soil stiffness of the site compared to a horizontally layered site possessing the same stratigraphy. This was to be expected owing to the presence of the stiff gypsum in closer proximity to the reactor foundation mat for the actual profile. In addition to increasing the site stiffness, the geometry of the interbedded gypsum layer leads to coupling of vertical and rocking motion of the reactor structure. However, the coupling effect, while present, does not introduce any significantly undesirable characteristics into the potential seismic

response of the reactor. The coupled motion together with the mat flexibility results in differential settlement of less than 12 percent of the mean vertical settlement under static loading.

The transfer functions for the free-field motion, shown in Figs 9 and 12 for horizontal and vertical excitation, indicate that the effect of the geometry of the interbedded gypsum layer is to increase the site stiffness as illustrated by the shift in the resonant peaks to higher frequencies, which is consistent with the results of the static analyses. However, as noted by the higher resonant peaks for horizontal motion in the neighborhood of 1 Hz, 3.5 Hz and 5 Hz compared to the horizontally layered site, the effect of the gypsum layer appears to be one of decreasing the radiation damping effects as a result of multiple wave reflections from the lower stiff and more pure gypsum layer. For vertical motion shown in Fig 12, the differences in amplitudes are less significant and primarily associated with a frequency shift of about 1 Hz.

The general effect of sloping rock interfaces has been found to lead to standing wave patterns such that regions of attenuation and amplification are established along the surface of an alluvial deposit bounded by sloping rock layers. (7) This effect can be observed from Figs 9 and 12 where the response functions for the free-field are different for a point to the left of the reactor structure and a point to the right. Neither free-field response of the actual soil profile differs from the horizontally layered model to an extent sufficient to revise the design ground response spectra.

Comparison of the horizontal and vertical foundation mat response functions, shown in Figs 8 and 11 respectively, again illustrates the slight stiffening effect of the geometry of the interbedded gypsum layer through an increase in the frequencies of the resonant peaks. Analogous to the free-field response functions, the amplification factors for horizontal excitation are slightly greater for the actual profile layer in the neighborhood of 5 Hz, suggesting less radiation damping resulting from multiple wave reflections between the foundation mat and stiff gypsum profile. However, the maximum horizontal amplification factors in the frequency range of 0.8 Hz to 1.0 Hz are practically identical for the actual profile and horizontally layered model. For the vertical excitation shown in Fig 11, the general effect of the gypsum layer, in addition to increasing the stiffness, is to slightly attenuate the response of the foundation mat in the range of 2 to 3 Hz, while having no significant effect on the mat response elsewhere.

Since the dynamic response characteristics of the reactor structural components are determined not only by the soil-structure interaction effects, but also by the dynamic characteristics of the structure itself, the response functions shown in Fig 7 for the horizontal excitation and Fig 10 for the vertical excitation are included only for information. However, these figures serve to illustrate possible resonant frequencies to be considered in the design. Even though the response functions in Fig 7 is highly dependent on the structure, some observations are possible. At the lower frequency where soil-structure interaction is predominant, the somewhat higher amplitude of response is attributed to lower radiation damping.

As expected, the layering and wave scatter tend to increase the response. For the vertical excitation, the results in Fig 10 indicate that the amplitude of response for the actual soil profile is somewhat less than that for a horizontally layered site, especially when one recognizes the slight frequency shift of about 1.0 Hz. In the higher frequency range around 10 Hz, the two response amplitudes are in closer agreement.

REFERENCES

1. Liu, L.K., Child, C.L. and Nowotny, B., "Effects of Parameter Variations on Floor Response Spectra," Journal of the Geotechnical Engineering Division, ASCE, October 1974.
2. Lysmer, J., Udaka, T., Bolton H., Seed, H.B. and R. Hwang, "LUSH - A Computer Program for Complex Response Analysis of Soil-Structure Systems," Report No. EERC 74-4, University of California, Berkeley, California.
3. Papadakis, C.N., Streeter, V.L., Wylie, E.B., "Bedrock Motions Computed from Surface Seismograms," Journal of the Geotechnical Engineering Division, ASCE, October 1974.
4. Schnabel, P.B., Lysmer, J. and Seed, H.B., "SHAKE - A Computer Program for Earthquake Response Analysis of Horizontally Layered Sites," Report No. EERC 72-12, College of Engineering, University of California, Berkeley, California, December 1972.
5. Swanson, J.A. and DeSalvo, G.J. ANSYS Engineering Analysis System User's Manual, Swanson Analysis Systems, Inc., Elizabeth, Pennsylvania, October 1972.
6. United States Atomic Energy Commission, "Design Response Spectra for Seismic Design of Nuclear Power Plants," Regulatory Guide 1.60, December 1973.
7. Wong, H.L. and Trifunac, M.D. "Surface Motion of a Semi-Elliptical Alluvial Valley for Incident Plane SH Waves," Bulletin of the Seismological Society of America, Vol. 64, No. 5, pp. 1389-1408, October 1974.

TABLE 1
SUMMARY OF DYNAMIC AND STRAIN COMPATIBLE SOIL PROPERTIES

Layer Number	Soil Type	Unit Weight (PCF)	Poisson's Ratio	Shear Modulus for Small Strain (KSF)	Strain Compatible Soil Properties	
					Shear Modulus (KSF)	Damping (%)
7	Sand Above Water Table	130.	0.26	7000.	5770.	2.6
6	Sand Below Water Table	130.	0.42	16000.	13350.	3.0
5	Clay	125.	0.48	5000.	955.	8.3
4	Sandstone	140.	0.38	70000.	68800.	0.8
3	Clay	125.	0.48	7400.	1370.	8.4
2	Clay Plus Gypsum	125.	0.43	43000.	15920.	5.1
1	Gypsum	130.	0.44	100000.	93240.	1.3

TABLE 2
SOIL SPRING CONSTANT

Model Identification	Displacement Direction	Vertical Soil Spring Constant	Horizontal Soil Spring Constant	Rotational Soil Spring Constant
Horizontal Layered Model	Vertical	2.02×10^6 k/ft	0	0
	Horizontal	0	1.11×10^6 k/ft	26.61×10^6 k/rad
	Rotation	0	26.61×10^6 k	9.57×10^9 k-ft/rad
Actual Profile Model	Vertical	2.56×10^6 k/ft	-0.024×10^6 k/ft	8.98×10^6 k/rad
	Horizontal	-0.024×10^6 k/ft	1.29×10^6 k/ft	32.33×10^6 k/rad
	Rotation	8.98×10^6 k	32.33×10^6 k	11.00×10^9 k-ft/rad

Sign Convention: Refer to Figs 5 and 6.
 Positive horizontal corresponds to positive X-axis.
 Positive vertical corresponds to positive Y-axis.
 Positive rotation if counter-clockwise (right hand rule).

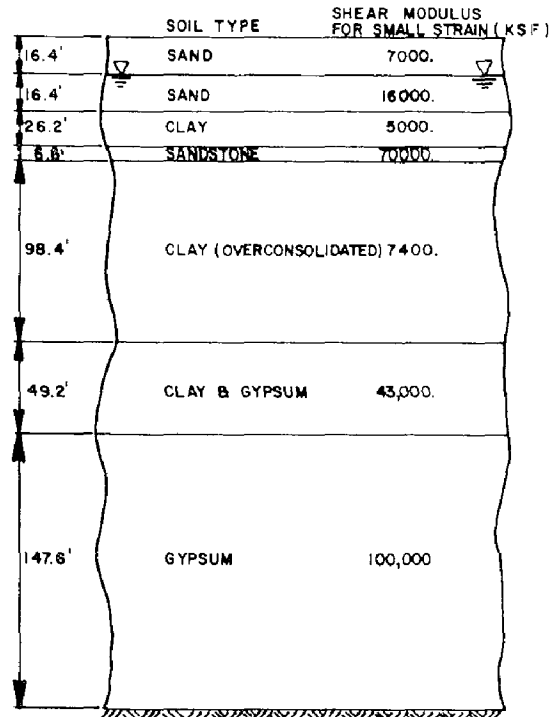
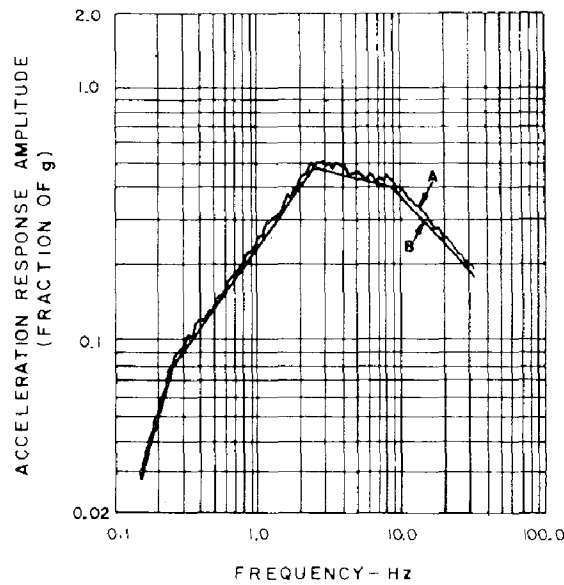


FIGURE 1-LAYER FORMATION



A: RESPONSE SPECTRUM BASED ON ARTIFICIAL TIME HISTORY, DAMPING = 7%

B: SMOOTH GROUND DESIGN RESPONSE SPECTRUM, USAEC REG. GUIDE 1.60, PEAK GROUND ACCELERATION = 0.18g, DAMPING = 7%

FIGURE 2-SMOOTH GROUND DESIGN RESPONSE SPECTRUM VS. ARTIFICIAL TIME HISTORY RESPONSE SPECTRUM

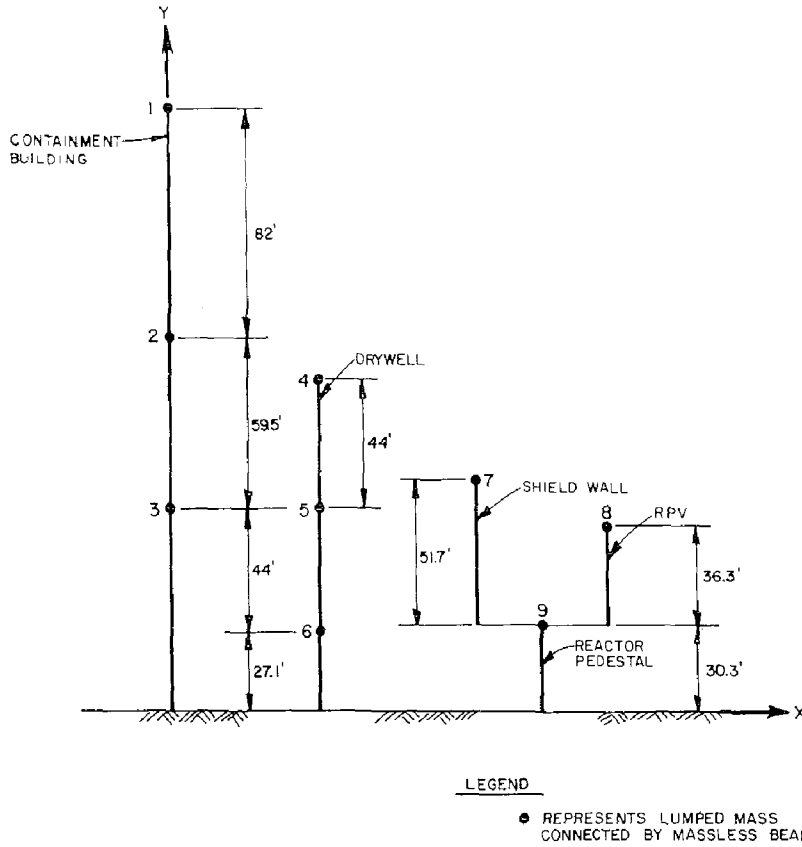


FIGURE 3—LUMPED MASS MODEL OF REACTOR BUILDING

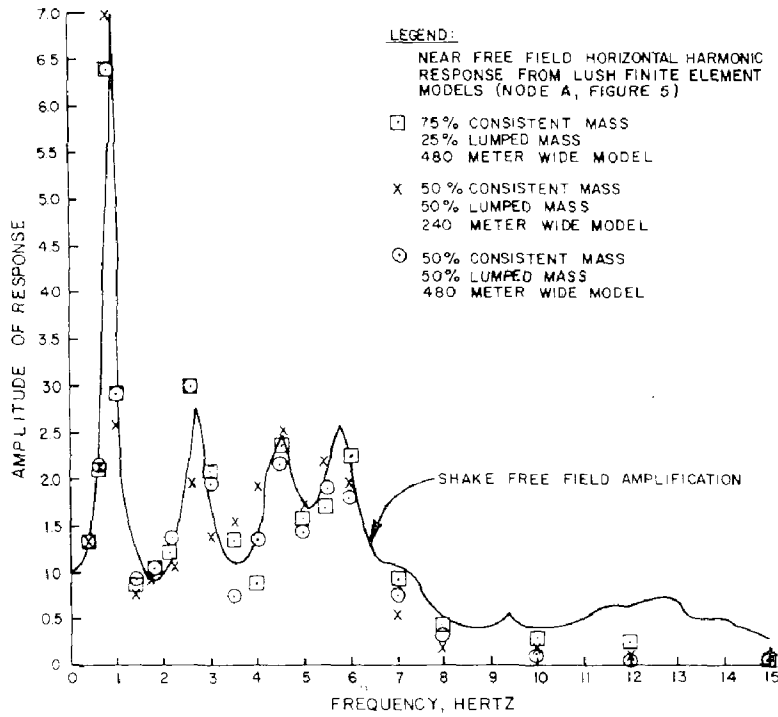


FIGURE 4—COMPARISON OF FREE FIELD RESPONSE FROM LUSH AND SHAKE

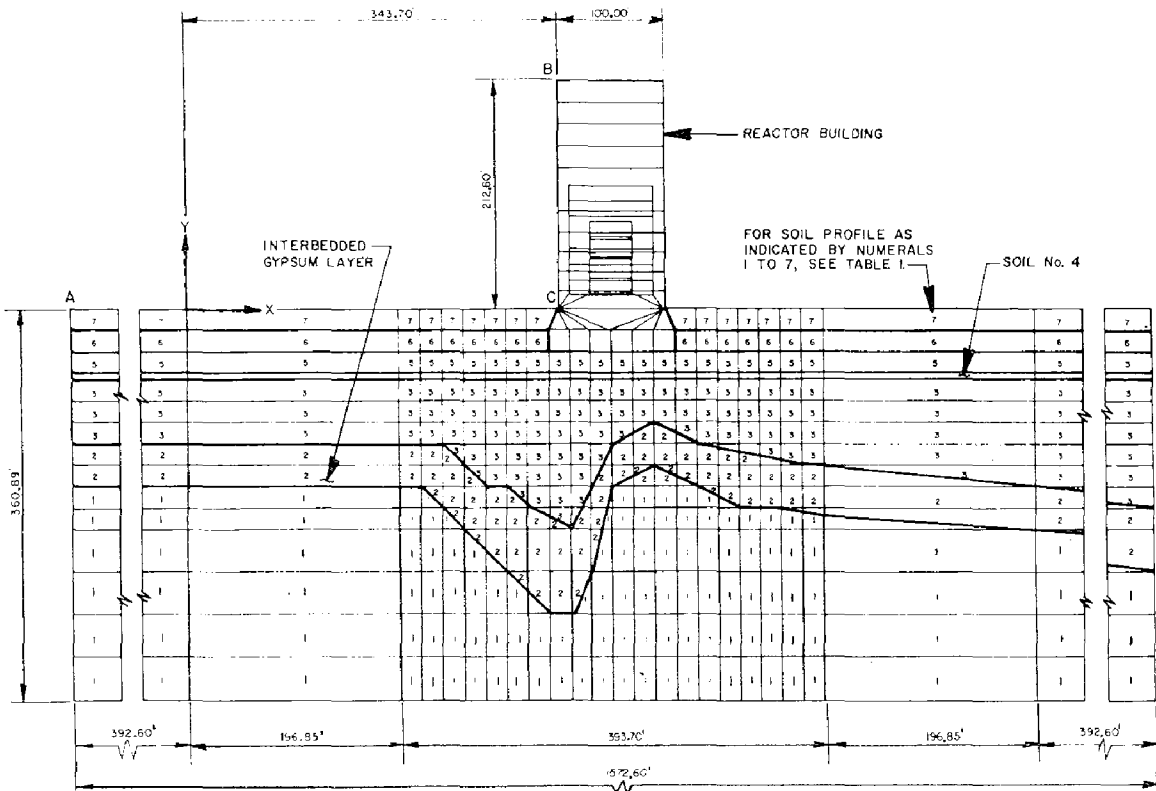


FIGURE 6- PLANE STRAIN FINITE ELEMENT MODEL,
ACTUAL SOIL PROFILE

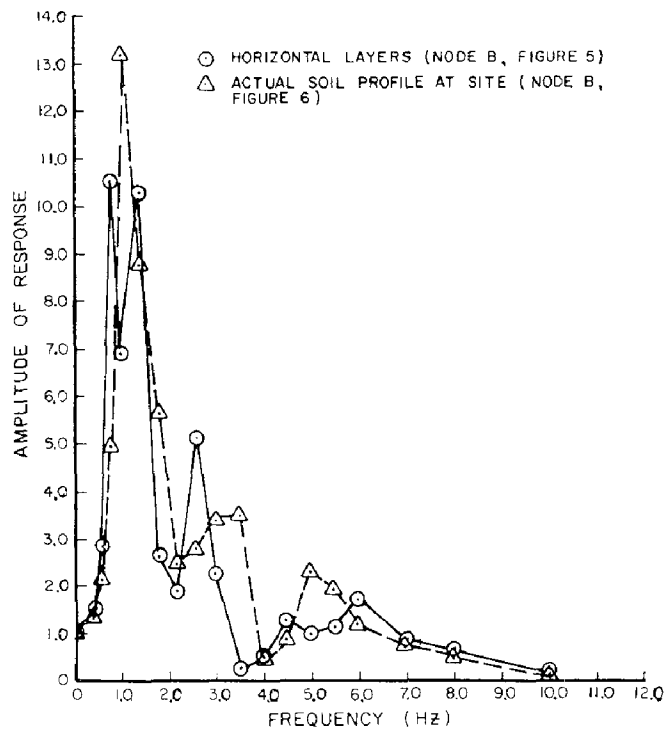


FIGURE 7-HORIZONTAL HARMONIC RESPONSE AT TOP OF REACTOR BUILDING

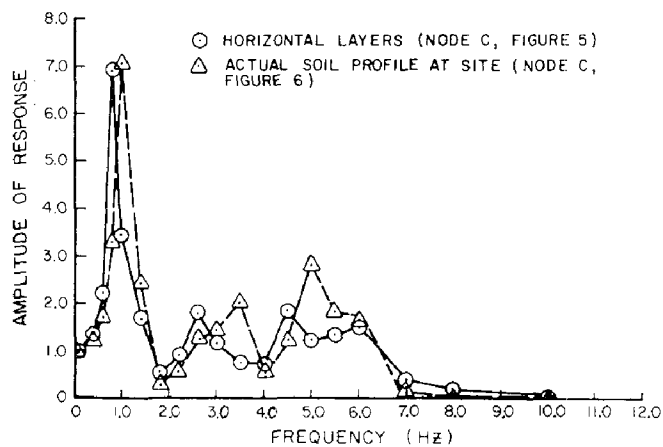


FIGURE 8-HORIZONTAL HARMONIC RESPONSE AT FOUNDATION MAT

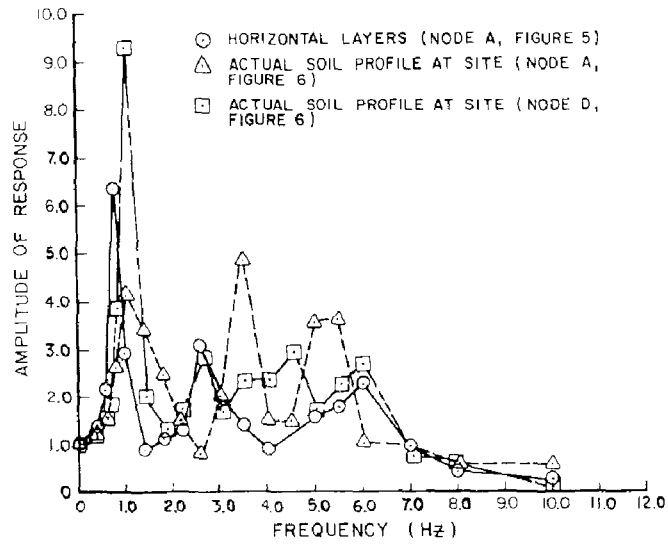


FIGURE 9—HORIZONTAL HARMONIC RESPONSE AT FREE FIELD

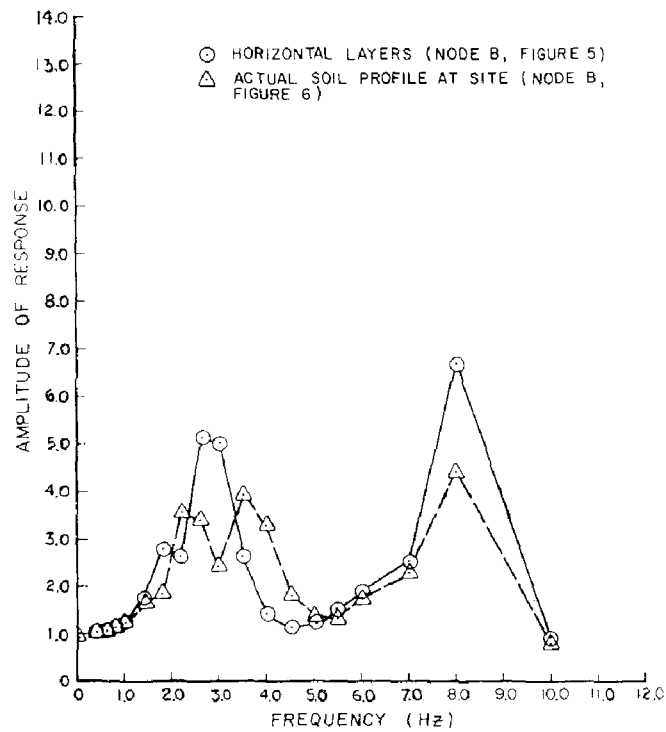


FIGURE 10—VERTICAL HARMONIC RESPONSE AT TOP OF REACTOR BUILDING

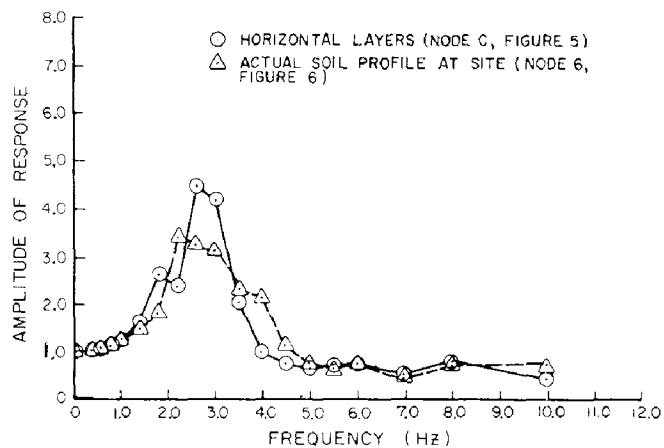


FIGURE 11—VERTICAL HARMONIC RESPONSE AT FOUNDATION MAT

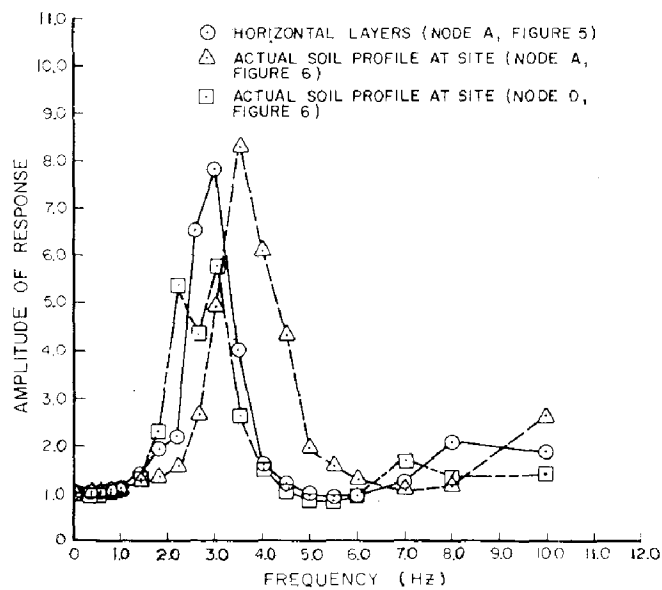


FIGURE 12—VERTICAL HARMONIC RESPONSE AT FREE FIELD

INTERNATIONAL SYMPOSIUM ON
EARTHQUAKE STRUCTURAL ENGINEERING

233

St. Louis, Missouri, USA, August, 1976

THE SOIL-FOUNDATION-STRUCTURE INTERACTION
UNDER THE ACTION OF EARTHQUAKE LOADS

I. CIONGRADI

Dr. Eng. Prof. of
Structural Engineering

N. UNGUREANU

Dr. Eng. Prof. of
Structural Engineering

Polytechnic Institute of Jassy
Romania

Summary

In this paper the interaction among structure, substructure and soil is analysed for dynamic and seismic actions.

The equations of motion of the structural system are written by taking into account the interaction with the soil; the corrections involved in comparison with the case when the interaction is ignored are also emphasized. Besides, the substructure is introduced into structural system and the influence of the soil is included by means of its stiffness matrix which improves the stiffness matrix of the structural system.

The way of determining the elements of the soil flexibility matrix referring to the contact surface with structural system is shown for different soil models.

The obtained results are used for the determination of conventional seismic loads, according to present seismic codes.

The proposed solution is particularized for framed structures with isolated foundation or with foundation beams.

A dynamic and seismic analysis is carried out by means of computers for a framed structure with consideration of the two mentioned types of foundation and the two types of soils differentiated each other by their deformability modulus. Finally, some of the obtained results are discussed.

1. Introduction.

Dynamic structural analysis is commonly performed by assuming the structure supporting base as a rigid body, the dynamic behaviour depending mainly on the deformation properties of the structure. In some cases, the supporting base is considered to undergo certain deformations, their effects being approximated in a whole manner, as done elsewhere [3] [5] .

In the majority of present codes, the seismic design requires that determination of stress and displacement state to be performed by considering the static action of some conventional loads obtained as functions of the vibration mode periods as well as of the mode shapes, the damping and the seismic intensity degree of the considered zone. This method was successfully used and was continuously improved.

This paper follows the same manner of treating the subject, except that interaction effect among structure, substructure (foundation system) and soil is moreover taken into consideration. This effect influences the behaviour of the structural system (structure - substructure) on two ways: 1) through dynamic characteristics and 2) through static interaction.

The equation of motion for a structural system with interaction are firstly presented and for a practical application the system is assumed to be discretized in order to use a finite element computation procedure.

The damping was not introduced in the dynamic equation of motion, firstly in order not to increase much the extend of this study and secondly because the numerical examples which are presented do not take directly into consideration the damping effects, the damping been introduced by means of a conventional seismic load. However, the analysis by means of the temporal steps with consideration of the damping, can

be performed without great difficulties, pursuing the views presented in paragraph 2 of the paper.

The interaction effect is introduced in the idea of maintaining permanently the contact between the structural system and the soil.

Some models with linear behaviour were adopted for the soil: homogeneous, isotropic or anisotropic linear deformable halfspace, halfspace having the deformability modulus as variable with depth, and the Winkler's model.

Particularly, the case of framed structures with isolated or continuous foundations are discussed.

The paper is based on a series of previous results [1] [4] [7] [8] , without resuming the problems treated there.

2. The Equation of Motion of Structural Systems With Interaction.

The differential equations will be derived for a structural system with interaction which may be considered as composed of a finite number of component members.

The displacement components about reference axis of a point from the structural system are denoted by u , v and w . These displacements can be expressed for any point of the structural system, as functions of an arbitrary number of displacements selected so that to be capable to describe the deflected configuration of the structure. The points where those displacement are selected become the structure joints, while the corresponding displacements are called the nodal displacements. The following relation can be written with respect to displacements q and nodal displacements q_N

$$q = a q_N \quad (1)$$

in which a is a matrix depending on x , y and z variables. If all displacements, q , are known, the specific deformations may be determined in the form of a vector ε .

$$\varepsilon = b q_N \quad (2)$$

where b is a matrix obtained from matrix a by a differentiation procedure. In the most general case, the vector ε has the form $\varepsilon^T = \{ \varepsilon_x \ \varepsilon_y \ \varepsilon_z \ \gamma_{xy} \ \gamma_{yz} \ \gamma_{zx} \}$. By using the Hooke's law, the tensions are determined

$$\sigma = C \varepsilon = C b q_N \quad (3)$$

in which C is the elasticity matrix, and

$$\sigma^T = \{ \sigma_x \ \sigma_y \ \sigma_z \ \tau_{xy} \ \tau_{yz} \ \tau_{zx} \}$$

If the displacements q as functions of time t , are known, the acceleration components may be found

$$\ddot{q}^T = \{ \ddot{u} \ \ddot{v} \ \ddot{w} \} = \left\{ \frac{\partial^2 u}{\partial t^2} \ \frac{\partial^2 v}{\partial t^2} \ \frac{\partial^2 w}{\partial t^2} \right\} \quad (4)$$

In order to establish the equation of motion of the structural system, the virtual work concept applied to elastic systems and the d'Alembert's principle are used

$$\delta U = \delta L - \int_V \rho \delta q^T \ddot{q} dV \quad (5)$$

in which δU is the variation of internal deformation energy of the structural system, δL is the virtual work of the applied and of the constraint forces, while $\int_V \rho \delta q^T \ddot{q} dV$ in the variation of virtual work done by inertial forces.

The variation of internal deformation energy may be written in the form

$$\delta U = \int_V \delta \varepsilon^T \sigma dV \quad (6)$$

which, by considering the equation (2) and (3), becomes

$$\delta U = \int_V \delta q_N^T b^T C b q_N dV \quad (7)$$

The virtual work of applied as well as of the constraint forces is composed of the following terms: the variation of the virtual work due to surface concentrated and distributed

forces, the variation of forces from connections without total constraints (which can also be concentrated and distributed) and the variation of the virtual work of volumetric forces. These terms are as follows:

$$\delta L = \delta q_N^T P + \int_S \delta q^T p dS + \delta q_{N_1}^T Y + \int_{\Omega} \delta q^T y d\Omega + \int_V \delta q^T Q dV \quad (8)$$

The concentrated forces were supposed to be applied at joints, while for the concentrated forces from connections only the interaction joints N, common both to structural system and to supporting base were considered. If the division of the structure in finite elements is practiced, the distributed applied and constraint forces along the body boundaries as well as the volumetric forces can be replaced by equivalent nodal forces, so that all applied forces set up a vector P^* while the constraint forces form a vector Y. In this case the virtual work of external forces takes a simple form

$$\delta L = \delta q_N^T P^* + \delta q_{N_1}^T Y \quad (9)$$

and the equation (5) may be written as

$$\int_V \delta q_N^T b^T C b q_N dV = \delta q_N^T P^* + \delta q_{N_1}^T Y - \int_V \rho \delta q_N^T a^T a \ddot{q}_N dV \quad (10)$$

Supposing that all nodal displacement influencing directly the interaction are grouped, the term $\delta q_{N_1}^T Y$ may be written as a function of $\delta q_N^T = \left\{ \delta q_{N_1} \quad \delta q_{N_2} \right\}$, as follows

$$\left\{ \delta q_{N_1} \quad \delta q_{N_2} \right\} \begin{Bmatrix} Y \\ 0 \end{Bmatrix} = \delta q_N^T Y^* \quad (11)$$

As δq_N is an arbitrary quantity, it may be left out and the equation (10) becomes

$$\left(\int_V b^T C b dV \right) q_N = P^* + Y^* - \left(\int_V \rho a^T a dV \right) \ddot{q}_N \quad (12)$$

In the above equation, the term

$$\int_V b^T C b dV = K \quad (13)$$

is the stiffness matrix of the structural system, or pointing out once more, of the system composed of structure and sub-structure, while the term

$$\int_V \rho a^T a dV = M \tag{14}$$

is mass matrix of the equivalent discrete system.

With those specifications the Equation (12) takes the form

$$Kq_N + M\ddot{q}_N = P^* + Y^* \tag{15}$$

In the case of free vibrations $P^* = 0$ so that the Equation (15) becomes

$$Kq_N + M\ddot{q}_N = Y^* \tag{16}$$

3 The Interaction Forces.

The contact between structural system and supporting base is permanently maintained; the displacements of the contact surface of the structural system and of the supporting medium are equal. Connection forces appears on the contact surface, under the form of the contact pressures, which are equivalently replaced by nodal force on the structural system. The pressures on a finite element of soil surface are assumed to be distributed according to certain simple laws. The smaller those finite elements are, the less the pressure distribution law influences the final results. The resultant of pressures on these subdomains (finite elements) must be equal but of a contrar sense to the reactive nodal forces applied to the structural system.

The structure horizontal displacements are supposed to be locked through friction effect and by the embedding into the soil.

Since some linear relationship were assumed to exist between vertical displacements on the soil surface and the applied forces, their general form will be

$$\begin{aligned} W_1 &= \beta_{11}\bar{Y}_1 + \beta_{12}\bar{Y}_2 + \dots + \beta_{1N_1}\bar{Y}_{N_1} \\ W_2 &= \beta_{21}\bar{Y}_1 + \beta_{22}\bar{Y}_2 + \dots + \beta_{2N_1}\bar{Y}_{N_1} \\ &\dots \end{aligned} \tag{17}$$

$$w_{N_1} = \beta_{N_1} \bar{Y} + \dots + \beta_{N_1 N_1} Y_{N_1}$$

or, under a condensed form

$$W = \beta \bar{Y} \quad (18)$$

in which w is the vertical displacement vector at the interaction nodal points, q_{N_1} and β is the soil flexibility matrix, its elements depending on the mechanical model adopted for the soil and, in to a certain extent on the laws adopted with respect to the pressure distribution on a surface finite element.

By the inversion of β matrix, the \bar{Y} vector is obtained from (18)

$$\bar{Y} = \beta^{-1} W = K_T W = K_T q_{N_1} \quad (19)$$

K_T being the stiffness matrix of the soil on the contact surface. By changing its sign, \bar{Y} becomes the interaction nodal force vector Y of the structural system

$$Y^* = \begin{Bmatrix} Y \\ 0 \end{Bmatrix} = - \begin{bmatrix} K_T & 0 \\ 0 & 0 \end{bmatrix} \begin{Bmatrix} q_{N_1} \\ q_{N_2} \end{Bmatrix} \quad (20)$$

or

$$Y^* = -K_T^* q_N \quad (21)$$

Returning to Equation (15), with Y^* given by (21) it can be written

$$K q_N + M \ddot{q}_N = P^* - K_T^* q_N \quad (22)$$

or

$$K_S q_N + M \ddot{q}_N = P^* \quad (23)$$

Particularly, in case of the free vibrations, the vector $P^* = 0$ and Eq. (23) becomes

$$K_S q_N + M \ddot{q}_N = 0 \quad (24)$$

in which K_S is called the stiffness matrix of the structural system and takes the form

$$K_S = \begin{bmatrix} K_{11} + K_T & K_{12} \\ K_{21} & K_{22} \end{bmatrix} \quad (25)$$

Therefore, the stiffness matrix of the system characterizes the behaviour of the structure, substructure and the soil.

In case when the dynamic analysis is used for the seismic design and besides the horizontal component of the earthquake is considered as predominant, the structural lateral matrix is then used, which can be obtained as follows

$$\begin{bmatrix} K_{S11} & K_{S12} \\ K_{S21} & K_{S22} \end{bmatrix} \begin{Bmatrix} q_H \\ q_o \end{Bmatrix} = \begin{Bmatrix} R_H \\ 0 \end{Bmatrix} \quad (26)$$

in which q_H represents the displacements about the directions of the adopted dynamic degree of freedom, R_H are the corresponding inertial forces, and q are the other displacements. By solving the matrix system (26) and eliminating q the lateral stiffness matrix of the system composed of the structure, substructure and the soil, K_{SL} , is obtained as

$$K_{SL} = K_{S11} - K_{S21}^T K_{S22}^{-1} K_{S21} \quad (27)$$

4. The Soil Flexibility Matrix.

As it was already showed the soil stiffness matrix K_T , on the contact zone is obtained by inversion of the soil flexibility matrix β . This matrix depends on the mechanical model adopted for the soil, i.e.

1^o. The soil is considered as a homogeneous isotropic linear deformable halfspace. Supposing that contact pressures are constant on a subdomain Ω_j , the elements of β matrix are calculated with relation

$$\beta_{ij} = \frac{1-\nu_o^2}{\pi E_o} \frac{1}{\Omega_j} \iint_{\Omega_j} \frac{d\Omega}{\sqrt{(x_{ij} + \xi)^2 + (y_{ij} + \eta)^2}} \quad (28)$$

in which E_o and ν_o are the deformation modulus and Poisson's coefficient respectively, the other quantities being showed in Fig.1. For the case of a rectangular element Ω_j , a computer program was elaborated for calculation of β matrix

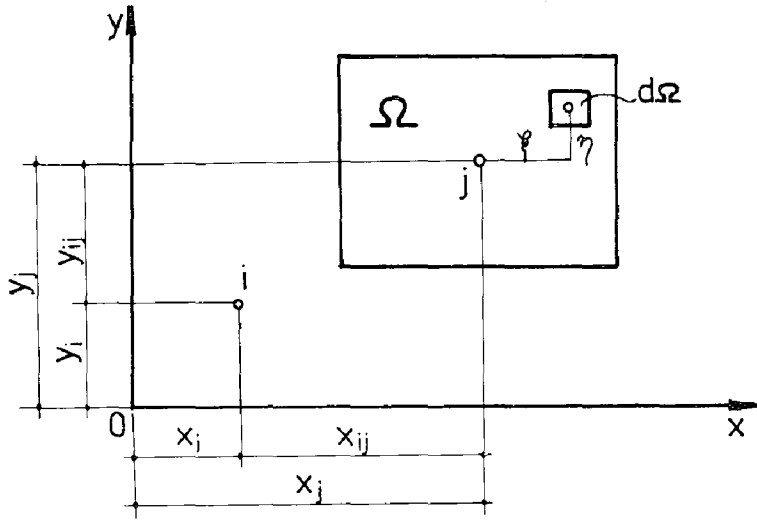


Fig.1. Co-ordinate system for β - matrix elements.

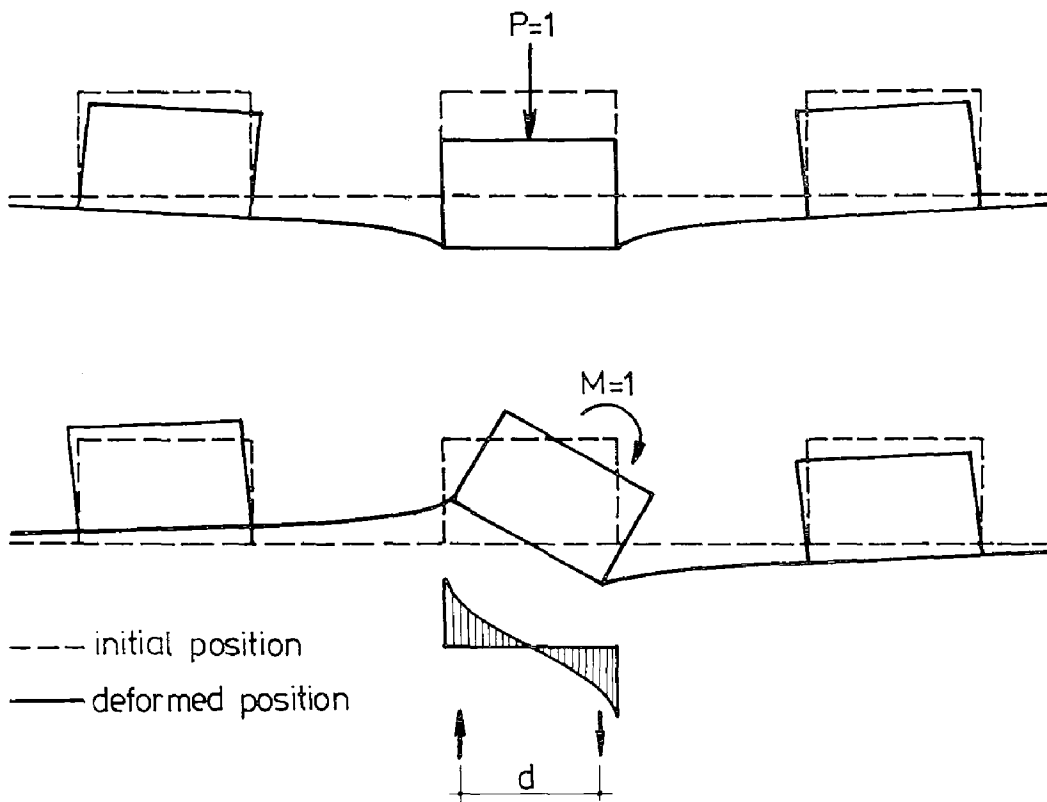


Fig.2. Interaction of isolated foundations.

elements.

2°. The soil is considered as a transversal anisotropic, homogeneous and linear deformable halfspace in the sense given by Michell. In case of the transversal anisotropy, according to the Michell's solution, the displacements on the halfspace limit surface due to a normal load P may be determined with

$$W = \frac{J}{E} \cdot \frac{P}{r} \quad (29)$$

where r is the distance between the point of application of P and the point corresponding to displacement w; J is a nondimensional factor characterizing the anisotropy of the term

$$J = \sqrt{\frac{\frac{nE}{G\Phi}(1-n\nu_2^2)}{\frac{nE^2}{\Phi^2}[(1-\nu_1^2)(1-n\nu_2^2)^2+G]^2 - \left[\frac{E}{\Phi}(1+\nu_1)+G\right]^2}} \quad (30)$$

in which E is the deformation modulus on a vertical direction, G is the shear modulus, $n = \frac{E_H}{E} = \frac{\nu_2}{\nu_3}$ denotes the anisotropy degree, E_H is the soil deformation modulus in transversal direction, ν_1, ν_2, ν_3 are the Poisson's coefficients, namely, ν_1 - for horizontal contraction due to the tensions in horizontal planes ν_2 - vertical contraction due to the tensions in horizontal plane, ν_3 - horizontal contraction due to the tensions in vertical planes; $\Phi = (1+\nu_1)(1-\nu_1-2n\nu_2)$

In the case of transversal anisotropic halfspace, the displacements on the limit surface can be obtained in the same manner as in the case of a homogeneous isotropic halfspace, by replacing the factor $\frac{1-\nu_0}{11E_0}$ by $\frac{J}{E}$.

3°. The soil is considered as a halfspace having its modulus of deformability as variable with the depth. The following law is used for the variation of $E = E_0 \pm E_1 z^m$ in which E_0 is the soil deformation modulus on the limit surface, E_1 is the soil deformation modulus at a depth of 1 m; the index m takes into consideration the manner of

nonhomogeneity propagation along the depth. Particularly, the values used in practice are $m = 1$, $m = \frac{1}{2}$ and $m = 2$, depending on the soil characteristics.

The soil surface displacements produced by a normal concentrated loads may be calculated with

$$W = \frac{P}{\pi \cdot r E_0^* (1 + E_1^* r^m)} \quad (31)$$

in which

$$E_0^* = \frac{E_0}{1 - \gamma_0^2} ; E_1^* = \frac{2E_1}{E_0} \frac{(1 + \gamma_0)(1 + m)}{3 + m} \quad (32)$$

By considering constant pressures on a surface finite element Ω_j , the coefficients β_{ij} may be calculated as follows:

$$\beta_{ij} = \frac{1}{\pi E_0^*} \frac{1}{\Omega_j} \iint_{\Omega_j} \frac{d\Omega}{\sqrt{(x_{ij} + \xi)^2 + (y_{ij} + \eta)^2 + E_1^* \sqrt{[(x_{ij} + \xi)^2 + (y_{ij} + \eta)^2]^{m+1}}} \quad (33)$$

4°. The soil is considered of the form of a field of springs (Winkler model). In contrast with the previous cases in which β was a full matrix, in this case it becomes a diagonal matrix. The elements of β matrix may be calculated with relation $\beta_{jj} = \Omega_j / k_j$

k_j being the stiffness coefficient (settlement coefficient) of the soil, k_j is supposed as constant on Ω_j surface. Sometimes the coefficient k_j is considered as constant on the whole contact surface.

5. Solutions for Framed Structures.

A detailed analysis was carried out for framed structures having as foundation a) continuous beam foundation or b)

isolated blocks under columns. The soil was assumed as a homogeneous, isotropic or anisotropic linear deformable half-space. Computer programs were elaborated for seismic analysis of these structural systems on the basis of considerations presented in this paper.

In the case of foundations of continuous beam form, the soil flexibility matrix β , is generated on the basis of the relation (28) depending on the nodal points of the structural system.

As for the framed structures with isolated foundation, the solution of halfspace deformations under a rigid block, subjected to a concentrated force or to a couple were used for determining the matrix β .

In Fig. 2 the foundation block deformations produced by a unity centric force or by an unity couple respectively, as well as the deformed soil shape and the influences on the surrounding foundations are shown. The following relations are used for the calculation of the displacements $\beta_{jj}(P=1)$, $\beta_{kk}(M=1)$ [6]:

$$\beta_{jj}(P=1) = \frac{1-\nu_0^2}{E_0} \frac{C_0}{\sqrt{A}} \quad ; \quad \beta_{kk}(M=1) = \frac{8k_1(1-\nu_0^2)}{E_0 L^3}$$

in which A is the contact surface between the foundation and the soil, L is the contact surface dimension respective to bending plane, C_0 and k_1 are coefficients depending on $\frac{L}{B}$ ration (B being the other dimension of the contact surface, assumed of a rectangular form); C_0 and k_1 may be found in the mentioned paper.

The computation of the lateral coefficients is performed by means of the relation that gives the limit surface displacements of the halfspace under the action of a normal load,

$$w = \frac{1-\nu_0^2}{\pi E_0} \frac{P}{r}$$

particularized for $P = 1$ in the case of centric loads and $P = \pm \frac{1}{d}$ in the case of couples, d being the couple arm of

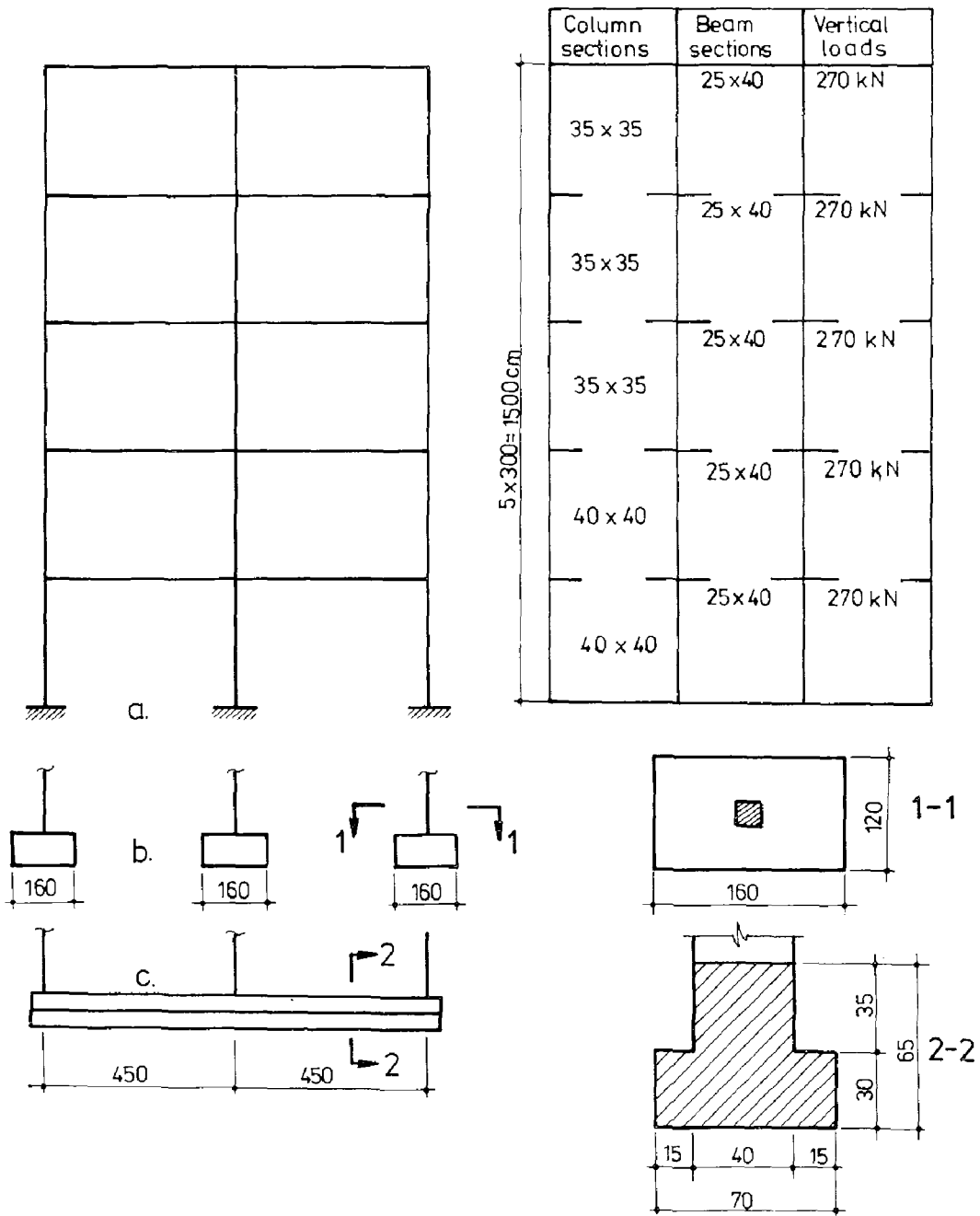


Fig.3. Geometric characteristics of the structural system.

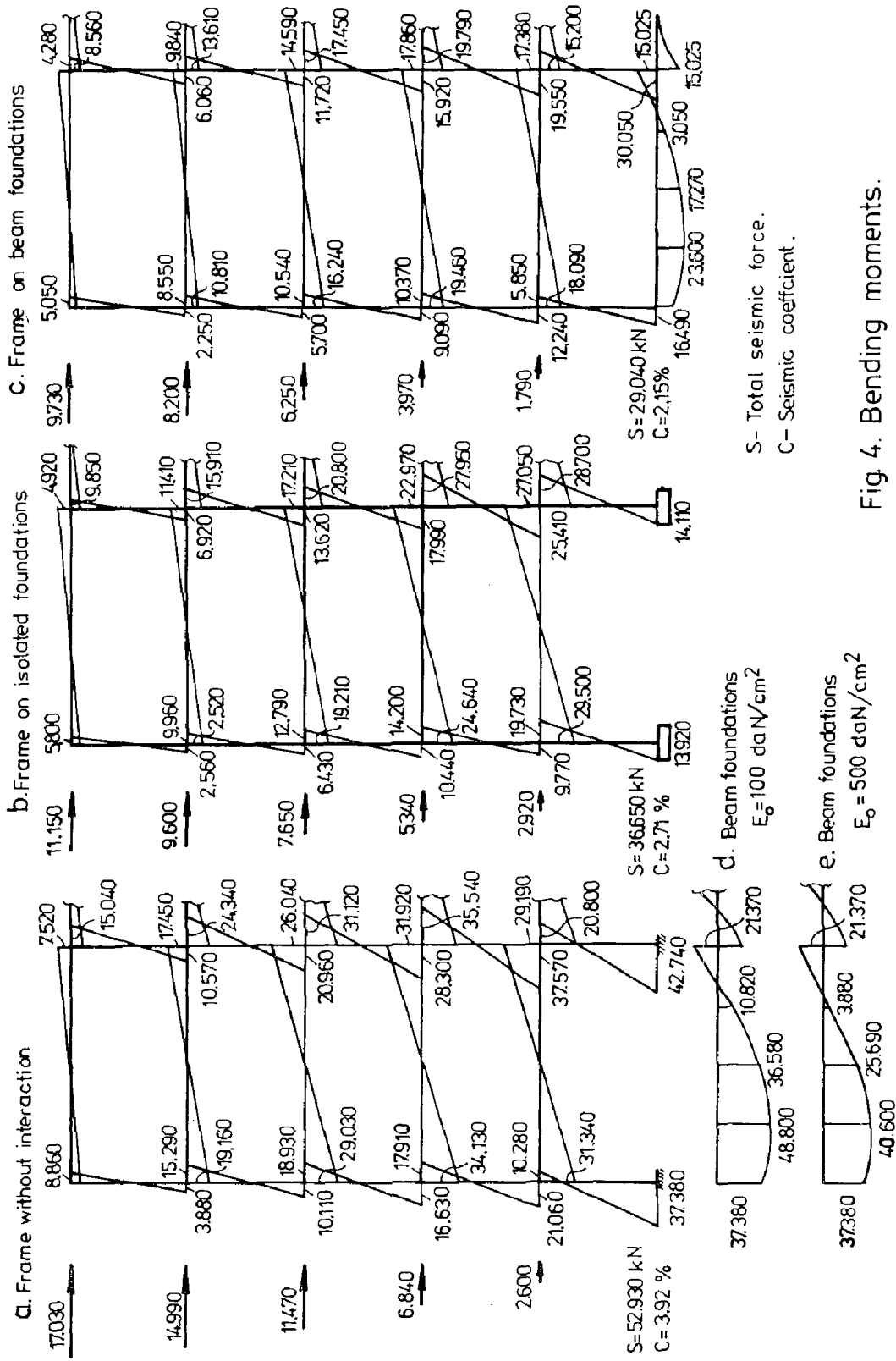


Fig 4. Bending moments.

the contact surface pressures due to the action of $M = 1$, Fig. 2.

6. Numerical Examples.

The dynamic and seismic analysis of a two bay, five story frame, considering two foundation solution: a) isolated foundations, b) continuous beams foundations. Two types of soil were assumed, differentiated by their deformation modulus E_0 for which the values of 100 da N/cm^2 and 500 da N/cm^2 respectively, were adopted. The Poisson's coefficient of the soil was assumed $\nu_0 = 0,35$.

The geometrical dimensions of the structure and the foundation as well as the gravity loads are shown in Fig.3. The reinforced concrete modulus of elasticity, for the structural system was chosen $E_b = 285.000$ da N/cm^2 .

In Fig. 4 and 5 the dynamic characteristics for the first three vibration modes (Fig.5 a) are presented together with the bending moment diagram, under the action of the seismic conventional forces, corresponding to the 1st mode of vibration, are presented as follows:

- frame without interaction (Fig. 4 a)
- foundation beams considered independent and loaded with connection loads transmitted by frames (from the analysis without interaction), (Fig.4 d and e),
- frame on isolated foundation with interaction (Fig. 4 b and 5 b),
- frame on foundation beam with interaction (Fig. 4 c and 5 c).

Conclusions.

With the assumption adopted a formulation for the dynamic and seismic analysis of structures was presented by taking into consideration the interaction with the sub-

structure and the foundation soil.

By using a finite element technique, the supplementary factors involved due to interaction, their way of evaluation, the corrections introduced in a structural analysis and especially the manner in which the soil takes part at this process, were emphasized.

Particularly some procedures for obtaining real solutions are indicated.

A computer program analysis was carried out for several examples, emphasizing the interaction effects on the dynamic behaviour of the structural systems considered and on the stress state in these systems.

From this analysis the following conclusions were drawn up:

The general shape of the three modes of vibrations is the same in the both case considered, with and without interaction.

As it was expected, an increase was found in the natural periods of vibration; more significant increases were observed to fundamental mode of vibration for the structural system having beam foundations, i.e. 80% for the soil with $E_0 = 100 \text{ da N/cm}^2$ and 43% for the soil with $E_0 = 500 \text{ da N/cm}^2$. In the case of isolated foundations, the increases of first mode period for the structural system are 55% greater for the soil with $E_0 = 100 \text{ da N/cm}^2$ and 17% for the soil with $E_0 = 500 \text{ da N/cm}^2$.

Some increases of the periods of vibration are found also to higher modes.

Therefore, both the foundation system and the soil type will influence the dynamic characteristics of the structure.

Because of the changes in the dynamic characteristics of the structural system, in the case of interaction, smaller seismic coefficients were obtained and implicitly decreased

conventional seismic loads have resulted.

Because of the decreasing in the seismic loads and as a result of the static interaction effect, the stress state of the studied structural systems undergoes some changes in comparison with the situation in which the interaction is neglected.

The most stressed sections are not always at the structure base, where the bending moments decrease with 18-300%. By comparing the most stressed members in the structure, it may be found differences ranging from 19% to 45%.

This effect is differentiated in function of the soil type, for base sections and the soil with $E_0 = 100 \text{ da N/cm}^2$ being more important for the structure with isolated foundation, while in the case of $E_0 = 500 \text{ da N/cm}^2$, the structure with foundation beams proved more sensitive.

All interaction effects are diminished at higher levels.

The decrease of the structure base section stresses leads to modification of the stress state in the foundation beams and the soil.

The effects of the interaction depend on structure, foundation system, type of the soil, so that the results obtained on the presented examples can not be extended to any practical situation. By including the interaction it is however possible to influence the way of elaborating some types of structures.

References

1. Ciongradi, I., Ungureanu, N., Ciongradi, Camelia, The Effect of Interaction between Structure, Foundation and Soil, upon the Standard Earthquake Response of Reinforced Concrete Buildings, Proc. 7th Conf. Reinforced Concrete Tall Buildings, Jassy, Oct., 1975, I, 73-83, (in Rumanian).
2. Lee, I.K., Valliappan, S., Analysis of Soil Settlement, Soil Mechanics-New Horizons, London, Newnes - Butterworths, 1974, 158-204.
3. Roesset, M.J., Whitman, V.R., Dolery, R., Modal Analysis for Structures with Foundation Interaction, Jour. Struct. Div., ASCE, 99, ST 3, 1973.
4. Sillion, T., Ungureanu, N., Ciongradi, I., Planar Frames on the Isolated Foundation in Cooperation with Foundation Soil, Proc. 3rd Conf. on Soil Mech. and Fndn. Eng., Timișoara, Romania, Sept., 1975, 258-267, (in Rumanian).
5. Singhal, A.C., Inelastic Earthquake of Multistorey Buildings, Jour. Inst. Struct. Eng., 49, Sept., 1971.
6. Tsyтович, N., Berezantsev, V., D., Dalmatov, B., Abelev, M., Foundation Soils and Substructures, MIR Publishers, Moscow, 1974.
7. Ungureanu, N., Ciongradi, I., Analysis of Plane Frames in the Cooperation with Bed Plates Foundations and Support Ground, Bul. Polyt. Inst. of Jassy, XX (XXIV), 1-2, V, 1974, 7-13, (in Rumanian).
8. Ungureanu, N., Ciongradi, I., Missir, I., The Soil-Structure Interaction for Spatial Multistorey Concrete Framed Structures, Proc. 7th Conf. Reinforced Concrete Tall Buildings, Jassy, Oct., 1975, I, 353-362, (in Rumanian).

INTERNATIONAL SYMPOSIUM ON
EARTHQUAKE STRUCTURAL ENGINEERING

253

St. Louis, Missouri, USA, August, 1976

PROTECTION OF COMMUNICATIONS FACILITIES IN EARTHQUAKE AREAS

N. J. DECAPUA

S. C. LIU

Bell Laboratories
Whippany, N. J., U.S.A.

National Science Foundation
Washington, D. C., U.S.A.

ABSTRACT

The continued reliable operation of telephone equipment in earthquake-prone areas depends on the equipment's ability to survive earthquakes of a realistic magnitude. This paper presents a procedure for developing regional earthquake protection practices in a cost-effective manner.

Maintaining system reliability requires extensive knowledge of the earthquake environment of a particular area and the response-damage-failure mechanism of the equipment and its supporting frame during earthquakes. The earthquake environment is determined by a regional microzonation analysis, which is translated into isoseismic acceleration maps of the area being studied. The seismic response of the communications equipment is determined by a comprehensive analysis of the coupled foundation-building system and dynamic testing of the equipment assembly, employing a regional test environment.

The procedure is applied to electronic, electromechanical, and reserved-power equipment for both a single system and multiple systems within an earthquake area.

INTRODUCTION

Telephone communications facilities are so vital to public health and safety that special efforts must be made to prevent disruption of these services by a major earthquake. At present, building codes have only rudimentary provisions regulating the planning and design of communications lifelines. The primary reason for this is a lack of understanding of the dynamic behavior of different communications systems under seismic loadings. Recently, the earthquake behavior of several types of communications facilities has been investigated to determine the dynamic characteristics and earthquake vulnerability of a variety of equipment supported in single-story and multistory telephone buildings.

In addition, microzonation studies, which delineate the risk potential of telephone systems in various seismic regions, and cost/loss analyses, which characterize the earthquake safety and economic consequences of these

Preceding page blank

systems, also have been performed. Based on the results of these studies, a procedure has been established for developing earthquake protection practices in communications facilities. The pertinent elements of this procedure, such as the characterization of earthquake environment, tests of equipment and framework assemblies, cost/loss considerations, and the interfacing of these elements will be described in this paper.

BASIC EARTHQUAKE PROTECTION PROCEDURE

The decision to protect a new or existing facility in a seismic environment can be made on the basis of maintaining system reliability against earthquake failure independent of the protection cost, or consideration of a proper balance between the earthquake loss and protection cost among various feasible protection schemes. (We refer to the former procedure as a reliability-based procedure and the latter one as a cost-based procedure.) These two approaches, along with the required data and information, are shown in Figure 1. The reliability-based decision requires information on the earthquake environment and knowledge of the system's response-damage-failure behavior during earthquakes. The earthquake environment information is provided by a microzonation analysis^{1*} and the resulting isoseismic intensity (or acceleration) maps of the area of interest. Such maps define the seismic risk within an area in terms of the intensity or acceleration level. The earthquake behavior of the equipment assembly is predicted by a comprehensive dynamic testing program² that identifies the failure modes and damage states associated with various ground excitation levels.

The cost-based decision (see Figure 1) combines system reliability and cost information to develop cost-effective earthquake protection. If the protection cost of the system is extremely small compared with other cost items, a cost-based decision usually becomes a reliability-based decision because the protection cost is no longer a controlling factor for decision making.

EARTHQUAKE ENVIRONMENT

The actual earthquake motion environment that a specific communications facility must survive is a function of the facility's geographic location and its location within a building. The expected peak ground acceleration is determined by microzonation studies that depict the regional earthquake environment as a function of geographic location. Peak in-building values are examined for two cases, i.e., ground/first floor locations and upper floor locations. An amplification factor that relates ground values to in-building values is employed. The appropriate test environment at the equipment support is achieved by linearly scaling a typical waveform for upper-bound in-building motion down to the expected acceleration level.

Microzonation Analysis

Microzonation maps show expected peak accelerations as a function of geographic location. In general, a microzonation study yields a

* References are listed as the last paragraph of this paper.

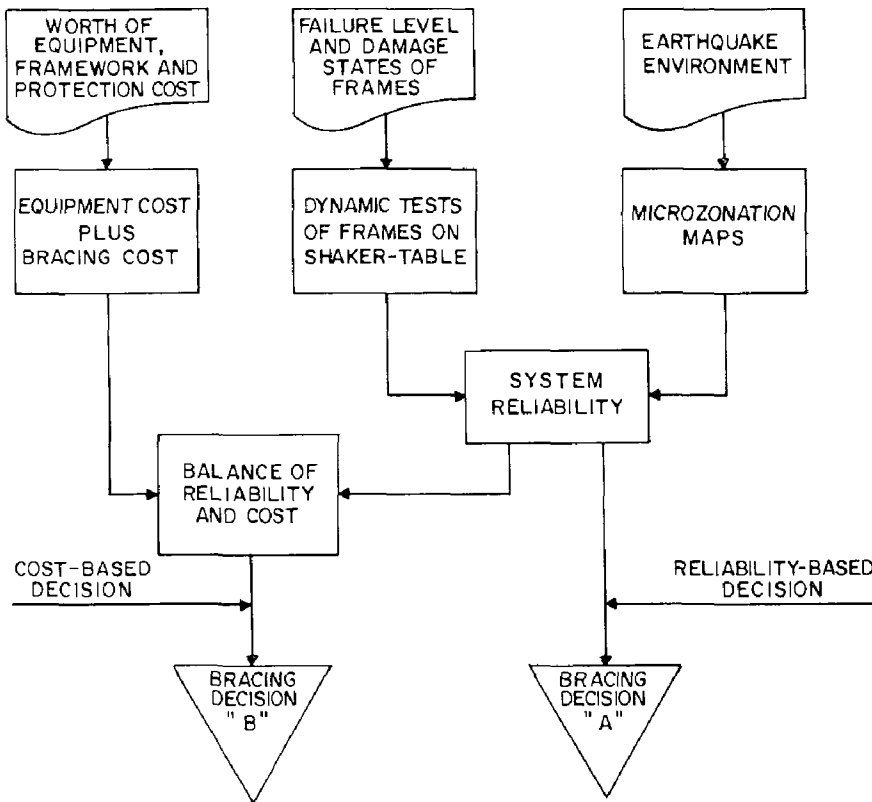


Figure 1. Decision Process for Earthquake Protection

probabilistic characterization of the earthquake environment in a particular region. It combines historical data, seismological and geological information, and a sound statistical model to determine the expected environment at a given facility. This information may be represented by a contour map with a 90-percent probability that the contour acceleration levels indicated will not be exceeded during the service life of a given communications facility.

As an example, the acceleration contours resulting from a microzonation analysis of the Rocky Mountain states¹ are shown in Figure 2. This contour map indicates the expected peak ground acceleration for every location in the study area with a 90-percent probability that these levels will not be exceeded during the 50-year service life of the equipment. The 10-percent exceedance probability is a generally accepted level in the earthquake engineering profession and is considered adequate for communications facilities. For extremely critical installations, such as nuclear power plants, a much lower exceedance probability — from 2 to 5 percent — most likely would be employed. This, of course, results in higher acceleration values.

Upper-Bound Response Spectra

Equipment located on upper floors of multistory buildings generally is subjected to stronger shaking than equipment on ground floors, since earthquake motion is amplified as it travels through the coupled

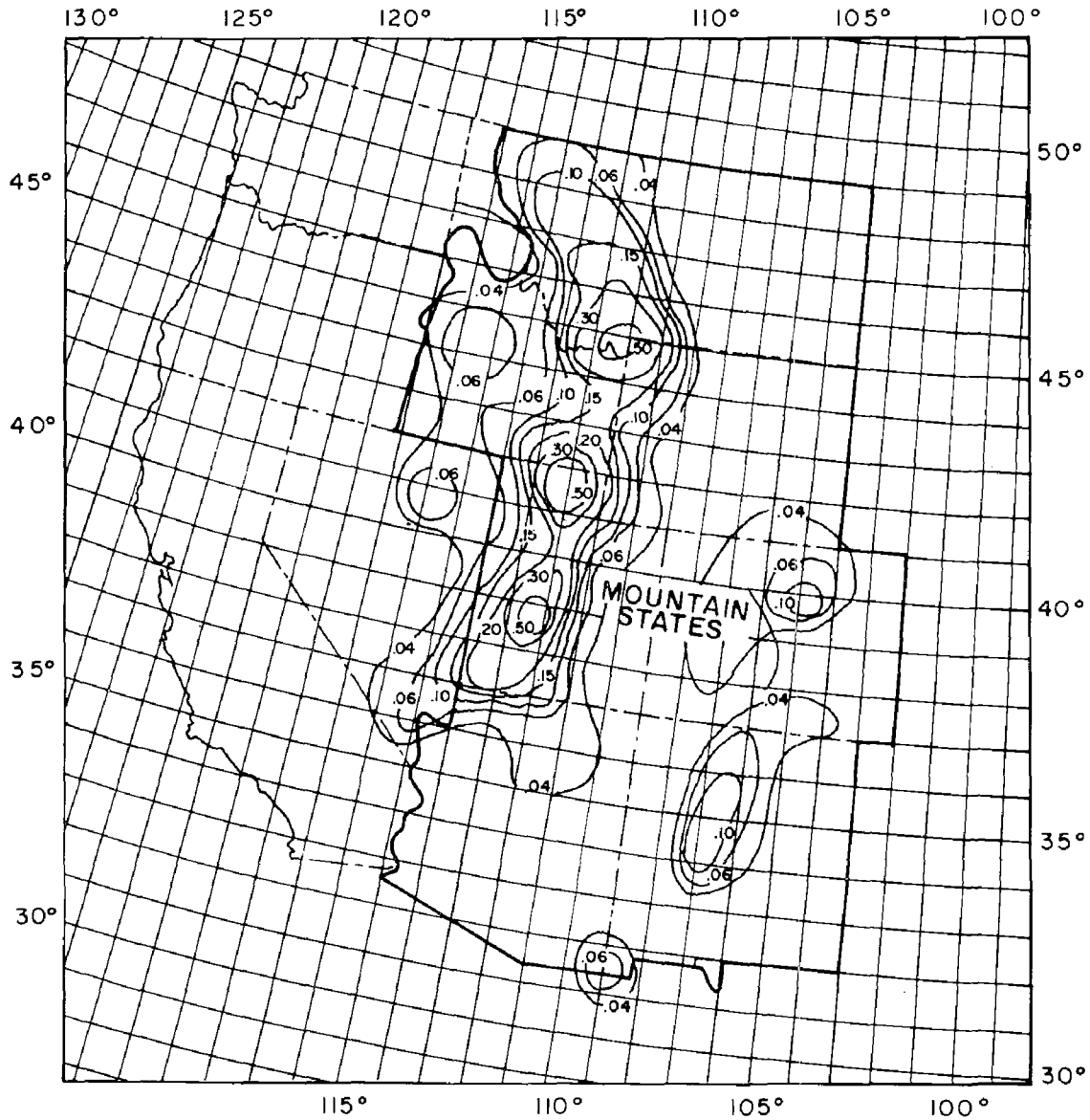


Figure 2. Peak Earthquake Ground Acceleration "g" Contours with a 90-Percent Probability of Not Being Exceeded in 50 Years

ground-building-equipment system. In an analytical study of earthquake-induced in-building motion,³ the motion time histories for the upper floors of representative multistory telephone buildings with different building characteristics and soil conditions were calculated for earthquakes with Modified Mercalli Intensities of V to X. The results were expressed in terms of motion histories. The envelope response spectra for different damping ratios are shown in Figure 3. These spectra indicate the floor response characteristics of telephone buildings in earthquake environments. The average peak floor acceleration level corresponding to such spectra is approximately 0.8 to 1.0 g, and the predominant frequency band is

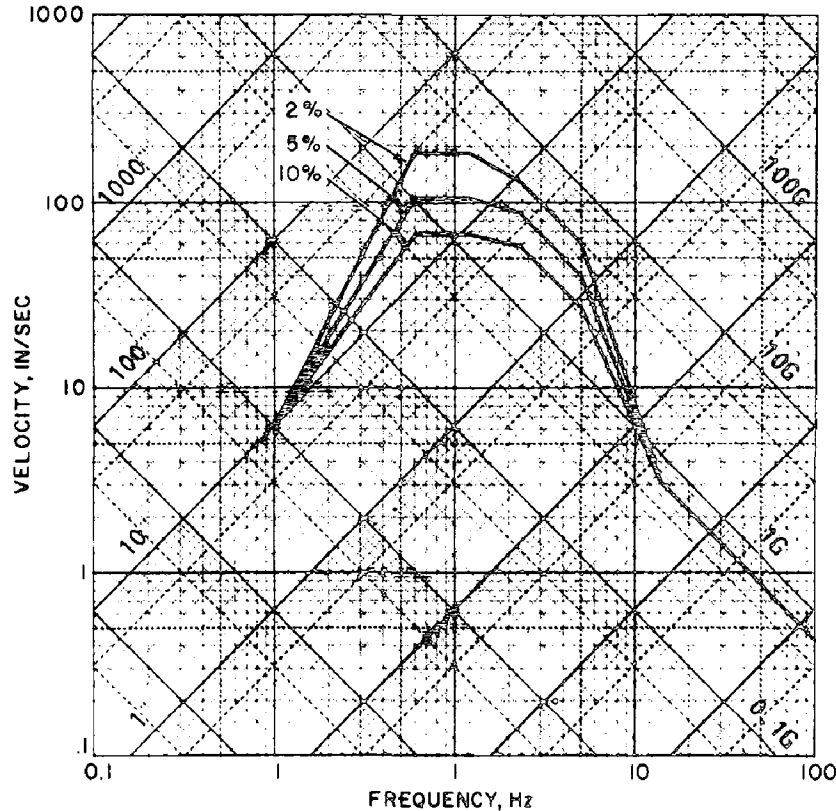


Figure 3. Envelope of In-Building Damped Response Spectra

approximately 2 to 6 Hz. This frequency range includes the fundamental frequencies of most communications equipment and framework assemblies.

Upper-Bound Time History

Ideally, a simulated earthquake motion used for equipment testing should resemble an actual earthquake motion as closely as possible in response spectra, peak accelerations, peak velocities, peak displacements, durations, and appearance of waveforms. A number of different test methods can be used to simulate an earthquake environment, including sine beat, decaying sine, sine sweep, and random waveforms. The random waveform method was chosen since it satisfies more of the above requirements than any other method.

The appropriate acceleration time history is generated on a digital computer using the techniques established earlier.⁴ Basically, the technique starts with a filtered Gaussian white noise; then an envelope function is used to shape the initial, middle, and final phases of the simulated motion into a typical earthquake accelogram. The predominant frequency content is adjusted through parameters related to the ground motion transfer function. An upper-bound earthquake environment is generated by matching, as closely as possible, the 2-percent spectrum of the synthesized earthquake to the in-building spectra shown in Figure 3.

The resulting acceleration history of this synthesized earthquake, shown in Figure 4, qualifies as the upper-bound criterion since it approximately matches the upper-bound in-building response spectrum and has a peak acceleration close to 1 g. This peak acceleration value is consistent with the maximum in-building accelerations determined in Reference 3.

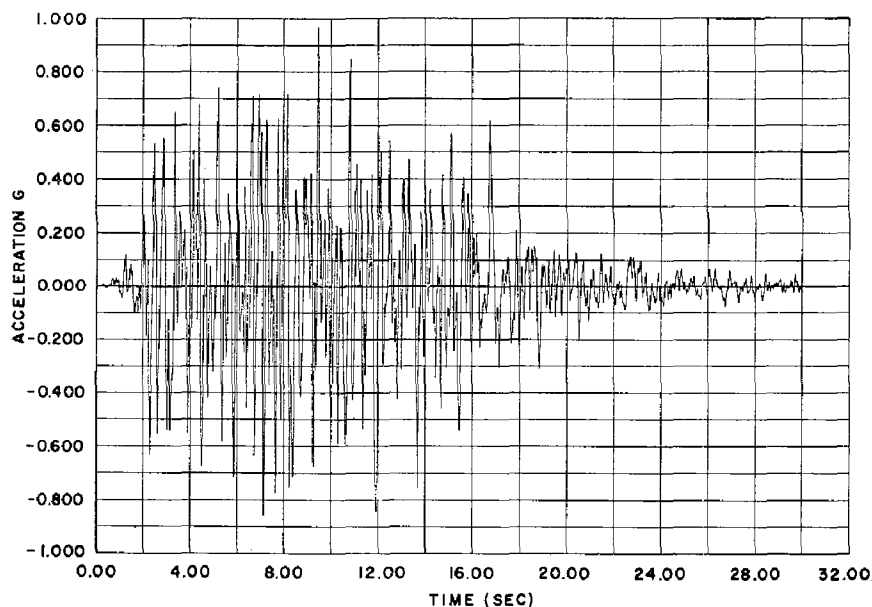


Figure 4. Analytically Developed Artificial Earthquake Accelerogram

In Figure 5 the in-building upper-bound spectrum (Figure 3) is compared to the spectrum of the, analytically generated time history. As indicated, the spectra match reasonably well within the frequency range of interest, i.e., approximately 2.3 to 6 Hz, which bounds the fundamental frequencies of most communications equipment-framework systems. At frequencies below 2 Hz, the time history spectrum is lower, and for frequencies above 6 Hz, somewhat higher than specified.

Building Amplification of Free-Field Motions

The large collection of ground-motion data recorded during the San Fernando earthquake was analyzed,³ and the results showed that the ratio of upper floor acceleration to ground/first floor acceleration (amplification factor) varied with the amplitude of the ground motion. Figure 6 shows the amplification factor for the mean plus-one standard deviation acceleration for moderate to large intensities and for conditions common to most telephone buildings. This amplification (one standard deviation above the mean) is judged sufficiently, yet not overly conservative for determining how to protect the equipment. As indicated in Figure 6, the amplification factor varies from 3.0 at 0.1 g ground acceleration down to 1.0 at 0.5 g. For ground accelerations higher than 0.5 g, the amplification factor remains unity — i.e., there is no amplification.

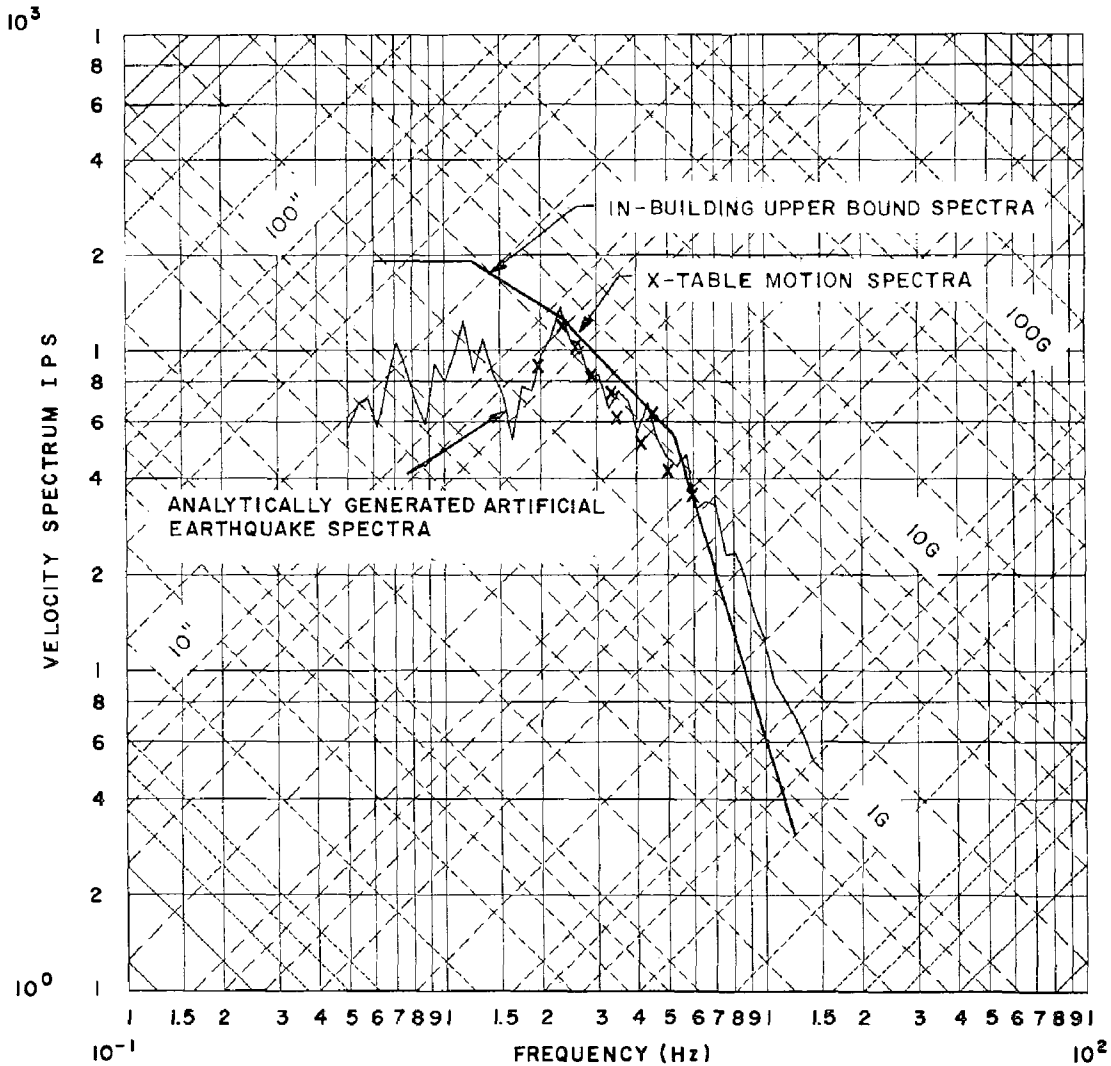


Figure 5. Comparison of 2-Percent Damped Shock Spectra

Earthquake Environment for a Specific Location

An earthquake environment used for testing can now be generated for a specific location. As an example, consider a communications facility located geographically on the microzonation map (Figure 2) such that the peak ground acceleration is 0.2 g. If the equipment is to be installed on the upper floors of the building, then the amplification factor in Figure 6 is approximately 2.0, so that the peak upper floor acceleration is 0.4 g.

The earthquake environment for this specific facility can be determined by linearly scaling the accelogram of Figure 4, which has a peak acceleration of approximately 1 g, down to a peak acceleration of 0.4 g. If the equipment were on the ground/first floor, there would be no building amplification and the test environment would have been scaled to 0.2 g instead of to 0.4 g.

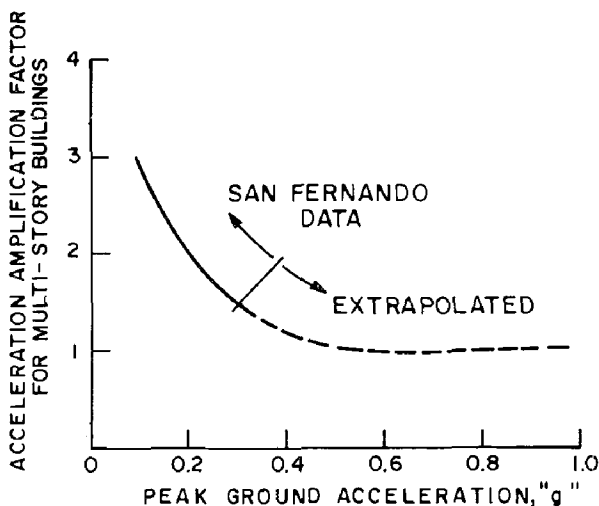


Figure 6. Building Amplification vs. Earthquake Ground Acceleration

TESTS OF VARIOUS TYPES OF EQUIPMENT

The regional earthquake environment discussed in the preceding sections has been used to test a variety of communications equipment. The tests are performed to determine the earthquake vulnerability — i.e., the failure modes, lateral strength and damage profile — of the equipment assembly. The equipment tested includes 7-ft floor-supported electronic equipment, 11-1/2 ft ceiling-braced electromechanical equipment, and the battery plant of the reserved power system. The basic concern is with the integrity of the equipment framework assemblies and their supports, such as holddown bolts and braces. If these supports fail, the entire communications system is vulnerable to a catastrophic collapse.

The basic test procedure for each category of equipment can be summarized as follows:

- Program a shaker table motion using the upper-bound synthesized earthquake waveform shown in Figure 4.
- Test the equipment framework by using linearly scaled table inputs of progressively increasing peak amplitude from 0.1 to 1.0 g.
- During each test, observe and record the frame responses. In particular, determine the peak table acceleration levels a_i , corresponding to initial damage, and a_f , corresponding to total failure. These characterize the damage profile of the equipment-framework assembly.

Electronic Equipment

The No. 1, 2, 3, and 4 Electronic Switching Systems (ESS) make up the latest vintage of telephone switching facilities. These systems are replacing the electromechanical equipment, which presently comprises the bulk of the existing telephone plant.



Figure 7. Typical 7-ft Electronic Equipment

Figure 7 shows a typical electronic switching office. The equipment frameworks are 7 ft tall and generally are self-supported — i.e., anchored to the floor. As a result of this support system the configuration is basically an inverted pendulum with a fundamental frequency that varies between 2 and 6 Hz, depending on the specific type of equipment.

The electronic equipment tests are performed for three different frameworks and three different weight categories, for a total of nine cases. Two failure levels are determined: the initial failure level, which is defined as the input acceleration level that causes a permanent frame distortion (as measured by strain gauges) or loosening of the anchor bolts in the floor; and the total failure level, which corresponds to frame buckling or pulling out of the anchor bolts.

The test results are used to construct the damage profile in terms of base equipment acceleration, as shown in Figure 8. In general, lightweight electronic equipment located on ground floors is less vulnerable than heavy equipment located on upper floors. The damage profile for each of the nine cases considered and the ground acceleration contours of Figure 2 are used to determine the regional floor anchor bolt requirements for equipment on ground/first floors and on upper floors of telephone buildings. In some cases, i.e., heavy equipment in high-risk areas (see Figure 2), it is necessary to include overhead bracing to ensure protection of the equipment.

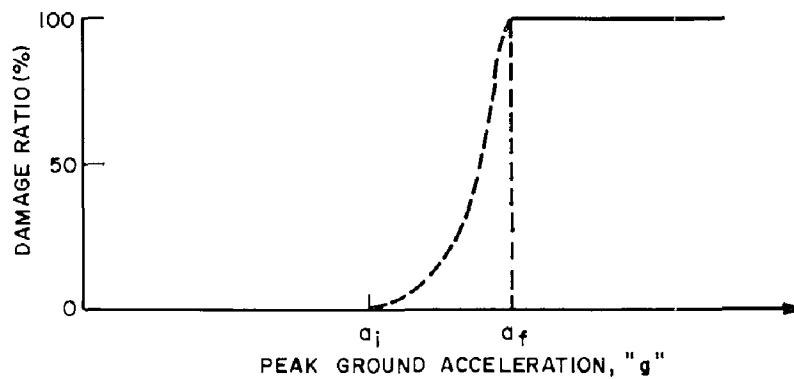


Figure 8. Typical Profile of Damage to Communications Equipment
Electromechanical Equipment

Electromechanical equipment, which consists primarily of crossbar switching facilities, is mounted on 11-1/2 ft frameworks anchored to the floor and braced to the ceiling, as shown in Figure 9. This configuration results in a fundamental frequency of 4 to 8 Hz for the equipment-framework-bracing, depending on the specific mix of equipment weights and frameworks.

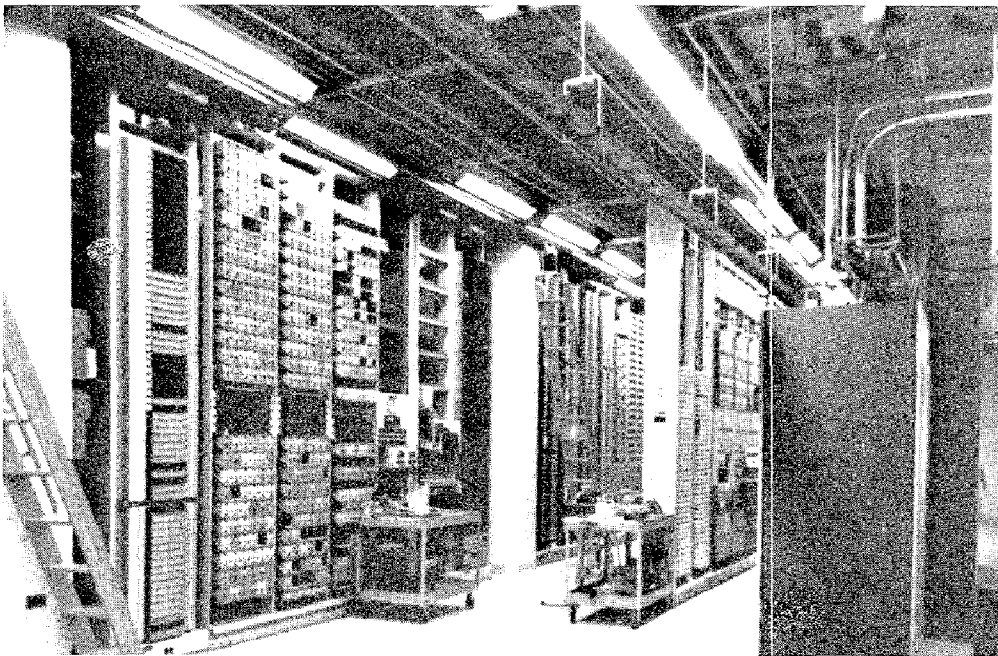


Figure 9. Typical 11-1/2 ft Electromechanical Equipment

The tests are the same as those performed on electronic equipment, i.e., varying the weight, framework, and input environment. In addition, a special structure was built to simulate overhead bracing on the shaker table, as shown schematically in Figure 10.

The results of the electromechanical equipment tests are expressed in terms of damage profiles. By keying these damage profiles to the micro-zonation map, regional earthquake protection practices were developed. The results show that the standard nonearthquake installations are satisfactory for low to moderate seismic risk areas and that present earthquake practices are adequate for the high-risk regions. These earthquake practices include a more substantial overhead bracing configuration than the nonearthquake installations use.

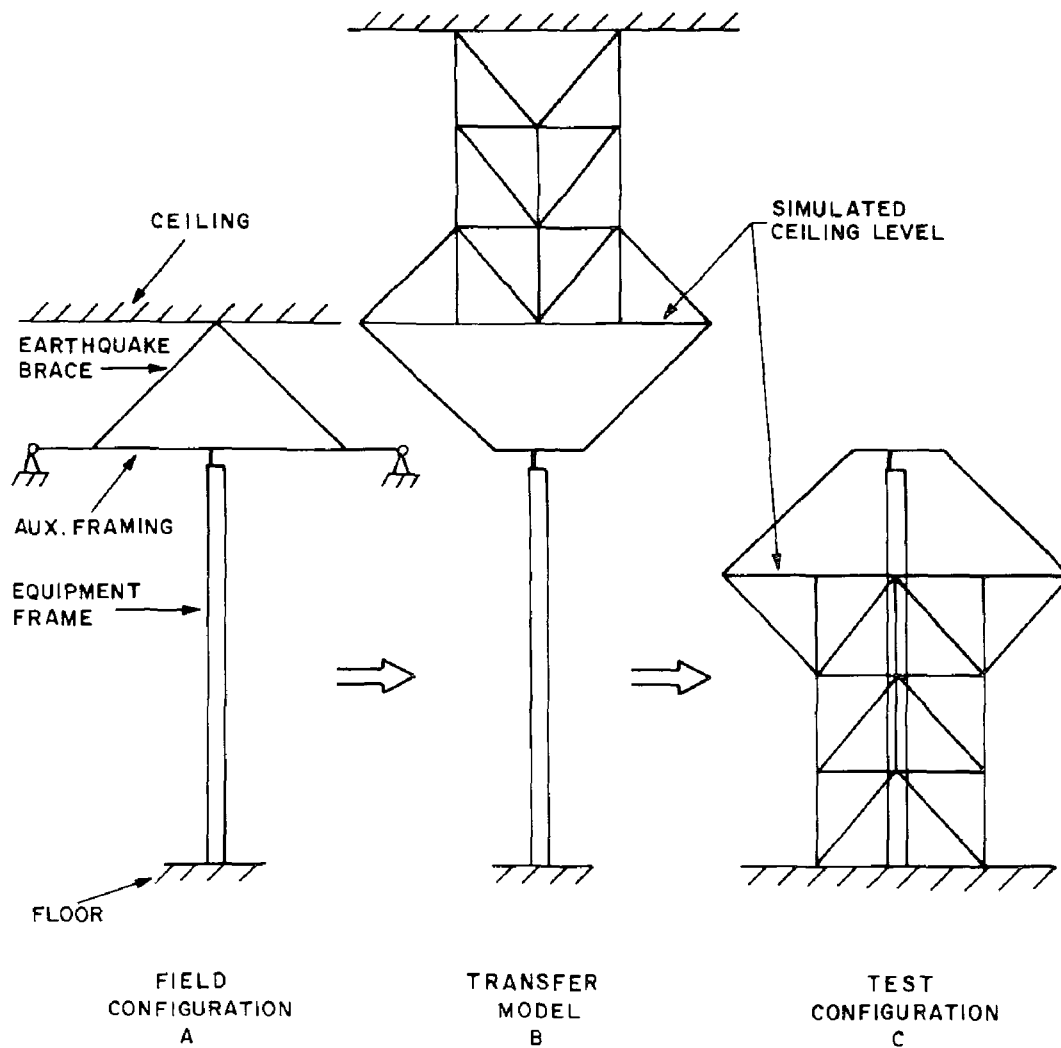


Figure 10. Evolution of Field Configuration to Test Configuration

Reserved Power Systems

The primary component of the telephone reserved power system is the battery plant. The newest battery plant consists of polyester-glass stands with round cells, as shown in Figure 11. There are several earthquake protection measures that can be employed with this stand-cell configuration — for example, epoxy all joints in the stand and lock the cells in place, and/or place a harness over the stand and anchor it to the floor, as shown in Figure 12.

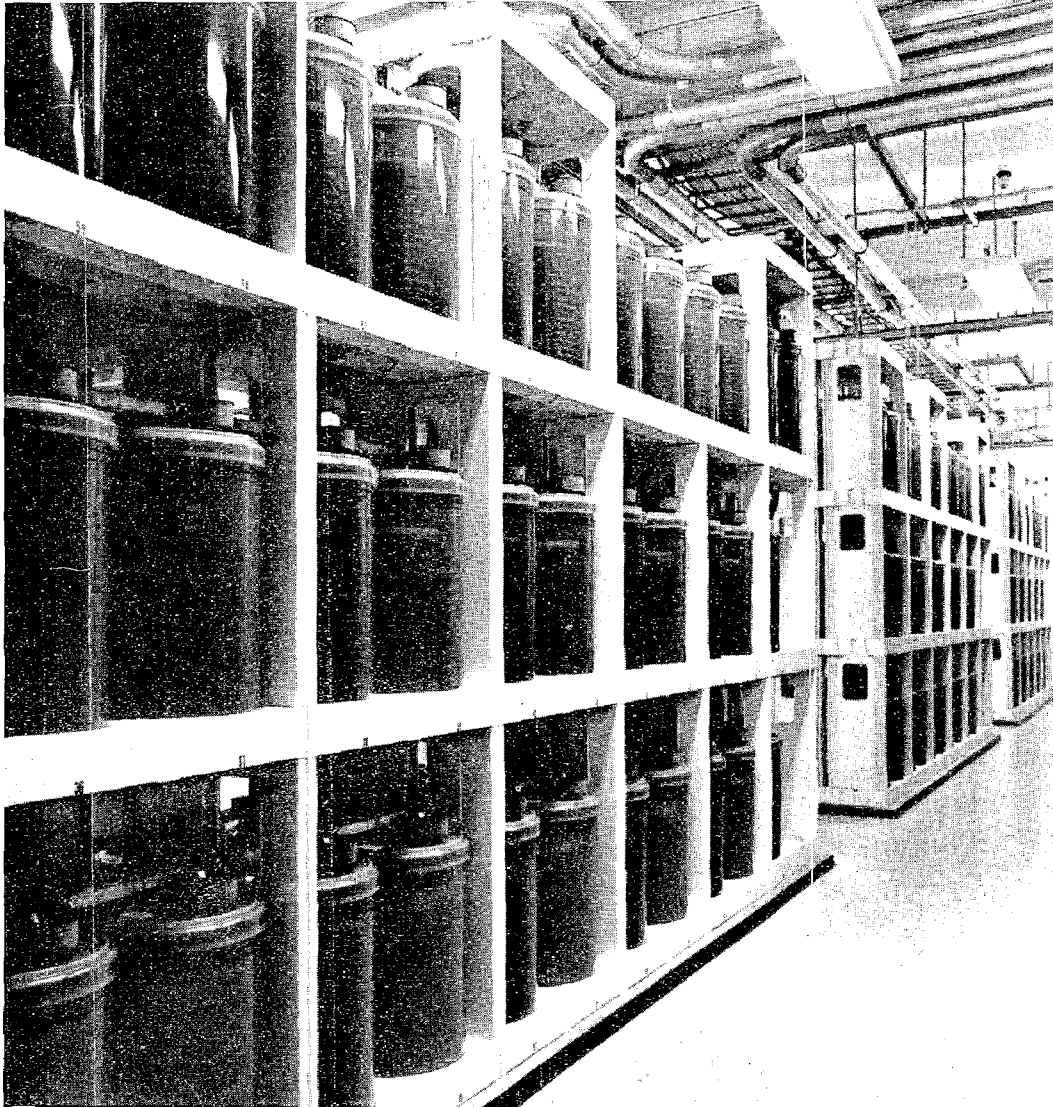


Figure 11. Nonearthquake Installation of Polyester Glass Stands with Round Cells

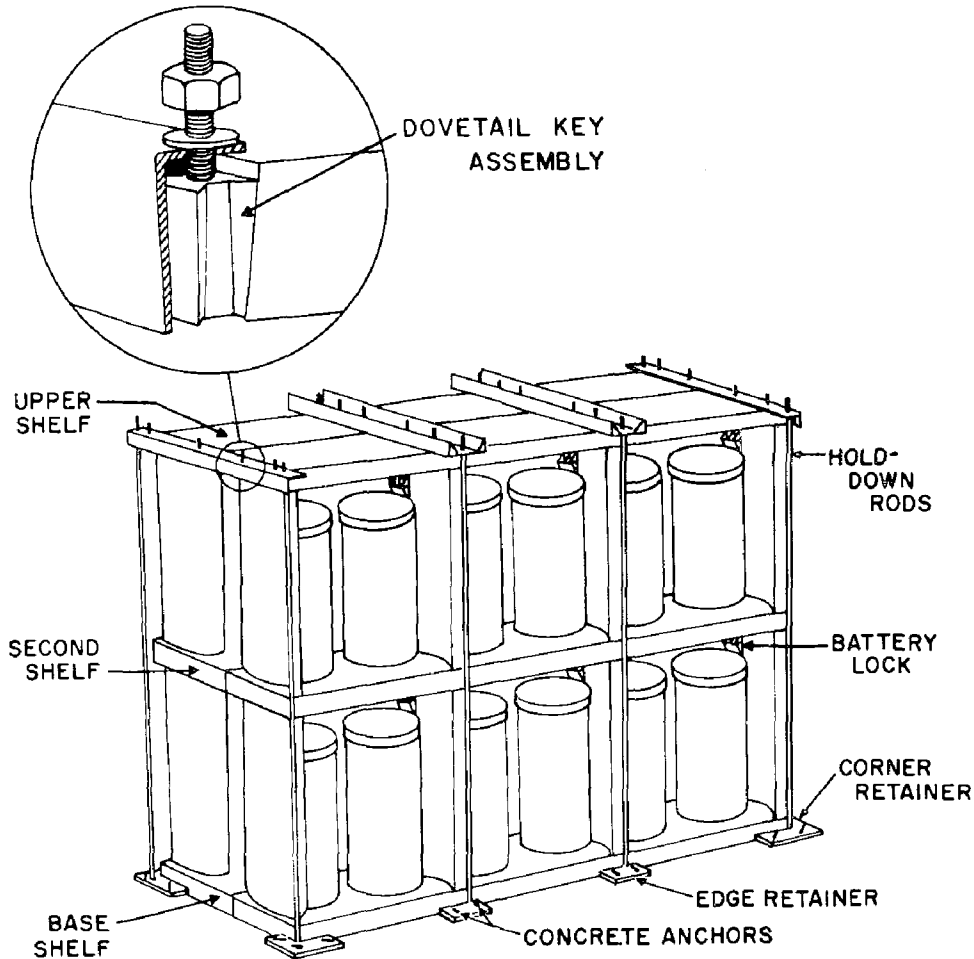


Figure 12. Earthquake Holddown Harness Assembly

A series of tests were performed with variations in the stand-cell configuration — i.e., 2-row 2-tier, 1-row 2-tier, 2-row 3-tier, etc. — different earthquake protection measures and variable earthquake input. The fundamental frequency varied from 4 to 7 Hz, depending on stand-cell configuration and earthquake protection. The resulting damage profiles were keyed to the microzonation map, and regional earthquake protection guidelines were developed. This study shows that the harness and epoxy are required for all battery stand configurations in moderate- and high-risk areas, and the harness is required for certain configurations on upper floors in low-risk areas.

COST AND LOSS ANALYSIS

The above analysis shows that an earthquake protection policy can be based on reliability considerations. While improving the reliability of the structure tends to lower the loss due to earthquake damage, it also could result in a significant increase in the total cost of the structure. When the additional protection cost becomes substantial, it is necessary to consider the cost and loss factors during the design protection decision

process. Some recent papers have been published addressing such problems in the context of optimal design^{5,6} or decision analysis.⁷ Since cost and reliability are key factors, estimates of these quantities must be truly representative of the actual environment to preclude both grossly conservative and marginal design practices. Because of uncertainties in the earthquake and structural parameters involved in such complex problems, the degree of precision in the cost and loss estimates depends on the sophistication of the analysis procedure. However, for practical purposes, simple but reliable procedures are more desirable. One such cost/loss analysis procedure is described below.

Cost/Loss Analysis Procedure

The expected dollar loss of an equipment system due to earthquakes depends on the earthquake risk and the total worth of the system. The following two situations are considered: one communications system in a given seismic risk area, and "n" of these systems in that area.

Single System Cost/Loss Analysis - Consider the situation where there is one communications system located within a given contour, as illustrated in Figure 13A. Assume that regional earthquake protection is incorporated to ensure survival of the system for the environment indicated by its location on the contour map (Figure 2). The specific earthquake protection installed is determined by the damage profile (Figure 8) of the equipment-framework system.

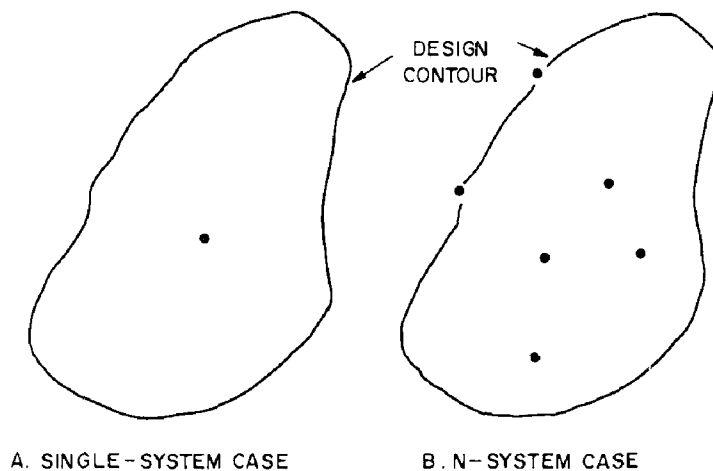


Figure 13. Monetary Losses for Communications Systems during Earthquake

If earthquake protection were not incorporated in the system, the expected losses over the 50-year facility service life would be equal to the value of the equipment, i.e., c_i . When earthquake protection is included, this loss is reduced to

$$L_e = p_f c_i, \quad (1)$$

where p_f is the probability that the design environment will be exceeded during the facility service life, i.e., the exceedance probability is 0.10.

Thus, the expected loss is

$$L_e = 0.10 c_i . \quad (2)$$

The earthquake protection cost ratio δ (i.e., protection cost divided by equipment value) for communications facilities is typically 0.004 to 0.02, depending on the type of equipment and its protection design level. Therefore, an expenditure

$$P = 0.004 c_i \text{ to } 0.02 c_i \quad (3)$$

results in a reduction of expected losses, L_e , from c_i to $0.10 c_i$, which obviously makes the earthquake protection cost-effective.

Multiple Systems Cost/Loss Analysis - When there is more than one system within a given contour (Figure 13B), the situation is different. Each system is equally vulnerable and has a certain likelihood of failure during a given time period. Furthermore, joint failures of a number of systems also may occur.

Let the "n" similar systems in Figure 13B be denoted as a,b,c,...; let $p_f(a), p_f(b), \dots$ - be the respective failure probabilities; $p_f(ab), p_f(bc), \dots, p_f(mn)$ the joint failure probabilities for two systems; and $p_f(abc), p_f(bcd), \dots, p_f(lmn)$ the joint failure probabilities for three systems, etc. Then the total expected earthquake loss for these "n" systems is

$$L_e = c_i [p_f(a) + p_f(b) + \dots + p_f(n)] \\ + 2c_i [p_f(ab) + p_f(bc) + \dots + p_f(mn)] + \dots + nc_i [p_f(ab\dots n)] . \quad (4)$$

If each system has earthquake protection to ensure survival for the environment indicated by its contour location, then the failure probabilities of single systems within the contour are identical - i.e., $p_f(a) = p_f(b) = \dots = p_f(n) \equiv p_f = 0.1$ - but the joint failure probabilities of two or more systems are not known. The calculation of these joint failure probabilities is complicated, because the correlation between events of multiple failures is difficult to evaluate. However, if these systems are geographically separated so that their failure can be treated as independent events, then it can be assumed that $p_f(ab) = p_f(a)p_f(b)$, $p_f(abc) = p_f(a)p_f(b)p_f(c)$, etc. and the expected loss can be expressed as

$$L_e = c_i \left[np_f + 2 \binom{n}{2} p_f^2 + 3 \binom{n}{3} p_f^3 + \dots + n \binom{n}{n} p_f^n \right] . \quad (5)$$

From the equation above note that higher-order terms contribute very little to the total loss; this is expected because these terms correspond to higher-order joint failures, which are extremely small. If these terms are neglected for $n \geq 2$ in the above equation, then a lower-bound estimate

of the earthquake loss is given by

$$L_e \geq nc_i p_f = 0.10 nc_i . \quad (6)$$

Therefore, since the protection cost for "n" similar systems is $P = n\delta c_i$, where δ is typically 0.004 to 0.02, it can be concluded that earthquake protection is cost-effective.

The relatively simple cost models described above demonstrate that earthquake protection of communications facilities increases system reliability, and can be incorporated into the system in a cost-effective manner.

CONCLUSION

This paper has described procedures developed to ensure telephone equipment reliability in various earthquake-risk regions. For a given system the following elements must be determined: the nature of the earthquake environment, equipment tests, and the cost of the protection as opposed to the possible system loss. The study showed that earthquake protection practices that were designed according to these prerequisites increased system reliability in a cost-effective manner.

REFERENCES

- ¹Liu, S. C. and DeCapua, N. J., "Microzonation of Rocky Mountain States," Procedures of the U.S. National Conference on Earthquake Engineering, University of Michigan, June 1975, pp. 128 - 35.
- ²DeCapua, N. J., Hetman, M. and Liu, S. C., "Earthquake Test Environment - Simulation and Procedure for Communications Equipment," to be published in Shock and Vibration Bulletin, Bulletin No. 46, June 1976.
- ³Liu, S. C., Fagel, L. W. and Dougherty, M. D., "Synthesis of Earthquake Motion in Multistory Buildings," to be published in the ASCE Journal of Structural Division, 1976.
- ⁴Liu, S. C. and Fagel, L. W., "Earthquake Environment for Physical Design," Bell System Technical Journal, Vol. 51, No. 9, November 1972, pp. 1957 - 82.
- ⁵Liu, S. C. and Neghabat, F., "A Cost Optimization Model for Seismic Design of Structures," Bell System Technical Journal, Vol. 51, No. 10, 1972, pp. 2209 - 25.
- ⁶Liu, S. C., Dougherty, M. D., and Neghabat, F., "Optimal Aseismic Design of Buildings and Equipment," to be published in the ASCE Journal of Engineering Mechanics Division, June 1976.
- ⁷Whitman, R. V., et al., "Seismic Design Decision Analysis - Methodology and Pilot Application," Department of Civil Engineering Research Report R74-15, MIT, July 1974.

INTERNATIONAL SYMPOSIUM ON
EARTHQUAKE STRUCTURAL ENGINEERING

269

St. Louis, Missouri, USA, August, 1976

CRITICAL EXCITATION AND RESPONSE
OF FREE STANDING CHIMNEYS

P. C. WANG, Prof. of Civil Engineering, Polytechnic Institute of N. Y.
W. WANG, Assist. Prof. of Civil Engineering, Polytechnic Institute of N. Y.
R. DRENICK, Prof. of System Engineering, Polytechnic Institute of N. Y.
J. VELLOZZI, Assoc., Ammann & Whitney, N. Y.

U. S. A.

SUMMARY

This paper deals with the problem of the seismic design of free standing chimneys, of constant as well as tapered cross sections. It is more particularly shown that seismic designs based on the so-called critical excitations of these structures are conservative, but not overly conservative, and that they should be appropriate either for localities in which ground motion records are scarce or for structures whose loss would have serious consequences, economically or socially. This conclusion is based on computed "critical design factors" which are the ratios of the response peaks generated by a critical excitation to those produced by an actual ground acceleration of same intensity. These factors were found to be in the order of 0.93 to 1.3 for at least one structural design variable of each of the two structures, implying the conclusion that design based on the critical excitation method would be more, but not greatly more, conservative than one based on an already observed ground motion. Design calculations for the additional steel reinforcement implied by those factors confirm this conclusion.

INTRODUCTION

Free standing chimney are comparatively susceptible to seismic damages due to their inherent weak supporting condition and lack of structural redundancy. The most damaging (critical) ground excitation for an assigned design variable (moments, shears, or deflections) possesses characteristic frequency contents, duration, and energy level. The first two characteristics are dependent on the structural properties while the other depends on the nature and intensity of the ground motion.

Structural response is characterized by the frequencies of the modes of its free vibrations. Intuitively, one should expect the most damaging (i. e., the critical) excitation of a structure to have a frequency spectrum that matches that of the structure. This is actually the case, as experience indicated. It is known, for instance, that ground motion matching in frequency with the lower vibration modes of a structure is likely to cause

severe damage in it. It is also well known that excitations at short distances from the epicenter which exhibit intense vibrations at high frequencies may induce damage in apparently strong but rigid structures, yet light or no damage to seemingly weaker but flexible structures. Mathematical confirmation [3] of these observations shows that the critical excitation of an elastic structure, for a given intensity and relative to one of the design variables, is the time-reversed impulse response of that variable.

It develops however, that the kind of precise frequency matching which is afforded by the time-reversed impulse response is not in general achieved by realistic ground motions. In other words, the response peaks to which it leads are typically much too large, and the designs that would escape damage, much too conservative to be useful. It has accordingly been necessary in this study to modify the time-reversed impulse response and to treat the modified excitation as the critical. To distinguish the original and its modification, they are called the "first-class" and the second-class" critical excitations in what follows.

This paper starts with a discussion of the first-class critical excitation for structures with a single-degree-of-freedom, as well as some assumptions and concepts that are pertinent to it, and then proceeds to the case of multi-degree-of-freedom systems. The idea of the second-class critical is introduced next. The succeeding sections present the methods and the results of the analyses of the two types of chimney, namely one with constant and the other with tapered cross sections. A critical discussion of the results is contained in the concluding section.

EFFECTIVE DURATION AND INTENSITY OF GROUND EXCITATION

The response $y(t)$ of a design variable of an elastic structure to a ground acceleration $\ddot{x}_g(t)$ is given by the Duhamel integral

$$y(t) = \int_0^t \ddot{x}_g(\tau) h(t-\tau) d\tau \quad (1)$$

in which $h(t-\tau)$ is the unit impulse response at a time $(t-\tau)$. For a structure with a single degree of freedom it is given by

$$h(t-\tau) = \frac{1}{\omega_D} e^{-\xi\omega(t-\tau)} \sin \omega_D(t-\tau) \quad (2)$$

where $\omega_D = \omega\sqrt{1-\xi^2}$ is the damped frequency, ω is the undamped frequency, and ξ is the damping ratio. Thus, if the maximum response of a structure occurs at time t_e , the duration of excitation needs not be taken longer than the value of (t_e-t_0) so that $h(t_e-t_0) = 0$, or more practically $h(t_e-t_0)$ decays to a certain percentage of the maximum of $h(t)$. The decay percentage can often be left to the judgment of the designers. For example, if the decay to a ten percent was assigned to a structure based on its fundamental period of vibration of 2 seconds, with a damping ratio of 5% then the duration of excitation need not be taken greater than

$$(t_e-t_0) = \frac{-\ln 0.1}{\xi\omega} = \frac{2.3}{0.05 \frac{2\pi}{2}} = 14.6 \text{ seconds} \quad (2a)$$

The definition of the intensity of ground excitation has been the subject of extensive discussions. In this paper, following the derivation of reference [3], the intensity of an excitation was defined as

$$E = \left[\int_{t_0}^{t_e} \ddot{x}_g^2(t) dt \right]^{\frac{1}{2}} \quad (3)$$

Since the duration of excitation ($t_e - t_0$) used for the critical excitations and the comparative recorded excitations, as will be seen in the later discussions, are the same, the intensity of excitation defined here is similar to that defined by Housner [6].

$$E = \frac{1}{t} \int_0^t \ddot{x}_g^2(t) dt \quad (4)$$

FIRST-CLASS CRITICAL EXCITATION

The maximum response of a multi-degree-of-freedom system represented by modal superposition is as follows:

$$\begin{aligned} y_k(t_e) &= \sum_i \phi_{ki} \eta_i(t_e) = \int_{t_0}^{t_e} \ddot{x}_g(\tau) \sum_i \phi_{ki} P_i h_i(t_e - \tau) d\tau \\ &= \int_{t_0}^{t_e} \ddot{x}_g(\tau) \bar{h}(t_e - \tau) d\tau \end{aligned} \quad (5)$$

where $y_k(t_e)$ is the k^{th} response variable, ϕ_{ki} is the k^{th} element of the i^{th} mode shape, $\eta_i(t_e)$ is the normal coordinate of i^{th} mode, $P_i = \phi_i^T M \hat{I} / \phi_i^T M \phi_i$ is the i^{th} mode participation factor with M as the mass matrix and \hat{I} is a vector with 1's or 0's to indicate the existence or not of excitation in the vector elements of y . Squaring the response y_k and setting up the inequality, the following relation is obtained.

$$\begin{aligned} y_k^2(t_e) &= \left[\int_{t_0}^{t_e} \ddot{x}_g(\tau) \bar{h}(t_e - \tau) d\tau \right]^2 \\ &\leq \left[\int_{t_0}^{t_e} \ddot{x}_g^2(\tau) d\tau \right] \left[\int_{t_0}^{t_e} \bar{h}^2(t_e - \tau) d\tau \right] \\ &\leq E^2 N^2 \end{aligned} \quad (6)$$

or $y_k(t_e) \leq EN$

where E is the intensity of excitation as defined in Eq. (3) and N^2 is the square integral of the unit impulse response. The maximum response is the product EN and can be obtained by applying a first-class critical excitation $\ddot{x}_{c1}(t)$, so that

$$\ddot{x}_{c1}(\tau) = \frac{E}{N} \bar{h}(t_e - \tau) \quad (7)$$

The shape of the unit impulse $\bar{h}(t)$ and $\ddot{x}_{c1}(t)$ are shown in Fig. 1.

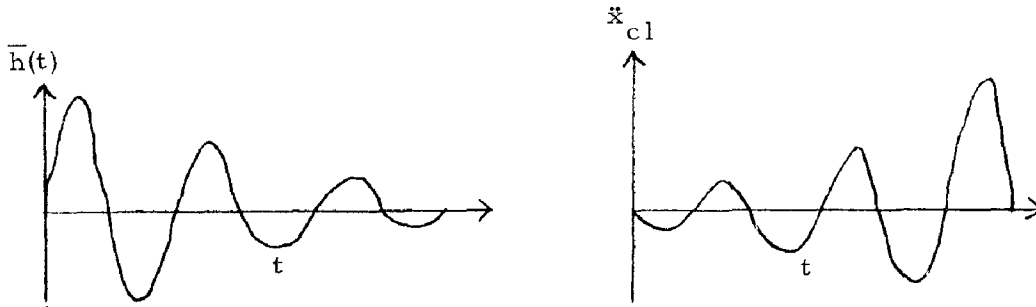


Fig. 1. SHAPE OF $\bar{h}(t)$ AND \ddot{x}_{c1}

The maximum response due to the first class critical excitation is

$$y_{c1} = \frac{E}{N} \int_{t_0}^t \bar{h}(t_e - \tau) \cdot \bar{h}(t_e - \tau) d\tau$$

$$= EN \quad (8)$$

The intuitive interpretation of this result was already mentioned in the Introduction. It indicates that the frequency content of the first class critical excitation matches exactly with that of the structural vibration and therefore that the corresponding critical response y_{c1} is the maximum peak among those produced by all the excitations with same intensity E .

SECOND-CLASS CRITICAL EXCITATION

It has been mentioned in the introduction, that the response peaks produced by the first-class critical excitations often are too large to be realistic, and the results reported below for two free-standing chimney will be seen to confirm this. It has therefore been found necessary to introduce a modification which is called the "second-class critical excitation" here.

The second-class critical excitation is obtained by superposition of a number of recorded ground excitations (or artificially generated excitations) and least-square fitted with the first class critical excitation as follows:

$$\ddot{x}_{c2}(t) = \sum_{i=1}^n c_i \ddot{x}_i(t) \quad (9)$$

and

$$\int_{t_0}^t [\ddot{x}_{c1}(t) - \ddot{x}_{c2}(t)]^2 dt = \text{minimum}$$

$$\int_{t_0}^{t_e} \ddot{x}_{c2}^2(t) dt = E^2$$

The response to the second-class critical excitation is

$$y_{c2} = \int_{t_0}^{t_e} \bar{h}(t_e - \tau) \ddot{x}_{c2}(\tau) d\tau \quad (10)$$

The second-class critical excitation \ddot{x}_{c2} resembles the recorded excitations more closely than the first-class one and the peak of its resultant response y_{c2} is more reasonable. However it is still larger than that of any of the responses due to the component excitations used for the least-squares of it.

In order to find the first-class critical excitation \ddot{x}_{c1} and the corresponding response y_{c1} for a particular structural design variable based on the time-reversed unit impulse response, the designer only needs the specification of a reference ground motion intensity E . However, in order to obtain the second-class critical excitation \ddot{x}_{c2} which is a least-squares fit, a number of appropriate ground motions must be selected to make the combination as shown by Eq. (9). Finally, in order to have a basis of comparison, a few recorded accelerograms must be selected and structural responses calculated for them as well. This section describes the choices that were made for these purposes.

In regard to the first requirement of obtaining the least-squares fitted excitation \ddot{x}_{c2} , twelve accelerograms were selected including two of the three selected for comparative studies. These accelerograms were chosen with the following stipulations:

1. The ground excitations are characterized by relatively short epicentral distances, say 25 to 30 kilometers.
2. The shape of the accelerogram should have a gradual build-up period.
3. The site conditions of the selected earthquakes should resemble as much as possible the condition prevailing at the location of the structure.

The third stipulation may be difficult to satisfy unless a choice can be made from a rather large variety of accelerograms, probably larger than now exists. At any rate, in the present study twelve ground motions recorded in Southern California were chosen and assumed to be representative for the locations of the chimneys to be analyzed below. Appendix 1 lists these twelve earthquakes and their intensities E .

Typical examples of second-class critical excitation obtained in this way are shown in Fig. 2.

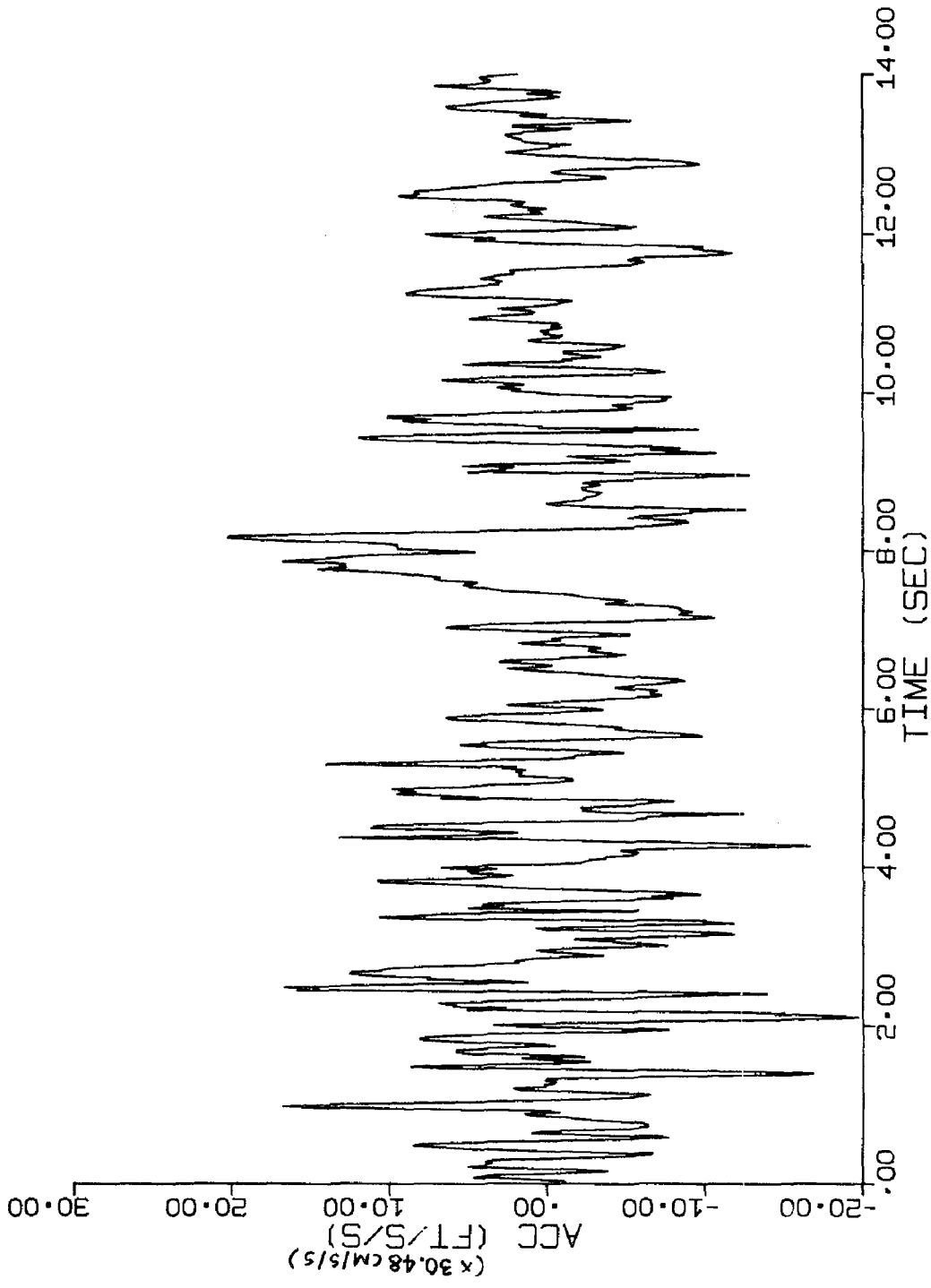


FIG. 2. TYPICAL 2ND CLASS CRITICAL EXCITATION
WITH SAN FERNANDO, PACOIMA DAM INTENSITY

For comparative studies, three accelerograms were selected from the published results [2], namely, (1) 1971 San Fernando, Pacoima S14W, (2) 1940 Imperial Valley, El Centro S00E, (3) 1954 Eureka N79E. Each of these three accelerograms has certain special characteristics: the first is the strongest (1.17g) that has ever been recorded, the second one is strong and of relatively long duration, while the third one is moderately intense and of relatively short duration.

CHIMNEYS WITH CONSTANT CROSS SECTIONS

Chimneys with constant cross sections are simple prismatic cantilevers. Its natural frequency of vibration of the i^{th} mode is given by [1]:

$$\omega_i = \alpha_i^2 \sqrt{\frac{EI}{mL^4}} \quad (11)$$

where α_i is obtained from the transcendental equation

$$\cos \alpha_i \cosh \alpha_i = -1 \quad (12)$$

The mode shapes are given by

$$\phi_i\left(\frac{x}{L}\right) = \sin \alpha_i \frac{x}{L} - \sinh \alpha_i \frac{x}{L} + A_i (\cosh \alpha_i \frac{x}{L} - \cos \alpha_i \frac{x}{L})$$

with

$$A_i = \frac{\sin \alpha_i + \sinh \alpha_i}{\cos \alpha_i + \cosh \alpha_i} \quad (13)$$

In the above expressions, E is the modulus of elasticity, I is the moment of inertia, m is the distributed mass per unit height, L is the height of the chimney, and x is the distance from the base of the chimney.

For a reinforced concrete chimney of 304.80 m in height, 18.288 m in outside diameter, and 0.4572 m in thickness, the mass per unit height is 1910.677 Kg-sec²/m². Based on modulus of elasticity 2.9489 x 10⁹ kg/m² and moment of inertia 1018.5 m⁴, the period of vibration in seconds of the first six modes are 2.400, 0.383, 0.137, 0.070, 0.042 and 0.028. The participation

factors $\int_0^L \phi_i dx / \int_0^L \phi_i^2 dx$ are 0.783, 0.434, 0.251, 0.001 for the first

four modes. The design variables selected are top deflection Δ , base moment M, and base shear V. The results of the dynamic analysis for the three reference earthquakes are shown in Table 1. The entries in the table are more specifically the response peaks generated by these excitations shown in the left column. The peaks to which the first-class critical excitation leads are seen to be consistently much higher than those due to the actual ground motion.

Those produced by the second-class critical are however much more realistic. The ratios of those peaks to the ones generated by the actual

ground motions are listed in Table 2, under the heading of "critical design factors." These factors are seen to range over values from 1 to 3.

TABLE 1. RESPONSE PEAKS OF CHIMNEY WITH CONSTANT CROSS SECTION

Excitations	Intensity E (cm/sec ^{3/2})	Response Variables		
		Top Deflection Δ (m)	Base Moment $10^5 M$ (Kg-m)	Base Shear $10^3 V$ (Kg)
Pacoima Dam	6.471	0.676	10288.8	1280.2
1st cl. critical		2.396	26151.1	1194.3
2nd cl. critical		5.101	59678.2	3565.7
El Centro	2.572	0.432	4967.4	349.9
1st cl. critical		0.953	10394.4	474.7
2nd cl. critical		2.028	23720.6	1417.3
Eureka	2.008	0.243	3423.3	286.6
1st cl. critical		0.744	8115.5	370.6
2nd cl. critical		1.583	18519.9	1106.5

TABLE 2. CRITICAL DESIGN FACTORS OF THE CHIMNEY WITH CONSTANT CROSS SECTIONS

Excitations	Top Deflection Δ	Base Moment M	Base Shear V
Pacoima Dam	3.54	2.54	0.93
El Centro	2.21	2.09	1.36
Eureka	3.06	2.37	1.29

TAPERED CHIMNEYS

Most chimneys have tapered shapes. Although expressions similar to (11) and (13) for frequency and mode shapes can be derived, it is simpler to use discrete lumped mass approach.

The chimney selected for this study is a 304.8 m free standing tapered reinforced concrete cylinder. The bottom outside diameter is 25.298 m with wall thickness of 0.889 m. The top outside diameter is 10.262 m with a thickness of 0.216 m. The 0.64 cm steel lining is not considered as the integrated structural element. The detailed vertical chimney wall cross section is shown in Figure 3.

A discrete finite element method was used to find the free vibration as well as dynamic analysis. The height of the chimney is divided into 17 sections with the respective horizontal cross sectional area and moment of inertia computed as shown in Table 3. The lumped masses at the nodal points are also shown in Table 3. The condensed stiffness matrix refers to the horizontal displacements at the nodal points corresponding to each mass point. The mode shapes and periods of vibration are shown in Figure 4. The design variables selected for study are again the top deflection Δ , the base moment M, and the base shear V. The dynamic

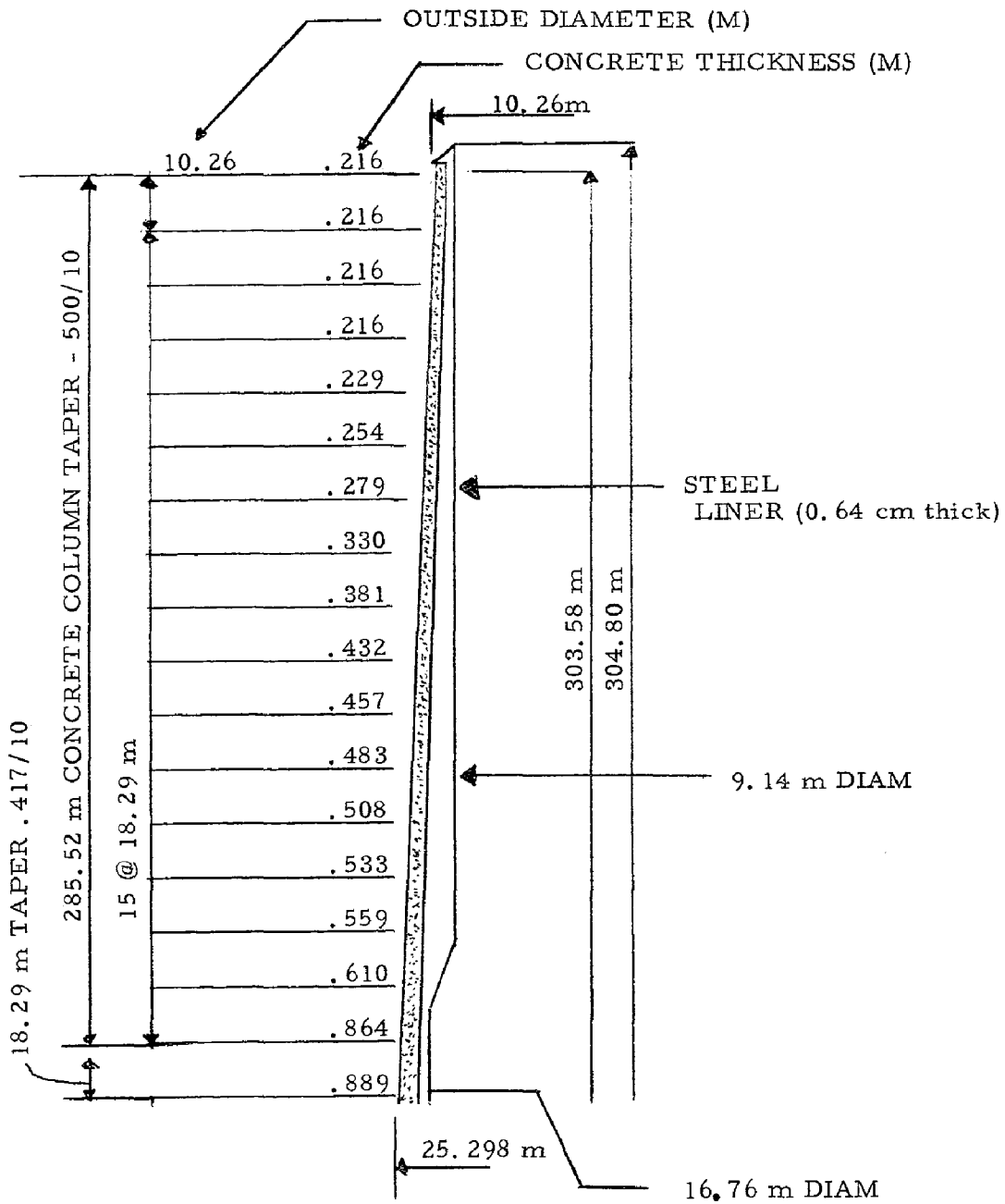


FIG. 3. VERTICAL CROSS SECTION OF CHIMNEY WITH TAPERED CROSS SECTIONS

TABLE 3. AREA, MOMENT OF INERTIA AND
LUMPED MASSES OF TAPERED CHIMNEY

Element	Area (m ²)	Moment of Inertia (m ⁴)	Node	Lumped Mass (Kg-sec ² /m)
17	7.005	93.420	18	10119.08
16	7.505	114.90	17	27976.28
15	8.125	145.791	16	37648.93
14	8.999	186.856	15	40476.32
13	10.448	24.652	14	45535.86
12	12.293	330.866	13	53571.6
11	14.888	450.039	12	62053.77
10	18.334	617.540	11	76934.77
9	22.956	823.209	10	93006.25
8	25.348	1044.520	9	110268.21
7	28.108	1274.539	8	122321.82
6	31.010	1540.536	7	134970.67
5	34.056	1846.109	6	148363.57
4	37.242	2194.955	5	162351.71
3	41.448	2644.194	4	176935.09
2	54.024	3684.179	3	200149.45
1	66.189	4788.865	2	290477.12
			1	

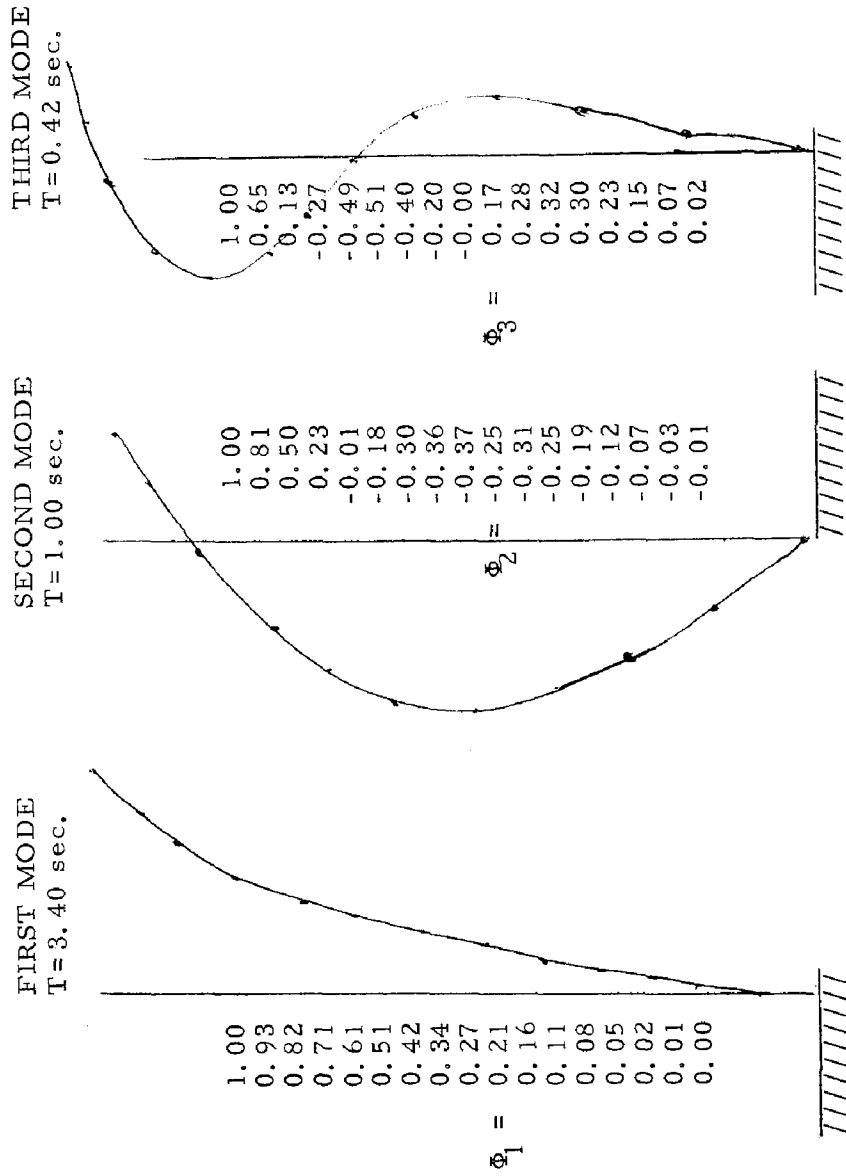


FIG. 4. MODE SHAPES AND PERIODS FOR THE TAPERED CHIMNEY

analyses of this chimney led to results which are summarized in Tables 4 and 5. Table 4 lists the response peaks that were generated by the actual ground motions, along with those due to the first-class and second-class critical excitations of the same intensities. Table 5 presents the critical design factors.

TABLE 4. RESPONSE PEAKS OF CHIMNEY WITH TAPERED CROSS SECTIONS

Excitation	Intensity E (m/sec ^{3/2})	Response Variables		
		Top Deflection Δ (m)	Base Moment M (10 ⁵ Kg-m)	Base Shear V (10 ⁴ Kg)
Pacoima Dam	6.996	1.383	5536.6	703.6
1st cl. critical		3.849	10930.4	1044.0
2nd cl. critical		21.924	58122.5	5191.0
El Centro	2.895	0.694	2134.7	313.3
1st cl. critical		1.594	4523.7	432.1
2nd cl. critical		9.074	22684.8	2148.4
Eureka	2.034	0.448	1580.3	2307.4
1st cl. critical		1.119	3177.9	3035.3
2nd cl. critical		6.373	15935.9	15092.2

TABLE 5. CRITICAL DESIGN FACTORS OF THE CHIMNEY WITH TAPERED CROSS SECTIONS

Excitations	Top Deflection Δ	Base Moment M	Base Shear V
Pacoima Dam	2.78	1.97	1.48
El Centro	2.51	2.12	1.33
Eureka	2.50	2.01	1.32

A design of the base cross section of the chimney was also made, based on the elastic design approach as well as on an inelastic one with ductility factor of $\mu = 4$. The results are shown in Table 6. The reinforcing that would be required for adequate strength against the second-class critical is considered to be rather high, but not beyond reason, when compared with that needed against the El Centro ground motion.

CONCLUSIONS

The proposed method of assessing seismic resistance of structures, based on the second-class critical excitation, was applied to uniform cross sectional and tapered chimneys. The conclusions from this study are as follows.

1. The method proposed here is an upper bound analysis in view of the fact that precise nature of earthquake, frequency of occurrence, interaction of structure and soil, and other earthquake related factors are not

TABLE 6. REINFORCEMENT FOR THE TAPERED CHIMNEY

	Excitations	Steel Ratio p%	$A_s(\text{req})(\text{cm}^2)$	Reinforcement	$A_s(\text{cm}^2)$ provided
F = 1 (elastic)	E1-Centro	0.60	4070.5	632-#9 bars, both sides, at 24.26 cm dist.	4077.4
	2nd cl. critical	5.00	32499.1	1260-#18S bars, both sides, at 12.19 cm dist.	32516.3
F = 4 (inelastic)	E1-Centro	0.06	409.22	578-#3 bars, both sides, at 26.7 cm dist.	410.2
	2nd cl. critical	0.90	6087.5	944-#9 bars, both sides, at 16.3 cm dist.	6090.4

readily available.

2. In the structural design of the two chimneys, the method appears to be effective, though still somewhat conservative. If desired, further reduction of the bound can be achieved by the judgment of the design engineer in reducing the specified intensity E , or in eliminating some of the selected component earthquakes in the least-squares fitting process. By observation of the coefficient of the least-squares fitting process, it appears that the earthquakes which most resemble the shape of the time-reversed unit impulse response excitation are the ones which may cause larger response. If these earthquakes are not likely to occur at a given location, they can be profitably omitted.

3. Both the intensity of the earthquake E , and the square integral N depend on the effective duration $t_e - t_0$ used in the integration process. In general, the duration depends on the fundamental period of vibration and the damping of the structure, being shorter for shorter period and larger damping. It is suggested that one may use the duration of decay of the unit impulse response to a judiciously selected percentage (say 20%) of the peak.

4. When plastic behavior is considered by using a ductility factor of 3 for a recorded earthquake, a ductility factor of roughly 6(=2x3) is required for the same structural strength against the least-squares fitted excitation. This ductility factor appears somewhat on the high side but not entirely out of proportion.

5. Based on the above discussions, it is suggested that the assessment of seismic resistance based on critical excitation be used for structures with major importance the destruction of which would cause severe human and economic losses. Another instance for adopting this approach is for those localities where seismicity is active but reliable ground motion data are scarce.

6. The practicality of the method is still undergoing examination by applying to various realistic structures at the time of this writing. Hopefully, consistent comprehensive recommendations can be drawn from these results in the near future.

ACKNOWLEDGMENT

The research on which this paper is based was supported by the National Science Foundation under Grant No. AEN72-00219 A01. This support is gratefully acknowledged.

APPENDIX 1

12 EARTHQUAKES USED FOR LEAST-SQUARES FITTING

File #	Quake	Record	Comp	$(\text{m}/\text{sec}^3/2)$ $E = \left(\int_0^{.14} x_g^2 dt \right)^{1/2}$
IIA 1	Imperial Valley	El Centro	S00E	2.895
IIA 10	San Jose	San Jose	N31W	0.660
IIA 13	San Francisco	San Francisco	N45E	0.340
IIA 14	San Francisco	San Francisco	N09W	0.293
IIA 15	San Francisco	San Francisco	N10E	0.397
IIA 16	San Francisco	San Francisco	S09E	0.543
IIA 17	San Francisco	San Francisco	N26E	0.234
IIA 18	Hollister	Hollister	S01W	0.838
IIA 19	Borrego Mt.	El Centro	S00W	0.875
IIC 41	San Fernando	Pacoima	S14W	6.996
IIC 48	San Fernando	Los Angeles	N00W	2.565
IID 56	San Fernando	Castaic	N21E	1.929

BIBLIOGRAPHY

1. Clough, R. W., Penzien, J., *Dynamic of Structures*, McGraw-Hill Hill Book Company, (1975); pp. 312-314.
 2. California Institute of Technology, Strong Earthquake Accelerograms Vol. II, corrected accelerogram.
 3. Drenick, R. F., "Model-Free Design of A seismic Structure," *Jour. Eng. Mech.*, ASCE, Vol. 96 (1970); pp. 483-493.
 4. Drenick, R. F., "A Seismic Design by Way of Critical Excitation," *Jour. Eng. Mech.*, ASCE, Vol. 49 (1973), pp. 649-667.
 5. Drenick, R. F., Prediction of Earthquake Resistance of Structures, Final Report to NSF, Grant GK14550, Polytechnic Institute of Brooklyn (1973).
 6. Housner, G. W., "Measures of Severity of Earthquake Ground Shaking," *Proceedings of U. S. National Conference on Earthquake Engineering*, Ann Arbor, Mich., June, 1975.
 7. Miller, C.A., Constantino, C. J., "Structure-Foundation Interaction of a Nuclear Power Plant with a Seismic Disturbance," *Nuclear Eng. and Design* 14 (1970), pp. 332-342, North-Holland Publishing Company.
 8. "Specification for the Design and Construction of Reinforced Concrete Chimneys," (ACI. 307-69), ACI Committee 307, ACI, 1969.
-

INTERNATIONAL SYMPOSIUM ON
EARTHQUAKE STRUCTURAL ENGINEERING

285

St. Louis, Missouri, USA, August, 1976

DYNAMIC ANALYSIS OF ELASTIC-PLASTIC SPACE FRAMES

NICHOLAS F. MORRIS

Associate Professor
Manhattan College
Riverdale, New York

SUMMARY

A method is presented for the nonlinear dynamic analysis of three dimensional space structures stressed into the elastic-plastic range. The procedure is an extension and modification of previously published static analyses. These modifications take place in the description of the stiffness matrix and in the interaction equations required for three dimensional elastic-plastic flow. The modal superposition method is used to reduce the order of the nonlinear dynamic equations to a more manageable form.

INTRODUCTION

The more efficient use of structural materials has led to design based on the ultimate capacity of structures, rather than their elastic limit. This has created a need for computational procedures to evaluate structural response in the complete range of material behavior. While a large amount of effort has been expended on the computation of planar elastic-plastic response, very little work has been published on the elastic-plastic analysis of three dimensional frameworks, even under static load (1). The dynamic response problem has been considered in (2) and (13). However, the latter paper was restricted to linear response computations. Herein will be presented a procedure for the computation of the nonlinear elastic-plastic response of arbitrary frameworks whose members can be struts, beams or cables.

MATHEMATICAL FORMULATION

The approach utilized herein is basically that employed in static analyses by Jonatowski and Birnstiel (7). However, certain modifications to their procedure have been made. First of all, it should be noted that, whereas in (7) stability functions are used, this work uses the usual stiffness values unmodified by the effect of thrust. While stability functions were applied in some of the early static analyses, their use did not make a difference in the final results. It was felt that the large amount of computer time required to generate the stiffness values in dynamic analyses did not justify the refinement of stability functions. The dynamic equations can be written in the following matrix form

$$[M] \left\{ \overset{\circ}{\overset{\circ}{D}} \right\} + [C] \left\{ \overset{\circ}{D} \right\} + [K] \left\{ D \right\} = \left\{ P \right\} \quad (1)$$

in which $[M]$ = mass matrix. It is made up of the lumped masses consisting of half the weight of each member framing into a node. The rotary inertia contribution was computed by assuming that half of each member rotates as a rigid bar about the node, while the torsional inertia is computed as the product of the polar moment of inertia and the mass density of the beam. Matrix $[C]$ = the damping matrix and $\{D\}$ = the displacement matrix ($u, v, w, \theta_x, \theta_y$ and θ_z at each node). The elements of $\{D\}$ are the velocities at the nodes while the $\{\overset{\circ}{D}\}$ matrix contains the accelerations. Matrix $\{P\}$ = the force matrix, made up of concentrated forces and couples at the nodes. The matrix $[K]$ is formed from member stiffness matrices $[k]$ evaluated at the deformed position of the member. The matrix elements of Eq. 1 are referred to a global system of coordinates; therefore, the elements of $[k]$ are referred to these coordinates as well. Matrix $[k]$ may be determined from

$$[k] = [r]^T [k^*] [r] \quad (2)$$

where $[r]$ is the member rotation matrix (4,7) and $[k^*]$ is the member stiffness matrix in local coordinates. The basic difficulty in the analysis concerns the evaluation of $[k^*]$ so attention will be focused on this problem.

It is assumed that all plastic behavior, when it occurs, is concentrated at the nodes of the system. Since loads are applied only at the nodes, these are the sections at which maximum bending stresses will occur. The stress-strain equation for the material is defined by (5,7)

$$\sigma = \frac{E \epsilon}{\left(1 + \left| \frac{E \epsilon}{\sigma_v} \right|^b\right)^{1/b}} \quad (3)$$

in which E = modulus of elasticity, b = constant defining the shape of the stress-strain curve, σ = unit stress, ϵ = unit strain and σ_u = the ultimate stress. For an elastic-perfectly plastic material σ_u will be taken as σ_y , the yield point of the material. The moment at the node is expressed by a relationship similar to Eq. 3 (5,7)

$$M = \frac{M_E}{(1 + \left| \frac{M_E}{M_P} \right| b)^{1/b}} \quad (4)$$

Jonatowski and Birnstiel derived a matrix $[k^*]$ based on Eq. 4. However, their procedure has two defects: one practical, the other theoretical. The practical defect is that their member stiffness matrix is not symmetrical. This means that a complete band width algorithm must be used in all computations, rather than the half band width procedures customarily employed in structural analysis. A second defect in their matrix is that it violates statics. This is easily proven by computing the shear at a node directly from their stiffness matrix and comparing that value with the shear computed by dividing the sum of node moments, obtained from the same matrix, by the member length. The two values should coincide but in the elastic-plastic case they do not. It must be emphasized, however, that the error in statics arises only when the member undergoes plastic flow. The error cannot be large because their results compare very favorably with those of other workers. A modified symmetrical form of the $[k^*]$ matrix is expressed by the following elements

$$k_{11}^* = k_{77}^* = -k_{17}^* = \frac{AE}{gL} \quad k_{22}^* = k_{88}^* = -k_{28}^* = \frac{B_1 + B_2}{L} \quad (5a)$$

$$k_{26}^* = -k_{68}^* = B_1 \quad k_{2,12}^* = -k_{8,12}^* = B_2 \quad (5b)$$

$$k_{33}^* = -k_{39}^* = k_{99}^* = \frac{C_1 + C_2}{L} \quad k_{35}^* = -k_{59}^* = C_1 \quad (5c)$$

$$k_{3,11}^* = -k_{9,11}^* = -C_2 \quad k_{4,4}^* = -k_{4,10}^* = k_{10,10}^* = \frac{GJ}{L} \quad (5d)$$

$$k_{5,5}^* = \frac{4EI_V}{Lh} \quad k_{5,11}^* = \frac{2EI_V}{Lr_V} \quad k_{66}^* = \frac{4EI_W}{p} \quad k_{6,12}^* = \frac{2EI_W}{r_W} \quad (5e)$$

$$k_{11,11}^* = \frac{4EI_V}{d} \quad k_{12,12}^* = \frac{4EI_W}{s} \quad (5f)$$

where

$$B_1 = \frac{EI_W}{L^2} \left(\frac{4}{p} + \frac{2}{r_W} \right) \quad B_2 = \frac{EI_W}{L^2} \left(\frac{4}{s} + \frac{2}{r_W} \right) \quad (6a)$$

$$C_1 = \frac{EI_V}{L^2} \left(\frac{4}{h} + \frac{2}{r_V} \right) \quad C_2 = \frac{EI_V}{L^2} \left(\frac{4}{d} + \frac{2}{r_V} \right) \quad (6b)$$

and

$$g = \left(1 + \left| \frac{F}{P_p} \right|^b \right)^{1/b} \quad h = \left(1 + \left| \frac{a_i (M'_V)_i}{(M_{pV})_i} \right|^b \right)^{1/b} \quad (7a)$$

$$p = \left(1 + \left| \frac{a_i (M'_W)_i}{(M_{pW})_i} \right|^b \right)^{1/b} \quad d = \left(1 + \left| \frac{a_j (M'_V)_j}{(M_{pV})_j} \right|^b \right)^{1/b} \quad (7b)$$

$$s = \left(1 + \left| \frac{a_j (M'_W)_j}{(M_{pW})_j} \right|^b \right)^{1/b} \quad r_V = \frac{2hd}{(h+d)} \quad r_W = \frac{2ps}{(p+s)} \quad (7c)$$

U, V and W denote the principal axes for the member. The a_i and a_j values will be defined later. For the present they can be taken as 1.00. Then the plastic factors g , h , p , d and s are identical to those developed in (7) while r_V is an averaging factor introduced to insure that the stiffness matrix satisfies statics and is symmetrical. In this formulation, unlike that of Jonatowski and Birnstiel, the existence of plastic flow at a node i influences the stiffness at the opposite member node j . This is reasonable, although it is possible to describe this influence in other ways (2).

The primed stress resultants in Eqs. 8 are those computed as if the member were completely elastic. Terms with P subscripts denote the yield values of the stress resultants.

(If the member is a cable, P_p is the ultimate force.) P_p is easily computed, but the yield moments depend on the interaction of the moments about both axes and the thrust acting on the section. This requires an interaction equation of some type. Both Jonatowski and Birnstiel, and Bockholdt and Weaver utilized the interaction equations developed by Santathadaporn and Chen (11). However, the solution of these equations requires a trial and error procedure, and is quite time-consuming, even for simple static problems. In a dynamic analysis, the computer time would seem to be prohibitive. It was decided to employ an approximate solution to the problem of interaction. In their work on H columns under biaxial loading, Tebedge and Chen introduce the following interaction equation (12)

$$\left(\frac{M_V}{M_{PV}}\right)^e + \left(\frac{M_W}{M_{PW}}\right)^e = 1.0 \quad (8)$$

wherein

$$M_{PW} = 1.18 F_Y Z_W (1 - \frac{F}{P}) \leq F_Y Z_W \quad (9a)$$

$$M_{PV} = 1.19 F_Y Z_V (1 - (\frac{F}{P})^2) \leq F_Y Z_V \quad (9b)$$

$$e = 1.60 - \frac{F/P}{2 \ln F/P} \quad (10)$$

Eq. 8 was used in the following manner: at nodes i and j the left hand side of Eq. 8 was computed and called a_i and a_j . If a_i or a_j is less than 1.00, it is set equal to 1.00, while if it is greater than 1.00 its computed value was used in Eqs. 7 along with values of M_{PV} and M_{PW} found from Eq. 9. This procedure insures interaction between the various moments only when Eq. 8 results in a value greater than 1.00. Since Eq. 8 is an upper bound equation, it can be expected that its use will result in an over-estimation of the yield load on a section. This defect was corrected somewhat by substituting M'_V for M_V and M'_W for M_W .

In order to solve dynamic problems it is necessary that unloading of a section be properly defined. If unloading is to occur at a point O on the moment-rotation curve, a residual moment, ΔM_O , the difference between the elastic-plastic moment at O and the elastic moment, M' , is introduced. Along the unloading curve, ΔM_O is taken as a residual moment in the definition of M' . For example, in Eq. 7, M'_V becomes $M_V - \Delta M_{VO}$ where, as usual, M_V is computed as if the member were elastic. This insures that unloading occurs the proper curve. Along this unloading curve, M_O remains as previously defined and Eqs. 5, 6 and 7 are again used with this modification.

All operations with the $[r]$ matrices are identical to those described in (7) and will not be reproduced here. It should be noted, however, that the geometric nonlinearities are introduced in the $[r]$ matrices; these matrices are functions of the deformed position of each member. The influence of member thrusts on the

stiffness matrix can be added to the member stiffness after it has been expressed in global coordinates

$$k_{i,i} = k_{i,i} - \frac{FL}{AE} \quad (i=1,2,3,7,8,9,) \quad (11a)$$

$$k_{i,i+6} = k_{i,i+6} + \frac{FL}{AE} \quad (i=1,2,3) \quad (11b)$$

The value of F is the compressive force acting on the member. It can be expressed by

$$F = F_0 - \frac{AE}{L} \Delta L \quad (12)$$

in which F_0 = the initial compressive force and

$$\Delta L = \frac{1}{L} \left((x_j - x_i)(u_j - u_i) + (y_j - y_i)(v_j - v_i) + (z_j - z_i)(w_j - w_i) + 0.50 \left((u_i - u_j)^2 + (v_i - v_j)^2 + (w_j - w_i)^2 \right) \right) \quad (13)$$

Eqs. 11 introduce the second geometric nonlinearity into the stiffness matrix as F is a nonlinear function of the displacements.

Once the stiffness and mass matrices have been adequately described, the dynamic response computations differ little from those required for the nonlinear elastic case (9). Eqs. 1 were solved with the aid of the modal response method and Newmark's linear acceleration method (3,9). The mode shapes were determined with the aid of the Givens-Householder method (10).

NUMERICAL RESULTS

The theory developed in the previous section was programmed and run on an IBM 360 computer. Several problems were run; the most informative example is presented in Fig. 1. The simple three dimensional frame of Fig. 1 was analyzed as a check on the static formulation (2,8). A comparison of previous work (8) and that proposed herein is presented in the figure. It cannot be claimed that the agreement is very good; however, in view of the assumptions made, the results are as could be expected. Jonatowski and Birnstiel used the interaction equations of (11); they are lower bound values. In this work, Eq. 9 represents an upper bound. Therefore, the point at which yield will occur differs for each model. This is evident from the figure. However, once yielding occurs for each system, the behavior becomes the same for both solutions. It can be concluded, therefore, that the description of plastic flow proposed herein is adequate but that the

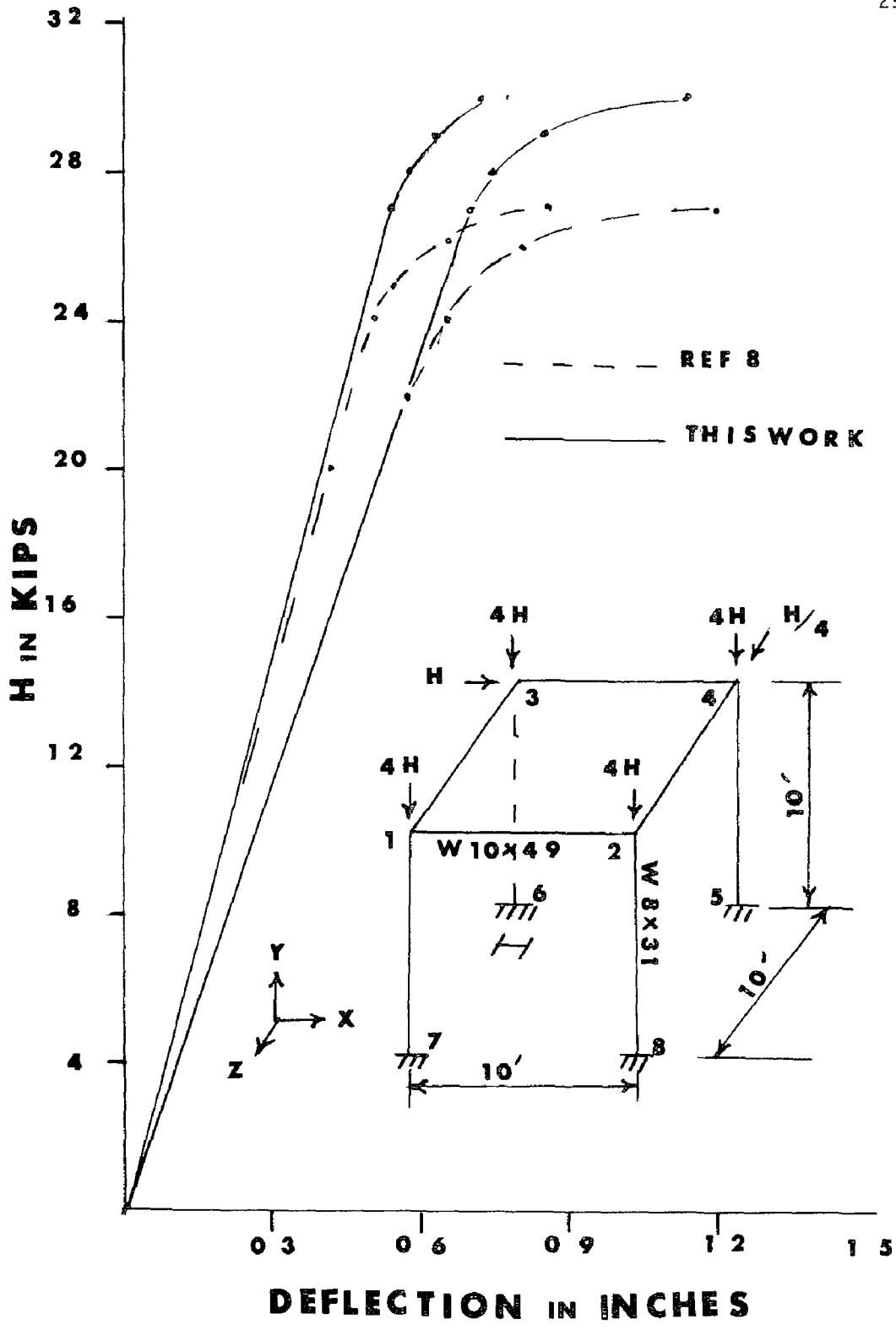


FIG.1 SMALL FRAME

stress state at which flow starts may be overestimated. It may be of some interest to note that the same frame was analyzed in (2) using a yield point stress of 33 ksi. The values obtained plotted slightly above those in (8).

Dynamic analyses were carried out for the frames presented in Figs. 1 and 2. In both cases $F_y = 36$ ksi (248 MN/m^2) and $b = 10$. Damping was 2.5 per cent of critical in each mode. A dead load of 100 kips (445 kN) was taken at each node of the simple frame of Fig. 1. In computing the mode shapes, inertia terms corresponding to rotational accelerations were multiplied by the factor 0.01. This corresponds to neglecting rotational accelerations. The mode shapes take the familiar configurations for a simple frame: the fundamental mode is a displacement in the Z direction at a frequency of 0.790 Hz while the mode corresponding to motion in the X direction is the third at a frequency of 1.34 Hz. Modes 2 and 4 correspond to combined motions in the X and Z directions at frequencies of 1.06 and 2.25 Hz. It should be noted that modes 5 through 8 describe motion in the Y direction at frequencies bunched around 14.9 Hz.

As a test case for the simple frame, it was analyzed for a harmonic load of 5 kips (22.25 kN) acting at a frequency of 4.70 radps applied at node 2 in the Z direction. This load is close to that required for resonance of the first mode. The response amplitudes are given in Table 1. The linear elastic solution employed the first 4 mode shapes at a time step of 0.07 seconds, corresponding to 1/6 the period of the highest mode, in this case, mode 4. It is evident that in order for the modal response method to be applicable to an elastic-plastic solution, all stress resultants must be found with great accuracy. The linear elastic four mode response satisfied this requirement. Elastic-plastic 1 denotes a four mode elastic-plastic response using $\Delta t = 0.07$ sec. The solution failed to converge at the step $N = 47$. However, the structure revealed an instability at the previous time step. This is found from an investigation of the moment values in the columns and the girders. It is obvious that for this frame the moment about the W axis for member 4-5, call it M_7 , should just about equal the moment about the V axis for member 3-4, call it M_2 . At $N=45$, $M_7 = -479$ in-kips while $M_2 = -482$ in-kips (54,500 N-m). At $N=46$, $M_7 = -1.0$ in-kips while $M_2 = -520.4$ in-kips; the results are completely wrong. This form of instability revealed itself in all elastic-plastic analyses of the frame.

In previous work on the nonlinear elastic analysis of cable stiffened structures (9), it has been found that, when the number of mode shapes needed to describe a response has been chosen, the time interval corresponding

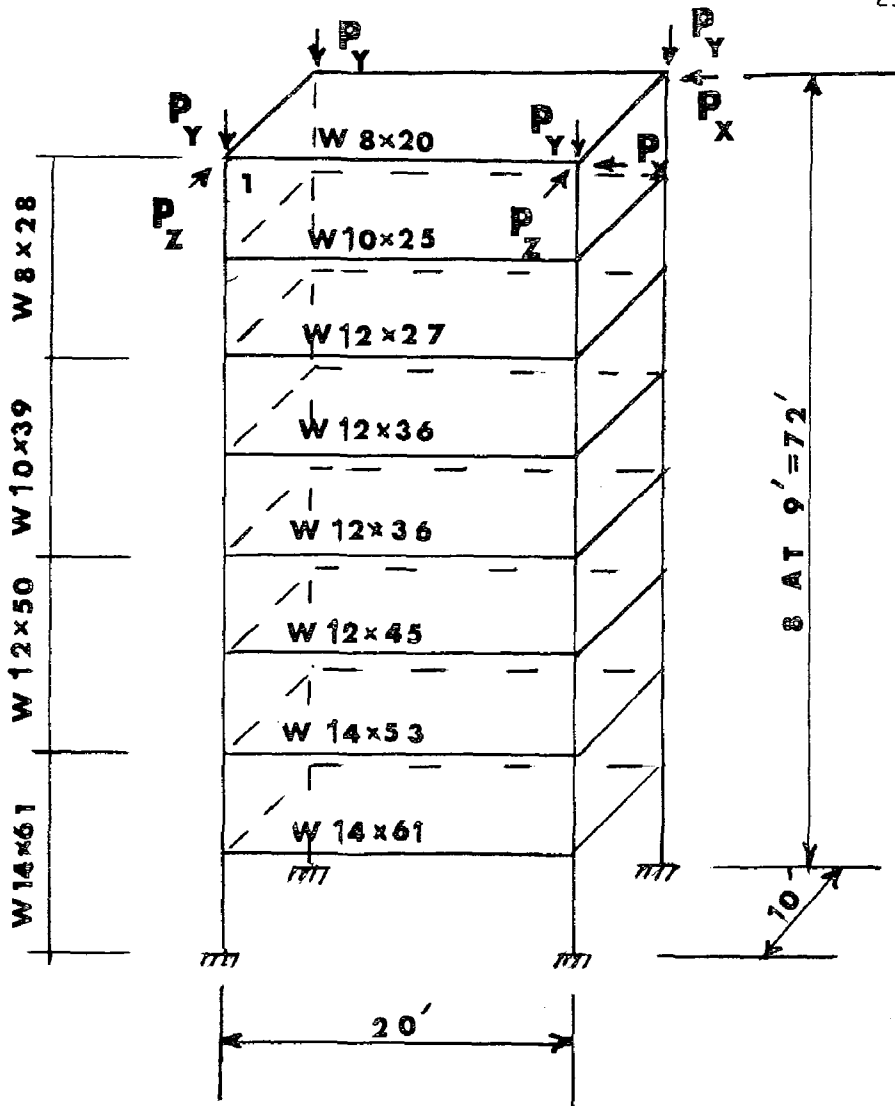


FIG. 2 LARGE FRAME

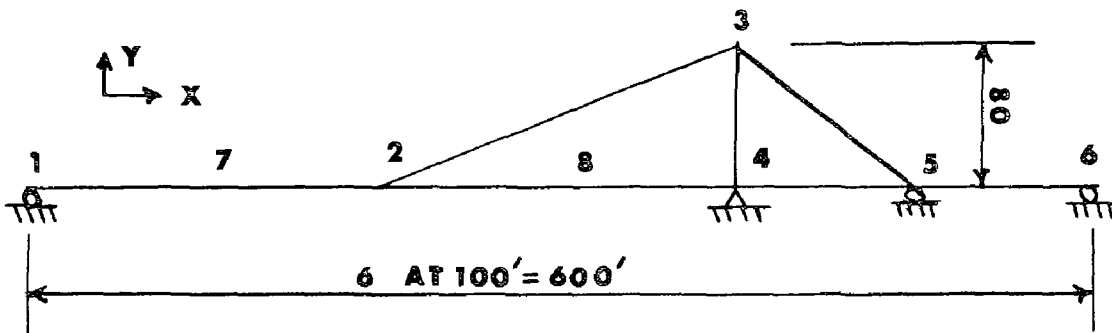


FIG. 3 CABLE STAYED BRIDGE

TABLE 1 - COMPARISON OF SOLUTIONS FOR SIMPLE FRAME

PEAK AMPLITUDE (1)	LINEAR ELASTIC		ELASTIC-PLASTIC 1		ELASTIC-PLASTIC 3		ELASTIC-PLASTIC 3	
	TIME STEP OF PEAK (2)	AMPLITUDE (IN) (3)	TIME STEP OF PEAK (3)	AMPLITUDE (IN) (5)	TIME STEP OF PEAK (6)	AMPLITUDE (IN) (7)	TIME STEP OF PEAK (8)	AMPLITUDE (IN) (9)
1st	9	.406	9	.406	8.5	.410	8.7	.412
2nd	18	-.702	18	-.703	17.5	-.707	17.7	-.709
3rd	27	.889	27	.890	27	.892	27	.892
4th	37	-1.055	37	-1.059	37	-1.067	36.8	-1.073
5th	46	1.280	46	1.231	45.5	1.234	45.9	1.260

ALL TIME STEPS ARE AT 0.07 SEC.

TABLE 2 - COMPARISON OF ELASTIC AND ELASTIC-PLASTIC SOLUTIONS FOR CABLE-STAYED BRIDGE

PEAK V 7 (1)	ELASTIC		ELASTIC-PLASTIC	
	TIME OF PEAK (SEC.) (2)	AMPLITUDE (FT.) (3)	TIME OF PEAK (SEC.) (4)	AMPLITUDE (FT.) (5)
1st	0.9	-.770	0.9	-.821
2nd	1.8	1.215	1.8	1.284
3rd	2.8	-1.590	2.8	-1.598
4th	3.7	1.805	3.8	1.857
5th	4.7	-1.690	4.8	-1.961
6th	5.7	1.485	5.8	1.827
7th	6.7	-1.205	6.7	-1.493
8th	7.8	.850	7.8	1.361
9th	9.1	-.900	8.8	-1.150

DATA WAS WRITTEN OUT AT $\Delta T = 0.10$ SEC.

to the accuracy of this description is fixed at $T_{min}/6$. That is, if not enough modes are chosen, the analysis will not yield an accurate description. However, its accuracy can be improved only by using more modes, not by decreasing the time step. For the elastic-plastic solution this may not be true. For that reason elastic-plastic 2 was run with four modes and a time step of 0.035 seconds. As can be seen, the results are basically the same as the previous case, indicating that the maximum time step for numerical stability is accurate enough for the description of elastic-plastic behavior.

Unlike the case for the linear elastic solution, the two elastic-plastic response solutions did not describe all the stress resultants accurately. The moment values checked out until instability occurred, but the thrusts in the columns were off somewhat. The vertical accelerations are very small; therefore the column thrusts should add up to around 400 kips (1789 kN). At $N=37$ in Elastic-plastic 1, their sum was 356.6 kips, a significant error. In order to determine how important an influence this defect in the solution has on the description of the structure's behavior, Elastic-plastic 3 was run. This response computation utilized 8 modes and a time step of 0.01 seconds. The column thrusts balanced completely, but other than this change, no differences exist between this solution and the previous two. It was decided that only four modes would be needed in elastic-plastic solutions.

An attempt was made to analyze the frame's response when subjected to earthquake loading. This was accomplished with the artificial accelerograms of (6). These accelerograms were generated by multiplying a stationary Gaussian process by a time dependent deterministic function. The stationary process and deterministic functions are chosen on the basis of statistical properties of the desired earthquake. Artificial earthquake 3 of (6) was chosen and 5 seconds of response were computed. The maximum acceleration of the quake in this time interval is around 0.108 gravity but this value was increased or decreased by multiplying the accelerogram by the necessary factor. Quake directions along the X axis and at an angle of 45 degrees with the X and Z axes were chosen. Very little plastic flow occurred in the frame prior to instability. However, when flow did occur in the columns, enough hinges were formed to start a collapse mechanism. The biaxial quake did not lead to any interaction effect on u_4 until failure occurred. That is, u_4 is basically a plot of the response of the frame to an accelerogram 0.707 times that of the artificial quake. Interaction, however, did lead to failure at a smaller amplitude.

The large frame (192 degrees of freedom) of Fig. 2

was also analyzed. Every floor has the same size girders while the columns change every two stories. Its static capacity was checked under the proportional loading system shown. The loads are in the ratios $P_y = 6P_x$ and $P_z = 2 P_x$ with half loads applied at the top story. Instability occurred at a load of $P_x = 2.06$ kips (9.16 kN); yield moments were exceeded at all columns in the bottom two stories. The displacements at node 1 were $u = 1.71$ inches (4.35 cm) and $w = 6.03$ inches (15.3 cm); very little non-linear behavior was revealed prior to the collapse load. The mode shapes for the structure were computed using an assumed dead load of 20 psf (958 N/m^2) on each floor. The fundamental frequency was 0.646 Hz corresponding to motion in the Z direction, while the second mode's frequency was .687 Hz and its displacement pattern indicates motion in the X-Z plane. All the mode shapes are what one would expect for the frame. Only the first nine mode shapes were computed ($f_g = 2.73$ Hz) and no vertical motion mode appeared among them. Response was computed for an earthquake acting in the Z direction with the acceleration of 0.486 gravity. The first 9 modes were used at a time step of 0.06 seconds. Again instability arose suddenly with little difference between the linear elastic solution and the nonlinear elastic-plastic solution until failure. Just as for the static case failure arose due to yielding of all the columns in the bottom two stories. In this solution, the column thrusts balanced out so that no error existed in the stress resultants. Until the final time step iterations converged in at most three trials; at the final step no convergence was reached after 20 iterations.

The dynamic analyses of the two frames were somewhat unsatisfactory in that their behavior could be described quite well by a linear elastic analysis. Such frames have no overload capacity when subjected to earthquake loadings. All columns yield together and form a collapse mechanism. A structure which does not reveal this type of behavior is shown in Fig. 3. This figure represents a planar cable-stayed bridge analysed elastically in a previous work (9). Its dead load was taken as 16 K/ft. The girder area is 8 sq. ft. (0.7 m^2) and its moment of inertia is 45 ft^4 (0.39 m^4) while the corresponding tower properties are 3 sq. ft. (0.3 m^2) and 20 ft^4 (0.173 m^4). A cable cross sectional area of 1.10 sq. ft. (0.1 m^2) was assumed; the cable tensions are 9696 kips (43 MN) in cable 2-3 and 11,500 kips (51 MN) in cable 3-5. Plastic properties were chosen to make the system yield under the applied dynamic load; $F_y = 2000$ ksf (95.8 MN/m^2) for the girder, 5000 ksf (239.4 MN/m^2) for the tower and 21,800 ksf ($1,050,000 \text{ MN/m}^2$) for the cable, along with $Z_w = 45 \text{ ft}^4$ (0.39 m^4) for the girder and 18 ft^4 for the tower. A comparison of solutions obtained

for a load of 500 kips (2.2 MN) applied at node 7 and varying as $\cos 3.00 t$ is shown in Table 2. 3 modes were all that is required for accurate results. The elastic solution was obtained from a previous nonlinear solution, where in 100 kips (450 kN) were applied, by multiplying the response by 5.00. This structure is basically linear so this would not introduce any error. Any correction would make the elastic solution larger because a cable-stayed bridge behaves as a softening spring. The results of the analysis are presented in Table 2. Behavior is as could be expected. However, it must be noted that significant plastic flow occurred in the system even in the first cycle. This is because the dead load moments must be included in the dynamic analysis. The interaction of thrust and moment resulted in large amounts of plastic flow at moments slightly larger than the dead load moments.

CONCLUSION

A method has been presented for the computation of the static and dynamic response of three dimensional space frameworks. While certain modifications were made in accepted static analysis procedures, these modifications appear to have a minor influence on the accuracy of the solutions obtained. On the other hand, complete nonlinear elastic-plastic solutions are possible with the use of little more computer time than is required for nonlinear elastic solutions. Of course, this does not mean that the amount of computer time needed to solve such dynamic problems is small; even nonlinear elastic solutions are quite time-consuming. The use of the modal superposition method does lead to a great saving in computer time because it makes it possible to use a much larger time step than the direct solution of the dynamic equations would permit.

BIBLIOGRAPHY

1. Adams, P. F., "Stability of Asymmetric Structures- Research Needs," Journal of the Structural Division, ASCE, Vol. 100, No. ST 11, Nov. 1974, pp. 2271-2274.
2. Bockholdt, J. L., and Weaver, W., "Inelastic Dynamic Analysis of Tier Buildings," Journal of Computers and Structures, Vol. 4, No. 3, May 1974, pp. 627-646.
3. Clough, R. W. and Penzien, J., "Dynamic of Structures," McGraw-Hill Book Company, Inc., 1974.
4. Gere, J. M. and Weaver, W., "Analysis of Frames Structures," D. Van Nostrand Company, Inc., 1965.

5. Goldberg, J. E. and Richard, R. M., "Analysis of Non-linear Structures," Journal of the Structural Division, ASCE, Vol. 89, No. ST 4, Aug. 1963, pp. 333-351.
6. Iyengar, R. N. and Iyengar, K.T.S.R., "Probabilistic Response Analysis to Earthquakes," Journal of the Engineering Mechanics Division, ASCE, Vol. 96, No. EM 3, June 1970, pp. 207-224.
7. Jonatowski, J. J. and Birnstiel, C., "Inelastic Stiffened Suspension Space Structures," Journal of the Structural Division, ASCE, Vol. 96, No. ST 6, June 1970, pp. 1143-1166.
8. Jonatowski, J. J. and Birnstiel, C., "Elasto-Plastic Analysis of Space Frameworks," Research Division Report, New York University, School of Engineering and Science, Bronx, N. Y., Sept. 1969.
9. Morris, N. F., "Dynamic Analysis of Cable-Stiffened Structures," Journal of the Structural Division, ASCE, Vol. 100, No. ST 5, May 1974, pp. 971-981.
10. Ortega, J., "The Givens-Householder Method for Symmetric Matrices," Mathematical Methods for Digital Computers, Vol. 2, Ralson, A. and Wilf, H.S. (ed.), John Wiley and Sons, Inc., 1967.
11. Santathadaporn, S. and Chen, W. F., "Interaction Curves for Sections Under Combined Biaxial Bending and Axial Force," Fritz Engineering Laboratory Report No. 331.3, Lehigh University, Bethlehem, Pa., Aug. 1968.
12. Tebedge, N. and Chen, W. F., "Design Criteria for H Columns Under Biaxial Loading," Journal of the Structural Division, Vol. 100, No. ST 3, March 1974, pp. 579-598.
13. Wen, R. K. and Farhoomand, F., "Dynamic Analysis of Inelastic Space Frames," Journal of the Engineering Mechanics Division, ASCE, Vol. 96, No. EM 5, Oct. 1970, pp. 667-686.

INTERNATIONAL SYMPOSIUM ON
EARTHQUAKE STRUCTURAL ENGINEERING

299

St. Louis, Missouri, USA, August, 1976

ON THE LIMIT ANALYSIS OF BOX-UNIT BUILDINGS UNDER STATIC
AND DYNAMIC EFFECTS

T.I.NASSONOVA, Dipl.Eng.,
M.J.FRAINT, Techn.M.

TSNIIEP zhyllischa
Moscow, USSR

SUMMARY

Some simple examples are given to show how the limit equilibrium extreme principles of elastic-plastic systems can be used to calculate box-unit buildings. The box-unit buildings are presented in the form of the system of imbound boxes i.e. in form of system with single-side ties.

INTRODUCTION

To calculate the ultimate load for the box-unit building one can use the limit equilibrium methods, devised by A.A.Gvozdev [3] and developed by S.M.Bernshtein [2] for systems with single-side ties.

The calculations of stability against overturning commonly used are particular cases of static (or kinematic) limit equilibrium principles application. These principles can be used to find destruction mechanism of the systems with single-side ties.

It is also important to take into account the fact that reactions in ties between boxes can have only one direction under dynamic load and vibrations. Application of extreme principles of the systems with single-side ties may simplify calculation in this case.

Structural system of box-unit building may be considered as a system with single-side ties.

BOX-UNIT COLUMN UNDER STATIC HORIZONTAL LOADS

The limit equilibrium box-unit column is considered. It is assumed that all boxes are identical. Calculation scheme, dimensions, loads and possible destruction mechanism are shown in Fig.1.

The load factor P_i , corresponding to i -th possible destruction mechanism can be obtained using the equation

$$A_{load} + A_{vez} = 0, \quad (1)$$

where A_{load} - action of load

A_{vez} - action of vertical forces of stability against overturning.

For the i -th possible destruction mechanism these effects are expressed as follows:

$$A_{load} = P_i \int_0^{h_i} q(x)(h_i - x) \varphi dx = P_i m_i^{load} \varphi \quad (2)$$

$$A_{vez} = -G_i \frac{b}{2} \varphi = -M_i^{vez} \varphi \quad (3)$$

in which h - storey height

m_i^{load} - moment of load unit $q(x)$

M_i^{vez} - moment of stability against overturning

(other symbols are given in Fig.1).

From equations (1), (2) and (3) the result is

$$P_i = \frac{M_i^{vez}}{m_i^{load}} \quad (4)$$

The limit value of load factor can be obtained from the following extreme problem

$$\bar{P}_i = \min P_i \quad (5)$$

If $q(x)$ sign is not changed along axis x minimum P_i is reached by $i = n$

Normally the necessary reliability of structure is secured introducing into formula the respective reliability factors. In above formular reliability factors of materials resistance can not be used. Therefore value of \bar{P} should be decreased 1.5 times and design load value P^{des} should be determined from the following equation:

$$P^{des} = 0.67 \frac{M_n^{vez}}{m_n^{load}} \quad (4')$$

and weight of boxes has to be taken into account with the coefficient of correction 0.9.

The values of summarized wind pressure - Q^{wind} and design load by (4') Q^{des} acting on a box - unit building diameter made of two box-unit columns are shown in Fig.2. For those calculations the following initial data is accepted: $G = 9.55t.$, $b = 5.2m.$, $h = 2.75m.$

As appears from Fig.2 ultimate height of box-unit building should not exceed 16 storeys, if boxes are not tied together

The above mechanism corresponds to a rotation of column around the edge of lower joint, the contact area of lower box being equal to zero and compressive stresses being infinitely large.

It would be correct to take into account deformations and limited strength of materials and so bi-linear stress-strain diagram for mortar joint should be taken into consideration (Fig.3).

This diagram is characterized by 3 values: σ_y - yield stress, U_y - displacement of beginning yield, U_u - maximum displacement.

The limitation on displacements by U_u is equal to limitation stipulating failure of concrete or mortar joint.

To simplify let us assume that all joints are identical. In this case the box-unit column strength has to be determined by strength of lower joint as given above. However, forces of stability produce moment M_i about center of gravity of compressive stress epure in contact area. It leads to decrease in the load bearing capacity.

So, load factor is to be calculated by formula (4'), but ultimate load has to be reduced by coefficient β which is

$$\beta = \frac{2Z_0}{b} \quad (6)$$

Where Z_0 - distance between above centre of gravity and center of the column.

If boxes rest upon each other with 4 sides, value β , as a rule, can be about 1. If boxes rest with 2 longitudinal sides, the value β can be obtained thus:

$$\beta = 1 - \frac{\gamma(\psi^2 - 3\psi + 3)}{1.5(2 - \psi)^2} \quad (7)$$

$$\gamma = \frac{2nG}{\sigma_y \delta_{joint} b}, \quad b = \frac{U_y}{U_u}$$

δ_{joint} - summarized width of joints

As regards the above example, the values Q_{des} were calculated by accounting for the coefficient β which was calculated by (6), where $\sigma_y = 130 \text{ kg/cm}^2$, $\delta_{joint} = 20 \text{ cm}$, $\psi = 1$ or 0.1

These values are shown in Fig.2.

The decrease in the load bearing capacity is 10-15%.

NATURAL VIBRATIONS OF BOX-UNIT COLUMN

The static load upon the box-unit column was considered above.

There is under consideration single-degree of freedom system shown in fig.4.

If small natural vibrations are considered equation of mass motion to the right can be written as follows

$$\ddot{\varphi} = f(\varphi) \lambda^2 \quad (8)$$

$$\lambda^2 = \frac{0.5 \cdot \beta \cdot g}{(H^2 + 0.25 \beta^2)} \quad (9)$$

$$f(\varphi) = \text{Sign}(\varphi) \quad (10)$$

g - gravity acceleration
(Cf. Fig.4).

Since $f(\varphi) = -f(-\varphi)$ non-linear equation (9) can be sufficiently precisely replaced by the linear equation [1]

$$\ddot{\varphi} + k^2 \varphi = 0 \quad (11)$$

in which

$$k^2 \approx \frac{4 \lambda^2}{3A}$$

A - amplitude of vibrations

As it is followed from (11) the frequency of natural vibrations depends on the amplitude and not on the mass. The diagram frequency of natural vibrations - amplitude is shown in Fig.5. In the design scheme under consideration the value H was accepted as equal $2/3$ of the building height. Experimental results obtained by vibration tests are shown in Fig.5 too.

As it follows from Fig.5 the experimental values can become equal to theoretical values when the amplitude is 2-3cm.

Hence, it is necessary when calculating to take into account the considered above vibration form.

CONCLUSION

The simple example dealt with in this paper show, that the box-unit building can be calculated by means of the limit equilibrium method.

More complicated cases require using linear programming and extreme properties of ultimate load [1,2], deformation time and residual deformation [4].

These examples confirm the fact, calculations of the elastic-plastic systems and systems with single-side ties are analogous.

The authors express their deep acknowledgement to their scientific adviser prof.G.A.Shapiro D.Sc.(Eng.) for his kind suggestion in carrying out this work.

REFERENCES

1. Бабаков И.М. Теория колебаний. "Наука", Ф.М.Л., М., 1968.
2. Бернштейн М.С. Расчет конструкций с односторонними связями. Стройиздат, 1947.
3. Гвоздев А.А. Расчет несущей способности конструкций по методу предельного равновесия. Госстройиздат, 1949.
4. Ерхов М.И. О приближенном решении задач динамики жестко-пластических конструкций. В сборнике "Новые методы расчета строительных конструкций" под редакцией проф. А.Р.Ржаницина, Стройиздат, 1968.

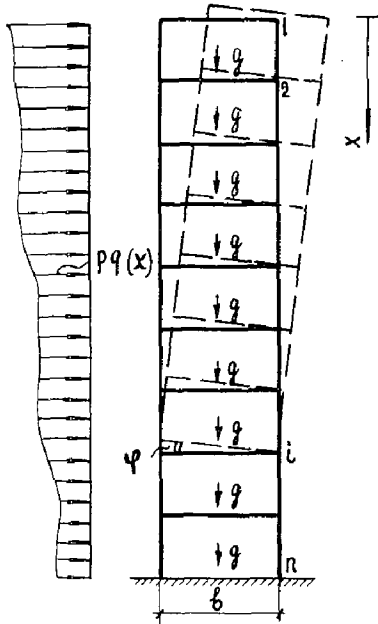


Fig. 1

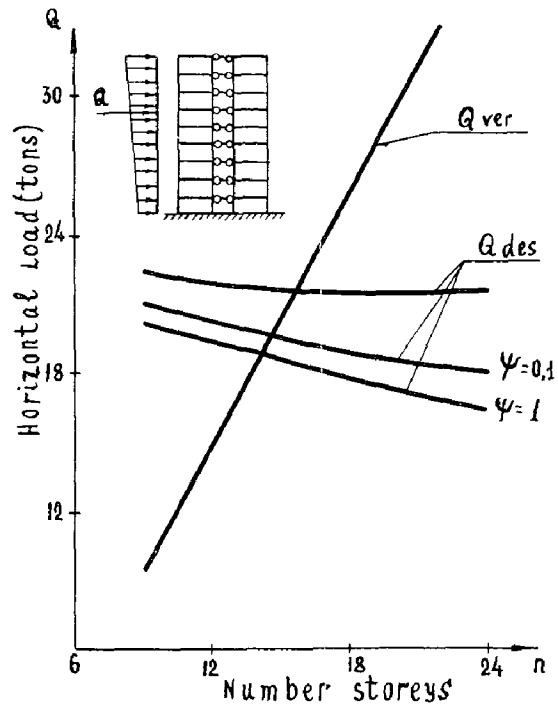


Fig. 2

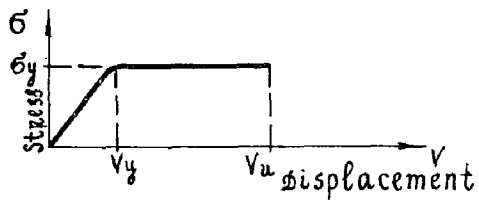


Fig. 3

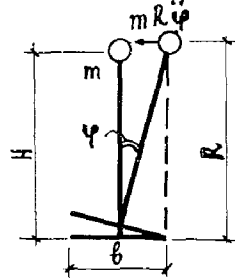


Fig. 5

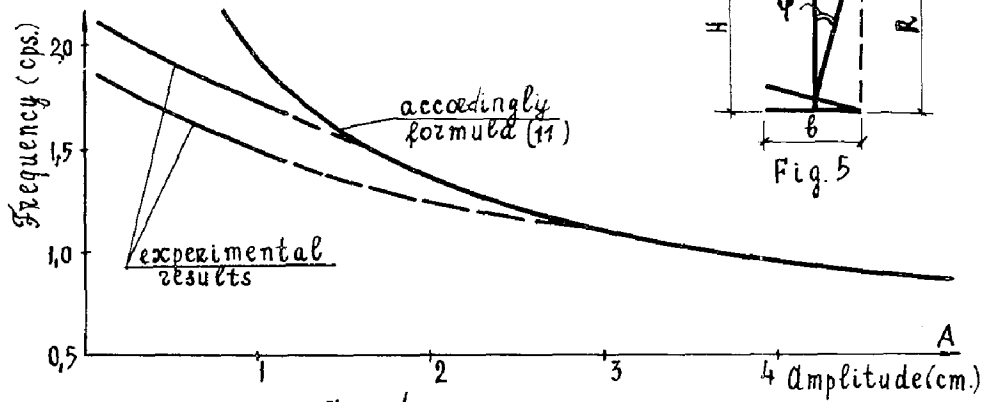


Fig. 4

DYNAMIC RESPONSE OF CANTILEVER BEAM - COLUMNS
WITH ATTACHED MASSES SUPPORTED ON A FLEXIBLE FOUNDATION

ANTHONY N. KOUNADIS

ASSOCIATE PROFESSOR

Nat. Techn. University of Athens

Athens, Greece

Summary

In this paper, the dynamic response of steel multi-story buildings with a concrete-core, supported on a flexible foundation and subjected to an arbitrary dynamic force or to a horizontal movement of the ground induced by an earthquake, is established by analyzing an equivalent continuous model. This model consists of a cantilever with translational and rotational springs at its support, carrying n concentrated masses at the floor levels. The influence of the rotatory inertia of the masses as well as of an initial constant compressive force acting at the free end of the cantilever, are also included. The free and forced motion of the aforementioned model is investigated, using generalized functions.

It is found that: a) the effect of the translational spring on the eigenfrequencies of the first three modes is considerably higher than that of the rotational spring; b) the effect of the translational and the rotatory inertia of the mass of the foundation on the frequency of the fundamental mode is appreciable.

Introduction

Recently, for economic and structural reasons, a great number of high-rise steel buildings with a reinforced concrete-core, resisting the wind and earthquake forces, have been constructed. The dynamic response of such buildings is usually established by analyzing an equivalent model made up of a massless cantilever with concentrated masses at the floor levels. A more accurate model will include the effect of the mass distribution of the core. Moreover, if the building is constructed on relatively soft soil, it may be necessary to consider the effect of the displacement of the foundation. Investigations of earthquake response have shown that the support flexibility has little effect on the stress distribution in the building; however, it may have a significant influence on the eigenfrequencies⁽²⁾.

In this investigation, a rigorous analysis of the dynamic response of a cantilever beam with translational and rotational elastic springs at its support, carrying n concentrated masses, is presented. The influences of the rotatory inertia of the masses and of an initial constant axial compressive force P are also included.

A closed form solution for the determination of eigenfrequencies and mode shapes, is given in matrix form. Furthermore, the differential equation for establishing the modal amplitude of the cantilever beam-column, subjected to an arbitrary dynamic force or to a horizontal movement of the support induced by an earthquake, is also presented using generalized functions^{(1) (3)}.

Mathematical analysis

Assuming that the concentrated masses M_1, M_2, \dots, M_n are attached at points located at $\alpha_1, \alpha_2, \dots, \alpha_n = l$ respectively from the support of the cantilever (Fig. 1), the equation of motion is

$$Ely'''' + \left[m + \sum_{i=1}^{n-1} M_i \delta(x-\alpha_i) \right] \ddot{y} - \sum_{i=1}^{n-1} J_i \delta'(x-\alpha_i) \dot{y}' + Py'' = f(t) \left[p(x) + \sum_{i=1}^{n-1} F_i \delta(x-\alpha_i) \right] \quad (1)$$

where $f(t)$ is the forcing function taken the same for all applied forces ; $p(x) = p_0 [H(x-x_j)-H(x-x_k)]$ is a distributed lateral load per unit length extending over a portion of the length of the beam x_k-x_j ($x_k > x_j$) ; F_i (1, 2, ..., n) is a concentrated lateral force acting on the i th concentrated mass.

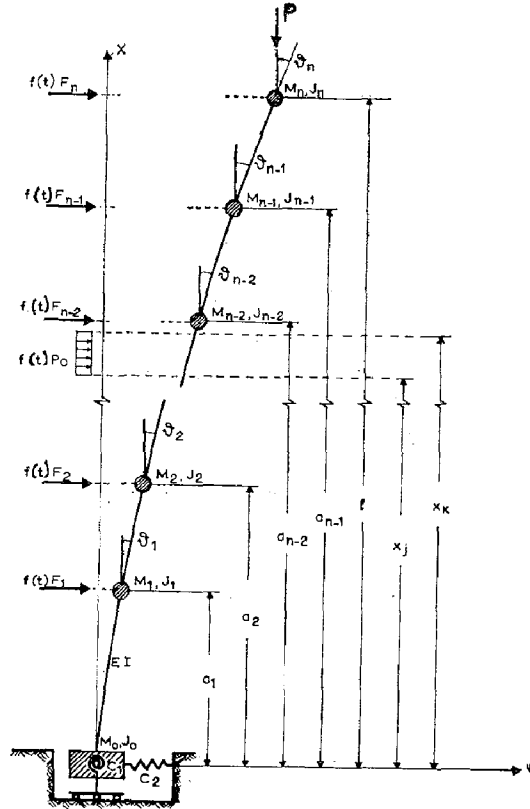


Fig 1. Cantilever beam - column with attached masses supported on flexible afoundation

The solution of equation(1) must satisfy the following conditions at the ends of the cantilever beam - column :

$$\left. \begin{aligned} \text{at } x=0 : & \quad Ely''(0, t) = C_1 y'(0, t) + J_0 \ddot{y}''(0, t), & \quad Ely'''(0, t) = -C_2 y(0, t) - Py'(0, t) - M_0 \ddot{y}(0, t) \\ \text{at } x=l : & \quad Ely''(l, t) = -J_n \ddot{y}''(l, t), & \quad Ely'''(l, t) = M_n \ddot{y}(l, t) - Py'(l, t) - f(t)F_n \end{aligned} \right\} \quad (2)$$

where C_1, C_2 are the rotational and translational spring constants, respectively. In the case of a lateral movement y_s of the support of the cantilever beam - column, as for example in motion induced by an earthquake, the acceleration of the support is usually a known function of time $\ddot{y}_s = \ddot{y}_{s0} f(t)$, where \ddot{y}_{s0} is the maximum support acceleration and $f(t)$ is the time function for support acceleration. Equations (1) and (2) are valid for this case, if y is taken as the relative displacement of the axis of the beam with re-

spect to its support, while the term in brackets on the right - hand side of equation (1) is replaced by $\left[-m\ddot{y}_{so} - \ddot{y}_{so} \sum_{i=1}^{n-1} M_i \delta(x-\alpha_i) \right]$ and F_n in equation (2) is replaced by $-\ddot{y}_{so}M_n$.

Free Vibrations

For free vibrations, the solution of equation (1) is of the form

$$y(x, t) = \bar{Y}(x)e^{i\omega t} \quad (3)$$

Introducing the nondimensional coordinates

$$\xi = \frac{x}{l}, \quad Y(\xi) = \frac{\bar{Y}}{l}, \quad \bar{\alpha}_i = \frac{\alpha_i}{l} \quad (4)$$

and substituting (3) into (1) and (2), the following relations are obtained

$$-\frac{d^4 Y(\xi)}{d\xi^4} - k^4 \left[1 + \sum_{i=1}^{n-1} \bar{M}_i \delta(\xi - \bar{\alpha}_i) \right] Y(\xi) + k^4 \left[\sum_{i=1}^{n-1} \bar{J}_i \delta'(\xi - \bar{\alpha}_i) \right] \frac{dY(\xi)}{d\xi} + \beta^2 \frac{d^2 Y(\xi)}{d\xi^2} = 0 \quad (5)$$

$$\left. \begin{aligned} \text{at } \xi = 0: \quad & \frac{d^2 Y(0)}{d\xi^2} = \bar{C}_1 \frac{dY(0)}{d\xi} - k^4 \bar{J}_0 \frac{dY(0)}{d\xi}, \quad \frac{d^3 Y(0)}{d\xi^3} = -\bar{C}_2 Y(0) - \beta^2 \frac{dY(0)}{d\xi} + k^4 \bar{M}_0 Y(0) \\ \text{at } \xi = 1: \quad & \frac{d^2 Y(1)}{d\xi^2} = k^4 \bar{J}_n \frac{dY(1)}{d\xi}, \quad \frac{d^3 Y(1)}{d\xi^3} = -k^4 \bar{M}_n Y(1) - \beta^2 \frac{dY(0)}{d\xi} \end{aligned} \right\} \quad (6)$$

where

$$\left. \begin{aligned} k^4 &= \frac{m\omega^2}{EI} l^4, \quad \bar{M}_i = \frac{M_i}{ml}, \quad \bar{J}_i = \frac{J_i}{ml^3} \quad (i=0, 1, \dots, n) \\ \beta^2 &= \frac{Pl^2}{EI}, \quad \bar{C}_1 = \frac{C_1 l}{EI}, \quad \bar{C}_2 = \frac{C_2 l^3}{EI} \end{aligned} \right\} \quad (7)$$

Taking the Laplace transform of the differential equation (5) and the kinematic boundary conditions of (6), solving for the Laplace transform and inverting the result, the following solution is obtained

$$Y(\xi) = \varphi_1(\xi)Y(0) + \varphi_2(\xi)Y'(0) + \sum_{i=1}^{n-1} H(\xi - \bar{\alpha}_i) [\bar{M}_i Y(\bar{\alpha}_i) F_2(\xi - \bar{\alpha}_i) - \bar{J}_i Y'(\bar{\alpha}_i) F'_2(\xi - \bar{\alpha}_i)] \quad (8)$$

where H is the Heaviside function and

$$\left. \begin{aligned} \varphi_1(\xi) &= F_1(\xi) - (\bar{C}_2 - \bar{J}_0) F_2(\xi), \quad \varphi_2(\xi) = F'_2(\xi) + (\bar{C}_1 - \bar{J}_0) F'_2(\xi) \\ F_1(\xi) &= \frac{1}{\varepsilon^2 + \zeta^2} (\varepsilon^2 \cosh \zeta \xi + \zeta^2 \cos \varepsilon \xi), \quad F_2(\xi) = \frac{1}{\varepsilon^2 + \zeta^2} \left(\frac{1}{\zeta} \sinh \zeta \xi - \frac{1}{\varepsilon} \sin \varepsilon \xi \right) \\ \zeta &= \sqrt{-\frac{\beta^2}{2} + \sqrt{\frac{\beta^4}{4} + k^4}}, \quad \varepsilon = \sqrt{\frac{\beta^2}{2} + \sqrt{\frac{\beta^4}{4} + k^4}} \\ \bar{M}_i^* &= k^4 \bar{M}_i, \quad \bar{J}_i^* = k^4 \bar{J}_i, \quad i = 0, 1, 2, \dots, n \end{aligned} \right\} \quad (9)$$

Differentiation of equation (8) yields

$$Y'(\xi) = \varphi'_1(\xi)Y(0) + \varphi'_2(\xi)Y'(0) + \sum_{i=1}^{n-1} H(\xi - \bar{\alpha}_i) [\bar{M}_i^* Y(\bar{\alpha}_i) F'_2(\xi - \bar{\alpha}_i) - \bar{J}_i^* Y'(\bar{\alpha}_i) F''_2(\xi - \bar{\alpha}_i)] \quad (10)$$

Using equation (8), the natural boundary conditions in relations (6) give

$$\left. \begin{aligned} f_1(1)Y(0) + f_2(1)Y'(0) + \sum_{i=1}^{n-1} [\bar{M}_i^* Y(\bar{\alpha}_i) \Phi_1(1 - \bar{\alpha}_i) - \bar{J}_i^* Y'(\bar{\alpha}_i) \Phi'_1(1 - \bar{\alpha}_i)] &= 0 \\ f_3(1)Y(0) + f_4(1)Y'(0) + \sum_{i=1}^{n-1} [\bar{M}_i^* Y(\bar{\alpha}_i) \Phi_2(1 - \bar{\alpha}_i) - \bar{J}_i^* Y'(\bar{\alpha}_i) \Phi'_2(1 - \bar{\alpha}_i)] &= 0 \end{aligned} \right\} \quad (11)$$

where

$$\left. \begin{aligned} f_1(1) &= \varphi_1''(1) - J_n^* \varphi_1'(1) & , & & f_2(1) &= \varphi_2''(1) - J_n^* \varphi_2'(1) \\ f_3(1) &= \varphi_1'''(1) + M_n^* \varphi_1(1) + \beta^2 \varphi_1'(1) & , & & f_4(1) &= \varphi_2'''(1) + M_n^* \varphi_2(1) + \beta^2 \varphi_2'(1) \\ \Phi_1(1 - \bar{\alpha}_i) &= F_2''(1 - \bar{\alpha}_i) - J_n^* F_2'(1 - \bar{\alpha}_i) & , & & \Phi_2(1 - \bar{\alpha}_i) &= F_2'''(1 - \bar{\alpha}_i) + M_n^* F_2(1 - \bar{\alpha}_i) + \beta^2 F_2'(1 - \bar{\alpha}_i) \end{aligned} \right\} (12)$$

By evaluating equations (8) and (10) for $\xi = \bar{\alpha}_1, \dots, \bar{\alpha}_{n-1}$ and using equations (11), the following system of $2n$ homogeneous equations is obtained on the unknowns $Y(0), Y(\bar{\alpha}_1), \dots, Y(\bar{\alpha}_{n-1}), Y'(0), Y'(\bar{\alpha}_1), \dots, Y'(\bar{\alpha}_{n-1})$.

$$\begin{bmatrix} A_{11} & A_{12} \\ A_{21} & A_{22} \end{bmatrix} \begin{bmatrix} Y \\ Y' \end{bmatrix} = 0 \tag{13}$$

where

$$A_{11} = \begin{bmatrix} \varphi_1(\bar{\alpha}_1) & -1 \dots & \dots & 0 \\ \varphi_1(\bar{\alpha}_2) & M_1^* F_2(\bar{\alpha}_2 - \bar{\alpha}_1) & -1 \dots & \dots & 0 \\ \dots & \dots & \dots & \dots & \dots \\ \varphi_1(\bar{\alpha}_{n-1}) & M_1^* F_2(\bar{\alpha}_{n-1} - \bar{\alpha}_1) & M_2^* F_2(\bar{\alpha}_{n-1} - \bar{\alpha}_2) \dots M_{n-2}^* F_2(\bar{\alpha}_{n-1} - \bar{\alpha}_{n-2}) & -1 & \dots \\ f_1(1) & M_1^* \Phi_1(1 - \bar{\alpha}_1) & M_2^* \Phi_1(1 - \bar{\alpha}_2) \dots \dots M_{n-2}^* \Phi_1(1 - \bar{\alpha}_{n-2}) & M_{n-1}^* \Phi_1(1 - \bar{\alpha}_{n-1}) & \dots \end{bmatrix} \tag{14}$$

$$A_{12} = \begin{bmatrix} \varphi_2(\bar{\alpha}_1) & 0 \dots & \dots & 0 \\ \varphi_2(\bar{\alpha}_2) & -J_1^* F_2'(\bar{\alpha}_2 - \bar{\alpha}_1) & 0 \dots & \dots & 0 \\ \dots & \dots & \dots & \dots & \dots \\ \varphi_2(\bar{\alpha}_{n-1}) & -J_1^* F_2'(\bar{\alpha}_{n-1} - \bar{\alpha}_1) & -J_2^* F_2'(\bar{\alpha}_{n-1} - \bar{\alpha}_2) \dots -J_{n-2}^* F_2'(\bar{\alpha}_{n-1} - \bar{\alpha}_{n-2}) & 0 & \dots \\ f_2(1) & -J_1^* \Phi_1'(1 - \bar{\alpha}_1) & -J_2^* \Phi_1'(1 - \bar{\alpha}_2) \dots \dots -J_{n-2}^* \Phi_1'(1 - \bar{\alpha}_{n-2}) -J_{n-1}^* \Phi_1'(1 - \bar{\alpha}_{n-1}) & \dots & \dots \end{bmatrix} \tag{15}$$

$$A_{21} = \begin{bmatrix} \varphi_1'(\bar{\alpha}_1) & 0 \dots & \dots & 0 \\ \varphi_1'(\bar{\alpha}_2) & M_1^* F_2'(\bar{\alpha}_2 - \bar{\alpha}_1) & 0 \dots & \dots & 0 \\ \dots & \dots & \dots & \dots & \dots \\ \varphi_1'(\bar{\alpha}_{n-1}) & M_1^* F_2'(\bar{\alpha}_{n-1} - \bar{\alpha}_1) & M_2^* F_2'(\bar{\alpha}_{n-1} - \bar{\alpha}_2) \dots M_{n-2}^* F_2'(\bar{\alpha}_{n-1} - \bar{\alpha}_{n-2}) & 0 & \dots \\ f_3(1) & M_1^* \Phi_2(1 - \bar{\alpha}_1) & M_2^* \Phi_2(1 - \bar{\alpha}_2) \dots \dots M_{n-2}^* \Phi_2(1 - \bar{\alpha}_{n-2}) & M_{n-1}^* \Phi_2(1 - \bar{\alpha}_{n-1}) & \dots \end{bmatrix} \tag{16}$$

$$A_{22} = \begin{bmatrix} \varphi_2'(\bar{\alpha}_1) & -1 \dots & \dots & 0 \\ \varphi_2'(\bar{\alpha}_2) & -J_1^* F_2''(\bar{\alpha}_2 - \bar{\alpha}_1) & -1 \dots & \dots & 0 \\ \dots & \dots & \dots & \dots & \dots \\ \varphi_2'(\bar{\alpha}_{n-1}) & -J_1^* F_2''(\bar{\alpha}_{n-1} - \bar{\alpha}_1) & -J_2^* F_2''(\bar{\alpha}_{n-1} - \bar{\alpha}_2) \dots \dots -J_{n-2}^* F_2''(\bar{\alpha}_{n-1} - \bar{\alpha}_{n-2}) & -1 & \dots \\ f_4(1) & -J_1^* \Phi_2'(1 - \bar{\alpha}_1) & -J_2^* \Phi_2'(1 - \bar{\alpha}_2) \dots \dots \dots -J_{n-2}^* \Phi_2'(1 - \bar{\alpha}_{n-2}) -J_{n-1}^* \Phi_2'(1 - \bar{\alpha}_{n-1}) & \dots & \dots \end{bmatrix} \tag{17}$$

$$\left. \begin{aligned} Y &= \{Y(0) \ Y(\bar{\alpha}_1), \dots, Y(\bar{\alpha}_{n-1})\}^T \\ Y' &= \{Y'(0) \ Y'(\bar{\alpha}_1), \dots, Y'(\bar{\alpha}_{n-1})\}^T \end{aligned} \right\} \tag{18}$$

where the superscript τ indicates the transpose of the matrix. For a non-trivial solution, the determinant of the system (13) must vanish, resulting in the following frequency equation

$$\begin{bmatrix} A_{11} & A_{12} \\ A_{21} & A_{22} \end{bmatrix} = 0 \tag{19}$$

Computation of Mode Shapes

When the natural frequencies ω_n are established, the corresponding mode shapes of the cantilever beam - column may be obtained as follows :

By evaluating equation (8) for $\xi = \bar{\alpha}_1, \bar{\alpha}_2, \dots, \bar{\alpha}_{n-1}$, equation (10) for $\xi = \bar{\alpha}_1, \bar{\alpha}_2, \dots, \bar{\alpha}_{n-1}, 1$ and using the first of equations (11), the following system of $2n$ equations is obtained

$$\begin{bmatrix} A_{11}^m & A_{12}^m \\ \bar{A}_{21}^m & \bar{A}_{22}^m \end{bmatrix} \begin{bmatrix} Y_m \\ Y'_m \end{bmatrix} = \begin{bmatrix} 0 \\ \Psi'_m \end{bmatrix} \tag{20}$$

where the matrices A_{11}^m, A_{12}^m are given by equations (14), (15) for $\omega = \omega_m$ respectively, the column matrices Y_m, Y'_m are given by equations (18) and

$$\bar{A}_{21}^m = \begin{bmatrix} \varphi'_1(\bar{\alpha}_1) & 0 \dots & \dots & 0 \\ \varphi'_1(\bar{\alpha}_2) & \bar{M}_1 F'_2(\bar{\alpha}_2 - \bar{\alpha}_1) & 0 \dots & \dots & 0 \\ \dots & \dots & \dots & \dots & \dots \\ \varphi'_1(\bar{\alpha}_{n-1}) & \bar{M}_1 F'_2(\bar{\alpha}_{n-1} - \bar{\alpha}_1) & \bar{M}_2 F'_2(\bar{\alpha}_{n-1} - \bar{\alpha}_2) \dots & \bar{M}_{n-2} F'_2(\bar{\alpha}_{n-1} - \bar{\alpha}_{n-2}) & 0 \\ \varphi'_1(1) & \bar{M}_1 F'_2(1 - \bar{\alpha}_1) & \bar{M}_2 F'_2(1 - \bar{\alpha}_2) \dots \dots & \bar{M}_{n-2} F'_2(1 - \bar{\alpha}_{n-2}) & \bar{M}_{n-1} F'_2(1 - \bar{\alpha}_{n-1}) \end{bmatrix} \tag{21}$$

$$\bar{A}_{22}^m = \begin{bmatrix} \varphi'_2(\bar{\alpha}_1) & -1 \dots & \dots & 0 \\ \varphi'_2(\bar{\alpha}_2) & -\bar{J}_1 F_2''(\bar{\alpha}_2 - \bar{\alpha}_1) & -1 \dots & \dots & 0 \\ \dots & \dots & \dots & \dots & \dots \\ \varphi'_2(\bar{\alpha}_{n-1}) & -\bar{J}_1 F_2''(\bar{\alpha}_{n-1} - \bar{\alpha}_1) & -\bar{J}_2 F_2''(\bar{\alpha}_{n-1} - \bar{\alpha}_2) \dots & -\bar{J}_{n-2} F_2''(\bar{\alpha}_{n-1} - \bar{\alpha}_{n-2}) & -1 \\ \varphi'_2(1) & -\bar{J}_1 F_2''(1 - \bar{\alpha}_1) & -\bar{J}_2 F_2''(1 - \bar{\alpha}_2) \dots \dots & -\bar{J}_{n-2} F_2''(1 - \bar{\alpha}_{n-2}) & -\bar{J}_{n-1} F_2''(1 - \bar{\alpha}_{n-1}) \end{bmatrix} \tag{22}$$

$$\Psi'_m = \{0, 0, \dots, Y'_m(1)\}^T \tag{23}$$

The above system of equations may be inverted to yield

$$\begin{bmatrix} Y_m \\ Y'_m \end{bmatrix} = \begin{bmatrix} A_{11}^m & A_{12}^m \\ \bar{A}_{21}^m & \bar{A}_{22}^m \end{bmatrix}^{-1} \begin{bmatrix} 0 \\ \Psi'_m \end{bmatrix} \tag{24}$$

Consequently Y_m, Y'_m are determined as functions of the arbitrary constant $Y'_m(1) \neq 0$. Y_m, Y'_m determined, as discussed above, may be substituted in equation (8) to yield the corresponding mode shapes. The general solution obtained by superimposing the characteristic shapes is

$$\bar{y}(\xi, t) = \sum_{m=1}^{\infty} Y_m(\xi) [C_m \sin \omega_m t + D_m \cos \omega_m t] \tag{25}$$

where $\bar{y} = y/l$ is the dimensionless deflection and C_m, D_m are constants which are determined from the initial conditions.

Forced Motion

The dynamic deflection may be expressed in series of the characteristic mode shapes

$$y(x, t) = \sum_{m=1}^{\infty} \bar{Y}_m(x) A_m(t) \tag{26}$$

where $A_m(t)$ is the modal amplitude.

Using the Lagrange equation of motion, the following differential equation for establishing the modal amplitude $A_m(t)$ may be obtained

$$\ddot{A}_m(t) + \omega_m^2 A_m(t) = \frac{f(t) \left[\int_0^l p(x) \bar{Y}_m(x) dx + \sum_{i=1}^n F_i \bar{Y}_m(\alpha_i) \right]}{m \int_0^l \bar{Y}_m^2(x) dx + \sum_{i=1}^n [M_i \bar{Y}_m^2(\alpha_i) + J_i \bar{Y}_m'^2(\alpha_i)]} \tag{27}$$

In the case of lateral motion of the support having a $\ddot{y}_s = \ddot{y}_{s0} f(t)$ acceleration, the term in the brackets in the numerator of the right-hand side of equation (27) must be replaced by $-[m \ddot{y}_{s0} \int_0^l \bar{Y}_m(x) dx +$

$\ddot{y}_{so} \sum_{i=1}^n M_i \bar{Y}_m(\alpha_i) \left. \right\}$ For this case, equation (27) may be rewritten in nondimensionalized coordinates as

$$\ddot{A}_m(\tau) + 4\pi^2 A_m(\tau) = -f(\tau) \ddot{\eta}(\tau) \Gamma_m \quad (28)$$

where

$$\eta = \frac{y_s}{l}, \quad \tau = \frac{t}{T_m} \quad (29)$$

$A_m(\tau)$ is the modal amplitude of the relative displacement of the axis of the cantilever with respect to its support; T_m is the natural period of the m th mode; Γ_m is the modal participation factor defined as

$$\Gamma_m = \frac{\int_0^1 Y_m(\xi) d\xi + \sum_{i=1}^n \bar{M}_i Y_m(\alpha_i)}{\int_0^1 Y_m^2(\xi) d\xi + \sum_{i=1}^n [M_i Y_m^2(\bar{\alpha}_i) + J_i Y_m^2(\bar{\alpha}_i)]} \quad (30)$$

The integrals in the above expression for Γ_m are evaluated as follows

$$\int_0^1 Y_m(\xi) d\xi = [Y_m \ Y'_m] \{r_m \ S_m\}^T, \quad \int_0^1 Y_m^2(\xi) d\xi = [Y_m \ Y'_m] \begin{bmatrix} R_m & Q_m \\ Q_m^T & S_m \end{bmatrix} \begin{bmatrix} Y_m \\ Y'_m \end{bmatrix} \quad (31)$$

where

$$\left. \begin{aligned} r_m &= \{r_1^m \ r_2^m \ \dots \ r_{n-1}^m\}^T, & S_m &= \{S_1^m \ S_2^m \ \dots \ S_{n-1}^m\}^T \\ r_1^m &= \int_0^1 \varphi_1(\xi) d\xi, & S_1^m &= \int_0^1 \varphi_2(\xi) d\xi, \\ r_i^m &= \bar{M}_i \int_{\bar{\alpha}_i}^1 F_2(\xi - \bar{\alpha}_i) d\xi, & S_j^m &= -J_j \int_{\bar{\alpha}_j}^1 F'_2(\xi - \bar{\alpha}_j) d\xi, \quad (i=2, \dots, n-1) \end{aligned} \right\} \quad (32)$$

$$R_m = \begin{bmatrix} r_{11}^m & r_{12}^m \dots r_{1, n-1}^m \\ & r_{22}^m \dots r_{2, n-1}^m \\ \text{Symmetr.} & \dots \\ & r_{n-1, n-1}^m \end{bmatrix} \quad \text{with: } \left. \begin{aligned} r_{11}^m &= \int_0^1 \varphi_1^2(\xi) d\xi \\ r_{1j}^m &= \bar{M}_j \int_{\bar{\alpha}_j}^1 \varphi_1(\xi) F_2(\xi - \bar{\alpha}_j) d\xi \quad (j=2, \dots, n-1) \\ r_{ij}^m &= \bar{M}_i \bar{M}_j \int_{\bar{\alpha}_i}^1 F_2(\xi - \bar{\alpha}_i) F_2(\xi - \bar{\alpha}_j) d\xi \quad (j \geq i \text{ and } j, i=2, \dots, n-1) \end{aligned} \right\} \quad (33)$$

$$S_m = \begin{bmatrix} S_{11}^m & S_{12}^m \dots S_{1, n-1}^m \\ & S_{22}^m \dots S_{2, n-1}^m \\ \text{Symmetr.} & \dots \\ & S_{n-1, n-1}^m \end{bmatrix} \quad \text{with: } \left. \begin{aligned} S_{11}^m &= \int_0^1 \varphi_2^2(\xi) d\xi \\ S_{1j}^m &= -J_j \int_{\bar{\alpha}_j}^1 \varphi_2(\xi) F'_2(\xi - \bar{\alpha}_j) d\xi, \quad (j=2, \dots, n-1) \\ S_{ij}^m &= J_i J_j \int_{\bar{\alpha}_j}^1 F'_2(\xi - \bar{\alpha}_i) F'_2(\xi - \bar{\alpha}_j) d\xi \quad (j \geq i \text{ and } j, i=2, \dots, n-1) \end{aligned} \right\} \quad (34)$$

$$Q_m = \begin{bmatrix} q_{11}^m & q_{12}^m \dots q_{1, n-1}^m \\ & q_{22}^m \dots q_{2, n-1}^m \\ \text{Symmetr.} & \dots \\ & q_{n-1, n-1}^m \end{bmatrix} \quad \text{with: } \left. \begin{aligned} q_{11}^m &= \int_0^1 \varphi_1(\xi) \varphi_2(\xi) d\xi \\ q_{1j}^m &= -J_j \int_{\bar{\alpha}_j}^1 \varphi_1(\xi) F'_2(\xi - \bar{\alpha}_j) d\xi \quad (j=2, \dots, n-1) \\ q_{ij}^m &= -\bar{M}_i J_j \int_{\bar{\alpha}_j}^1 F_2(\xi - \bar{\alpha}_i) F'_2(\xi - \bar{\alpha}_j) d\xi \quad (j \geq i \text{ and } j, i=2, \dots, n-1) \end{aligned} \right\} \quad (35)$$

In case the cantiliver beam-column is initially at rest ($t = 0$) the solution of equation (28) is given by the Duhamel integral as

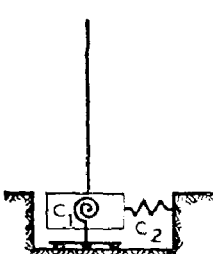
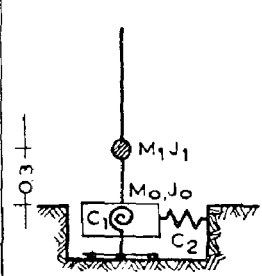
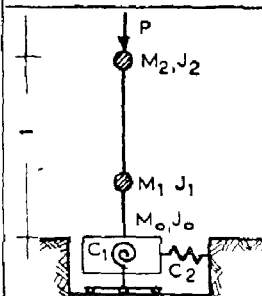
$$A_m(\tau) = -\frac{\ddot{n}(\tau)}{2\pi} \Gamma_m \int_0^\tau f(\tau') \sin 2\pi(\tau - \tau') d\tau' \quad (36)$$

Numerical Results

The frequency equation (19) depends on the stiffness ratios $\bar{C}_1 = C_1 l / EI$, $\bar{C}_2 = C_2 l^3 / EI$, the mass and the moment of inertia ratios $\bar{M}_i = M_i / ml$, $\bar{J}_i = J_i / ml^3$ ($i = 0, 1, 2, \dots, n$) respectively, the length ratios $\bar{\alpha}_i = \alpha_i / l$ ($i = 1, 2, \dots, n$) and the nondimensional axial force $\bar{p} = \beta^2 = Pl^2 / EI$.

The frequency equation (19) is evaluated numerically for cantilever beam - columns carrying up to two attached masses ; the nondimensionalized frequencies Ω_m ($m = 1, 2, 3$) of the first three modes are

Table I. Nondimensionalized Eigenfrequencies Ω_m ($m=1, 2, 3$)

	Numerical data									$\Omega_m = \frac{\omega_m}{\sqrt{\frac{EI}{m l^4}}}$
	\bar{C}_1	\bar{C}_2	\bar{p}	\bar{M}_0	\bar{M}_1	\bar{M}_2	\bar{J}_0	\bar{J}_1	\bar{J}_2	
	∞	∞	0	0	0	0	0	0	0	3.516 22.034 61.701
	1	∞	0	0.5	0	0	0.5	0	0	1.074 4.583 22.218
	1	1	0	0.5	0	0	0.5	0	0	0.743 1.326 5.306
	∞	∞	0	0	0.5	0	0	0.5	0	2.128 6.302 22.911
	1	∞	0	0.5	0.5	0	0.5	0.5	0	0.810 3.642 8.314
	1	1	0	0.5	0.5	0	0.5	0.5	0	0.632 0.987 3.659
	∞	∞	0	0	0.5	0.25	0	0.5	0.25	1.461 3.331 9.658
	1	∞	0	0.5	0.5	0.25	0.5	0.5	0.25	0.672 2.499 4.007
	1	1	0.5	0.5	0.5	0.25	0.5	0.5	0.25	0.370 0.773 2.446

obtained numerically on a G. E. 235 digital computer by a trial and error technique, and are given in Table I. As evident from Table I, the effects of the translational and rotational inertia of the concentrated masses, of the axial constant compressive force, of the translational and rotational springs as well as of the translational and rotatory inertia of the mass of the foundation, tend to decrease the natural frequencies and to bring them closer together. This implies that in the solution for forced motion of cantilever beam - columns having rotational and translational springs at their support and carrying concentrated masses, it will be necessary to retain more terms in the expansion of the displacement components in series of the characteristic shapes than in the case of fixed - end cantilever beams without concentrated masses.

In Table II, the frequencies of the first three modes of vibration of a cantilever beam without concentrated masses and with a translational and a rotational spring at its support, are presented. It can be seen that the effect of both springs on the frequency of the first mode is appreciable. However, only the translational spring has an appreciable effect on the frequencies of the second and third modes.

In case of an elastic support, the effect on the fundamental frequency of the mass of the foundation and of its rotatory inertia is presented in Table III. As it can be seen, for $\bar{C}_1 \sim 0$, $\bar{C}_2 \geq 0.10$ or

Table II. Effect of Springs on the Eigenfrequencies Ω_m ($m=1, 2, 3$)

Numerical Values of \bar{C}_1, \bar{C}_2	Rotational spring		Translational spring	
	$\Omega_m = \frac{\omega_m}{\sqrt{\frac{EI}{m \cdot l^4}}}$	% change of Ω_m from that of rigid support	$\Omega_m = \frac{\omega_m}{\sqrt{\frac{EI}{m \cdot l^4}}}$	% change of Ω_m from that of rigid support
∞	3.516	0	3.516	0
	22.044	0	22.034	0
	61.701	0	61.701	0
1000	3.509	0.2	3.504	0.3
	21.991	0.2	21.013	4.6
	51.575	0.2	53.173	13.8
100	3.438	1.9	3.386	3.7
	21.620	1.9	14.304	35.1
	60.570	1.8	33.954	45.0
10	2.968	15.6	2.447	29.6
	19.356	12.2	7.017	68.2
	55.519	10.0	30.570	50.4
1	1.557	55.7	0.976	72.2
	16.250	26.2	5.731	74.0
	50.897	17.5	30.261	51.0
0.1	0.541	84.6	0.315	91.0
	15.512	29.6	5.605	74.6
	50.065	18.9	30.233	51.0
0.01	0.173	95.1	0.100	97.1
	15.428	30.0	5.595	74.6
	49.975	19.0	30.221	51.0
0.001	0.055	98.4	0.031	99.1
	15.420	30.0	5.595	54.6
	49.966	19.0	30.221	51.0

$\bar{C}_1=0.10$, $\bar{C}_2 \geq 10$ or $\bar{C}_1=10$, $\bar{C}_2 \sim \infty$ the effect of the translational inertia of the mass of the foundation is negligible, whereas the effect of its rotatory inertia is appreciable. Conversely, for $\bar{C}_2 \sim 0$, $\bar{C}_1 \geq 0.10$ or $\bar{C}_2=0.10$, $\bar{C}_1 \geq 10$ or $\bar{C}_2=10$, $\bar{C}_1 \sim \infty$ the effect of the translational inertia of the mass of the foundation is appreciable, whereas the effect of its rotatory inertia is negligible. Finally, if both spring constants \bar{C}_1, \bar{C}_2 have the same numerical value, less than 1000, the effect of the translational and rotatory inertia of the masse of the foundation is substantial.

Table III. Effect of \bar{M}_0, \bar{J}_0 of the Mass of the Foundation on the Fundamental Frequency

		$\bar{C}_r = 0.001$					$\bar{C}_r = 0.1$					
\bar{C}_2	$\bar{M}_0 \setminus \bar{J}_0$.001	.01	.1	1	10	$\bar{M}_0 \setminus \bar{J}_0$	arbitrary				
0.001	.001	0.028	0.028	0.028	0.024	0.010	.001	0.032				
	.01	0.028	0.028	0.028	0.024	0.010	.01	0.031				
	.1	0.027	0.027	0.027	0.024	0.010	.1	0.030				
	1	0.021	0.021	0.021	0.021	0.010	1.	0.022				
	10	0.009	0.009	0.009	0.009	0.008	10.	0.009				
0.1	$\bar{M}_0 \setminus \bar{J}_0$.001	.01	.1	1	10	$\bar{M}_0 \setminus \bar{J}_0$.001	.01	.1	1	10
	arbitrary						.001	0.280	0.280	0.278	0.243	0.098
		0.054	0.053	0.048	0.027	0.010	.01	0.279	0.279	0.277	0.242	0.098
							.1	0.272	0.272	0.270	0.240	0.098
							1.	0.216	0.216	0.216	0.210	0.098
						10.	0.095	0.095	0.095	0.095	0.094	0.094
10	$\bar{M}_0 \setminus \bar{J}_0$.001	.01	.1	1	10	$\bar{M}_0 \setminus \bar{J}_0$.001	.01	.1	1	10
	arbitrary	0.055	0.054	0.048	0.027	0.010	arbitrary	0.535	0.528	0.473	0.273	0.098
1000	arbitrary	0.055	0.054	0.048	0.027	0.010	arbitrary	0.541	0.534	0.477	0.274	0.098

		$\bar{C}_1 = 10$					$\bar{C}_1 = 1000$					
\bar{C}_2	$\bar{J}_0 \setminus \bar{M}_0$.001	.01	.1	1	10	$\bar{J}_0 \setminus \bar{M}_0$	0.01	.01	.1	1	10
0.001	arbitrary	0.032	0.031	0.030	0.022	0.009	arbitrary	0.032	0.031	0.030	0.022	0.009
	arbitrary	0.315	0.314	0.300	0.223	0.095	arbitrary	0.315	0.314	0.310	0.223	0.095
10	$\bar{J}_0 \setminus \bar{M}_0$.001	.01	.1	1	10	$\bar{J}_0 \setminus \bar{M}_0$.001	.01	.1	1	10
	.001	2.273	2.271	2.246	1.986	0.950	arbitrary					
	.01	2.273	2.270	2.245	1.986	0.950						
	.1	2.263	2.261	2.237	1.983	0.950	2.464	2.480	2.441	2.072	0.951	
	1	2.131	2.130	2.115	1.935	0.950						
10	0.981	0.981	0.981	0.981	0.981							
1000	$\bar{J}_0 \setminus \bar{M}_0$	arbitrary					$\bar{J}_0 \setminus \bar{M}_0$	arbitrary				
	.001	2.959					arbitrary	~ 3.495.				
	.01	2.955										
	.1	2.920										
	1	2.462										
10	0.982											

Conclusions

A rigorous analysis of the dynamic response of a cantilever beam--column with translational and rotational spring at its support, carrying concentrated masses, is presented. The effects of the rotatory inertia of the masses, as well as of the translational and rotatory inertia of the mass of the foundation are also included.

A closed-form solution for the determination of natural frequencies is established in matrix form. The effect of various parameters on the frequency of the first three modes has been established by numerical evaluation of the results for cantilever beam - columns having up to two attached masses. Furthermore, it is found that in case of an elastic support, the effects of the mass of the foundation and of its rotatory inertia on the fundamental frequency of the cantilever are appreciable. A procedure for determining the mode shapes is also given.

Finally, the differential equation for establishing the modal amplitudes of cantilever beam - columns subjected to an arbitrary dynamic force or to a movement of the support, is presented.

Bibliography

1. Biggs, M. J., *«Introduction to Structural Dynamics»*, McGraw-Hill Book Co. Inc., N. York, 1964.
2. Kounadis, A.N., *«Dynamic Response of Cantilevers with Attached Masses»*, Journal of the Engineering Mechanics Division, A. S. C. E., Vol. 101, Proc. paper, 11616, pp. 695 - 706.
3. Pan, H. H., *«Some Applications of Symbolic Functions of Beam Problems»*, Journal of the Franklin Institute, Vol. 303, March 1963, pp. 303 - 313.

INTERNATIONAL SYMPOSIUM ON
EARTHQUAKE STRUCTURAL ENGINEERING

315

St. Louis, Missouri, USA, August, 1976

VIBRATIONS AND INTERACTIONS OF LAYERED BEAM FOUNDATIONS

Vikram N. Shah
Senior Engineer, Westinghouse Electric Co.
Pittsburgh, Pennsylvania, USA

T. C. Huang
Professor, Department of Engineering Mechanics
University of Wisconsin
Madison, Wisconsin, USA

Summary A beam and its supporting soil foundation are represented by a layered beam system. Each beam in this system is either a classical beam or a shear beam, and each is separated from its adjacent beams by spring layers. Natural frequencies and normal modes are obtained by two different methods: the state space method and power series method. Numerical examples are given. In a succeeding paper, orthogonality conditions will be derived for these modes and applied to the investigation of forced vibrations.

INTRODUCTION

The interaction between the soil foundation and the supported structure is of great importance in many engineering problems such as earthquake structural engineering and high speed ground transportation. This paper concerns the vertical reaction of the soil foundation on the supported structure. Generally, the Winkler foundation model [13] is used for this purpose. This model assumes that the foundation consists of closely spaced, independent linear springs. Pasternak proposed a foundation model [3] which includes the shear interaction between the spring elements of the Winkler foundation. Later, Kerr [4] proposed a two-layered foundation model which is a modification of the Pasternak model.

In this paper, the general case of a two-dimensional, n-layered foundation is considered. As a first phase of this type of investigation, the supported structure is replaced, for simplicity, by a beam. The length and width of the foundation are assumed to be the same as those of the supported beam. This beam-foundation system is referred to as a layered beam foundation. Analytical methods are developed for the study of free and forced vibrations of this foundation.

The natural frequencies and the normal modes for the layered beam foundation are obtained by two different methods: the state space method [10] and power series method [1]. Numerical examples are given.

For the forced vibration analysis of a structure, orthogonality and normalizing conditions for the modes of the structure are needed. In the succeeding paper [2], these conditions will be found and applied to the investigation of the forced vibrations of the layered beam foundation.

1. EQUATIONS OF MOTION

The layered beam foundation shown in Fig. 1 consists of n beams. Each beam is either a classical beam or a shear beam and is separated from the adjacent ones by the spring layers.

The mass of the spring layer introduces dynamic coupling terms in the governing equations for the system. The mass density is assumed to be constant across the thickness of each layer. The mass and stiffness of the elastic layers and the beams are allowed to vary along the length.

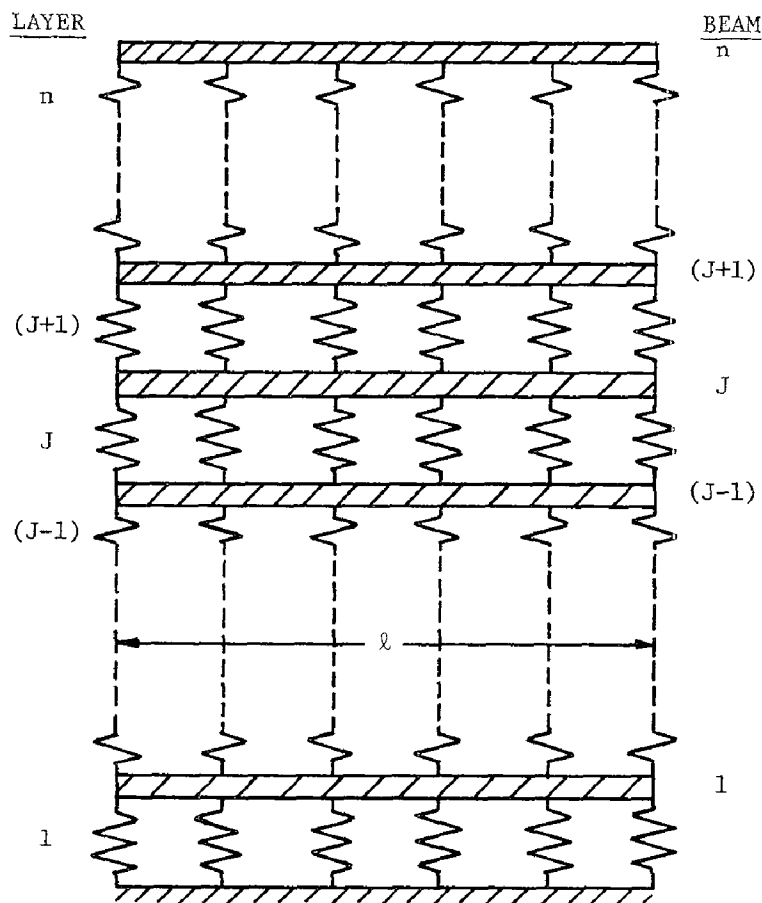


Fig. 1 System of Layered Beams

The equation of motion for the j^{th} beam is derived as follows: First the potential energy and the kinetic energy for the j^{th} beam, j^{th} layer, and $(j+1)^{\text{st}}$ layer are obtained; then the Hamilton principle [5] is applied to derive the equation of motion.

The potential energies of the classical beams and layers are expressed as follows:

$$V_{bj} = \int_0^{\ell} \frac{1}{2} E_j I_j(x) \left(\frac{\partial^2 y_j}{\partial x^2} \right)^2 dx \quad (1)$$

$$V_{\ell j} = \int_0^{\ell} \frac{1}{2} bk_j(x) (y_j - y_{j-1})^2 dx \quad (2)$$

$$V_{\ell(j+1)} = \int_0^{\ell} \frac{1}{2} bk_{j+1}(x) (y_{j+1} - y_j)^2 dx \quad (3)$$

$$T_{bj} = \frac{1}{2} \int_0^{\ell} m_{bj}(x) \left(\frac{\partial y_j}{\partial t} \right)^2 dx \quad (4)$$

To find the kinetic energy of the j^{th} layer, it is assumed that the displacement is linearly distributed along the thickness of the layer. The kinetic energy, $\Delta T_{\ell j}$, in the section of the layer of length Δx , shown in Fig. 2, is expressed as

$$\begin{aligned} \Delta T_{\ell j} &= \frac{1}{2} bm_j(x) \Delta x \int_0^{h_j} \frac{1}{h_j} \left(\frac{t_j}{h_j} \dot{y}_{j-1} + \frac{h_j - t_j}{h_j} \dot{y}_j \right)^2 dt_j \\ &= \frac{1}{2} \frac{bm_j(x) \Delta x}{3} (\dot{y}_j^2 + \dot{y}_{j-1}^2 + \dot{y}_j \dot{y}_{j-1}) \end{aligned} \quad (5)$$

Therefore,

$$T_{\ell j} = \int_0^{\ell} \frac{1}{2} \frac{bm_j(x)}{3} (\dot{y}_j^2 + \dot{y}_{j-1}^2 + \dot{y}_j \dot{y}_{j-1}) dx \quad (6)$$

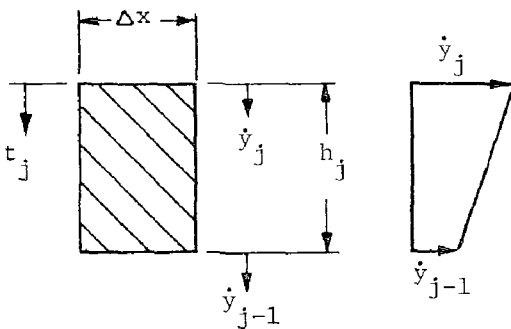


Fig. 2 An Element of the j^{th} layer.

Similarly,

$$T_{\ell(j+1)} = \frac{1}{2} \int_0^{\ell} \frac{bm_{j+1}(x)}{3} (\dot{y}_j^2 + \dot{y}_{j+1}^2 + \dot{y}_j \dot{y}_{j+1}) dx \quad (7)$$

Let

$$\bar{v}_j = v_{bj} + v_{\ell j} + v_{\ell(j+1)} \quad (8)$$

$$\bar{T}_j = T_{bj} + T_{\ell j} + T_{\ell(j+1)} \quad (9)$$

and

$$\bar{L}_j = \bar{T}_j - \bar{v}_j \quad (10)$$

Then

$$A_j = \text{action integral} = \int_{t_0}^{t_1} \bar{L}_j dt \quad (11)$$

and, according to Hamilton's principle,

$$\delta A_j = 0. \quad (12)$$

Equation (12) implies that the Euler equation for the integral A_j is the differential equation of motion for the j^{th} beam. The Euler equation [6] is as follows:

$$\begin{aligned} \frac{\partial \bar{L}_j}{\partial y_j} - \frac{\partial}{\partial x} \left(\frac{\partial \bar{L}_j}{\partial y_j'} \right) - \frac{\partial}{\partial t} \left(\frac{\partial \bar{L}_j}{\partial \dot{y}_j} \right) + \frac{\partial^2}{\partial x^2} \left(\frac{\partial \bar{L}_j}{\partial y_j''} \right) + \frac{\partial^2}{\partial x \partial t} \left(\frac{\partial \bar{L}_j}{\partial \dot{y}_j'} \right) \\ + \frac{\partial^2}{\partial t^2} \left(\frac{\partial \bar{L}_j}{\partial \dot{y}_j} \right) = 0 \end{aligned} \quad (13)$$

The substitution of expression (10) for \bar{L}_j in equation (13) gives:

$$\begin{aligned} -bk_j(x) (y_j - y_{j-1}) + bk_{j+1}(x) (y_{j+1} - y_j) \\ -m_{bj}(x) \ddot{y}_j - \frac{bm_j(x)}{3} \ddot{y}_j - \frac{bm_j(x)}{6} \ddot{y}_{j-1} \\ - \frac{bm_{j+1}(x)}{3} \ddot{y}_j - \frac{bm_{j+1}(x)}{6} \ddot{y}_{j+1} \\ - \frac{\partial^2}{\partial x^2} \left(E_j I_j(x) \frac{\partial^2 y_j}{\partial x^2} \right) = 0 \end{aligned} \quad (14)$$

If the j^{th} beam is a shear beam, then

$$V_{bj} = \int_0^l \frac{1}{2} bG_j(x) \left(\frac{\partial y_j}{\partial x} \right)^2 dx \quad (15)$$

and the second term in equation (13) becomes

$$- \frac{\partial}{\partial x} \left(\frac{\partial \bar{L}_j}{\partial y_j'} \right) = \left(bG_j(x) \frac{\partial y_j}{\partial x} \right)' \quad (16)$$

The equation of motion for the j^{th} shear beam is obtained by replacing the last term in equation (14) by the right-hand side of equation (16). The equations of motion for the j^{th} beam are re-arranged as follows:

Classical beam:

$$\begin{aligned} (f_j(x) y_j'')'' + bk_j(x) (y_j - y_{j-1}) + bk_{j+1}(x) (y_j - y_{j-1}) \\ + m_{bj}(x) \ddot{y}_j + \left(\frac{m_j(x) + m_{j+1}(x)}{3} \right) \ddot{y}_j + \frac{m_j(x)}{6} \ddot{y}_{j-1} \\ + \frac{m_{j+1}(x)}{6} \ddot{y}_{j+1} = 0 \end{aligned} \quad (17)$$

where

$$f_j(x) = E_j I_j(x) \quad (18)$$

Shear beam:

$$\begin{aligned} - (g_j(x) y_j')' + bk_j(x) (y_j - y_{j-1}) + bk_{j+1}(x) (y_j - y_{j+1}) \\ + m_{bj}(x) \ddot{y}_j + \left(\frac{m_j(x) + m_{j+1}(x)}{3} \right) \ddot{y}_j + \frac{m_j(x)}{6} \ddot{y}_{j-1} \\ + \frac{m_{j+1}(x)}{6} \ddot{y}_{j+1} = 0 \end{aligned} \quad (19)$$

where

$$g_j(x) = bG_j(x) \quad (20)$$

2. FREE VIBRATIONS

For free vibration analysis

$$y_j(x,t) = w_j(x) e^{i\lambda t} \quad (21)$$

After equation (19) is substituted in equation (17), the resulting fourth-order equation is reduced to the following four first-order ordinary differential equations:

$$\begin{aligned}
\frac{dw_j}{dx} &= \psi_j \\
E_j I_j(x) \frac{d\psi_j}{dx} &= -M_j \\
\frac{d(M_j)}{dx} &= V_j \\
\frac{d(V_j)}{dx} &= bk_j(x) (w_j - w_{j-1}) + bk_{j+1}(x) (w_j - w_{j+1}) \\
&\quad - m_{bj}(x) w_j \lambda^2 - \frac{[m_j(x) + m_{j+1}(x)] \lambda^2}{3} w_j \\
&\quad - \frac{m_j(x) \lambda^2}{6} w_{j-1} - \frac{m_{j+1}(x) \lambda^2}{6} w_{j+1}
\end{aligned} \tag{22}$$

Similarly, equation (19) can be reduced to the following two equations:

$$\begin{aligned}
bG_j(x) \frac{dw_j}{dx} &= V_j \\
\frac{dv_j}{dx} &= bk_j(x) (w_j - w_{j-1}) + bk_{j+1}(x) (w_j - w_{j+1}) \\
&\quad - m_{bj}(x) w_j \lambda^2 - \frac{[m_j(x) + m_{j+1}(x)] \lambda^2}{3} w_j \\
&\quad - \frac{m_j(x) \lambda^2}{6} w_{j-1} - \frac{m_{j+1}(x) \lambda^2}{6} w_{j+1}
\end{aligned} \tag{23}$$

In this way, the layered beam system can be represented by a system of N linear, first-order, ordinary differential equations. N is given by the following expression:

$$N = 4 n_b + 2 n_s \tag{24}$$

where

$$\begin{aligned}
n_b &= \text{number of beams in the system,} \\
n_s &= \text{number of shear beams in the system.}
\end{aligned}$$

These N equations can be expressed in matrix form as

$$\frac{d}{dx} \{Y\} = [A] \{Y\} \tag{25}$$

where

$$\{Y\} = [N \times 1] \text{ state vector}$$

$$= \{u_1, u_2, \dots, u_j, \dots, u_N\} \quad (26)$$

$$\{u_j\} = \{w_j, \psi_j, m_j, V_j\} \quad \text{for beam} \quad (27)$$

$$= \{w_j, V_j\} \quad \text{for shear beam} \quad (28)$$

and

[A] = coefficient matrix.

Two methods, the state space method and power series method, are used to solve equation (25).

3. STATE SPACE METHOD

This method is used for the cases where the matrix [A] is constant. Let $\Phi(x)$ be a fundamental matrix of equation (25) at $x = 0$. Then the solution of equation (25) is

$$\begin{aligned} \{Y\}_{x=x} &= \Phi(x)\Phi^{-1}(0)\{Y\}_{x=0} \\ &= \phi_N(x)\{Y\}_{x=0} \end{aligned} \quad (29)$$

where

$$\{Y\}_{x=x} = \text{state vector at } x=x$$

$$\{Y\}_{x=0} = \text{state vector at } x=0$$

and

$$\begin{aligned} \phi_N(x) &= \Phi(x)\Phi^{-1}(0) \\ &= \text{normalized fundamental matrix at } x=0 \\ &= \text{transfer matrix [7]}. \end{aligned}$$

For $x=l$, equation (29) becomes

$$\{Y\}_{x=l} = \phi_N(l)\{Y\}_{x=0} \quad (30)$$

Based on the boundary conditions at $x=0$ and $x=l$, the submatrix $[\phi]_D$ which is $(N/2 \times N/2)$, is derived from the matrix $\phi_N(l)$. The value of λ , which makes the determinant of $[\phi]_D$ equal to zero, is the eigenvalue of the system. The corresponding eigenfunction is obtained from equation (29).

Examples 1 & 2. These examples illustrate the state space method. In both examples, a beam supported by a two-layered foundation model, a modified Pasternak model as shown in Fig. 3, is used. In the first example, the beam and the shear beam are simply supported. In the second example the beam and the shear beam have free-free boundary conditions. The data for these two examples are the same, as follows:

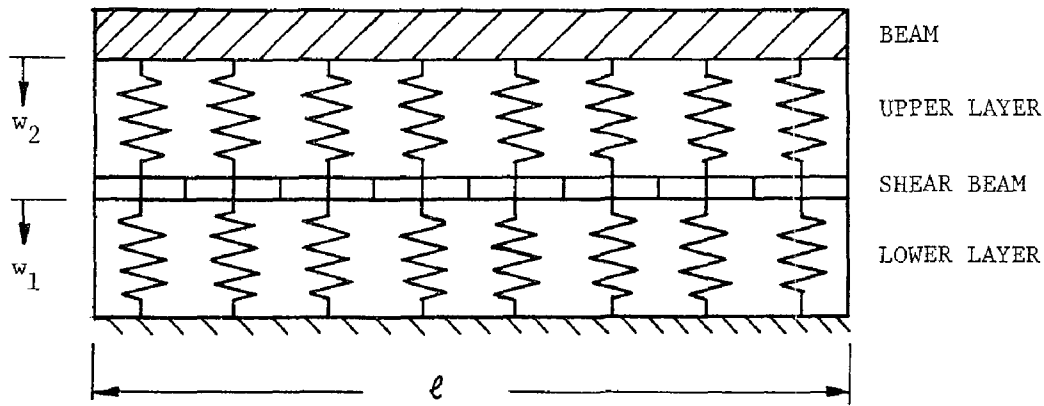


Fig. 3 Beam on Elastic Foundation (Modified Pasternak Model) of same Width and Length

$$\begin{aligned}
 E_2 I_2 &= 10^5 \text{ lbs-ft}^2 & G_1 &= 2 \times 10^5 \text{ lbs/ft} \\
 m_{b2} &= .5 \text{ lbs-sec}^2/\text{ft}^2 & m_2 &= 6 \text{ lbs-sec}^2/\text{ft}^3 \\
 m_{b1} &= 0 & m_1 &= 18 \text{ lbs-sec}^2/\text{ft}^3 \\
 k_2 &= 10^5 \text{ lbs/ft}^3 & b &= 1 \text{ ft} \\
 k_1 &= 33,333.3 \text{ lbs/ft}^3 & l &= 10 \text{ ft}
 \end{aligned}$$

Tables 1 and 2 give the first eight eigenvalues for Examples 1 and 2, respectively. To obtain the accurate eigenfunctions, it is necessary to calculate the corresponding eigenvalues for eight significant digits. Since the eigenfunctions are symmetric or anti-symmetric with respect to the midspan, their accuracy can easily be checked. The orthogonality conditions of these eigenfunctions, derived in paper [2], provide another check.

Table 1. Eigenvalues for Example 1.

Mode	Eigenvalue, rad/sec	
	State Space Method	Finite Element Method
1	64.5031	64.5968
2	99.5431	100.4874
3	152.2749	155.7791
4	212.2243	222.0954
5	262.7208	262.7381
6	267.2531	278.1600
7	277.8812	288.8704
8	317.7203	322.9463

Table 2. Eigenvalues for Example 2.

Mode	Eigenvalue, rad/sec	
	State Space Method	Finite Element Method
1	50.9513	50.9516
2	64.0285	64.1241
3	94.5255	95.4871
4	139.5464	142.7728
5	198.7639	207.2009
6	256.6565	259.9604
7	259.9603	261.9398
8	263.0352	273.1839

For comparison purposes, the finite element method developed in [9] is used to find the eigenvalues and eigenfunctions for these two examples. The eigenvalues found by the finite element method are included in Tables 1 and 2. As the consistent mass matrix is used in the finite element development, the eigenvalues obtained by this method are larger than the exact ones.

For a beam on the Winkler foundation the difference between n^{th} and $(n+1)^{\text{st}}$ eigenvalues is monotonically increased as n increases [11]. This is not true for the two examples considered here. Because the state space method is based on the trial-and-error approach, it would be easy to miss two eigenvalues which are close to each other. One way to reduce this difficulty is to consider a small increase in the value of λ at every step. Computationally, this is an expensive approach. Another way to eliminate this difficulty is to use a Sturm sequence, as discussed below.

Let $[M]$ be the mass matrix and $[K]$ be the stiffness matrix of the beam-foundation system. These matrices are developed by the finite element method discussed in [9]. $[M]$ and $[K]$ are symmetric and positive definite. The leading principal minors, $f_r(\lambda)$ of $[[M]-\lambda[K]]$, possess the Sturm sequence property [8]. Consequently, the number of changes in sign of consecutive members of the sequence $f_r(\lambda)$, starting with $f_0(\lambda) = 1$, is equal to the number of eigenvalues of $[[M]-\lambda[K]]$ which are smaller than λ . This property provides a test to check whether any eigenvalue has been missed. The leading principal minors of $[[M]-\lambda[K]]$ are computed using a variant of Gaussian elimination [12] which preserves information necessary for evaluating the required determinants.

Because some natural frequencies are close, a beating phenomenon may take place between the two beams during free vibrations.

Figures for eight corresponding eigenfunctions for each example are drawn in the Appendix. The eigenfunctions of Example 1 are divided into two groups, in-phase and out-of-phase groups, as there are two layers in the beam-foundation system. Eigenfunctions 1-4, 6, and 8 belong to the in-phase group and the eigenfunctions 5 and 7 belong to the out-of-phase group. The first and fifth eigenfunctions constitute a pair. There is an infinite number of such pairs. In each pair, the one belonging to the out-of-phase group has a higher eigenvalue. For an n -layered beam-foundation system, there are n such groups. In the first group, the individual normal modes of the beams are in-phase. In the second group, only one individual normal mode is out-of-phase. In the i^{th} ($i \leq n$) group, a total of $(i-1)$ individual mode shapes are out-of-phase. Similarly, the eigenfunctions of Example 2 can be divided into two groups.

4. POWER SERIES METHOD

When the matrix $[A]$ is not constant, the state space method cannot be applied. However, the power series method can be used if matrix $[A]$ is analytic for $0 \leq x \leq \ell$. This means $k_j(x)$, $m_j(x)$, $m_{bj}(x)$, $f_j^{-1}(x)$, and $g_j^{-1}(x)$, $j=1,2,\dots,n$, are analytic for $0 \leq x \leq \ell$. Under this condition,

there exists a unique solution $Y(x)$ of equation (25) which is analytic for $0 \leq x \leq \ell$. Thus, this solution has the following power series representation:

$$Y(x) = \sum_{k=0}^{\infty} Y_k (x-x_0)^k \quad 0 \leq x - x_0 \leq \ell \quad (31)$$

where

Y_k is a constant $(N \times 1)$ vector and $x_0 = 0$.

According to Taylor's theorem,

$$Y_{k+1} = \frac{1}{(k+1)!} Y^{(k+1)}(x_0) \quad (32)$$

$$= \frac{1}{(k+1)!} \left[\frac{d^k}{dx^k} Y'(x) \right]_{x=x_0} \quad (33)$$

Substitution of equation (25) in equation (33) gives

$$Y_{k+1} = \frac{1}{(k+1)!} \left[\frac{d^k}{dx^k} (A(x) Y(x)) \right]_{x=x_0} \quad (34)$$

$$k = 0, 1, 2, 3, \dots$$

Applying Leibnitz's rule, equation (34) reduces to

$$Y_{k+1} = \frac{1}{(k+1)!} \left[\sum_{i=0}^k \binom{k}{i} A^{(i)}(x_0) Y^{(k-i)}(x_0) \right] \quad (35)$$

As $[A]$ is analytic, according to Taylor's theorem,

$$[A(x)] = \sum_{k=0}^{\infty} [A_k] (x-x_0)^k \quad (36)$$

where

$$[A_k] = \frac{[A^{(k)}(x_0)]}{k!} \quad (37)$$

Substitution of equations (33) and (36) in equation (35) gives

$$Y_{k+1} = \frac{1}{k+1} \sum_{i=0}^k [A_i] Y_{k-i} \quad k = 0, 1, 2, \dots \quad (38)$$

where

$$Y_0 = Y(x_0) \quad (39)$$

Substitution of equations (38) and (39) in equation (31) gives

$$Y(x) = \sum_{k=0}^{\infty} [B_k(x)] (x-x_0)^k \quad 0 \leq x \leq \ell \quad (40)$$

where

$$[B_k(x)] = \frac{1}{k} \left[\sum_{i=0}^{k-1} [A_i] Y_{k-i-1} \right] \quad k = 1, 2, 3, \dots$$

and

$$[B_0(x)] = [I]Y_0$$

The series in equation (40) converges absolutely and uniformly to $Y(x)$. This implies that this series can be rounded-off to any desired accuracy. So the equation (40) can be expressed as

$$Y(x) \approx [\psi(x)]Y_0 \quad (41)$$

in which $[\psi(x)]$ is the partial sum of the series which gives the desired accuracy.

For $x = l$, equation (41) becomes

$$Y(l) \approx [\psi(l)]Y_0 \quad (42)$$

As before, a sub-matrix $[\psi(l)]_D$ is derived from the matrix $[\psi(l)]$, according to the boundary conditions at $x=0$ and $x=l$. The value of λ which makes the determinant of $[\psi(l)]_D$ zero is an eigenvalue. The corresponding eigenfunction can be obtained from equation (41). Three examples are solved to illustrate the power series method.

Examples 3 & 4. A simply supported beam is resting on the Winkler foundation as shown in Fig. 4. The following data is common to these two examples:

$$E_1 I_1 = 10^5 \text{ lbs-ft}^2 \quad L = 10 \text{ ft} \quad m_1 = 0$$

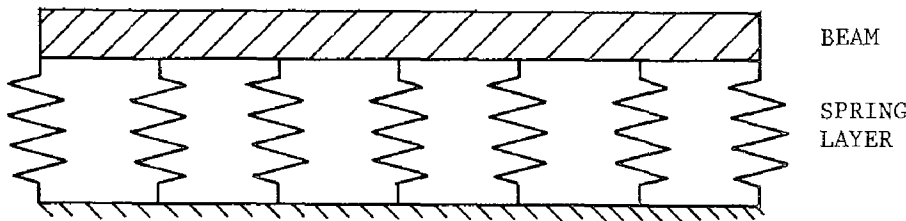


Fig. 4 Beam on Winkler Foundation

In Example 3,

$$k_1(x) = 10^4 \left(1 + \frac{x}{L} \right) \text{ lbs/ft}^3 \quad 0 \leq x \leq 10'$$

and

$$m_{b1} = 0.5 \text{ lbs-sec}^2/\text{ft}^2$$

In Example 4,

$$k_1 = 10^4 \text{ lbs/ft}^3$$

and

$$m_{b1}(x) = 0.5 \left(1 + \frac{x}{L} \right) \text{ lbs-sec}^2/\text{ft}^2 \quad 0 \leq x \leq 10'$$

The first four eigenvalues in radians/second, for Example 3, are 177.5078, 247.9721, 433.4473, and 727.1568. For Example 4, they are 55.776, 86.0725, 162.2364, and 273.6375. The corresponding eigenfunctions, calculated from eigenvalues with eight significant digits, are drawn in the Appendix. The eigenfunctions are no longer symmetric or anti-symmetric with respect to the midspan. Only the first eigenfunction can be predicted qualitatively. This is not true for the other eigenfunctions. In Example 3, stiffness of the foundation increases as x increases. Thus, the modal deflection for the first eigenfunction should be smaller at $x = 8'$ than at $x = 2'$. For the second mode it is completely opposite. This is necessary so that the second eigenfunction is orthogonal to the first one. Similar comments are applicable to Example 4.

Example 5. In this example, a two-layered beam, represented by a modified Pasternak model, as shown in Fig. 3, is considered. The stiffness of each layer increases linearly. The data for this example are as follows:

$$\begin{aligned} E_2 I_2 &= 10^5 \text{ lbs-ft}^2 & m_{b2} &= 0.5 \text{ lbs-sec}^2/\text{ft} \\ \ell &= 10 \text{ ft} & m_{b1} &= 0 \\ k_2(x) &= \left(1 + \frac{x}{\ell} \right) 10^5 \text{ lbs/ft}^3 & m_2 &= 2.0 \text{ lbs-sec}^2/\text{ft}^3 \\ k_1(x) &= \frac{1}{3} k_2(x) & m_1 &= 6.0 \text{ lbs-sec}^2/\text{ft}^3 \\ G_1 &= 2 \times 10^5 \ell \text{ lbs/ft.} \end{aligned}$$

The first eight eigenvalues in radians/second obtained by the power series method are 73.6654, 106.081, 156.5450, 217.072, 274.4609, 304.1648, 326.2989, 339.0188. Figures representing the corresponding eigenfunctions are allotted in the Appendix. Comments regarding the eigenvalues and the eigenfunctions obtained by the state space method in Example 1 are also applicable here.

CONCLUSION

The problem of interaction between a structure and its supporting foundation is of current interest. In this paper, the structure (represented by a beam) and its supporting soil foundation are modelled by a layered beam system for free vibration analysis. In a forthcoming paper, forced vibration will be analyzed. With this background, we are currently investigating the problem of a moving elastic system on a beam supported by a layered foundation. We may also extend our research to investigate the interaction between a complex structure and its supporting soil foundation.

Acknowledgment This research was supported in part by the Wisconsin Alumni Research Foundation.

REFERENCES

1. Goldberg, J. L. and Schwartz, A. J., Systems of Ordinary Differential Equations: An Introduction, Harper & Row, 1972.
2. Huang, T. C. and Shah, Vikram N., "Forced Vibrations and Interactions of Layered Beam Foundation," in preparation.
3. Kerr, A. D., "Elastic and Viscoelastic Foundation Models," Journal of Applied Mechanics, Sept. 1964, pp. 491-498.
4. Kerr, A. D., "A Study of a New Foundation Model," ACTA Mechanica, 1966, pp. 135-147.
5. Langhaar, H. L., Energy Methods in Applied Mechanics, John Wiley, 1962, p. 234.
6. Ibid., p. 96.
7. Pestel, E. C. and Leckie, F. A., Matrix Methods in Elastodynamics, McGraw-Hill, 1963, pp. 130-148.
8. Peters, G. and Wilkinson, J. H., "Eigenvalues of $A_x = \lambda B_x$ with Band Symmetric A and B," Computer Journal, 12, 1969, pp. 398-404.
9. Shah, Vikram N., Elastic Systems Moving on a Beam Supported by Soil or Fluid Foundation, Ph.D. Thesis, University of Wisconsin-Madison, 1974.
10. Thompson, W. T., Vibration Theory and Applications, Prentice-Hall, 1972.
11. Timoshenko, S., Vibration Problems in Engineering, D. Van Nostrand, 1955, p. 377.
12. Wilkinson, J. H., The Algebraic Eigenvalue Problem, Clarendon Press, Oxford, 1965, p. 237.
13. Winkler, E., "Die Lehre von der Elastizitat und Festigkeit," Prag. 1867, p. 182.

NOMENCLATURE

b	= width of the beam-foundation system
$E_j(x)$	= modulus of elasticity of the j^{th} beam
$G_j(x)$	= shear modulus of the j^{th} shear beam, lbs/ft
$I_j(x)$	= area moment of inertia of the j^{th} beam
$k_j(x)$	= stiffness of the j^{th} layer, lbs/ft ³
l	= length of the beam-foundation system
$m_{bj}(x)$	= mass per unit length of the j^{th} beam
$m_j(x)$	= mass of the j^{th} layer per unit contact area
$M_j(x)$	= moment in the j^{th} beam
T_{bj}	= kinetic energy of the j^{th} beam
T_{lj}	= kinetic energy of the j^{th} layer
V_{bj}	= potential energy of the j^{th} beam

V_j	= potential energy of the j^{th} layer
$V_j(x)$	= shear force in the j^{th} beam
$w_j(x)$	= deflection of the j^{th} beam
$y_j(x,t)$	= deflection of the j^{th} beam
$\psi_j(x)$	= slope of the j^{th} beam
λ	= frequency of harmonic vibration

APPENDIX

Normal modes for Examples 1-5, reduced and simplified from [9], are plotted here as Figs. 5-9, respectively. The mode numbers are indicated within the figures.

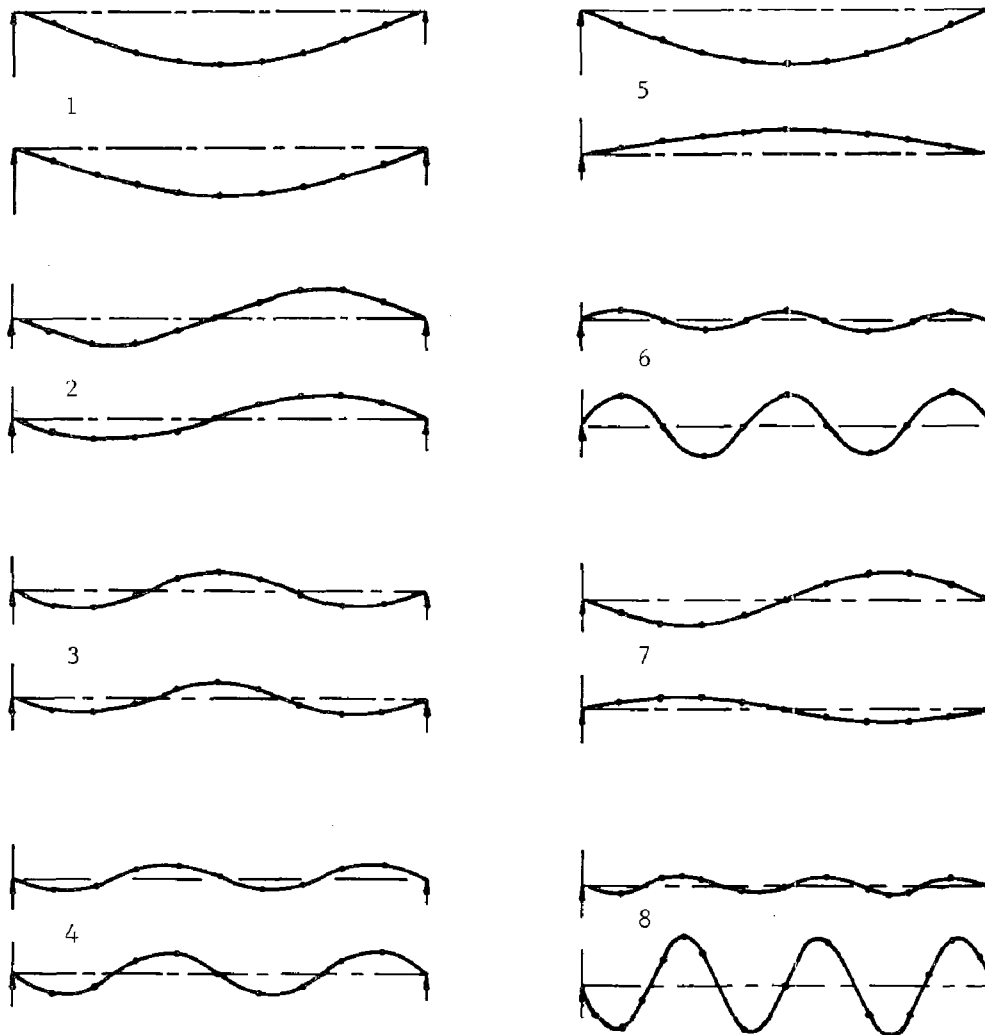


Fig. 5 Eight Normal Modes of Example 1

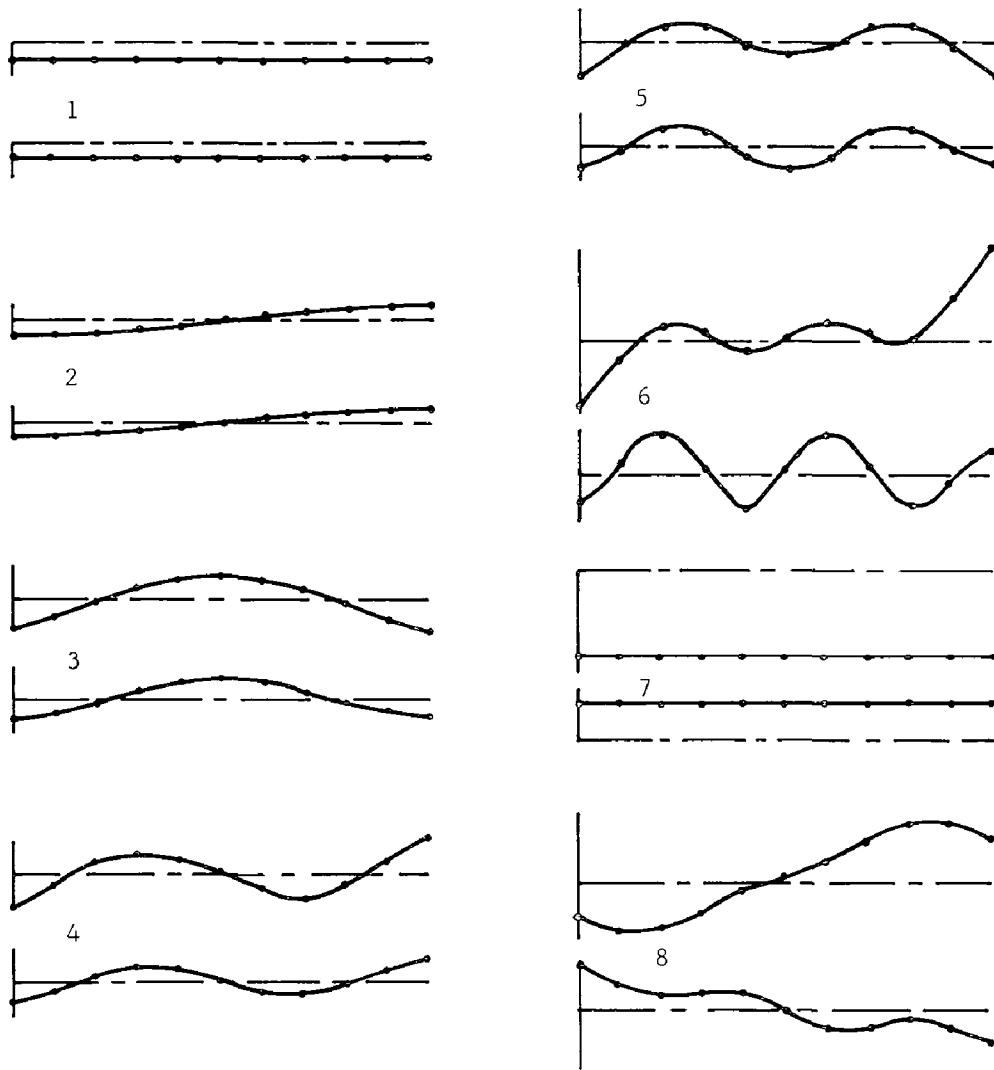


Fig. 6 Eight Normal Modes of Example 2

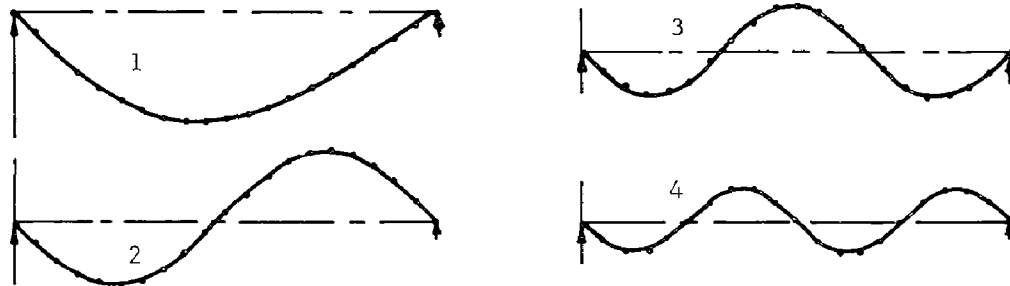


Fig. 7 Four Normal Modes of Example 3

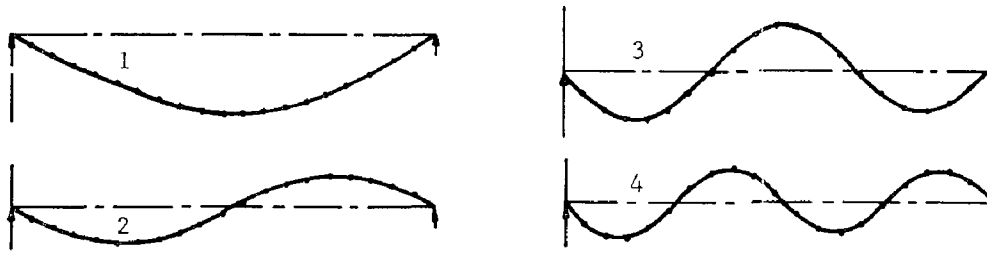


Fig. 8 Four Normal Modes of Example 4

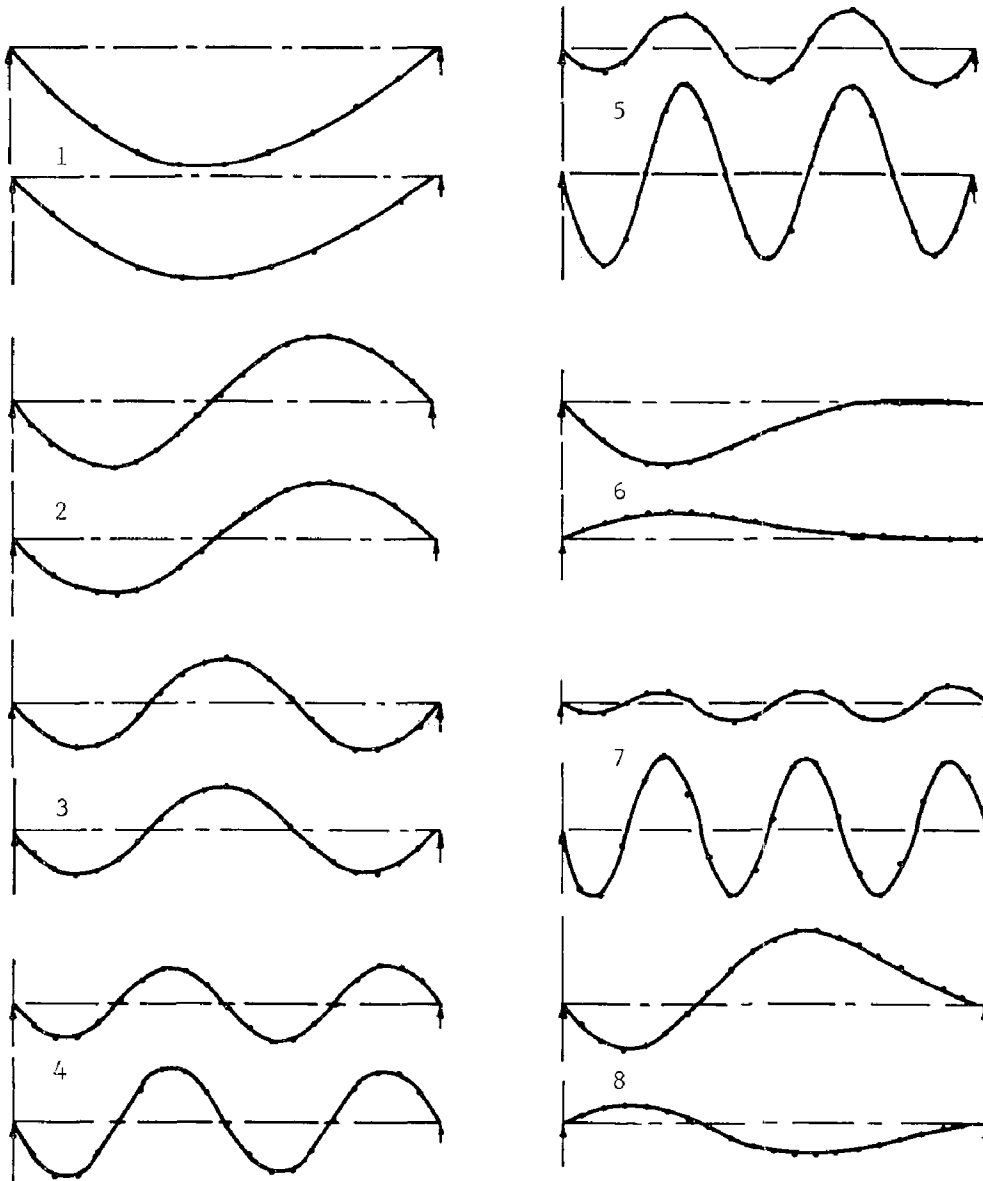


Fig. 9 Eight Normal Modes of Example 5

INTERNATIONAL SYMPOSIUM ON
EARTHQUAKE STRUCTURAL ENGINEERING

331

St. Louis, Missouri, USA, August, 1976

GENERATING RESPONSE SPECTRA FROM DISPLACEMENT AND VELOCITY
TIME HISTORY INPUT

A. CHUANG, T. H. LEE, D. A. WESLEY, and S. LU

General Atomic Company

San Diego, California, United States

ABSTRACT

An investigation has been made to explore a method of generating response spectra from displacement and velocity time history input instead of acceleration time history. The ability to generate response spectra from digitized displacement and velocity time history input is required in order to show that the displacement input used for some component tests or analyses is, in fact, equivalent to the input when specified in terms of acceleration.

In many instances, the component structure analysts use dynamic models which utilize displacement and velocity input. This is often the case of the tests where digitized displacement is specified. Since the floor response spectra are usually determined in a conventional analysis by using acceleration input, it is necessary to ascertain that the response data produced by using displacement and velocity input are consistent with those generated by using acceleration excitation.

The analytical approach used in this investigation was successively to integrate by parts the expression of the absolute acceleration response of a single degree-of-freedom oscillator and the final results are in terms of Duhamel's integrals involving only displacement and velocity excitations. The numerical computations of these integrals were facilitated by making use of recurrence relations. The response spectra obtained were compared with those generated by conventional methods using acceleration input.

1. INTRODUCTION

The determination of seismic response through the use of the response spectrum method has long been a standard practice in dealing with linear systems. However, in recent years many structural components are modelled as nonlinear systems whose governing equations are formulated in absolute coordinates. The expressions of these equations contain boundary displacement and velocity as excitation input rather than the support acceleration terms as commonly encountered in the conventional linear analysis methods. For the same reason, when these nonlinear component structures are qualified by test methods, the excitation is usually specified by digitized displacement input. Since the support motion of a component structure is usually defined by acceleration time history data along with the floor response spectra, it is necessary to establish the equivalency of using displacement excitation input.

A response spectrum is defined as the maximum response of a damped, single degree of freedom linear oscillator to a specified support motion plotted versus the natural frequency or period. The calculations are then repeated for various damping values. These curves provide a description of the frequency characteristics of the support motion and give the maximum response of single-degree of freedom systems to the excitation. By modal super-position, the response spectrum techniques can be applied to the analysis of complex multi-degree of freedom structures such as buildings, nuclear power plants, and equipment.

The generation of response spectra normally requires the numerical computation of the response of a simple oscillator to a specified base acceleration. The motion of the oscillator is described by a second order, linear, inhomogeneous differential equation, and if a digital description of the support excitation is available, the response can be obtained by numerical integration.

For some engineering applications, dynamic models for the component structures are used where displacement and velocity time history inputs are required. This is often the case of tests where digitized displacement is specified. In this case, the response spectra must be generated from the displacement and velocity time history records.

In this investigation, the acceleration response is in terms of displacement and velocity time history. Therefore, the analytical approach used in this study was successively to integrate by parts the expression of the absolute acceleration response to a single-degree of freedom oscillator, and the final results are in terms of Duhamel's integrals involving only displacement and velocity excitations.

2. MATHEMATICAL FORMULATION

The exact expression for the relative displacement of a single degree of freedom, damped, linear system with zero initial conditions excited by base motion $\ddot{y}(t)$ is [1]:

$$S(t) = -\frac{1}{\omega\sqrt{1-\zeta^2}} \int_0^t \ddot{y}(\tau) e^{-\omega\zeta(t-\tau)} \sin \omega\sqrt{1-\zeta^2} (t-\tau) d\tau \quad (1)$$

where ω is the undamped natural frequency, and ζ is the fraction of critical damping.

By differentiating equation (1), the exact expression for the relative velocity can be obtained:

$$\begin{aligned} V(t) = & -\int_0^t \ddot{y}(\tau) e^{-\omega\zeta(t-\tau)} \cos \omega\sqrt{1-\zeta^2} (t-\tau) d\tau \\ & + \frac{\zeta}{\sqrt{1-\zeta^2}} \int_0^t \ddot{y}(\tau) e^{-\omega\zeta(t-\tau)} \sin \omega\sqrt{1-\zeta^2} (t-\tau) d\tau \quad . \quad (2) \end{aligned}$$

The "absolute" acceleration of the mass may be derived by further differentiating equation (2) with respect to t :

$$\begin{aligned} a(t) = & \frac{\omega(1-2\zeta^2)}{\sqrt{1-\zeta^2}} \int_0^t \ddot{y}(\tau) e^{-\omega\zeta(t-\tau)} \sin \omega\sqrt{1-\zeta^2} (t-\tau) d\tau \\ & + 2\omega\zeta \int_0^t \ddot{y}(\tau) e^{-\omega\zeta(t-\tau)} \cos \omega\sqrt{1-\zeta^2} (t-\tau) d\tau \quad . \quad (3) \end{aligned}$$

If we let $c = \omega\zeta$, $B = \omega\sqrt{1-\zeta^2}$, the first integral yields:

$$\begin{aligned} \int_0^t \ddot{y}(\tau) e^{-c(t-\tau)} \sin \omega B(t-\tau) d\tau = & [U(t-\tau)\dot{y}(\tau)]_0^t \\ & - \int_0^t \dot{y}(\tau) \frac{\partial}{\partial \tau} U(t-\tau) d\tau \end{aligned}$$

where $U(t-\tau) = e^{-c(t-\tau)} \sin \omega B(t-\tau)$ (4)

The expression $\int_0^t \dot{y}(\tau) \frac{\partial}{\partial \tau} U(t-\tau) d\tau$ can be successively

integrated by parts, so that the first integral can be written as:

$$\begin{aligned} \int_0^t \ddot{y}(\tau) e^{-c(t-\tau)} \sin \omega B(t-\tau) d\tau &= \dot{y}(t)U(0) - \dot{y}(0)U(t) \\ &- \left. \frac{\partial}{\partial \tau} U(t-\tau) \right|_{\tau=t} y(t) + \left. \frac{\partial}{\partial \tau} U(t-\tau) \right|_{\tau=0} y(0) \\ &+ \int_0^t y(\tau) \frac{\partial^2}{\partial \tau^2} U(t-\tau) d\tau \end{aligned} \quad (5)$$

Since the initial velocity and displacement are usually zero and

$$\left. \frac{\partial}{\partial \tau} U(t-\tau) \right|_{\tau=t} y(t) = -\omega B y(t)$$

equation (3) is reduced to the following expression:

$$\begin{aligned} a(t) &= AB\omega^2 y(t) + A\omega \int_0^t y(\tau) \frac{\partial^2}{\partial \tau^2} U(t-\tau) d\tau \\ &+ 2c \int_0^t \ddot{y}(\tau) e^{-c(t-\tau)} \cos \omega B(t-\tau) d\tau \end{aligned} \quad (6)$$

where $A = \frac{(1 - 2\zeta^2)}{\sqrt{1 - \zeta^2}}$.

The second integral $2c \int_0^t \ddot{y}(\tau) e^{-c(t-\tau)} \cos \omega B(t-\tau) d\tau$,

may also be successively integrated by parts and after a somewhat lengthy derivation the final expression may be written as:

$$\begin{aligned} a(t) &= AB\omega^2 y(t) + 2c\dot{y}(t) - 2c^2 y(t) + A\omega \int_0^t y(\tau) \frac{\partial^2}{\partial \tau^2} U(t-\tau) d\tau \\ &+ 2c \int_0^t y(\tau) \frac{\partial^2}{\partial \tau^2} \bar{U}(t-\tau) d\tau \end{aligned} \quad (7)$$

where $\bar{U}(t-\tau) = e^{-c(t-\tau)} \cos \omega B(t-\tau)$.

The expression for $a(t)$ is finally given as:

$$\begin{aligned} a(t) &= (1 - 2\zeta^2) \omega^2 y(t) + 2\omega\zeta\dot{y}(t) - 2\omega^2\zeta^2 y(t) \\ &- D \int_0^t e^{-\omega\zeta(t-\tau)} \sin \omega \sqrt{1 - \zeta^2} (t-\tau) y(\tau) d\tau \\ &- E \int_0^t e^{-\omega\zeta(t-\tau)} \cos \omega \sqrt{1 - \zeta^2} (t-\tau) y(\tau) d\tau \end{aligned} \quad (8)$$

where

$$D = \frac{\omega^3(1 - 2\zeta^2)^2}{\sqrt{1 - \zeta^2}} - 4\omega^3\zeta^2 \sqrt{1 - \zeta^2} \quad ,$$

and

$$E = 2\omega^3\zeta(1 - 2\zeta^2) + 2\zeta^2(1 - 2\zeta^2)\omega^3 \quad ,$$

$y(t)$ is the displacement time history and $\dot{y}(t)$ is the velocity time history. Since $y(t)$ and $\dot{y}(t)$ are known, $a(t)$ can be evaluated as soon as the values of the two Duhamel's integrals

$$\int_0^t e^{-\omega\zeta(t-\tau)} \sin \omega \sqrt{1 - \zeta^2} (t - \tau)y(\tau)d\tau \quad ,$$

and

$$\int_0^t e^{-\omega\zeta(t-\tau)} \cos \omega \sqrt{1 - \zeta^2} (t - \tau)y(\tau)d\tau \quad , \quad (9)$$

are determined.

3. EVALUATION OF DUHAMEL'S INTEGRALS

The two Duhamel's integrals as shown in Equation (9), can be evaluated by using a numerical integration technique [2]. However, for excitations of longer duration, an accurate computation for these integrals is almost prohibitive due to the cost of the computer time unless a recurrence relation can be found.

For a small time increment Δt , the expression of the first integral in Equation (9) may be written as:

$$\int_0^{t+\Delta t} e^{-c(t+\Delta t-\tau)} \sin \omega B(t + \Delta t - \tau) y(\tau)d\tau$$

or

$$\int_0^{t+\Delta t} e^{-c(t-\tau)} \cdot e^{-c\Delta t} [\sin \omega B(t-\tau) \cos \omega B\Delta t + \cos \omega B(t-\tau) \sin \omega B\Delta t] y(\tau)d\tau \quad (10)$$

which can be written as

$$P \int_0^t e^{-c(t-\tau)} \sin \omega B(t-\tau)y(\tau)d\tau + P \int_t^{t+\Delta t} e^{-c(t-\tau)} \sin \omega B(t-\tau)y(\tau)d\tau \\ + Q \int_0^t e^{-c(t-\tau)} \cos \omega B(t-\tau)y(\tau)d\tau + Q \int_t^{t+\Delta t} e^{-c(t-\tau)} \cos \omega B(t-\tau)y(\tau)d\tau \quad (11)$$

where P and Q are constants defined by

$$P = e^{-c\Delta t} \cos \omega B\Delta t$$

$$Q = e^{-c\Delta t} \sin \omega B\Delta t \quad .$$

In the same manner, the second integral, for a small increment, yields

$$\int_0^{t+\Delta t} e^{-c(t-\tau+\Delta t)} \cos \omega B(t - \tau + \Delta t) y(\tau) d\tau \quad (12)$$

which may be expressed as:

$$\begin{aligned} & P \int_0^t e^{-c(t-\tau)} \cos \omega B(t - \tau) y(\tau) d\tau \\ & + P \int_t^{t+\Delta t} e^{-c(t-\tau)} \cos \omega B(t - \tau) y(\tau) d\tau \\ & - Q \int_0^t e^{-c(t-\tau)} \sin \omega B(t - \tau) y(\tau) d\tau \\ & - Q \int_t^{t+\Delta t} e^{-c(t-\tau)} \sin \omega B(t - \tau) y(\tau) d\tau \end{aligned} \quad (13)$$

By examining the eight integrals in Equations (11) and (13), one can conclude that there is a recurrence relation in each of the Duhamel's integral for a small time increment. Therefore, the numerical data of the four integrals may be stored in the computer in the form of the original Duhamel's integrals multiplied by a constant P or Q.

For each time increment, there are only two integrals to be evaluated for the particular small time increment only. The integrals are:

$$(P - Q) \int_t^{t+\Delta t} e^{-c(t-\tau)} \sin \omega B(t - \tau) y(\tau) d\tau$$

and

$$(P + Q) \int_t^{t+\Delta t} e^{-c(t-\tau)} \cos \omega B(t - \tau) y(\tau) d\tau$$

Since the integration for the two integrals is limited from (t) to (t + Δt), both the computation time and core storage are drastically reduced. The trapezoidal rule is usually accurate enough to evaluate these two integrals for small time increment Δt.

4. NUMERICAL RESULTS

In this section, results are obtained to demonstrate that the response spectra generated by digitized displacement and velocity time history input are essentially the same as the ones generated by acceleration time history. Moreover, the results will be compared between the response spectra generated by acceleration input and those generated by displacement time history alone, i.e., with velocity time history neglected, for a low damping case.

In order to perform the numerical calculations described in the previous section, a computer code, DISPEC, was developed. The output of the code includes numerical values and graphical displays of the computed response spectra. The input data are digitized time history values of displacement and velocity input generated by integrating an acceleration trace whose response spectra are known. The accuracy of the DISPEC code has been tested against an existing computer program EQUAL [9] which generates response spectra from acceleration time history input, and the comparison shows that the agreement is excellent.

A. Comparison of Response Spectra (using both displacement and velocity input for DISPEC).

Two response spectra plots as well as a numerical tabulation due to a 1 g horizontal ground motion of an artificial earthquake are shown. One is the result from the program using acceleration input (Figure 2), and the other is the result of DISPEC code using displacement and velocity time history input (Figure 1). In both cases, the damping factor is 5%.

For the purpose of improving the accuracy of the integration process in the high frequency range, the time step Δt for integration was chosen for this test case, as 0.0001 second when the period is less than 0.06 second. For all other period values, satisfactory accuracy can be achieved with a more economical integration step of 0.001 second.

B. Comparison of Response Spectra (using only displacement input for DISPEC).

It was shown in the equation (8) for the undamped case that the response spectra can be generated from displacement time history alone. For a lightly damped structure, such as a steel structure, or an uncracked concrete building [3], it is also possible to generate an approximate response spectra of acceptable accuracy from only the displacement time history input by using Equation (8).

A series of comparisons was made to find a maximum damping value for which the response spectra generated from acceleration can be approximately generated by displacement time history alone. The need for this investigation is due to the fact that the velocity input trace in a test is sometimes unavailable.

By comparing Figure 2 and Figure 3 as well as Table 2, one can easily conclude that the spectra for 0.05 damping computed by DISPEC without $\dot{y}(t)$ input is quite different from the one computed by EQUAL. In the high frequency range the difference is quite large but decreases to an acceptable region when the period reaches approximately 0.2 second. Above this period, the difference is considered to be acceptable from the engineering point of view.

As shown in Equation (8), the term $2\omega\zeta y(t)$ is the only term containing the velocity time input $\dot{y}(t)$. The effect of this term is obviously quite small if the product of ω and ζ is small. The smaller of the damping value ζ , the less effect this term has on the overall response $a(t)$. Since the circular frequency ω is a variable its effect at low frequencies will be small.

It is shown in Figure 4, Figure 5 and Table 3 that the difference of the response spectra, computed respectively by DISPEC and by EQUAL has been improved considerably as the damping is reduced from 0.05 to 0.01. The maximum deviation at the lowest period of 0.03 second is 17.6%. However; the difference decreases rapidly as the period increases until the discrepancy is only 2.12% at a period of 0.1 second. As shown in Table 6, some steel, reinforced or prestressed concrete structures without cracking or joint slip where the stress level is low or well below proportional limits are representative of structures with critical damping in the neighborhood of 1.0%.

Similar results are obtained for 0.008 damping as can be seen by an examination of Table 4, Figure 6 and Figure 7. The difference of the response spectra computed by DISPEC and computed by EQUAL has been reduced slightly. The maximum discrepancy is about 14 percent, and it decreases to 2.02% at $T = 0.1$ second.

For a structure with 0.005 damping value or lower, the response spectra can be generated by using displacement time history alone. From Figure 8, Figure 9 and Table 5, the response spectra generated by DISPEC and by EQUAL are almost identical except in the low period range which still has some minor differences. From Table 6, steel structures with a low stress level of $\sigma < 1/4 \sigma_y$ and without joint slip, reinforced or prestressed concrete structures without cracking, with the stress level well below proportional limit, etc., are structures typically encountered in this damping range.

5. CONCLUSIONS

An analytical technique has been developed for generating response spectra from displacement and velocity time history input instead of acceleration time history. Recurrence relations are developed which provide an economical means of solution for the numerical evaluations of the Duhamel's integrals involved. A comparison shows that agreement between spectra generated by the two methods is excellent.

It is further shown, that for very lightly damped cases, the response spectra may be generated by displacement time history input alone. At 0.5% critical damping or lower, the response spectra for a structure may be generated by displacement time history alone with only minor error (of the order of 5%) in the low period range ($T < 0.08$ second).

For a structure with damping values in the 0.008 to 0.01 range, one can expect about 15% error introduced for a period T less than 0.06 second. For damping values higher than 0.01, the response spectra generated by displacement time alone are not recommended for use and the contributions from the relative velocity terms must be included.

COMPARISON OF RESPONSE SPECTRA DUE TO 1 G HORIZONTAL COMPONENT
OF GA ARTIFICIAL EARTHQUAKE

.05 Damping

TABLE 1

Spectra Computed by DISPEC		Spectra Computed by EQUAL
Period, Sec.	Max. Acc. (g)	Max. Acc. (g)
.03	1.21	1.14
.04	1.27	1.24
.06	1.87	1.83
.08	2.04	2.20
.1	2.47	2.58
.2	3.35	3.37
.3	3.03	3.03
.4	4.19	4.19
.6	2.95	2.95
.8	2.09	2.09
1.	1.57	1.57
1.2	1.79	1.79
1.4	1.13	1.13
1.6	1.35	1.35
1.8	1.39	1.39
2.0	1.20	1.20

COMPARISON OF RESPONSE SPECTRA DUE TO 1 G HORIZONTAL COMPONENT
OF GA ARTIFICIAL EARTHQUAKE

.05 Damping

TABLE 2

Spectra Computed by DISPEC (without y(t) input)		Spectra Computed by EQUAL
Period, Sec.	Max. Acc. (g)	Max. Acc. (g)
.03	5.38	1.14
.04	4.14	1.24
.06	3.40	1.83
.08	2.98	2.20
.1	2.84	2.58
.2	3.40	3.37
.3	3.10	3.03
.4	4.07	4.19
.6	2.91	2.95
.8	2.18	2.09
1.	1.55	1.57
1.2	1.77	1.79
1.4	1.12	1.13
1.6	1.36	1.35
1.8	1.40	1.39
2.0	1.21	1.20

COMPARISON OF RESPONSE SPECTRA DUE TO 1 G HORIZONTAL COMPONENT
OF GA ARTIFICIAL EARTHQUAKE

0.01 Damping

TABLE 3

Spectra Computed by DISPEC (without y(t) input)		Spectra Computed by EQUAL
Period, Sec.	Max. Acc. (g)	Max. Acc. (g)
.03	1.93	1.59
.04	1.80	1.53
.06	2.84	2.40
.08	3.63	3.84
.1	4.51	4.71
.2	6.36	6.42
.3	6.62	6.62
.4	6.25	6.24
.6	4.01	4.02
.8	3.39	3.40
1.	2.31	2.31
1.2	2.33	2.33
1.4	1.96	1.96
1.6	1.79	1.79
1.8	1.67	1.67
2.0	1.41	1.41

COMPARISON OF RESPONSE SPECTRA DUE TO 1 G HORIZONTAL COMPONENT
OF GA ARTIFICIAL EARTHQUAKE

.008 Damping

TABLE 4

Spectra Computed by DISPEC (without g(t) input)		Spectra Computed by EQUAL
Period, Sec.	Max. Acc. (g)	Max. Acc. (g)
.03	1.77	1.64
.04	1.76	1.56
.06	2.84	2.43
.08	3.77	3.97
.1	4.85	4.95
.2	6.88	6.89
.3	7.15	7.15
.4	6.41	6.39
.6	4.06	4.06
.8	3.49	3.50
1.	2.40	2.41
1.2	2.37	2.37
1.4	2.05	2.05
1.6	1.85	1.84
1.8	1.69	1.69
2.0	1.42	1.42

COMPARISON OF RESPONSE SPECTRA DUE TO 1 G HORIZONTAL COMPONENT OF GA ARTIFICIAL EARTHQUAKE

.005 Damping

TABLE 5

Spectra Computed by DISPEC (without $\dot{y}(t)$ input)		Spectra Computed by EQUAL	
Period, Sec.	Max. Acc. (g)	Max. Acc. (g)	
.03	1.72	1.72	
.04	1.74	1.62	
.06	2.74	2.54	
.08	4.31	4.52	
.1	5.30	5.41	
.2	7.64	7.63	
.3	8.10	8.10	
.4	7.01	7.00	
.6	4.13	4.13	
.8	3.65	3.65	
1.	2.54	2.59	
1.2	2.41	2.41	
1.4	2.20	2.20	
1.6	1.96	1.96	
1.8	1.71	1.71	
2.0	1.44	1.44	

DAMPING VALUES

TABLE 6

STRESS LEVEL	TYPE AND CONDITION OF STRUCTURE	PERCENTAGE OF CRITICAL DAMPING
1. Low, well below proportional limit ($\sigma \leq 1/4 \sigma_y$)	Steel - Reinforced or Prestressed Concrete (no cracking) (no joint slip)	0.5 - 1.0
2. Working Stresses ($\sigma_{all} \leq 1/2 \sigma_y$)	Steel (welded) and P. Concrete and well R. Concrete (no cracking or very small)	2.0
	R. Concrete with considerable cracking	3.0 - 5.0
	Bolted and Riveted Steel wood structures with nailed or bolted joints	5.0 - 7.0
3. At or just below σ_y	Steel (welded), P. Concrete (without loss in Prestress)	5.0
	R. Concrete and P. Concrete with loss in prestress	7.0 - 10.0
4. Beyond σ_y with permanent strain greater than ϵ_y	Welded Steel	7.0 - 10.0
	Prestressed and R. Concrete	10.0 - 15.0
	Bolted and Riveted Steel or Wood Structures	20.0

RESPONSE SPECTRA, DISPLACEMENT AND VELOCITY TIME HISTORY INPUT
0.05 Damping

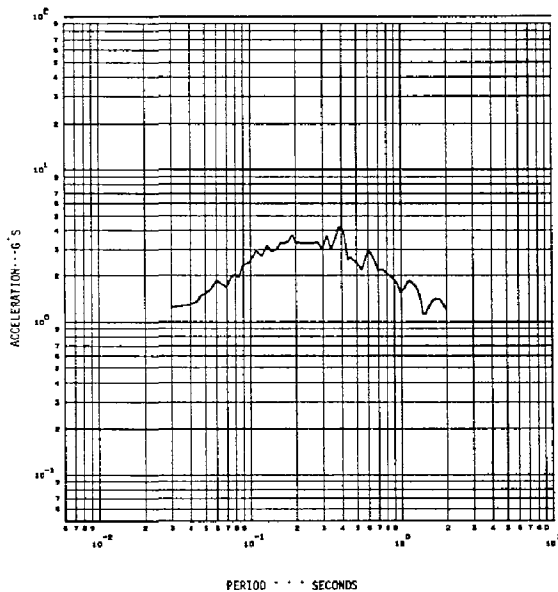


FIGURE 1

RESPONSE SPECTRA, ACCELERATION TIME HISTORY INPUT
0.05 Damping

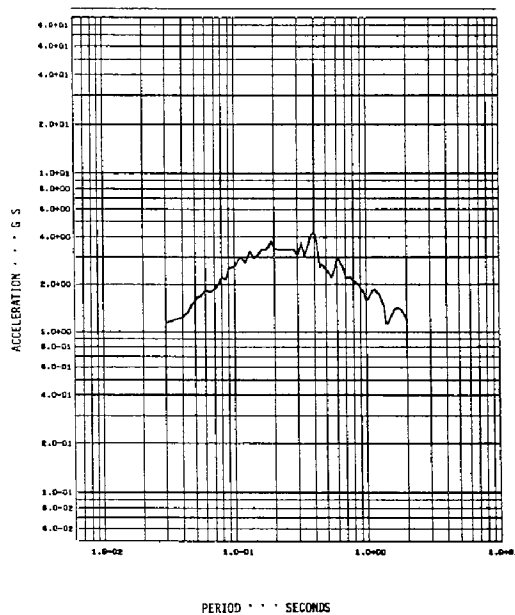


FIGURE 2

RESPONSE SPECTRA, DISPLACEMENT TIME HISTORY INPUT
0.05 Damping

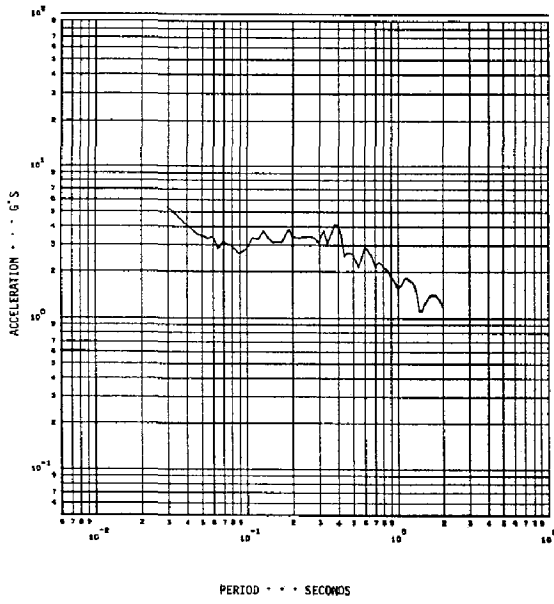


FIGURE 3

RESPONSE SPECTRA, DISPLACEMENT TIME HISTORY INPUT
0.01 Damping

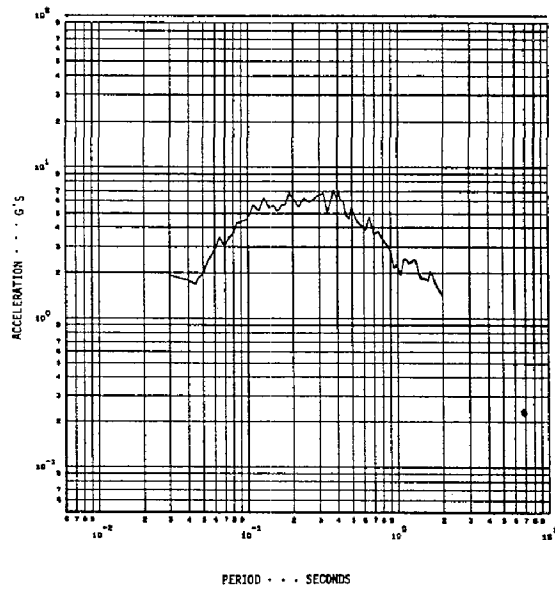


FIGURE 4

RESPONSE SPECTRA, ACCELERATION TIME HISTORY INPUT
0.01 Damping

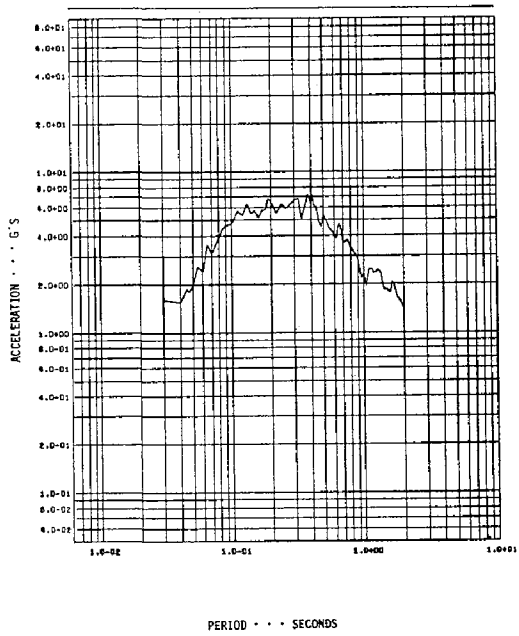


FIGURE 5

RESPONSE SPECTRA, DISPLACEMENT TIME HISTORY INPUT
0.008 Damping

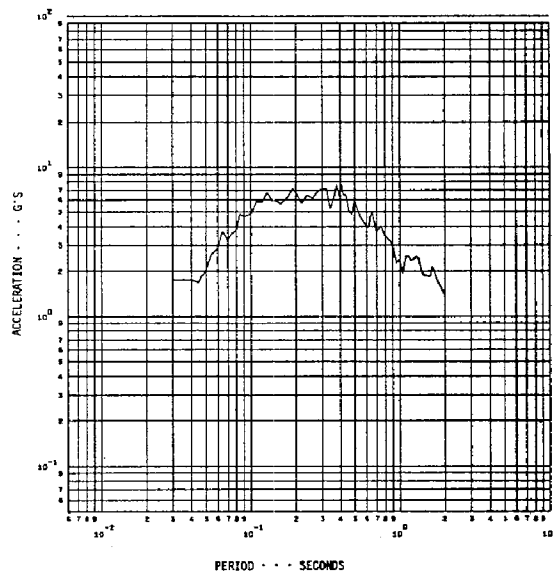


FIGURE 6

RESPONSE SPECTRA, ACCELERATION TIME HISTORY
0.008 Damping

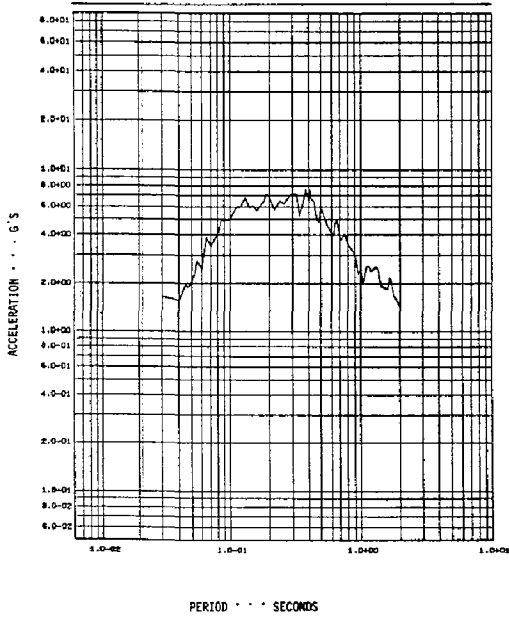


FIGURE 7

RESPONSE SPECTRA, DISPLACEMENT TIME HISTORY INPUT
0.005 Damping

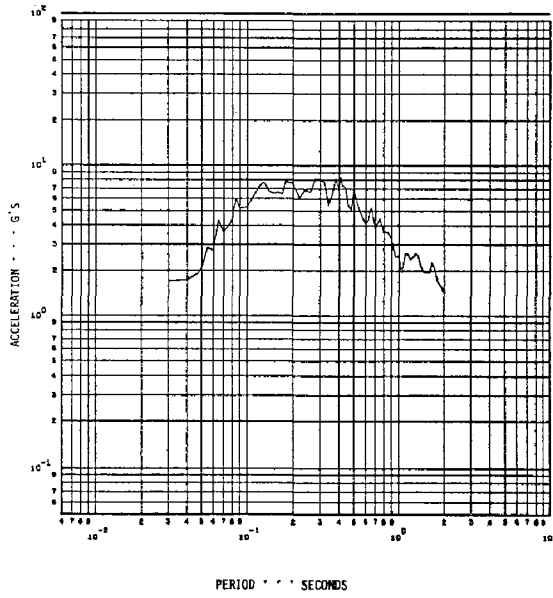


FIGURE 8

RESPONSE SPECTRA, ACCELERATION TIME HISTORY INPUT
0.005 Damping

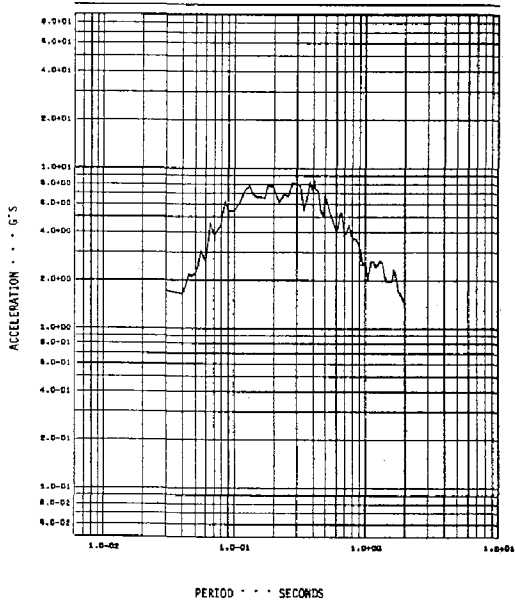


FIGURE 9

REFERENCES

1. Hudson, D. E. "Some Problems in the Application of Spectrum Techniques to Strong-Motion Earthquake Analysis," Bulletin of the Seismological Society of America, Vol. 52, No. 2, pp. 417-430, April, 1962.
2. Salvador, M. G. and Baron, M. L., "Numerical Methods in Engineering," 2nd Edition, Prentice Hall, 1961.
3. Katayama, T. "A Review of Theoretical and Experimental Investigations of Damping in Structures," UNICIV Report No. 1-4, July 1965.
4. Lazan, B. J. "Damping of Materials and Members in Structural Mechanics," Pergamon Press, Inc., 1968.
5. Newmark, N. M. and Hall, W. J., "Seismic Design Criteria for Nuclear Reactor Facilities," Preprint of 4WCEE, Section B4, pp. 37-50.
6. Rea, D., Bouwkamp, J. G., and Clough, R., "The Dynamic Behavior of Steel Frame and Truss Buildings," Structure and Materials Research Report No. 66-22, University of California, Berkeley, California.
7. Jennings, P. C., "Equivalent Viscous Damping for Yielding Structures," Journal of the Engineering Mechanics Division, ASCE Vol. 94, No. EM1, Proc. Paper 5793, February, 1968, pp. 103-116.
8. Rea, D., Clough, R. W., Bouwkamp, J. G. and Vogel, U., "Damping Capacity of a Model Steel Structure," Preprint of 4WCEE, Chile, January, 1969, pp. B-2 (63-74).
9. Tow, D. "EQUAL" and "UNEQUAL," two computer programs for calculating response spectra from strong-motion acceleration records, General Atomic Company, unpublished data, November, 1970.

INTERNATIONAL SYMPOSIUM ON
EARTHQUAKE STRUCTURAL ENGINEERING

345

St. Louis, Missouri, USA, August, 1976

A SIMPLIFIED
NONLINEAR SEISMIC RESPONSE
ANALYSIS OF STRUCTURES
INCLUDING VERTICAL GROUND MOTION

D. R. BERVIG

Structural Systems Consultant

Black & Veatch

Kansas City, Missouri, USA

SUMMARY

The seismic response of structures was studied by using a small and large displacement analysis for a one and two story model. Both the small and large displacement analyses used in this study include the effect of a bilinear or elasto-plastic force-displacement relationship. In addition, the large displacement analysis includes the large displacement coupling term relating the horizontal and vertical displacement, the P-delta effect and vertical ground motion.

The P-delta effect in the analysis evolves from a consideration of the stiffness of a fixed-fixed column with axial forces applied at the ends. In the dynamic analysis, the axial forces acting on the columns include the gravity, or dead loads of the structure, in addition to the vertical inertia loads resulting from vertical accelerations. The vertical acceleration of the structural mass depends not only on the vertical ground motion but also on the large displacement coupling term. Due to axial forces, the horizontal restoring force of the columns will decrease for large horizontal distortions.

The objective of the study was to determine the significance of these additional effects on the seismic response of the one and two story models. In order to evaluate the effect of these additional terms the small displacement differential equations of motion were solved and used as a baseline for comparison with the solutions from the large displacement differential equations of motion.

A complete parametric study was conducted over the frequency range of .2 cps to 10 cps. The effects of various levels of elastic and plastic action, damping and vertical ground motion on the response of the one and two story models were investigated.

The results showed that the large displacement considerations included in the analysis do have an effect on the seismic response of structures. This was found to be particularly true for the lower

frequencies (2 cps or less) when a large amount of plastic action was allowed to take place.

The seismic response studies for the one and two story models strongly indicate that vertical ground motion could be a significant factor for tall structures.

INTRODUCTION

When a structure is subjected to an earthquake, the base of the structure essentially moves with the ground while the upper stories move relative to the ground. These relative motions can be of such large magnitudes that plastic deformations occur causing permanent offsets in the structure. The extent of the damage, especially the amount of permanent offset, will determine the useability of the structure.

The problem of designing a structure to minimize damage caused by earthquakes has been of considerable interest for some time. Some of the earliest published work done in this area was by Martel (1)* and Green (2)* on the flexible first story concept. Martel studied the response of a single bent excited harmonically. His studies show that the flexible first story concept will not reduce the accelerations of the upper stories if the period of the fundamental frequency of the earthquake is greater than the fundamental period of the bent. Essentially the same conclusion was reached by Green. By using a single degree of freedom spring and mass system, he showed it would be very difficult to isolate the upper stories from low frequency ground motions.

A more recent publication, that of Fintel and Khan (3)* extends the flexible first story concept by designing a shock absorbing system into the structure of the first floor. Their studies show that by using a shock absorbing system with a bilinear force-displacement characteristic, it is possible to keep the force input to the upper stories below a specified level as well as confine the damage to the first floor. They analyzed the response characteristics of their one story model within the completely plastic to 10 percent elastic range. For clarification of the plastic and elastic terms refer to page 10.

Thomaides (4), made a study of bilinear single degree of freedom systems. He investigated the response characteristics over a much wider range, from zero to 25 percent elastic action. One of his conclusions which is of particular interest in regards to this study is that a structure will sustain less permanent offset when the amount of elastic action is increased in a structure.

None of the references previously cited included the effect of vertical ground motion.

*The number in parenthesis refers to a reference included in the bibliography.

The existing seismic building codes are reviewed in references (5), (6) and (7). They are primarily based on the concept of absorbing energy to prevent catastrophic failures by allowing large amounts of plastic action to take place within the structure. This requires designing buildings with high ductility factors. The code also requires a quasi-static earthquake loads analysis which consists of applying lateral loads at the different floor levels of the structure. These lateral loads are based on a number of considerations. Some of those considered are gravity plus dynamic loads, seismic zone factors, site soil factors, etc. The dynamic loads used in the code are based essentially on results obtained from single degree of freedom models. The effects of large displacement coupling, P-delta effect and vertical ground motion, have not been considered in arriving at the present codes.

The analytical work by Smith, Ernst and Maheshwari (12) points out the importance of designing with steel that does not have a yield plateau. They show that the use of this type of steel in the design of structures will significantly reduce the amount of permanent offset. The results from the experimental work at Nebraska, conducted by Smith, Ernst, Riveland, and Pierce (13) substantiates their analytical results. From this work, a new design philosophy has evolved which is the designing of buildings with as much reserve elasticity (elastic action) as possible in order to minimize permanent offset and damage.

An area in which a lot of development work has taken place is use of the finite element technique to study the linear and non-linear seismic response of structures. A number of large scale linear three dimensional and non-linear two dimensional programs are available. To the writer's knowledge, no large scale non-linear three dimensional frame analysis programs are available at this time. A large scale two dimensional non-linear program was not used in this study because of the difficulty of conducting simplified parametric studies. It was also felt the cost involved would be prohibitive.

The objective of this study is to determine the combined effect of large displacement coupling, P-delta effect, vertical ground motion, and bilinear action, on the following structural response characteristics:

- (1) Distortion
- (2) Permanent offset
- (3) Lateral force coefficients

DERIVATION OF THE EQUATIONS OF MOTION FOR THE ONE AND TWO STORY MODELS

The differential equation of motion which include the large displacement coupling term, the P-delta effect, and the vertical ground motion was derived as follows for the one story structure which is shown schematically in figure 1a. The equation was derived with the restriction that the mass m_1 moves parallel with the horizontal plane. This restriction is realistic since most buildings are built such that this type of motion will predominate. This restriction is substantiated by pictorial documentation of earthquake damaged structures. For instance, figure 3.15 page 156 of reference (11) shows the deformed shape of a reinforced concrete structure damaged by the San Fernando earthquake of February 9, 1971.

This figure shows that the columns are deformed approximately in the fixed-fixed mode shape while the first floor remains horizontal. It is further assumed in the derivation that the inertial effects of the column and its axial deformation are negligible.

The large displacement coupling term relating the vertical (Δ_V) and horizontal (Δ_H) displacements, shown in figure 2, was obtained by using an approximation method. First, the shape function, equation 1, which represents the deformed shape of a fixed-fixed column was determined.

$$y(x) = \left(\frac{3x^2}{\ell^2} - \frac{2x^3}{\ell^3} \right) \Delta_H \quad (1)$$

Next, the integral $\frac{1}{2} \int_0^\ell \left(\frac{dx}{dx} \right)^2 dx$ was used to approximate the vertical displacement (Δ_V) caused by the horizontal displacement (Δ_H). The resulting equation relating these two displacements is;

$$\Delta_V = \frac{9}{15\ell} (\Delta_H)^2 \quad (2)$$

This equation shows that large horizontal displacements, which a structure will experience during severe earthquakes, will cause significant vertical displacements. The validity of the above equation was substantiated by experimental tests. A comparison of the experimental and theoretical curves is given in figure 3.

The P-delta effect is included in the analysis by using a geometric stiffness term for a fixed-fixed column with axial forces applied at the ends. The important effect included in the analysis, by using the geometric stiffness, is that the columns horizontal stiffness decreases as the axial load increases. In the dynamic analysis the axial load is the sum of the dead loads (gravity loads) plus live loads which herein are considered to include inertia loads.

The input to the mathematical models include the horizontal and vertical acceleration, velocity and displacement time histories.

The equation for the horizontal motion of the mass m_1 was obtained by using the concept of dynamic equilibrium, or D'Alembert's principle. The coordinates δ_{H1} , y_V and y_H shown in figure 1 are independent. δ_{H1} represents the horizontal displacement of the mass m_1 while y_V and y_H define the vertical and horizontal displacement of the ground. Vertical displacement of the mass is defined by δ_{V1} and is expressed in terms of δ_{H1} , y_V and y_H . The horizontal restoring force due to the relative displacement of a column is;

$$Q = \left(\frac{12EI}{\ell^3} - \frac{6P_T}{5} \right) (\delta_{H1} - y_H) \quad (3)$$

where the first term in parenthesis is the geometric stiffness and the second term in parenthesis is the relative horizontal displacement between

the mass m_1 and the ground. The relative displacement term is referred to as distortion,

The free body diagram of the mass m_1 is given in figure 1b. By summing moments about points a and b which represent the inflection points of the columns, equations are obtained for the axial loads (P_R and P_L) in the right and left columns. These equations are:

$$P_R = -\frac{m_1 \ddot{\delta}_{H1}}{w} \left(\frac{\ell}{2} - \frac{\Delta_V}{2} \right) - \frac{m_1 \ddot{\delta}_{V1}}{w} \left[\frac{w}{2} + \left(\frac{\delta_{H1} - y_H}{2} \right) \right] \quad (4)$$

$$+ \frac{m_1 g}{w} \left[\frac{w}{2} + \left(\frac{\delta_{H1} - y_H}{2} \right) \right]$$

$$P_L = \frac{m_1 \ddot{\delta}_{H1}}{w} \left(\frac{\ell}{2} - \frac{\Delta_V}{2} \right) - \frac{m_1 \ddot{\delta}_{V1}}{w} \left[\frac{w}{2} - \left(\frac{\delta_{H1} - y_H}{2} \right) \right]$$

$$+ \frac{m_1 g}{w} \left[\frac{w}{2} - \left(\frac{\delta_{H1} - y_H}{2} \right) \right] \quad (5)$$

where
$$\Delta_V = \frac{9}{15\ell} (\delta_{H1} - y_H)^2$$

The differential equation for the horizontal motion of mass m_1 was derived by summing the horizontal forces which gives;

$$m_1 \ddot{\delta}_{H1} + k_L (\delta_{H1} - y_H) + k_R (\delta_{H1} - y_H) = 0 \quad (6)$$

where
$$k_L = \left(\frac{12EI}{\ell^3} - \frac{6P_L}{5\ell} \right)$$

$$k_R = \left(\frac{12EI}{\ell^3} - \frac{6P_R}{5\ell} \right)$$

Now, by substituting for the axial column loads P_R and P_L and rearranging, equation 6 becomes:

$$m_1 \ddot{\delta}_{H1} + 2 \left[\frac{12EI}{\ell^3} - \frac{6}{5\ell} \left(\frac{m_1 g}{2} - \frac{m_1 \ddot{\delta}_{V1}}{2} \right) \right] (\delta_{H1} - y_H) = 0 \quad (7)$$

This equation gives an interesting insight into the problem. For instance, the restoring force in the above equation is decreased by the static gravity term $\left(\frac{m_1 g}{2} \right)$ and increased by the large displacement coupling acceleration term $\frac{m_1 \ddot{\delta}_{V1}}{2}$.

Noting that $\ddot{\delta}_{V1} = (18/15\ell)[\delta_{H1}-y_H](\ddot{\delta}_{H1}-\ddot{y}_H) + (\dot{\delta}_{H1}-\dot{y}_H)^2] + \ddot{y}_V$ and adding a viscous damping term, the large displacement response equation for a one story structure is;

$$\begin{aligned} \ddot{\delta}_{H1} = & -\alpha \frac{\omega_n^2}{D} (\delta_{H1}-y_H) - \beta \frac{\omega_n^2}{D} (\delta_{H1}-y_H)^2 \\ & - \frac{2\xi\omega_n}{D} (\dot{\delta}_{H1}-\dot{y}_H) + \frac{6g}{5\ell D} (\delta_{H1}-y_H) + \frac{108}{75\ell^2 D} (\delta_{H1}-y_H)^2 \ddot{y}_H \\ & - \frac{108}{75\ell^2 D} (\dot{\delta}_{H1}-\dot{y}_H)^2 (\delta_{H1}-y_H) - \frac{108}{75\ell D} (\delta_{H1}-y_H) \ddot{y}_V \end{aligned} \quad (8)$$

where:

α = percent elastic action

β = percent plastic action

$$D = 1 + \frac{108}{75\ell^2} (\delta_{H1}-y_H)^2$$

δ_{H1} = horizontal displacement of mass m_1 (in)

y_H = horizontal ground motion (in)

y_V = vertical ground motion (in)

g = acceleration of gravity (in/sec²)

ξ = damping factor

ℓ = length of columns (in)

$$\omega_n = \sqrt{\frac{2(12EI)}{m_1 \ell^3}} \quad \text{fundamental frequency of one story model for small displacements (rad/sec)}$$

The first three terms on the right hand side of the equal sign, when (D=1), is the equation of motion for mass m_1 considering small displacements. This is the equation which G. M. Smith, G. Ernst, and Maheshwari (12) have investigated quite thoroughly. The next three terms are due to large displacement coupling and P-delta considerations while the last term comes from including vertical ground motion.

Equations for the two story model were derived in the same manner as for the one story model. A set of coupled non-linear differential equations was obtained which defines the motion of masses m_1 and m_2 as shown in figure 4. The independent coordinates used in the analysis are δ_{H1} and δ_{H2} which represent the horizontal motion of masses m_1 and m_2 while the horizontal and vertical ground motions are defined by y_H and y_V , respectively.

The vertical displacements of masses m_1 and m_2 can be expressed as a summation in terms of the independent coordinates. These equations are:

$$\delta_{V1} = \frac{9}{15\ell_1} (\delta_{H1} - y_H)^2 + y_V \quad (9)$$

$$\delta_{V2} = \frac{9}{15\ell_1} (\delta_{H1} - y_H)^2 + \frac{9}{15\ell_2} (\delta_{H2} - \delta_{H1})^2 + y_V \quad (10)$$

The differential equation of motion for mass m_2 is determined by summing forces in the horizontal direction in figure 5a. After making the necessary substitutions, we obtain;

$$m_2 \ddot{\delta}_{H2} + 2 \left\{ \left(\frac{12EI}{\ell^3} \right) (\delta_{H2} - \delta_{H1}) - \frac{6}{5\ell_2} \left[\left(\frac{m_2 g}{w} \left(\frac{w}{2} \right) - \frac{m_2 \ddot{\delta}_{V2}}{w} \left(\frac{w}{2} \right) \right] \right\} (\delta_{H2} - \delta_{H1}) = 0 \quad (11)$$

Again, we find that the horizontal restoring force is decreased by the gravity term and increased by the vertical acceleration term.

The differential equation of motion for mass m_1 is derived by summing the horizontal forces in figure 5b. Upon substituting for the axial column loads P_{L1} , P_{R1} , P_{L2} , and P_{R2} , the equation becomes;

$$m_1 \ddot{\delta}_{H1} + \left[2 \left(\frac{12EI}{\ell_1^3} - \frac{6}{5\ell_1} (m_1 g - m_1 \ddot{\delta}_{V1} + m_2 g + m_2 \ddot{\delta}_{V2}) \right) \right] (\delta_{H1} - y_H) - \left[2 \left(\frac{12EI}{\ell_2^3} \right) - \frac{6}{5\ell_2} (m_2 g - m_2 \ddot{\delta}_{V2}) \right] (\delta_{H2} - \delta_{H1}) = 0 \quad (12)$$

Again it is noted, for the first set of terms in brackets, the gravity term reduces the restoring force while the vertical acceleration increases the restoring force. However, for the last set of terms in brackets, the gravity term increases the restoring force while the vertical acceleration decreases it.

After substituting for the vertical accelerations and the addition of the forces due to viscous damping, the differential equation for masses m_2 and m_1 are;

$$\begin{aligned}
\ddot{\delta}_{H2} = & -\frac{2}{m_2 D_2} \left(\frac{12EI}{3} \right) \frac{1}{\ell_2} (\delta_{H2} - \delta_{H1}) - \frac{C_2}{D_2} (\dot{\delta}_{H2} - \dot{\delta}_{H1}) + \frac{6g}{5\ell_2 D_2} (\delta_{H2} - \delta_{H1}) \\
& - \frac{108}{75\ell_1 \ell_2 D_2} (\ddot{\delta}_{H1} - \ddot{y}_H) (\delta_{H2} - \delta_{H1}) (\delta_{H1} - y_H) - \frac{108}{75\ell_1 \ell_2 D_2} (\dot{\delta}_{H1} - \dot{y}_H)^2 (\delta_{H2} - \delta_{H1}) \\
& + \frac{108}{75\ell_2^2 D_2} (\delta_{H2} - \delta_{H1})^2 \ddot{\delta}_{H1} - \frac{108}{75\ell_2^2 D_2} (\dot{\delta}_{H2} - \dot{\delta}_{H1})^2 (\delta_{H2} - \delta_{H1}) \\
& - \frac{6}{5\ell_2 D_2} (\delta_{H2} - \delta_{H1}) \ddot{y}_V
\end{aligned} \tag{13}$$

$$\begin{aligned}
\ddot{\delta}_{H1} = & -\frac{\alpha(2)}{m_1 D_1} \left(\frac{12EI}{3} \right) \frac{1}{\ell_1} (\delta_{H1} - y_H) - \frac{\beta(2)}{m_1 D_1} \left(\frac{12EI}{3} \right) \frac{1}{\ell_1} (\delta_{H1} - y_H) \\
& + \frac{2}{m_1 D_1} \left(\frac{12EI}{\ell_2^3} \right) (\delta_{H2} - \delta_{H1}) - \frac{C_1}{D_1} (\dot{\delta}_{H1} - \dot{y}_H) + \frac{C_2}{D_1} (\dot{\delta}_{H2} - \dot{\delta}_{H1}) \\
& + \frac{6}{5} \frac{g}{\ell_1 D_1} (\delta_{H1} - y_H) + \frac{6}{5\ell_1} \left(\frac{m_2}{m_1} \right) \frac{g}{D_1} (\delta_{H1} - y_H) - \frac{6}{5\ell_2} \left(\frac{m_2}{m_1} \right) \frac{g}{D_1} (\delta_{H2} - \delta_{H1}) \\
& + \frac{6}{5\ell_2} \left(\frac{m_2}{m_1} \right) (\delta_{H2} - \delta_{H1}) \ddot{y}_V - \frac{6}{5\ell_1 D_1} (\delta_{H1} - y_H) \ddot{y}_V + \frac{108}{75\ell_1^2 D_1} (\delta_{H1} - y_H)^2 \ddot{y}_H \\
& + \frac{108}{75\ell_1^2 D_1} \left(\frac{m_2}{m_1} \right) (\delta_{H1} - y_H)^2 \ddot{y}_H - \frac{108}{75\ell_1^2 D_1} \left(\frac{m_2}{m_1} \right) (\dot{\delta}_{H1} - \dot{y}_H)^2 (\delta_{H1} - y_H) \\
& - \frac{6}{5\ell_1 \ell_2 D_1} \left(\frac{m_2}{m_1} \right) (\delta_{H2} - \delta_{H1}) (\delta_{H1} - y_H) \ddot{\delta}_{H2} - \frac{108}{75\ell_1 \ell_2 D_1} \left(\frac{m_2}{m_1} \right) (\dot{\delta}_{H2} - \dot{\delta}_{H1}) (\delta_{H1} - y_H) \\
& - \frac{6}{5\ell_1} \left(\frac{m_2}{m_1} \right) (\delta_{H1} - y_H) \ddot{y}_V - \frac{108}{75\ell_1 \ell_2 D_1} \left(\frac{m_2}{m_1} \right) (\delta_{H1} - y_H) (\delta_{H2} - \delta_{H1}) \ddot{y}_H \\
& + \frac{108}{75\ell_2^2 D_1} \left(\frac{m_2}{m_1} \right) (\dot{\delta}_{H2} - \dot{\delta}_{H1})^2 (\delta_{H2} - \delta_{H1}) + \frac{108}{75\ell_1 \ell_2 D_1} \left(\frac{m_2}{m_1} \right) (\dot{\delta}_{H1} - \dot{y}_H)^2 (\delta_{H2} - \delta_{H1}) \\
& + \frac{108}{75\ell_2^2 D_1} \left(\frac{m_2}{m_1} \right) (\delta_{H2} - \delta_{H1})^2 \ddot{\delta}_{H2}
\end{aligned} \tag{14}$$

where

$$D_2 = \left[1 + \frac{108}{75\ell_2^2} (\delta_{H2} - \delta_{H1})^2 \right]$$

$$D_1 = \left[1 + \frac{108}{75\ell_1^2} (\delta_{H1} - y_H)^2 + \frac{108}{75\ell_1^2} \left(\frac{m_2}{m_1} \right) (\delta_{H1} - y_H)^2 \right. \\ \left. - \frac{216}{75\ell_1\ell_2} \left(\frac{m_2}{m_1} \right) (\delta_{H2} - \delta_{H1}) (\delta_{H1} - y_H) + \frac{108}{75\ell_2^2} \left(\frac{m_2}{m_1} \right) (\delta_{H2} - \delta_{H1})^2 \right]$$

$$C_1 = C_2 = 2\xi\omega_n$$

ξ = percent of critical damping

$$\omega_n = \sqrt{0.293 \left(\frac{24EI}{3\ell_1} \right)}$$

fundamental frequency of two story model (Rad/sec) with $m_2 = m_1/2$.

m_2 = lumped mass representing second floor (lb-sec²/in) = $m_1/2$

m_1 = lumped mass representing first floor (lb-sec²/in)

δ_{H2} = horizontal displacement of mass m_2 (in)

δ_{H1} = horizontal displacement mass m_1 (in)

ℓ_2 = length of columns supporting mass m_2 (in)

ℓ_1 = length of columns supporting mass m_1 (in)

y_V = vertical displacement of ground (in)

y_H = horizontal displacement of ground (in)

g = acceleration of gravity (in/sec²)

The two equations, 13 and 14, are referred to as the large displacement equations for the two story model.

The small displacement equations for the two story model are obtained by setting $D_1 = D_2 = 1$, and keeping the first two terms on the right hand side of equation 13 and the first five terms on the right hand side of equation 14. All the other terms in equations 13 and 14 come from considering the large displacement coupling term, the P-delta effect and vertical ground motion.

PROCEDURES FOR THE SOLUTION OF THE ONE AND TWO STORY MODEL EQUATIONS

The differential equations of motion were solved using a digital computer program which functions as an analog computer. For the one and two story models, the computer program uses an idealized bilinear hysteresis loop to represent the force-deflection property of reinforced concrete. In order to mathematically define the bilinear hysteresis loop α and β parameters were used. Smith, Ernst and Maheshwari (12) give a detailed discussion on the various interpretations that may be given to the α and β parameters. Herein, the α and β parameters simply represent the percent of elastic and plastic action, respectively, allowed for a particular structure. By using these terms, the restoring force Q can be expressed as:

$$Q = Q\alpha + Q\beta$$

where $Q\alpha = \alpha(Q) =$ elastic restoring force

$Q\beta = \beta(Q) =$ plastic restoring force

$$\alpha + \beta = 1$$

The bilinear restoring force as related to the α and β parameters is shown in figure 6. Initially, at point 0, the structure is unloaded. With increasing distortion, the structure will go partially plastic which is shown to occur at point a. For any additional distortion, the $Q\beta$ term remains constant while $Q\alpha$ continues to increase. The sum of $Q\alpha$ and $Q\beta$ gives the total restoring force Q .

Corrected versions of the San Fernando earthquake of February 9, 1971 were used to excite the one and two story models. These records were obtained from the National Earthquake center at the California Institute of Technology in Los Angeles. Information regarding this earthquake data is given in references (14) and (15). The data points defining the acceleration-time histories are supplied at time increments of .02 seconds. The velocity and displacement time histories of the earthquake, which are required for the solution of the non-linear differential equations, were obtained by integrating the acceleration-time histories.

As stated in the introduction, the objective was to determine the significance of the additional terms on the response of the one and two story dynamic models. In order to evaluate the effect of the additional terms the differential equations for small displacements were solved and used for comparison purposes.

A parametric study was made for the following parameter values:

α = percent elastic action (0., .5, 1.0)

β = percent plastic action (1., .5, 0.)

ξ = damping factor (.03, .1)

$f_n = \omega_n / 2\pi$ = fundamental frequency (one story model) (.2 to 10 cps)

$f_n = \omega_n / 2\pi = \sqrt{.293 \left(\frac{2(12EI)}{l^3} \right)}$ = Fundamental frequency (two story model)
(.3 to 10 cps)

$U_p = K(U_e)$

where U_p = distortion level at which plastic action starts

K = fraction of maximum linear distortion (.4, .6, .8, 1.)

U_e = maximum elastic distortion

The parameter K determines the level of distortion at which plastic action occurs (U_p). For example, the completely elastic ($\alpha=1.0$, $\beta=0.0$) response for the one story model is shown in figure 7. Thus, when bilinear runs are made for a particular β value, distortions above the line $K = .6$ would cause plastic action to occur in the structure.

All the response-time histories for the one and two story models were solved using the 4th order Runge-kutta integration method. The computer program was checked by comparing the small displacement response solutions with those obtained by Smith, Ernst and Maheshwari (12) for linear and bilinear cases. For a linear case, the analog solution of Smith, Ernst and Maheshwari gave a maximum distortion of 5 inches while the program used gave 5.12 inches maximum distortion. This small difference in distortion is representative of all the cases run. When considering the possible errors in the analog simulation approach and the round off errors, etc. for digital computation, the writer feels that the agreement between the two solutions is very good.

An exact check on the solution of the large displacement problem was not possible because no published results were available for comparison. Since the main harmonic components of the San Fernando earthquake are below 0.3 cps it was felt that a high frequency model should respond about the same for either a small or large displacement analysis. Therefore, check runs were made using the small or large displacement analyses for a high frequency model. Since the results for the two solutions compared almost exactly, it is an indication that the large displacement differential equation was programmed correctly.

The equations for the two story model were solved using a mass ratio of $\left(\frac{m_1}{m_2} = 2\right)$ for the first and second floors. The damping in the model

is the same viscous damping term $(2\xi\omega_n)$ used in the one story model. The ω_n term is the first mode frequency of the two story model and was used as the basis for plotting the results. The computer codes for the two story model (small and large displacement analyses) were checked in the same manner as the one story model.

COMPARISON OF RESULTS BETWEEN THE SMALL AND LARGE DISPLACEMENT ANALYSES

The response characteristics of the one and two story models were investigated over a frequency range of .2 to 10 cps. It was found that for frequencies over 4 cps, the small and large displacement analysis gave essentially the same results. Therefore, the response information for the one and two story models is plotted for a frequency range of 0.2 to 4.0 cps. The results obtained for cases where $K = .6$ or $K = .8$ compared closely with the results for the completely linear cases ($\alpha = 1$ and $\beta = 0$). Because of this, response information on the cases where $K = .6$ or $K = .8$ has not been included since they would have added very little useful information.

The maximum distortion response solutions for the first story of the one and two story models are shown in figures 8, 9 and 10. For the completely elastic cases shown in figure 8, the small and large displacement analyses compare very closely for frequencies above 0.7 cps. Below this frequency, the two solutions differ. For example, the small displacement analysis for the one story, figure 8a, shows a sharp increase in distortion below 0.7 cps while the large displacement analysis shows a decrease to .5 cps. For the two story model, the difference in the first story distortion determined by the two analyses is shown in figure 8b. Again, the differences occur below 0.7 cps.

As the amount of plastic action is increased, the large displacement terms become more significant. This can be seen by comparing figures 8 and 9. The difference in distortion between the small and large displacement analyses for the one story model has increased significantly for frequencies below 1.0 cps. For example, at .75 cps the large displacement analysis shows an increase of 35 percent. For the two story model, the point at which the small and large displacement analyses differ considerably in first story distortion has moved up from .7 cps to about 1.7 cps. The effect of reserve elasticity on distortion is shown in figure 10. For the case with $\alpha = \beta = .5$, the region of difference between the small and large displacement analyses for maximum distortion has dropped below 0.7 cps. This compares very closely with the completely elastic case.

A comparison of the results obtained for permanent offset for the small and large displacement analyses are shown in figures 11 and 12. There is a considerable difference between the small and large displacement analyses in the amount of offset for the one story model. This is shown in figure 11a. For example, at 0.75 cps the large displacement analysis

shows an increase of 72 percent in the amount of permanent offset. The two story model also shows a large difference in offset of the first floor up to about 1.6 cps. When the amount of elastic action is increased, the magnitude of permanent offset is significantly reduced. These results, when $\alpha = \beta = .5$ for the one and two story models, are shown in figure 12. For the one story model, the large displacement analysis, in comparison to the small displacement analysis, shows an increase in offset below 0.9 cps and a decrease in offset from 0.9, to 1.5 cps. For the two story model, the large displacement analysis shows an increase in permanent offset over the small displacement analysis for frequencies below 2.7 cps.

While investigating the maximum distortion and permanent offset characteristics for the large displacement analysis, runs were made to determine which large displacement terms were significant. It was found that the static gravity term, which is the P-delta effect, accounted for most of the differences between the small and large displacement analyses.

The vertical acceleration caused by the large displacement coupling term was evaluated for the one and two story models. The maximum vertical first floor accelerations due to the large displacement coupling term for structural models with a fundamental frequency of 1.3 cps was found to be 0.06 G's and 0.074 G's, respectively, while the maximum acceleration for the second floor was 0.076 G's. These acceleration levels are quite low in comparison to the maximum vertical ground motion acceleration of 0.71 G's for the San Fernando earthquake.

The lateral force coefficients, $C = \frac{(\ddot{\delta}_{H1})_{\max}}{g}$, for the case ($\alpha = 0.0$, $\beta = 1.0$) are shown in figure 13. There is a slight increase in the lateral force coefficient when large displacements are included in the analysis for the one story model. However, for the two story model, the opposite situation is true. In general, the large displacement analysis shows a reduction in the lateral force coefficient.

The effect of vertical ground motion for the case when ($\alpha = 0.0$, $\beta = 1.0$) is shown in figure 14. Cases were run with and without vertical ground motion using the large displacement analysis. No difference in maximum distortion was found for the one story model. However, for the two story model, the vertical ground motion did have an effect on the horizontal distortion. For instance, a 1.3 cps building showed an increase of 21 percent in maximum distortion for the first story when vertical ground motion was included.

CONCLUSIONS AND DISCUSSION

The results obtained from the small and large displacement analyses show that the large displacement terms and vertical ground motion do have an effect on the seismic response of buildings under certain conditions. As the amount of plastic action increases in a structure the more significant their effect becomes. In general, the large displacement terms have a significant effect at low frequencies.

For the one story model the maximum distortion and permanent offset show a difference between the small and large displacement analyses for frequencies below 1 cps while the two story model shows a difference below 1.7 cps. The fact that the frequency range, which shows this difference, has moved from .7 cps for a one story structure to 1.7 cps for a two story structure indicates that large displacement terms including vertical ground motion could become even more significant for taller buildings which would have frequencies within this range.

It should be kept in mind, when considering these results, that one and two story structures usually do not have fundamental frequencies under 2.0 cps.

Results from the small and large displacement analyses also show a difference for the lateral force coefficients. This difference extends over the frequency range of 1 to 4 cps for the one story model and 0.2 to 4 cps for the two story model. A maximum difference of 29 percent was calculated for the two story model which has a frequency of 1.9 cps. This also indicates that large displacement terms including vertical ground motion should be used in the dynamic analysis for the determination of lateral force coefficients.

The results showed that the vertical ground motion had essentially no effect on the horizontal response for the one story model. For the two story model the results obtained from the vertical ground motion effect study showed a difference over a frequency range from 1 cps to 4 cps. A maximum difference in distortion of 21 percent was obtained for the two story model. These results strongly indicate that taller buildings could be effected significantly by vertical ground motion.

BIBLIOGRAPHY

1. Martel, R. R., "The Effects of Earthquakes on Buildings with a Flexible First Story". Bulletin of the Seismological Society of America, Vol. 19, No. 3, September 1929.
2. Green, N. B., "Flexible First Story Construction for Earthquake Resistance". Transactions ASCE, Vol. 100, pp. 645-647, 1935.
3. Fintel, M., and Khan, F. R., "Shock-Absorbing Soft Story Concept for Multi-Story Earthquake Structures". ACI Journal, Proceedings Vol. 66, No. 5, May 1969, pp. 381-390.
4. Thomaides, Spiro S., "Earthquake Response of Systems with Bilinear Hysteresis", Journal Structural Division, ASCE No. ST4, August 1964.
5. Newmark, N. M., and Hall, W. J., "Procedures and Criteria for Earthquake Resistant Design", National Bureau of Standards Building Science Series 46, Building Practices for Disaster Mitigation, Proceedings of a Workshop sponsored by the National Science Foundation and the National Bureau of Standards, August 28-September 1, 1972, Boulder, Colorado. (Issued February 1973).
6. Sharpe, R. L., Garrison, K., and Lord, J., "Behavior of Structural Systems under Dynamic Loads", Science Series 46, Building Practices for Disaster Mitigation, Proceedings of a Workshop sponsored by the National Science Foundation and the National Bureau of Standards, August 28-September 1, 1972, Boulder, Colorado. (Issued February, 1973).
7. Blume, J. A., "Building Columns Under Strong Earthquake Exposure", Journal Structural Division, ASCE, No. ST9, September, 1971, pp. 2351-2368.
8. Martin, H. C., "On the Derivation of Stiffness Matrices for the Analysis of Large Deflections and Stability Problems", AFFDL-TR-66-80.
9. American Concrete Institute Committee 442, "Response of Buildings to Lateral Forces", ACI Journal, No. 2, Proc. Vol. 68, February, 1971, pp. 81-106.
10. Degenkolb, J. J., "Codes, Research and Engineering Practices in Earthquake Resistance Construction", ASCE Structural Engineering Conference, San Francisco, April 1973.
11. California Institute of Technology, EERL 71-02, "Engineering Features of the San Fernando Earthquake of February 9, 1971", June, 1971.
12. Smith, G. M., Ernst, G. C., and Maheshwari, M., "Seismic and Cyclonic Response of Continuous Frames", Journal Structural Division, ASCE, Vol. 100, No. ST2, February 1974.

13. Ernst, G. C., Smith, G. M., Riveland, A. R., and Pierce, D. N., "Basic Reinforced Concrete Frame Performance Under Vertical and Lateral Loads", *Journal American Concrete Institute*, No. 4, Proc. Vol. 70, April 1973, pp. 261-269.
14. California Institute of Technology, EERL 72-51, "Strong Motion Earthquake Accelerograms", February 1973.
15. California Institute of Technology, EERL 71-50, "Strong Motion Earthquake Accelerograms", September, 1971.

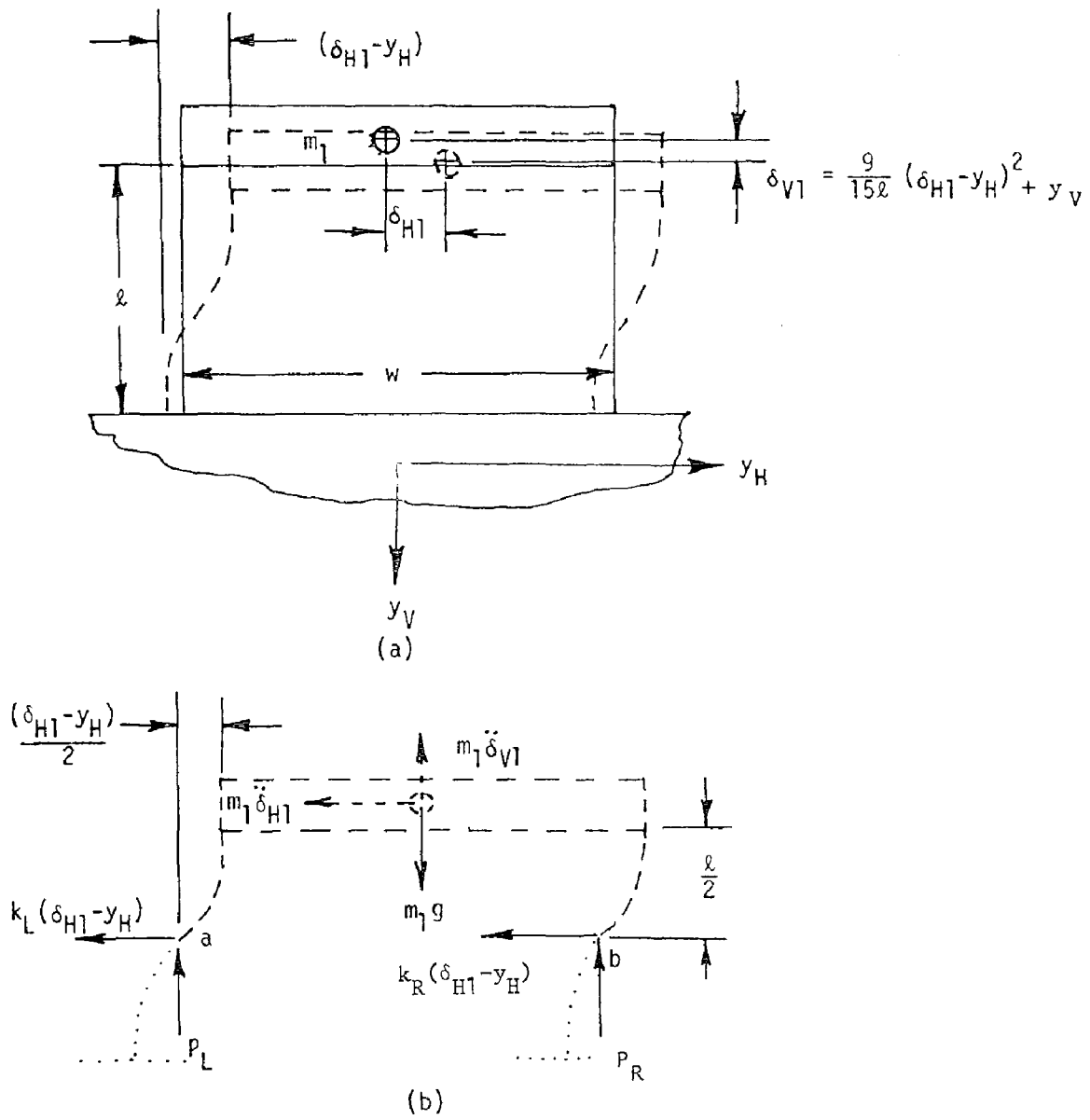


Figure 1

Schematic of one story model
and free body diagram

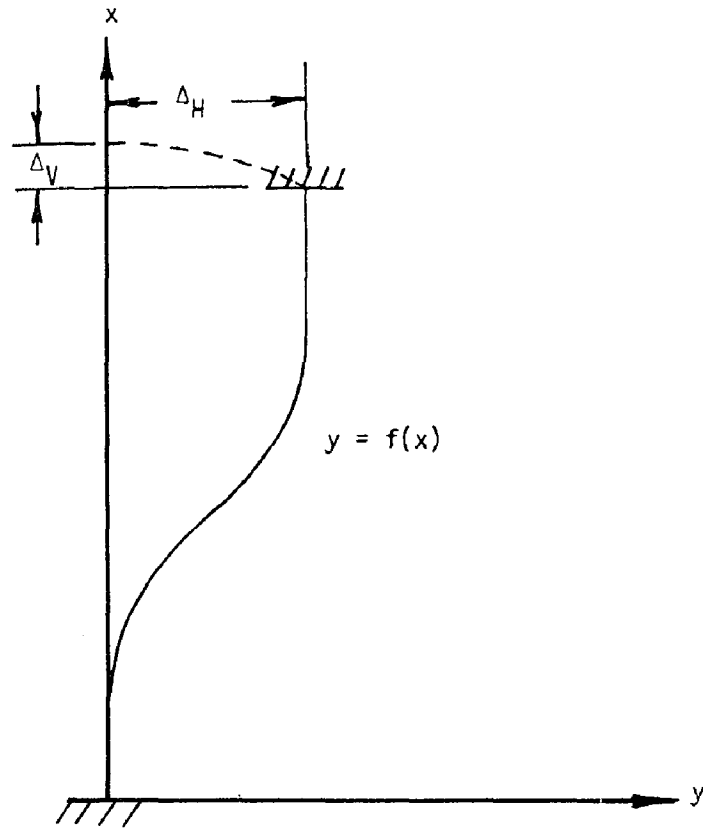


Figure 2

Column deformed in fixed-fixed mode

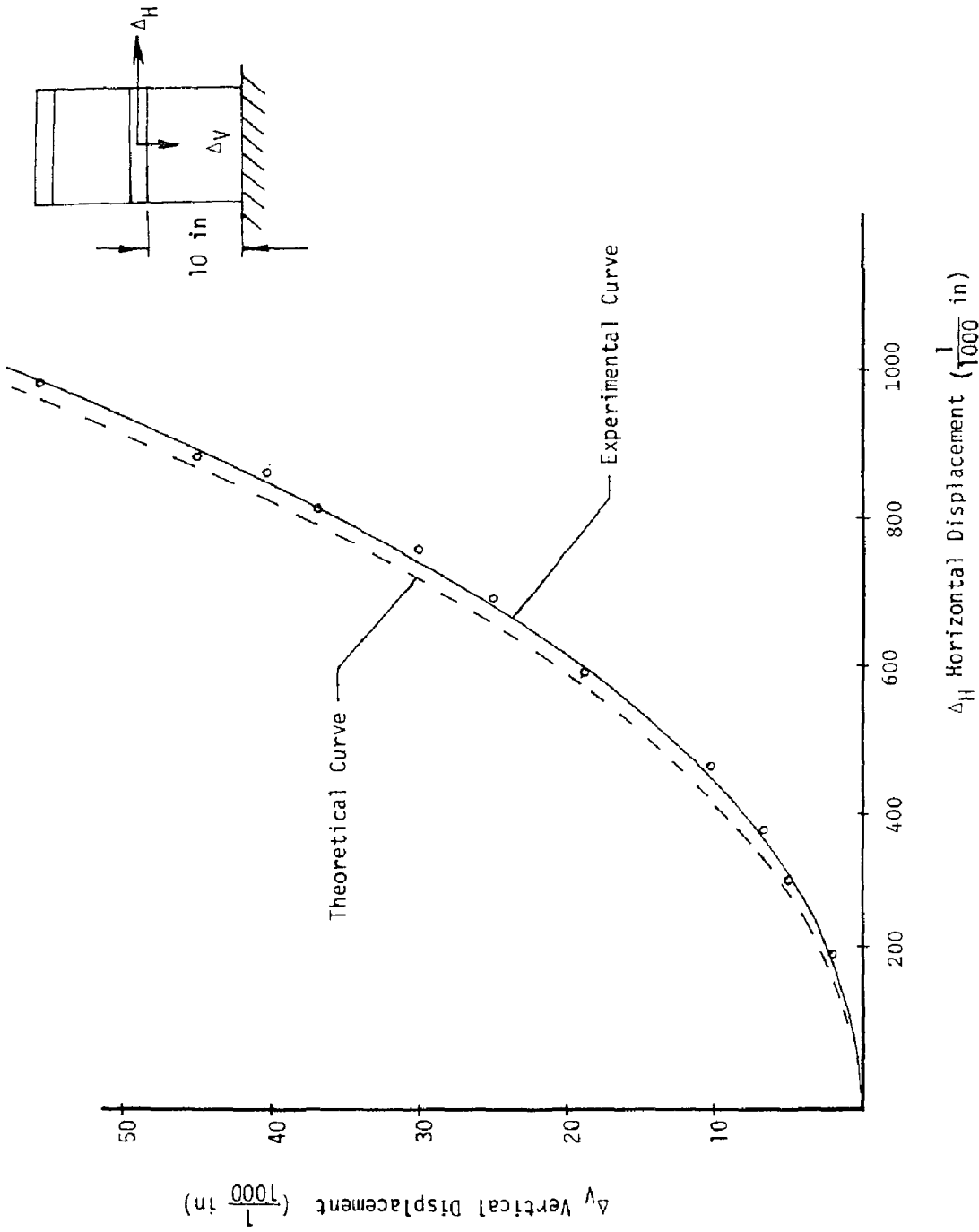


Figure 3

Large displacement coupling curve

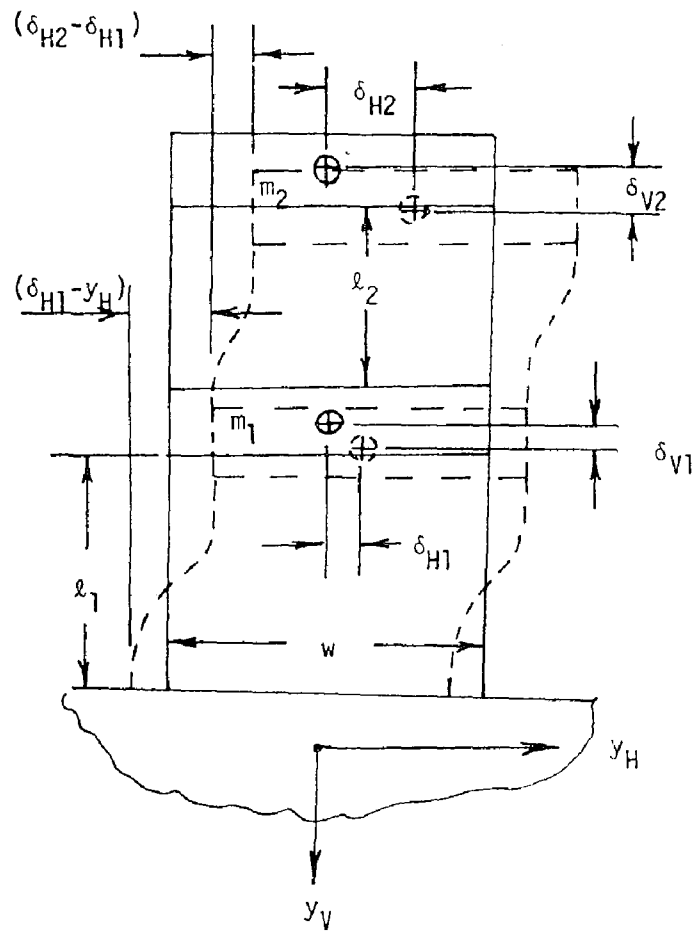


Figure 4
Schematic of two story model

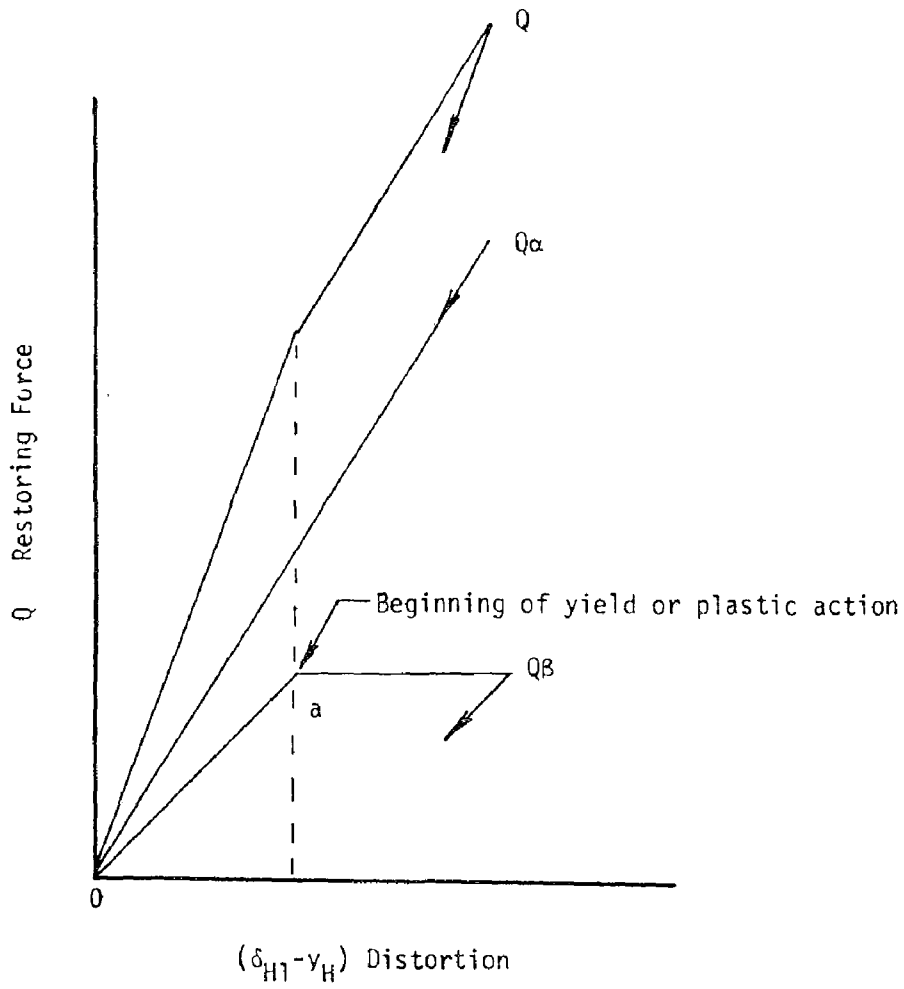


Figure 6

Relation between restoring force and distortion

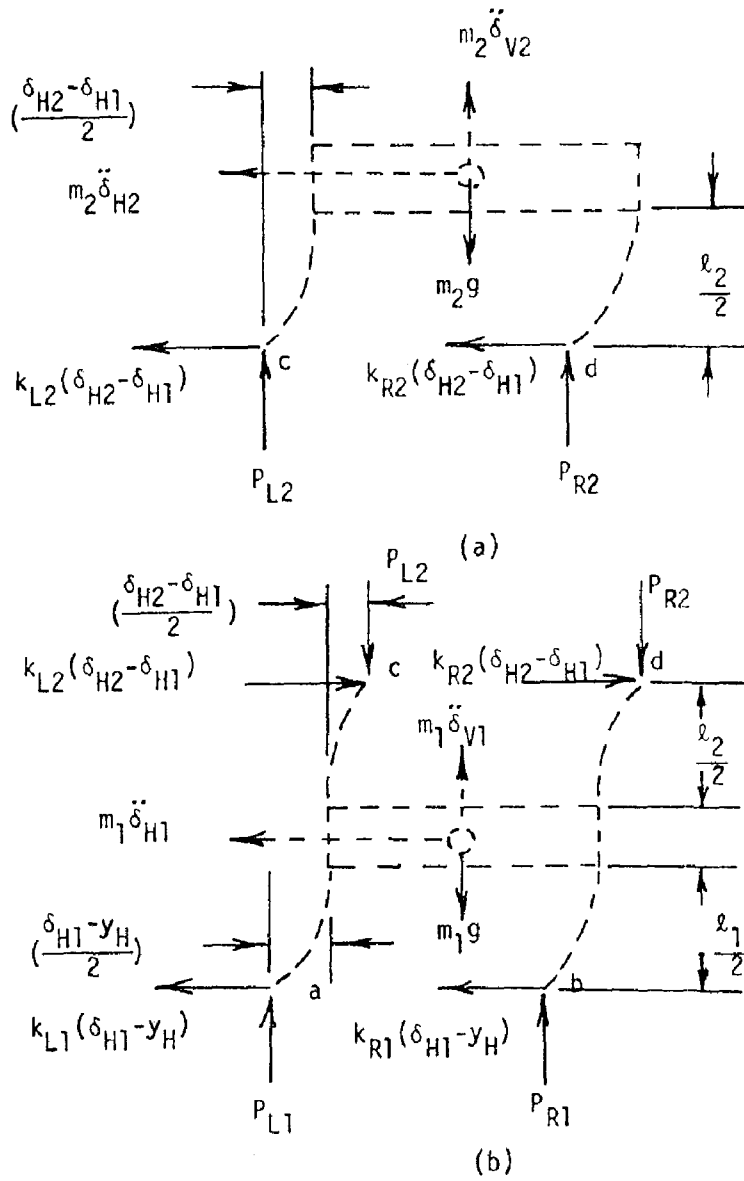


Figure 5

Free body diagrams for two story model

$\alpha = 1.0, \beta = 0.0, \xi = .03, \omega_n = 2.0 \text{ cps}$

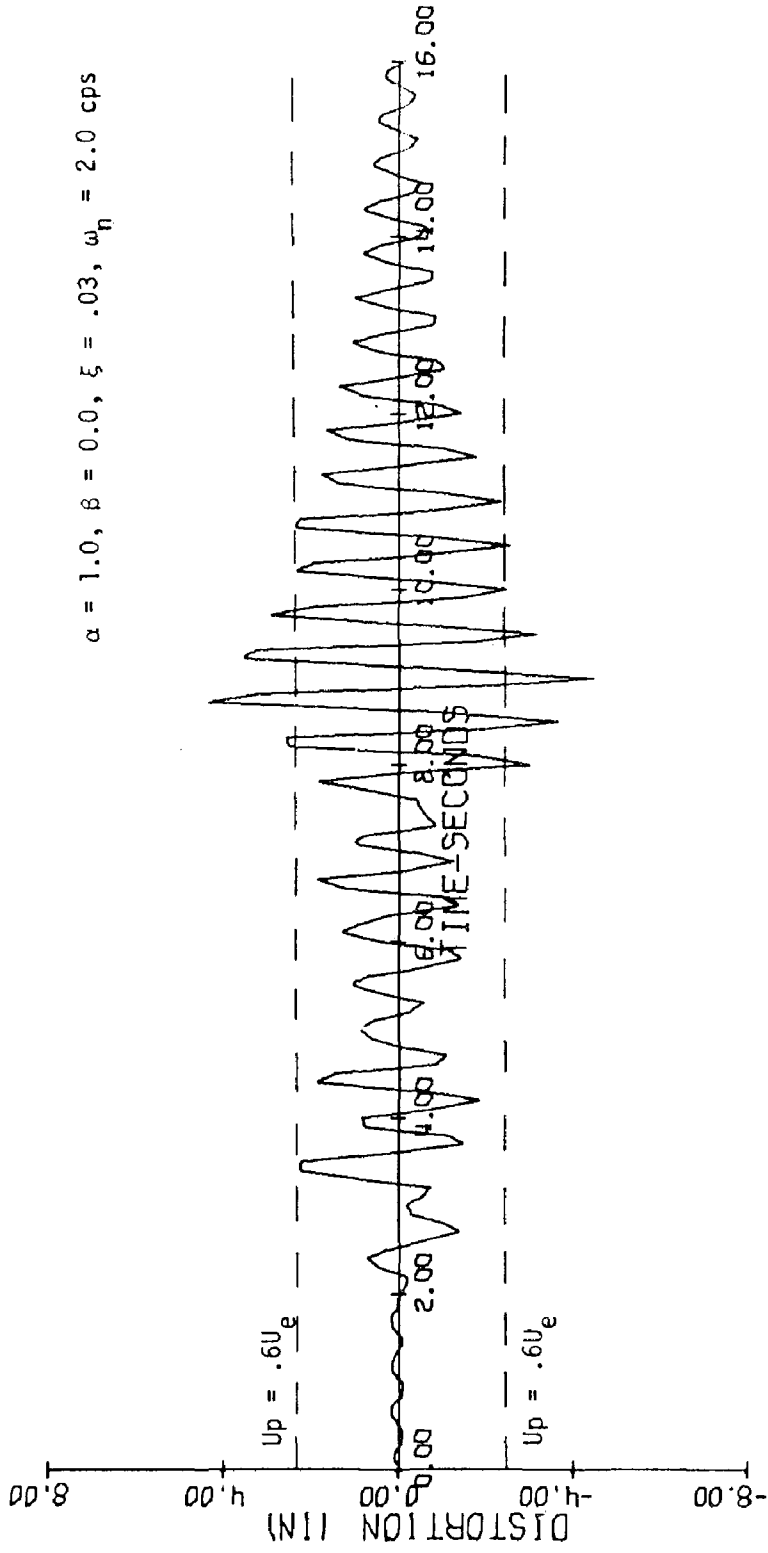
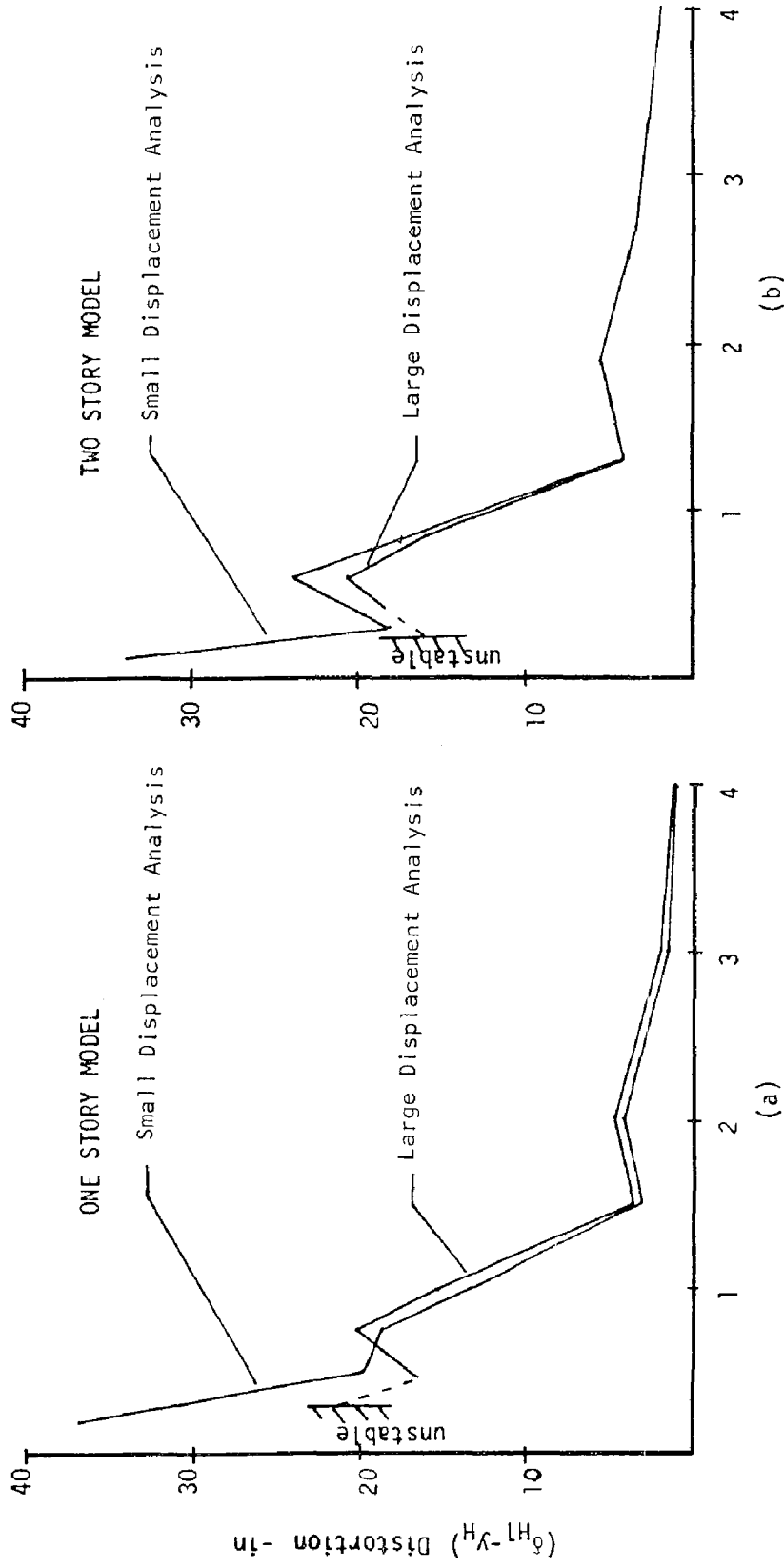


Figure 7

Elastic Response of One Story Model

$\alpha = 1.0, \beta = 0.0, \xi = .03$



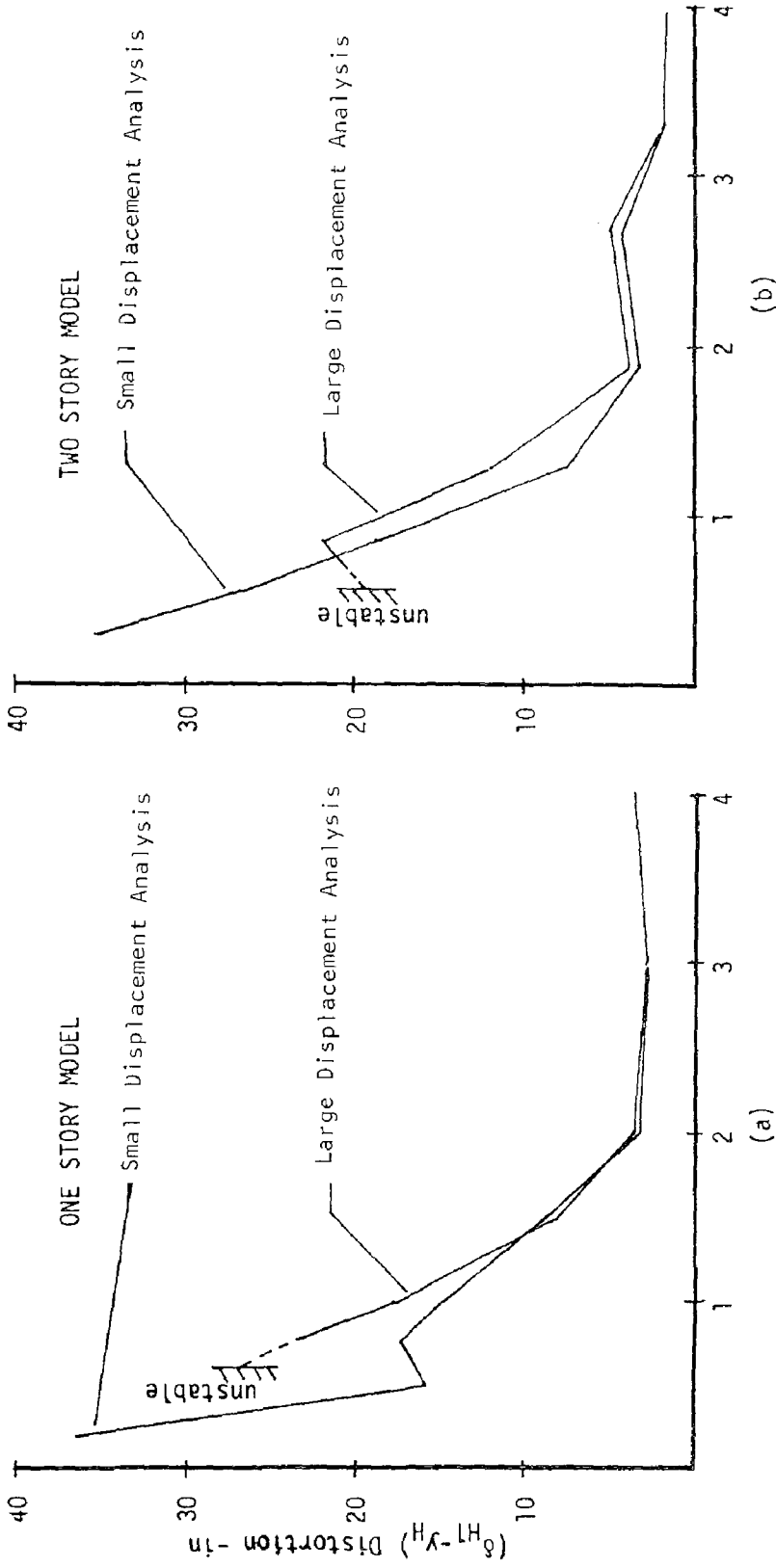
Frequency - cps

Figure 8

Maximum distortion of first story

$\alpha = 0.0, \beta = 1.0, \xi = .03$

$U_p = .4U_e$



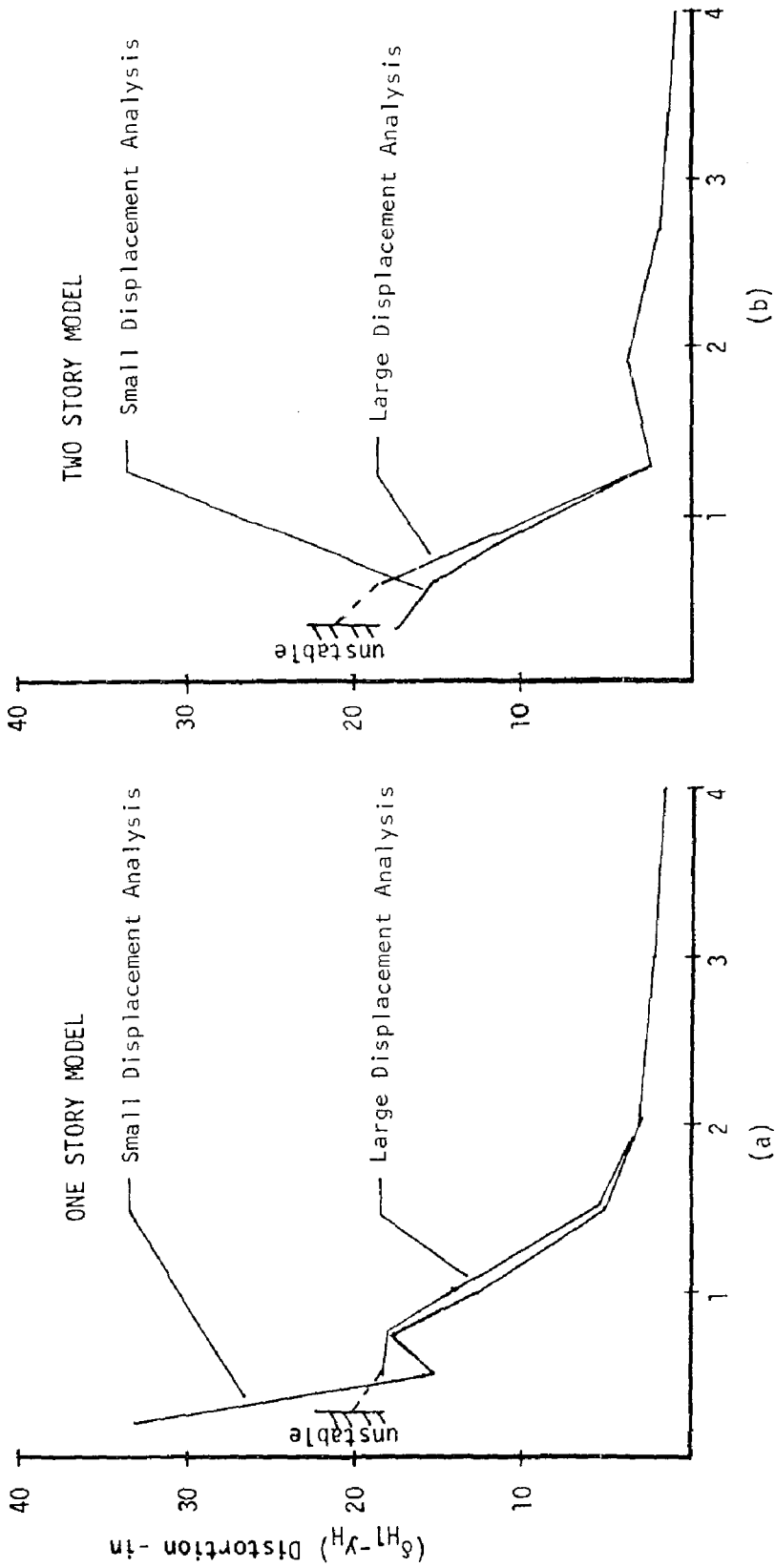
Frequency - cps

Figure 9

Maximum distortion of first story

$\alpha = 0.5, \beta = 0.5, \xi = .03$

$U_p = .4U_e$



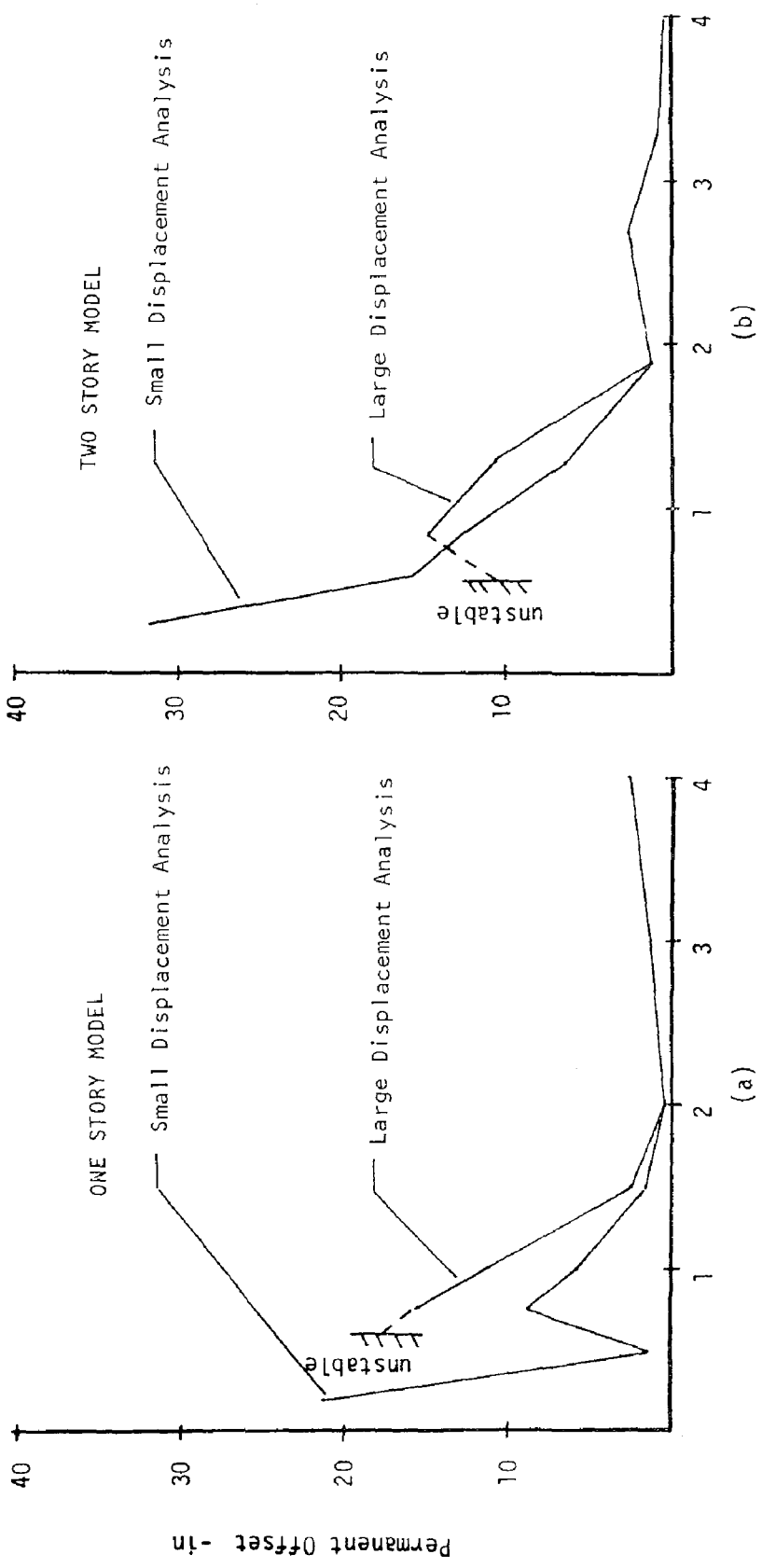
Frequency - cps

Figure 10

Maximum distortion of first story

$\alpha = 0., \beta = 1.0, \xi = .03$

$U_p = .4U_e$

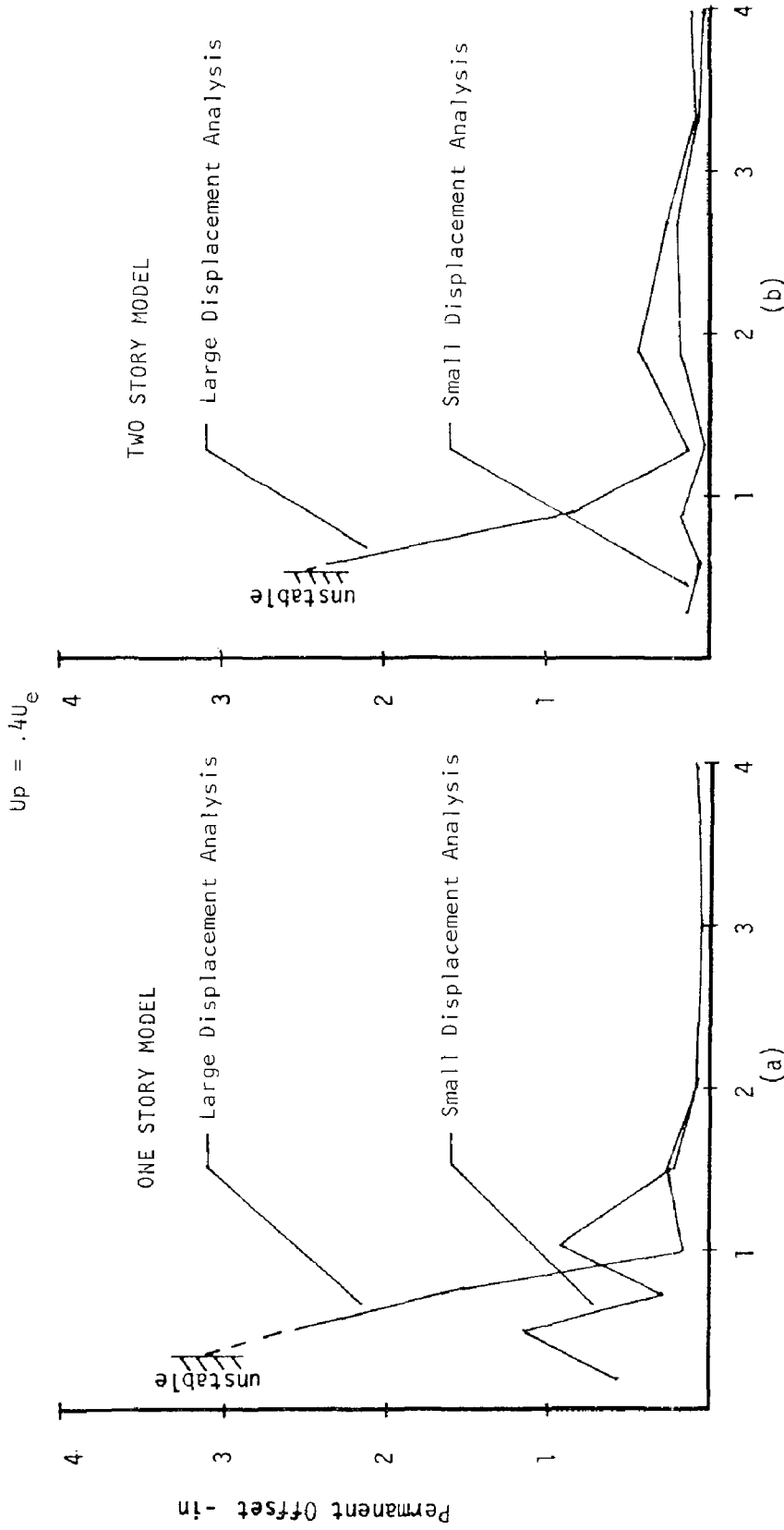


Frequency - cps

Figure II

Permanent offset of first story

$$\alpha = 0.5, \beta = 0.5, \xi = .03$$



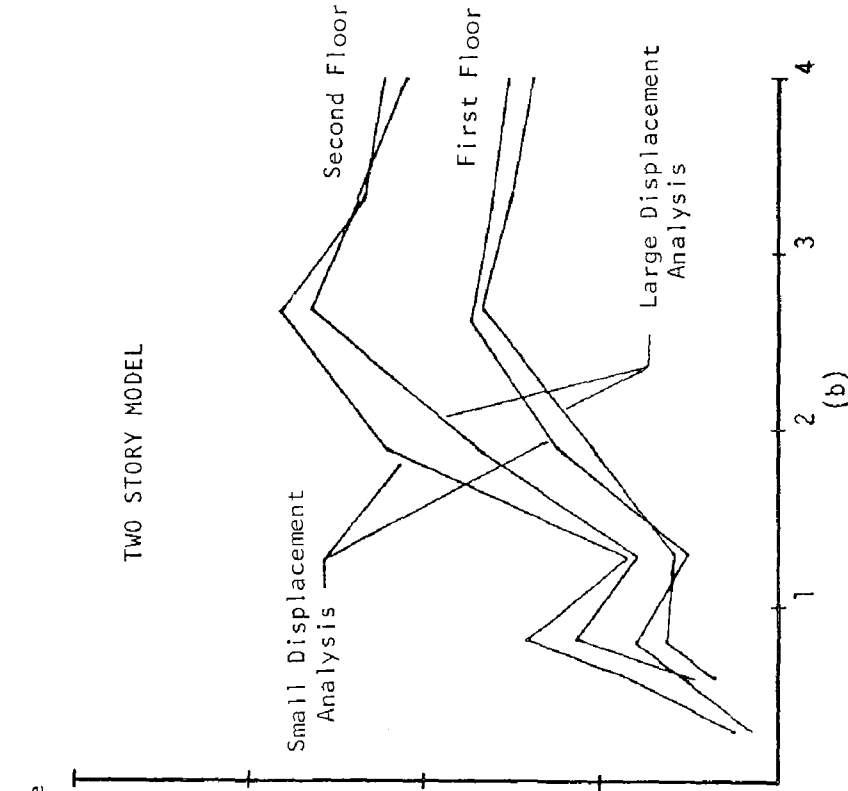
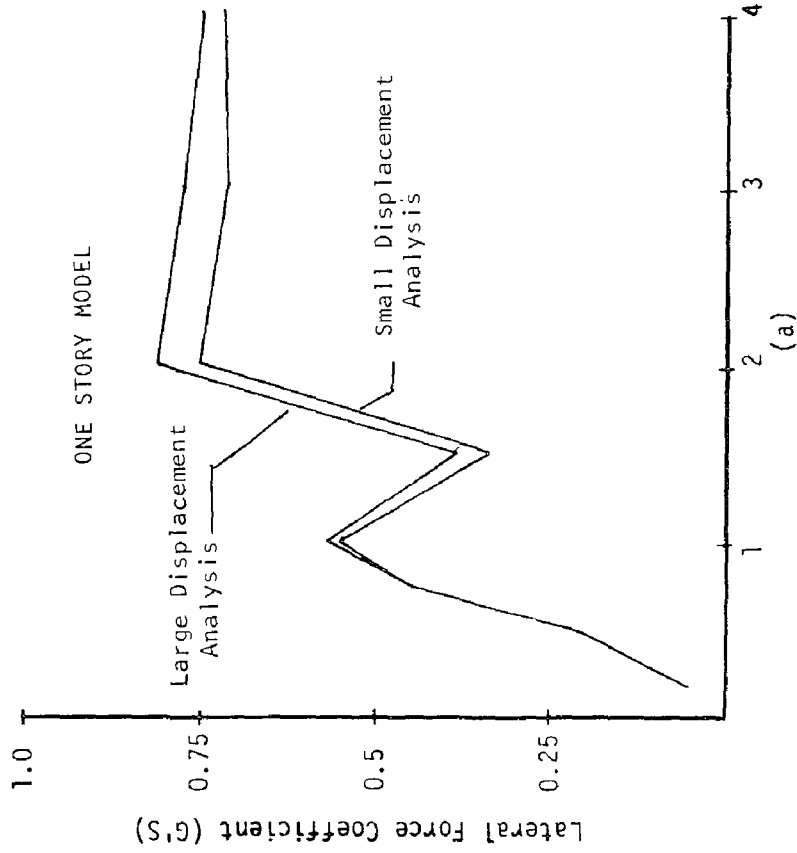
Frequency - cps

Figure 12

Permanent offset of first story

$\alpha=0.0$ $\beta = 1.0$, $\xi = .03$

$U_p = .4U_e$



Frequency - cps

Figure 13

Lateral force coefficients

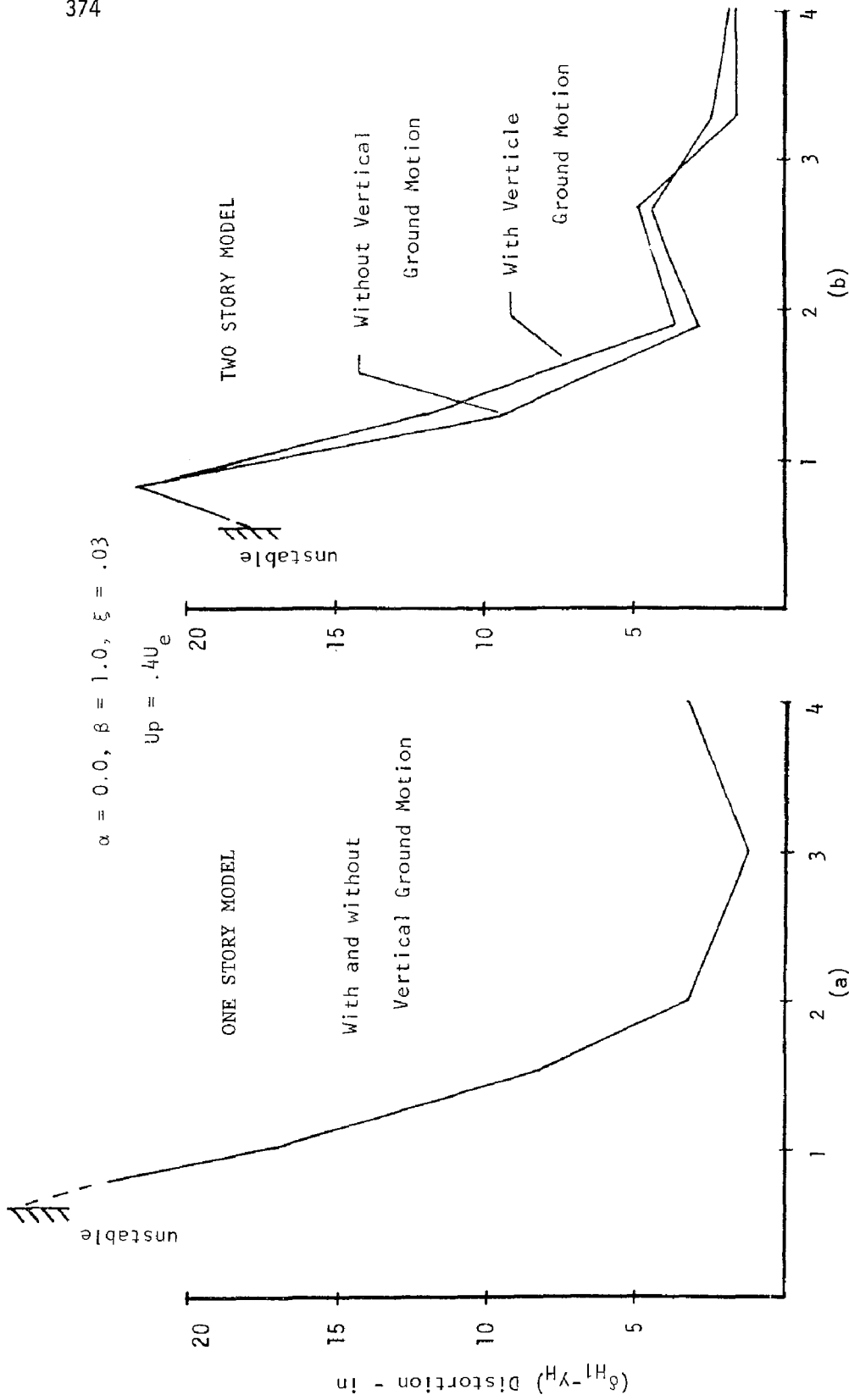


Figure 14
Maximum distortion of first story
(Large Displacement Analysis)

INTERNATIONAL SYMPOSIUM ON
EARTHQUAKE STRUCTURAL ENGINEERING

375

St. Louis, Missouri, USA, August, 1976

RESPONSE OF AN ELASTO-PLASTIC SPHERICAL
STRUCTURE IN A FLUID TO EARTHQUAKE MOTIONS

DAVID SRIMAHACHOTA
Engineer
Sigma Company Limited
Bangkok, Thailand

TONGCHAT HONGLADAROMP
Associate Professor of Civil Engineering
Asian Institute of Technology
Bangkok, Thailand

SENG-LIP LEE
Professor and Head
Department of Civil Engineering
University of Singapore
Singapore
SUMMARY

The dynamic response of a single degree of freedom spherical structure restrained elastic-plastically and submerged in a fluid of infinite extent is investigated by taking into account the fluid resistance given by Basset in terms of added mass, viscous drag and Basset history integral. The elastic-plastic behavior of the structure is characterized by a bilinear resisting force displacement relationship. The governing equation of motion is solved numerically for the response of the submerged system subjected to El Centro earthquake.

The study covers the effects of the ductility factor, Stokes number, diameter and density of the sphere and natural frequency. To facilitate the design of such structural system, response spectra for the N-S component of the El Centro earthquake May 1940 are generated for different values of the parameter in practical ranges. Response spectra in terms of the optimum yield displacement which may be used as a guide in selecting the member when the displacement is an important constraint in design are also generated.

INTRODUCTION

The dynamic response of a structure submerged in a fluid depends on physical properties of the fluid as well as those of the structure itself. The forces exerted by a real fluid on a submerged body moving arbitrarily are very complicated and, in principle, they can be determined by integrating stresses acting on the structure around the surface of the structure. However, it involves solving the nonlinear Navier-Stokes equations and an exact solution even for a sphere is not known.

A solution for the forces acting on an accelerating sphere submerged in a viscous fluid of infinite extent derived by neglecting the convective acceleration terms from the Navier-Stokes equations was given by Basset (1,2) in 1888. Such a solution is valid for high acceleration and small motions and for oscillation of small amplitude (3,6,7,10 and 11). Basset's

analysis gives the fluid resistance F in the form

$$F = \frac{1}{2} \rho_f \frac{\pi d^3}{6} \ddot{x} + 3 \rho_f \nu \pi d \dot{x} + \frac{3}{2} d^2 \rho_f \sqrt{\pi \nu} \int_0^t \frac{\ddot{x} d\tau}{\sqrt{t-\tau}} \quad (1)$$

in which ρ_f and ν are the density and kinematic viscosity of the fluid, d the diameter of the sphere, t the time, x the displacement of the sphere and the dot denotes derivative with respect to time. The first term represents the added mass, the second is the steady state viscous drag, and the last term is known as Basset history integral.

Basset's expression for forces acting on a sphere was used in the study of dynamic behavior of elastic spherical structures submerged in a viscous fluid (4,5 and 8). Basset's expression is used again here in the study of dynamic response of an elastic-plastic spherical structure submerged in a viscous fluid shown in Fig. 1 to earthquake motions.

In this study, inelastic deformations are taken into account in the analysis of a single degree of freedom spherical structure submerged in a viscous fluid of infinite extent. The elastic-plastic behavior of the structure is described by a bilinear resisting force displacement relationship shown in Fig. 2. in which its limiting cases are the elastic and elastic perfectly plastic. Response spectra and the optimum response spectra (12) for the N-S component of the May 1940 El Centro earthquake are generated for the elastic perfectly plastic case for different values of the density ratio of fluid to sphere, Stokes number, and ductility factor (13).

EQUATION OF MOTION

The equation of motion of a spherical structure submerged in a fluid shown in Fig. 1 and obeying the bilinear resisting force-displacement relationship shown in Fig. 2 can be written in the form

$$M\ddot{u} + (3\rho_f \nu \pi d + c)\dot{u} + Q + \frac{3}{2} d^2 \rho_f \sqrt{\pi \nu} \int_0^t \frac{\ddot{u} d\tau}{\sqrt{t-\tau}} = - (M\dot{y} + 3\rho_f \nu \pi d \dot{y} + \frac{3}{2} d^2 \rho_f \sqrt{\pi \nu} \int_0^t \frac{\ddot{y} d\tau}{\sqrt{t-\tau}}) \quad (2)$$

in which $M = (\rho_s + \frac{1}{2}\rho_f) \frac{\pi d^3}{6}$ is the virtual mass, ρ_s and u are the density and relative displacement of the sphere respectively, y the displacement of the base, c the structural damping coefficient, and Q the resisting force which can be expressed as

$$Q = Q_j + ak(u - v_j) \quad (3)$$

in which

$$a = \delta(\alpha - 1) + 1 \quad (4)$$

and

$$\left. \begin{aligned} \delta &= 0 && \text{in the elastic phase} \\ \delta &= 1 && \text{in the plastic phase} \end{aligned} \right\} \quad (5)$$

In the above equations, α is the strain hardening coefficient, k the elastic stiffness, and Q_j and v_j are the phase constants which denote the

coordinates of the phase change in the resisting force-displacement relation of the system. Introducing damping ratio $\zeta = c/(2\sqrt{kM_s})$, density ratio $\rho_o = \rho_f/\rho_s$ and Stokes number $N_s = \sqrt{v/(\omega d^2)}$, Eq. 2 can be written in the form

$$\begin{aligned} \ddot{u} + \left[\frac{2\zeta\omega}{\sqrt{1+\frac{1}{2}\rho_o}} + \frac{18\rho_o\omega N_s^2}{1+\frac{1}{2}\rho_o} \right] \dot{u} + a\omega^2 u + \frac{9\rho_o\sqrt{\omega N_s}}{\sqrt{\pi}(1+\frac{1}{2}\rho_o)} \int_0^t \frac{\ddot{u}d\tau}{\sqrt{t-\tau}} = -\ddot{y} \\ - \frac{18\rho_o\omega N_s^2}{1+\frac{1}{2}\rho_o} \dot{y} - \frac{Q_j\omega^2}{k} + a\omega^2 v_j - \frac{9\rho_o\sqrt{\omega N_s}}{\sqrt{\pi}(1+\frac{1}{2}\rho_o)} \int_0^t \frac{\ddot{y}d\tau}{\sqrt{t-\tau}} \end{aligned} \quad (6)$$

where M_s is the mass of the sphere and $\omega = \sqrt{k/M}$ is the natural frequency of the submerged system in the absence of damping and effect of fluid history.

PHASE TRANSITION

Starting from the system at rest where $Q_o = v_o = 0$, the first phase change from elastic to plastic takes place when $|Q| > Q_1$ where Q_1 is the yield resisting force. Plastic to elastic phase transitions will occur whenever $\dot{u} = 0$. Further elastic to plastic transitions will occur if $|Q - Q_j| > 2Q_1$.

It is also necessary to check whether reversal of direction occurs within the elastic phase. This occurs when $\dot{u} = 0$ during the elastic phase, and the elastic to plastic transitions occur when $(u - v_j)$ changes sign.

NUMERICAL INTEGRATION

The acceleration is assumed to vary linearly over a small time interval $\Delta t = t(l) - t(l-1)$. The displacement and velocity can thus be expressed as

$$u(l) = u(l-1) + \Delta t \dot{u}(l-1) + \frac{(\Delta t)^2}{6} [2\ddot{u}(l-1) + \ddot{u}(l)] \quad (7)$$

$$\dot{u}(l) = \dot{u}(l-1) + \frac{\Delta t}{2} [\ddot{u}(l-1) + \ddot{u}(l)] \quad (8)$$

The Basset history integral can be decomposed into two terms to avoid the problem of singularity as

$$\int_0^t \frac{\ddot{u}d\tau}{\sqrt{t-\tau}} = \int_0^{t-\Delta t} \frac{\ddot{u}d\tau}{\sqrt{t-\tau}} + \int_{t-\Delta t}^t \frac{\ddot{u}d\tau}{\sqrt{t-\tau}} \quad (9)$$

Integrating the first term on the right side of Eq. 9 numerically and expressing \ddot{u} in the last term as a linear function of τ and integrating yield

$$\int_0^t \frac{\ddot{u} d\tau}{\sqrt{t-\tau}} = \frac{1}{2} \sum_{p=1}^{\ell-1} \left[\frac{\ddot{u}(p-1)}{\sqrt{t(\ell)-t(p-1)}} + \frac{\ddot{u}(p)}{\sqrt{t(\ell)-t(p)}} \right] [t(p) - t(p-1)] + \sqrt{\Delta t} \left[\frac{4}{3} \ddot{u}(\ell) + \frac{2}{3} \ddot{u}(\ell-1) \right] \quad (10)$$

Substituting Eqs. 7, 8 and 10 into Eq. 6 leads to

$$\begin{aligned} & \left[1 + \frac{\zeta \omega \Delta t}{\sqrt{1 + \frac{1}{2} \rho_0}} + \frac{9 \rho_0 \omega N_s^2 \Delta t}{1 + \frac{1}{2} \rho_0} + \frac{a \omega^2 (\Delta t)^2}{6} + \frac{12 \rho_0 \sqrt{\omega} N_s \sqrt{\Delta t}}{\sqrt{\pi} (1 + \frac{1}{2} \rho_0)} \right] \ddot{u}(\ell) \\ & = - \left[\frac{\zeta \omega \Delta t}{\sqrt{1 + \frac{1}{2} \rho_0}} + \frac{9 \rho_0 \omega N_s^2 \Delta t}{1 + \frac{1}{2} \rho_0} + \frac{a \omega^2 (\Delta t)^2}{3} + \frac{6 \rho_0 \sqrt{\omega} N_s \sqrt{\Delta t}}{\sqrt{\pi} (1 + \frac{1}{2} \rho_0)} \right] \ddot{u}(\ell-1) \\ & - \left[\frac{2 \zeta \omega}{\sqrt{1 + \frac{1}{2} \rho_0}} + \frac{18 \rho_0 \omega N_s^2}{1 + \frac{1}{2} \rho_0} + a \omega^2 \Delta t \right] \dot{u}(\ell-1) - a \omega^2 u(\ell-1) - \ddot{y}(\ell) \\ & - \frac{18 \rho_0 \omega N_s^2}{1 + \frac{1}{2} \rho_0} \dot{y}(\ell) + a \omega^2 v_j - \frac{Q_j \omega^2}{k} - \frac{9 \rho_0 \sqrt{\omega} N_s}{\sqrt{\pi} (1 + \frac{1}{2} \rho_0)} \left\{ \frac{1}{2} \sum_{p=1}^{\ell-1} \left[\frac{\ddot{u}(p-1) + \ddot{y}(p-1)}{\sqrt{t(\ell)-t(p-1)}} \right] \right. \\ & \left. + \frac{\ddot{u}(p) + \ddot{y}(p)}{\sqrt{t(\ell)-t(p)}} \right\} [t(p) - t(p-1)] + \sqrt{\Delta t} \left[\frac{4}{3} \ddot{y}(\ell) + \frac{2}{3} \ddot{y}(\ell-1) \right] \quad (11) \end{aligned}$$

starting from a system at rest where the initial displacement, velocity and phase constants are zero and $\ddot{u} = -\ddot{y}$ at $t = 0$ in accordance with Eq. 6, the acceleration at time $t = t(\ell)$ can be determined from Eq. 11 and the corresponding displacement and velocity can then be determined from Eqs. 7 and 8 respectively.

In carrying out the numerical integration, the time increment of $0.1T_0$, where T_0 is the undamped natural period in vacuum, was normally used and whenever T_0 is greater than 0.5 second $\Delta t = 0.05$ second was employed.

LATERAL FORCE COEFFICIENT

The lateral force coefficient spectra for the elastic perfectly plastic case ($\alpha = 0$) with Stokes number $N_s = 0.0001$ and damping ratio $\zeta = 0.02$ are generated for different values of the density ratio and ductility factor, $\mu = u_{\max}/v_1$ where u_{\max} is the maximum displacement and, v_1 the yield displacement which is the displacement at the first phase change. The lateral force coefficient C , defined as the ratio of the maximum resisting force to the weight of the sphere, for the bilinear system can be expressed as

$$C = 4\pi^2 v_1 [1 + \alpha(\mu-1)] / (gT_0^2) \quad (12)$$

where g is the acceleration of gravity.

For each set of damping ratio, Stokes number, density ratio, strain hardening coefficient and undamped natural period in vacuum, the maximum relative displacements were obtained for various values of the yield displacements. The yield displacements corresponding to ductility factors of 2, 4 and 6 were then determined by graphical interpolation as illustrated in Fig. 3. Lateral force coefficient spectra for $\mu = 1$ (elastic), 2, 4 and 6 corresponding to $\rho_0 = 0.25, 1$ and 2 are computed by Eq. 12 and given in Figs. 4, 5 and 6 respectively.

OPTIMUM YIELD DISPLACEMENT

For each set of the damping ratio, Stokes number, density ratio and undamped natural period in vacuum, there exists an optimum value of the yield displacement at which the response in term of maximum displacement is a minimum (12). This optimum yield displacement can be determined graphically (9) as shown in Fig. 3. The response spectra in terms of the optimum yield displacement and the corresponding maximum displacement are given in Figs. 7(a) and 7(b).

CONCLUSIONS

Based on the results obtained in this study, the dynamic response of a spherical structure submerged in a fluid is significantly influenced by the density ratio and ductility factor. An increase in the density ratio leads to increasing period of vibration but does not necessarily lead to a higher response. The range of Stokes number in civil engineering field lies between 0.0001 and 0.001. Studies on the response in this range of Stokes number reveal that there is no significant difference in the response from the case of zero Stokes number, and hence only the spectra for the case where $N_s = 0.0001$ are given here.

The result obtained for the elastic perfectly plastic system shows that the lateral force coefficient decreases appreciably as the ductility factor increases as shown in Figs. 4 to 6. This behavior is somewhat similar to the effect of damping on the response of the elastic system. For the optimum response spectra, the results shown in Fig. 7 indicate that the maximum displacement of the elastic perfectly plastic system corresponding to the optimum yield displacement is always less than that of the corresponding elastic system.

Although no parametric study was carried out for elastic strain hardening submerged structures, the analysis can be performed readily by the proposed formulation.

For the range of parameters in civil engineering purposes, the lateral force for the elastic perfectly plastic systems submerged in a fluid is in general larger than that vibrating in vacuum or in air. Consequently, the structural system submerged in a fluid such as water should be made stronger than its counterpart in air. In case where the displacement is an important constraint in the design, the optimum response spectra given in Fig. 8 may be used as a guide in selecting the structural members.

REFERENCES

1. Basset, A.B., "On the Motion of a Sphere in a Viscous Fluid", Philosophical Transactions, Royal Society of London, Vol. 179, 1888, pp. 43-63.
2. Basset, A.B., A Treatise on Hydrodynamics, Vol. 2, Dover Publications, Inc., New York, N.Y., 1961, Chapter 22, pp. 285-303.
3. Brush, L.M., Ho, H.W. and Yen, B.C., "Accelerated Motion of a Sphere in a Viscous Fluid", Journal of the Hydraulics Division, ASCE, Vol. 90, No. HY1, Proc. Paper 3764, January 1964, pp. 149-160.
4. Carney, J.F., Mockros, L.F. and Lee, S.L., "Dynamic Response of a Two Degree of Freedom Spherical System in a Fluid", Ingenieur-Archiv, Vol. 35, No. 6, 1967, pp. 351-361.
5. Carney, J.F., Mockros, L.F. and Lee, S.L., "Dynamic Stability of Discrete Spherical Structural Systems in Fluid Media", Ingenieur-Archiv, Vol. 36, No. 4, 1967, pp. 237-245.
6. Hamilton, W.S. and Lindell, J.E., "Fluid Force Analysis and Accelerating Sphere Tests", Journal of the Hydraulics Division, ASCE, Vol. 97, HY6, Proc. Paper 8195, June 1971, pp. 805-817.
7. Hjelmfelt, A.T. and Mockros, L.F., "Stokes Flow Behavior of an Accelerating Sphere", Journal of the Engineering Mechanics Division, ASCE, Vol. 93, No. EM6, Proc. Paper 5647, December 1967, pp. 87-102.
8. Hjelmfelt, A.T., et al., "Dynamic Response of a Restrained Sphere in a Fluid", Journal of the Engineering Mechanics Division, ASCE, Vol. 93, No. EM1, Proc. Paper 5107, February 1967, pp. 41-56.
9. Hongladaromp, T., Srimahachota, D. and Lee, S.L., "Response Spectra of Strain Hardening Structural Systems to Earthquake Motions", Journal of Engineering for Industry, ASME, Vol. 96, Series B., No. 2, Paper No. 73-DET-25, May 1974, pp. 399-404.
10. Keulegan, G.H. and Carpenter, L.H., "Forces on Cylinders and Plates in an Oscillating Fluid", Journal of Research of the National Bureau of Standards, Research Paper No. 2856, Vol. 60, No. 5, May 1958.
11. Mockros, L.F. and Lai, R.Y.S., "Validity of Stokes Theory for Accelerating Sphere", Journal of the Engineering Mechanics Division, ASCE, Vol. 95, No. EM3, Proc. Paper 6613, June 1969, pp. 629-640.
12. Odaka, T. and Horie, F., "A Study on the Optimum Value of a Seismic Coefficient", Proceedings, III World Conference on Earthquake Engineering, New Zealand, Vol. 2, 1965, pp. 399-420.
13. Veletsos, A.S. and Newmark, N.M., "Effect of Inelastic Behavior on the Response of Simple Systems to Earthquake Motions", Proceedings, II World Conference on Earthquake Engineering, Japan, Vol. 2, 1960, pp. 815-831.

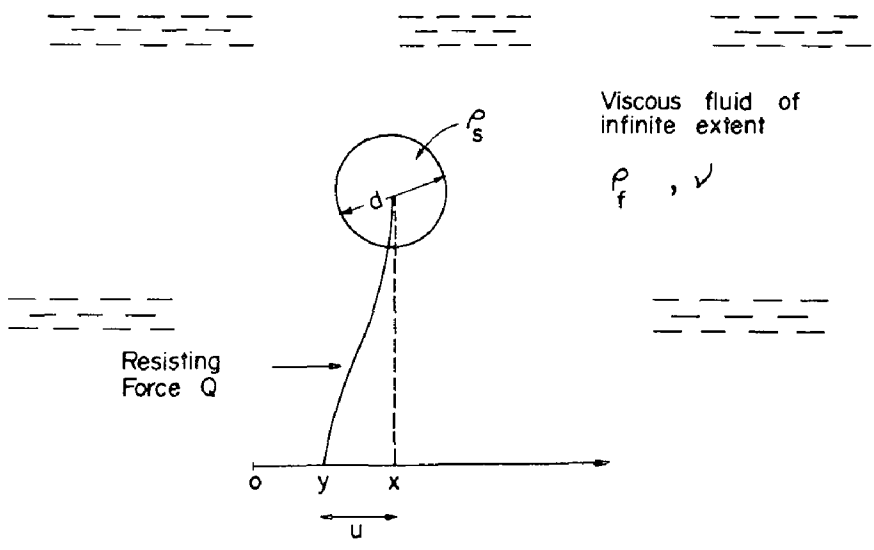


Fig. 1 - Single Degree of Freedom System Submerged in Fluid

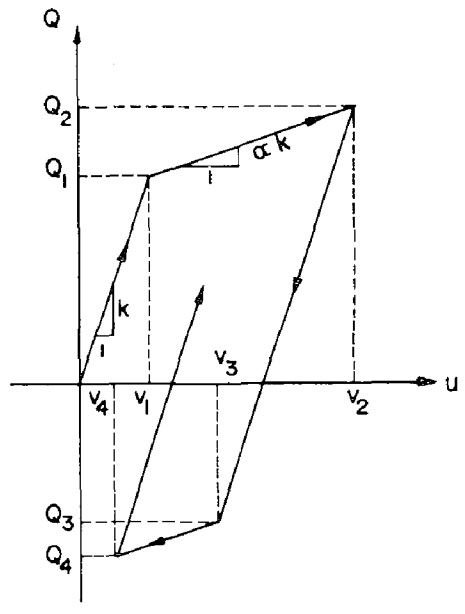


Fig. 2 - Resisting Force - Displacement Relation

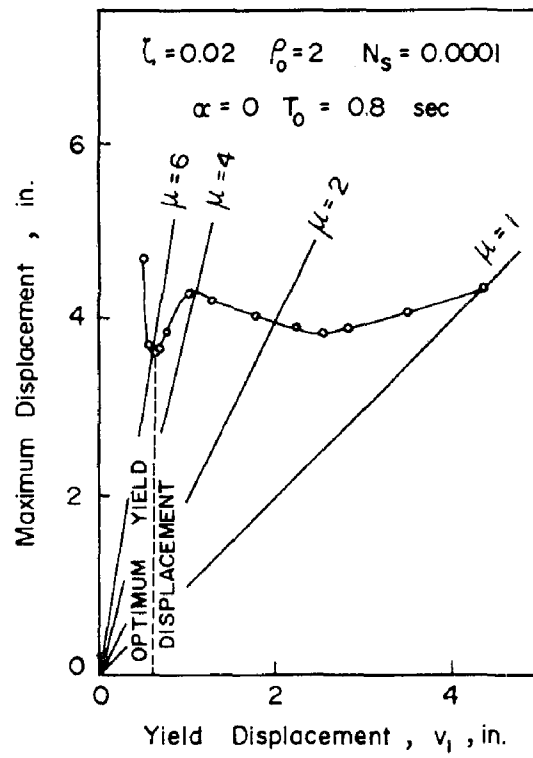


Fig.3 - Optimum Yield Displacement

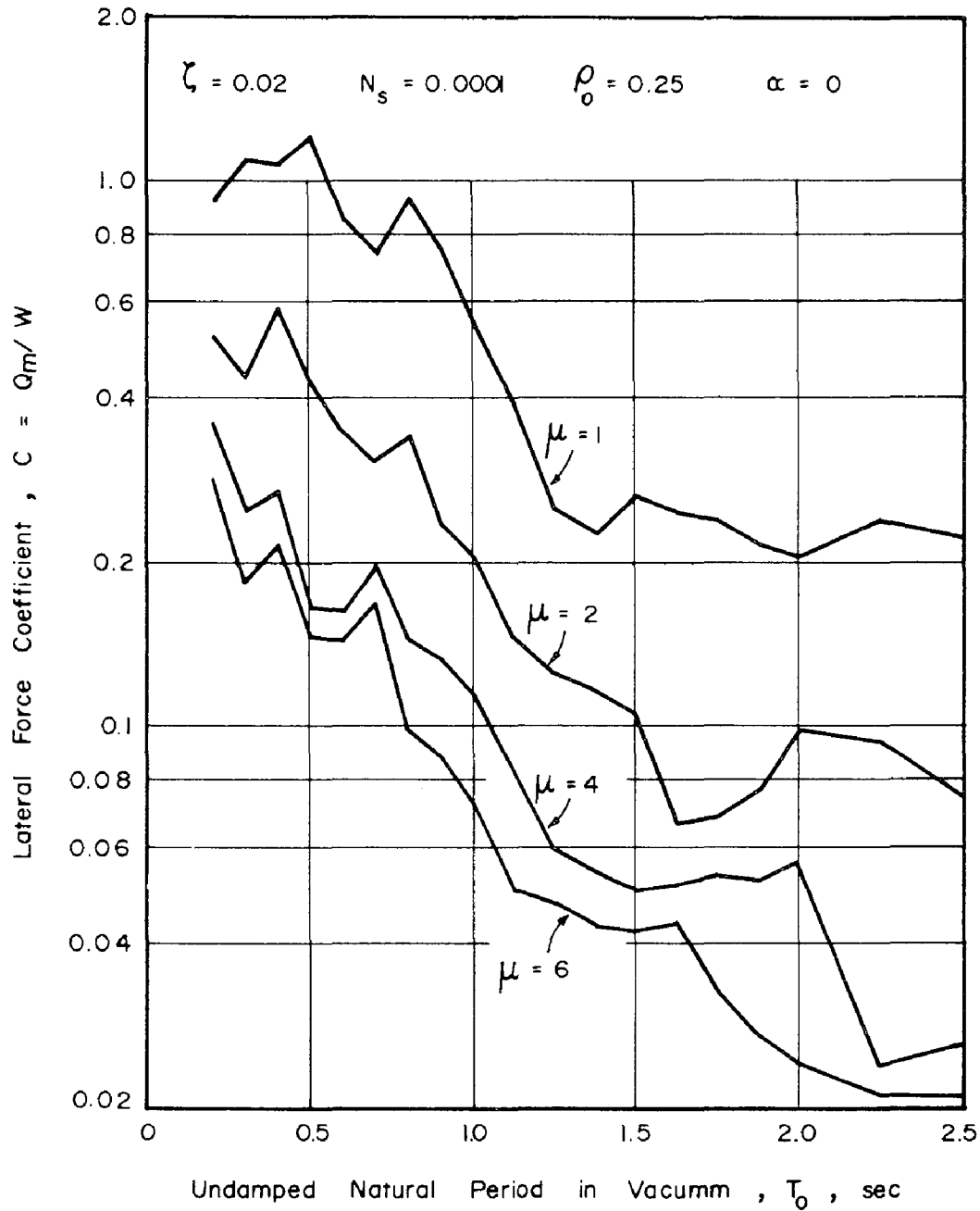


Fig. 4 - Lateral Force Coefficient of Elastic Perfectly Plastic Spherical Structure in Flood for N-S component of May 1940 El Centro Earthquake ($\rho_0 = 0.25$)

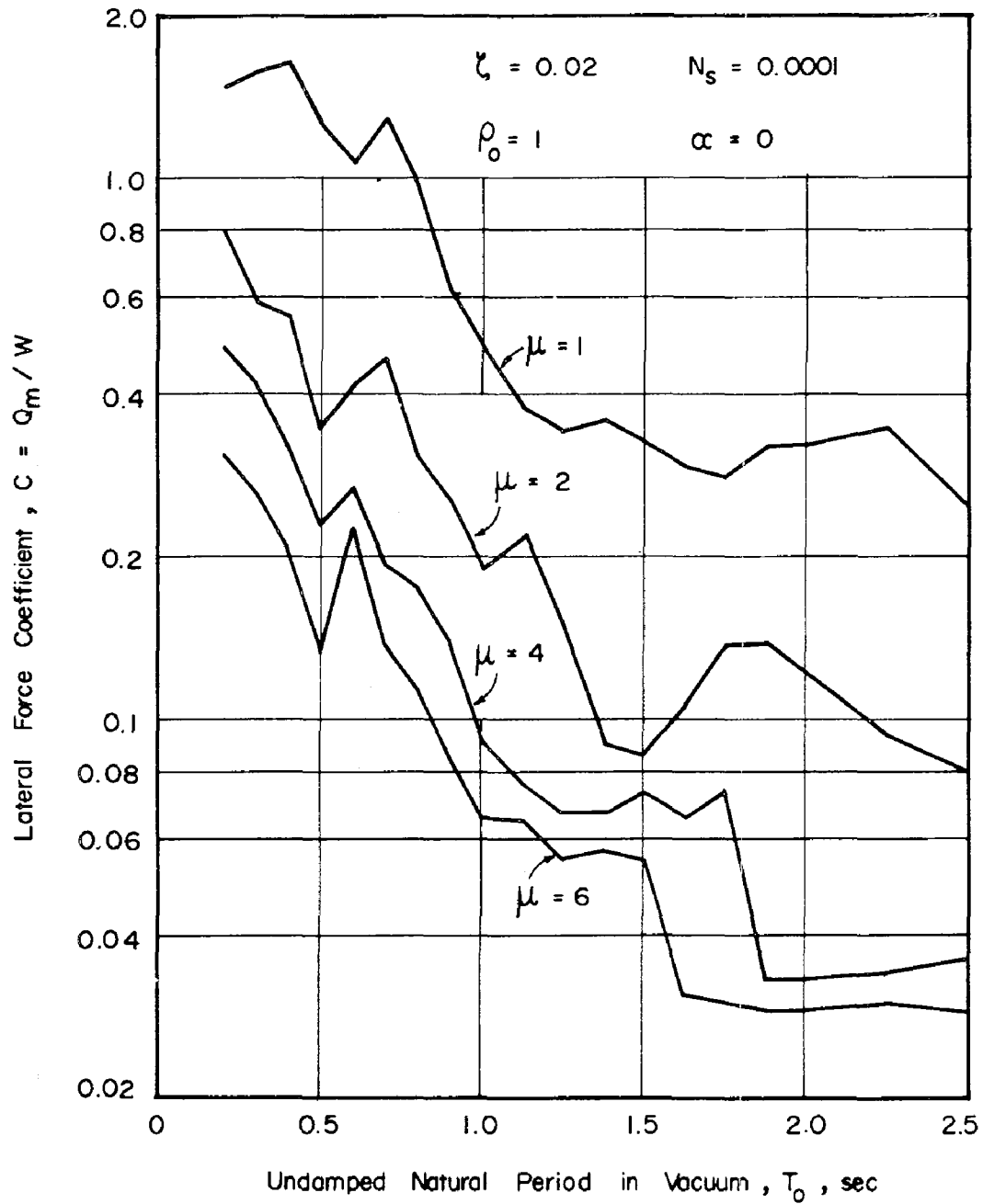


Fig.5 - Lateral Force Coefficient of Elastic Perfectly Plastic Spherical Structure in Fluid for N-S Component of May 1940 El Centro Earthquake ($\rho_0 = 1$)

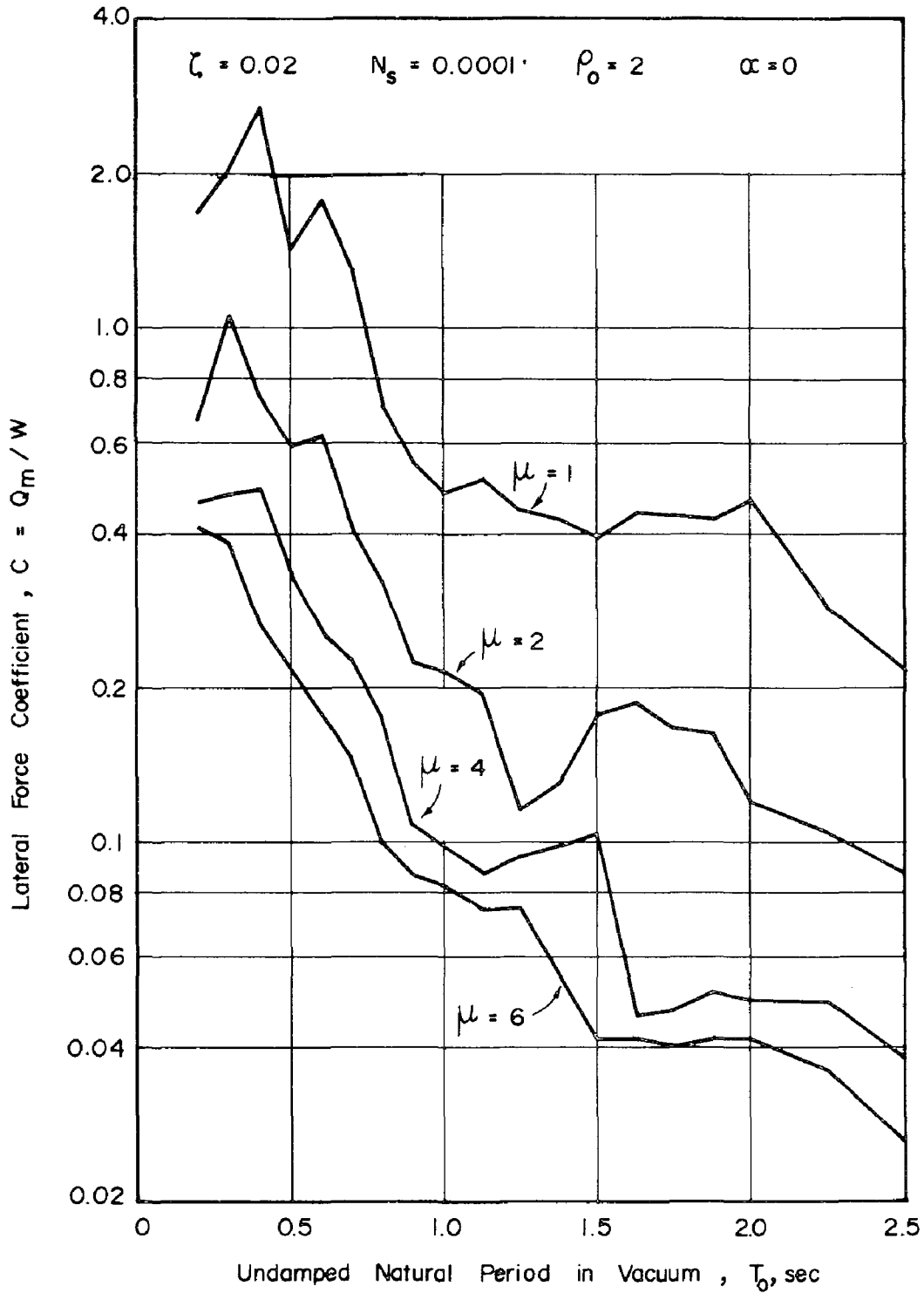


Fig. 6 - Lateral Force Coefficient of Elastic Perfectly Plastic Spherical Structure in Fluid for N-S Component of May 1940 El Centro Earthquake ($\rho_0 = 2$)

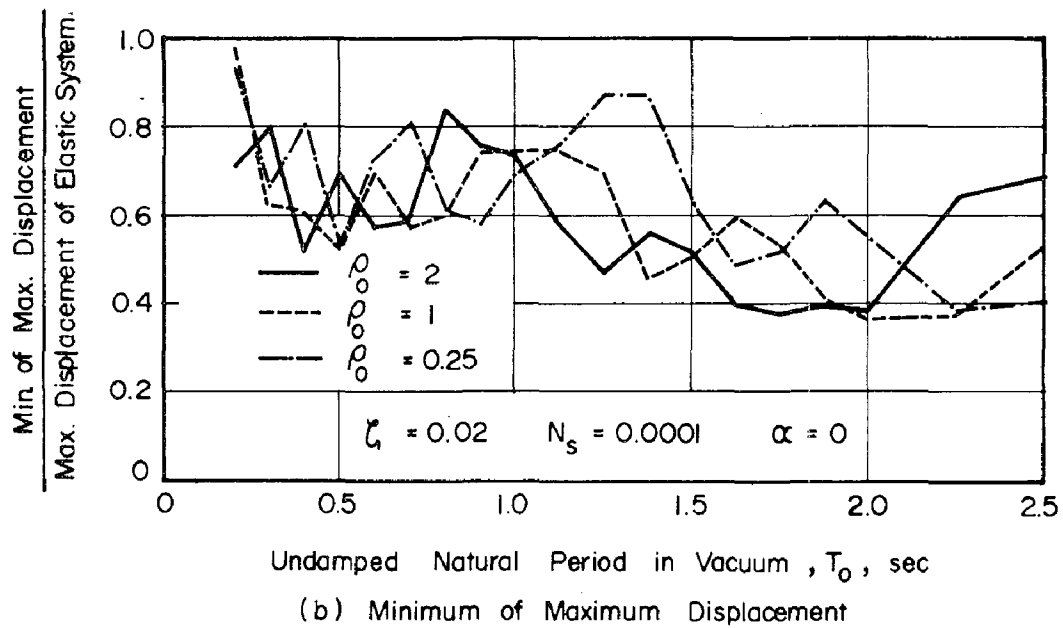
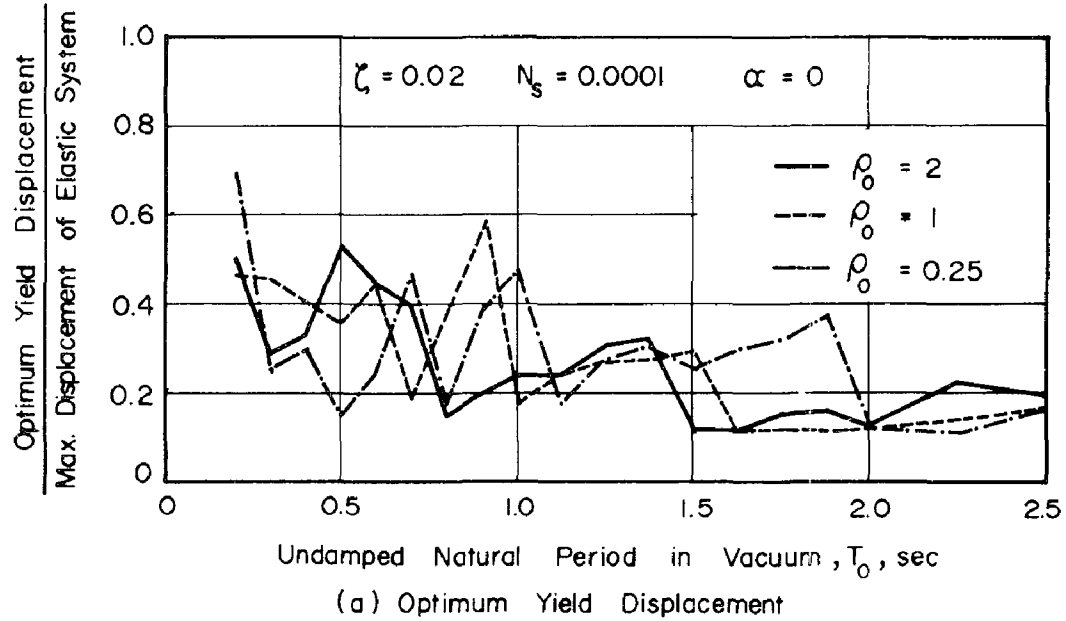


Fig.7 - Optimum Response Spectra of Elastic Perfectly Plastic Spherical Structure in Fluid for N-S Component of May 1940 El Centro Earthquake

INTERNATIONAL SYMPOSIUM ON
EARTHQUAKE STRUCTURAL ENGINEERING

387

St. Louis, Missouri, USA, August, 1976

DYNAMIC RESPONSE OF RETAINING WALLS DURING EARTHQUAKE

CHAU-SHIOUNG YEH

Associate Professor
Department of Civil Engineering
National Taiwan University
Taipei, Taiwan, Republic of China

SUMMARY

A model of the shear beam-Winkler spring-retaining wall system is employed to describe the interaction between the backfill and the wall. The wall is assumed to be a rigid body and undergoes horizontally translational and rocking motions. A set of coupled integro-partial differential equations describing the vibration of the whole system is reduced into a set of coupled ordinary differential equations by employing Galerkin's method. Then the model analysis is served to solve the equations. For certain cases the frequencies and the corresponding mode shape are calculated. The force and moment on the wall during design earthquake are also presented. The significance of the effect of wall motion on the responses is also shown.

INTRODUCTION

The pressure developed on a retaining wall during earthquake is usually calculated by mononobe-Okabe method^{(2),(3)}. The analysis basing on this method shows that the pressure distribution increases linearly as the depth and the total force locates at 1/3 height from the base of wall. Recently, Scott⁽⁴⁾ proposed an alternative approach in which he considered the backfill as an one-dimensional shear beam attached to the wall by springs representing the soil-wall interaction. The results evaluated by employing the model show that the point of action of force is at $2h/3$ instead of $h/3$. This result is close to $0.6h$ that is measured by Seed and Whitman⁽⁵⁾ with small scale experiments. However, in Scott's approach, the effect of wall motion on the earthquake-induced force and moment is neglected. In this paper, Scott's model is adopted, and the translational and rocking motion of wall are taken into consideration such that the significance of the effect of wall motion can be investigated.

THEORETICAL ANALYSIS

As shown in Fig. 1, consider a cross-section of an infinitely long

rigid wall and backfill with horizontal surface. The backfill is modelled as a shear beam. The shear beam is connected to both wall and original soil with a continuous Winkler spring material which has infinitesimal thickness with spring constant, k . The foundation material is assumed to be rigid and to undergo a horizontal earthquake motion specified by $\ddot{U}_0(t)$, where the dot denotes differentiation with respect to time, t . The equations of motion for the backfill, horizontal translation and rocking of the wall are, respectively

$$\rho_1 \frac{\partial^2 u}{\partial t^2} - G \gamma \frac{\partial^2 u}{\partial t^2} + 2ku - kU + (x - ah)V/h = - \rho_1 \ddot{U}_0 \quad (1)$$

$$\rho_0 bh\ddot{U} + khU - \frac{kh}{2} (1 - 2a)V - k \int_0^h u dx = - \rho_0 bh\ddot{U}_0 \quad (2)$$

$$\begin{aligned} & \frac{1}{3} \rho_0 bh^2(1 - 3a + 3a^2)V + \frac{1}{3} kh^2(1 - 3a + 3a^2)V \\ & - \frac{1}{2} kh^2(1 - 2a)U + k \int_0^h (x - ah)u dx = 0 \end{aligned} \quad (3)$$

with boundary conditions

$$\frac{\partial u(0,t)}{\partial x} = 0, \quad u(h, t) = 0 \quad (4)$$

where

- ah = distance between the top and the mass center of wall
- b = thickness of wall
- G = shear modulus of backfill
- h = height of wall
- γ = length of backfill
- $u(x,t)$ = relative horizontal displacement of shear beam to foundation
- $U(t)$ = relative horizontal displacement of wall to foundation
- $U_0(t)$ = earthquake horizontal displacement of foundation
- $V(t)$ = horizontal displacement induced by $\Omega(t)$, rotation of mass center of wall
- ρ = mass density of backfill
- ρ_0 = mass density of wall

The equations (1), (2) and (3) are coupled integro-partial differential equations. Galerkin's method(1) is adopted to reduce them into a set of ordinary differential equations. Let

$$u(x, t) = \sum_1^n q_j(t) \cos \lambda_j x \quad (5)$$

with $\lambda_j = (2j - 1)\pi / 2h$. The function $q_j(t)$ is the amplitude varying with time and $\cos \lambda_j x$ satisfies boundary conditions (4). Substitution of Eq.(5) into Eq.(1), then multiplying both sides by $\cos \lambda_j x$ and integrating from 0 to h gives n equations

$$\begin{aligned} \frac{\rho}{2} \frac{1}{h} \ddot{q}_i + \frac{h}{2} (G \lambda_i^2 + 2k) q_i + \frac{k}{\lambda_i} (-1)^i U + \frac{k}{h \lambda_i} \left[h(1-a)(-1)^{i-1} - \frac{1}{\lambda_i} \right] V \\ = - \frac{\rho}{\lambda_i} (-1)^{i-1} \ddot{U}_0 \quad i = 1, 2, \dots, n \end{aligned} \quad (6)$$

Substitution of Eq. (5) into Eqs. (1) and (2) gives

$$\rho_0 b h U + k h U - \frac{k h}{2} (1 - 2a) V - k \sum_1^n \frac{1}{\lambda_j} (-1)^{j-1} q_j = - \rho_0 b h U_0 \quad (7)$$

$$\begin{aligned} \frac{1}{3} \rho_0 b h^2 (1 - 3a + 3a^2) \dot{V} + \frac{1}{3} k h^2 (1 - 3a + 3a^2) V \\ - \frac{1}{2} k h^2 (1 - 2a) U + k \sum_1^n \frac{1}{\lambda_j} \left[h(1-a)(-1)^{j-1} - \frac{1}{\lambda_j} \right] q_j = 0 \end{aligned} \quad (8)$$

As identified by Scott, k may be taken as $8G(1 - \nu)/1(1 - 2\nu)$ in which ν is Poisson's ratio. The standard procedure applied in modal analysis⁽¹⁾ may be employed to solve $(n + 2)$ coupled ordinary differential equations of which n equations, (6), contribute n modes of shear beam vibration and two equations, (7) and (8), contribute wall vibration. However, for simplicity but without lossing to show the effect of the wall motion, only the first equation in (6) will be chosen to couple with eqs. (7) and (8) with $n = 1$. For convenience, three coupled equations are written in matrix form

$$[m] \{\ddot{q}\} + k \{q\} = \{Q\} \ddot{U}_0 \quad (9)$$

where

$$\begin{aligned} [m] = \rho_0 \begin{bmatrix} 1/2 & & \\ & \rho_0 b / \rho_1 & \\ & & \rho_0 b (1 - 3a + 3a^2) / 3 \rho_1 \end{bmatrix} \\ [k] = k \begin{bmatrix} (G \pi^2 / 4 k h^2 + 2) / 2 & -2/\pi & 2(1 - a - 2/\pi) / \pi \\ -2/\pi & 1 & -(1 - 2a) / 2 \\ 2(1 - a - 2/\pi) / \pi & -(1 - 2a) / 2 & (1 - 3a + 3a^2) / 3 \end{bmatrix} \\ \{q\} = \begin{Bmatrix} q_1 \\ U \\ V \end{Bmatrix}, \quad \{Q\} = \rho_0 \begin{Bmatrix} -2/\pi \\ \rho_0 b / \rho_1 \\ 0 \end{Bmatrix} \end{aligned}$$

Employing the expansion theorem the response can be described as a superposition of the normal modes in the form

$$\{q\} = [\phi]\{\zeta\} \quad (10)$$

where ϕ is the modal matrix obtained from the solution of eigenvalue problem

$$[m_s][\phi][\omega^2] = [k][\phi] \quad (11)$$

in which the natural frequency, ω^2 , is the eigenvalue determined from the above equation, and $\{\zeta\}$ is the generalized coordinates which is the solution of the equation

$$\{\ddot{\zeta}\} + [\omega^2]\{\zeta\} = \{N\} \ddot{u}_0 \quad (12)$$

with the participation factor

$$\{N\} = [\phi]^T \{Q\} \quad (13)$$

The maximum displacement q_{im} due to a specified design earthquake can be found from the equation

$$q_{im} = \sum_1^3 (\phi_{ij} S_{vj} N_j / \omega_j) \quad (14)$$

where S_{vj} is the maximum relative velocity at the frequency ω_j . Thus the most probably maximum forces $\{F\}_m$ is given by the expression

$$F_{im} = \left[\sum_1^3 (K_{ij} q_{jm})^2 \right]^{1/2}$$

where K_{ij} is the element of the matrix

$$K = k \begin{bmatrix} h(G + \pi^2/4kh^2 + 2)/2 & -2h/\pi & 2h(1-a-2/\pi)/\pi \\ -2h/\pi & h & -h(1-2a)/2 \\ 2h^2(1-a-2/\pi)/\pi & -h^2(1-2a)/2 & h^2(1-3a+3a^2)/3 \end{bmatrix}$$

To illustrate the significance of the effect of wall motion, two cases with the same $\rho/\rho_0 = 0.8$, $h/l = 0.8$, $a = 1$, $\nu = 1/3$, $h(\rho/G)^{1/2} = 0.1$ sec and with different h/b are calculated in detail. The case for $h/b = 15$ gives the results: the frequencies, $\omega_1 = 33.93$ rad/sec, $\omega_2 = 47.32$ rad/sec, $\omega_3 = 171$ rad/sec, the most probably maximum force, $P_m = 4.86G$, the most probably moment, $M_m = 3.07Gh$ and the point of action of force, $0.63h$ from base. For the other case, $h/b = 10$, the results is $\omega_1 = 33.1$ rad/sec, $\omega_2 = 39$ rad/sec, $\omega_3 = 142$ rad/sec, $P_m = 4.83G$, $M_m = 2.92Gh$ and the point of action of force is located at $0.605h$ from the base. It is mentioned that P_m and M_m are calculated by employing a response spectra curve in Ref. 6.

It is noted that both the frequencies of fundamental modes are lower than 48.1 rad/sec predicted by Scott's formula without considering the effect of wall motion. The frequency of second mode of the thinner wall is close to 48.1 rad/sec but the frequency for the thicker wall is much lower than it. The point of action of the forces P_m for the two cases are both close to that calculated by Scott's formula, $0.637h (=2h/\pi)$ from the base. However, it should be pointed out that the magnitude of the force and moment of two cases are much higher than those calculated by Scott's formula, $P_m = 1.73G$, and $M_m = 1.1Gh$, respectively.

CONCLUSION AND REMARK

A model of the shear beam-Winkler spring-retaining wall system is employed to investigate the dynamic responses of the wall during earthquake. The wall motion as well as the soil motion is taken into consideration. The calculated results show that the effect of wall motion is essential in the evaluation of the earthquake-induced force and moment. However, the effect of flexibility of wall is neglected in this investigation. In many soils, the soil properties vary with depth. The study of earthquake responses of a wall interacting with such soils is also necessary. The two subjects mentioned above are currently investigated and the results will be presented in due course.

ACKNOWLEDGEMENTS

The author gratefully acknowledges the support of the National Science Council.

REFERENCES

- (1) Meirovitch, L., "Analytical Methods in Vibrations", MacMillan Comp., London, (1967)
- (2) Mononobe, N., & Matuo, H., "On the Determination of Earth Pressure during Earthquakes", World Engineering Congress, (1929)
- (3) Okabe, S., "General Theory of Earth Pressure and Seismic Stability of Retaining Wall and Dam" J. Japanese Soc. Civil Eng., Vol. 12, No. 1 (1924)
- (4) Scott, R.F., "Earthquake-induced Earth Pressures on Retaining Walls", Proc. of Fifth World Conf. on Earthquake Eng., Paper No. 202, (1973)
- (5) Seed, H.B. and Whitman, R.V., Conf. on Lateral Stresses and Earth-Retaining Structures, ASCE, (1970) pp 103-147.
- (6) Wiegel, R.L., (ed.), "Earthquake Engineering" Prentice-Hall Inc., N.J. (1970), p 320

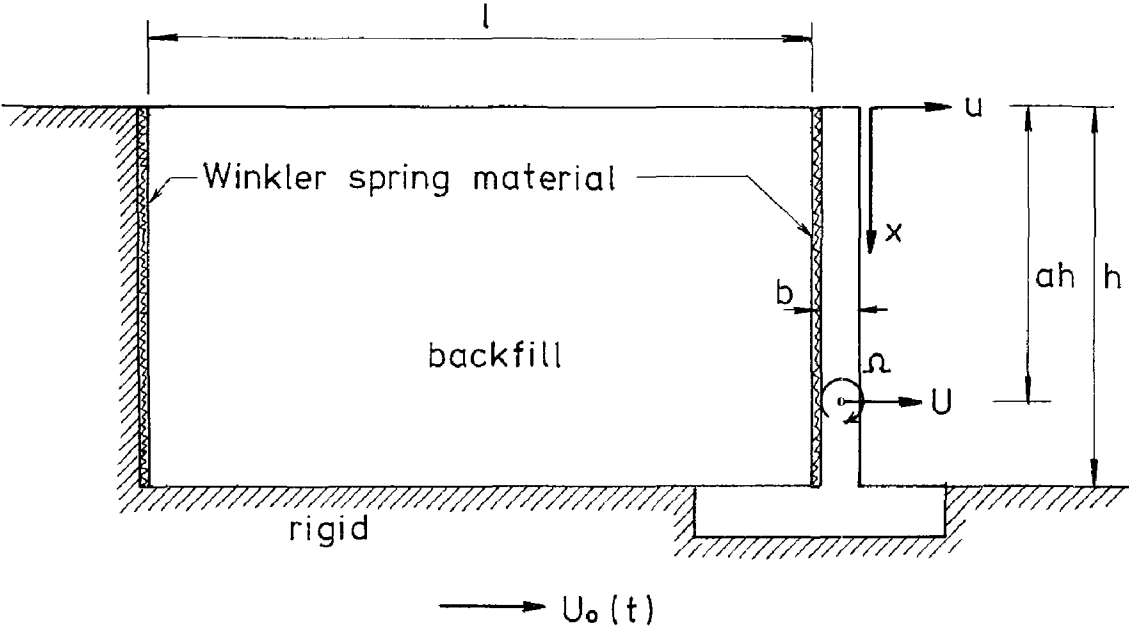


Fig. 1

DYNAMIC RESPONSE OF BRIDGE GRID
UNDER MOVING FORCE

N. MUNIRUDRAPPA,
Lecturer in Civil Engineering
Bangalore University,
Bangalore-560056
INDIA

SUMMARY

This paper deals with the analytical and experimental verification of an orthogonal bridge grid (consisting of longitudinal beams and cross beams) subjected to a moving force under constant velocities. The natural frequency, mode shapes and the dynamic response of the bridge grid are carried out for two cases, lumping the masses at the joints, in one case for the self weight of grid and in the second case, for the self weight of grid plus the weight of the slab. The modal analysis is used for the evaluation of dynamic response of the bridge. The moving force is treated as a transient pulse which is triangular in nature and assumed to be acting at the modal points. The resulting differential equation is solved by using laplace transformation, taking into account the two dimensional behaviour of the structure. Theoretical and experimental comparisons are carried for forced vibration. The results have been compared with Timoshenko's beam theory. The variation in impact factors are studied for the load moving on different beams.

INTRODUCTION

The study of the vibration of bridges caused by the moving

force is very essential for the design of any bridge. For the calculation of response under moving force or any earthquake force the accurate knowledge of force and forced vibration is very essential. The existing method of analysis for the open grid structure can be broadly classified as follows: a) Treating the bridge grid with masses lumped at joints (lumped mass approach), b) By orthotropic plate theory.

The bridge impact problem has been recognised at least from 1848. WILLIE R.⁽¹⁵⁾ obtained a mathematical theory for a load crossing the beam, the self weight of the beam being neglected. In 1905 KRYLOV⁽⁹⁾ obtained a solution for the case in which the mass of the load was negligible. A more generalised solution was obtained by considering masses of the load as well as the beam. The solution was obtained by JEFFCOTT⁽⁸⁾ in 1929. In connection with the Railway bridges impact problem much work has been done by early 1890's. Most of the work on railway bridge are carried out by TIMOSHENKO's⁽¹⁴⁾ and INGLIS⁽⁶⁾ for the dynamic behaviour of the structure considering the case of a moving force which was intended to represent the hammer blows of a steam locomotive. Recently SCHALLAR-KAMP⁽¹²⁾ and HILLEBORG⁽⁵⁾ A. presented some refinements to the theory. Though all of the above said solutions are theoretically useful, none have been successfully used or applied to the practical problems of highway bridge vibrations under actual conditions.

For highway bridges on the other hand very little theoretical work and much experimental details are available, based on the fact, that the highway bridges are extremely complicated by virtue of their complicated assembly of elements, varying geometry, different material constants and spans. WISE, J.A.⁽¹⁶⁾ BIGGS, J.M., HERBERT, S. and LOAW, J.M.,⁽⁴⁾ LINGARI, J.S. and WILSON⁽¹⁰⁾ and GESUND, H and YOUNG, D⁽⁴⁾ contributed in detail to the dynamic response of highway bridges. In each of these the investi-

gators treated the bridge as a prismatic beam simply supported on either ends subjected to a moving load and loads moving at tandem. The solution of the equations formulated are solved by finite difference method or by solving the actual differential equation obtained.

FLEMING AND ROMUALDI⁽²⁾, WEN R.K. and TORIDIS⁽¹⁷⁾ and F.V.FILHO⁽³⁾ developed methods for calculating the response of beams and frames subjected to time dependant force moving with constant velocity. The mass distribution is constituted by lumped masses with translational degrees of freedom. The methods followed by the above investigators used for the solution of simply supported beams, continuous beams and frames for different geometrical parameters and for different constant velocities. In all these methods, lumped mass scheme for the mass distribution of the structure is assumed.

THEORETICAL DEVELOPMENT

In the present analysis, the bridge grid is idealised, as open grid with masses lumped at various nodal points. Analysis is made both for free and forced vibration³. The response of the grid is analysed by modal analysis.

For the forced vibrations, the modal is traversed by a vertical force moving with a constant velocity V , while the force crosses the structure each mass point is excited by a transient force of triangular variation(Fig.1). This results in n number of differential equation equivalent to the number of masses excited by the moving force. The solution of these equations are obtained by laplace transformation technique. By the superposition of the modal values to the foregoing solution, time deflection relationships are obtained.

The differential equation of motion in the 'w' co-ordinate system takes the matrix form.

$$[M]\{\ddot{w}\} + [K]\{w\} = \{P(t)\} \quad \dots (1)$$

Applying co-ordinate transformation,

$$w(t) = [\phi] \eta(t) \quad \dots (2)$$

in which $[\phi]^*$ = the (nxn) matrix, the columns that are formed by the amplitudes of the normal modes, and $\eta(t)$ the (n x 1) column matrix of the dynamic factors relative to each normal mode.

From equation (2) we have

$$\{w\} = [\phi] \eta(t) \quad \dots (3)$$

and

$$\{\ddot{w}\} = [\phi] \{\ddot{\eta}(t)\} \quad \dots (4)$$

substituting equation (3) and (4) in equation (1) we get,

$$[m][\phi] \{\ddot{\eta}(t)\} + [K][\phi] \{\eta(t)\} = \{p(t)\} \quad \dots (5)$$

Now premultiplying the equation (5) by the transpose of ϕ , equation (5) becomes

$$[\phi]^T [m] [\phi] \{\ddot{\eta}\} + [\phi]^T [K] [\phi] \{\eta\} = [\phi]^T \{p(t)\} \quad \dots (6)$$

from the orthogonality relationship, it follows that

$$[\phi]^T [m] [\phi] = [M_K] \quad \dots (7)$$

$$[\phi]^T [K] [\phi] = [\omega_K^2] [M_K] \quad \dots (8)$$

substituting equation (7) and (8) in (6) we get

$$[M_K] \{\ddot{\eta}(t)\} + [\omega_K^2] [M_K] \{\eta(t)\} = [\phi]^T \{p(t)\} \quad \dots (9)$$

where $[m]$ = the (nxn) diagonal matrix formed by the lumped masses $m_i = (i = 1, 2, \dots, n)$.

$[M_K]$ is the (nxn) diagonal matrix formed by the generalised elastic masses relative to each normal mode $\{p(t)\}$ = the (n x 1) column matrix formed by the forces that excite the masses.

Hence the differential equation for the dynamic displacement relative to the K^{th} normal mode $\eta_K(t)$ is

* (An element ϕ_{ij} represent the displacements at i in the J th normal mode)

** ω_K = Natural frequency of the mode K

$$M_k \ddot{\eta}_k(t) + \omega_k^2 M_k \eta_k(t) = \sum_{i=J}^n \phi_{ik}^T P_i(t) \quad \dots (10)$$

After applying the Laplace transformation, the final differential equation reduces to

$$\begin{aligned} w_i(t) = P_0 & \sum_{k=1}^m \frac{\phi_{ik}}{M_k \omega_k^2} \sum_{i=J}^n \phi_{ik} \left\{ \frac{1}{\Delta t_i} U(t-t_{i-1}) \right. \\ & \left[(t-t_{i-1}) - \frac{1}{\omega_k} \sin \omega_k (t-t_{i-1}) \right] - \\ & - \left[\frac{1}{\Delta t_i} + \frac{1}{\Delta t_{i+1}} \right] U(t-t_i) \left[(t-t_i) - \right. \\ & - \left. \frac{1}{\omega_k} \sin \omega_k (t-t_i) \right] + \frac{1}{\Delta t_{i+1}} U(t-t_{i+1}) \\ & \left. \left[(t-t_{i+1}) - \frac{1}{\omega_k} \sin \omega_k (t-t_{i+1}) \right] \right\} \quad \dots (11) \end{aligned}$$

in which m = the number of modes that are taken in to account and $J=1$. The equation gives the displacement for a particular mass point i for different positions of the load.

ANALYSIS

The computations of the dynamic influence of the bridge grid under the passage of moving load are made through Fortran programmes. These programmes are carried out on CDC 3600-160A. (Digital computer). The following parameters are taken into account in the analysis (The mode shapes and the frequencies obtained from the free vibration data* has been used in the study of forced vibrations).

- 1) The dynamic response of the bridge grid under moving force is studied for different velocities (Fig. 2(a) and 2(b).
- 2) The action of the slab is taken by distributing its mass towards the joints.

*** $w_i(t)$ = Deflection associated with t^{th} degree of freedom

* B.C. Rajanna, B.K. Ramiah, and N. Munimdrappa. (1972) "Free vibration of Bridge grids". Presented @ the Seminar on role of computers in structural Analysis and optimization. Held at I.I.T. Madras.

3) By taking the ratio of the dynamic deflection to that of static deflection the respective impact factors are calculated for different velocities.

Fig. 3,4,5 and 6 shows the variation of impact factors without lumping the mass resulting due to the slab and taking into account the additional masses resulting due to the slab. The graphs are drawn for a particular position of the mass point.

EXPERIMENTAL VERIFICATION

Experimental verification is carried out on prespex model to verify the correctness of the theoretical analysis. Prespex is chosen as a model material since it satisfies the theoretical assumption of load moving on a smooth surface. Fig. 7 and 8 shows the track layout the instrumentation arrangement for the forced vibration study. The observed values are compared with theoretical values and are shown in Fig.10 and 11.

DISCUSSION AND CONCLUSIONS

i) Referring to Fig.3 it is observed that the maximum impact factor of 1.56 is obtained for the velocity of 150 cm/sec. theoretically.

ii) Referring to Fig.4 the impact factor is observed to be more for the load moving on the end beam CD than on the central beam AB, the values being 1.56 and 1.36.

iii) From the Fig.5 and Fig.6 it is observed that impact factor reduced considerably by considering the effect of lumping the self weight of the deck slab in the form of additional masses at each nodal point of the grid. By comparing the impact factors the difference was found to be 0.20. The experimental result shows the same results with impact factor of 1.37 for additional masses lumped and impact factors of 1.57 without lumping any additional masses(as observed from Figs. 10 and 11).

iv) The observed impact factors are compared with Timoshenko's beam theory and with the moment impact factors of I.S. code of practice. The values obtained by the authors are more than the values obtained by Timoshenko and I.S. code of practice. This difference may be due to vehicle and structural damping.

v) As the theory is general the results have to be interpreted with respect to a definite relation which has to be brought out with respect to specific prototype of the bridge grid of any material. The analysis has to be done taking into account their respective geometrical properties and simulate the actual loading conditions.

TABLE - 1
COMPARISON OF IMPACT FACTORS

Load Position	Velocity (cm/sec)	Theoretical Impact Factor	Impact/Factors by Beam Approach	I.S. Code (Moment Impact factors)
a) Without lumping any additional mass				
AB	150	1.48	0.98	1.35
	120	1.41	0.96	
	100	1.35	0.92	
	30	1.29	0.90	
CD	150	1.560	0.98	1.35
	120	1.532	0.96	
	100	1.465	0.91	
	30	1.320	0.88	
b) By lumping additional masses of 0.3 Kg. to the nodal points of the grid.				
AB	150	1.280	0.92	1.35
	120	1.180	0.90	
	100	1.140	0.88	
	30	1.100	0.84	
CD	150	1.356	0.92	1.25
	120	1.301	0.98	
	100	1.240	0.89	
	30	0.225	0.94	

BIBLIOGRAPHY

1. J.M. Bigge, Herberts Suer, and J.M. Louw,
A Theoretical and experimental investigation of
of the simple span highway bridges, Bridge Vibration
Progress Report No.2, Cambridge M.I.T.(1956)
2. Fleming J.F. and Romuldi, J.P.,
Dynamic of highway bridges, Journal of the Structural
Division, ASCE, Vol.37, Proc. Paper 2955, pp.31-61
(1963)
3. F.V.Filho
Dynamic influence lines of beams and frames, Journal
of the Structural Division, ASCE, Vol.92, No.ST-2,
Proc. Paper 4797, pp.371-378(1966)
4. H.Gesund and D.Young,
Dynamic analysis of beams to moving loads, Interna-
tional Association for Bridges and Structural Engi-
neering, Vol.21, pp.95-100
5. A.Hilleborg
Dynamic influence of smoothly running loads on simply
supported girders, Institution of structural Engineer-
ing and Bridge Building, Royal Institute of Techno-
logy, Stockholm, Sweeden(1951)
6. C.E.Inglis
A mathematical treatise on vibration in railway
bridges, Cambridge University Press, London(1934)
7. K.T.S.Iyengar and K.S.Jagadish
The response of beam and slab bridges to moving forces,
Publications, IABSE, Vol.28, No.2, pp.69-86(1968)
8. H.H.Jeffcott
On the vibration of beams under the action of moving
loads, Philosophical Magazine-7, Series V-8(1929)
9. A.N.Krylov
Mathematische Anaalen V.61, p.211(1905)

10. Lincari, J.S. and Wilson,
Dynamic response of bridge subjected to moving
forcing systems, Proc. of 4th U.S.National Conference
on Applied Mechanics, Vol.19, ASME(1962)
11. N.Munirudrappa
Dynamic response of orthogonal bridge grid under
moving force, M.Tech. thesis submitted to the
I.I.T., Bombay(1969)
12. A.Schallenkamp
Schwingungen von tragern bei bewegten hasten,
Rasten Ingenien, Archiv, Vol.8, pp.182-198(1937)
13. Smith, J.W.,
Finite strip analysis of the dynamic response of
beam and slab highway bridges, Int. Journ. of Earth-
quake Engineering and Structural Dynamics, Vol.1,
pp.357-370(1973)
14. Timoshenko, S.,
Vibration of highway bridges, Trans. ASME., Vol.23,
pp.108-110(1928)
15. R.Willis
Report of the commissioners appointed to enquire
into the Application of Iron to railway structures,
Appendix, B., London(1849)
16. Wise, J.A.,
Dynamics of highway bridges, Proc. of Highway Research
Board, Vol.32.
17. Wen, R.K. and Toridis, T.,
Dynamic behaviour of cantilever bridges, Journal of
Engineering Mechanics Division, ASCE, Vol.88, No.EM-4,
Proc. paper 3220, pp.27-43(1962).

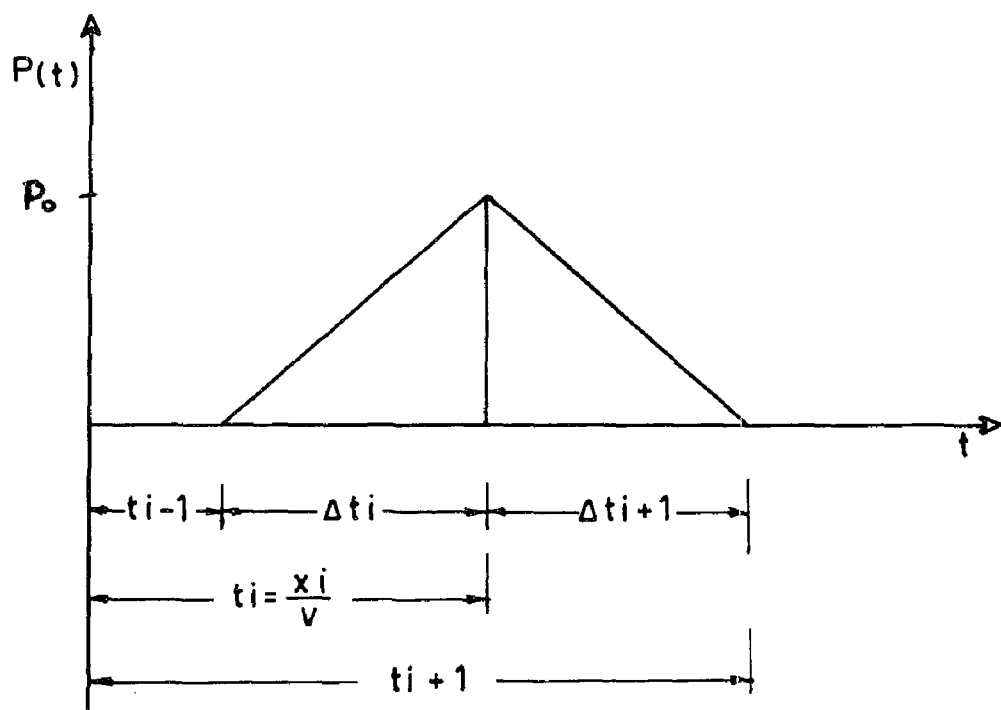
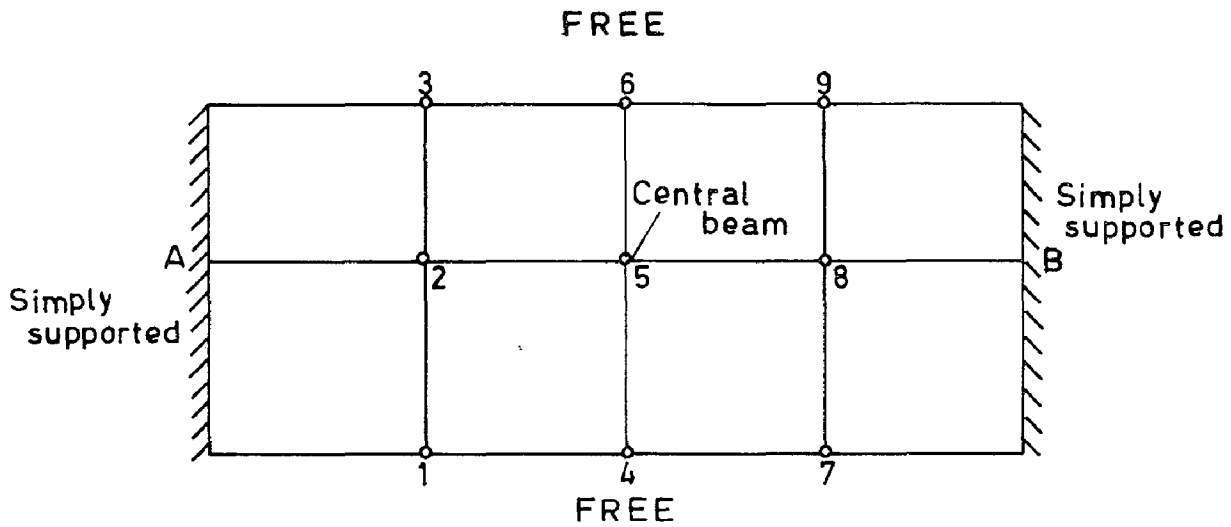
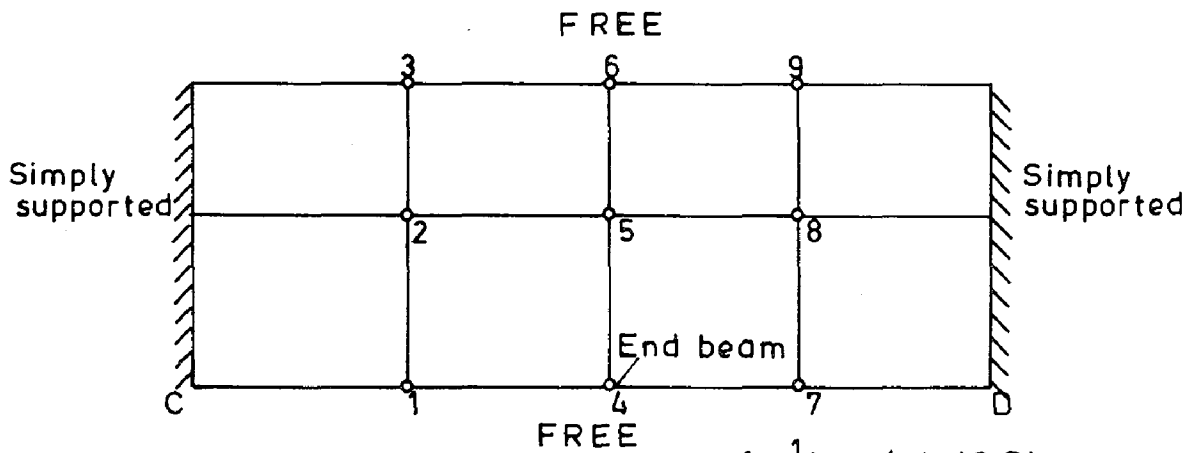


FIG. 1. TIME VARIATION OF FORCE ACTING ON MASS POINT i



- 2 - $\frac{1}{4}$ point (A-B)
- 5 - Central point (AB)
- 4 - Central point (C-D)

FIG. 2(a) FORCE MOVING ON THE CENTRAL BEAM A-B



- 1 - $\frac{1}{4}$ point (C-D)
- 4 - Central point (C-D)
- 5 - Central point (A B)

FIG. 2(b) FORCE MOVING ON THE END BEAM C-D

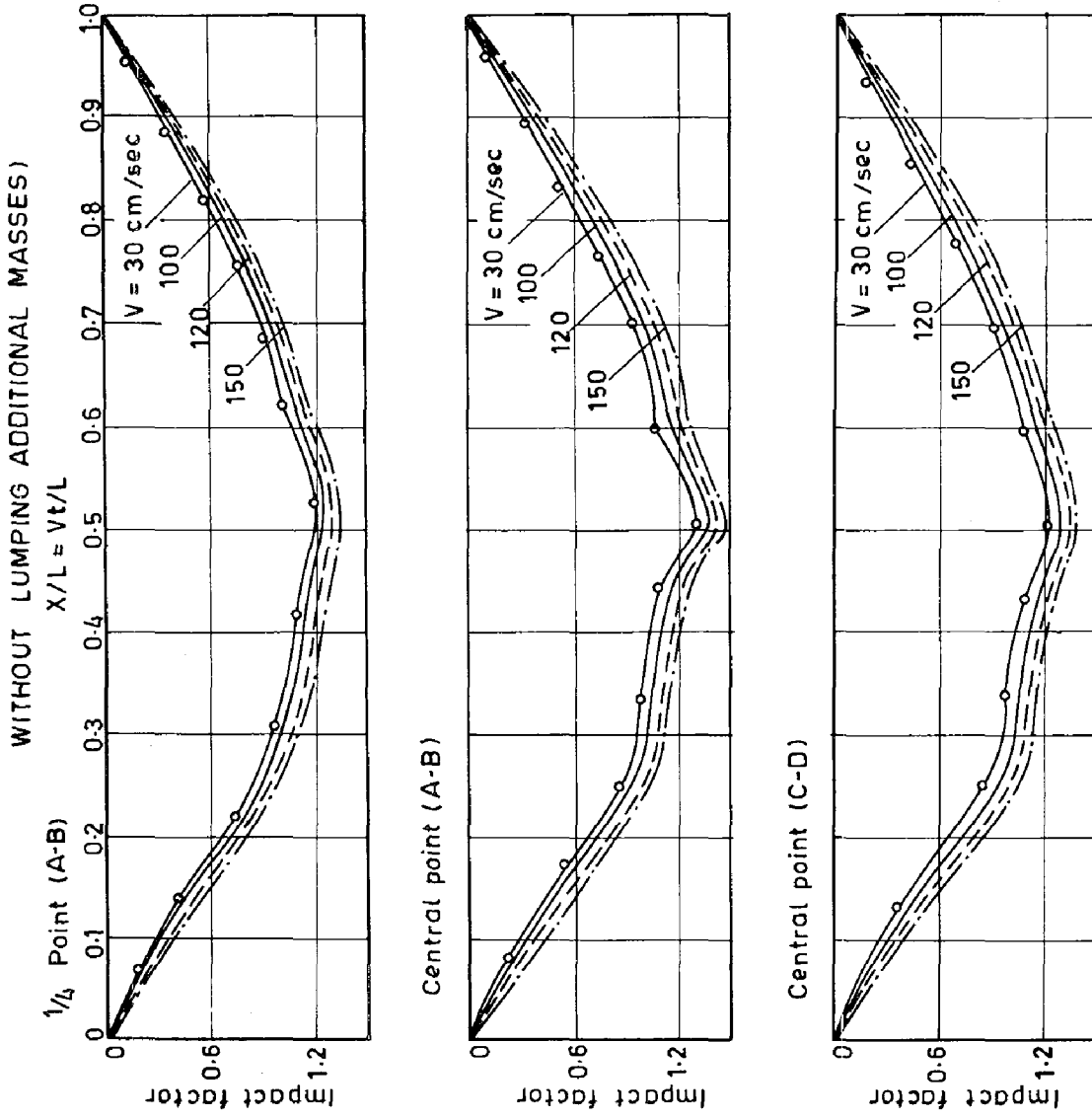


FIG. 3. VARIATION OF IMPACT FACTORS. FORCE MOVING ON THE CENTRAL BEAM (A-B)

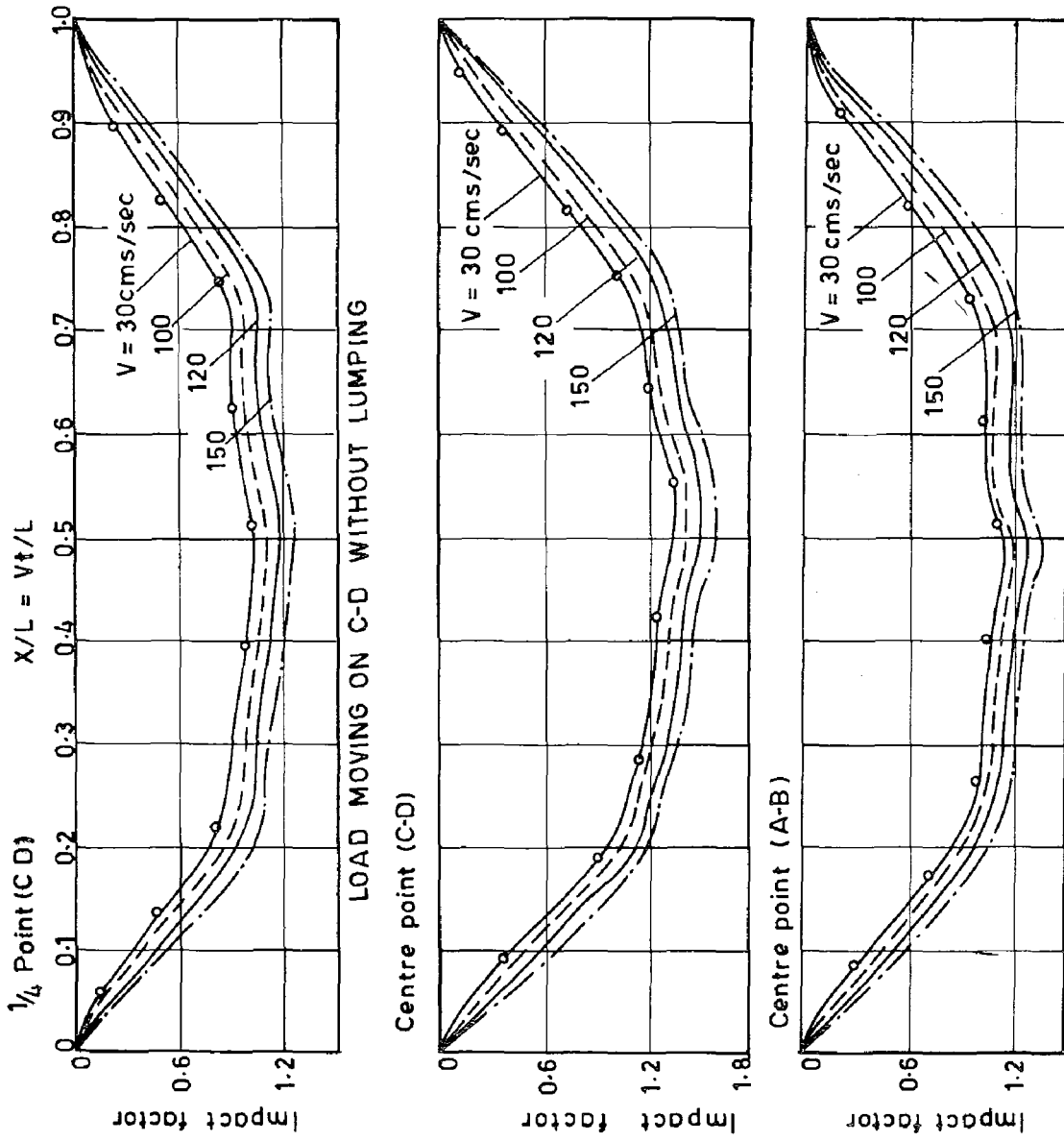


FIG.4 . VARIATION OF IMPACT FACTORS. FORCE MOVING ON THE END BEAM (C-D)

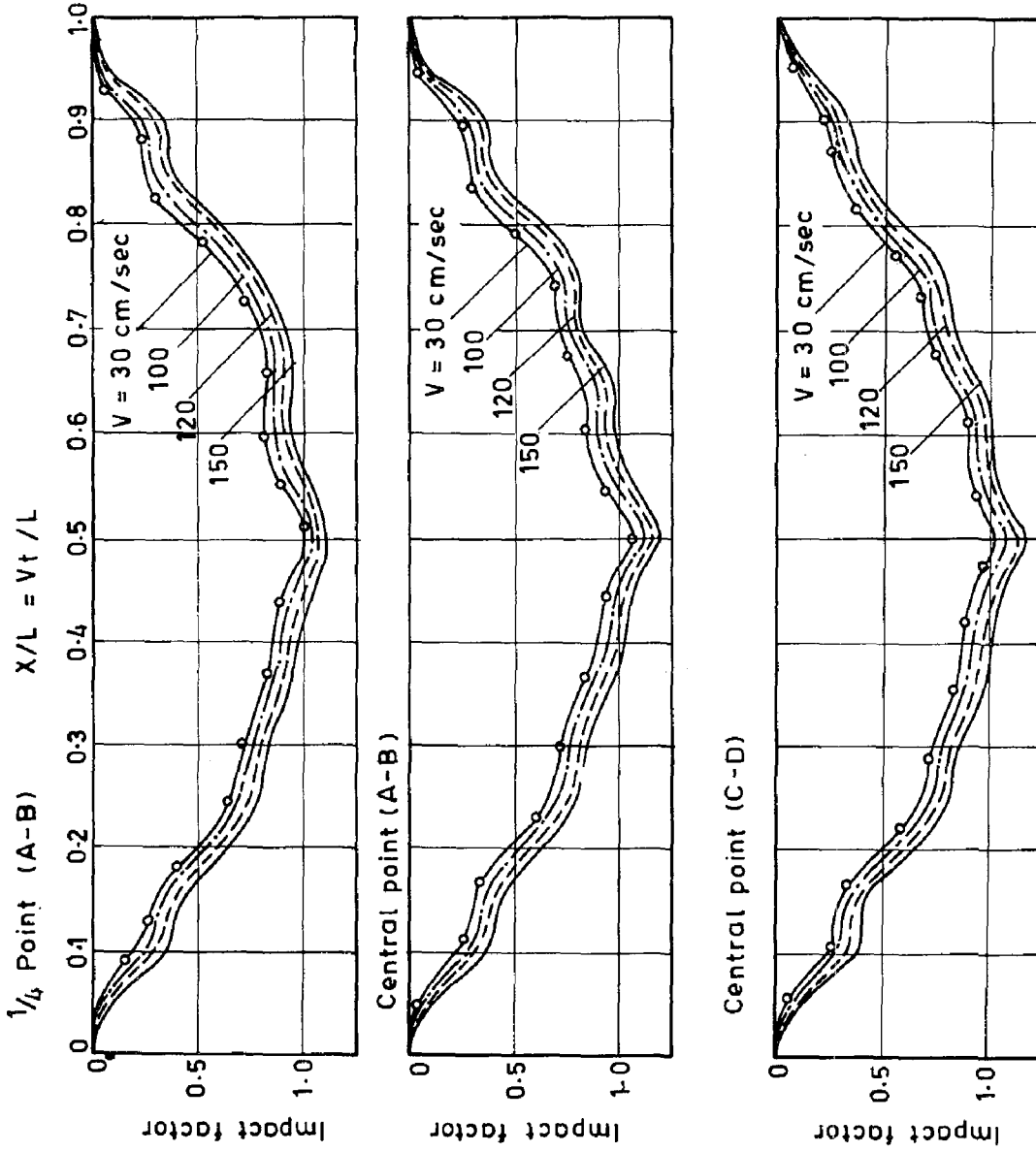


FIG. 5 . VARIATION OF IMPACT FACTORS. FORCE MOVING ON THE CENTRAL BEAM (A-B) BY LUMPING ADDITIONAL MASSES OF 0.3 kg.

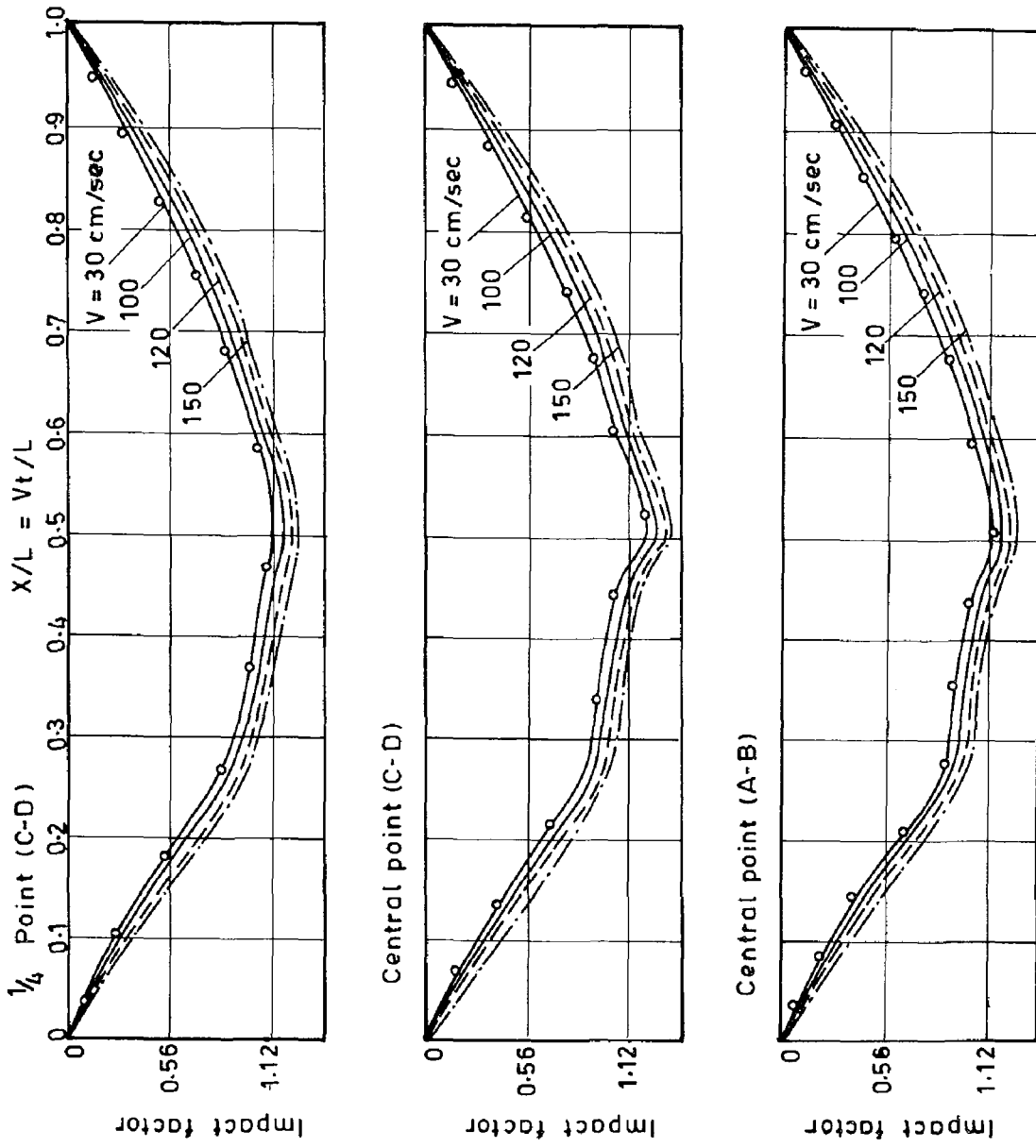


FIG. 6 . VARIATION OF IMPACT FACTORS. FORCE MOVING ON THE END BEAM (C-D) BY LUMPING ADDITIONAL MASSES OF 0.3 Kg.

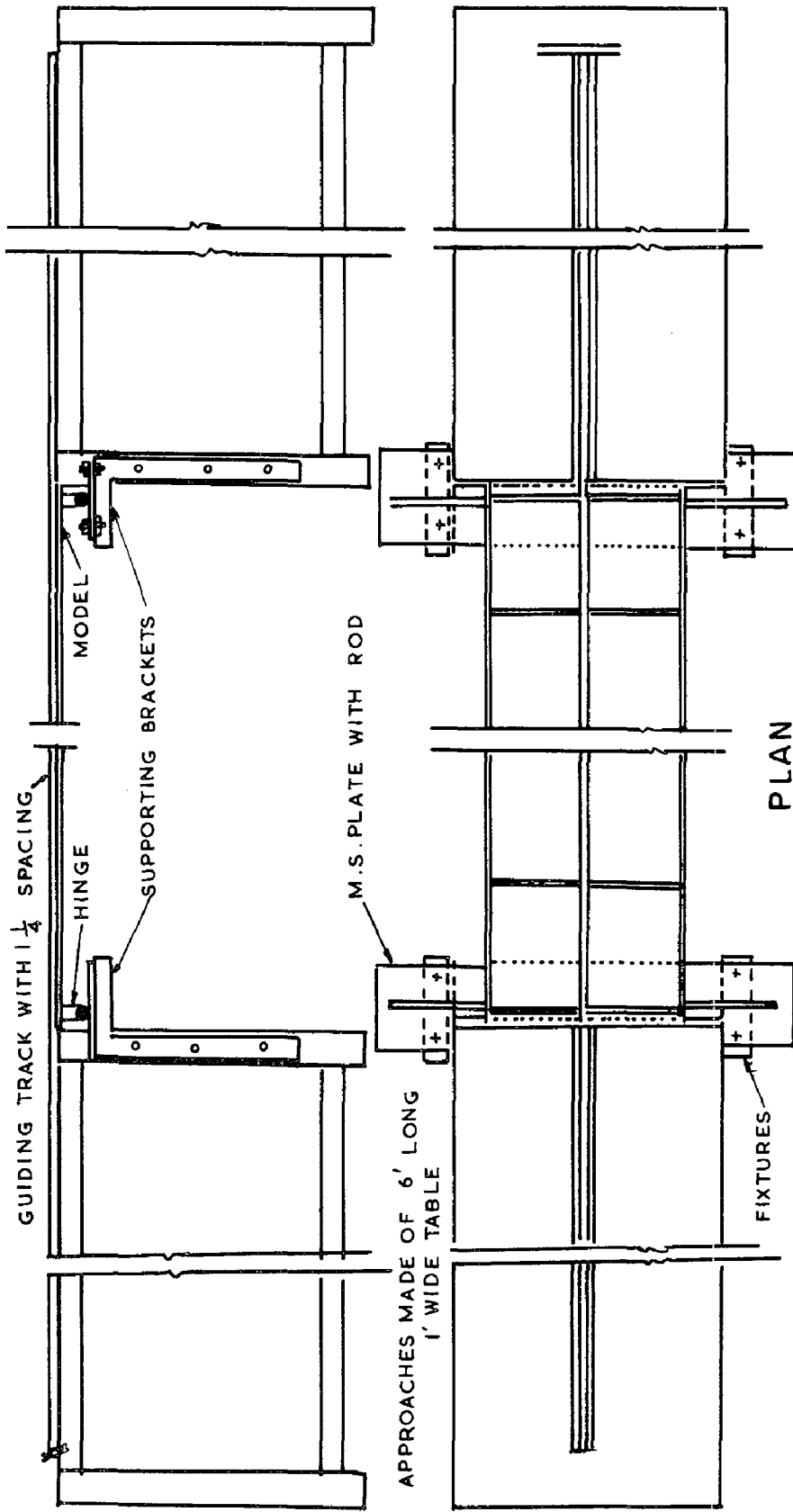


FIG.7. TRACK LAYOUT AND THE LAYOUT OF THE MODEL .

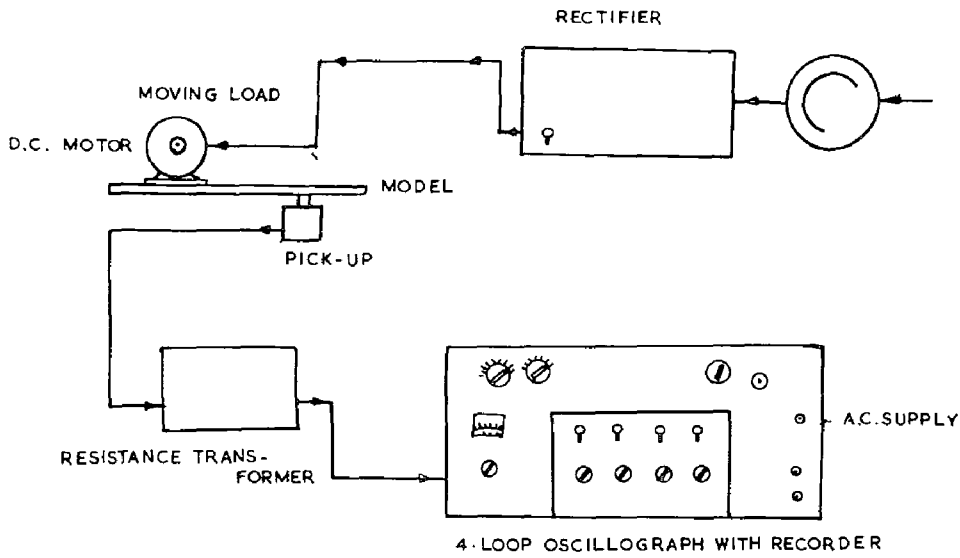
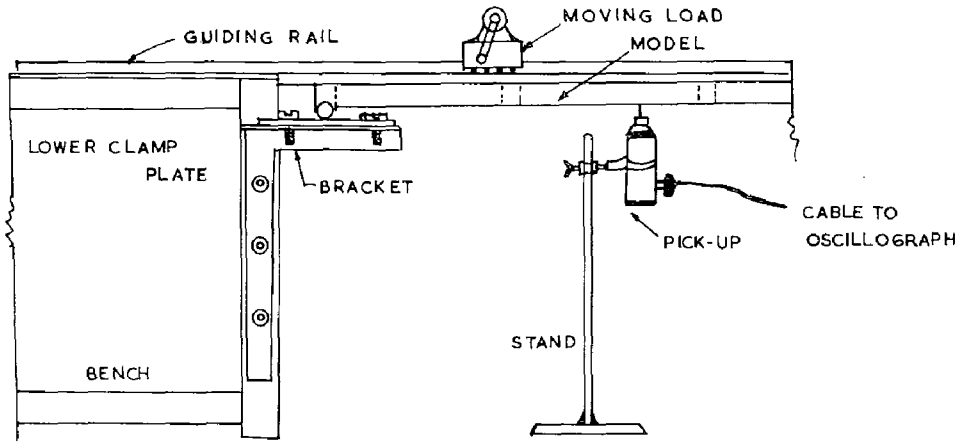
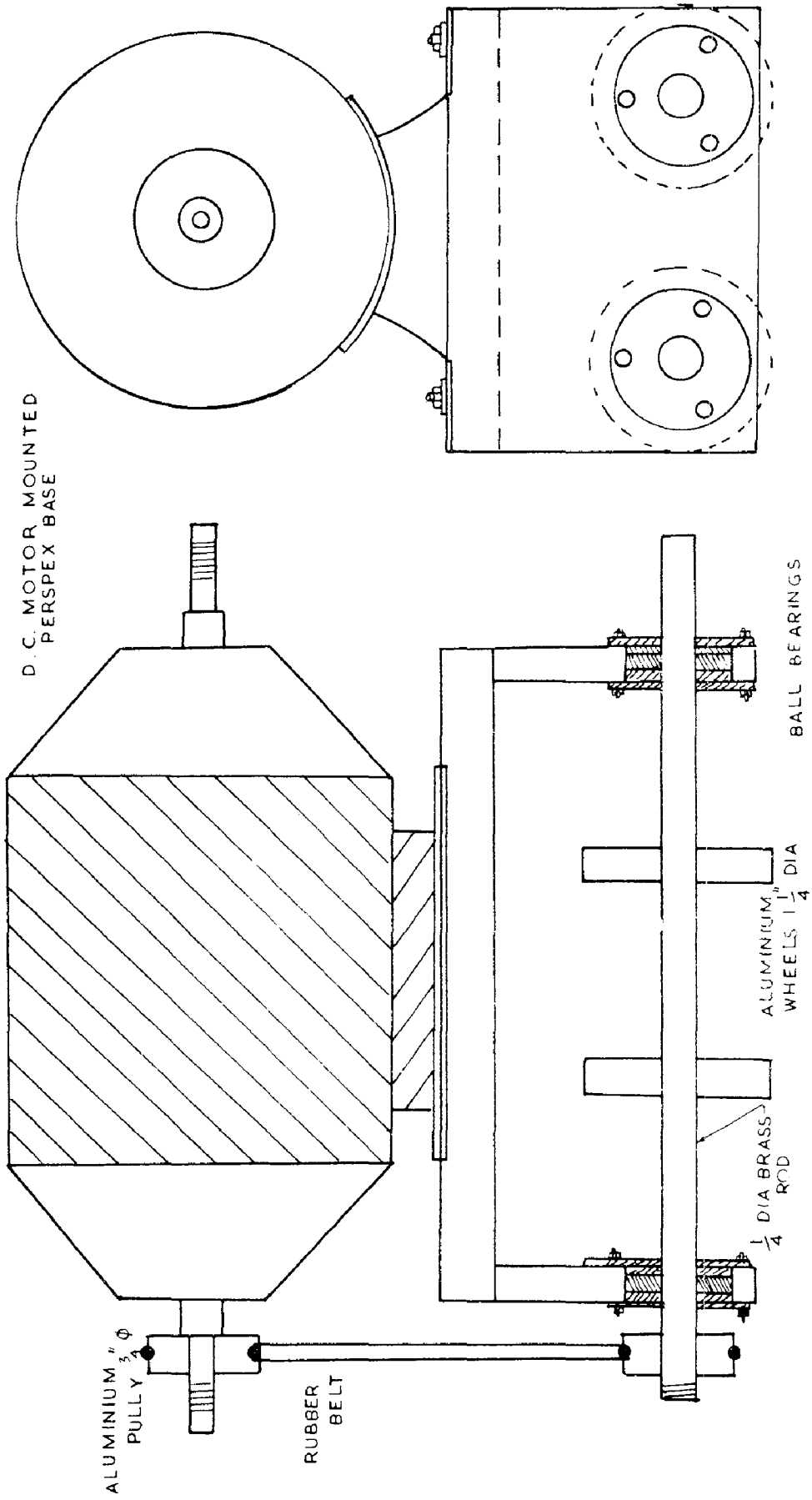


FIG. 8. INSTRUMENTATION ARRANGEMENT FOR THE DYNAMIC RESPONSE .



Side elevation

Sectional elevation

FIG.9. MOVING LOAD ASSEMBLY.

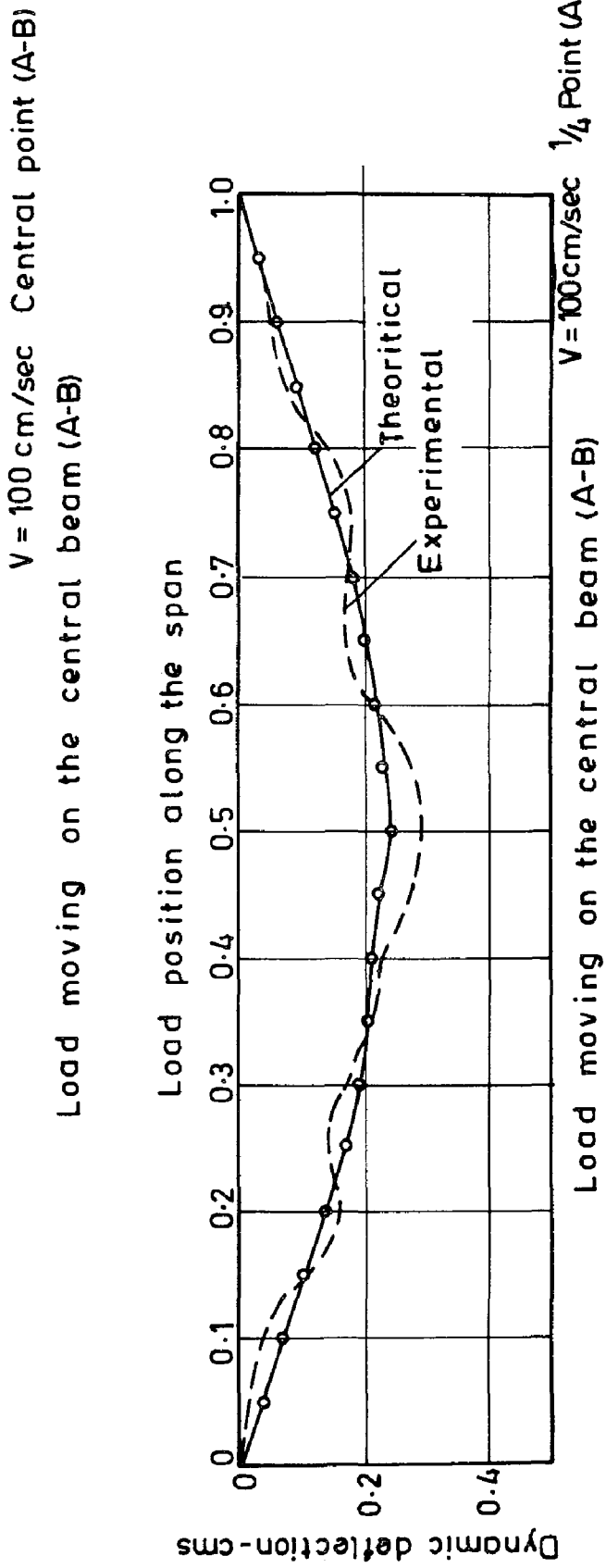
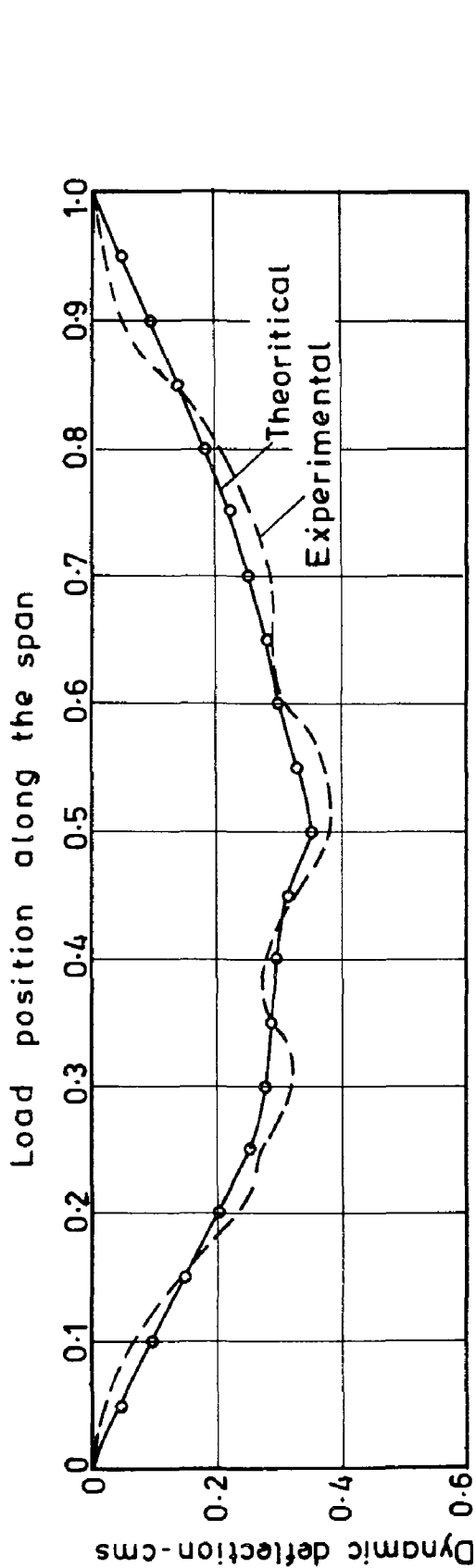


FIG. 10. COMPARISON OF EXPERIMENTAL AND THEORETICAL DYNAMIC RESPONSE

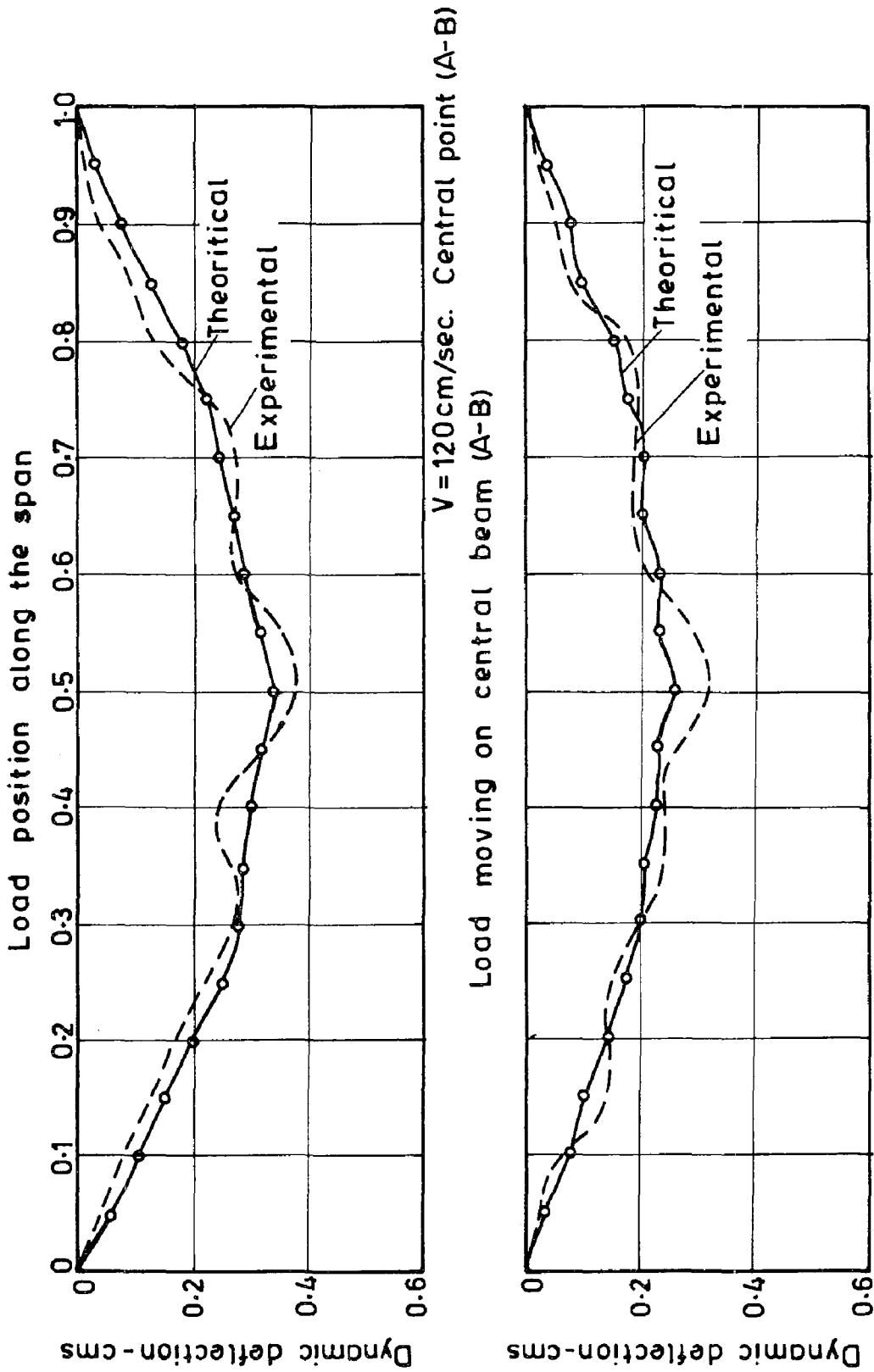


FIG. 11. COMPARISON OF EXPERIMENTAL AND THEORETICAL DYNAMIC RESPONSE

INTERNATIONAL SYMPOSIUM ON
EARTHQUAKE STRUCTURAL ENGINEERING

413

St. Louis, Missouri, USA, August, 1976

A NEW METHOD FOR NUMERICAL INTEGRATION
OF EQUATIONS OF MOTION

by

John E. Goldberg

Introduction

Several of the techniques currently employed in earthquake design of structures depend, at one stage or another, upon numerical integration of the equation of motion. For example, if the spectral approach is used, the response spectra are generated by numerical integration using the recorded ground motion of a real earthquake as a forcing function and determining the response of damped simple oscillators--that is, damped single-degree-of-freedom systems--over a broad range of natural frequencies and damping ratios of these systems. Alternatively, ensembles of recorded earthquake ground motions or of artificially generated hypothetical earthquakes are sometimes used. Another possible technique is to integrate numerically the response of a structure in each of its several significantly responsive modes to a real or artificial earthquake and then to combine these responses either by superposing the individual responses in real time or combining, in some presumably judicious manner, the maximums of the model responses.

A number of numerical integration processes already exist and, depending to some extent upon the desired or expected accuracy or upon the familiarity of the engineer with the various processes, these are used in connection with the design techniques mentioned above or in connection with other techniques and problems. Some of these numerical integration processes have found favor among engineers. Among these are finite differences, the Runge-Kutta methods, Newmark's beta-method and certain methods which have the character of predictor-corrector methods. These well-known processes have been adequately described in the literature and it is therefore unnecessary to deal at length with them.

The purpose of this presentation is to describe, in the context of earthquake engineering problems, a new method for numerical integration of differential equations. The new method appears to have certain advantages over some of the methods that are currently in use.

The process is self-starting and the interval or step size may be varied arbitrarily during the computation. Properties of the system and characteristics of the forcing function may also vary during the computation. These are advantages that do not accrue to all methods which are in current use. The method does not require more than one pass over each time-step as predictor-corrector and iterative processes require. The process is stable. Accuracy is high and may be further increased as will be discussed later.

Theory

The equation of motion for a damped one-degree-of-freedom system is

$$m\ddot{y} + c\dot{y} + ky = f(t) \quad (1)$$

in which

m = mass

c = damping coefficient

k = spring stiffness

f = forcing function

and each dot over a variable represents one differentiation with respect to time ($\dot{y} = dy/dt$, $\ddot{y} = d^2y/dt^2$). The system coefficients (m , c and k) may vary with time. The procedure may be modified to take into account, at least approximately and with a fair degree of accuracy, variations of these coefficients with displacement, velocity and acceleration.

Equation (1) is transformed into a Volterra integral equation of the second kind by introducing the following substitution:

$$\ddot{y}(t) = Y(t) \quad (2)$$

Then

$$\dot{y}(t) = \int_0^t Y(\tau) d\tau + C_1 \quad (3)$$

$$y(t) = \int_0^t (t-\tau) Y(\tau) + C_1 t + C_2 \quad (4)$$

It is easily seen that

$$C_1 = \dot{y}(0) \quad (5)$$

$$C_2 = y(0) \quad (6)$$

For convenience, these initial values will be written respectively as \dot{y}_0 and y_0 . Similarly $Y(0)$ will be written as Y_0 . In general, the integrations will be carried out over each time-step or interval so that Y_0 , \dot{y}_0 and y_0 will be the starting values at the beginning of that step or interval; and generally will change from interval to interval.

Substitution of Equations (2) - (6) into Equation (1) transforms the latter into a Volterra integral equation of the second kind:

$$mY + \int_0^t [c + k(t-\tau)]Y d\tau + (c + kt)\dot{y}_0 + ky_0 = f \quad (7)$$

or

$$mY + (c + kt) \int_0^t Y d\tau - k \int_0^t \tau Y d\tau + (c + kt)\dot{y}_0 + ky_0 = f \quad (8)$$

There are several ways in which Equation (7) or (8) can be solved numerically, the choice depending upon circumstances and desired accuracy. One class of approaches is to represent $Y(\tau)$ by a truncated series of appropriately chosen functions:

$$Y(\tau) = Y_0 + A_1\phi_1(t) + A_2\phi_2(t) + A_3\phi_3(t) + \dots + A_n\phi_n(t) \quad (9)$$

in which A_1, \dots, A_n are arbitrary constants, the values of which will be chosen in some way so as to obtain a good approximation to the exact solution. An obvious simple and, it turns out, convenient choice is to take the functions to be powers of the independent variable, t , within the interval:

$$Y(\tau) = Y_0 + A_1t + A_2t^2 + A_3t^3 + \dots + A_nt^n \quad (10)$$

Substitution of Equation (9) or (10) into Equation (7) or (8) transforms this equation into an equation involving the n arbitrary constants, A_1 to A_n and the chosen time functions. There are now several ways in which to arrive at the values of these constants which will give a good solution over the interval. A particularly straightforward and useful way is the collocation method. The interval is divided into n subdivisions. It is convenient but not necessary to make these subdivisions of equal length. The division points together with the end of the interval will constitute a set of n instants (t_1, t_2, \dots, t_n) . Substitution of each of these times into the equation obtained by substituting Equation (9) or (10) into Equation (8) or (9) will yield a set of n simultaneous algebraic equations in the unknown coefficients, A_1 to A_n , from which the values for these coefficients are readily obtained. These values are now to be substituted into Equation (9) or (10). Having, now, the interpolating function for Y , values of Y , \dot{y} and y at the end of the interval (and at interior points if desired) can be calculated by means of Equations (2), (3) and (4). If there are no discrete jumps in Y , \dot{y} or y at the end of the interval as a consequence of impulses, change in system coefficients or so on, the terminal values at the end of the interval become the initial values $(Y_0, \dot{y}_0, \text{ and } y_0)$ for the next interval.

If, for example, Y is taken in the general quadratic form

$$Y = Y_0 + A_1 t + A_2 t^2 \quad (0 \leq t \leq \lambda) \quad (11)$$

then

$$\int_0^t Y d\tau = Y_0 t + \frac{1}{2} A_1 t^2 + \frac{1}{3} A_2 t^3$$

$$\int \tau Y d\tau = \frac{1}{2} Y_0 t^2 + \frac{1}{3} A_1 t^3 + \frac{1}{4} A_2 t^4$$

so that Equations (7) and (8) become

$$m(Y_0 + A_1 t + A_2 t^2) + c(Y_0 t + \frac{1}{2} A_1 t^2 + \frac{1}{3} A_2 t^3) + k(\frac{1}{2} Y_0 t^2 + \frac{1}{6} A_1 t^3 + \frac{1}{12} A_2 t^4) + c\dot{y}_0 + k t \dot{y}_0 + k y_0 = f \quad (12)$$

Denoting the length of the time-step or interval by λ and taking the collocation points at $t = \lambda/2$ and $t = \lambda$ (i.e., substituting $t = \lambda/2$ and $t = \lambda$ into Equation (12)), the following pair of simultaneous equations in A_1 and A_2 is obtained:

$$\left. \begin{aligned} G_{11}A_1 + G_{12}A_2 &= f(\lambda/2) - G_{13}Y_0 - G_{14}\dot{Y}_0 - G_{15}Y_0 \\ G_{21}A_1 + G_{22}A_2 &+ f(\lambda) - G_{23}Y_0 - G_{24}\dot{Y}_0 - G_{25}Y_0 \end{aligned} \right\} \quad (13)$$

in which

$$\left. \begin{aligned} G_{11} &= \frac{\lambda}{2} \left[m + \frac{1}{4}c\lambda + \frac{1}{24}k\lambda^2 \right] & G_{21} &= \lambda \left[m + \frac{1}{2}c\lambda + \frac{1}{6}k\lambda^2 \right] \\ G_{12} &= \frac{\lambda^2}{4} \left[m + \frac{1}{6}c\lambda + \frac{1}{48}k\lambda^2 \right] & G_{22} &= \lambda^2 \left[m + \frac{1}{3}c\lambda + \frac{1}{12}k\lambda^2 \right] \\ G_{13} &= m + \frac{1}{2}c\lambda + \frac{1}{8}k\lambda^2 & G_{23} &= m + c\lambda + \frac{1}{2}k\lambda^2 \\ G_{14} &= c + \frac{1}{2}k\lambda & G_{24} &= c + k\lambda \\ G_{15} &= G_{25} = k \end{aligned} \right\} \quad (14)$$

Then, by Cramer's rule, the following formulas for A_1 and A_2 are obtained:

$$\left. \begin{aligned} A_1 &= \frac{1}{\Delta} [G_{22}F_1 - G_{12}F_2] \\ A_2 &= \frac{1}{\Delta} [G_{11}F_2 - G_{21}F_1] \end{aligned} \right\} \quad (15)$$

in which

$$\Delta = G_{11}G_{22} - G_{12}G_{21} \quad (16)$$

$$\left. \begin{aligned} F_1 &= f(\lambda/2) - G_{13}Y_0 - G_{14}\dot{Y}_0 - G_{15}Y_0 \\ F_2 &= f(\lambda) - G_{23}Y_0 - G_{24}\dot{Y}_0 - G_{25}Y_0 \end{aligned} \right\} \quad (17)$$

The calculated values of A_1 and A_2 can now be substituted into Equations (3), (4) and (10) to obtain expressions for the acceleration, velocity and displacements within and at the end of the interval, λ :

$$\left. \begin{aligned} \ddot{y} &= Y = Y_0 + A_1 t + A_2 t^2 \\ \dot{y} &= Y_0 t + \frac{1}{2} A_1 t^2 + \frac{1}{3} A_2 t^3 + \dot{y}_0 \\ y &= \frac{1}{2} Y_0 t^2 + \frac{1}{6} A_1 t^3 + \frac{1}{12} A_2 t^4 + \dot{y}_0 t + y_0 \end{aligned} \right\} \quad (18)$$

Using these formulas, the values at the end of the interval, $t = \lambda$, can be calculated. If the motion is continuous into the next time-step or interval, the values thus obtained at $t = \lambda$ become the starting values for the next interval.

It may be noted, in passing, that the necessary formulas are easily obtained if one desires to use interpolating polynomials of higher or lower degree. For example, a cubic or quartic polynomial may be used in place of the quadratic expression represented by Equation (11). Collocation will be established at the end of the interval and at either two or three intermediate points, depending on whether the cubic or quartic form is used. In either case, the subdivisions within the interval can be taken to be either equal or unequal. Equations (13) will be replaced by new sets of either three or four simultaneous equations involving the appropriate number of undetermined coefficients with corresponding changes in Equations (14) - (17).

If, for any reason, results are desired for the simpler assumption of a piecewise linear variation in the acceleration, it is only necessary to set A_2 equal to zero in Equations (11), (12) and the second of (13) and to use the formula,

$$A_1 = \frac{1}{G_{21}} (F_2)$$

in which F_2 and G_{21} have the definitions given by Equations (14) and the second of (17).

Still higher order polynomials may be used as the interpolating functionals to further increase the accuracy obtainable with given interval sizes. The computing effort and cost will increase correspondingly. Alternatively, functions other than simple powers of t may be used in the interpolating functional.

A computer program is easily written for running at a regular computer installation. Programs may be written for running on a desk-top computer. Programs may also be written and successfully ran on some of the currently available programmable hand calculators, depending of course, and the amount of interval memory.

Example

For purposes of an illustrative example, the motion of a system for which

$$m = 1 \quad c = 0 \quad k = 4$$

is computed for the range $0 \leq t \leq 2\pi$ with initial values $\ddot{y}(0) = 0$, $\dot{y}(0) = 2$, and $y(0) = 0$ and with $f = 0$. The example is simple, but serves nevertheless to demonstrate the accuracy and rate of convergence that can be obtained.

A computer program was written based on the quadratic form of Equation (11). The program was run on a CDC 6500 and results were obtained for five different interval sizes: $\pi/8$, $\pi/16$, $\pi/32$, $\pi/64$, $\pi/128$. The program calculates and prints results at the end of each interval and, if desired, at intermediate points. Tables 1a, 1b and 1c present abridged results transcribed from the complete printout along with the exact solution for this problem. It may be mentioned that the total computer charge for input-output, central processing and printing for the five runs was \$0.21.

Results were also obtained using the piecewise linear assumption so that the accuracies of the linear and quadratic assumptions could be compared. Abridged results are presented in Tables 2a, 2b and 2c. It can be seen that these results are quite good for the smaller interval sizes and show that results obtained with the coarser divisions may also be useful. It is worth noting that the savings in computer charges with respect to the charges for the quadratic calculation was less than two cents.

Table 1a. Calculated Accelerations -- Quadratic Analysis

Time t	Time-Step Size					Exact
	$\pi/4$	$\pi/8$	$\pi/16$	$\pi/32$	$\pi/64$	
0	0	0	0	0	0	0
$\pi/8$		-2.82700396	-2.82834050	-2.82842174	-2.82842679	-2.82842713
$2\pi/8$	-3.97181123	-3.99858865	-3.99991608	-3.99999482	-3.99999968	-4.00000000
$3\pi/8$		-2.82870483	-2.82844963	-2.82842861	-2.82842722	-2.82842713
$4\pi/8$	-0.03425563	-0.00240575	-0.00015434	-0.00000971	-0.00000061	0.00000000
$5\pi/8$		2.82530207	2.82823137	2.82841488	2.82842636	2.82842713
$6\pi/8$	3.97151579	3.99858720	3.99991607	3.99999482	3.99999968	4.00000000
$7\pi/8$		2.83040467	2.82855875	2.82843547	2.82842765	2.82842713
π	0.06850872	0.00481150	0.00030867	0.00001941	-0.00000121	0.00000000
$9\pi/8$		-2.82359916	-2.82812223	-2.82840802	-2.82842593	-2.82842713
$10\pi/8$	-3.97092492	-3.99858431	-3.99991605	-3.99999482	-3.99999968	-4.00000000
$11\pi/8$		-2.83210349	-2.82866788	-2.82844233	-2.82842807	-2.82842713
$12\pi/8$	-0.10275671	-0.00721725	-0.00046301	-0.00002912	-0.00000182	0.00000000
$13\pi/8$		2.81289522	2.82801308	2.82840116	2.82842550	2.82842713
$14\pi/8$	3.97003868	3.99857996	3.99991604	3.99999482	3.99999968	4.00000000
$15\pi/8$		2.83380129	2.82877700	2.82844920	2.82842850	2.82842713
2π	0.13699716	0.00962300	0.00061734	0.00003882	0.00000242	0.00000000

Table 1b. Calculated Velocities -- Quadratic Analysis

Time t	Time-Step Size					Exact
	$\pi/4$	$\pi/8$	$\pi/16$	$\pi/32$	$\pi/64$	
0	2.00000000	2.00000000	2.00000000	2.00000000	2.00000000	2.00000000
$\pi/8$		1.41442626	1.41422720	1.41421442	1.41421362	1.41421356
$2\pi/8$	0.00862469	0.00060165	0.00003858	0.00000243	0.00000015	0.00000000
$3\pi/8$		-1.41357527	-1.41417264	-1.41421099	-1.41421340	-1.41421356
$4\pi/8$	-1.99992561	-1.99999964	-2.00000000	-2.00000000	-2.00000000	-2.00000000
$5\pi/8$		-1.41527674	-1.41428177	-1.41421785	-1.41421383	-1.41421356
$6\pi/8$	-0.02587342	-0.00180495	-0.00011575	-0.00000728	-0.00000045	0.00000000
$7\pi/8$		1.41272377	1.41411807	1.41420756	1.41421319	1.41421356
π	1.99970246	1.99999855	1.99999999	2.00000000	2.00000000	2.00000000
$9\pi/8$		1.41612670	1.41433633	1.41422128	1.41421404	1.41421356
$10\pi/8$	0.04312023	0.00300825	0.00019292	0.00001213	0.00000075	0.00000000
$11\pi/8$		-1.41187176	-1.41406350	-1.41420413	-1.41421297	-1.41421356
$12\pi/8$	-1.99933057	-1.99999674	-1.99999999	-2.00000000	-2.00000000	-2.00000000
$13\pi/8$		-1.41697616	-1.41439089	-1.41422471	-1.41421426	-1.41421356
$14\pi/8$	-0.06036384	-0.00421155	-0.00027009	-0.00001699	-0.00000106	0.00000000
$15\pi/8$		1.41101923	1.41400892	1.41420069	1.41421276	1.41421356
2π	1.99880995	1.99999421	1.99999998	2.00000000	2.00000000	2.00000000

Table 1c. Calculated Displacements - Quadratic Analysis

Time t	Time-Step Size					Exact
	$\pi/4$	$\pi/8$	$\pi/16$	$\pi/32$	$\pi/64$	
0	0.00000000	0.00000000	0.00000000	0.00000000	0.00000000	0.00000000
$\pi/8$		0.70675099	0.70708513	0.70710544	0.70710670	0.70710678
$2\pi/8$	0.99295281	0.99964716	0.99997902	0.99999870	0.99999992	1.00000000
$3\pi/8$		0.70717621	0.70711241	0.70710715	0.70710670	0.70710678
$4\pi/8$	0.00856391	0.00060144	0.00003858	0.00000243	0.00000015	0.00000000
$5\pi/8$		-0.70632552	-0.70705784	-0.70710372	-0.70710659	-0.70710678
$6\pi/8$	-0.99287895	-0.99964680	-0.99997902	-0.99999870	-0.99999992	-1.00000000
$7\pi/8$		-0.70760117	-0.70713969	-0.70710887	-0.70710691	-0.70710678
π	-0.01712718	-0.00120288	-0.00007717	-0.00000485	-0.00000030	0.00000000
$9\pi/8$		0.70589979	0.70703056	0.70710200	0.70710648	0.70710678
$10\pi/8$	0.99273123	0.99964608	0.99997902	0.99999870	0.99999992	1.00000000
$11\pi/8$		0.70802587	0.70716697	0.70711058	0.70710702	0.70710678
$12\pi/8$	0.02568918	0.00180431	0.00011575	0.00000728	0.00000045	0.00000000
$13\pi/8$		-0.70547381	-0.70700327	-0.70710029	-0.70710638	-0.70710678
$14\pi/8$	-0.99250967	-0.99964499	-0.99997901	-0.99999870	-0.99999992	-1.00000000
$15\pi/8$		-0.70845032	-0.70719425	-0.70711230	-0.70710713	-0.70710678
2π	-0.03424926	-0.00240575	-0.00015434	-0.00000971	-0.00000061	0.00000000

Table 2a. Calculated Accelerations -- Linear Analysis

Time t	Time-Step Size					Exact
	$\pi/4$	$\pi/8$	$\pi/16$	$\pi/32$	$\pi/64$	
0	0.0000	0.0000	0.0000	0.0000	0.0000	0.0000
$\pi/8$		-2.6058	-2.7689	-2.8133	-2.8246	-2.8284
$2\pi/8$	-3.4476	-3.8783	-3.9728	-3.9935	-3.9984	-4.0000
$3\pi/8$	-3.1666	-2.9314	-2.9314	-2.8555	-2.8353	-2.8284
$4\pi/8$	-2.2276	-0.8346	-0.2333	-0.0600	-0.0151	0.0000
$5\pi/8$		1.9244	2.5968	2.7704	2.8139	2.8284
$6\pi/8$	2.0083	3.6987	3.9591	3.9926	3.9983	4.0000
$7\pi/8$		3.5807	3.0839	2.8971	2.8459	2.8284
π	3.5252	1.6305	0.4657	0.1200	0.0302	0.0000
$9\pi/8$		-1.1538	-2.4157	-2.7269	-2.8032	-2.8284
$10\pi/8$	0.2694	-3.3479	-3.9318	-3.9908	-3.9982	-4.0000
$11\pi/8$		-3.8290	-3.2257	-2.9381	-2.8565	-2.8284
$12\pi/8$	-3.3512	-2.3510	-0.6965	-0.1799	-0.0453	0.0000
$13\pi/8$		0.3299	2.2263	2.6827	2.7924	2.8284
$14\pi/8$	-2.4346	2.8419	3.8909	3.9881	3.9980	4.0000
$15\pi/8$		3.8999	3.3564	2.9784	2.8671	2.8284
2π	1.7781	2.9626	0.9250	0.2398	0.0604	0.0000

Table 2b. Calculated Velocities -- Linear Analysis

Time t	Time-Step Size					Exact
	$\pi/4$	$\pi/8$	$\pi/16$	$\pi/32$	$\pi/64$	
0	2.0000	2.0000	2.0000	2.0000	2.0000	2.0000
$\pi/8$		1.4884	1.4348	1.4195	1.4155	1.4142
$2\pi/8$	0.6461	0.0587	0.0587	0.0150	0.0038	0.0000
$3\pi/8$		-1.1681	-1.3506	-1.3982	-1.4102	-1.4142
$4\pi/8$	-1.5825	-1.9537	-1.9966	-1.9998	-2.0000	-2.0000
$5\pi/8$		-1.7397	-1.5141	-1.4405	-1.4209	-1.4142
$6\pi/8$	-1.6686	-0.6356	-0.1759	-0.0451	-0.0113	0.0000
$7\pi/8$		0.7937	1.2617	1.3766	1.4048	1.4142
π	0.5044	1.8169	1.9862	1.9991	1.9999	2.0000
$9\pi/8$		1.9105	1.5882	1.4612	1.4262	1.4142
$10\pi/8$	1.9945	1.0266	0.2925	0.0751	0.0189	0.0000
$11\pi/8$		-0.3826	-1.1684	-1.3546	-1.3994	-1.4142
$12\pi/8$	0.7843	-1.5960	-1.9690	-1.9980	-1.9999	-2.0000
$13\pi/8$		-1.9928	-1.6568	-1.4815	-1.4315	-1.4142
$14\pi/8$	-1.4878	-1.3701	-0.4082	-0.1051	-0.0264	0.0000
$15\pi/8$		-0.0463	1.0712	1.3323	1.3940	1.4142
$16\pi/8$	-1.7456	1.3012	1.9451	1.9964	1.9998	2.0000

Table 2c. Calculated Displacements -- Linear Analysis

Time t	Time-Step Size					Exact
	$\pi/4$	$\pi/8$	$\pi/16$	$\pi/32$	$\pi/64$	
0	0.0000	0.0000	0.0000	0.0000	0.0000	0.0000
$\pi/8$		0.6519	0.6922	0.7033	0.7062	0.7071
$2\pi/8$	0.8619	0.9696	0.9932	0.9984	0.9996	1.0000
$3\pi/8$		0.7916	0.7329	0.7139	0.7088	0.7071
$4\pi/8$	0.5569	0.2086	0.0583	0.0150	0.0038	0.0000
$5\pi/8$		-0.4811	-0.6492	-0.6926	-0.7035	-0.7071
$6\pi/8$	-0.5021	-0.9247	-0.9998	-0.9981	-0.9996	-1.0000
$7\pi/8$		-0.8952	-0.7710	-0.7243	-0.7115	-0.7071
π	-0.8813	-0.4076	-0.1164	-0.0300	-0.0076	0.0000
$9\pi/8$		0.2885	0.6039	0.6817	0.7008	0.7071
$10\pi/8$	-0.0673	0.8370	0.9829	0.9977	0.9996	1.0000
$11\pi/8$		0.9572	0.8064	0.7345	0.7141	0.7071
$12\pi/8$	0.8378	0.5877	0.1741	0.0450	0.0113	0.0000
$13\pi/8$		-0.0825	-0.5566	-0.6707	-0.6981	-0.7071
$14\pi/8$	0.6087	-0.7105	-0.9727	-0.9970	-0.9995	-1.0000
$15\pi/8$		-0.9750	-0.8391	-0.7446	-0.7168	-0.7071
$16\pi/8$	-0.4445	-0.7406	-0.2312	0.0600	-0.0151	0.0000

INTERNATIONAL SYMPOSIUM ON
EARTHQUAKE STRUCTURAL ENGINEERING

423

St. Louis, Missouri, USA, August, 1976

SHERATON HOTEL IN SANTO DOMINGO, DOM. REP.:
ANALYSIS, DESIGN, AND CONSTRUCTION TECHNIQUES

BY

ALFREDO A. RICART NOUEL

Exec. Vice-president

Ricart & Maluf, S. A.

Prof. Universidad Autonoma de Santo Domingo

Santo Domingo, Dom. Rep.

SUMMARY

Analysis and design techniques are herein described for a 11-story RC building, part of the Sheraton Hotel project in Santo Domingo, Dom. Rep.; construction methods are briefly outlined. Main features of the structure are the typical 9 stories high pierced shear walls on top of 2-story frames.

Wind forces, UBC earthquake forces, and those obtained from an elasto-dynamic analysis were compared using programs written for an IBM 1130 with 8-K core capacity. The Equivalent Half Frame Method was used for lateral loads analysis, and the design was based on the ACI 318-71 Building Code.

INTRODUCTION

The Caracas earthquake in 1967 (a) made quite evident, in certain cases, the poor detailing of beam-column joints and the adverse effect of abrupt changes in building stiffness from floor to floor, when not comprehensively considered in planning and design (dramatic shear failures occurred in columns of the Macuto Sheraton Hotel). Recognition of these facts is present in the Special Provisions for Seismic Design, incorporated for the first time in the ACI Building Code in 1971.

Several architectural premises were dominant in selecting the final structural scheme: a) all rooms were planned to have seashore view; and b) first two stories were mainly for commercial use. Seismic probability in the D. R., occupying the eastern 2/3 of Hispaniola, can be classified as equal to that of the neighboring Puerto Rico, that is, Zone 2, according to UBC standards. Conditions were then similar to that of buildings affected in the Caracas earthquake.

The purpose of this paper is to describe a seismic design application of a complex structure, following ACI latest requirements, and to show the existence of a simple accurate method for handling the corresponding lateral loads effects.

GENERAL DESCRIPTION OF 11 - STORY BUILDING

Layout of reinforced concrete columns two stories high are shown in fig. 1 , together with the concrete shafts and shear walls extending the 11 stories of the building. All columns are 0.70 meters (27.56") square; concrete shafts are mainly 0.178 m. (7") thick , other shear walls are 0.254 m. (10") thick. Slab thicknesses are : a) 0.14 meters (5.51") for the first two floor levels, each slab being supported by beams on the four sides; and b) 0.17 meters (6.69") for all other floors, without beams.

A typical floor plan for the 9 top stories is shown in fig. 2 ; pierced shear walls are inclined 60 degrees at the ends, with respect to the longitudinal axis. Corbelling of the 9 top stories shear walls can be observed in the vertical section of the building in fig. 3 . There is no basement and foundations (fig. 4) are resting on a heterogeneous thick layer of calcareous fractured rocks with scattered small "pockets" of sand and clay; mortar injections were necessary for stabilizing the soil conditions.

ANALYSIS

Three computer programs written for IBM 1130 with 8-K core capacity were used for the analysis of the structure (b):

1) TORSO - Three Dimensional Seismic Analysis.

The purpose of the program is to perform the elasto-dynamic analysis of the building subjected to a prescribed earthquake taking into consideration horizontal rotation at floor levels due to structural eccentricity. The program was also used to estimate the building torsional response related to the spatial derivatives of the ground motion, that is, the floor inertia torques developed by ground rotation.

The Equivalent Half Frame Method (c) was used for substituting the actual frames (APPENDIX I-A), taking into consideration the axial deformation of the columns supporting the shear walls (APPENDIX I-B). Special input forms (b) greatly reduced the task of compiling pertinent data for the 3 programs herein described.

Floor loads, story shears and overturning moments were obtained corresponding to the elasto-dynamic analysis and the Uniform Building Code criteria. Comparison of both sets of values indicated the degree of ductility required for final design. Ultimate transverse seismic loads were taken as (1/2.4) of elasto-dynamic response to Taft Earthquake, 1952, with 7% of critical damping and 1550 m/sec (5000 ft/sec) shear wave velocity. These forces are slightly larger than minimum values of UBC, Zone 2, times 1.87 (ACI factor), just above the 3rd floor level and smaller below that level; base shear is higher than UBC value.

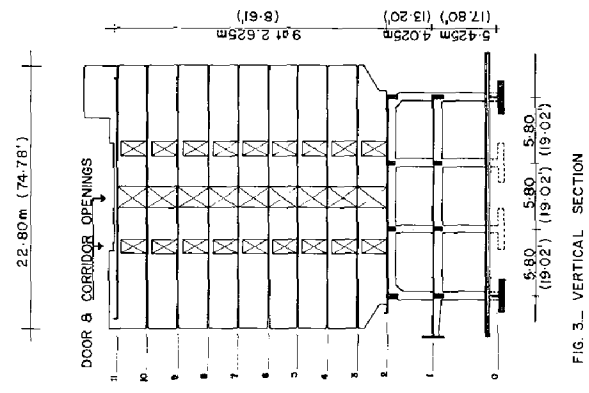
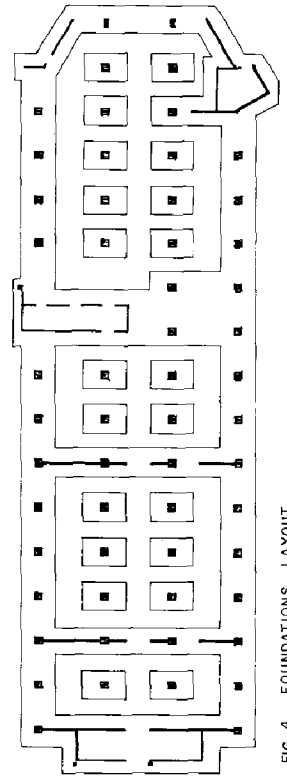
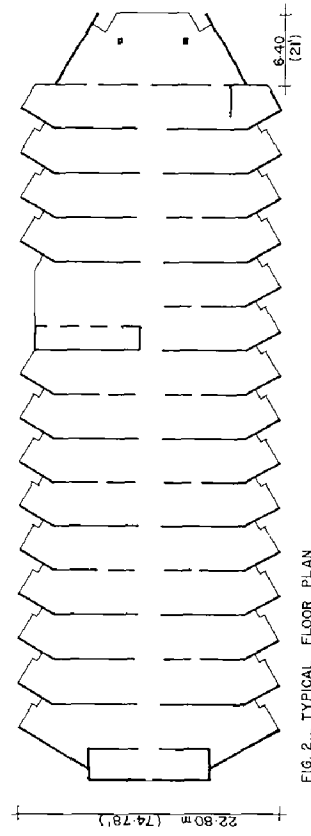
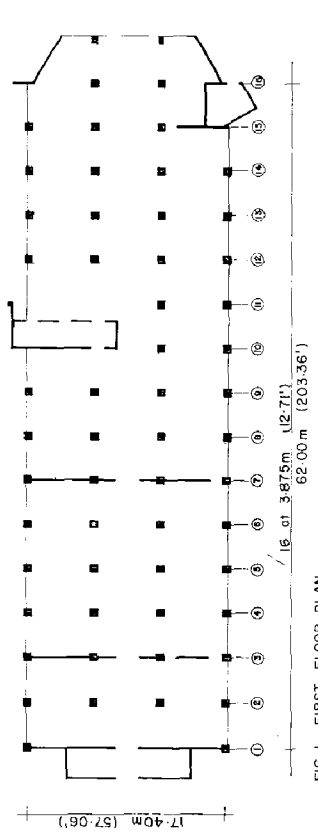


FIG. 4... FOUNDATIONS LAYOUT

FIG. 3... VERTICAL SECTION

FIG. 1... FIRST FLOOR PLAN

FIG. 2... TYPICAL FLOOR PLAN

2) ANA3D - Three Dimensional Distribution of Lateral Loads.

This program was used to obtain the distribution of the total wind and/or seismic loads between the different resistant frames and shear walls of the building, taking into consideration horizontal rotation at floor levels due to torsion related to eccentricity of the lateral load.

The resistant elements were also described in terms of Equivalent Half Frames taking into account, as before, axial and shear deformations of the equivalent column. Output data included, at all floors and for each load case, the force distributed to the resistant element and its corresponding horizontal displacement. The floor forces, and their moments with respect to the base, were also accumulated by the program to yield shear and overturning moment at base level.

3) BERNI - General Analysis of Frames Loaded in Their Planes.

This program is quite similar to STRESS, but admits actual stiffness of coupling beams for shear walls, and orthogonal rigid arms needed for simulation of special conditions in pierced shear walls (APPENDIXES I-C, and I-D).

There are 16 transverse lines of "frames" for resisting vertical and lateral loads in that direction; in the longitudinal direction only the concrete shafts and walls having a significant component were assumed for resisting lateral loads. Only 10 lines of frames were analysed in the transverse direction, some of which are shown in fig.5. Three loading conditions were considered for each symmetrical frame, and five, for unsymmetrical frames for obtaining reversed stresses; maximum horizontal load cases were selected from the output of ANA3D program. Total computer time for the 3 programs was 10 hours.

DESIGN TECHNIQUES

Minimum reinforcement on the gross section of typical 9-story shear walls (indicated as closed stirrups in both directions) was governed by the torsional stresses induced by the discontinued balcony slabs supported at the inclined ends. Corbels were designed following the "shear-friction" criteria. "Transition" beams supporting the pierced shear walls, were haunched at the ends, thus allowing a reduced section of columns on the "façade"; special confinement reinforcement details were indicated at these beam-column connections. Longitudinal beams in the first two stories, were indicated for increasing resistance of beam-column connections.

Coupling Beams with axial tension and moments were designed by "extending" the interaction diagrams available for columns. Eight coupling beams were made of welded plates, totally encased in concrete (fig.6); plastic design was used for these steel beams.

Concrete classes included 240 Kg/cm^2 (3500 psi) concrete for footings and 280 Kg/cm^2 (4000 psi) concrete for all other structural members. Grade 40 reinforcing steel was selected throughout.

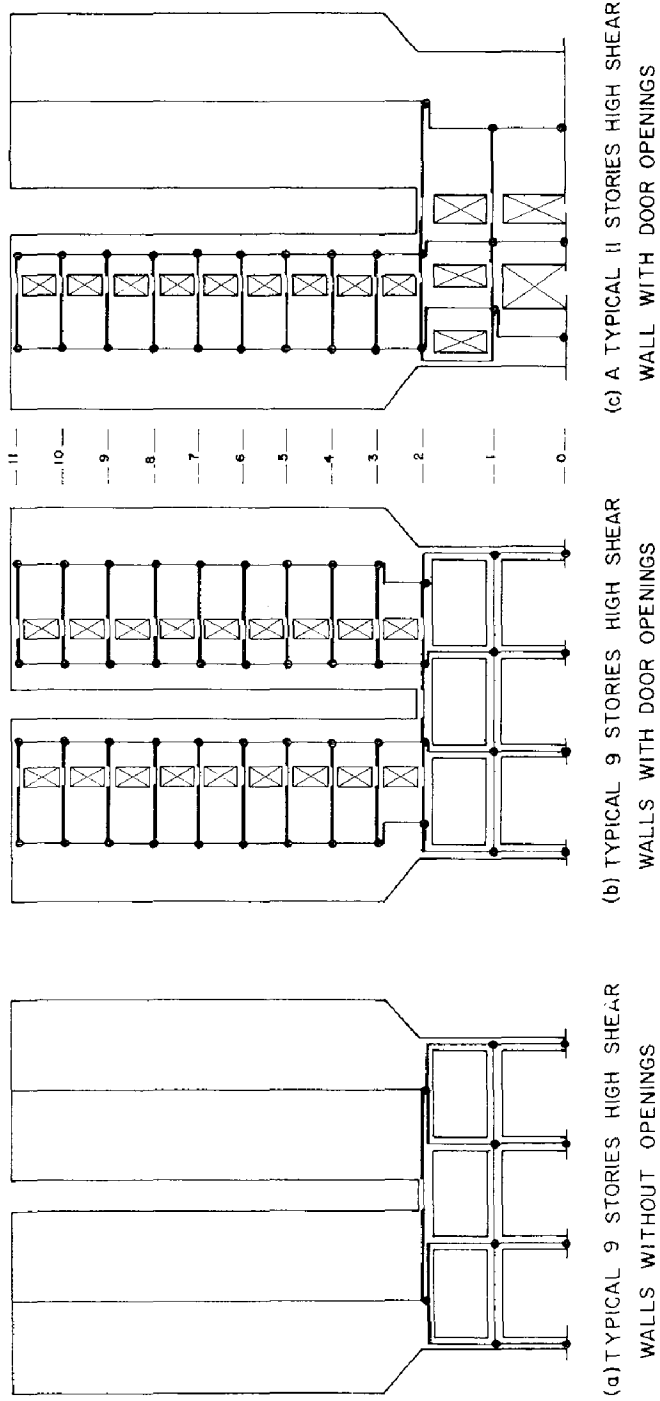
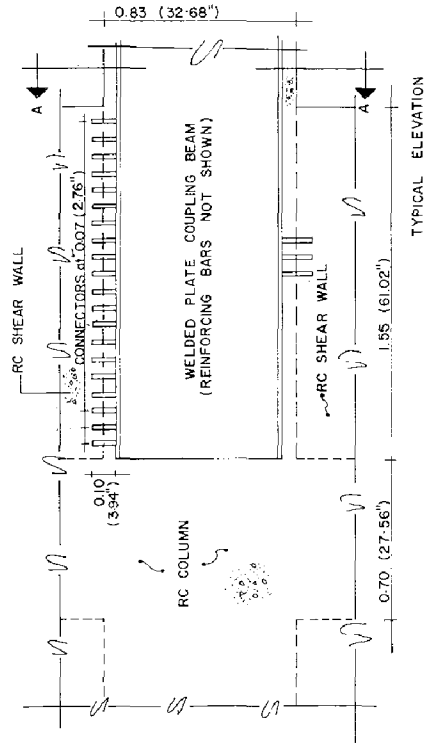
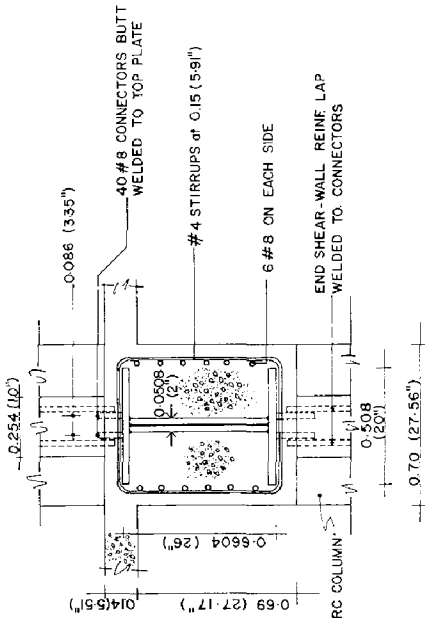


FIGURE 5

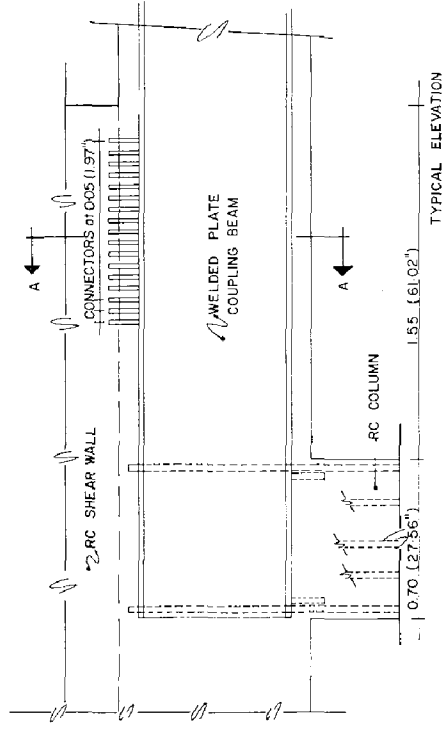


TYPICAL ELEVATION

WALL TO WALL COUPLING BEAMS

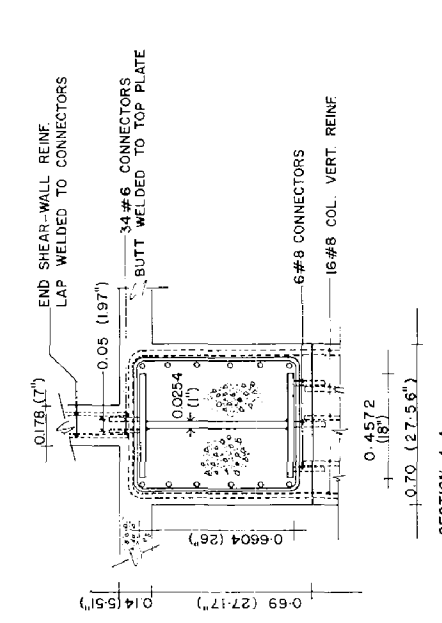


SECTION A-A



TYPICAL ELEVATION

COLUMN TO COLUMN COUPLING BEAMS AT 2ND FLOOR



SECTION A-A

FIGURE 6

CONSTRUCTION FEATURES

Conventional formworks were used for the first two stories. The 9 top stories are being constructed with "flying," or travelling forms for the slabs handled by a climbing crane (fig.7).-

Shrinkage effects in this 67 meters (220') long building will be minimized by using: 1) a temporary "control strip" (d), 2) controlled quantities of mixing water and cement, 3) retarders, and 4) curing compounds. Since total annual temperature change is approximately 15 degrees centigrade (27°F) its effects were neglected. Concrete masonry partition walls, although fixed at the bottom, will be separated from the rest of the structure by using standard dovetail slots and anchors.

CONCLUDING REMARKS

International meetings on earthquake structural engineering are spreading present knowledge on the subject. This is mainly needed in developing countries, where tall buildings are now appearing (recent news of earthquakes are catastrophic). It is hoped that known institutions sponsor special educational programs in order to be more effective in preventing excessive distress in earthquakes.

ACKNOWLEDGEMENTS

The author wishes to thank Mr. Christian Maluf, who shared the task of the structural design in question, and Prof. Bernardo Deschappelles (G.P.O. Box 4167, San Juan, Puerto Rico, 00936) who kindly authorized that part of his lecture notes (b) were included herein as Appendix I.

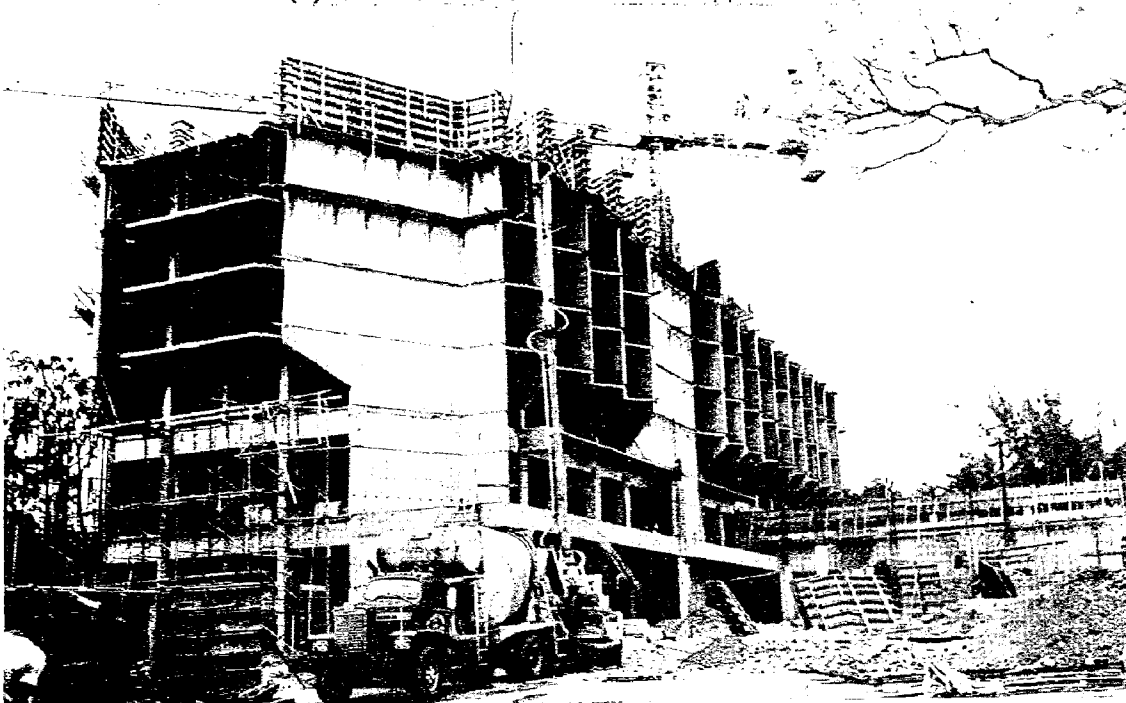
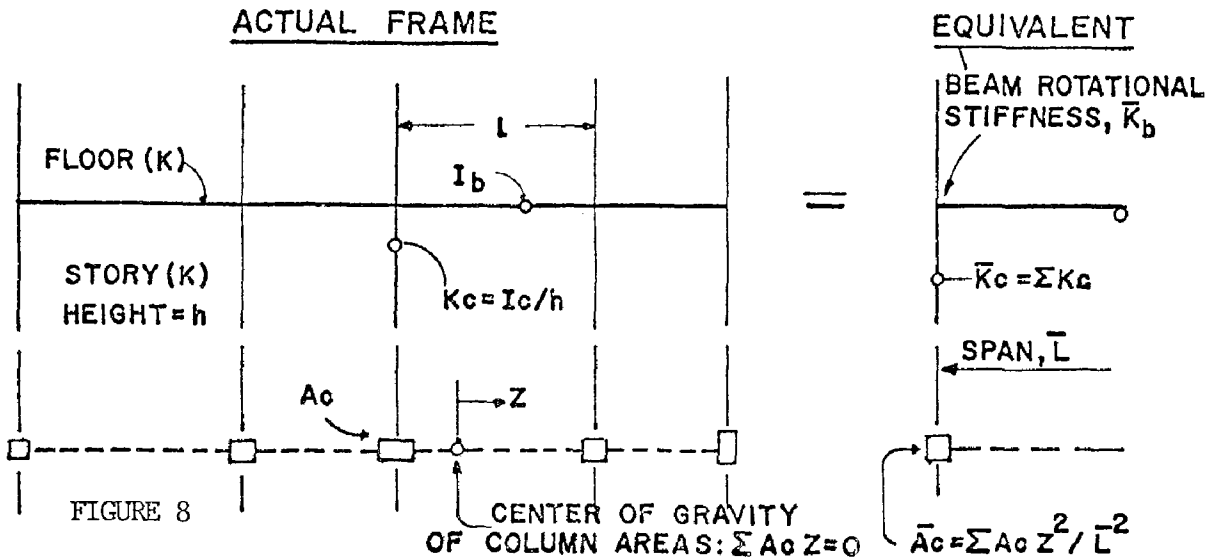


FIGURE 7

APPENDIX I-A) DEFINITION OF THE EQUIVALENT HALF FRAME, FOR LATERAL STIFFNESS CALCULATIONS



1.- Equivalent Column Properties at Story (k):

a) Inertia/story height=Sum of (Inertia/story height) values of all columns

$$\bar{K}_c = \sum K_c$$

b) Area x Span²=Second moment of all column areas, with respect to their center of gravity:

$$\bar{A}_c \bar{L}^2 = \sum A_c Z^2$$

For any arbitrary length of the span \bar{L} , area \bar{A}_c may be calculated.

c) Shear area, \bar{A}_s of the equivalent column could be included as:

$$\bar{A}_s = \sum A_s$$

Sum all shear column areas.

2.- Equivalent Beam Properties at Floor (k):

Rotational stiffness at end rigidly connected to the column, that is, ratio of moment applied to rotation produced, is approximately equal to the sum of antisymmetrical bending stiffness of all floor beams:

a) Case in which column width may be ignored:

Contribution of each beam is $6EI_b/l$ for each end; then, $\bar{K}_b = \sum (12EI_b/l)$



Fig. 9 Beam antisymmetrical bending, with unit rotation at each end.

b) Case in which column width can not be neglected:

This is the typical case of a lintel connecting two walls; the walls are then said to be "coupled" and the lintel is called the "coupling beam." A pierced shear wall may be considered as coupled walls acting in the same plane.

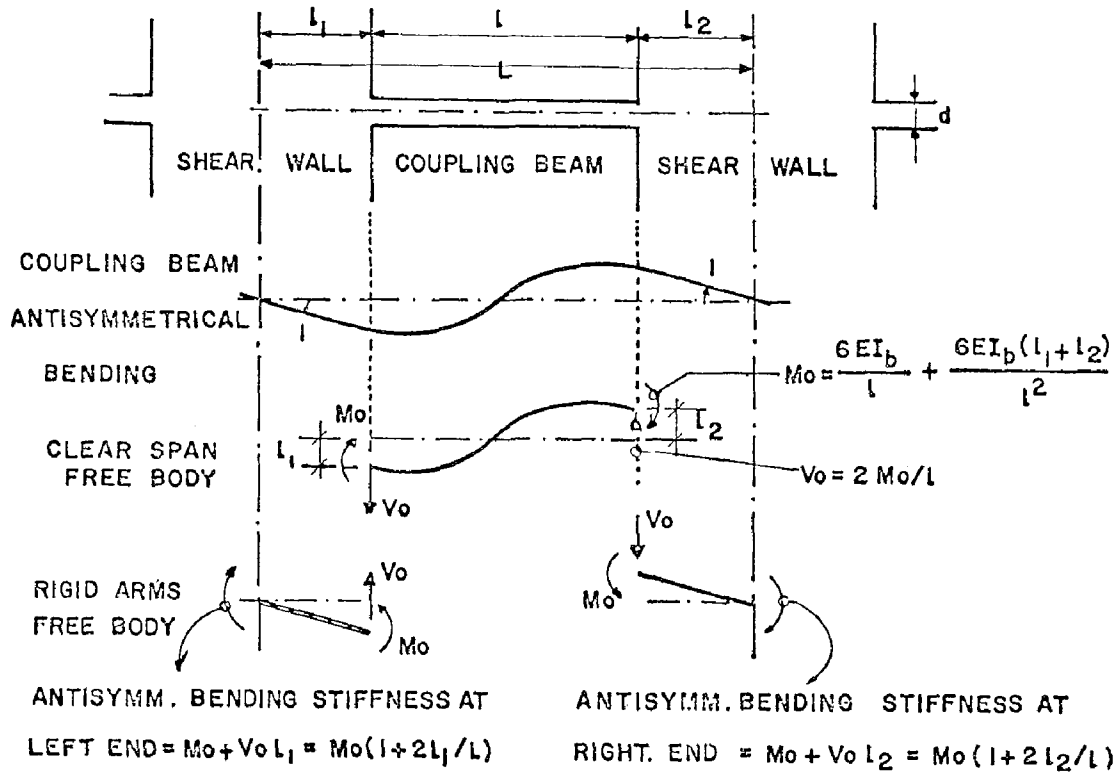


FIGURE 10

Contribution of the coupling beam (fig. 10) to the Equivalent Beam Rotational Stiffness is then,

$$M_o \left(1 + \frac{2l_1}{L}\right) + M_o \left(1 + \frac{2l_2}{L}\right) = \frac{12EI_b}{L} \times \left[\frac{L}{L}\right]^2$$

The Equivalent Beam Rotational Stiffness, calculated as described above, is a reasonable approximate value. More accurate result can be obtained using the particular moment distribution technique described elsewhere (c).

If shear deformations are considered, the Equivalent Beam Rotational Stiffness should be divided by $1 + \bar{\Phi}$, where,

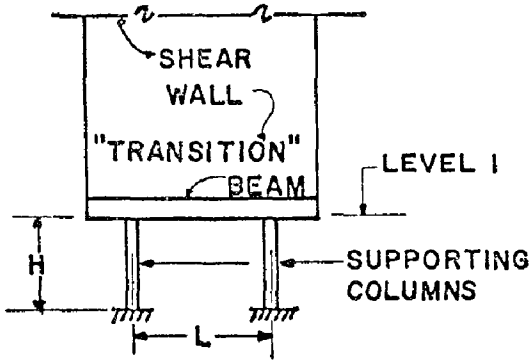
$$\bar{\Phi} = \frac{12EI}{GAsL^2}$$

Shear strain parameter (Przemieniecki J. "Theory of Matrix Structural Analysis," McGraw-Hill Co., P.71)

Assuming $E=2.5 G$, as for concrete and $A_s=1.2 A_c$, form factor in rectangular sections, it can be obtained:

$$\Phi = 2.7 (d/L)^2$$

APPENDIX I-B) EQUIVALENT WALL PANEL FOR COLUMN SUPPORTING A SHEAR WALL FOR LATERAL STIFFNESS CALCULATIONS



Let A , A_s and I represent the geometrical properties of the column related to axial shear and bending strains.

Let A_w and I_w stand for shear area and moment of inertia of the wall panel equivalent to the supporting columns.

FIGURE 11

Consider two degrees of freedom that define the state of deformation of the shear wall at level 1, due to the action of lateral loads: u_1 will represent horizontal displacement while u_2 will stand for rotation. First, we shall recall the elastic constants corresponding to the stiffness matrix of a beam element, including shear strain, with moment of inertia I , shear area A_s , and length H : the shear deformation depends on a "form factor," f , that is equal to $6/5$ in rectangular sections; assuming a shear modulus of elasticity G equal to $0.4E$, the so-called "shear factor," g , is expressed by:

$$g = 6fEI / GA_s H^2 = 18 I / A_s H^2$$

(Gere, J. M. "Moment Distribution," D. Van Nostrand Co., Chapter 6). The terms of the stiffness matrix related to transverse and rotational displacements at one end, with fixity at the other end, are shown below:

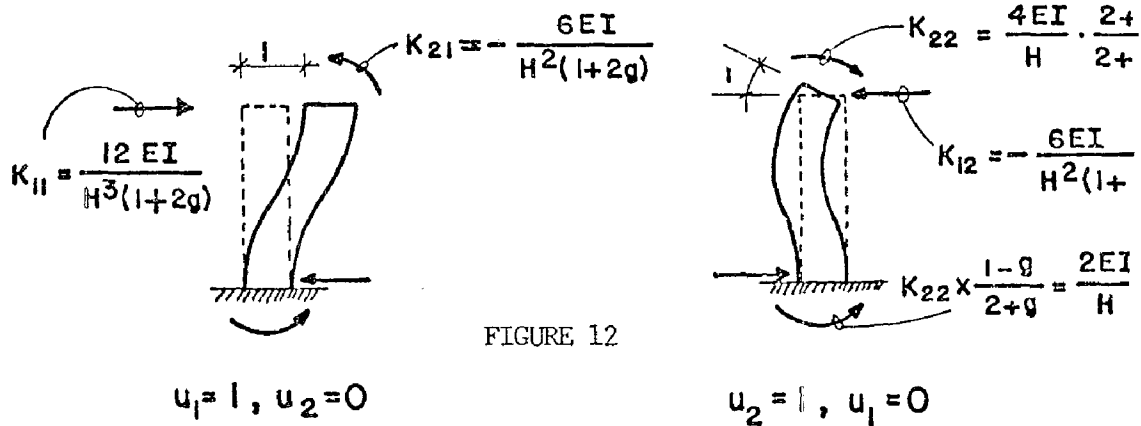


FIGURE 12

Contributions of the Supporting Columns to the Stiffness Matrix Related to Horizontal and Rotational Displacements, Will Then Be as Shown:

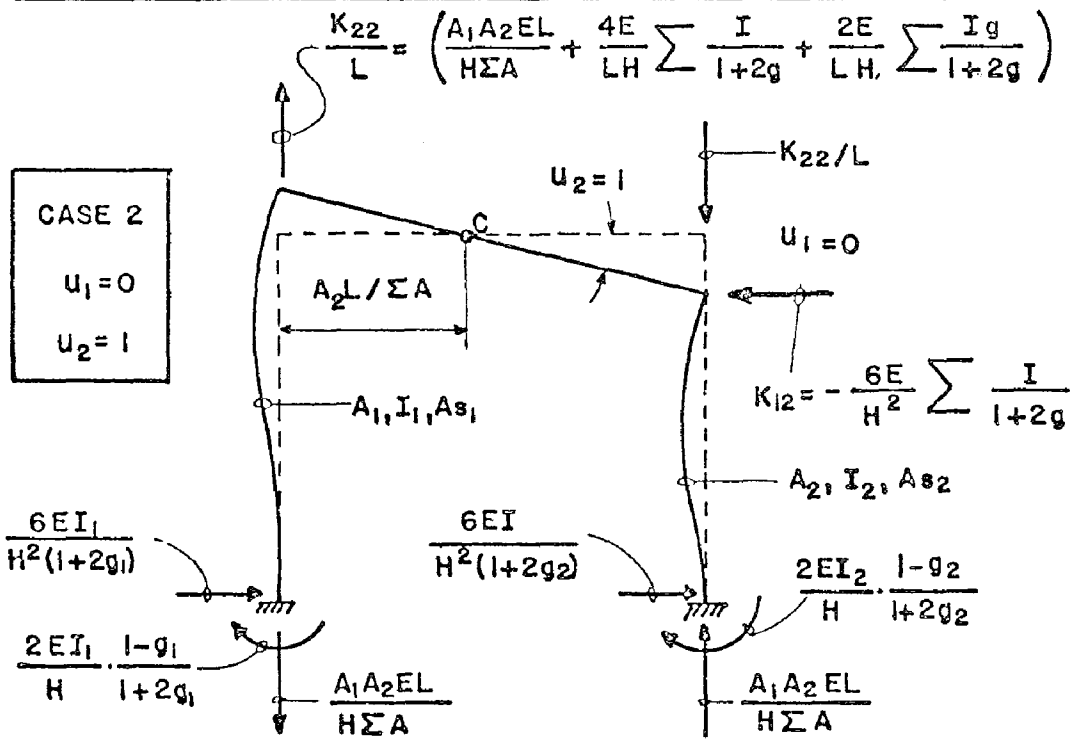
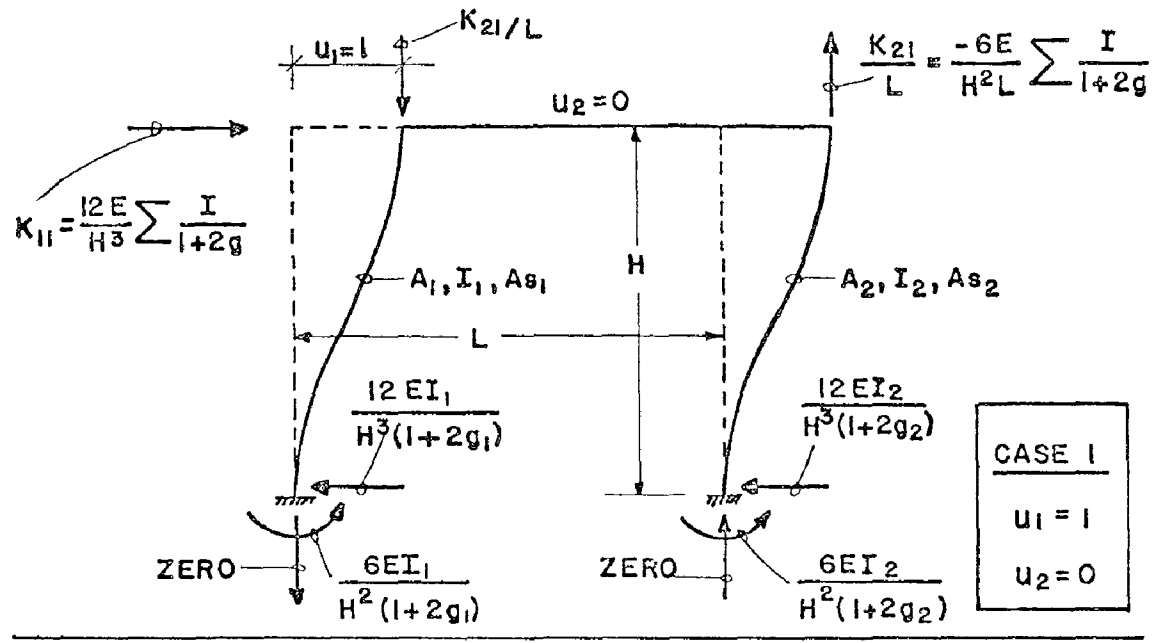


FIGURE 13

General expressions for properties of equivalent wall panel will then be obtained as follows: let I_w and A_w represent moment of inertia and shear area of the equivalent wall panel. The corresponding "shear factor," g_w , has the value $18I_w/(A_w H^2)$ and the diagonal terms of the stiffness matrix, related to horizontal and rotational displacements at level 1, have expressions:

$$K_{11} = \frac{12EI_w}{H^3(1+2g_w)} \quad \text{and} \quad K_{22} = \frac{4EI_w}{H} \cdot \frac{2+g_w}{2+4g_w}$$

In accordance with previous discussion, the contributions of the supporting columns to the same stiffness matrix are as follows

$$K_{11} = \frac{12E}{H^3} \sum I'_c \quad \text{and} \quad K_{22} = E\bar{I} + \frac{4E}{H} \sum I'_c + \frac{2E}{H} \sum g_c I'_c$$

where I'_c stands for $I_c/(1+2g_c)$ and $\bar{I} = A_1 A_2 L^2 / \sum A$ represents the 2nd moment of the column areas, A_1 , and A_2 , with respect to their common center of gravity.

Equating both expressions of the same term unknowns I_w and A_w may be calculated in terms of the data that describe the actual supporting columns. The reader is urged to verify the following:

$$I_w = \bar{I} + \sum I'_c + 2 \sum g_c I'_c$$

$$A_w = \frac{36 \sum I'_c}{H^2} \cdot \frac{I_w}{I_w - \sum I'_c}$$

APPENDIX I-C) COUPLING BEAM ELASTIC CONSTANTS, EXPRESSED BY MEANS OF THE STIFFNESS MATRIX.

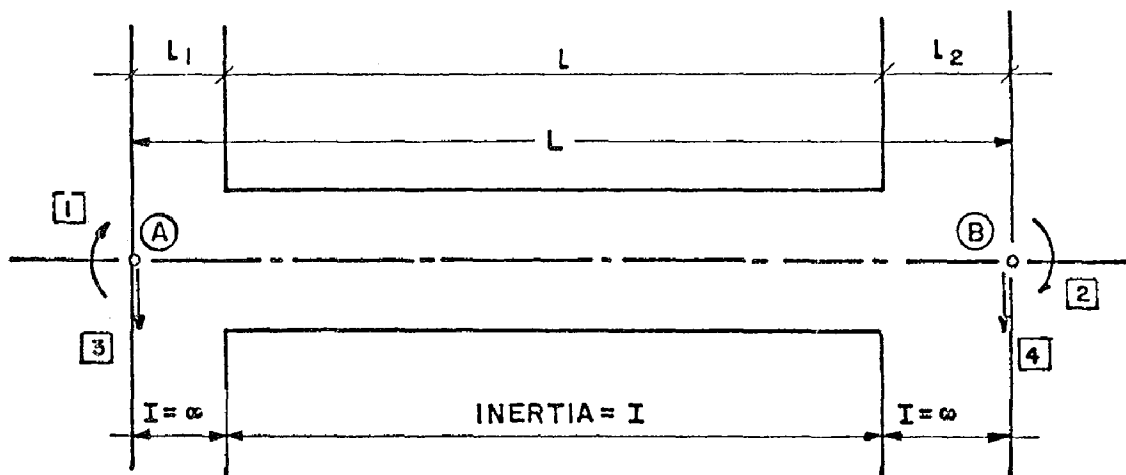


FIGURE 14

$$F_1 = 4 \left(1 + 3L_1/L + 3L_1^2/L^2 \right) \quad F_2 = 2 \left(1 + 3L_1/L + 3L_2/L + 6L_1L_2/L^2 \right)$$

$$F_3 = 4 \left(1 + 3L_2/L + 3L_2^2/L^2 \right)$$

	1 ⊖ _A	2 ⊖ _B	3 Δ _A	4 Δ _B
1	$F_1 I$	$F_2 I$	$(F_1 + F_2) \frac{I}{L}$	$-(F_1 + F_2) \frac{I}{L}$
2		$F_3 I$	$(F_2 + F_3) \frac{I}{L}$	$-(F_2 + F_3) \frac{I}{L}$
3			$(F_1 + 2F_2 + F_3) \frac{I}{L^2}$	$-(F_1 + 2F_2 + F_3) \frac{I}{L^2}$
4				$(F_1 + 2F_2 + F_3) \frac{I}{L^2}$

$\times \frac{E}{L}$

APPENDIX I-D) STIFFNESS MATRIX OF A BEAM WITH RIGID ANGLE AT EACH END

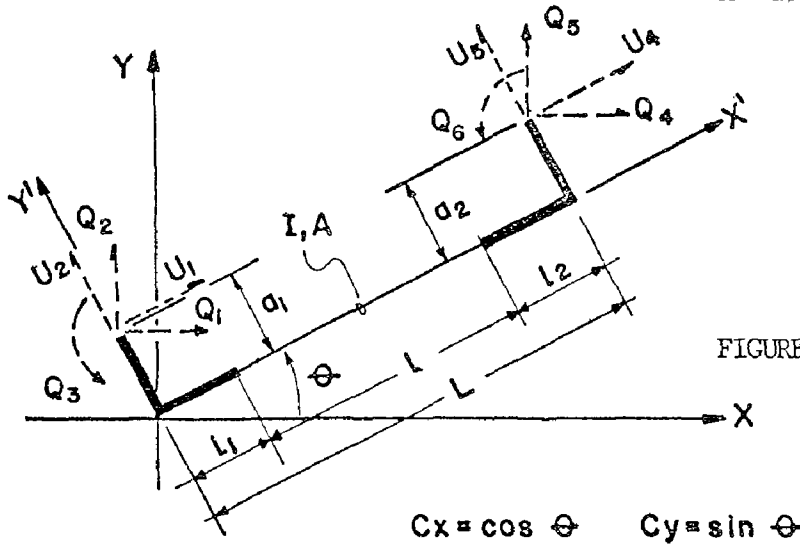


FIGURE 15

Q ₁	Q ₂	Q ₃	Q ₄	Q ₅	Q ₆
ACx ² +	ACxCy -	Aa ₁ Cx -	-ACx -	-ACxCy +	-Aa ₂ Cx -
$\frac{G_1 I}{L^2} Cy^2$	$\frac{G_1 I}{L^2} CxCy$	$\frac{G_2 I}{L} Cy$	$\frac{G_1 I}{L^2} Cy^2$	$\frac{G_1 I}{L^2} CxCy$	$\frac{G_3 I}{L} Cy$
	ACy ² +	Aa ₁ Cy +	-ACxCy +	-ACy ² -	-Aa ₂ Cy +
	$\frac{G_1 I}{L^2} Cx^2$	$\frac{G_2 I}{L} Cx$	$\frac{G_1 I}{L^2} CxCy$	$\frac{G_1 I}{L^2} Cx^2$	$\frac{G_3 I}{L} Cx$
		F ₁ I +	-Aa ₁ Cx +	-Aa ₁ Cy -	-Aa ₁ a ₂ +
		Aa ₁ ²	$\frac{G_2 I}{L} Cy$	$\frac{G_2 I}{L} Cx$	F ₂ I
			ACx ² +	ACxCy -	Aa ₂ Cx +
			$\frac{G_1 I}{L^2} Cy^2$	$\frac{G_1 I}{L^2} CxCy$	$\frac{G_3 I}{L} Cy$
				ACy ² +	Aa ₂ Cy -
				$\frac{G_1 I}{L^2} Cx^2$	$\frac{G_3 I}{L} Cx$
					Aa ₂ ² +
					F ₃ I

$$F_1 = 4(1 + 3L_1/L + 3L_1^2/L^2)$$

$$F_2 = 2(1 + 3L_1/L + 3L_2/L + 6L_1L_2/L^2)$$

$$F_3 = 4(1 + 3L_2/L + 3L_2^2/L^2)$$

$$G_1 = F_1 + 2F_2 + F_3$$

$$G_2 = F_1 + F_2$$

$$G_3 = F_2 + F_3$$

APPENDIX II.- REFERENCES

- (a).- Fintel, M. "Behavior os Structures in the Caracas Earthquake," Civil Eng. ASCE, Feb. 1968
- (b).- Deschappelles, B. "Lecture Notes for Advanced Course in Seismic Engineering," Unpublished, Santo Domingo, D. R., Jan-Feb 1975
- (c).- Deschappelles, B., "Analytical Model for Lateral Loads Effectson Buildings," journal of the Structural Division, ASCE, vol. 96, No. st. 6, June 1970
- (d).- Fintel, M. "Theme Report: Creep, Shrinkage and Temperature Effects," Proceedings of the International Conference on Planning and Design of Tall Buildings, Vol III, Pag. 741, 1972

INTERNATIONAL SYMPOSIUM ON
EARTHQUAKE STRUCTURAL ENGINEERING

437

St. Louis, Missouri, USA, August, 1976

REVERSING LOAD TESTS OF FIVE ISOLATED STRUCTURAL WALLS

A. E. FIORATO, R. G. OESTERLE, Jr., and J. E. CARPENTER

Senior Structural Engineer, Associate Structural Engineer
and Former Principal Structural Engineer

Structural Development Section

Portland Cement Association

Skokie, Ill. U.S.A.

SUMMARY

An experimental program is being carried out to develop design criteria for reinforced concrete walls used as lateral bracing in earthquake resistant buildings. Primary items of interest include the ductility, energy dissipation, and strength of the walls.

Tests of five walls are described. The model walls were 15-ft. (4.57 m) high and 6-ft. 3-in. (1.91 m) wide. Wall thicknesses were 4 in. (102 mm). All specimens were subjected to in-plane horizontal reversing loads.

Controlled variables included the shape of the wall cross section, the amount of main flexural reinforcement, and the amount of hoop reinforcement around the main flexural reinforcement.

Two specimens were subjected to high nominal shear stresses. The failure mode for these specimens was associated with web shear distress.

Three specimens were loaded with low nominal shear stresses. Two of these had ordinary column ties. One had lateral confinement reinforcement around the main flexural reinforcement in the boundary elements. Capacities of these specimens were governed by damage to the boundary elements as alternate tensile yielding and compressive buckling of the main flexural reinforcement occurred.

Lateral confinement reinforcement in the boundary elements helped to limit bar buckling and to contain cracked concrete within the core. Confinement provided a wall with somewhat greater ductility, but no significant increase in strength.

INTRODUCTION

A combined experimental and analytical investigation of structural walls is being carried out by the Portland Cement Association. The investigation is sponsored in part by the National Science Foundation through Grant No. GI-43880. This investigation is intended to develop design criteria for reinforced concrete walls used as lateral bracing in earthquake resistant structures. As part of the experimental program, tests of isolated structural walls subjected to reversing loads are being carried out. Primary items of interest in this investigation are the ductility, energy dissipation and strength of the walls.

OBJECTIVES AND SCOPE

The following are overall objectives of the investigation of isolated walls:

1. To determine load versus deformation characteristics for a wide range of configurations of wall specimens.
2. To determine the ductility and energy dissipation capacity of walls subjected to reversing loads.
3. To determine the flexural and shear strengths of walls subjected to reversing loads, and to compare these strengths with the strengths under monotonic loading.
4. To determine means of increasing the energy dissipation capacity of walls where required.
5. To develop design procedures for walls of adequate strength and energy dissipation capacity.

In this paper, tests on five reinforced concrete walls are reported. The test specimens represent approximately 1/3-scale models of full-size walls, although no specific prototype walls were modeled. Test specimens were subjected to in-plane lateral reversing loads. The controlled variables in the program have been the shape of the wall cross-section, the amount of main flexural reinforcement, and the amount of hoop reinforcement around the main flexural reinforcement.

Table 1 provides a summary of the test specimens and their material properties.

TEST PROGRAM

Geometric and material properties of the specimens tested are given in this section. In addition, construction, instrumentation, and testing procedures are described.

TABLE 1. SUMMARY OF MATERIAL PROPERTIES*

Specimen	Shape	Reinforcement										Concrete**			
		Boundary Element				Web						Confinement	f' _c (psi)	f _r (psi)	E _c (ksi)
		f _y (ksi)	f _{su} (ksi)	ρ _f (%)	f _y (ksi)	f _{su} (ksi)	ρ _h (%)	ρ _n (%)	f _y (ksi)	f _{su} (ksi)	ρ _s (%)				
F1		64.5	102.6	3.89	76.2	102.2	0.71	0.30	-	-	-	5575	635	3690	
B1		65.2	102.7	1.11	75.5	100.8	0.31	0.29	-	-	-	7685	730	4080	
B2		59.5	100.8	3.67	77.2	101.6	0.63	0.29	-	-	-	7775	710	4200	
R1		74.2	111.0	1.47	75.7	101.5	0.31	0.25	-	-	-	6490	655	4030	
B3		63.5	101.0	1.11	69.4	95.5	0.31	0.29	69.4	95.5	1.28	6860	635	3960	

* 1000 psi = 1.0 ksi = 70.3 kgf/sq.cm.

** Average properties for lower 6 ft. (1.83m) of wall.

Description of Test Specimens

The dimensions of the test specimens are shown in Fig. 1. Height of each wall, from the top of the base block to the center of the top slab, was 15 ft. (4.57 m). The horizontal length of the wall was 6 ft. 3 in. (1.91 m) and its web thickness was 4 in. (102 mm).

Three different wall cross-sections were investigated. These are flanged, barbell, and rectangular sections. The nominal cross-sectional dimensions of the three sections are shown in Fig. 2.

The base block shown in Fig. 1 was used to secure the specimens to the laboratory floor during testing. The slab on top of the wall, also shown in Fig. 1, was used to transfer the loads to the test specimen.

Design of Test Specimens

The first step in design of the test specimens was to select a nominal percentage of main flexural reinforcement. This was either 1% or 4% based on the area of the boundary element. For rectangular sections, the "boundary element" was considered to extend 7.5 in. (191 mm) from each end of the wall. The percentages of flexural reinforcement were chosen to give section moment capacities corresponding to both low and high nominal shear stresses.

Nominal vertical web reinforcement provided in the walls was 0.25% of the gross concrete area of the horizontal wall section. This is the minimum amount permitted by the 1971 ACI Building Code.⁽¹⁾

Once the vertical reinforcement was selected, bar sizes and locations were determined based on construction requirements. The moment capacity of the section was then calculated according to the 1971 ACI Building Code, Section 10.2.⁽¹⁾ Design yield stress of the steel was 60,000 psi (4218 kgf/sq.cm) and design concrete strength was 6000 psi (422 kgf/sq.cm). Following ACI Building Code assumptions, strain hardening of the steel was neglected in calculating the moment capacity.

Horizontal shear reinforcement was provided so that the calculated moment capacity would be developed. The shear design was made according to the 1971 ACI Building Code, Section 11.16.⁽¹⁾

The vertical and horizontal reinforcement was constant over the height of each specimen.

Reinforcement

Reinforcing details for the five specimens tested are shown in Fig. 3. All reinforcing steel was detailed and fabricated according to standard practice.^(1,2)

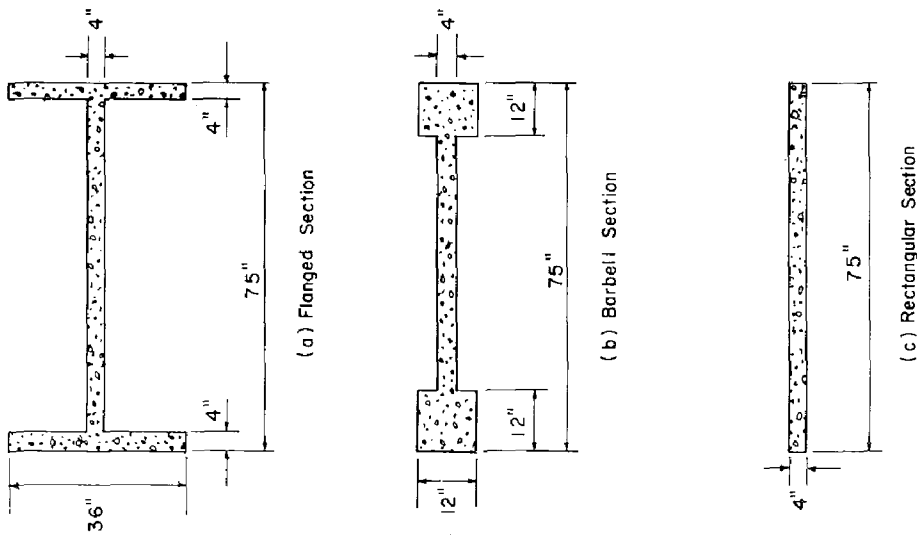


Fig. 2 Nominal Cross-Sectional Dimensions of Test Specimens (1 in. = 25.4 mm)

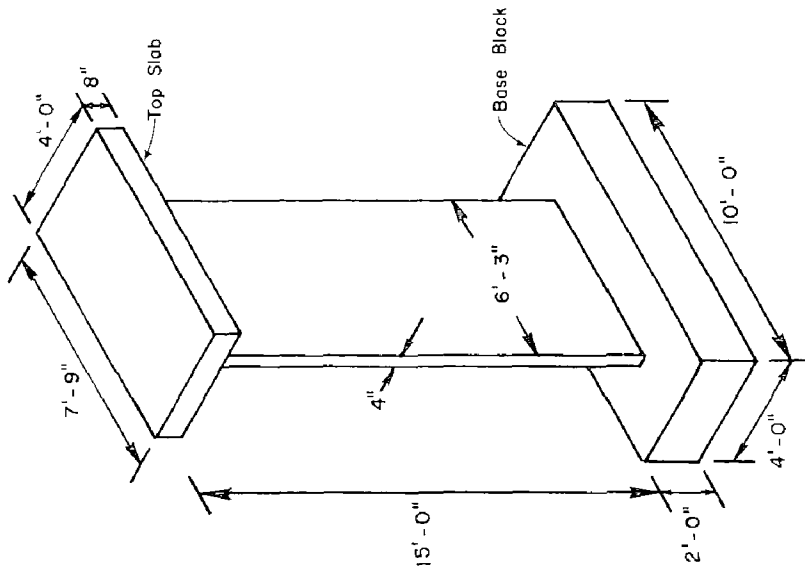
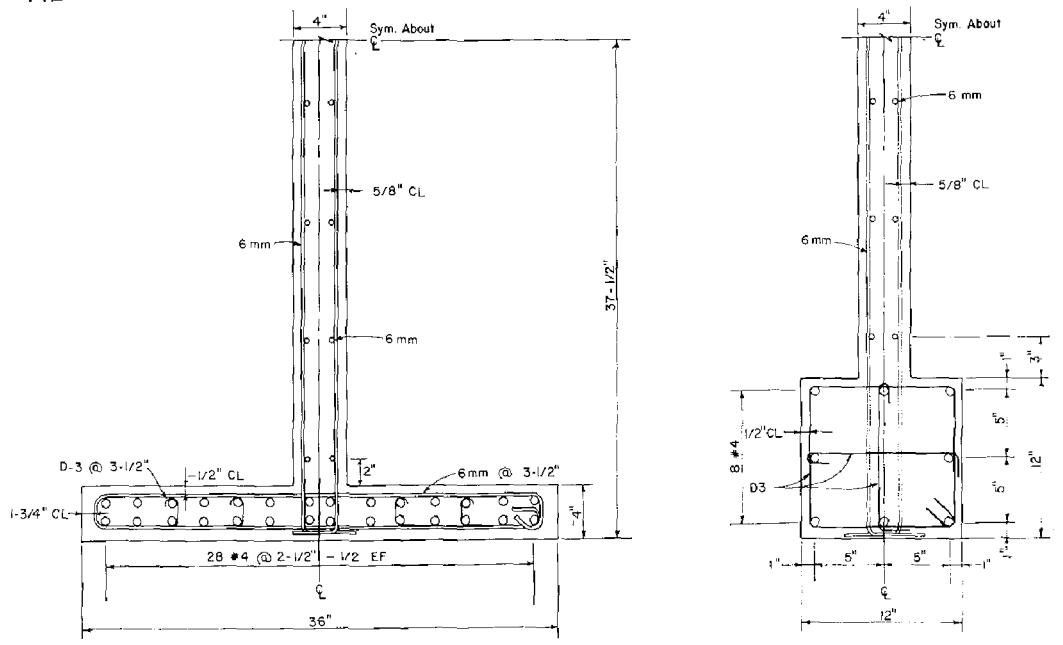
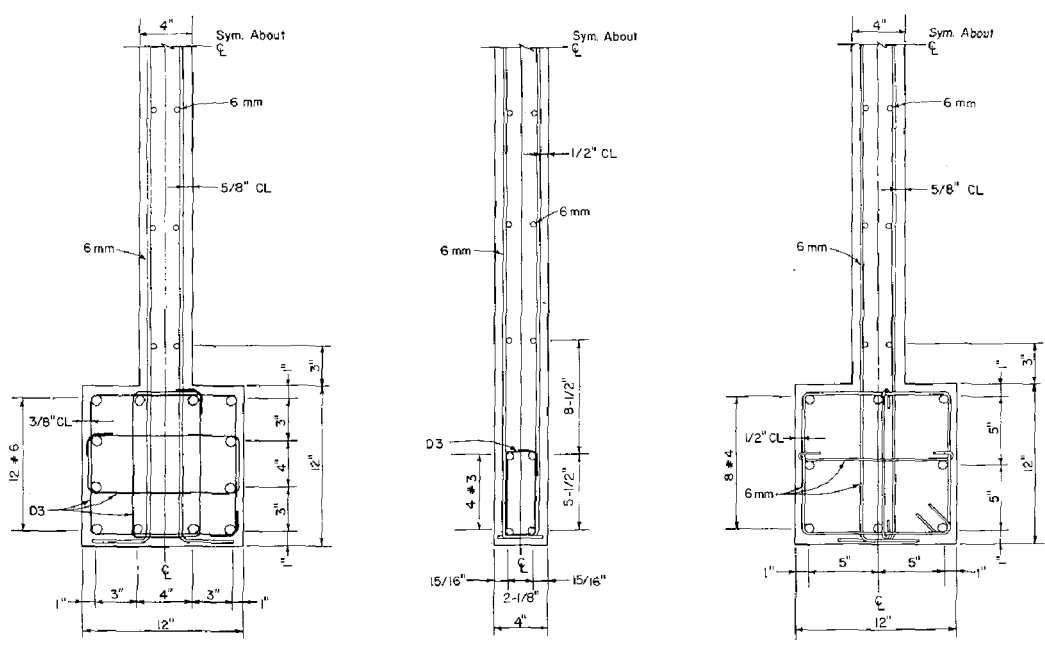


Fig. 1 Nominal Dimensions of Test Specimen With Rectangular Cross Section (1 in. = 25.4 mm)



a) Specimen F1

b) Specimen B1



c) Specimen B2

d) Specimen R1

e) Specimen B3

Fig. 3 Cross Sections of Test Specimens (1 in. = 25.4 mm)

Except for Specimen B3, no special reinforcing details were used. Tie spacings were selected according to the 1971 ACI Building Code, Section 7.12.⁽¹⁾

Specimen B3 was constructed with confinement reinforcement in the lower 6 ft. (1.83 m) of the boundary elements. In all other respects, Specimen B3 was similar to Specimen B1. The confinement hoops were designed according to Appendix A of the 1971 ACI Building Code⁽¹⁾ and were spaced at 1-1/3 in. (34 mm) center-to-center.

In the specimens, bars conforming to ASTM Designation A615 Grade 60 were used as reinforcement. Deformed 6mm hot rolled bars with properties similar to Grade 60 bars were also used. Deformed wire, size D-3, was used to represent smaller bar sizes. This wire was heat-treated to obtain stress versus strain characteristics similar to those of Grade 60 bars.

The physical properties of the reinforcement used in the test specimens are summarized in Table 1.

Concrete

A concrete mix using a maximum aggregate size of 3/8 in. (10 mm) was selected for the walls. Type I cement, sand, coarse aggregate and water were combined to provide concrete with a slump of 3 1/2 in. (76±13 mm).

Physical properties of the concrete used in each specimen are given in Table 1.

Construction of Test Specimens

Test specimens were constructed in the vertical position. Each wall was cast in six lifts.

At the start of construction, a heavy reinforcing cage for the base block was constructed. This cage was placed on a level base platform. The vertical wall reinforcement was then placed in the base cage and secured in position. After the vertical reinforcement was placed, the base block was cast.

Following casting of the base block, the construction joint was prepared and the horizontal reinforcement for the next lift was placed. Formwork for the lift was then set, and the concrete was cast. Subsequent wall lifts were constructed in the same manner. Each wall lift was 36-in. (914 mm) in height. Figure 4 shows Specimen B1 during construction.

Construction joints between lifts were made following procedures described in ACI Specifications 301-72.⁽³⁾ The surface of the concrete was

roughened with a cold chisel, and cleaned of laitance and loose particles prior to placing the adjoining concrete.

Test Apparatus

The apparatus for testing the walls is shown in Fig. 5. Each specimen was post-tensioned to the floor. The specimen was loaded as a vertical cantilever with concentrated forces at the top. Hydraulic rams on each side of the specimen alternately applied force first to one side then the other side of the top slab.

Instrumentation

During each test, applied loads, displacements, rotations, and steel strains were measured.

The applied loads were measured by load cells attached to one end of each ram. The load cells have a capacity of 200 kips (90,719 kgf) in compression and can measure loads to within about 20 lb. (9.1 kgf).

Horizontal displacements were measured at six levels, as shown in Fig. 5(a). For the lower three levels, measurements were made at each end of the wall. Diagonal displacements were also measured at the lower three levels to define the geometry of the deformed wall. Using this system, both flexural and shearing distortions were determined.

As shown in Fig. 5(a), the horizontal and vertical displacement gages were supported on reference planes located on each side of the test specimen. As a check, the reference planes were instrumented to monitor any possible movement. For the five tests reported in this paper, movements of the reference planes were negligible.

Rotations in the lower 6 ft. (1.83 m) of the wall were obtained by measuring vertical displacements along each end of the wall. Three sets of measurements were made. One set was made between the top of the base block and the bottom of the wall over a nominal gage length of 3 in. (76 mm). The other two sets of measurements were made over nominal gage lengths of 36 in. (914 mm).

Displacement measurements were obtained using linear potentiometers and direct current differential transducers (DCDT). These gages have sensitivities from 0.001 in. (0.025 mm) to 0.003 in. (0.076 mm).

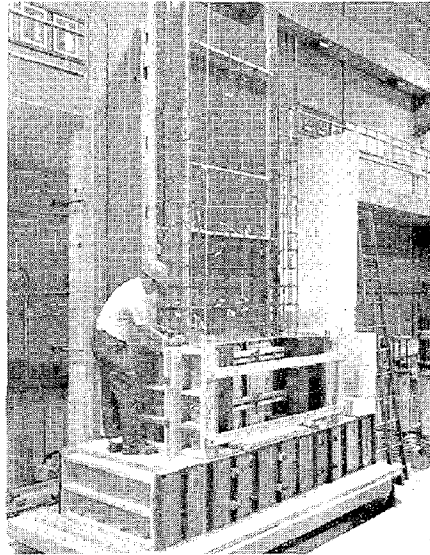
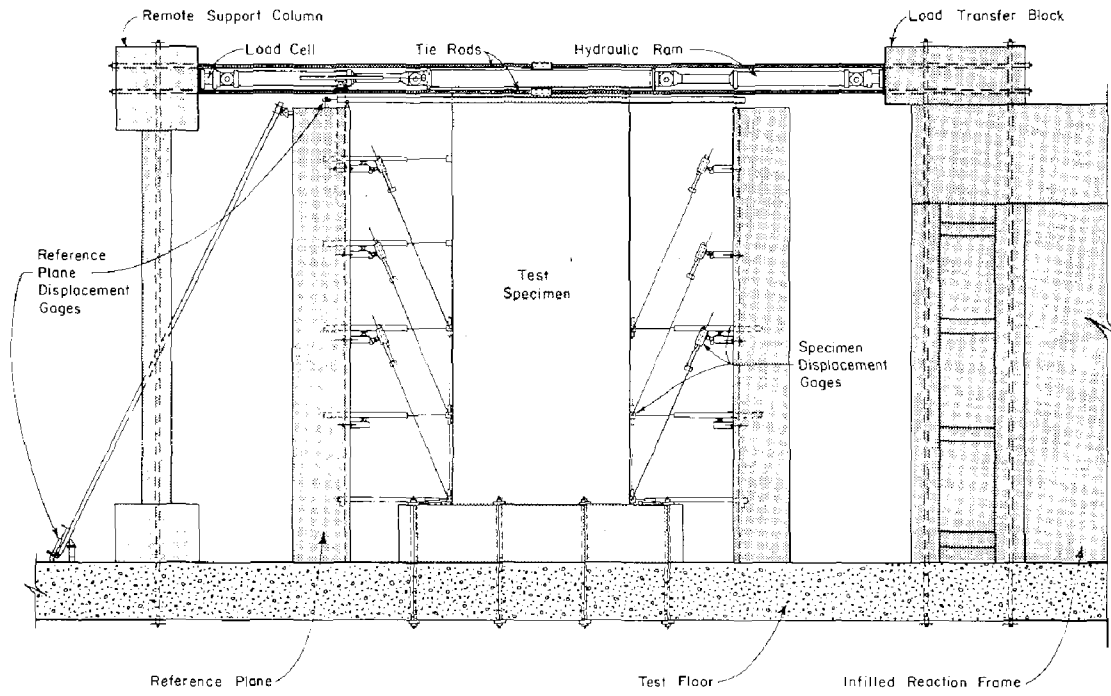
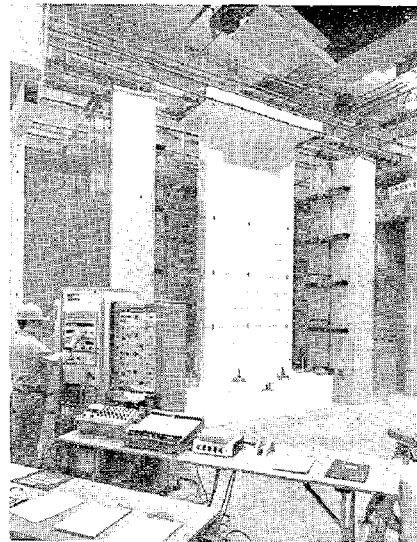


Fig. 4 Specimen B1 During Construction



a) Test Apparatus



b) Isolated Wall Test

Fig. 5 Isolated Wall Testing Arrangement

Strain gages were placed both on the vertical and on the horizontal reinforcement. In addition, strains were measured on several of the hoops and supplementary cross ties of the confinement reinforcement of Specimen B3.

In addition to the instrumentation previously described, dial gages were used to measure relative slip at construction joints. Crack widths were measured during testing with a hand microscope containing a scale with graduations of 0.001 in. (0.025 mm). A complete photographic record was obtained for each test. In addition to color slides and black and white photographs, three time-lapse cameras recorded each cycle of loading.

Test Procedure

Each of the first five test specimens was loaded in about three increments of force until yielding occurred. At each force increment, three complete cycles of loading were applied. Subsequent to yielding, loading was controlled by deflections in 1-in. (25.4 mm) increments. Three complete cycles were again applied at each deflection increment.

TEST RESULTS

A load versus deflection relationship for Specimen B3 is shown in Fig. 6. The deflection is that at the top of the specimen. Only the first cycle of each increment and only new maximum increments were plotted. Numbers on the figure refer to the sequential number of the load cycle. The envelope of the load versus deflection relationship was obtained by passing lines through the peak points of each new maximum loading cycle.

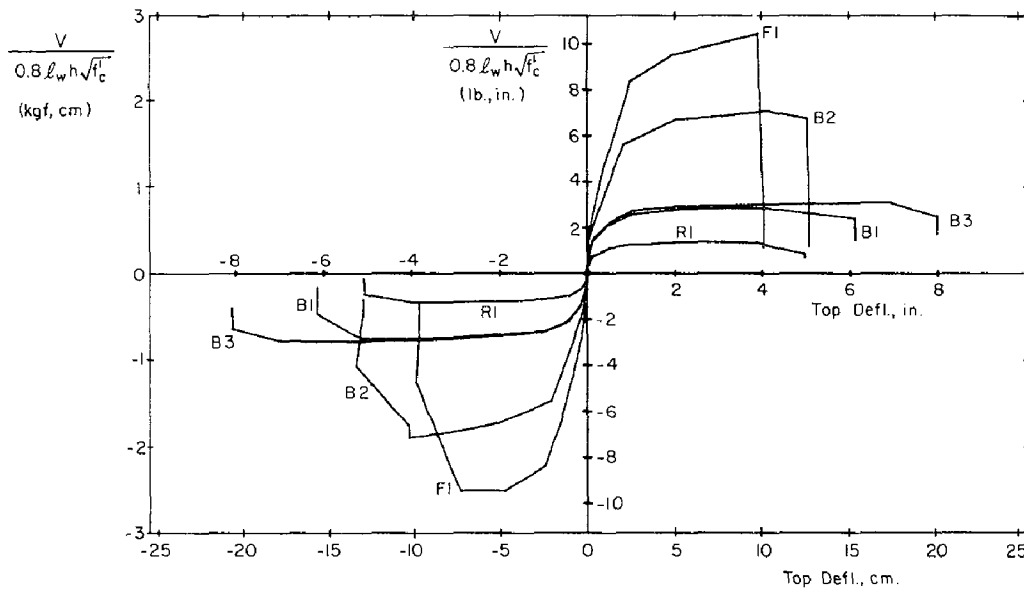
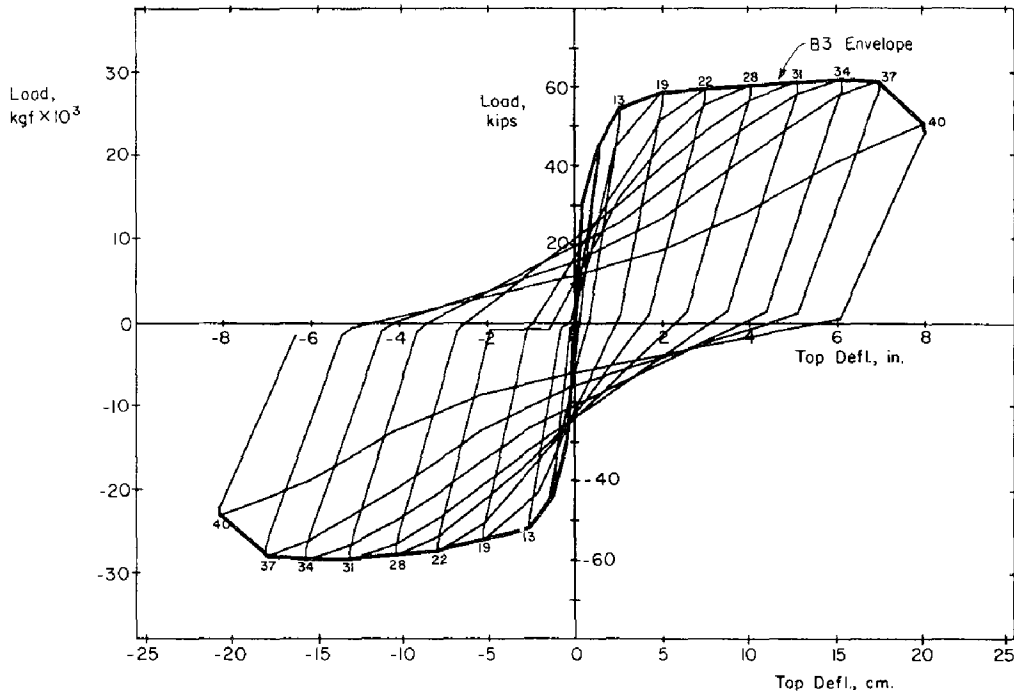
Load versus deflection envelopes for all five specimens are compared in Fig. 7. In general, two types of behavior were observed in the walls. These types were distinguished by the magnitude of the applied shear stress.

Walls Subjected to High Shear Stress

Specimens F1 and B2 were subjected to high shear stress. Maximum nominal shear stresses $v_{max} > 7 \sqrt{f'_c}$ ($1.86 \sqrt{f'_c}$) were applied. In these specimens the cracking patterns and failure modes indicated that the effects of shear predominated.

The test of Specimen F1 was terminated by web crushing at a nominal shear stress corresponding to $10.5 \sqrt{f'_c}$ ($2.78 \sqrt{f'_c}$). The load observed after web crushing was 50% of that prior to crushing. Six complete inelastic cycles were applied to the specimen before web crushing occurred. Figure 8 shows the specimen after web crushing.

The test of Specimen B2 was terminated by a shear-compression failure. Capacity of the specimen then dropped by about 40%. Specimen B2 carried a maximum load corresponding to $7.2 \sqrt{f'_c}$ ($1.91 \sqrt{f'_c}$). A photograph of the specimen is shown in Fig. 9.



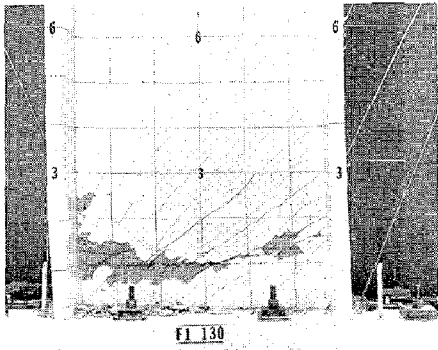


Fig. 8 Specimen F1 After Web Crushing

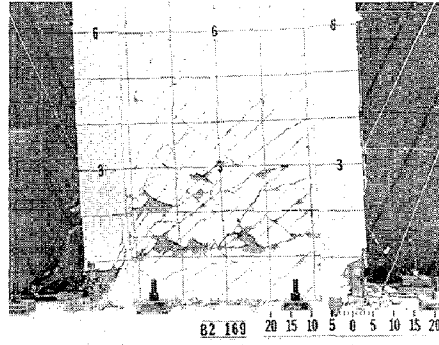


Fig. 9 Specimen B2 After Shear-Compression Crushing

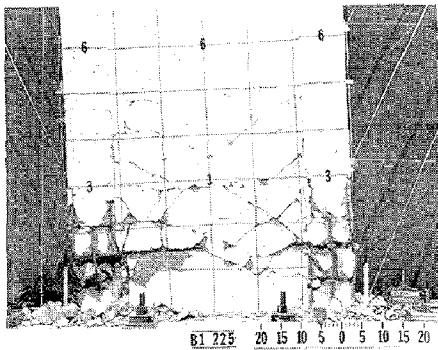


Fig. 10 Specimen B1 After Testing to Destruction

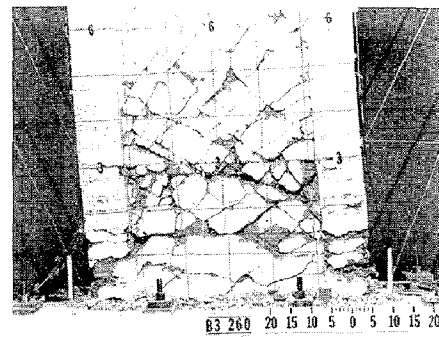


Fig. 11 Specimen B3 After Testing to Destruction

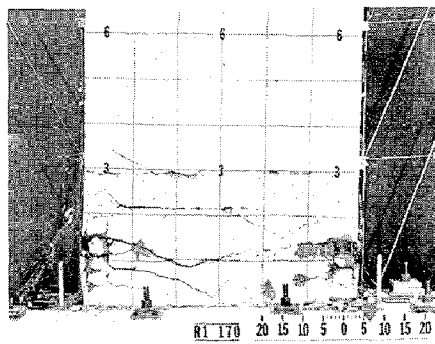


Fig. 12 Specimen R1 After Testing to Destruction

Walls Subjected to Low Shear Stress

The three specimens subjected to low shear stress were B1, R1, and B3. Maximum nominal shear stresses $v_{\max} < 3.1 \sqrt{f'_c}$ ($0.82 \sqrt{f'_c}$) were applied. In these specimens the cracking patterns and observed failure modes indicated that flexure predominated. For these specimens, deterioration of the boundary elements by alternate tensile yielding and compressive buckling of the main tensile reinforcement was observed. Eventually the main reinforcing bars fractured. The fractures were undoubtedly influenced by prior bar buckling. Loss of load capacity in these specimens was gradual as bars fractured and as broken concrete pieces in the boundary elements were lost.

Specimen B3 was similar to Specimen B1 except that confinement reinforcement was provided in the lower 6 ft. (1.83 m) of each column. As indicated in Fig. 7, ductility was significantly greater in the specimen with confinement. Photographs showing Specimens B1 and B3 after testing to destruction are shown in Fig. 10 and 11, respectively.

Because of the confinement reinforcement, the concrete in the core of the columns of Specimen B3 was contained. The confinement hoops also helped to limit, but did not prevent bar buckling. However, the length of the buckled portion of the bar was shorter in the confined specimen. The specimen with confinement underwent 29 inelastic cycles prior to bar fractures. The specimen without confinement withstood 21 inelastic cycles.

Web concrete in Specimen B3 was more extensively damaged than that in Specimen B1. However, the primary zone of damage in the walls did not extend above the 6-ft. (1.83 m) level where the confinement hoops were terminated.

Figure 12 shows Specimen R1 after testing to destruction. This specimen carried a maximum load corresponding to a very light shear stress of $1.4 \sqrt{f'_c}$ ($0.37 \sqrt{f'_c}$). Because the specimen was lightly reinforced in flexure, the concrete in the wall was not crushed prior to bar fracture.

Observed and Calculated Loads

Design loads for each specimen calculated according to the 1971 ACI Building Code⁽¹⁾ are given in Table 2. Also listed in Table 2 are the observed and calculated values of the yield and maximum loads.

The ACI design does not account for strain hardening of the reinforcement. It should be noted that in three of the specimens, maximum bar spacing requirements led to a significant over-design for shear. The intent was to design the shear reinforcement to permit development of the design flexural capacity. All specimens exceeded the calculated ACI design strengths.

TABLE 2 TEST RESULTS

Specimen	ACI Design Strength				Yield Load				Maximum Load				V _{test} (5) V _{calc.}	M _{test} (4) M _{calc.}	Failure Mode (6)	
	Flexural		Shear		Calculated		Observed		Calculated (4)		Observed					
	kips (1)	$\sqrt{f'_c}$ (2)	kips $\sqrt{f'_c}$	$\sqrt{f'_c}$	kips $\sqrt{f'_c}$	$\sqrt{f'_c}$	kips $\sqrt{f'_c}$	$\sqrt{f'_c}$	kips $\sqrt{f'_c}$	$\sqrt{f'_c}$	kips $\sqrt{f'_c}$	$\sqrt{f'_c}$				
F1	145	8.1	140	7.8	145.6	8.1	150.6	8.4	12.7	227.1	12.7	187.9 ⁽⁵⁾	10.5	1.34	0.83	WC
B1	46	2.2	82 ⁽³⁾	3.9	39.7	1.9	45.1	2.1	3.5	72.8	3.5	61.0	2.9	0.74	0.84	F
B2	129	6.1	127	6.0	105.8	5.0	119.7	5.7	8.1	170.9	8.1	152.8	7.2	1.20	0.89	SC
R1	18	0.9	82 ⁽³⁾	4.2	16.1	0.8	20.1	1.0	1.5	29.4	1.5	26.6	1.4	0.32	0.90	F
B3	46	2.3	82 ⁽³⁾	4.1	38.7	1.9	45.2	2.3	3.5	70.0	3.5	62.0	3.1	0.76	0.89	F

(1) 1.0 kip = 0.454 kgf

(2) Shear stress, v (psi), $1.0\sqrt{f'_c}$ (psi) = $0.265\sqrt{f'_c}$ (kgf/sq.cm)

(3) Shear reinforcement governed by maximum bar spacing requirements.

(4) Based on flexural capacity including strain hardening

(5) Calculated ACI shear design strength

(6) WC = web crushing, F = flexure, SC = shear compression

The calculated yield and maximum loads were obtained from a flexural analysis of each cross section for monotonic loading. Analysis of the section was based on satisfying the applicable conditions of equilibrium and strain compatibility. A linear distribution of strain over the section was assumed. Measured material properties were used. The analysis considered complete stress versus strain relationships for concrete and steel, including strain hardening of the reinforcement. Yielding was defined as first yield of the main flexural reinforcement. A limiting concrete strain of 0.004 was selected for the calculations. The maximum calculated loads were taken at this limiting strain unless the maximum capacity occurred at a lower strain.

When calculating loads, no attempt was made to account for variation in strength resulting from load reversals. All the walls reached a maximum load within 17% of the calculated flexural capacity for a monotonically loaded wall. Specimens F1 and B2, which failed in shear, reached capacities in excess of that which could be carried by the horizontal reinforcement alone. Thus, even with reversing loads, the concrete contributed to the shear capacity.

CONCLUSIONS

The following observations are based on data from tests of five isolated wall specimens:

1. All specimens had a capacity greater than that indicated by the strength provisions of the 1971 ACI Building Code.⁽¹⁾ This was the case even though the walls were subjected to a large number of inelastic cycles of load.
2. Two specimens were loaded to produce relatively high nominal shear stress. The failure mode for these specimens was associated with web shear distress. In one of these specimens, the test ended with severe web crushing at a nominal shear stress $v_{\max} = 10.5 \sqrt{f'_c}$ ($2.78 \sqrt{f'_c}$). For both specimens, observed maximum loads indicated that the concrete contributed to the shear strength.
3. Two specimens were loaded to produce relatively low nominal shear stress and had ordinary column ties. Capacities of these specimens were governed by damage to the boundary elements. Tensile yielding and compressive buckling of the main flexural reinforcement in these specimens led to bar fractures. This along with the loss of broken concrete not contained by the reinforcing cage caused the specimens to lose strength.
4. Lateral confinement hoops were added around the main flexural reinforcement in the boundary elements of a third wall loaded with a low nominal shear stress. These hoops helped to limit

bar buckling and contained broken concrete within the core of the boundary elements.

5. The load capacity of the confined specimen was approximately the same as that for a companion specimen without confinement.
6. The confined specimen had an overall top deflection ductility factor about 50% greater than that for the companion specimen without confinement.
7. For all specimens, the primary area of distress was within a height equal to the horizontal length of the wall.
8. All specimens had post-yield deflection capabilities under reversing load.

ACKNOWLEDGMENTS

This investigation was carried out in the Structural Development Section of the Portland Cement Association under the direction of Dr. H. G. Russell, Manager. Fabrication and testing of the specimens were performed by the Technical Staff of the Section with the assistance of the Staff of the Transportation Development Section.

The work formed part of a combined experimental and analytical investigation sponsored in part by the National Science Foundation through Grant No. GI-43880. M. Fintel, Director, Engineering Services Department is overall Project Investigator. Dr. W. G. Corley, Director, Engineering Development Department, heads the experimental investigation.

BIBLIOGRAPHY

1. "Building Code Requirements for Reinforced Concrete (ACI 318-71)," American Concrete Institute, Detroit, 78 pp.
2. "Manual of Standard Practice for Detailing Reinforced Concrete Structures (ACI 318-74)," American Concrete Institute, Detroit, 1974, 167 pp.
3. "Specifications for Structural Concrete for Buildings (ACI 301-72)," American Concrete Institute, Detroit, 1972, 36 pp.

NOTATION

- A_{sh} = Area of transverse hoop bar (one leg)
 E_c = Modulus of elasticity of concrete
 f'_c = Compressive strength of standard 6x12-in. concrete cylinders

f_r = Modulus of rupture of concrete

f_y = Yield strength of reinforcement

f_{su} = Tensile strength of reinforcement

h = Wall thickness

l_h = Maximum unsupported length of rectangular hoop

l_w = Horizontal length of wall

s_h = Center-to-center spacing of hoops

V = Shear force

v = Nominal shear stress = $\frac{V}{0.8l_w h}$

v_{max} = Maximum nominal shear stress

ρ_f = Ratio of main flexural reinforcement area to the gross concrete area of the boundary element. For rectangular sections, the boundary element was taken to extend $0.1 l_w$ from each end of the wall.

ρ_h = Ratio of horizontal shear reinforcement area to the gross concrete area of a vertical section of the wall web.

ρ_n = Ratio of vertical reinforcement area to the gross concrete area of a horizontal section of the wall web.

ρ_s = Ratio of effective volume of confinement reinforcement to total

$$\text{volume of core} = \frac{2 A_{sh}}{l_h s_h}$$

INTERNATIONAL SYMPOSIUM ON
EARTHQUAKE STRUCTURAL ENGINEERING

455

St. Louis, Missouri, USA, August, 1976

DYNAMIC BEHAVIOR OF A REINFORCED
CONCRETE SPRAY TOWER

TIMOTHY J. FOWLER
Senior Engineering Fellow
Monsanto Company
St. Louis, Missouri
U.S.A.

DON M. WILLIAMS
Senior Civil Engineer
Ford, Bacon & Davis Utah, Inc.
Salt Lake City, Utah
U.S.A.

SUMMARY

The paper reports results of dynamic tests and complementary dynamic analyses of a reinforced concrete spray tower. The tower has an overall height of 80 feet (24.38m). The 25' (7.62m) diameter x 54' (16.46m) high cylindrical section is supported on four 42" (1.07m) diameter columns. The structure is founded on 42" (1.07m) diameter caissons carried to lava bedrock 20 feet (6.10m) below grade.

The structure was excited by cyclic air pressure waves in an associated redwood demister. The structural response was determined at the top of the support columns and at the top of the tower. The primary natural frequency, mode shape, and an estimate of the damping were determined.

A series of theoretical dynamic analyses of the structure were carried out using a finite element computer program. The analyses gave good agreement with the measured primary natural frequency and mode shape. The effect of varying some of the analytical assumptions is also reported.

A second dynamic test of the structure was carried out approximately 4 years after the first test. The primary natural frequency of the structure was found to be unchanged. The results of a response spectrum earthquake analysis of the spray tower are also reported.

Preceding page blank

INTRODUCTION

Seismic design, in contrast to design for other load conditions, is highly dependent on theoretical concepts and analyses. This is because documented experience of the response of structures to earthquakes is very limited. Only a few structures designed by modern earthquake design methods have been subjected to severe earthquake loads. It is also extremely difficult and expensive to apply simulated earthquake loads to structures and to observe field performance.

Because of the dependence of seismic design on theoretical analyses, it is important that the analytical methods and assumptions be correct. One of the most important aspects of earthquake design is correct determination of the structure's natural frequency. This paper reports results of dynamic tests of a reinforced concrete spray tower located at Soda Springs, Idaho. The results of the dynamic tests are compared with theoretical analyses of the structure. Good agreement is found between the two. The relative importance of some of the analytical assumptions is also discussed.

STRUCTURE

Fig. 1 shows the spray tower during construction. The view is from the south southwest. Fig. 2 shows details of the structure, together with the arrangement of the associated redwood demister, demister support structure, and the fan which drives the air through the system. The spray tower is built of reinforced concrete and consists of a 25'-4" (7.72m) dia. x 53'-7" (16.33m) high cylindrical portion supported on four 42" (1.07m) diameter columns. The columns are 26 ft. (7.93m) long and are founded on 42 inch (1.07m) diameter caissons each of which is approximately 20 ft. (6.10m) long. Type III A high early strength cement was used for all concrete.

A fan and drive motor are mounted on the top of the spray tower. The fan serves to drive air through the spray tower and into the adjacent redwood demister. The fan and motor support pedestals and the supporting slab are designed with natural frequencies three times the 710 rpm fan operating speed. In this manner, resonant pedestal and floor vibrations are avoided.

The demister is made of redwood staves tied together by intermediate stiffening bands. The demister is tied to a steel support structure which is itself partly supported on the reinforced concrete spray tower.

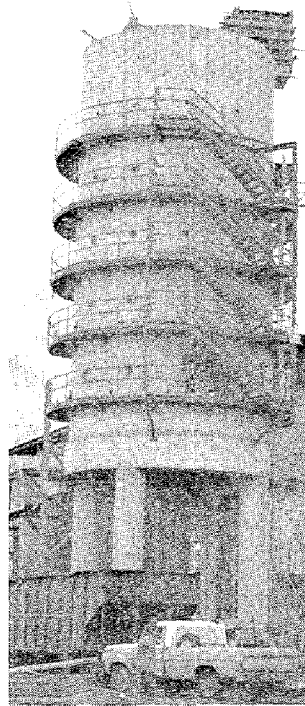


FIG. 1 - SPRAY TOWER STRUCTURE - SOUTH SOUTHWEST VIEW

VIBRATION EXCITATION

On start-up, it was observed that vibrations were set up in the demister. It was also observed that the frequency and severity of the vibrations could be altered by opening and closing the air stream damper. Adjusting the damper also affected the indicated fan amperes. In order to define the source and nature of the vibration, pressure probes were installed in the demister. These probes indicated a regular rotating pressure wave. Seismometers were installed on the top of the spray tower and on the demister, and a series of readings were taken relating indicated fan amperes to frequency and peak to peak pressure. The results of these tests are shown in Fig. 3. As can be seen from the figure, the relationship between indicated fan amperes and pressure, and between indicated fan amperes and frequency is approximately linear. The vibration and pressure readings also confirmed that the pressure wave frequency and the structural vibration frequency were the same.

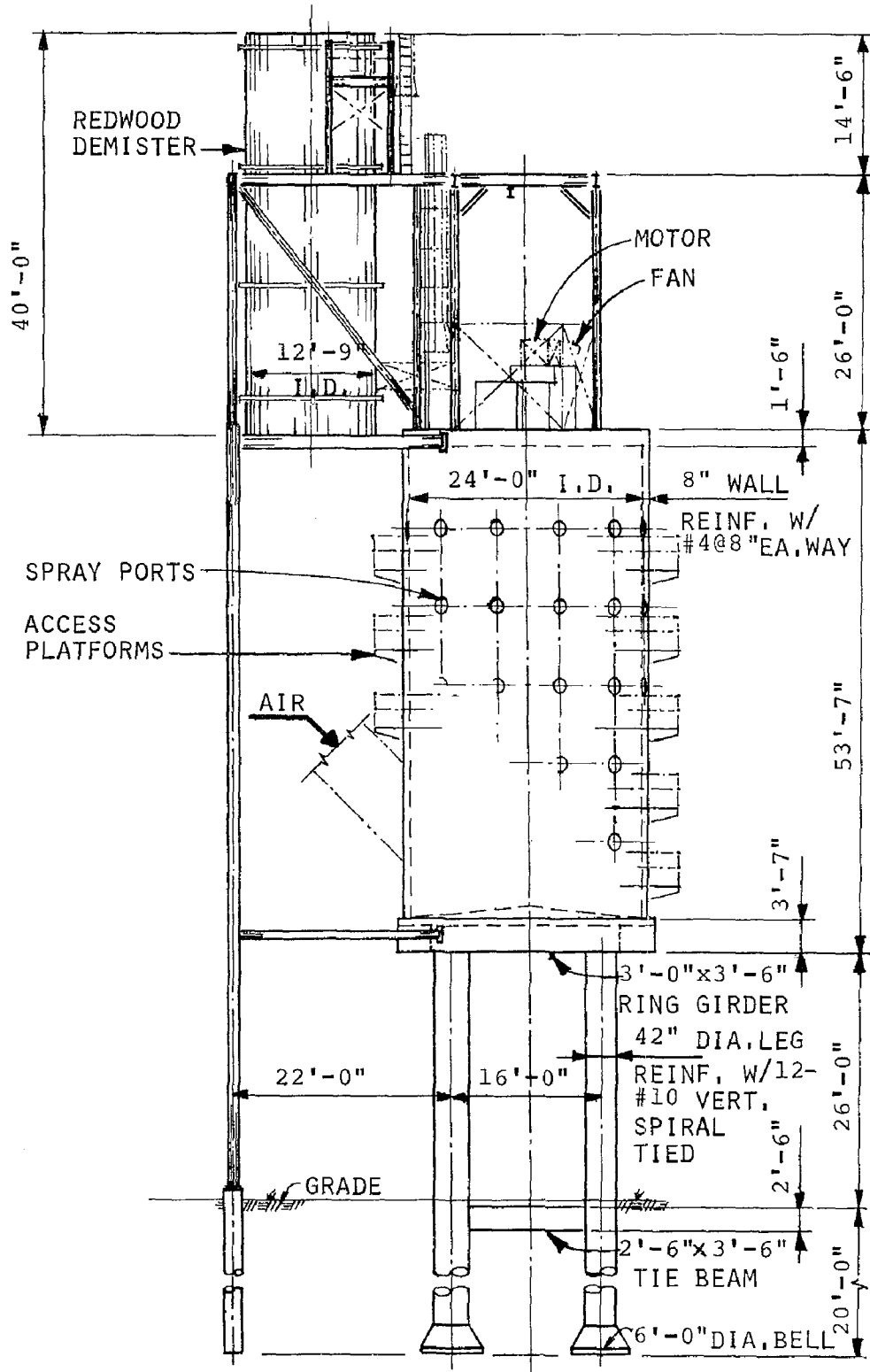


FIG. 2 - SPRAY TOWER STRUCTURE-WEST ELEVATION

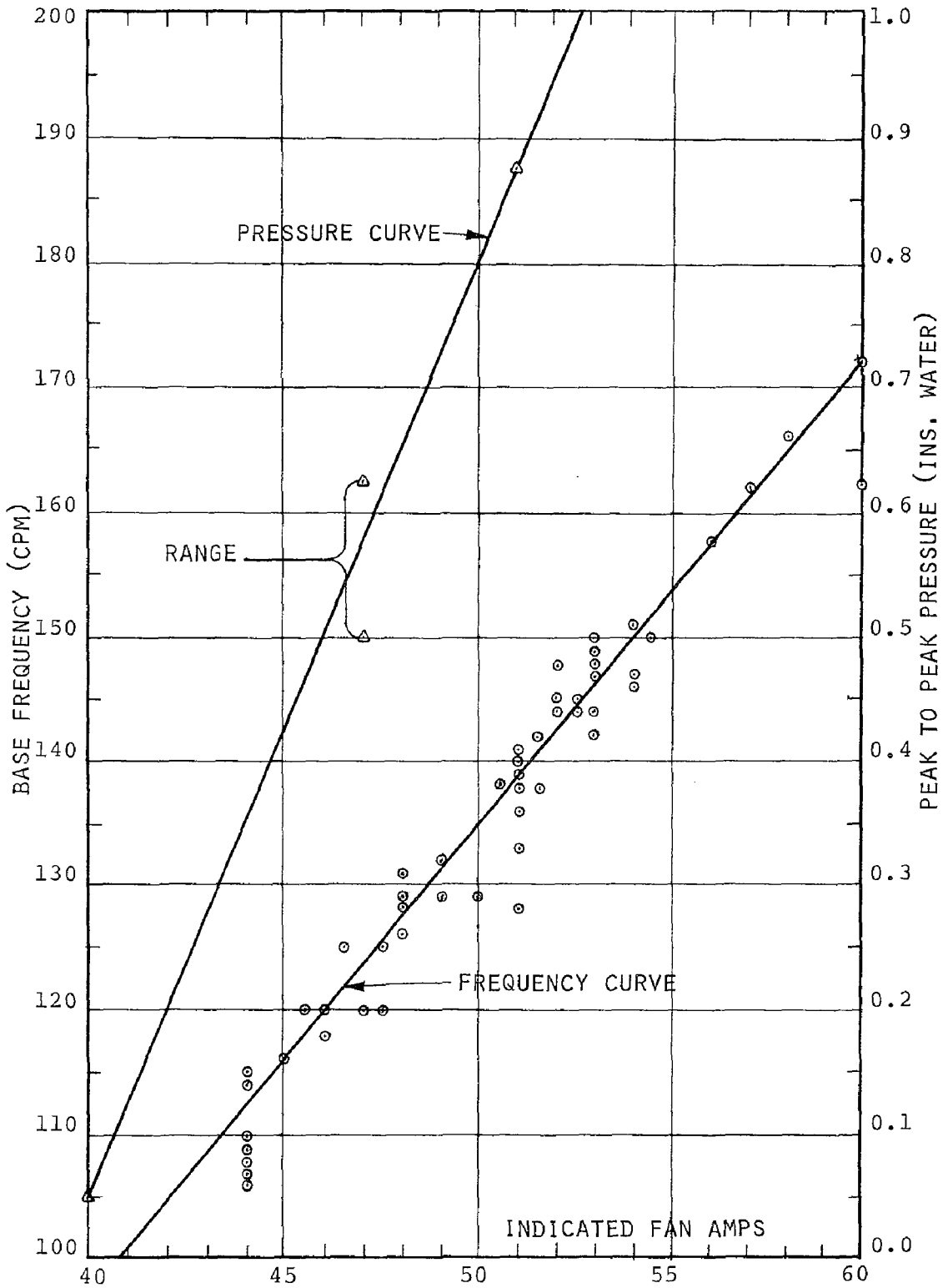


FIG. 3 - EFFECT OF FAN LOAD ON BASE FREQUENCY AND DEMISTER PRESSURE WAVE

A dynamic characterization of the structure was undertaken using seismometers mounted on the top of the structure and at the top of the reinforced concrete columns. Vibration of the structure was observed for different damper settings. Fig. 4 is a series of plots of amplitude of vibration vs natural frequency. In some cases, it was not possible to determine the predominant frequency from the vibration traces. Accordingly, the relationship shown in Fig. 3 for fan amperes vs frequency were used to determine the disturbing frequency.

DYNAMIC TEST RESULTS

Two series of tests were carried out. The first series was affected by an overhanging resonance of the demister at a frequency of approximately 157 cpm. This resonance can be seen as a peak on the Fig. 4 response curve for the NE leg. A program of stiffening the demister to eliminate this resonance was carried out, and a second series of dynamic tests performed. The spray tower response curves after stiffening of the demister, are also shown on Fig. 4. All three curves indicate a resonance in the range of 126 to 129 cpm. Damping values can be calculated from response curves by use of the following formula (Ref. 3):

$$d = \frac{\Delta f}{2f}$$

in which,

d = damping factor (%)

f = resonant frequency

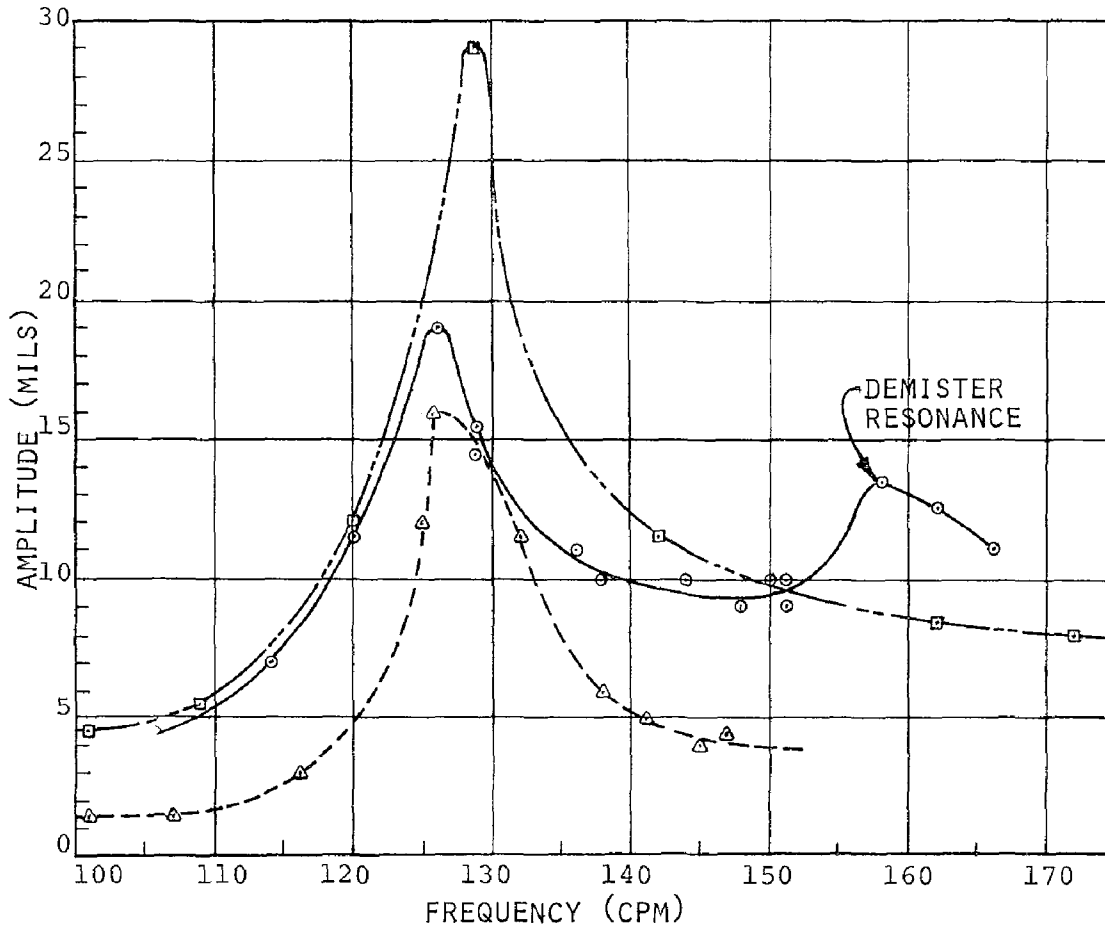
Δf = difference in frequency of the two points
on the response curve with amplitudes of
 $1/\sqrt{2}$ times the resonant amplitude.

Applying the above formula to the three curves in Fig. 4, the following values of damping are obtained:

NE leg NS direction - no stiffening	= 3.4%
NE leg NS direction - after stiffening	= 2.8%
Top of tower EW direction - after stiffening	= 2.3%

The higher value of damping that occurs with the unstiffened demister is to be expected because, in this case, there are larger movements and a greater working between the redwood staves. The tests indicate a damping value of between 2% and 3% for the reinforced concrete spray tower.

Fig. 5 shows the variation of displacement with direction at the top of the reinforced concrete columns. The increase in displacement in the SW-NE direction is explained by the different lengths of the caissons, and by the caissons on the west side being offset 2 ft. (.61m) in an easterly direction. The different length caissons were required because of the varying depth of bedrock.



LEGEND: —○— = NE LEG, N-S DIRECTION NO STIFFENING
 - - -△- - - = TOP OF NE LEG, N-S DIRECTION AFTER STIFFENING
 - · - ·□- · - · = TOP OF TOWER, E-W DIRECTION AFTER STIFFENING

FIG. 4 - SPRAY TOWER RESPONSE CURVES

DYNAMIC ANALYSIS

A finite element model of the structure was developed and a theoretical analysis was carried out using the McDonnell Automation Company version of the STRUDL DYNAL Program. The finite element model is shown in Fig. 6 (a). This model has the caissons included. A separate model, without caissons included, was also analyzed. Concentrated masses were added at the top of the structure to account for the fan, concrete pedestals and the demister. For member properties, gross cross section moments of inertia and transformed areas were used. 28 day cylinder strengths showed an average concrete strength of 4500 psi (31026 kPa). From this value, a modulus of elasticity of 3875 ksi was calculated using the standard ACI formula (Ref. 1).

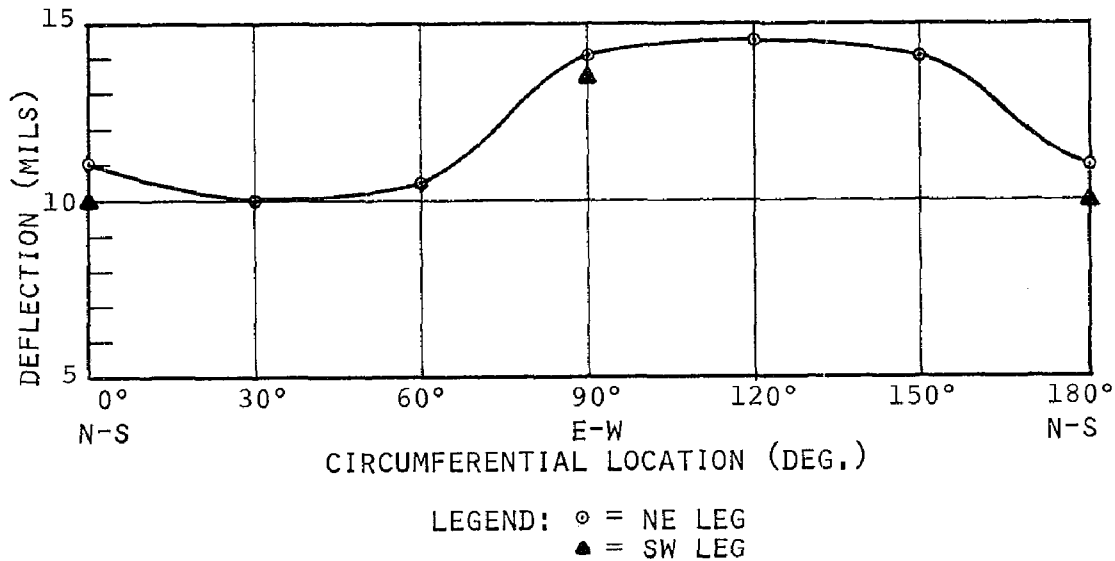


FIG: 5 - HORIZONTAL DEFLECTION IN NE & SW LEGS

As can be seen, a relatively coarse model was used for the analysis and a number of simplifying assumptions were made. In particular, no increase for dynamic effects was included in the modulus of elasticity and for bending, gross cross section moments of inertia were used.

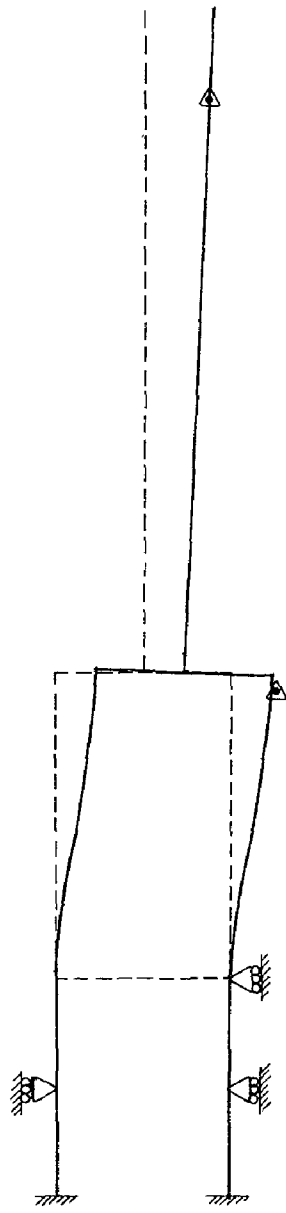
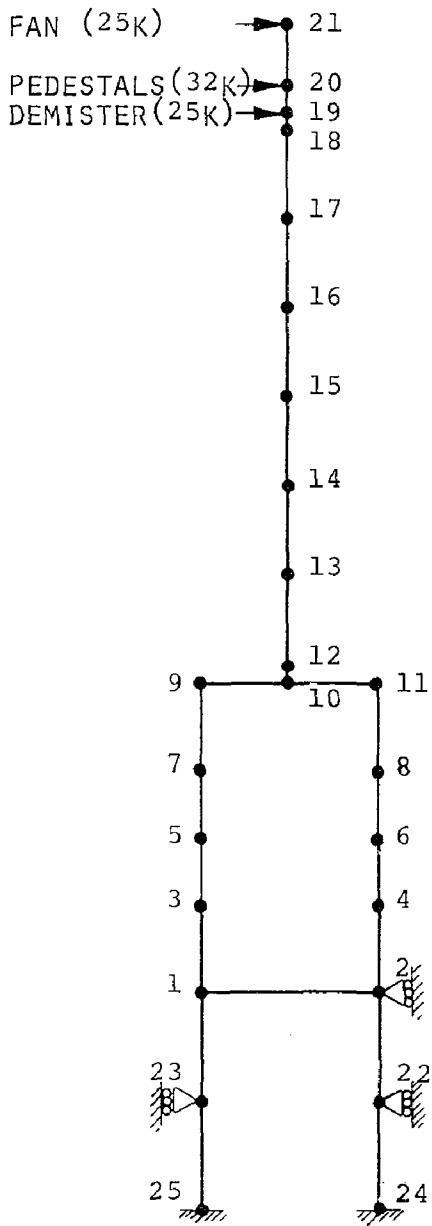
A normal mode analysis gave the following frequencies for the first mode of vibration.

Spray tower, caissons not considered	= 155 cpm
Spray tower, caissons included	= 135 cpm

for comparison;

Measured natural frequency = 126-129 cpm.

As can be seen, the theoretical analysis, even with simplifying assumptions, gives good agreement with the measured natural frequency. The effect of length change of the caissons is significant. The analytical assumption that the caissons are laterally supported was confirmed by dynamic test measurements. Fig. 6 (b) shows the spray tower's first mode deflected shape. The largest contribution to lateral deflection is bending and axial change of the columns. Because of its stiffness, the cylindrical spray section acts as a rigid body. Fig. 6 (b) is a normalized deflected shape upon which two measured deflections have been superimposed. The measured deflections confirm the rigid body behavior of the cylindrical spray section.



Δ MEASURED DEFLECTIONS

FIG. 6 - (A) FINITE ELEMENT MODED

(B) DEFLECTED SHAPE

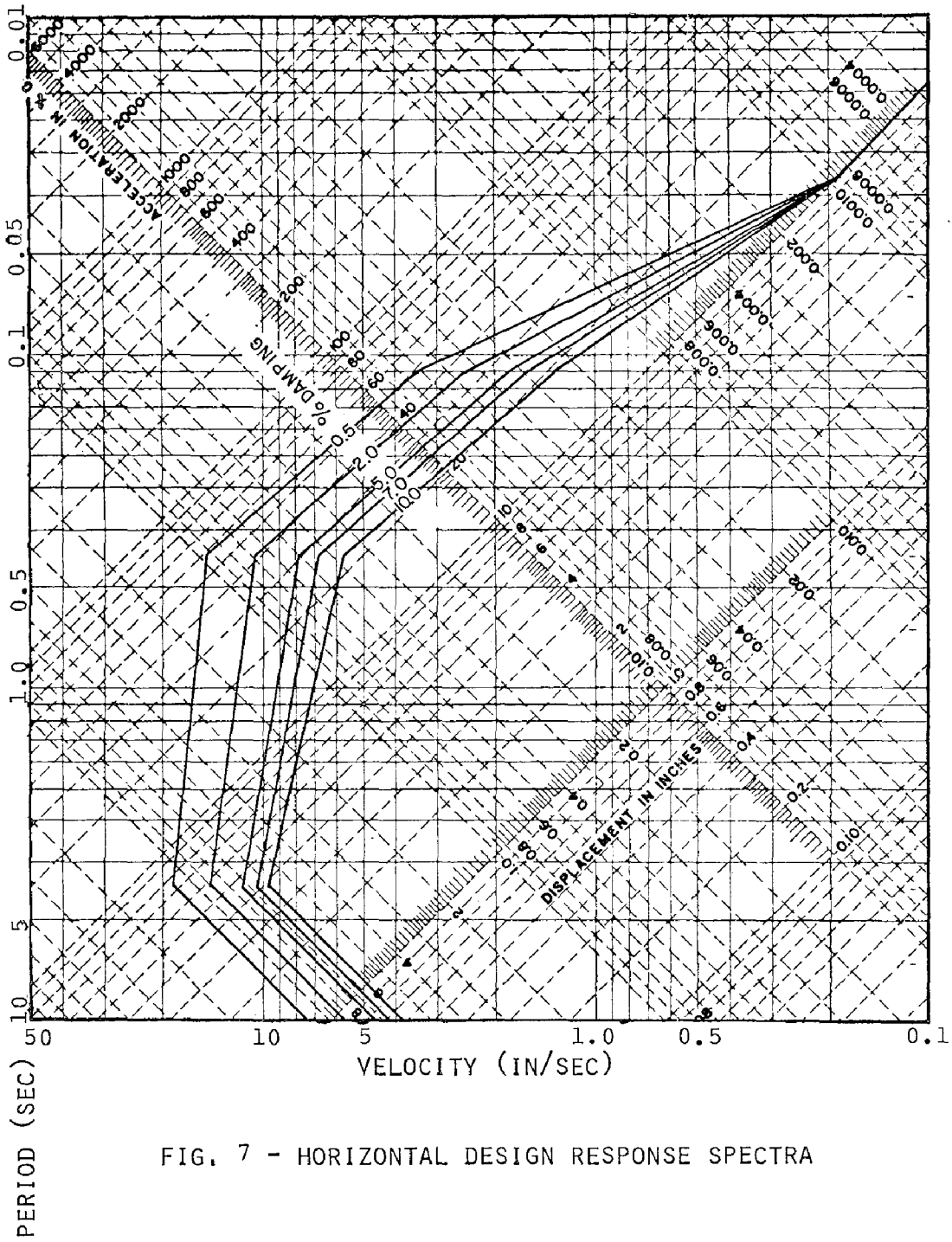


FIG. 7 - HORIZONTAL DESIGN RESPONSE SPECTRA

SEISMIC ANALYSIS

Design spectra for southeast Idaho are shown in Fig. 7. Based on 7% damping and the model shown in Fig. 6 (a), a response spectrum analysis was carried out. The deflections and tower and column forces and moments which result, are shown in Fig. 8. For the spray tower structure, the minimum factor of safety on ultimate load is 1.23 at the critical section at the base of the columns. The value of 7% damping is based on the recommendations of Newmark, Blume and Kapur (Ref. 2). Taking into account the large displacement that occurs under the maximum earthquake condition, the 7% value is consistent with the measured 2-3% for low amplitude vibrations.

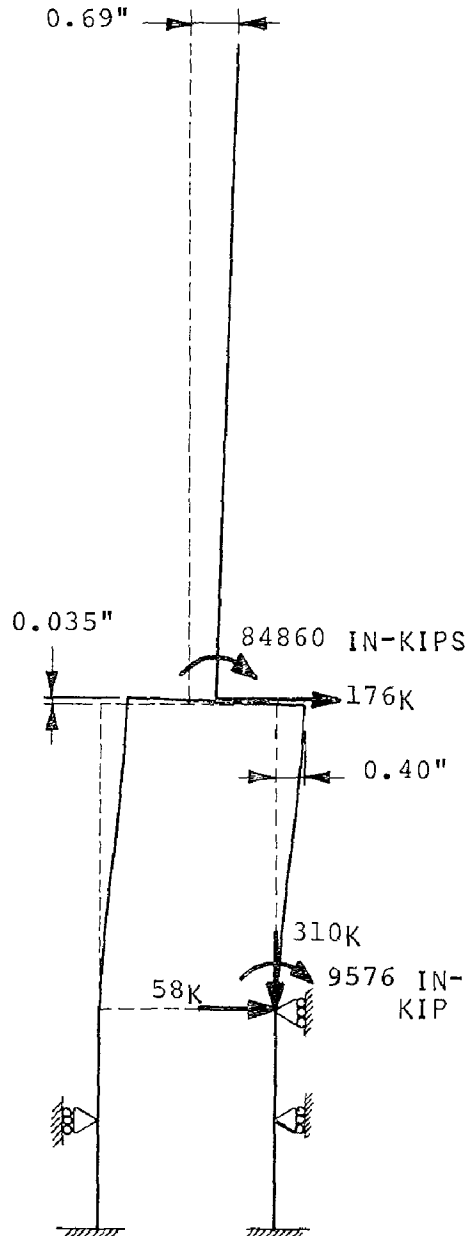


FIG. 8 - EARTHQUAKE RESPONSE

EFFECT OF CONCRETE STRENGTH

Separate analyses were made using the modulus of elasticity for 3000 psi (20684 kPa) and 5000 psi (34473 kPa) concrete. The first mode natural frequency was 18% higher for the 5000 psi (34473 kPa) concrete than for 3000 psi (20684 kPa) concrete.

EFFECT OF TIME

The spray tower structure was constructed during the period August through December 1970. Dynamic testing was carried out in February 1971. In April 1975, a second dynamic test was carried out and the primary natural frequency of the structure was found to be unchanged.

CONCLUSIONS

1. For the reinforced concrete spray tower described in the paper, a relatively coarse dynamic analysis gives good agreement with observed dynamic performance.
2. The dynamic tests indicate a damping value in the range of 2-3% for low amplitude vibrations.
3. After four years of service, the measured natural frequency of the spray tower structure remains unchanged from the value measured one month after construction.

BIBLIOGRAPHY

1. "Building Requirements for Reinforced Concrete (ACI 318-71)", American Concrete Institute, 1971.
2. Newmark, N. M., Blume, J. A., Kapur, K. K., "Seismic Design Spectra for Nuclear Power Plants", Journal of Power Division, American Society of Civil Engineers, November 1973.
3. Wiegel, R. L., "Earthquake Engineering", pg. 153, Prentiss Hall 1970.

INTERNATIONAL SYMPOSIUM ON
EARTHQUAKE STRUCTURAL ENGINEERING

467

St. Louis, Missouri, USA, August, 1976

EXPERIMENTAL STUDIES ON HYSTERETIC CHARACTERISTICS
OF STEEL REINFORCED CONCRETE COLUMNS AND FRAMES

Minoru WAKABAYASHI
Professor
Disaster Prevention Research Institute
Kyoto University
Kyoto, Japan

Koichi MINAMI
Lecturer
Osaka Institute of Technology
Osaka, Japan

SUMMARY

In order to obtain the information on the hysteretic characteristics in the inelastic range of steel reinforced concrete (SRC) columns and frames, a parametric experimental study was carried out on the strength, deformability, failure mechanism and shapes of hysteresis curves under repeatedly applied, well-defined loads using 27 column and 9 frame specimens. Variables chosen for the experiments were the magnitude of the constant axial load and the composition of column cross section; full-web (H-shaped) steel component, open-web (battened) steel component and reinforced concrete sections (without steel component) for the comparison of the characteristics with SRC counterparts. All column specimens were of the rectangular cross section ($15^{\text{cm}} \times 15^{\text{cm}}$). Well-defined cyclic loading was applied to all the specimens by controlling the deflection amplitude. Main discussion was concentrated on the strength, the behavior before and after the attainment of the maximum strength, failure mechanism and hysteretic characteristics involved in the large deformation range under repeated loading.

1. INTRODUCTION

Recently, dynamic analyses and designs are increasingly made on steel reinforced concrete (hereinafter abbreviated to SRC*) structures. In order to establish a reasonable dynamic design method, researches are required to clarify not only ultimate strength of structural members and frames but also their inelastic behavior up to fracture. Especially required is the knowledge of hysteretic characteristics of SRC members and frames under repeatedly applied external forces that alter with the range beyond the yield strength of the members or the frames (1~4).

* Also, reinforced concrete structure, member, etc. will be abbreviated to RC structure, member, etc. throughout this paper.

The intended by this paper is to experimentally clarify the elastic-plastic deformation behavior of SRC columns, which are regarded to involve most substantial ductility problems among the structural members, under repeatedly applied external loads.

2. EXPERIMENTS

2. 1 Outline of Experiments

The total of 36 specimens were tested under repeatedly applied, well-defined loads; 27 column specimens and 9 frame specimens.

Features of the test specimens are tabulated in Table, and their cross sections are shown in Fig. 1. Test specimens were grouped into four series. Series 1 was to know the deformation behavior of columns subjected to constant axial compression and repeatedly applied pure bending. Series 2 was to know the deformation behavior of columns with $h/D=6$, where h is the column length and D is the column depth, subjected to constant axial compression and repeatedly applied bending and shear. Column specimens were designed so that the flexural failure was predominant. Tests of Series 3 were very similar to those of Series 2 except that the column dimensions were such that $h/D=3$, and shear failure was predominant over flexural failure. Series 4 was to investigate the behavior of one-story, one-bay portal frame when subjected simultaneously to constant vertical load on columns and repeatedly applied horizontal load. The column members were the same as the specimens in Series 2, hence the flexural type of failure should take place prior to shear failure.

Variables chosen for the series of experiments were the magnitude of the constant axial compression and the composition of member cross section. Test specimens were denoted in such a manner that the combination of the experimental variables could be easily recognized from the specimen names. In the names of test specimens, the first numerals, 1, 2, 3, or 4, represent the series number and the second characters, F, B, or R, represent the cross sectional composition; F for SRC column with full-web (H-shaped) steel component, B for SRC members with open-web (battened) steel component, and R for RC members (without steel component) for the comparison of the structural characteristics with SRC counterparts. The third numerals indicate the magnitude of constant axial compression loaded on the specimens. The numerals, 0, 3, and 6 correspond to $n=0, 0.3$, and 0.6 , respectively, where n is the ratio of applied axial compression, N , to the load carrying capacity of centrally loaded SRC column, N_0 , which is obtained by superimposing the capacity of RC cross section upon that of steel cross section.

2. 2 Configuration and Dimensions of Test Specimens

All the test specimens had the same square cross section of $150\text{mm} \times 150\text{mm}$, as is shown in Fig. 1. Full-web steel section was the nominal H-100 \times 50 \times 4 \times 6 of SS41 grade steel (min. yield point = 25 kg/mm^2). Open-web steel section was the same size and material only with flame-cut, rectangular openings of $75\text{mm} \times 74\text{mm}$ in the web, as is illustrated in Fig. 2.

The numbers and the diameters of the longitudinal reinforcements were so chosen that the moment capacities of SRC and RC columns in each series of experiments were approximately the same. The longitudinal bars used were D10 and D13 of SD35 grade (min. yield point = 35 kg/mm^2). Web reinforcements

had the diameter of 3mm and were of annealed mild steel equivalent to SR 24 grade (min. yield point = 24 kg/mm^2). Web reinforcements were spaced at every 50mm in all the RC specimens and all the column specimens of Series 3. For the RC specimens in Series 1, 2 and 4, the spacing of web reinforcements was reduced to half, in order to prevent the transition of failure mode from flexural type to shear type. For the column specimens in Series 1, 2, and 3, rigid anchor blocks were provided at both ends of each specimens as shown in Fig. 3(a) and (b). For the frame specimens of Series 4, the amount of longitudinal reinforcements in the beams were twice as much as that in the columns, and the steel shapes of the same dimensions were used in both beams and columns, as is shown in Fig. 3(c). This was to let the flexural failure occur only in columns. To provide the column bases with enough rigidity, the base beams were designed to have the sections of $150\text{mm} \times 200\text{mm}$ and to contain the steel wide flange shape of H-150 \times 75 \times 6 \times 9. Thus, the base beams were more rigid and stronger than beams and columns. Anchor blocks were provided on the outside of the beam-to-column connections, 150mm long each, and longitudinal reinforcements of beams and columns were anchored, in order to prevent the failure at the reinforcement anchors from occurring in the region of beam-to-column connections.

2.3 Materials and Making of Test Specimens

Mix design of concrete was common to all the specimens; water-cement ratio was 65%, mix ratio in weight was cement 1 : sand 2.95 : gravel 2.82, and the slump was 21cm. Concrete was cast in vertical position for all the specimens. The age of the concrete when the specimens were tested was approximately two months for all specimens. Mechanical properties of concrete material were obtained by testing concrete cylinders of $150\text{mm} \times 300\text{mm}$ for compressive strength, F_c , and split tensile strength, F_t , when corresponding specimens were tested.

2.4 Testing Apparatus

Test set-ups for each of the test series and different loading systems are shown in Figs. 4(a), (b) and (c), and their theoretical models are sketched in Figs. 5(a), (b) and (c).

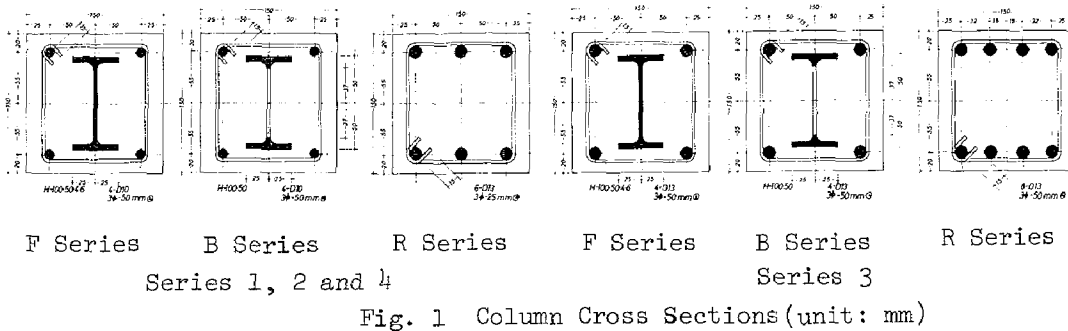
For Series 1, steel loading beams were bolted with high strength bolts to the anchor blocks on the ends of the specimen as is shown in Fig. 4(a). The load was applied on these beams by a pair of manual oil jacks, to introduce the external moments on the column ends. By changing the point of load application, cyclic external moments were applied on the specimens. Constant axial compression was applied by a manual oil jack.

For Series 2 and 3, referring to Fig. 4(b), another set of steel loading beams were bolted to end anchor blocks with high strength bolts. The lower loading beam was fixed to the rigid testing floor through a universal joint, and the upper loading beam was jointed, through another universal joint, to a reversible manual oil jack, with which cyclic load was introduced to the test specimen. Constant axial compression was put on by a manual oil jack located at a specimen end. With all of the above test set-up, the specimens of Series 2 and 3 were tested under repeatedly applied bending and shear as well as the constant axial compression.

Table Test Program

	Name of Test Specimen	Type of Specimen	Loading Condition	Planned Failure Mode	Column Length (mm)	Experimental Variables		Reinforcements	
						Sectional composition	Axial Compression Ratio n	Longitudinal Reinforcements	Web Reinforcements
Series 1	1 F 0 1 F 3 1 F 6	column	Constant axial compression and alternately applied pure bending	Flexural failure	600	F *	0 0.3 0.6	4-D10	3 ϕ -50 ^{mm@}
	B					0 0.3 0.6	4-D10	3 ϕ -50 ^{mm@}	
	R					0 0.3 0.6	6-D13	3 ϕ -25 ^{mm@}	
Series 2	2 F 0 2 F 3 2 F 6		Constant axial compression and alternately applied bending and shear	Flexural failure	900	F	0 0.3 0.6	4-D10	3 ϕ -50 ^{mm@}
	B					0 0.3 0.6	4-D10	3 ϕ -50 ^{mm@}	
	R					0 0.3 0.6	6-D13	3 ϕ -25 ^{mm@}	
Series 3	3 F 0 3 F 3 3 F 6	Shear failure	450	F	0 0.3 0.6	4-D13	3 ϕ -50 ^{mm@}		
	B			0 0.3 0.6	4-D13	3 ϕ -50 ^{mm@}			
	R			0 0.3 0.6	8-D13	3 ϕ -50 ^{mm@}			
Series 4	4 F 0 4 F 3 4 F 6	Frame	Constant vertical load and alternately applied horizontal load	Flexural failure	900	F	0 0.3 0.6	4-D10 (8-D13)**	3 ϕ -50 ^{mm@}
	B					0 0.3 0.6	4-D10 (8-D13)	3 ϕ -50 ^{mm@}	
	R					0 0.3 0.6	6-D13 (12-D13)	3 ϕ -25 ^{mm@}	

* F denotes full-web type SRC member, B for battened-web type SRC member, and R for RC member provided for comparison purpose.
 ** Numerals in parentheses are the reinforcements in the beams.



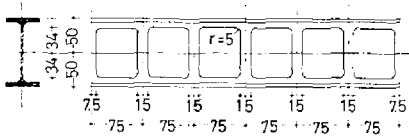
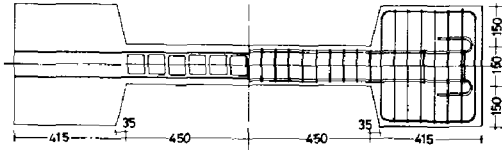
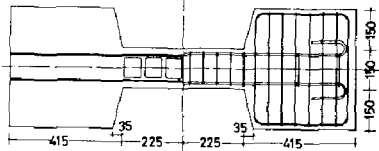


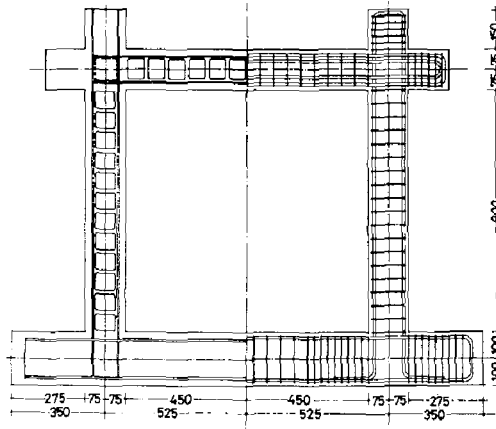
Fig. 2 Dimensions of Open-web Steel Component(unit: mm)



(a) Series 2



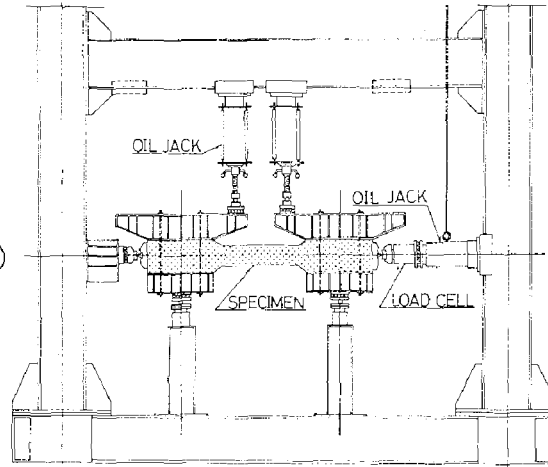
(b) Series 3



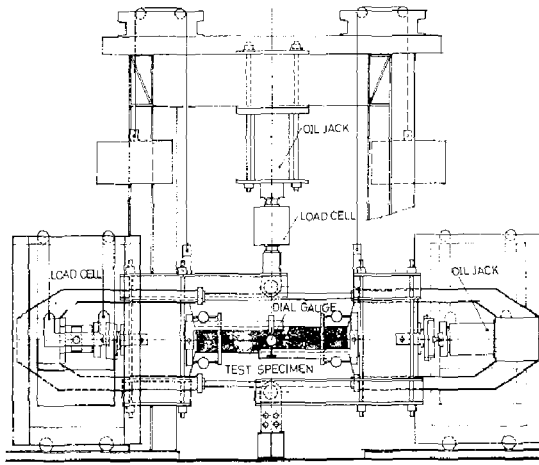
(c) Series 4

Fig. 3 Dimensions and Arrangement of Reinforcement(unit: mm)

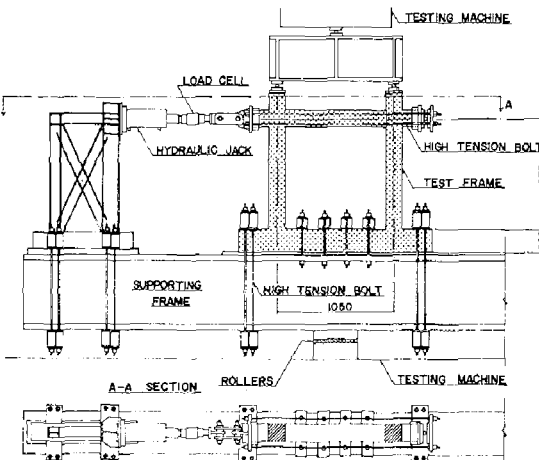
Note: The SRC columns and frame with open-web(batten) steel component are shown in Fig. 3.



(a) Series 1



(b) Series 2 and 3



(c) Series 4

Fig. 4 Loading Apparatus

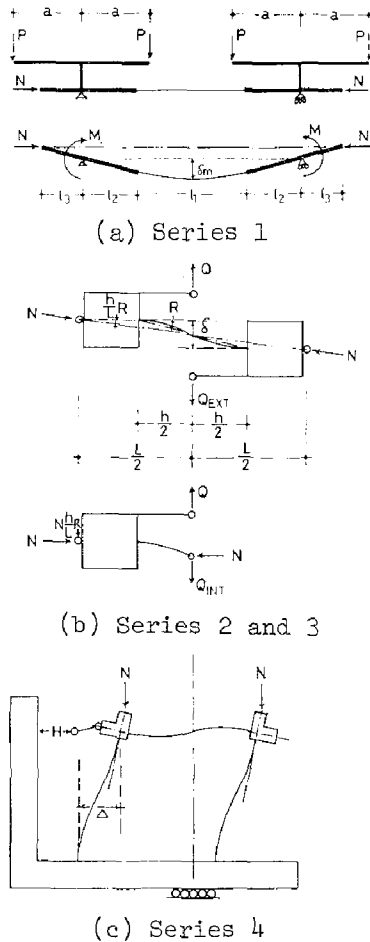


Fig. 5 Loading System

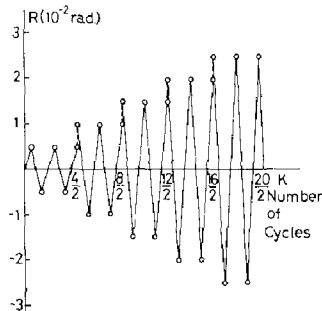


Fig. 6 Loading Program

at the column ends, and abscissa gives the mid-point deflection, δ , or the curvature ϕ . Figures 8 and 9 show the hysteresis loops for Series 2 and 3. Ordinate is the load, Q , applied to the column specimen by the oil jack, and abscissa represents the measured slope deflection, R . Hysteresis curves of test frames in Series 4 are shown in Fig. 10. Ordinate represents the applied horizontal force, H , and abscissa gives the horizontal displacement (sway), Δ , of the test frame.

For the tests of frame specimens of Series 4, loading apparatus is shown in Fig. 4(c). The frame specimen and the horizontal load applicator frame were fixed onto the supporting frame with high strength bolts. The rollers were placed between the supporting frame and testing machine to prevent any resistance to horizontal displacement of the supporting frame. Constant vertical load was applied on two columns of the test frame by a hydraulic testing machine. Care was taken to load the two columns equally. Cyclic loading of the horizontal force was accomplished by a reversible oil jack attached to the horizontal load applicator frame. Horizontal displacement (sway) of the frame was measured at the mid-point of the beam.

In all tests, applied loads were censored by load cells, and deflections and displacements were measured by electrical displacements gages and/or mechanical dial gages. Also, in Series 2 and 4, average curvature and average axial strain were measured by mechanical dial gages over the column length of 150mm from the ends.

2. 5 Loading Programs

One of the loading programs for the tests is shown in Fig. 6. This was the one for Series 2. Well-defined cyclic load was applied to all the test specimens by controlling the deformation, that is, deflection or displacement and the deformation amplitude was increased at every other cycles of loading.

3. RESULTS OF EXPERIMENTS

3. 1 Hysteresis Loops and Failure Modes

Hysteresis curves obtained from the tests are shown in Fig. 7, 8, 9 and 10 for Series 1, 2, 3 and 4, respectively. Shown in Fig. 7 are the hysteresis curves obtained for each test specimens in Series 1. Ordinate of the diagrams represents the external moment M , applied

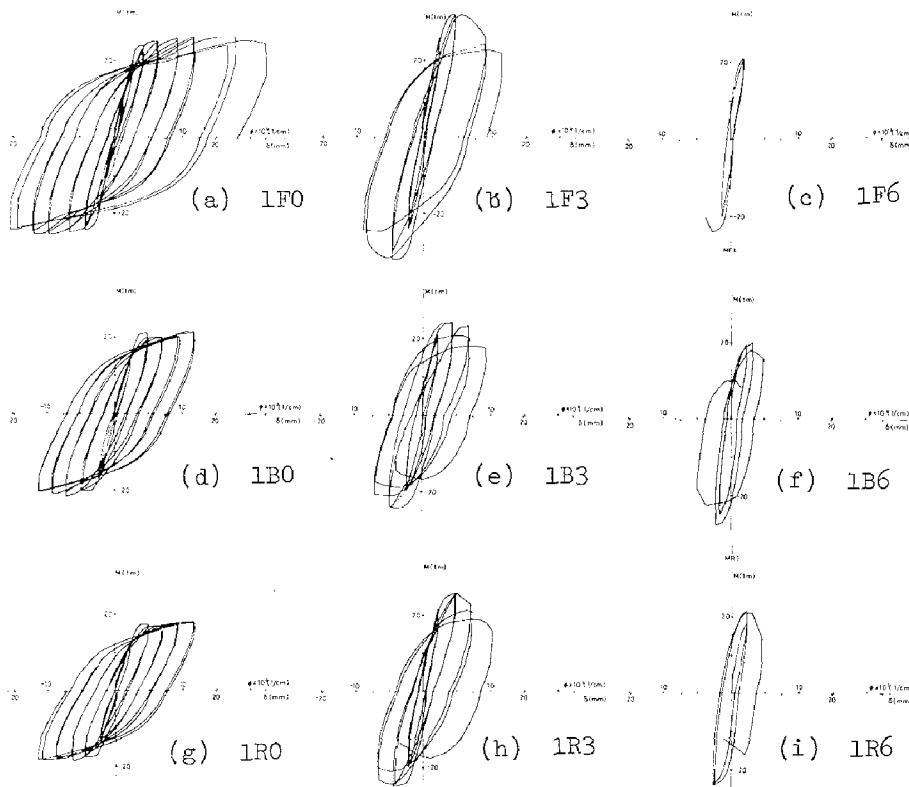


Fig. 7
Hysteresis
Loops
for
Series 1

For the column specimens in Series 1 on which no axial compression was loaded ($n=0$), there was no strength deterioration observed due to the effect of cyclic bending up to the deflection amplitude of five times the elastic deflection, and the hysteresis loop obtained was the spindle-shaped one that implied the large capacity of energy absorption. When $n=0.3$, the load carrying capacity was improved with the help of axial compression, whereas the deflection at the maximum strength was considerably small and was found to be approximately twice the elastic deflection. After the attainment of the maximum strength, considerable deterioration in strength due to the influence of cyclic bending was observed, and the column collapsed by the fracture in compression concrete and the buckling of compression reinforcements at the deflection amplitude of four times the elastic deflection. This tendency was further emphasized in the columns of $n=0.6$, which showed very limited amount of deformability. When the load carrying capacity was reached, compression concrete fractured suddenly and accompanied overall buckling lead to the collapse of the column. The deformation after the collapse exhibited a very unstable hysteretic characteristics. Therefore, in the hysteresis loops of the Series 1 columns, there was no appreciable difference observed between the SRC columns with full- or open-web steel and the RC columns owing to the difference in the composition of cross section, and only the effect of the magnitude of axial compression was clearly seen. For Series 2 and 3, however, hysteresis curves indicated the apparent difference between the full-web type SRC columns, open-web type SRC columns and RC columns owing to the influence of applied shear force.

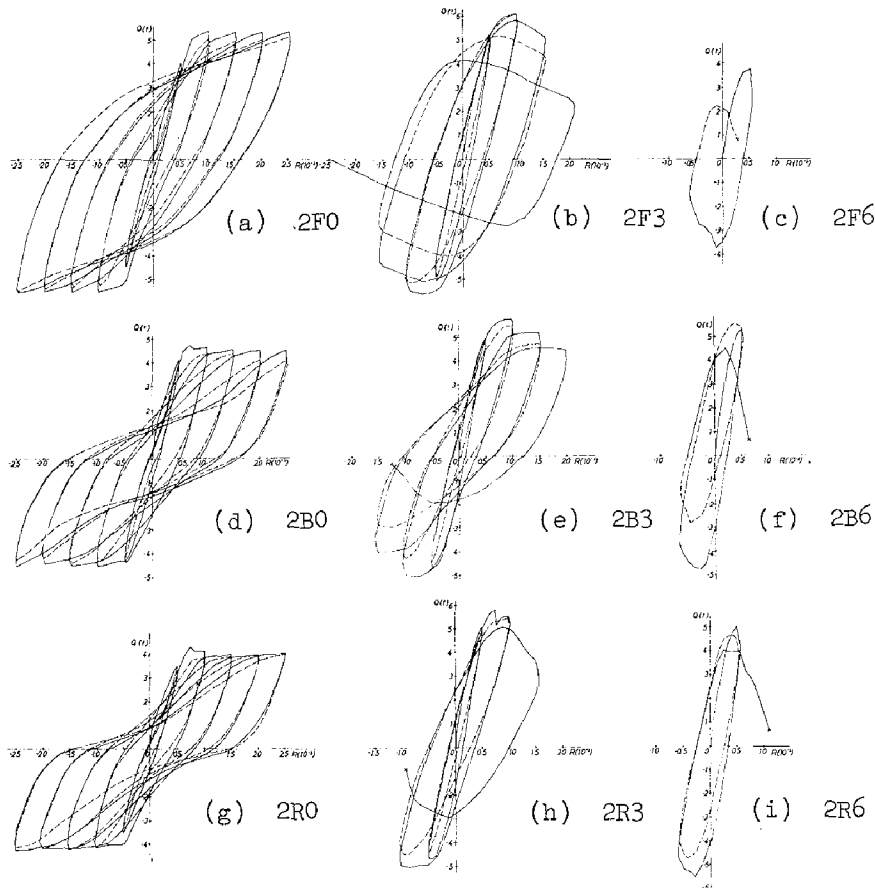


Fig. 8
Hysteresis
Loops
for
Series 2

For the column specimens 2R0 and 2B0 ($n=0$) in Series 2 ($h/D = 6$), flexural and diagonal tension cracks were created and developed with the increase of deformation amplitude and of the number of loading cycles. Even in last stages of cyclic loading, no perceptible deterioration in strength occurred. The load-deformation curves showed reversed S-shaped loops with the increasing amplitude. One of the reasons to this lies in the plastic hinge formed at the column end; the plastic hinge was not the one due to pure bending but was apparently the shear type hinge with diagonal tension cracks. On the other hand, no diagonal tension crack was formed in the full-web type SRC column 2F0 through the entire life of cyclic loading, and the flexural cracks developed in the direction approximately perpendicular to the column axis. Hysteresis loops showed very stable spindle-like shape when the slope deflection reached 0.015 rad., and showed the tendency of gradually approaching to the loops of pure steel columns as the deflection amplitude increased. When $n=0.3$, for all the column specimens 2F3, 2B3 and 2R3, the occurrence of flexural cracks, diagonal tension cracks and concrete failure were limited in the region approximately 150mm, equal to the column depth, away from the column ends. The column fracture followed by the buckling of compression reinforcements showed apparent shear-compression type of failure. All of the above three column specimens reached their load carrying capacities within the cycle of the deformation amplitude of $R=0.01$ rad., and did not show the reversed S-shaped loops after the attainment of the maximum capacities. When $n=0.6$, all the column specimens

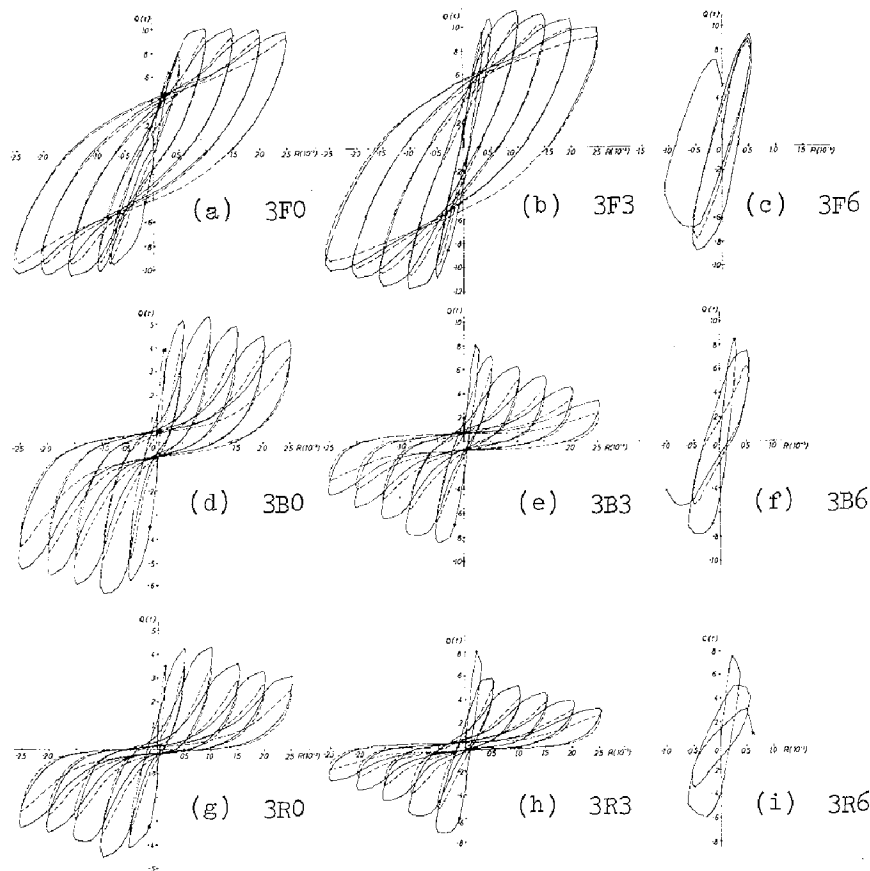


Fig. 9
Hysteresis
Loops
for
Series 3

exhibited very limited capability of deformation, and collapsed when $R=0.005$ rad. due to the local failure in compression concrete and the buckling of compression reinforcements.

As is shown in Fig. 11(a), the pattern of crack development in the column specimens of Series 3 ($h/D = 3$) were, despite the difference in cross sectional composition and the magnitude of applied axial compression such that the diagonal tension cracks were formed first and developed into shear-bond cracks along the longitudinal reinforcements and steel flanges with the increase in the deformation amplitude and the number of loading cycles, finally to exhibit shear-bond type of column fracture. This was one of the reasons why the hysteresis loops had the reversed S-shape. The hysteresis loops of the columns 3R0 and 3B0 ($n=0$) were very similar to each other; the slope deflection at the maximum load capacity was approximately equal to 0.01 rad. and very gradual deterioration in strength was observed after the maximum capacity, showing apparent reversed S-shaped hysteresis loops. Diagonal tension cracks were found in the specimen 3F0 at the load larger than those found in 3R0 and 3B0. The steel web was considered to have carried some shear until the diagonal tension cracks were formed. With the increase of deformation amplitude, shear-bond cracks developed along the longitudinal reinforcements and the steel flanges. Rather stable shape of the hysteresis loop was obtained, different from the reversed S-shaped loops of 3B0 and 3R0, and the loops indicated the tendency to con-

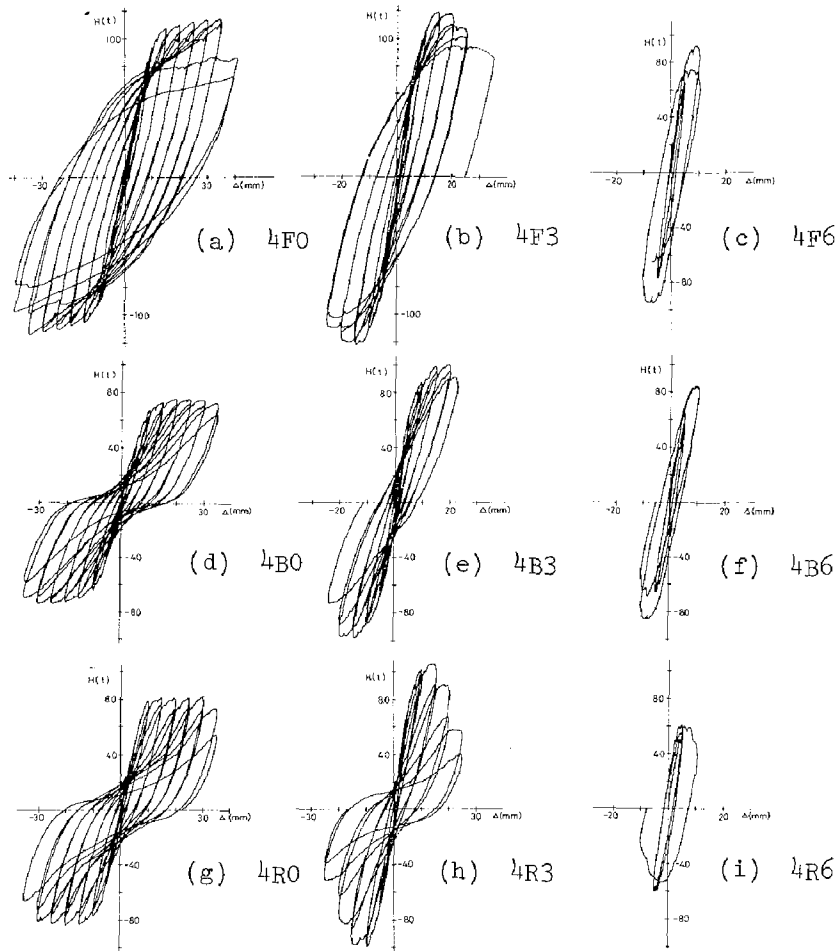


Fig. 10
Hysteresis
Loops
for
Series 4

verge to the ones of the pure steel columns. Deterioration in strength after the attainment of the maximum capacity was very small. When $n=0.3$, the loads at which the diagonal tension cracks took place were larger than the specimens with $n=0$. This means that the compressive stress in concrete due to axial compression helped raise the diagonal tension crack loads. The diagonal tension crack loads themselves, however, were approximately equal to the maximum strength of the columns, and the column specimens 3R3 and 3F3 showed considerable deterioration in strength after this stage, giving apparent reversed S-shaped loops. For 3F3, the deterioration was not large and the hysteresis loops were spindle-shape. In all the columns of 3R6, 3B6 and 3F6 ($n=0.6$), shear-bond cracks along the longitudinal reinforcements and the steel flanges occurred along with diagonal tension cracks, and the columns collapsed at $R=0.005$ rad. One of the most distinctive features brought up by the shear failure modes of the columns in Series 3 is that the bondage between concrete and steel flanges can not be expected in the SRC columns in which the shear-bond cracks cause the shear-bond failure of columns when subjected simultaneously to cyclic bending and shear. The shear capacity of a steel shape with battened web is only equal to that of Vierendeel beam. Therefore, the SRC members tested had very small shear capacity, and the hysteretic characteristics of the RC columns and the SRC columns with battened steel web were very similar to each other.

For the frame specimens in Series 4, regardless of SRC or RC frames, the maximum load carrying capacity was maintained up to $\Delta=30\text{mm}$ when $n=0$, the deterioration in strength initiated at $\Delta=15\sim 20\text{mm}$ when $n=0.3$, and the frame collapsed in the loading cycle of $\Delta=10\text{mm}$ when $n=0.6$. Failure modes at the column bottom portions of these frame specimens were very similar to those at the member ends in Series 2. Shear-bond cracks were formed along the longitudinal reinforcements and developed all the way through the entire column length. This caused the hysteresis loops to be of reversed S-shape and the strength deterioration was considerably large. Hysteresis loops of the full-web type SRC frames of $n=0$ and 0.3 showed spindle-like shapes which were very similar to those of the pure steel frames. They had better quality in both strength capacity and ductility than that of other frame specimens. Locations of failure in columns, which lead to the collapse of the entire frames, differed depending on the magnitude of applied constant vertical loads. That is, the failure occurred in the column ends when $n=0$, and in the regions approximately 150mm (equal to the column depth) away from the ends when $n=0.3$ and 0.6 as shown in Fig. 11(b). Local flexural cracks and diagonal tension cracks took place also in the beams of all the frame specimens, but they did not induce the frame collapse.

Shown in Fig. 12 are the nondimensionalized average curvatures, ϕD (ϕ is the average curvature measured over the column length of 150mm , and D is the column depth) and the average normal strain, ϵ , at column ends, which were the top ends when concrete was cast, obtained from the tests in Series 2. In the figure, ordinate represents the applied load, Q , and abscissa represents either the nondimensionalized average curvature, ϕD , or the average normal strain, ϵ . Hysteretic behavior of all the specimens in Series 2 as shown in the figures for the nondimensionalized curvature are very similar to that obtained for the column slope deflection, R . The hysteretic behavior for the average normal strain, however, were different depending on the magnitude of axial compression; normal tensile strain was accumulated when $n=0$, and compressive strain was accumulated when $n=0.3$ and 0.6 , regardless of the cross sectional composition. The accumulation of compressive strain was accelerated as the deformation approached to the amplitude of the member failure.

3. 2 Relationship between the Specific Damping Capacity and the Number of Loading Cycles

Shown in Fig. 13 is the relationship between the magnitude of energy consumed within every half cycle of loading and the number of loading cycles, computed from the hysteresis loops of Series 2 and 3. In the figure, ordinate represents the specific damping capacity, $\psi = \Delta w/w$, which is in proportion to the amount of energy consumption and is nondimensionalized, where Δw is the amount of energy consumed within a half cycle of loading, and w is the potential energy in the same loading cycle. Abscissa represents the number of cycles. For the open-web type SRC columns and RC columns in Series 3, the specific damping capacity, ψ , decreased from 1.50 to 0.40 with the increase in the number of loading cycles and in the deformation amplitude. Within the same cycle of loading, the values ψ for the reloaded loops were smaller than that in the virgin loop, and this tendency was more clearly seen in the loops of the smaller amplitude of deformation. For the full-web type SRC columns in Series 3, the value of ψ increased from 0.80 to 1.10 as the deformation amplitude increased. For the open-web SRC column and RC

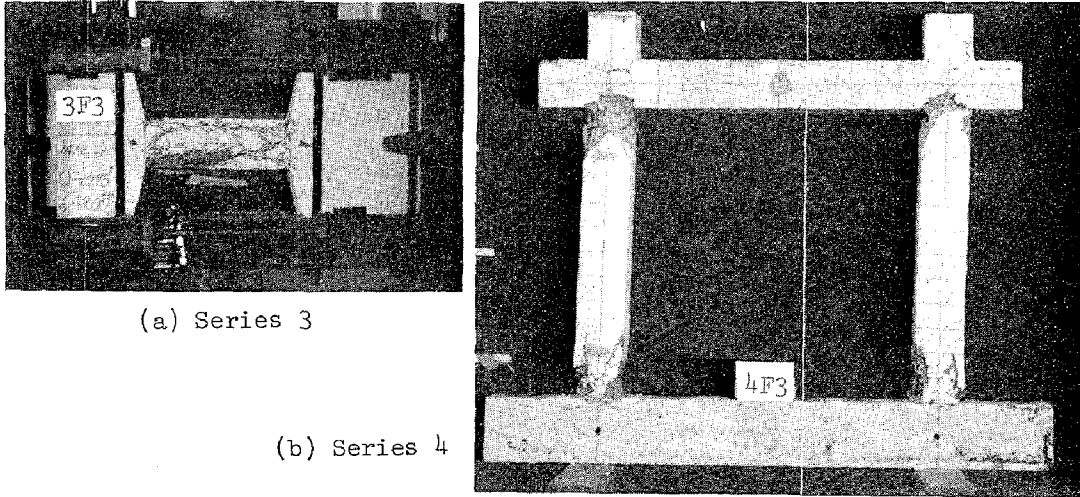


Fig. 11 Test Specimen after Test

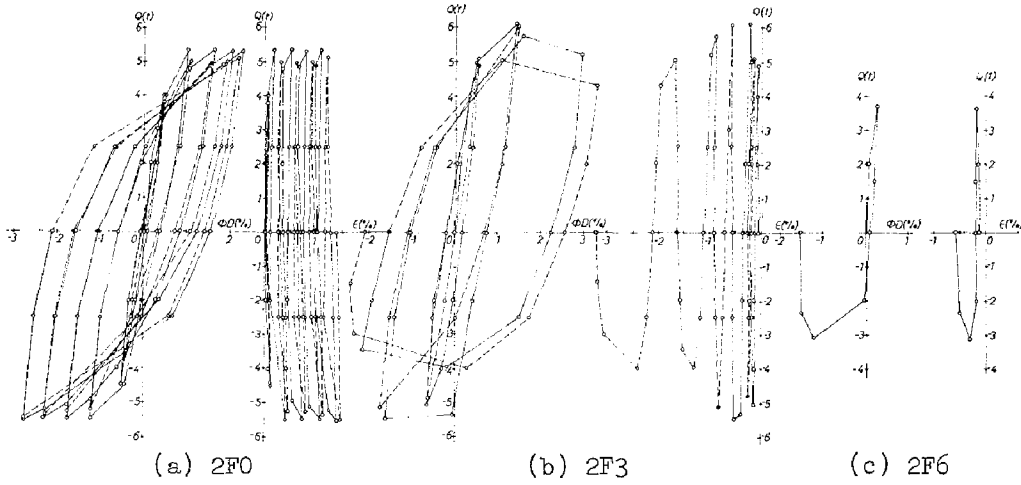


Fig. 12 Curvature and Normal Strain History for Series 2

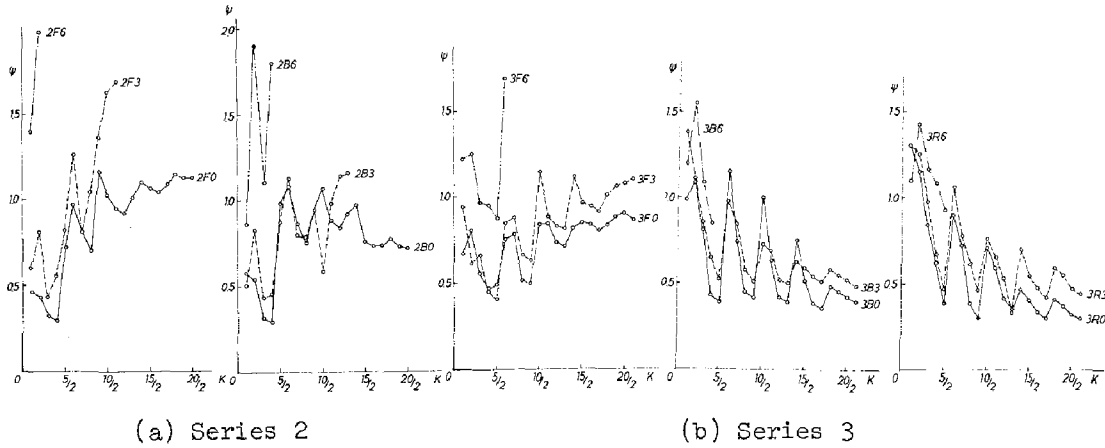


Fig. 13 Specific Damping Capacity

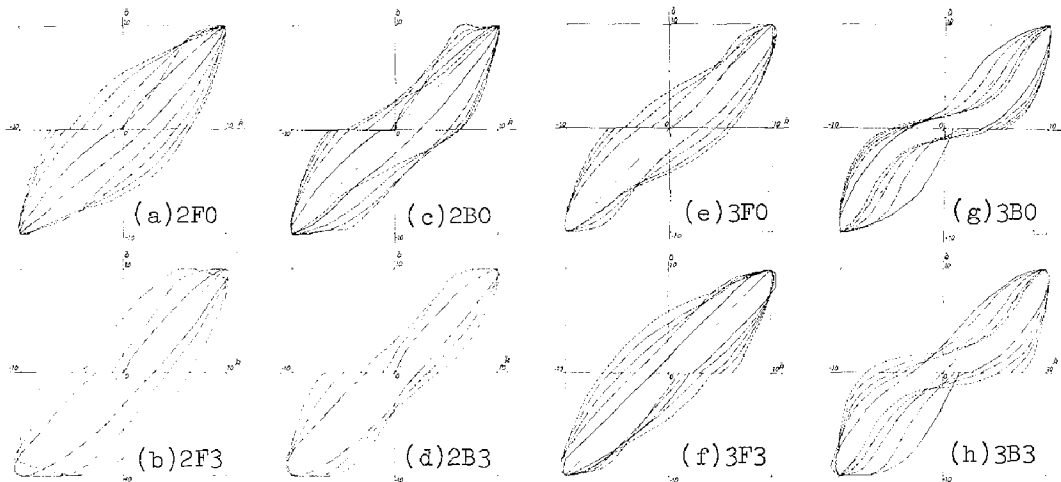


Fig. 14 Normalized Characteristic Loops

columns in Series 2, except those of $n=0.6$, the value of the specific damping capacity increased from 0.70 to 1.20, and for the full-web SRC columns, the value increased from 0.60 to 1.15.

3. 3 Normalized Characteristic loops

Some of the normalized characteristic loops obtained from the tests of column specimens with $n=0$ and 0.3 in Series 2 and 3 are shown in Fig. 14. In the figure, ordinate represents the nondimensionalized load carrying capacity, \bar{Q} , which is the ratio of the load carrying capacity at each loading stage to the maximum strength in the corresponding loading cycle. Abscissa represents the nondimensionalized slope deflection, \bar{R} , which is the ratio of the column slope deflection at each loading stage to the maximum slope deflection of the corresponding loading cycle. For both cases of flexural failure and shear failure, the normalized characteristic loops of the battened-web SRC columns and RC columns had reversed S-shapes and were similar to each other, while the loops of full-web type SRC columns expanded the spindle-like shape with the increase of deformation amplitude and converged to those of pure steel columns, for both cases of flexural failure and shear failure.

4. CONCLUSIONS

Stated below are the conclusions drawn from the experimentally obtained hysteretic characteristics of the SRC columns and frames under well-defined, repeatedly applied loads.

- 1) If the column is subjected to repeatedly applied bending and shear as well as constant axial compression, there are obvious differences in the hysteretic characteristics between SRC columns with full-web steel shapes, those with open-web steel shapes and RC columns, due to the shear deformation in the elastic-plastic region caused by applied shear force and to the shear failure.
- 2) Among the failure modes of SRC and RC members, there is the shear-bond failure besides the ordinary diagonal tension failure and shear-compression failure. In the SRC member that shows the shear-bond failure, the

- bondage strength between concrete and steel flanges can hardly be expected.
- 3) Therefore, the steel section with battened-web in an SRC member has the property equivalent to that of a *Vierendeel member*. Hence the hysteresis loop of an SRC member with usual configuration and dimension containing battened steel section is very similar to that of an RC member, and is of reversed S-shape with very small capability of energy consumption.
 - 4) As to the full-web type SRC member under repeatedly applied bending and shear, the hysteresis loop shows very stable, spindle-like shape with large capability of energy consumption. This is true for both cases of flexural-type and shear-type failures.
 - 5) The deformability of an SRC column containing either full-web or battened-web type steel shape, however, is highly dependent upon the magnitude of the axial compression working on it. When the working axial compression is equal to 60% of the load carrying capacity of centrally loaded column, no ductility shall possibly be expected.
 - 6) The hysteretic characteristics of an SRC frame, in which the column failure is predominant, when subjected to well-defined, alternately applied horizontal load, is very similar to that of a single column member.

ACKNOWLEDGMENT

Research work reported here was a research project supported by a Japanese Government subsidy for promoting scientific researches and conducted by a research group headed by the senior author. Series 1 was tested by Mr. Ryoichi Sasaki of Setsunan University, Series 2 and Series 3 were tested by Mr. Takeshi Nakamura of Kyoto University and the coauthor, and Series 4 was tested by Dr. Chiaki Matsui, Isao Mitani and Kazuo Matsumura of Kyushu University. Authors wish to express sincere appreciations for their contributions.

BIBLIOGRAPHY

- 1) Naka, T., Wakabayashi, M., and Murata, T., : Steel Reinforced Concrete Construction, Preliminary Report, International Association for Bridge and Structural Engineering, Ninth Congress, Amsterdam, May, 1972, pp. 165-172.
- 2) Wakabayashi, M., Naka, T., and Kato, B., : Elasto-Plastic Behavior of Encased Structures, Proceedings of the International Conference on Planning and Design of Tall Buildings, Lehigh University, Bethlehem, Pennsylvania, August, 21-26, 1972, vol. 2, pp. 525-544.
- 3) Wakabayashi, M., : Steel-Reinforced Concrete --- Elastic Plastic Behaviour of Members, Connections and Frames, Proceedings of the National Conference on the Planning and Design of Tall Buildings, vol. 3, Mixed steel-and-Concrete Buildings, Architectural Institute of Japan, August, 1973, pp. 23-26.
- 4) Wakabayashi, M., Shibata, M., Matsui, C. and Minami, K., : A Study on the Behavior of Steel Reinforced Concrete Columns and Frames, Preliminary Report of IABSE-Québec Symposium, Design and Safety of Reinforced Concrete Compression Members, August, 1974, pp. 53-60.

INTERNATIONAL SYMPOSIUM ON
EARTHQUAKE STRUCTURAL ENGINEERING

481

St. Louis, Missouri, USA, August, 1976

STATIC AND DYNAMIC TESTS OF A LARGE-SIZE MODEL OF A
FRAMELESS IN-SITU REINFORCED CONCRETE RESIDENTIAL
BUILDING

Yu. V. BARKOV, Yu. V. GLINA
Dipl. Engineers

TSNIIEP zhylysha
Moscow, USSR

SUMMARY

The report presents the objectives, methods and results of static and dynamic tests of a large-size 10-storey model of a frameless seismic resistant building, built from in-situ reinforced concrete on a natural soil foundation.

Brief description of the model structure and its erection methods is given. The results of the model design considering the actual physical and mechanical characteristics of the structure materials and the yielding of the soil foundation are shown. The joint behaviour of piers and lintels as well as the interaction between the model and its soil foundation at different intensities of horizontal inertia loads applied by means of vibrators is analysed.

INTRODUCTION

The expanding volume of construction of frameless in-situ reinforced concrete public and residential buildings in seismic active zones of the Soviet Union and the increase of their height has required that safe seismic resistance of these buildings should be provided in combination with rational material consumption for supporting structures and, first of all, of reinforcing steel and concrete. The investigations into the behaviour of building structures under the effect of earthquake loads are carried out by the TSNIIEP zhylysha Institute in three directions: theoretical research, tests of fullscale buildings and their structural elements, tests of large-size models.

STATIC AND DYNAMIC TESTS

The tests of a 10-storey model have been aimed at studying the features of actual behaviour of frameless in-situ reinforced concrete buildings under force effects of different nature and intensities and at making more accurate the methods of their design and calculation on these bases, including design schemes at different stages of behaviour. The erection of the model on a natural soil foundation also offered the opportunity to study the interaction between the supporting structure system and soil foundation.

The model presented a section of the building with load bearing transverse and interior longitudinal walls which was built in a scale of one fourth of the natural size of the building (Fig.1). The model dimensions in plan were 3.3m x 3.34 m, the height was 7m. The thickness of walls and floors was 4cm according to the adopted scale of geometrical dimensions.

The areas of in-situ reinforced concrete transverse walls along both sides of an interior longitudinal corridor were joined by in-situ reinforced concrete lintels into transverse load bearing membranes. Horizontal membranes were in-situ reinforced concrete floor slabs. The model foundation was a solid reinforced concrete slab.

The model walls and floors were reinforced with flat welded reinforcing meshes, the lintels - with flat welded reinforcing cages. The principal reinforcement of meshes and cages was made from hot-rolled steel, its design resistance being 2100 kgf/sq.cm.

Preliminary approximated design for the model was carried out as for a full-scale building considering vertical service and horizontal earthquake loads.

The rigidity and dynamic parameters of the system were determined taking into consideration flexure and shear of structures assuming their behaviour being at an elastic stage as well as allowing for foundation yielding at rocking vibrations of the model. The initial characteristics were the modulus of deformation of the model concrete, E_c , being equal to 140,000 kgf/sq.cm, and the coefficient of foundation rigidity, K_f , calculated for the soil of standard compressive strength 2 kgf/sq.cm.

The period of the first tone of rocking vibrations in a transverse direction was 0.195 sec which corresponds to the frequency of 5.1 hertz.

The carrying capacity of the model at an elastic stage was provided, according to the preliminary design, for an earthquake load not less than 8 MSK-64 points.

The moulding of the model structures was carried out by means of metal progressive gang forms. During one cycle, walls or a floor slab for one storey was concreted. As a result of breaks between two adjoining cycles of concreting which amounted to 2-3 days, horizontal construction joints were formed at places of contact with lower and upper planes of floor slabs.

The model was tested by applying horizontal loads -

static and dynamic ones. Separate fragments of the model (walls and lintels) were also statically tested which made it possible to analyse the influence of different structural factors on the behaviour of the system as a whole.

Static tests of the model were carried out by means of a frame-strainer. Horizontal loads were applied at the level of floors. At the end of static tests the value of the total horizontal load was increased up to a half of the design load, i.e. it was equivalent to 7 MSK-64 points in total transverse force, applied at the top level of the foundation slab. At this load value as well as at lower loads, non-linearity of structure deformation was not considerable, indicating their behaviour at an elastic stage.

Dynamic tests were carried out by means of vibrators designed at the TSNIEP zhylyshcha. During dynamic tests the dynamic parameters of the system, including the nature of vibrations, were determined and the nature of joint behaviour of structural elements as well as the interaction between the model and its soil foundation was studied depending upon the intensity of force effect.

Horizontal and vertical displacements of the superstructure, vertical displacements of the foundation slab bottom relative to the ground level and stresses at separate points of the walls were recorded by recording apparatus including vibrometers, tensors and oscillographs.

A vibrator was placed on the top floor of the model.

The first series of tests was carried out by means of a vibrator of low capacity, the second series of tests-with a vibrator of high capacity.

Each series of tests consisted of several stages differing in the value of a horizontal inertia load. The load was increased from stage to stage, its maximum value exceeded the design one by more than three times.

The process of changes in the nature of the interaction between the model structure and its soil foundation can be conditionally divided into three phases. At the first phase the behaviour of all structures was at an elastic stage while the soil under boundary zones of the foundation slab was partially compressed due to elastic-plastic deformations. The initial parts of the charts for rigidity parameters variation correspond to this phase, Fig.3.

The initial part of the chart for rigidity variations of the model has the shape being near to a linear one while that of the charts for rigidity variations of the foundation

and the whole system is curvilinear, which indicates the appearance of the first signs of non-linearity in the behaviour of the system, mainly, due to the soil foundation.

At the second phase, due to crack formation at the abutting of lintels and walls and over the planes of construction joints, non-linear reduction of the system rigidity occurred due to both the soil foundation and the structure. Soil compression under the foundation boundary zones during rocking vibrations of the model continued with the increase of horizontal inertia loads which resulted in the formation and gradual opening of a gap between the foundation and the soil.

At the third phase oblique cracks appeared and developed in the walls of the ground and first floors. With further increase of loading the concrete in the zone of wall and foundation junction failed, and then concrete splintering at the extreme areas of the ground floor walls occurred as well as crack formation in the walls of two lower floors over the whole their surface. The integrity of walls being broken, the deformability of the model greatly increased. This was the major cause that non-linearity in the system behaviour continued to increase even in a greater degree than at the previous phases.

By the moment the inertia load has achieved its maximum value, the first tone frequency of the system natural vibrations, amounting to 5 hertz at the beginning of tests, decreased 2.63 times as compared to the initial one, and the amplitude increased 33 times, as is shown in the charts, Fig.4.

A substantial reduction of rigidity of the model and of the system as a whole changed the nature of dependence between the amplitude and the inertia load: an ascending branch of the curve was replaced by a descending one. This principal change reflected the process when despite the increase of counterweights on the vibrator and the growth of vibration amplitude of the model top, the total inertia force was not already increasing but was decreasing. Such phenomenon was predicted earlier theoretically.

The loss of the carrying capacity by the system occurred due to failure of the model ground floor walls at cyclic loading during which in the boundary zones of piers eccentric tension, which caused concrete failure in piers, alternated with eccentric compression, which led to concrete splintering and buckling of exposed reinforcement.

CONCLUSIONS

1. Construction joints in walls, being formed following the breaks in concreting at cyclic erection of walls and floors, contributed to deformability increase of in-situ load bearing structures of the model. The same joints in the lower floors of the model were the zones of local damage (cracks).

2. Lintels were the most vulnerable elements of the frameless in-situ reinforced concrete model. The first cracks appeared in lintels earlier than in other elements of the structure.

3. Non-linearity in the behaviour of the whole system increased with the growth of horizontal inertia loads. The degree of non-linearity influence in the behaviour of the foundation or the model structure varied due to the irregular development of non-elastic processes in them depending upon the value of horizontal inertia loads.

4. As regards the load bearing capacity, the limit state of the "building-soil foundation" system can depend upon the fact whether the carrying capacity of superstructure or foundation is exhausted, depending upon their rigidity parameter relationship.

The authors express their deep acknowledgement to their scientific adviser Prof. G.A.Shapiro, D.Sc.(Eng.), and to all researchers of the Strength Test Laboratory of the TSNIIEP zhylishcha working under his guidance, who took part in conducting model tests and treatment of test results.

REFERENCES

1. Ashkinadze G.N., eng. Recommendations for the Methods of Vibration Tests and Determination of Residential Building Parameters for the Design of Vibrations and Horizontal Loads. Moskva, TSNIIEP zhylishcha, 1972.

2. Prof. Drozdov P.F., D.Sc.(Eng.); Sebekin I.M., Cand. Sc.(Eng.). Design of Large-Panel Buildings (Framed and Frameless). Moskva, Stroyizdat, 1967.

3. SNiP II-A.12-69. Construction in Seismic Regions. Design Code of Practice.

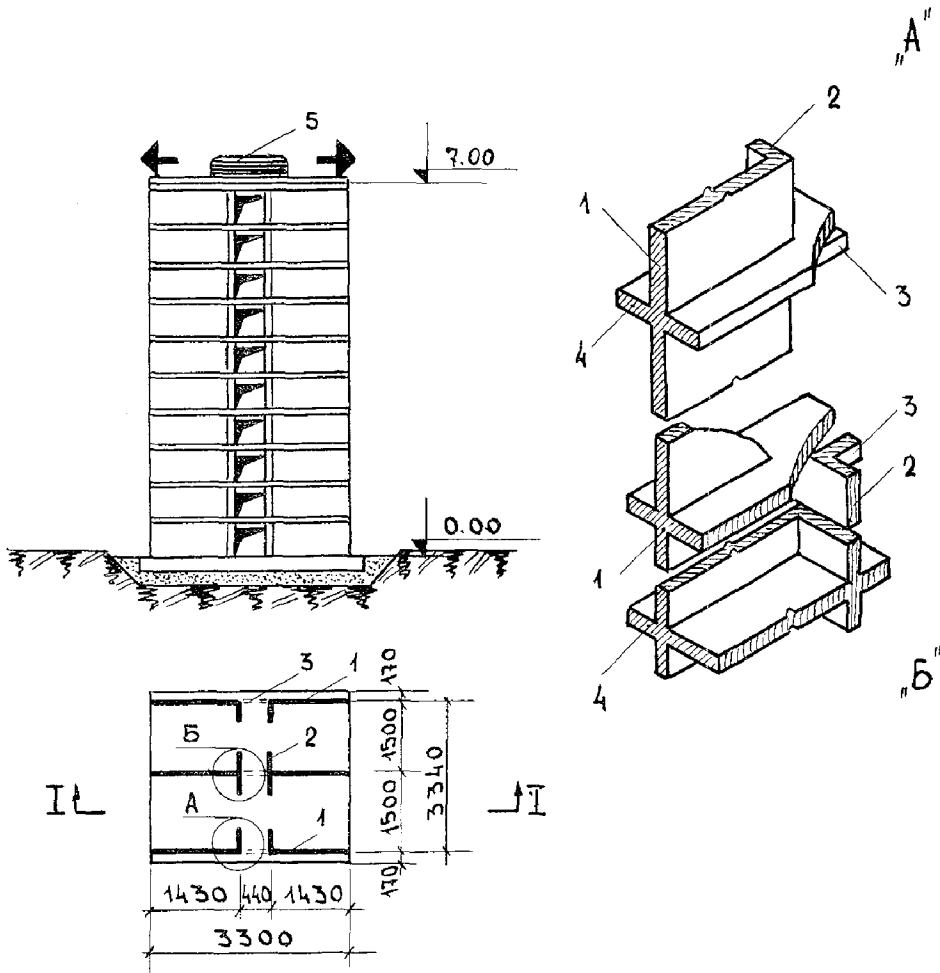


Fig. 1. General view and structural nodes of the model
 1-transverse walls,
 2-longitudinal walls,
 3-lintels,
 4-floors.

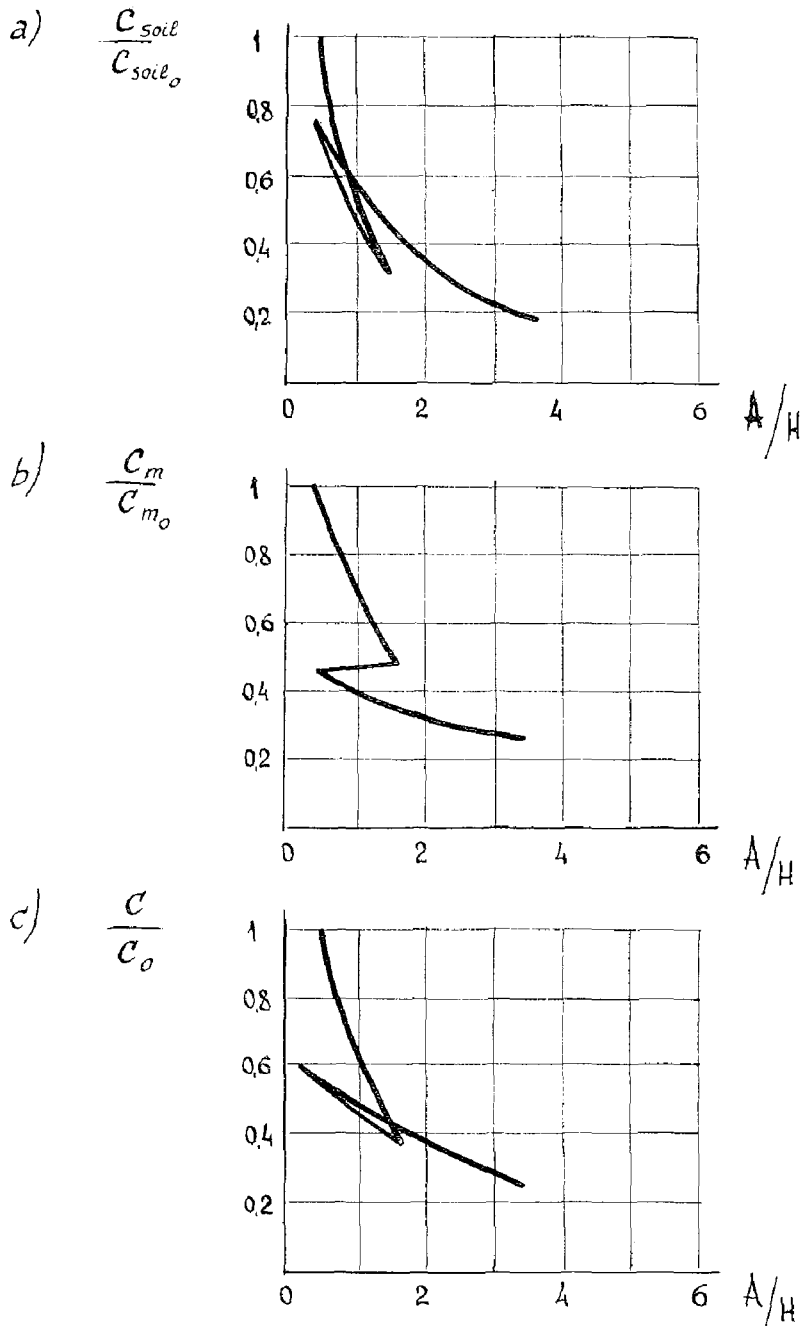


Fig. 2. Charts for rigity parameter variations of the system: a - soil, b - model, c - „model-soil“ system.

C_{soil}, C_m, C - rigidities of the soil, the model and a generalised rigidity of the „model-soil“ system;
 C_{soil_0}, C_{m_0}, C_0 - their initial values, respectively;
 A - amplitude of the model top;
 H - model height.

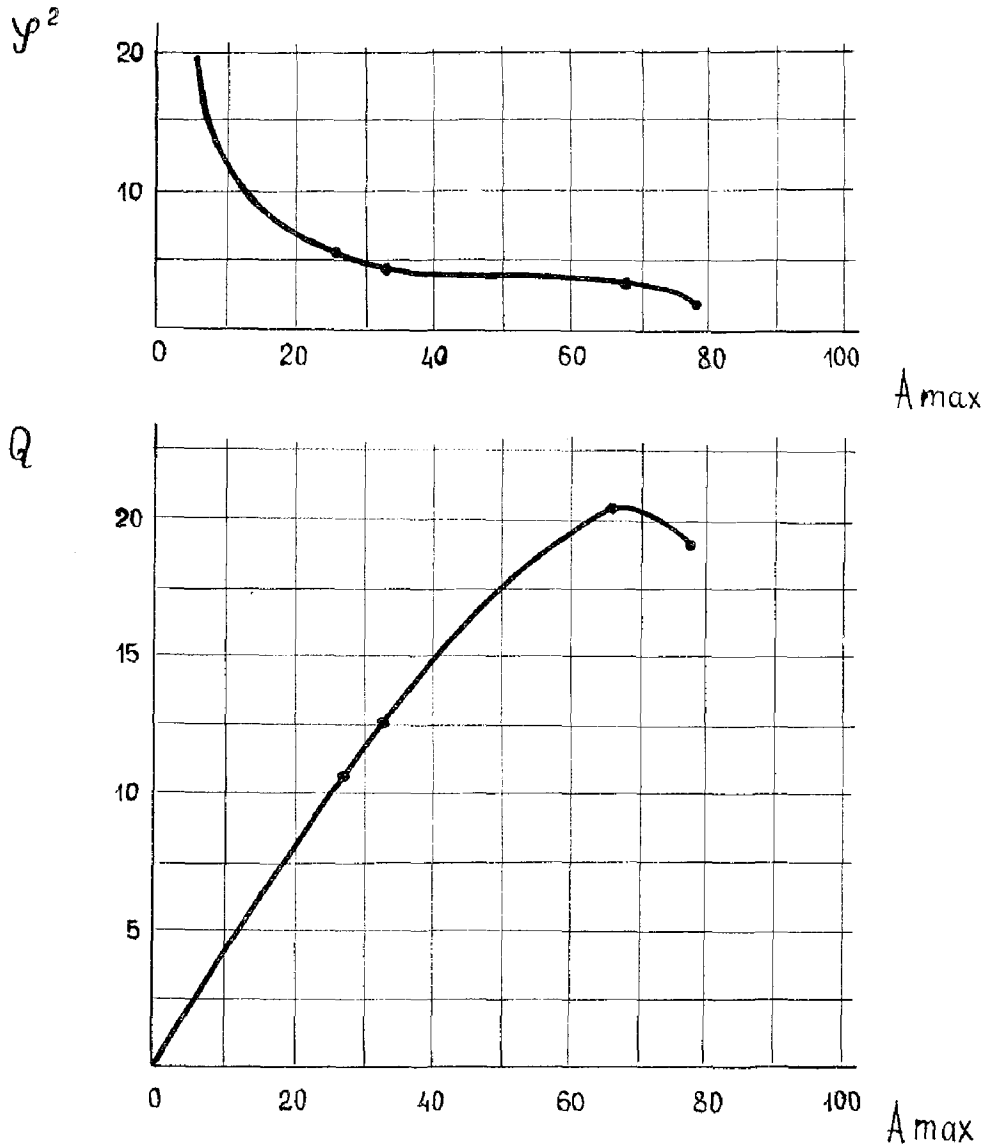


Fig. 3. Relationship between $\varphi^2 - A_{max}$ and $Q - A_{max}$.

φ - resonance frequency of vibrations;
 A_{max} - amplitude of vibrations of the model top;
 Q - total inertia force acting in soil foundation.

INTERNATIONAL SYMPOSIUM ON
EARTHQUAKE STRUCTURAL ENGINEERING

489

St. Louis, Missouri, USA, August, 1976

EXPERIMENTAL STUDY ON REINFORCED CONCRETE TRUSS
FRAMES AS EARTHQUAKE RESISTANCE ELEMENTS

by

TAKAYUKI SHIMAZU

Assoc.Prof. University of Hiroshima, Hiroshima,
Japan

and

YASUHIRO FUKUHARA

Assis.Prof. Technical College of Kure, Hiroshima,
Japan

SUMMARY

More than twenty of one-storied and one-spanned reinforced concrete braced frames with small size, were tested, subjected to alternating repeated horizontal loads at the top beam level with constant axial load at the two tops of the columns. These tests were intended for obtaining some basic data on earthquake resistance capacities of reinforced concrete truss frames.

The variables considered in this investigation are the slenderness of the members composing a frame, the longitudinal reinforcement ratios of the members, the level of axial load and the reinforcement arrangements in connections.

The test results show that braced frames have considerable ductility in addition to high stiffness and high strength.

INTRODUCTION

In such countries having the large temporary load (seismic load) as Japan, it is necessary to have such strong members or frames which can resist against the above load as earthquake resistance walls. The objective of this paper is to review recent research⁽²⁾ carried out at Hiroshima University and to use

these results to provide a means of determining seismic design for truss frames of reinforced concrete, including braced frames which can be arranged more freely in buildings than walls.

TEST PROGRAM

Two series of tests have been conducted. Usual reinforcement arrangements were used at connections of braced frames in the Series A, while special arrangements were made in the Series B as shown in Fig.1.

1) Series A: A specimen consists of two symmetrical braced frames, the size of which is about one-fifth - tenth of prototype with the dimensions of the height, the span of frames and the standard section of members being 60cm, 60cm and 10cm x 10cm respectively. Seventeen frames were tested in total as shown in Table 1. Five frames (I) including one rahmen frame were subjected to monotonic horizontal load at beam level while eight frames (II, and III) subjected to alternating reversed horizontal load. The other three frames (N) were subjected to alternating reversed horizontal load, with constant vertical loads at the tops of columns. Only the specimens designated B-H and B-Hp have the members of non-standard sections (5cm x 10cm). The reinforcement ratio of main bars ranged from about 1 - 3.8 %, with the hoop reinforcement ratio being about 0.1 % and 0.2 % for the members having standard section and non-standard section respectively. Much more amount of hoops were, on the other hand, used to enclose main bars in connections against anchor failure except for five frames (I) of monotonic loading as shown in Fig.1. Maximum size of aggregate of concrete was 5 mm and the cylinder strength at test was 0.21 - 0.23 t/cm². Main bars were 6 ϕ with yield strength of about 2.70 t/cm² except for two frames (4.65 t/cm² for B-I, R-I). Hoops were 2 ϕ . Horizontal displacement at beam level as well as elongation of each member and strains of main bars embedded were measured by dial gauges and wire strain gauges respectively.

2) Series B : Six frames including a wall and a rahmen were subjected to alternating reversed horizontal loads with constant vertical loads at the tops of columns except for the specimen of B-H-I without vertical loads. Structural round bars SR 35 (9 ϕ) were used as main bars with special arrangements in connections as shown in Fig.1 (d) and (e). Loading and measuring methods as well as materials were nearly the same as in the Series A.

TEST RESULTS

In Table 2 are listed up the results of tests on strength. In Figs.3 - 8 , are shown typical load-deflection curves and failure patterns. Based on the results of 23 tests, the following trend were observed:

1) The stiffness before crack can be estimated for braced frames, by assuming every connection as a pin-joint and both concrete and main bars in every member as linearly effective. The calculated value as rigid joint is only 6% higher even for the specimens with the depth to length ratio of 5 than that as pin-joint.(Fig. 9).

2) First cracks were observed at the bottom of column subjected to tension. The stress at first crack is about 0.08 - 0.125 F_c (F_c ; cylinder strength),obtained by assuming as rigid joints. The deflection (ratio to height) at first crack is about 0.15 mm (0.25×10^{-3} rad.) for the specimens without axial loads and about 0.30 mm (0.5×10^{-3} rad.) for the specimens with axial load of 40 kg/cm².(Table 2 and Fig.10).

3) The yielding load is 14 - 40 % higher for the specimens (II,III and N) of the Series A except for the I type specimens,than that calculated by assuming every connection as a pin-joint and all main bars in tension members as yielding, that means that yielding strength is proportional to the reinforcement ratios of main bars. These percentage can be attributed mainly to bending and shear resistances of compression

members. The deflection (ratio to height) at yielding load is about 1.5 - 2.1 mm ($2.5 - 3.6 \times 10^{-3}$ rad.), increasing with main bar reinforcement ratios and with axial loads (Table 2).

4) The I type specimens in the Series A failed at connections before or about reaching the yielding strength calculated as pin-joints. The specimens of braced frames in the Series B, on the other hand, failed at compression members. For the former, being preliminary test specimens, the failure at connections might be able to be avoided if projecting parts were made at loading points in the same way as the specimens (II, III and N), but test results indicate, at the same time, that some amount of hoops are needed to prevent the breaking out of main bars in connections. The cause of the premature failures for the latter will be explained below. (Table 2, Fig. 1)

5) The specimens (II, III and N) in the Series A hold the load higher than the yielding load calculated as pin-joints, up to the deformation angle of frames (ratio of deflection to height) of 1/50, except for the specimens of B-3-N. It should be noted that truss frames of reinforced concrete have considerable ductility, compared with shear walls, usually having the deformation angle of only 1/250 at ultimate. This can be inferred from the fact that the members composing truss frames have much larger ratio of length to depth than walls (Fig. 12).

6) It is found desirable for braced frames having the members with little amount of hoops to obtain sufficient ductility, that axial force (ratio to cylinder strength times concrete area) of the compression members at the yielding load, calculated as pin-joints mentioned above, is below 0.4, which is the axial force level at balanced point in axial force - moment diagram, although there were the ductile specimens having the members with the axial force ratio of more than 0.4 (B-2-N and B-3-II). It is also clarified that maximum shear stress (nominal) for the members of braced frames should be

within $0.1 F_c$ (F_c = cylinder strength⁽¹⁾) to obtain sufficient ductility. (Figs. 13,14 and 15)

7) The column of B-H-II specimen failed in buckling, shortly after the negative horizontal load following unloading at the deformation angle of $1/40$ in the positive loading were applied. The load of this specimen was not well recovered even at the reversal of small deflection. The scale of the specimen leaves room for discussion but members with the length to depth ratio of more than 10 seem undesirable for truss frames.

8) Simpler anchor methods(one bolting or plate welding) in connections than usual arrangements were tested. These specimens failed at compression members below the yielding load calculated as pin-joints because of the axial force ratios' being far beyond 0.4 for compression members at yielding load, although main bars of larger diameter than in the Series A were used. It is, however, found that braced frames have higher resistance capacities than walls having the same volume of concrete and reinforcements (Fig. 8)

CONCLUSIONS

The main conclusions of these experimental studies are as follows; The truss frames of reinforced concrete including braced frames can be considerably ductile in addition to high stiffness and high strength if much care is taken of the both compression members and connections. Further researches are needed on practical simple anchor methods in connections.

BIBLIOGRAPHY

(1) Morrow, J., et al, " Shear Strength of Reinforced Concrete Frame Members Without Web Reinforcement", Journal of A. C. I. No. 10 Vol. 28 Apr. 1957.

(2) Shimazu, T., " Ultimate Strength of Reinforced Concrete Truss Frames" 18th National Sym. on Bridge and Structural Engineering, 1972 pp 113 - 122.

TABLE 1 PROPERTIES OF SPECIMENS

Series	Symbols of Specimens		Section of Members				Axial Stress Applied (kg/cm ²)	
			Columns and Bracings		Beams			
	Kind ¹⁾	Type ²⁾	b×D (cm ²)	Pg (%)	b×D (cm ²)	Pg (%)		
A	B-H	I	10 × 5	2.07	10 × 5	2.07	0	
		II						
	B-Hp	I	Column	10×10	1.03	10 × 10	1.03	0
		II	Bracing	10×5	2.07			
	B-I	I	10 × 10		0.96	10 × 10	0.96	0
		II			1.03			
		III						
		N						
	B-2	I	10 × 10		1.93	10 × 10	0.96	0
		II			2.07			
		III						
		N						
	B-3	I	10 × 10	3.86	10 × 10	1.03	0	
		II	13 × 10	3.18	13 × 10	0.80		
III								
N		40						
R	I	10 × 10	0.96	10 × 10	0.96	0		
B	B-H	I	7 × 7	4.16	7 × 7	4.16	0	
		II					40	
	B-Hp	I	Columns	10×10	2.08	10 × 10	2.08	40
		II	Bracings	7×7	4.18			
	W	I	Frame bD=10×10, Pg=2.08%		Plate t=2.5cm, Pw=1.26%		40	
R	I	10 × 10	2.08	10 × 10	2.08	40		

Note 1) B=Braced Frame R=Rahmen W=Wall

2) See Fig. 1 for Braced Frames

TABLE 2 RESULTS OF TESTS

Series	Symbols of Specimens		First Crack		Yield Load			Maximum Load			
			Load	Deflection	Load	1) Ratio to Calculated Value	Deflection	Load	1) Ratio to Calculated Value	Deflection	
	Kind	Ty.	(ton)	(mm)	(ton)		(mm)	(ton)		(mm)	
A	B-H	I	3.0	0.14	7.0	0.73	1.5	8	0.83	4.0	
		II	2.6	0.12	11.0	1.14	1.6	12.8	1.33	1.7	
	B-Hp	I	3.5	0.14	9.0	0.94	1.5	9.8	1.02	4.0	
		II	3.5	0.16	13.0	1.36	1.6	13.7	1.42	2.2	
	B-1	I	5.0	0.15	16.0	1.05	2.1	16.0	1.05	3.0	
		II	5.5	0.14	13.5	1.40	1.6	13.7	1.43	5.0	
		III	6.0	0.16	13.2	1.38	1.7	13.7	1.43	3.0	
		N	12.0	0.3	24.0	1.36	1.7	24.0	1.36	1.8	
	B-2	I	5.5	0.14	18.0	0.92	1.8	23.0	1.17	6.0	
		II	7.0	0.16	25.0	1.30	1.9	26.0	1.35	3.5	
		III	6.0	0.14	23.0	1.19	1.9	23.3	1.21	4.5	
		N	16.0	0.3	35.0	1.28	1.9	36.0	1.32	2.1	
	B-3	I	7.0	0.16	36.0	0.96	2.2	40.0	1.06	3.6	
		II	8.5	0.17	46.0	1.19	2.1	48.0	1.25	7.0	
		III	10.0	0.14	45.0	1.17	2.0	47.7	1.24	7.5	
		N	21.0	0.3	60.0	1.22	2.1	60.0	1.22	2.2	
	R	I	0.9	0.13	2.3	0.92	4.0	3.27	1.31	12.0	
	B	B-H	I	8.0	0.2	18.0	0.56	1.0	—	—	—
			II	8.0	0.19	26.0	0.82	3.6	27.5	0.86	9.4
		B-Hp	I	12.0	0.30	30.0	0.85	3.9	32.2	0.89	7.1
II			12.0	0.30	29.5	0.81	3.7	31.0	0.86	4.8	
W		I	8.0	0.2	18.0	1.18	1.4	22.5	0.48	2.9	
R		I	2.0	0.14	4.5	1.37	2.0	5.7	1.73	2.6	

Note 1) Calculated values for braced frames were obtained by assuming every connection as a pin-joint and all main bars in tension members as yielding.

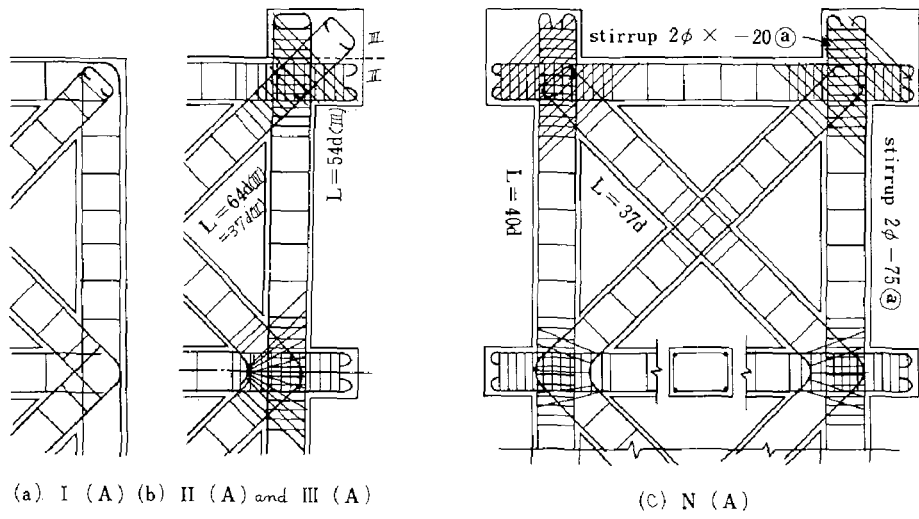


Fig. 1 Reinforcement Arrangements for Test Specimens

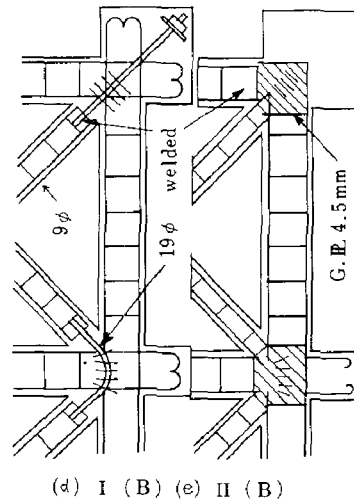
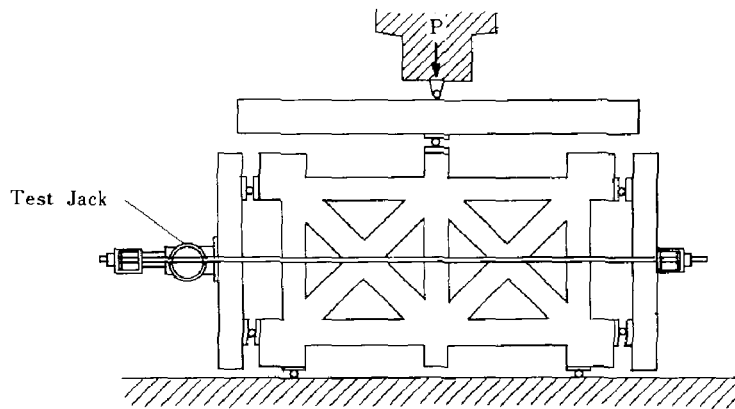


Fig. 2 Test Set-up



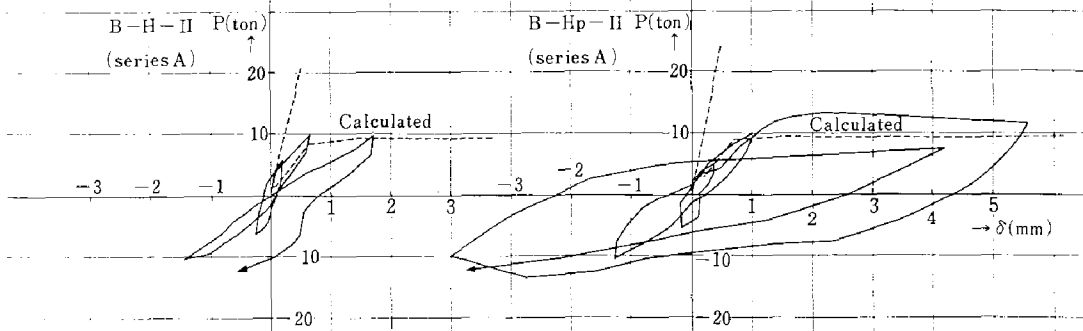


Fig. 3 Load-Deflection Curves (B-H-II, B-HP-II)

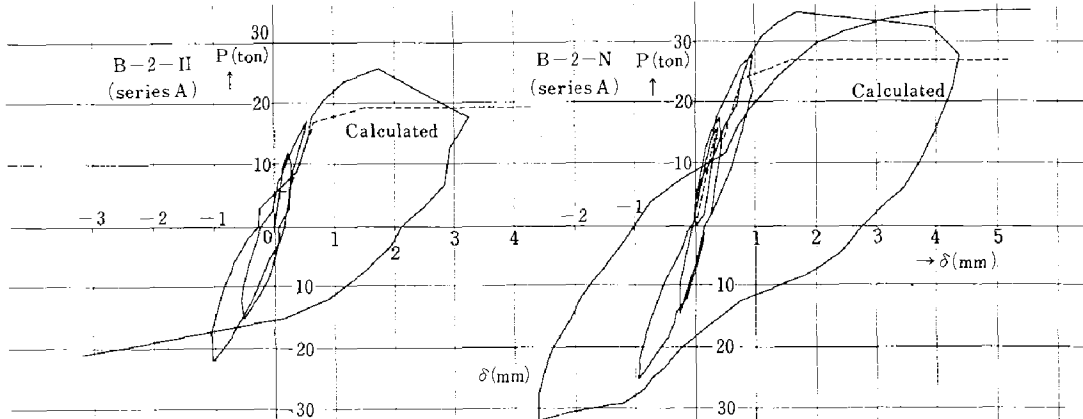


Fig. 4 Load-Deflection Curves (B-2-II, B-2-N)

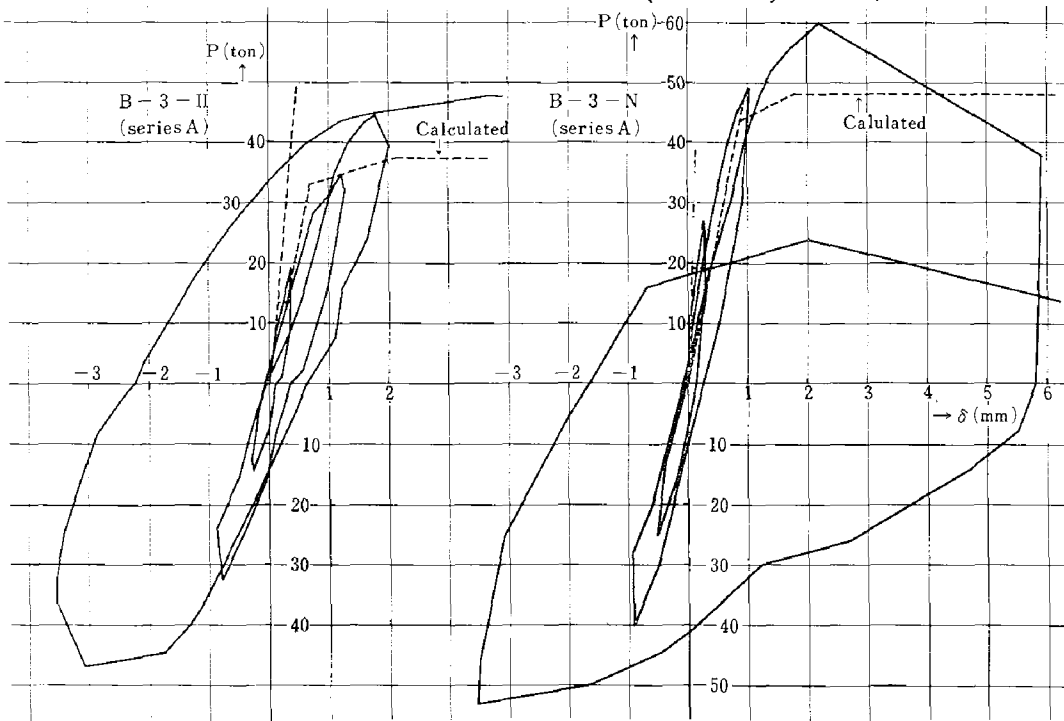


Fig. 5 Load-Deflection Curves (B-3-II, B-3-N)

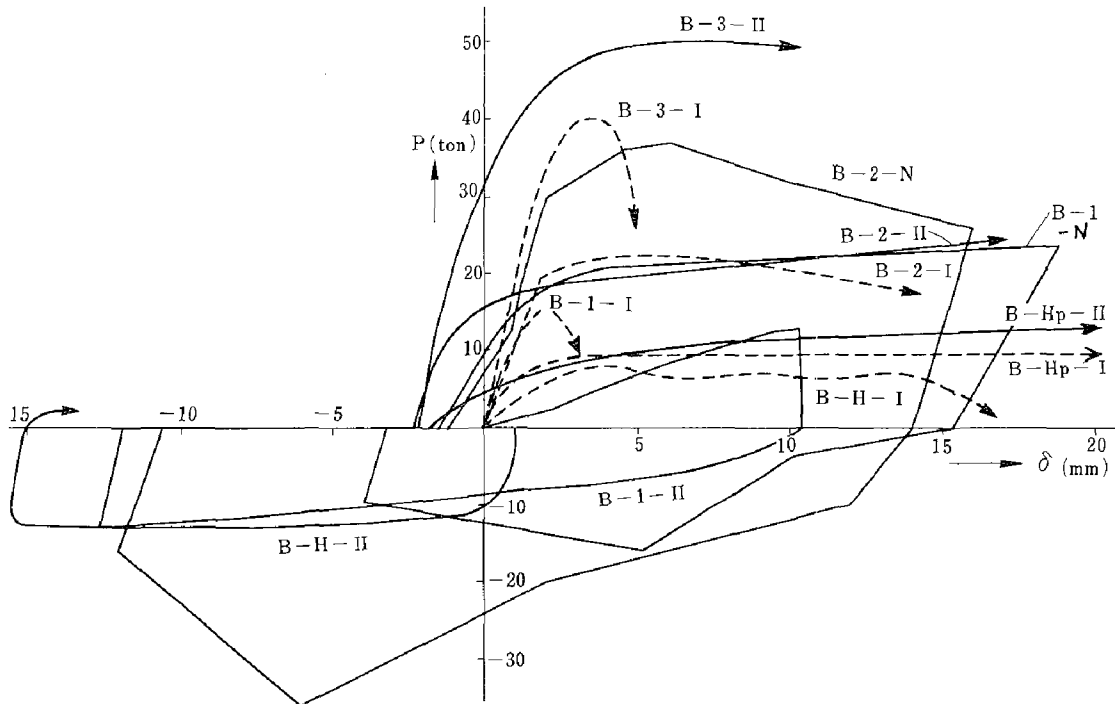


Fig.6 Load-Deflection Curves(in the Range of Large Deflection)

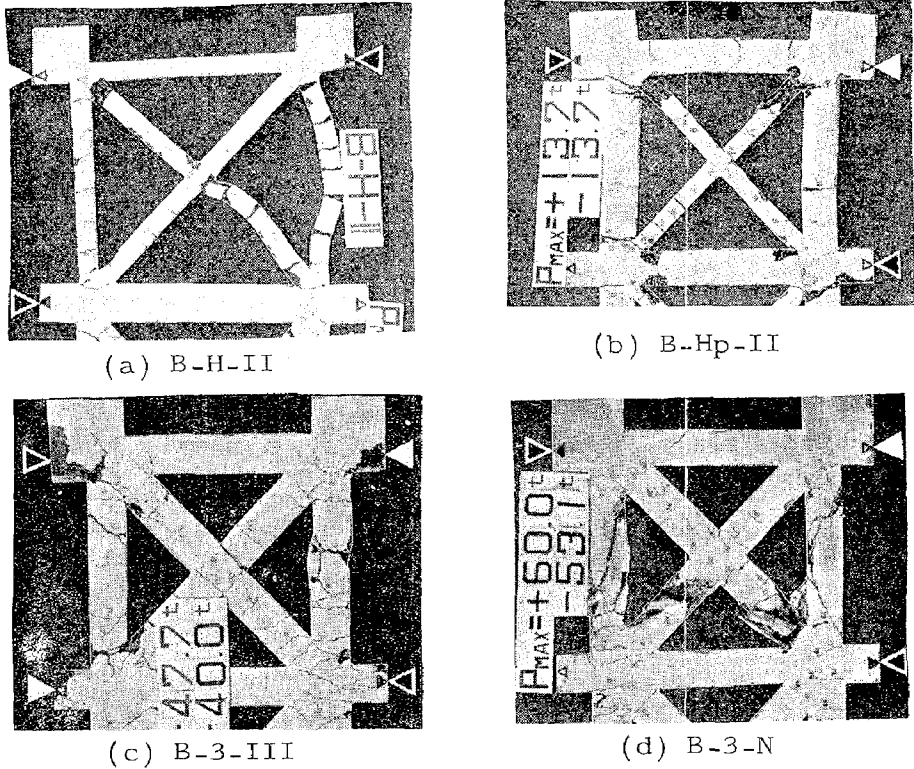


Fig.7 Failure Patterns

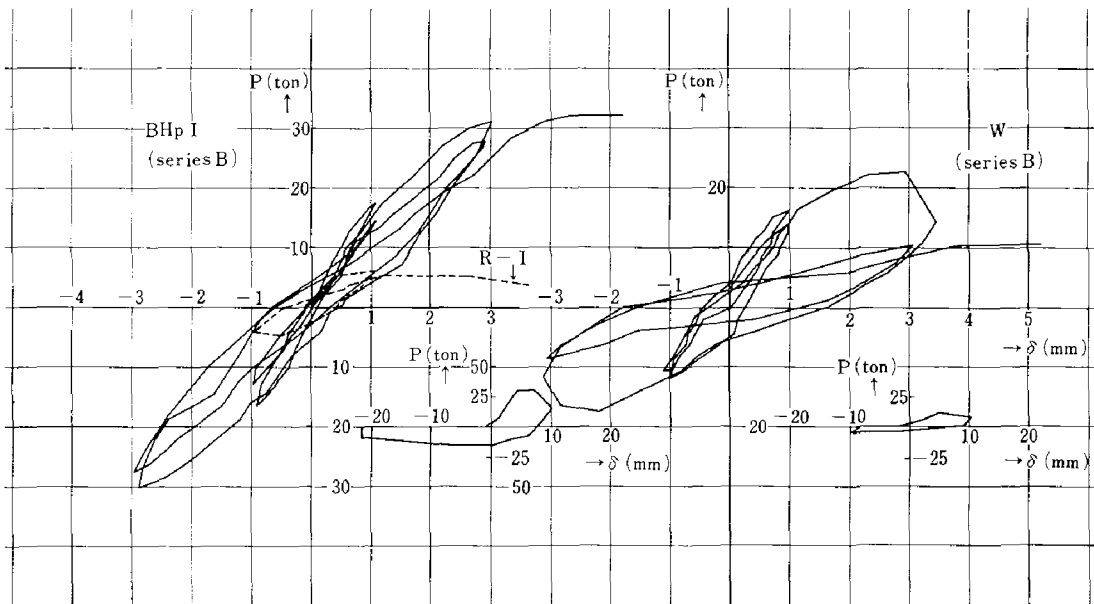


Fig. 8 Load-Deflection Curves (B-HP-I, W-1, Series B)

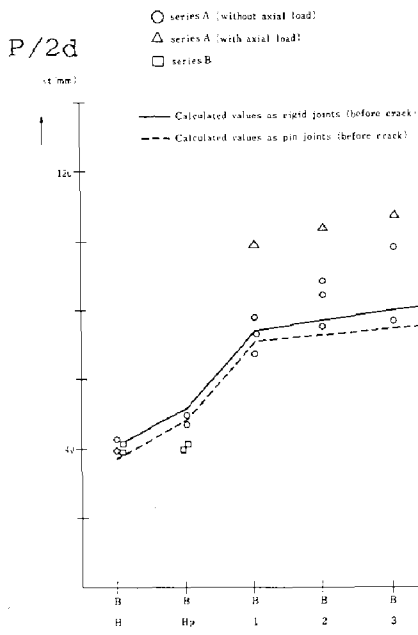


Fig.9 Stiffness Before Crack

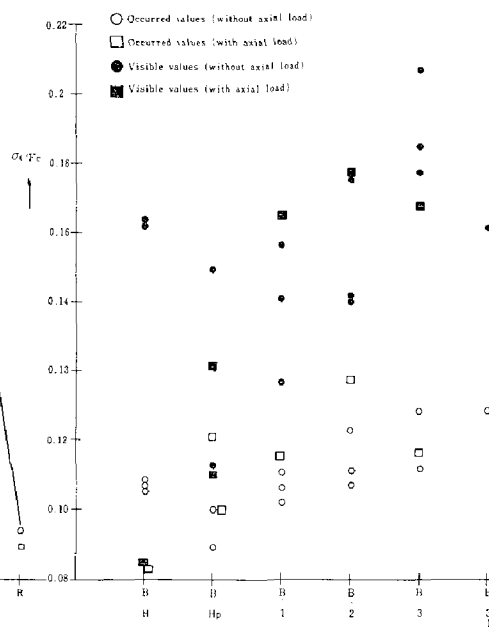


Fig.10 First Crack Stresses

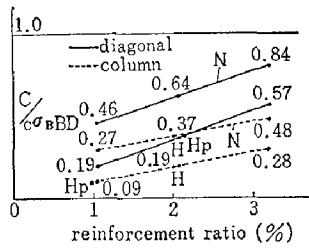


Fig. 11 Axial Force Ratio of Both Compression Members at Ultimate

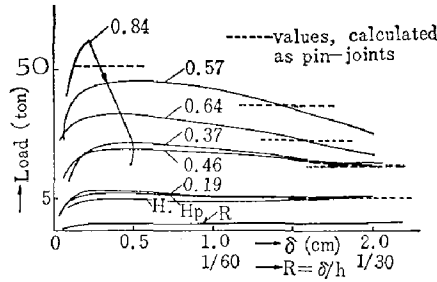


Fig. 12 Envelope Curves of Braced Frames at Ultimate

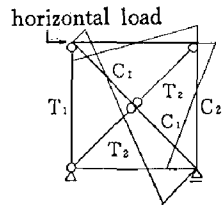


Fig. 13 Resistance Mechanism at Ultimate

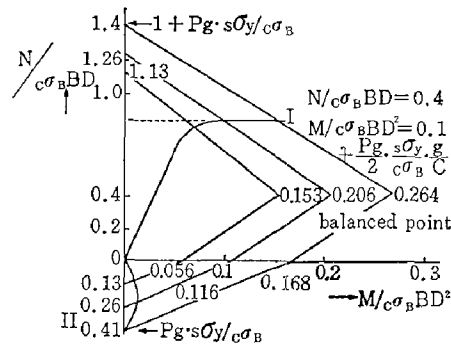


Fig. 14 Bending Capacities of Members Sections at Ultimate

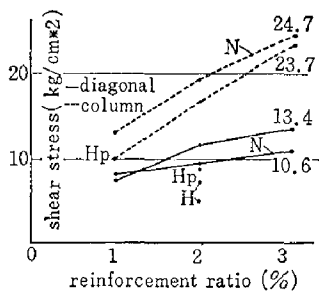


Fig. 15 Shear Stresses of Members at Ultimate

DUCTILE BEHAVIOUR OF COUPLED SHEAR WALLS
SUBJECTED TO REVERSED CYCLIC LOADING

A.R.SANTHAKUMAR

Lecturer in Civil Engineering
College of Engineering, Guindy
Madras, India.

SUMMARY

The behaviour of two quarter full size seven storey reinforced concrete coupled shear walls, with conventionally and diagonally reinforced coupling beams, subjected to static reversed cyclic loading to simulate seismic effects, is compared in terms of stiffness degradation, ductilities attained and energy absorption capacity. In the walls coupled by conventionally reinforced coupling beams, the sliding shear failure of the beams limits the energy absorption capacity of the structure. In every respect the superior performance of the structure containing diagonally reinforced beams is established. The use of ductile diagonally reinforced coupling beams enabled a considerable portion of the total energy to be dissipated by the coupling system thereby relieving plastic hinges in the walls. The results show that with careful detailing, coupled shear wall structures can be made to possess all the desirable features of an effective earthquake resistant structure.

INTRODUCTION

In many tall buildings coupled shear walls provide the required stiffness and strength to resist lateral loads resulting from gravity, wind and earthquake effects. The fundamental behaviour of the typical coupled shear wall structures has been identified in numerous studies (5,7,8 and 9). It is now recognised that it is not economical to resist forces generated by seismic disturbances within the elastic range of behaviour. Therefore, for most earthquake resistant structures ductile behaviour is an essential prerequisite. Building codes (1,4) generally require the shear walls to be designed for resisting larger equivalent lateral forces compared to the rigid jointed frames of identical fundamental periods of vibration.

However, definite experimental evidence (6) is now available to show that carefully designed and detailed shear walls can be made to behave in a ductile manner. This paper reports briefly the results of this investigation (3).

Quarter full size shear wall models (Figures 1) one with conventionally reinforced beams and the other with diagonally reinforced spandrels, were subjected to high intensity alternating cyclic loading simulating seismic effects. The reinforcements in the walls of both these specimens were identical.

Both the walls were designed in such a way that yielding could be expected to occur at the base of the walls only after all the coupling beams had yielded. This was in accordance with the sequence of plastification desired in a proto type structure where the designer would wish to protect the walls against permanent damage (2). Lateral point loads of equal intensity were applied at the 3rd, 5th and 7th floors in alternate directions. This simulated a triangular distributed load commonly used in building codes (1,4). Some of the load was limited to produce stresses within the elastic range, but generally large yielding was imposed upon the structure in a cyclic fashion.

For convenience the models were tested in a horizontal position. As Figure 2 shows wall B was attached to a steel truss which provided the base fixity required. In the background is wall A which was erected after destruction.

LOAD-DISPLACEMENT RELATIONSHIPS

The most revealing comparison of the two structures can be made by studying the load-displacement relationships obtained during the test for each model. Figure 3, giving the deflection at the top floor level of Wall A with conventional beams, shows that considerable ductility was attained with little loss of strength during cyclic loading. However, the pinching of the hysteresis loops, characteristic of the breakdown of shear resisting mechanisms in reinforced concrete members, and the loss of overall stiffness are evident.

Figure 4 presents the load-roof deflection relationship for Wall B with diagonally reinforced coupling beams. It shows convincingly the superior performance of this structure. The hysteresis loops not only show large ductilities with no loss of strength but also indicate the stable characteristics of a ductile steel structure.

When the difference in the responses of the two test structures are examined it becomes evident that the pinching in the hysteresis loops, i.e., the inferior energy absorption capacity, of Wall A results from the inferior performance of conventionally reinforced coupling beams.

It is inevitable that with each excursion past yield some damage occurs in a reinforced concrete structure. The damage and the consequent loss of stiffness of each of the components in a coupled shear wall will determine the overall structural stiffness. A progressive softening, as a result of high intensity cyclic loading, particularly at low levels of loading, may lead to undesirable dynamic response during certain instants of the seismic excitation.

It is desirable therefore to design and detail the structure in such a way that a reasonable stability in stiffness is ensured. As the reinforcing of all the walls of the two test specimens were the same, the degradation of overall stiffness during similar load cycles can be attributed to the performance of the coupling beams.

DUCTILITIES ATTAINED

The displacement ductility with respect to the top floor level of the test specimens is defined in Figure 5a. The displacement ductility in the first load cycle is $\mu_1 = \Delta_1/\Delta_y$. In the second and third load cycles the imposed ductilities may be defined as $\mu_2 = \Delta_2/\Delta_y$ and $\mu_3 = \Delta_3/\Delta_y$ respectively.

Displacement ductilities, that correspond with positive or negative (reversed) loadings, are plotted for each of the two test specimens in Figure 5b. The peak loads, associated with the maximum ductilities imposed in the "plastic" cycles, are also recorded. It is seen that cycles 5 and 9 are the first high intensity cycles for Walls A and B respectively. In both walls the imposed ductilities in the final cycles were of the order of 10 to 15. The ductility in Wall B during the final cycle would have been much larger had an unexpected buckling failure at ground floor level not occurred.

To demonstrate once more the ability of these coupled shear walls to be ductile Figure 5c is presented. In this the maximum static load sustained is plotted against the cumulative ductility as the test loading progressed. Because of the strain hardening of the reinforcement, for which no allowance was made in the prediction of the ultimate load capacity $P_U^*(A)$ and $P_U^*(B)$ of the models, upto 18% higher loads were attained in the tests. According to the Code definition of "adequate" ductility the minimum cumulative ductility required in each direction is $4 \times 4 = 16$ with a strength loss of not more than 20%. Figure 5b shows that the superior wall suffered negligible loss of strength while twice the minimum cumulative ductility (i.e. $2 \times 16 = 32$) was imposed upon it. This demonstrates a remarkable performance for a reinforced concrete structure. It suggests that carefully detailed ductile coupled shear walls are likely to offer the highest degree of protection against both moderate and very large seismic disturbances.

ENERGY ABSORPTION PROPERTIES

The term "ductility", discussed in the previous section, is generally used to indicate the overall energy absorption capacity of the structure. However, in real structures this evaluation is incorrect, for there is no allowance made in it for the possible loss of strength and the degradation of stiffness, both of which will reduce the ability to dissipate energy.

To quantify the energy absorption characteristics the total energy E , absorbed by the models, was expressed in terms of the base shear P and the top floor displacement Δ , based on an assumed linear deflection profile of the walls as shown in insert of Figure 6.

Numerous measurements showed that nearly the entire lateral wall deflection resulted from elastic and plastic deformations near the base and that above first floor level the walls remained practically straight.

The energy absorbed by the model is thus:

$E = 0.70 \times$ area enclosed by the hysteresis loops of Figure 3 and Figure 4 for Walls A and B respectively.

The factor 0.70 has been introduced to take into account the work done by the resultant force P at fifth floor level.

Figure 6 shows the relationship between the cumulative energy absorbed and the cumulative displacement ductility for each of the models which appears to be linear. During the final cycles the energy absorbed up to the maximum loads attained, and the estimated energy recovery were considered to assess the cumulative energy dissipated. The figure shows that for the same cumulative displacement ductility the energy absorbed by wall B is nearly twice as much as that by Wall A.

ENERGY DISSIPATION BY THE COMPONENTS OF WALL B

Extensive strain and displacement measurement at all stages of the loading of model Wall B enabled the approximate evaluation of the energies stored during the elastic part of the response and also the energies dissipated by the components during postelastic deformations. The total energy absorbed at any stage of the loading E may be expressed as the sum of the energies absorbed by the coupling beams E_p and by the Walls E_w . In each of these two sets of components the energy absorbed may be divided into two parts. One originates from energy stored during the elastic range of behaviour. i.e. E_{pe} and E_{we} , and the other is the energy dissipated during excursions into the plastic range of deformation, i.e. E_{bp} and E_{wp} .

For a typical elasto-plastic load cycle (such as cycle 9 shown in Figure 4), the four energy components defined above, are shown in separate bands in Figure 7. A detailed analysis for obtaining these energy components has been reported elsewhere (8). For convenience the energy absorbed by the structure at any load is expressed as a percentage of the total energy absorbed at the attainment of the theoretical ultimate load P_u^* . The load is shown as a fraction of the theoretical ultimate value. The energy stored during the elastic part of the response and the energy dissipated through plastic deformations are separated into two

broad bands. The total energy absorbed by the model structure was obtained from the area under the load-deflection curve for cycle 9 given in Figure 4. As expected, this was a little larger than the sum of the four energy components derived independently. This is because the energy absorption due to axial and shear forces in the walls and anchorage displacements at foundation level were not included. The major part of the energy absorption due to these causes, denoted in Figure 7 as "others", is likely to be irrecoverable. It was found to be less than 10% of the total energy at any stage of the loading. Figure 7 reveals that at the onset of yielding in the walls 20% of the energy was already dissipated, mainly by the coupling beams. The dissipation due to plastic distortions increased to over 30% when the theoretical ultimate load was reached. At the maximum load attained in this cycle, corresponding with a displacement ductility factor of 2, over 60% of the total energy was dissipated and this dissipated energy was over 150% of the total energy absorbed at the theoretical ultimate load. It is also seen that the major source of the energy dissipation till the attainment of over 110% of the theoretical strength of the structure originated from the coupling system and not from the walls. This must be considered as a desirable feature of the elasto-plastic behaviour.

ENERGY - STIFFNESS CONSTANT

The energy absorption capacity E may be computed as explained previously. To evaluate quantitatively the loss of stiffness during progressive cyclic loading, the load sustained by each of the models in the corresponding cycles at a displacement equal to twice the theoretical top floor yield displacement i.e. 1 inch (2.54 cm), is taken as the representative stiffness S during that cycle. Generally, researchers have found it difficult to quantitatively assess the performance of structures based on the dual criteria of stiffness during service load and ductile behaviour at ultimate stages. This difficulty may be overcome by devising a constant termed Energy Stiffness Constant. This energy-stiffness constant ESC is defined as the product of total energy E and the representative stiffness S during the cycle under consideration divided by the square of the theoretical ultimate load P_U^* , i.e. $ESC = (E \times s) / (P_U^*)^2$. Figure 8 shows the cumulative energy stiffness constant for the various cycles for the two models. The larger the value of energy stiffness constant, the better is the performance. The performance of Wall B is about 3 times better when compared with that of Wall A.

FAILURE MECHANISMS

Wall-A: During the final load cycles the deterioration and the consequent spalling of concrete in the narrow compression zone of the tension wall was severe near the inner single layer of compression reinforcement. (Figure 1). These two vertical bars buckled outward. Probably even larger ductilities could be

attained by providing at least two layers of vertical bars in the inner faces of the walls and by effectively containing the concrete in this region by binding steel. The average slope of the structure at failure was approximately 1:15.

Wall B: The failure was initiated in the compression wall during the final load cycle. An inadvertent misalignment in the form-work resulted in a kink at the junction of the base block and the wall, and this caused the compression wall to buckle. The line of failure at ground floor level is clearly visible in Figure 1. In prototype structures, this type of failure cannot occur because of the restraint offered by the floor slabs. Hence this wall could have exhibited considerably more ductility. The average slope of the structure at failure was approximately 1:28.

Figure 1 shows the models after test. It is evident that in Wall A during the final cycle all the beams failed by sliding shear.

In spite of large yielding in the beams of Wall B, the beam distortions were much smaller and the damage was much less than in Wall A.

APPLICATION TO DESIGN

The improved performance of wall B results from the behaviour of diagonally reinforced coupling beams. Thus adequately detailed coupled walls, with diagonally reinforced coupling beams, fail predominantly in flexural mode. For such walls higher lateral forces when compared with rigid jointed frames as required by the code (4), need not be considered. This would result in the reduction in the cost of the shear core because of the savings in the quantity of steel.

CONCLUSIONS

The performance of the two models, upon which very severe displacements were imposed, were compared in terms of stiffness degradation, ductilities attained and energy-stiffness criteria. In every respect the superior performance of Wall B, containing diagonally reinforced coupling beams, was identified. The reason for this was the arrangement of reinforcement, particularly in the beams, which enabled the major parts of the critical internal forces to be carried by steel rather than concrete.

With careful detailing, particularly in areas where yielding can occur, coupled shear wall structures could be made to possess all the desirable features of an effective earthquake resistant structure.

The improved performance of the coupled shear wall with diagonally reinforced spandrel beams could be made use of and the coupled shear cores may be designed for approximately the same equivalent lateral seismic force as rigid jointed frames. This

would lead to considerable reduction in the cost of shear core because of the savings in the quantity of steel.

ACKNOWLEDGEMENTS

The above investigation was carried out in the Department of Civil Engineering, University of Canterbury, Christchurch, New Zealand when the author was a Commonwealth Research Scholar under the supervision of Prof.T. Paulay and the financial assistance was provided by the New Zealand University Grants Committee.

APPENDIX I - REFERENCES

1. "Building Code Requirements for Reinforced Concrete, (ACI 317-71)", American Concrete Institute, Detroit, 1971, 78 pp.
2. Paulay, T., "Some Aspects of Shear Wall Design", Bulletin of the New Zealand Society for Earthquake Engineering, Vol.5, No.3, Sept. 1972, pp. 89-105.
3. Paulay, T and Santhakumar, A.R., "Ductile Behaviour of Coupled Shear Walls", Journal of the Structural Division, ASCE, Accepted for Publication.
4. "Recommended Lateral Force Requirements and Commentary", Seismologic Committee, Structural Engineers, Association of California, (SRAOC), 1968.
5. "Response of Multistorey Concrete Structures to Lateral Forces", Publication SP 36, American Concrete Institute, Detroit, 1973. 314, pp.
6. Santhakumar, A.R., "The Ductility of Coupled Shear Walls", Ph.D. Thesis, University of Canterbury, Christchurch, New Zealand, Oct. 1974, 412 pp.
7. Stafford Smith, B. and Coull, A., "Elastic Analysis of Tall Concrete Buildings", State of the Art Report No.1, Technical Committee 21, Joint Committee for Tall Buildings Reports, Vol.III-21, pp.9-23.
8. "Symposium on Tall Buildings with Particular Reference to Shear Wall Structures", University of Southampton, April, 1966, Oxford, Pergamon Press, 1967.
9. Winokur, A. and Gluck, J., "Ultimate Strength Analysis of Coupled Shear Walls", Proceedings, American Concrete Institute Journal, Vol.63, No.12, Dec. 1968, PP.1029-1035.

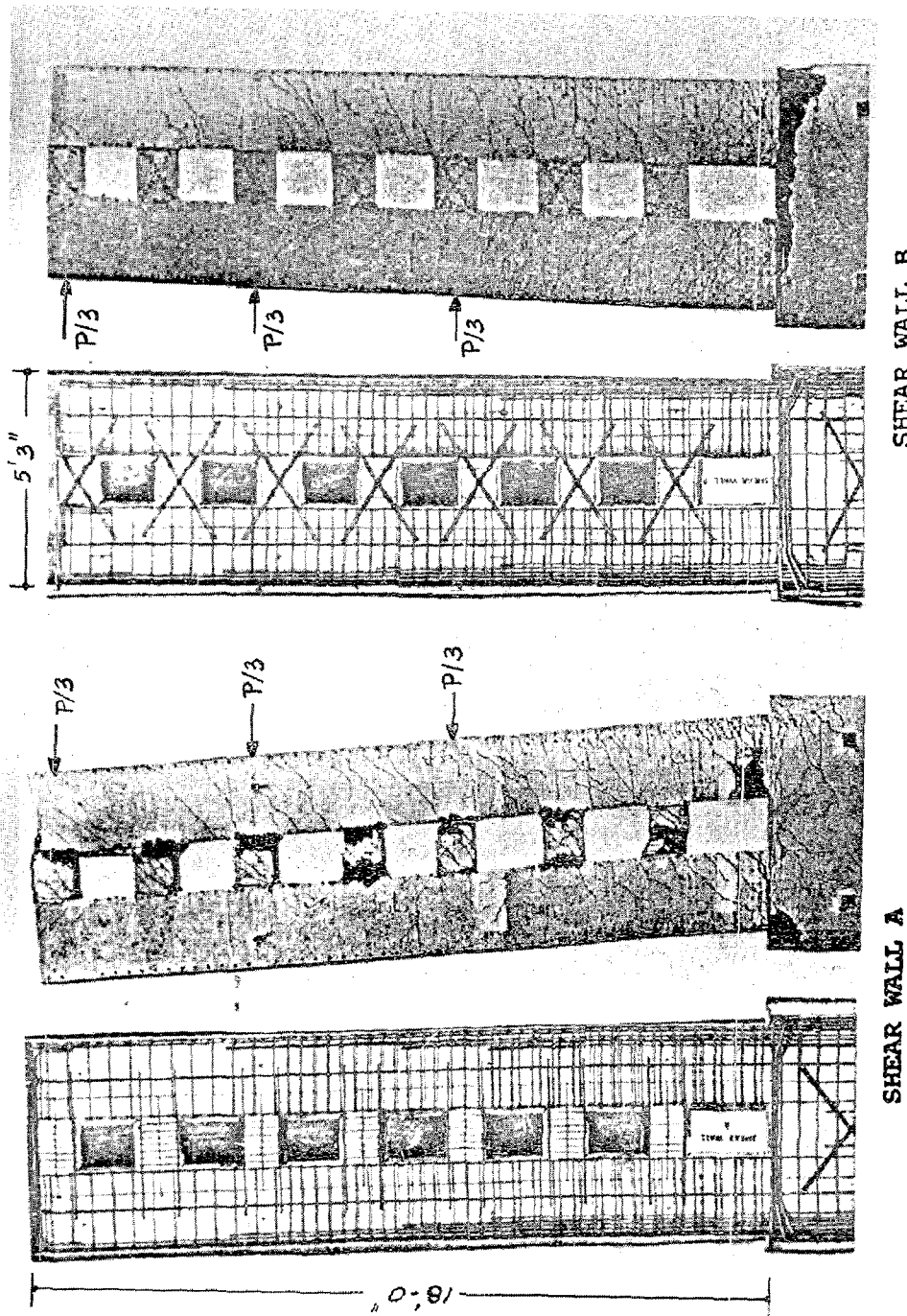
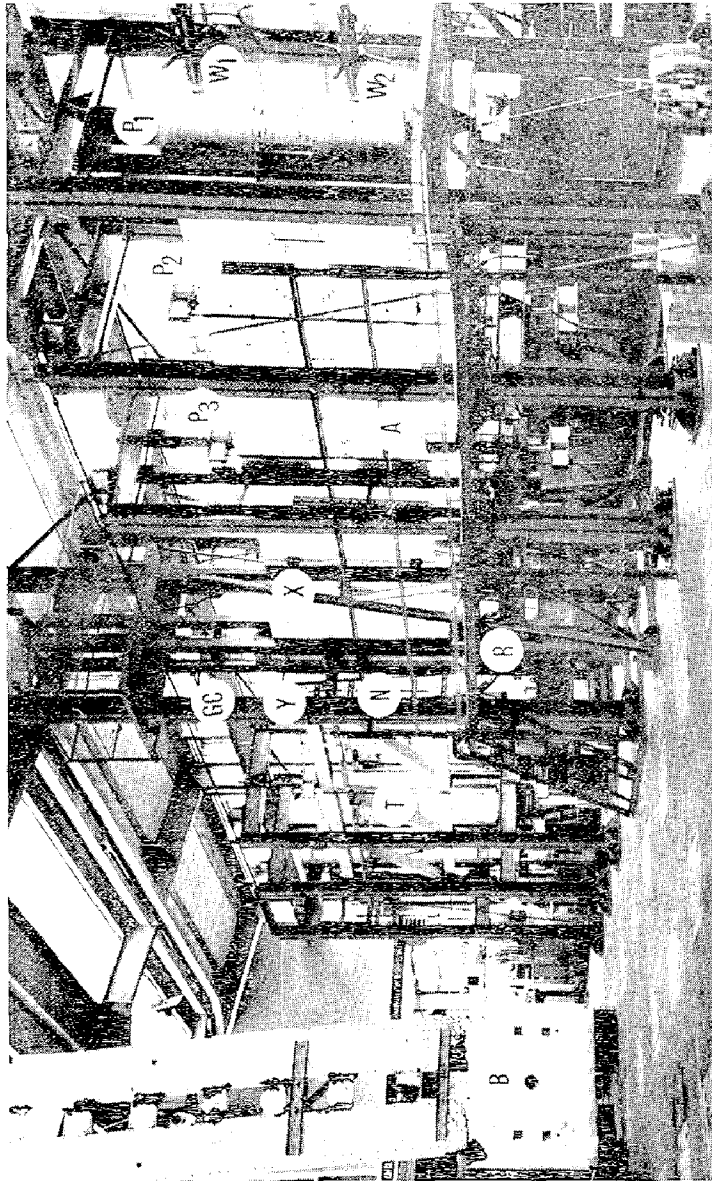


FIGURE 1 THE REINFORCEMENT IN, AND THE CRACK PATTERNS OF, QUARTER FULL SIZE SHEAR WALL MODELS SUBJECTED TO REVERSED CYCLIC LOADING



A	Model Shear Wall
T	Balancing Truss
P ₁ P ₂ P ₃	Static Loads
W ₁ W ₂	Simulation of Gravity Loads
GC	Guiding Channels
R	Central Reaction
Y	Yoke
N	Central Pin
B	Base Block

FIGURE 2 DOUBLE CANTILEVER LOADING SYSTEM

WALL A AFTER FAILURE AND WALL B SET UP FOR TESTING

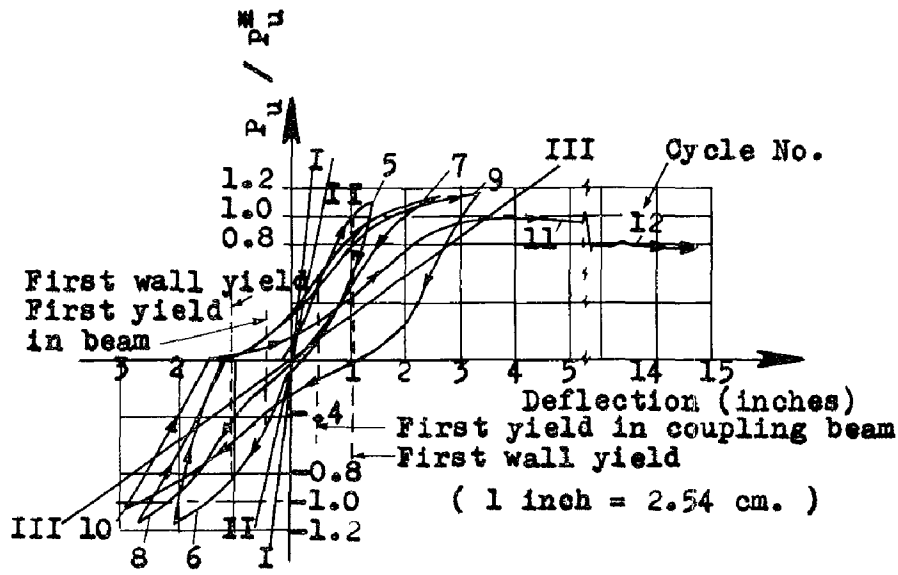


FIGURE 3 LOAD-ROOF DEFLECTION RELATIONSHIP FOR WALL A

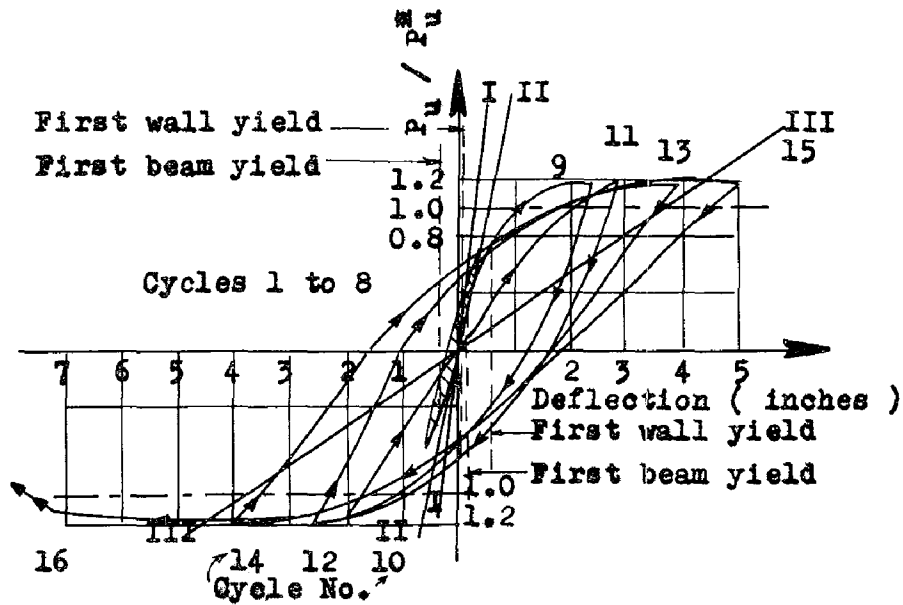


FIGURE 4 LOAD-ROOF DEFLECTION RELATIONSHIP FOR WALL B

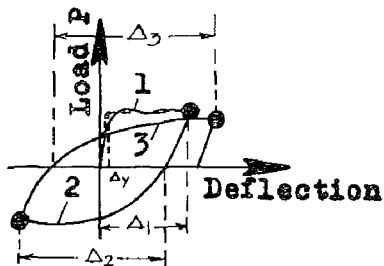


FIGURE 5a A DEFINITION OF DISPLACEMENT DUCTILITY

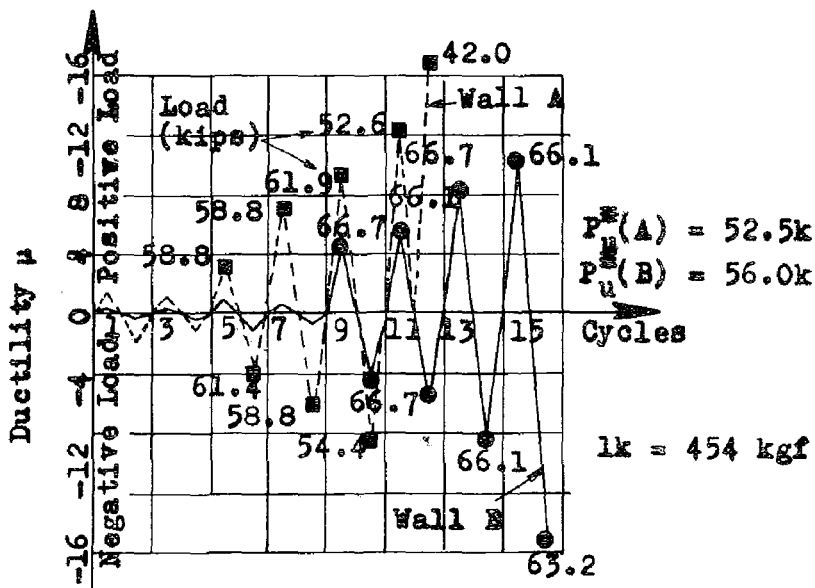


FIGURE 5b OVERALL DUCTILITIES ATTAINED

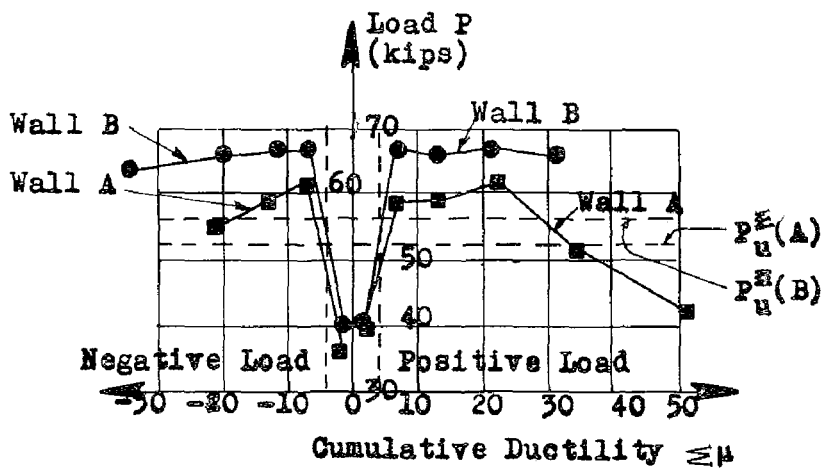


FIGURE 5c COMPARISON OF CUMULATIVE DUCTILITIES

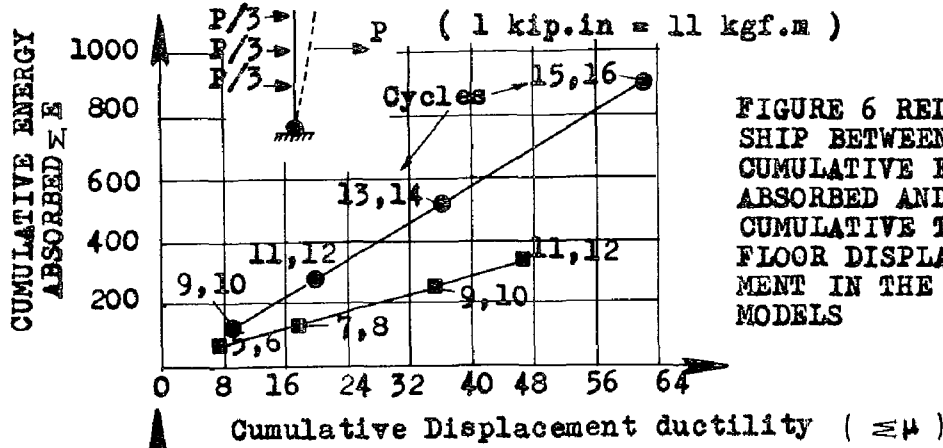


FIGURE 6 RELATIONSHIP BETWEEN THE CUMULATIVE ENERGY ABSORBED AND THE CUMULATIVE TOP FLOOR DISPLACEMENT IN THE MODELS

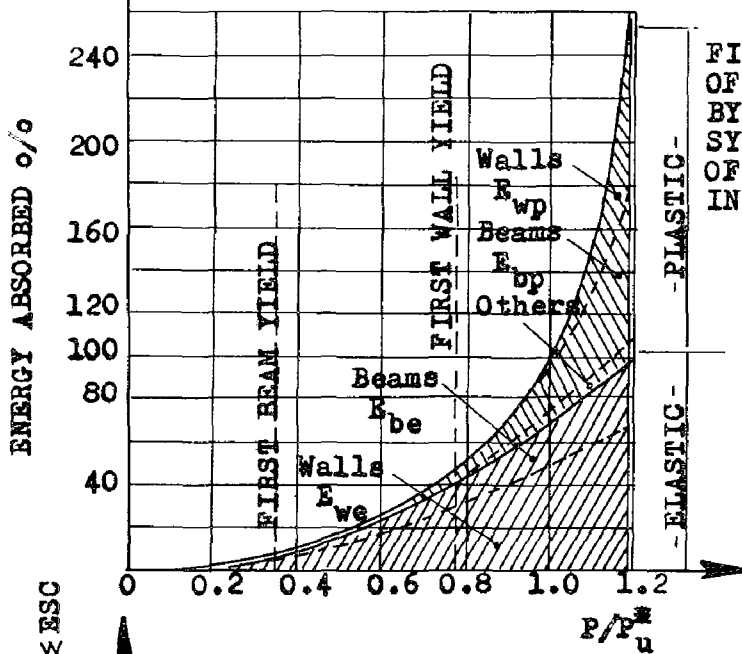


FIGURE 7 PROPORTIONS OF ENERGY ABSORBED BY THE COUPLING SYSTEM AND WALLS OF SHEAR WALL B IN CYCLE 9

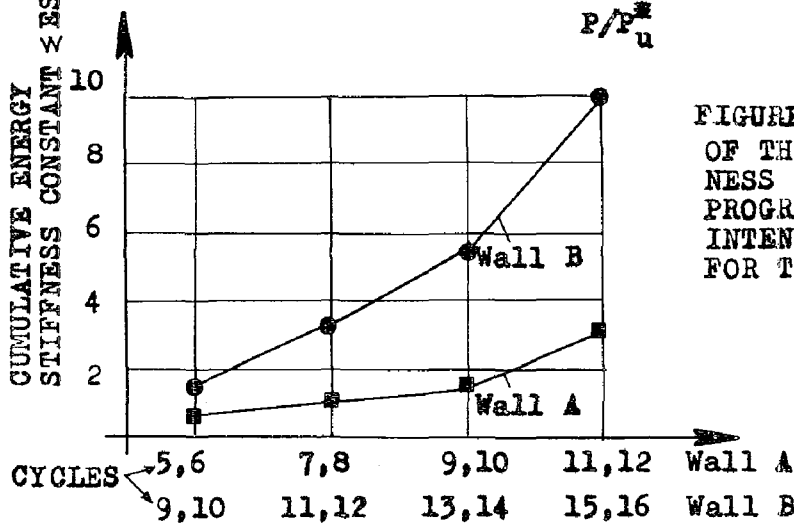


FIGURE 8 A COMPARISON OF THE ENERGY STIFFNESS CONSTANT DURING PROGRESSIVE HIGH INTENSITY CYCLES FOR THE TWO MODELS

INTERNATIONAL SYMPOSIUM ON
EARTHQUAKE STRUCTURAL ENGINEERING

513

St. Louis, Missouri, USA, August, 1976

EARTHQUAKE RESPONSE OF GUYED TOWERS

ANDRES V. DU BOUCHET

Assistant Professor
Department of Civil and Environmental Engineering
College of Engineering
Rutgers University
New Brunswick, New Jersey 08903, U.S.A.

SUMMARY

A structural model of a guyed tower (scaled by dimensional analysis principles) is subjected to simulated earthquake ground motion, by means of a shake table driven by electro-hydraulic apparatus.

The guyed tower structural model has been scaled from a prototype previously reported in the literature. A total of fifteen variables are scaled, including ground and structure acceleration, velocity, and displacement, material constants and density, structure geometry, stress levels and gravitational constant.

Brass in commercially available sizes is the material selected to model the tower mast and guy cables.

The prototype structure is 1200 ft (365.8 m) in height, and the structural model (with a length scale factor of 106.4) therefore stands 135.3 in (3.438 m) high.

The shake table upon which the model is mounted consists of a 3 ft (0.914 m) by 3 ft (0.914 m) by 3 in (7.62 cm) steel plate (with aluminum struts to anchor the guy cables) mounted on linear bearings.

The structural model is subjected to a series of sinusoidal base motions of constant frequency and maximum amplitude, for successively larger amplitudes of base motion.

The guyed tower mast is instrumented with five accelerometers at the mast top and base, and at the three cable junctions. The tower mast is supported by a force transducer which senses the dynamic base shear of the tower mast in the direction parallel to the base motion.

The acceleration and force signals are amplified by charge amplifiers and recorded on a multi-channel tape recorder. The raw data is then digitized, and velocities and displacements obtained by numerical

integration.

Curves are plotted for maximum transverse mast displacement versus driving frequency, for successively larger amplitudes of base motion. A series of curves is also constructed for the magnitude of the maximum dynamic base shear (a measure of energy input) as a function of forcing frequency for given amplitude of base motion.

INTRODUCTION

The dynamic response of a structure subjected to earthquake-induced ground motion may typically be generated in one of three ways:

1. by instrumenting a prototype structure, and recording and processing any subsequent ground motion. Many important structures have been permanently instrumented in this manner.
2. by subjecting a mathematical model of a structure to simulated earthquake ground motion, which may consist of digitized records of actual ground motion, or a statistically generated earthquake record.
3. by subjecting a structural model (scaled by dimensional analysis principles) to simulated earthquake ground motion, by means of a shake table driven by electro-hydraulic apparatus.

For structures such as guyed towers, the approach outlined in (3) is particularly valuable. Guyed towers are of simple geometric configuration, and contain relatively few secondary and non-structural components. A structural model of the prototype structure may therefore be constructed with reasonable accuracy.

Moreover, the geometrically nonlinear response of guyed tower structures to earthquake ground motion renders mathematical modelling infeasible (no suitable mathematical model of a guyed tower structure has as yet been generated).

Model testing, in the absence of data recorded from existing prototype structures (1), is therefore currently the most feasible method of determining the response of guyed towers to earthquake ground motion.

STRUCTURAL MODEL

The prototype guyed tower structure parameters used to perform the dimensional analysis (1,7,8) are excerpted from a paper by Goldberg and Gaunt (6). The overall geometry of the prototype tower is given in Fig. 1, while the prototype cables and mast parameters are summarized in Table 1. Symbol definitions are tabulated under Appendix II. - Notation.

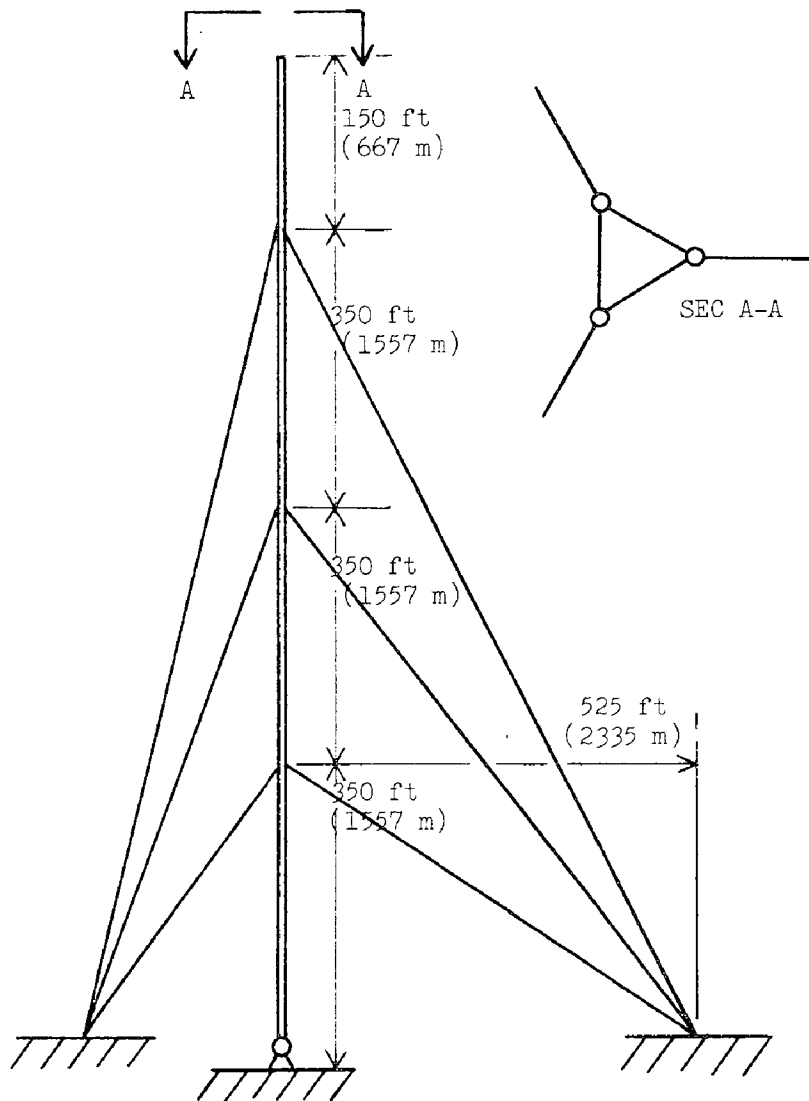


FIG. 1. - PROTOTYPE TOWER CONFIGURATION

TABLE 1. - PROTOTYPE TOWER PARAMETERS

Parameter (1)	Level 1 (2)	Level 2 (3)	Level 3 (4)
D_c , in inches (millimeters)	1.375 (34.93)	1.750 (44.45)	2.250 (57.15)
W_c , in pounds per foot (newtons per meter)	3.94 (57.5)	6.38 (93.1)	10.55 (154.0)
$E_c A_c$, in kilopounds (kilonewtons)	28,400 (126,000)	46,000 (205,000)	76,000 (338,000)
A_m , in square inches (centimeters squared)	64.0 (413.0)	64.0 (413.0)	64.0 (413.0)
I_m , in inches to the fourth power (centimeters to the fourth power)	3.455×10^5 (1.438×10^7)	3.455×10^5 (1.438×10^7)	3.455×10^5 (1.438×10^7)
P_m , in kilopounds (kilonewtons)	5,790 (25,750)	5,790 (25,750)	5,790 (25,750)
H_c , in kilopounds (kilonewtons)	15.3 (68.1)	18.6 (82.7)	20.1 (89.4)

Table 2 summarizes the results of the dimensional analysis, as a function of the length and elastic modulus scale factors λ_ℓ and λ_e .

TABLE 2. - MODEL SCALE FACTORS

Scale Factor (1)	Function (2)
Ground, structure displacement, λ_{ug} , λ_{us}	λ_ℓ
Ground, structure velocity, λ_{vg} , λ_{vs}	$\lambda_\ell^{1/2}$
Ground, structure acceleration, λ_{ag} , λ_{as}	1
Cross-sectional area, λ_a	λ_ℓ^2
Moment of inertia, λ_i	λ_ℓ^4
Material density, λ_ρ	$\lambda_e \lambda_\ell^{-1}$
Stress level, λ_σ	λ_e

The relationships given in Table 2 for the assumption of unit gravity scale factor may be verified, for example, in Newmark and Rosenblueth (8).

Brass in commercially available sizes is the material used to fabricate the structural model. Based on the selection of .049 in (1.24 mm) brass wire for the model mast elements, the length scale factor λ_l is computed as 1/106.4, and the overall height of the structural model is therefore 135.3 in (3.438 m).

Table 3 summarizes the structural model parameters computed on the basis of the data summarized in Tables 1 and 2. The cable anchor tension is computed as a function of the cable geometry and the horizontal component of cable pretension (9,12).

TABLE 3. - MODEL PARAMETERS

Parameter (1)		Exact Scale (2)	Actual (3)
Mast inertia, inches to the fourth (centimeters to the fourth)		2.70×10^{-3} (0.112)	2.70×10^{-3} (0.112)
Mast weight, pounds (newtons)		11.5 (51.2)	11.5 (51.2)
Buckling Load P_m , pounds (newtons)		257 (1140)	257 (1140)
Cable diameters, inches (millimeters)	level 1 2 3	.013 (.330) .016 (.406) .021 (.533)	.018 (.457) .020 (.508) .022 (.559)
Cable unit weights, pounds per foot (newtons per meter)	level 1 2 3	.00153 (.0223) .00248 (.0362) .00411 (.0600)	.00153 (.0223) .00248 (.0362) .00411 (.0600)
Cable anchor tension, pounds (newtons)	level 1 2 3	0.781 (3.47) 1.27 (5.65) 1.74 (7.74)	0.781 (3.47) 1.27 (5.65) 1.74 (7.74)
Cable anchor stress, kilopounds per sq in (newtons per sq meter)	level 1 2 3	5.97 (4.12×10^7) 5.98 (4.12×10^7) 4.96 (3.42×10^7)	3.06 (2.11×10^7) 4.05 (2.79×10^7) 4.58 (3.16×10^7)

Inspection of Table 3 indicates that, with the exception of the cable stresses, the structural model satisfies all scale factors identically.

The cable anchor tensions are computed in order to properly pretension the model guys during installation of the structural model. Wherever required, lead stripping and bead is utilized to obtain the required mass magnitude and distribution.

Figs. 2 and 3 indicate the overall configuration and detailed geometry of the installed guy tower structural model.

SHAKE TABLE AND DRIVING APPARATUS

The shake table upon which the model is mounted consists of a 3 ft. (0.914 m) by 3 ft. (0.914 m) by 3 in. (7.62 cm) steel plate (with aluminum struts to anchor the guy cables) mounted on linear bearings. A hydraulic actuator capable of providing a stroke of plus or minus 0.25 in. (0.635 cm) in the frequency range 0 - 10 Hz drives the shake table. Fig. 4 illustrates the test configuration.

SIMULATED GROUND MOTION

The structural model is subjected to sinusoidal base motion of constant frequency and maximum amplitude. For a given load cycle, steady-state response is generated for 10 sec. duration. The input signal is then cut and the transient response of the model is recorded for an additional 20 sec. duration.

In this manner, the dynamic response of the structural model is monitored, for given maximum base double amplitudes of .005 in. (.127 mm), .010 in. (.254 mm), and .015 in. (.381 mm), over the frequency range 2.0 - 9.0 Hz at 1.0 Hz intervals.

SIGNAL GENERATION AND DATA PROCESSING

The guyed tower mast is instrumented with five accelerometers at the mast top and base, and at the three cable junctions.

The tower mast is supported by a force transducer which senses the dynamic base shear of the tower mast in the direction parallel to the base motion. Fig. 3 illustrates the method of support of the tower mast, which rests on a knife edge (oriented normal to the direction of motion) supported by a vee-block secured to the force transducer. The accelerometer mounted at the tower base is also visible in Fig. 3.

The acceleration and force signals are amplified by charge amplifiers and recorded on a seven-track magnetic tape recorder.

The raw data is then digitized at a rate of 103 samples per second, resulting in a Nyquist (cutoff) frequency (2,4,5,13) of approximately 50 Hz.

Prior to performing the numerical integration, the raw acceleration data are smoothed using Hanning's weighing coefficients (4,5,13).

$$a_{i\text{new}} = 0.25a_{i-1} + 0.50a_i + 0.25a_{i+1} \quad (1)$$

Accelerations are assumed to vary linearly within a time increment h , yielding a parabolic variation in velocity and a cubic variation in displacement.

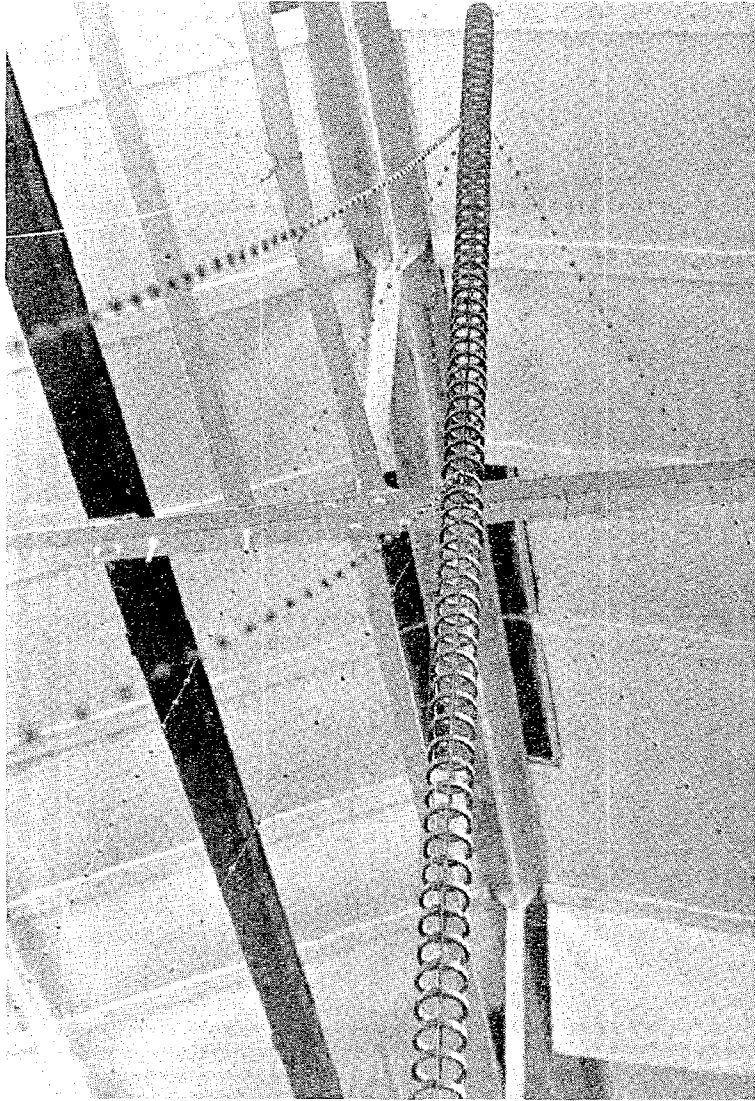


FIG. 2. - MODEL TOWER CONFIGURATION

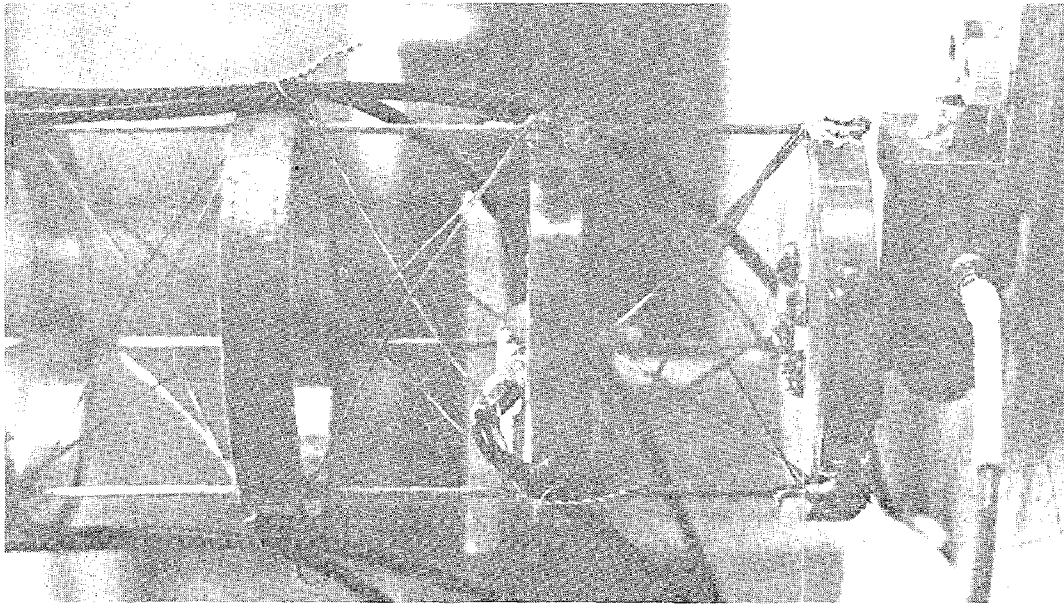


FIG. 3. - MODEL GEOMETRY

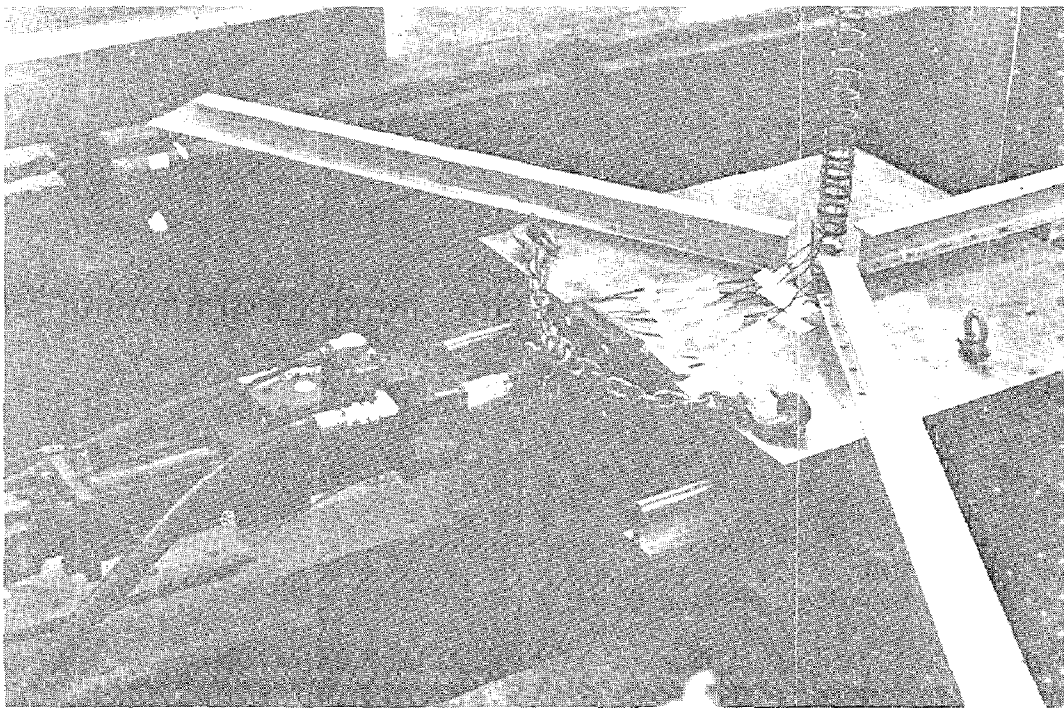


FIG. 4. - SHAKE TABLE CONFIGURATION

$$v_{i+1} = v_i + \frac{h}{2}(a_i + a_{i+1}) \quad (2)$$

$$x_{i+1} = x_i + hv_i + \frac{h^2}{6}(2a_i + a_{i+1}) \quad (3)$$

Zero initial conditions for displacement and velocity are assumed to hold at the beginning of each steady-state run.

After computing the uncorrected velocities (Eq. 2), a least-squares minimization procedure is applied in order to adjust the uncorrected accelerations (3,4,5,10,13).

$$a_{icorr} = a_i + C_0 + C_1(ih) + C_2(ih)^2 \quad (4)$$

where, for

$$A = \int_0^T v(t)dt \quad B = \int_0^T v(t)t^2dt \quad (5)$$

$$C = \int_0^T v(t)t^3dt$$

the correction coefficients C_0 , C_1 , C_2 are given by (10)

$$C_0 = -\frac{300A}{T^3} + \frac{900B}{T^4} - \frac{630C}{T^5}$$

$$C_1 = +\frac{1800A}{T^4} - \frac{5760B}{T^5} + \frac{4200C}{T^6} \quad (6)$$

$$C_2 = -\frac{1890A}{T^5} + \frac{6300B}{T^6} - \frac{4725C}{T^7}$$

where T represents the time duration of processed velocities.

In order to generate the integrals A, B, C , Waddle's formula (with an error of order h^8) is used (11).

$$E_6 = \frac{3h}{10}(a_{i-3} + 5a_{i-2} + a_{i-1} + 6a_i + a_{i+1} + 5a_{i+2} + a_{i+3}) \quad (7)$$

The smoothed, uncorrected accelerations are then adjusted using Eq. 4, and the subsequent corrected accelerations are integrated twice to obtain velocities and displacements.

Because of drift generated by the integration, it is necessary to compute and remove the mean accelerations and velocities prior to integration. This is physically equivalent to zero mean displacement drift, which characterizes the system under consideration.

TOWER RESPONSE

Figures 5 and 6 summarize envelopes of maximum dynamic base shear and maximum mast tip displacement for the double amplitudes ± 0.005 in. (.127 mm), ± 0.010 in. (.254 mm), and ± 0.015 in. (.381 mm) over the frequency range 2.0 Hz to 9.0 Hz at 1.0-Hz intervals.

These curves may be interpreted as "inverse" response spectra, since the model structure parameters are held constant, while the amplitude and frequency of the harmonic forcing function are varied.

For a condition of steady-state oscillation, the dynamic base shear is proportional to the energy absorbed (and therefore dissipated) by the structure. As Fig. 5 indicates, the magnitude of the maximum base shear is clearly a function of the amplitude of base motion.

Note that the maximum recorded magnitude of base shear, 7.7 lb (34 N), is approximately half the total model structure weight of 14.2 lb (63.2 N).

Examination of Fig. 6 indicates that the envelopes of maximum mast tip displacement are also clearly related to the magnitude of base motion. Moreover, the overall maximum displacements are seen to occur at the low end of the driving frequencies. This reflects tower mast response to the cable fundamental frequencies, which fall in the range 1.7-2.5 Hz (perturbation and visual count during pretensioning).

CONCLUSIONS

A guyed tower structural model has been designed, fabricated, instrumented and subjected to harmonic base motion.

Envelopes of maximum dynamic base shear and maximum transverse mast tip displacement as a function of amplitude and frequency of base excitation have been presented.

The data presented therein are directly applicable to earthquake design of guyed towers in areas prone to long ground motion exhibiting prevailing periods of vibration.

ACKNOWLEDGMENTS

The writer acknowledges the assistance of the following Rutgers University students and staff: Donald A. Molony and Louis J. Rosenthal, Professors of Electrical Engineering; Andrew Moskal and John Machuzak, students in the Department of Electrical Engineering; Harold Greve, graduate student in the Department of Civil and Environmental Engineering; and Annamary McCann, of the Physics Department.

The writer would like to thank Joel Wiesenfeld, Chairman of the Department of Civil and Environmental Engineering, for advice and encouragement rendered during the course of this project.

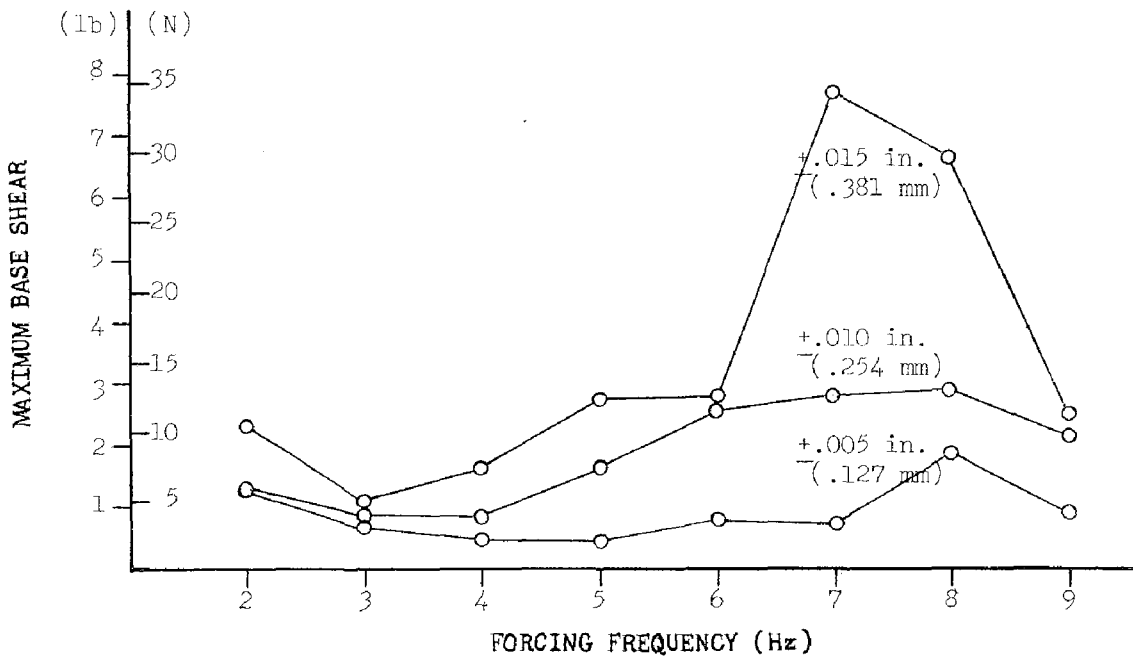


FIG. 5. - ENVELOPES OF MAXIMUM BASE SHEAR

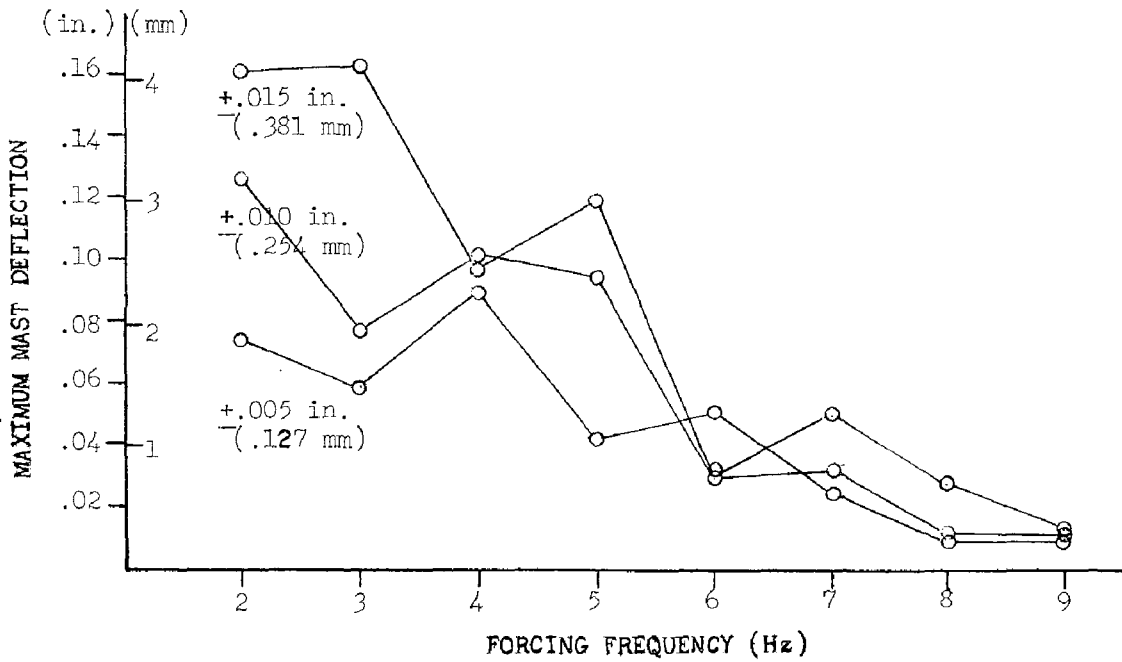


FIG. 6. - ENVELOPES OF MAXIMUM MAST DISPLACEMENT

The research summarized herein was supported by NSF Grant GK-42126 and by funds provided by the Department of Civil and Environmental Engineering, Rutgers University.

APPENDIX I. - REFERENCES

1. Baker, W. E., Westine, P. S., and Dodge, F. T., Similarity Methods in Engineering Dynamics, Hayden Books, Inc., Rochelle Park, N. J., 1973.
2. Bendat, J. S., and Piersol, A. G., Random Data: Analysis and Measurement Procedures, Wiley - Interscience, New York, N. Y., 1971.
3. Berg, G. V., and Housner, G. W., "Integrated Velocity and Displacement of Strong Earthquake Ground Motion," Bulletin of the Seismological Society of America, Vol. 51, No. 2, April, 1961, pp. 175-189.
4. Chiu, A. N. L., and Taoka, G. T., "Tower Response to Actual and Simulated Wind Forces," Journal of the Structural Division, ASCE, Vol. 99, No. ST9, Proc. Paper 10012, September, 1973, pp. 1911-1929.
5. Chiu, A. N. L., Santo, P. T., and Taoka, G. T., "Structure Response to Wind Forces," IABSE ASCE AIA IFHP UIA Regional Conference on Tall Buildings, Bangkok, Thailand, January, 1974, pp. 589-603.
6. Goldberg, J. E., and Gaunt, J. T., "Stability of Guyed Towers," Journal of the Structural Division, ASCE, Vol. 99, No. ST4, Proc. Paper 9683, April, 1973, pp. 741-756.
7. Hudson, D. E., "Scale Model Principles," Shock and Vibration Handbook, Chapter 27, McGraw-Hill, Inc., New York, N. Y., 1961.
8. Newmark, N. M., and Rosenblueth, E., Fundamentals of Earthquake Engineering, Prentice-Hall, Inc., Englewood Cliffs, N. J., 1971.
9. Odley, E. G., "Analysis of High Guyed Towers," Journal of the Structural Division, ASCE, Vol. 92, No. ST1, Proc. Paper 4671, February, 1966, pp. 169-197.
10. Poppitz, J. V., "Velocity and Displacement of Explosion - Induced Earth Tremors Derived From Acceleration," Bulletin of the Seismological Society of America, Vol. 58, No. 5, October, 1968, pp. 1573 - 1582.
11. Salvadori, M. G., and Baron, M. L., Numerical Methods in Engineering, Prentice-Hall, Inc., Englewood Cliffs, N. J., 1952.
12. Steinman, D. B., Suspension Bridges, John Wiley & Sons, Inc., New York, N. Y., 1949.
13. Taoka, G. T., Hogan, M., Khan, F., Scanlon, R. H., "Ambient Response Analysis of Some Tall Structures," Journal of the Structural Division, ASCE, Vol. 101, No. ST1, Proc. Paper 11051, January, 1975, pp. 49-65.

APPENDIX II. - NOTATION

The following symbols are used in this paper:

a_i = acceleration at time interval i

v_i = velocity at time interval i

x_i = displacement at time interval i

h = time increment

D_c = cable diameter

W_c = cable weight

E_c = mast elastic modulus

A_c = mast cross-sectional area

I_m = mast moment of inertia

P_m = mast buckling load

H_c = horizontal component of cable tension

λ_l = length scale factor

λ_e = elastic modulus scale factor

$\lambda_{ug}, \lambda_{us}$ = ground, structure displacement scale factor

$\lambda_{vg}, \lambda_{vs}$ = ground, structure velocity scale factor

$\lambda_{ag}, \lambda_{as}$ = ground, structure acceleration scale factor

λ_a = cross-sectional area scale factor

λ_i = moment of inertia scale factor

λ_ρ = material density scale factor

λ_σ = stress level scale factor

INTERNATIONAL SYMPOSIUM ON
EARTHQUAKE STRUCTURAL ENGINEERING

527

St. Louis, Missouri, USA, August, 1976

EXPERIMENTAL STUDY ON REINFORCED CONCRETE COLUMNS
WITH SPECIAL WEB REINFORCEMENTS*

by

HAJIME UMEMURA

Prof., University of Tokyo, Tokyo, Japan

TAKAYUKI SHIMAZU

Assoc. Prof., University of Hiroshima, Hiroshima

SINICHI TADEHARA

Assist., Hiroshima Institute of Technology, Hiroshima

TERUHIKO KONISHI

Senior Chief Eng., Japan Public Corp. of Housing, Tokyo

YUHEI ABE

Chief Eng., Japan Public Corp. of Housing, Tokyo

SUMMARY

This paper presents the experimental studies carried out on reinforced concrete columns with double spiral web-reinforcements wound and welded on longitudinal bars by the machine which has been developed, aiming at the prefabrication of reinforcement bars assemblages as well as the improvement of columns as regards as earthquake resistance capacities.

About thirty specimens have been tested, subjected to alternating repeated anti-symmetrical loads with constant axial load. The variables considered in this investigation, are shear span ratio, axial load level, the amount and diameter of web reinforcement, the angle between web and longitudinal reinforcements and the with or without welding between both the reinforcements.

It has been found from the tests that double spiral web reinforcements are much more effective for reinforced concrete columns than conventional web reinforcements.

* This study is sponsored by Japan Public Corp. of Housing with the supports of The Ministry of Education of Japan.

INTRODUCTION

One of the most important factors in the design of tall buildings in such countries having large seismic loads as Japan, is how to obtain sufficient shear strength for the columns with small shear span ratio.

The objective of this paper is to review recent research⁽⁴⁾ carried out at University of Hiroshima, on reinforced concrete columns, fabricated by the machine⁽²⁾ as shown in Fig.1 and to use these results to provide a means of determining seismic design for columns with double spiral web reinforcements.

TEST PROGRAM

The tests specimens, as shown in Fig.2, are one-third full scale of the columns which are subjected to anti-symmetrical lateral loading with or without constant axial load as shown in Fig.4. The variable elements of the specimens are shown in Table 1. Structural deformed bars SD35 (D25, $\sigma_Y = 3.82$ t/cm² and D29, $\sigma_Y = 3.75$ t/cm²) were used as longitudinal reinforcements in columns and steel wire (6 ϕ , 9 ϕ) and structural round bars SR24 (9 ϕ) were used as double spiral hoops (web reinforcements) and conventional hoops respectively. The stress strain curves for these hoop materials are shown in Fig.3. The ordinary mixed concrete consisted of portland cement, river sands and usual size aggregates were used and their compressive strength of cylinder are shown in Table 1.

Specimens were subjected to more than ten times alternating lateral loads up to ultimate to study their hysteretic loop characteristics. The relative displacements due to the rotation between both up and down gauge holders were measured as shown in Fig.4. The strains for both reinforcements and concrete were also measured by using wire strain gauges.

* KB1504 in JIS (Japan Industrial Standard)

TEST RESULTS

The results of tests are shown in Table 2 and Fig. 5-13. Based on the results of 26 tests, the following trends were observed:

(1) The maximum load of double spiral hoop specimens without axial load is about 30% higher, regardless of the shear span ratio and web reinforcement ratio, than that of conventional hoop specimens with the same ratio of web reinforcement. It is about 24% and 15% higher for the specimens with axial load of 36.7 kg/cm² and 73.3 kg/cm² respectively (Table 2, 8) col.).

(2) The maximum load is not influenced by the diameter of web reinforcement or the angle between web and longitudinal reinforcements (Table 2, 8) col. No. 3 - 10 specimens).

(3) The loop of load-deflection is nearly the same in positive and negative loadings for double spiral specimens while it is smaller in negative loadings for conventional hoop specimens (Figs. 5 - 13).

(4) The resisting load does not decrease so much even in the range of large deflection for the double spiral hoop specimens with the web reinforcement ratios of 1.2% and 1.8% (Figs. 5 - 13).

(5) The maximum load of the specimens with web reinforcement ratio of 1.8% is nearly the same with that of specimens with w.r.r. of 1.2% but the resisting load at large deflections does not decrease even under high axial stresses of 73.3 kg/cm² (Table 2, 6) col. Fig.10).

(6) The resisting load at small deflection is small for the specimens without welding, compared with that of specimens with welding but they are nearly the same at large deflection (Figs. 5,6).

(7) The difference of loops between double spiral hoop and conventional hoop is larger for the shear span ratio of 1.5 partly due to the fact that the double spiral hoop specimens reached their bending capacities (Figs 11 - 13).

General examinations were made into the test results, on the crack strength, maximum strength and ductility.

(8) There is little difference between double spiral hoop specimens and conventional hoop specimens regarding stress levels of bending crack, bending shear crack or middle inclined crack from which loads deflections increase more remarkably than before. Diagonal line crack or shear compression loads are, however, higher for double spiral hoop specimens. The relations among bending crack stress, middle inclined crack stress, axial stress applied and web reinforcement ratios are shown in Figs. 15 - 16. Calculated value in these figures are based on Arakawa formula⁽¹⁾. (Table 2 and Fig.14)

(9) Web reinforcement share, τ_w , in ultimate shear strength of double spiral hoop specimens can be estimated by

$$\tau_w = 0.5 \cdot p_w \cdot s \sigma_y \quad (p_w \cdot s \sigma_y \leq 80 \text{ kg/cm}^2) \quad (1)$$

in which p_w is web reinforcement ratio and $s \sigma_y$ is effective yielding strength for steel wire not having a definite yield point ($0.85 \cdot s \sigma_B$) while concrete share τ_{uc} is calculated by Ono-Arakawa formula⁽³⁾. The above equation is also supported by the results of embedded strain gauges for steel wire as shown in Fig. 21 - 23 . (Fig. 19)

(10) The deflection at maximum load increase with the va-

$$\tau_c = k_c (500 + F_c) \frac{0.085}{M/Qd + 1.7}$$

**

$$\tau_{uc} = (0.90 + \sigma/250) \cdot k_u \cdot k_p \frac{0.115}{M/Qd + 0.115} (180 + F_c)$$

k_c, k_u, k_p : Coefficients dependent on $d, d,$ and $p_t,$ respectively

lues of $p_w \cdot s_{\sigma y}$, which is approximately calculated by the truss analogy as shown in Fig.20). It is also found that there is considerable confinement effects of double spiral hoop on the diagonal members in increasing ductility but little effects in increasing strength in the range of over 50 kg/cm² in $p_w \cdot s_{\sigma y}$ values (Figs. 17 and 18).

CONCLUSIONS

The results from these tests are summarized as follows:

(1) The maximum load of the specimens with double spiral hoop is much higher than that of conventional hoop specimens and the loop of load deflection curves is much more stabilized even at large deflections.

(2) The web reinforcements share in ultimate shear strength for double spiral hoop specimens can be calculated by assuming the half of reinforcements reaching the effective yielding strength ($s_{\sigma B}$).

(3) Further researches are needed to establish design formula of taking into considerations the loop stabilities at large deflections.

BIBLIOGRAPHY

(1) Arakawa, T., " Experimental Studies on Shear Strength of Reinforced Concrete Beams, Conclusions", No.66 Trans. of Architectural Institute of Japan, Oct. 1960.

(2) Konishi, T., et al., " Horizontal Load Test on the Frames Erected with Preassembled Bars", Report of Experimental Lab. of Mass Product, Public Corp. of Housing of Japan, Mar.1973.

(3) Ono, K., et al., " Shear Strength and Ductility of Reinforced Concrete Columns", Proc. of A.I.J., Oct. 1972.

(4) Shimazu, T., et al., " Experimental Study on Double Spiral Hoop Columns (Parts 1,2 and 3) and (Parts 4,5,6 and 7)", Proc. of A.I.J. Oct. 1974 and Oct. 1975 Respectively.

TABLE 1—PROPERTIES OF SPECIMENS

Symbol of Specimens No.	h/2D.	Main Bar		Web Reinforcement				8) $c\sigma_B$ (kg/cm ²)	9) σ_o (kg/cm ²)
		2) Pt (%)	3) P _w (%)	4) ϕ (mm)	5) θ (deg.)	6) Weld.	7) $s\sigma_y$ (kg/cm ²)		
1	1.0	1.69	0.	---	---	---	---	203	0.
2	1.0	1.69	0.	---	---	---	---	203	73.3
3	1.0	1.69	0.6	9	65	Weld	5630	220	0.
4	1.0	1.69	0.6	9	65	Weld	5630	218	73.3
5	1.0	1.69	0.6	6	63	Weld	5504	203	0.
6	1.0	1.69	0.6	6	63	Weld	5504	203	36.7
7	1.0	1.69	0.6	6	63	Weld	5504	203	73.3
8	1.0	1.69	0.55	9	45	Weld	4490	173	0.
9	1.0	1.69	0.55	9	45	Weld	4490	173	73.3
10	1.0	1.69	0.6	9	90	No Weld	3057	203	73.3
11	1.0	1.69	1.2	9	65	Weld	5630	220	0.
12	1.0	1.69	1.2	9	65	Weld	4490	173	36.7
13	1.0	1.69	1.2	9	65	Weld	5630	218	73.3
14	1.0	1.69	1.2	9	65	No Weld	4490	173	0.
15	1.0	1.69	1.2	9	65	No Weld	4490	173	73.3
16	1.0	1.69	1.2	9	90	No Weld	2943	220	0.
17	1.0	1.69	1.2	9	90	No Weld	2943	218	73.3
18	1.0	2.14	1.8	9	65	Weld	4490	173	0.
19	1.0	2.14	1.8	9	65	Weld	4490	173	73.3
20	1.5	1.69	0.6	9	65	Weld	5630	203	0.
21	1.5	1.69	0.6	9	65	Weld	5630	211	73.3
22	1.5	1.69	0.6	9	90	No Weld	3057	231	73.3
23	1.5	1.69	1.2	9	65	Weld	5630	203	0.
24	1.5	1.69	1.2	9	65	Weld	5630	211	73.3
25	1.5	1.69	1.2	9	90	No Weld	2943	203	0.
26	1.5	1.69	1.2	9	90	No Weld	2943	211	73.3

Note --- 1) Shear Span Ratio, h : Clear Length of Column, D : Depth of Column.

2) Tension Reinforcement Ratio, $P_t = a_t/bD$, a_t : Tension Reinforcement Area, b : Width of Column.

3) Web Reinforcement Ratio, $P_w = \frac{\sum a_w}{bx} \sin\theta$, a_w : Web Reinforcement Area, x : Pitch, θ : Angle of Web Reinforcement against Main Bar. 4) Diameter.

5) \rightarrow 3). 6) Spot Welding between Web Reinforcements and Main Bars

7) Yield Point or Effective Yield Point ($0.85 s\sigma_B$)

8) Cylinder Strength. 9) Average Stress of Axial Load Applied.

TABLE 2—RESULTS OF TESTS

Specimen No.	1) P.B.C. (ton)	2) P.B.S.C. (ton)	3) τ B.S.C. (kg/cm ²)	4) P M.I.C. (ton)	5) τ M.I.C. (kg/cm ²)	6) P _{max.} (ton)	7) $\tau_{max.}$ (kg/cm ²)	8) $\frac{P_{max.}}{C.H.P_{max.}}$	9) $\frac{P_{max.}}{Ca.P.B.Y.}$	10) $\delta_{P_{max.}}$ (cm)	11) Failure Mode
1	17.8	17.8	13.0	17.8	13.0	39.1	28.6	—	0.46	0.50	S.C.
2	—	44.9	32.9	35.0	25.6	44.9	32.9	—	0.32	0.25	S.C.
3	20.0	30.0	22.0	41.8	30.6	70.8	51.9	1.30	0.82	1.06	S.C.
4	40.0	46.5	34.1	50.0	36.6	67.3	49.3	1.12	0.57	0.50	S.L.B.
5	17.2	20.0	14.7	30.0	22.0	70.8	51.9	1.30	0.83	0.50	S.C.
6	29.5	40.0	29.3	56.0	41.0	70.0	51.4	1.22	0.62	0.50	S.C.
7	30.0	50.0	36.6	30.0	22.0	70.0	51.4	1.16	0.50	0.20	S.C.
8	14.0	18.0	13.2	20.0	14.7	65.7	48.1	1.32	0.77	0.52	S.C.
9	28.5	65.0	50.0	47.6	36.6	69.5	50.9	1.27	0.56	0.25	S.C.
10	45.0	45.0	33.0	28.5	20.9	60.0	44.0	1.00	0.43	0.25	S.C.
11	20.0	20.0	14.7	15.3	11.2	89.5	65.6	1.28	1.03	0.97	S.C.
12	28.0	50.0	36.6	57.0	41.8	92.7	67.9	1.26	0.89	1.03	S.C.
13	74.0	74.0	54.2	63.5	46.5	91.5	67.0	1.14	0.70	0.50	S.C.
14	20.0	30.0	22.0	42.0	30.8	77.8	57.0	1.12	0.91	2.04	S.C.
15	40.0	48.3	35.4	48.3	35.4	75.0	55.0	0.97	0.61	1.14	S.C.
16	25.0	18.0	13.2	30.0	22.0	70.0	51.3	1.00	0.82	0.50	S.C.
17	62.8	49.0	35.9	60.0	44.0	77.2	56.6	1.00	0.59	0.50	S.L.B.
18	20.0	30.0	22.0	40.0	29.3	92.4	67.7	—	0.87	0.85	S.C.
19	30.0	50.0	36.6	58.0	42.5	91.3	66.9	—	0.64	1.00	S.C.
20	15.0	15.0	11.0	30.0	22.0	55.0	40.3	1.32	0.95	1.50	S.C.
21	36.0	42.0	30.8	42.0	30.8	57.0	41.8	1.08	0.66	1.50	S.L.B.
22	27.5	50.0	36.6	40.0	29.7	53.0	38.8	1.00	0.61	0.75	S.C.
23	15.0	30.0	22.0	30.0	22.0	68.8	50.4	1.30	1.19	3.08	B.
24	46.0	50.0	36.6	50.0	36.6	76.8	56.3	1.14	0.89	1.50	S.C.L.B.
25	14.0	22.5	16.5	37.5	27.5	53.0	38.8	1.00	0.91	1.50	S.C.
26	26.6	48.8	35.8	56.0	41.0	68.0	49.8	1.00	0.79	1.50	S.L.B.

Note — 1) Bending Crack Load (Initially Observed).

2) Bending Shear Crack Load. 3) Average Shear Stress at 2).

4) Middle Inclined Crack Load. 5) Average Shear Stress at 4).

6) Maximum Load. 7) Average Shear Stress at 6).

8) Ratio to Max. Load of Conventional Hoop's Specimen with the Same Web Reinforcement Ratio.

9) Ratio to Bending Yield Load Calculated.

10) Deflection at Max. Load. 11) S : Shear Failure Type, S.C. : Shear Compression Failure Type,

B : Bending Failure Type, L.B. : Lateral Buckling.

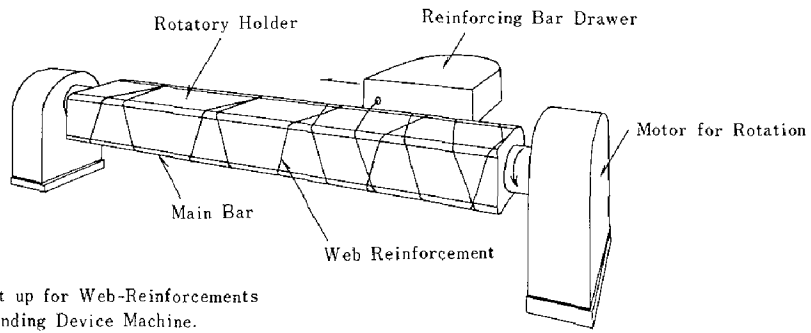


Fig. 1 Set up for Web-Reinforcements Winding Device Machine.

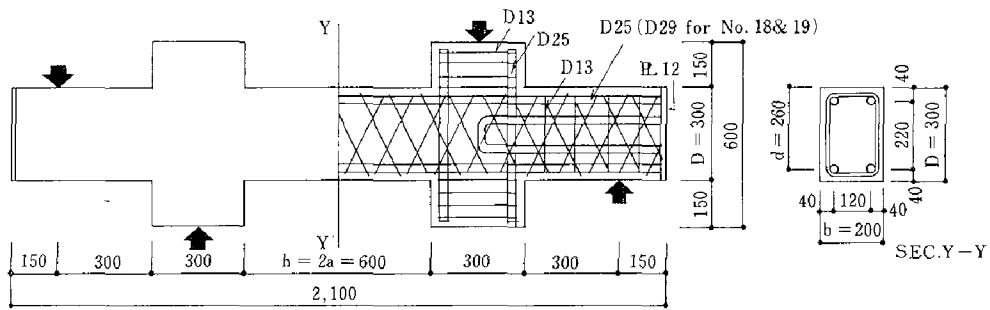


Fig. 2 Test Specimen

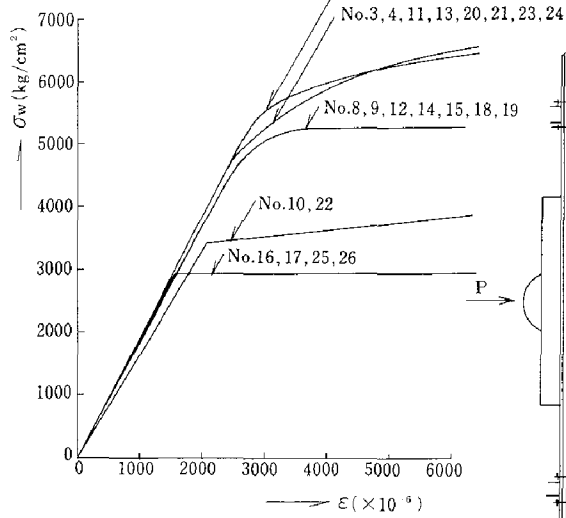


Fig. 3 Stress-Strain Curves of Web-Reinforcements

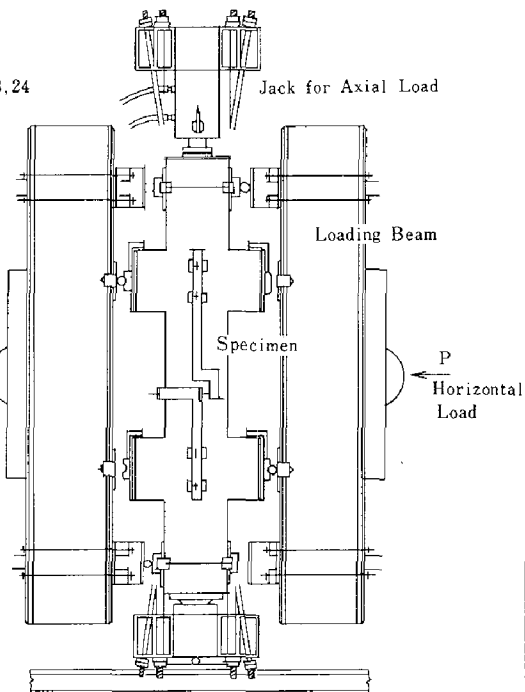


Fig. 4 Test Set-up

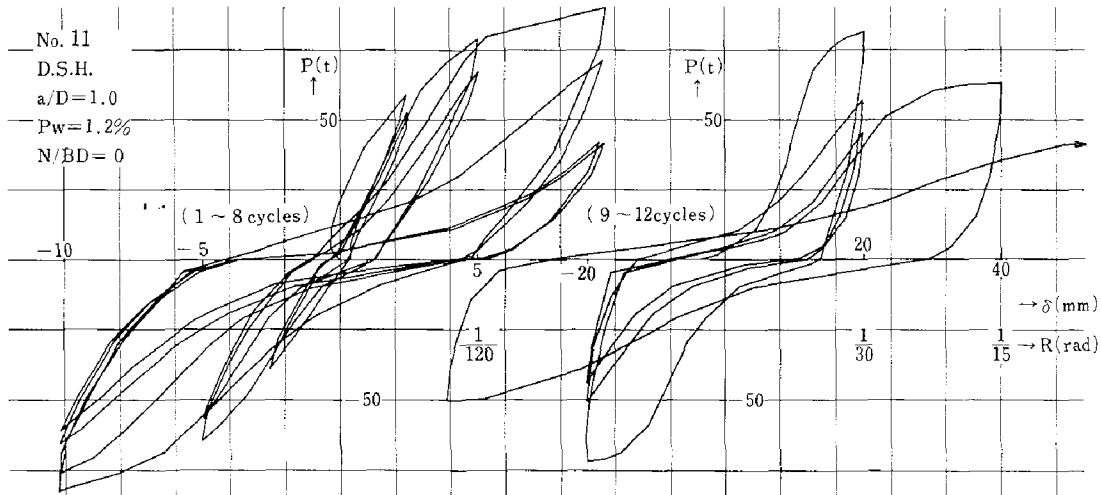


Fig. 5 Load-Deflection Curves(No.11)

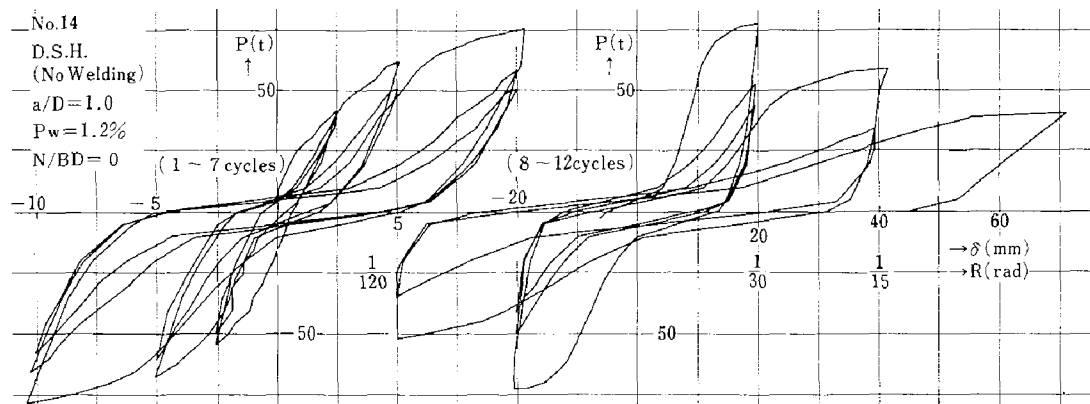


Fig. 6 Load-Deflection Curves(No.14)

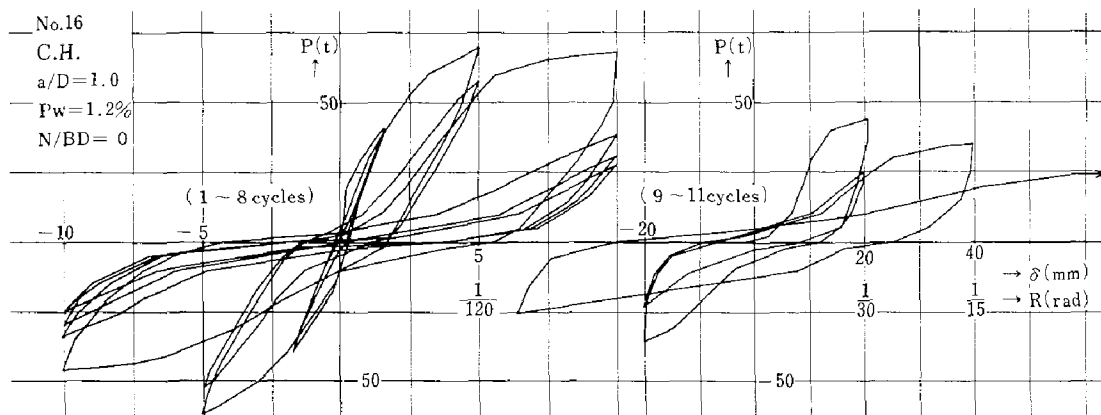


Fig. 7 Load-Deflection Curves(No.16)

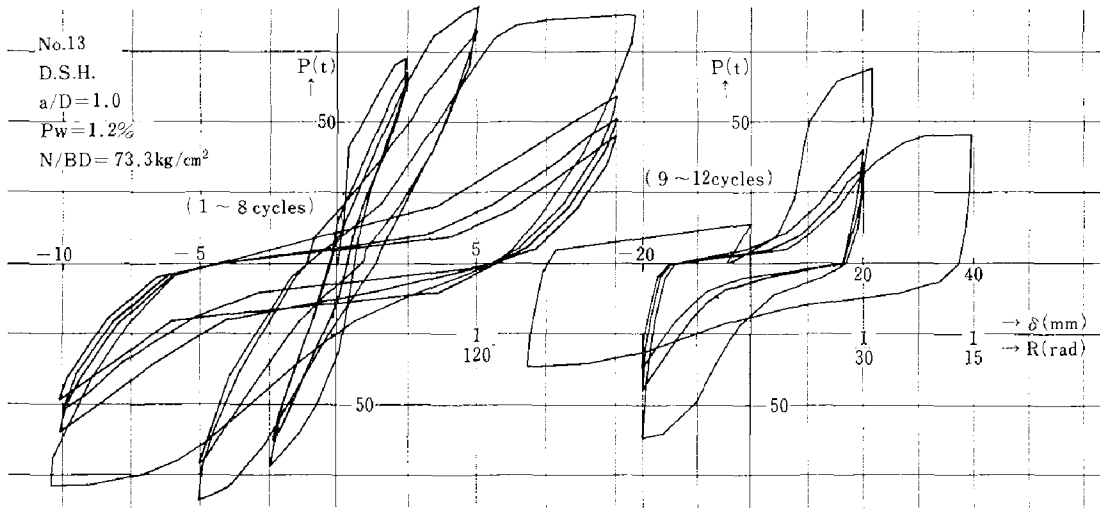


Fig. 8 Load-Deflection Curves(No.13)

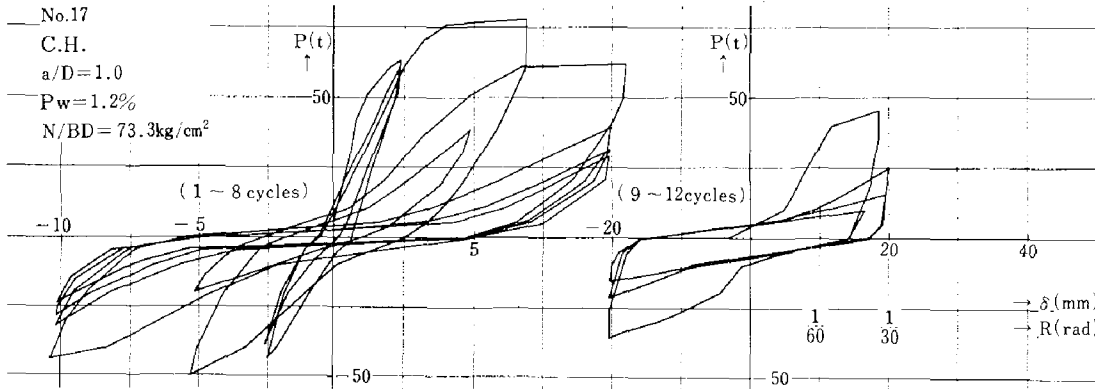


Fig. 9 Load-Deflection Curves(No.17)

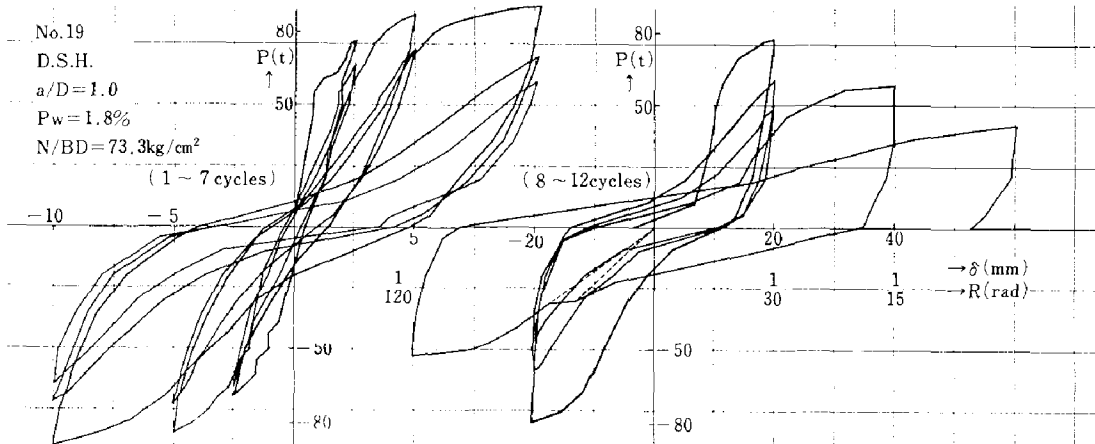


Fig.10 Load-Deflection Curves(No.19)

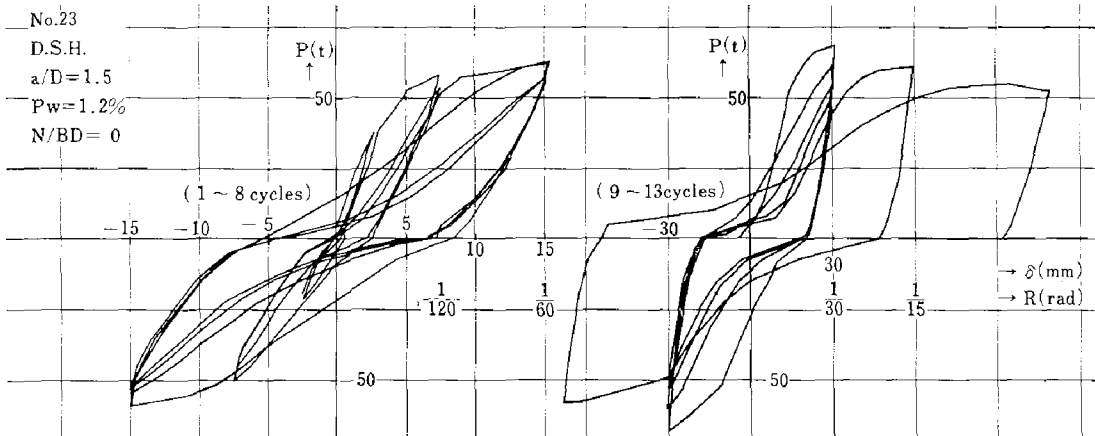


Fig.11 Load-Deflection Curves(No.23)

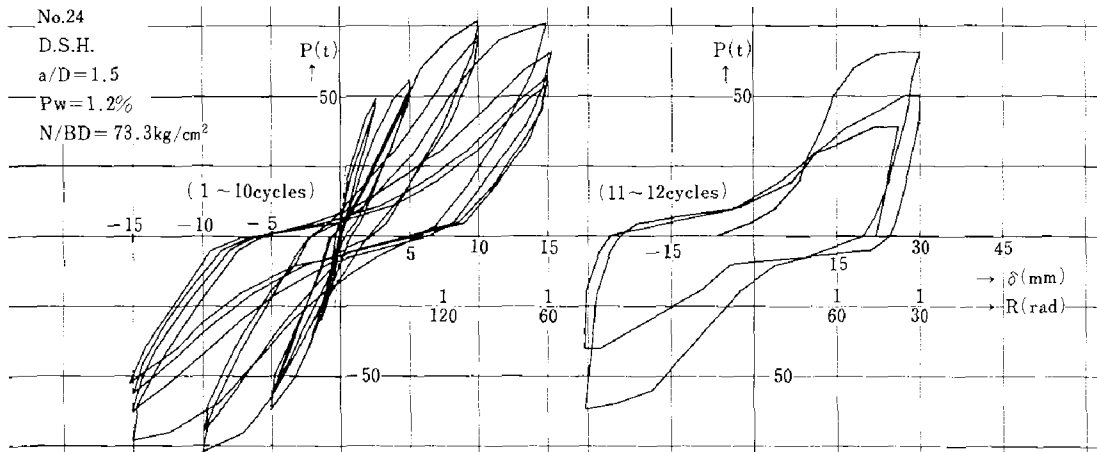


Fig.12 Load-Deflection Curves(No.24)

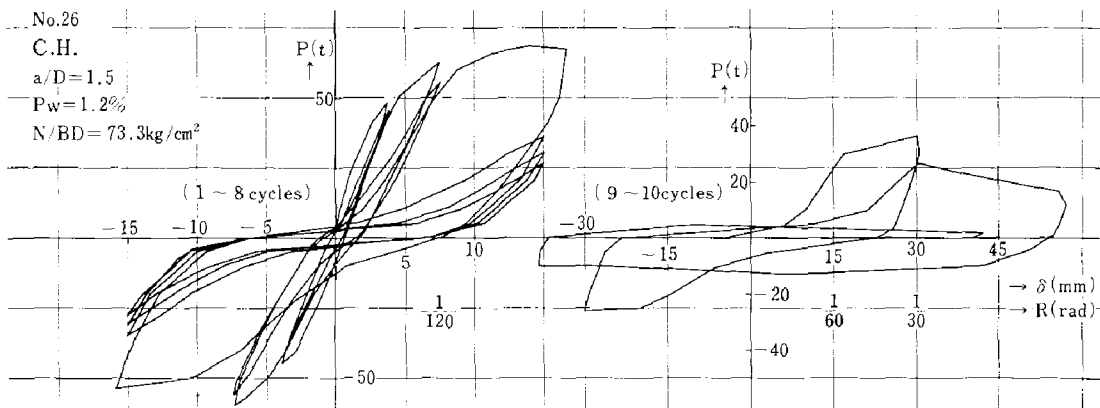


Fig.13 Load-Deflection Curves(No.26)

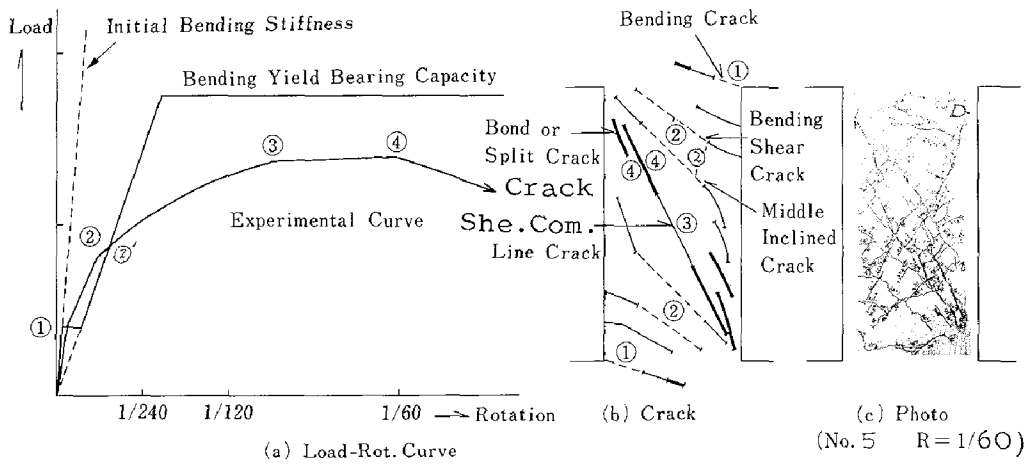


Fig. 14 Shear Failure Type Model

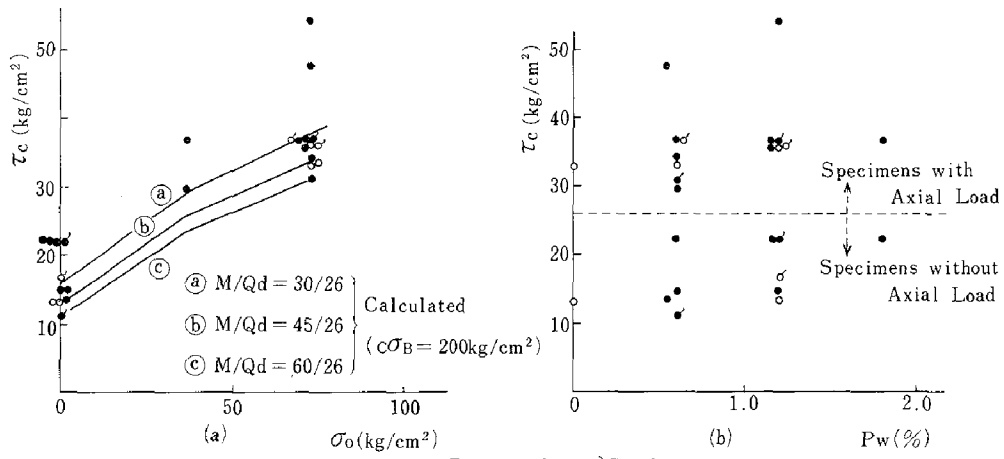


Fig. 15 Bending Shear Crack Stress

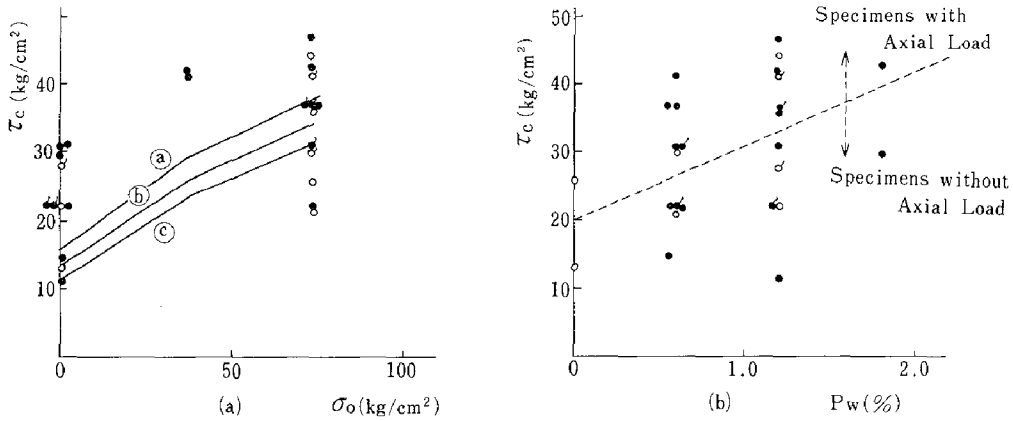


Fig. 16 Middle Inclined Crack Stress

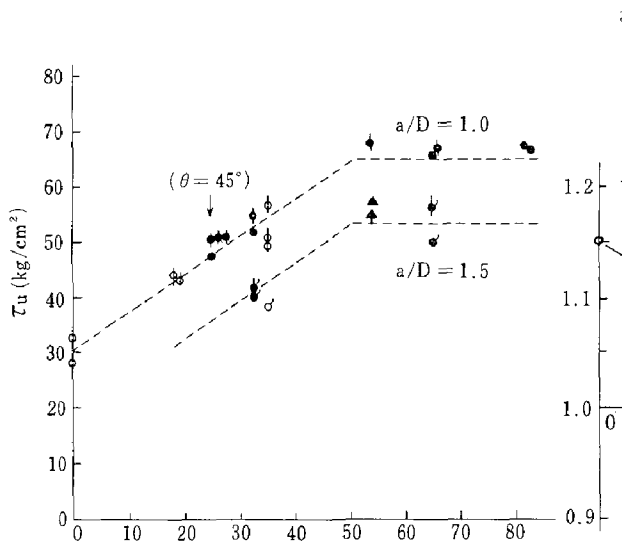


Fig. 17 Ultimate Shear Strength $P_w \cdot s \cdot \sigma_y$ (kg/cm²)

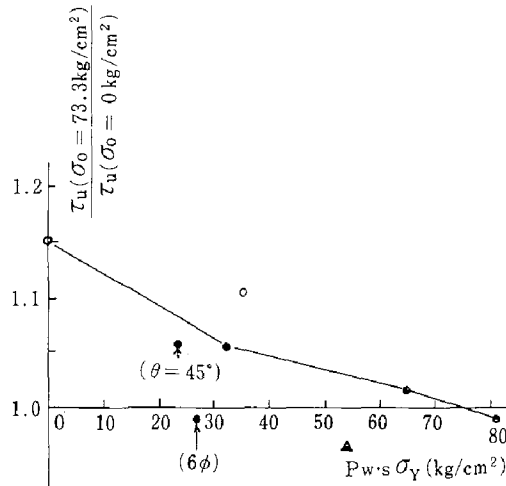


Fig. 18 Ultimate Shear Strength Ratio on Axial Load

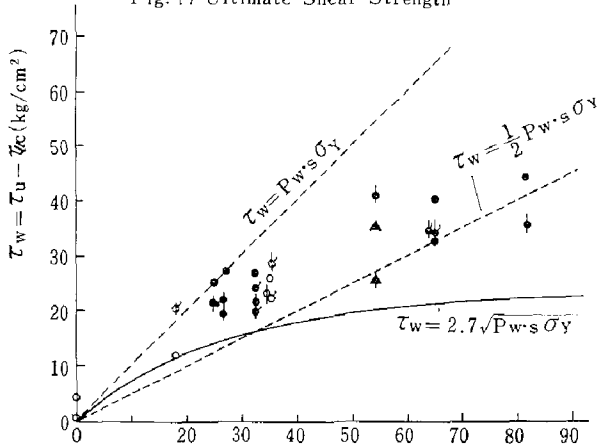


Fig. 19 Web Reinforcement's Share $P_w \cdot s \cdot \sigma_y$ (kg/cm²) in Ultimate Shear Strength

Symbol	
●	Double Spiral Hoop Specimen
○	Conventional Hoop Specimen
◊	$a/D = 1.5$
◆◆◆	Specimens with Axial Load
▲	No Weld

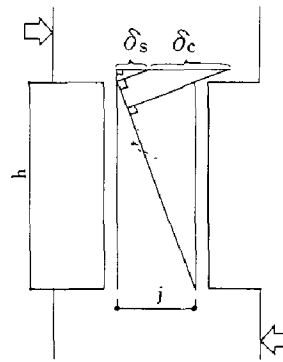


Fig. 2 (b) Truss Analogy

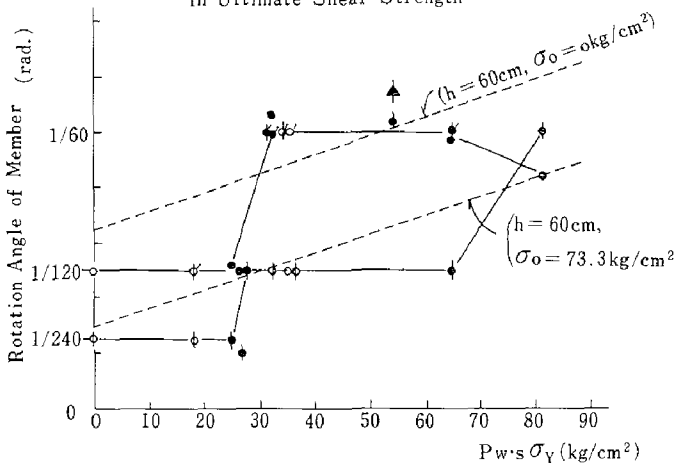


Fig. 20(a) Rotation Angle of Member

Note.

$$\delta_c/h = c \epsilon_B (j/h + h/j)$$

$$\delta_s/h = s \epsilon_t h/j$$

Rotation Angle of Member $= \delta/h = \frac{\delta_c + \delta_s}{h}$

$$c \epsilon_B = (0.2 + \frac{0.3}{80} P_w \cdot s \cdot \sigma_y) \%$$

$$s \epsilon_t = \begin{cases} 0.18\% & (\sigma_o = 0 \text{ kg/cm}^2) \\ \frac{0.18}{4}\% & (\sigma_o = 73.3 \text{ kg/cm}^2) \end{cases}$$

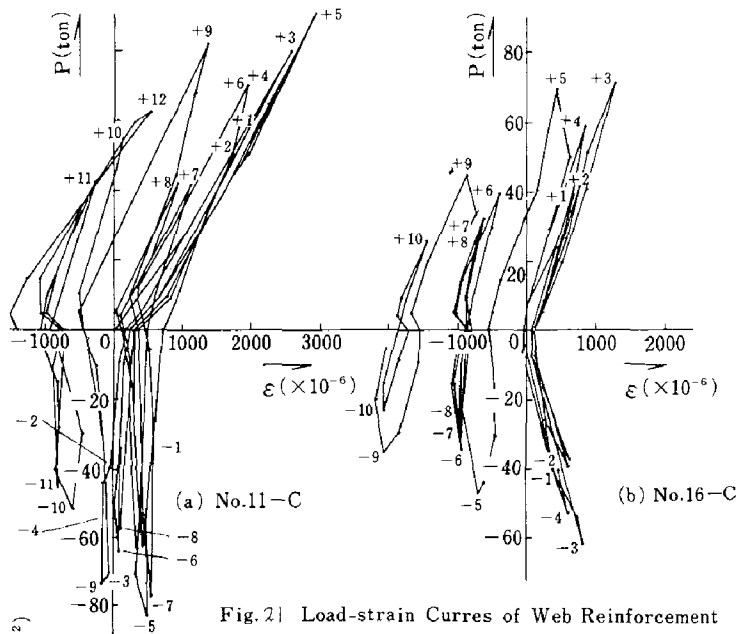


Fig. 21 Load-strain Curves of Web Reinforcement

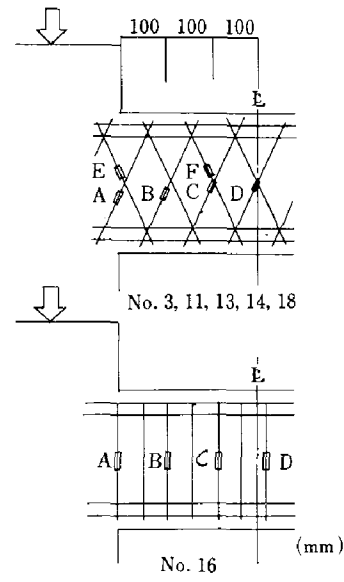


Fig. 22 Location of Embedded strain Gages

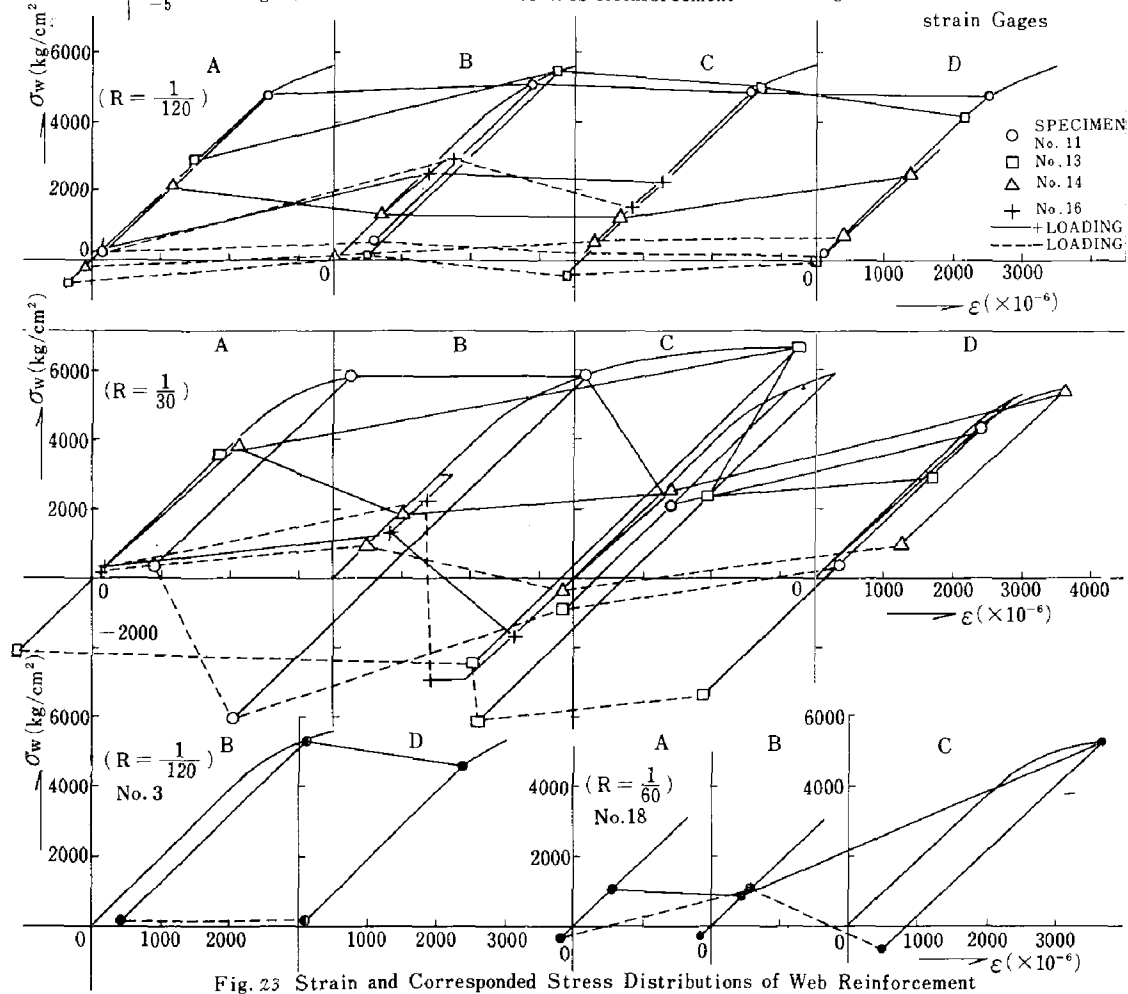


Fig. 23 Strain and Corresponded Stress Distributions of Web Reinforcement

INTERNATIONAL SYMPOSIUM ON
EARTHQUAKE STRUCTURAL ENGINEERING

541

St. Louis, Missouri, USA, August, 1976

TORSIONAL RESPONSE AT LARGE ECCENTRICITIES

K. J. MEYER AND I. J. OPPENHEIM

Department of Civil Engineering

Carnegie-Mellon University

Pittsburgh, Pa. 15213

The induced torsional response of a one storey structure was studied. The authors proposed and tested a simplified analysis technique. The technique properly recreated the periodicity of the torsional motion, but was disappointing in not accurately predicting the peak response. Examination of these somewhat "negative" results still revealed some interesting patterns of behavior. The main positive results are an extension of some well known earlier work, and an insight into probable response at large eccentricities.

Introduction

Torsional response of structures to earthquake ground motion is of increasing concern to structural engineers. One cause of torsional motion is an eccentricity between the center of stiffness and center of mass of the structure. This torsional response occurs even when the ground motion is purely translational, and is known as induced torsion. It is the subject of this study.

Newmark and Rosenblueth report in their text the results of several earlier studies. Most significant are the results originally published by Rosenblueth and Elorduy. These results show that an analysis neglecting the eccentricity (a purely translational analysis) always produce conservative values for the storey shears. This, however, leaves the analyst with the necessity of estimating the induced torsional moment. Typically, this is done by the "static method" where the moment is estimated as the storey shear times the plan eccentricity. This method may drastically underestimate the storey torque. The authors hoped to obtain better results with their "simplified analysis" which will be described in the following section. Unfortunately, the "simplified analysis" was not as immediately successful as the authors might have wished.

The Model and the Simplified Analysis

The general configuration of the model is shown in Figure 1. The structure is a one storey, square rigid slab supported by four corner columns. The three independent variables are the two translations and the rotation at the geometric center of the slab. This point is coincident with the mass center. The total lateral stiffness for the four columns remains constant; the ratio of stiffnesses between pairs of columns will vary to move the center of stiffness and thus create the eccentricity. The equation of motion for the system is

$$[M]\{\ddot{u}\} + [C]\{\dot{u}\} + [K]\{u\} = \{F(t)\}$$

In this formulation the mass matrix $[M]$ is diagonal. The off diagonal terms of the stiffness matrix represent the effect of the eccentricity. The eccentricity is modeled in only one direction, normal to the applied ground motion. The damping matrix, $[C]$, is selected to produce Rayleigh damping of 2.5% of critical.

The Excitation

Unlike the earlier study, (Rosenblueth and Elorduy) which used a spectrum analysis, the loading is a time dependent acceleration record representing a strong motion earthquake. The record is an artificial one produced by the program PSEQGN. It has a peak surface acceleration of 0.5g and a duration of 10 seconds. Its spectrum resembles those produced by real earthquake records.

Methods of Analysis

The basic analysis method is a straight-forward numerical solution using the Wilson- θ method. Theta was always set to 1.37 and the time interval was less than one tenth the shortest structural period.

The static method of estimating storey torque has already been mentioned. In this method a solution is required only for the lateral response of the structure. The torsional moment is then estimated as the maximum lateral force times the eccentricity.

The authors' "simplified analysis" was intended to replace the three-dimensional "exact" analysis with a series of steps involving one-dimensional analyses. The first step consists of finding the lateral force (as a function of time) for the purely translational structure. The second step multiplies this record by the eccentricity, resulting in a time-varying torsional moment forcing function. In the third step the torsional forcing function is applied to the purely torsional structure, giving a torsional response as a function of time. These steps may be restated as:

- 1) Find $H(t)$ from $M\ddot{u} + C\dot{u} + Ku = -M\ddot{u}_g$

2) Find $M_t(t)$ as $M_t(t) = H(t) * \text{Eccentricity}$

3) Find $\theta(t)$ from $I_p \ddot{\theta} + C \dot{\theta} + K_t \theta = M_t(t)$

Results

Fifteen cases were analyzed. The ratio of rotational to translational modal natural frequencies took five different values; for each ratio eccentricities of 10, 20, and 30% of the plan dimension were used. The ratio was expressed as MK/Jk which is the square of the ratio of the frequencies. This ratio took the values 3, 2, 1, 0.96 and 0.5.

The results of the proposed analysis method were disappointing when compared to the exact results. The amplitude of the maximum torsional moment was often more accurately predicted by the static method. The error was found to increase with the eccentricity for modal ratios greater than 1 and decrease with the eccentricity for modal ratios less than 1. When the moment records are compared (Figure 2) it is seen that the moment-time plots are similar; this is true as long as the system is removed from resonance. Work is being done to see if the proposed method can be corrected, maintaining its accurate periodicity and upgrading its estimation of peak response.

The results from the exact analysis are presented in Figures 3 and 4. This presentation is the same one used by Rosenblueth and Elorduy. Figure 3 shows the dynamic shear (from the exact analyses) divided by the "static" shear, which is obtained from analyzing a one degree of freedom translational structure. Figure 4 shows the ratio of dynamic torsional moment (from the exact analysis) to the static moment, which is simply the static shear times the eccentricity.

There are, however, some results which may not have been suspected. The static shear is always conservative as an estimate of lateral force, but the curves in Figure 3 change shape for different values of the eccentricity. Structures with low eccentricity are characterized by a sharply increasing curve near resonance, while other structures display much less of a peak. The results from Rosenblueth and Elorduy (for 5% eccentricity) indicate a ratio fairly close to 1 except in the area near resonance; for larger values of eccentricity this is not the case.

Figure 4 shows good general agreement with the other authors' results for the eccentricity magnification factor. These curves drop off more sharply than the corresponding plots of shear force. This implies that, outside of the resonance region, the static method is adequate for estimating torsional moments.

Results are further displayed in Table I, listing the torsional moments from the exact analysis and from the simplified approach. As already mentioned, the correspondence is not good. Of great interest, however, is that in the resonant region ($MK/Jk=1, =0.96$)

the moment produced at 30% eccentricity is less than that produced at 20% eccentricity. This is explained by the fact that the eccentricity alters the natural frequencies of the system, separating the two modes. Resonance should be defined with respect to the true frequencies, including the effects of eccentricity.

Conclusions

The last mentioned result is significant in assessing the non-linear performance of structures. Were a structure, with its original eccentricity, near the resonant state, an earthquake loading would immediately produce severe torsional moments. This loading, however, could be expected to cause non-linear action, resulting in a re-distribution of stiffness. A migration of the shear center would be expected. Therefore, the resonant state will be only temporary. This will be the subject of future work.

The results of the time history analyses themselves compare closely with results of the earlier study where smooth spectra were used. Those results have now been somewhat extended to include systems with greater eccentricities. It was shown that the translational analysis for "static shear" may err more than expected for large eccentricities, though the error is conservative. The static method of analysis for storey torques still is unsuitable in the region near resonance. The method developed by the authors, based on an interesting physical model, was in error. The method still retains some promise, and further work is needed.

References

Meyer, K. J., Some Aspects of the Analysis of Story Torques Induced by Translational Strong Ground Motions, M. S. Thesis, Carnegie-Mellon University, Pittsburgh, Pa. 1975.

Newmark, N. M., and Rosenblueth, E., Fundamentals of Earthquake Engineering, New Jersey, Prentice-Hall, 1971

Rosenblueth, E., and Elorduy, J., "Responses of Linear Systems to Certain Transient Disturbances," Proc. Fourth World Conf. Earthq. Eng'g., Santiago, Chile, 1969.

TABLE I

Torsional Moments - Exact Method and Simplified Method

MK/Jk	Eccentricity %	M _{exact} x 10 ⁷	M _{simpl.} x 10 ⁷	M _{exact} /M _{simpl.}
2	10	0.4414	0.7311	0.60
	20	0.5429	1.358	0.40
	30	0.6498	2.068	0.31
1	10	1.307	2.920	0.45
	20	1.430	5.422	0.26
	30	0.9420	8.261	0.11
0.96	10	1.247	2.939	0.42
	20	1.446	5.458	0.26
	30	1.034	8.312	0.12
0.5	10	0.6420	0.3952	1.62
	20	0.9429	0.7339	1.28
	30	1.253	1.118	1.12

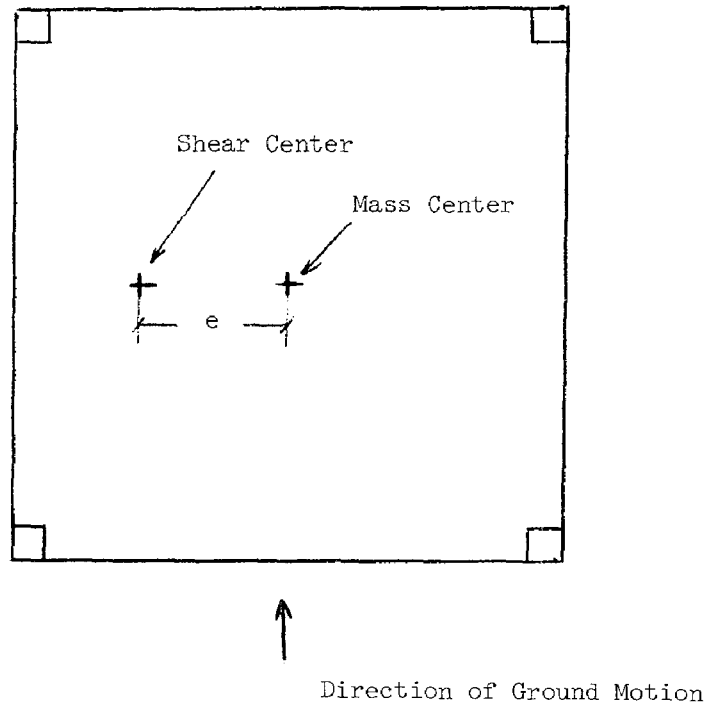


Figure 1. Structural Plan

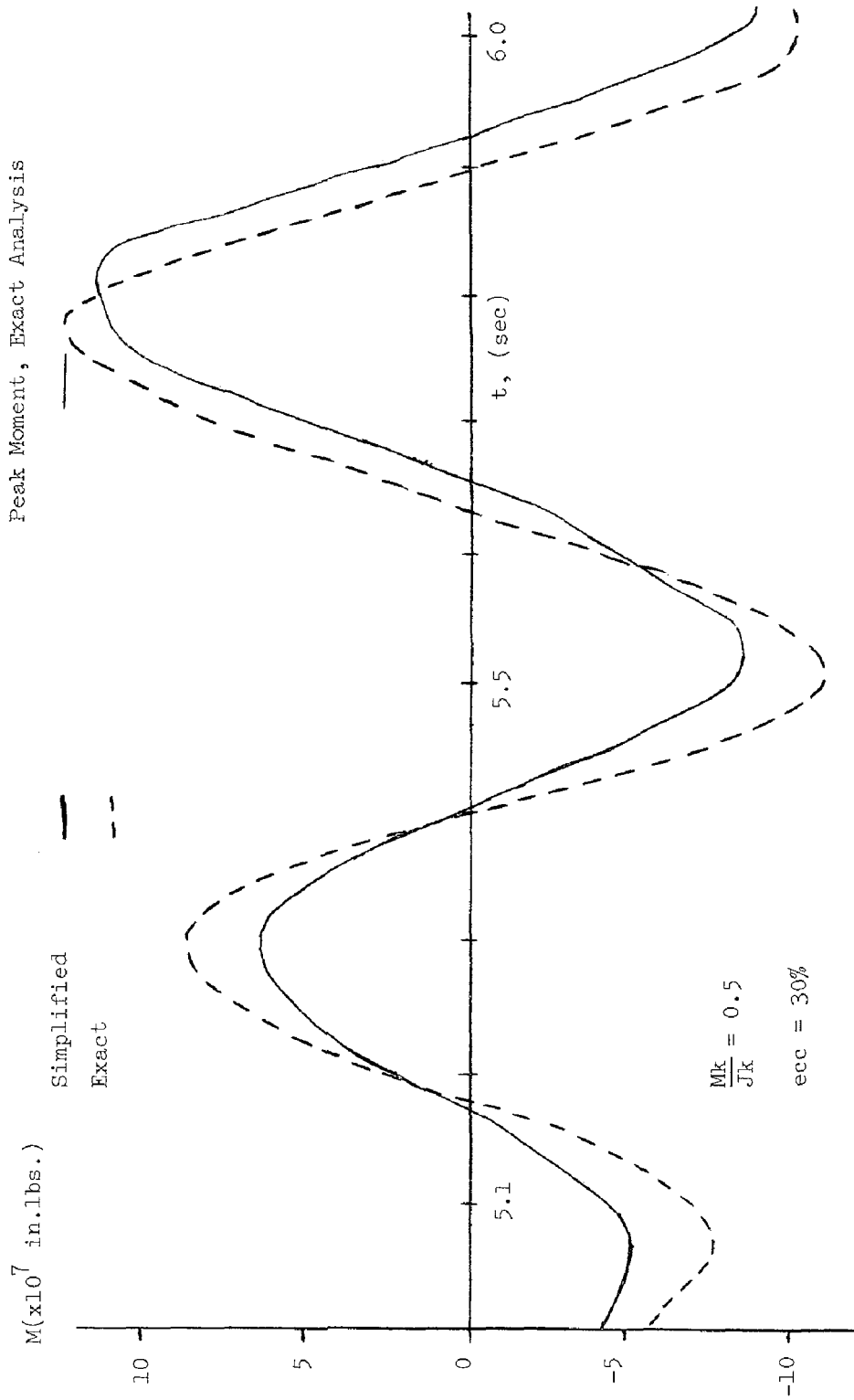


Figure 2. Exact and Simplified Moment Records

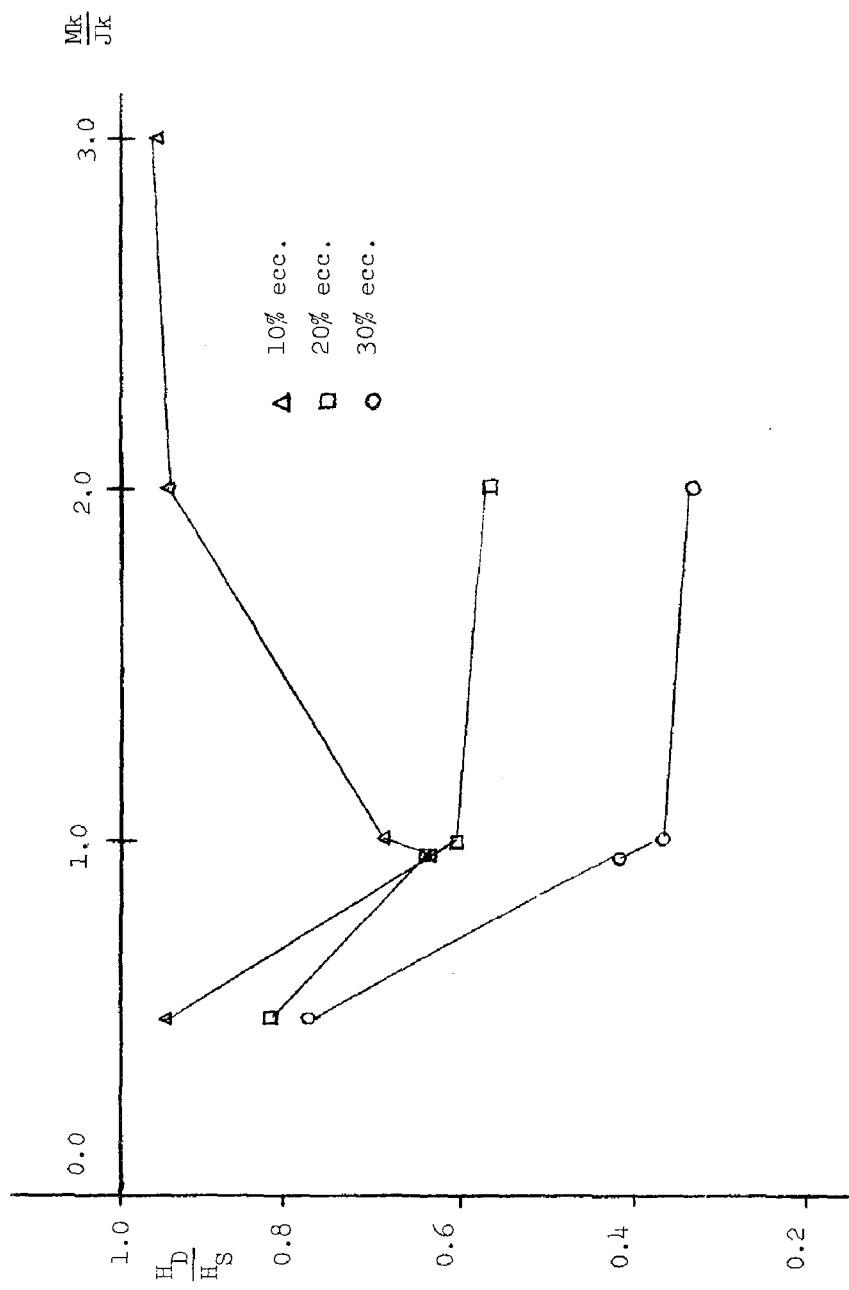


Figure 3. Plot of Dynamic Shear/Static Shear

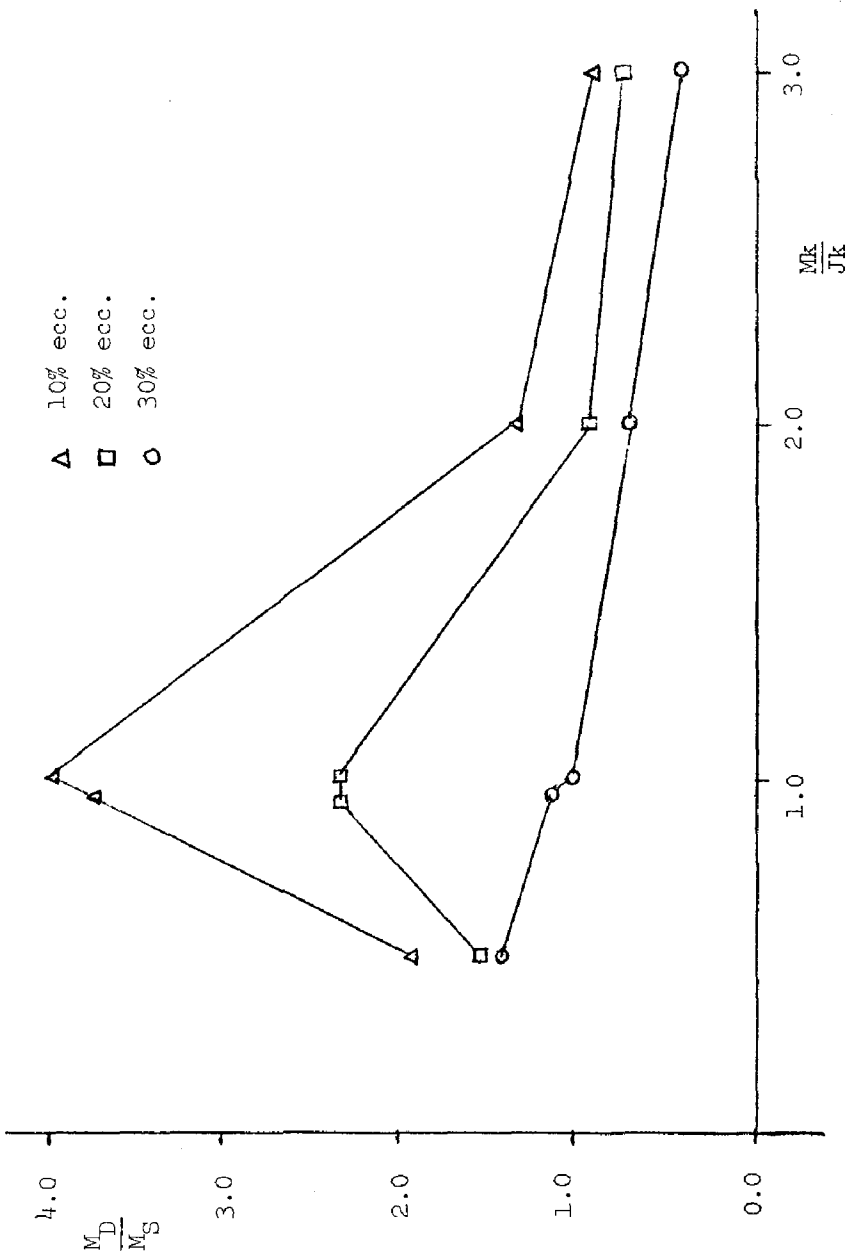


Figure 4. Plot of Dynamic (Torsional) Moment/Static Moment



INTERNATIONAL SYMPOSIUM ON
EARTHQUAKE STRUCTURAL ENGINEERING

551

St. Louis, Missouri, USA, August, 1976

ESTABLISHMENT OF DESIGN EARTHQUAKES -
EVALUATION OF PRESENT METHODS

by V. V. Bertero
Professor of Civil Engineering

In collaboration with

R. A. Herrera
Junior Specialist

S. A. Mahin
Assistant Research Engineer

University of California

Berkeley, USA

SUMMARY

This paper evaluates the reliability of current methods of establishing design earthquakes for structures located at sites near potential source(s) of major earthquakes. Problems associated with the establishment of such earthquakes are reviewed and present methods are summarized. Emphasis is placed on assessing the reliability of the method which derives inelastic design response spectra directly from a linear-elastic design response spectrum. The suggested spectra are compared with response spectra, computed for accelerograms derived from records obtained near the fault rupture of the 1971 San Fernando earthquake. The aseismic design implications of the results of this comparison are evaluated on the basis of the dynamic responses of single and multiple degree-of-freedom systems subjected to available accelerograms of near-fault ground motions. Guidelines for improving present methods of establishing design earthquakes are suggested and recommendations for future research are offered.

INTRODUCTION

One of the most challenging problems for a structural designer is to achieve an economical, serviceable, and safe design for a building located at a high seismic risk site. To achieve such an efficient aseismic design, it is necessary to predict the mechanical behavior of the structure under the critical earthquake conditions. Building damage may result from different effects of an earthquake, e.g. (1) ground failures due to fault ruptures or those due to the effects of seismic waves (soil vibrations creating fissures, landslides, lurching, nonuniform compaction and associated differential settlement, and liquefaction); (2) vibrations transmitted from the ground to the structure; (3) seismic sea waves (tsunami) and tsunami-like disturbances and seiches in lakes; and (4) other consequential phenomena such as fires, and floods caused by dam failures and by landslides plugging rivers or increasing the water level of lakes. The effect which usually concerns the structural engineer, and is presently accounted for by seismic resistant design provisions of building codes, is the response of a structure to ground shaking. This is the only source of damage that will be considered in this paper.

Preceding page blank

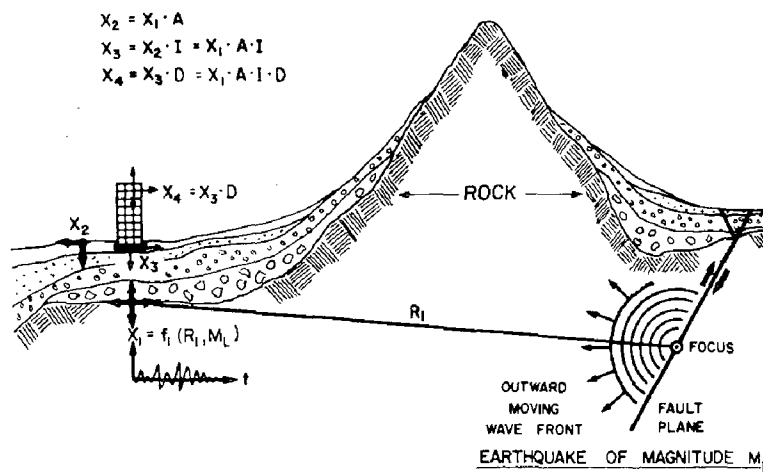


FIG. 1 FACTORS USED TO PREDICT SEISMIC RESPONSE

this is a simple expression, the uncertainties involved in a realistic estimation of X_3 and D give rise to serious difficulties in obtaining an accurate numerical evaluation of X_4 .

For an earthquake of specified magnitude, M_L , and focal distance, R_1 , it seems analytically feasible to estimate the base rock motion at the given site, X_1 (Fig. 1), if the fault type is known [$X_1 = f(R_1, M_L)$] [10]. Prediction of X_3 , however, must account for the effects of the soil layers underlying and/or surrounding a building. These effects can be classified in two groups: one is related to the influence of the dynamic characteristics of the different soil layers during the transmission of X_1 to the free ground surface, indicated in Fig. 1 by an attenuation or amplification factor, A [$X_2 = A \cdot X_1$]; the other is related to the interaction between structure and soil foundation, symbolically represented by a factor, I . At present, large uncertainties exist regarding the realistic values of A and I , and major errors could be introduced by trying to quantify these two factors using available analytical techniques. Even if X_1 could be predicted with engineering accuracy, attempts to quantify the influence of soil conditions on X_1 to attain X_2 and X_3 would result in a wide range of predicted values. Thus, the designer should not rely exclusively on results obtained from a single deterministic analysis. Bounds on the possible variations in A and I should also be considered.

The precise evaluation of X_4 at any point in the structure would require the establishment of its three translational and three rotational components. To simplify the discussion, however, it is assumed that for aseismic design the only significant components are the two horizontal translational ones, and that each of these components can be considered independently. Thus, X_4 can be defined by evaluating the total lateral displacement, ΔH_i , of each floor (Fig. 2). The prediction of the lateral displacement response of a particular building to a specific ground motion will depend upon the excitations acting on the structure and on the dynamic characteristics of the whole soil-structure system. In general, the main excitations acting on a structure during an extreme earthquake are due to: (1) gravity forces,

The general problems involved in predicting the seismic response of a building are symbolically defined and schematically illustrated in Fig. 1. As stated above, the structural engineer is concerned with predicting the response, X_4 (Fig. 1), which results from shaking at the foundation, X_3 . As indicated in Fig. 1, the term X_4 can be obtained by multiplying X_3 by a dynamic operator, D . Although

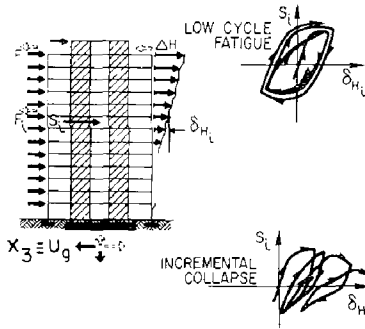


FIG. 2 LATERAL STORY SHEAR-DISPLACEMENT RELATIONSHIP

$G(t)$, with the associated effects due to creep of the material, especially in the case of concrete structures; (2) changes in environmental conditions, $\Delta E(t)$, such as the stresses produced by changes in temperature; and (3) at least the three translational components of the foundation shaking, $X_3(t)$. As shown in Eq. 1(a), the dynamic characteristics of the whole system, which change continuously as the structure is deformed into its inelastic range, might be summarized by representing them symbolically as the instantaneous values of: (1) mass, $M(t)$; (2) damping coefficient, $\xi(t)$; and (3) resistance function, $(R \text{ vs. } \Delta H_i)(t)$. As illustrated in

Eq. 1(b), the dynamic characteristics of the soil-structure system can also be symbolically represented by the instantaneous values of: (1) fundamental period, $T(t)$; (2) damping coefficient, $\xi(t)$; (3) yielding strength, $R_y(t)$; and (4) energy absorption and dissipation capacity as represented by the instantaneous available ductility, $\mu(t)$, which is a function of $\Delta H_i(t)$. Thus:

$$X_4 = \Delta H_i(t) = F \left\{ [G(t), \Delta E(t), X_3(t)], [M(t), \xi(t), (R \text{ vs. } \Delta H_i)(t)] \right\} \quad [1(a)]$$

$$X_4 = \Delta H_i(t) = F \left\{ [G(t), \Delta E(t), X_3(t)], [T(t), \xi(t), R_y(t), \mu(t)] \right\} \quad [1(b)]$$

Dynamic Characteristics of Excitations
Dynamic Characteristics of Whole Soil-structure System

Analysis of the parameters included in Eqs. 1(a) and (b) clearly indicates the magnitude of the problems involved in trying to predict response to earthquake ground motions. One problem arises from the fact that all these parameters are functions of time, although the gravity forces and changes in environmental conditions usually remain nearly constant for the duration of an earthquake. In general, therefore, this is a dynamic problem for which it is necessary to consider two important effects of the time variation of the excitations and of the response: first, the effect of inertial forces developed by the mass; and second, the effect of rate of change in the intensity of strains with time (rate of loading or straining). This rate may be high enough to considerably affect the so-called static-mechanical characteristics of the materials on which the dynamic characteristics of the structure [$T(t)$, $\xi(t)$, $R_y(t)$, and $\mu(t)$] are usually predicted.

Another problem is that $\Delta H_i(t)$ depends on the response of the whole soil-structure system rather than that on the structural system alone. Soil-structure interaction affects the so-called free-field ground motion, $X_2(t)$ (Fig. 1), which is the ground motion usually measured. Furthermore, the response of the building depends, to a considerable extent, on the interaction between structural elements and nonstructural components, and this interaction is very difficult to predict accurately.

To carry out an efficient aseismic design, it is necessary to predict the building's response to the worst combination of excitations that can occur. To do this it is necessary to establish the controlling (critical)

ground motions, X_3 , commonly referred to as "design earthquakes," and to obtain information regarding the dynamic characteristics of the whole soil-structure system. More specifically, it is necessary to know the actual excitation-deformation relationship or restoring force characteristics of the whole soil-structure system which include stiffness, strength, energy absorption and energy dissipation capacities, and the different sources of damping. Although it is not possible to study independently the problems associated with establishing design earthquakes from those problems associated with the dynamic characteristics of the building, in this paper, emphasis is placed on the problems associated with the establishment of design earthquakes.

OBJECTIVES AND SCOPE. - The main objectives of the study reported herein are, first, to evaluate the reliability of present methods for specifying design earthquakes for structures located at sites near [less than about 10 mi. (16 km)] potential source(s) of major earthquakes, and, second, to assess the implications of the results obtained in order to improve such methods.

To achieve the above objectives, different methods of specifying the design earthquakes are briefly reviewed. Emphasis is placed on the method which derives an inelastic design response spectrum (IDRS) directly from a linear-elastic design response spectrum (LEDRS). The suggested LEDR and IDR spectra are compared with the response spectra derived from the records obtained near the fault rupture of the 1971 San Fernando earthquake. The implications of the differences identified from this comparison are evaluated based on the results obtained in a series of analyses on the linear-elastic and nonlinear dynamic responses of single and multiple degree-of-freedom systems to some of the ground motions either directly recorded or derived from the San Fernando earthquake records.

ESTABLISHMENT OF DESIGN EARTHQUAKES

The general philosophy of earthquake-resistant design for buildings other than essential facilities has been well established. Significant aspects of this philosophy are: (1) to prevent nonstructural damage in minor earthquake ground shakings, which may frequently occur during the service life of the structure; (2) to prevent structural damage and minimize nonstructural damage in moderate earthquake shakings, which may occasionally occur; and (3) to avoid collapse or serious damage in major earthquake ground shakings, which may rarely occur.

Before this philosophy can be implemented for a given building, it is necessary to establish what constitutes minor, moderate and major ground shaking at the building site and to describe quantitatively the corresponding earthquake ground motions that should be considered as the critical excitations at the building foundation. In other words, it is necessary to establish the design earthquake(s).

EVALUATION OF PRESENT METHODS. - In the past, the design earthquake has been specified in terms of a building code zone, site intensity, or site acceleration [14]. In aseismic design, it is generally recommended that a structure be proportioned to withstand the effects of horizontal base translation assumed to take place nonconcurrently along each of the two main horizontal axes of the structure. Thus, the structure is usually designed for the envelope, rather than for the effects of the two horizontal

excitations acting simultaneously [23].

Ground motions actually have six components: three translational and three rotational. For sites located near active faults (or, more generally, near the earthquake source), each of the six components can have a significant effect on the overall response of a building, and prediction of response should be based on the simultaneous action of all six components. Actual records of all ground motion components should be obtained in future earthquakes in order to study their effects on building response and to determine the minimum data required by structural engineers to adequately define design earthquakes. Determination of these data is not simple because they vary according to the limit states controlling the design of the structure. Depending on the function and type of structure, different limits of usefulness can control the design. At least two main cases should be considered; one in which the design is controlled by service limit states, and the other, by ultimate limit states. In the former case, the structure should essentially remain in its linear-elastic range of behavior to avoid functional failure; in the latter, inelastic behavior up to the point of incipient dynamic collapse could be tolerated.

Service Limit State Design Earthquakes. - One of the most common practices is to specify the design earthquake by only a peak site acceleration. The reliance on such an acceleration alone, however, is generally inadequate. From available ground motions and building response data, it is now generally accepted that one of the best ways to describe quantitatively the service level design earthquake is through an average or smooth response spectrum [2]. This spectrum is best obtained by a statistical analysis of the linear-elastic response spectra of ground motion records resulting from earthquakes with comparable magnitudes and obtained at sites with similar epicentral distances and soil conditions. Analyses of this type conducted by Newmark, Blume, and Kapur [20] show that the basic data necessary to construct possible design response spectra are the peak acceleration, velocity, and dynamic or transient displacement of the critical ground shaking at the site of the structure. Therefore, to establish the design spectra the following questions must be answered: (1) what reasonably expected types of earthquakes represent the most severe seismic hazard at the site; and (2) for these types of earthquakes, what ground motions are reasonably expected at the site?

Although there are sufficient seismic and geological data to estimate the minor, moderate, and major expected earthquakes for certain sites [21, 29], in most cases, these data are unavailable or insufficient, particularly for major earthquakes. If the peak ground acceleration, velocity and displacement at a site are known, it will be possible to construct smoothed LEDRS for selected values of damping using spectral amplification factors [20]. When only the peak ground acceleration is available, it has been suggested that reasonable estimates of the peak ground velocity and displacement may be made "for a number of areas in the world...either on firm ground, soft rock or competent sediments of various kinds," by multiplying the ground acceleration (expressed as a fraction of gravity) by 48 in./sec. (122 cm/sec.) and 36 in. (91 cm), respectively [18].

Ultimate State Design Earthquakes. - Comparison of lateral design forces derived from LEDRS for major earthquakes with those specified by present

code regulations indicates that it would generally be uneconomical to design all structures to resist elastically a major earthquake. Design forces lower than those derived from LEDRS may be used by taking advantage of the structure's inelastic energy dissipation capacity. The inelastic deformations, however, must be kept within the acceptable limits imposed by the available structural deformation capacity and/or by the degree of nonstructural damage usually associated with such large inelastic deformations that can be tolerated. Preliminary design loads can be obtained from IDRS that are derived by evaluating the nonlinear dynamic response of structural models with realistic hysteretic idealizations subjected to various ground motions having characteristics appropriate to the site, e.g. see Ref. 16. Because of the complexities involved in such nonlinear dynamic analyses, simpler methods which derive the IDRS by directly modifying a LEDRS are more commonly used [2,19]. The LEDRS is modified by using factors obtained from analyses of the elasto-perfectly plastic response of single degree-of-freedom systems [18]. These methods, however, are based on results obtained with limited numbers of ground motion records and caution should be exercised when applying them to sites that can be subjected to significantly different kinds of ground motions. Furthermore, such methods may not be suitable for multiple degree-of-freedom systems, or in cases where the actual hysteretic behavior is likely to differ from the assumed elasto-plastic idealization [6,18].

The validity of deriving the IDRS directly from the LEDRS can be seriously questioned because the types of excitations that induce the maximum response in elastic and inelastic systems are fundamentally different. The information used for computing (and therefore contained in) an LEDRS, although necessary, is insufficient for predicting the maximum inelastic dynamic response. This information should be complemented with data on the duration of strong ground shaking and the number, sequence and characteristics of intense, relatively long acceleration pulses (i.e. pulses inducing large ground velocity increments) that can be expected.

The need for this additional information can be found by reviewing the results obtained by applying the vibration theory to single degree-of-freedom systems. In the case of a linear-elastic system, the critical dynamic excitation is of a periodic type having a frequency equal to that of the system because this induces an engineering resonance phenomenon. For this type of excitation, the dynamic magnification operator, D , can reach a maximum value approximately equal to $\frac{1}{2\xi}$. Thus, for values of ξ ranging from 2 to 10 percent, D can attain values ranging from 25 to 5. Since the largest value of D for an impulsive excitation is only 2, severe long acceleration pulses are usually not critical for linear-elastic response. In an inelastic system, however, such long pulses can become critical. This is particularly true for a structure having a hysteretic yielding resistance, R_y , equal to or less than the inertial force corresponding to the effective ground acceleration of the pulse, i.e., $R_y \leq M\ddot{x}_g$, where M is the mass of the structure. In the case of elasto-plastic systems, the existence of periodic short acceleration pulses in the ground motion contributes only to building the response of the system up to its yielding level. Once the system begins to yield, the phenomenon of engineering resonance is depressed since the energy dissipated through even small inelastic deformations is equivalent to very large values of ξ . Therefore, very large inelastic deformations are not expected during each yielding excursion. Although the existence of periodic short pulses can induce a series of yielding reversals, it is doubtful that the number of these reversals can lead to a phenomenon of

low cycle fatigue. This is because the amount of inelastic strain developed in each reversal will usually be so small that the number of reversal cycles required to induce fracture would even exceed the number which can occur in the longest conceivable strong motion of an actual earthquake.

The above discussion indicates that the amplification factors to be applied to the maximum ground accelerations in order to obtain the maximum linear-elastic response of a structure are usually controlled by the engineering resonance phenomenon. On the other hand, considerably larger deformations can be induced by the presence of just one, long pulse with an effective acceleration equal to or just greater than that corresponding to the yielding strength of the structure. Furthermore, repeated applications of severe long acceleration pulses can lead to the accumulation of sufficiently large inelastic strains which could induce one or a combination of the two types of failure illustrated in Fig. 2, i.e. low cycle fatigue and incremental (crawling) collapse. Of these two, the author believes that the critical failure against which the structure should be designed is the crawling type of collapse. This is because the number of cycles of large inelastic strain reversals necessary to attain fracture of the structural material is usually so great that it is doubtful that it can be developed by the number of severe long pulses that could exist in even the longest conceivable strong motion of an actual earthquake.

It should be clear from the above discussion, that even for a given site, the design earthquake is not unique. The critical ground motion depends on the type of behavior that is expected to control the response of the building at the site or on the limit state(s) controlling the design.

From results already available on the response of single degree-of-freedom systems to impulsive forces, it becomes clear that in the case of seismic ground motions, the larger the intensity of the effective acceleration of a pulse with respect to the yielding strength of the structure and the longer the duration of the pulse relative to the fundamental period of the structure, the larger the amount of inelastic deformations that will develop. In order to specify quantitatively the inelastic design earthquake, however, it is necessary to determine: (1) the severity of the long acceleration pulses that can be developed during an earthquake; and (2) the manner in which these pulses can be defined. An attempt to resolve these problems follows.

Analysis of 1971 San Fernando Earthquake Records. - It is possible to address the first problem by analyzing the records of the two strongest motions obtained from the San Fernando earthquake of February 9, 1971. The only strong motion accelerograph record near the fault rupture of this earthquake was obtained at Pacoima Dam (PD), Fig. 3. A seismoscope record was also obtained at the abutment of the lower Van Norman Dam (VND) which was located near the fault zone.

Pacoima Dam Record. - This record [Fig. 4(a)] contains the highest ground acceleration registered to date, 1.25g. Several investigators [22,27,] have indicated that the irregular surface topography in the vicinity of the accelerometer significantly affected the frequency content of the record, especially for frequencies greater than 1 Hz. Analysis of the dam and adjacent geological structures has led to a derivation of the ground

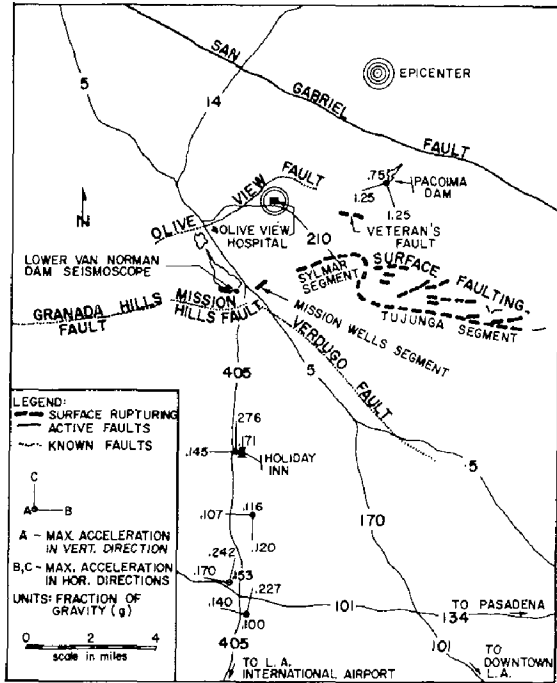


FIG. 3 LOCATION OF STRONG MOTION SEISMOGRAPHS IN SAN FERNANDO AREA

motion at sites below the base of the dam [Fig. 4(b)] [27]. Since the effects of local surface and interaction of the dam with its foundation have been removed from the derived record, it is probably more representative of ground motions at other nearby sites than the actual PD accelerogram. (Note that the derived record was based on an erroneous orientation initially reported for the PD record.)

The derived Pacoima Dam (DPD) record [Fig. 4(b)] indicates that the high peak accelerations registered at the PD after 6 sec. may not be characteristic of ground motions experienced at other sites. Both records, however, contain two severe acceleration pulses, each of about 2/3 sec. duration, at about

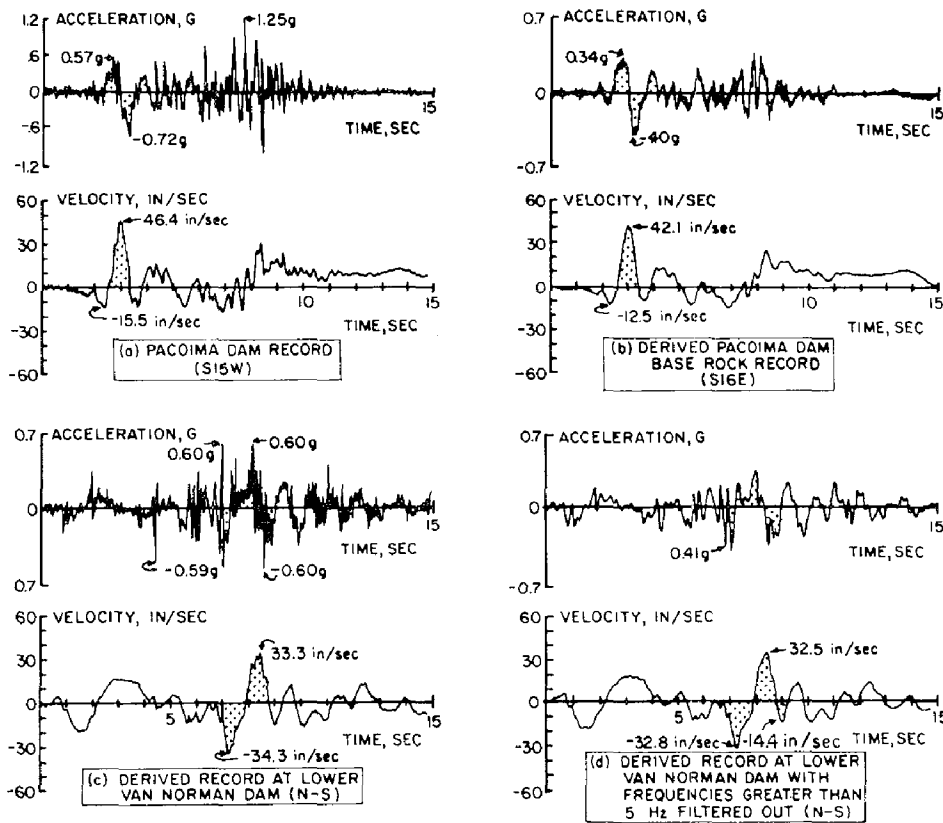


FIG. 4 NEAR-FAULT GROUND MOTION RECORDS OF SAN FERNANDO EARTHQUAKE

2-4 sec. These unusual acceleration pulses resulted in very large incremental ground velocities [PD, 61.9 in./sec. (157 cm/sec.); DPD, 54.6 in./sec. (139 cm/sec.)] and ground velocities (Fig. 4). They also led to unusually large linear-elastic response spectrum values for periods larger than 0.8 sec. (Fig. 5).

Van Norman Dam Records. - The ground motion necessary to produce the seismoscope trace obtained at the abutment of the lower Van Norman Dam [located near the fault zone about 6 mi. (10 km) from Pacoima Dam] has been computed [24]. The north components of this record and one which resulted by filtering out the frequencies above 5 Hz, are shown in Figs. 4(c) and (d). Although many of the characteristics of this ground motion are different from those of the PD record, as would be expected, the VND contains a series of long acceleration pulses that led to large incremental ground velocities, the largest being 67.6 in./sec. (172 cm/sec.).

Characteristics of Near-fault Records. - For the second problem stated above, it may be possible to determine the characteristics of long acceleration pulses by examining the records of near-fault ground motions. Some studies have already indicated that the severe long acceleration pulses recorded during the San Fernando earthquake may be typical of near-fault ground motions. Similar ground motion characteristics have been reported

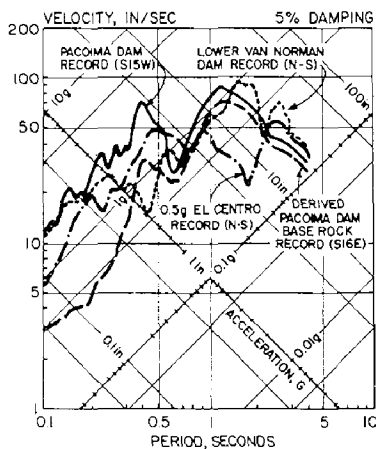


FIG. 5 LINEAR-ELASTIC RESPONSE SPECTRA FOR NEAR-FAULT RECORDS

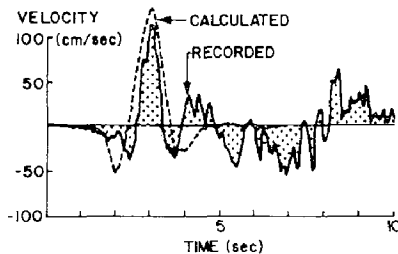


FIG. 6 COMPARISON OF THEORETICAL GROUND VELOCITY FOR STICK-SLIP FAULTING WITH PD RECORD [10]

for several other earthquakes at sites close to the fault zone on firm ground [17]. Analytical studies based on simple two- and three-dimensional fault dislocation models [8,27] have verified that the near-fault ground motions of the San Fernando earthquake were characterized by large ground velocity pulses of the type exhibited by the records in Fig. 4. These pulses are directly related to the faulting process and are not a result of local geological conditions. Studies of stick-slip faulting [7,10,28] have also indicated that such pulses are not peculiar only to thrust faulting (Fig. 6). Such studies have led Boore and Zoback [7] to conclude that the peak particle velocity may be a better basis for establishing the design earthquake than peak acceleration, and the initial portions of the PD records containing the large velocity pulse shown in Fig. 4 may be appropriate for the aseismic design of structures located close to potential faults.

To have an idea of the severity of the structural effect that can be induced by long acceleration pulses developed as a consequence of fault ruptures, it is at least necessary to estimate the maximum incremental velocity and the associated effective acceleration of such long pulses. Another important factor is the rise time of each pulse.

In a recent study, Seed et al. [25] determined the relationships between peak accelerations and peak velocities for earthquakes with magnitudes of about 6.5 and epicentral distances equal to or greater than 9.3 mi. (15 km). Unfortunately, little empirical data are currently available on the peak ground acceleration and velocity for epicentral distances less than 9.3 mi. (15 km).

Ambraseys [1] and Brune [9] have conducted some theoretical studies which enabled them to place the upper limit for the peak near-fault particle velocity in the range of 39.4 in./sec. (100 cm/sec.) to 58.7 in./sec. (150 cm/sec.). Newmark and Hall [18] have also indicated that it is unlikely for the maximum ground velocity to exceed 4 ft/sec. (122 cm/sec.) or 5 ft/sec. (152 cm/sec.). Although significant, this information is insufficient. What is needed is the estimation of the maximum incremental, rather than the maximum, velocity and the associated acceleration that can be developed for different soil conditions taking into account the mechanical characteristics of each type of soil. If this can be established, the structural designer will at least know the upper bound of the energy input that can be transmitted to the foundations of the structure and can design the structure accordingly. The solution to this problem will require close cooperation between geologists, seismologists, soil engineers and structural designers. Integrated experimental and analytical studies should be carried out in this area.

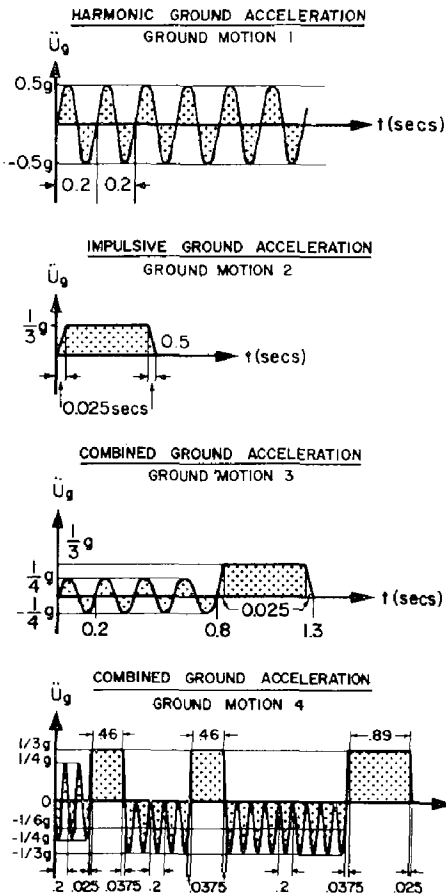


FIG. 7 SIMPLE IDEALIZED GROUND MOTIONS

EFFECTS OF GROUND MOTION RECORDS WITH SEVERE LONG ACCELERATION PULSES ON INELASTIC RESPONSE OF STRUCTURES

The importance of considering the interrelationship between types of ground motions and the mechanical behavior of the structure in selecting design earthquakes is best illustrated by the results of a series of analyses on a single degree-of-freedom system subjected to the simple idealized ground accelerations shown in Fig. 7 [4]. Some of these results are presented in Figs. 8 and 9 and permit comparison of the relative displacement time-histories of the mechanical behavior (linear-elastic and elasto-perfectly plastic) of a structure when subjected to ground motions having different dynamic characteristics such as those specified as 1, 2, 3 and 4 of Fig. 7. The yielding strength of the elasto-perfectly plastic hysteretic model was selected to be equal to $Mg/3$. The main results obtained from Figs. 8 and 9 are compared in Fig. 10.

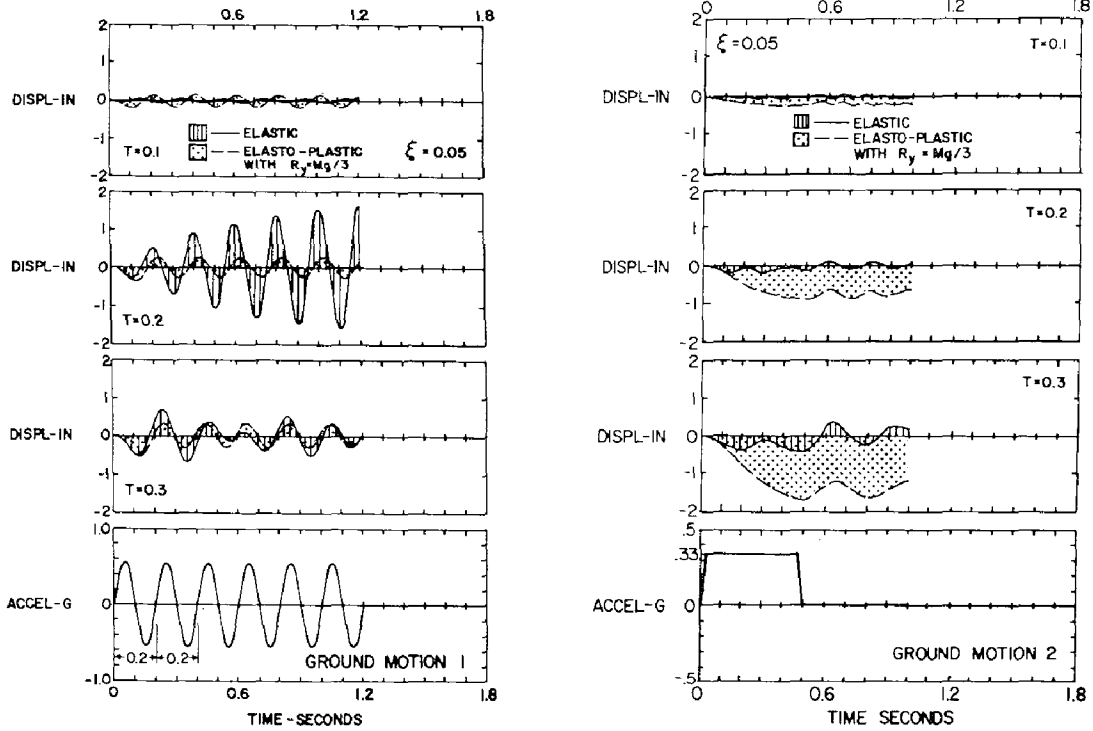


FIG. 8 RELATIVE DISPLACEMENT TIME-HISTORIES - GROUND MOTIONS 1 AND 2

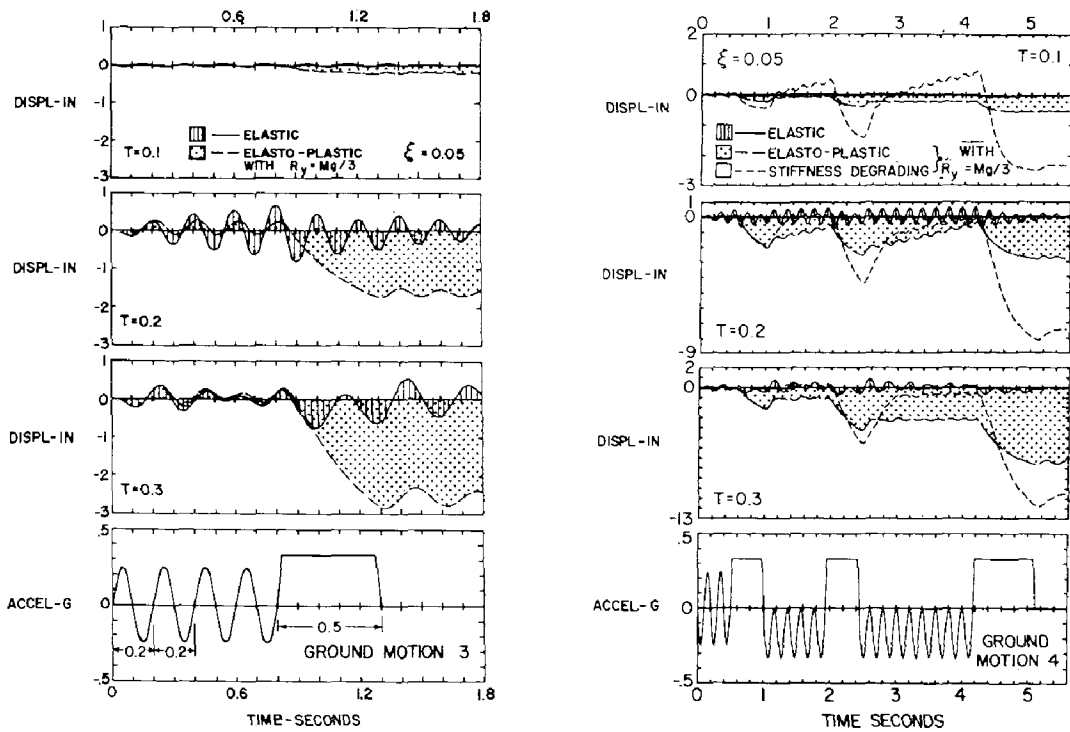


FIG. 9 RELATIVE DISPLACEMENT TIME-HISTORIES - GROUND MOTIONS 3 AND 4

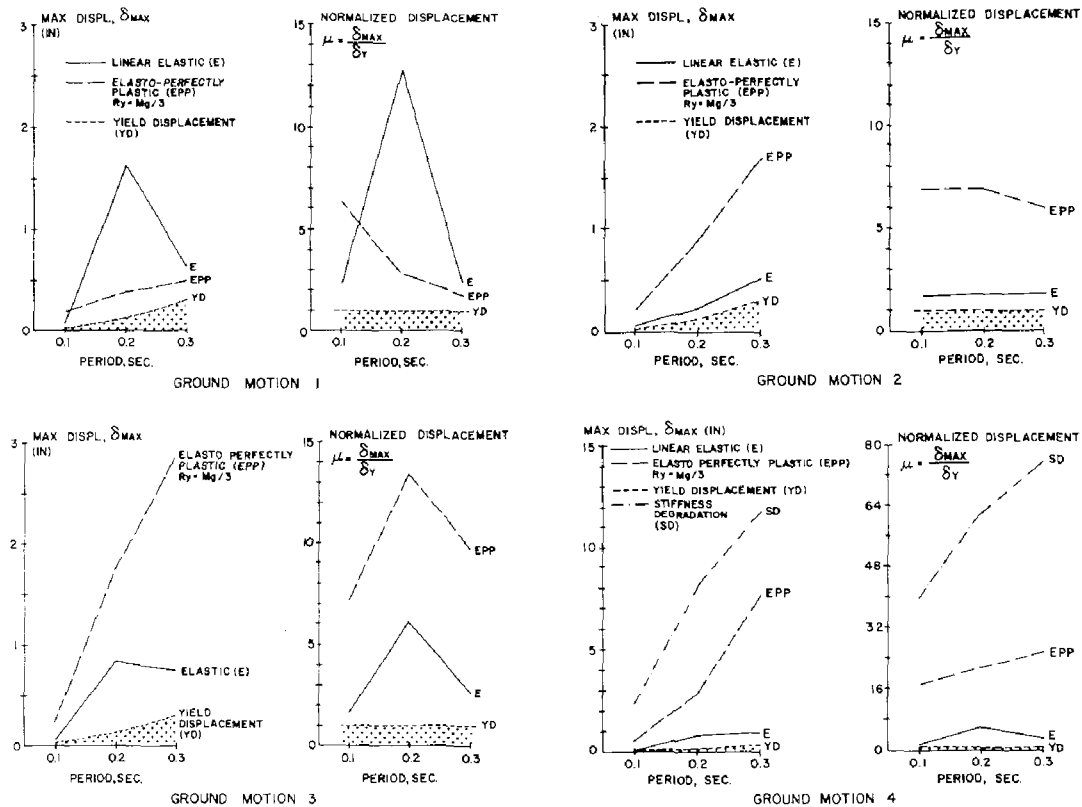


FIG. 10 MAXIMUM DISPLACEMENT AND DUCTILITY VS. PERIOD

Analysis of the results presented in Figs. 8 through 10 not only confirms the observation that the critical ground motion depends on the type of behavior expected to control the response of a structure, but also indicates the difficulty of finding simple relations that can be used to derive the inelastic deformations directly from results obtained assuming only linear-elastic behavior. Furthermore, if the ground motion can contain long acceleration pulses, it would be necessary to design the structure with a yielding strength somewhat greater than the inertial forces corresponding to the largest effective acceleration of these pulses. This need is accentuated when one considers the possibility that the ground motion can contain two or even more of these long pulses having the same acceleration sign, as clearly illustrated by the comparison of the results obtained in the elasto-plastic model when subjected to ground motions 3 and 4. This type of motion can undoubtedly lead to incremental collapse, Fig. 2. The results presented in Fig. 9 for ground motion 4 also illustrates the detrimental effect of a stiffness degrading system when subjected to this type of motion. Comparison of results between ground motions 2 and 3 or 4 also points out how the building up of the response due to a periodic motion can contribute significantly to an increase in the inelastic response to a long severe pulse.

Evidence of the effects of severe long acceleration pulses contained in actual earthquake motions was obtained from the analytical studies of the damage induced in the newly constructed buildings of the Olive View Medical Center, located near the fault rupture of the San Fernando

earthquake. A discussion of these studies follows.

ANALYTICAL STUDIES OF OLIVE VIEW EARTHQUAKE DAMAGE. - An analysis of the capacities of the buildings of the Olive View Medical Center complex show that they had seismic resistance coefficients far in excess of then existing code requirements [3]. For example, the six-story main building had story seismic resistance coefficients exceeding 0.3. In spite of this, the permanent drifts [greater than 30 in. (76 cm)] and the associated damage suffered by this reinforced concrete building were so large that it had to be demolished.

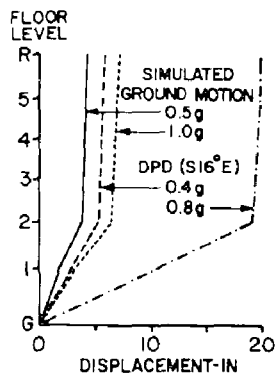


FIG. 11 MAXIMUM DISPLACEMENTS FOR OLIVE VIEW HOSPITAL MAIN BUILDING

Maximum displacements (Fig. 11) computed for a simplified model of the main building were much smaller than the actual residual displacements for the S16°E component of the DPD record and for a simulated ground motion (based on the dynamic characteristics of records obtained at sites other than Pacoima Dam) with a 0.5g peak ground acceleration [11]. However, the computed response to the simulated ground motion consisted of many displacement oscillations having amplitudes close to the maximum one. This was not compatible with the observed damage which was primarily the result of a few, large displacement excursions. The response to the DPD record, although smaller than that observed, was consistent with the actual damage. When the intensities of the two records were arbitrarily doubled, the displacements for the DPD record significantly increased and were characterized by a single, large displacement excursion coinciding with the largest amplitude pulse in the ground velocity. The displacements for the amplified simulated record were still smaller than the observed damage, however. Although some of the local structural damage to the main building was attributable to the inadequacy of the structural system, poor member detailing and deficient construction workmanship, it is believed that the overall damage pattern and the large residual displacements observed were primarily a consequence of severe long acceleration pulses similar to those experienced at the Pacoima and Van Norman Dams.

RELIABILITY OF NONLINEAR ASEISMIC DESIGN OF STRUCTURES USING SUGGESTED INELASTIC DESIGN SPECTRA

The reliability of aseismic designs using IDRS derived directly from LEDRS for structures whose sites are located near possible source(s) of major earthquakes, is evaluated by analyzing the nonlinear responses of several single degree-of-freedom systems and of a ten-story moment-resisting frame to the San Fernando records of Fig. 4 and then by comparing these responses to those obtained under some of the more standard records used in the derivation of LEDRS.

SINGLE DEGREE-OF-FREEDOM (SDOF) SYSTEMS. - The basic equilibrium equation controlling the motion of a viscously damped, SDOF system subjected to a ground acceleration time-history, \ddot{u}_g , is given by:

$$M\ddot{u} + 2M\omega\xi\dot{u} + R = -M\ddot{u}_g \quad (2)$$

in which M is the mass of the system; ξ is its viscous damping ratio; ω is the system's natural circular frequency; R is the force resisted by the system; and \ddot{u} and \dot{u} are the system acceleration and system velocity, respectively, at any time. For elastic systems, R is equal to the product of the stiffness, K and displacement, u , of the system. In the elastic case, Eq. 2 reduces to:

$$\ddot{u} + 2\omega\xi\dot{u} + \omega^2 u = -\ddot{u}_g \quad (3)$$

which is convenient for design purposes since the response of all systems with given values of period, $T = 2\pi/\omega$, and damping to a particular ground excitation can be determined using a single analysis.

To obtain useful design charts for nonlinear structures, it is desirable to rewrite Eq. 2 in a nondimensional form which accounts for yielding. To do this, Eq. 2 is divided by u_y (the yield displacement of the system's load-displacement relationship) and M to obtain:

$$\frac{u}{u_y} + 2\xi\omega\frac{\dot{u}}{u_y} + \frac{R}{Mu_y} = -\frac{\ddot{u}_g}{u_y} \quad (4)$$

By noting that $K = \omega^2 M$ and $R_y = Ku_y$ and by introducing variable transformations $\mu = u/u_y$ and $\rho = R/R_y$, Eq. 4 becomes:

$$\ddot{\mu} + 2\xi\omega\dot{\mu} + \omega^2\rho = -\omega^2\left(\frac{M}{R_y}\right)\ddot{u}_g \quad (5)$$

It is useful to express the ground acceleration as a fraction of the peak ground acceleration in the record, $\ddot{u}_{g\max}$. In this case, the nondimensionalized equation of motion, Eq. 5, can be written as:

$$\ddot{\mu} + 2\xi\omega\dot{\mu} + \omega^2\rho = -\frac{\omega^2}{\eta}\frac{\ddot{u}_g}{\ddot{u}_{g\max}} \quad (6)$$

In the above equation, the value of η is the ratio of the seismic resistance coefficient to the peak ground acceleration expressed as a fraction of gravity, i.e.:

$$\eta = \frac{R_y}{M\ddot{u}_{g\max}} = \frac{C_y}{\ddot{u}_{g\max}/g} \quad (7)$$

in which g is the acceleration of gravity, and C_y is the system's seismic resistance coefficient (i.e., the yield resistance, R_y , divided by its weight, $M \cdot g$). Thus, the nondimensional hysteretic response of a nonlinear system (μ and ρ) to a particular nondimensionalized ground motion ($\ddot{u}_g(t)/\ddot{u}_{g\max}$), can be evaluated in terms of η in addition to the parameters ω and

ξ needed for an elastic system. From this relationship, it is possible to construct charts in which the required displacement ductility, μ , of an SDOF system to a given ground motion is a function of ξ , T and η . Using such charts for a given ground motion record, μ can be determined if T , ξ , C_y , and $\ddot{u}_{g_{\max}}$ are known. Alternatively, the value of C_y required to obtain a desired value of μ can be derived if T and ξ of the system and $\ddot{u}_{g_{\max}}$ of the ground motion are known.

The response of elasto-perfectly plastic SDOF systems, with values of ξ equal to 0.02, 0.05 and 0.10; with η varying between 0.2 and 1.0; and with periods ranging between 0.1 sec. and 2.0 sec. were computed for the DPD, the original and filtered VND, and the El Centro ground motion records. The main results of these computations are presented in the charts shown in Fig. 12. In these charts the maximum absolute values of the computed displacement ductility, μ , for each of the values of ξ and for each of the ground motion records are plotted as a function of period in a series of curves. Each curve corresponds to a constant value of η . These charts can be useful for design purposes, as shown in the following example.

GIVEN: A building to be designed in a region of high seismic risk with a maximum expected ground motion similar to the DPD record having a $\ddot{u}_{g_{\max}}$ of 0.4g and where, according to the function of the building, the limit state of collapse controls the design. The structure can be modeled as an SDOF system with an effective M , with an ξ of 5 percent, and with a first estimation of T resulting in a value of 0.4 sec.

REQUIRED: Assuming that the structure can develop a maximum displacement ductility, μ_{\max} , of 6, it is necessary to determine the value of R_y to be provided to the structure.

SOLUTION: The required value of R_y is obtained from Fig. 12(b) as follows:

Using $T = 0.4$ and $\mu = 6$, Fig. 12(b) gives $\eta = 0.8$, and

$$\eta = 0.8 = \frac{C_y}{\ddot{u}_{g_{\max}}/g} = \frac{C_y}{0.4} . \quad \text{Then } C_y = 0.8 \times 0.4 = 0.32.$$

Since $C_y = \frac{R_y}{Mg}$, the required $R_y = 0.32Mg = 0.32W$

The charts of Fig. 12 can also be used to determine the parameters necessary for establishing ultimate state design earthquakes. This figure shows that for the three ground motions considered, ductility demands generally increase with decreasing values of η and T . For any given value of η , the ductility demands for both the DPD and VND records are generally much greater than for the El Centro record, except when η approaches unity in the short period range ($T < 0.5$ sec.).

The results of Fig. 12 indicate that if the ductility demands are to be kept at presently acceptable levels (4 to 6), the value of η must be

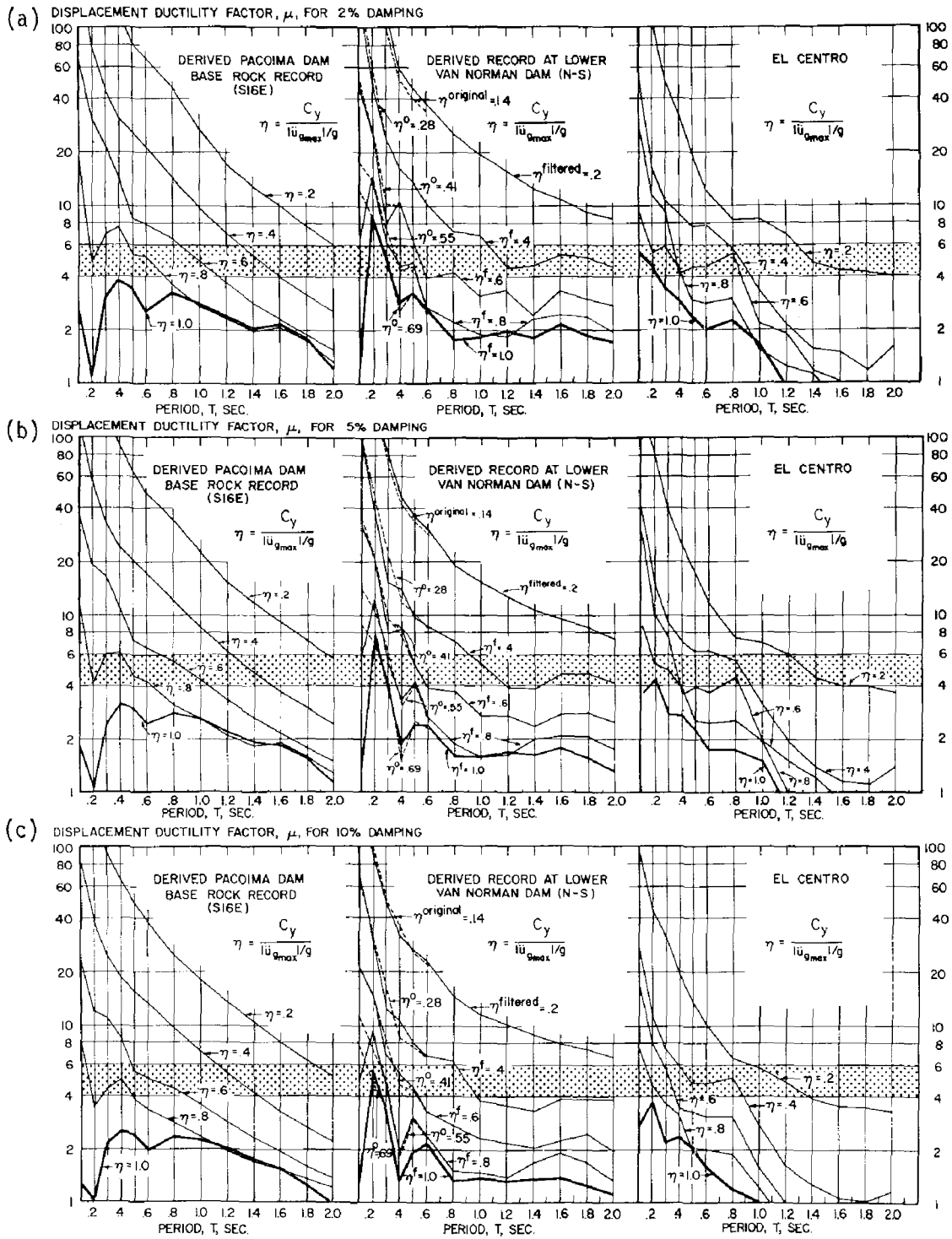


FIG. 12 DISPLACEMENT DUCTILITY REQUIREMENTS FOR 2%, 5% AND 10% DAMPING

near unity in the short period range for any of these ground motions. This value of η must also be maintained at this level at longer periods for the DPD and VND records than for the El Centro record.

The required ductilities shown in Fig. 12 generally decrease for constant values of η as the period becomes longer. The relatively lower ductility values for the high period structures should not be interpreted as justification for selecting flexible, rather than rigid, structures. The following observations should be kept in mind when the ductility factors represented in Fig. 12 are used. First, the design base shear required by current building code provisions generally decreases as the period increases. Thus, for a specific design earthquake, the value of η used in practice is likely to decrease with increasing periods, rather than remain constant as in each of the curves plotted in Fig. 12. In this case, differences between present ductility requirements for short and long period structures may not be as great as implied by the curves of constant η in Fig. 12. Second, one of the main reasons for presently using considerably lower values of η for long period buildings is the fact that in obtaining IDRS from LEDRS, the allowable design ductility factors are usually assumed to remain constant over the entire range of periods. The value of the acceptable ductility factor should depend, however, on whether structural or nonstructural damage controls the design. While the use of a constant ductility factor may be appropriate if structural damage controls the design, it is not so in cases where nonstructural damage is the controlling factor. The latter usually depends on the total amount of tangential story drifts [15]. For example, story drifts corresponding to a constant value of ductility will generally increase with period for similar buildings. Thus, where nonstructural damage must be considered, acceptable design ductility values should decrease with increasing period to account for this.

For the level of C_y currently required by building codes, Fig. 12 indicates that very large ductility factors will result if peak ground accelerations greater than 0.3g occur, particularly for short period buildings. Furthermore, for structures near active faults, if IDRS based on values of effective ground accelerations lower than the expected peak values or on ground velocities obtained assuming standard ground spectrum shapes [2,18] are used, undesirably large ductilities could result if these structures are subjected to ground motions similar to the DPD or VND.

Code commentaries usually refer to effective damping ratios (2 to 10 percent) and allowable ductility ratios (4 to 6) as justification for the low specified seismic design forces. If these ratios cannot be increased, it will be necessary to design structures located near the source of potential major earthquakes for forces considerably higher than those presently specified by building codes. To illustrate this, the C_y values required by elasto-perfectly plastic systems, with 5 percent damping to achieve a ductility of 4 for a peak ground acceleration of 0.5g, were interpolated from Fig. 12 and compared in Fig. 13 with current SEAOC recommendations [26]. The C_y values obtained from two IDRS, derived according to the procedure described in Ref. 18, for peak accelerations of 0.5g and using two different ground spectrum shapes are also plotted in this figure. The IDRS curve labeled 24 in./sec. (61 cm/sec.) was based on the shape recommended in Ref. 18, and the curve labeled 53 in./sec. (134 cm/sec.) was obtained by scaling the ground spectrum values for the DPD to 0.5g. While the C_y values required

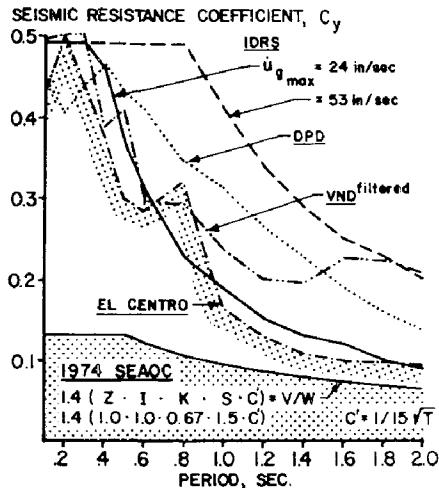


FIG. 13 SEISMIC RESISTANCE COEFFICIENT FOR 0.5g PEAK ACCELERATION GROUND MOTIONS, $\xi = 5\%$, AND $\mu = 4$

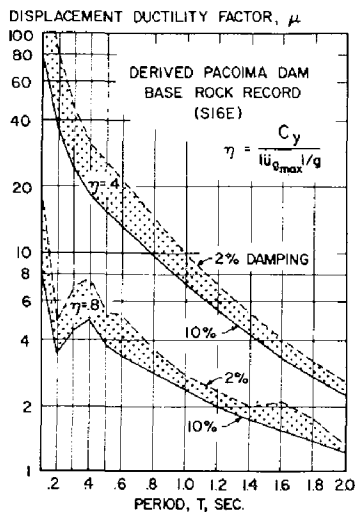


FIG. 14 EFFECT OF CRITICAL DAMPING ON DISPLACEMENT DUCTILITY REQUIREMENTS

erably less than 2. For example, for an $\eta = 0.8$, the average value of the ratio for all periods except $T = 0.1$ sec. is 1.3^4 . If this value is compared with the ratio between the relative values of spectrum amplification factors for the different amounts of damping suggested in Ref. 18 (for smoothed LEDRS) and reproduced in the table, it can be seen that under the actual inelastic response, the ratio between the amplification factors for $\xi = 0.02$ and 0.10 is 2.86 for the acceleration region and 2.15 for the amplified velocity region.

by the 24 in./sec. (61 cm/sec.) IDRS are acceptable for the El Centro record, they are generally unconservative for the DPD and VND records. The 53 in./sec. (134 cm/sec.) IDRS results in C_y values that, except for $T < 0.4$ sec., are too conservative for all the ground motions, as seen in Fig. 13. In all of these cases, the forces required to achieve a ductility of 4 are significantly higher than those currently recommended by the SEAOC.

Although structures could be detailed and constructed to accommodate the large ductility demands that would result if they were designed for the SEAOC or similar low design forces, this may not be desirable except for short period structures. In more flexible buildings, large ductility factors would lead to large lateral deflections resulting in non-structural damage to the building. Comprehensive studies or more rational methods for determining the acceptable ductility factor, particularly its variation with the flexibility of the structure, are needed, as are investigations into the economic impact of designing structures either for higher seismic resistance coefficients or for design ductility ratios higher than those presently assumed.

It is also helpful to compare the curves of μ vs. T with the same η corresponding to different values of ξ for any of the ground motions considered in Fig. 12. In order to facilitate such comparison, the curves, $\eta = 0.8$ and 0.4 , for the DPD motion with $\xi = 0.02$ and 0.10 , are compared in Fig. 14. Except for values of $T = 0.1$ sec. and 0.2 sec. where the values of the ratio between the response for $\xi = 0.02$ and 0.10 exceed 2, all ratios for values of T are consid-

frame for the 0.5g El Centro, DPD, and VND accelerograms are shown in Fig. 16; also shown in this figure are the input accelerograms. It is evident from examination of Fig. 16 that the inelastic response of the frame to the DPD and VND records are more severe than the response to the El Centro record: the maximum roof displacements under the VND and DPD

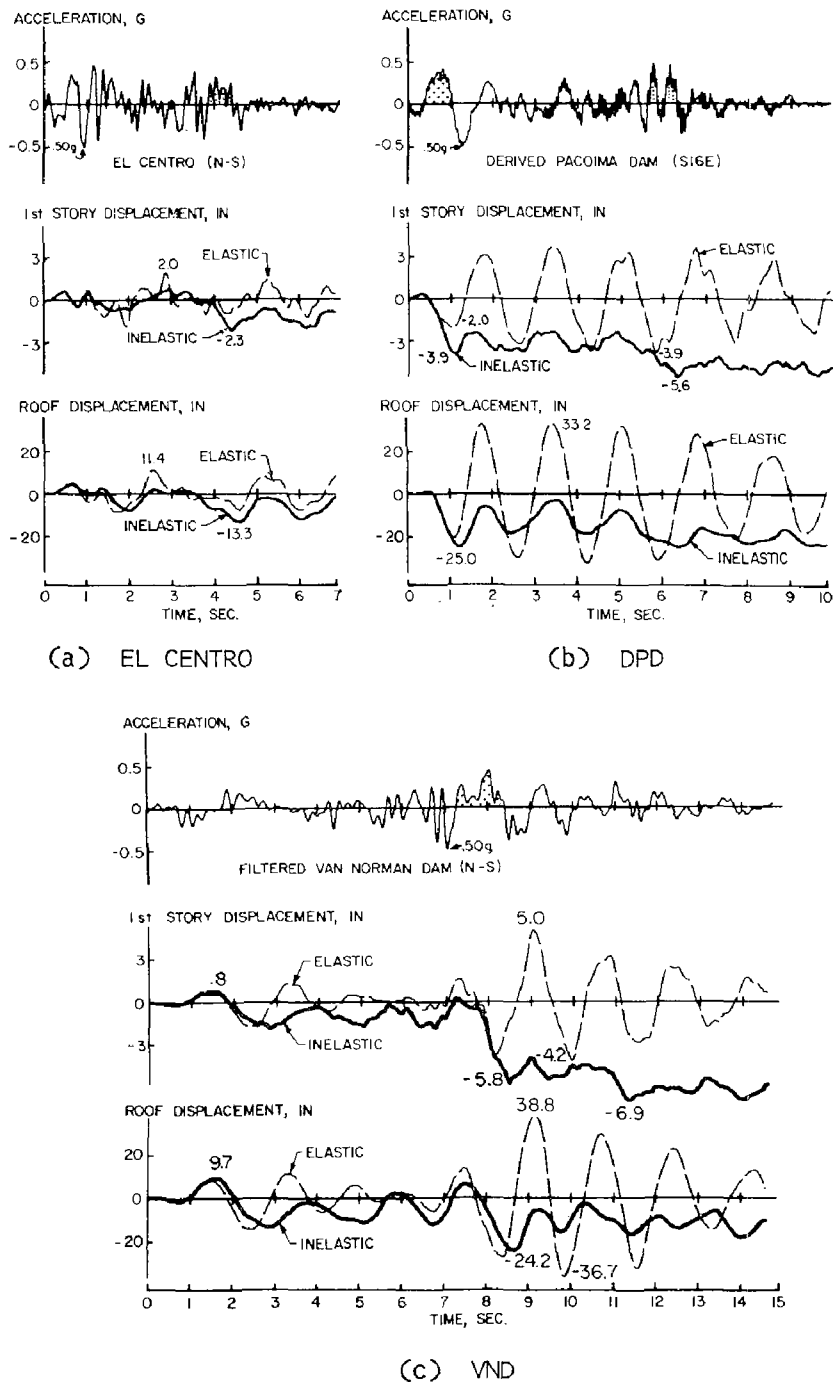


FIG. 16 DISPLACEMENT TIME-HISTORIES OF TEN-STORY FRAME FOR 5% DAMPING

motions were 24.2 in. (61 cm) and 25.0 in. (64 cm), respectively, while it was only 13.3 in. (34 cm) for El Centro. Thus, the DPD results in a maximum total roof displacement nearly 1.9 times larger than that obtained under El Centro. The difference is even greater for the first floor displacement, where the severity of response to the VND and DPD was about 3 and 2.4 times the value for El Centro, respectively: 6.9 in. (17.5 cm) for the VND, 5.6 in. (14.2 cm) for the DPD and 2.3 in./sec. (5.8 cm/sec.) for El Centro.

The results presented in Fig. 16 also permit the elastic and inelastic responses to these ground motions to be compared. A brief discussion of this comparison for each of the ground motions follows.

Response to 0.5g El Centro. - Although there are differences, the overall inelastic response during El Centro is generally similar to the linear-elastic response. Initially, the inelastic response is smaller than the elastic. This difference may be attributed to the fact that at the initial stages of the responses, the ground motion consists of a periodic type of input with relatively short pulses. The dynamic magnifications of the displacements in the elastic, as well as inelastic, models are essentially the result of an engineering resonance phenomenon. The inelastic model's displacement could therefore not reach large values in this initial phase because each time the model response was building up, the resonance phenomenon was depressed at the point of yielding by the energy dissipated through the small plastic deformations that started to develop. Energy dissipation, through even small plastic deformations, has effects similar to that of considerably increasing the damping in an elastic response.

Greater differences between the elastic and inelastic response under El Centro begin to develop at about 4 sec. At this time, considerable inelastic increases in the response of the first floor and roof can be observed. Comparison of these response time-histories with the input accelerogram reveals that the increases coincide with a relatively long pulse having an initial peak acceleration of 0.26g, an effective (average) acceleration of about 0.16g, and a velocity increment of 36 in./sec. (91 cm/sec.). Although this pulse had an effective peak acceleration, normalized by the gravity acceleration, somewhat smaller than the seismic resistance coefficient of the frame, 0.18, it induced a large increase in the lateral displacement of the first floor of about 2 in. (5 cm) in the negative direction. At the time it was hit by the long pulse, the frame was already building up its motion in this direction. This combined effect resulted in a total lateral displacement for the first floor of $|-2.3|$ in. (5.8 cm) which was the maximum value computed. The long pulse also caused an increase of about $|-6.5|$ in. (16.5 cm) in the roof displacement, resulting in a maximum inelastic roof displacement of $|-13.3|$ in. (33.8 cm). This was the maximum value of inelastic roof displacement obtained for the frame under the El Centro motion and it was only about 16 percent larger than the maximum computed displacement of the elastic model [11.4 in. (28 cm)]. It is believed that the fairly close agreement between the elastic and inelastic response time-histories explains why this frame, designed using the derived IDRS, performed relatively well under the El Centro ground motion.

Response to 0.5g DPD. - There is quite a discrepancy between the response time-histories for the elastic and inelastic models. The elastic

displacement of the roof appears to be an almost first mode type of response which in no way resembles the response of the inelastic structure. In the latter case, the frame underwent a mostly inelastic, lateral displacement under the action of the first large pulse that occurred at about 2.4 sec. of the input ground motion.

The damaging effect of large pulses is well illustrated by the first story response. After the first pulse, the first floor displacement increases in absolute value to $|-3.9|$ in. (9.6 cm), which corresponds to a story drift index of 0.022, already an unacceptably high value. A further increase in displacement is prevented by the second pulse, which is opposite in sign to the first; the second pulse forces the structure back to a displacement of $|-2.3|$ in. (5.8 cm). Oscillation of the structure subsequently occurs about a displacement of -3.1 in. (7.8 cm). No significant increases in the first floor lateral displacement occur until near the end of the ground motion. At about 7.6 sec. this displacement increases from $|-3.8|$ in. (9.6 cm) to $|-5.6|$ in. (14.2 cm), the latter being the maximum computed value, corresponding to a story drift index of 0.032. This increase was induced by two successive acceleration pulses, having the same sign, which began at about 7.6 sec. Subsequent oscillation of the first floor occurs about a deformation of -4.9 in. (12 cm) corresponding to a story drift index of 0.027.

A closer look at the elastic and inelastic displacement time-histories of the first floor reveals that the respective maximum values up to 7.6 sec. are similar, both being about 4 in. (10.2 cm), although they are the results of completely different phenomena. A large inelastic displacement of -3.9 in. (9.9 cm), 70 percent of the maximum, results from the first large, long acceleration pulse; at the end of this pulse, the elastic displacement is -2 in. (5.1 cm), only about half the inelastic value. The elastic maximum is reached at about 7.9 sec. in the fourth cycle of an increasing oscillation induced by engineering resonance. Note that during the series of acceleration pulses after 7 sec., the displacement of the elastic model decreases, whereas the displacement of the inelastic model increases by more than 43 percent.

The roof response shows similar trends to those already noted for the first floor, although the response is smoother and the effect of the two pulses after 7.6 sec. is not as distinct. Toward the end of the response, the roof oscillates at about 20.3 in. (51.6 cm), of which almost 25 percent is due to the displacement of the first floor.

Response to 0.5g VND. - The findings from a comparison of the response time-histories of the elastic and inelastic models under the VND motion are similar to those made for the response under the DPD record. The damaging effect of large pulses is again demonstrated by the first story displacement response. Until 8 sec. the displacement response of the elastic and inelastic models are not dissimilar and the maximum values do not exceed 1.9 in. (4.8 cm), despite that the maximum ground peak acceleration already occurred at about 7 sec. Only after the first large acceleration pulse occurred, corresponding to an incremental velocity of about 80 in./sec. (202 cm/sec.), did the first story displacement of the inelastic model undergo a considerable increase, to a value of $|-5.8|$ in. (14.7 cm) while the elastic increased to a value of only $|-3.7|$ in. (9.4 cm). Comparison

of the increases obtained under the first large pulse of the DPD and VND [3.9 in. (9.9 cm) vs. 5.8 in. (14.7 cm)] confirms the previous statement that the larger the incremental velocity of the pulse, the larger the inelastic response if the effective acceleration of the pulse is equal to or greater than that required to produce yielding in the system. This observation is generally true except in cases involving different rise times.

Concluding Remarks. - The response of this frame indicates that elastic response cannot be used to predict a reliable inelastic response. The type of response expected from ground motions with long acceleration pulses is characterized, not, as inferred from elastic response, by numerous intense oscillations, but rather, by a few large displacement excursions.

With respect to application of results obtained using the SDOF system to the analysis of the response of the ten-story frame, it should be noted that for a structure with a period of 1.67 sec., the C_y value required to obtain a ductility of 4 for an $\xi = 0.05$ for the 0.5g El Centro motion would be close to 0.10. For the 0.5g DPD record, this value would be slightly less than 0.20; for the 0.5g VND, it would be slightly greater than 0.20. Although the frame had a C_y value of 0.18 (close to the upper bound for all three records), the response was still rather poor. Such differences are to be expected, since the analysis of SDOF systems neglects the effects of gravity loads, geometric nonlinearities, etc. Furthermore, the lateral load-deflection relationship for multistory frames is not generally elasto-perfectly plastic. Extrapolation of results for SDOF systems to multiple degree-of-freedom systems should therefore be done with great caution.

EFFECTS OF DIFFERENT AMOUNTS OF DAMPING. - After first establishing the critical ground motion controlling the design of a building, it is necessary to determine the effect of damping in order to obtain the seismic design forces. This is usually done by estimating an equivalent viscous damping factor and accounting for its effect on the response of the building by directly modifying the design response spectra. Thus, the effect of damping for designs of linear-elastic systems is accounted for by using spectrum amplification factors as shown in the table [18]. By multiplying the values of the ground spectrum--the effective ground acceleration, velocity and displacement--by these amplification factors, a LEDRS can be obtained which accounts for the effect of the estimated damping.

Since the IDRS is presently obtained by dividing the values of the LEDRS by either μ or $\sqrt{2\mu-1}$, this method assumes that for a given or selected structural system, the damping is the same for both service and ultimate limit state designs. This assumption is questionable, however, since critical excitations for ultimate limit state designs have been shown to differ from those for service limit state designs and the effect of damping in structural response is known to differ depending on whether the dynamic ground excitation is periodic or impulsive and on whether the response is strictly elastic or demands significant inelastic deformation.

To illustrate this point, the ten-story frame was analyzed using different amounts of damping. The time-histories of the lateral displacement of the first floor and roof under the VND and DPD are plotted in Fig. 17 for 2 percent and 10 percent damping. A brief evaluation of the effects

of these amounts of damping follows.

On Elastic Response to DPD. - From analysis of the elastic response time-histories shown in Fig. 17(a), it is clear that as the damping increased from 2 to 10 percent, the responses of the first story and roof were significantly suppressed. For example, while the maximum response of the first story for $\xi = 2\%$ is 4.8 in. (12.2 cm) and occurs at 6.8 sec. after four complete oscillations, the maximum response for $\xi = 10\%$ is only 2.6 in. (6.5 cm) and occurs at 1.8 sec., just after the first complete oscillation. The ratio between these maximum values, $4.8/2.6 = 1.85$, clearly shows the importance of damping in the elastic response and, therefore, in the aseismic design for service limit states. It should be noted, however, that this ratio is smaller than the ratio between the suggested values of the spectrum amplification factors for 2 percent and 10 percent critical damping ($2.8/1.3 = 2.15$ for the velocity region of the LEDRS, see table). Similar conclusions can be drawn by analyzing the responses of the roof with similar percentages of damping. The ratio between the values for the maximum response is $40.0/27.6 = 1.45$.

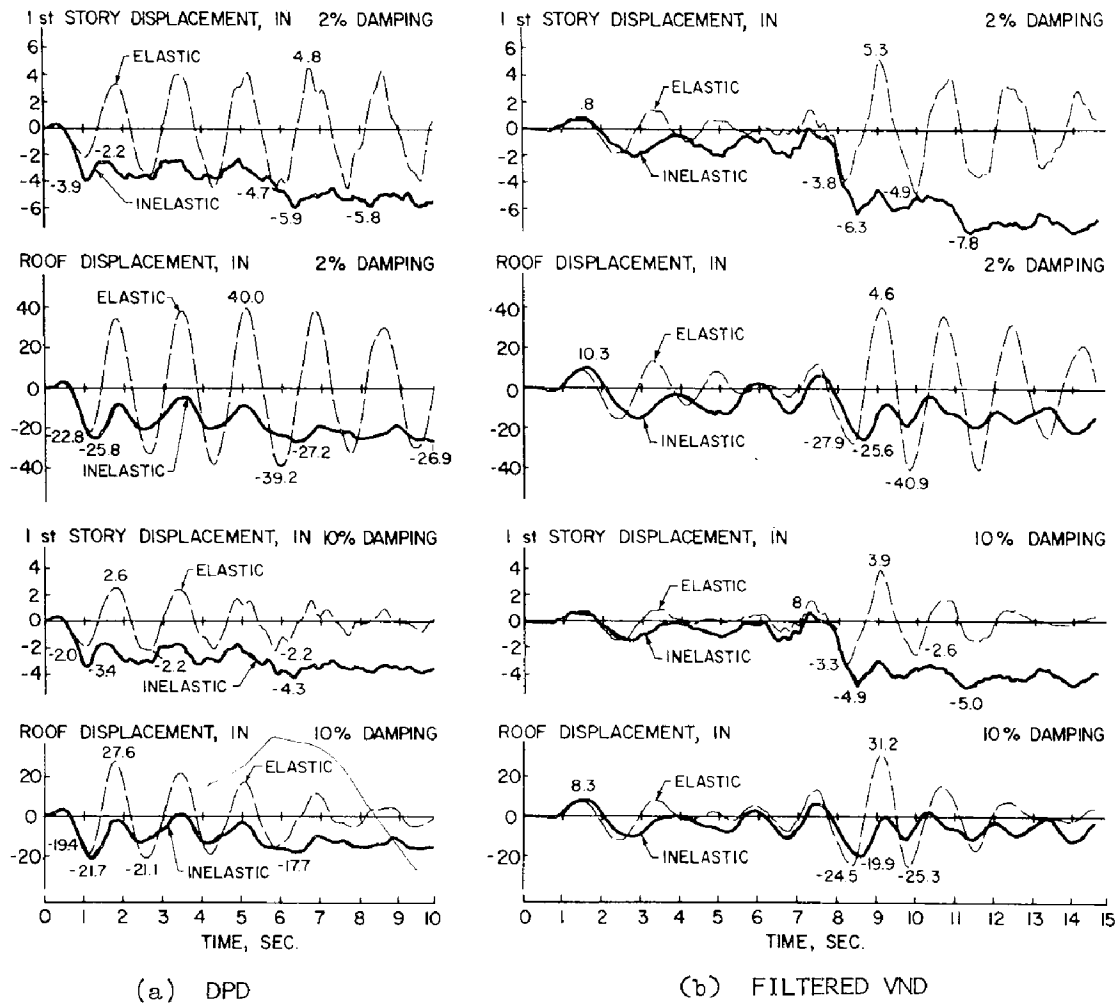


FIG. 17 DISPLACEMENT TIME-HISTORIES OF TEN-STORY FRAME FOR 2 & 10% DAMPING

On Inelastic Response to DPD. - The curves shown in Fig. 17(a) reveal that each of the inelastic response time-histories of this figure had two main peak responses; one at about 1.1 sec. after the first, long severe acceleration pulse (Fig. 16) and another at about 6.5 sec., just after the last, long severe pulse.

The ratio between the values of the first main peak for 2 percent and 10 percent damping for the first story and roof are as follows:

$$\text{First story: } \frac{-3.9}{-3.4} = 1.15 \qquad \text{Roof: } \frac{-25.8}{-21.7} = 1.19$$

These values indicate the extremely small effects of damping in the response to an impulsive load.

Similar ratios between the values of the second main peak lead to the following:

$$\text{First story: } \frac{-5.9}{-4.3} = 1.37 \qquad \text{Roof: } \frac{-27.2}{-17.7} = 1.54$$

These ratios are considerably higher than the previous values, and thus reflect the effects of different amounts of damping on the building up of the elastic response that takes place between 1.1 sec. and 6.5 sec.

The values for the ratio between the maximum responses are:

$$\text{First story: } \frac{-5.9}{-4.3} = 1.37 \qquad \text{Roof: } \frac{-27.2}{-21.7} = 1.25$$

These values are smaller than the corresponding values for the elastic response, particularly the value corresponding to the first story (1.37 vs. 1.85).

On Elastic Response to VND. - By increasing the damping from 2 to 10 percent, there was a considerable decrease in the oscillations of the system during the part of the ground motion containing the long severe pulses, i.e. at 7 sec., 17(b). By comparing the values of the successive response peaks for the first floor, the following ratios can be determined:

$$\frac{-3.8}{-3.3} = 1.15 \qquad \frac{5.3}{3.9} = 1.36 \qquad \frac{-4.9}{-2.5} = 1.96$$

where 1.36 is the ratio between the maximum values of the response. Corresponding ratios for the roof displacement are:

$$\frac{-27.9}{-24.5} = 1.14 \qquad \frac{40.6}{31.2} = 1.30 \qquad \frac{-40.9}{-25.3} = 1.62$$

where the ratio between the maximum peak values is equal to $|-40.9|/31.2 = 1.31$.

As expected, analysis of these values indicates that the effect of

damping increases with the number of oscillations. However, the ratios (1.36 and 1.31) between the maximum peak values are considerably smaller than the ratios between the suggested values for the spectral amplification factors (2.15 for the velocity region and 2.86 for the acceleration region, see table).

On Inelastic Response to VND. - From comparison of the curves shown in Fig. 17(b), it is evident that the effect of higher damping for the inelastic model is not as well-defined as for the elastic model. After the first long acceleration pulse, the ratio between the peak first floor displacement values is equal to $-6.3/-4.9 = 1.28$. Although this ratio is as high as that for the elastic model, it cannot be directly attributable to the effect of damping during the response to the pulse. Rather, it is due to the fact that yielding began much earlier for the case of 2 percent damping than for 10 percent damping. This is because the elastic response that occurred before the initiation of long severe pulses for 10 percent damping was considerably more suppressed than that for the 2 percent case. This observation re-emphasizes that by building up the motion of the structure, due to the elastic engineering resonance phenomenon, short periodic pulses preceding a long severe pulse can significantly increase the inelastic response that the long pulse alone could have induced. Similarly, the ratio between the maximum values of the first floor response, $-7.8/-5.0 = 1.56$, is more a consequence of the effect of damping on the elastic response that takes place between 8.5 sec. and 11.4 sec., than on the effect of damping on the response to the severe pulse alone. Similar observations can be made for the roof displacement by comparing the corresponding peak values. In this case, the ratio between the maximum values for displacement with 2 and 10 percent damping is equal to $-25.6/-19.9 = 1.28$.

SUMMARY AND CONCLUSIONS

The results of the studies reported herein have permitted evaluation of the reliability of present methods for establishing design earthquakes when their use is extended to building located near potential source(s) of major earthquakes. These methods have been assessed in view of the dynamic characteristics of ground motions observed in accelerograms directly obtained or derived from records of the 1971 San Fernando earthquake, and on the basis of the observed building damage caused by this earthquake.

Conceptually, the design earthquake should be that ground motion which is "critical," i.e. which drives the structure to its critical response. The application of this simple concept in practice meets with serious difficulties, however, because even for a specific structural system, the critical response will vary according to the different limit state(s) that could control its design.

DESIGN EARTHQUAKES FOR SERVICE LIMIT STATES. - In cases where service limit states control design, structures should remain essentially in their elastic range. In these cases, the most effective way of defining the design earthquake is through the use of a LEDRS. Simple methods have already been suggested for the construction of such a spectrum. These methods have been based on so-called standard severe earthquake motions at moderate distances from the causative fault. For building sites located near these faults, however, the LEDRS should be based on the actual maximum values that can be

expected for the parameters defining the ground spectrum: effective ground acceleration, velocity and displacement. These values should be determined from analysis of available records and/or from theoretical predictions based on the faulting process at the causative fault. Estimates of the peak ground velocity and displacement obtained by multiplying the expected ground acceleration by suggested coefficients obtained from analysis of standard earthquake ground motions alone can lead to unconservative LEDRS. If no records are available for sites near causative faults, and if acceptable predictions of the effective peak values for the ground acceleration, velocity and displacement cannot be made, then establishment of the "critical" earthquake ground motion can be based on techniques suggested by Drenik, Wang, and Wang [12] or Hoshiya, Shibata, and Nishiwaka [13].

Further studies on the subject of spectral amplification factors for different amounts of damping are needed. Significant differences were found between the values of the ratio of maximum elastic responses corresponding to different amounts of damping (obtained for the DPD and VND ground motions) and those corresponding to presently suggested amplification factors.

DESIGN EARTHQUAKES FOR ULTIMATE STATES. - When safety rather than serviceability controls the design, large but controllable inelastic deformations can be tolerated. The amount of nonstructural and structural damage should be limited so as to prevent loss of human life and personal injury during, as well as after, the earthquake. One of the most pressing problems in establishing design earthquakes for ultimate states involves determining whether the damage or collapse of nonstructural or structural elements controls the criteria for acceptable deformations, and in each of these cases, the type of deformation inducing the damage.

Use of IDRS derived directly from recommended LEDRS through displacement ductility factors as suggested by present methods, does not appear to be conservative for buildings located in the immediate area of causative faults. The LEDRS and, therefore, the derived IDRS do not account for the duration of strong motions during major earthquakes. Determining the maximum inelastic deformation excursion, as well as the maximum number of reversals of inelastic deformations, for the structure's critical regions is essential for the proportioning and detailing of these regions. Although some information has recently become available on the duration of strong shaking for certain areas [29], data for most seismic regions of the U. S. remain scarce.

The main drawback of present methods is that direct derivation of IDRS from LEDRS has been shown to be basically untenable due to the fact that the dynamic characteristics of the critical ground excitations for elastic and inelastic responses are completely different. While periodic pulses having frequencies equal to those of the predominant modes of the vibration of the building constitute the critical ground motions for linear-elastic systems, a critical inelastic response can be induced by just one or a few long acceleration pulses with effective (average) peak accelerations of equal to greater value than the effective seismic resistance coefficient of the structure.

Near-fault records of the San Fernando earthquake, such as those for the Paccima and Van Norman Dams contain severe long acceleration pulses which resulted in large velocity increments. This was found to be characteristic of near-fault motions. Results of an analytical study of a building near the fault zone using the DPD record correlated well with the observed damage. This damage appears to have been the result of only a few large displacement excursions rather than of numerous oscillations.

Unusually large ground velocities may be developed at near-fault sites. Methods for constructing elastic and inelastic design response spectra should reflect the larger values recorded at such sites. Additional research is needed to establish bounds on the different parameters that define the characteristics of severe long pulses, i.e. the largest incremental velocity and the associated effective acceleration that can be developed according to the mechanical dynamic characteristics of the soil present at a site. These values will enable the design engineer to determine an upper bound on the energy that can be transmitted to the foundation of the structure so that the structure can be designed accordingly. It is also necessary to know the number of long severe pulses that can occur at the site since repeated pulses can lead to an incremental (crawling) type of collapse.

Obtaining all the information considered necessary for the establishment of reliable design earthquakes for near-fault sites will require extensive investigation and research. Until this is done, the following procedure may be implemented.

For the case of single degree-of-freedom systems, charts similar to those presented in Fig. 12 should be prepared. These charts should take into account the different hysteretic models (at least the bounds of all possible stiffness degradation and strain-hardening) and all earthquake ground motions previously recorded at sites near faults as well as those which can be obtained from theoretical consideration of fault mechanisms. Once sufficient records are available, statistical analysis of the results obtained should be conducted in order to formulate inelastic design earthquakes in the form of IDRS (C_y vs. T). This will require the establishment of acceptable ductility factors. Current methods usually recommend the use of a constant ductility. Even for a specific structural system, however, the amount of acceptable ductility will vary depending on whether non-structural or structural damage controls the design. If design is controlled by nonstructural damage, the allowable ductility will decrease with increases in the flexibility (period) of the selected structure. Since present methods do not distinguish between the types of damage controlling a design, the first step in formulating inelastic design earthquakes as an IDRS should be to seek more reliable methods for establishing values of acceptable ductility.

For multiple degree-of-freedom systems, the charts derived for SDOF systems may be used only as design guidelines. The response of different multiple degree-of-freedom systems to severe ground motions like those resulting from the San Fernando earthquake should be extensively investigated. At present, it is common to evaluate the reliability of an aseismic design by analyzing the designed structure under numerous ground motions obtained by normalizing recorded earthquake accelerograms to some maximum

selected value of the peak acceleration. Unfortunately, in many cases, these ground motions are the result of earthquakes with different magnitudes, and recorded at sites located at different distances from the earthquake sources and having different soil conditions. Indiscriminate use of such a technique, when significant inelastic behavior is expected under severe ground motions, can lead to highly misleading results. For example, accelerograms obtained on soft soil at sites distant from the earthquake source usually contain very long pulses. If these accelerograms are normalized to a large peak acceleration, these pulses may become unrealistically severe.

In view of the results of this study, there is an urgent need to obtain actual records for all six ground motion components and to study their simultaneous effect on the response of structures located near sources of possible major earthquakes.

ACKNOWLEDGEMENTS

Appreciation is expressed to the National Science Foundation for the financial support of the studies reported in this paper under Grant No. AEN-07732 A02, Sub-project 0-21983 and Grant No. ENV 7601-419.

REFERENCES

1. Ambraseys, N. N., "Maximum Intensity of Ground Movements Caused by Faulting," Proc. of the 4th Wld. Conf. on Earthq. Engng., Vol. 1, Santiago, Chile, 1969.
2. ATC, An Evaluation of a Response Spectrum Approach to Seismic Design of Buildings, San Francisco, 1974.
3. Bertero, V. V., et al., "Design Implications of Damage Observed in the Olive View Medical Center Buildings," Proc. of the 5th Wld Conf. on Earthq. Engng., Vol. 1, Rome, June 1973.
4. Bertero, V. V., "Identification of Research Needs for Improving Aseismic Design of Building Structures," Rept. No. EERC 75-27, EERC, Univ. of Calif., Berkeley, Sept. 1973.
5. Bertero, V. V. and Kamil, H., "Nonlinear Seismic Design of Multistory Frames," Canadian Jnl. of Civ. Engng., Vol. 2, Ottawa, Dec. 1975.
6. Bertero, V. V., Herrera, R. A., and Mahin, S. A., "Reliability of Nonlinear Aseismic Design of Structures using Inelastic Design Spectra," paper pres. at 5th Pan-Am. Symp. of Struc. and 17th So. Am. Conf. on Struc. Engng., Caracas, Dec. 8-12, 1975.
7. Boore, D. M. and Zoback, M. D., "Near-field Motions from Kinematic Models of Propagating Faults," Bul. of the Seis. Soc. of Amer., Vol. 64, No. 2, April 1974.
8. Boore, D. M. and Zoback, M. D., "Two-dimensional Kinematic Fault Modeling of the Pacoima Dam Strong-motion Recording of the February 9, 1971, San Fernando Earthquake," Bul. of the Seis. Soc. of Amer., Vol. 64, No. 3, June 1974.
9. Brune, J. N., "Tectonic Stress and the Spectra of Seismic Shear Waves from Earthquakes," Jnl. of Geophys. Res., Vol. 75, 1970.
10. Cherry, T. J., Halda, E. J., and Hamilton, K. G., "A Deterministic Approach to the Prediction of Free Field Ground Motions and Response Spectra from Stick-slip Earthquakes," Earthq. Engng. & Struc. Dyn., Int'l. Assn. for Earthq. Engng., Vol. 4, No. 4, April-June 1976.

11. Chopra, A. K., Bertero, V. V., and Mahin, S. A., "Response of the Olive View Medical Center Main Building during the San Fernando Earthquake," Proc. of the 5th Wld. Conf. on Earthq. Engng., Vol. 1, Rome, June 1973.
12. Drenik, R. F., Wang, P. C., and Wang, W., "Case Study of Critical Excitations and Response Structures," Rept. No. POLY EE/EP-75-DID, Polytechnic Inst. of N. Y., Nov. 1975.
13. Hoshiya, M., Shibata, S., and Nishiwaka, T., "Upper Bound of Response Spectrum," Proc. of the 5th Euro. Conf. on Earthq. Engng., Vol. 1, Istanbul, Sept. 1975.
14. Leeds, D. J., "The Design Earthquake," Geol. Seismicity and Environmental Impact, Spec. Publ., Assn. of Engng Geols., Univ. Publ., Los Angeles, October, 1973.
15. Mahin, S. A. and Bertero, V. V., "Problems in Establishing and Predicting Ductility in Aseismic Design," paper submitted to Int'l. Symp. on Earthq. Struc. Engng., St. Louis, Aug. 19-21, 1976.
16. Murakami, M. and Penzien, J., "Nonlinear Response Spectra for Probabilistic Seismic Design of Reinforced Concrete Structures," Proc. of the U.S.-Japan Coop. Res. Prog. in Earthq. Engng., Assn. for Sci. Documents Inf., Tokyo, 1976.
17. Newmark, N. M. and Rosenblueth, E., Fundamentals of Earthquake Engineering, Prentice-Hall, Inc., Englewood Cliffs, N. J., 1971.
18. Newmark, N. M. and Hall, W. J., "Procedures and Criteria for Earthquake Resistant Design," Bldg. Prac. for Disas. Mitig., Bldg. Sci. Series 45, NBS, Feb. 1973.
19. Newmark, N. M., "Seismic Design Criteria for Structures and Facilities of the Trans-Alaska Pipeline System," Proc. of U. S. Natl. Conf. on Earthq. Engng., EERI, Oakland, 1975.
20. Newmark, N., Blume, J., and Kapur, K., "Seismic Design Spectra for Nuclear Power Plants," Jnl. of the Power Div., ASCE, Vol. 99, No. P02, Proc. Paper 10142, Nov. 1973.
21. Page, R. A., et al., "Ground Motion Value for Use in the Seismic Design of the Trans-Alaska Pipeline System," Circular 762, USGS, 1972.
22. Reimer, R. B., "Deconvolution of Seismic Response for Linear Systems," Rept. No. EERC 73-10, EERC, Univ. of Calif., Berkeley, Oct. 1973.
23. Rosenblueth, E., "The Six Components of Earthquakes," Proc. of the Austrl. Conf. on Plan. and Des. of Tall Bldgs., Sidney, Aug. 14-17, 1973; also publ. in Jnl. of Struc. Div., ASCE, Vol. 102, No. ST2, 1976.
24. Scott, R. F., "The Calculation of Horizontal Accelerations from Seismoscope Records," Bul. of Seis. Soc. of Amer., Vol. 63, No. 5, 1973.
25. Seed, H. B., et al., "Relationship between Maximum Acceleration, Maximum Velocity, Distance from Source and Local Site Conditions for Moderately Strong Earthquakes," Rept. No. EERC 75-17, EERC, Univ. of Calif., Berkeley, July 1975.
26. SEAOC, Recommended Lateral Force Requirements and Commentary, Seis. Comm., San Francisco, 1974.
27. Trifunac, M. D., "A Three-dimensional Dislocation Model for the San Fernando, California, Earthquake of February 9, 1971," Bul. of the Seis. Soc. of Amer., Vol. 64, No. 1, Feb. 1974.
28. Tsai, T. B. and Patton, H. J., "Near-field Small Earthquakes - Dislocation Motion," Semi-annual Rept. 1, Texas Instr., Inc., 1972.
29. Wesson, R. L., et al., "Expectable Earthquakes and their Ground Motions in the Van Norman Reservoir Area," Circular 269-A,B, USGS.

mode of vibration for the three components of earthquake⁽¹⁾

$$R_e^2 = R_{in} R_{in} \quad (1)$$

where

R_e = effective response value (any displacement, stress or force)

R_{in} = maximum response in nth mode of vibration due to excitation in ith direction ($i = 1, 2, 3$)

The repeated sub or superscripts in Equation (1) and later in this report imply summation. For example, in the case of Equation (1),

$$R_{in} R_{in} = \sum_i \sum_n (R_{in})^2$$

For modes with closely spaced frequencies, Equation (1) is modified to include a coupling matrix ϵ_{mn} ⁽²⁾

$$R_e^2 = \epsilon_{mn} R_{im} R_{in} \quad (2)$$

When frequencies of all the modes are sufficiently apart

$$\epsilon_{mn} = \delta_{mn}$$

where δ_{mn} is the Kronecker delta

$$\delta_{mn} = 1 \quad \text{when } m = n$$

$$\delta_{mn} = 0 \quad \text{when } m \neq n$$

In this case

$$\begin{aligned} R_e^2 &= \delta_{mn} R_{im} R_{in} \\ &= R_{in} R_{in} \end{aligned}$$

which is the same as in Equation (1). Obviously, Equation (2) is more general and Equation (1) is a special case of Equation (2); therefore, in further discussions only Equation (2) will be used.

In many design problems, the strength criterion is based on values of more than one quantity at an instance. However, Equation (2) gives the maximum probable value of each of the quantities, which in general do not occur simultaneously. For the lack of a better approach in many current design practices, the structure is conservatively designed as if these probable maximum values were occurring simultaneously.

In the next section a theory is presented by which simultaneous variation of various quantities can be postulated within the framework of

the definition given by Equation (2). In Section III it is shown that the response in several modes of vibration under three components of earthquake can be represented by the response in a small number of Equivalent Modes, thus reducing the number of calculations required in the design analysis. Using the concept of Equivalent Modes, it is shown in Section IV that the variation of responses contributing to a design criterion can be represented by an Interaction Surface. Application of the theories presented in this paper to the design problems is illustrated in Section V.

It is observed in this paper that the modal vectors lie in a Riemannian Space designated as Modal Space. The Equivalent Modal Vectors represent a Cartesian Space, which is designated as Modal Subspace.

In three sections (II, III and IV), seemingly three different methods have been presented, which can be derived independently of each other (not presented in this paper). However, it is shown in this paper that all three methods are interconnected and essentially follow the same basic theory developed in Section II; hence, the nomenclature "Unified Approach" in the title of this paper.

II. Probable Simultaneous Response: The Modal Space

In the response spectrum method of analysis, the maximum value of any response quantity R is known in any mode n due to i th direction of excitation, denoted here by R_{in} . At a given instance the response can be expressed as the weighted algebraic sum of response in various modes due to various excitations:

$$R(t) = \sum_{in} K_{in}(t) R_{in} \quad (3)$$

The value of $R(t)$ given by Equation (3) is bounded by value of R_e given by Equation (2), or

$$|R(t)| \leq R_e \quad (4)$$

Now consider the instance at which a given response at a specified location, U , reaches its maximum value U_e . Equation (3) gives:

$$\sum_{in} K_{in} U_{in} = U_e$$

or

$$\sum_{in} K_{in} u_{in} = 1 \quad (5)$$

where

$$u_{in} = U_{in} / U_e \quad (6)$$

Equations (2) and (6) give

$$\sum_{mn} \epsilon_{mn} u_{im} u_{in} = 1 \quad (7)$$

If there are N modes excited in each of the three components of earthquake, then according to Equation (7) u_{im} is a unit vector in a $3N$ Riemannian space⁽³⁾ whose metric tensor is represented by ϵ_{mn} . This space is designated here as the Modal Space. Consider, another arbitrary unit vector v_{in} in the same space. Again

$$\epsilon_{mn} v_{im} v_{in} = 1 \quad (8)$$

According to Equation (4)

$$|K_{in} v_{in}| \leq 1 \quad (9)$$

Since, v_{in} is any arbitrary unit vector, without loss of generality one can write

$$K_{im} = C \epsilon_{mn} v_{in} \quad (10)$$

Equations (9) and (10) give

$$|C \epsilon_{mn} v_{im} v_{in}| \leq 1 \quad (11)$$

which with Equation (8) yields

$$|C| \leq 1 \quad (12)$$

Now, substitution of Equation (10) into Equation (5) gives

$$C \epsilon_{mn} u_{im} v_{in} = 1 \quad (13)$$

The angle between the vectors u and v is given by

$$\cos(u, v) = \epsilon_{mn} u_{im} v_{in} \quad (14)$$

Therefore, Equations (13) and (14) give

$$C = 1/\cos(u, v)$$

or

$$|C| \geq 1 \quad (15)$$

The only way to satisfy both Equations (12) and (15) is to set

$$|C| = 1 \quad (16)$$

Therefore,

$$|\cos(u, v)| = 1$$

or

$$|\epsilon_{mn} u_{im} v_{in}| = 1 \quad (17)$$

which is possible only when

$$v_{im} = u_{im} \quad (18)$$

Equations (10) and (18) yield

$$K_{im} = \epsilon_{mn} u_{in} \quad (19)$$

Since ϵ_{mn} is positive-definite by definition⁽²⁾, it can be inverted to obtain γ_{mn} , such that

$$\gamma_{mi} \epsilon_{in} = \delta_{mn} \quad (20)$$

Now, Equations (7), (19) and (20) give

$$\gamma_{mn} K_{im} K_{in} = 1 \quad (21)$$

Finally, therefore, Equation (3) gives the values of all relevant responses $R(t)$ at any instance which may cause extreme probable effects on the structure when K_{in} varies according to Equation (21).

To check if Equations (3) and (21) are compatible with Equation (2), consider the following extremum problem:

$$R = K_{in} R_{in} + \lambda (\gamma_{mn} K_{im} K_{in} - 1)$$

where λ is a Lagrangian multiplier. For R to be maximum,

$$\frac{\partial R}{\partial K_{in}} = R_{in} + 2 \lambda \gamma_{mn} K_{im} = 0 \quad (22)$$

Multiplying Equation (22) by K_{in} , one gets

$$R + 2\lambda = 0 \quad (23)$$

Multiplying Equation (22) by $\epsilon_{ln} R_{il}$ one gets

$$\epsilon_{ln} R_{il} R_{in} + 2 \lambda \epsilon_{ln} R_{il} \gamma_{mn} K_{im} = 0$$

or by Equations (3) and (20),

$$\epsilon_{ln} R_{il} R_{in} + 2 \lambda R = 0 \quad (24)$$

Equations (23) and (24) give

$$R^2 = \epsilon_{ln} R_{il} R_{in}$$

which is same as Equation (2) with

$$R = R_e$$

thus proving the validity of Equation (21). Equations (22) and (23) also give

$$K_{im} = \frac{\epsilon_{mn} R_{in}}{R_e} \quad (25)$$

when R is maximum ($=R_e$). Note, Equation (25) can also be derived from Equation (19).

III. The Equivalent Modal Response Method

Consider a design problem in which only a small number, M, of the response values R^r ($r = 1, M$) contribute. For instance, for a beam column subjected to combined axial force and bending moment

$$\begin{aligned} M &= 2 \\ R^1 &= \text{Axial force} \\ R^2 &= \text{Bending moment} \end{aligned}$$

Obviously, there are many design problems with $M=2, 3$ etc. Let the design criterion be specified as

$$\phi \leq \phi_{\text{allowable}} \quad (26)$$

where

$$\phi = A^r R^r \quad (27)$$

In Equation (27), A^r represents M influence coefficients, which have been assumed to be locally constant to make Equation (27) linear. In other words, even if the actual design criterion is nonlinear in R^r , it is still valid to use it in locally linear form, such as Equation (27), if the response spectrum analysis is applicable.

For nth mode, ith excitation,

$$\phi_{in} = A^r R_{in}^r \quad (28)$$

Equations (2) and (28) give

$$\phi_e^2 = A^r A^s \epsilon_{mn} R_{im}^r R_{in}^s \quad (29)$$

or

$$\phi_e^2 = A^r A^s G^{rs} \quad (30)$$

where

$$G^{rs} = \epsilon_{mn} R_{im}^r R_{in}^s \quad (31)$$

It is obvious from Equation (30) that for design purposes it is sufficient to know G^{rs} and it is not necessary to know R_{in}^r . The array G^{rs} is symmetric, as defined by Equation (31) and has $M(M+1)/2$ unique elements, which is equal to 3 for $M=2$. If the total number of modes in each of the three excitations of earthquake is N , then R_{in}^r has $3MN$ elements, which is equal to 60 for $M=2$ and $N=10$.

For convenience, as will be apparent later, Equivalent Modal Response, \bar{R}_α^r , is introduced here, such that

$$G^{rs} = \bar{R}_\alpha^r \bar{R}_\alpha^s \quad (32)$$

The Greek subscripts have a range equal to the number of Equivalent Modes, say M' . In terms of the Equivalent Modal Response

$$R_e^2 = \bar{R}_\alpha \bar{R}_\alpha \quad (33)$$

$$\phi_e^2 = A^r A^s \bar{R}_\alpha^r \bar{R}_\alpha^s \quad (34)$$

which follow directly from Equation (32).

The values of \bar{R}_α^r are arbitrary except that Equation (32) must be satisfied. Equation (32) represents $M(M+1)/2$ equations; however, as will be shown here, there are more conditions to be satisfied. The \bar{R}_α^r can be represented in terms of unit vectors and their amplitudes as

$$\bar{R}_\alpha^r = R_e^{(r)} r_\alpha^r \quad (35)$$

The superscript in parenthesis means that the implied summation has been suppressed. Substituting Equation (35) into Equation (32) one gets

$$\begin{aligned} G^{rs} &= R_e^{(r)} R_e^{(s)} r_\alpha^r r_\alpha^s \\ &= R_e^{(r)} R_e^{(s)} \cos(r,s) \end{aligned} \quad (36)$$

where (r, s) represents the angle between r th and s th vectors.

It is observed from Equation (36) that there are $(M-1)(M-2)/2$ equations of the type

$$(r, t) = (r, s) + (s, t) \quad (37)$$

where $M \geq t > s > r \geq 1$

Therefore, Equivalent Modal Response \bar{R}_α^r should satisfy a total of $M(M+1)/2$ equations represented by Equation (32) or (36) and $(M-1)(M-2)/2$

equations represented by Equation (37). The number of elements \overline{R}_α^r to be determined is $M \cdot M'$. Therefore,

$$M \cdot M' \geq \frac{M(M+1)}{2} + \frac{(M-1)(M-2)}{2}$$

or

$$M \cdot M' \geq M^2 - M + 1$$

or

$$M' \geq M \quad (38)$$

or

$$M'_{\min} = M \quad (39)$$

When $M' = M$, \overline{R}_α^r is a square array of the size $M \times M$. The number of elements which can be selected arbitrarily are:

$$M^2 - (M^2 - M + 1) = M - 1 \quad (40)$$

As shown above, usually one will choose to have the minimum number of Equivalent Modes which is equal to the number of responses which contribute to a given design criterion, M . Examples of Equivalent Modes are given later.

The Equivalent Modal Responses \overline{R}_α^r can be considered as a Modal Subspace of the order M in the original Modal Space, R_{in}^r of the order $3N$. The Modal Space R_{in}^r in general is a Riemannian Space with a positive definite metric tensor ϵ_{mn} , the Modal Subspace \overline{R}_α^r is Cartesian (Equation 35), which is a special case of the Riemannian Space. The Modal Subspace also satisfies Equations (3) and (21), derived earlier with proper substitutions.

$$R^r = \overline{K}_\alpha \overline{R}_\alpha^r \quad (41)$$

with

$$\overline{K}_\alpha \overline{K}_\alpha = 1 \quad (42)$$

IV. Interaction Surface

Equations (41) and (42) represent a surface in the Modal Subspace. The points on this surface represent the values of R^r that can be expected to occur simultaneously to cause the extreme probable effect. The equation of this surface can also be written explicitly as discussed below.

Assuming that \overline{R}_α^r is a square array of the order M , one can write from Equation (4)

$$\overline{K}_\alpha = R^r T_\alpha^r \quad (43)$$

where

$$\overline{R}_\alpha^r T_\alpha^s = \delta^{\alpha rs} \quad (44a)$$

and

$$\overline{R}_\alpha^r T_\beta^r = \delta_{\alpha\beta} \quad (44b)$$

Substituting Equation (43) into Equation (42) one gets

$$\overline{K}_\alpha \overline{K}_\alpha = R_\alpha^r T_\alpha^r R^s T_\alpha^s = 1$$

or

$$H^{rs} R^r R^s = 1 \quad (45)$$

where

$$H^{rs} = T_\alpha^r T_\alpha^s \quad (46)$$

Equation (45) gives the desired Interaction Surface. The coefficient matrix H^{rs} given by Equation (46) can be represented in more direct form without calculating the Equivalent Modal Response \overline{R}_α^r . Equations (32) and (46) give

$$H^{rs} G^{st} = T_\alpha^r T_\alpha^s \overline{R}_\beta^s \overline{R}_\beta^t$$

which with Equation (44) gives

$$H^{rs} G^{st} = \delta^{rt} \quad (47)$$

Therefore, H^{rs} is inverse of the matrix G^{st} , which is given by Equation (31).

V. Application to Design Problems

With the theories presented in the preceding three sections one should be able to design any type of structure analyzed by the response spectrum method. Application of these theories to some frequently encountered design problems is illustrated below. However, the application is not intended to be limited to these problems.

A. Design of Building Cross Section

Figure 1 shows a building cross section which is subjected to axial force SN and the story overturning moments SM_x , SM_y . Vertical reinforcement is designed to resist the vertical stresses which are given by

$$\sigma = \frac{SN}{A} + \frac{SM_x (y I_y - x I_{xy}) + SM_y (x I_{xy} - y I_{xy})}{I_x I_y - I_{xy}^2} \quad (48)$$

where

A = area of cross section

I_x = moment of inertia about x axis

I_y = moment of inertia about y axis

I_{xy} = product of inertia

One way of calculating the effective stress distribution is to calculate stresses at various locations in the cross-section using Equation (48) for each mode of vibration under each excitation of earthquake. If there are 10 modes and 3 directions of earthquake, this calculation will have to be performed 30 times for each location in the building cross section. Then, the effective stress at any location can be calculated using Equation (2).

The obvious alternative is to use the Equivalent Modal Response method presented in Section III of this paper.

Following the notations of Section III

$$R^r = (SN, SM_x, SM_y)^T \quad (49)$$

$$G_{11} = \epsilon_{mn} SN_{im} SN_{in} = SN_e^2$$

$$G_{22} = \epsilon_{mn} SM_{xim} SM_{xin} = SM_{xe}^2$$

$$G_{33} = \epsilon_{mn} SM_{yim} SM_{yin} = SM_{ye}^2$$

$$G_{12} = G_{21} = \epsilon_{mn} SN_{im} SM_{xin}$$

$$G_{13} = G_{31} = \epsilon_{mn} SN_{im} SM_{yin}$$

$$G_{23} = G_{32} = \epsilon_{mn} SM_{xim}, SM_{yin} \quad (50)$$

The Equivalent Modes are

$$R_\alpha^r = (SN_\alpha, SM_{x\alpha}, SM_{y\alpha})^T \quad (51)$$

Equation (51) has 9 unknowns. Two of the unknowns can be selected arbitrarily (Equation 40).

Let the first arbitrary selection be

$$SN_1 = SN_e \quad (52a)$$

Therefore, appropriate conditions from Equation (32) yield

$$SN_2 = SN_3 = 0 \quad (52b, c)$$

and

$$SM_{x1} = G_{12}/SN_e \quad (52d)$$

$$SM_{y1} = G_{13}/SN_e \quad (52e)$$

Next, let the other arbitrary selection be

$$SM_{x2} = (SM_{xe}^2 - SM_{x1}^2)^{1/2} \quad (52f)$$

Again, Equation (32) gives

$$SM_{x3} = 0 \quad (52g)$$

$$SM_{y2} = (G_{23} - SM_{x1} SM_{y1})/SM_{x2} \quad (52h)$$

$$SM_{y3} = (SM_{ye}^2 - SM_{y1}^2 - SM_{y2}^2)^{1/2} \quad (52i)$$

The above values of the Equivalent Modes are also given in Table 1.

TABLE 1 Equivalent Modes For The
Design of Building Cross Sections

Equivalent Mode	SN	SM_x	SM_y
1	SN_e	$\frac{G_{12}}{SN_e}$	$\frac{G_{13}}{SN_e}$
2	0	$(SM_{xe}^2 - SM_{x1}^2)^{1/2}$	$\frac{(G_{23} - SM_{x1} SM_{y1})}{SM_{x2}}$
3	0	0	$(SM_{ye}^2 - SM_{y1}^2 - SM_{y2}^2)^{1/2}$

Once the three Equivalent Modes have been determined as above, one can compute the stress at any location in the section for each Equivalent Mode. The effective stress can then be obtained using Equation (1) or (33). Simplification of the problem is obvious.

B. Design of Base Slab

Consider a building whose cross section is shown in Figure 1, supported on a base slab on a soil subgrade. The slab is subjected to the

same axial force and overturning moments which the building cross-section is subjected to. Once again, the three Equivalent Modes are determined as discussed in the previous problem. The slab is analyzed individually for each Equivalent Mode, thus giving at any slab section three moments: M_x , M_y , M_{xy} , Figure 2. If the failure direction is θ , the design flexural capacities⁽⁴⁾ in x and y directions are given by

$$M_x^* = \frac{\sum M_{\theta\alpha} (M_x + M_{xy} \tan\theta)_\alpha}{M_{\theta e}} \quad (53a)$$

$$M_y^* = \frac{\sum M_{\theta\alpha} (M_y + M_{xy} \cot\theta)_\alpha}{M_{\theta e}} \quad (53b)$$

where

$$M_\theta = M_x \cos^2\theta + M_y \sin^2\theta + 2 M_{xy} \sin\theta \cos\theta \quad (54)$$

The critical direction θ is arbitrary, except that, it should satisfy the following conditions

$$M_x^* \geq M_{xe} \quad (55a)$$

$$M_y^* \geq M_{ye} \quad (55b)$$

More detailed treatment of the problem is provided in Reference 4.

C. Design of Reinforced Concrete Column

Consider a reinforced concrete column subjected to axial forces N and bending moment, M , shown in Figure 3. One common method of designing such column sections is to draw the N - M capacity interaction diagram and to ensure that all of the N - M load points are within the capacity interaction diagram. For seismic loading the variation of seismic N - M is given by Equation (45), which for the present problem can be rewritten as

$$H_{11} N^2 + H_{22} M^2 + 2 H_{12} NM = 1 \quad (56)$$

where

$$H_{11} = \frac{M_e^2}{N_e^2 M_e^2 - G_{12}^2} \quad (57a)$$

$$H_{22} = \frac{N_e^2}{N_e^2 M_e^2 - G_{12}^2} \quad (57b)$$

$$H_{12} = \frac{G_{12}}{N_e^2 M_e^2 - G_{12}^2} \quad (57c)$$

and

$$G_{12} = \epsilon_{mn} N_{im} M_{in} \quad (57d)$$

Equation (56) represents an ellipse, designated here as Interaction Ellipse. As shown in Figure 4, the Interaction Ellipse should be completely enveloped by the capacity interaction diagram.

When the design procedure is digitized on computer, then the comparison between the capacity and the loading is made using several points on the interaction diagram. Any point on the Interaction Ellipse is given by (Equation 41)

$$N = \bar{K}_1 \bar{N}_1 + \bar{K}_2 \bar{N}_2 \quad (58a)$$

$$M = \bar{K}_1 \bar{M}_1 + \bar{K}_2 \bar{N}_2 \quad (58b)$$

in which \bar{K}_1 and \bar{K}_2 should satisfy the following condition (Equation 42)

$$\bar{K}_1^2 + \bar{K}_2^2 = 1 \quad (59)$$

\bar{N}_α and \bar{M}_α ($\alpha = 1, 2$) in Equations (58) represent Equivalent Modes and may be calculated as described in this Section and in Section III.

Several well distributed sets of the values of \bar{K}_1 and \bar{K}_2 are selected which satisfy Equation (59); each set of \bar{K}_1 and \bar{K}_2 gives a point on the Interaction Ellipse by substituting it into Equations (58).

Procedures similar to those described above can be used for the design of reinforced concrete columns subjected to axial force and biaxial bending moments. Similar methods can also be used for the design of steel columns.

D. Analysis and Design of Base Slab With Local Uplift

It is possible that under the combined action of static and seismic loads the base slab uplift in certain areas. If the uplifted area is significant a detailed nonlinear analysis of the complete structure-base slab-soil system may be required which is beyond the scope of the present discussion. However, if the uplift is local in nature, it can be assumed that the actual dynamic behavior of the building does not significantly depart from that predicted by the response spectrum analysis of the decoupled building system.

In the latter case the seismic axial force and the overturning moments acting on the base slab can again be represented by three Equivalent Modes,

derived in Subsection V-A above. Values of axial force and overturning moments expected to occur simultaneously are then given by

$$SN = \bar{K}_\alpha \bar{SN}_\alpha \quad (60a)$$

$$SM_x = \bar{K}_\alpha \bar{SM}_{x\alpha} \quad (60b)$$

$$SM_y = \bar{K}_\alpha \bar{SM}_{y\alpha} \quad (60c)$$

and

$$\bar{K}_\alpha \bar{K}_\alpha = 1 \quad (61)$$

Where subscript α has a range 1 to 3. Various sets of \bar{K}_α can be selected which satisfy Equation (61), and the corresponding values of SN, SM_x and SM_y are calculated from Equations (60). For each set of SN, SM_x , SM_y so calculated, the base slab should be analyzed nonlinearly accounting for the uplift. Such an analysis should include all the other static loads together with the seismic loads.

Since the nonlinear analysis is usually expensive, an effort should be made to reduce the number of such analyses. This may be achieved by first analyzing the base slab linearly under each of the three equivalent modes. Maximum probable deflection at various locations in the base slab is calculated using the standard procedures. Locations most critical to uplift can thus be determined. At such a location P, the seismic deflection is given by

$$W^P = \bar{K}_\alpha \bar{W}_\alpha^P \quad (62)$$

This deflection is maximum when

$$\bar{K}_\alpha = \frac{\bar{W}_\alpha^P}{W_e^P} \quad (63a)$$

where

$$(W_e^P)^2 = \bar{W}_\alpha^P \bar{W}_\alpha^P \quad (63b)$$

according to Equations (1), (25) and (35). The set of SN, SM_x , SM_y which would cause this maximum displacement can be determined by substituting the value of \bar{K}_α from Equation (63a) into Equations (60). The slab is then analyzed nonlinearly applying the values of seismic SN, SM_x , SM_y so calculated. The above process should be repeated considering as many locations critical to uplift as necessary.

Conclusions

A theory which postulates simultaneous variation in various responses of a structure based on the response spectrum method of analysis has been presented. Furthermore, it is shown that the response in several modes of

vibration under three components of earthquake can be represented by the response in a small number of Equivalent Modes, thus reducing the number of calculations required in the design analysis.

The modal vectors lie in a Riemannian Space designated as Modal Space. The Equivalent Modal Vectors lie in a Cartesian Space which is designated as Modal Subspace. The order of Modal Subspace is equal to the number of responses included in a design criterion. The response values which are expected to occur simultaneously to cause extreme probable effect lie on an Interaction Surface in the Modal Subspace. This concept facilitates the use of a graphical design procedure when the design criterion can be represented in terms of a capacity interaction diagram as in the case of the design of a reinforced concrete beam column section.

Application of the theories developed in this paper has been illustrated for four design problems. However, application of these theories is not limited to these illustrations. Indeed any structure which can be analyzed by the response spectrum method can also be designed using the methods presented in this paper.

Within the assumptions of Equation (1) or (2), the theories and the methods in this paper are exact thus eliminating the conservatism inherent in many of the existing practices.

References

1. Chu, S. L., Amin, H. and Singh, S., "Spectral Treatment of Actions of Three Earthquake Components on Structures", Nuclear Engineering and Design, Vol. 21, 1972, pp. 126-136.
2. Singh, A. K., Chu, S. L. and Singh, S., "Influence of Closely Spaced Modes in Response Spectrum Method of Analysis", Proceedings, ASCE Specialty Conference on Structural Design of Nuclear Power Plant Facilities, Chicago, Illinois, December, 1973.
3. Synge, J. L. and Schild, A., Tensor Calculus, University of Toronto Press, 1949.
4. Gupta, A. K. and Chu, S. L., "Design of Reinforced Concrete Structures Subjected to Three Components of Earthquake", Nuclear Engineering and Design, to be published.

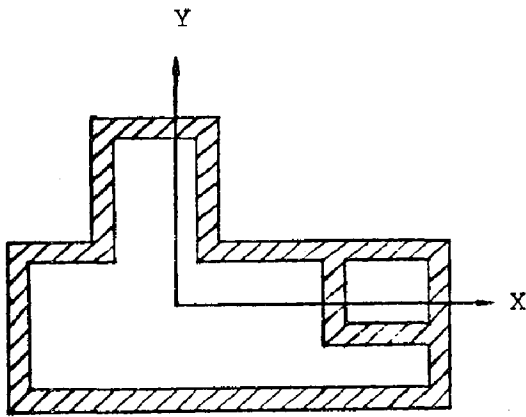


Fig. 1. A Building Cross Section

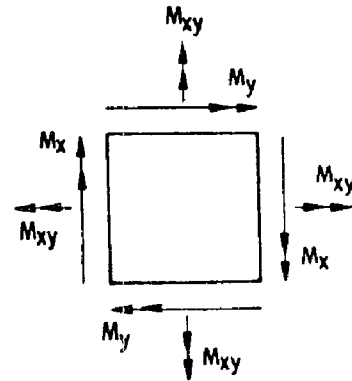


Fig. 2. A Slab Element Subjected to Flexural Moments

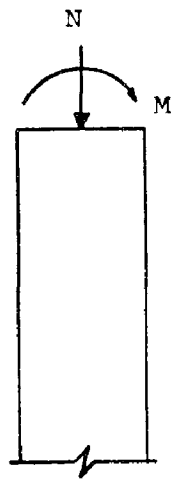


Fig. 3. Column Subjected to Axial Force and Uniaxial Moment

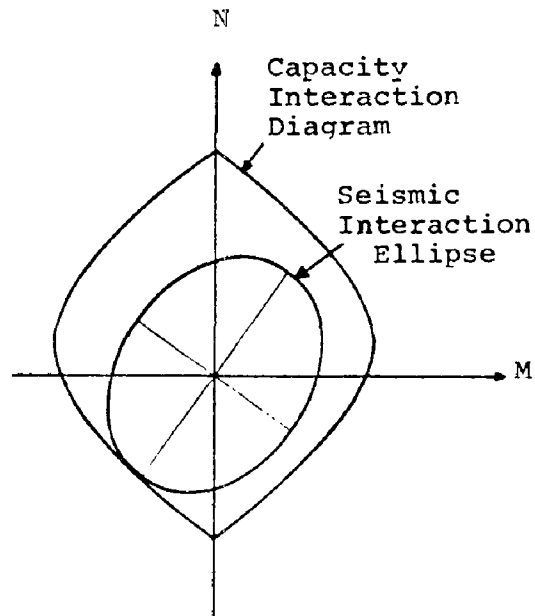


Fig. 4. Design of Reinforced Concrete Column

INTERNATIONAL SYMPOSIUM ON
EARTHQUAKE STRUCTURAL ENGINEERING

St. Louis, Missouri, USA, August, 1976

597

RESIZING OF FRAMES SUBJECTED TO GROUND MOTION

V.B. VENKAYYA¹ and F.Y. CHENG²

1. Aerospace Engineer, Flight Dynamics Laboratory, Wright-Patterson, AFB, Ohio, U.S.A.
2. Professor of Civil Engineering, University of Missouri-Rolla, Missouri, U.S.A.

SUMMARY

The object of this paper is to present a design procedure based on optimality criteria, treating the expected ground motion as a dynamic force on the structure. Elastic systems are designed for minimum weight while satisfying all the design requirements. The design requirements are in general strength and stiffness under all loading conditions including those resulting from expected ground motion.

INTRODUCTION

The pressure for building bigger and safer structures is relentlessly increasing because of the ever increasing population around the world. Large high-rise buildings, nuclear reactors, storage tanks with inflammable substances and toxic gases and water retaining structures such as dams are the prime candidates for catastrophic failure due to ground motion induced by seismic conditions. The problem becomes even more acute as the population centers move closer to the fault regions in search of open space and untapped resources. There is a great deal of effort around the world to develop rational design criteria for seismic design. This effort is greatly enhanced by the revolutionary development in digital computers and the design methods. Even before computers, the successful design of Latino Americano Tower in Mexico provides evidence that it is feasible to evolve an adequate design criteria to withstand moderate to severe seismic motions(1).

In addition to the seismic conditions, ground motions are induced by waves coming from underground blasts. The motion on uneven pavement surfaces may also be treated as ground motion in designing landing gears and

other wheel bays in vehicles. The ground motion effects are in general dynamic and random in nature. The rapid ground motion generates inertia forces which in turn produce differential displacements and stresses in the structure. The adequacy of the structure to withstand these forces depends on the intensity of the ground motion, the natural frequencies and the ductility of the structure. In addition the soil structure interaction can be a major factor.

The normal practice is to design structures to dead and live loads (other than those induced by ground motion) and check the adequacy of the resulting structure to the expected intensity of ground motion. Depending on the region in which the structure is to be located the past history of the ground motion can provide a deterministic condition for checking the design. With the increased analytical capabilities it is now possible to include this expected ground motion condition with all the other dead and live load conditions.

Whether it is stated explicitly or not, design has always been an optimization problem. The simplest and probably the most useful objective function is the weight of structure. Then the objective is to minimize the weight of the structure while satisfying all the design requirements. The design requirements are in general strength and stiffness under all loading conditions (including those resulting from expected ground motion).

The object of this paper is to present a design procedure based on optimality criteria (2), treating the expected ground motion as a dynamic force on the structure. Only elastic case is considered here. However, it is realized that a realistic design procedure must consider elastoplastic behavior of the structure (3). It is also tacitly assumed that the structure has adequate ductility. The optimization procedure pertaining to dynamic case is discussed here and the discussion for the static case is given in Reference (5).

ANALYSIS FOR GROUND MOTION

The generalized displacements of a structure subjected to ground motion can be represented by

$$\underline{r}_c = \underline{r}_G + \underline{r} \quad (1)$$

where \underline{r}_c is the vector of the total displacements of the structure. \underline{r}_G is the vector of displacements imparted by the ground to the structure as

rigid body motion. The vector \underline{r} represents elastic deformation of the structure.

The dynamic equation governing the motion of the structure due to ground motion can be written as

$$\underline{M} \ddot{\underline{r}} + \underline{C} \dot{\underline{r}} + \underline{K} \underline{r} = 0 \quad (2)$$

In Equation (2) no other forces other than ground motion is acting on the structure. The matrices \underline{M} , \underline{C} and \underline{K} represent the generalized mass, damping and elastic stiffness of the structure. The mass and stiffness matrices of the structure are given by

$$\underline{M} = \sum_{i=1}^n \underline{a}_i^t m_i \underline{a}_i + \underline{M}_C \quad (3)$$

$$\underline{K} = \sum_{i=1}^n \underline{a}_i^t k_i \underline{a}_i \quad (4)$$

where \underline{a}_i is the compatibility matrix of the i^{th} element (4). The matrix \underline{M}_C represents concentrated or lumped masses due to non-structural attachments such as floors, equipment, etc. This non-structural mass matrix is assembled by adding the mass of the attachments to the diagonal elements of \underline{M}_C corresponding to their points of application. If they are lumped masses without specific geometric dimensions, only the translational degrees of freedom will be effected. When the masses are located between the discrete points of the structure the equivalent effect on the generalized mass can be derived by D'Alembert's principle and the principle of virtual work.

The damping matrix \underline{C} is assumed to be proportional to the mass and stiffness matrices by the following relation

$$\underline{C} = 2\theta \underline{M} + \alpha \underline{K} \quad (5)$$

where θ and α are the proportionality constants. This proportionality assumption facilitates decoupling of the dynamic equations by a modal analysis.

It is evident from Equation (2) that the last two terms are effected by only the relative motion of the structure and not the ground motion. It

is further assumed that no other dynamic force other than ground motion is acting on the structure. However, in actual design additional loading conditions including some static and dynamic cases must be considered. An extensive discussion of optimization for static loads and periodic dynamic forces was presented in References 5 and 6 respectively.

Substitution of Equation (1) in (2) gives the dynamic equation in the form

$$\underline{M} \ddot{\underline{r}} + \underline{C} \dot{\underline{r}} + \underline{K} \underline{r} = - \underline{M} \ddot{\underline{r}}_G \quad (6)$$

The response of the structure can be represented by a finite number of normal coordinates in the form

$$\underline{r} = \underline{\psi} \underline{q} \quad (7)$$

where each column of the matrix $\underline{\psi}$ is a normal mode and is obtained by a standard eigenvalue analysis of the problem

$$\omega^2 \underline{M} \underline{\psi} = \underline{K} \underline{\psi} \quad (8)$$

The vector \underline{q} represents a set of normal coordinates. Substitution of Equation (7) in (6) and premultiplication by $\underline{\psi}^t$ gives

$$\underline{\psi}^t \underline{M} \underline{\psi} \ddot{\underline{q}} + \underline{\psi}^t \underline{C} \underline{\psi} \dot{\underline{q}} + \underline{\psi}^t \underline{K} \underline{\psi} \underline{q} = - \underline{\psi}^t \underline{M} \ddot{\underline{r}}_G \quad (9)$$

The uncoupled Equation (9) may be written as

$$\ddot{q}_i + (2\theta + \alpha \omega_i^2) \dot{q}_i + \omega_i^2 q_i = - \underline{\psi}_i^t \underline{M} \ddot{\underline{r}}_G / \underline{\psi}_i^t \underline{M} \underline{\psi}_i \quad (10)$$

If β is represented as

$$\beta_i = \theta + 1/2 \alpha \omega_i^2 \quad (11)$$

then the characteristic equation becomes

$$(S^2 + 2\beta S + \omega_i^2) q = 0 \quad (12)$$

The roots of Equation (12) are given by

$$S = -\beta_i \pm \sqrt{\beta_i^2 - \omega_i^2} \quad (13)$$

Then β can be written as

$$\beta_i = \left(\frac{\theta}{\theta_0} + \frac{\alpha}{\alpha_0} \right) \omega_i \quad (14)$$

where $\theta_0 = \omega_i$ and $\alpha_0 = 2/\omega_i$ and

$$\frac{\theta}{\theta_0} + \frac{\alpha}{\alpha_0} \begin{cases} < \\ = \\ > \end{cases} 1 \quad (15)$$

represents underdamped, critically damped and overdamped cases respectively. Only the underdamped case is of interest in this paper. The parameters θ_0 and α_0 represent the cases when the damping is proportional to the mass and stiffness matrices respectively.

In Equation (10) the ground acceleration \ddot{r}_G may be represented as

$$\ddot{r}_G = -r_G f(t) \quad (16)$$

where r_G is a vector with elements in the direction of the ground motion while all other elements are zero. Unless the dimensions of the body imparting the mass at a point is specified, the elements corresponding to the rotational degrees of freedom are all zero. The function $f(t)$ represents time variation of the ground acceleration. Now Equation (10) can be written as

$$\ddot{q}_i + 2\beta_i\omega_i\dot{q}_i + \omega_i^2q_i = \frac{\psi_i^t M r_G}{M_i} f(t) \quad (17)$$

The solution of this uncoupled equation can be obtained by the use of the convolution integral in the following form:

$$q_i(t) = \frac{\psi_i^t M r_G}{\omega_i^2 M_i} D_i(t) \quad (18)$$

where $D_i(t)$, the dynamic load factor, is given by

$$D_i(t) = \int_0^t \frac{\omega_i^2}{(\omega_i^2 - \beta_i^2)^{1/2}} e^{-\beta_i(t-\tau)} \sin[(\omega_i^2 - \beta_i^2)^{1/2}(t-\tau)] f(\tau) d\tau \quad (19)$$

Here t represents the time at which the response is desired and τ is the intermediate variable. Substitution of Equation (19) in (7) gives the response of the structure in the following form

$$\tilde{r} = \sum_{i=1}^p C_i \psi_i \quad (20)$$

where p is the number of modes required to represent dynamic response. The parameter C_i is given by

$$C_i = \frac{\psi_i^t M r G}{\omega_i M_i} D_i(t) \quad (21)$$

In Equation (20) the total response is represented as the sum of the modal responses. The nature of the ground motion and mass distribution determine the number and type of modes that participate in the response.

The dynamic load factors in each mode require evaluation of the integral in Equation (19). If the function $f(t)$ is periodic, the integral can be evaluated by expanding the function in a Fourier Series. On the other hand if $f(t)$ is aperiodic but a known analytic function, the Fourier integral representation can precede integration. But in the case of ground motion neither of these procedures is feasible because the ground motion information is often available as accelogram readings at discrete time steps. In such cases a numerical integration scheme would be more convenient.

The numerical integration scheme consists of slicing the duration of the forcing function into a number of intervals. Each interval covers a number of accelogram readings. At the end of each interval all the dynamic load factors are evaluated by Simpson's rule as follows:

$$D_i = \frac{h_i}{3} [D_{i0} + 4 D_{i1} + 2 D_{i2} + \dots + 4 D_{in-1} + D_{in}] \quad (22)$$

where h_i is the interval at which accelogram records are available. D_{ij} is

the value of the integrand in Equation (19) at the j^{th} accelogram record. It is possible by using this procedure, to determine at least approximately the values of the dynamic load factors during different instances of the ground motion. The load factors for all the modes can be determined at equal intervals of time during the ground motion. The peak response of the structure is needed for design. However, the peak values of the dynamic load factors may not be reached at the same time for all the modes. Even if they do the peak response may not be the critical response for all the components (elements) of the structure. An actual design must consider the response at various time slices as being that of multiple loading conditions and design the structure accordingly. Normally design for multiple loading conditions can be quite cumbersome and this effect of peaks reaching at different times becomes significant only when a large number of modes participate in the dynamic response. However, in most practical cases only a few modes would be significant, and the assumption that all dynamic load factors reach their peak values at the same time would at best yield conservative results. This is the procedure adopted in this paper.

CONDITIONS OF OPTIMALITY

Basically the procedure presented here is similar to that discussed in Reference 6. The optimality criteria is derived for a structure vibrating in one of its natural modes, and it is subjected to a dynamic stiffness requirement which is expressed as a Rayleigh quotient in the vibrating mode.

Most structural optimization problems can be stated as follows:

Minimize the objective function

$$W = W(A) = \sum_{i=1}^n e_i A_i \ell_i \quad (23)$$

subject to the constraints

$$Z_j \leq E_j \quad (24)$$

where W is the weight of the structure, A is the design vector that represents the sizes of the structural elements and Z_j is the constraint expressed as a stiffness requirement involving the entire structure. In a finite element formulation the weight of the structure can be expressed as the sum of

the weights of the elements. If the stiffness of the structure can also be expressed as the sum of the stiffnesses of the individual components, then an optimality criterion involving uniformity of an energy functional across the elements can be established.

Combining Equations (23) and (24) a new function ϕ can be written as

$$\phi = W(A) + \sum_{j=1}^p \frac{1}{\lambda_j} Y_j \quad (25)$$

where λ_j is the Lagrangian multiplier and Y_j is given by

$$Y_j = Z_j(A) - E_j \leq 0 \quad (26)$$

The summation is over the number of stiffness constraints involved.

The necessary condition for a stationary value of ϕ is obtained by

$$\frac{\partial \phi}{\partial A_i} = \frac{\partial}{\partial A_i} [W(A)] + \sum_{j=1}^p \frac{1}{\lambda_j} \frac{\partial}{\partial A_i} (Y_j) = 0 \quad (27)$$

After simplifying Equation (23) the optimality condition can be written as follows:

$$\sum_{j=1}^p \frac{e_{ji}}{\lambda_j} = 1 \quad (28)$$

where e_{ji} can be interpreted as an energy density function and is of the form

$$e_{ji} = \frac{\frac{\partial}{\partial A_i} [Z_j(A)]}{\frac{\partial}{\partial A_i} [W(A)]} \quad (29)$$

The quantities e_{ji} are the ratio of the gradients of the constraint and objective functions. They can be interpreted as some energy density functions in the structure depending on the type of constraint conditions (2).

The sufficient condition for a minimum is obtained by

$$\frac{\partial^2 \phi}{\partial A_i^2} > 0 \quad (30)$$

Both the necessary and sufficient conditions assure only relative minimums in the neighborhood.

The dynamic stiffness of the structure vibrating in the natural mode is defined as

$$Z_j = \omega_j^2 = \frac{\psi_j^t K \psi_j}{\psi_j^t M \psi_j} \quad (31)$$

where ψ_j is the j^{th} natural mode of the structure. The matrices K and M are the stiffness and mass matrices of the structure respectively. Substitution of this stiffness requirement in Equation (27) gives the optimality condition as follows:

$$\lambda = \frac{e_i}{\psi_j^t M \psi_j} \quad (32)$$

where e_i is the ratio of the difference in strain and kinetic energy densities to the mass density of the i^{th} element in the given mode and it is given by

$$e_i = (\psi_j^t K_i \psi_j - \omega_j^2 \psi_j^t M_i \psi_j) / \rho_i A_i l_i \quad (33)$$

where K_i and M_i are the stiffness and mass matrices of the i^{th} element in the structure coordinate system.

Since the Lagrangian multiplier is constant, Equation (32) can be true only when all the elements of the structure have the same e value in the given mode. This means that a structure has optimum distribution of the material if the quantity e has the same value in all its elements in a given mode of vibration.

From Equations (23) and (32) the Lagrangian multiplier λ can also be written as a total system parameter as follows:

$$\lambda = \frac{Z(1-\eta)}{W} \quad (34)$$

where W is the weight of the structure and η is the ratio of the structural modal mass to the total modal mass and it is given by

$$\eta = \frac{\psi_j^t M_s \psi_j}{\psi_j^t M \psi_j} \quad (35)$$

where M_s is the structural mass only. The case of a zero nonstructural mass results in the trivial case of zero weight structure.

The optimality criteria as expressed in Equation (32) is valid only for a structure vibrating in one of its natural modes. However, the same criterion will be used as an approximation to a general dynamic response case (6). The Rayleigh quotient in such a case is defined as

$$Z = \frac{r^t K r}{r^t M r} \quad (36)$$

The response r is designated as the dynamic mode and it is represented as the sum of the modal responses in Equation (20). The quantity e_i in this case is defined as the ratio of the difference in strain and kinetic energy densities to the mass density of the i^{th} element in the dynamic mode, and it is given by

$$e_i = (r^t K_i r - Z r^t M_i r) / \rho_i A_i \ell_i \quad (37)$$

where Z is the Rayleigh quotient in the dynamic mode.

OPTIMIZATION ALGORITHM

A recursion relation to achieve the optimality criterion can be derived by writing Equation (32) as follows:

$$\lambda = \frac{1}{r^t M r} \frac{[r^t K_i r - Z r^t M_i r]}{\rho_i A_i \ell_i} \quad (38)$$

The design variable vector A is written as

$$A = \Lambda \alpha \quad (39)$$

where Λ is the normalizing or scaling parameter and α is the relative design variable vector. Multiplying both sides of Equation (38) by Λ^2 , we can write it as

$$\Lambda^2 = \frac{1}{\lambda \tilde{r}^t \tilde{M} \tilde{r}} \frac{[\tilde{r}^t \tilde{K}_i \tilde{r} - Z \tilde{r}^t \tilde{M}_i \tilde{r}]}{\rho_i \alpha_i \ell_i} \quad (40)$$

After multiplying both sides of Equation (40) by α_i^2 and taking the square root the expression for the design variable may be written as

$$\alpha_i \Lambda = C \alpha_i (U_i' / \tau_i')^{1/2} \quad (41)$$

where τ_i' and U_i' are the relative volume and energy terms of the element and they are given by

$$\tau_i' = \rho_i \alpha_i \ell_i \quad (42)$$

$$U_i' = [\tilde{r}^t \tilde{K}_i \tilde{r} - Z \tilde{r}^t \tilde{M}_i \tilde{r}] \Lambda \quad (43)$$

C is a constant term and it is the same for all the elements. It is given by

$$C = \frac{1}{\lambda \tilde{r}^t \tilde{M} \tilde{r}} \quad (44)$$

Since α_i exists on both sides of Equation (41), the resizing formula may be written as

$$(\alpha_i \Lambda)_{v+1} = C (\alpha_i)_{\nu} [U_i' / \tau_i']_{\nu}^{1/2} \quad (45)$$

where ν refers to the cycle of iteration. In the case of multiple loading conditions the resizing formula may be written as

$$(\alpha_i \Lambda)_{v+1} = (\alpha_i)_{\nu} \left[\sum_{j=1}^p C_j (U_i(j) / \tau_i(j))' \right]^{1/2} \quad (46)$$

where C_j are the weighting constants for the individual loading conditions

and they are given by Equation (44). A recursion relation similar to Equation (46) was used on a number of occasions for designing for static loading conditions involving displacement as well as uniform stress constraints (5) acting separately. However, when the constraints are mixed, convergence to the optimum is not as smooth as it is when they are treated separately. Also Equation (46) was hardly ever tried for designing with multiple dynamic loading conditions.

It should be noted that structures are hardly ever designed just for ground motion. It is more likely that ground motion is considered as one of the loading conditions along with a host of other static and dynamic loading conditions. The only dynamic case considered in this paper is the ground motion. Structures are designed for this case in conjunction with other static loading conditions. When the static and dynamic loading conditions are combined, the weighting constants and energy terms for the static case are given by (5)

$$C_j = \frac{Z}{W} \quad (47)$$

$$U_i^{(j)'} = \tilde{r}^t \tilde{K}_i \tilde{r} \quad (48)$$

where \tilde{r} is the displacement vector due to the static loading case and Z is the generalized stiffness requirement as defined by (5)

$$Z = \frac{1}{2} \tilde{R}^t \tilde{r} \quad (49)$$

or

$$Z = \tilde{R}^t \tilde{f} \quad (50)$$

for displacement constraint problems. In both Equations (49) and (50) \tilde{R} is the applied load vector. In Equation (49) \tilde{r} is the displacement vector resulting from the applied loads. In Equation (50) \tilde{f} is the displacement vector due to a unit load at the point and direction of the constraint displacement.

DESIGN PROCEDURE AND EXAMPLES

An outline of the resizing procedure using optimality criteria algorithm is given here:

1. The design starts with an initial solution of equal sizes for all the elements.

2. The structure is analyzed for static loads.

3. The structure is scaled to satisfy static stress and displacement requirements. The details and implications of scaling in static case are discussed in Reference 5.

4. The eigenvalues of the structure are determined.

5. The dynamic load factors for the ground motion are determined by Equation 22.

6. The eigenvectors of the structure are determined by inverse iteration.

7. The dynamic response due to ground motion is determined by using Equation 20.

8. The ground motion response is then added to the static response determined in Step 2.

9. The structure is again scaled to satisfy the combined static and dynamic stress requirements. The proportion of structural to nonstructural mass determines the effect of this scaling on eigenvalues (6). The three possible cases are as follows:

Case 1. No non-structural mass.

The eigenvalues and modes are unaffected by scaling.

Case 2. Structural mass is insignificant.

The eigenvalues can be scaled in the same proportion as the design but the eigenvectors have to be modified.

Case 3. Structural and non-structural masses are of similar proportions

Both eigenvalues and eigenvectors of the scaled structure have to be up-dated.

In the first case the design can proceed to the next step. In the second case Steps 5 thru 8 have to be repeated. In the last case Steps 4 thru 8 have to be repeated.

10. The feasible weight of the structure is determined.

11. The structure is resized using combined static and ground motion response in Equation 46.

12. Repeat Steps 2 thru 11 so long as the design improves.

EXAMPLES

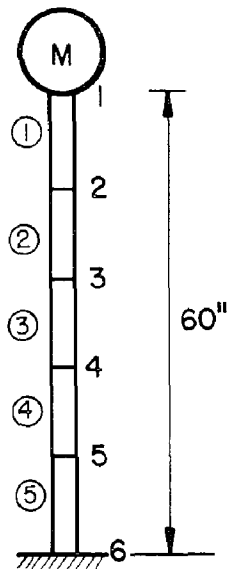
A cantilever column and a portal frame shown in Figures 1 and 2 are subjected to ground acceleration representative of 1940 El Centro, California Earthquake (North South motion). The duration of the earthquake is 29.32 seconds. The accelogram readings are available at 0.005 seconds interval. The total number of readings are 5864. For numerical integration of load factors the duration is sliced at 60 division increments (see Fig. 3). For

the cantilever problem only the first two modes are considered. Actually the first mode is significant. For the portal frame the first six modes are considered. The qualitative distribution of the moment of inertia is given in Tables 1 and 2.

The procedure presented in this paper fits quite well with the popular finite element analysis methods. The adequacy of the designs however, have to be checked with procedures that take into account the behavior in the elasto-plastic range. The ductility and the soil structure interaction are additionally important parameters left out in this design. An empirical procedure must augment this elastic design to introduce these parameters into the design.

REFERENCES

1. Newmark, N.M., and Hall, W.H., "Procedures and Criteria for Earthquake Resistant Design", National Bureau of Standards Building Science Series 46, February 1973.
2. Venkayya, V.B., Knot, N.S., and Berke, L., "Application of Optimality Criteria Approaches to Automated Design of Large Practical Structures". AGARD Second Symposium on Structural Optimization, April 2-6, 1973, Milan, Italy, Conference Proceedings No. 123.
3. Cheng, F.Y., and Botkin, M.E., "Second-Order Elasto-Plastic Analysis of Tall Buildings with Damped Dynamic Excitations", Proceedings, Specialty Conference on Finite Element Method in Civil Engineering held at Montreal, Canada, 1972, pp. 549-563.
4. Przemieniecki, J.S., "Theory of Matrix Structural Analysis", McGraw-Hill Book Company, New York, 1968.
5. Venkayya, V.B., "Design of Optimum Structures", Journal of Computers and Structures, Vol. I, pp. 265-304, 1971.
6. Venkayya, V.B., Khot, N.S., "Design of Optimum Structures to Impulse Type Loading", AIAA Journal, Vol. 13, No. 8, August 1975, pp. 989-994.



$M = 100 \text{ lbs-sec}^2/\text{ft}$
 $\rho = .00884 \text{ lbs-sec}^2/\text{ft-in}^3$
 $r = \text{rad. gyration} = 4.474$
 $E = 30. \times 10^6 \text{ psi}$
 $f_s = \text{allowable stress} = 30 \times 10^3 \text{ psi}$

} both problems

Fig. 1. Cantilever Column

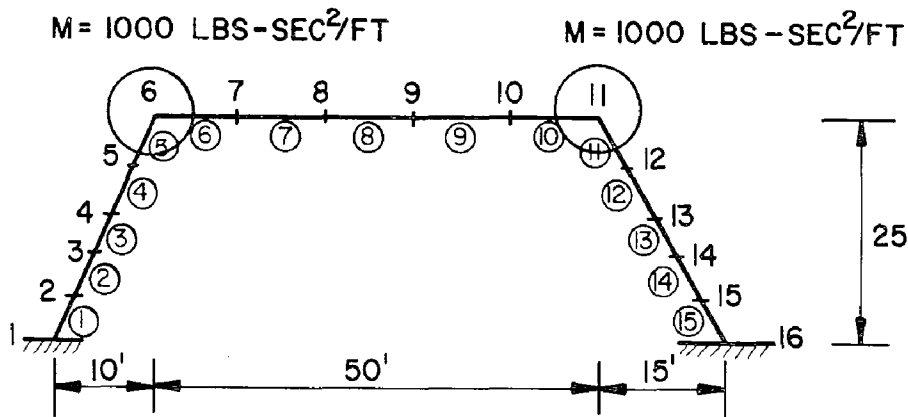


Fig. 2. Portal Frame

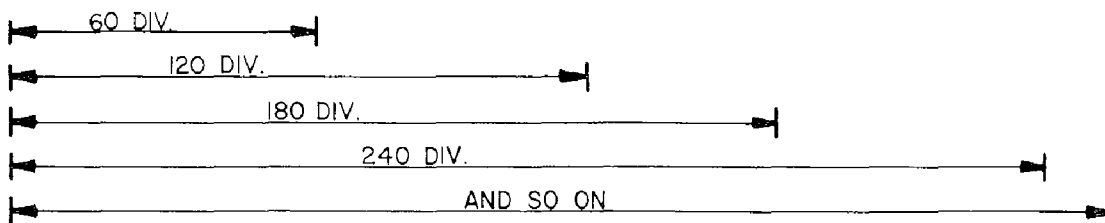


Fig. 3. Time Slices for Numerical Integration

Table 1. Moment of Inertia Distribution-Cantilever

El. No.	1	2	3	4	5
I	3.00	7.96	13.10	18.28	23.48

Table 2. Moment of Inertia Distribution-Portal Frame

El. No.	1	2	3	4	5	6	7	8
I	189.25	112.75	45.77	61.07	131.00	130.92	67.20	19.56
El. No.	9	10	11	12	13	14	15	
I	60.12	130.68	141.23	76.89	58.15	112.43	184.07	

INTERNATIONAL SYMPOSIUM ON
EARTHQUAKE STRUCTURAL ENGINEERING

613

St. Louis, Missouri, USA, August, 1976

PROBLEMS IN ESTABLISHING AND PREDICTING
DUCTILITY IN ASEISMIC DESIGN

S. A. MAHIN
Assistant Research Engineer

V. V. Bertero
Professor of Civil Engineering

University of California

Berkeley, USA

SUMMARY

Ductility factors are commonly used in inelastic analyses of building structures to quantitatively describe maximum deformations. Improved methods based on such factors have recently been suggested for preliminary seismic-resistant design and for detailing of critical regions. Definitions of several basic ductility factors are examined in detail in this paper noting problems that may be encountered in applying them to real structural systems. Alternative definitions are suggested for systems subjected to reversed plastification. The reliability of curvature ductility estimates obtained using conventional lumped, rather than more realistic spread, plasticity models is investigated. Systematic errors introduced by two-component models are examined. The implications of these results for the analysis and design of seismic-resistant structures are discussed.

INTRODUCTION

Economic considerations generally require that some of the energy input to a structural system during severe earthquake ground motions be dissipated by inelastic deformations. Because of uncertainties regarding the nature of future ground motions and the dynamic behavioral characteristics of actual structure-foundation systems, buildings must be capable of dissipating substantial energy. While large inelastic deformations may be tolerated for seismic events that occur infrequently, these deformations must be controlled to prevent loss of strength, large deflections or other actions that can lead to structural collapse or loss of life. To evaluate the seismic response of a structure, it is desirable to describe the main features of its hysteretic behavior using a few numerical indices. Since the hysteretic behavior of actual structural systems is complex, its precise quantitative description is difficult.

It has been common in inelastic structural analyses to express maximum required deformations in terms of ductility factors [Mahin & Bertero, 1975]. Such factors are generally defined as a particular system deformation divided by the corresponding deformation present when yielding occurs. If

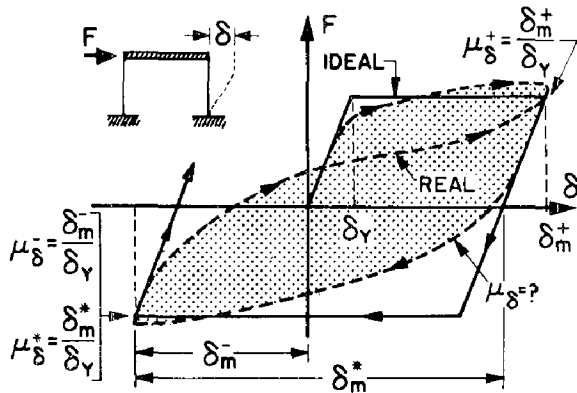


FIG. 1 DEFINITION OF DUCTILITY FACTORS

the load-deformation relationship under study can be idealized as being elasto-perfectly plastic, the history of the corresponding ductility demand will precisely define the complete hysteretic behavior. Unfortunately, the hysteretic behavior of real systems usually differs significantly from this simple idealization (Fig. 1), and although ductility factors can be used to describe maximum deformations, they generally fail to quantify energy dissipation.

PROBLEMS IN ESTABLISHING DUCTILITY FACTORS

In most cases it is neither convenient nor even possible to examine the hysteretic behavior of a system in detail. Ductility factors as previously defined are useful comparative indices of the severity of inelastic deformations. As such, ductility factors may be applied to nearly any response parameter including displacements, relative displacements (drifts), rotations, curvatures, and strains. It must be realized, however, that ductility factors based on different response parameters will generally not have similar numerical values. Furthermore, the load-deformation relationship for each of these parameters does not usually exhibit a definite yielding point. Consequently, the response parameters used as the basis of a particular ductility factor and the method used to determine its yield value must be clearly identified.

DEFINING DUCTILITY FACTORS. - Real structural systems may not have distinct yield points (Fig. 1). This may be due to material mechanical properties or because yielding in multistory structures does not generally occur instantaneously at all locations necessary to develop a collapse mechanism. Structures may therefore experience gradual, rather than sudden, reductions in their stiffness. For example, the base shear-roof deflection relationship computed for a two-story reinforced concrete frame (Fig. 2) differs significantly from an ideal elasto-perfectly plastic shape. The lateral load-deflection relationship for such multiple degree-of-freedom systems is not unique and depends on the distribution and history of loading. Many other parameters, such as variations in gravity loading, high rates of loading, changing environmental conditions, stress redistribution due to long-term loading, and so on, can also substantially affect the lateral load-deflection relationship. Precise determination of a yield value may not be possible in such cases. Possible estimates of the yield value include the deflection when yielding first occurs, the deflection corresponding to the collapse load had the structure remained elastic, or the yield deflection of an elasto-plastic system with the same energy absorption as the real structure (Fig. 3). In many cases the physical significance of the yield displacement may be lost.

Additional problems arise when cyclic inelastic deformations occur.

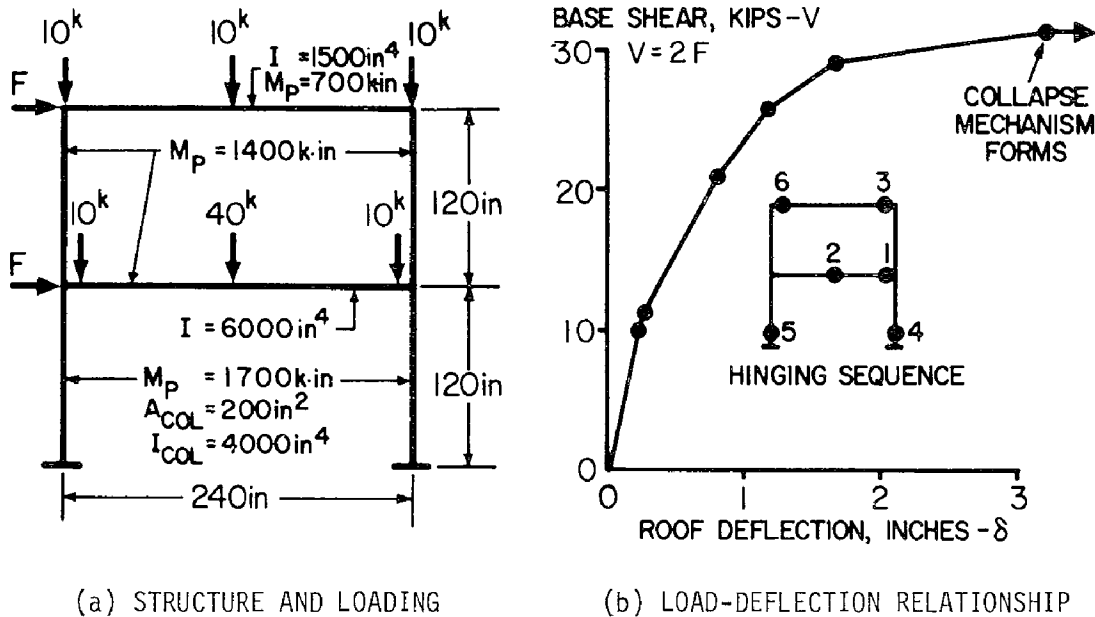


FIG. 2 NONLINEAR RESPONSE OF A STRUCTURE TO MONOTONICALLY INCREASING LATERAL LOADS (1 k = 4.45kN; 1 in. = 25.4mm)

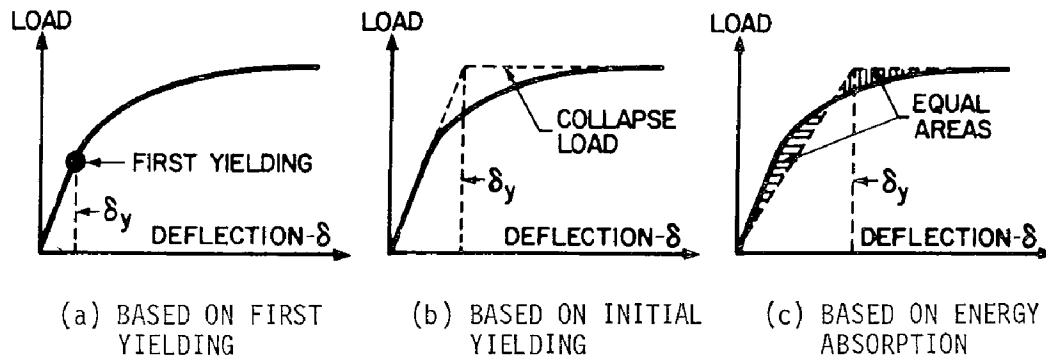


FIG. 3 ALTERNATIVE DEFINITIONS OF YIELD DISPLACEMENT

While ductility factors as previously defined are good indices of the maximum deflection of the system, they do not necessarily measure the severity of the largest inelastic deformation. To resolve this problem, schematically illustrated in Fig. 1, a cyclic ductility factor, μ^* , may be used [Mahin & Bertero, 1975]. The origin used to measure the system deformation in this case shifts to account for prior inelastic action.

The sum of the absolute values of all inelastic deformations divided by the yield value is also a useful index of the severity of the total inelastic deformation [Goel, 1968]. A definition of ductility which more directly measures the total inelastic energy dissipation would be useful, particularly for systems which substantially degrade in stiffness and/or strength. One such definition equates the total hysteretic energy, E_H ,

dissipated by the real system with that dissipated by an equivalent elasto-perfectly plastic system having the same yield strength, R_y , and yield deformation, δ_y , as the real system. The ductility factor for the equivalent system is given as:

$$u_{\text{equiv}} = \frac{E_H}{R_y \delta_y} + 1 \quad (1)$$

Furthermore, it is desirable to supplement information regarding the ductility of a system with the number of cycles of severe inelastic deformation and reversal. This data combined with the various ductility factors provides a better basis for assessing the hysteretic behavior of a system than the use of a specific ductility factor alone.

DUCTILITY FACTORS FOR OVERALL RESPONSE. - Ductility factors can be classified in two general categories: (1) factors used to describe the overall response of a structural system, and (2) factors used to describe the behavior of individual critical regions. The first category generally comprises ductility factors based on displacement and drift.

Displacement Ductility Factors. - Comprehensive preliminary aseismic design methods have recently been suggested in which equivalent static lateral design forces are determined using a selected value of overall lateral displacement ductility factor [Bertero & Kamil, 1975]. These design forces are established using ductility factors computed for single degree-of-freedom systems with different mechanical and dynamic characteristics subjected to various earthquake ground motions [Newmark & Hall, 1973; Anagnostopoulos, 1972; Murakami & Penzien, 1975].

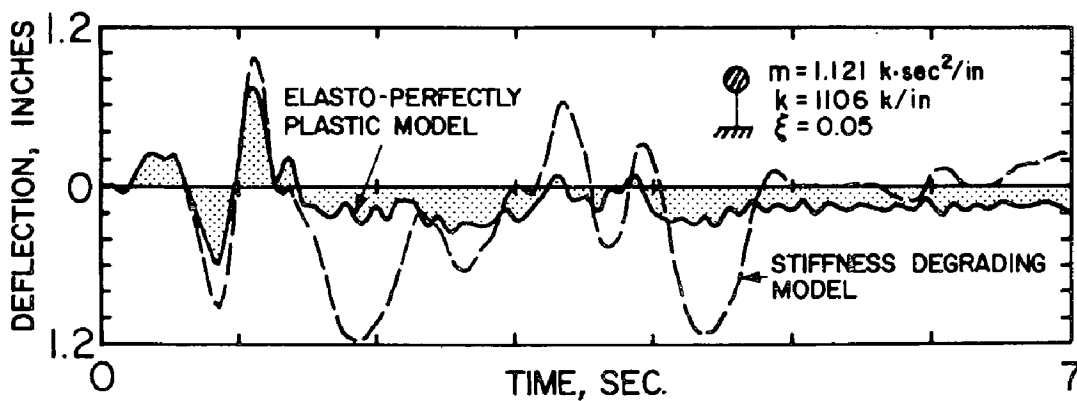
There are a number of problems inherent in this approach (see Bertero, Herrera and Mahin, 1975). For example, the complex inertial loadings that occur in multiple degree-of-freedom systems during earthquakes makes it impossible to identify a unique single degree-of-freedom system with nonlinear dynamic characteristics equivalent to those of the actual structure. Specifically, the actual structural hysteretic behavior may not be adequately represented by the elasto-perfectly plastic mechanical idealization generally assumed to derive design forces. For this idealization to be valid, all of the plastic hinges participating in a collapse mechanism would have to form instantaneously. Plastic hinging usually develops only in critical regions located in a few stories at a particular time; the stories that experience yielding change with time [Mahin & Bertero, 1975]. It has also been found that higher mode effects may prevent the formation of a complete collapse mechanism. Design forces based on assumed elasto-perfectly plastic behavior may not be appropriate in such cases.

Design procedures based on a selected overall displacement ductility factor do not account for the cumulative damage that may occur due to reversed inelastic deformation. Where low cycle fatigue may be critical, design might be more appropriately based on the cyclic or equivalent ductility factors previously defined, or on other types of factors that account for the total energy dissipation demand on the structure.

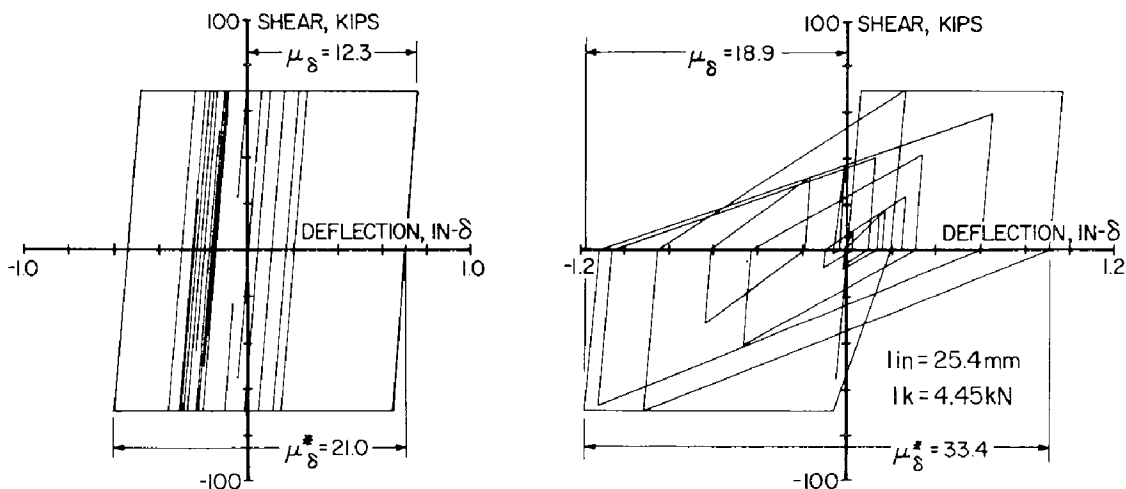
To quantitatively inspect the implications of the various types of ductility factors, the nonlinear behavior of two single degree-of-freedom

systems is discussed. Both of these systems had initial periods of 0.2 sec. and an effective seismic resistance coefficient ($C = V_{ULT}/W$) of 0.16. For the 1940 El Centro (N-S) accelerogram, used as the seismic excitation, the ratio of the resistance coefficient to the peak ground acceleration (expressed as a fraction of gravity) was 0.48. Viscous damping in both models was assumed to be equal to 5 percent of critical. A simple stiffness degrading hysteretic model was assumed for one of the systems and the other system was based on a conventional elasto-perfectly plastic model.

Response time-histories computed for the two systems are shown in Fig. 4(a). The apparent period exhibited by the stiffness degrading system was considerably longer than the initial period and its maximum deflections were larger than those for the elasto-perfectly plastic system. Considerable inelastic deformation including many cycles with reversed plastification occurred in both nonlinear systems as indicated by the hysteretic



(a) DEFLECTION RESPONSE HISTORIES



(b) HYSTERETIC CURVE FOR ELASTO-PERFECTLY PLASTIC MODEL

(c) HYSTERETIC CURVE FOR STIFFNESS DEGRADING MODEL

FIG. 4 RESPONSE OF TWO SINGLE DEGREE-OF-FREEDOM SYSTEMS WITH $T = 0.2$ SEC. TO 1940 EL CENTRO (N-S)

curves in Figs. 4(b) and 4(c). Maximum displacement ductilities computed for the elasto-plastic and stiffness degrading models were 12.3 and 18.9, respectively. The cyclic displacement ductility factors computed for the elasto-plastic and stiffness degrading systems were 21.0 and 33.4, respectively. While these values indicate that severe inelastic reversals do occur, they still fail to reflect quantitatively the large number of severe inelastic reversals indicated by the hysteretic curves. As shown in the

NUMBER OF EVENTS	ELASTO-PLASTIC SYSTEM	STIFF. DEGRAD. SYSTEM
POS. YIELD EXCURSIONS	12	2
NEG. YIELD EXCURSIONS	12	2
YIELD REVERSALS	13	3

accompanying table, the initial yield shear is reached considerably more often by the elasto-plastic system. The stiffness degrading system nevertheless experiences numerous cycles with large inelastic deflections [Fig. 4(c)]. Because of the degraded stiffness, the initial yield shear is not developed during these deflections. Consequently, the number of yield excursions and yield

reversals obtained for stiffness degrading systems may be misleading. A better indication of the total inelastic deformation is given by the computed hysteretic energy. The hysteretic energy dissipated by the elasto-plastic system was 316 k-in. (35.7 kNm) and the value for the stiffness degrading system was 407 k-in. (46.0 kNm). The stiffness degrading system dissipates substantial energy during cycles in which shears remain well below the yield level. Equivalent displacement ductility factors (Eq. 1) of 74.4 and 95.4 were computed for the elasto-plastic and stiffness degrading systems, respectively. Comparison of these values with the previously reported maximum displacement ductility factors clearly indicates that the systems developed substantial inelastic reversals.

Drift Ductility Factors. - While displacement ductility factors generally provide a good indication of structural damage, they do not usually reflect adequately the damage to nonstructural elements. This is an important limitation in aseismic design since a significant portion of the hazard to occupants and of the total cost of repairing earthquake damage is a consequence of nonstructural damage. Nonstructural damage is more dependent on the relative displacements (drift) than on the overall displacements. To obtain a reliable measure of nonstructural damage, maximum drifts must remain unnormalized or be divided by the value of drift corresponding to the damage threshold. Nonstructural damage estimates based on drift ductilities may be misleading. For example, nonstructural damage for relatively rigid structures may be small even for large values of displacement ductility since the yield displacement may be well below the nonstructural damage threshold. On the other hand, the nonstructural damage and lateral displacements for flexible structures may become intolerably large even before significant yielding develops.

To produce safe and economical structures, aseismic design methods must incorporate drift (damage) control in addition to lateral displacement ductility as design constraints. Story drifts and drift ductility factors may also be useful in providing information on the distribution of structural

damage. Unfortunately, conventionally computed story drifts may not adequately reflect the potential structural or nonstructural damage to multi-story buildings. In some structures, a substantial portion of the horizontal displacements results from axial deformations in columns. Story drifts due to these deformations are not usually a source of damage [Fig. 5(a)].

A better index of both structural and nonstructural damage is the tangential story drift index, R . As schematically indicated in Fig. 5(b), the intent of this index is to measure the shearing distortion within a story. For the displacement components shown in Fig. 5(c) and assuming that floor diaphragms are rigid in their own plane, the average tangential drift index is equal to:

$$R = \frac{1}{H} (u_3 - u_1) + \frac{1}{2L} (u_6 + u_8 - u_2 - u_4) \quad (2)$$

in which L is the bay width and H is the story height. The first term on the right-hand side of Eq. 2 is the conventional story drift index and the second is a correction applied for each bay accounting for the slope of the floors above and below the story. It may not be appropriate to average the values of R for a story when the pattern of axial column deformations varies greatly across the structure (e.g., frames with structural walls).

Although drift indices and, in particular, tangential drift indices, provide a good measure of the distribution of structural deformations, it may be difficult to compute corresponding yield drifts. One possible method for computing the yield drift includes taking the drift present at the appropriate location when the building, loaded with equivalent seismic lateral forces, reaches its yield displacement; another is by computing a story shear-drift relationship for a subassembly consisting of the story in question with appropriate boundary conditions.

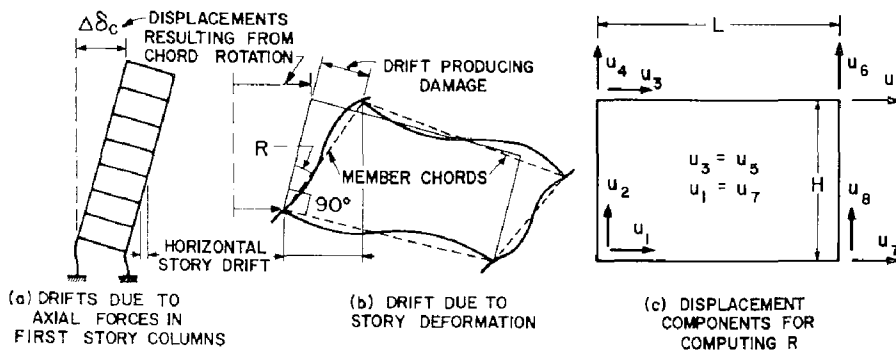


FIG. 5 COMPUTATION OF DRIFT INDICES

DUCTILITY FACTORS FOR CRITICAL REGIONS. - A comprehensive evaluation of the seismic response of a structure, as required in the final stages of design, may require thorough analysis of the behavior of individual critical regions. In flexural members, plastic rotations and curvatures are commonly used to monitor inelastic deformations at these regions. To design and detail critical regions, it would be ideal to examine their entire hysteretic behavior. Since this is generally impractical for large structural

systems, it is desirable to have at least a measure of the maximum inelastic reversals that may be required at a particular critical region.

Rotation Ductility Factors. - Joint rotations and plastic hinge rotations are response parameters commonly used as the basis of ductility factors. It is, however, difficult to determine meaningful values of yield rotations, particularly when inelastic deformations in critical regions are idealized by concentrated plastic hinges [Anderson & Bertero, 1973]. The rotation at a critical section corresponding to yielding depends on the stiffness, strength and loading of the structure as a whole. While yield rotations for members with simple loading conditions may be readily calculated, such factors as gravity loads, nonuniform cross-sectional properties, unsymmetric boundary conditions and so on, make such computations more difficult. Moreover, it is possible that a member's boundary conditions and/or gravity loadings are such that the joint rotation at yield is zero, resulting in infinite rotation ductility factors for all plastic rotations.

When the spreading of plastic deformations along a member is considered, the yield rotation may be based on the rotation that develops over the yielded region when yielding first occurs. Computation of this yield rotation, as well as the plastic rotation capacity, requires knowledge of the plastic hinge length, the moment variation and the moment-curvature relationships for the member. Because of these complexities, plastic rotations are usually presented unnormalized rather than in terms of rotation ductility factors. These unnormalized values may then be compared directly with rotation capacities obtained from experiments on similar regions under similar loading conditions.

Curvature Ductility Factors. - Yield and ultimate curvatures depend only on material and section properties. Moment-curvature relationships for most structural steel wide flange shapes can be adequately represented by an elasto-plastic idealization. The yield curvature can be established without difficulty. For some structural steel and many reinforced concrete sections, however, such idealizations may not be appropriate. An additional problem in defining curvature ductilities is that the ultimate flexural capacity of a steel or reinforced concrete section is generally a function of the applied axial load. Thus, it is possible for the flexural capacity to change during a yield excursion and for the moment at which yielding initiates to change from cycle to cycle due to variations in axial load. In such cases, it is difficult to establish meaningful definitions for yield moment. An equivalent curvature ductility factor based on Eq. 1 may be appropriate [Mahin & Bertero, 1975].

Evaluation of the possible behavior of individual critical regions to seismic excitations is complex since there are currently no adequate failure criteria based on curvature (or rotation) ductilities. Ultimate curvatures and plastic rotations may be estimated assuming monotonically increasing deformations. It is not clear whether these estimates are appropriate for cyclic loading, however, and only limited experimental data are currently available regarding energy dissipation or cumulative ductilities. To compensate for the lack of precise failure criteria and for uncertainties in the predicted nonlinear response, critical regions should be designed and detailed to have substantially larger energy dissipation

capacities than computed. Nonetheless, it appears that curvatures and curvature ductility factors are quite useful comparative indices of the severity of inelastic behavior in critical regions.

ANALYTICAL PREDICTION OF CURVATURE DUCTILITY FACTORS

In nonlinear structural analyses, inelastic deformations in flexural members are usually assumed to occur at concentrated plastic hinges (lumped plasticity models). One of the most extensively used analytical techniques to simulate the flexural behavior of members with bilinear hysteretic moment-curvature, $M-\phi$, characteristics is the two-component model shown in Fig. 6. One of these components is an infinitely elastic element with a

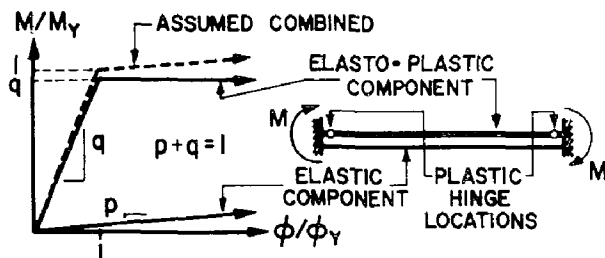


FIG. 6 TWO-COMPONENT MODEL

fraction p of the actual $M-\phi$ stiffness, and can be interpreted to represent the real $M-\phi$ strain-hardening stiffness. The other component has an elasto-perfectly plastic $M-\phi$ relationship with the remaining elastic stiffness and strength fraction q ($q = 1-p$). Inelastic deformations are concentrated in plastic hinges at the ends of the elasto-

perfectly plastic component. When flexural members with bilinear $M-\phi$ relationships are subjected to moment gradients, however, plastic deformations will be concentrated at discrete points only if the rate of strain-hardening, p , equals zero. Thus, idealizations such as the two-component model cannot exactly represent the behavior of flexural members with bilinear sectional stiffness characteristics [Powell, 1972].

The reasons for this can be clarified by noting that while the combined $M-\phi$ relationship for the two-component model is identical to the real member's bilinear $M-\phi$ relationship, this relationship is only applied at the end sections of the model. At other sections, the curvatures developed after both ends of the beam have yielded are controlled by the $M-\phi$ stiffness of the elastic component alone. In a member with bilinear moment-curvature relationships, the curvatures developed outside the critical regions are controlled by the initial $M-\phi$ stiffness of the member. This discrepancy usually leads to errors in evaluating curvature ductilities.

Effects of assuming lumped, rather than the more realistic spread, plasticity can be quantitatively evaluated by comparing results obtained using a two-component model with the exact solution based on bilinear sectional stiffnesses.

RESULTS FOR STATIC LOADING. - To simplify these discussions, a beam with constant plastic strength, M_p , and stiffness, EI , over its length, L , will be examined for the case of monotonically increasing antisymmetric end moments. Differences in the post-yielding moment-end rotation relationships computed for this example beam will be examined, and the reliability of curvature ductility factors obtained with two-component models will be assessed. Due to the antisymmetric loading, only half of the example beam (Fig. 7) need be considered. To facilitate the following discussions, the two-component model will be referred to as the model beam and the

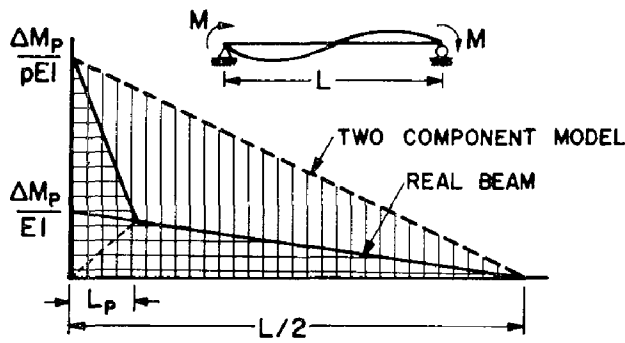


FIG. 7 INCREASE IN CURVATURES AFTER YIELDING
 post-yielding end rotation, $\Delta\theta_p^M$, is given by:

$$\Delta\theta_p^M = \frac{L}{6pEI} \Delta M_p^M \tag{3}$$

where ΔM_p^M is the amount by which the applied moment acting on the two-component model exceeds the plastic moment (i.e., $\Delta M_p^M = M - M_p$). In the case of the real beam, the post-yielding deformations are controlled by the incremental curvature distribution shown in Fig. 7. Thus,

$$\Delta\theta_p^R = \frac{\Delta M_p^R L}{6EI} + \left(\frac{\Delta M_p^R}{pEI} - \frac{\Delta M_p^R}{EI} \right) \frac{L_p}{2} \left(\frac{L}{2} - \frac{L_p}{3} \right) \frac{2}{L} \tag{4}$$

where L_p is the length of the plastic region and the superscript R denotes the real beam. The total moment-end rotation relationships for the real and model beams can be computed by adding the appropriate yield values to the post-yielding moments and end rotations obtained in Eqs. 3 and 4. Reference to Fig. 8, or comparison of Eqs. 3 and 4, clearly indicates that

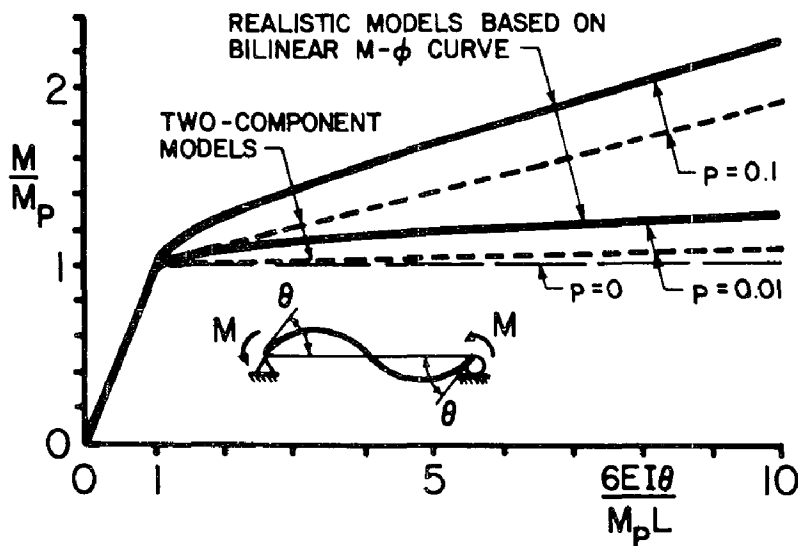


FIG. 8 MOMENT-END ROTATION RELATIONSHIPS

idealization with bilinear moment-curvature relationships as the real beam.

Post-yielding Moment-End Rotation Relationships.-

As soon as the yield moment is reached in the two-component idealization of the example beam, the stiffness of the member is controlled entirely by the elastic component, and the

the end rotation predicted by the two-component model can be substantially larger than that for the real beam if the same moments are applied to both (i.e., $\Delta M_p^M = \Delta M_p^R$). On the other hand, if the same end rotations are imposed on both (i.e., $\Delta \theta_p^M = \Delta \theta_p^R$), the two-component model will underestimate the resisting moment.

Differences between the beam and model can be further clarified by examining the beam's post-yielding secant stiffness, $K_T = \Delta M_p / \Delta \theta_p$. For the real beam, this stiffness may be expressed in terms of the curvature ductility factor, μ_ϕ , by noting that:

$$\frac{L_p}{L} = \frac{\Delta M_p^R}{2(M_p + \Delta M_p^R)} = \frac{p(\mu_\phi^R - 1)}{2[1 + p(\mu_\phi^R - 1)]} \approx \frac{\Delta M_p^R}{2M_p} = (\mu_\phi^R - 1)p/2 \quad (5)$$

thus,

$$\frac{K_T^R}{K_{EL}^R} = p \left[p + 3(1-p) \frac{p(\mu_\phi^R - 1)}{2[1 + p(\mu_\phi^R - 1)]} - 2(1-p) \left[\frac{p(\mu_\phi^R - 1)}{2[1 + p(\mu_\phi^R - 1)]} \right]^2 \right]^{-1} \quad (6)$$

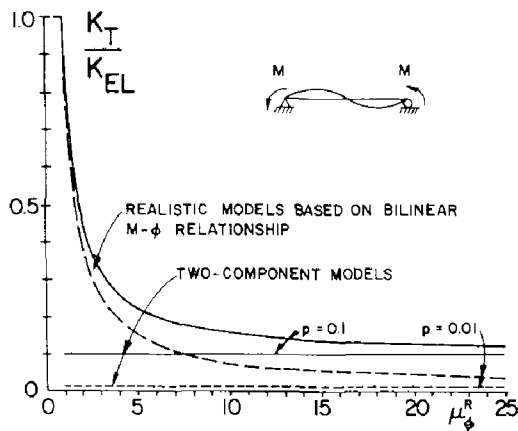


FIG. 9 TANGENT STIFFNESS VS. CURVATURE DUCTILITY FACTOR

in which K_{EL} is the beam's initial elastic stiffness, $K_{EL} = 6EI/L$.

Results of Eq. 6 are plotted in Fig. 9 which illustrates that the real beam's post-yielding stiffness decreases rapidly with the onset of yielding. On the other hand, the two-component model's tangent stiffness reduces immediately with the initiation of yielding to p times the initial elastic stiffness.

To analyze the errors involved in using the two-component model, it is convenient to compute the following ratio :

$$\frac{K_T^M}{K_T^R} = p + 3(1-p) \frac{p(\mu_\phi^R - 1)}{2[1 + p(\mu_\phi^R - 1)]} - 2(1-p) \left[\frac{p(\mu_\phi^R - 1)}{2[1 + p(\mu_\phi^R - 1)]} \right]^2 \approx p \left(\frac{3}{2} \mu_\phi^R - \frac{1}{2} \right) \quad (7)$$

where the approximate linear relationship is obtained by assuming $L_p \ll L$ and by disregarding higher order terms of p . Examination of the results of Eq. 7, plotted in Fig. 10, reveals that the two-component idealization may substantially underestimate the post-yielding stiffness of the member.

Plastic Rotations. - It is important to note that $\Delta \theta_p^M$ and $\Delta \theta_p^R$ given by

Eqs. 3 and 4 represent the end rotation of the member and not the actual plastic rotation. Plastic rotation is generally defined as the permanent rotation present at the end of the member when the end moment is reduced to zero. For this definition a rotation equal to $\Delta M_p^M/6EI$ and $\Delta M_p^R/6EI$ must be subtracted from Eqs. 3 and 4, respectively, to determine the actual plastic rotation. Plastic rotations usually reported for two-component models are generally based on Eq. 3 (this represents the rotation developed in the plastic hinge), and they will differ from the plastic rotations by a small amount for typical values of strain-hardening.

Because of the differences between the flexural stiffness of the model and real beams, it might appear that the seismic response predicted using two-component models would differ significantly from that predicted using realistic elements. If the flexural stiffness of a yielding member is small in comparison to adjacent elastic members, however, the incremental structural displacements and the nonlinear member deformations are controlled by the elastic deformations of the stiffer adjacent members; thus, the post-yield rotations computed using two-component models should be nearly correct. This may not be so for structures consisting of only a few elements or when a collapse mechanism forms.

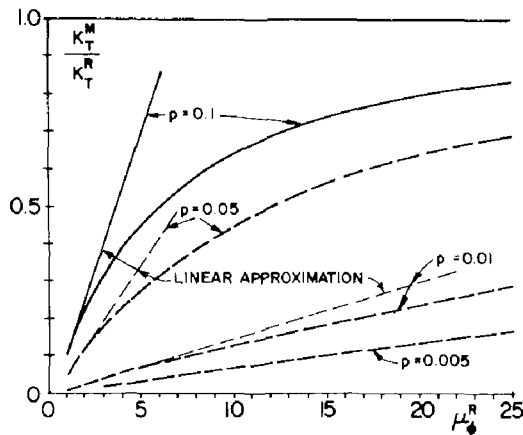


FIG. 10 VARIATION OF K_T^M/K_T^R WITH μ_ϕ^R

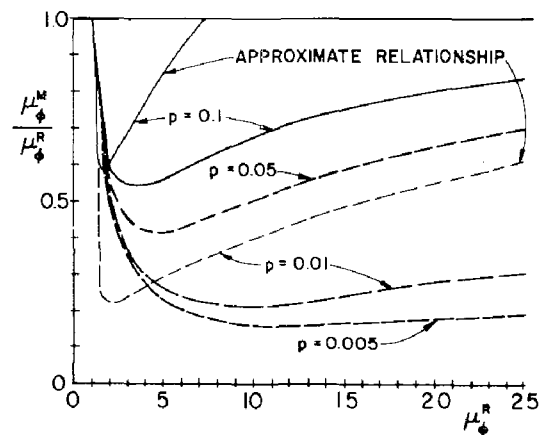


FIG. 11 VARIATION OF μ_ϕ^M/μ_ϕ^R WITH μ_ϕ^R

Moments and Curvature Ductilities. - If the incremental rotations developed at the ends of the real beam and the model are assumed to be identical, the following relationships apply :

$$\frac{K_T^M}{K_T^R} = \frac{\Delta M_p^M / \Delta \theta_p^M}{\Delta M_p^R / \Delta \theta_p^R} = \frac{\Delta M_p^M}{\Delta M_p^R} = \frac{\mu_\phi^M - 1}{\mu_\phi^R - 1} \quad (8)$$

From this equation, it is clear that relationships between incremental moments and curvature ductilities are also given by Eq. 7. As seen in Figs. 8 and 10, the two-component model would underestimate the maximum strain-hardening moments and curvature ductilities developed in a member for a given end rotation. Since the rate of strain-hardening is generally small, the error in the total moment (i.e., $M = M_p + \Delta M_p$) may not be

significant for most practical applications. However, curvature ductility estimates made on the basis of two-component idealizations may substantially underestimate actual ductility requirements, particularly at low values of ductility and strain-hardening. This is clearly shown in Fig. 11, which plots the following relationships obtained from Eqs. 7 and 8 :

$$\mu_{\phi}^R + \frac{1}{2} \left(\frac{3}{p} - 2\mu_{\phi}^M - 3 \right) \mu_{\phi}^R - \frac{2\mu_{\phi}^M}{p} (1-p) \mu_{\phi}^R - \frac{\mu_{\phi}^M}{p} (1-2p+p^2) + \frac{1}{2p^2} (2-3p+p^2) = 0 \quad (9a)$$

$$\text{or for } L_p \ll L, \quad \mu_{\phi}^R \approx \frac{2}{3} + \frac{1}{3} \left[1 + 6 \frac{(\mu_{\phi}^M - 1)}{p} \right]^{-2} \quad (9b)$$

Relationship between Curvature, Plastic Hinge Rotation and End Rotation Ductility Factors. - The simplicity of the example beam permits ductility factors based on response parameters other than curvature to be readily calculated. Comparisons of these factors further illustrates the differences between the model and real beams. For example, the rotation over the length of the plastic hinge can be divided by the rotation developed over that length at first yield to give a ductility factor based on the plastic hinge rotation. The basis of this definition for the real beam is shown in Fig. 12. Using Eq. 5, the relationship between curvature and plastic hinge rotation ductilities is given by

$$\mu_{\theta_p}^R = \frac{p(\mu_{\phi}^R - 1) + \mu_{\phi}^R + 1}{p(\mu_{\phi}^R - 1) + 2} \quad (10)$$

Since the length of the plastic hinge is zero for the two-component model, this definition cannot be applied to the model beam.

Ductility factors can also be based on end rotations. Such a factor is a measure of the overall deformation of the beam. The end rotation ductility factor is equal to $\mu_{\theta} = (\Delta\theta_p/\theta_y) + 1$, in which $\Delta\theta_p$ may be taken from Eqs. 3 or 4 and θ_y is equal to $M_p L / 6EI$. For the real beam, the relationship between the end rotation and curvature ductilities is given (using Eq. 5) by:

$$\mu_{\theta_p}^R = 1 + p(\mu_{\phi}^R - 1) \left[1 + \frac{(1-p)(\mu_{\phi}^R - 1)}{2[1+p(\mu_{\phi}^R - 1)]} \left(3 - \frac{p(\mu_{\phi}^R - 1)}{1+p(\mu_{\phi}^R - 1)} \right) \right] \quad (11)$$

Corresponding computations for the two-component model indicate that the end rotation ductility factor is numerically equal to the curvature ductility factor (i.e., $\mu_{\theta}^M = \mu_{\phi}^M$).

Results obtained from Eqs. 10 and 11 are plotted in Fig. 13. This figure clearly shows that the curvature ductility for the real beam can be considerably larger than ductilities based on plastic hinge rotation. These in turn are usually much larger than ductilities based on end rotation. This simple example reaffirms the need for explicit identification of the

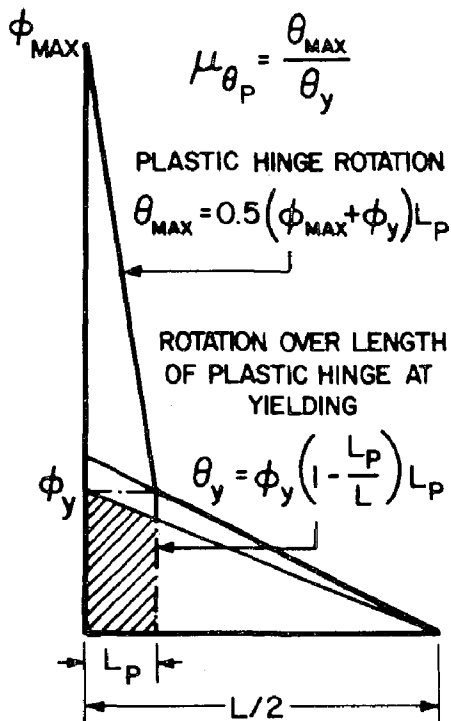


FIG. 12. DEFINITION OF DUCTILITY FACTOR BASED ON PLASTIC HINGE ROTATION

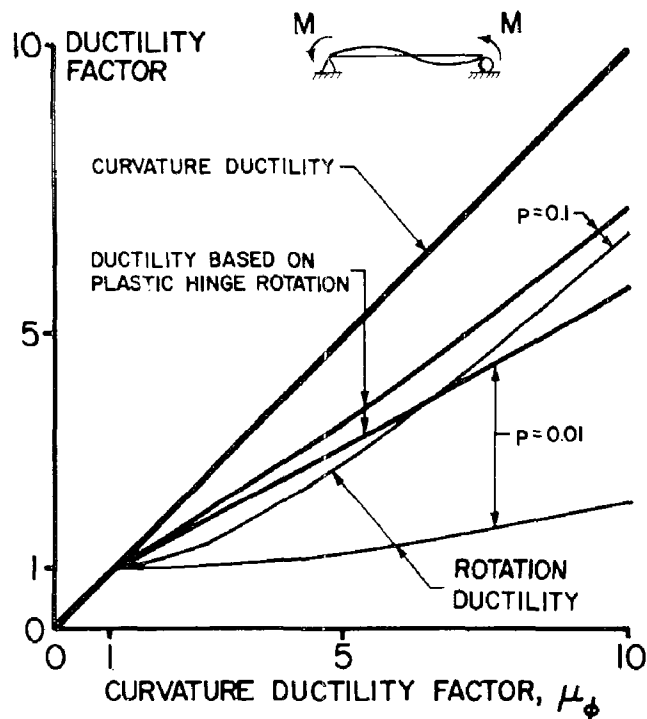


FIG. 13. COMPARISON OF DUCTILITY FACTORS BASED ON DIFFERENT RESPONSE PARAMETERS FOR REAL BEAM

definition of a ductility factor.

RELIABILITY OF TWO-COMPONENT MODELS. - In view of the results obtained for the preceding example, it is necessary to carefully evaluate and interpret analytical results based on two-component models. If the loading conditions and member properties found in practice resemble those shown in Fig. 7, analytical results obtained using two-component models can be interpreted using the above relationships. It must be remembered, however, that these relationships are only approximate for other loading conditions. Moreover, the relatively large difference between the post-yielding tangent stiffness of real and model beams may have a significant effect on the overall response of structures to both static and dynamic loading. In this case the assumption that plastic rotations in model and real beams are identical may not be justifiable and it will be difficult to estimate ductility requirements on the basis of results of two-component models.

Improvement of Reliability. - A simple method for reducing the error between the moment-end rotation relationships for the real and model example beams (see Fig. 8) might be to increase the yield moment assumed for the two-component model (i.e., $M_p^M > M_p^R$). The optimum magnitude of this increase, however, is not known and this approach may not be applicable to other loading conditions. Another method for improving the reliability of two-component models is to subdivide a member (especially the critical regions)

into a series of elements. It is expected that as the size of the subdivisions becomes smaller, the results would approach those for a member with bilinear moment-curvature relationships, but at the cost of increasing computational effort. Significant improvement may be obtained, however, by representing each critical region by a single element.

Implications for Aseismic Design and Analysis. - The seismic response of simple framed structures computed using lumped plasticity models with no strain-hardening has been compared with results obtained using refined nonlinear finite element structural idealizations [Latona, 1970]. The correlation between the results was poor. An investigation is currently being conducted by the authors to further assess the reliability of plastic rotations and curvature ductilities predicted using two-component models and to ascertain methods for interpreting these results.

It is believed that two-component models should provide valuable information regarding seismic response. Because of uncertainties involved with response prediction based on the two-component model and its tendency to underestimate curvature ductility requirements, critical regions must be detailed to have considerable reserve ductility capacity.

CONCLUSIONS

Ductility factors are useful indices of inelastic deformation for aseismic design and analysis. Because of the complex hysteretic behavior that may develop in real structural systems during seismic excitations, ductility factors require careful definition and interpretation. It is generally necessary to supplement ductility requirements with information regarding the number of severe yield excursions and reversals. Definitions for cyclic and equivalent ductility factors have been presented as possible indices of reversed plastification. Problems in implementing ductility factors based on displacement, drift, rotation and curvature have been discussed. While ductility factors based on curvature were comparatively easy to define, conventional methods for analyzing the nonlinear response of structures were found to introduce systematic errors in curvature ductility predictions. In spite of their limitation, properly interpreted, ductility factors can be useful design guidelines.

ACKNOWLEDGEMENTS

The work presented in this paper was sponsored by the National Science Foundation, Grant No. AEN73-07732 A02. The assistance of L. Tsai and L. Hashizume in the preparation of this paper is greatly appreciated.

REFERENCES

- Anagnostopoulos, S. A., "Nonlinear Dynamic Response and Ductility Requirements of Building Structures Subjected to Earthquakes," Department of Civil Engineering Research Report R72-54, Massachusetts Institute of Technology, Cambridge, Mass., September 1972.
- Anderson, J. C. and Bertero, V. V., "Seismic Behavior of Multistory Frames Designed by Different Philosophies," Earthquake Engineering Research Center Report No. EERC 69-11, University of California, Berkeley, June 1969.

- Bertero, V. V., Herrera, R. A., and Mahin, S. A., "Reliability of Nonlinear Aseismic Design of Structures using Inelastic Design Spectra," paper presented at the combined Fifth Pan-American Symposium of Structures and Seventeenth South American Conference of Structural Engineering, held in Caracas, Venezuela, December 8-12, 1975.
- Bertero, V. V. and Kamil, H., "Nonlinear Seismic Design of Multistory Frames," Canadian Journal of Civil Engineering, Vol. 2, National Research Council, Ottawa, Ontario, Canada, December 1975.
- Goel, S. C., "Response of Multistory Steel Frames to Earthquake Forces," AISI, Bulletin No. 12, November 1968.
- Latona, R. W., "Nonlinear Analyses of Building Frames for Earthquake Loading," Department of Civil Engineering Research Report R70-65, Massachusetts Institute of Technology, Cambridge Mass., September 1970.
- Mahin, S. A. and Bertero, V. V., "An Evaluation of Some Methods for Predicting Seismic Behavior of Reinforced Concrete Buildings," Earthquake Engineering Research Center Report No. EERC 75-5, University of California, Berkeley, February 1975.
- Murakami, M. and Penzien, J., "Nonlinear Response Spectra for Probabilistic Seismic Design of Reinforced Concrete Structures," Proceedings of the Review Meeting, U. S. - Japan Cooperative Research Program in Earthquake Engineering with Emphasis on the Safety of School Buildings, held in Hawaii, August 1975, Association for Science Documents Information, Tokyo, 1976.
- Newmark, N. M. and Hall, W. J., "Procedures and Criteria for Earthquake Resistant Design," Building Practices for Disaster Mitigation, Building Science Series 46, U. S. Department of Commerce, February 1973.
- Powell, G. H., "Notes on Inelastic Dynamic Analysis of Tall Buildings," University of California, Berkeley, June 1972.

INTERNATIONAL SYMPOSIUM ON
EARTHQUAKE STRUCTURAL ENGINEERING

629

St. Louis, Missouri, USA, August, 1976

SHEAR COEFFICIENT AND SHEAR FORCE DISTRIBUTION
IN NUCLEAR POWER PLANT STRUCTURES DUE TO SEISMIC LOADING

N. C. CHOKSHI¹ AND J. P. LEE²

¹Dynamic Analysis Engineer
²Head, Dynamic Analysis Section

Brown & Root, Inc.

Houston, Texas

Summary

In the earthquake-resistant design of Nuclear Power Plant facilities, structures are sometimes modeled by lumped-mass method. Due to this simplification, the shear coefficient has to be calculated and the total shear forces properly distributed. The shear coefficient is important because the deformations due to shear effect are generally significant. The distribution of the total shear force is a highly statically indeterminate problem and requires solutions of a large number of simultaneous equations for complex wall configurations. In this paper, the results of shear coefficient and shear distribution calculations due to both the thin wall beam theory method and the rigidity method are presented for several elementary structural shapes. These results are compared with those obtained by Cowper through the integration of the equations of three-dimensional elastic theory.

Dynamic Analysis is performed on a two story structure by using above two approaches to generate lumped-mass model. The results of dynamic analysis are compared with those obtained by constructing a finite element model. The Dynamic Analysis is performed in two orthogonal directions. Results and applicability of each approach are discussed.

Introduction

In the earthquake resistant design of nuclear power plant facilities, the shear forces and moments are obtained from the dynamic analysis of a structural model subject to the earthquake ground motion. Due to the labor, large computer core storage space and high computer cost involved in the dynamic finite element analysis, structures are frequently simplified by using a lumped - mass stick model. By simulating the wall system or portion of it by a single stick, it is necessary to determine the equivalent effective shear coefficient and the shear flow for each floor elevation.

The shear coefficient, which defines the effective shear area for a particular floor plane, is important in the analysis of nuclear power plant facilities because of the low aspect ratio of these structures. The deformation due to shear effect is generally significant in comparison to that due to bending effect. The shear coefficient will not only affect the

magnitude of the resulting shear forces due to ground motion but will affect the calculated natural frequencies as well.

The shear flow diagram, which show the distribution of a unit shear force acting at the shear center of a wall system, is important in the design application. The results obtained from the seismic analysis of the lumped-mass model are total shear forces for the entire wall system. This force should be distributed properly to each wall element for design. The distribution of shear force is a highly statically indeterminate problem and requires solutions of a large number of simultaneous equations for complex wall configurations. In this paper, both the rigidity approach (1) and the thin wall beam approach (3, 4, 5) are presented.

For the thin wall beam theory approach, the shear flow for each wall element at a particular floor elevation is calculated using the beam theory and the principle of virtual work (3, 4). The detailed theoretical procedure will be discussed under the Approximate Methods section. In the rigidity approach, one simplifying assumption is made, i.e. only the in-plane rigidity of the wall is considered. The relatively small out-of-plane rigidity is neglected. Thus, the overall effective coefficient in an apparent principal direction is directly proportional to the ratio of the area of wall elements parallel to the direction of interest to the total cross-sectional area.

The results obtained using the above two approaches are compared in a tabulated form with those obtained by Cowper (2) through the integration of the equations of three-dimensional elastic theory. The resulting shear coefficients and distribution of the shear forces are presented for various structural shapes such as box, I, T, angle, etc., for engineering design application.

A case study, including modal analysis and structural response analysis is performed, using the thin wall theory approach, the rigidity approach and the finite element approach. When the thin wall theory approach is used the stick representing the characteristics of the wall system is placed at the shear center about which the summation of moment of all the wall elements vanishes. Consistently, the torsional constant is also calculated using the same approach. When the rigidity method is used, the members are located at the rigidity center and the torsional constant is calculated about that point. A finite element model is constructed for this structure and subjected to same time-history motion. Results due to two lumped mass methods are compared with those due to finite element analysis under the Case Study section. Conclusions are drawn with regards to accuracy and applicability of each approximate method.

Approximate Methods for Computing Sectional Properties:

In this section two approximate approaches, viz, the thin wall beam theory approach and the rigidity approach are outlined. The procedure used for calculating the shear coefficient and torsional constant is indicated. Results from these approximate methods are compared with those due to three-dimensional elasticity approach. Fig. 1 shows floor plans of a two-story Diesel Generator building of a Nuclear Power Plant. Discussions in the following sections pertain to such shear wall cross-sections.

Thin Wall Beam Theory Approach: Following step wise procedure is used in this study to compute shear coefficient. Detailed mathematical derivation

can be found in Ref. 4. For the sake of discussion only one direction (x-direction) will be considered, same procedure is used to obtain the shear coefficient in other direction.

1. First, the shear flow in each wall element (such as AB, BC, etc. in Fig. 1a), due to shear force, V_x , acting through the shear center along the x-direction, is calculated using the thin wall beam theory. For the section which has closed loops (such as A' B' C' D' in Fig. 1b), this problem becomes indeterminate since the continuity at each junction of the wall elements must be maintained. This indeterminacy is solved from the condition that the rotation of each closed loop must be zero since the shear force is acting through shear center. Note that this results into as many number of simultaneous equations as closed loops in the section.
2. Secondly, the shear strain in each wall element, due to shear force of one unit in x-direction, is calculated. This is done by first obtaining the shear stress in each element and then dividing it by the shear modulus, G . The shear stress and shear strain have parabolic distribution along the length, s (fig. 1a), of a rectangular wall element.
3. The virtual displacement (of entire cross-section) per unit height, δx , due to shear force V_x can now be expressed in terms of the integral of the product of shear stress and strain over the entire cross-sectional area, A . For a cross-section consistency of n wall elements, this integral can be replaced by summation over the n terms.
4. From the basic beam theory:

$$\delta x = \frac{V_x}{G A_{sx}} \quad \text{--- (1)}$$

where, A_{sx} = effective shear area in x-direction

5. Equating the δx of eq. (1) and that obtained in step 3, one can compute A_{sx} .
6. Finally, shear coefficient, K_x , is defined by following relationship

$$K_x = \frac{A_{sx}}{A} \quad \text{--- (2)}$$

similarly, K_y is obtained.

The torsional constant for the open sections is calculated by using the familiar formula,

$$J = \sum_{i=1}^n \frac{b_i t_i^3}{3} \quad \text{--- (3)}$$

where, J - torsional constant, b_i = length of i th element, t_i = thickness of the i th element and n = no. of elements in a cross-section. For the sections with closed loops, torsional constant is calculated from the condition that under pure torque the angle of rotation of each closed loop will be the same. Again, this results into a set of simultaneous equations of size one less than the number of closed loops.

Rigidity Approach: In this approach, assumptions are generally made to simplify the calculations and to eliminate solving simultaneous equations. Continuity of intersecting walls is neglected.

The rigidity of the wall element is considered only along the length of the wall and this rigidity is calculated using the simple formula (1):

$$\lambda = \frac{1}{\delta} ; \quad \delta = \frac{h^3}{12EI} + \frac{h}{G A_s} \quad \text{-----(4)}$$

where, λ = rigidity of the wall element, δ = deflection of the wall element due to unit load, h = height of the wall, E = elastic modulus, A_s = effective shear area, and I = moment of inertia of the wall element about the axis perpendicular to the length of the wall.

The effective shear area in the x -direction (or y -direction) is obtained, by first summing the areas of the wall elements whose longer dimension is parallel to x -axis (or y -axis), and then dividing by 1.2 for the rectangular wall section. Again, shear coefficient is calculated from Eq. (2).

Total rotational stiffness, λ_R , is obtained from the following relationship:

$$\lambda_R = \sum_j \lambda_{xj} \cdot (Y_j - Y_{cr})^2 + \sum_k \lambda_{yk} \cdot (X_k - X_{cr})^2 \quad \text{-----(5)}$$

where, j walls are parallel to x -axis and k walls are parallel to y -axis, and, X_k , Y_j , X_{cr} , Y_{cr} = coordinates of center of wall elements and the rigidity center from a reference point. X_{cr} and Y_{cr} are obtained in similar manner as center of gravity. Here, the moments of rigidities are taken about the reference point:

$$X_{cr} = \frac{\sum_k \lambda_{yk} \cdot X_k}{\sum_k \lambda_k} ; \quad Y_{cr} = \frac{\sum_j \lambda_{xj} \cdot Y_j}{\sum_j \lambda_{xj}} \quad \text{-----(6)}$$

Torsional constant is calculated from elementary relationship:

$$\lambda_R = \frac{GJ}{h} \quad \text{-----(7)}$$

From eq. (4), it is evident that torsional constant for this method is dependent on height, h , of the cross-section. However, for structures with low aspect ratio, second term in eq. (4) will be the governing term, and J will be relatively independent of height.

Theory of Elasticity Approach - Cowper (2) derived the Timoshenko beam equation by integration of the equations of three-dimensional elasticity theory. From this approach he derived a formula for the shear coefficient, K , which takes into account the shear stress distribution in both cross-sectional directions. He presented results for many cross-sectional shapes.

Discussion of Shear Properties Calculations: Table 1 lists the results of shear coefficient calculations for some common shapes. Results from beam theory compare quite well with those from the Cowper's formula. The differences range from the 0.5% for the Tee-section to 2.6% for the thin-walled square box. For the same shapes, the differences from the rigidity approach are 7.8% and 2.7%. It is found that for symmetrical and relatively elementary shapes two approximate methods give closer results. However, for complex unsymmetrical sections, these results differ greatly as shown in the case study.

Shear coefficients resulting from beam theory are independent of Poisson's ratio, ν . The value of ν used here for Cowper's formula in Table 1 is 0.17. This value is selected as representative of the structural concrete. Ebner and Billington (3) compared the shear coefficient for two W shapes using beam theory and Cowper's formula. They also found very good agreement.

Because of the relatively low height to width ratios of nuclear power plant structures, one would expect that the natural frequencies of these structures will be affected by the shear coefficient. Ebner and Billington investigated the effect of K on natural frequencies for a fixed-fixed beam. For the case investigated, a difference of 2.1% in the K -values gave a difference of 1.75% in the fundamental frequency and 3.87% in the fifth natural frequency.

Table 2 shows the shear force distribution over the section for some simple shapes. It is noted that the zero forces in an element does not necessarily mean zero stress everywhere in the element, for the beam theory approach. These two methods give quite different distributions in case of complex sections as shown in case study. Torsional constant for open sections could differ very greatly from two approximate methods. Thin wall beam theory gives much lower values for this particular case. Locations of shear center and rigidity center will also be radically different for open sections. These aspects will be illustrated in case study.

Case Study:

In this section, a case study involving the first two stories of a Diesel Generator building of a Nuclear Power plant is undertaken. A Dynamic Analysis, using time history load, is performed.

The floor plans are shown in Figs. 1a and 1b. The height of the first story is 24' (7.32m), and that of the second story is 20' (6.10m). The thickness of the slab at each floor is 2' (.61m). Two three dimensional lumped-mass models according to the beam theory and the rigidity approach are developed for this structure. A finite element model is also developed for the same structure. The foundation is considered fixed for all three models.

Lumped-mass Models: In the lumped-mass technique the shear walls running between floors are combined as one structural member. Thus, there are two structural members for the case under consideration. For the beam theory members are located at the shear center, and for the rigidity approach they are located at rigidity center. The location of mass concentration is characterized as a mass center (or joint) in the lumped-mass model. Mass centers are located at each floor level. These mass centers include the dead load of slab and half the dead load of walls above and below. No live load is considered in this study since the finite element used is not capable of generating rotatory masses. However, it was found that the effect of rotatory inertia was negligible in the lumped-mass model due to the rigidity approach. These mass centers and elastic members are connected by rigid links. Thus, the eccentricity of the mass in both x and y direction is taken into account. Fig. 2 show the location of mass-center, rigidity center, and shear center for the first floor. The second floor has a symmetrical cross-section and all three centers coincide with geometric center.

Table 3 shows the calculation of shear properties. For the first floor, which is unsymmetrical about x-axis, the shear coefficient values differ greatly. However, for the symmetrical sections these values are close to each other. The major difference in two models is the torsional constant and eccentricity between the mass and elastic member of the first floor. However, for the second floor, the torsional constant from both the approach are much closer. One should note that torsional constant from rigidity approach is height dependent, unless the structure has a very low aspect ratio.

Fig. 3 shows the shear force distribution in each wall element of the first floor, due to a force of 100kips (45360.0 kg) acting though the shear center in x and y direction. As seen in figs. 3a and 3b, these results are significantly different for unsymmetrical axis. The rigidity approach gives zero forces in the walls perpendicular to the applied force. The distribution of shear force in each wall has significant impact in the design of those walls.

Finite Element Model: A three dimensional finite element model was generated for this building. The model consisted of 264 joints and 544 elements. The element used is triangular plate bending and stretching type. It has five degree-of-freedom and considers both the in-plan and plate bending forces. A sixth degree of freedom is added so that the element can be used to model the three dimensional structure (6).

Discussion of Results: Table 4 shows the natural frequencies calculation for all three models. The agreement between the rigidity approach and the finite element model is quite good in general. It should be noted

that the finite element model has a number of localized modes reflecting the local bending of walls. The first frequency of the thin wall beam model is extremely low. This is primarily due to low torsional stiffness of the first floor. The higher frequencies from the thin wall beam model are in reasonable agreement with those due to other models.

All three models are subjected to the same acceleration time history with duration of 14 seconds and maximum acceleration of $0.1g$. This time history is applied in both x and y direction separately. The response spectra of this time history envelops the response spectra specified by the NRC Regulatory Guide 1.60 (Revision 1).

Fig. 4 (a, b, c, d) shows the results of these time history analyses for both x and y directions.

Due to very flexible lower story, the maximum acceleration response of the thin wall model is much lower than the maximum ground acceleration (Fig. 4a). The results due to the rigidity approach are in good agreement with those due to the finite element model. In the y-direction (the structure is essentially symmetric, W.R.T. y-axis), the acceleration responses due to the all three models show better agreement (Fig. 4c). Due to the high flexibility, the thin wall beam model gives higher displacements (Fig. 4d). However, the shear forces from the two lumped-mass models show good agreement in y-direction (results not shown here). It was shown in a previous case study (ref. 4) that both the approximate methods give close results, for the structure consisting of closed wall sections.

Conclusions:

Following conclusions are made in this study. It should be noted that the following remarks, generally apply to the case under consideration.

1. For symmetrical sections, both the thin wall beam method and the rigidity method give close values for shear coefficients. However, for unsymmetrical section, these values may differ considerably.
2. Again, the shear force distribution will vary greatly for unsymmetrical sections.
3. For open sections, the thin wall beam method gives very low torsional constant. For the structures with open wall configurations similar to the case studied, the rigidity approach appears to generate results which correlate better with those due to the finite element model.

It must be pointed out that, great care is needed in introducing fictitious cuts to the cross-section for calculating the sectional properties. For the thin wall beam theory approach, the fictitious cut is taken care of by adjustment to satisfy the deformation requirements. However, for the rigidity approach, the results will be affected by the cuts.

Acknowledgments:

The authors would like to thank N. D. Fulton for his encouragement. They would also like to thank G. L. Fisher, M. B. Chan and I. K. Ghosh for helpful discussions. Thanks are also extended to A. H. Kotara, D. J. Olver and E. H. Bomke who helped to make this publication possible.

Bibliography:

1. Blume, J. A., Newmark, N. M., and Corning, L. H., 'Design of Multistory Reinforced Concrete Buildings for Earthquake Motions', PCA, 1961.
2. Cowper, G. R., 'The Shear Coefficient in Timoshenko Beam Theory', Journal of Applied Mechanics, Vol. 33, 1966, pp. 335-340.
3. Ebner, A. M., and Billington, D. P., 'Steady State Vibrations of Damped Timoshenko Beams', ASCE, Vol. 94, No. ST3, March 1968, pp. 737-759.
4. Lee, J. P., Chokshi, N. C., and Chan, M. B., 'Shear Coefficient and Distribution of Shear Force Due to Earthquake Load', Second ASCE specialty conference on Structural Design of Nuclear Plant Facilities, New Orleans, December 1975, Volume 1-B, pp. 1085-1105.
5. Maugh, L. C., 'Statically Indeterminate Structures', John Wiley & Sons, Inc., 1964.
6. 'ICES STRUDL Improvements', McDonnell-ECI, 1972, p. 24.

TABLE 1

SHAPE	SHEAR COEFFICIENTS		
	COOPER*	BEAM THEORY	RIGIDITY THEORY
	$K_x = 0.2391$	$K_x = 0.2960$ $K_y = 0.5559$	$K_x = 0.2778$ $K_y = 0.5556$
	$K_x = 0.4283$ $K_y = 0.4283$	$K_x = 0.4172$ $K_y = 0.4172$	$K_x = 0.4167$ $K_y = 0.4167$
	$K_x = 0.6601$	$K_x = 0.6460$ $K_y = 0.2079$	$K_x = 0.6250$ $K_y = 0.2083$
	$K_x = 0.4637$	$K_x = 0.4661$ $K_y = 0.3390$	$K_x = 0.5000$ $K_y = 0.3333$
	—	$K_x = 0.5735$ $K_y = 0.2610$	$K_x = 0.5556$ $K_y = 0.2778$

TABLE 2

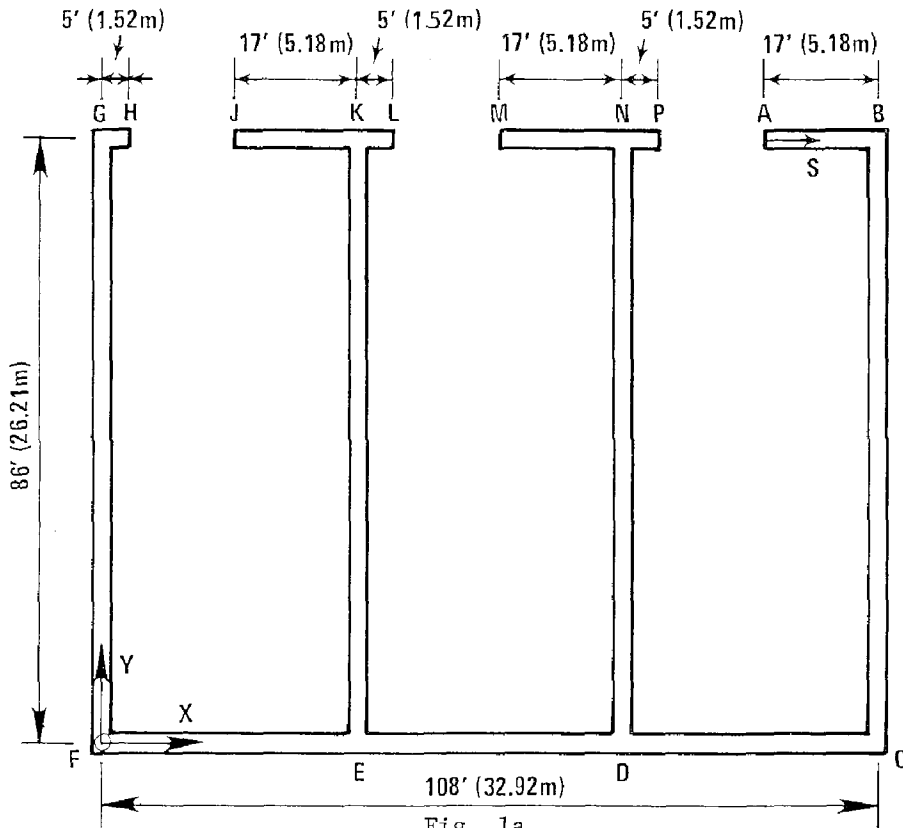
SHAPE	SHEAR FORCE DUE TO 100% BEAM THEORY		SHEAR FORCE DUE TO 100% RIGIDITY THEORY	
	X - DIREC.	Y - DIREC.	X - DIREC.	Y - DIREC.
	10.71 10.71 99.99 10.71 10.71	25.0 25.0 25.0 25.0	100.0	25.0 25.0
	49.99 49.99	49.99	50.0 50.0	50.0 50.0
	50.0 50.0	50.0	50.0 50.0	50.0 50.0
	99.93 13.63 13.63	49.6 49.6	100.0	50.0 50.0
	99.99	99.9	100	100

TABLE 3. SHEAR PROPERTIES

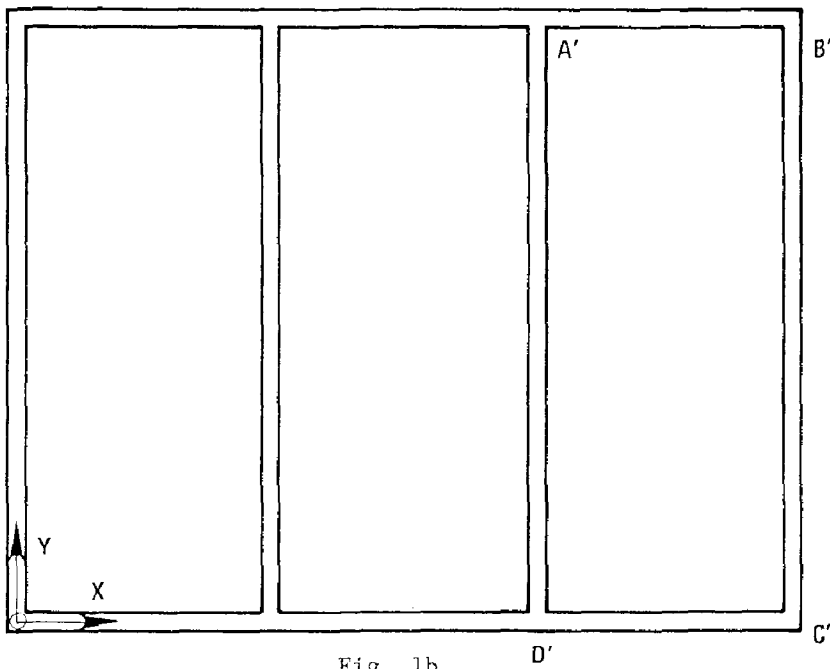
METHOD	FLOOR	SHEAR COEFFICIENT		TORSIONAL CONSTANT, $10^4 \text{ Ft.}^4 (10^4 \cdot \text{M}^4)$
		Kx	Ky	
THIN WALL BEAM APPROACH	1	0.14432	0.59492	.1381 (.0012)
RIGIDITY APPROACH	1	0.27993	0.55341	127.05 (1.0966)
THIN WALL BEAM APPROACH	2	0.33000	0.57011	184.40 (1.5916)
RIGIDITY APPROACH	2	0.32143	0.51190	156.88 (1.3540)

TABLE 4. NATURAL FREQUENCIES (GPS)

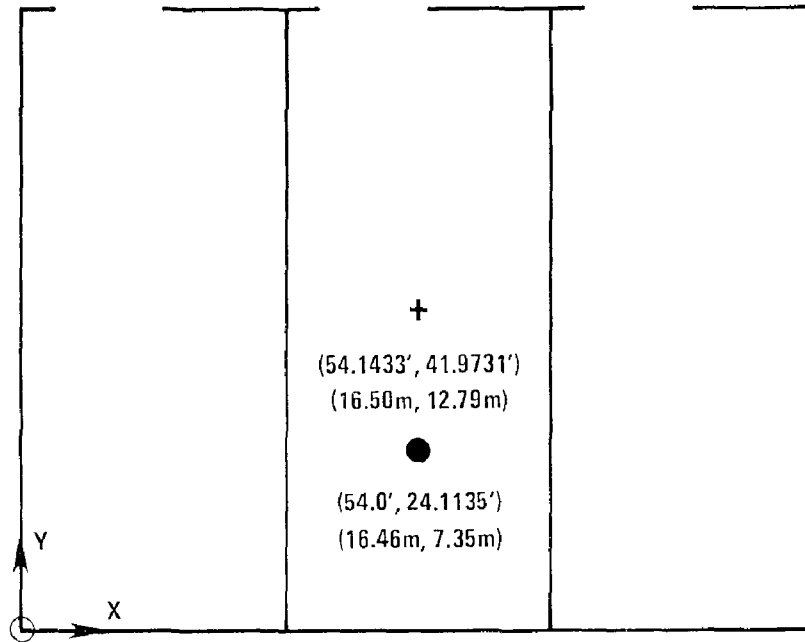
MODE	DIRECTION	MODEL		
		FINITE ELEMENT	RIGIDITY APPROACH	THIN WALL BEAM APPROACH
1	X	13.235	12.435	0.323
2	Y	20.860	17.215	16.720
3	X	34.665	35.540	31.570
4	Y	46.653	44.568	40.283



FIRST FLOOR PLAN
NOTE: ALL WALLS ARE 2 FT. THICK



SECOND FLOOR PLAN



⊙ (60.988', -41.369')
(18.59m, -12.61m)

+ MASS CENTER; ● RIGIDITY CENTER; ⊙ SHEAR CENTER

FIRST FLOOR: LOCATIONS OF MASS CENTER;
RIGIDITY CENTER AND
SHEAR CENTER

Fig. 2

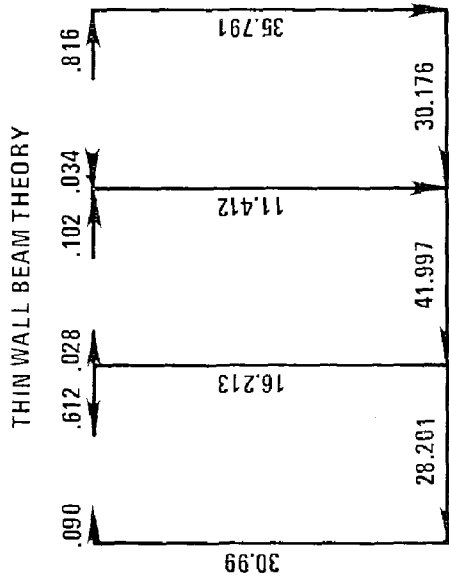


Fig. 3a

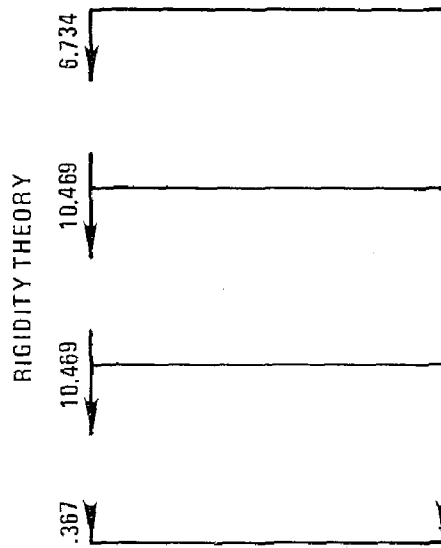


Fig. 3b

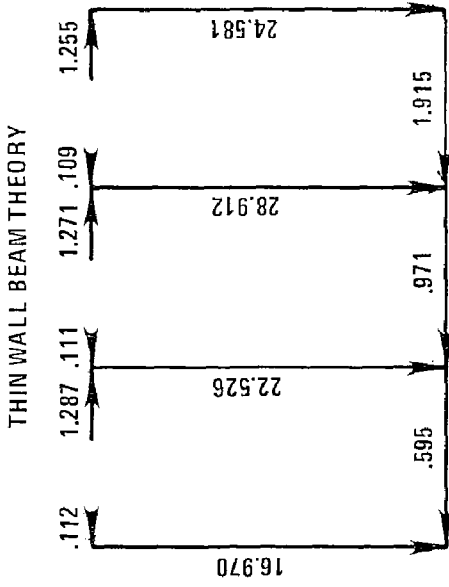


Fig. 3c

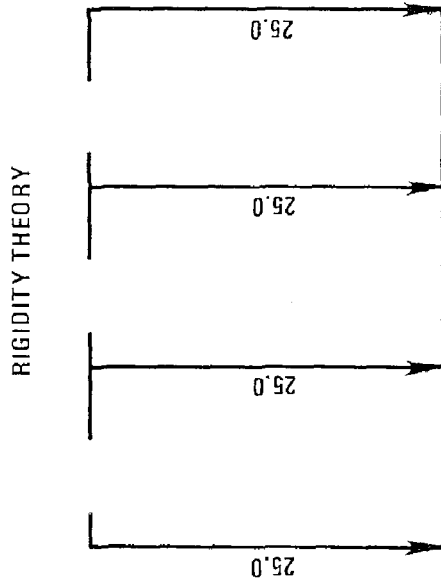


Fig. 3d

SHEAR FORCE DISTRIBUTION DUE TO 100 KIPS IN Y-DIRECTION

SHEAR FORCE DISTRIBUTION DUE TO 100 KIPS IN X-DIRECTION

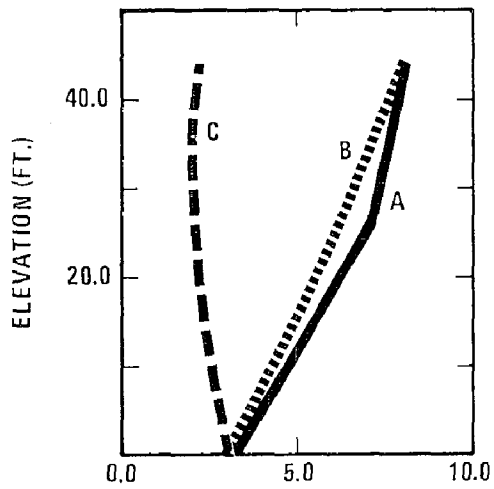


Fig. 4a

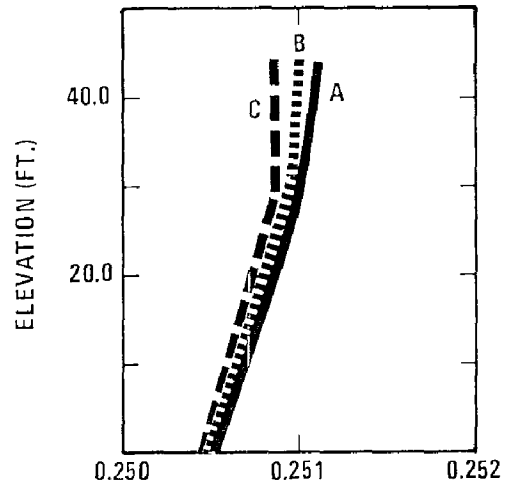


Fig. 4b

TOTAL ACCELERATION (FT.)

TOTAL DISPLACEMENT (FT.)

X - DIRECTION

A = FINITE ELEMENT; B = RIGIDITY APPROACH; C = THIN WALL BEAM THEORY

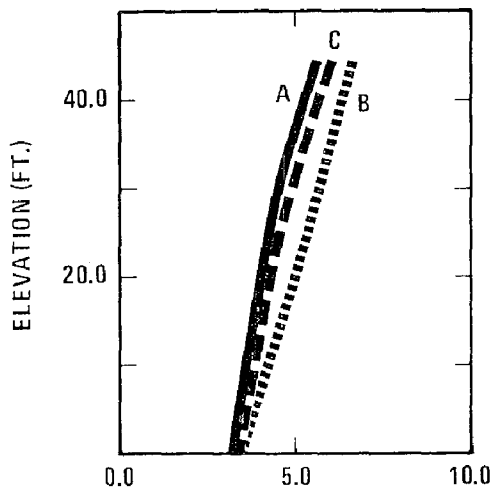


Fig. 4c

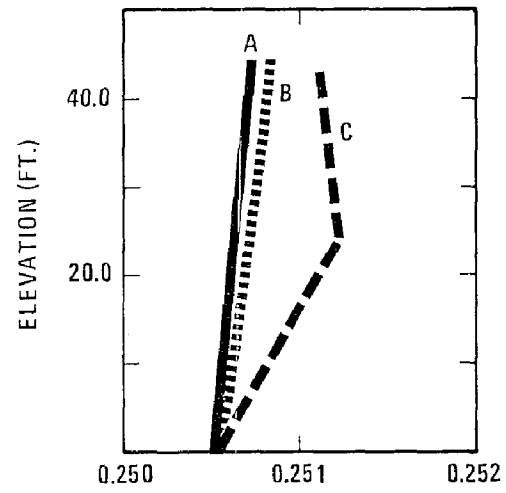


Fig. 4d

TOTAL ACCELERATION (FT.)

TOTAL DISPLACEMENT (FT.)

Y - DIRECTION

INTERNATIONAL SYMPOSIUM ON
EARTHQUAKE STRUCTURAL ENGINEERING

643

St. Louis, Missouri, USA, August, 1976

EVALUATION OF THE RESERVOIR EFFECT
ON THE DYNAMICS OF DAMS

H. U. AKAY and P. GÜLKAN

Department of Civil Engineering
Middle East Technical University
Ankara, Turkey

SUMMARY

A finite element procedure is presented for obtaining the approximate mass coefficients of two-dimensional dam-reservoir systems. The procedure is applied to obtain the dynamic response of a specific dam. The results are compared with the case in which the presence of the reservoir is not considered. It is concluded that for the large rockfill dam studied in the example, the added mass terms do not alter the dynamic response significantly when water is assumed to be incompressible.

INTRODUCTION

A problem of practical interest in the earthquake analysis of dams is determination of the effects of the reservoir on the dynamic response of the structure. The presence of a body of water affects the vibrational properties of a dam in two ways. First, the hydrodynamic pressure exerted by the reservoir during vibration caused by an earthquake alter the period of the structure, and may force a change in its frequency response. This effect is more important in tall arch dams which are relatively light. Secondly, the seepage of water into the body of an earth or rockfill dam changes the state of stress there as well as the properties of the constituent materials.

The finite element method has been used extensively for the earthquake analysis of earth, gravity and arch dams (e.g. 5,4,6,3,9) where the body of the dam is idealized into an assemblage of two or three dimensional elements. The presence of the reservoir is generally incorporated into the analysis in one of three different ways: One is to idealize the water as a structural finite element with zero shearing modulus (11). This method is computationally costly since one has to choose a grid layout for the reservoir as well as for the dam and the grid size grows rapidly. The second approach is to solve the coupled fluid and soil problem by taking into account the compressibility of water (14). Inasmuch as the governing equations for both components must be solved simultaneously, this procedure is also computationally difficult.

Also, it leads to non-symmetric matrices. The third approach is a special case of the previous one, and can be applied only if water is assumed to be incompressible. This leads to an uncoupled problem and is termed the "added mass" approach (14). In this, the effect of hydrodynamic pressure is approximately included in the analysis by calculating a set of influence coefficients which are simply added to the mass matrix of the dam.

The purpose of this paper is to present a method of calculating the added mass coefficients using a finite element code and to obtain the comparative dynamic response of a particular dam with and without the inclusion of these coefficients in the mass matrix. The method is also applicable to other two dimensional submerged structures.

ANALYSIS OF EARTHQUAKE RESPONSE

The cross section and the finite element arrangement selected for the dynamic analysis of Keban Dam, studied without the incorporation of reservoir effects in a previous paper (1) are shown in Fig. 1. The dam, which ranks among the largest in the world, has a height of approximately 210.0 m above the foundation and actually comprises a gravity section as well. The materials used in the rockfill portion can be grouped in three main categories : compacted rockfill, an impervious clay core, and a concrete core at the bottom of the axis (1).

Macroseismic data does not indicate the occurrence of an earthquake with a magnitude larger than $M=6.0$ within an 80 km radius of the dam (13). Although the location of the dam falls within a relatively earthquake-free zone in the earthquake categorization map of Turkey, an extension of the North Anatolian Fault is situated at a distance of approximately 100 km to the north. It would be a justifiable exercise to consider the long distance effects of a very large earthquake directly associated with this fault or the effects of a smaller magnitude event centered more closely. In order that comparisons may be made with results presented earlier (1), the same earthquake excitation was employed in the present study. Examination of the design calculations for the dam has shown that a slope stability analysis considering an equivalent lateral load of 15 percent of gravity has been done but no dynamic analysis was carried out (7). In this paper the results of a discrete parameter dynamic analysis considering an artificially generated earthquake intended to describe the ground motion for a magnitude 7.5 event at an epicentral distance of 40 km will be presented.

The mathematical model which was employed to portray the ground motion at the dam site is the same as that suggested in (2) and (8) : an approximation of white noise of a chosen duration was passed through a second order filter, and this process was followed by multiplying the ordinates by an envelope function to make the process nonstationary and to scale the maximum ground acceleration peak to a desired value. Although the total duration to the generated base motion in both the horizontal and vertical directions was 30 seconds, response calculations will be presented only for the approximately 9 second long portion of both components depicted in Fig.2.

METHOD OF ANALYSIS

A consistent way of calculating the added mass matrix due to reservoir effects with finite elements involves the solution of the appropriate boundary value problem as outlined in (14). For a two dimensional reservoir model, if the water is assumed to be incompressible, the excess dynamic pressures developed due to the motion of the boundaries are obtained from

$$\frac{\partial^2 p}{\partial x^2} + \frac{\partial^2 p}{\partial y^2} = 0 \quad (1)$$

in the reservoir, with boundary conditions

$$\frac{\partial p}{\partial n} = -\rho a_n \quad (2)$$

on the dam surface, and

$$p = 0 \quad (3)$$

on the free surface of the reservoir. In Eqs. 1-3, p denotes the dynamic pressure, ρ is the density of water and a_n is the component of the acceleration of the boundary in the direction of the unit normal n . Solving Eq. 1 successively by giving each node on the dam-reservoir interface a unit acceleration in the normal direction, the relation between the pressures p_1, p_2, \dots, p_m developed at m nodes on the boundary and the applied acceleration can be obtained as

$$p = \underline{M}_a a_n \quad (4)$$

where \underline{M}_a represents the added mass matrix. Further if a suitable interpolation matrix \underline{N} is used, the normal forces \underline{f}_{na} are obtained from

$$\underline{f}_{na} = \underline{N} \underline{M}_a a_n \quad (5)$$

By using an appropriate coordinate transformation matrix \underline{A} for the x - and y - directions, Eq.5 is transformed into

$$\begin{aligned} \underline{f}_a &= \underline{A}^T \underline{N} \underline{M}_a \underline{A} a \\ &= \underline{\bar{M}}_a a \end{aligned} \quad (6)$$

Here, it should be noted that the m by m added mass matrix \bar{M}_a is not necessarily symmetric unless the interpolating matrix \bar{N} is of the same order as the finite element approximation for p and unless the mesh is uniform at the interface. Only the uniformity of the mesh guarantees a symmetric \bar{N} with equal diagonal elements and symmetric matrix \bar{M}_a , and yields a symmetric matrix $\bar{N} \bar{M}_a$.

The equation of motion for the discrete structure is

$$\underline{M} \ddot{\underline{r}} + \underline{C} \dot{\underline{r}} + \underline{K} \underline{r} = \underline{f}(t) \quad (7)$$

where

\underline{M} = the mass matrix which is a diagonal lumped matrix in the present analysis

\underline{C} = damping matrix

\underline{K} = stiffness matrix

\underline{r} = relative displacement vector with (') indicating time differentiation

$\ddot{\underline{r}} = \underline{a}$ = acceleration vector

$\underline{f}(t)$ = time dependant load vector.

Under an earthquake loading

$$\underline{f}(t) = -\underline{M} \ddot{\underline{r}}_g \quad (8)$$

where

$\ddot{\underline{r}}_g$ = ground acceleration vector.

Equation (6) now can be coupled with Eq. 7 by modifying the mass matrix term to include the sum $\underline{M} + \bar{M}_a$ to yield

$$(\underline{M} + \bar{M}_a) \ddot{\underline{r}} + \underline{C} \dot{\underline{r}} + \underline{K} \underline{r} = -\underline{M} \ddot{\underline{r}}_g \quad (9)$$

A mode superposition algorithm was adopted in solving Eq.(9) to obtain the response of the structure, for which the undamped free vibrational eigenproblem.

$$\underline{K} \underline{\phi}_n = \omega^2 (\underline{M} + \bar{M}_a) \underline{\phi}_n \quad (10)$$

must be solved, which yields the n th mode shape ϕ_n and the n th natural frequency ω_n . Here, although \underline{M} is diagonal, \underline{M}_a is not, and therefore $\underline{M} + \underline{M}_a$ is a banded matrix with maximum band width of m .

FINITE ELEMENT IDEALIZATIONS

The finite element mesh of the dam cross-section is given in Fig.1. The structure is treated as a plane strain problem. For the dynamic structural problem, an arbitrary four-node isoparametric quadrilateral with u and v displacements as unknowns at each node was used (14). For the static analysis of the structure under body forces and hydrostatic pressure, an improved version of this element with an additional internal degree-of-freedom was used (12).

For the calculation of the added mass matrix, a separate finite element mesh for the reservoir cross-section was chosen so that the nodal points at the dam reservoir interface coincide for both the solid and the fluid. The reservoir was assumed to have a length to height ratio of four in the upstream direction. An arbitrary four-node isoparametric element with p as a degree-of-freedom was used in solving Eq.1 to obtain the added mass coefficients.

A computer program was coded to solve Eq.1 for m times ($m = 10$ in this case) for the reservoir and to calculate \underline{M}_a . The program then forms and solves response equation (Eq.7) by the mode superposition method. The method given in (10) was used for the time integration of modal equations.

As seen in Fig.1, the chosen mesh was not uniform at the interface; consequently the matrix \underline{M}_a was not symmetric. For computational convenience however, it was made symmetric here simply by taking the averages of the off-diagonal terms.

DISCUSSION OF RESULTS

The elastic material constants assumed for the different zones of the dam cross-section are indicated in Fig.1. Inasmuch as experimental data was not available, these constants were based on the known general average characteristics of similar materials. A viscous damping of 10 percent of critical in each mode was assumed, and the contribution of the lowest seven modes were included. For the numerical integration of response for each mode the linear acceleration scheme with 0.02 second time interval was used.

The lowest four free vibration mode shapes and the corresponding circular frequencies with and without the added mass effect are shown in Fig. 3. There was insignificant difference in the normalized mode shapes and this difference could not be indicated in the figures. The differences for the frequencies are generally within 5 percent, and can be explained by noting that the massive structure is insensitive to mass property variations caused by the presence of a body of water on the upstream face. The two dimensional behavior of the cross-section is apparent from Fig.3.

A comparison of the magnitude of the resultant acceleration at the tip of the dam (point A in Fig.1) may be seen in Fig.4. Except for small shifts in the extremum points, this figure indicates a general agreement between the two cases. Both the periodicity of the motion as well as the peaks are generally the same. The maximum absolute acceleration is reached near time $t = 7.5$ sec. with a magnitude of 0.60 g. The dam appears to be vibrating almost entirely in the first mode for which the period is about 1.0 sec.

In Fig.5 the variation of the normal stress component in x-direction for point B (Fig.1) is indicated. In the figure, the stress at $t = 0$ is due to self weight plus static water pressure. While the time variation of the stresses generally conform to the case where the presence of the reservoir is not considered, tensile stresses of significant magnitude are experienced at $t = 7.5$ sec. This would seem to indicate local failures in the cross-section during the strong ground motion.

CONCLUSIONS

This paper has presented a comparative dynamic study for the rockfill part of Keban dam which is presently in operation. The free vibration properties and the response, in terms of absolute acceleration and a normal stress component at selected points in the cross section, to a fairly strong artificial earthquake are given. It is noted that consideration of the hydrodynamic effects of the reservoir (under the assumption that water is incompressible) as an additional body of mass associated with the upstream face of the dam does not cause significant differences either in the mode shapes or in the general response. For a massive structure such as a large rockfill dam the interaction between the reservoir and the solid phase may be neglected without serious error. This effect however, may be significant for a gravity or an arch dam.

REFERENCES

1. Akay, H. U., and Gülkan, P., "Earthquake Analysis of Keban Dam", Proceedings of the Fifth European Conference on Earthquake Engineering, paper no.36, Istanbul, 1975.
2. Amin, M., and Ang, A. H. - S., "A Nonstationary Stochastic Model for Strong Motion Earthquakes", Civil Engineering Studies, Structural Research No.306, University of Illinois, Urbana, 1966.
3. Balsara, J. P., and Norman, C. D., "Vibration Tests and Analysis of a Model Arch Dam", International Journal of Earthquake Engineering and Structural Dynamics, Vol.4, 163-167, 1975.
4. Chakrabarti, P., and Chopra, A. K., "Earthquake Analysis of Gravity Dams Including Hydrodynamic Interaction", International Journal of Earthquake Engineering and Structural Dynamics, Vol.2, No.2, 143-160, 1973.
5. Clough, R. W., and Chopra, A. K., "Earthquake Stress Analysis in Earth Dams", Journal of the Engineering Mechanics Division, ASCE, Vol.92, No.EM2, April 1966.

6. Clough, R. W., Raphael, J. M., and Mojtahadi, S., "ADAP-A Computer Program for Static and Dynamic Analysis of Arch Dams", Earthquake Engineering Research Center Report No.73-14, University of California, Berkeley, 1973.
7. EBASCO Services Inc., "Keban Dam and Hydroelectric Power Plant - "As-Built" Design Drawings", State Waterworks Authority, Ankara, 1975.
8. Jennings, P. C., Housner, G. W., and Tsai, N. C., "Simulated Earthquake Motions", Earthquake Engineering Research Laboratory, California Institute of Technology, Pasadena, 1968.
9. Lefebvre, G., Duncan, J. M., and Wilson E. L., "Three Dimensional Finite Element Analysis of Dams" Journal of the Soil Mechanics and Foundation Division, ASCE, 495-507, July 1973.
10. Newmark, N. M., "A Method of Computation for Structural Dynamics", Journal of the Engineering Mechanics Division, ASCE, Vol.85, 1959.
11. Wilson, E. L., "A Method of Analysis for the Evaluation of Foundation-Structure Interaction", Earthquake Engineering Research at Berkeley, Report No. EERC 69-1, University of California, Berkeley, January, 1969.
12. Wilson, E. L., "SAP-A General Structural Analysis Program", SESM Report No. 70-20, University of California, Berkeley, 1970.
13. Yaralıoğlu, M., "Seismic Activity Investigation at Keban Dam, Turkey", Engineering Geology, 8:53-58, 1974.
14. Zienkiewicz, O. C., The Finite Element Method in Engineering Science, McGraw Hill, 1971.

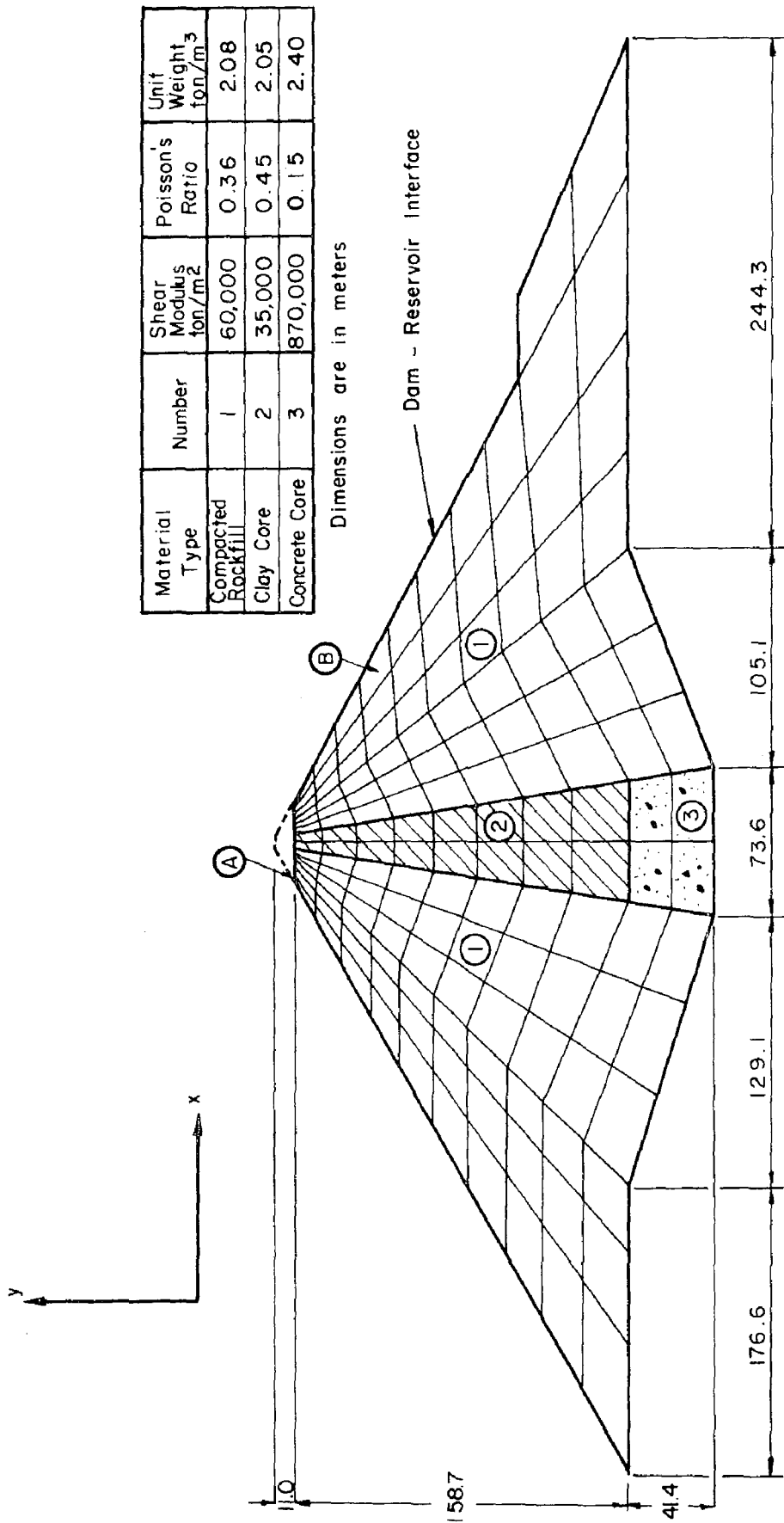


Fig. 1 - Mesh Arrangement of the Dam Cross Section

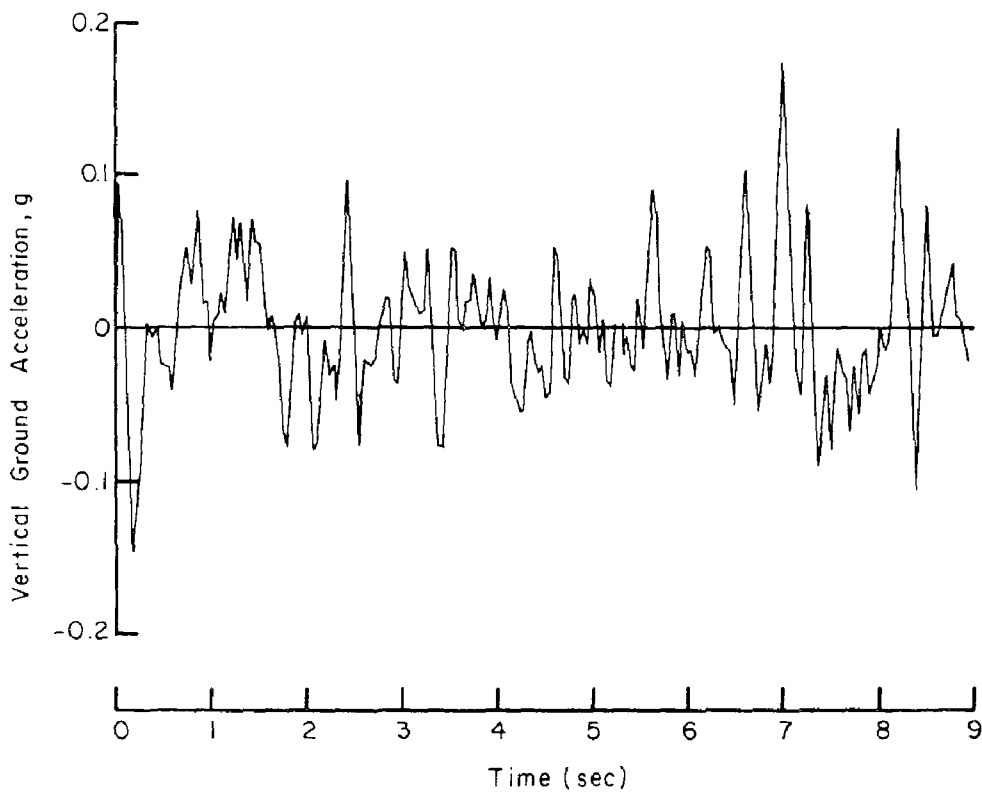
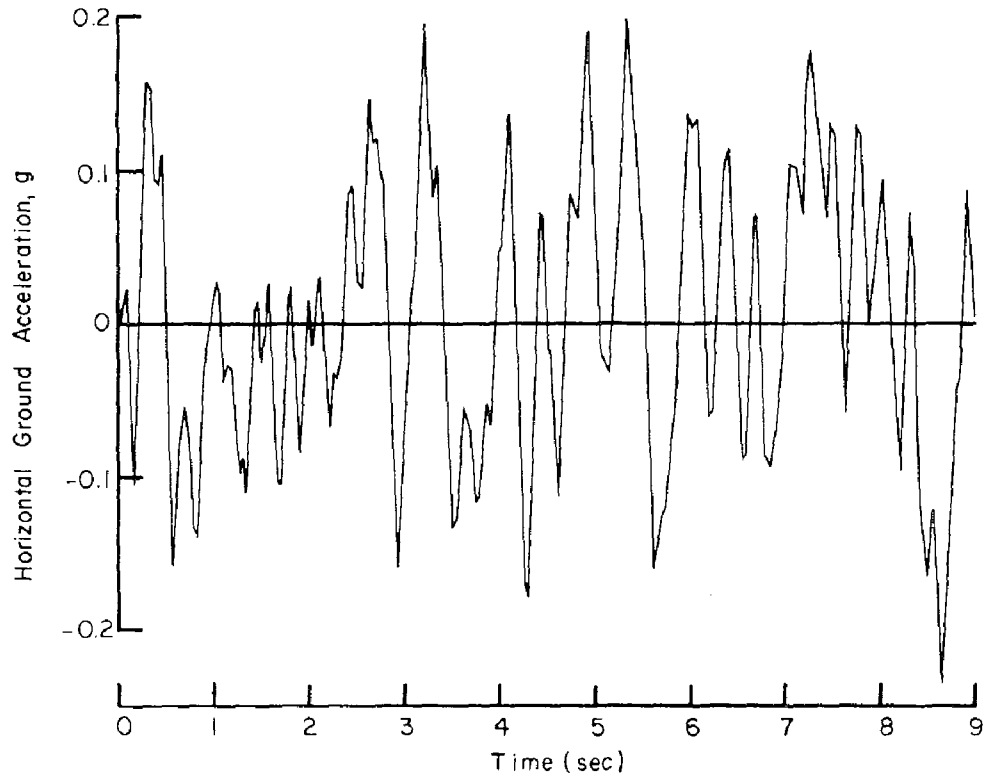


Fig. 2 - Horizontal and Vertical Ground Motion

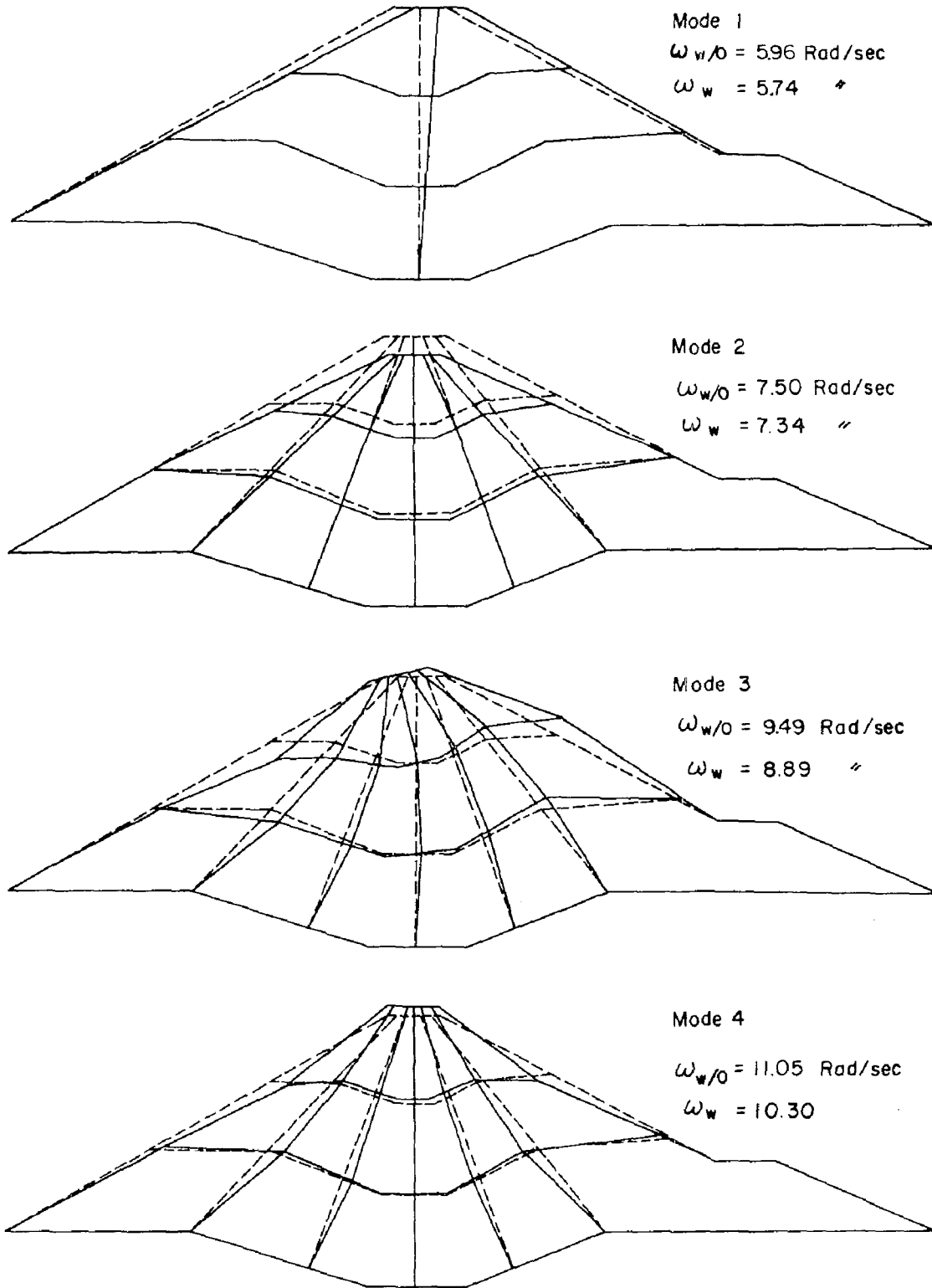


Fig. 3 - Free Vibration Mode Shapes and Frequencies (Modes 1 to 4)

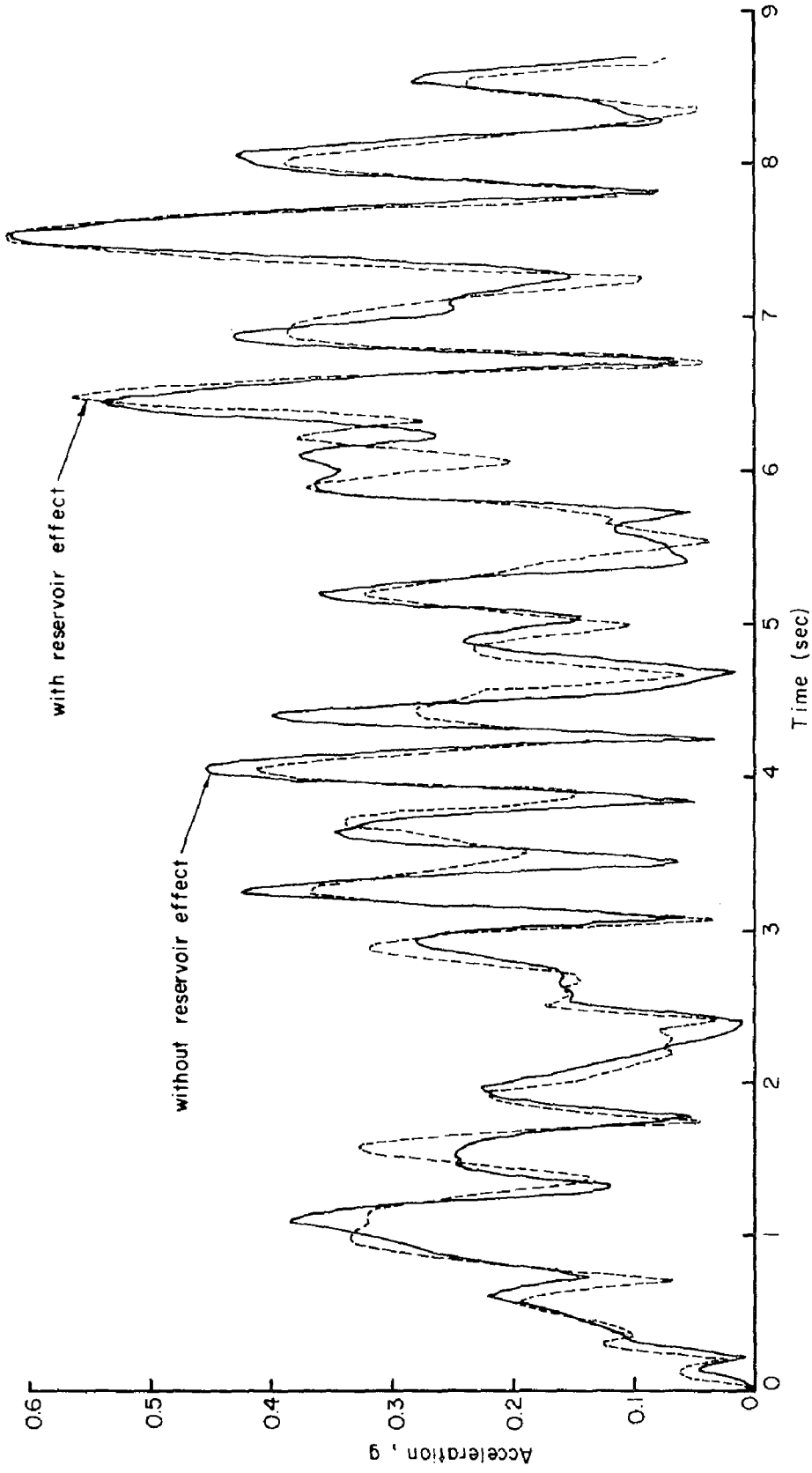


Fig. 4 - Time History of Total Acceleration at Point A

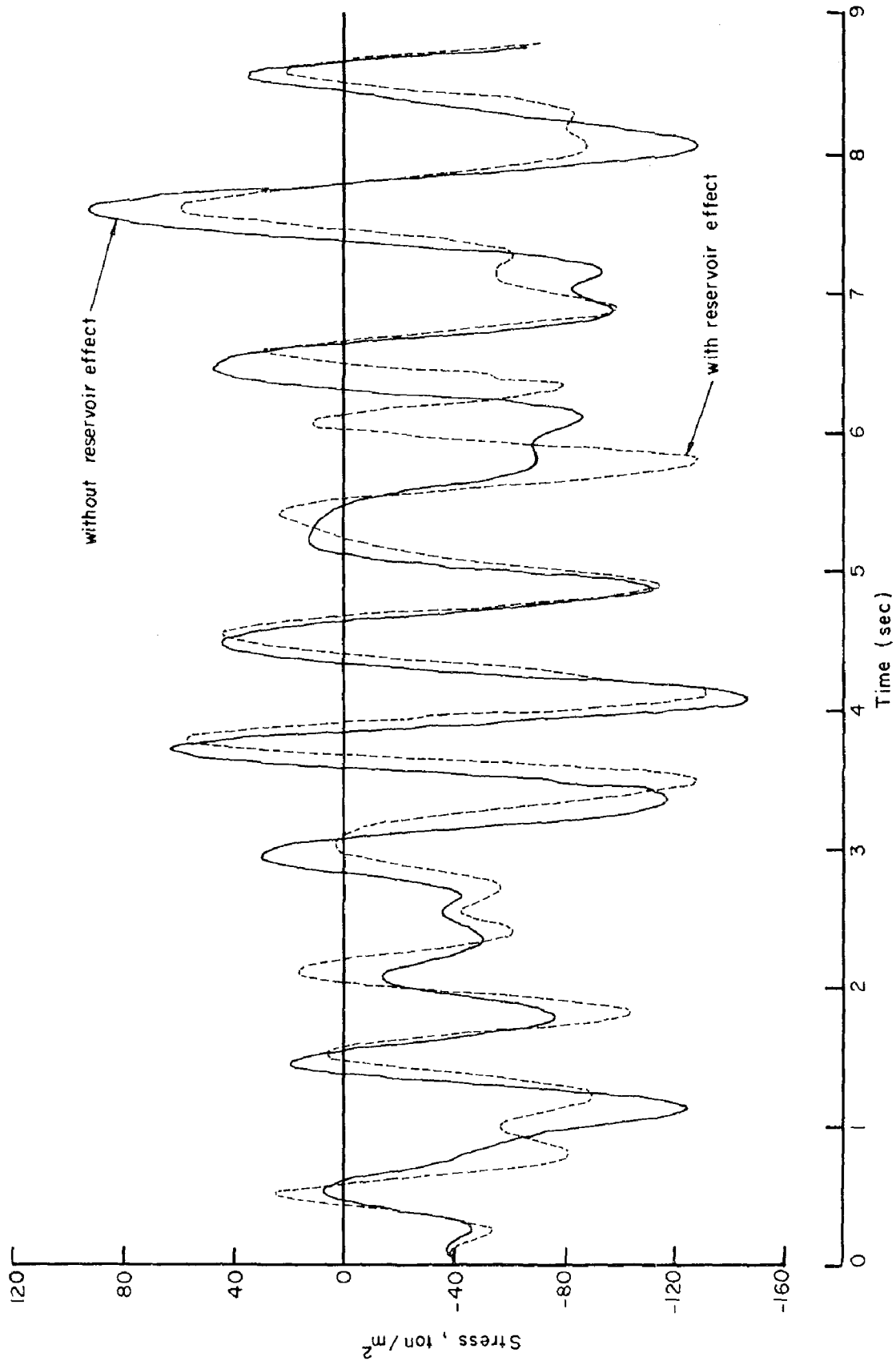


Fig. 5 - Time History of Normal Stress in x - Direction at Point B